



HAL
open science

Les bassins carbonifères-permiens et leur couverture mésocénozoïque - Mise à jour des connaissances, applications et perspectives

Laurent Beccaletto

► To cite this version:

Laurent Beccaletto. Les bassins carbonifères-permiens et leur couverture méso-cénozoïque - Mise à jour des connaissances, applications et perspectives. Sciences de la Terre. Université de Montpellier 2, 2023. tel-04639083

HAL Id: tel-04639083

<https://hal.science/tel-04639083>

Submitted on 8 Jul 2024

HAL is a multi-disciplinary open access archive for the deposit and dissemination of scientific research documents, whether they are published or not. The documents may come from teaching and research institutions in France or abroad, or from public or private research centers.

L'archive ouverte pluridisciplinaire **HAL**, est destinée au dépôt et à la diffusion de documents scientifiques de niveau recherche, publiés ou non, émanant des établissements d'enseignement et de recherche français ou étrangers, des laboratoires publics ou privés.



UNIVERSITE DE MONTPELLIER
GEOSCIENCES MONTPELLIER

LES BASSINS CARBONIFERES- PERMIENS

ET

LEUR COUVERTURE MESO- CENOZOÏQUE

Mise à jour des connaissances,
applications, perspectives

- Laurent BECCALETTO -

Habilitation à diriger des recherches

Soutenu le 06/12/2023

Composition du jury

Dominique Frizon de Lamotte	Pr. Emér., Cergy Paris Université	Rapporteur
Sophie Leleu	MdC, Université de Bordeaux - INP	Rapporteuse
Michel Séranne	CR, Université de Montpellier	Rapporteur
Sylvie Bourquin	DR, Université de Rennes	Examinatrice
Philippe Hervé Leloup (Président)	DR, Université Claude Bernard Lyon 1	Examinateur
Catherine Homberg	MdC, Sorbonne Université	Examinatrice
Michel Lopez	Pr. Emer., Université de Montpellier	Examinateur

" Je déclare avoir respecté, dans la conception et la rédaction de ce mémoire d'HDR, les valeurs et principes d'intégrité scientifique destinés à garantir le caractère honnête et scientifiquement rigoureux de tout travail de recherche, visés à l'article L.211-2 du Code de la recherche et énoncés par la Charte nationale de déontologie des métiers de la recherche et la Charte d'intégrité scientifique de l'Université de Montpellier. Je m'engage à les promouvoir dans le cadre de mes activités futures d'encadrement de recherche."

Avant-propos

De par son statut d'Etablissement Public à Caractère Industriel et Commercial (EPIC) à la croisée des mondes académiques et industriels, le **BRGM - Service Géologique National** - a une position stratégique dans le paysage de la recherche française et européenne. Par définition, il se doit de mieux connaître et comprendre le sol et le sous-sol de notre territoire, en France métropolitaine et en outre-mer. Cette connaissance est essentielle car au-delà des aspects scientifiques, elle aide à (i) une meilleure utilisation des ressources (eau, production et stockage d'énergie, minéraux industriels, métaux...), et (ii) une anticipation et gestion des risques naturels et des pollutions (dans une optique d'aménagement du territoire).

En particulier, les défis du changement climatique (voir les derniers rapports du GIEC), les tensions géopolitiques récentes, la croissance de la demande d'énergie, se traduisent par une demande accrue de connaissance du sous-sol pour produire différemment en émettant moins de CO₂.

Le BRGM est au cœur de ces enjeux scientifiques forts, et mon parcours depuis mon arrivée dans cette institution en 2007 s'insère parfaitement dans l'objectif d'accroître la connaissance géologique et en tirer des applications utiles.

Les bassins sédimentaires et les roches qui les composent sont des zones à forts enjeux socio-économiques (i.e. bassins de population), contenant de nombreuses ressources à la fois en surface (e.g. granulats, pierres ornementales) et en profondeur (e.g. eau potable, hélium et hydrogène, géothermies, hydrocarbures) ; leur sous-sol pourrait aussi servir de lieu de stockage pour le CO₂ ou l'hydrogène ; ils sont donc au cœur des enjeux mentionnés ci-dessus.

Mon domaine d'étude porte plus spécifiquement sur les **bassins continentaux à remplissage silicoclastique d'âge Carbonifère et Permien** et leur **couverture sédimentaire méso-cénozoïque** en France métropolitaine. Ces bassins fini-paléozoïques ont été largement étudiés et exploités par le passé pour leurs ressources en charbon et parfois en uranium jusqu'à la fermeture des mines à partir des années 1980. D'un point de vue académique, ces bassins ont été identifiés comme des témoins de la fin de l'orogène varisque, et ont fait l'objet de nombreuses publications, quand les concepts de d'effondrement tardi-orogénique et de désépaississement crustal se sont développés. L'état des connaissances a ensuite stagné et leur étude est entrée en sommeil, hormis quelques travaux isolés. C'était l'âge d'or de l'étude des bassins carbonifères-permiens qui s'est conclu au BRGM par la publication de synthèses géologiques faisant encore aujourd'hui référence (synthèse géologique du bassin houiller lorrain en 1981, synthèse sur le bassin houiller du Nord-Pas-de-Calais en 1983, synthèse géologique des bassins permien français en 1989). Dès mon arrivée au BRGM, j'ai choisi de poursuivre le travail sur ces bassins et j'ai été un des tout premiers en France (et le premier au BRGM) à braquer à nouveau à la fin des années 2000 les projecteurs sur ces objets, alors délaissés. Je les ai abordés en utilisant des données de subsurface nouvellement accessibles (profils sismiques retraités), afin de mieux les localiser et comprendre leur mode de formation.

Les données qui permettent d'imager ces bassins en profondeur m'ont aussi offert l'opportunité d'étudier leur couverture sédimentaire méso-cénozoïque, à l'exemple de mes travaux passés et

actuels dans le bassin de Paris et le fossé Rhéna. L'objectif de mes études est de mieux connaître leur géométrie profonde et d'étudier leur déformation en réponse à des événements géodynamiques lointains. Avec en fil conducteur ce besoin de connaissance croissant en réponse aux nouveaux usages du sous-sol (géothermie, hydrogéologie...), thèmes qui émailleront mon manuscrit.

En résumé, la démarche scientifique développée dans ce mémoire s'organise autour de trois piliers :

- **Les outils** - L'interprétation de profils sismiques retraités par le BRGM (dans le but d'imager les bassins sédimentaires en subsurface).
- **Les objets géologiques** - Les bassins sédimentaires comme marqueurs de la déformation :
 - Les bassins carbonifères-permiens : marqueurs de la transition syn- à post-orogénique varisque.
 - Le bassin de Paris et le fossé Rhéna: marqueur de la déformation far-field.
- **Les applications** - Les ressources des bassins sédimentaires, les usages de leur sous-sol.

Motivations

La rédaction de cette HDR est à la fois une démarche professionnelle et personnelle. C'est bien sûr l'opportunité de faire le point sur ma carrière en réalisant un bilan de mes activités scientifiques (recherche et encadrement d'étudiant). Se retourner sur son parcours après vingt ans d'activité n'est pas inutile, cela permet d'en dégager la cohérence, de valider ses acquis, et de poser l'état de l'art sur quelques sujets centraux. C'est aussi un solide point de d'ancrage, terreau fertile des idées et projets qui bâtiront mes futures recherches.

J'ai souhaité me rattacher à Géosciences Montpellier et présenter mon dossier à l'Ecole Doctorale GAIA de l'Université de Montpellier. En effet, située à proximité des bassins sédimentaires de Graissessac-Lodève-Saint-Affrique et de la Montagne Noire, Géosciences Montpellier est une place forte historique de l'étude de bassins carbonifères-permiens, toujours très active dans ce domaine. Ce laboratoire a par ailleurs développé depuis plus de vingt ans une expertise reconnue sur l'étude des bassins sédimentaires via les données de subsurface (apport de la sismique), données et méthode que j'ai largement utilisées au cours de mes travaux de recherche. Il me semblait important de présenter mon dossier HDR dans un laboratoire pionnier dans ce domaine. Je suis par ailleurs certain qu'obtenir mon HDR à Geosciences Montpellier ne peut être que bénéfique pour ma progression scientifique, le laboratoire étant reconnu en France et à l'étranger dans divers domaines des Géosciences, notamment celui de la Géologie des réservoirs et des ressources dans les bassins sédimentaires, sujet qui m'est cher. Cela me donnera également la possibilité de renforcer certaines collaborations et développer de futurs projets de recherche (e.g. avec l'équipe Géologie des réservoirs et ressources). Enfin d'un point de vue plus personnel, j'ai effectué mon cursus jusqu'au DEA à Geosciences Montpellier, et je suis ravi de pouvoir soutenir mon HDR dans ce même laboratoire, vingt-cinq ans plus tard.

Remerciements

Obtenir l'HDR était jusqu'à récemment un objectif assez lointain mais toujours enviable. La politique d'encouragement et de soutien aux agents BRGM en vue de les aider à obtenir ce diplôme a été le déclencheur de mon passage à l'acte, car l'enchaînement sans fin des projets ne me permettait pas de dégager le temps nécessaire ; que le BRGM en soit largement remercié.

Mes travaux n'auraient eu aucune réalité sans le soutien des personnels scientifiques, techniques et administratifs de l'Université de Lausanne et du BRGM ; un très grand merci à eux.

Je remercie chaleureusement tous les collègues avec qui j'ai directement échangé et collaboré depuis 25 ans, à Montpellier, à Lausanne, au BRGM et ailleurs.

Je remercie vivement mes rapporteurs Dominique Frizon de Lamotte, Sophie Leleu et Michel Séranne, ainsi que mes examinateurs Sylvie Bourquin, Hervé Leloup, Catherine Homberg et Michel Lopez, d'avoir accepté de participer à mon jury et pris le temps de lire ce manuscrit.

Mon parcours doit beaucoup au regretté Gilles Merzeraud (MCF à Géosciences Montpellier), à Gérard M. Stampfli (Pr. retraité de l'université de Lausanne) et Jean-Paul Cadet (Pr. retraité de l'Univ. P. et M. Curie), qui chacun à leur manière m'ont encouragé à poursuivre mon aventure géoscientifique.

Plan du manuscrit

Ce manuscrit s'organise comme suit :

- Une première partie présente mon CV et détaille mes activités pédagogiques et d'encadrement, ma production scientifique et mes projets de recherche.
- Présentation de mes activités de recherche, scindées en trois volets :
 - Un premier volet méthodologique sur le retraitement et l'interprétation des profils de sismique réflexion.
 - Un second volet sur les bassins carbonifères-permiens, le cœur de mon manuscrit.
 - Un troisième volet sur leur couverture méso-cénozoïque.
- Une dernière partie présente mes perspectives de recherches à court et plus long terme.

J'ai délibérément choisi de mettre les objets géologiques au centre de mon HDR. Les différentes grandes sections de mon manuscrit correspondent donc aux cas d'études successifs (les différents bassins, fini-paléozoïques, puis méso-cénozoïques). Pour chacun d'entre eux, la problématique scientifique et appliquée est posée, après un rappel du cadre collaboratif ; le contexte géologique régional est ensuite décrit afin de mieux appréhender les principaux résultats ; ces derniers sont résumés avant que l'ensemble de la démarche et des résultats soient exposés, le plus souvent sous formes d'articles insérés dans le corps du texte.

Ma sélection d'articles illustre mes activités des recherche (i) avec mes collègues universitaires (encadrements d'étudiants en M2, thèse et post-doc), (ii) en interne au BRGM, et (iii) pendant ma période lausannoise (en annexes).

Table des matières

Avant-propos	3
1. Curriculum Vitae	13
Situation actuelle	14
Situation antérieure	14
Diplômes	14
Formation continue	14
1.1. Activités pédagogiques	16
1.1.1. Depuis 2007, au BRGM	16
1.1.2. Avant 2007, à l'Université de Lausanne.....	16
09/2003-11/2006 1 ^{er} assistant	16
09/1999-08/2003 Assistant diplômé.....	18
1.1.3. Divers	18
1.2. Production scientifique	19
1.2.1. Articles publiés dans des revues à comité de lecture (au 01/03/2023).....	19
ACL	19
ACLN.....	21
Articles soumis dans des revues ACL	22
1.2.2. Numéros thématiques	22
1.2.3. Rapports BRGM (au 01/03/2023)	22
1.2.4. Mémoires universitaires	25
1.2.5. Actes de colloques (au 01/03/2023).....	25
Communications à des congrès internationaux.....	25
Communications à des congrès nationaux	30
1.2.6. Conférencier invité	35
1.2.7. Organisation et animation de colloques et workshop.....	35
1.2.8. Divers	36
1.3. Encadrement de la recherche	37
1.3.1. Synthèse de l'encadrement doctoral et participation aux jury de thèses	37
Encadrements principaux	37
Participation à l'encadrement et suivi de thèses	38
1.3.2. Encadrements post-doctoral	38
1.3.3. Encadrements de stages de recherche de Master 2 et 3A ingénieur	39
Au BRGM.....	39
A l'Institut de Géologie et de Paléontologie, Faculté des Géosciences et de l'Environnement, Université de Lausanne, Suisse.....	39
1.3.4. Encadrements de stage de recherche de Master 1	39
1.3.5. Encadrements de stage de recherche de L3	40
1.4. Projets de recherche	41
1.4.1. Au BRGM, projets en rapport direct avec les volets 2 et 3	41
Volet 2 - Les bassins carbonifères-permiens sous couverture sédimentaire méso-cénozoïque	41
Volet 3 - L'interprétation sismique au service des nouveaux usages du sous-sol : exemples du bassin de Paris et du fossé Rhénan.....	42
1.4.2. Au BRGM, projets à finalité appliquée.....	42
Ressource en eau	43
Ressources minérales.....	43
Risques naturels.....	43
Géothermie	43
Stockage souterrain	43

Hydrocarbures	43
1.4.3. A l'Université de Lausanne.....	44
1.4.4. Projets INSU financés en collaborations avec les partenaires académiques.....	44
1.4.5. Missions scientifiques.....	44
Au BRGM (depuis 2007).....	44
A l'Université de Lausanne.....	45
1.4.6. Activités synergétiques - Valorisation de la recherche	46
1.4.7. Collaborations scientifiques	46
ACTIVITES DE RECHERCHE.....	47
Introduction - Déroulement de mes activités de recherche.....	48
2. Volet 1 - Le destockage, le retraitement et l'interprétation de profils de sismique réflexion	51
2.1. La sismique réflexion.....	51
2.2. Déstockage des données sismiques brutes	52
2.3. Séquence de traitement	52
2.4. Les lignes retraitées au BRGM	53
2.5. L'interprétation sismique	54
2.6. Retraitement et interprétation sismique dans le bassin de Paris - Publication 1	57
2.6.1. Principaux résultats de la publication 1.....	57
2.6.2. Publication 1	59
3. Volet 2 - Les bassins carbonifères-permiens sous couverture sédimentaire méso-cénozoïque.....	77
3.1. Problématique générale.....	78
3.2. Les BCP en France métropolitaine et en Europe de l'ouest - cadre géodynamique interne et externe.....	78
3.2.1. Contexte géodynamique interne : la chaîne varisque d'Europe occidentale	78
La phase orogénique varisque sensu stricto (340-305 Ma)	79
Déformations tardi-varisques (305-270 Ma)	80
3.2.2. Contexte géodynamique externe - Transition icehouse - greenhouse.....	82
3.3. Les bassins carbonifères-permiens en France et en Europe occidentale	83
3.3.1. Les bassins syn-orogéniques westphaliens.....	83
3.3.2. Les bassins post-orogéniques stéphano-permiens.....	84
3.3.3. Localisation et âge des bassins carbonifères-permiens en Europe	85
3.4. Le bassin houiller du Nord-Pas-de-Calais, son substratum et la déformation du front nord varisque	90
3.4.1. Cadre collaboratif	90
3.4.2. Problématiques appliquée et scientifique	90
3.4.3. Contexte géologique du front orogénique nord varisque	93
Socle Brabançon.....	93
Parautochtone Brabançon et séries syn-orogéniques varisques.....	93
Ecaillés et Massifs Renversés (EMR)	94
Allochtone Ardennais, séries syn- et post-rifts rhéno-hercyniennes.....	94

3.4.4.	Le front nord varisque : structuration et évolution géodynamique - Publication 2	95
	Principaux résultats de la publication 2	95
	Publication 2	97
3.4.5.	Modélisation 3D des réservoirs dinantiens - Publication 3	130
	Principaux résultats de la publication 3	130
	Publication 3	131
3.5.	Le bassin sarro-lorrain, transition syn- à -post-orogénique varisque	145
3.5.1.	Cadre collaboratif	145
3.5.2.	Problématiques appliquée et scientifique	146
3.5.3.	Contexte géologique du bassin de Lorraine-Saar-Nahe (BLSN)	147
	The LSNB in the Variscan geodynamic context	147
	Stratigraphy of the LSNB	149
3.5.4.	Données sismiques et de forage, interprétation sismique	151
3.5.5.	Principaux résultats	153
3.6.	Les bassins stéphano-permiens du sud du bassin de Paris et du nord du Massif Central, évolution structurale et paléo-environnements en contexte post-orogénique	157
3.6.1.	Cadre collaboratif	157
3.6.2.	Problématiques appliquée et scientifique	158
3.6.3.	Contexte géologique des bassins stéphano-permiens du sud du bassin de Paris et du nord du Massif Central.....	159
3.6.4.	Evolution structurale et enregistrement sédimentaire des bassins stéphano-permiens du SO du bassin de Paris - Publication 4	160
	Principaux résultats issus de la publication 4.....	160
	Publication 4	161
3.6.5.	Le bassin de Decize-La Machine / Lucenay-lès-Aix	183
	Contexte géologique.....	183
	Géométrie et reconstitutions paléoenvironnementales du bassin de Decize-La Machine - Publication 5	183
3.6.6.	Le bassin d'Autun.....	211
	Contexte géologique.....	211
	Le bassin d'Autun : faciès, stratigraphie séquentielle et paléoenvironnements - Publication 6	211
4.	Volet 3 - La couverture sédimentaire méso-cénozoïque : interprétation sismique et nouveaux usages du sous-sol	247
4.1.	Le Mésozoïque du bassin de Paris.....	248
4.1.1.	Cadre collaboratif	248
4.1.2.	Problématiques appliquée et scientifique	249
4.1.3.	Contexte géologique du bassin de Paris	250
	Héritage varisque et subsidence mésozoïque	250
	Remplissage sédimentaire et déformations	251
4.1.4.	Résultats	255
	Schéma structural du bassin de Paris	255
	Impact des structures géologiques sur les anomalies thermiques du bassin de Paris	256
	Modélisation 3D à visée géothermique des aquifères en région Centre-Val-de-Loire - Publication 7..	258
	Ressource en eau - Caractérisation d'un système karstique dans la craie du sud du bassin de Paris...	278
4.2.	Le fossé Rhénan	281
4.2.1.	Cadre collaboratif	281
4.2.2.	Problématique scientifique et appliquée.....	281
4.2.3.	Contexte géologique du fossé Rhénan	282
	Evolution pré-rift du fossé Rhénan	283
	Evolution syn- et post-rift du fossé Rhénan.....	284

4.2.4.	Résultats	285
	Schéma structural, héritage structural, failles bordières et calendrier des déformations	285
	Conditions thermiques pré-rift du fossé Rhénan - Publication 8.....	290
5.	Perspectives de recherche	311
5.1.	Perspectives de recherche sur les bassins sédimentaires carbonifères-permiens	313
5.1.1.	Mise à jour de la connaissance et modalités de mise en place des bassins stéphano-permiens sur le pourtour du Massif Central	313
	Les bassins en bordure occidentale du Massif Central	313
	Les bassins en bordure orientale du Massif Central et la phase saalienne.....	313
	Les bassins du sud du Massif Central, connexions Lodève-Alès	314
	Datations absolues et corrélations inter-bassins	315
5.1.2.	Le projet Deepdust - Explorer le climat continental à la transition icehouse-greenhouse de la fin du Paléozoïque	318
5.1.3.	Bassins carbonifères-permiens et ressources.....	321
	L'Interprétation Quantitative appliquée aux bassins carbonifères-permiens	321
	La structuration du bassin houiller du Nord-Pas-de-Calais, entre géothermie profonde et hydrogéologie	323
	Le bassin sarro-lorrain comme cible géothermique ?.....	324
	Les bassins carbonifères-permiens comme réservoir d'hélium naturel	325
5.1.4.	Pour aller plus loin	326
5.2.	Perspectives de recherche sur la couverture sédimentaire méso-cénozoïque	327
5.2.1.	Les déformations multi-échelles cénozoïques du bassin de Paris	327
5.2.2.	Tectonique du Trias évaporitique et carbonaté du Haut-Var - Implications en terme d'aléa gravitaire (effondrement-dissolution).....	328
5.2.3.	Pour aller plus loin	330

Liste des Figures

<i>Figure 1 - Exemple de séquence de traitement PSTM simplifiée (Source BRGM).....</i>	<i>53</i>
<i>Figure 2 - Profils sismiques interprétés par moi-même ou interprétation suivie dans le cadre de projets à forte implication (en bleu foncé) ; profils co-interprétés en appui expertise à l'interprétation (en marron foncé) ; profils consultés lors de synthèses géologiques (en vert). En noir profils retraités disponibles au BRGM ; en rosé, profils industriels acquis en France métropolitaine. En fond carte géologique de la France au 1 :1000000^{ème} (BRGM, 2003).....</i>	<i>54</i>
<i>Figure 3 - Même carte et légende que la Figure 2 ; en violet, les forages profonds d'exploration-production d'hydrocarbures en France métropolitaine (source http://www.minergies.fr).....</i>	<i>55</i>
<i>Figure 4 - Exemple de calage de la sismique au forage par l'intermédiaire d'un séismogramme synthétique (bassin sarro-lorrain) ; en noir, bleu, rouge, rose et vert : horizons sismiques.....</i>	<i>56</i>
<i>Figure 5 - Evolution géodynamique varisque selon Averbuch et Piromallo (2012), depuis la phase éovarisque (c) jusqu'à la phase post-varisque et l'initiation du bassin de Paris (g, h).....</i>	<i>80</i>
<i>Figure 6 - Cadre temporel et processus de mise ne place des bassins carbonifères-permiens (coupes lithosphériques modifiées par M. Mercuzot et moi-même de Malavielle, 1993).....</i>	<i>81</i>
<i>Figure 7 - Proposition schématique de différents modes de mise en place des bassins Stéphaniens-Permien inférieur en France (Faure, 1995).....</i>	<i>82</i>
<i>Figure 8 - LPIA et transition icehouse-greenhouse à la fin du Paléozoïque (modifié par M. Mercuzot et moi-même de Scotese, 2002).....</i>	<i>83</i>
<i>Figure 9 - Localisation actuelle des bassins syn-orogéniques varisques westphaliens (Doornenbal et Stevenson, 2010).....</i>	<i>84</i>
<i>Figure 10 - Localisation des bassins post-orogéniques varisques vers 300 Ma (Pochat et Van den Driessche, 2011).....</i>	<i>85</i>

Figure 11 - Carte tectonique simplifiée de l'Europe occidentale montrant la localisation des principaux bassins syn- et post-varisques en surface (resp. au nord et au sud du front nord varisque) et les principales structures tectoniques (Oplustil et Schneider, 2023). 1, South Wales; 2, Forest of Dean; 3, Bristol–Somerset; 4, Kent; 5, Pennine; 6, Midland Valley of Scotland; 7, Nord et Pas-de-Calais + Namur Synclinorium; 8, Campine; 9, Aachen; 10, Ruhr; 11, Ibbenbühen et Piesberg; 16, NW Spain (Cantabrian Mountains); 17, Carnic et Karawanke Alps; 19, Peñarroya; 20, Puertollano; 21, Pyrenees; 22, Saint Étienne; 23, Autun; 24, Commentry; 25, Graissessac–Lodève; 26, Lorraine–Saar–Nahe; 27, Saale; 28, Erzgebirge (Flöha + Zwickau); 29, Thüringian Forest. 30, Pilsen–Trutnov Basin Complex – western part (e.g. Kladno–Rakovník, Radnice et Pilsen basins); 33, Salvan–Doréaz; 34, La Mûre; 35, Briançon; 36, Ollano; 37, North Switzerland; 38, Schwarzwald (Oppenau, Geroldseck, Baden-Baden, Breisgau, Schramberg); 39, Val Sanagra (Como, Ticino), 40, Gurktal.	86
Figure 12 - Intervalle de dépôt et lithologies simplifiées de quelques bassins syn-varisques français et européens (Oplustil et Schneider, 2023).	87
Figure 13 - Intervalle de dépôt et lithologies simplifiées de quelques bassin post-varisques français et européens (Oplustil et Schneider, 2023) ; même légende que Figure 13.	88
Figure 14 - Carte de synthèse des bassins carbonifères-permiens en France à l'affleurement et en subsurface, classés par âge. Bassins à l'affleurement : 1: Carentan/Littry ; 2: St-Pierre-la-Cour ; 3: Doué-la-Fontaine ; 4: Sillon Vendéen, Chantonay, Faymoreau ; 5: Villé ; 6: St-Dié ; 7: Ronchamp-Giromagny ; 8: Autun ; 9: Decize La Machine ; 10: Blanzay-Le Creusot ; 11: Bert ; 12: Aumance ; 13: Commentry, Doyet, Deneuille ; 14: Ahun ; 15: Bosmoreau-les-Mines ; 16: Bassins du Sillon-Houiller ; 17: Brive ; 18: Brassac, Brioude ; 19: St-Etienne ; 20: Prades-Jaujac ; 21: Alès ; 22: Graissessac, Lodève ; 23: St-Affrique ; 24: Figeac, Decazeville, Rodez ; 25: Quercy-Albigeois, La Grésigne ; 26: La Rhune-Bidarray ; 27: Ossau ; 28: Sierra del Cadi ; 29: Var ; 30 Barrot, Argentera ; 31: Corse ; 32: Alpes zones externes ; 33: Alpes zones internes. Bassins en subsurface : A: Nibas ; B: Saint-Maur ; C: Coulommès ; D: Villequier ; E: Vernon ; F: Champigny ; G: Vacherauville ; H: Lorraine ; I: Centre bassin de Paris ; J: Arpheuilles ; K: Contres ; L: Brécly ; M: Bresse sud ; N: Bresse nord ; O: Beaune ; P: Bourgogne ; Q: Bugey ; R: Périgord, Quercy ; S: St-Géry ; T: Bouglon-Ste-Marthe ; U: Castelsarrasin ; V: Castrais ; W: Gabian-Garrigues ; Y: Carces ; X: Vallon.....	89
Figure 15 - a : carte géologique simplifiée du nord de la France ; b : carte structurale du substratum varisque dans le nord de la France (Laurent et al., 2021 et références incluses); localisation du Bassin Houiller du Nord-Pas-de-Calais et de la coupe de la Figure 16.	92
Figure 16 - Coupe équilibrée du profile sismique M146 dans la région de Valenciennes illustrant la structure de premier ordre du front nord varisque (modifié de Lacquement et al., 1999; Mansy et Lacquement, 2006 et Laurent et al., 2021a). AA: Allochtone Ardennais, AMBT: Allochthon Main Basal Thrust, PB: Parautochtone Brabançon, EMR: Ecailles et Massifs Renversés, BEMR: Chevauchement Basal des EMR. Trait de coupe sur la Figure 15.....	93
Figure 17 - Carte géologique de l'est de la France avec la couverture sédimentaire mésozoïque représentée en transparence. Les limites classiquement proposées pour les bassins carbonifères-permiens en subsurface sont également reportées (Delmas et al., 2002). Les transects correspondent aux profils sismiques ECORS et DEKORP ainsi qu'à la coupe du bassin de Paris représentée dessous. L'encart montre la localisation du bassin sarro-lorrain et de Saar-Nahe au sein des principaux domaines tectoniques varisques (**Hemelsdaël et al., 2022 soumis à Tectonics ; compilé à partir de Faure, 1995 ; Franke, 2014 ; Guillot et al., 2020 ; Schneider & Romer, 2010).....	148
Figure 18 - Stratigraphie synthétique du Permo-Carbonifère du bassin Lorraine-Saar-Nahe (**Hemelsdaël et al., 2022 soumis à Tectonics).	151
Figure 19 - Localisation des profils sismiques et des puits avec leur succession sédimentaire permo-carbonifères simplifiée (**Hemelsdaël et al., 2022 soumis à Tectonics).	152
Figure 20 - Interprétation de deux profils transverses au bassin sarro-lorrain ; on note l'épaisseur maximale du déposé syn-rift au droit de la partie la plus érodée des séries westphaliennes plissées, témoignant d'un processus majeur d'inversion topographique et tectonique négative (**Hemelsdaël et al., 2022 soumis à Tectonics).	153
Figure 21 - Coupe schématique NW-SE illustrant le modèle d'évolution du bassin permo-carbonifère lorrain, subdivisé en 6 étapes: (a) développement d'un bassin syn-orogénique (ici au Westphalien C); (b) propagation de chevauchements à vergence SE et plissements associés pendant le Westphalien D; (c) inversion tectonique négative post-orogénique contrôlant le développement de déposécentres syn-rift (Stéphanien à Permien	

inférieur); (d) volcanisme syn-rift du Permien inférieur; (e) réactivation locale des chevauchements pendant la phase de compression saalienne; (f) subsidence thermique post-rift à la fin du Permien inférieur et au Permien moyen (**Hemelsdaël et al., 2022 soumis à Tectonics).....	155
Figure 22 - Carte structurale révisée du bassin permo-carbonifère sarro-lorrain dans le prolongement du bassin Saar-Nahe (Allemagne), basée sur l'interprétation des profils sismiques (**Hemelsdaël et al., 2022 soumis à Tectonics).....	156
Figure 23 - Localisation des bassins stéphano-permiens du sud du bassin de Paris et du nord du Massif Central (en bleu foncé à l'affleurement, en bleu clair en subsurface).....	159
Figure 24 - Regroupement des doublets géothermiques au Bathonien suivant leur distribution spatiale et la présence de structures tectoniques (**Dentzer et al., 2018).....	250
Figure 25 - Schéma structural de la zonation de la chaîne varisque sous le bassin de Paris méso-cénozoïque et ses bordures varisques et cadomiennes (Baptiste, 2016).....	251
Figure 26 - Le bassin de Paris (**Mas et al., 2022). Carte géologique localisant les failles principales (*Beccaletto et al., 2011). Coupe ouest-modifiée de AGBP (2014). Log lithostratigraphique avec les principaux aquifères (modifié de Delmas et al., 2002).....	252
Figure 27 - Evolution géodynamique du bassin de Paris (*Beccaletto et al., 2011).....	253
Figure 28 - Schéma structural consolidé du bassin de Paris ; en rouge, failles au toit du Trias ; en bleu failles au toit du Dogger Calcaire, en vert failles au toit du Kimméridgien ; en fond carte géologique de la France au 1/1000000 ^{ème} (BRGM, 2003).....	255
Figure 29 - Structuration et anomalies thermiques dans le bassin de Paris ; (i) des isothermes ; (ii) des isosalinités au Bathonien ; (iii) des propositions d'interprétations géologiques (en vert et bleu) à partir des lignes sismiques ; iv) de la coupe de référence 2D en orange (Dentzer, 2016).....	256
Figure 30 - Ligne sismique interprétée au nord de Paris montrant en bleu un conduit subvertical caractérisé par un faciès sismique transparent ; horizons interprétés en noir ; BTr base Trias, L1 toit Trias, Dac toit des Marnes à Ostrea Acuminata, D1 toit du Dogger calcaire « Dalle nacrée », C1 limite Bériasien inférieur/supérieur, C4 toit de l'Albien (**Dentzer et al., 2018).....	257
Figure 31 - Carte géologique simplifiée de la zone d'étude ; les lignes de vol de l'acquisition TDEM sont représentées en gris ; triangles noirs : forages ; ligne noire en pointillés : une des lignes sismiques interprétées (** Reninger et al., 2014).....	278
Figure 32 - Comparaison entre un profil de résistivité et la ligne sismique E-O (localisation sur la Figure 31). Les forages situés à une distance de 50 m du profil sont également représentés. Les argiles sont représentées en blanc dans les forages et la craie en noir. Les lignes pointillées blanches et noires représentent le sommet interprété de la craie et l'interface entre C1 et C2 respectivement. Les contours noirs en pointillés et les flèches noires mettent en évidence les zones de résistivité intermédiaire et leur lien suggéré avec les failles interprétées en sismique (** Reninger et al., 2014).....	279
Figure 33 - Schéma structural de l'ECRIS (Modifié de Dèzes et al. (2004) dans Bourgeois et al., 2007) ; BF Black Forest, EG Eger Graben, FP Franconian Platform, HG Hessian grabens, LG Limagne Graben, LRG Lower Rhine (Roer Valley) Graben, LRhG Lower Rhône; Grabens, NRG Northern Bresse Graben, RG Roanne Graben, SBG ; Southern Bresse Graben, URG Upper Rhine Graben, V Vosges, VG ; Valence Graben.....	283
Figure 34 - Remplissage sédimentaire cénozoïque du fossé Rhénan, cinématique et champ de contraintes régionaux (σ_1 en noir, σ_2 en gris, σ_3 en blanc) (Schumacher, 2002).....	285
Figure 35 - Schéma structural du fossé Rhénan pour la base du Tertiaire (projet GeORG); en arrière-plan, profils sismiques interprétés en mauve, orange et vert ; en fond, carte géologique au 1/1000000 ^{ème} de l'Allemagne (BGR, 1993).....	286
Figure 36 - Profil sismique interprété dans le nord du Fossé rhénan ; séries syn-rift en orange foncé (Beccaletto et al., 2014, confidentiel).....	287
Figure 37 - Profil sismique interprété dans le nord du Fossé rhénan ; séries syn-rift en orange foncé (Beccaletto et al., 2014, confidentiel).....	287
Figure 38 - Schéma structural du fossé Rhénan pour la base de la série post-rift (projet GeORG); en noir tracé de la faille de Lalaye-Lubine-Baden-Baden ; en fond carte géologique au 1/1000000 ^{ème} de l'Allemagne (BGR, 1993).....	288
Figure 39 - Différentes géométries de la faille bordière occidentale du fossé Rhénan (à gauche sur les profils) ; série syn-rift entre les horizons rouges et jaunes (Beccaletto et al., 2013).....	288

Figure 40 - Schéma structural hiérarchisé du fossé Rhénan (Team GeORG, 2013).....	289
Figure 41 - Localisation des bassins permien (en bleu) et stéphanien (en noir) de Brive, Blanzey-Le Creusot, St-Étienne et Alès. Plan de position des profils sismiques retraités au BRGM en vert, disponibles pour retraitement en marron. En fond carte géologique de la France au 1:1000000 ^{ème} (BRGM, 2003).	314
Figure 42 - Localisation des bassins permien (en bleu) et stéphanien (en noir) de Decazeville-Rodez, St-Affrique, Graissessac-Lodève et Alès. Plan de position des profils sismiques retraités au BRGM en noir, disponibles pour retraitement en marron. En fond carte géologique de la France au 1:1000000 ^{ème} (BRGM, 2003).	315
Figure 43 - Exemple de corrélations inter-bassins entre les bassins de Lucenay-lès-Aix, d'Autun et de Lodève (**Ducassou et al., 2019).	316
Figure 44 - Localisation des bassins permien (en bleu) et stéphanien (en noir) des Vosges. En fond carte géologique de la France au 1:1000000 ^{ème} (BRGM, 2003).	317
Figure 45 - Paléogéographie au Permien inférieur et supérieur, d'après les reconstructions de (A) Domeier et Torsvik (2014), (B) Muttoni et Kent (2019), et (c) Tomezzoli et al. (2018). Les points rouges indiquent les 2 cibles de forages en Pangée équatoriale (USA et Europe occidentale), dans *Soreghan et al., 2020).	318
Figure 46 - Fiche synthétique pour la cible Deepdust en France (Source : full proposal ICDP, 2021).	320
Figure 47 - Illustration simplifiée de la réflexion et de la transmission d'une onde sismique dans le sous-sol. L'interprétation quantitative consiste à retrouver les propriétés du sous-sol à partir de la trace sismique (Capar et al., 2021).	321
Figure 48 - Exemple d'Interprétation Quantitative sur une zone test dans le bassin houiller du Nord-Pas-de-Calais ; les couleurs bleu vert blanc correspondent à trois lithologies (Toussaint, 2020).	322
Figure 49 - Géothermie et hydrogéologie dans le bassin houiller du Nord-Pas-de-Calais, une démarche intégrée.	323
Figure 50 - Profils sismiques interprétés dans le bassin sarro-lorrain vus en 3D (source Post-doc R. Hemelsdaël).	325
Figure 51 - Dépoctrène permien identifié sous couverture méso-cénozoïque ; le profil sismique correspond à une longueur de quelques kilomètres (Jacob et al., 2021).	326
Figure 52 - Approche multi-échelles et multi-techniques pour établir le corpus structural du bassin de Paris pour le Tertiaire.	328
Figure 53 - Alignement selon une direction N110 des fontis sur la commune de Bargemon (Marçot et al., 2022) ; en fond carte géologique harmonisée au 1/50000 ^{ème} (source BRGM).	329

Annexes

Annexe 1 - Publication 9.....	346
Annexe 2 - Publication 10.....	381

1. Curriculum Vitae

Laurent Beccaletto

Né le 25 novembre 1972 à Versailles (78)
Nationalité française, marié, 2 enfants

Situation actuelle

Ingénieur géologue au BRGM
Direction des Géoressources / Unité Géologie des Bassins Sédimentaires

Centre Scientifique et Technique du BRGM à Orléans, 3 avenue Claude-Guillemin - BP 36009
45060 Orléans Cedex 2.

l.beccaletto@brgm.fr / 02.38.64.39.85

Domaines de recherche : géologie des bassins sédimentaires, étude des modes de remplissage et de déformation à partir des données de subsurface (forages et sismique réflexion), spécialiste des bassins carbonifères-permiens français et de leur couverture méso-cénozoïque.

Situation antérieure

2003-2006 Premier Assistant, Institut de Géologie et de Paléontologie, Faculté des Sciences, Université de Lausanne, Suisse.
1999-2003 Doctorant en Sciences de la Terre, Institut de Géologie et de Paléontologie, Faculté des Sciences, Université de Lausanne, Suisse.

Diplômes

2003 Docteur ès Sciences, mention géologie, Institut de Géologie et de Paléontologie, Faculté des Sciences, Université de Lausanne, Suisse. Titre de la thèse "Geology, correlations, and geodynamic evolution of the Biga Peninsula (NW Turkey)" [en anglais].
Thèse soutenue à Lausanne le 11/06/2003 (séance d'épreuve, en anglais) et le 14/07/2003 (séance publique, en français).
1998 DEA *Structure et Evolution de la Lithosphère*, Univ. Montpellier II, France, mention AB.
1996 Maîtrise des Sciences de la Terre, Université Montpellier II, France (2/21).
1995 Licence des Sciences de la Terre, Université Montpellier II, France (13/60).
1994 DEUG A, option Mathématique-Physique, Université Montpellier II, France.
1992 Baccalauréat série C, Lycée P. Valéry, Sète (mention AB).

Formation continue

Le BRGM dispose d'une offre de formation continue étoffée qui permet à ses agents de développer des compétences dans des domaines connexes aux Sciences de la Terre à vocation appliquée et opérationnelle. J'ai ainsi bénéficié des formations suivantes :

- 2023 Géologie et économie des ressources minérales (2 j.)
- 2022 SIG - QGIS (3 j.)
- 2021 Conversion sismique – Temps-profondeur (3 j.)
- 2019 Appréhender la complexité des réservoirs carbonatés (3 j.)
- 2019 Vitesses et calage de données de puits en sismique (1.5 j.)
- 2018 Geographix - Interprétation sismique (5 j.)
- 2016 Outils et méthodes connaissance des risques littoraux (2 j.)
- 2015 Introduction à la géothermie (1 j.)

- 2015 Sensibilisation aux risques naturels géologiques (1 j.)
 - 2013 SIG - ArcGIS (4 j.)
 - 2014 Sensibilisation aux méthodes géophysiques (3 j.)
 - 2012 Géologie structurale (5 j. Béta testeur)
 - 2011 Formation de formateurs (3 j.)
 - 2010 Sensibilisation à l'hydrogéologie (2 j.)
 - 2009 Geomodeller[®] - Modélisation 3D (3 j.)
 - 2008 Stratigraphie séquentielle, approche terrain (5 j.)
 - 2008 Formations superficielles autochtones (5 j.)
- 1997 Formation à distance certifiée d'écologie générale (CNED) pendant mon Service militaire.

1.1. Activités pédagogiques

Mon implication dans les activités pédagogiques ne s'est jamais démentie ; elles concernaient les étudiants quand j'étais doctorant puis Premier Assistant à l'Université de Lausanne ; elles concernent désormais principalement les adultes en formation continue, le BRGM n'étant pas un organisme d'enseignement universitaire.

1.1.1. Depuis 2007, au BRGM

- 2010-Présent Formateur BRGM pour adultes « Géologie : théorie et pratique » (1 à 2 sem./an).
- 2013-14-15 Formateur BRGM pour étudiants de Master 2 de l'Université de Brazzaville, Congo-Brazzaville (3 sem./an), école de terrain sur place.

1.1.2. Avant 2007, à l'Université de Lausanne

09/2003-11/2006 1^{er} assistant

Responsable des TP, Institut de Géologie et de Paléontologie, Faculté des Géosciences et de l'Environnement, Université de Lausanne, Suisse.

En 2003/2004 j'ai été responsable de la refonte totale des TP de 1^{ère} année (conception, élaboration et mise en œuvre des exercices), suite à la création de la nouvelle Faculté de Géosciences et de l'Environnement de l'Université de Lausanne (passage de 30 à 110 étudiants répartis sur 4 salles simultanément pendant 4 heures). A la rentrée 2004, j'ai été nommé responsable des TP de 1^{ère} année de géologie générale/sédimentologie (logistique, mise en œuvre, correction des exercices, animation d'une équipe de 6 assistants).

Je souhaite m'attarder quelques instants sur cette réorganisation pédagogique, à la fois conceptuelle et dans sa mise en œuvre, pionnière à l'époque.

Cette réforme visait à intégrer la géologie dans une vision globale du « système Terre » en favorisant l'interdisciplinarité. Nous avons mené cette réflexion en parallèle à la conception par une équipe voisine d'un cours de géosciences en ligne ("Objectif Terre"), une rareté au début des années 2000. La logique de l'ensemble des enseignements (cours ex-cathedra, cours en ligne, travaux pratiques, stages de terrain) reposait sur le principe de contextualisation de l'apprentissage et de décloisonnement des disciplines.

Cela s'est exprimé au niveau des TP par une volonté de faire participer au maximum les étudiants (travail en groupe, autonomie accrue) en leur proposant de résoudre des problèmes concrets, basés sur la **mise en situation des objets géologiques** (e.g. reconstruire l'histoire d'une marge active).

Dans la pratique, chaque groupe d'étudiants disposait en TP d'un ordinateur portable, distribué en début de séance au moyen d'unités mobiles (chariots équipés de 10 PC). L'ordinateur était utilisé pour la distribution des consignes du travail, la mise à disposition de divers documents,

et le rendu du travail demandé. L'ensemble de ces activités se faisait au moyen de la plateforme d'enseignement Moodle (nouvelle à l'époque).

La remise du travail se faisait selon diverses interfaces qui facilitaient l'archivage puisque l'ensemble des devoirs remis était stocké sur serveur. Une partie des questions ont pu être adaptées sous la forme de QCM et étaient dès lors corrigées automatiquement. D'autres, dont les réponses nécessitaient un argumentaire, étaient directement rédigées sur Moodle. Enfin l'intégration de l'ordinateur renforçait **l'apprentissage coopératif** au sein du groupe puisqu'un ou plusieurs étudiants durant le TP avait pour tâche de transmettre les informations du TP au reste du groupe, d'utiliser les ressources électroniques mises à disposition ou de rédiger le rendu du travail.

Les étudiants ont été particulièrement motivés par ce type d'approche. Comparé à un TP classique, les avantages étaient nombreux: (i) mise à disposition d'un plus grand nombre de documents, facilement éditables et réutilisables les années suivantes; (ii) mise à disposition de documents qu'il était auparavant impossible de distribuer (e.g. des images en couleurs de qualité, des animations ou des vidéos); (iii) accès à des ressources en ligne supplémentaires (sur internet).

Les TP concernaient le tronc commun géologie/géographie de 1ère année, 110 étudiants - 54 h/an :

Cycle des roches, aspect sédimentologique.

- Approfondissement/comblement en milieu détritique et carbonaté.
- Introduction à la paléontologie.
- Les roches en tant qu'indicateurs climatiques.
- Introduction aux diagraphies.
- Roches des croûtes océaniques et continentales.
- Evolution d'une marge passive: géométrie et répartition des milieux de dépôts, reconstitution de son évolution géologique. Basé sur l'interprétation d'un profil sismique et des corrélations de forages carottés fictifs.
- Evolution d'une marge active: idem ci-dessus.

Répartition des autres enseignements auxquels j'ai participé :

Filière géologie, 3^{ème} année :

- Excursions journalières - 45 étudiants.
 - Introduction à la géologie alpine.
 - Géologie du Jura.
 - Géologie des Préalpes I.
 - Géologie des Préalpes II.
- Camp de terrain - 20 étudiants - 2003/2004. Alpes Carniques, Italie (10 jours)

Filière géologie, 3^{ème} année :

- Cours « les mélanges d'accrétion » - 15 étudiants - 2 heures.

Filière géologie, 4^{ème} année

- Module monothématique sur 3 jours « Géodynamique des bassins » - 15 étudiants.
 - Rifting: modèle et application à la Mer Rouge.

- Flexuration de la lithosphère: reconstitution de la géométrie de la plaque subduite à l'aide du logiciel FLEX, application à un cas actuel (plaque Nazca) et ancien (Téthys Alpine).
- Subsidence: aspect théorique et application au domaine Briançonnais à l'aide du logiciel EASYSUB.
- Camp de terrain - 8 étudiants - 2006. Montagne Noire (1 sem.): géologie structurale en domaine ductile.

09/1999-08/2003 Assistant diplômé

Institut de Géologie et de Paléontologie, Faculté des Sciences, Université de Lausanne, Suisse.

Répartition des enseignements

Filière géologie, 1^{ère} année :

- Travaux Pratiques de géologie générale/sédimentologie – 30 étudiants - 48 h/an : Idem 2003-2006.
- Excursions journalières - 45 étudiants : Idem 2003-2006.
- Camp de terrain - 20 étudiants - 2000/2001. Col du Galibier, Alpes, domaine sub-briançonnais (10 jours): cartographie géologique en terrain sédimentaire tectonisé; approche paléogéographique.

Filière géologie, 4^{ème} année :

- Camp de terrain dans le cadre du cours de géodynamique - 15 étudiants –2001/2002. Crète (1 semaine): relations sédimentologie/tectonique/géodynamique en domaine de fore-arc, approche paléogéographique et paléotectonique.
- Module monothématique sur trois jours, Géodynamique des bassins : Idem 2003-2006.

A ces enseignements s'ajoutent l'évaluation de mémoires de Master Recherche de géologie :

- 2006 - Etude géologique des Tyros Beds de la région de Tyros-Leonidion, Péloponnèse, Grèce.
- 2005 - Les unités infra-ophiolitiques de l'île de Lesbos, Grèce.
- 2004 - Le mélange ophiolitique de Mersin (sud Anatolie), un fragment de marge Néotéthys ?

1.1.3. Divers

1998 Jury d'oral pour l'examen de géologie au concours d'entrée de l'Ecole Nationale du Génie de l'Eau et de l'Environnement de Strasbourg (ENGEES).

Représentant des assistants (Faculté des Géosciences et de l'Environnement, Université de Lausanne, Suisse):

- Au conseil de faculté (2005-2006).
- A la commission de l'enseignement de la faculté 2006.

1.2. Production scientifique

1.2.1. Articles publiés dans des revues à comité de lecture (au 01/03/2023)

ORCID <https://orcid.org/0000-0003-2132-1738>

24 publications de rang A = revues internationales à comité de lecture (ACL WoS), IF>1.

5 publications de rang B = revues nationales à com. de lecture non indexées WoS (ACLN WoS).

Citation Index (hors auto-citation): 960 (Google Scholar), 593 (WoS).

H-Index: 13 (Google Scholar), 10 (WoS).

Les **noms en gras** correspondent aux étudiants (co-)encadrés en doctorat ou master (i.e. publications liées à la thèse ou au master).

ACL

- 1) **Tchang-Tchong L.**, Michels R., Beccaletto L., Bossennec C., Lorgeoux C., Faure P. (2023) Pre- to early-rift thermal conditions of the Upper Rhine Graben using geological and organic geochemical controls, *Marine & Petroleum Geology*, 151. <https://doi.org/10.1016/j.marpetgeo.2023.106202> - IF=4.348.
- 2) **Mas P.**, Calcagno P., Caritg-Monnot S., Beccaletto L., Capar L. & Hamm V. (2022) A 3D geomodel of the deep aquifers in the Orléans area of the southern Paris Basin (France), *Scientif Data*, <https://doi.org/10.1038/s41597-022-01876-4> - IF=8.501.
- 3) Poujol M., Mercuzot M., Lopez M., Bourquin S., Bruguier O., Hallot E. and Beccaletto L. (2023) Insights on the Permian tuff beds from the Saint-Affrique Basin (Massif Central, France): an integrated geochemical and geochronological study, accepted to *CR Geosciences*, waiting for volume n° + DOI - IF=2.241.
- 4) **Mercuzot M.**, Bourquin S., Pellenard P., Beccaletto L., Schnyder J., Baudin F., Ducassou C., Garel S., Gand G. (2022) Reconsidering Carboniferous–Permian continental paleoenvironments in eastern equatorial Pangea: facies and sequence stratigraphy investigations in the Autun Basin (France), *International Journal of Earth Sciences*, 111, 1663-1696. <https://doi.org/10.1007/s00531-022-02200-6> - IF=2.698.
- 5) **Laurent A.**, Averbuch O., Beccaletto L., Graveleau F., Lacquement F., Capar L., & Marc S. (2021). 3-D structure of the Variscan thrust front in northern France: New insights from seismic reflection profiles. *Tectonics*, 40, e2020TC006642. <https://doi.org/10.1029/2020TC006642> - IF=5.261.
- 6) **Mercuzot M.**, Thomazo C., Schnyder J., Pellenard P., Baudin F., Pierson-Wickmann A-C., Sans-Jofre P., Bourquin S., Beccaletto L., Santoni A-L., Gand G., Buisson M., Glé L., Munier T., Saloume A., Boussaid M. and Boucher T. (2021) Carbon and Nitrogen Cycle Dynamic in Continental Late- Carboniferous to Early Permian Basins of Eastern Pangea (Northeastern Massif Central, France). *Frontiers in Earth Sciences* 9, <https://doi.org/10.3389/feart.2021.705351> - IF = 3.661.
- 7) Soreghan G.S., Beccaletto L., Benison K.C., Bourquin S., Feulner G., Hamamura N., Hamilton M., Heavens N.G., Hinnov L., Huttenlocker A., Looy C., Pfeifer L.S., Pochat S., Abadi M.S. , Zambito J., and the Deep Dust workshop participants (2020) Report on ICDP Deep Dust

- workshops: probing continental climate of the late Paleozoic icehouse-greenhouse transition and beyond, *Scientific Drilling*, 28, 93-112, <https://doi.org/10.5194/sd-28-93-2020> - IF=1.54.
- 8) **Mercuzot M.**, Bourquin S., Beccaletto L., Ducassou C., Rubi R., Pellenard P., (2021) Palaeoenvironmental reconstitutions at the Carboniferous Permian transition south of the Paris Basin, France: implications on the stratigraphic evolution and basin geometry, *International Journal of Earth Sciences*. <https://doi.org/10.1007/s00531-020-01940-7> - IF=2.698.
 - 9) Ducassou C., **Mercuzot M.**, Bourquin S., Rossignol C., Pellenard P., Beccaletto L., Poujol M., Hallot E., Pierson-Wickmann A.-C., Hue C., Ravier E. (2019) Sedimentology and U-Pb dating of Carboniferous to Permian continental series of the northern Massif Central (France): Local palaeogeographic evolution and larger scale correlations, *Palaeogeography, Palaeoclimatology, Palaeoecology* 533. <https://doi.org/10.1016/j.palaeo.2019.06.001> - IF=3.565.
 - 10) Juncal M. A., Bourquin S., Beccaletto L., Bienvenido Diez J. (2018) New sedimentological and palynological data from the Permian and Triassic series of the Sancerre-Couy core, Paris Basin, France, *Geobios* 51, 517-535. <https://doi.org/10.1016/j.geobios.2018.06.007> - IF=2.115.
 - 11) **Dentzer J.**, Bruel D., Delescluse M., Chamot-Rooke N., Beccaletto L., Lopez S., Courrioux G., Violette S. (2018) Thermal and seismic hints for chimney type cross-stratal fluid flow in onshore basins, *Nature Scientific Reports*. <http://dx.doi.org/10.1038/s41598-018-33581-x> - IF=4.996.
 - 12) **Roche V.**, Bouchot V., Beccaletto L., Jolivet L., Guillou-Frottier L., Tuduri J., Bozkurt E., Oguz K., Tokay B. (2018) Structural, lithological, and geodynamic controls on geothermal activity in the Menderes geothermal Province (Western Anatolia, Turkey), *International Journal of Earth Sciences*, vol. 108, 301-328. <https://doi.org/10.1007/s00531-018-1655-1> - IF=2.698.
 - 13) **Baptiste J.**, Martelet G., Faure M., Beccaletto L., Reninger P.-A. & Chen Y. (2016) Mapping of a buried basement combining aeromagnetic, gravity and petrophysical data: The substratum of southwest Paris Basin, France, *Tectonophysics* 683, 333-348. <https://doi.org/10.1016/j.tecto.2016.05.049> - IF=3.660.
 - 14) Beccaletto L., Capar L., Serrano O., Marc S. (2015), Structural evolution and sedimentary record of the Stephano-Permian basins occurring beneath the Mesozoic sedimentary cover in the southwestern Paris basin (France), *Bull. Soc. géol. France*, t. 186, n°6, 429-450. <https://doi.org/10.2113/gssgfbull.186.6.429> - IF=3.192.
 - 15) Reninger P.-A., Martelet G., Lasseur E., Beccaletto L., Deparis J., Perrin J., Chen Y. (2014) Geological environment of karst within chalk using airborne time domain electromagnetic data cross-interpreted with boreholes, *Journal of Applied Geophysics*. <https://doi.org/10.1016/j.jappgeo.2014.04.020> - IF=2.121.
 - 16) Lenoir F., Guillocheau F., Robin, C., Lasseur E., Serrano O., Beccaletto L. (2014) Seismic study of the Jurassic deformation and sedimentation of the southwestern Paris basin: a low subsiding domain transition to the Aquitaine basin, *Bull. Soc. géol. France* 185/3, 191-204. <https://doi.org/10.2113/gssgfbull.185.3.191> - IF=3.192.
 - 17) Beccaletto L., Hanot F., Serrano O., Marc S. (2011). Overview of the subsurface structural pattern of the Paris Basin (France): insights from the reprocessing and interpretation of regional seismic lines. *Marine and Petroleum Geology* 28, 861-879. <https://doi.org/10.1016/j.marpetgeo.2010.11.006> - IF=4.348.

- 18) Moix P., Beccaletto L., Masset O., Kozur H. W., Dumitrică P., Vachard D., Martini R. & Stampfli G. M. (2011) Geology and Correlation of the Mersin Mélanges, Southern Turkey. *Turkish Journal of Earth Sciences* 20, 57-98 - IF=1.543.
- 19) Bonev N., Beccaletto L., Robyr M., Monié P. (2009) Metamorphic and age constraints on the Alakeçi shear zone: implications for the extensional exhumation history of the northern Kazdağ Massif, NW Turkey, *Lithos* 113, 331-345. <https://doi.org/10.1016/j.lithos.2009.02.010> - IF=4.02.
- 20) Moix P., Beccaletto L., Kozur H.W., Hochard C., Rosselet F., Stampfli G.M. (2008) A New Classification of the Turkish Terranes and Sutures and its Implication for the Paleotectonic History of the Region, *Tectonophysics* 451, 7–39. <https://doi.org/10.1016/j.tecto.2007.11.044> - IF=3.933.
- 21) Bonev N. and Beccaletto L. (2007) From syn- to post-orogenic Tertiary extension in the north Aegean region: constraints on the kinematics in the eastern Rhodope-Thrace, Bulgaria-Greece and the Biga Peninsula, northwest Turkey. *Geological Society, London, Special Publications* 291; p. 113-142. <https://doi.org/10.1144/sp291.6> - IF=2.322.
- 22) Beccaletto L., Bonev, N., Bosch, D and Bruguier, O. (2007), Record of a Palaeogene syn-collisional extension in the north Aegean region: evidence from the Kemer micaschists (NW Turkey) *Micaschists, NW Turkey. Geological Magazine* 144 (2), 2007, pp. 393–400. <https://doi.org/10.1017/s001675680700310x> - IF=2.656.
- 23) Beccaletto L., Bartolini A-C, Martini R, Hochuli P. and Kozur H. (2005) Biostratigraphic data from the Çetmi melange, northwest Turkey: palaeogeographic and tectonic implications. *Palaeogeography, Palaeoclimatology, Palaeoecology* 221, 215-244. <https://doi.org/10.1016/j.palaeo.2005.02.011> - IF=3.565.
- 24) Beccaletto L. and Steiner C. (2005) Evidences of Two-stage Extensional Tectonics from the Northern Edge of the Edremit Graben (NW Turkey). *Geodinamica Acta* 18/3-4, 283-297. <https://doi.org/10.3166/ga.18.283-297> - IF=3.235.

ACLN

- 1) **Laurent A.**, Beccaletto L., Averbuch O., Graveleau F., Lacquement F., Caritg S., Marc S. & Capar L. (2021) Modelling the 3D geometry of the Dinantian carbonate geothermal reservoir in northern France, *Z. Dt. Ges. Geowiss. (J. Appl. Reg. Geol.)*, 172 (3), 293-305. <https://doi.org/10.1127/zdgg/2021/0284> - IF=1.
- 2) Lacquement F., Trautmann F., Beccaletto L., Vernhet Y. (2011) – Carte géol. France (1/50 000), feuille Vitré (318). Orléans : BRGM. Notice explicative par Trautmann F., Lacquement F., Vernhet Y., Pivette B., avec la collaboration de Cocherie A., Guerrot C., Thiéblemont D., Tegye M., Denis É. (2011), 131 p.
- 3) Sokol, G; Nitsch, E; Anders, B; Franz, M; Oliviero, G; Prestel, R; Rupf, Isabel; Wielandt-Schuster, Ulrike; Wirsing, Gunther; Zumsprekel, H; Kaercher, T; Haneke, J; Kryzanowski, J; Storz, R; Tesch, J; Weidenfeller, Michael; Elsass, P; Beccaletto L.; Capar, L; Cruz-Mermy, D; Huggenberger, P; Dresmann, H. (2010) The Upper Rhine Graben; assessing geopotentials and geohazards by a transnational study. *Schriftenreihe der Deutschen Gesellschaft für Geowissenschaften, (Eds) Hoppe, Andreas; Roehling, Heinz-Gerd; Schueth, Christoph, vol. 68, p.524.*

- 4) Beccaletto L. and Lagasquie J.-J. (2007) Failles de détachement et morphologie en roches métamorphiques, dans "du continent au bassin versant, théories et pratiques en géographie physique", Presses Universitaires Blaise Pascal, Université de Clermont-Ferrand, 33-37.
- 5) Beccaletto L. and Jenny C. (2004) Geology and Correlation of the Ezine Zone: a Rhodope Fragment in NW Turkey? Turkish Journal of Earth Sciences, vol. 13/2, p 145-176. IF=1.543.

Articles soumis dans des revues ACL

Hemelsdaël R., Averbuch O., Beccaletto L., Izart, A. Marc S., Capar L., Michels R. (2023) A deformed wedge-top basin inverted during the collapse of the Variscan belt: the Permo-Carboniferous Lorraine Basin (NE France), submitted to Tectonics.

1.2.2. Numéros thématiques

Dossier thématique Géochronique « les bassins carbonifères-permiens, avancées scientifiques, enjeux et perspectives », en cours, parution 12/2023.

Beccaletto L., Lasseur E, Paquet F., Capar, L. (2014) Evolution méso-cénozoïque du fossé Rhénan : apport du démonstrateur RGF, Géochronique n°129, 32-33.

1.2.3. Rapports BRGM (au 01/03/2023)

- 1) N. Marçot, M. Genevier, J. Abad, G. Aslan, L. Beccaletto, A. Bitri, R. Coueffe, M. De Michele, E. Equilbey, I. Gaudot, A. Portal, M. Lombard, M. Ibbi, B. Ladouche, B. Maurice, B. Ladouche et R. Wright (2022) – Gestion du risque affaissement-effondrement lié à la dissolution de gypse - Commune de Bargemon (Var). Rapport final. BRGM/RP-71427-FR, 283 p.
- 2) E. Husson, M. Genevier, B. Dewandel, M. Moulin coll. L. Beccaletto (2021) – PROVEN-KARSTS - Karsts profonds et ressources en eau en région Provence: état des connaissances et zones à investiguer. Rapport final Version 2. BRGM/RP-71300-FR, 295 p., 160 ill., 11 tabl., 5 ann.
- 3) Portal, A. ; Coppo, N. ; Jacob, T. ; Maurice, B. ; Beccaletto, L. (2021) - Investigations géophysiques au sein du PER « Fonts-Bouillants » (Saint-Parize-le-Châtel, 58) - Phase 3.1 : Tomographie de Résistivité Electrique ciblée sur « Les Fonts Bouillants » - Rapport final. BRGM/RC-71164-FR, 31 p., 1 ann.
- 4) Peter-Borie M., Dominique P., Beccaletto, L. (2021) – Expertise relative à l'évaluation du risque sismique associé au projet de géothermie profonde dans le Puy-de-Dôme (63) - Rapport final. BRGM/RC-71111-FR, 54 p., 4 Fig., 9 tab. (Confidentiel).
- 5) Jacob T., Portal A., Gal F., Beccaletto, L., Bitri A., Gaudot I. (2021) – Acquisitions géophysiques et Radon le long d'un linéaire au sein du PER « Fonts-Bouillants » - Phase II (Saint-Parize-le-Châtel, 58). Rapport final. BRGM/RC-70801-FR, 97 p., 23 ill., 4 ann.
- 6) Schroëtter J-M., Boisson A., Lucassou F., Bader A-G., Beccaletto, L., Ouergui Y. et Tourliere B. (2020) - ANAFORE : ANALYse multicritère des données de FORages les plus productifs de bretagnE, Rapport final, BRGM/RP-70280-FR, 156 p., 105ill., 2 ann.
- 7) Bourbon, P., Wuilleumier A., Barrière, J, Grataloup S., Beccaletto, L., (2020) Etude des ressources géothermiques potentielles dans plusieurs secteurs stratégiques de l'Agglomération Pau Béarn Pyrénées (64) - Rapport final, BRGM/RP-69745-FR, 47 p., 3 ann (Confidentiel).

- 8) Schroëtter J.-M., Bader A.-G., Beccaletto, L., Boisson A., Lucassou F., Ouergui Y. et Tourlière B. (2017) - ANAFORE : ANALYse multicritère des données de FORages les plus productifs de bretagnE, Rapport intermédiaire 2017, BRGM/RP-68479-FR, 77p., 45 ill., 2 ann.
- 9) Beccaletto, L. (2018) - Définition du bloc structural et identification des propriétés pétrographiques de la matrice et des objets structuraux aux échelles appropriées - Livrable 3.1.4 - Projet FONGEOSEC. Rapport final. BRGM/RC-68038-FR, 79 p., 47 fig., 11 tabl., 2 ann. (Confidentiel).
- 10) Bader A-G. et Beccaletto, L. (2017) Inventaire du potentiel français en cavités salines - tâche 1 projet ANR Fluidstory. Rapport final BRGM/RP-66725-FR, 160 p.
- 11) Beccaletto, L. 2016 Synthèse géologique et structurale du bassin d'Aquitaine - Livrable 3.1.1.a - Projet FONGEOSEC. Rapport final BRGM/RC-65827-FR, 82p. (Confidentiel).
- 12) Van Gessel S., Bader A-G., Bialkowski A, Beccaletto, L., Begemann E. (2016) ESTMAP Energy Storage Data Collection Report, EC ESTMAP project WP3 final report, 140p. (Confidentiel)
- 13) N. Charles, S. Colin, L. Beccaletto, H. Bauer under the coordination of F. Prognon (2015) - Study on the Protection against Floods for the Cities, Villages and Facilities throughout KSA - Evaluation of Potential Construction Materials. Final report BRGM/RC-64194-FR. (Confidentiel).
- 14) Couëffé R., Bauer H., Beccaletto, L., Bialkowski A., Capar L., Lasseur E., Paquet F. Serrano O., Thinon I., Tourlière B. (2016) Projet METROCENE. Bilan des activités sur l'exercice 2015, Rapport final BRGM/RP-65648-FR, 52 p., 5 ann.
- 15) Beccaletto, L., Capar L., Badinier G., Marc S. (2014) Étude sismique Non-Exclusive du Fossé rhénan français Rapport de traitement et d'interprétation. Apport de la sismique à la connaissance géologique du Fossé rhénan français, BRGM/RC-63950-FR, 147p. (Confidentiel).
- 16) Bouchot V., Bonijoly D. avec la collaboration de L. Beccaletto, S. Grataloup, S. Lopez, L. Vaute (2014) - Evaluation des ressources géothermales dans le Buntsandstein et le Permocarbone sous le site de Bure et sa région. Rapport d'expertise BRGM/RP-63598-FR, 50 p. (Confidentiel).
- 17) L. Beccaletto avec la collaboration de S. Marc (2014) - Potentiel en hydrocarbures non conventionnels du secteur Meuse/Haute Marne - Approche sismique. Rapport final BRGM/RC-63704-FR, 51p (IRSN). (Confidentiel).
- 18) Equipe GeORG (dont Beccaletto, L.) (2013) - Potentiel géologique profond du Fossé rhénan supérieur, projet GeORG INTERREG IV. Partie 1 résumé - Rapport Final BRGM/RP-61945-FR.
- 19) Equipe GeORG (dont Beccaletto, L.) (2013) - Potentiel géologique profond du Fossé rhénan supérieur, projet GeORG INTERREG IV. Partie 2 résultats - Rapport Final BRGM/RP-61945-FR.
- 20) Equipe GeORG (dont Beccaletto, L.) (2013) - Potentiel géologique profond du Fossé rhénan supérieur, projet GeORG INTERREG IV. Partie 3 méthodes - Rapport Final BRGM/RP-61945-FR.
- 21) Equipe GeORG (dont Beccaletto, L.) (2013) - Potentiel géologique profond du Fossé rhénan supérieur, projet GeORG INTERREG IV. Partie 4 Atlas - Rapport Final BRGM/RP-61945-FR.

- 22) Equipe RGF (dont Beccaletto, L.) (2013) - Elaboration d'un chantier RGF: retour d'expérience du chantier pilote Vosges - Fossé rhénan. Rapport final BRGM/RP-63008-FR.
- 23) Beccaletto, L., E. Lasseur, F. Paquet, L. Capar (2013) - Géométrie et contrôle structural des dépôts syn-rifts du Fossé rhénan: Démonstrateur RGF Vosges/Fossé rhénan. Rapport final BRGM/RP-62896-FR.
- 24) S. Grataloup, O. Serrano et Beccaletto, L. (2012) - Stockage de gaz en cavités salines, diapir de Dax Bénesse Saint-Pandelon, Bas-Adour. Rapport final BRGM/RP-60914-FR, 53 p., 26 fig., 3 tabl., 7 ann. (Confidentiel).
- 25) Bouchot V., Bader A.G., Bialkowski A., Bonté D., Bourguine B., Caritg S., Castillo C., Dezayes C., Gabalda S., Guillou-Frottier L., Haffen S., Hamm V., Kervévan C., Lopez S., Peter-Borie M. et collaborateurs (dont Beccaletto L.) (2012) - CLASTIQ-2 : programme de recherche sur les ressources géothermales des réservoirs clastiques en France (bassin de Paris et fossé rhénan). Rapport final. BRGM/RP-61472-FR, 207 p., 80 fig., 9 tabl., 2 ann.
- 26) Lasseur. E., Vedrine. S., Bauer. H., Beccaletto L., Capar. L., Flehoc. C., Gabalda. S. (2011) 3D geometry, paleogeography and facies distribution of the Paris Basin Lias deposits (France). Rapport final BRGM/RP-59611-FR, 341 p. (Confidentiel).
- 27) S. Grataloup, O. Serrano et L. Beccaletto (2011) - Stockage de gaz en cavités salines, diapir de Dax Bénesse Saint-Pandelon, Bas-Adour. Rapport final BRGM/RP-60279-FR, 53 p., 25 fig., 2 tabl., 6 ann. (Confidentiel).
- 28) Y. Callec, L. Beccaletto, J. Le Métour, J. Roger, C. Zammit, F. Chêne, P. Vinauger (2011). Reconnaissance géologique des zones d'El Ghallâouiya et Bir Amrane, au Nord du Bloc Ta-07 (Bassin de Taoudéni, Mauritanie). Rapport BRGM RC-59976-FR. (Confidentiel).
- 29) A-G Bader et L. Beccaletto (2011) Fournitures de données géologiques pour le programme de simulation "Hydraulique champ lointain" – Caractérisation des formations de l'unité hydrogéologique du Buntsandstein à l'échelle du secteur Meuse Haute-Marne étendu - TACHE 3, Rapport BRGM/RC-59602-FR, 25 p. (Confidentiel).
- 30) V. Bouchot, L. Beccaletto, A. Bialkowski, L. Capar, S. Caritg, C. Castagnac, A. Colnot, C. Castillo, C. Dezayes, S. Gabalda, V. Hamm, C. Kervévan, S. Lopez, C. Lerouge, C. Rigollet, A. Veillerette (2010) - CLASTIQ-2 : projet de recherche sur les ressources géothermales des réservoirs clastiques en France. Rapport d'avancement n° 2. BRGM/RP-59077-FR, 115 p., 60 fig., 17 tabl., 1 ann.
- 31) G. Badinier, L. Beccaletto et B. Tourlière, avec les participations d'O. Rouzeau et J.-P. Quinquis, coordination L. Beccaletto (2010) Inventaire des données géologiques nécessaires à la réalisation d'une étude d'implantation de sites de stockage d'énergie (CAES), Rapport BRGM/RP-58922-FR, 97 p. (Confidentiel).
- 32) L. Beccaletto (2010) Fournitures de données géologiques pour le programme de simulation "Hydraulique champ lointain" – Construction d'un écorché géologique du toit du substratum pré-Mésozoïque du bassin de Paris, tâche 4, Rapport BRGM/RC-59023-FR, 70 p. (Confidentiel).
- 33) L. Beccaletto, F. Hanot, S. Marc, avec la participation d'A. Perrin, coordination F. Hanot (2007). Etude structurale des réservoirs du Bassin de Paris Retraitement et interprétation de 14 lignes sismiques régionales - Non Exclusive Survey, Rapport BRGM/RC56407-FR, 41 p. (Confidentiel).

- 34) L. Beccaletto, F. Chapuis, B. Tourlière avec les participations de P. Graviou et O. Serrano, coordination L. Beccaletto (2010). Fournitures de données géologiques pour le programme de simulation "Hydraulique champ lointain" - Construction de la grille du toit du substratum pré-Mésozoïque - Echelle Bassin de Paris et secteur MHM étendu, tâche 2, Rapport BRGM/RC-58684-FR, 75 p. (Confidentiel).
- 35) L. Beccaletto, B. Tourlière avec les participations de P. Graviou, E. Lasseur et O. Serrano, coordination L. Beccaletto (2010). Fournitures de données géologiques pour le programme de simulation "Hydraulique champ lointain" - Construction de la grille du toit du substratum pré-Mésozoïque - Echelle Bassin de Paris et secteur MHM étendu, tâche 1, Rapport BRGM/RC-58644-FR, 36 p. (Confidentiel).
- 36) L. Beccaletto, F. Hanot, C. Robelin, avec les participations de L. Denis, S. Grataloup, D. Rambourg et B. Tourlière, coordination F. Hanot (2008). Fourniture de données géologiques pour le programme "Hydraulique Champ Lointain, Echelle bassin de Paris - Cartographie structurale de surfaces géologiques de référence, caractérisation des failles majeures, Rapport BRGM/RP56305-FR, 625 p. (Confidentiel).
- 37) L. Beccaletto, C. Robelin, F. Hanot, avec les participations de L. Denis et S. Grataloup, D. Rambourg et B. Tourlière, coordination F. Hanot (2008). Fourniture de données géologiques pour le programme "Hydraulique Champ Lointain, Echelle Meuse Haute-Marne étendu - Cartographie structurale de surfaces géologiques de référence, caractérisation des failles majeures, Rapport BRGM/RP56355-FR, 379 p. (Confidentiel).

1.2.4. Mémoires universitaires

- 1) Beccaletto L. (2004) Geology, correlations, and geodynamic evolution of the Biga Peninsula (NW Turkey). Mémoires de Géologie (Lausanne), Suisse, vol 43, 146p (+ 7 annexes et 14 planches).
- 2) Beccaletto L. (1998) Etude intégrée et stratigraphie génétique des réservoirs silicoclastiques de Villefranche-sur-Cher (sud du bassin de Paris), Mémoire de DEA, Université Montpellier II, 40 p.
- 3) Beccaletto L. et Colombié C. (1996) Reconstitution tridimensionnelle des niveaux réservoirs silicoclastiques de l'Hettangien de Sologne: exemple du site de stockage Gaz de France de Céré-la-Ronde (sud-ouest du Bassin de Paris), Mémoire de Maîtrise, Université Montpellier II, 39 p.

1.2.5. Actes de colloques (au 01/03/2023)

Communications à des congrès internationaux

Présentations orales

- 1) **Tchang-Tchong L.**, Michels R., Beccaletto L., Bossennec C., Lorgeoux C., Faure-Catteloin P. (2022) Energy transition in a petroleum rich area: the case study of the Pechelbronn sub-basin, DeepSurf Intern. Conference, Nancy, France.
- 2) **Hemelsdaël R.**, Allouti S., Averbuch O., Beccaletto L., Izard A., Michels R., Pironon J. (2022) 3D exploration of sedimentary basins in the context of energy transition : example of the Permo-Carboniferous Lorraine Basin, DeepSurf Intern. Conference, Nancy, France.
- 3) **Laurent A.**, Averbuch O., Beccaletto L., Graveleau F., Lacquement F., Capar L., Marc S. (2021) 3D geometry and kinematics of the Northern Variscan Thrust Front in Northern France: new

- insights based on reprocessing and interpretation of seismic reflection profiles, EUG 2021, On-line conference.
- 4) **Laurent, A.**, Averbuch, O., Beccaletto L., Graveleau, F., Lacquement, F., Caritg, S., Marc, S., Capar, L. (2021) 3D structural modelling of the Dinantian deep geothermal reservoir in the Nord-Pas-de-Calais coal district area (Northern France). MEET - Multi-sites EGS Demonstration - Geothermal Winter School, On-line conference.
 - 5) **Laurent, A.**, Averbuch, O., Beccaletto L., Graveleau, F., Lacquement, F., Caritg, S., Marc, S., Capar, L. (2021) 3D structural modelling of the Dinantian carbonates reservoir in the Nord-Pas-de-Calais coal basin area: towards a better characterization of the deep geothermal resource in Northern France. European Geothermal Phd Days 2021, On-line conference.
 - 6) Soreghan G., (2021), Benison K., Bourquin S., Hamamura N., Hamilton M., Heavens N., Hinnov L., Looy C., Pfeifer L., and Pochat S. (2020) DeepDust - A Proposed Drilling Project to Probe Continental Climate of the Late Paleozoic Icehouse-Greenhouse Transition, EGU2020: Sharing Geoscience Online, <https://doi.org/10.5194/egusphere-egu2020-11830>
 - 7) **Mercuzot M.**, Bourquin S., Pellenard P., Thomazo C., Beccaletto L., Schnyder J., Baudin F., Ducassou C., and Pierson-Wickmann A.-C. (2020) Contribution of sedimentology, organic geochemistry and clay mineralogy to reconstruct the palaeoenvironments of late Carboniferous to Permian of the northeastern Massif central, France, EGU2020: Sharing Geoscience Online, <https://doi.org/10.5194/egusphere-egu2020-14346>
 - 8) Schnyder J., Martinez M., Baudin F., Mercuzot M., Pellenard P., Thomazo C., Bourquin S., and Beccaletto L. (2020) Long-term lacustrine paleo-productivity and/or paleo-anoxia trends controlled by eccentricity cycles in the continental Autun Basin (France) at the Carboniferous/Permian boundary, EGU2020: Sharing Geoscience Online, <https://doi.org/10.5194/egusphere-egu2020-19962>
 - 9) Beccaletto L., Averbuch O., Izart A. (2019) The Lorraine-Saar Basin (E. France) in the frame of the Variscan orogeny: structure and tectono-sedimentary evolution, ICCP19, Köln, Germany.
 - 10) **Laurent A.**, Averbuch O., Beccaletto L., Capar L., Graveleau F., Lacquement F., Marc S. (2019) New insight on the 3D geometry of the Nord-Pas-de-Calais coal basin (N France) and its Devono-Carboniferous substratum by seismic imaging - contribution to a better definition of the low-energy geothermal resources, ICCP19, Köln, Germany.
 - 11) **Mercuzot M.**, Bourquin S., Ducassou C., Pellenard P., Beccaletto L., Pierson-Wickmann A.-C., Thomazo C., Schnyder J., Baudin F. (2019) Palaeoenvironmental reconstitutions of the late Carboniferous to Permian intracratonic basins of the north-eastern Massif Central (France), ICCP19, Köln, Germany.
 - 12) Bourquin S., Beccaletto L., Pochat S., **Mercuzot M.**, Ducassou C., Le Carlier de Veslud C. (2019) New sedimentological and well-log data from the Permian of the southern Paris Basin (France): a complete sedimentary succession underestimated? , ICCP19, Köln, Germany.
 - 13) Beccaletto L., **Baptiste J.**, Martelet G., Faure M. and Chen Y. (2016) Unravelling the geology beneath the Meso-Cenozoic sedimentary cover of the intracratonic Paris Basin - Part 1: new insights from seismic and potential field methods, 35IGC, Cape Town, South Africa.
 - 14) **Roche V.**, Jolivet L., Guillou-Frottier L., Tuduri J., Bouchot V., Beccaletto L., Lahfid A. (2016) Geometry and thermal structure of the Menderes Massif Core Complex (Western Turkey), implications for thermal evolution of Hellenic subduction zone, EUG 2016, Vienna, Austria.

- 15) **Baptiste J.**, Martelet G., Faure M., Beccaletto L., Chen Y., Reninger P.A. (2016) Detailed petrophysical characterization enhances geological mapping of a buried substratum using aeromagnetic and gravity data; application to the southwestern Paris basin, EUG 2016, Vienna, Austria.
- 16) **Baptiste J.**, Martelet G., Faure M., Beccaletto L. (2015) Up-to-date regional gravity and aeromagnetic data to unravel the geological pattern of the pre-Mesozoic substratum of the Paris Basin, Variscan 2015, Rennes, France.
- 17) Audigane P., Gentier S., Bader A-G., Beccaletto L., and Bellenfant G. (2014) The role of the underground for massive storage of energy: a preliminary glance of the French case, EUG 2014, Vienna, Austria. PICO.
- 18) Grataloup S., Beccaletto L., Serrano O., Courrioux G. (2013) Modelling of salt structures in South-West France - European 3D Geomodeller User Meeting, Orléans, France.
- 19) Beccaletto L., Lasseur, E. Martelet, G., Serrano O., Capar L., Marc S (2013) Pre-Mesozoic basement of the SW Paris Basin (France): The structural pattern of the Stephano-permian basins revisited using combined seismic, aeromagnetic and gravimetric methods, EUG 2013, Vienna, Austria. PICO.
- 20) Beccaletto L., Nitsch E., Anders B., Dresmann H., Rupf I., Tesch J., Zumsprekel H., Capar L. & The Georg Project Team (2013) Structural control and 3D modelling of a wrench rift basin: the Upper Rhine Graben of NW Europe as a case study - Contribution of the EU GeORG project, EUG 2013, Vienna, Austria. PICO.
- 21) Beccaletto L., Nitsch E., Anders B., Dresmann H., Rupf I., Tesch J., Zumsprekel H., Capar L. & The Georg Project Team (2012) 3D structural modelling of a wrench rift basin: the Upper Rhine Graben of NW Europe as a case study - Contribution of the EU GeORG project. 34IGC, Brisbane, Australia.
- 22) Nitsch E., Wielandt-Schuster U., Beccaletto L. (2011) Climatic vs. tectonic control on facies and salinity changes in an Eocene rift lake, Upper Rhine Graben, Central Europe. 5th International Limnogeology Congress, Konstanz, Germany.
- 23) Nitsch E., Anders B., Beccaletto L., Dresmann H., Rupf I., Tesch J., Zumsprekel H. (2011) Anatomy of a wrench rift revisited: Toward a 3D structural model of the Upper Rhine Graben. Fragile Earth Joint Meeting GV-DGG-GSA, München, Germany.
- 24) Rupf I., Anders B., Beccaletto L., Dresmann H., Nitsch E., Tesch J., Zumsprekel H. (2011) Regional/transnational 3D modeling in the Upper Rhine Graben within the Interreg GeORG Project. Fragile Earth Joint Meeting GV-DGG-GSA, München, Germany.
- 25) Dezayes C., Beccaletto L., **Oliviero G.**, Baillieux P., Capar L., Schill E (2011) 3-D visualization of a fractured geothermal field: the example of the EGS Soultz site (Northern Upper Rhine Graben, France). Proceedings of the Thirty-Sixth Workshop on Geothermal Reservoir Engineering Stanford University, Stanford, California, USA.
- 26) Bonev N., Beccaletto L., Robyr M., Monié P. (2008) Metamorphic and Ar/Ar geochronology constraints on the Alakeçi shear zone: implications for the extensional exhumation history of the northern Kazdağ Massif, NW Turkey, Donald D. Harrington Symposium, Geology of the Aegean, Austin, USA.
- 27) Beccaletto L. and Bonev N. (2006) Tertiary exhumation processes and related kinematic record in the northern Aegean: evidence from the Eastern Rhodope- Thrace (Bulgaria-Greece) and the Biga Peninsula (NW Turkey), EGU General Assembly, Vienne, Autriche.

- 28) Beccaletto L. and Bonev N. (2005) Bivergent extensional unroofing in northwest Turkey: kinematic evidence from the Kazdag Massif, International Symposium on the Geodynamics of Eastern Mediterranean: Active Tectonics of the Aegean, Istanbul, Turquie.
- 29) Bonev N. and Beccaletto L. (2005) Northeastward ductile shear in the Kemer micaschists, Biga Peninsula (NW Turkey), International Symposium on the Geodynamics of Eastern Mediterranean: Active Tectonics of the Aegean, Istanbul, Turquie.
- 30) Beccaletto L. and Stampfli G. M., (2004) Paleotectonic and paleogeographic significance of melanges: examples from the Tethyan realm, 20th Réunion des Sciences de la Terre, International session SGF-GV, Strasbourg, France.
- 31) Beccaletto L. and Steiner C. (2004) Tectonic and sedimentary Evidence of the Two stage Extensional evolution of the Edremit Graben (NW Turkey), 20th Réunion des Sciences de la Terre, International session SGF-GV, Strasbourg, France.
- 32) Beccaletto L. and Stampfli G. M., (2004) Toward a geodynamic significance of mélanges: examples from the Tethyan realm, 32th International Geological Congress, Florence, Italie.
- 33) Beccaletto L. and Stampfli G. M., (2002) Origin of the Çetmi mélange (NW Turkey), 1st International Symposium of Istanbul Technical University, Istanbul, Turkey.
- 34) Beccaletto L. and Stampfli G. M., (2001) Geodynamic evolution of the Biga Peninsula (NW Turkey), *EUG XI*, Strasbourg, France.

Posters

- 1) Portal A., Maurice B., Ibba M., Beccaletto L., Coueffe R., Genevier M., Abad J., Equilbey E., Marçot N. (2022) Enlighten the Triassic geological setting favourable to large gypsum dissolution-related collapses through geophysics, EAGE, Belgrade, Serbia.
- 2) **Laurent A.**, Averbuch O., Beccaletto L., Graveleau F., Lacquement F., Caritg S., Marc S., Capar L. (2021) 3D structural modelling of the Dinantian carbonates reservoir in the Nord-Pas-de-Calais coal basin area: towards a better characterization of the deep geothermal resource in Northern France, European Geothermal PhD Days - EGPD2021, Distanciel.
- 3) **Mas P.**, Calcagno P., Caritg-Monnot S., Capar L., Beccaletto L., Hamm V., Saada A. (2021) Seismic interpretation and 3D geomodelling of the Dogger and Triassic aquifers for a geothermal application in the metropolis of Orléans, France, European Geothermal PhD Days - EGPD2021, Distanciel.
- 4) Beccaletto L., Bader A.G, Bialkowski A., Jaudin F., Van Gessel S., Hopman J. (2017) Collecting geological subsurface data for energy storage assessment as a part of the European ESTMAP project (Energy STORAGE Mapping and Planning), IMS2017, Toulouse, France.
- 5) Bader A-G., Beccaletto L. (2017) Inventory of the French salt formations for energy storage in salt cavities (FLUIDSTORY ANR project), IMS2017, Toulouse, France.
- 6) **Dentzer J.**, Bruel D., Delescluse M., Chamot-Rooke N., Beccaletto L., Lopez S., Courrioux G., Violette S. (2017) Pervasive faulting revealed by acoustic blanking: a potential explanation for large thermal anomalies in the Anglo-Paris Basin? EUG 2017, Vienna, Austria.
- 7) Briais J., Lasseur E., Homberg C., Beccaletto L., Couëffé R., Bellahsen N., Chateaufneuf J-J. (2017) Sedimentary record and structural analysis of the opening of the European Cenozoic Rift System: The case of the Upper Rhine Graben, EUG 2017, Vienna, Austria.
- 8) Beccaletto L., Capar L., Serrano O., and Marc S. (2016) Unravelling the geology beneath the Meso-Cenozoic sedimentary cover of the intracratonic Paris Basin - Part 3: using seismic data

to decipher the structural evolution and sedimentary record of the Stephano-Permian basins, 35IGC, Cape Town, South Africa.

- 9) **Baptiste J.**, Martelet G., Faure M., Beccaletto L., Chen Y., and Reninger P-A. (2016) Unravelling the geology beneath the Meso-Cenozoic sedimentary cover of the intracratonic Paris Basin - Part 2: geological mapping of the buried Variscan basement combining aeromagnetic, gravity and petrophysical data, 35IGC, Cape Town, South Africa.
- 10) **Roche V.**, Bouchot V., Beccaletto L., Jolivet L., Guillou-Frottier L. (2016). Structural controls on geothermal activity in eastern Mediterranean region: example of the Main Menderes area, 35IGC, Cape Town, South Africa.
- 11) Beccaletto L., Bader A-G., Bialkowski A., Jaudin F., Hladík V., Holeček J., Van Gessel S., Meinke-Hubeny F., and Mulder A. (2016) Geological subsurface data collection as a part of the European ESTMAP Project (Energy STORAGE Mapping and Planning), 35IGC, Cape Town, South Africa.
- 12) Bader A.G., Beccaletto L., Bialkowski A., Jaudin F., Hladík, V., Holeček J., Van Gessel S., Wiersma F., Meinke-Hubeny F., (2016) The ESTMAP Project (Energy storage Mapping and Planning): focus on the subsurface data collection, EUG 2016, Vienna, Austria.
- 13) **Roche V.**, Jolivet L., Guillou-Frottier L., Tuduri J., Lahfid A., Bouchot V., Beccaletto L. (2015) Geometry and thermal structure of the Menderes Massif Core Complex (Turkey), implications for thermal evolution of Hellenic subduction zone, Annual TOPO-EUROPE workshop, Antibes, France.
- 14) Beccaletto L., Lasseur, E. Martelet, G., Serrano O., Coueffe R., Capar L., Marc S. (2012) The Pre-Mesozoic basement of the SW Paris Basin (France) revisited using combined seismic, aeromagnetic and gravimetric methods - Focus on the Stephano-permian basins. 34IGC, Brisbane, Australia.
- 15) Beccaletto L., Serrano O., Coueffe R., Capar L., Marc S. (2012) The response of the French sedimentary basins to the Pyrenean and Alpine compressive phases: insights from the reprocessing and interpretation of regional seismic lines. 34IGC, Brisbane, Australia.
- 16) Lasseur E., Beccaletto L., Martelet G., Ona Ona L., Baudouin V., Serrano O. (2012) Jurassic palaeogeography and subsidence of the Poitou high (western France), influence of the Variscan orogene structural inheritance on the onset of a Mesozoic sedimentary basin. 34IGC, Brisbane, Australia.
- 17) Nitsch E., Wielandt-Schuster U., Rupf I, Beccaletto L. (2011) Climatic VS Tectonic control on facies and salinity changes in an Eocene rift lake, Upper Rhine Graben, Central Europe. Fragile Earth Joint Meeting GV-DGG-GSA, München, Germany.
- 18) Moix P., Beccaletto L., Masset O., Kozur H. W., Dumitrica P., Vachard D., Martini R., Stampfli G. M. (2010) Geology, correlation and geodynamic evolution of the Mersin mélanges, Southern Turkey. GSA Meeting "Tectonics Crossroads: Evolving Orogens of Eurasia-Africa-Arabia", Ankara, Turkey.
- 19) Beccaletto L., Stampfli G. M. (2010) Paleotectonic and paleogeographic signification of melanges: examples from the Tethyan realm. GSA Meeting "Tectonics Crossroads: Evolving Orogens of Eurasia-Africa-Arabia", Ankara, Turkey.
- 20) Beccaletto L., Hanot F., Serrano O., Marc S. (2008) Structural frame of the Paris Basin (France) based on the reprocessing and interpretation of regional seismic lines, 33rd IGC – Oslo – Norvège.

- 21) Lasseur E., Guillocheau F., Robin C., Beccaletto L. (2008) 3D geometry and palaeogeography of the Paris Basin Chalk (Cenomanian to Campanian) - Tectonics and eustatic implications, 33rd IGC – Oslo – Norvège.
- 22) Serrano O., Hanot F., Delmas J., Vially R., Beccaletto L. (2008) The Aquitaine Basin: seismic data valorization, structural mapping and petroleum potential, 33rd IGC – Oslo – Norvège.
- 23) Beccaletto L. and Stampfli G.M. (2005) Permo-Cretaceous geodynamic evolution of the Biga Peninsula (NW Turkey) and adjacent areas - Part I: field observations, International Earth Sciences Colloquium on the Aegean Regions, Izmir, Turquie.
- 24) Stampfli G.M., Hochard C., Beccaletto L. (2005) Permo-Cretaceous geodynamic evolution of the Biga Peninsula (NW Turkey) and adjacent areas - Part II: paleotectonic model, International Earth Sciences Colloquium on the Aegean Regions, Izmir, Turquie.
- 25) Beccaletto L. and Stampfli, G. M. (2004) Does the Ezine zone, Biga Peninsula, represent a fragment of Rhodope in NW Turkey ?, 32th International Geological Congress, Florence, Italie.
- 26) Beccaletto L., Rosselet F. and Stampfli G. M., (2003) (5 posters) Tethyan Evolution of the Aegean Domain from Early Jurassic to Late Cretaceous: Examples from Turkey, AAPG International Conference and Exhibition, Barcelone, Espagne.
- 27) Rosselet F., Beccaletto L. and Stampfli G. M., (2003) (5 posters) Tethyan Evolution of the Aegean Domain from Paleozoic to Late Triassic: Examples from Turkey, AAPG International Conference and Exhibition, Barcelone, Espagne.
- 28) Beccaletto L. and Stampfli G. M., (2003) Unexpected implications of Anisian limestones blocks in the Çetmi mélange (NW Turkey): younger ocean or mixing processes, EGS-AGU-EUG Joint Assembly, Nice, France.
- 29) Beccaletto L. and Stampfli G. M., (2000) New data on the Çetmi mélange (Biga Peninsula, NW Turkey), 4th International Earth Sciences Colloquium on the Aegean Region, Izmir, Turkey.

Communications à des congrès nationaux

Présentations orales

- 1) **Brown S.**, Missenard Y., Robion, Ph, Beccaletto L., , Allanic C., Haurine F. (2023) How and when do intraplate basins record deformations, TSGF, Leeds, England.
- 2) Beccaletto L., Bourquin S. (2021) Le bassin sous couverture de Brécly (sud du bassin de Paris): plus de 3500 m de sédiments permien préservés - quelles implications? 27^{ème} RST, Lyon, France.
- 3) Beccaletto L., (2021) Les bassins carbonifères-permiens en France imagés par les données de subsurface: vers une meilleure compréhension des dynamiques syn- et post-varisques, 27^{ème} RST, Lyon, France.
- 4) **Mercuzot M.**, Bourquin S., Beccaletto L., Pellenard P., Ducassou C., Rubi R., Gand G. (2021) Reconstitutions paléoenvironnementales des bassins fini-carbonifères à permien en contexte tardi-orogénique (N-E du Massif central) : implications paléogéographiques et géodynamiques, 27^{ème} RST, Lyon, France.

- 5) **Mercuzot M.**, Pellenard P., Bourquin S., Thomazo C., Martinez M., Beccaletto L., Schnyder J., Baudin F. (2021) Étude paléoenvironnementale et paléoclimatique multi-proxies des bassins fini-carbonifères à permien du N-E du Massif central, 27^{ème} RST, Lyon, France.
- 6) Pellenard P., **Mercuzot M.**, Gand G., Schmitz M., Ducassou C., Bourquin S., Beccaletto L. (2021) Un nouveau modèle d'âge pour l'Autunien du bassin d'Autun à partir de datations U-Pb sur des tonsteins, 27^{ème} RST, Lyon, France.
- 7) **Mercuzot, M.**, Thomazo, C., Pellenard, P., Bourquin, S., Martinez, M., Schnyder, J., Beccaletto L., (2020). Enregistrement climatique dans les séries lacustres fini-carbonifère à permien du domaine intertropical d'Europe de l'ouest (bassin d'Autun). Journées climat et impact, grandes échelles de temps, Paris, France (vidéoconférence).
- 8) **Laurent A.**, Averbuch O., Beccaletto L., Capar L., Graveleau F., Lacquement F., Marc S. (2019) Structuration et faciès sédimentaires des potentiels réservoirs géothermiques profonds du Dévonien et du Dinantien dans la région du bassin houiller du Nord-Pas-de-Calais, 17^{ème} ASF, Beauvais, France.
- 9) **Mercuzot M.**, Bourquin S., Ducassou C, Beccaletto L., Pellenard P., Poujol M. (2019) Le bassin intracontinental fini-carbonifère à permien de Lucenay-lès-Aix (nord-est du Massif Central) réévaluations sédimentologiques implications paléoenvironnementales, 17^{ème} ASF, Beauvais, France.
- 10) Bourquin S., Beccaletto L., Pochat S., **Mercuzot M.**, Ducassou C., (2019) Nouvelles données sédimentologiques et réévaluation des anciens forages du Sud du bassin de Paris : une succession permienne complète sous-estimée ? 17^{ème} ASF, Beauvais, France.
- 11) Beccaletto L., Pochat S., Bourquin (2019) The ICDP Deepdust project - Probing continental climate of the Late Paleozoic icehouse-greenhouse transition, les forages scientifiques IODP et ICDP, outils majeurs au service des géosciences, MNHN Paris, France.
- 12) **Mercuzot M.**, Bourquin S., Ducassou C, Beccaletto L., Pellenard P., Pierson-Wickmann, A.-C., (2019) Apport des forages profonds aux reconstitutions paléoenvironnementales et paléoclimatiques des bassins carbonifères à permien du nord-est du Massif Central, Réunion SGF Forages profonds en France: 30 ans de résultats, Paris, France.
- 13) Beccaletto L., Pochat S., Soreghan L., et collaborateurs. (2019) The Permian of the Paris Basin (ICDP "DeepDust" project), Réunion spécialisée de la SGF - Forages profonds en France: 30 ans de résultat, Paris, France.
- 14) **Mercuzot M.**, Bourquin S., Pellenard P., Pierson-Wickmann A.-C., Thomazo C., Beccaletto L., Ducassou C., Schnyder J., Baudin F., Ravier E. (2018) Reconstitutions paléoenvironnementales et enregistrement paléoclimatique fini-carbonifère à permien du bassin d'Autun (Nord-Est du Massif Central), RST2018, Lille, France.
- 15) Averbuch O., Lacquement F., Meilliez F., Graveleau F., Beccaletto L., Vendeville B. (2018) La chaîne varisque vue depuis son front nord : dynamique du front de chaîne, sous-charriage crustal de la marge avalonienne et délamination associée de la lithosphère supra-subduction, RST2018, Lille, France.
- 16) **Baptiste J.**, Martelet G., Beccaletto L., Faure M., Chen Y. (2018) Géométrie, nature et origine de l'Anomalie Magnétique du Bassin de Paris (AMBP) : apport de nouvelles modélisations 2D, RST2018, Lille, France.
- 17) Beccaletto L., Averbuch O., Izart A. (2018) La place du Bassin Sarro-Lorrain dans la chaîne varisque: structure et timing de mise en place, RST2018, Lille, France.

- 18) Ducassou C., Bourquin S., Pellenard P., Beccaletto L., **Mercuzot M.**, Rossignol C., Poujol M., Hallot E., Pierson-Wickmann A.-C., and Gand G. (2018) Caractérisation pétro-géochimique et datation U/Pb du volcanisme contemporain des bassins d'âge fini-Carbonifère à Permien du Nord du Massif Central, RST2018, Lille, France.
- 19) **Baptiste J.**, Martelet G., Faure M., Beccaletto L., Reninger P-A, Perrin J., Chen Y. (2016) Structures, lithologie et géométries d'un substratum enfoui : application au sud-ouest du bassin parisien, RST2016, Caen, France.
- 20) Averbuch O., Beccaletto L., Izart A. Piromallo C. (2016) Le processus de délamination lithosphérique tardi-orogénique : un modèle intégrateur pour expliquer l'effondrement de la chaîne varisque et l'initiation du bassin de Paris ? RST2016, Caen, France.
- 21) Briais J., Couëffé R.1, Lasseur E., Bauer H., Beccaletto L., Bialkowski A., Capar L., Paquet F., Serrano O., Thinon I., Tourlière B. (2016) Le projet METROCENE : vers une synthèse nationale actualisée des bassins sédimentaires tertiaires sur la base des travaux récents du BRGM à terre et en mer, RST2016, Caen, France.
- 22) Briais J., Lasseur E., Homberg C., Beccaletto L., Couëffé R., Bellahsen N., Chateauneuf J-J., (2016) Enregistrement sédimentaire et analyse structurale de la dynamique de l'ouverture du système de rift ouest européen (ECRIS), exemple du fossé rhénan, RST2016, Caen, France.
- 23) Hue C., Rossignol C., Bourquin S., Beccaletto L., Pellenard P., Poujol M., Ferrand M., Le Carlier de Veslud C., and Gastineau R. (2016) Reconstitution des environnements de dépôt du Carbonifère supérieur/ Permien inférieur au Sud du bassin de Paris : implication géodynamique, RST2016, Caen, France.
- 24) Pellenard P., Ferrand M., Rossignol C., Gand G., Bourquin S., Beccaletto L., Poujol M., Hue C. (2016) Volcanisme explosif aérien au passage Carbonifère-Permien dans les bassins stéphanos-autuniens d'Europe de l'Ouest, RST2016, Caen, France.
- 25) **Roche V.**, Bouchot V., Beccaletto L., Jolivet L., Guillou-Frottier L., Oguz K., Tuduri J., Tokay B. (2016) - Structural, lithological and geodynamic controls on geothermal activity in the Main Menderes geothermal Province (Western Anatolia, Turkey), RST2016, Caen, France.
- 26) Beccaletto L., Serrano O., Capar L., Marc S. (2014) Le substratum pré-mésozoïque du bassin de Paris revisité: évolution structurale des bassins permo-carbonifères sous couverture sédimentaire, 50 ans de l'AGBP, Paris, France.
- 27) **Baptiste J.**, Martelet G. ; Faure M., Beccaletto L., Perrin J. (2014) Regard sur la structure géologique du substratum pré-Mésozoïque du Bassin de Paris, 50 ans de l'AGBP, Paris, France.
- 28) Beccaletto L., Serrano O., Capar L., Marc S (2014) The pre-Mesozoic basement of the SW Paris basin (France) revisited - Focus on the structural evolution of the Late Carboniferous-Early Permian sedimentary basins under their post depositional sedimentary cover, RST2014, Pau, France.
- 29) **Baptiste J.**, Martelet G. ; Faure M., Beccaletto L., Perrin J. (2014) Geological patterns of the pre-Mesozoic substratum of the Paris Basin revealed by recent regional geophysical data, RST2014, Pau, France.
- 30) **Beccaletto L.**, Lasseur E., Paquet F., Capar L. (2013) Geometry of the sedimentary filling and role of present-day the border faults during the Cenozoic rifting phase of the Upper Rhine graben of Western Europe. ASF2013, Paris, France.

- 31) Zumsprekel H., Anders B., Fehn, C., Nitsch E., Rupf I., Sokol G., Wirsing G., Ellwanger D., Franz M., Prestel R., Rodat C., Schuff J., Wielandt-Schuster U., Kaercher T., Haneke J., Krzyzanowski J., Storz R., Tesch, J., Wiedenfeller M., Capar L., Beccaletto L., Cruz-Mermy D., Dezayes C., Urban S., Huggenberger P., Dresmann H. (2012) The GeORG geoportal; interoperable web distribution of harmonized geological data, German Society for Geosciences Annual Meeting; Hannover, Germany.
- 32) Anders B., Fehn, C., Nitsch E., Rupf I., Sokol G., Wirsing G., Zumsprekel H., Ellwanger D., Franz M., Prestel R., Rodat C., Schuff J., Wielandt-Schuster U., Kaercher T., Haneke J., Krzyzanowski J., Storz R., Tesch, J., Wiedenfeller M., Capar L., Beccaletto L., Cruz-Mermy D., Dezayes C., Urban S., Huggenberger P., Dresmann H. (2012) Geopotentials of the Upper Rhine Graben; results of the GeORG project, German Society for Geosciences Annual Meeting; Hannover, Germany.
- 33) Wielandt-Schuster U., Nitsch E. Anders B., Beccaletto L., Dresmann H., Ellwanger D., Haneke J., Huggenberger P., Wiedenfeller M., Sokol G., Franz M., Prestel R., Rodat C., Rupf I., Schuff J., Wirsing G., Zumsprekel H., Kaercher T., Krzyzanowski J., Storz R., Tesch, J., Capar L., Cruz-Mermy D., Dezayes C., Urban S. (2012) Towards a harmonized lithostratigraphic nomenclature for the Cenozoic of the Upper Rhine Graben of Germany, France and Switzerland, German Society for Geosciences Annual Meeting; Hannover, Germany.
- 34) Beccaletto L., Lasseur E., Capar L., Martelet G. (2011). Pre-Mesozoic Basement of the SW Paris Basin (France) - Focus on The Stephano-Permian Basins. ASF2011, Dijon, France.
- 35) Lasseur E., Ona Ona L., Lenoir F., Baudouin V., Serrano O., Guillocheau F., Beccaletto L. (2011). Paléogéographie, géométrie et évolution jurassique de la partie sud du seuil du Poitou. Influence de la Structuration Varisque héritées sur la sédimentation jurassique. ASF2011, Dijon, France.
- 36) Rupf I., Anders B., Nitsch E., Zumsprekel H., Beccaletto L., Capar L., Kärcher T., Tesch J. (2010). Exploring deep subsurface: Techniques, workflow, data processing and status of the GeORG-project. GeORG Technical Workshop, Freiburg, Germany.
- 37) Beccaletto L., Capar L., Cruz-Mermy D., **Oliviero G.**, Elsass P., Perrin A., Rupf I., Nitsch E., Tesch J. (2010). The GeORG project – Seismic interpretation, structural pattern and 3D modeling of the Upper Rhine Graben - first scientific results. GeORG Technical Workshop, Freiburg, Germany.
- 38) Beccaletto L., Capar L., Cruz-Mermy, D., Rupf I., Nitsch E., **Oliviero G.**, Elsass P., Perrin A., Marc S. (2010). The GeORG project - Geological Potential of the Upper Rhine Graben - Situation, goals and first scientific results, RST2010, Bordeaux, France.
- 39) Lasseur E, Beccaletto L., Callec Y, Couëffé R, Paquet F, Platel JP, Serrano O, Thinin I (2009) The RGF program (geological reference map of France); a geodynamic geologic map. 5th thematic meeting of the French Working Group on the Cretaceous, Paris, France.
- 40) Lasseur.E., Callec.Y., Beccaletto L., Couëffé.R., Paquet.F., Platel.J.P., Serrano.O., Thinin.I., Baudin.T. (2009) Evénements géodynamiques, enregistrement des grandes phases de déformation méso-cénozoïque dans les bassins sédimentaires français, 12^{ème} ASF, Rennes, France.
- 41) Beccaletto L., Hanot, F., Serrano, O., Marc, S. (2009) Building, reprocessing and interpretation of regional seismic lines in the Paris Basin (France): methodology and developments, 12^{ème} ASF, Rennes, France.

- 42) Beccaletto L. and Stampfli G. M., (2002) Le prisme d'accrétion fossile de Çetmi (Turquie du N-O): approche méthodologique et évolution paléogéographique, 19th Réunion des Sciences de la Terre, Nantes, France.

Posters

- 1) **Mercuzot M.**, Vennin E., Pellenard P., Steiner S., Bourquin S., Gand G., Beccaletto L., Theriez G. (2021) Late Carboniferous to early Permian microbial deposits of the Massif Central, France: paleoenvironment and paleoclimatic implications, M-Fed, Paris, France.
- 2) **Hemelsdaël R.**, Beccaletto L., Averbuch O., Michels R., Izart A., Laouici I. (2021) Tectono-stratigraphic evolution of the Permo-Carboniferous Lorraine-Saar basin constrained by 3D geological modeling (France, Germany), 27^{ème} RST, Lyon, France.
- 3) Jacob T., Coppo N., Dubois F., Wawrzyniak P., Portal A., Bitri A., Gaudot I., Beccaletto L., Le Maire P., Laine C., Hauville B., Pellissier N. (2021) Exploration géophysique au sein du PER "Fonts-Bouillants": apport des méthodes gravimétriques, audiomagnétotelluriques et électromagnétiques à source contrôlée, 27^{ème} RST, Lyon, France.
- 4) **Brown S.**, Beccaletto L., Jullien-Sicre A., Missenard Y., Robion P., Allanic C. (2021) A synthetic structural map of Tertiary formations in the Paris Basin, 27^{ème} RST, Lyon, France.
- 5) Graveleau F., Antoine P., Jomard H. Camelbeeck T., Lecocq T., Manchuel K., Averbuch O., Laurent A., Meilliez F., Beccaletto L., Chanier F., Watremez L., Gaullier V., Laurencin M., Duperret A., Vandycke S., Arroucau P., Bergerat F., Loch J-L. (2021) Activities Of The Resif-Ats-Fact Group For Northern France Region To Improve The Knowledge On Potential Active Faults, International workshop on "Active tectonics and dating, Praz-sur-Arly, France.
- 6) **Ducassou C.**, Rossignol C., Bourquin S., Pellenard P., Beccaletto L., Poujol M., **Hue C.**, Mercuzot M. (2018) Différentes approches pour la datation U/Pb des tonsteins intercalés dans les séries continentales d'âge fini-carbonifère à permien de Lucenay-lès-Aix (Sud du Bassin de Paris, France), RST2018, Lille, France.
- 7) **Baptiste J.**, Melleton J., Beccaletto L., Faure M., Poujol M., Lach P. (2018) Premières données géochronologiques sur les granites du substratum pré-mésozoïque du Bassin parisien, RST2018, Lille, France.
- 8) Beccaletto L. (2016) The French Stephano-Permian basins as witnesses of the Variscan-Mesozoic transition - compilation map and open scientific questions. RST2016, Caen, France.
- 9) Bialkowski A., Bader A-G., Beccaletto L., Jaudin F., Van Gessel S. and Hopman J. (2016) The ESTMAP Project (Energy STORAGE Mapping and Planning): Focus on the subsurface data collection, RST2016, Caen, France.
- 10) Briaïs J., Beccaletto L., Tourlière B., Lasseur E., Bauer H., Beccaletto L., Bialkowski A., Capar L., Paquet F., Serrano O., Thinon I. (2016) Géométrie des bassins cénozoïques métropolitains : premier aperçu fourni par la carte des épaisseurs de leur remplissage sédimentaire (projet METROCENE), RST2016, Caen, France.
- 11) Briaïs J., Lasseur E., Beccaletto L., Couëffe R., Bellahsen N., (2015). Enregistrement sédimentaire de la dynamique de l'ouverture du système de rift ouest européen (ECRIS), exemple du fosse rhénan, ASF 2015, Chambéry, France.
- 12) Beccaletto L., Lasseur E., Martelet G. Serrano O., Capar L., Marc S. (2013). The structural pattern and geological evolution of the Stephano-Permian basins under the pre-Mesozoic basement of the SW Paris Basin (France). ASF2013, Paris, France.

- 13) Capar L., Beccaletto L., Elsass P., Marc S., Rupf I., Nitsch E., et le Groupe Georg. (2011). Failles Transverses dans le fossé rhéna. ASF2011, Dijon, France.
- 14) Capar L., Beccaletto L., Elsass P., Oliviero G., Perrin A., Marc S., Rupf I., Nitsch E. (2010) Structures tectoniques dans la région de Pechelbronn par interprétation sismique: leur rôle dans le rifting du fossé rhéna, RST2010, Bordeaux, France.
- 15) Capar L., Beccaletto L., Elsass P., Marc S., Perrin A., Oliviero G. (2009) Apport du retraitement sismique à l'étude des bassins sédimentaires : exemple du fossé rhéna, 12^{ème} ASF, Rennes, France.
- 16) Beccaletto L. and Stampfli G. M., (2004) The role of accretion-related melanges to reconstruct past plate tectonics. Examples from the western Tethyan realm, 2th Swiss Geoscience Meeting, Lausanne, Suisse.
- 17) Beccaletto L. and Stampfli G. M., (2001) La séquence de Karadag (Turquie du N-O): sédimentologie et implications géodynamiques, 8ème congrès de l'ASF, Orléans, France.
- 18) Beccaletto L. and Stampfli G. M., (2001) New constraints on the exhumation of the Kazdag Massif (Biga Peninsula, N-W Turkey), 18th Swiss Tectonic Studies Group Meeting, Neuchâtel, Suisse.
- 19) Beccaletto L., Merzeraud G., Larqué P., Rauscher R., Hoffert M. and Leroy E., (2000) Etude sédimentologique intégrée et organisation séquentielle des réservoirs silicoclastiques de Villefranche/Cher (S-O du Bassin de Paris), 18th Réunion des Sciences de la Terre, Paris, France.

1.2.6. Conférencier invité

- 11/2019 Géosciences Rennes, Réunion thématique de la SGF « Histoire Carbonifère Permien du domaine intertropical ». A la recherche des bassins carbonifères et permien cachés sous couverture - Importance des données de subsurface pour la compréhension des bassins syn- et post-varisques.
- 12/2014 GECergy-Pontoise. Evolution structurale des bassins permo-carbonifères sous couverture sédimentaire mésozoïque.
- 01/2004 Ecole Doctorale de Montpellier (ISTEEM). Les mélanges d'accrétion fossiles dans une perspective paléogéographique: exemple du mélange de Çetmi (Turquie du NO).
- 03/2004 Ecole Doctorale de Lyon (PEPS). Les mélanges d'accrétion fossiles dans une perspective paléogéographique: exemple du mélange de Çetmi (Turquie du NO).

1.2.7. Organisation et animation de colloques et workshop

Co-organisateur avec S. Bourquin du Workshop ICDP Deepdust 2.0 à Paris les 27 et 28 janvier 2020 ; 32 participants de 10 pays européens + USA.

Co-chairman avec A. Gébelin, J-M. Lardeaux, K. Schulmann, M-I. Spalla, O. Vanderhaeghe de la session « La chaîne varisque » à la RST Lille 2018.

Co-chairman avec J. Herrle, D. Bajnai, S. Bourquin, M. Simmons, W. Dummann, I. Montañez, D. Ray de la session « Phanerozoic Stratigraphy, Paleoenvironments, Eustasy and Paleoclimate » à l'EGU 2020.

1.2.8. Divers

Review d'articles (Journal of Geodynamics, Journal of Structural Geology, BSGF - Earth Sciences Bulletin).

Expertise d'un projet pour l'appel d'offre du Programme TelluS INSU-CNRS en 2019.

1.3. Encadrement de la recherche

Depuis mon recrutement au BRGM en 2007 j'ai directement participé au montage de quatre thèses (« encadrements principaux ») : (i) la thèse de J. Baptiste à l'ISTOrléans (2013-2016) a permis de dresser une cartographie détaillée du substratum anté-mésozoïque du bassin de Paris à partir de données magnétiques et gravimétriques ; (ii) la thèse de M. Mercuzot à Géosciences Rennes (2017-2020) a revisité la géologie des bassins stéphano-permiens du nord du Massif Central à partir de données de subsurface (carottes, diagraphies, sismique) ; (iii) la thèse d'A. Laurent au LOG de Lille (2018-2021) a totalement modernisé la compréhension du front nord varisque dans le nord de la France à partir de données sismiques. Ces trois thèses ont donné lieu à plusieurs publications (voir section 1.2). Les résultats de ces deux dernières thèses seront détaillés dans la suite du manuscrit ; (iv) je participe actuellement à l'encadrement de la thèse de S. Brown à GEOPSSaclay sur les « Déformations multi-échelles cénozoïques du bassin de Paris », dans le cadre du projet BRGM RGF chantier bassin de Paris, dans laquelle j'interviens en tant que spécialiste des déformations d'échelle sismique dans ce bassin.

Je suis également impliqué dans l'encadrement de la thèse de L. Tchang Tchong à Géoressources Nancy, pour laquelle je mets à profit mon expertise sur la géologie du fossé Rhénan. Je suis aussi intervenu dans la thèse de J. Dentzer à Mines Paris Tech, à qui j'ai apporté mon savoir-faire sur l'interprétation sismique dans le bassin de Paris, et dans celle de V. Roche à l'ISTEParis, à qui j'ai apporté ma connaissance sur les métamorphisme core-complex de Turquie occidentale. Je suis co-auteur d'une publication pour chacune de ces trois thèses (voir section 1.2).

1.3.1. Synthèse de l'encadrement doctoral et participation aux jury de thèses

Encadrements principaux

- 1) 2020- Co-encadrement de la thèse de Stephen Brown (25%), inscrit à l'Université de Cergy; cofi. 50-50 BRGM-Université Cergy-Pontoise (projet RGF bassin de Paris) : « Déformations multi-échelles cénozoïques du Bassin parisien » ; directeur habilité Y. Missenard, GEOPS, ED Sciences mécaniques et énergétiques, matériaux et géosciences.
- 2) 2018-2021 Co-encadrement de la thèse d'Aurore Laurent (40%), inscrite à l'Université de Lille ; cofi. 50-50 BRGM-Région Hauts-de-France : « Modélisation géologique 3D du bassin houiller du Nord-Pas-de-Calais et de son substratum dévonien-carbonifère inférieur: vers une meilleure définition des réservoirs géothermiques profonds » ; directeur habilité O. Averbuch, LOG Lille, ED Sciences de la Matière, du Rayonnement et de l'Environnement.

Situation actuelle : en post-doc au Service géologie du Canada depuis 01/2023.

- 3) 2017-2020 Co-encadrement de la thèse de Mathilde Mercuzot (40%), inscrite à l'Université de Rennes ; cofi. 50-50 BRGM-Région Bretagne : « Reconstitutions paléoenvironnementales et paléoclimatiques en contexte tardi-orogénique: cas des bassins fini-carbonifères à permien du nord-est du Massif Central, France » ; directrice habilitée S. Bourquin, Géosciences Rennes, ED Ecole doctorale Sciences de la matière.

Situation actuelle : en post-doc à l'ENSEGID Bordeaux.

- 4) 2013-2016 Co-encadrement de la thèse de Julien Baptiste (30%), inscrit à l'Université d'Orléans ; cofi. 50-50 BRGM-Région Centre-Val-de-Loire : « Cartographie structurale et lithologique du substratum du Bassin parisien et sa place dans la chaîne varisque de l'Europe de l'Ouest. Approches combinées : géophysiques, pétrophysiques, géochronologiques et modélisations 2D » ; directeur habilité M. Faure, ISTOrléans, ED Energie, Matériaux, Sciences de la Terre et de l'Univers.

Situation actuelle : géologue au BRGM depuis 2017.

Participation à l'encadrement et suivi de thèses

- 5) 2019- Participation à l'encadrement de la thèse de Laurie Tchang Tchong (20%), inscrite à l'Université de Lorraine, Nancy, financement 100% projet DEEPSURF: « Les hydrocarbures comme marqueurs des transferts entre réservoirs profonds et zone critique : exemple du Fossé Rhéna » ; directeurs habilités R. Michels et P. Faure, ED Science et ingénierie des ressources naturelles.
- 6) 2013-2016 Participation à l'encadrement de la thèse de Jacques Dentzer (10%), inscrit à l'UPMC et à l'ENS Paris, cofi. Région IdF-Agence de l'Eau : « Forçages environnementaux et contrôles structuraux sur le régime thermique actuel du bassin de Paris - Enjeux pour la compréhension du potentiel géothermique en Île-de-France » ; directeur habilité D. Bruel, ED Géosciences, ressources naturelles et environnement.

Situation actuelle : aménagement du territoire, Ile-de-France.

- 7) 2014-2017 Co-encadrement de la thèse de Vincent Roche (20%), inscrit à l'Université d'Orléans ; cofi. BRGM-Labex Voltaire : « Du manteau au système géothermal de haute température : dynamique de subduction et anomalies thermiques en Méditerranée orientale » ; Directeurs habilités L. Jolivet, UPMC et L. Guillou-Frottier, BRGM, ED Energie, Matériaux, Sciences de la Terre et de l'Univers.

Situation actuelle : en post-doc à l'ISTEP Sorbonne Université.

Je suis aussi intervenu en appui ponctuel en tant qu'expert interprétation sismique/structuration du bassin de Paris dans les deux thèses suivantes (avec à chaque fois une publication en co-auteur à la clé):

- Pierre-Alexandre Reninger (2009-2012): « Méthodologie d'analyse de levés électromagnétiques aéroportés en domaine temporel pour la caractérisation géologique et hydrogéologique » ; encadrement BRGM/ISTOrléans, financement BRGM/Région Centre-Val-de-Loire.
- Fabien Lenoir (2009-2012): « Faciès, géométries et déformations du Jurassique du Sud-Ouest du bassin de Paris : un domaine faiblement subsident, transition avec le bassin d'Aquitaine » ; encadrement et financement Géosciences Rennes/BRGM.

1.3.2. Encadrements post-doctoral

- 1) 2021-2022 Co-encadrement à 50% du Post-Doc de Romain Hemelsdaël avec R. Michels (Géoressources Nancy), inscrit à L'université de Lorraine, Nancy ; cofi 50-50 BRGM-Université de Lorraine (projet DEEPSURF Nancy), sur la « Modélisation structurale 3D et l'évolution thermique du bassin Carbonifère-Permien sarro-lorrain ».

Situation actuelle : contrat IODP à Géoressources Nancy.

- 2) 2017-2018 Co-encadrement à 20% du Post-Doc de Céline Ducassou, inscrite à l'Université de Rennes, financement Univ. Rennes 100%, sur la « Datation U/Pb et la caractérisation du volcanisme à la limite Carbonifère-Permien dans le nord du Massif Central ».

Situation actuelle : Enseignante dans le secondaire (32).

1.3.3. Encadrements de stages de recherche de Master 2 et 3A ingénieur

Au BRGM

- 1) 2020 Nicolas Nguyen, Stage 3A ENSG, Nancy, « Caractérisation de la fracturation affectant les calcaires lutétiens d'une carrière souterraine et de ses alentours (Soissonais, bassin de Paris) ».
- 2) 2020 Axelle Pantiga, Stage 3A ENSG, Nancy, « Caractérisation à haute résolution des faciès, des architectures et de la diagenèse des calcaires lutétiens du soissonais ».
- 3) 2016 Charline Hue, Géosciences Rennes, « Reconstitution des environnements de dépôt du carbonifère supérieur/permien inférieur au sud du bassin de Paris ».
- 4) 2015 Marylou Vines, Dépt Sc. de la Terre, Université de Nantes, « Nouvelles données sur les cycles magmatiques paléozoïques post-varisque de la chaîne pyrénéenne ».
- 5) 2013 Maeva Berger, Géosciences Rennes, « Traitement, interprétation et modélisation de géophysique régionale (aéromagnétisme, gravimétrie, sismique pétrolière) pour la reconnaissance du substratum pré-mésozoïque dans le sud-ouest du bassin de Paris ».
- 6) 2012 Jérémy Bureau, Géosciences Rennes, « Sédimentologie et stratigraphie des dépôts permien du sud-ouest du bassin de Paris (France) ».
- 7) 2009 Gwénnolé Oliviero, EGID Bordeaux, « Potentiel géologique profond du Fossé Rhénan Supérieur, Interprétation sismique et schéma structural du nord du Fossé rhénan ».

A l'Institut de Géologie et de Paléontologie, Faculté des Géosciences et de l'Environnement, Université de Lausanne, Suisse.

- 8) 2006 Laurent Thum et Renato De Paoli, « Implications géodynamiques de l'étude pétrographique des flyschs du Crétacé supérieur du Piolit, du Pelat et de Baiardo (Alpes occidentales) ».
- 9) 2005 Pauline Renaud, Université de Lausanne, « Les unités infra-ophiolitiques de l'île de Lesbos, Grèce ».

1.3.4. Encadrements de stage de recherche de Master 1

- 10) 2014 Mathias Lebaudy, Géosciences Rennes, « Corrélations diagraphiques et sismiques dans les bassins permien du Sud-Ouest du bassin de Paris ».
- 11) 2011 Alexandre Houdu, Dépt Sc. de la Terre, Université de Nantes, « Les bassins permien sous couverture, exemple de la prolongation du bassin de Lodève-Graissessac ».

1.3.5. Encadrements de stage de recherche de L3

- 12) 2017 Eôle Paulin, Dépt. Géosc. & Envirt., Université de Tours, « Le bassin permocarbonifère d'Alès et ses prolongements sous couverture sédimentaire méso-cénozoïque ».
- 13) 2009 Alexis Nutz, EOSTrasbourg, « Interprétation du profil sismique régional EW03, Fossé rhénan ».

1.4. Projets de recherche

1.4.1. Au BRGM, projets en rapport direct avec les volets 2 et 3

Mes activités de recherche au BRGM sont le plus souvent financées par la Direction de la Recherche et la Direction des Géoressources dans laquelle je travaille.

Les projets au BRGM se répartissent entre projets de recherche s.s. (RP pour Recherche Publique), projets d'Appui aux Politiques Publiques (APP) et projets commerciaux (Com. France ou International, incluant la recherche partenariale). Quels qu'ils soient, ces projets nécessitent une compétence et une expertise scientifiques et peuvent amener à des communications à congrès et/ou publications scientifiques, même pour des projets « commerciaux » en fonction des clauses de confidentialité; dans tous les cas ils sont validés par un rapport final, vérifiés et approuvés en interne au BRGM avant diffusion (Système de Management de la Qualité, norme ISO9001, liste des rapports en section 1.2).

C'est tout l'intérêt du BRGM que d'être situé à l'interface entre les mondes académique et industriel : la diversité des projets est un atout indéniable car elle permet d'appliquer dans le cadre de projets plus opérationnels et/ou appliqués (risque naturel, hydrogéologie, géothermie, ou projets commerciaux à l'International) les connaissances plus fondamentales acquises par ailleurs. Ces activités se nourrissent l'une de l'autre et sont intimement liées, mon parcours aurait été bien différent sans mes expériences autres que purement scientifiques.

Un projet est piloté par un Chef de projet (CdP ; au sens BRGM) qui est garant du montage budgétaire et administratif, de la coordination des agents constituant l'équipe projet, de la gestion des budgets, des délais et des livrables internes ou externes. Le montant géré et le nombre de personnes composant l'équipe projet est indiqué pour les projets pour lesquels j'étais [CdP].

En dehors des projets de thèse et de post-doc (dont l'accompagnement est considéré comme un projet à part entière au BRGM, voir section 1.3), mes activités de recherche ont été financées par les projets suivants, classés selon les volets 2 et 3 (pour les projets non financés à 100 % par le BRGM, les commanditaires/clients sont soulignés) :

Volet 2 - Les bassins carbonifères-permiens sous couverture sédimentaire méso-cénozoïque

2017-	Projet ICDP Deepdust, Co-PI pour la cible Europe de l'ouest (RP).
2021	Projet Fonts-Bouillants - <u>45-8 Energie</u> , caractérisation des réservoirs d'He dans le sud du bassin de Paris (Com. France) / expert bassins sédimentaires, interprétation sismique.
2020	Projet Incrémental DGR « bassins carbonifères-permiens » (RP) / [CdP] + expert bassins sédimentaires / budget 30 k€ / équipe projet : 3 personnes.
2015-2017	Projet LogIso (APP), synthèse forages et sismique du bassin de Paris / expert bassins sédimentaires, interprétation sismique.

- 2014 Projet IRSN, identification des géométries des séries sédimentaires carbonifères et permienues dans l'est de la France (Com. France) / [CdP] + géologue expert, interprétation sismique / budget 26 k€ / équipe projet : 2 personnes.
- 2014 Expertise CLIS Bure, évaluation de la ressource géothermale dans le Trias et l'anté Trias dans la région de Bure (Com. France) / géologue expert.
- 2009-2010 Projet ANDRA Socle (Com. France), caractérisation du substratum anté-mésozoïque du bassin de Paris / [CdP] + expert bassins sédimentaires, cartographie structurale / budget 120 k€ / équipe projet : 8 personnes.

Volet 3 - L'interprétation sismique au service des nouveaux usages du sous-sol : exemples du bassin de Paris et du fossé Rhénan

Bassin de Paris

- 2019-2023 RGF bassin de Paris (RP), responsable de la tâche « structuration ».
- 2012-2014 LogIso (APP), synthèse forages et sismique du bassin de Paris / expert bassins sédimentaires.
- 2007-2008 Projet ANDRA BP (Com. France), cartographie structurale de subsurface dans le bassin de Paris / [CdP] + expert bassins sédimentaires / budget 200 k€ / équipe projet : 7 personnes.
- 2007 Non Exclusive bassin de Paris (APP + Com. France) / expert bassins sédimentaires, interprétation sismique de 14 transects régionaux soit 2500 km.

Fossé Rhénan

- 2016 Métrocène (RP), synthèse des bassins tertiaires en France.
- 2014 Non Exclusive Alsace (Com. France) / expert bassins sédimentaires, interprétation sismique de 26 transects régionaux soit 840 km.
- 2013-2014 RGF Vosges-Fossé rhénan (RP) / expert bassins sédimentaires, interprétation sismique, cartographie structurale.
- 2008-2013 GeORG (Europe - programme Interreg), Potentiel géologique profond du Fossé rhénan supérieur / Géologue référent pour la France et responsable du volet interprétation sismique (supervision de 7 collègues français, allemands et suisses); expert bassins sédimentaires et cartographie structurale.

1.4.2. Au BRGM, projets à finalité appliquée

Mes axes de recherche développés au BRGM se sont nourris de projets à finalité appliquée en dehors des champs thématiques des volets 2 et 3. Mon intervention était alors liée à mon expertise de géologue des bassins sédimentaires - que ce soit sur le terrain ou en interprétation sismique - en géologie structurale en domaine cassant, ou tout simplement en tant que géologue généraliste. Ces projets sont listés ci-après, par finalité (pour les projets non financés à 100% par le BRGM, les commanditaires/clients sont soulignés ; ces derniers ne sont pas cités si la confidentialité l'exige) :

Ressource en eau

- 2021-2023 Projet Hydro Alpilles, Parc Régional des Alpilles (APP) / cartographie géologique en domaine sédimentaire structuré, caractérisation de la fracturation, coupes géologiques.
- 2016-2019 Projet Anafore, Collectivités territoriales et agence de l'eau (APP) / cartographie géologique en domaine de socle altéré, caractérisation des réservoirs fracturés.

Ressources minérales

- 2022-2023 Numérisation de l'Inventaire minier France / [CdP] + géologue expert/ budget 60 k€ / équipe projet : 5 personnes.
- 2018 Inventaire Minier Tchad, Ministère des Mines du Tchad (projet porté par la Dir. Intern.) / reconnaissance géologique en terrains magmatiques et métamorphiques.

Risques naturels

- 2020-2022 Gestion du risque gypse, Bargemon ; collectivités territoriales (APP) / cartographie géologique en domaine sédimentaire structuré, coupes géologiques, interprétation géophysique proche surface.
- 2014-2015 FLOOD Arabie, Ministère des Mines de l'Eau du Royaume d'Arabie Saoudite (projet porté par la Dir. Intern.) / reconnaissance géologique en terrains magmatiques et métamorphiques (granulats pour barrages).

Géothermie

- 2015-2018 FONGEOSEC, Fonroche Géothermie (RP partenariale), projet géothermique Béarn / synthèse géologique, interprétation sismique et structurale.

Stockage souterrain

- 2010-2011 Stockage en cavités salines (Com. France) / [CdP] + géologue expert/ budget 150 k€ / équipe projet : 7 personnes.
- 2017 FluidStory-stockage d'énergie (ANR) / inventaire du potentiel français de stockage en cavités salines.
- 2016 ESTMAP (Financement Commission Européenne) / inventaire du potentiel européen de stockage en subsurface.
- 2021 Stockage en cavités salines (RP partenariale) / synthèse géologique, interprétation sismique.

Hydrocarbures

- 2010 Mauritanie (projet porté par la Dir. Intern.) / cartographie géologique.

1.4.3. A l'Université de Lausanne

2003-2006 Post-doc sur l'exhumation des dômes métamorphiques tertiaires en Turquie du NO, comparaison avec le Rhodope (Bulgarie).

Financement 7.5 kCHF par le fond du 450^{ème} anniversaire de l'Université de Lausanne et la Société Académique Vaudoise.

1.4.4. Projets INSU financés en collaborations avec les partenaires académiques

J'ai participé dans le cadre de mes collaborations avec les collègues universitaires à la réalisation des projets INSU gagnés suivants :

2020 Projet INSU/SYSTER « Datation U-Pb CA-ID-TIMS de zircons et téphrostratigraphie des séries fini-Carbonifère – Permien du nord du Massif Central (porteur S. Bourquin, 5 k€).

2019 Projet INSU/CESUR « Caractérisation des aquifères géothermaux du front nord varisque en région Hauts-de-France (porteur F. Graveleau, 3.5 k€).

2018 Projet INSU/SYSTER « Apports de la Géochimie à la reconstitution du signal climatique des bassins Carbonifère - Permien du Massif Central » (porteur A.C. Pierson-Wickmann, 6 k€).

2016 Projet INSU/SYSTER sur « les bassins permien nord Massif Central » (porteur S. Bourquin, 5 k€).

2015 Projet INSU/SYSTER sur la « délamination lithosphérique tardi-orogénique comme marqueur de l'effondrement de la chaîne varisque » (porteur O. Averbuch, 10 k€).

1.4.5. Missions scientifiques

Cette section liste les missions scientifiques effectuées depuis que je suis au BRGM et lors de mon passage à l'Université de Lausanne (hors activités pédagogiques et sans compter les nombreuses excursions de 1 ou 2 jours lors de divers projets français ou internationaux).

Au BRGM (depuis 2007)

06-2021 Mission de terrain dans les bassins de Lodève et Saint-Affrique (5 j.) : datation des cinérites / collaboration avec S. Bourquin, M. Poujol, M. Lopez, M. Mercuzot, O. Bruguier.

02/2021 Campagne de terrain dans les Alpilles (5 j.) : géologie structurale / projet Hydro Alpilles, CdP BRGM M. Moulin.

03/2020 Campagne de terrain dans le Var : étude du Trias (5 j.) / Projet Risque gypse Bargemon, CdP BRGM N. Marçot.

11/2018 Campagne de terrain au Tchad (1 m.) : reconnaissance géologique / Projet Tchad Ressources Minérales, CdP BRGM O. Rouzeau.

- 2018 Mission dans le bassin d'Autun pour l'étude du Permien (3 j.) / collaboration avec G. Gand, S. Bourquin, P. Pellenard, C. Thomazo, P. Sans-Jofre, F. Fluteau dans le cadre de la thèse de M. Mercuzot.
- 2018 Mission dans le Morvan pour la datation des roches éruptives permiennees du secteur de Montreuillon (3 j.) / collaboration avec G. Gand, M. Durand, S. Bourquin, P. Pellenard, dans le cadre du post-doctorat de C. Ducassou.
- 07-08/2017 Campagnes de terrain en Bretagne (3 sem.) : caractérisation de la fracturation des aquifères de socle / Projet Anafore, CdP BRGM M. Schroetter.
- 03/2017 Mission dans le bassin de l'Aumance (3 j.) : étude des séries stéphano-permiennes / collaboration avec S. Bourquin, P. Pellenard, A.C. Pierson-Wickman, C. Ducassou, P. Debriette dans le cadre de la thèse de M. Mercuzot.
- 02/2017 Mission à la carothèque Total à Boussens (3 j.) / échantillonnage, projet FONGEOSEC.
- 07-08/2016 Campagnes de terrain en Bretagne (3 sem.) : caractérisation de la fracturation des aquifères de socle / Projet Anafore, CdP BRGM M. Schroetter.
- 02/2014 Mission à la carothèque Total à Boussens (3.) / échantillonnage, dans le cadre de la thèse de J. Baptiste.
- 03/2014 Campagne de terrain en Arabie Saoudite (1 m.) : prospection et échantillonnage pour caractérisation des granulats / projet FLOOD, CdP BRGM F. Prognon.
- 07/2011 Programme de cartographie géologique de la France au 1/50000, feuille de Vitry (1 m.).
- 02/2010 Campagne de terrain en Mauritanie (1 m.) : exploration géologique en domaine sédimentaire / projet Total, CdP BRGM Y. Callec.

A l'Université de Lausanne

- 08/2006 Campagne de terrain dans les Hautes-Alpes (5 j.) : étude des flyschs créacés supérieur / Encadrement Diplôme (M2) L. Thum et R. De Paoli / collaboration avec G.M. Stampfli, O. Ferrari.
- 09/2005 Post-Doc - Campagne de terrain dans la Péninsule de Biga, Turquie du NO (2 sem.) : dômes métamorphiques syn- à post-orogéniques / collaboration avec N. Bonev.
- 10/2004 Post-Doc - Campagne de terrain dans la Péninsule de Biga, Turquie du NO (3 sem.) : dômes métamorphiques syn- à post-orogéniques / collaboration avec N. Bonev.
- 09/2004 Reconnaissance de terrain sur l'île de Lesbos (Grèce) dans les séries infra-ophiolitiques (1 sem.) / Encadrement diplôme P. Renaud / collaboration avec G.M. Stampfli.

02/2002 Excursion dans le Péloponnèse et l'Île de Tinos (1 sem.) : déformation ductile-cassante dans les core-complexes / collaboration avec L. Jolivet.

1999-2003 Thèse - 6 campagnes de terrain (6 m.) dans le Péninsule de Biga, Turquie du NO.

1.4.6. Activités synergétiques - Valorisation de la recherche

2018-Actuel Vice-Président de l'Association des Géologues du Permien et du Trias.

Affiliations professionnelles : Membre de la Société Géologique de France, de l'EGU, de la Société Géologique du Nord, du Groupe Français du Paléozoïque.

2011-13-21 Animateur scientifique à la Fête de la Science au BRGM.

2000 Stand "Géologie et tectonique des plaques", festival Science et Cité, Lausanne.

1.4.7. Collaborations scientifiques

(Hors collaborations internes au BRGM avec les collègues géophysiciens, géothermiciens, ingénieurs risques naturels, hydrogéologues, modélisateurs 3D...).

- Olivier Averbuch (MCF LOG Lille)
- Jocelyn Barbarand (Pr. GEOPS Paris-Saclay)
- Sylvie Bourquin (DR Géosciences Rennes)
- Olivier Bruguier (IR Géosciences Montpellier)
- Nicolas Espurt (MCF Géoazur Nice)
- Aude Gébelin, (Pr. Géoressources Nancy)
- Fabien Graveleau (MCF LOG Lille)
- Olivier Kaufman (Pr. Univ. Mons, Belgique)
- Michel Lopez (Pr. Emér. Géosciences Montpellier)
- Raymond Michels (CR Géoressources Nancy)
- Yves Missenard (MCF GEOPS Paris-Saclay)
- Pierre Pellenard (MCF Biogéosciences Dijon)
- Philippe Robion (MCF GE Cergy)
- Lynn Soreghan (Pr. Univ. Oklahoma, USA) + les PIs et Co-PIs de l'équipe DeepDust

Activités de recherche

Introduction - Déroulement de mes activités de recherche

Mon profil de chercheur s'est constitué en suivant le cheminement intellectuel et chronologique suivant.

1994-1998 - Géologie des bassins, géométrie et caractérisation des réservoirs silicoclastiques

Après l'obtention de mon bac scientifique C en 1992 j'ai tout naturellement poursuivi mes études en DEUG Maths-Physique-Chimie à l'Université Montpellier II. Passionné depuis l'enfance par l'astronomie et les planètes, je me suis mis en tête de bifurquer vers une Licence puis une Maîtrise de Sciences de la Terre. Le Pr. Adolphe Nicolas intervenait à l'époque en DEUG A dans l'option Sciences de la Terre ; il m'a encouragé dans ma démarche, non sans me donner du travail pour l'été à venir : ingurgiter « Géologie : objets et méthodes » et « Comprendre et enseigner la Planète Terre » afin de rattraper par la lecture mes lacunes. Ma Maîtrise, sous la direction de Gilles Merzeraud, avait pour sujet de recherche les séries triasiques du Pas de l'Escalette, comme analogues aux réservoirs de gaz hettangiens en Sologne. J'ai ensuite poursuivi en DEA avec Gilles, toujours en partenariat avec GDF, sur la caractérisation sédimentologique, minéralogique et géochimique et la stratigraphie génétique des réservoirs triasiques du site de stockage souterrain de Villefranche-sur-Cher.

1999-2006 - Mélanges et ophiolites téthysiens, transition syn- à post-orogénique dans le domaine égéen

Après l'obtention de mon DEA, j'ai poursuivi avec une thèse de doctorat à la Faculté des Sciences de l'Université de Lausanne (Suisse) sous la direction du Pr. G.M. Stampfli. Le projet portait sur l'étude des mélanges ophiolitiques et des ophiolites de la Péninsule de Biga dans le NO de la Turquie. L'objectif final consistait à proposer un scénario paléogéographique et paléotectonique pour l'histoire géodynamique régionale de ces objets géologiques complexes. J'ai cartographié ces objets alors mal connus (6 mois passés sur le terrain) et échantillonné pour réaliser des datations micropaléontologiques et radiochronologiques et caractériser le magmatisme omniprésent (5 mois au laboratoire, du DRX à l'attaque des radiolarites à l'HF et l'extraction des ostracodes à l'acide formique, en passant par la séparation des zircons de granodiorites et la géochimie des roches basiques). Ces quatre années passées en grande autonomie (durée d'une thèse en Suisse) ont confirmé mon goût pour la recherche et pour la géologie de terrain ; j'ai aimé l'aspect pluridisciplinaire, très formateur, qui s'est avéré essentiel pour la suite de mon parcours. Deux publications sont issues de ce travail, montrant que les domaines océaniques à l'origine de ces sutures étaient déconnectés de ceux connus en Turquie, et plutôt en lien avec ceux connus en Bulgarie ou en Grèce.

Suite à mes travaux de thèse G. M. Stampfli m'a proposé d'être son Premier Assistant à l'été 2003 (contrat de cinq ans), avec carte blanche sur mon projet de recherche. Il est apparu pendant ma thèse que les séries ophiolitiques investiguées reposaient structurellement sur des séries métamorphiques exhumées à l'Oligo-Miocène (« metamorphic core-complexes »). Cédant une fois de plus à l'attrait de la nouveauté, j'ai monté un projet d'étude de ces séries déformées en domaine fragile-ductile, sur la base d'une approche structurale multi-échelle classique (du terrain à la lame mince), complétée d'analyses de pétrographie métamorphique et radiochronologiques. Avec, à la

clé, une mise à jour complète de la compréhension de l'évolution du NO de la Turquie dans le contexte de la transition syn-orogénique à post-orogénique dans le domaine égéen. Et aussi la certitude que la curiosité et le goût de la nouveauté pouvaient compenser un déficit initial de connaissance. Ces travaux ont fait l'objet de cinq publications, montrant que la Péninsule de Biga enregistre toute l'histoire géodynamique égéenne depuis le Crétacé terminal jusqu'à l'actuel. Ces années lausannoises ont également été l'occasion de faire mes premiers pas d'encadrant de travaux de recherche, pour des stages de Master 2 ou en appui direct à plusieurs thésards de G.M. Stampfli. Mon histoire suisse-turque s'est conclue par la publication d'un article de référence qui résume à lui seul mes huit années à Lausanne, proposant une nouvelle classification des terranes en Turquie et ses implications paléotectoniques à l'échelle du domaine téthysien occidental (*Moix, Beccaletto et al., 2008 ; cf. annexe 1). Il est suivi en annexe 2 d'une publication caractéristique de mes travaux sur la géodynamique cénozoïque égéenne (*Beccaletto et Steiner, 2005), traitant de l'exhumation du dôme métamorphique du Kasdag et la formation du bassin supra-détachement associé, incluant une discussion sur les rôles respectifs de « l'orogenic collapse » et du « slab roll-back » comme éléments déclencheur de l'extension égéenne¹.

2007-présent - Bassins carbonifères-permiens, transition syn- à post-orogénique varisque, couverture méso-cénozoïque, et usages du sous-sols

Anticipant la fin de mon contrat à Lausanne, j'ai postulé au BRGM que j'ai rejoint en janvier 2007 au sein de l'équipe Géologie des Bassins Sédimentaires. Géologue des bassins ayant touché à de nombreuses disciplines des Géosciences, quoi de plus logique que de travailler au Service Géologique National. Le BRGM permet d'aborder des sujets appliqués (hydrogéologie, géothermie, stockages, risques naturels) tout en donnant l'occasion à qui la saisit de poursuivre une carrière orientée recherche. Une nouvelle vie scientifique a alors commencé, faites de profils sismiques, de forages, et toujours de terrain en France ou à l'International. Après huit ans d'exil en Suisse et le regard tourné vers le « monde téthysien », j'étais de retour en plein cœur de la géologie métropolitaine ; il ne m'a fallu que quelques mois pour comprendre que la connaissance géologique de notre territoire restait de manière générale encore bien parcellaire, loin de mes souvenirs d'étudiant.

Mes quatre premières années au BRGM ont été décisives pour l'orientation de mon parcours de chercheur. Pendant cette période, je me suis retrouvé au gré des projets (et à ma grande satisfaction) à interpréter plusieurs milliers de kilomètres de profils sismiques dans le bassin de Paris et dans la région Centre-Val-de-Loire. En parallèle je menais des projets avec l'agence nationale pour la gestion des déchets radioactifs (ANDRA) sur la structuration de ce même bassin depuis le Trias, et la nature de son « socle », avec à la clé une mise à jour du schéma structural grande maille, schéma toujours utilisé aujourd'hui au BRGM. Cette période m'a aussi permis d'interpréter 1500 km de profils sismiques dans le fossé Rhéan (projet européen Interreg GeORG) tout en supervisant l'interprétation de 3500 km de sismique du côté allemand du fossé ; avec à la clé un nouveau modèle structural du fossé, encore utilisé aujourd'hui en interne et en externe dans de nombreux projets de recherche à vocation géothermique.

¹ Note bibliographique: la bibliographie précédée d'un * correspond aux publications écrites ou co-écrites (hors rapports BRGM), la bibliographie précédée de ** aux publications co-écrites avec des étudiants co-encadrés ou pour lesquels je suis venu en appui expertise sismique/structuration.

La sismique réflexion industrielle tirée dans les bassins français enregistre généralement toute la pile sédimentaire depuis les bassins carbonifères et permians jusqu'aux dépôts cénozoïques en passant par la couverture mésozoïque. J'ai donc eu tout le loisir de parcourir la pile sédimentaire fini-paléozoïque/mésozoïque. Cependant très vite le « 300 Ma » m'a attiré : la transition syn- à post-orogénique varisque et son enregistrement dans les bassins sédimentaires. Les derniers travaux d'ampleurs sur les bassins houillers dataient des années 1980 (synthèses BRGM et fin du charbon en France) ; ces travaux caractérisaient les bassins aussi bien à l'affleurement qu'en subsurface, dans ce dernier cas sur la base de données sismiques antérieures à celles disponibles aujourd'hui. Beaucoup restait donc à faire et je me suis attelé, bassin après bassin, à remettre à jour leur connaissance, soit dans le cadre de projets internes au BRGM, soit le plus souvent dans le cadre de collaborations académiques prenant la forme de travaux de thèse ou de post-doc, dont les résultats sont présentés plus loin dans ce manuscrit. Le tout sans jamais perdre de vue les potentielles applications industrielles, parce je travaille au BRGM - et que derrière chaque projet de recherche, même le plus fondamental, se trouve en germe une application.

Un peu de recul

Je résumerais ainsi ces vingt dernières années. Ma période lausannoise m'a permis de me familiariser avec les concepts de transition syn- à post-orogénique, sur la base d'études de terrain - complétées par un large volet analytique - au cours desquelles j'ai croisé divers objets caractéristiques de ces contextes (bassins sédimentaires supra-détachement et roches métamorphiques déformées sous-jacentes, et leurs relations structurales). Une fois au BRGM, j'ai transposé ce bagage au cas d'étude de la chaîne varisque sur le territoire métropolitain, travaillant désormais principalement à partir des données de subsurface, indépassables pour littéralement voir comment s'enregistre dans les bassins sédimentaires la fin de cette orogène.

Quels points communs entre ces diverses expériences scientifiques ? Hors un goût prononcé pour la nouveauté, l'envie de comprendre le fonctionnement du système Terre, et la curiosité inhérente à nos parcours et nos métiers, je pense pouvoir dégager les quatre points cardinaux ayant guidé ma carrière scientifique jusqu'à aujourd'hui, et sans doute à l'avenir ; du particulier au général :

- L'étude des bassins sédimentaires, témoins par leur contenu et leur déformation des événements tectoniques near- et far-field.
- La déformation des roches, donc, à toutes les échelles, de la lame mince à la plaque tectonique, du ductile au cassant. La plupart de mes projets ont été ou sont liés à cette thématique.
- L'intérêt pour les sauts d'échelles spatiales, les échelles variables de temps et d'espace, l'influence d'une action à une échelle sur une échelle d'ordre différent.
- Le plaisir de raconter une histoire géologique, la succession des événements, et partant de là, la notion de temps géologique. Je suis venu à la géologie par goût pour l'astronomie et autant que je me souviens tout ce qui touchait au *temps* avait ma préférence.

2. Volet 1 - Le destockage, le retraitement et l'interprétation de profils de sismique réflexion

Préambule aux volets 2 et 3

Exemple du bassin de Paris

Tous les profils de sismique profonde que j'ai interprétés au BRGM ont été acquis à une époque antérieure aux différents projets sur lesquels j'ai travaillé; il a donc fallu récupérer les données sismiques brutes avant de les retraiter avec des méthodes actualisées pour ensuite les interpréter. Ces étapes, pilotées depuis plusieurs années au BRGM par Stéphane Marc et Laure Capar, sont primordiales pour mes travaux de recherche et méritent donc d'être exposées ici. Cette section donne aussi l'occasion au lecteur de se familiariser si nécessaire avec les profils de sismique réflexion, base de mes travaux exposés dans les volets 2 et 3.

2.1. La sismique réflexion

La sismique réflexion est une méthode géophysique non destructrice de prospection du sous-sol fournissant des images continues de ce dernier en 2D ou 3D, de quelques dizaines de mètres jusqu'à plusieurs dizaines de kilomètres en profondeur.

Cette technique est basée sur les lois physiques de propagation des ondes sismiques générées à la surface du sol - généralement par un camion vibreur (« Vibroseis ») ou à l'aide d'explosifs - dans la croûte terrestre, et de leur réflexion sur les discontinuités du sous-sol. Les ondes réfléchies sont enregistrées à la surface par une série de géophones. Les discontinuités correspondent à des interfaces entre deux couches géologiques d'impédances acoustiques différentes, généralement la base ou le sommet des couches sédimentaires - l'impédance acoustique Z correspond au produit de la densité (ρ) et de la vitesse de propagation (V) des ondes sismiques dans la roche ($Z=\rho*V$). L'impédance acoustique est influencée par plusieurs facteurs (cf. section 5.1), notamment la lithologie, la porosité, la perméabilité, la cimentation, le type de fluide présent dans les pores ou encore la pression lithostatique de la roche. Les variations d'amplitude des réflecteurs représentent les variations d'impédance plus ou moins fortes entre les différentes couches. La profondeur est

généralement exprimée en temps double (Two-Way-Travel Time ou TWT), c'est-à-dire le temps mis par l'onde sismique pour atteindre la discontinuité et revenir à la surface.

2.2. Déstockage des données sismiques brutes

En France, les données de sismique réflexion proviennent principalement des opérateurs pétroliers, qui ont acquis de nombreuses données depuis les années 1950 sur leurs titres miniers. D'après le Code minier français, une copie des données sismiques brutes est transmise à l'Administration française. Elles tombent dans le domaine public après un période de 10 ans. Quant aux données traitées (ou retraitées) elles appartiennent à vie à l'entité qui a financé le (re)traitement. La première étape d'un projet sismique est de récupérer ces données sismiques brutes ; c'est la phase de déstockage.

Les données sismiques brutes comprennent (i) le signal sismique (tir sismique) enregistré sur des supports analogiques ou magnétiques, (ii) des informations sur les paramètres d'enregistrement et du déploiement du dispositif d'acquisition (rapport d'enregistrement), (iii) les coordonnées des positions de tous les récepteurs (géophones) et de toutes les sources d'ondes (ou sources sismiques), issues de chutes de poids, de camions vibrateurs ou d'explosifs.

À leur réception, un premier travail de contrôle sur les données brutes est effectué afin de vérifier si les informations nécessaires sont cohérentes et complètes. Ensuite, les données de sismique réflexion sont envoyées au centre de traitement pour effectuer un retraitement sismique supervisé par le BRGM.

2.3. Séquence de traitement

La séquence et les paramètres de traitement sont choisis en fonction de l'objectif final du projet. La séquence de traitement comporte généralement quatre grandes phases, décomposées en de nombreuses étapes:

- Positionnement des sources sismiques et des récepteurs avec leurs coordonnées (« mise à jour de la géométrie »).
- Edition/atténuation des traces invalides et/ou bruitées pour garder les traces et les signaux sismiques valides.
- Correction du signal sismique pour compenser des effets de la topographie et des variations des vitesses de propagation des ondes sismiques dans la proche surface.
- Remise à leur place réelle des objets géologiques (« migration ») et addition des traces pour former l'image finale. Si la migration se fait après la sommation des traces, on parle de Post Stack Trace Migration ; si elle se fait avant, on parle de Pre Stack Time Migration (PSTM) ; cette dernière méthode a l'avantage de mieux imager la structure du sous-sol et est désormais systématiquement utilisée au BRGM (Figure 1).

SÉQUENCE DE TRAITEMENT	
1.	Corrélation des tirs sismiques
2.	Mise à jour de la géométrie
3.	Éditions ou atténuation des traces bruitées et/ou invalides
4.	Pointé des premières arrivées
5.	Compensation de la divergence sphérique
6.	Analyse de vitesses
7.	Déconvolution
8.	Corrections statiques grandes longueurs d'onde
9.	2 itérations d'analyse de vitesses
10.	2 itérations de corrections statiques résiduelles
11.	Atténuation des multiples
12.	Interpolation et régularisation des traces
13.	Analyse de vitesses en position migrée
14.	Migration en temps des traces individuelles (PSTM)
15.	Compensation des anomalies d'amplitudes résiduelles
16.	Addition des traces (Stack)
17.	Filtre variant en temps
18.	Contrôle automatique des amplitudes

Figure 1 - Exemple de séquence de traitement PSTM simplifiée (Source BRGM).

Les retraitements avec des algorithmes modernes donnent une image améliorée du sous-sol par rapport aux images issues des traitements originaux : en particulier concernant la définition et la continuité des réflecteurs, et l'identification des failles et des zones faillées.

2.4. Les lignes retraitées au BRGM

Plus de 372000 km de données sismiques brutes (onshore et offshore) sont tombés dans le domaine public en France métropolitaine. 1150 lignes sismiques représentant plus de 35000 km ont été retraitées au BRGM depuis le début des années 2000, pour un coût total de plusieurs millions d'euros. En vertu du code minier, ces lignes retraitées appartiennent au BRGM, qui les utilise à sa guise. Parmi ces lignes, j'ai eu l'occasion d'interpréter 612 lignes correspondant à une longueur de près de 10000 km (lignes sismiques en bleu foncé sur la Figure 2), principalement dans le bassin de Paris dans le fossé Rhénan.

Ces profils sismiques sont la matière de mon travail, sans elles pas de rampe latérale du chevauchement frontal nord-varisque (section 3.4), pas d'inversion tectonique négative en Lorraine (section 3.5), pas de structures en fleurs négatives dans le fossé Rhénan (section 4.2).

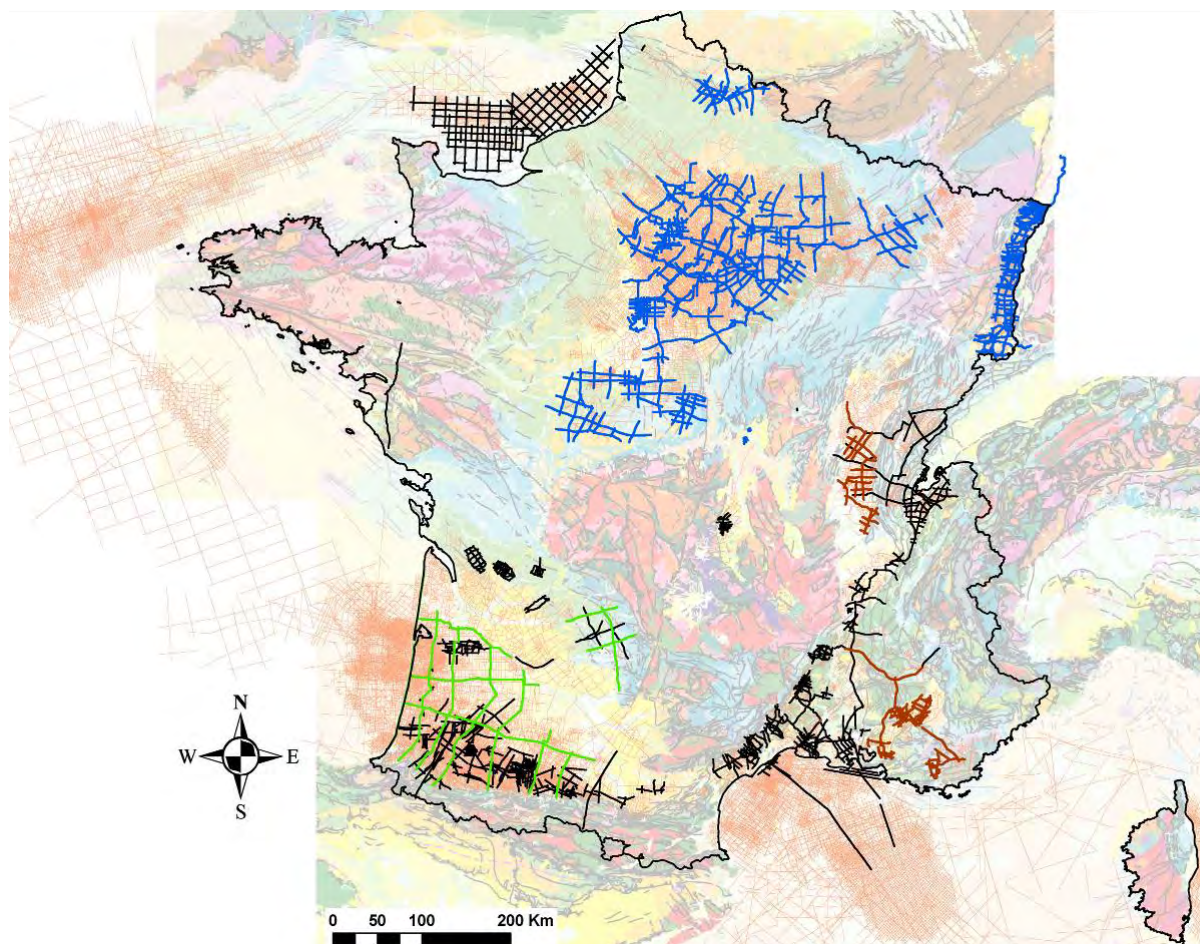


Figure 2 - Profils sismiques interprétés par moi-même ou interprétation suivie dans le cadre de projets à forte implication (en bleu foncé) ; profils co-interprétés en appui expertise à l'interprétation (en marron foncé) ; profils consultés lors de synthèses géologiques (en vert). En noir profils retraités disponibles au BRGM ; en rosé, profils industriels acquis en France métropolitaine. En fond carte géologique de la France au 1 :1000000^{ème} (BRGM, 2003).

2.5. L'interprétation sismique

L'interprétation des profils sismiques consiste (i) à repérer et suivre les réflecteurs sismiques correspondant aux marqueurs géologiques ciblés (les horizons sismiques), et (ii) identifier et pointer les structures géologiques qui affectent les horizons sismiques. Au BRGM les interprétations sismiques sont menées dans la suite logicielle Gverse GeoGraphix®.

Les structures géologiques recherchées sont des failles, des réseaux de failles (e.g. structures en fleurs, réseau de failles normales), des flexures anticlinales ou synclinales, etc...

L'interprétation sismique onshore utilise généralement de forages à proximité des lignes sismiques pour reporter tel marqueur géologique sur le profil sismique au droit du forage. Plusieurs milliers de forages existent ainsi sur le territoire métropolitain (Figure 3). Arrêtons-nous un instant sur le processus de calage au forage (« well-tie »). Pour ce faire, il est utile de disposer d'une loi de vitesse (ou checkshot) le long du forage, qui permet de convertir en temps double les cotes des marqueurs géologiques en mètres. Si un forage n'a pas de loi de vitesse, les logiciels d'interprétation utilisent généralement les lois de vitesses de forages à proximité ; il est aussi possible de créer pour un forage sa propre loi de vitesse.

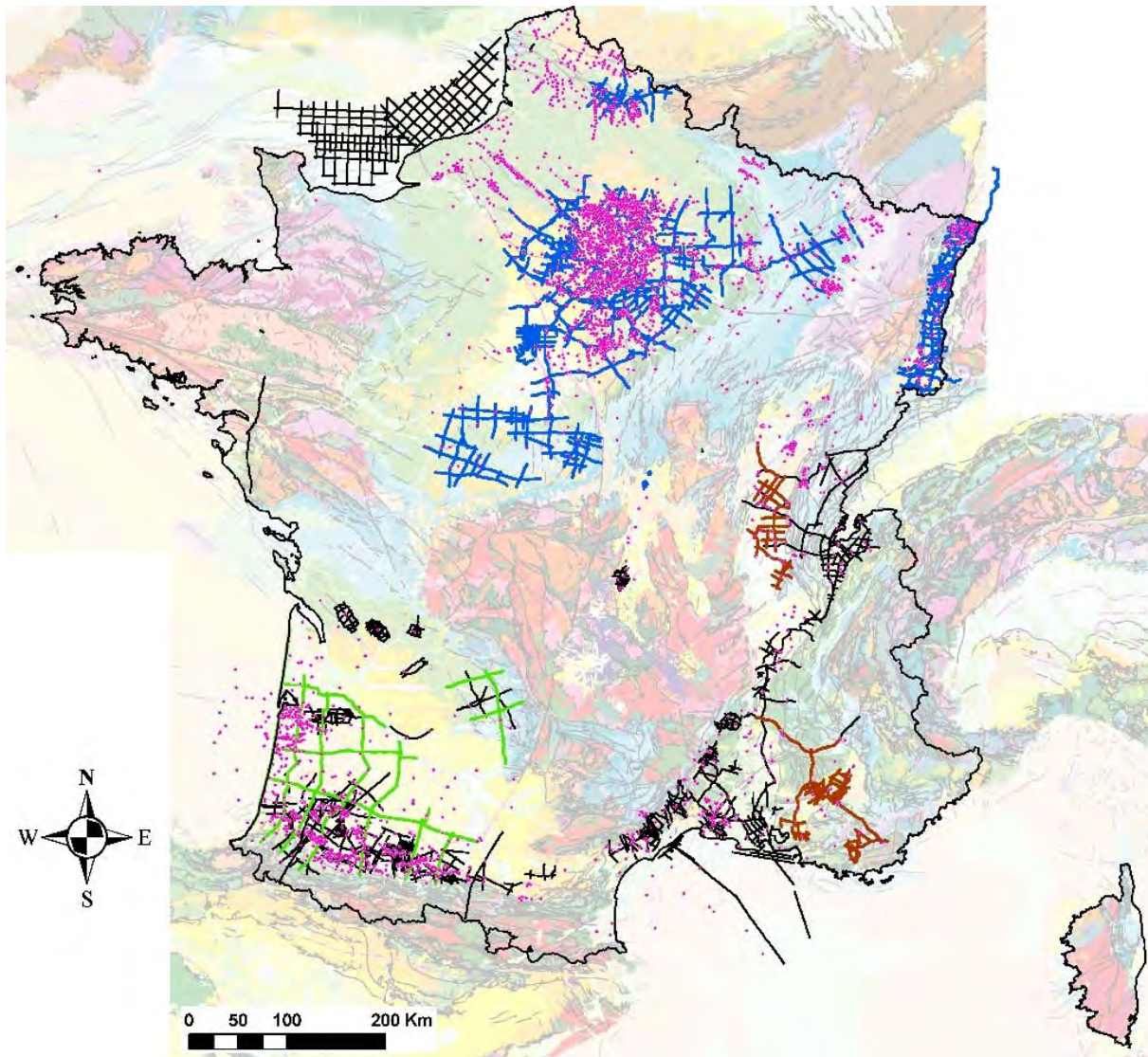


Figure 3 - Même carte et légende que la Figure 2 ; en violet, les forages profonds d'exploration-production d'hydrocarbures en France métropolitaine (source <http://www.mineries.fr>).

Idéalement, l'utilisation d'un sismogramme synthétique permet d'améliorer le calage des marqueurs géologiques d'un forage donné sur un profil sismique. En effet un film synthétique est défini comme la trace sismique théorique correspondant aux variations d'impédance acoustique au sein des différentes couches du sous-sol le long d'un puits donné. Différentes données d'entrée sont nécessaires afin de produire un sismogramme synthétique :

- Une loi temps-profondeur associée au puits. Elle est généralement disponible à partir de données de carottages sismiques (checkshots ou VSP). La loi temps-profondeur peut également être générée par l'intégration d'un log de vitesse (Sonic), moyennant une erreur (dérive) augmentant avec la profondeur.
- Une diagraphie de vitesse (Sonic).
- Une diagraphie de densité (RHOB).
- Une ondelette sismique, définissant les variations d'amplitude du sismogramme synthétique et représentant au mieux le signal sismique. Cette ondelette peut être théorique ou extraite à partir des données sismiques autour du puits.

Un sismogramme synthétique est généré selon les étapes suivantes. Dans un premier temps, l'échelle verticale des diagraphies de vitesse et de densité du forage est convertie en temps grâce à la loi temps-profondeur. Dans un second temps, l'impédance acoustique ($Z=\rho*V$) est calculée le long du forage à partir des logs de vitesse (V) et de densité (ρ). Le coefficient de réflexion RC , défini par la formule $RC=(Z_2-Z_1)/(Z_1+Z_2)$, est ensuite calculé. Il permet d'évaluer le contraste d'impédance acoustique entre deux couches 1 et 2, à l'origine de l'amplitude plus ou moins forte des réflecteurs. Enfin, le sismogramme synthétique est généré par convolution du coefficient de réflexion et de l'ondelette sismique.

Une fois le sismogramme synthétique créé, le profil sismique peut être calé au puits (Figure 4). Ce calage est réalisé en déplaçant, en étirant, ou en resserrant verticalement l'entièreté ou plusieurs intervalles du sismogramme synthétique, afin de correspondre à la trace sismique le long du puits. A l'issu du calage au puits, une nouvelle loi temps-profondeur associée au puits est générée.

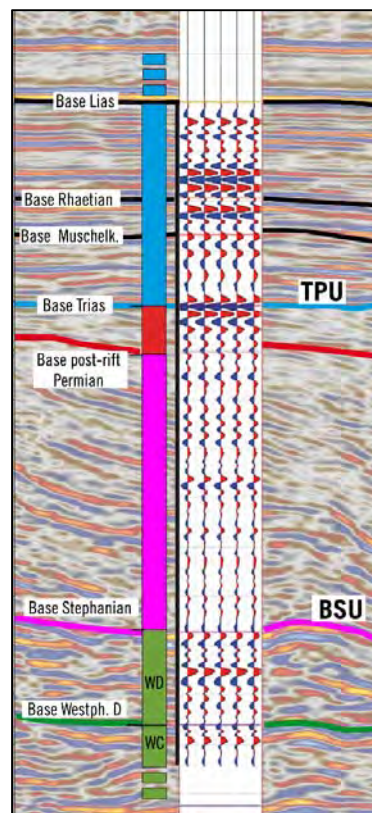


Figure 4 - Exemple de calage de la sismique au forage par l'intermédiaire d'un sismogramme synthétique (bassin sarro-lorrain) ; en noir, bleu, rouge, rose et vert : horizons sismiques.

Un dernier point important à prendre en compte lors de tout processus d'interprétation est la résolution sismique verticale ; elle est définie comme l'épaisseur minimale d'une couche, de manière à ce que les réflexions sismiques du toit et de la base de cette couche puissent être distinguées. Elle dépend de la fréquence et de la vitesse des ondes acoustiques dans le sous-sol (et donc des paramètres d'acquisition de la sismique). Les profils retraités au BRGM ont en moyenne des résolutions verticales de 20-25 m pour les faibles profondeurs d'investigation ($\approx 0.5-1$ km), et 30-35 m pour les profondeurs plus importantes ($\approx 2.5-3$ km). Cela signifie qu'une couche de moins

de 25 m d'épaisseur ne sera pas résolue si elle se trouve à 2 km de profondeur. Il en découle qu'une faille de rejet vertical réel de moins de 25 m ne sera pas non plus résolue pour la même profondeur.

2.6. Retraitement et interprétation sismique dans le bassin de Paris - Publication 1

Beccaletto L., Hanot F., Serrano O., Marc S. (2011). Overview of the subsurface structural pattern of the Paris Basin (France): Insights from the reprocessing and interpretation of regional seismic lines. *Marine and Petroleum Geology* 28, 861-879. <https://doi.org/10.1016/j.marpetgeo.2010.11.006>

Cette publication fondatrice concrétise mes deux premières années au BRGM et conditionne l'ensemble de mon activité de recherche jusqu'à ce jour, dont elle représente la matrice : elle formalise à la fois mon intérêt pour la géologie du territoire métropolitain (sur un objet emblématique, le bassin de Paris) et mon entrée dans le monde de la sismique réflexion ; elle mentionne pour la première fois les bassins carbonifères-permiens sous couverture méso-cénozoïque, et démontre mon intérêt pour les déformations extensives et compressives (tertiaires en particulier) vues depuis les profils sismiques. Il s'agit de la première étude régionale sur le bassin de Paris sur la base du retraitement et de l'interprétation de plus de 2500 km de profils de sismique réflexion ; ces données sismiques étaient habituellement réservées au monde industriel.

2.6.1. Principaux résultats de la publication 1

- Présentation de la méthodologie détaillée (i) de construction des 14 transects régionaux, construits à partir de 240 profils sismiques unitaires, et (ii) de la méthode de retraitement sismique, en particulier l'importance des corrections statiques primaires pour s'affranchir au mieux des effets perturbateurs de la couverture sédimentaire tertiaire. Le retraitement améliore l'image du sous-sol par rapport à celle issue du traitement original.
- Les 14 transects donnent de par leur longueur (le plus court : 75 km, le plus long : 339 km) un aperçu unique du sous-sol du bassin de Paris, en particulier pour tout ce qui touche à la continuité latérale des objets géologiques en subsurface (10 horizons interprétés sur la base de 27 forages avec des séismogrammes synthétiques).
- Le cadre tectonique régional est précisé:
 - Les discordances principales sont imagées, telles que la discordance du Crétacé terminal et celle de l'Aalénien (« Mid-Cimmérien phase »), vue en sismique pour la première fois.
 - Les inversions du Crétacé inférieur et pyrénéennes sont confirmées et illustrées.
 - Mise en évidence des relations étroites entre la géométrie des failles telle que vue en sismique, la densité des failles, et l'évolution géologique du bassin de Paris. En plus d'une subsidence thermique continue, la subsidence dépend principalement de l'activité de faille tardi-varisques polyphasées.

- Mise en évidence d'une tectonique tertiaire marquée par (i) la prolongation en subsurface vers le nord des Limagnes, et (ii) le développement de petits fossés d'effondrement dans le bassin de Paris oriental ; à ces endroits, les séries sédimentaires sont recoupées par des failles normales monophasées s'organisant parfois en structures décrochantes emboîtées.
- Enfin cette étude image et localise pour la première fois le long de grandes coupes régionales à l'échelle de l'ensemble du bassin de Paris les dépocentres carbonifères-permiens sous couverture méso-cénozoïque.

2.6.2. Publication 1

Marine and Petroleum Geology 28 (2011) 861–879



Contents lists available at ScienceDirect

Marine and Petroleum Geology

journal homepage: www.elsevier.com/locate/marpetgeo

Overview of the subsurface structural pattern of the Paris Basin (France): Insights from the reprocessing and interpretation of regional seismic lines

Laurent Beccaletto*, Franck Hanot¹, Olivier Serrano, Stéphane Marc

BRGM GEO, BP36009, 45060 Orléans Cedex 2, France

ARTICLE INFO

Article history:

Received 11 November 2010

Accepted 16 November 2010

Available online 25 November 2010

Keywords:

Paris Basin

Reprocessing and interpretation of regional seismic lines

Structural pattern

Variscan heritage

Mesozoic geological evolution

ABSTRACT

The study presents the methodology used by the French Geological Survey (BRGM) for the building, reprocessing and interpretation of selected regional seismic lines in the Paris intracratonic basin (France): the 14 constructed E–W and N–S regional transects represent a total of 2,516 km length, and are based on the merge of 240 seismic single profiles recorded by petroleum operators between 1971 and 1995. The regional lines have been selected to cross the main oil fields of the Paris Basin, as well as high potential areas for oil exploration. A first difficulty was to recover the raw data necessary to build-up the regional transects. The signal reprocessing, harmonization and merge of the single seismic lines, constituent of the regional transects, are then described; these operations represent the cornerstone of the study. We put the emphasis on the primary static corrections, as the targeted structures are commonly spatially associated with large seismic velocity variations in the upper Cretaceous chalk and Tertiary sedimentary cover.

The interpreted regional transects definitely give complementary information to the existing studies, which generally lack seismic (and therefore structural) data: we give an overview of the main structural and geometrical features of the Paris Basin: inversion structures, major unconformities, as well as Permo-Carboniferous basins. We also describe the structural pattern, and show the close relationships between the faults geometry, the faults density, and the geological evolution of the Paris Basin: we distinguish (1) few large-scale polyphase faults, with a Variscan origin, representing the first order structural frame of the Paris Basin; (2) monophasic normal faults, with strike-slip features, representing the subsurface prolongation of Cenozoic grabens cropping out in the neighbourhood; (3) deep normal faults, sealed by the base Calcareous Dogger sequence, related to the Permo-Liassic extensional tectonic regime. This large-scale view of the Paris Basin has highlighted several potential exploration targets.

© 2010 Elsevier Ltd. All rights reserved.

1. Introduction

There is an increasing interest in petroleum exploration in the Paris Basin of northern France: the number of exploration licences has increased significantly, and the future hydrocarbon potential for the basin may be anticipated with optimism (Chungkham, 2009). At the same time, the French Ministry of Industry delegated to the French Geological Survey (BRGM) the management of all the raw seismic and well data for the French territory. As a consequence, the BRGM has developed a valorisation activity of all the geological subsurface French data, with an emphasis on the seismic data. This has led to the recent creation of a dedicated

seismic pole, dealing with the entire seismic post acquisition process line. Several leading projects have been consecutively launched, such as the regional seismic study of the Paris Basin presented in the present paper.

We specifically aim (1) to introduce the methodology used by the BRGM in the building and reprocessing of selected regional seismic lines in the Paris Basin, and (2) to present the first results given by their interpretation. 14 regional transects representing a total of 2,516 km length, made of about 240 seismic profiles recorded by petroleum operators between 1971 and 1995 have been reprocessed and interpreted.

Public seismic regional studies on the Paris Basin are scarce (e.g. the pioneer work of Héritier and Villemin, 1971). The last similar study, focussing on petroleum interests, had a much less spatial extent (Bessereau et al., 1996), and the project was based on older lines with lower quality acquisition parameters, and no particular emphasis on the static corrections. For academic institutions, the

* Corresponding author. Tel.: +33 (2) 38 64 39 85; fax: +33 (2) 38 64 33 33.

E-mail addresses: l.beccaletto@brgm.fr (L. Beccaletto), f.hanot@cdpconsulting.fr (F. Hanot), o.serrano@brgm.fr (O. Serrano), s.marc@brgm.fr (S. Marc).

¹ Present address: CDP Consulting, 23 av. des droits de l'homme, 45000 Orléans, France.

seismic lines in the Paris Basin are only locally available, depending on the goodwill of petroleum companies. Let's mention yet the ECORS program, dedicated to the scientific study of the deep structures of the continental crust beneath the Meso-Cenozoic sedimentary cover of the basin (Cazes et al., 1985).

Our paper is planned as follows. We first give a concise description of the geological background of the Paris Basin, with a special focus on its three petroleum systems. We then explain the building of the regional transects and the specific job consisting in retrieving the useful raw seismic data. The signal reprocessing of the regional lines is then outlined, with a focus on the static corrections. Indeed, one of the difficulties of oil exploration in the Paris Basin is due to the very low relief of the structures (or mixed structural-stratigraphic traps), which stays within the resolving power of seismic methods; the structures are locally spatially associated with large seismic velocity variations in the upper Cretaceous chalk and Tertiary levels (Hanot, 1992); this implies to get reliable primary static corrections. After a description of the interpretation process (choice of the horizons and well-calibration), we give an overview of the main structural and geometrical features of the Paris Basin, depicted altogether for the first time: inversion structures, major unconformities, as well as Permo-Carboniferous basins. We then describe the fault pattern and show the close relationships between the faults geometry, the faults density, and the geological evolution of the Paris Basin. The interests for oil exploration are also depicted.

2. Geological background and tectonic settings of the Paris Basin

2.1. Geographic and geological backgrounds

The Paris Basin is an intraplate flexural basin covering a large part of northern France (Pomerol, 1978; Mégnien, 1980). It is made of local Permo-Carboniferous, Mesozoic then minor Cenozoic sediments lying with an unconformable contact over a Cadomian-Variscan (mainly low-grade metamorphic and granitic) basement. The latter presently crops out and surrounds the basin in four massifs: the Armorican Massif in the west, the Central Massif in the south, the Vosges in the east, and the Ardennes in the northeast. The geological boundary between the Armorican and Central Massifs is made by the Poitou High, that between the Central Massif and the Vosges by the Burgundy High. Eastwards, the Vosges basement and the Paris Basin are bounded by the Rhine and Bresse Grabens.

The present-day basin is characterized at the surface by a pattern of concentric outcrops of exhumed Meso-Cenozoic sediments and underlying basement (Fig. 1), resulting from Late Cretaceous and Tertiary deformation and erosion (e.g. Cavalier et al., 1979; Perrodon and Zabek, 1990). The Paris Basin is paleogeographically connected to the London and English Channel Basins in the northwest (at least since the Toarcian to the Paleogene, Dercourt et al., 2000), and to the Belgium Basin in the north.

2.2. Variscan inheritance

Most of the Meso-Cenozoic tectono-sedimentary evolution of the Paris Basin is genetically related to the paleogeography of the Variscan orogeny and the geometry of the resulting structural pattern (Debelmas, 1986; Le Roux, 2000; Lorenz, 1992; Mascle and Cazes, 1987; Lacombe and Obert, 2000).

The basement of the Paris Basin belongs to four paleogeographic Variscan domains, bounded by Variscan major faults and/or thrusts (Fig. 1 and Chantraine et al., 2003): (1) the Armorican domain (central-Armorican zone and Cadomian block) in the west

(bounded by the Bray fault in the north), the internal domain (Liguro-Arverne zone and Morvan-Vosges zone) in the south and southeast, the Saxo-Thuringian zone in the east (bounded by the Metz fault in the north and the Vittel fault in the south), and the Rheno-Hercynian zone in the north (bounded by the Bray-Vittel fault system in the south). In the same way, the structural pattern of the Paris Basin, with its characteristic Y-shape, is made of three basement faults systems: (1) the NE–SW (N60) faults (e.g. Metz fault); (2) the NW–SE (N120) faults (e.g. Bray and Seine faults); and (3) the meridian fault system (N90) (e.g. Etampes-Rambouillet, Sennely and Saint-Martin-de-Bossenay faults). The Bray fault is the only one cross-cutting through the upper continental crust and the Moho (ECORS deep seismic profile, Bois et al., 1994).

The initial thermal anomaly at the origin of the subsidence of the Paris Basin is most probably inherited from the Late Carboniferous–Early Permian Late Variscan history (Prijac et al., 2000). Literature proposes several mechanisms responsible for this anomaly, such as the extensional post-orogenic Variscan collapse, the delamination of the mantle lithosphere below the Variscan Belt, the detachment of the Variscan oceanic slab, or a combination of them (Burg et al., 1994; Le Solleuz et al., 2004; Lorenz and Nicholls, 1984; Prijac et al., 2000; Ziegler and Stampfli, 2001). At the same time (Stephanian–Autunian), present-day western Europe, including the area of the future Paris Basin, was characterized by the development of several intramontane coal-bearing basins, genetically related to the post-orogenic Variscan history (e.g. Saar-Lorraine Basin to the East; Jura-Burgundy and Contres Basin to the South, Carentan and Channel Basin to the West; Mascle, 1990).

The latest Variscan compressive Saalian phase (Deroin and Bonin, 2003), characterized by thrusting along the Metz fault and back-thrusting and large-scale folding of the Sarro-Lorraine through, occurred near the Autunian/Saxonian boundary (Lower Permian). Then, from the end of the Variscan orogeny onwards, the Paris Basin stayed far from strongly active margins, and the tectonic activity resulted only in medium to large wavelength deformations with low amplitudes (gentle folding and fault inversions). The Variscan faults were therefore reactivated at various epochs, controlling the Meso-Cenozoic sedimentation pattern. This tectonic activity played an important role in the formation of traps and for primary and secondary migration (Delmas et al., 2002).

2.3. Late Permian–Cenozoic tectono-sedimentary evolution

Following the demise of the Variscan orogen, the Late Permian–Cenozoic subsidence of the Paris Basin originated in a Late Permian–Triassic rifting phase (Brunet and Le Pichon, 1982; Loup and Wildi, 1994). This continental rifting stage, known at the scale of Western and Central Europe (van Wees et al., 2000; Ziegler et al., 2006), originated both in the southward propagation of the Arctic–North Atlantic rifts, and the westward propagation of the Tethyan s.l. rift systems (Ziegler et al., 2001).

The ongoing Meso-Cenozoic subsidence of the Paris Basin may then be seen as the combination of two superimposed processes: (1) a long-term thermal subsidence pattern (Brunet and Le Pichon, 1982), and (2) several short-lived tectonic pulses applied to the basin, related to the deformation of the western part of the Eurasian plate (Loup and Wildi, 1994; Robin et al., 2000). This two-scale evolution (long-term vs. short-term subsidence) is a regional key feature, controlling the development of most of the intracratonic basins of northwestern Europe (Loup and Wildi, 1994 and references therein; Ziegler and Dèzes, 2006).

In the Paris Basin, these regional geodynamic events mainly result in (1) particular deformational (fault activity, folding...) and sedimentary patterns, and (2) subsequent major erosional unconformities (e.g. Bourquin et al., 1997; Curnelle and Dubois, 1986;

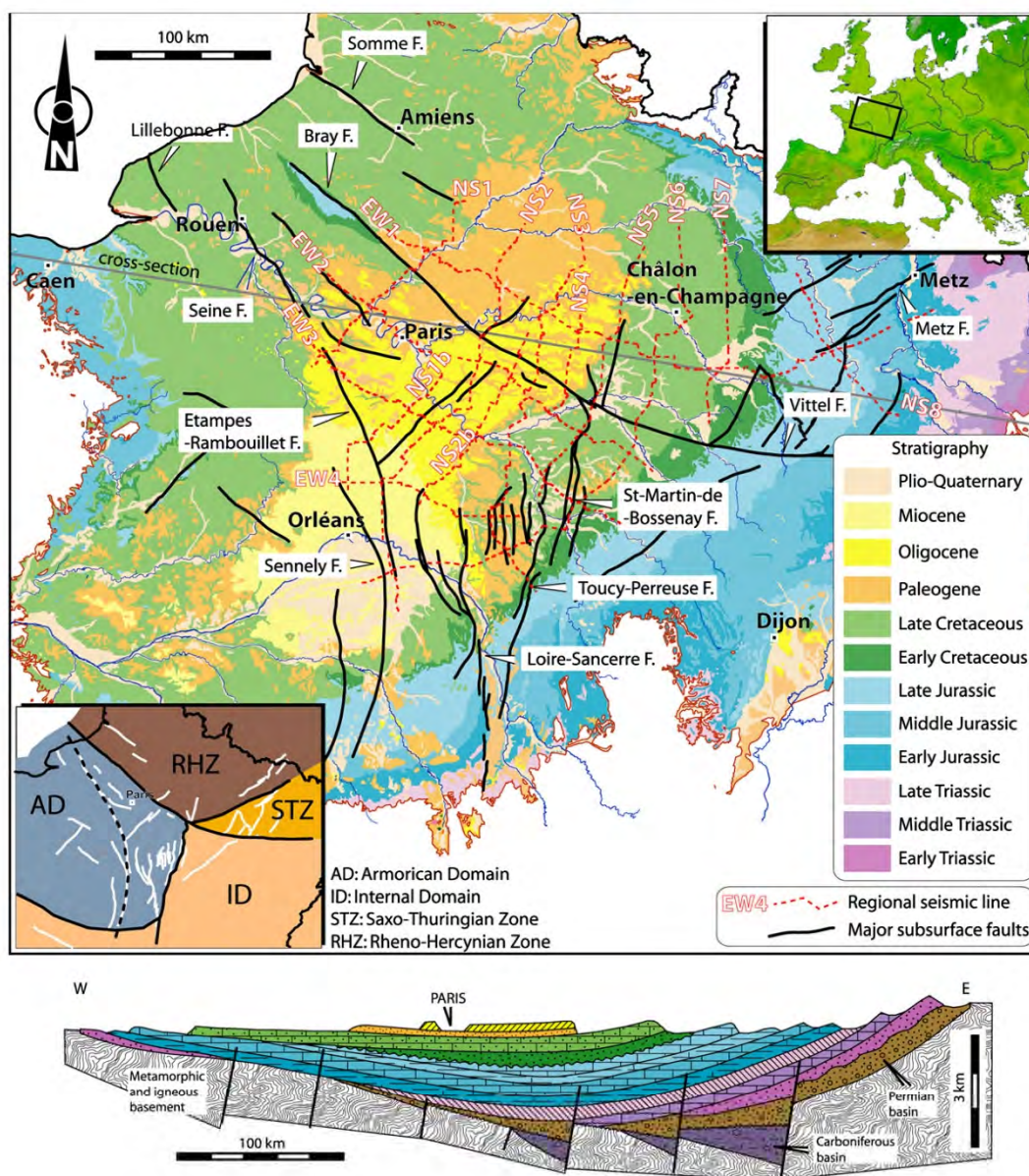


Fig. 1. Location of the 14 reprocessed and reinterpreted regional seismic lines in the geological frame of the Paris Basin. The major subsurface faults are mentioned; they are compiled from Héritier and Villemin (1971), Mégnien (1980), Perrodon and Zabek (1990), and Delmas et al. (2002), redrawn and modified by the present study. The geological background is from the 1:1000000 geological map of France (Chantraine et al., 2003). Top-right inset: the Paris Basin in Western Europe. Lower-left inset: Variscan paleogeographic domains of the Paris Basin. The schematic geologic cross-section of the Paris Basin is redrawn from Perrodon and Zabek (1990).

Gély, 1996; Mégnien, 1980; Robin, 1997 and Rusciadelli, 1996). In term of sequence stratigraphy, the Meso-Cenozoic sedimentary pile of the Paris Basin may be divided into 10 major stratigraphic cycles from the Scythian to the Maastrichtian (Guillocheau et al., 2000 and references therein; Lasseur, 2008 for the Late Cretaceous), and three cycles for the Tertiary.

We propose below an outline of the Meso-Cenozoic tectono-sedimentary evolution of the Paris Basin (Fig. 2), with a special focus on the fault activity. For further details the reader may refer to the already published works of Mégnien (1980), Perrodon and Zabek (1990), or Guillocheau et al. (2000). Following Guillocheau et al. (2000), we distinguish five mains stages for the basin evolution,

based on subsidence, sedimentary systems, accommodation variations (without eustatic corrections) and paleogeography; these stages are generally bounded by major unconformities. They are mainly of tectonic origin, and basically reflect the major geodynamic events affecting the western European plate (namely the opening of the Atlantic system and the opening to closure of the Alpine Tethys Ocean (Fig. 2 and Guillocheau, 1991; Guillocheau, 1995; Robin et al., 2000)).

2.3.1. Late Permian-Toarcian stage

As a consequence of the Permo-Triassic rifting, some of the previous Stephanian-Autunian basins of the Paris Basin were reactivated in Late Permian time (e.g. Saar-Lorraine and Contres

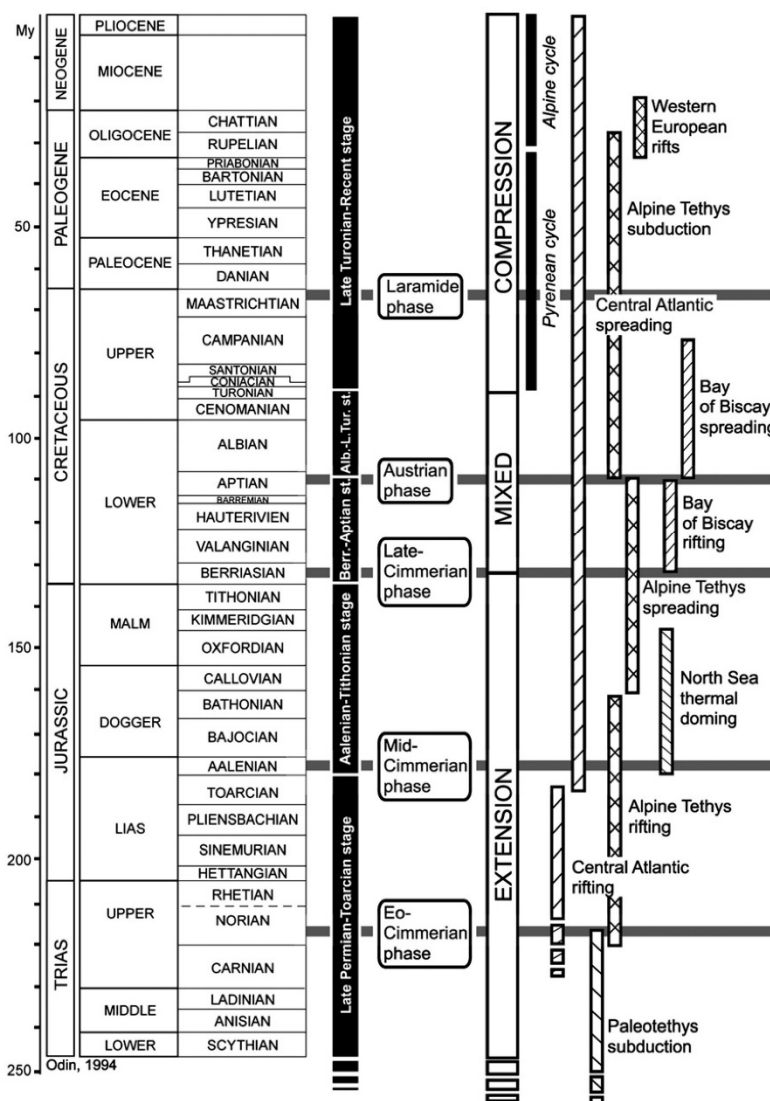


Fig. 2. Main stages of the tectono-sedimentary evolution of the Paris Basin, separated by their major unconformities (grey horizontal strokes), with the corresponding tectonic phases (explanations in the text). The major related regional geodynamic events, compiled from Guillocheau et al. (2000) and Stampfli and Borel (2002), are mentioned.

basins). These half-grabens, filled with continental lacustrine and coarse-grain sediments, developed under the control of the inherited NE–SW, NW–SE and meridian faults.

The Triassic deposits widely crop out in the eastern part of the Paris Basin (Lorraine region). During the Early and Middle Triassic, the Paris Basin formed the western end of the Germanic basin, under an overall continuing extensive tectonic regime (with strong fault activity). The deposits consist mainly of fluvial and playa sediments (Early Triassic, Buntsandstein facies), and evaporite and marine sediments (Middle Triassic, Muschelkalk facies). The Paris Basin has existed as an independent basin from the Middle Carnian onward (i.e. base of Keuper), with the occurrence of the “Grès à roseaux” unconformable deposits (Bourquin and Guillocheau, 1993, 1996). The Late Triassic period was then characterized by evaporitic and fluvial sediments (Keuper facies, Courel et al., 1980). A major unconformity occurred in the Norian (Bourquin and Guillocheau, 1993, 1996), possibly related to the southerly closure of the Paleotethys Ocean, a major regional event affecting the southern Eurasian margin in the Carnian–Norian times (Eo-Cimmerian orogeny of Stampfli and Kozur, 2006).

The Lias remained a period of extensive tectonic regime (Alpine Tethys rifting, Robin et al., 1996; Stampfli and Marchant, 1997). It is tectonically characterized by the reactivation of the meridian faults (Etampes-Rambouillet, Saint-Martin-de-Bossenay faults), the NW–SE faults (e.g. Bray fault), and the NE–SW faults. The transgressive deposits show correlated lateral variations of their thicknesses, and consist of open marine sediments (“calcaires à Gryphées”); the maximum flooding is represented by the Toarcian black shales (“schistes carton”), being the main source rocks of the basin. The Permian-Toarcian stage ended with the occurrence of the Aalenian unconformity (Mid Cimmerian phase of Ziegler, 1990), possibly related to the conjunction between the rifting of the Alpine Tethys, the end of rifting in the Central Atlantic, and thermal doming in the North Sea (Guillocheau et al., 2000).

2.3.2. Aalenian-Tithonian (middle–upper Jurassic) stage

The activity of the synsedimentary faults continued during the Dogger, to decrease significantly toward the upper Malm. This led to important facies variations of the associated sediments. The

Aalenian–Tithonian interval is subdivided into three major transgressive–regressive cycles (Guillocheau et al., 2000). The transgressive deposits consist of shallow marine bioclastic platforms, ooids and bioclastic deposits (e.g. the “Dalle Nacrée”, the main Dogger play in the Paris Basin, Delmas et al., 2002), or alternation of siliciclastic shales and muddy carbonates. The maximum floodings are represented by shaly to marly deposits. The regressive successions are also made of carbonate platforms and marine/littoral sediments (e.g. the oil-producer Portlandian facies), with siliciclastic inputs and evaporitic occurrences (Purberkian facies). The Aalenian–Tithonian stage ends with the major Berriasian unconformity (Late Cimmerian unconformity of Ziegler, 1990).

2.3.3. Berriasian–Aptian stage

The Berriasian unconformity marked a net decrease of the subsidence rate (Loup and Wildi, 1994), and a drastic change in the nature of the sediments: the Jurassic carbonates were unconformably overlain by siliciclastic deposits, such as alluvial (Griselles sandstones) or deltaic sediments (Wealdian facies), prograding from the Armorican domain. The Berriasian–Aptian stage ended with the Late Aptian unconformity (Austrian phase), preceding the transgressive deposits of the Albian tidal-dominated Greensands. Both unconformities, as well as the detrital sedimentary record, are directly related to the uplift of Western Europe, consecutive to the rifting and oceanic accretion of the Bay of Biscay (Montadert et al., 1979). The Berriasian–Aptian stage therefore displays the first compressional pattern in the Paris Basin (NE–SW compression), with inversions observed along the meridian faults in the southern part of the Paris Basin (e.g. Sennely and Saint-Martin-de-Bossenay faults, Benard et al., 1985; Trémolieres, 1981). The NW–SE faults stay active in continuity with the Jurassic tectonic regime. Both unconformities are the result of hundred meters scale vertical movements and erosion (Albian Greensands overlying unconformably the Paleozoic basement in the Artois region).

2.3.4. Albian–Late Turonian stage

The Albian–Late Turonian interval is characterized by a resumption of the accommodation, mainly controlled by a general transgressive trend (Haq et al., 1988); the tectonic activity was very moderate during this time interval (Lasseur et al., 2009; Robaszynski, 1981).

The Albian siliclastic Greensands sedimentation changed to carbonate platforms (Cenomano–Turonian Chalk), with a general onlap of the sediments toward the east and the northeast. Most of the thickness and facies variations, related to minor tectonic activity, are localized in the western part of the Paris Basin (e.g. Lillebonne and Bray fault, Mascle and Cazes, 1987).

2.3.5. Late Turonian–recent stage

In a general way, the Late Turonian to recent interval is characterized by a decrease of the subsidence rate (Loup and Wildi, 1994; Robin et al., 2000) under a compressive tectonic setting. The Late Turonian–Campanian is the period of the deposition of the Clayey and White Chalk (resp. Turonian and Late Turonian–Campanian). These sediments record the last important phase of subsidence in the Paris Basin, mainly due to high sea-level conditions until the Campanian (Hancock, 1989), following the Late Turonian sea-level drop (Haq et al., 1988). At the same time, the first long-wavelength deformations related to the Alpine cycle s.l. occurred in the Paris Basin (Lasseur, 2008 and reference therein). During the Campanian–Maastrichtian interval, the intensity of this long-wavelength deformation increased, under an overall N–S compressional regime (Castaing et al., 1984; Curnelle and Dubois, 1986; Guillocheau et al., 2000; Mégnién et al., 1980); NW–SE faults were inverted (e.g. Bray and Somme faults). The

compressional regime is directly related to a regional-scale plate tectonic reorganisation, with the onset of the northward drift of Iberia and the beginning the Pyrenean cycle s.l. (Olivet, 1996; Stampfli and Borel, 2002). The Late Cretaceous (Maastrichtian) unconformity (“Laramide phase”) marks the paroxysm of these Late Cretaceous deformations (total emersion of the Paris Basin).

During the Paleocene, only the central part of the Paris Basin was flooded by the sea, and recorded siliciclastic to carbonate proximal environments.

A second major phase of compression associated with various deformational patterns occurred from the middle Lutetian to the lower Oligocene (“Pyrenean phase” s.s.). It is characterized by (1) the reactivation of new E–W faults bounding in the north the Artois anticline (“epi-Cretaceous” faults in their former denomination); (2) short-wavelength folding in the central part of the basin (Desprez et al., 1980), with the development of asymmetrical anticlines (e.g. Bray, Margny-les-Compiègne, Beynes-Meudon or la Remarde anticlines); (3) the reactivation of meridian faults, with strike-slip to normal movements (e.g. Etampes–Rambouillet fault).

This compressional phase was then succeeded in the eastern and southern part of the Paris Basin by an extensional phase of Late Eocene–Oligocene age, coeval with the activity of the easterly Bresse and Rhine grabens (and its satellite grabens, such as the Gondrecourt Graben, Bergerat et al., 2007), and southerly Limagne grabens (Dèzes et al., 2004; Sissingh, 2006). Its western part still suffered a compressional regime (Lorenz, 1984).

Due to the decreasing subsidence rate, a change from accumulation to sediment by-pass occurred in the Upper Oligocene and lasted until the Pliocene (Guillocheau et al., 2000). A last major NW–SE compressional phase (with high wavelength deformations) occurred in the Late Miocene, in relation to the compression in the easterly Jura Mountains (Bergerat, 1987) and volcanic activity in the Central Massif (Maury et al., 1980). The present-day Paris Basin is not still a subsiding basin, but an uplifted area (Robin et al., 2003).

2.4. The three petroleum systems of the Paris Basin

The Paris Basin has been intensively explored since the 1950', with the drilling of more than 1000 exploration wells. In 2000, 39 fields produce about half of the French extracted oil (Fig. 3 and Delmas et al., 2002). The gas production represents 7% of the basin hydrocarbons. The three petroleum systems of the Paris Basin are briefly described below, from the base to the top (Delmas et al., 2002; Perrodon and Zabek, 1990):

- The Permo–Carboniferous–Middle Triassic petroleum system is represented by the Lettenkohle dolomite, lower Carnian in age (Forcelles field), and the middle Muschelkalk sandstones, upper Anisian in age (Trois-Fontaines field, conventional gas). The source rocks are the Permo–Carboniferous organic-rich sediments located in several troughs below the Triassic deposits. The vertical oil migration from the Permo–Carboniferous source rocks to the Triassic traps may have occurred during the lower Cretaceous (Delmas et al., 2002).
- The upper Trias–Middle Liassic Petroleum system, which produced about 50% of the basin oil in 2000, is represented by (1) the fluvatile Donnemarie sandstones, Carnian in age, the fluvatile Chaunoy sandstones, and the Vert-le-Grand dolomites, Norian in age. The oil fields (e.g. Chaunoy field) are located in the central part of the basin (Brie region); the traps are structural or mixed structural/stratigraphic; (2) the Rhaetian fluvatile (Boissy) and marine sandstones; the oil fields are located in the central part of the basin (Champagne, Brie, e.g. Soudron oil field); (3) The shallow marine Hettangian carbonates (L'Orme field); the trap is a faulted low-relief

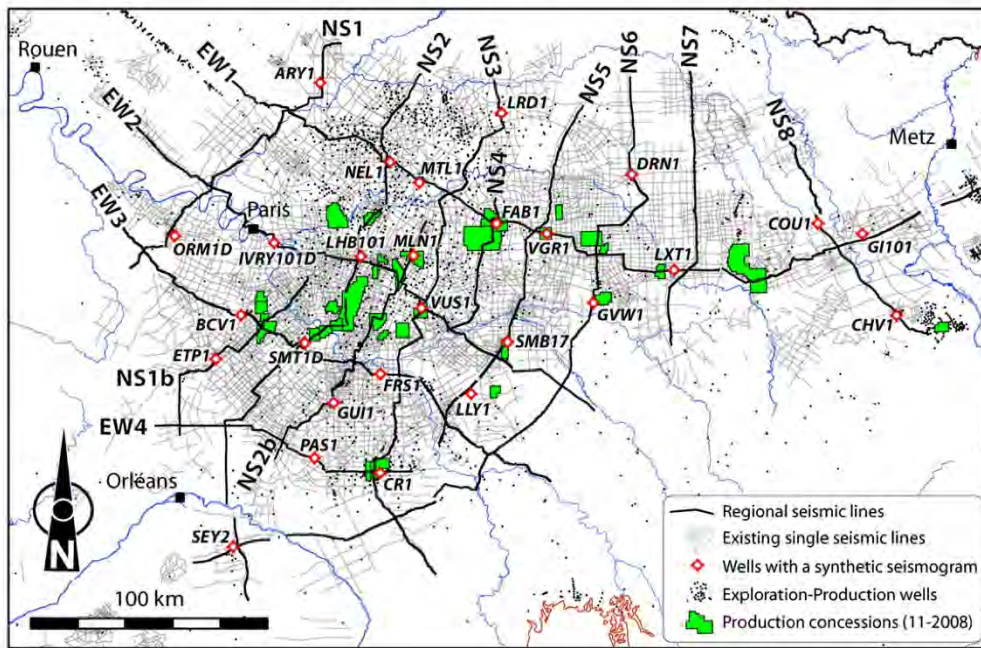


Fig. 3. Position of the regional seismic lines and the 27 wells with synthetic seismograms use to calibrate the interpretation. The regional lines cross the main oil fields of the Paris Basin.

anticline. The source rocks of the upper Trias-Middle Liassic Petroleum system are the lower and middle Liassic marine shales (Lotharingian and Domerian). The oil migration from the Liassic source rocks to the Triassic traps occurred mainly during the upper Cretaceous.

- The upper Liassic-Dogger-Neocomian petroleum system, which produced about 50% of the basin oil in 2000. It is represented by (1) the Dogger limestones, of Bathonian age (“Calcaire Comblanchien” and “Oolithe Blanche”) or Callovian age (“Dalle Nacrée”); the 13 Dogger oil fields (e.g. Villeperdue field) are located in the central part of the basin, in the Brie and Champagne regions; (2) the Malm limestones (Joigny field) in the south of the basin; (3) the Neocomian sandstones, Valanginian in age (Griselles sands) and Hauterivian age (Châteaurenard sands), which are located in a limited area in the south of the basin (four oil fields). The source rocks are the Toarcian shales (“schistes carton”), being the main petroleum source rocks of the basin. The vertical oil migration from the Toarcian source rocks to the Dogger traps occurred mainly during the upper Cretaceous along normal faults. A secondary oil migration from the Dogger reservoirs to the Malm and Neocomian traps occurred during the Oligocene rifting.

3. Retrieval of the field data and build-up of the regional seismic lines

3.1. Retrieving the data

The building of the regional seismic lines has been an iterative, long-term process, depending on the availability of the raw seismic data. The latter are composed of seismic shots recorded on magnetic tapes, associated with field documents (e.g. the shot and geophone coordinates, the observer reports...), generally archived on paper. Up to 2006, these data were managed either by the operators still present in France, or by the Office of Exploration and

Production of Hydrocarbons (BEPH) for the operators having left France. Since 2006, the BEPH delegates this data management to the BRGM, as well as the data management of the well data since 2008 (Hanot, 2002).

The selection of the single seismic lines, basic constituent of the regional lines, was done using a dedicated database, gathering the position and the “metadata” of all the lines acquired in the Paris Basin since the 1950’ (Fig. 3). The raw seismic data reprocessed during this project were historically recorded by 17 different operators: BP, BPF, CANYON, COPAREX, DPF, EAP, ERAP, ESSOREP, EURAFREP, EUROMIN, FINA, GDF, PETROREP, SNEA (P), SHELL, SUN, TRITON. By the set of alliances or repurchases of companies, the number of operators holding the data decreased. As an example, the TOTAL Company holds about half of the used data, and ESSOREP nearly a quarter. Once received, a first control on the data led to identify problematic seismic lines, not containing the necessary data for their reprocessing (partial seismic files due to degraded magnetic tapes, unknown data format, unrecoverable data media and incomplete field documents...). Therefore, some modifications on the original geometry of the regional transects were realized regarding (1) the answer of the operators concerning the availability or not of the originally selected data, and (2) the quality of the received data. In areas with a strong density of seismic data, these changes could be easily done. In the ultimate case where no replacement raw data were found, a digitalization of a previous processing work was used. As a final result, the quality of the field data covered a wide variety, from poor to good.

3.2. Building of the regional transects

The regional lines have been selected to cross the main oil fields of the Paris Basin, as well as high potential areas for oil exploration (Fig. 3). One may distinguish three areas each with their own characteristics: (1) the western domain and the main Armorican reversed structures. The latter are classically exploited for underground gas

Table 1
Main characteristics of the 14 regional lines, showing the heterogeneity of the original data.

Line Name	CDP length (km)	Nb. of single lines	Nb. of operators	Nb. of contractors	Acquisition year (min–max)	Source	Fold (min–max)	Geoph. interval (min–max)
NS1	130.7	15	7	4	1981–1992	Vibroseis	24–60	30 m–40 m
NS1BIS	115.3	7	4	3	1983–1993	Vibroseis	30–60	30 m–50 m
NS2	245.8	19	4	3	1980–1989	Vibroseis	24–60	25 m–50 m
NS2BIS	121.4	20	4	5	1978–1990	Vibroseis	24–80	40 m–100 m
NS3	240.0	20	5	3	1977–1991	Vibroseis	24–60	20 m–100 m
NS4	75.3	9	2	2	1978–1989	Vibroseis	12–60	30 m–75 m
NS5	150.5	12	4	2	1979–1995	Dynamite + Vibroseis	24–80	25 m–75 m
NS6	315.3	23	6	5	1974–1989	MiniSOSIE + Vibroseis	24–60	25 m–100 m
NS7	116.8	7	4	3	1975–1991	Vibroseis	24–48	30 m–100 m
NS8	101.9	5	3	3	1982–1991	Dynamite + Vibroseis	24–48	40 m–100 m
EW1	338.7	35	7	6	1978–1995	Dynamite + Vibroseis	24–120	20 m–75 m
EW2	237.3	30	4	6	1972–1991	Vibroseis	6–80	20 m–100 m
EW3	215.2	26	6	5	1977–1992	Vibroseis	12–80	25 m–100 m
EW4	112.1	9	3	2	1982–1989	Vibroseis	24–60	40 m–50 m

storage (e.g. Beynes and Saint Illiers fields) and may represent targets for structural or mixed traps for the upper Trias–Middle Liassic reservoirs; (2) the central domain, corresponding to the upper Trias–Middle Liassic and upper Liassic–Dogger major structural traps (e.g. Coulommès and Chaunoy fields) or mixed traps (e.g. Itteville and Villeperdue fields). The transects provide a corrected image from static anomalies related to the Tertiary and Cretaceous sedimentary cover (see section 4). The transects replace proven structures within a widened framework and clarify the potential of under-prospected areas; (3) the eastern domain, which is the area of Rhaetian trap discoveries (e.g. Soudron and Courdemanges fields), presents the potentialities of the Ardennes buttresses. The transects also recognize the Carboniferous proven gas system of Trois-Fontaines field, and the oil system of the Forcelles field.

3.3. Heterogeneity of the data

A specific problem, inherent in this kind of project, is the heterogeneity of the raw data (Table 1). The main sources of heterogeneity

(for a given regional line) are related to the number of operators and to the variety of the acquisition parameters (source, fold, geophone interval ...). This heterogeneity is amplified by the increasing number of single lines in the regional transect, as well as the quality and preservation of the raw data. One of the challenges of the reprocessing of the regional lines is therefore to make them homogeneous.

4. Signal reprocessing - focus on the static correction

The cornerstone of the present study is the signal reprocessing, harmonization and merge of the single seismic lines, constituent of the regional transects. That is, in other words, to create new (regional) seismic lines from heterogeneous (single) old ones.

4.1. Homogenization of the regional transects using modern processing methods

The use of modern processing methods, applied to old raw seismic data, significantly improves the quality of the resulting

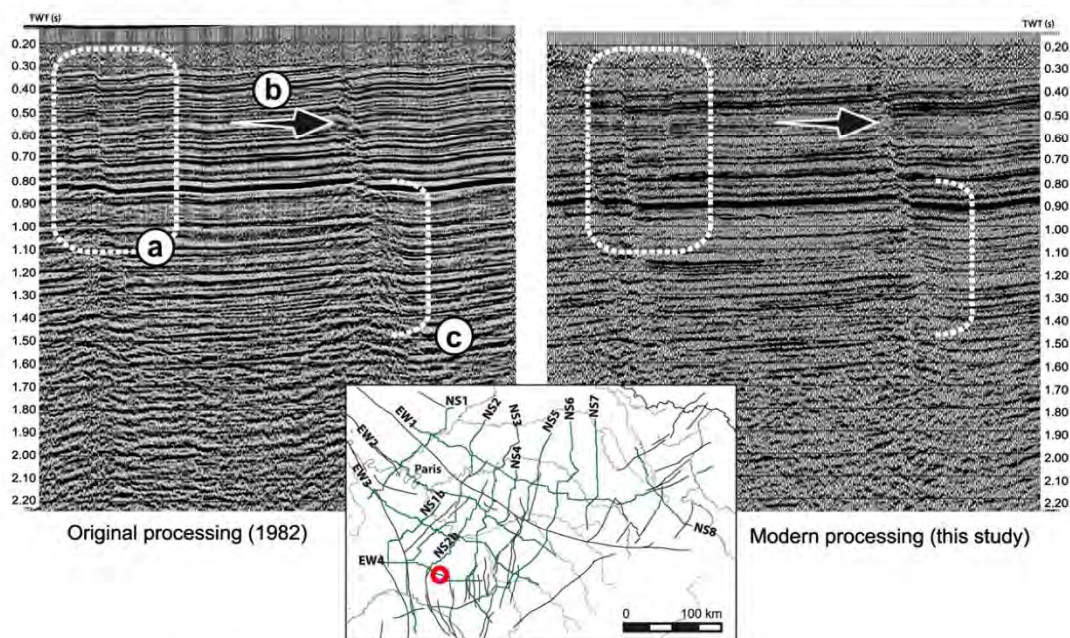


Fig. 4. Impact of modern seismic processing methods on the quality of the resulting seismic section, compared with the original processing (EW4 regional transect); the use of modern processing increases the resolution of the horizons, the fault zone (a), the single fault (b) and the related drag folds (c).

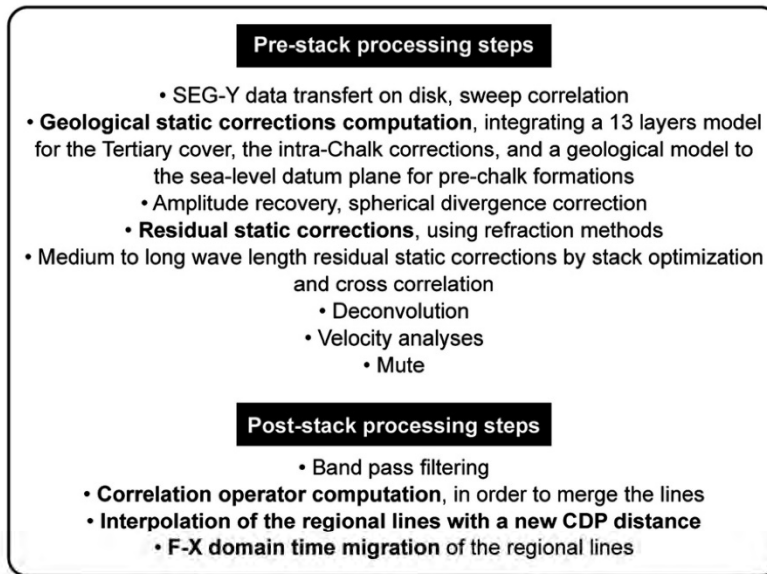


Fig. 5. Main steps of the modern processing sequence used in this study; specific steps dedicated to the homogenization of the regional lines are in bold.

seismic section, leading to enhanced descriptions of the geological structures. Compared with old-processed line, the newly processed lines display a better (1) continuity and horizontal-vertical resolution of the seismic horizons or groups of horizons (this is particularly true for the deepest horizons), (2) geometric characterization of faults and fault zones, and (3) description of the potential reservoir structures (Fig. 4).

The main steps of the processing sequence are summarized in Fig. 5. More specifically, the homogenization of the regional seismic lines is based on four specific processing steps:

(1) The use of a single and homogeneous static correction velocity model, in the purpose of eliminating the time shifts and the

velocities lateral variations in the Tertiary sedimentary cover, the Late Cretaceous chalk, and the Jurassic sequences. Static modelling (including residual statics) is a key issue for any reservoir-oriented seismic processing in the Paris Basin, and is addressed in a specific part below.

- (2) The stack sections (single lines) were interpolated to a new CDP distance of 20 m. New CDP numbering starting with 1 was assigned to the regional lines.
- (3) The use of matching filters, ensuring the homogenization of the features of two successive single lines, without damaging lines with high-frequency signatures (Fig. 6). Moreover, the polarity of some lines should have been reversed to get the best fit.
- (4) The time-migration of the regional seismic lines.

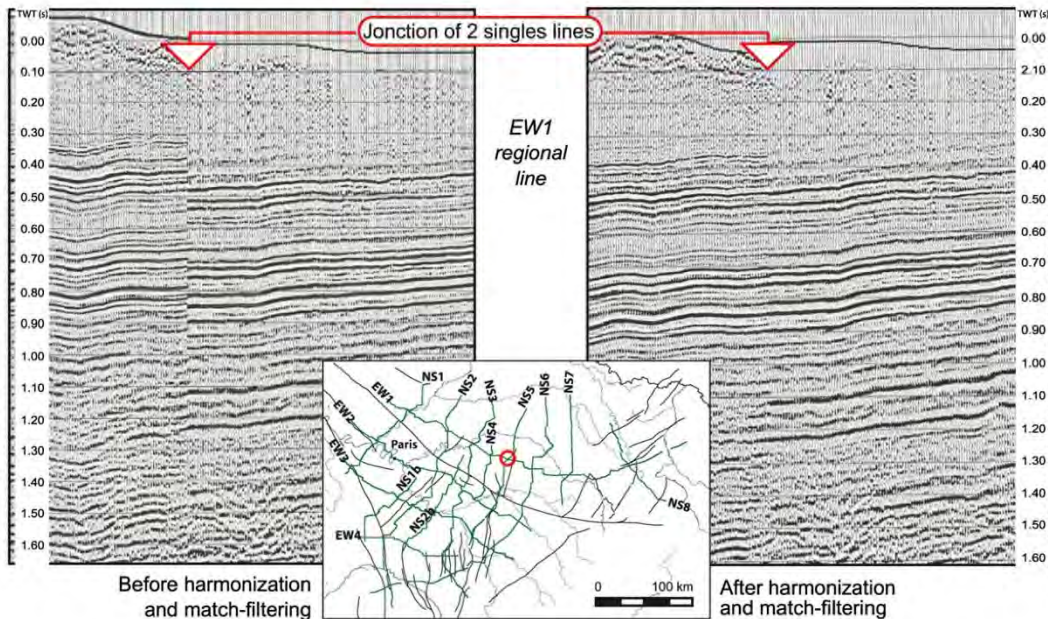


Fig. 6. Example of harmonization and match-filtering at the junction of 2 single seismic lines (EW1 regional transect).

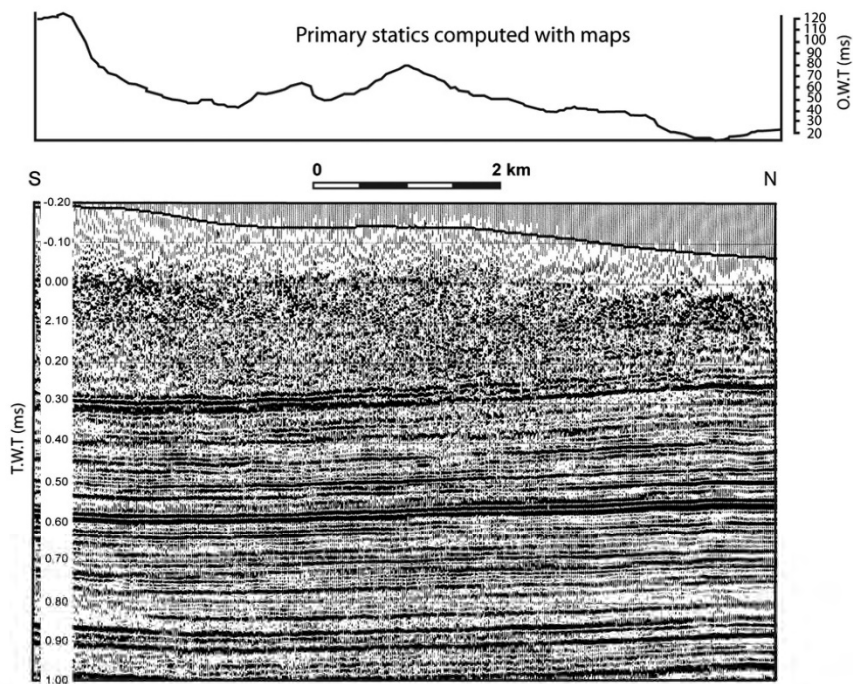


Fig. 7. Impact of the primary static corrections, with the example of a seismic section showing the southern flank of a known structure. Along the seismic line, the time differences of target horizons on the stack reach about 30 ms OWT, whereas the corresponding difference for statics is greater than 120 ms OWT.

4.2. Static corrections

In seismic processing, topography along the seismic lines and lateral velocity variations in the Low Velocity Zone (“LVZ” or weathered zone) highly disturb the seismic signal. The LVZ corresponds to the superficial rock layer, variable in thickness and in lithology, and characterized by heterogeneous acoustic velocities,

due for instance to rock alteration, diagenesis or water circulations. Static corrections basically aim to remove these topographic and velocity effects.

Despite significant technical advances, one of the main aspects of the seismic processing in the Paris Basin concerns the uncertainties in the calculation of primary static corrections (Hanot, 1992). Up to recently these uncertainties have remained of

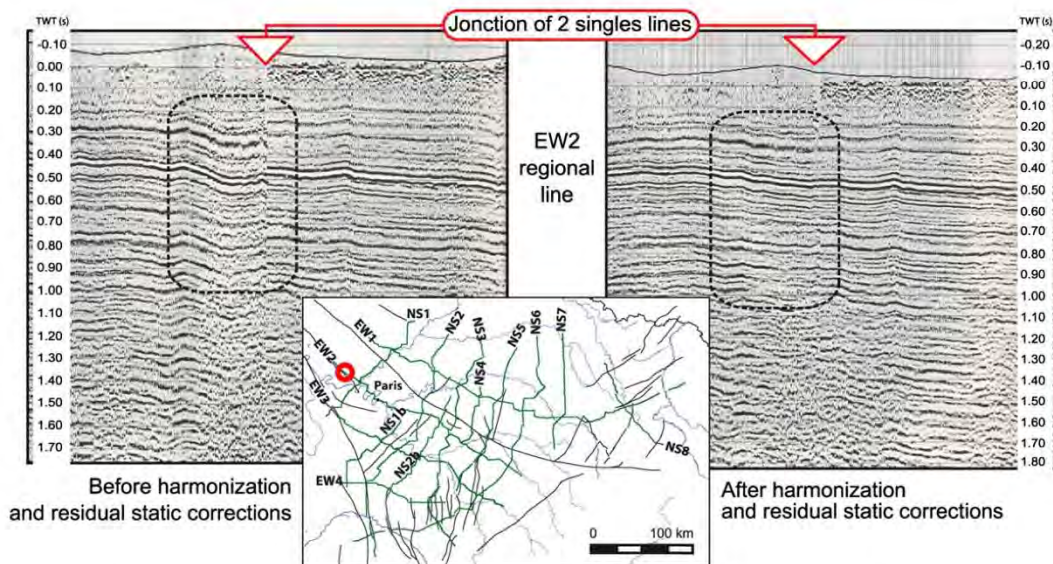


Fig. 8. Impact of the residual static corrections. The left picture shows a partial view of the EW2 regional transect directly below a Tertiary sand hill. Regardless of the phase problem at the junction of the single profiles, the under-correction below the hill generates a reverse dip (time artefact). The right picture shows the same area in stack version after the application of the residual static corrections.

a similar size compared to the investigated closures (usually 10–15 ms TWT). As a consequence, a large number of seismic prospects resulted in drilling of unreal structures. Fig. 7 illustrates the confidence in statics needed to produce reliable time sections.

In the Paris Basin, the various outcrops lithologies provide extreme contrasts of seismic interval velocity, which represent the main source of difficulty in computing primary field statics. For instance in the Lorraine region, the Cuesta of the Dogger is the result of the contact

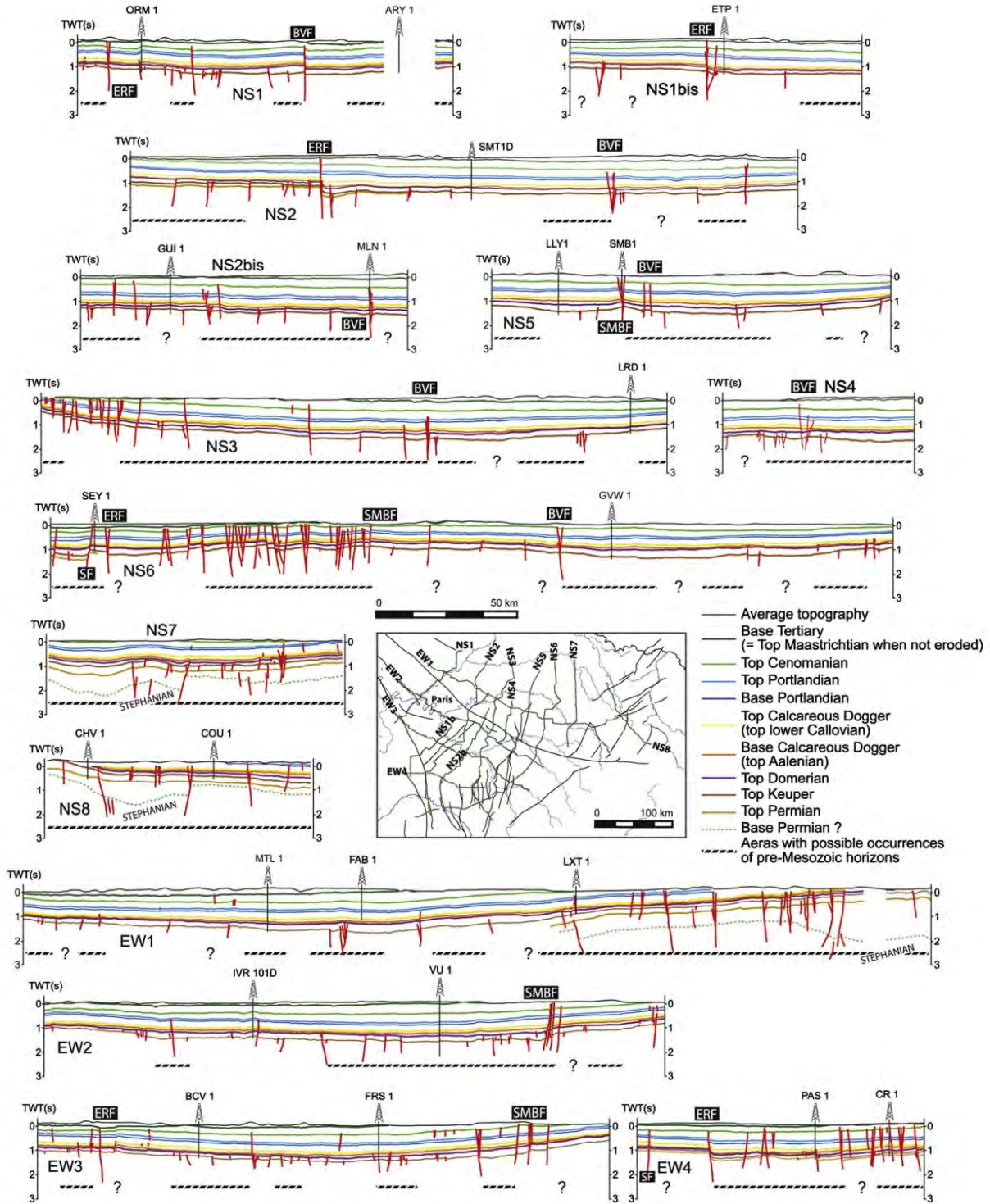


Fig. 9. Line drawings and locations of the 14 regional transects. The main faults and calibration-wells are shown: SF: Sennely fault; SMBF: Saint-Martin-de-Bossenay fault; ERF: Etampes-Rambouillet fault; BVF: Brav-Vittel fault. For the N–S lines, the South is at the left (except for NS7): For the E–W lines, the West is at the left.

between the Bajocian limestone (velocity of $3000\text{--}3500\text{ m s}^{-1}$) and the Toarcian marls (velocity of 2000 m s^{-1}). In the same way in the Champagne and Ile-de-France regions, diagenesis characterized by strong elevation variations ($200\text{--}300\text{ m}$) located within the Turonian chalk produces a strong velocity discontinuity (2800 m s^{-1} to over 3300 m s^{-1}), and generates various static corrections difficulties (Hanot and Renoux, 1991; Thiry et al., 2003).

However, the static problems of the previous examples are subordinate compared to the static effects generated by the Tertiary sedimentary cover in the Ile-de-France area, which is the main zone of oil-exploration activity in the Paris Basin (Hanot and Thiry, 1999). The total thickness of the 65 million years of Tertiary deposits in the Paris

Basin never exceeds 250 m . This period of sedimentation was contemporaneous with major tectonic periods, which structured the Mesozoic series (see section 2.3.5). This tectonic activity explains the great variability in thickness and petrography of facies of the Tertiary formations, where no lithological unit is more than 50 m thick. Therefore, the main purpose of the static corrections in the Paris Basin is to remove the disturbing effects of the Tertiary sedimentary cover.

4.3. Usefulness of the geology for calculating primary statics

Until recently static corrections in the Paris Basin were calculated by means of $50\text{--}80\text{ m}$ deep up-holes distributed on average

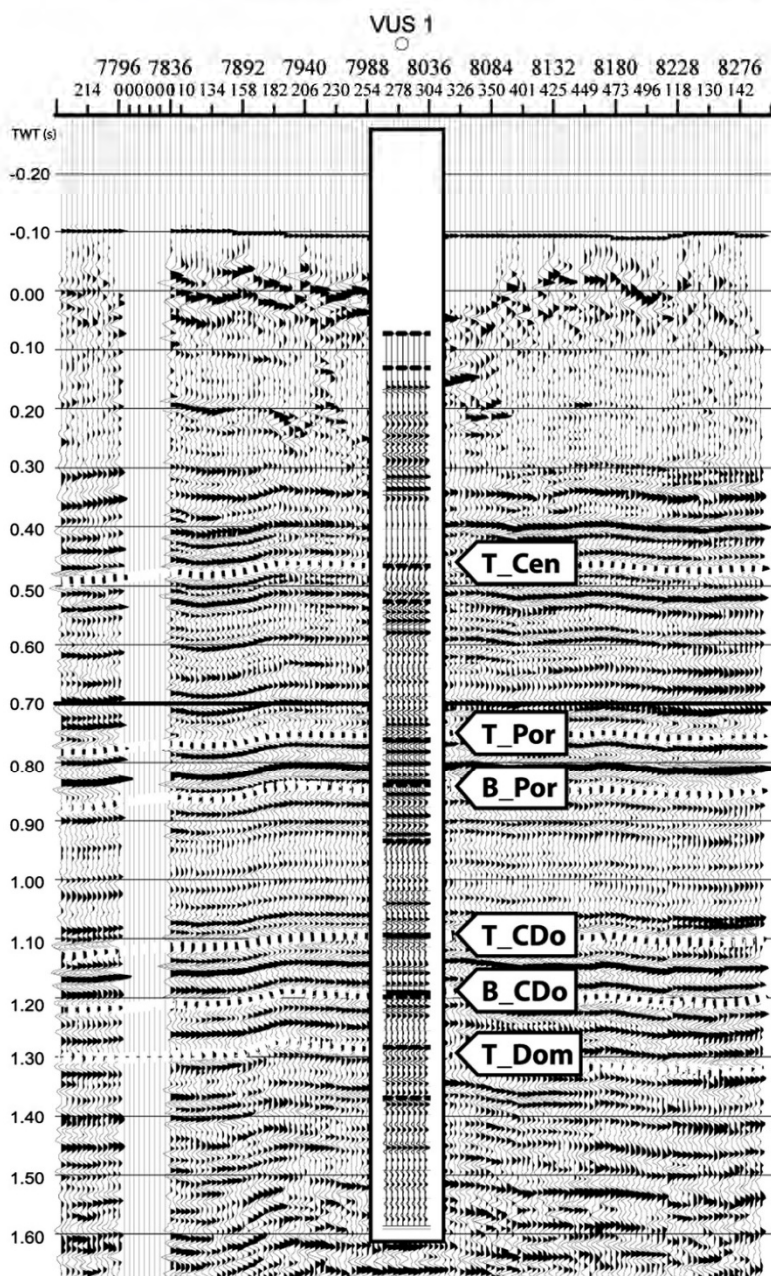


Fig. 10. Correlation between well Vulaines-1 and the line EW2. Legend: T_Cen; Top-Cenomanian; T_Por; Top-Portlandian; B_Por; Base-Portlandian; T_CDo; Top Calcareous Dogger; B_CDo; Base Calcareous Dogger; T_Dom; Top Domerian.

every 2 km. The classical method consisted of a linear interpolation of the up-hole final times in relation to the surface elevation.

However, it is possible to produce a geological interpretation of the velocity variations observed in the up-holes integrated with (1) external geological information (geological maps, water research

boreholes, etc...), (2) cuttings sampling in the up-holes, and (3) wireline logs (e.g. Gamma Ray). The resulting complex shallow layering shows that the base of the true Low Velocity Zone is at the top of the Late Cretaceous Chalk (i.e. the base of the Tertiary sequence) and continues beyond the final depth of the up-holes.

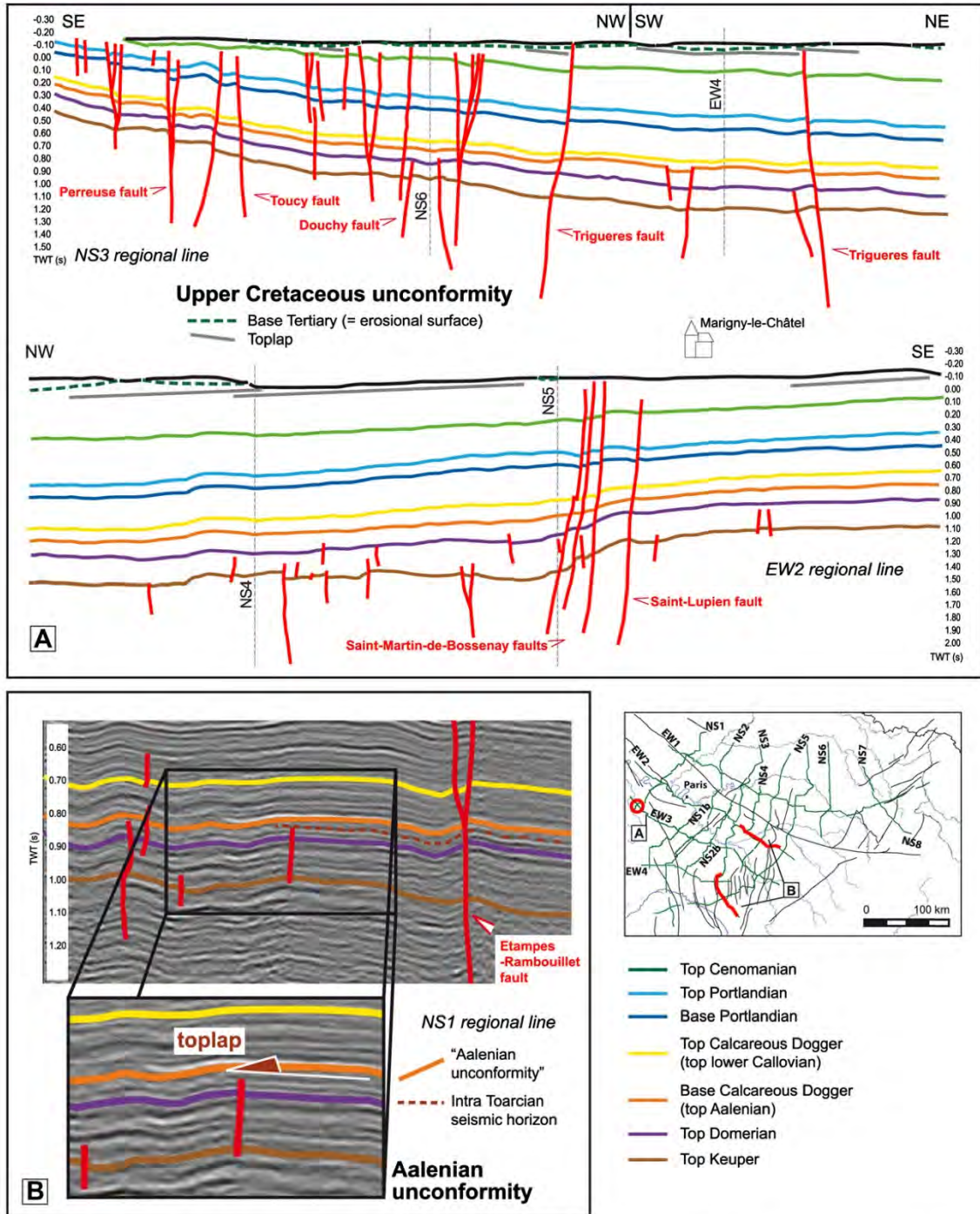


Fig. 11. A: geometry of the upper Cretaceous unconformity (lines drawings of EW3 and NS2 regional lines). The pictures show (1) the thickness variations and toplap geometries of the upper Cretaceous sequence due to the upper Cretaceous unconformity, and (2) the thickness variations of the lower Cretaceous sequence due to the Late Aptian unconformity; B: geometry of the Aalenian unconformity (NS1 regional line). The picture shows the toplap of an intra-Aalenian seismic horizon against the Base Calcareous Dogger horizon (top Aalenian).

Despite the fact that not all the up-holes reach the top of the Chalk, it is possible to work out a geological model down to this level by piling up all the different layers together with their own velocities. Moreover, this model is continuously enhanced with the information brought by the residual statics and new up-holes (Fig. 8). Compared to the standard method, this new model definitely improves the quality of the calculated statics, because of a more realistic velocity and geological model. This led to the elimination of the large wavelength anomalies under the Tertiary cover. For example, the already known structural traps distinctly appear, and we may therefore be confident in about twenty new observed structural features. Specific local seismic reprocessing could then be considered to improve the resolution.

5. Interpretation of the regional seismic lines: structural implications

The main interest of this regional seismic study is to acquire an overview of the major structural features of the Paris Basin. After a description of the interpretation process, we therefore aim to illustrate some of them, in relation to their geological and structural framework. All the interpreted seismic lines are shown on Fig. 9, together with the calibration-wells and major faults.

5.1. Choice of the horizons and well-calibration

5.1.1. Choice of the horizons

The selected horizons correspond either to bases and tops of known petroleum reservoirs or characteristic sedimentary units of the Paris Basin (see section 2). Somme of them therefore coincide with major unconformities know throughout the basin. From the base to the top, the picked horizons are: (1) the top of Carboniferous (i.e. base upper Permian), continuous in the eastern part of the Paris Basin, where these levels lie shallow enough to stay within the seismic resolution; (2) the top of Permian (i.e. the base of Trias), mainly in the eastern part of the basin, for the same previous reasons; (3) the top of Trias (i.e. the top Rhaetian); (4) the top of the Domerian (upper Pliensbaschian); (5) the base and top of the Dogger carbonates (i.e. resp. the top of Aalenian and the top of lower Callovian); (6) the base and top of Portlandian (latest Jurassic); (7) the base and top of the upper Cretaceous Chalk (i.e. resp. the top-Cenomanian and the top Maastrichtian = base Tertiary).

5.1.2. Well data - synthetic seismograms

In order to calibrate and tie well data to the corresponding seismic horizons, a total of 27 wells with good velocity information were selected to build synthetic seismograms (Figs. 3 and 9). The

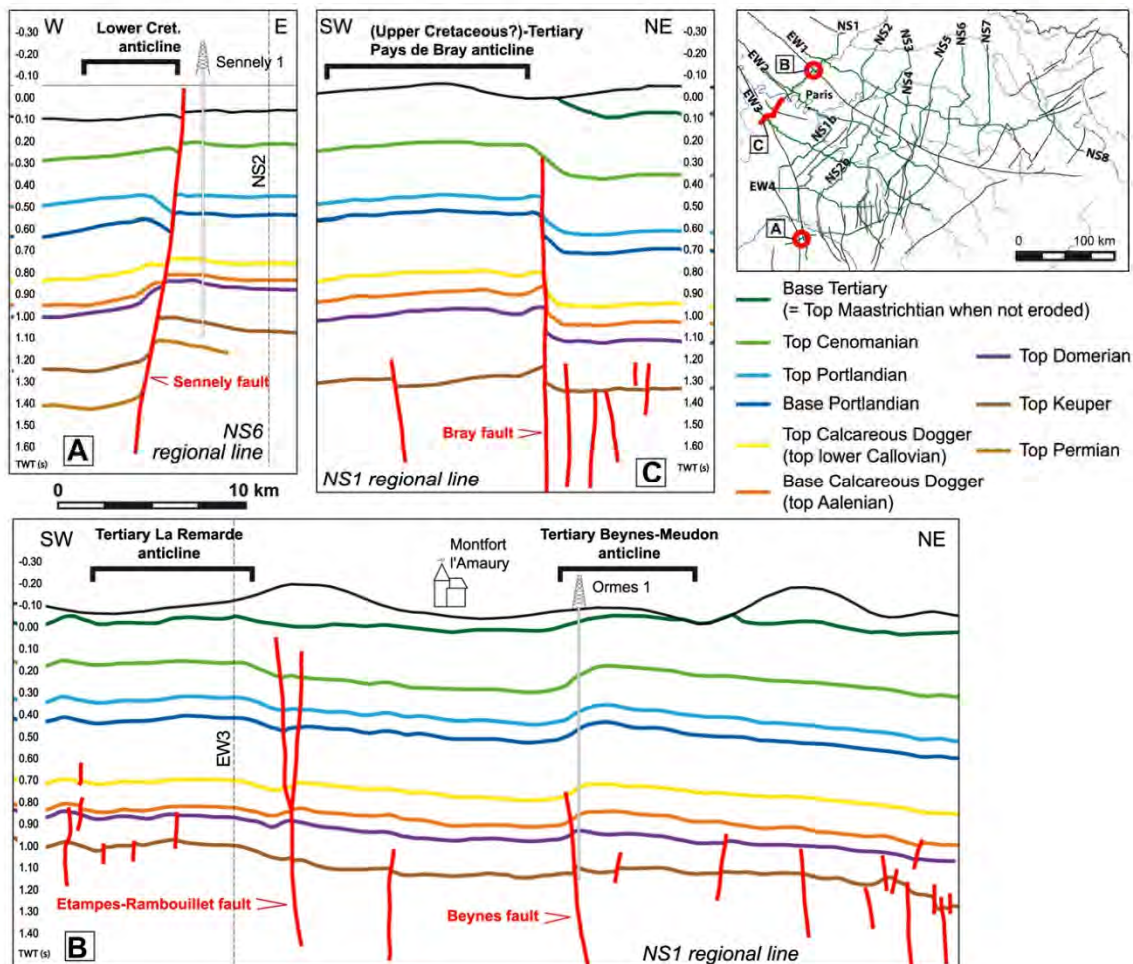


Fig. 12. Inversions structures in the Paris Basin: examples of line drawings taken from various regional lines. A: lower Cretaceous anticline along the Sennely fault (NS6 regional line); B: (upper Cretaceous ?)-lower Tertiary anticline along the Bray fault (Pays de Bray anticline, NS1 regional line); C: lower Tertiary anticlines along the Etampes-Rambouillet and Beynes faults (resp. La Remarde and Beynes-Meudon anticline, NS1 regional line).

latter aim to model the acoustic response of the rock layers along a given borehole. They were generated by convolving the reflectivity derived from digitized acoustic and density logs with a specific wavelet. The processing sequence followed the following steps: (1) editing of the Sonic log and the check-shot, (2) calibration of the Sonic log with the interpolated check-shots, (3) time-resampling and computation of the reflectivity, and (5) convolution of the latter with a Ricker wavelet; the heterogeneity of the seismic data leads us to chose frequencies of 40 and 50 Hz for the wavelet. Fig. 10 gives an example of tie between well Vulaines-1 and the regional line EW2. Previous seismic studies (Thinon and Grataloup, 2007) have also been used for the calibration process of the regional seismic lines.

5.2. Examples of regional-scale geological features

5.2.1. Unconformities

Our regional study highlights by nature regional-scale geometrical features, such as major unconformities.

The widely distributed Late Cretaceous unconformity (near the Cretaceous-Tertiary boundary, see section 2.3.5) is well illustrated, despite the poor quality of the near-surface seismic images (indeed, the seismic acquisition parameters for oil exploration in the Paris Basin were chosen to highlight deeper structures). Nice examples are given on the south-eastern ends of the NS3 and EW2 regional lines (Fig. 11A). Both transects clearly display the erosion and subsequent thickness variations of the Late Cretaceous sedimentary sequence prior to the deposition of the first Tertiary sediments. Note that because no horizon equivalent to the top Aptian has been picked, the Late Aptian unconformity/truncation (and a fortiori the Berriasian one, partly eroded by the Aptian one), is not directly visible. In a general way, Albian sediments overlie either unconformably the previous series (from the Variscan basement to the Wealdian sediments, northern and south-western part of the basin), or paraconformably the Aptian sediments (central part of the basin) (Guillocheau et al., 2000). However, a rough image of the Late Aptian unconformity may be given by the thickness variations of the sedimentary sequence between the top-Portlandian and top-

Cenomanian horizons (Fig. 11A, south-eastern part of the NS3 regional line).

The study also possibly recognizes the major Aalenian unconformity. In the Paris Basin, well data show that the latter is either characterized by condensation surfaces, or very local truncations of the underlying Toarcian sediments (Guillocheau et al., 2000). In addition, our study shows the truncation of an intra-Toarcian seismic horizon by the Base Calcareous Dogger horizon (Fig. 11B, south-western end of the NS1 regional line). We interpret this toplap geometry as the local record of the Aalenian unconformity.

5.2.2. Inversion structures

Two major inversion and folding episodes are confirmed and imaged by the present study (Early Cretaceous and Early Tertiary inversions, see section 2.3).

The Early Cretaceous (Aptian-Albian) deformation is characterized by the occurrence of N–S inverted faults under a roughly E–W compressional regime. A suitable example is given by the Sennely fault on the NS6 regional line (Fig. 12A); the fault dips strongly westward, with an overall normal fault present-day geometry. The normal activity is characterized by (1) the more important thickness of the western hanging-wall deposits (at least until the top-Portlandian horizon), compared to the other side of the fault, and (2) the important downthrows of the western flank. Then, the post base-Portlandian to pre top-Cenomanian sequence displays a striking anticline structure, which then prevails on the previous brittle normal deformation. Post-Cenomanian deposits are not affected. Another example may be found on Fig. 11A, on the NS3 regional line between Perreuse and Toucy faults.

The Pyrenean Tertiary deformation is characterized by the occurrence of short-wavelength folds in the central part of the basin (asymmetrical anticlines, generally related to the reverse reactivation of previous normal faults). The south-western end of the NS1 regional line displays two nice examples of these structures (Fig. 12B): the La Remarde anticline, which developed along the southern flank of the Etampes-Rambouillet fault, and the Beynes-Meudon anticline, which developed in relation with the Beynes

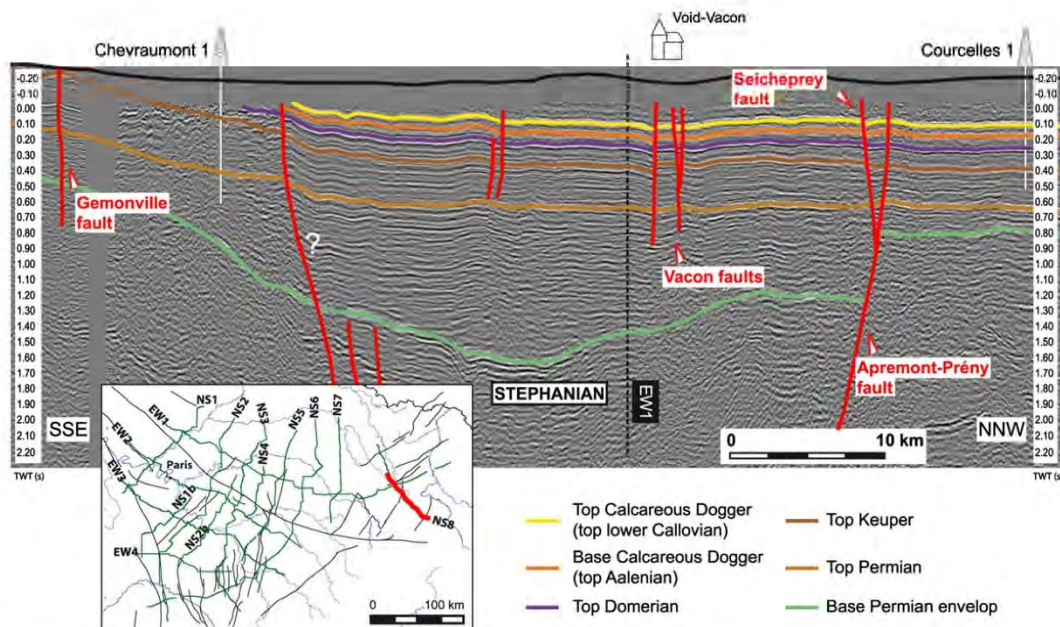


Fig. 13. The Permo-Carboniferous Saar-Lorraine basin illustrated by the NS8 regional line. Note the role of the Apremont-Prény fault in the growth of the basin.

fault. In both cases, the whole pre-Tertiary sequence shows undulations with pluri-km wavelengths.

Another appropriate example is given by the Bray fault, for instance on the NS1 regional line (Fig. 12C); the fault is subvertical with an overall reverse fault present-day geometry. At least from the Triassic until the Late Cretaceous, the Bray fault had shown synsedimentary normal activity, marked by the downshift of the southern flank; the Early Cretaceous inversion is not recorded by the E–W trending Bray fault, which may rather behaved as a strike-slip fault under the E–W compressional regime. The Pyrenean inversion is characterized by (1) the development of a flexure along the south-western flank of the fault (Pays de Bray anticline), and (2) important upthrows of the south-western flank. From the top-Cenomanian horizon upward, the fault disappears and is replaced by the flexuration of the sedimentary pile. Note that the Bray fault may have also previously suffered a compressional episode during the latest Cretaceous times (see section 2.3.5).

5.2.3. Permo-Carboniferous grabens

The pre-Mesozoic basement of the Paris Basin is characterized by the development of several fault-controlled Permo-Carboniferous grabens (see section 2.3), with high exploration potentials (Chungkham, 2009). Several regional transects have been selected to cross some of them, known in eastern France. An example is given by the NS8 NNW-SSW trending regional line, cross-cutting through the Permo-Carboniferous Saar-Lorraine Basin. The Fig. 13 shows the occurrence of the graben, more than 50 km wide, whose filling up has been controlled by the activity of the Apremont-Prény normal fault. Reflectors below the Base Permian horizon are attributed to the Stephanian and Westphalian coal layers. Compared to the Permian deposits, the post Permian sedimentary sequence shows more or less isopach thicknesses, with minor variations of the Triassic sequence. Permo-Carboniferous basins of the eastern Paris Basin are also imaged on the regional lines NS7 and EW1 (see Fig. 9).

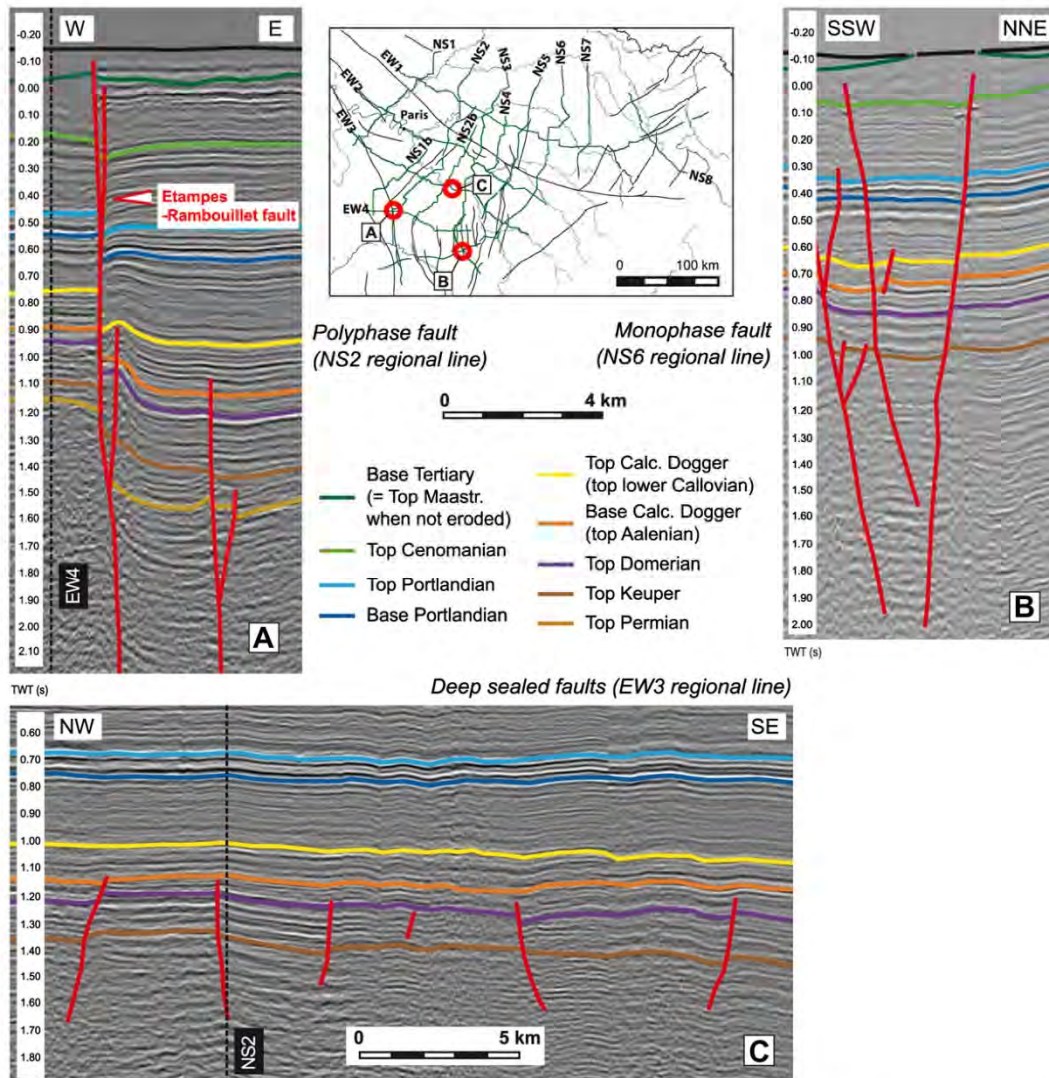


Fig. 14. Fault typology in the Paris Basin: examples taken from various regional lines, A: deep active polyphase faults; B: monophasic faults; C: deep sealed fault. See explanations in the text.

In addition to this well-known area, all the regional lines show deep seismic markers below the top Keuper horizons (Fig. 9). Due to the thickness distribution of the whole Triassic sedimentary sequence in the Paris Basin (Debrand-Passard, 1980; Delmas et al., 2002), these horizons cannot be attributed to the Triassic sequence alone (the Triassic sequence is not thick enough to match all the observed horizons). Therefore, these observations confirm the occurrence of widely distributed pre-Mesozoic sedimentary sequences (i.e. Permo-Carboniferous basins) under the Mesozoic cover of the Paris Basin (Delmas et al., 2002; Mégnien, 1980). Only long-enough regional seismic transects could have imaged such continuous deep sedimentary units.

5.3. Structural pattern of the Paris Basin

The interpretation of the regional seismic lines led us to find out connections between the 2D fault geometry, the faults density along the regional seismic transects, and their structural control during the geological evolution of the Paris Basin. Three main types of individual faults may be then distinguished:

- (1) Few large-scale deep active polyphase faults. They generally show normal present-day patterns (e.g. Etampes-Rambouillet fault, Fig. 14A); nevertheless reverse geometries are also observed (e.g. Bray fault, see Fig. 12C). They correspond to

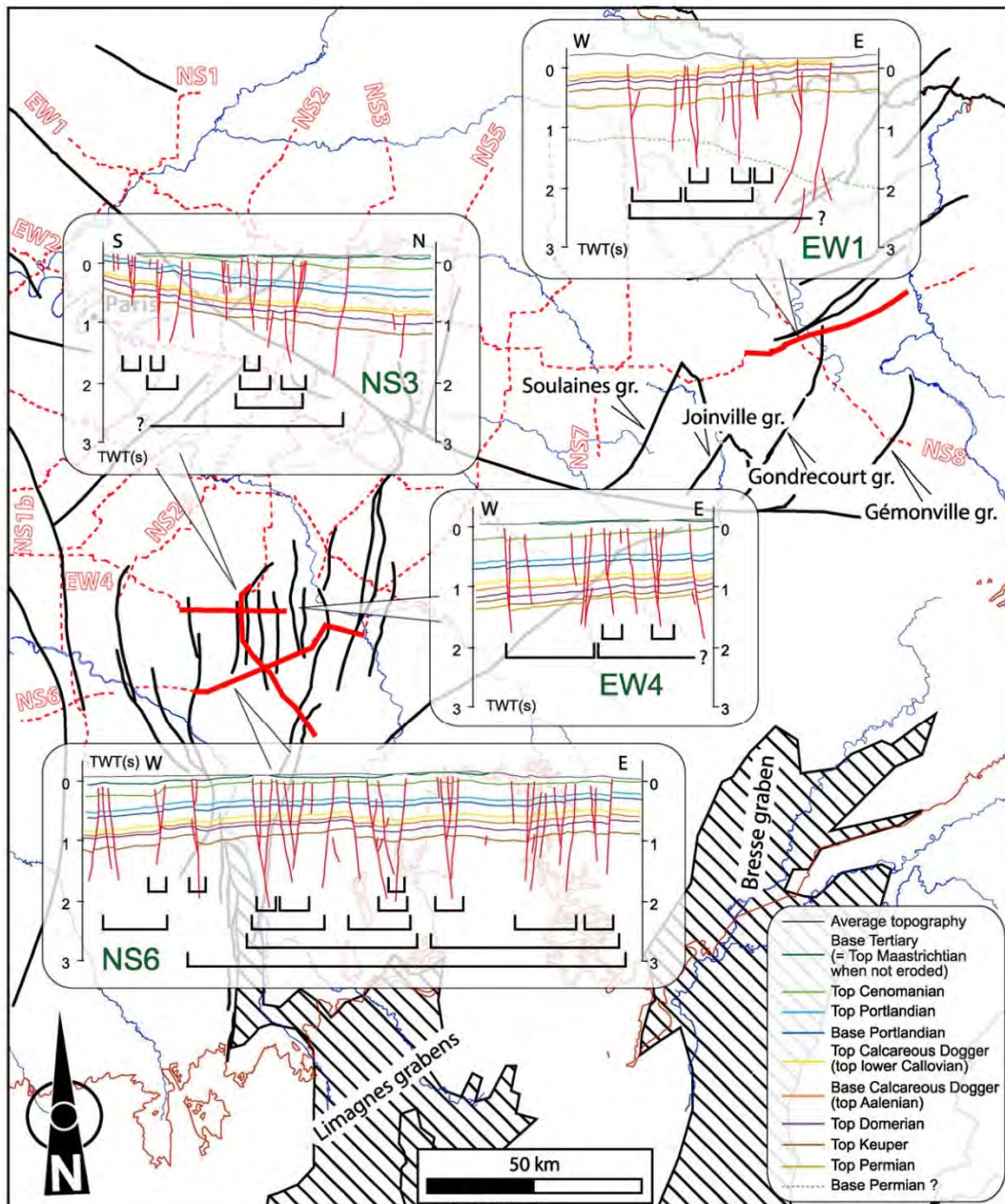


Fig. 15. Location and line drawings of the seismic lines displaying the monophase normal faults, occurring in the vicinity of the Cenozoic grabens. The strike-slip features and the related hierarchy of the structural pattern are also depicted; gr. is the abbreviation for graben. The faults are the same as in Fig. 1.

major basement faults, with at least a Variscan origin. Most of them are visible at the surface (e.g. Etampes-Rambouillet, Seine, Sennely, Bray-Vittel, and Saint-Martin-de-Bossenay faults). They represent the first order structural framework of the Paris Basin (Fig. 9). These faults were reactivated from the Permo-Carboniferous onwards, according to their original strike and in relation with the orientations of the stress regimes.

- (2) Monophase normal faults (Fig. 14B). They cross-cut the whole rock pile, from the basement up to the late Cretaceous reflectors, which are the topmost visible horizons where they occur; along each individual fault the downthrows are roughly the same.

These monophase faults are always grouped together to display the highest faults density throughout the Paris Basin, as exemplified in the southern area (Fig. 15, southern part of transect NS3 and NS6, eastern part of transect EW4), and in the eastern Paris Basin (eastern part of transect EW1).

These regions correspond to places potentially affected by the late Eocene-Oligocene rifting event (see section 2.3.5): the southern occurrence of monophase normal faults is located just north of the Limagne grabens, while the eastern occurrence is located in the area of the small Cenozoic grabens of the eastern Paris Basin (e.g. Soulaïnes, Joinville, Gondrecourt and Gémonville grabens, Fig. 15). In both cases, we interpret these structural zones as the subsurface prolongation of the outcropping graben geometries. In addition, a close view to the interpreted sections show typical transtensional strike-slip features (e.g. negative flower structures), occurring at various scales (structural hierarchy, Fig. 15). This is particularly true for the regional lines mentioned above and located in the south of the Paris Basin. In the hypothesis of a subsurface record of the Late Eocene-Oligocene graben formation, this observation strongly suggests the occurrence of a strike-slip component during their opening.

- (3) Deep sealed normal faults (Fig. 14C). They cross cut the basement of the Paris Basin and vanish in the Mesozoic sedimentary cover, most of time in the Liassic sequence. They are mainly occur south of the Bray-Vittel fault, east of the Etampes-Rambouillet fault, and west of the Saint-Martin-de-Bossenay fault, which are major late-Variscan structures (Fig. 9). Within this delimited area, their distribution is sparse. We interpret these deep sealed faults to be directly related to the long-lasting Permo-Liassic extensional tectonic regime known in the Paris Basin and surrounding areas (see section 2.3.1).

We also observe very rare cover faults, only cross-cutting the Meso-Cenozoic sedimentary cover, without any root in the basement rocks. They are most of time spatially related to the monophase faults (Fig. 15), suggesting that they belong to the same group. In that case, they are two possibilities to explain the absence of downward continuity of the faults: either the seismic resolution is not high enough to observe the vertical shift of the horizons, or the strike-slip component is much more large than the normal component, so that there is no significant vertical throw.

A direct consequence of all the previous observations is that the pre-Late Eocene-Oligocene structural pattern of the Paris Basin is similar to that observed today, except where high density monophase normal faults occur. It was chiefly characterized by a low faults density, with major faults inherited from the (late) Variscan history accommodating the vertical and strike-slip motions of the upper continental crust during the Permo-Mesozoic interval; deep sealed normal faults were locally present, but they were probably no active after the Liassic times.

6. Conclusions

The present study aims to present the methodology used by the French Geological Survey (BRGM) in the building, reprocessing and interpretation of selected regional seismic lines in the Paris Basin (France): the 14 E–W and N–S regional transects represent a total of 2,516 km length, based on the merge of 240 seismic single profiles recorded by petroleum operators between 1971 and 1995. The regional lines have been selected to cross the main oil fields of the Paris Basin, as well as high potential areas for oil exploration.

The signal reprocessing, harmonization and merge of the single seismic lines, constituent of the regional transects, represent the cornerstone of the study. We point out the decisive role of the primary static corrections, and the importance to apply specific velocity parameters to remove the strongly disturbing effects of the Tertiary sedimentary cover of the Paris Basin. In addition, modern processing methods strongly improve the quality of the seismic signal, leading to enhanced descriptions of the geological structures.

The interpreted regional transects definitely give complementary information to the existing studies, which generally lack of seismic (and therefore structural) data. They give a different image of the basin underground, with the emphasis on the lateral regional continuity of the geological information. Indeed, the density of the regional transects, added to modern reprocessing methods, make this study a step forward in the recognition of the subsurface structural framework of the Paris Basin: fault topology, inversion structures, major unconformities, as well as Permo-Carboniferous basins. For example, the Early Cretaceous and Pyrenean inversions are confirmed; the major unconformities are imaged, and the Aalenian unconformity is illustrated for the first time on a seismic section; in the same way, our study confirms the occurrence of widely distributed Permo-Carboniferous basins below the Mesozoic cover of the basin. The regional study also highlights the close relationships between the faults geometry, the faults density, and the geological evolution of the Paris Basin; the latter is characterized by a low density of faults (large-scale polyphase and deep sealed normal faults), except where the structural pattern represents the subsurface prolongation of Cenozoic grabens (e.g. Limagne area and eastern Paris Basin); in that last case, the monophase normal faults show transtensional strike-slip features, occurring at various scales.

Moreover, this modern view of the Paris Basin's underground shows the spatial relationships between the various oil fields, and has highlighted several exploration targets. In addition to academic research and oil & gas exploration, this regional work would also give an excellent frame for further studies in other topical domains (water exploration, geothermy, gas storage), by zooming in on specific locations and reinterpreting the seismic lines using a more detailed stratigraphic breakdown.

Acknowledgments

This publication was supported by the BRGM's Research, International and Public Services Divisions. The authors also would like to thank BRGM's colleagues for fruitful discussions. A special thank to the editors for their patience and support. The manuscript was improved following reviews by three anonymous reviewers; the authors wish to thank them for their helpful and constructive comments.

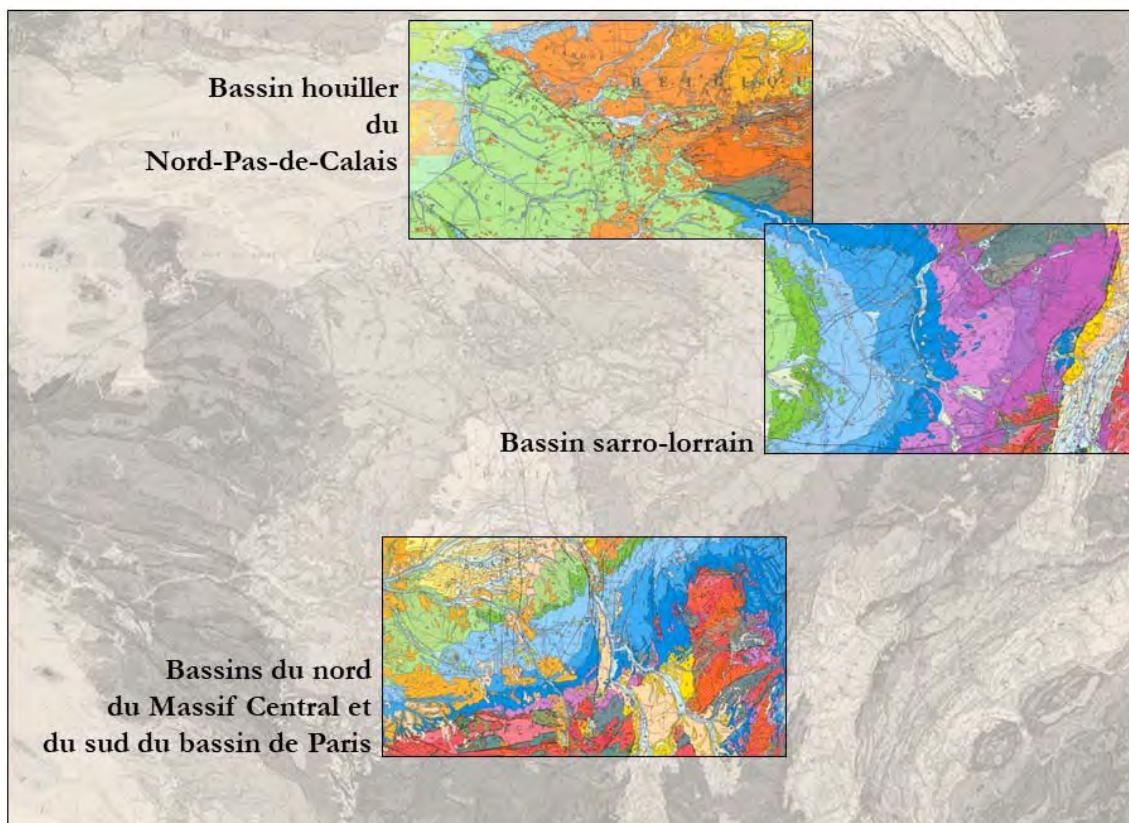
References

- Benard, F., de Charpal, O., Mascle, A., Trémoilères, P., 1985. Evidence for lower Cretaceous east-west shortening in western Europe. *Comptes Rendus des Séances de l'Académie des Sciences* 300, 765–768.

- Bergerat, F., 1987. Stress fields in the European platform at the time of Africa-Eurasia collision. *Tectonics* 6, 99–132.
- Bergerat, F., Elion, P., Frizon de Lamotte, D., Proudhon, B., Combes, P., Andre, G., Willeveau, Y., Laurent-Charvet, S., Kouradian, R., Lerouge, G., Ott d'Estevou, P., 2007. 3D multiscale structural analysis of the eastern Paris Basin; the ANDRA contribution; A multi-disciplinary approach to the eastern Jurassic border of the Paris Basin (Meuse/Haute-Marne). In: *Memoires de la Societe Geologique de France, Nouvelle Serie*, vol. 78, pp. 15–35.
- Bessereau G., Renoux P., Deville E., Ancel M., Jardin A, 1996. Paris Basin, IFP-CGG Regional Report.
- Bois, C., Cazes, M., Choukroune, P., Gariel, O., Hirn, A., Le Gall, B., Lefort, J.P., Matte, P., Pinet, B., 1994. Seismic Reflection Images of the Pre-Mesozoic Crust in France and Adjacent Areas. In: Keppie, J.D. (Ed.), *Pre-Mesozoic Geology in France and Related Areas*. Springer-Verlag, Berlin, pp. 3–48.
- Bourquin, S., Guillocheau, F., 1993. Geometry of Keuper (Ladinian to Rhaetian) depositional sequences of the Paris basin; geodynamic implications. *Comptes Rendus De L'Academie Des Sciences, Serie 2* (317), 1341–1348.
- Bourquin, S., Guillocheau, F., 1996. Keuper stratigraphic cycles in the Paris basin and comparison with cycles in other Peritethyan basins (German basin and Bresse-Jura basin). *Sedimentary Geology* 105, 159–182.
- Bourquin, S., Vairon, J., Le Strat, P., 1997. Three-dimensional evolution of the Keuper of the Paris Basin based on detailed isopach maps of the stratigraphic cycles; tectonic influences. *Geologische Rundschau* 86, 670–685.
- Brunet, M., Le Pichon, X., 1982. Subsidence of the Paris basin. *Journal of Geophysical Research* 87, 8547–8560.
- Burg, J.P., Van Den Driessche, J., Brun, J.P., 1994. Syn- to post-thickening extension in the Variscan Belt of Western Europe: modes and structural consequences. In: *Geologie De La France*, vol. 3, pp. 33–51.
- Castaing, C., Autran, A., Delpont, G., Turland, M., 1984. Evolution of different tectonic and geodynamic contexts of the Paris Basin bedrock since the Proterozoic; new hypotheses on the nature of the magnetic anomaly (Bassin de Paris). *Documents - B.R.G.M.*, 81-2, pp. 163–183.
- Cavelier, C., Megnien, C., Pomerol, D., Rat, P., 1979. Le bassin de Paris. *Bulletin D'Information Des Geologues Du Bassin De Paris* 16, 3–52.
- Cazes, M., Torrelles, G., Bois, C., Damotte, B., Galdeano, A., Hirn, A., Mascle, A., Matte, P., Van Ngoc, P., Raoult, J.F., Busson, G., 1985. Structure of the Hercynian crust of northern France; first results of the ECORS profile. *Bulletin de la Societe Geologique de France, Huitieme Serie* 1, 925–941.
- Chantraine, J., Autran, A., Cavelier, C., 2003. Carte géologique de la France au 1/100000. édition révisée. Bureau de Recherches Géologiques et Minières.
- Chungkham, P., 2009. Paris Basin offers opportunities for unconventional hydrocarbon resources. *First Break* 27, 45–52.
- Courel, L., Durand, M., Maget, P., Maiaux, C., Menillet, F., Pareyn, C., Dubois, P., Marchal, C., Yapaudjian, L., 1980. Geological Synthesis of the Paris Basin. In: *Stratigraphy and Paleogeography*, vol. 1, Mémoires du B.R.G.M., pp. 37–74.
- Curnelle, R., Dubois, P., 1986. Mesozoic evolution of large French sedimentary basins; Paris, Aquitaine, and southeastern basins. *Bulletin de la Société Géologique de France* 2, 529–546.
- Debelmas, J., 1986. Hercynian heritage of the origin of large sedimentary basins. *Bulletin des Centres de Recherches Exploration-Production Elf-Aquitaine* 10, 151–161.
- Debrand-Passard, S., 1980. Synthèse géologique du Bassin de Paris, II, Atlas. In: *Mémoires du Bureau de Recherches Géologiques et Minières*, vol. 102.
- Delmas, J., Houel, P., Vially, R., 2002. Paris Basin, Petroleum potential (IFP regional report).
- Dercourt, J., Gaetani, M., Vrielinck, B., Barrier, E., Biju-Duval, B., Brunet, M-F., Cadet, J-P., Crasquin, S. and Sandulescu M., 2000. Atlas peri-Tethys, Palaeogeographical maps CCGM/CGMM, Paris, 24 maps and explanatory notes, I-XX, 269 pp.
- Derooin, J.P., Bonin, B., 2003. Late Variscan tectonomagmatic activity in Western Europe and surrounding areas. *Bollettino Della Societa Geologica Italiana* 2, 169–184.
- Desprez, N., Labourguigne, J., Manivit, J., 1980. Evolution of principal structures of the Paris Basin from the end of the Dogger to the beginning of the Tertiary. *Bulletin d'Information des Géologues du Bassin de Paris* 17, 61–67.
- Dèzes, P., Schmid, S.M., Ziegler, P.A., 2004. Evolution of the European Cenozoic rift system: interaction of the Alpine and Pyrenean orogens with their foreland lithosphere. *Tectonophysics* 389, 1–33.
- Gély, J.-P., 1996. Le Lutétien du Bassin parisien: de l'analyse séquentielle haute résolution à la reconstitution paléogéographique. *Bulletin d'information des géologues du bassin de Paris* 34, 3–27.
- Guillocheau, F., 1991. Mesozoic large-scale transgressive-regressive cycles of tectonic origin in the Paris Basin. *Comptes Rendus de l'Académie des Sciences, Serie 2* (312), 1587–1593.
- Guillocheau, F., 1995. Nature, rank and origin of Phanerozoic sedimentary cycles. *Comptes Rendus de l'Académie des Sciences, Serie 2* (320), 1141–1157.
- Guillocheau, F., Robin, C., Allemand, P., Bourquin, S., Brault, N., Dromart, G., Friedenberg, R., Garcia, J., Gaulier, J., Gaumet, F., Grosdoy, B., Hanot, F., Le Strat, P., Mettraux, M., Nalpas, T., Prijac, C., Rigollet, C., Serrano, O., Grandjean, G., 2000. Meso-Cenozoic geodynamic evolution of the Paris Basin; 3D stratigraphic constraints. *Geodinamica Acta* 13, 189–245.
- Hancock, J. M., 1989. Sea-level changes in the British region during the Late Cretaceous. *Proceedings of the Geologists' Association*, 100/4, pp. 565–594.
- Hanot, F., 1992. Seismic applications of a Paris Basin shallow geology database. *First Break* 10, 175–188.
- Hanot, F., 2002. Plan de sauvegarde des données brutes concernant les profils sismiques terrestres enregistrés en France métropolitaine (confidential report), 55 pp.
- Hanot, F., Renoux, P., 1991. Petrophysical variations in the Senonian chalk of the Paris Basin and their influence on static corrections. *First Break* 9, 515–526.
- Hanot, F., Thiry, M., 1999. Seismic anomalies in chalk and superimposed deformation in the Tertiary formations of the southeastern Paris Basin. *Bulletin de la Société Géologique de France* 170, 915–926.
- Haq, B.U., Hardenbol, J., Vail, P.R., 1988. Mesozoic and Cenozoic chronostratigraphy and cycles of sea-level change. Sea-level changes: an integrated approach. In: *Special Publication of the Society of Economic Paleontologists and Mineralogists*, vol. 42 72–108.
- Héritier, F., Villemin, J., 1971. Evidence of deep tectonics in the Paris Basin from petroleum exploration. In: *Geologie de la France*, vol. 2, pp. 11–30.
- Lacombe, O., Obert, D., 2000. Héritage structural et déformation de couverture: plissement et fracturation tertiaires dans l'ouest du bassin de Paris. *Comptes Rendus de l'Académie des Sciences, Série 2* (330), 793–798.
- Lasseur, E., 2008. La craie du Bassin de Paris (Cénomaniens-Campanien, Crétacé supérieur); sédimentologie de faciès, stratigraphie séquentielle et géométrie 3D. In: *Mémoires de Géosciences Rennes*, vol. 129.
- Lasseur, E., Guillocheau, F., Robin, C., Hanot, F., Vaslet, D., Coueffe, R., Neraudeau, D., 2009. A relative water-depth model for the Normandy Chalk (Cenomanian-Middle Coniacian, Paris Basin, France) based on facies patterns of metre-scale cycles. *Sedimentary Geology* 213, 1–26.
- Le Roux, J., 2000. Structure of the northeastern Paris basin. *Bulletin d'Information des Géologues du Bassin de Paris* 37, 13–34.
- Le Solliez, A., Doin, M.P., Robin, C., Guillocheau, F., 2004. From a mountain belt collapse to a sedimentary basin development; 2-D thermal model based on inversion of stratigraphic data in the Paris Basin. *Tectonophysics* 386, 1–27.
- Loup, B., Wildi, W., 1994. Subsidence in the Paris Basin: a key to Northwest European intracratonic basins? *Basin Research* 6, 159–177.
- Lorenz, C., 1984. Manifestations tectoniques intrastampiennes dans le sud du Bassin de Paris. *Bulletin d'Information Des Géologues Du Bassin De Paris* 21, 89–91.
- Lorenz, C., 1992. Large deformations of the sedimentary cover in the west and southwest of the Paris Basin; their contribution to the understanding of the structure of the basement. *Bulletin d'Information des Géologues du Bassin de Paris* 29, 5–17.
- Lorenz, V., Nicholls, I.A., 1984. Plate and intraplate processes of Hercynian Europe during the late Paleozoic. *Tectonophysics* 107 (1–2), 25–56.
- Mascle, A., 1990. Petroleum geology of French Permian basins; comparison with the Permian basins of northern Europe. In: *Chronique De La Recherche Minière*, vol. 499, pp. 69–86.
- Mascle, A., Cazes, M., 1987. La couverture sédimentaire du bassin parisien le long du profil ECORS-Nord de la France. In: *Revue de l'Institut Français du Pétrole*, vol. 42, pp. 303–316.
- Maury, R.C., Varet, J., Autran, A., Dercourt, J., 1980. Tertiary and Quaternary volcanism in France. In: *Mémoires du B.R.G.M.*, vol.107, pp. 137–159.
- Mégénien, C., 1980. Synthèse géologique du Bassin de Paris, I, Stratigraphie et paléogéographie. In: *Mémoires du Bureau de Recherches Géologiques et Minières*, vol. 101, 466 pp.
- Mégénien, C., Cogne, J., Slansky, M., 1980. Tectogenesis of the Paris Basin; stages in evolution of the basin. In *Geology of Europe, from Precambrian to the post-Hercynian sedimentary basins*. In: *Mémoires du B.R.G.M.*, vol. 108, 295 pp.
- Montadert, L., Roberts, D. G., De Charpal, O., Guennoc, P., Montadert, L., Roberts, D. G., Auffret, G. A., Bock, W. D., Dupeuble, P. A., Hailwood, E. A., Harrison, W. E., Kagami, H., Lumsden, D. N., Muller, C. M., Schnitker, D., Thompson, R. W., Thompson, T. L., Timofeev, P. P., 1979. Rifting and subsidence of the northern continental margin of the Bay of Biscay: initial reports of the deep Sea drilling project covering Leg 48 of the cruises of the drilling Vessel Glomar Challenger, Initial Reports of the Deep Sea Drilling Project, 48, pp. 1025–1060.
- Odin, G.S., 1994. Geological time-scale. *Comptes Rendus de l'Académie des Sciences, Série 2* (318), 59–71.
- Olivet, J.L., 1996. La cinématique de la plaque ibérique. *Bulletin des Centres de Recherche et d'Exploration-Production d'Elf Aquitaine* 20, 131–195.
- Perridon, A., Zabeck, J., 1990. Paris Basin: Interior cratonic basins. In: *AAPG Memoir*, vol. 51 633–679.
- Pomerol, C., 1978. Paleogeographic and structural evolution of the Paris Basin, during the Precambrian to the present day, in relation to neighboring regions. *Geologie En Mijnbouw Journal of Geosciences* 57, 533–543.
- Prijac, C., Doin, M.P., Gaulier, J.M., Guillocheau, F., 2000. Subsidence of the Paris Basin and its bearing on the late Variscan lithosphere evolution; a comparison between plate and CHABLIS models. *Tectonophysics* 323, 1–38.
- Robaszynski, F., 1981. Moderation of Cretaceous transgressions by block tectonics; an example from the north and north-west of the Paris Basin. *Cretaceous Research* 2, 197–213.
- Robin, C., 1997. Stratigraphic measurement of deformation; application to Jurassic evolution of the Paris Basin. In: *Mémoire de Géosciences Rennes*, vol. 77, 293 pp.
- Robin, C., Guillocheau, F., Gaulier, J.M., 1996. Mesure des signaux eustatiques et tectoniques au sein de l'enregistrement sédimentaire d'un bassin intracratonique; application au Lias du Bassin de Paris. Measurement of tectonic and eustatic signals from stratigraphic information within an intracratonic basin; application to the Lower Jurassic of the Paris Basin. *Comptes Rendus De L'Académie Des Sciences* 322, 1079–1086.
- Robin, C., Guillocheau, F., Allemand, P., Bourquin, S., Dromart, G., Gaulier, J., Prijac, C., 2000. Time and space scales of tectonic control on a flexural intracratonic basin; the Paris Basin. *Bulletin de la Societe Géologique de France* 171, 181–196.

3. Volet 2 - Les bassins carbonifères-permiens sous couverture sédimentaire méso-cénozoïque

De la transition syn- à post-orogénique varisque
aux usages du sous-sol



3.1. Problématique générale

Les bassins sédimentaires continentaux à remplissage silicoclastique d'âge Carbonifère-Permien (syn- à post-orogéniques varisques) constituent un ensemble géologique hétérogène à l'échelle du territoire métropolitain. « Présents partout mais peu visibles », leur extension et épaisseur sous couverture méso-cénozoïque est généralement considérable - en tout cas bien plus importante que celle connue localement à l'affleurement: par exemple trois km d'épaisseur dans la région Centre Val-de-Loire et plus de huit km en Lorraine.

Les études que je mène actuellement au BRGM sont motivées par la double volonté :

- De rattraper le retard pris en France sur la connaissance géologique de ces bassins finipaléozoïques (localisation sous couverture, profondeur, épaisseur, style structural, mode de remplissage, calage temporel, contexte géodynamique...), les dernières synthèses scientifiques sur ces bassins datant des années 1980-90 (Donsimoni, 1981 ; Becq-Giraudon, 1983 ; Donsimoni, 1990). Les données de subsurface (sismique industrielle retraitée, forages...) et les moyens analytiques désormais disponibles, nouveaux ou dont la sensibilité a considérablement augmenté (datations radiochronologiques, minéralogie RX des argiles, isotopes stables du carbone et de l'azote, caractérisation de la matière organique...) permettent d'accroître sensiblement cette connaissance.
- De réfléchir en terme de ressources potentielles et promouvoir leur mise en œuvre (e.g. géothermie, hélium naturel).

Mes travaux ont principalement concerné les trois grands bassins carbonifères-permiens connus en subsurface sur le territoire métropolitain, chacun enregistrant une période clé de l'orogène varisque : le bassin houiller du Nord-Pas-de-Calais (phase syn-orogénique), le bassin sarro-lorrain (transition syn- à post-orogénique en position retro-wedge), et les bassins du sud du bassin de Paris et du nord du Massif Central (phase post-orogénique). Pour chaque cas d'étude, l'objectif est de déterminer la géométrie des remplissages sédimentaires, de relier la sédimentation aux structures imagées, pour in fine comprendre les mécanismes de la déformation régionale et la replacer dans le contexte de l'évolution finale de l'orogène varisque.

Les résultats issus de mes travaux sur ces trois bassins sont présentés ci-après, à la suite d'une brève introduction sur leur contexte géodynamique interne et externe et leur localisation en France et en Europe occidentale.

3.2. Les BCP en France métropolitaine et en Europe de l'ouest - cadre géodynamique interne et externe

3.2.1. Contexte géodynamique interne : la chaîne varisque d'Europe occidentale

Il n'est pas ici question de retracer l'histoire géologique varisque dans son ensemble, de discuter du calendrier des déformations, des phénomènes magmatiques et métamorphiques en jeu, du nombre de domaines océaniques et terranes impliqués lors de cette orogène majeure ; le lecteur est renvoyé aux nombreuses publications traitant du sujet (e.g. Matte, 1986, 2001; Van Raumer et al., 2003 ; Ballèvre et al., 2009, 2014; Franke et al., 2017, Martinez-Catalan et al., 2020).

J'apporterai seulement quelques éléments de compréhension sur la phase orogénique varisque s.s. (340-305 Ma) puis sur les déformations tardi-varisques, afin de replacer les bassins sur lesquels je travaille dans leur contexte général (Figure 5).

La phase orogénique varisque sensu stricto (340-305 Ma)

Du Dévonien au Mississippien la convergence N-S entre le continent Laurussia au nord et les microplaques Armorica-Saxo-Thuringia au sud entraîne la fermeture progressive de l'océan rhéno-hercynien par subduction vers le sud de la marge sud de Laurussia (i.e. Avalonia) sous les microplaques armoricaine et saxo-thuringienne (Cazes et al., 1985; Plesch et Oncken, 1999; Golonka, 2002 ; Averbuch et Piromallo, 2012; Golonka et Gaweda, 2012; Franke et al., 2017). Cette convergence a abouti à la collision de Laurussia et du complexe d'accrétion de Gondwana, Armorica et Saxo-Thuringia à partir du Viséen moyen (340 Ma) (e.g. Schulmann et al., 2002 ; Guillot et al., 2020). Cette deuxième phase de collision, aussi appelée phase asturienne ou phase majeure de l'orogénèse varisque, s'est poursuivie jusqu'à la transition Westphalien-Stéphanien. Elle est à l'origine de l'inversion tectonique de l'ensemble de la marge sud-laurussienne (dont fait partie la plate-forme carbonatée dinantienne discutée par la suite) et de l'écaillage progressif du bassin océanique rhéno-hercynien, aboutissant à la mise en place d'un second système de plis et de chevauchements (le premier système datant de la phase éovarisque au Dévonien), cette fois à vergence nord, dans la partie nord de la chaîne varisque, du Mississippien supérieur (Viséen) au Pennsylvanien moyen (Westphalien) (Cazes et al., 1985; Fielitz et Mansy, 1999; Plesch et Oncken, 1999; Franke, 2000; Oncken et al., 2000). Cette phase de collision finale et de surépaississement crustal s'accompagne d'un important magmatisme granitique et dioritique dans les zones internes de la chaîne (Henk et al., 2000 ; Timmerman, 2004), caractérisé localement par la présence de magmas ultra-potassiques et magnésiens typique d'une importante fusion partielle du manteau lithosphérique (vaugnérîtes; van Raumer et al., 2014, Guillot et al., 2020).

Les bassins syn-orogéniques d'avant-pays (molasse varisque) se développent au front de la chaîne avant d'être en partie incorporés dans les unités chevauchantes (**Laurent et al., 2021 ; Figure 6). La double subduction continentale de Gondwana (phase éovarisque) et Laurussia, accompagnée du développement de deux prismes d'accrétion crustaux diachrones, sont ainsi à l'origine de l'épaississement lithosphérique et de la surrection de la chaîne varisque.

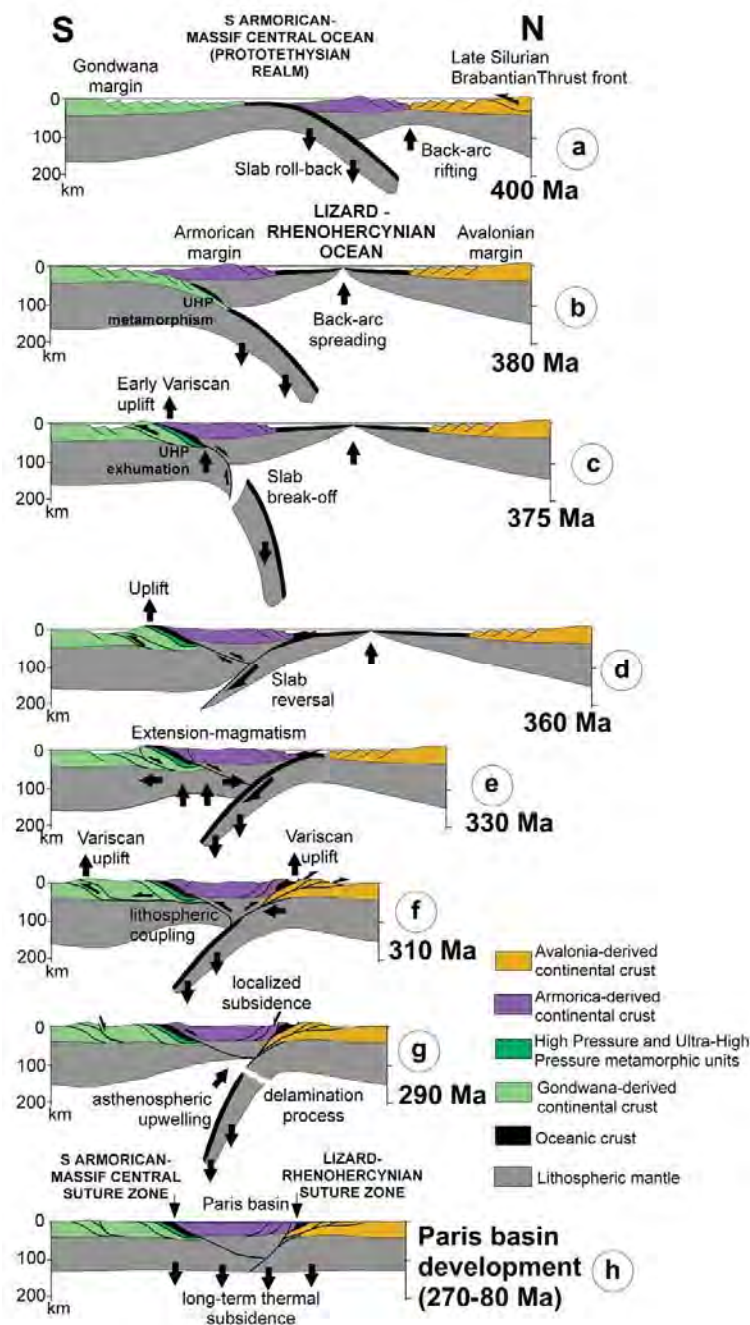


Figure 5 - Evolution géodynamique varisque selon Averbuch et Piromallo (2012), depuis la phase éovarisque (c) jusqu'à la phase post-varisque et l'initiation du bassin de Paris (g, h).

Déformations tardi-varisques (305-270 Ma)

Au Pennsylvanien supérieur (Stéphanien)-Permien, l'ensemble de la chaîne varisque est affecté par des déformations dites tardi-varisques. Elles sont contemporaines du réajustement thermique (métamorphisme de HT et magmatisme) et du rééquilibrage isostatique de la lithosphère, associés à l'effondrement de l'orogène (e.g. Ménard et Molnar, 1988; Malavieille et al., 1990; Burg et al., 1994 ; Figure 6). L'origine précise de cette évolution tardive de la chaîne reste encore débattue au sein de la communauté scientifique, mais les modèles les plus récents considèrent qu'elle se développe en lien avec la déstabilisation et le détachement de la racine orogénique varisque *via* le

processus de délamination lithosphérique tardi-orogénique (Lorenz et Nicholls, 1984; Schott et Schmeling, 1998; Henk et al., 2000; Arnold et al., 2001; Finger et al., 2009; Averbuch et Piromallo, 2012; Laurent et al., 2017; Guillot et al., 2020; Vanderhaeghe et al., 2020). Au sein des unités varisques, elle se matérialise par le développement de nombreux détachements syn-métamorphes (HT) ou syn-magmatiques (Burg et al., 1994; Costa et Rey, 1995; Faure, 1995; Gapais et al., 2015 ; Gardien et al., 2022), d'une intense fracturation en extension et subsidence du substratum paléozoïque induisant la formation d'épais bassin intra-montagneux à remplissage continental (e.g. Echtler et Malavieille, 1990; Henk, 1993, 1999; Allemand et al., 1997; Pochat et Van Den Driessche, 2011; *Beccaletto et al., 2015 ; Ballèvre et al., 2018 ; Saspiturry et al., 2019 ; **Mercuzot et al., 2021, 2022), et de la formation de décrochements de taille et d'orientation variables selon les régions (N20-40°, e.g. le Sillon Houiller ; N110-130°, e.g. les cisaillements armoricains ; N160°, e.g. la faille d'Argentat ; Arthaud et Matte, 1975, 1977 ; Matte, 1986 ; Ziegler, 1990).

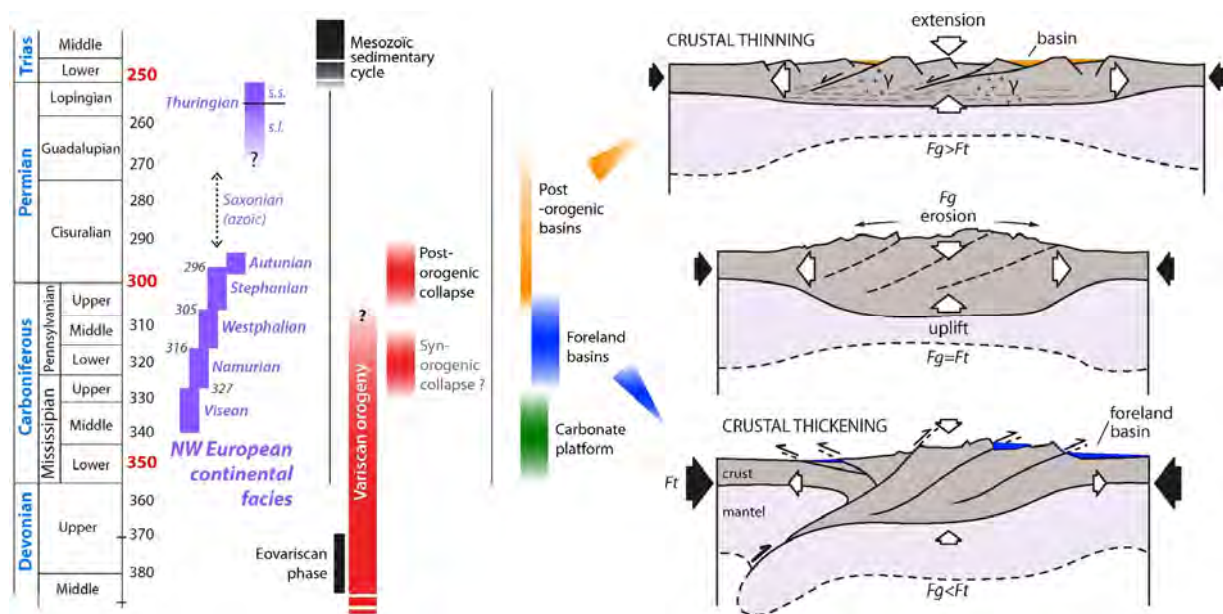


Figure 6 - Cadre temporel et processus de mise en place des bassins carbonifères-permiens (coupes lithosphériques modifiées par M. Mercuzot et moi-même de Malavieille, 1993).

Le magmatisme dérivé de la fusion partielle du manteau présente localement une contamination crustale notable (Bonin, 1990 ; Bonin et al., 1993 ; Neumann et al., 2004). Les produits magmatiques sont mafiques à felsiques et présentent des caractéristiques distinctes du domaine orogénique au domaine anorogénique, avec une tendance générale allant du mafique en Europe septentrionale au felsique en Europe occidentale et méridionale (Timmerman, 2004). Les roches ignées permienne sont principalement alcalines dans les zones externes et calco-alcalines à alcalines dans les zones internes (Spillmann et Büchi, 1993; Bonin et al., 1998). Des plutons mafiques permienne d'affinité tholéïtite sont également présents dans tous les niveaux crustaux (Vielzeuf et Pin, 1989; Hermann, 1997; Monjoie et al., 2007; Tribuzio et al., 2009, 1999).

La cinématique de déformation de ces systèmes de faille tardi-varisque (réseau de failles normales et décrochantes) a fait l'objet d'études détaillées dans nombres de régions de la chaîne varisque: en Grande-Bretagne (Hibsch et al., 1993; Shail et Alexander, 1997), dans le Boulonnais (Averbuch et al., 2001), en Lorraine-Sarre (Donsimoni, 1981; Stollhofen, 1998), dans le Massif

Central (Bonijoly et Castaing, 1984; Vallé et al., 1988, Faure, 1995 ; Figure 7), dans les Alpes occidentales (Handy et al., 1999), dans le sud de la France (Soula, 1984; Genna et Debriette, 1994). Elles suggèrent une tectonique tardi-varisque majoritairement extensive et transtensive, associée à une extension NNW-SSE et une compression ENE-WSW.

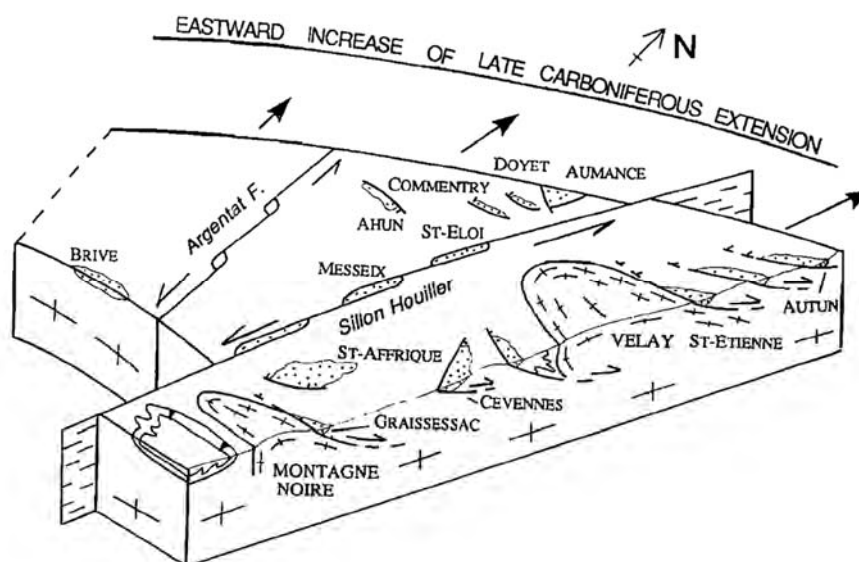


Figure 7 - Proposition schématique de différents modes de mise en place des bassins Stéphanien-Permien inférieur en France (Faure, 1995).

3.2.2. Contexte géodynamique externe - Transition icehouse - greenhouse

La période Carbonifère-Permien témoigne, au-delà du contexte géodynamique interne complexe décrit ci-dessus, d'un changement climatique majeur : les archives sédimentaires et géochimiques enregistrent la plus récente transition d'un climat de type icehouse (avec de la glace pérenne aux pôles) à un climat greenhouse (sans calotte glaciaire pérenne) (Figure 8). Cette ère glaciaire, connue sous le nom de Late Paleozoic Ice Age (LPIA), constitue la plus longue phase de glaciation du Phanérozoïque. S'étendant sur 50 à 90 Ma selon les études (Bishop et al., 2010; Montañez et Poulsen, 2013), cette transition s'amorce dès la fin du Dévonien, atteint son apogée durant la fin du Carbonifère-début du Permien (e.g. Fielding et al., 2008; Montañez et Poulsen, 2013), et connaît ses dernières pulsations à la fin du Permien moyen (260 Ma, Fielding et al., 2008).

Cette perturbation climatique est le seul témoin ancien d'une glaciation qui se produit dans des conditions d'une Terre végétalisée (Gastaldo et al., 1996), avec le développement de grandes forêts en zone intertropicale, et n'ayant jamais eu d'analogie comparable en termes d'étendue et de fonctionnement au cours du Phanérozoïque (Cleal et Thomas, 2005).

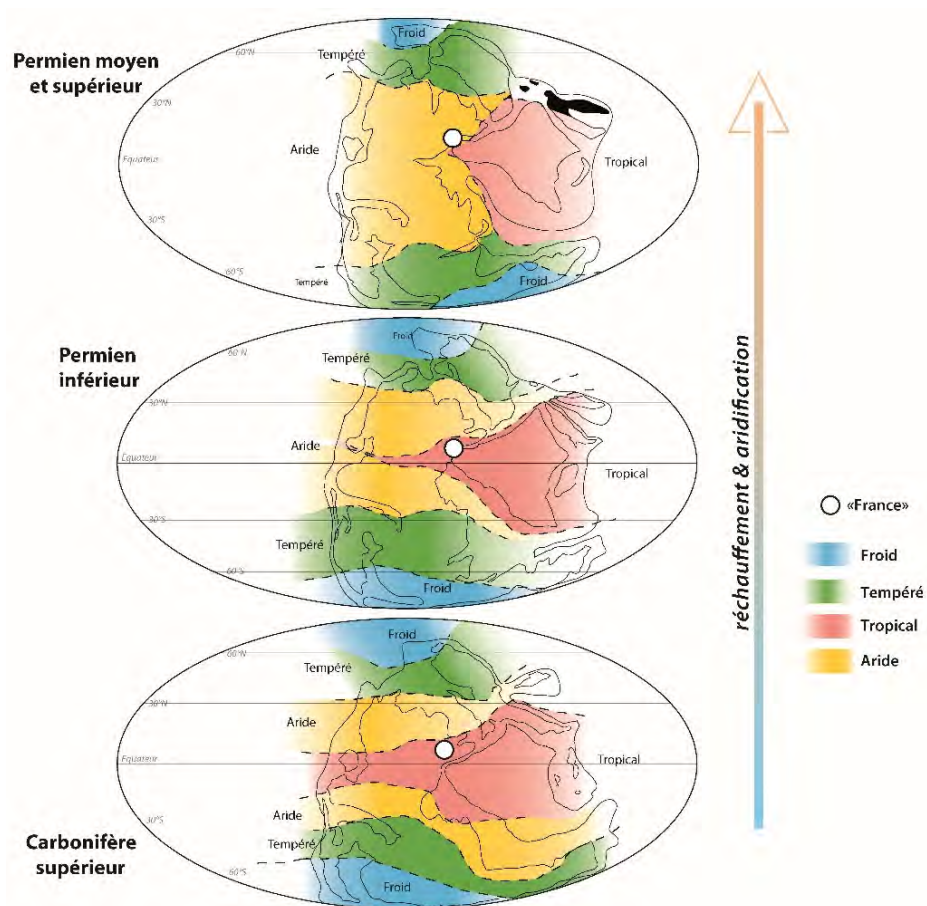


Figure 8 - LPLA et transition icebouse-greenhouse à la fin du Paléozoïque (modifié par M. Mercuzot et moi-même de Scotese, 2002).

3.3. Les bassins carbonifères-permiens en France et en Europe occidentale

Cette section présente des généralités sur la localisation, les modes de subsidence et les épaisseurs préservées des séries sédimentaires déposées en contexte syn-orogénique (i.e. molassique) et post-orogénique varisque.

3.3.1. Les bassins syn-orogéniques westphaliens

Les bassins carbonifères syn-orogéniques varisques (namuriens-westphaliens²) sont principalement connus en subsurface dans les pays d'Europe occidentale et du nord (France, Royaume Uni, Belgique, Pays-Bas, Danemark, Allemagne, Pologne), au nord du front nord varisque (Figure 9 ; Ziegler, 1990 ; Doornenbal et Stevenson, 2010). Les faciès silicoclastiques fluvio-lacustres à deltaïques, riches en charbon, se déposent en domaine continental (présence de rares incursions marines) sous l'effet de la subsidence tectonique au front nord de la chaîne. Les séries syn-orogéniques peuvent atteindre plus de trois km d'épaisseurs à proximité du front

² Pour les attributions d'âge, j'utiliserai indifféremment la nomenclature ouest-européenne et celle de l'International Chronostratigraphic Chart (Cohen et al., 2013) ; voir la Figure 6 pour la correspondance entre les deux.

de chaine (Becq-Giraudon, 1983; Delmer et al., 2001, **Laurent et al., 2021), et sont réduites à quelques centaines de mètres plus au nord (Doornenbal et Stevenson, 2010). Ces faciès sont distincts des faciès orogéniques de type flysch à wildflysch (environnements marins) connus par exemple dans le Massif Rhénan en Allemagne ou la Montagne Noire dans le sud de la France, qui leur sont antérieurs (Mississipien ; Aretz, 2016).

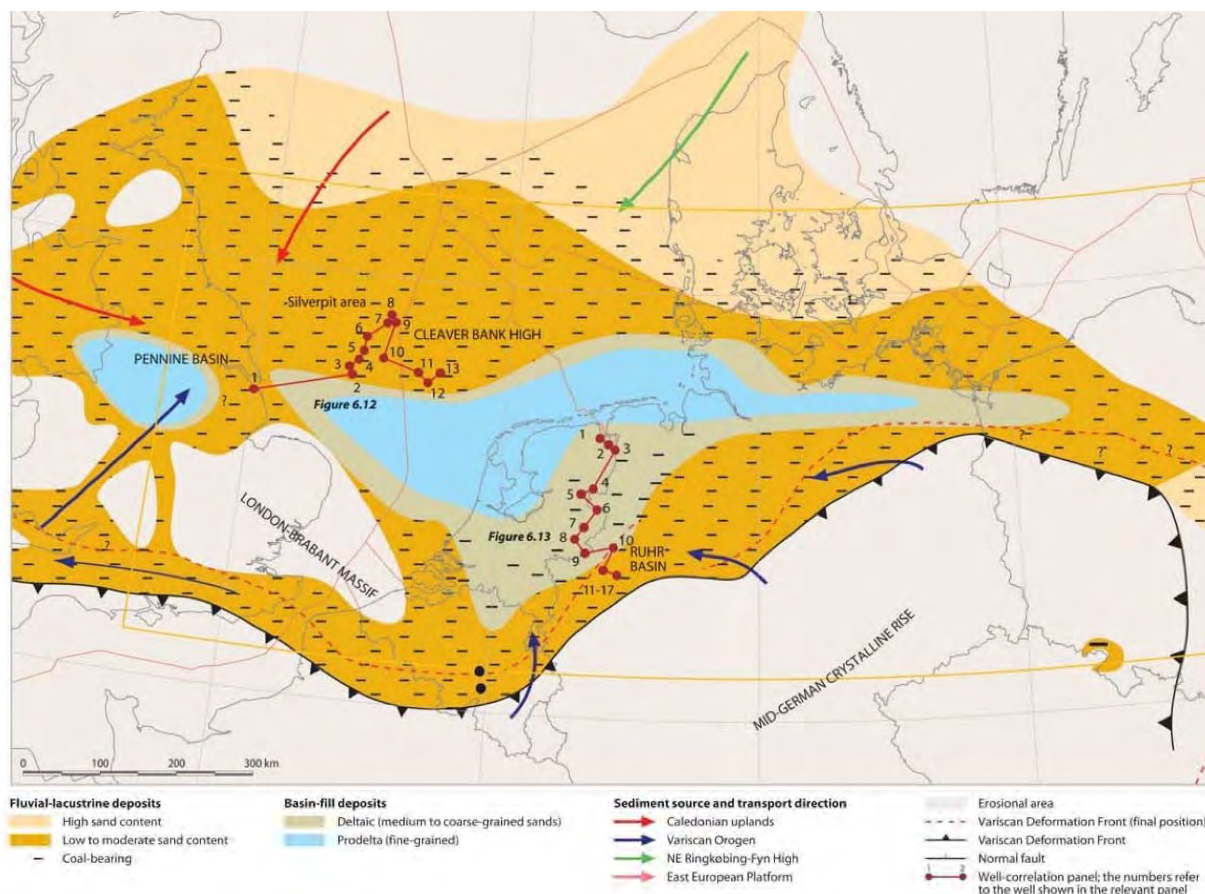


Figure 9 - Localisation actuelle des bassins syn-orogéniques varisques westphaliens (Doornenbal et Stevenson, 2010).

3.3.2. Les bassins post-orogéniques stéphano-permiens

Les bassins carbonifères-permiens post-varisques (ou tardi-varisques) affleurent au sud du front nord varisque en plusieurs endroits limités dans et autour le substratum métamorphique/magmatique varisque de l'Europe occidentale et centrale : Massif Central (France), Vosges-Forêt Noire (France, Allemagne), Pyrénées (France, Espagne), Alpes (France, Suisse), Harz (Allemagne), Massif de Bohême (République Tchèque) ; ils se trouvent à proximité des principales structures tectoniques varisques (e.g. Sillon Houiller, failles des Cévennes ; Figure 10)³. En carte, ils se présentent comme des "bassins" isolés de faible extension, déconnectés les uns des autres, dont les successions sédimentaires montrent de nombreuses lacunes de sédimentation et d'érosion. En effet, leur superficie actuelle ne reflète pas leur étendue et leur épaisseur initiales,

³ Le Northern Permian Basin et le Southern Permian Basin d'Europe du nord ne seront pas discutés ici. Ces bassins non présents en France enregistrent une histoire Permien supérieur (Rotliegend et Zeichstein), non *directement* liée à l'orogène varisque (Glennie et al., 2003 ; Doornenbal et Stevenson, 2010).

qui peuvent être explorées en étudiant leur prolongement en subsurface sous les couvertures sédimentaires méso-cénozoïques (Ziegler, 1990 ; *Beccaletto et al., 2015 ; Schneider et Scholze, 2018 ; **Mercuzot et al., 2021 ; cf. section 3.6). Sous couverture, les épaisseurs atteignent plusieurs centaines de mètres à plusieurs kilomètres, comme dans le sud du Massif Central (e.g. Lodève, Carmaux - La Grésine) ou dans le NO de l'Europe (e.g. Saar-Nahe et Thuringian Forest; Schneider et Romer, 2011).

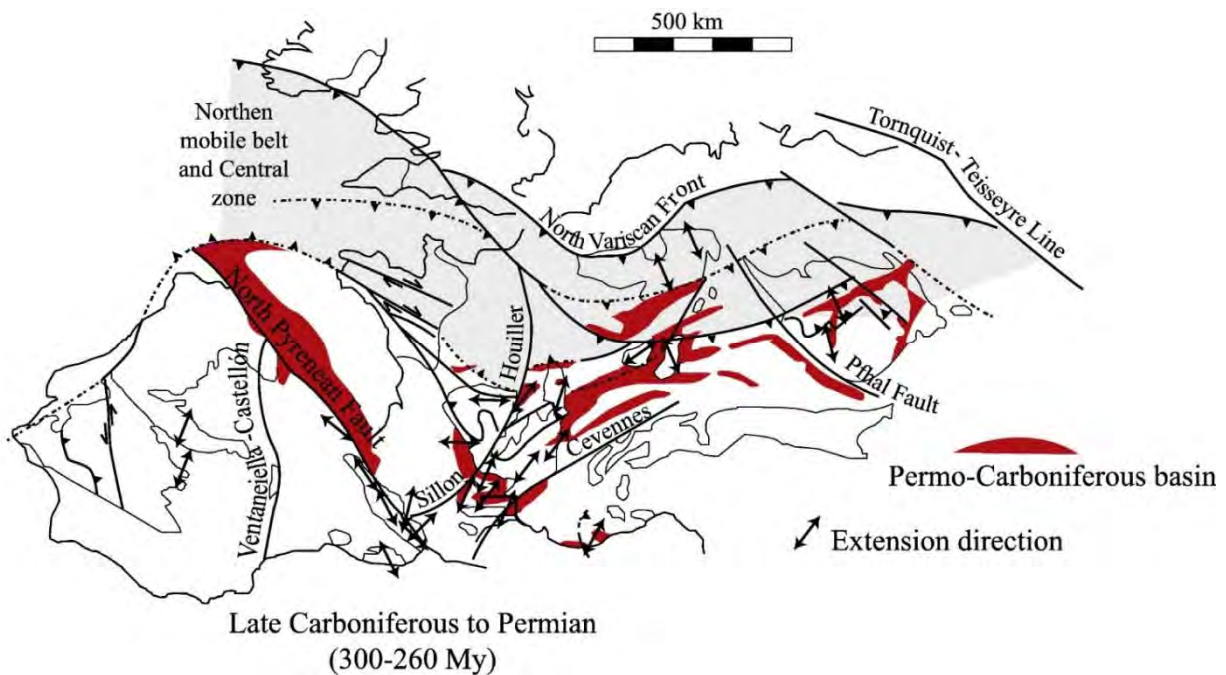


Figure 10 - Localisation des bassins post-orogéniques varisques vers 300 Ma (Pochat et Van den Driessche, 2011).

3.3.3. Localisation et âge des bassins carbonifères-permiens en Europe

Cette section, qui se veut purement descriptive, se présente sous la forme de deux cartes et deux tableaux de synthèse qui permettent de se faire une idée de la localisation et des âges et lithologies des bassins carbonifères-permiens en Europe :

- La carte de la Figure 11 localise à l'échelle de l'Europe occidentale les bassins syn- et post-orogéniques à l'affleurement sur un fond de carte tectonique simplifié de l'Europe (Oplustil et Schneider, 2023).
- Le tableau de la Figure 12 présente les intervalles de dépôt de quelques bassin syn-orogéniques varisque en Europe et en France (Oplustil et Schneider, 2023).
- Le tableau de la Figure 13 présente les intervalles de dépôt de quelques bassin post-orogéniques varisque en Europe et en France (Oplustil et Schneider, 2023).
- Enfin, j'ai initiée il y a quelques années une carte de synthèse des bassins carbonifères-permiens en France classés par âge (Figure 14). Il s'agit d'une carte à l'échelle du 1/000000^{ème} regroupant les bassins connus à l'affleurement issus de la carte géologique de la France au 1/000000^{ème} du BRGM (BRGM, 2003), avec ceux identifiés en subsurface (BRGM, 1984 ; BRGM, 1989 ; Delmas et al., 2002; Beccaletto et al., 2015).

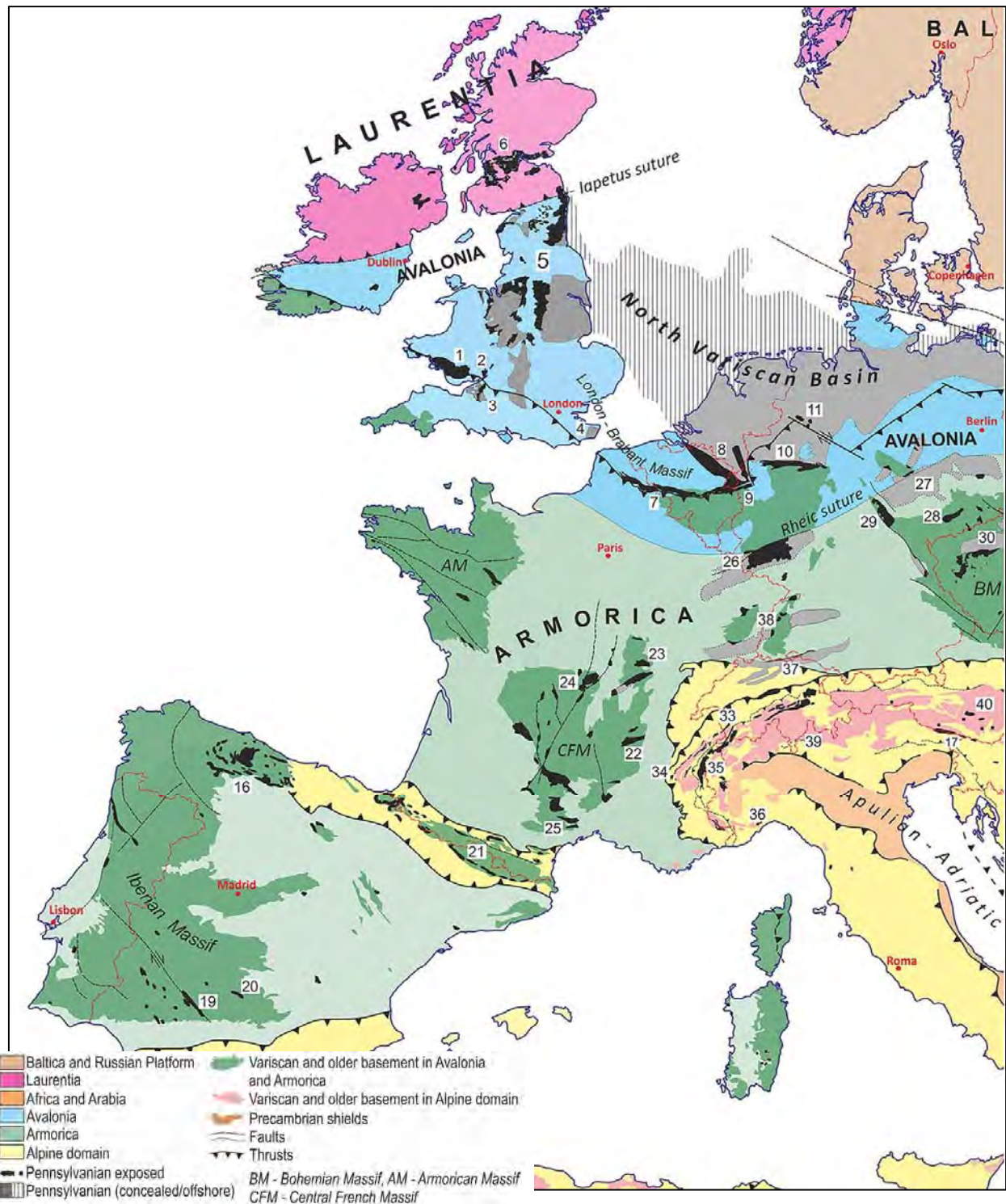


Figure 11 - Carte tectonique simplifiée de l'Europe occidentale montrant la localisation des principaux bassins syn- et post-varisques en surface (resp. au nord et au sud du front nord varisque) et les principales structures tectoniques (Oplustil et Schneider, 2023). 1, South Wales; 2, Forest of Dean; 3, Bristol–Somerset; 4, Kent; 5, Pennine; 6, Midland Valley of Scotland; 7, Nord et Pas-de-Calais + Namur Synclinorium; 8, Campine; 9, Aachen; 10, Rubr; 11, Ibbenbüren et Piesberg; 16, NW Spain (Cantabrian Mountains); 17, Carnic et Karawanke Alps; 19, Peñarroya; 20, Puertollano; 21, Pyrenees; 22, Saint Étienne; 23, Autun; 24, Commeny; 25, Graissessac–Lodève; 26, Lorraine–Saar–Nabe; 27, Saale; 28, Erzgebirge (Flöha + Zwickau); 29, Thüringian Forest. 30, Pilsen–Trutnov Basin Complex – western part (e.g. Kladno–Rakovník, Radnice et Pilsen basins); 33, Salvan–Doréna; 34, La Mûre; 35, Briançon; 36, Ollano; 37, North Switzerland; 38, Schwarzwald (Oppenau, Geroldseck, Baden-Baden, Breisgau, Schramberg); 39, Val Sanagra (Como, Ticino), 40, Gurktal.

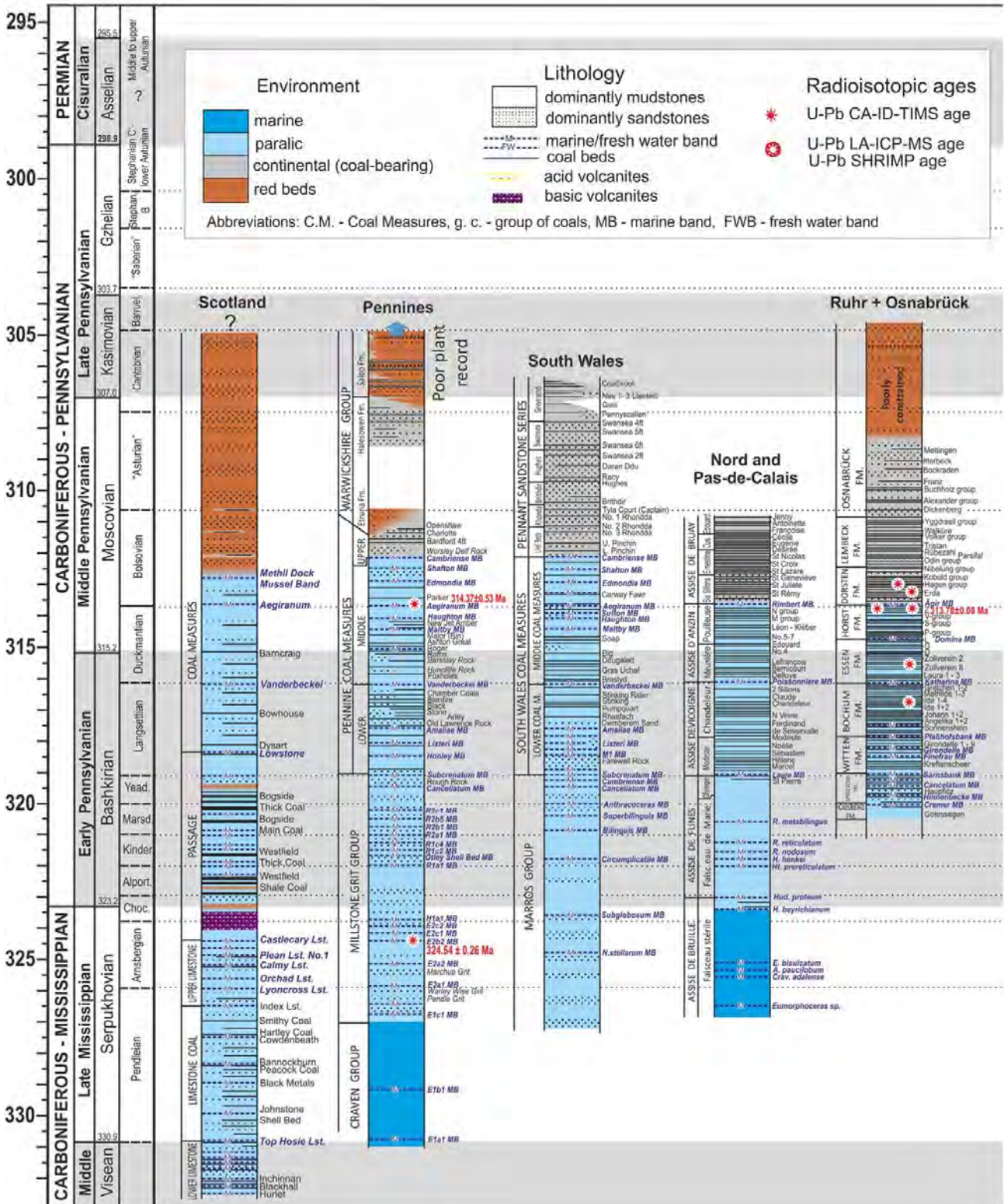


Figure 12 - Intervalle de dépôt et lithologies simplifiées de quelques bassins syn-varisques français et européens (Oplustil et Schneider, 2023).

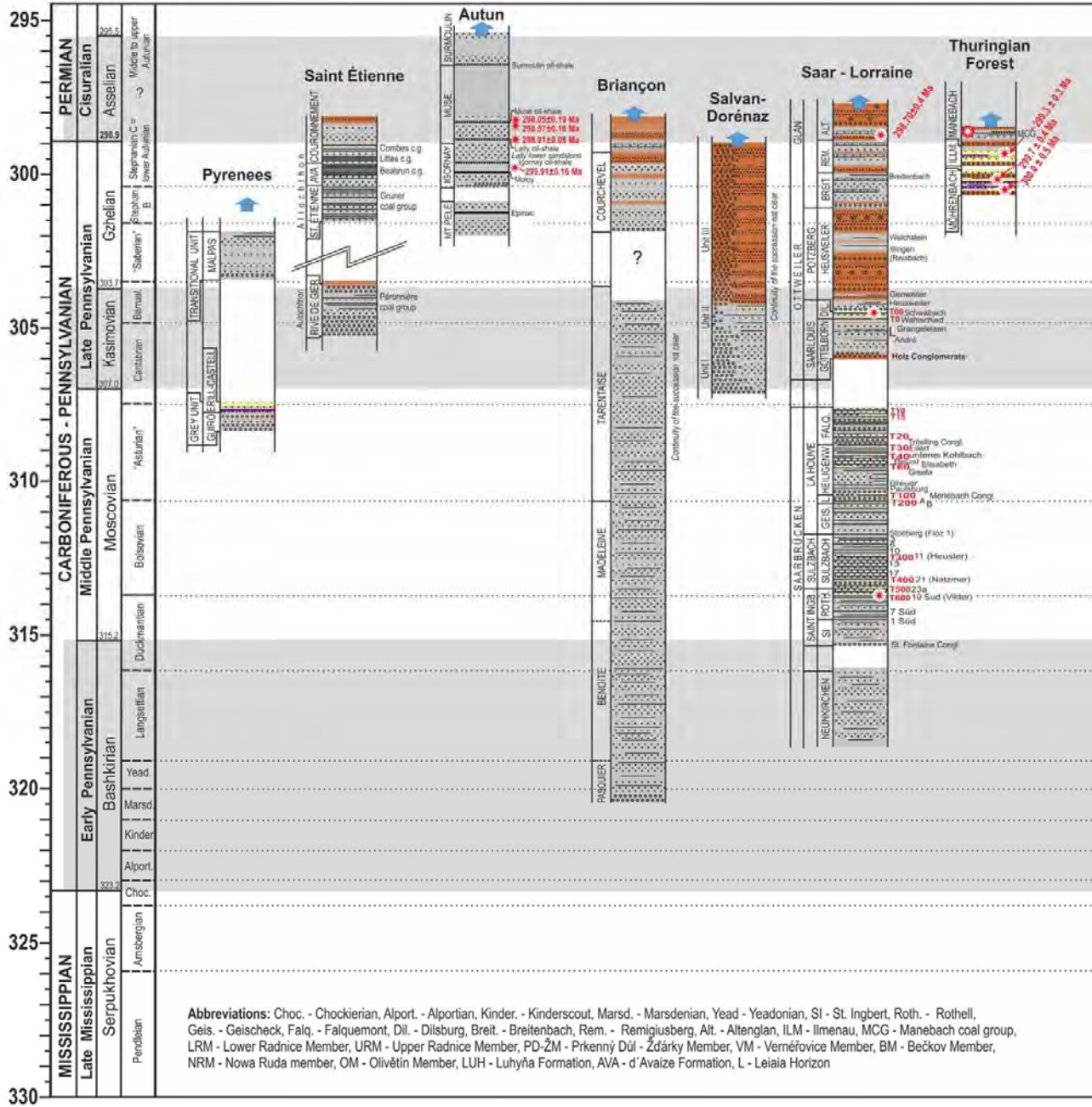


Figure 13 - Intervalle de dépôt et lithologies simplifiées de quelques bassin post-varisques français et européens (Oplustil et Schneider, 2023) ; même légende que Figure 13.

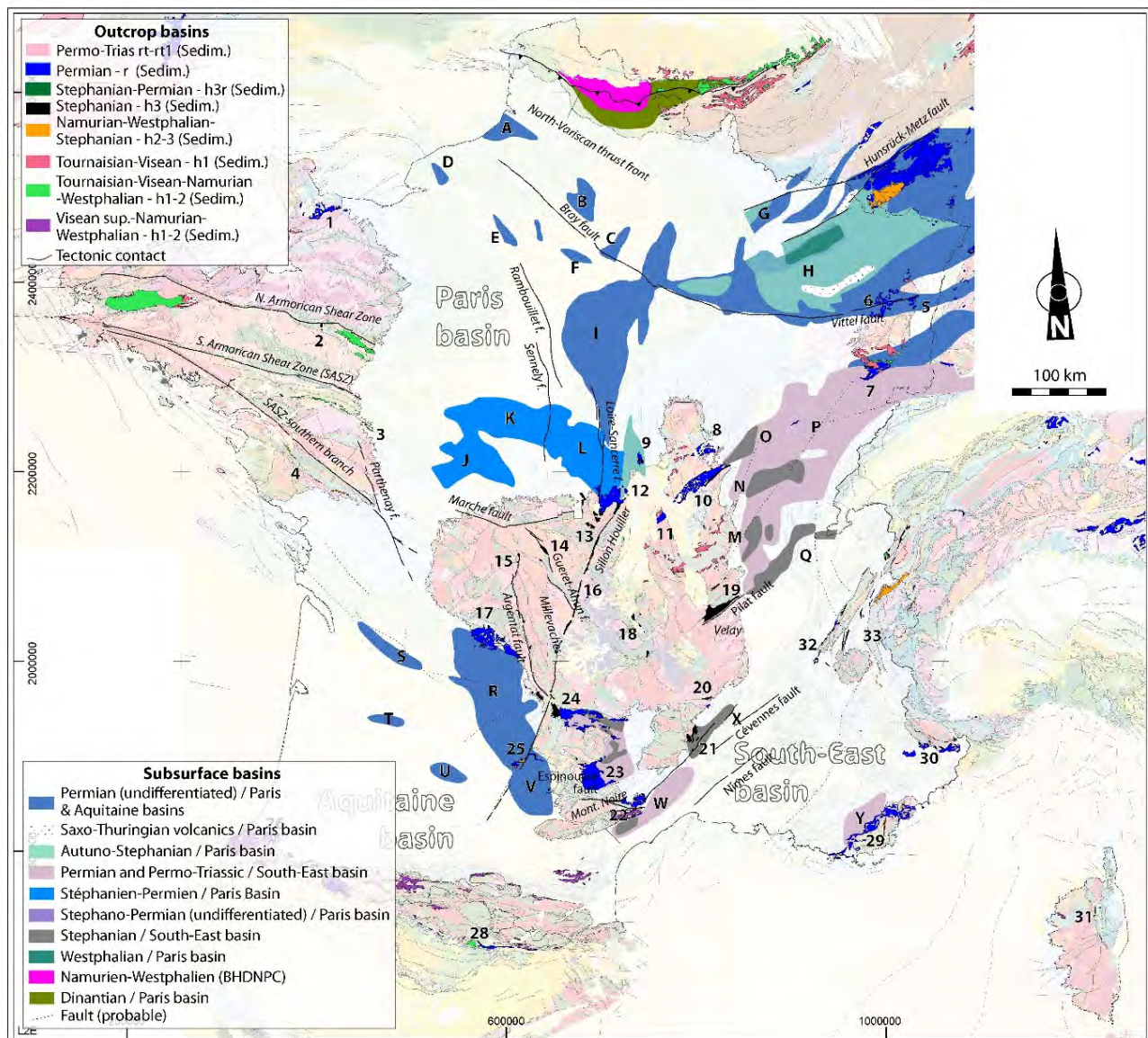
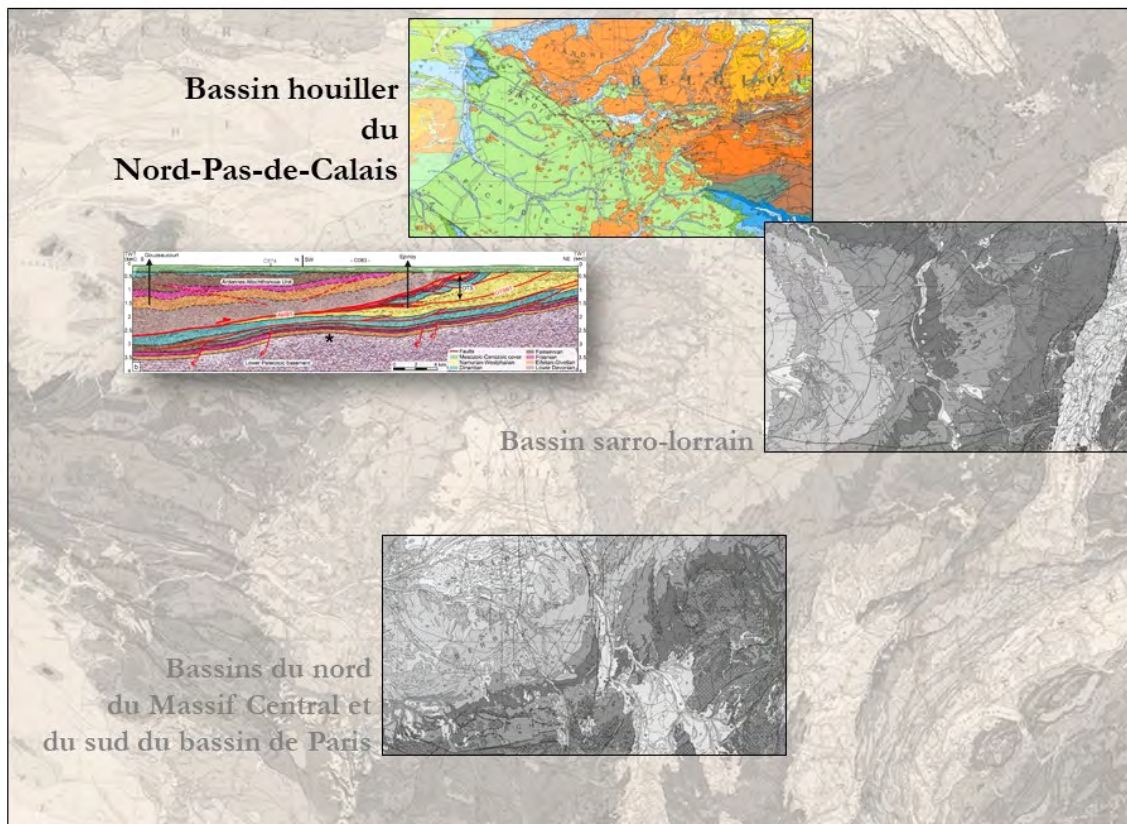


Figure 14 - Carte de synthèse des bassins carbonifères-permiens en France à l'affleurement et en subsurface, classés par âge. Bassins à l'affleurement : 1: Carentan/Littry ; 2: St-Pierre-la-Cour ; 3: Doué-la-Fontaine ; 4: Sillon Vendéen, Chantonmay, Faymoreau ; 5: Villé ; 6: St-Dié ; 7: Ronchamp-Giromagny ; 8: Autun ; 9: Decize La Machine ; 10: Blanzay-Le Creusot ; 11: Bert ; 12: Aumance ; 13: Commentry, Doyet, Deneuille ; 14: Abun ; 15: Bosmoreau-les-Mines ; 16: Bassins du Sillon-Houiller ; 17: Brive ; 18: Brassac, Brioude ; 19: St-Etienne ; 20: Prades-Jaujac ; 21: Alès ; 22: Graissessac, Lodève ; 23: St-Affrique ; 24: Figeac, Decazeville, Rodez ; 25: Quercy-Albigeois, La Grésigne ; 26: La Rhune-Bidarray ; 27: Ossau ; 28: Sierra del Cadi ; 29: Var ; 30: Barrot, Argentera ; 31: Corse ; 32: Alpes zones externes ; 33: Alpes zones internes. Bassins en subsurface : A: Nibas ; B: Saint-Maur ; C: Coulommès ; D: Villequier ; E: Vernon ; F: Champigny ; G: Vacherauville ; H: Lorraine ; I: Centre bassin de Paris ; J: Arpheilles ; K: Contres ; L: Brécy ; M: Bresse sud ; N: Bresse nord ; O: Beaune ; P: Bourgogne ; Q: Bugey ; R: Périgord, Quercy ; S: St-Géry ; T: Bouglon-Ste-Marthe ; U: Castelsarrasin ; V: Castrais ; W: Gabian-Garrigues ; Y: Carces ; X: Vallon.

3.4. Le bassin houiller du Nord-Pas-de-Calais, son substratum et la déformation du front nord varisque



3.4.1. Cadre collaboratif

La collaboration entamée il y a plusieurs années en interne au BRGM avec F. Lacquement et mes collègues O. Averbuch et F. Graveleau du LOG (Laboratoire d'Océanologie et de Géosciences) de l'Université de Lille, s'est concrétisée par la thèse d'A. Laurent, soutenue en 2021, cofinancée par le BRGM et la région Hauts-de-France. Cette thématique de recherche sur le front nord varisque se poursuit avec un stage de Master 2 en cours, en collaboration avec les mêmes collègues lillois et O. Kaufman (Université de Mons, Belgique) ; l'objectif est désormais de regrouper dans le même projet sismique les profils existant en France et dans le Hainaut belge afin d'obtenir une image transfrontalière des réservoirs géothermiques profonds carbonifères.

3.4.2. Problématiques appliquée et scientifique

Dans le cadre de la loi sur la transition énergétique votée par le gouvernement français en 2015, la région des Hauts-de-France s'est engagée à investir et développer considérablement les énergies renouvelables dans les prochaines décennies afin d'atteindre un objectif ambitieux de 100% d'énergies renouvelables à l'horizon 2050 (Projet « REV3: 3^{ème} révolution industrielle en Hauts-de-France »). Cet objectif requiert dès à présent le développement à l'échelle régionale la géothermie basse énergie (température des eaux comprises entre 30°C et 90°C), et le territoire du bassin houiller (Figure 15) constitue une région de fort potentiel pour son développement. En effet, deux

réservoirs carbonatés constituent des cibles potentielles au sein de son substratum dévono-carbonifère: les aquifères du Dinantien (Carbonifère inférieur, 360-330 Ma) et du Givétien-Frasnien (Dévonien moyen-supérieur, 388-372 Ma). Les eaux chaudes du réservoir dinantien sont exploitées depuis plus de trente ans dans la région de Mons en Belgique à des températures de 60-70°C. L'évaluation du potentiel géothermique dans le nord de la France nécessite tout d'abord la réalisation d'études de caractérisation (géométrique, hydrodynamique, thermique, etc...) de ces potentiels réservoirs géothermiques. L'objectif à visée appliquée de notre travail est de définir la géométrie (profondeur, extension, épaisseur, structuration) des potentiels réservoirs géothermiques profonds du Dinantien et du Givétien-Frasnien à l'échelle régionale des Hauts-de-France.

Outres ces enjeux énergétiques et sociétaux, l'étude de la géométrie du sous-sol du bassin houiller fournit un cadre scientifique exceptionnel pour analyser la dynamique du front de chaîne nord varisque, aujourd'hui érodé et enfoui sous la fine couverture sédimentaire crétacé-cénozoïque. Ce dernier résulte des interactions entre les processus de déformation (tectonique) et les processus de surface (érosion, sédimentation, climat) ; c'est un laboratoire idéal pour analyser les interactions entre flux sédimentaires, évolution des reliefs et activités des structures. L'enjeu scientifique majeur est ici de comprendre la dynamique sédimentaire et structurale du front nord varisque, essentiel pour améliorer la connaissance géologique des réservoirs profonds. Ce travail s'inscrit plus largement dans le champ d'étude des fronts de chaîne et de leurs bassins d'avant-pays, démontrant sur un exemple ancien l'importance de l'existence des structures préexistantes (héritage structural) et des contrastes lithologiques dans la plaque inférieure (stratigraphie mécanique) sur leur géométrie et cinématique de déformation (e.g. Butler, 1989; Gutscher et al., 1996; Ziegler et al., 2002; Lacquement et al., 2005; Butler et al., 2006; Ravaglia et al., 2006).

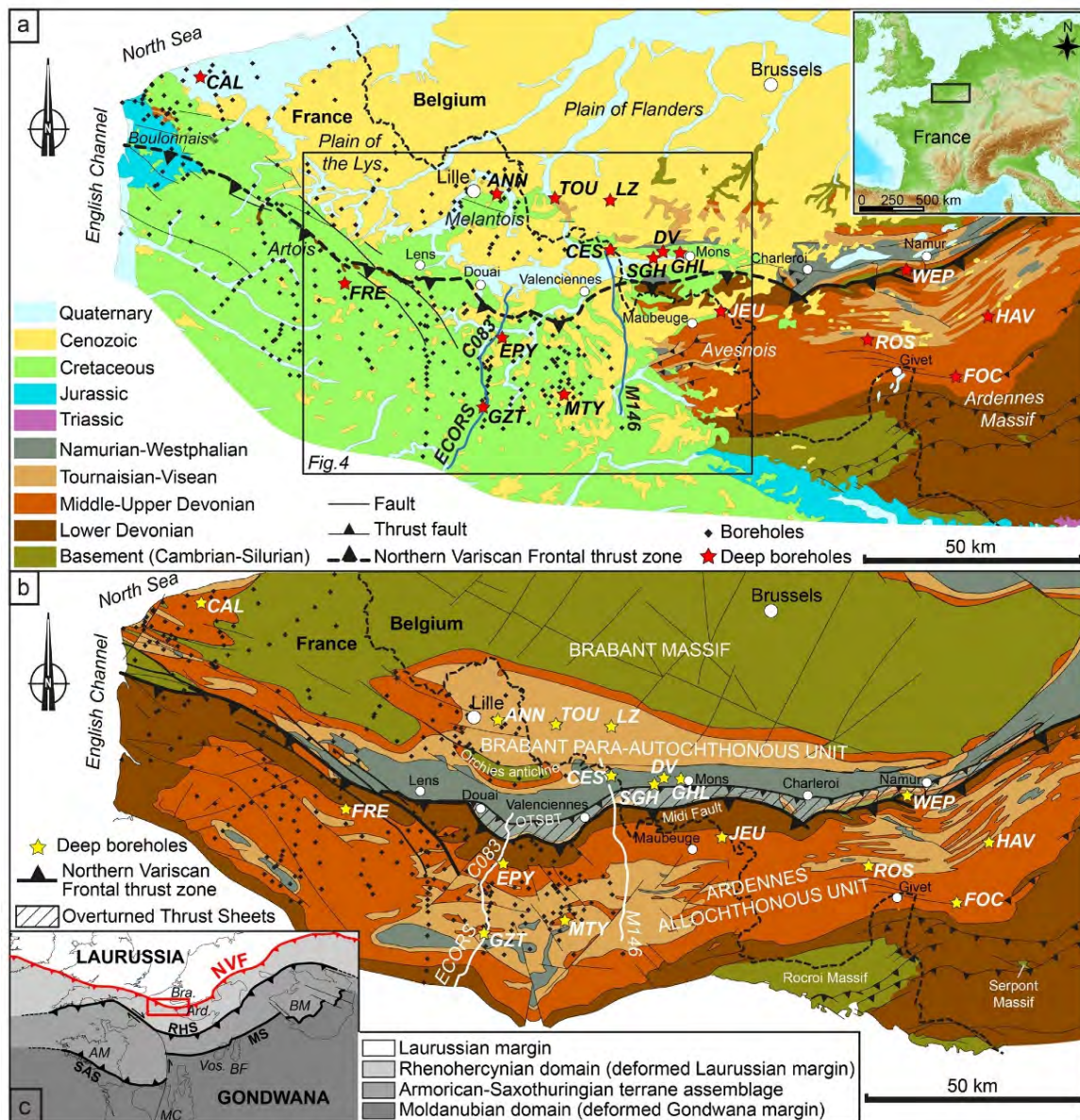


Figure 15 - a : carte géologique simplifiée du nord de la France ; b : carte structurale du substratum varisque dans le nord de la France (Laurent et al., 2021 et références incluses); localisation du Bassin Houiller du Nord-Pas-de-Calais et de la coupe de la Figure 16.

La définition de la géométrie et de la cinématique du front varisque dans le nord de la France n'avait pas fait l'objet d'une réactualisation dans le détail depuis la fin de l'exploitation des terrains houillers il y a plus de quarante ans (Becq-Giraudon, 1983). L'étude du front varisque se base sur le retraitement et l'interprétation de profils industriels de sismique réflexion et sur la réinterprétation structurale des nombreuses données géologiques disponibles dans le bassin houiller du Nord-Pas-de-Calais (forages, levés de galeries, plans et coupes d'exploitation, etc...) afin d'en proposer une version actualisée. Cette nouvelle vision est basée sur l'application de concepts géologiques développés ces dernières décennies et attachés à la compréhension des géométries des bassins d'avant-pays et de leur déformation en contexte de front orogénique (« tectonique chevauchante », inversion tectonique, etc...). L'ensemble des données (sismique, minières, forages, etc...) a été intégré au sein d'un modèle structural 3D définissant les géométries des couches sédimentaires du bassin houiller et de son substratum dévonien-carbonifère inférieur,

construit à l'aide du Geomodeller[®] du BRGM. La réalisation de ce modèle géologique a permis d'agrèger les deux volets de notre travail : (i) d'une part réinterpréter les géométries des différents ensembles sédimentaires et des discontinuités qui les affectent (mise en cohérence 3D des failles et chevauchements), et (ii) d'autre part mieux contraindre l'évolution cinématique du bassin houiller et du front de chevauchement nord de la chaîne varisque.

3.4.3. Contexte géologique du front orogénique nord varisque

Dans le nord de la France et le sud de la Belgique, le front de chevauchement nord varisque est formé de quatre unités structurales majeures (Meilliez et Mansy, 1990; Mansy et al., 1997; Lacquement et al., 1999; Belanger et al., 2012). Du nord au sud, ce sont : le Socle Brabançon, le Parautochtone Brabançon, les Ecailles et Massifs Renversés (EMR), et l'Allochtone Ardennais (Figure 15, Figure 16).

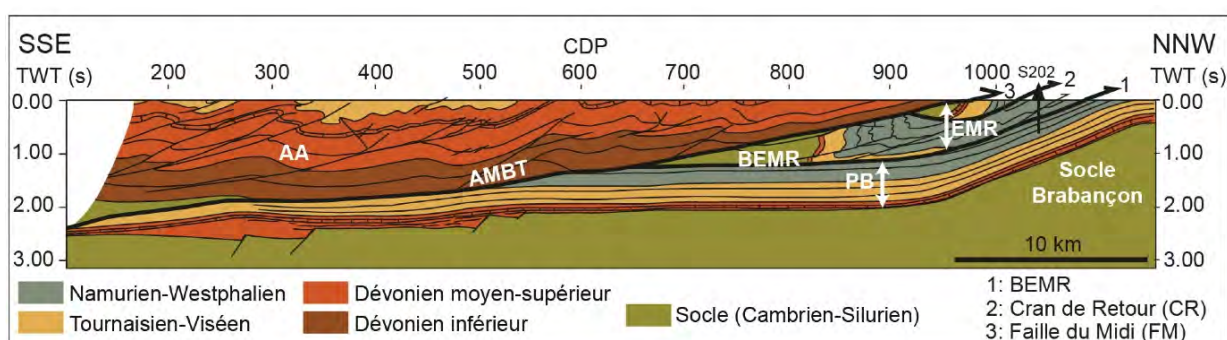


Figure 16 - Coupe équilibrée du profil sismique M146 dans la région de Valenciennes illustrant la structure de premier ordre du front nord varisque (modifié de Lacquement et al., 1999; Mansy et Lacquement, 2006 et Laurent et al., 2021a). AA: Allochtone Ardennais, AMBT: Allochtone Main Basal Thrust, PB: Parautochtone Brabançon, EMR: Ecailles et Massifs Renversés, BEMR: Chevauchement Basal des EMR. Trait de coupe sur la Figure 15.

Socle Brabançon

Le Socle Brabançon, également appelé Massif du Brabant ou Massif de Londres-Brabant (Legrand, 1968, Raoult, 1986; Ziegler, 1990; Verniers et al., 2001; Pharaoh, 2018), fait partie de la chaîne orogénique de l'Anglo-Brabant formée à la fin de l'orogénèse calédonienne au Silurien supérieur-Dévonien inférieur (Llandovery-Emsien). Il est constitué d'une succession sédimentaire majoritairement détritique (grès, siltites, pélites), d'âge cambro-silurien, traversée par de nombreuses intrusions magmatiques (Legrand, 1968; Verniers et al., 2001). Le Socle Brabançon est un domaine autochtone peu déformé par l'orogénèse varisque. Il est recouvert par une plateforme carbonatée post-rift discordante et transgressive, d'âge Eifélien à Viséen (ca. 400-330 Ma, voir la section Allochtone ardennais).

Parautochtone Brabançon et séries syn-orogéniques varisques

Le Parautochtone Brabançon repose en discordance sur le Massif calédonien du Brabant (Meilliez et Mansy, 1990 ; Mansy et Meilliez, 1993; Mansy et al., 1997, 1999; Hance et al., 1999). Il constitue la partie légèrement déformée de la marge continentale sud-laurussienne (Lacquement et al, 1999; Delmer, 2004; Mansy et Lacquement, 2006). Il est formé du bassin d'avant-pays

molassique syn-orogénique (Namurien-Westphalien) franco-belge et de la plateforme carbonatée post-rift sous-jacente, développée au Dévonien moyen-Mississippien. Le bassin d'avant-pays molassique franco-belge, défini comme le Bassin houiller du Nord-Pas-de-Calais dans sa portion française et les Bassins du Hainaut et de Namur dans sa portion belge, fait partie d'un large bassin flexural développé le long du front de chevauchement nord de la chaîne varisque au Carbonifère supérieur. Il se développe au cours de la phase majeure de l'orogénèse varisque au Mississippien supérieur-Pennsylvanien moyen (Namurien-Westphalien, ca. 331-307 Ma) ; il est formé d'une succession de niveaux de grès, d'argiles plus ou moins schisteuses et de veines de charbon, caractéristiques d'un environnement de dépôt paralic et fluvio-deltaïque, dont l'épaisseur peut atteindre 3500 m (Bouroz, 1969; Delmer, 2001).

Ecailles et Massifs Renversés (EMR)

Entre le Parautochtone Brabançon et l'Allochtone Ardennais s'intercale l'unité des Ecailles et Massifs Renversés (EMR) (Mansy et al., 1997; Lacquement et al. 1999; Lacquement et al., 2005). Les EMR sont formés de séries sédimentaires plissées siluriennes à carbonifères supérieur, caractérisées par une géométrie complexe, généralement renversée (Bouroz et al., 1961; Bouroz, 1969; Delmer, 1997, 2003; Mansy et al., 1997; Lacquement et al., 1999). Ces séries sont notamment décrites dans le sondage profond d'Epinoy (Raoult, 1986) au nord de Cambrai. Les EMR sont tronqués à leur sommet par la Faille du Midi (expression en surface du chevauchement nord varisque principal), et sont limités à leur base par une juxtaposition latérale de chevauchements à vergence NNO, tronquant les dépôts carbonifères supérieurs du bassin houiller molassique sous-jacent.

Allochtone Ardennais, séries syn- et post-rifts rhéno-hercyniennes

Au sud, le Parautochtone Brabançon et les EMR sont tronqués et chevauchés par l'Allochtone Ardennais, le long d'une zone de chevauchement crustale majeure nommée « chevauchement ardennais » (Lacquement, 2001). Ce dernier s'étend sur plus de 120 km vers le sud (Cazes et al., 1985 ; Raoult, 1986, 1988; Khatir et al., 1988; Meilliez et Mansy, 1990; Mansy et Meilliez, 1993) et est connue sous le nom de « Faille du Midi » dans sa partie émergente (Meilliez, 2019). L'allochtonne ardennais constituait au Dévonien-Carbonifère inférieur la partie distale de la marge sud-laurussienne (Mansy et al., 1999). Il est formé d'une série détritique syn-rift très épaisse d'âge Dévonien inférieur, recouverte d'une succession de dépôts carbonatés post-rift du Dévonien moyen-Mississippien et de dépôts molassiques syn-orogéniques du Mississippien supérieur-Pennsylvanien moyen (Mansy et al., 1997). Ces épaisses séries syn-rifts témoignent de la phase de rifting rhénohercynienne au Dévonien inférieur. Ces séries détritiques se sont déposées dans des environnements continentaux de cônes alluviaux et de systèmes fluviaux à littoraux au nord, évoluant vers une plateforme marine peu profonde au sud. Ces séries n'existent aujourd'hui qu'au sein de l'Allochtonne Ardennais et sont absentes du Parautochtone Brabançon. Quant aux séries post-rifts, elles témoignent d'une période d'expansion marine majeure du Dévonien moyen (Eifélien sup.) au Carbonifère inférieur (Dinantien), à l'origine du développement d'une plateforme carbonatée de grande ampleur sur la marge sud-laurussienne. Les dépôts de cette plateforme sont aujourd'hui observés au sein de l'Allochtonne Ardennais et du Parautochtone Brabançon (où ils représentent dans ce dernier cas les cibles géothermiques qui nous intéressent).

3.4.4. Le front nord varisque : structuration et évolution géodynamique - Publication 2

Laurent, A., Averbuch, O., Beccaletto, L., Graveleau, F., Lacquement, F., Capar, L., & Marc, S. (2021). 3-D structure of the Variscan thrust front in northern France: New insights from seismic reflection profiles. *Tectonics*, 40, e2020TC006642 <https://doi.org/10.1029/2020TC006642>

Cette publication concrétise les travaux de thèse d'A. Laurent ainsi que l'ensemble des réflexions menés à l'Université de Lille et au BRGM depuis plusieurs années sur la géométrie du front de chaîne nord varisque, les mécanismes de sa déformation et sa relation avec le bassin de foreland contemporain (le bassin houiller), le rôle de l'héritage structural sur la localisation et la configuration des structures chevauchantes, et son évolution cinématique. Les résultats s'appuient sur le retraitement et l'interprétation de 21 profils sismiques industriels représentant une longueur de 532 km, qui apportent de nouvelles contraintes sur la compréhension du front nord varisque. Ce travail montre toute l'importance de disposer de données sismiques de qualité et d'extension régionale, qui ont permis de s'extraire de la vision parcellaire qui prévalait jusqu'à présent.

Principaux résultats de la publication 2

- La zone de chevauchement frontal (AMBT : Allochthonous Main Basal Thrust) localise le déplacement de l'unité allochtone ardennaise sur plus de 50 km au-dessus de la marge laurussienne (appelée le Parautochtone Brabançon). Ce déplacement considérable a induit le sous-charriage du bassin d'avant-pays molassique et sa troncature par un chevauchement hors séquence majeur.
- Un vaste complexe d'écaïlles chevauchantes généralement renversées (OTS : Overturned Thrust Sheets complex, les EMR en français) est présent à la base de l'AMBT. Il est interprété comme le résultat de la troncature d'un anticlinal majeur au front de l'AMBT, dont le flanc inverse a été cisailé puis renversé en réponse au cisaillement basal lié à la propagation du chevauchement hors-séquence sus-jacent (AMBT).
- Les cartes structurales produites à partir de l'interprétation des horizons sismiques mettent en évidence pour la première fois une importante rampe latérale orientée NW-SE, approximativement le long d'une ligne Douai-Cambrai, et qui affecte à la fois le chevauchement frontal principal (AMBT) et le chevauchement basal du Massif des Ecaïlles Renversées (OTSBT : Overturned Thrust Sheets Basal Thrust). Cette rampe limite à l'ouest le complexe du OTS/EMR. Il s'agit d'une zone de relais majeure le long du front de chevauchement entre son segment oriental (orienté ENE-WSW entre Valenciennes et Douai), où le bassin molassique d'avant-pays est largement sous-charrié (sur plus de 20 km) sous l'unité allochtone, et son segment occidental (orienté WNW-ESE dans les régions du Boulonnais et de l'Artois) où il n'y a pas eu de sous-charriage.
- Un autre résultat important est la caractérisation en 3D de l'unité parautochtone brabançonne. Cette unité ainsi que les séries syn-orogéniques namuro-westphaliennes sus-jacentes du bassin d'avant-pays varisque sont déformées par une série de chevauchements de second-ordre vers le nord, souvent associés des plis de rampe développés à leur toit.
- A la base de l'unité parautochtone brabançonne, la séquence du Dévonien moyen-supérieur a été affectée par des failles normales syn-sédimentaires. Ces failles sont responsables de

l'épaississement généralisé de cette séquence dévonienne vers le sud et le sud-ouest. Leur orientation N60-80 et N110-130 correspond précisément à l'orientation des rampes frontales et latérales du prisme orogénique varisque. Nos interprétations sismiques confirment que de nombreux chevauchements varisques ont été initiés au droit des failles normales syn-sédimentaires. Ceci est vrai à la fois pour les rampes frontales et latérales, et souligne l'impact de ces hétérogénéités mécaniques sur la localisation des rampes chevauchantes postérieures.

- Le substratum paléozoïque, l'unité parautochtone et les séries molassiques sous-charriées montrent de larges plis ouverts. Ces ondulations pourraient trouver leur origine dans la réactivation de retro-chevauchements profonds calédoniens, tout comme la flexuration prononcée qui limite au nord le bassin d'avant-pays (qui fait remonter le substratum paléozoïque inférieur). Ces retro-chevauchements profonds pourraient alors avoir joué le rôle de butée au front des chevauchements varisques, et être à l'origine de leur dislocation hors séquence et de la localisation de la déformation le long d'un plan de chevauchement unique (l'AMBT).
- En guise de synthèse des différentes observations et conclusions ci-dessus nous proposons un scénario conceptuel d'évolution tectonique du front nord-varisque dans le nord de la France (Figure 15 de la publication ci-après).

Publication 2



Tectonics

RESEARCH ARTICLE

10.1029/2020TC006642

Key Points:

- Seismic data emphasize the large underthrusting of the Carboniferous foreland basin beneath the northern France Variscan thrust wedge
- 3-D imaging of the main thrust Allochthon Main Basal Thrust evidences a major lateral ramp segmenting the frontal thrust zone
- Inherited normal faults from the Laurussian margin exerted a major control on the dynamics and segmentation of the thrust front

Correspondence to:

A. Laurent,
aureore.laurent@univ-lille.fr

Citation:

Laurent, A., Averbuch, O., Beccaletto, L., Gravelleau, F., Lacquement, F., Capar, L., & Marc, S. (2021). 3-D structure of the Variscan thrust front in northern France: New insights from seismic reflection profiles. *Tectonics*, *40*, e2020TC006642. <https://doi.org/10.1029/2020TC006642>

Received 11 DEC 2020

Accepted 16 JUN 2021

© 2021. American Geophysical Union.
All Rights Reserved.

3-D Structure of the Variscan Thrust Front in Northern France: New Insights From Seismic Reflection Profiles

A. Laurent¹, O. Averbuch¹, L. Beccaletto², F. Gravelleau¹, F. Lacquement², L. Capar², and S. Marc²

¹Univ. Lille, CNRS, Univ. Littoral Côte d'Opale, UMR 8187-LOG-Laboratoire d'Océanologie et de Géosciences, Lille, France, ²BRGM, Orléans, France

Abstract In NW Europe, the late Carboniferous Variscan collision between the Laurussia and the Armorica-Gondwana continental blocks led to the development of a crustal-scale north-verging thrust system along the southern Laurussian margin. In northern France, the 3-D geometry and kinematics of the Variscan deformation front have been investigated on the basis of reprocessing and interpreting 532 km of industry-level seismic reflection profiles. This extensive seismic imaging provides new constraints on the structural and kinematic features of the orogenic front. It particularly emphasizes the localization of displacement along the main frontal thrust zone that accommodated more than 50 km of total displacement of the allochthonous units above the foreland. It also highlights the induced large underthrusting of the foreland basin below the frontal thrust zone, and its truncation in a general out-of-sequence mode of thrust propagation. We built structural maps that led to better delineating a major NW-SE lateral ramp along the main frontal thrust. The Mid-Upper Devonian series within the flexured foreland were deformed at depth by N060–080° trending and N110–130° trending syn-sedimentary normal faults that led to their south-to southwestward thickening. These pre-existing structures along the margin have exerted a primary control on the ensuing dynamics and geometry of the Northern Variscan Front by localizing both the frontal and lateral ramps during thrust wedge growth.

1. Introduction

Mountain fronts and foreland basins have been extensively studied in the past 50 years (e.g., Nemcok et al., 2005; Lacombe et al., 2007; Poblet & Lisle, 2011; Hammerstein et al., 2020 and references herein). They provide a record of the kinematic history of thrust propagation into the foreland, as well as of the orogenic relief erosion (e.g., Allen et al., 1986; Vann et al., 1986; DeCelles & Giles, 1996; Ziegler et al., 2002; Ford, 2004; Ortner et al., 2015). The dynamics of mountain-belt formation has been investigated in the frame of the accretionary wedge model that compares (for good mechanical reasons) the formation of a mountain belt with a pile of gravels pushed by a moving bulldozer (Chapple, 1978; Dahlen et al., 1984; Davis et al., 1983). Additionally, the style of deformation propagation of the thrust front within the foreland has been often investigated either in a first-order thin-skinned or a thick-skinned mode (e.g., Bally et al., 1966; Dahlstrom, 1969; Boyer & Elliott, 1982; Butler, 1987; Lacombe & Mouthereau, 2002), depending on the effect of basement structure on the deformed cover in the orogenic wedge.

One of the main parameters controlling the structural diversity of a foldbelt front is the rheology of the foreland rocks. Changes in the mechanical coupling between the propagating thrust wedge and its foreland sequence, along with regional structural inheritance (pre-existing basement faults and 3-D configuration of décollements) exert a primary control on the evolution of mountain-belts (e.g., Butler, 1989; Moore, 1989; Huiqi et al., 1992; Gutscher et al., 1996; Kley et al., 1999; Ziegler et al., 2002; Lacquement et al., 2005; Butler et al., 2006; Ravaglia et al., 2006). The importance of mechanical stratigraphy and structural inheritance has been demonstrated in numerous mountain fronts (e.g., Fitz-Diaz et al., 2011; Butler et al., 2018; Legeay et al., 2020) and by different analog and numerical modeling approaches (e.g., Ravaglia et al., 2006; Gravelleau et al., 2012; Hughes, 2020). Surface processes (erosion and sedimentation) are also important factors controlling the structural evolution of mountain belts (Fillon et al., 2013; Konstantinovskaya & Malavieille, 2005; Malavieille, 2010; Storti & McClay, 1995) because they determine the sedimentary fluxes between the hinterland and the foreland. As a result of these heterogeneities in foreland rheological properties and changes in erosion and sedimentation rates, a large diversity of 3-D geometries and kinematics

can be observed in fold-and-thrust belts. It includes for examples triangle zones, buried thrust fronts, in-sequence versus out-of-sequence thrusting, duplexes, fore-versus back-thrusting, folding versus faulting, etc (e.g., Jones, 1982; Banks & Warburton, 1986; Price, 1986; Vann et al., 1986; Morley, 1986, 1988; Averbuch et al., 1995; Tozer et al., 2006; Ortner et al., 2015; Von Hagke & Malz, 2018).

Mountain fronts represent also a very privileged target for the exploration and exploitation of natural resources because subsidence of the foreland basin associated to the combined effects of thrusting and syn-orogenic sedimentation, have allowed the development, migration and trapping of hydrocarbons (Lacombe et al., 2007; McClay, 2004; Needham et al., 2004; Nemcok et al., 2005). Recently, studies of foreland basin geology found also some additional applications for renewable energy and particularly geothermal energy. Thus, high temperature waters have been investigated and drilled in reservoirs buried a few kilometers in foreland basins. This is the case in the Alps, where temperatures reach about 80–140°C under the molassic foreland basin in Germany (Farquharson et al., 2016), or along the fossil Variscan belt of northern Europe, where warm waters around 60–70°C are exploited in southern Belgium (Delmer et al., 1982; Licour, 2012).

In order to gain insights on foreland fold-and-thrust belt dynamics, we investigated the geometry and kinematics of the Northern Variscan Front in northern France. This mountain front is an ancient, deeply eroded fold-and-thrust belt that was active 300 Ma ago. Our study is based on the interpretation of 532 km of reprocessed seismic reflection profiles covering a 5,130 km² area. The various orientations of the seismic profiles allow to intersect the main regional structural features and to build for the first time a comprehensive 3-D view of this portion of the Northern Variscan thrust front. Results highlight the geometry of a major lateral ramp segmenting the main frontal thrust. They also emphasize the control of structural inheritance (normal faults) of the underthrust margin on the deformation pattern of the thrust wedge.

2. Geological Setting

2.1. Outline of the Devonian-Carboniferous Geodynamic Evolution in Northern France

The late Paleozoic geodynamics of northern France was controlled by the growth of the Variscan mountain belt, a major orogenic system that extends across several thousands of kilometers across Europe (Figure 1). The Variscan orogen resulted from a polyphased collisional process between the Laurussia and Gondwana paleocontinents from Mid-Devonian (ca 380 Ma) to late Carboniferous times (ca 305 Ma). This accounted for the progressive closure of a complex set of interacting oceanic basins and the accretion of microcontinents (e.g., Matte, 2001; Franke, 2006; Ballèvre et al., 2009). The northern deformation front corresponds to the inverted southern Laurussian margin (Figure 1).

The latter was primarily structured during a major rifting phase from Early (Lochkovian) to Middle Devonian (Eifelian) that resulted in the opening of a relatively narrow oceanic realm called the Rheno-Hercynian Ocean (Franke, 1992, 2000; Franke et al., 1995; Meilliez et al., 1991; Oncken et al., 2000; Shail & Leveridge, 2009). The Rheno-Hercynian oceanic basin is considered to have formed in a back-arc tectonic setting above the north-verging subducting slab of the South Armorican-Moldanubian Ocean (Averbuch & Piromallo, 2012; Cobert et al., 2018; Franke, 1992; Franke et al., 1995; Golonka, 2020; Oncken et al., 1999; Shail & Leveridge, 2009; Ziegler, 1989).

Extensional deformation, although of lesser importance than during the rifting stage, persisted until the end of the Devonian (Famennian) as demonstrated by tectono-sedimentary studies in the Belgian Ardennes (Préat & Boulvain, 1988; Thorez & Dreesen, 1986) and in southern England (Leveridge, 2011; Shail & Leveridge, 2009). The southern Laurussian margin was dissected by a series of N50–70° and N110–130° striking normal faults that delimited the Dutch-Belgian Brabant continental high along its south-eastern and south-western borders (Meilliez et al., 1991; Smit et al., 2018; Van Hulten, 2012). During the syn-rift subsidence, thick Lower Devonian siliciclastics sediments were deposited in the distal part of the Laurussian margin (Ardennes, Rhenish Slate belt) (Figure 2). During the post-rift phase that lasted from Mid-Late Devonian to early Carboniferous times, a large-scale transgressive carbonate platform formed above the slowly subsiding Laurussian margin and Brabant basement high (Figure 2).

During the Late Devonian and Mississippian, a general N–S convergence caused the gradual closure of the Rheno-Hercynian Ocean by southward subduction beneath the Armorican-Saxothuringian block (Averbuch

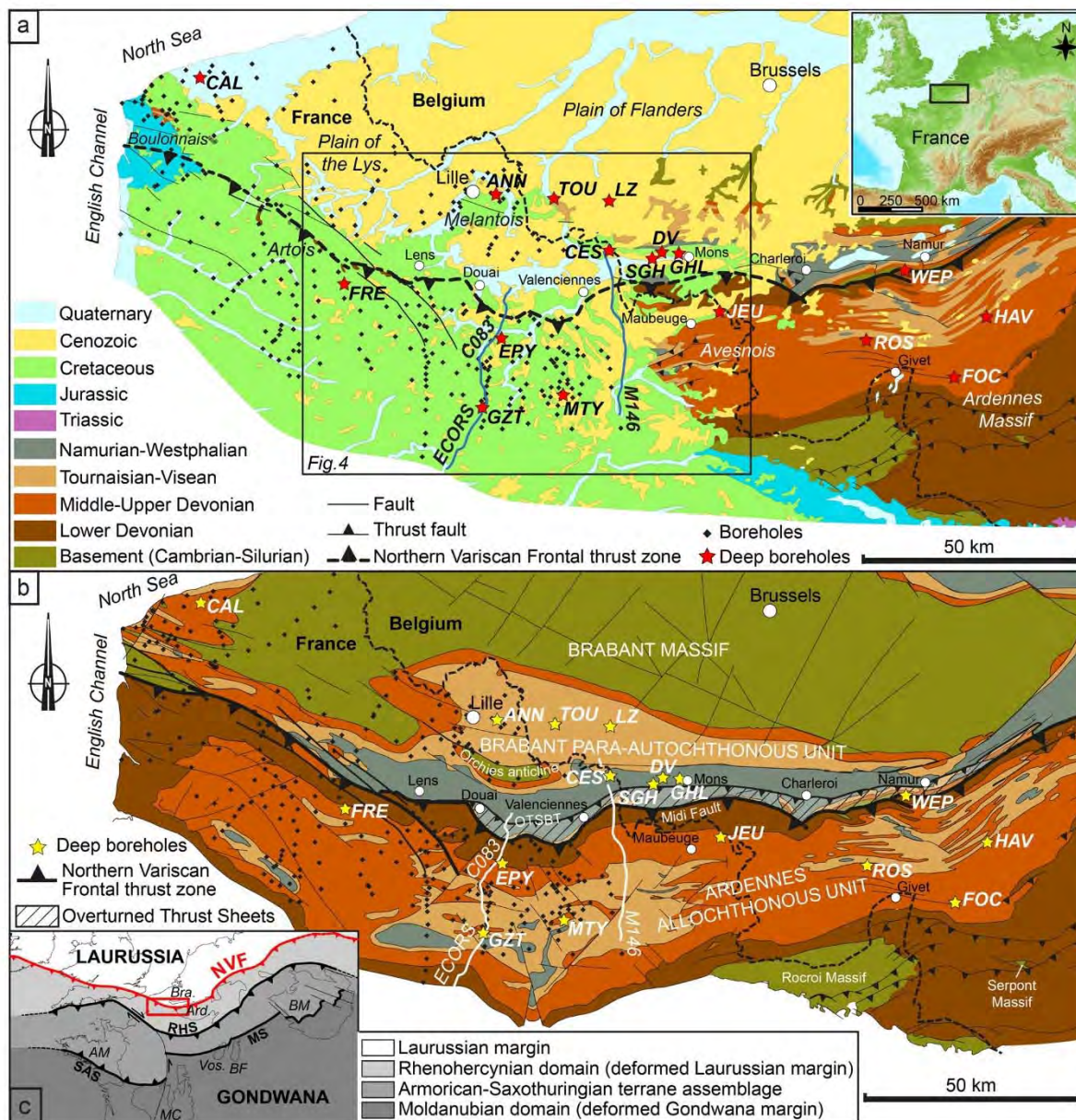


Figure 1. (a) Simplified geological map of northern France-southern Belgium (modified from the geological map of France, scale 1:1,000,000, Chantraine et al., 2003). The black frame corresponds to the location of Figure 4. (b) Structural map of the Variscan basement in northern France-southern Belgium (modified from C.F.P. et al., 1965 and Averbuch et al., 2004). This map is based on outcrop, well and geophysical data. The location of the Northern Variscan Front is based on previous studies. Borehole legend: ANN: Annappes; CAL: Calais; CES: Condé-sur-l'Escaut; DV: Douvrain; EPY: Epinoy; FOC: Focant; FRE: Frevillers; GHL: Ghlin; GZT: Gouzeaucourt; HAV: Havelange; JEU: Jeumont; LZ: Leuze; MTY: Montigny-en-Cambrésis; ROS: Rosières; SGH: Saint-Ghislain; TOU: Tournai; WEP: Wépion. c. Sketch map of the Variscan orogenic system in NW Europe (modified from Guillot et al., 2020). NVF: Northern Variscan deformation front; MS: Moldanubian suture; RHS: Rhenohercynian suture; SAS: South Armorican suture; AM: Armorican Massif; Ard.: Ardennes; BF: Black Forest; BM: Bohemian Massif; Bra: Brabant Massif; MC: Massif Central; Vos.: Vosges.

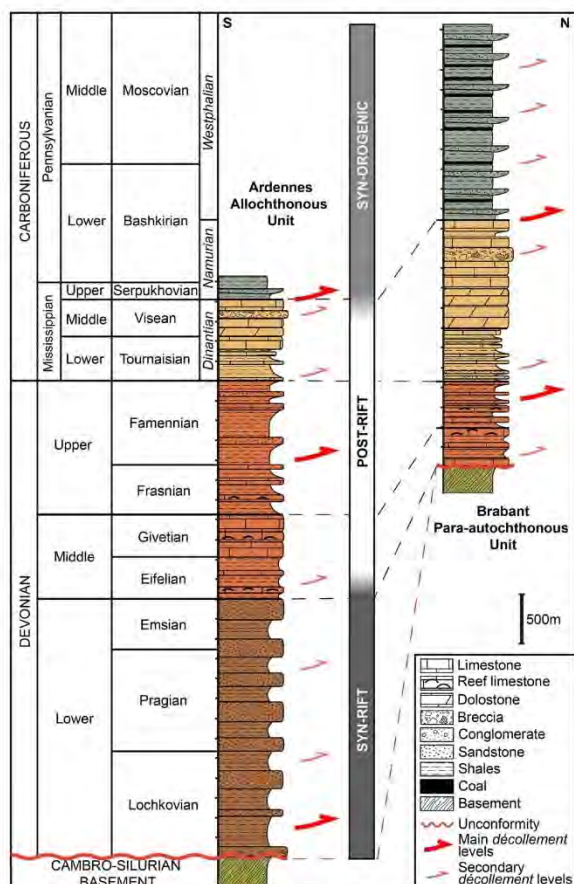


Figure 2. Synthetic lithostratigraphic logs of the Ardennes Allochthonous Unit and the Brabant Para-autochthonous Unit in northern France-southern Belgium. The thicknesses are based on data from deep boreholes in the region (see Figure 1).

& Piromallo, 2012; Cazes et al., 1985; Franke et al., 2017; Golonka, 2002; Golonka & Gaweda, 2012) (Figure 1). Starting from the middle Viséan times onwards (ca 340 Ma), this ultimately led to the collision of Laurussia with the Armorica-Gondwana accretionary complex (e.g., Schulmann et al., 2002; Guillot et al., 2020). The Variscan collision stage is characterized by an overall NNW-SSE shortening (e.g., Corfield et al., 1996; Oncken et al., 2000; Averbuch et al., 2004; Averbuch & Piromallo, 2012) that was responsible for the tectonic inversion of the southern Laurussian margin. This resulted in the formation of a crustal-scale north-verging thrust system that propagated outward from the Late Mississippian (Viséan) to the Middle Pennsylvanian (Westphalian) (Cazes et al., 1985; Fielitz and Mansy, 1999; Franke, 2000; Oncken et al., 2000; Plesch and Oncken, 1999). Tectonic stresses exerted on the lithosphere by the continental subduction and the increasing orogenic load led to flexural bending of the Laurussian continental lithosphere (e.g., Karner & Watts, 1983) and to the formation of a large-scale foredeep along the Northern Variscan Front. The latter can be tracked from Ireland to Northern Germany (Burgess & Gayer, 2000; Oncken et al., 2000; Plesch & Oncken, 1999; Tanner et al., 2011) and is likely to extend eastward to SE Poland (Lublin basin area) through a major bend along the Teisseyre-Tornquist zone (Krzywiec et al., 2017; Mazur et al., 2020) (Figure 1c). In northern France and southern Belgium, this foredeep was filled with up to 3.5 kilometers of synorogenic, coal-bearing, deposits during the Late Mississippian-Middle Pennsylvanian (Namurian-Westphalian 325–305 Ma) (Becq-Giraudon, 1983; Bourou, 1969; Delmer et al., 2001) (Figure 2).

2.2. Basic Structural Features of the Northern Variscan Thrust Front in Northern France

In northern France, the Northern Variscan Front is almost never visible at the surface because it is covered by 100-to-200 meters of unconformable Mid-Cretaceous to Eocene sedimentary layers (Figure 1a). Apart from scarce outcrops of Paleozoic rocks exhumed in the Boulonnais and Artois hills resulting from Tertiary uplift (Mansy et al., 2003; Minguely et al., 2010), the most prominent outcrops of Paleozoic substratum are found in the Ardennes Massif and the Avesnois region. The Northern Variscan Front was discovered and extensively studied during the 19th–20th centuries during the intensive coal-mining activity. These first exploration data allowed to draw a general map of the thrust front at depth showing that its strike varies progressively from WNW-ESE (N110–120°) in the Boulonnais and Artois regions to ENE-WSW (N60–70°) in the Avesnois region and the Ardennes Massif (i.e., the classical V-shape of the Variscan belt) (Figures 1b and 1c). Some second-order trend changes have been defined in this general structural framework, such as the reentrant to the south of Douai and Valenciennes in the French coal-basin district.

The deep structure of the thrust wedge remained poorly known until new geophysical data (mainly seismic reflection profiles) and exploration wells were acquired during the 1980's by the ECORS program and hydrocarbons exploration (Cazes et al., 1985; Le Gall, 1992; Raoult, 1986, 1988; Raoult & Meilliez, 1987). These data considerably improved the knowledge on the deep structure of this orogenic front and showed the first-order geometry of the fold-thrust system. More recently, reprocessing and interpretation of a selected seismic profile (M146) along the French-Belgian border (Averbuch et al., 2018; Lacquement, 2001; Lacquement et al., 1999; Mansy et al., 1997) allowed to better define these first observations and better characterize the current structural model of the thrust front, as illustrated in Figures 1b and 3.

The structure of the thrust front in northern France and southern Belgium is classically subdivided into four major tectonic units (Figures 1b and 3a). In the following parts of our text, and essentially based on

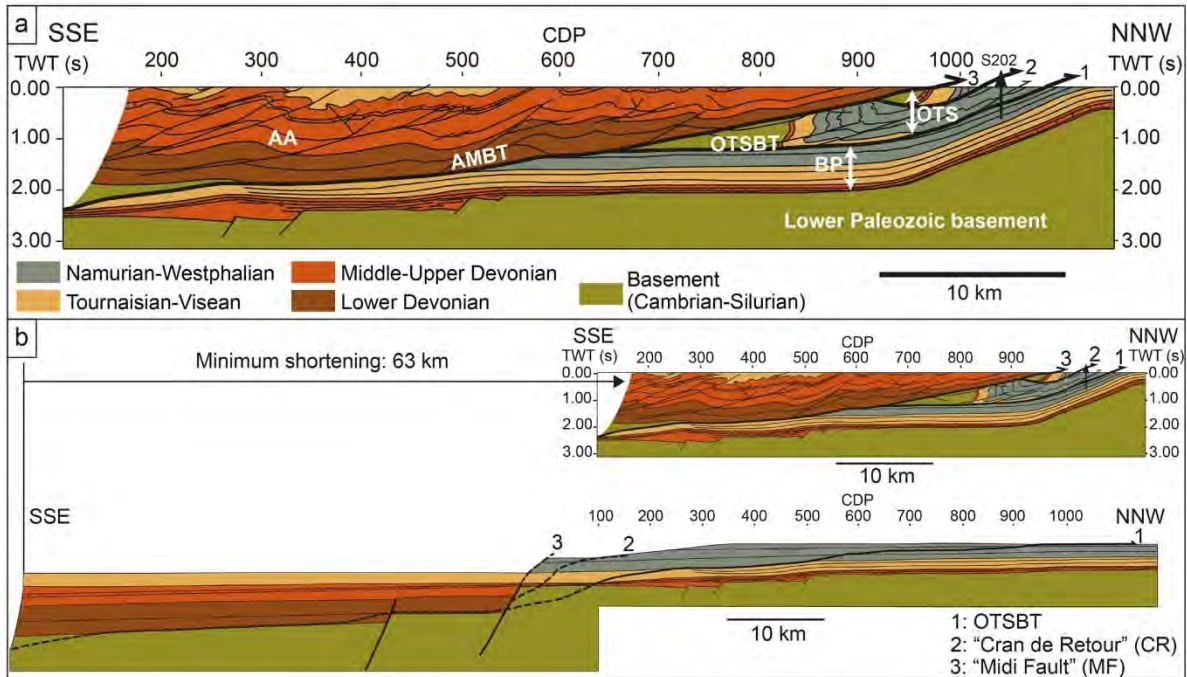


Figure 3. (a) Balanced cross-section along the M146 seismic profile in the area of Valenciennes (location in Figure 1b) illustrating the main structural features of the thrust front. Modified from Lacquement et al. (1999) and Mansy & Lacquement (2006). AA: Ardennes Allochthonous Unit, AMBT: Allochthon Main Basal Thrust, BP: Brabant Para-autochthonous Unit, OTS: Overturned Thrust Sheets, OTSBT: Overturned Thrust Sheets Basal Thrust. (b) Balanced and restored cross-section of the interpreted seismic profile showing the southern Laurussian margin before the Variscan shortening event (modified from Averbuch et al., 2018). Numbers 1, 2 and 3 correspond to the order of activity of the different thrust faults.

French terminology, we will follow this classical structural nomenclature to ensure a comprehensive link with previous works in this region. From north to south, these units are the Brabant Massif, the Brabant Para-autochthonous Unit, the Overturned Thrust Sheets complex (OTS) and the Ardennes Allochthonous Unit (Belanger et al., 2012; Lacquement et al., 1999; Mansy et al., 1997; Meilliez & Mansy, 1990).

The Brabant Massif is part of the Anglo-Brabant deformation belt (Pharaoh, 2018) that was deformed during a late Caledonian orogenic event from Late Silurian to possibly Early Devonian as a result of tectonic inversion of an old Cambro-Ordovician basin (Debacker et al., 2005; Sintubin et al., 2009). It consists of a predominantly silico-clastic sedimentary sequence (sandstone, siltites, pelites) of Cambro-Silurian age, intruded by numerous deep syn-sedimentary magmatic intrusions (Legrand, 1968; Verniers et al., 2001). The lower Paleozoic substratum is unconformably overlaid to the south by a transgressive Mid-Devonian to lower Carboniferous carbonate platform sequence (Eifelian-Visean, ca. 400–330 Ma) (Bultynck et al., 1991; Mansy et al., 1999; Ziegler, 1990).

The upper Carboniferous Nord-Pas-de-Calais (NPC) coal-bearing basin overlies the Brabant lower Paleozoic basement and the Mid-Devonian to lower Carboniferous platform sequences (Figure 2). All these units constitute the foreland of the Northern Variscan thrust system. The NPC coal basin and its Devonian-lower Carboniferous substratum constitute the slightly deformed part of the Laurussian continental margin, which is classically referred to as the Brabant Para-autochthonous Unit (Figure 2a) (Hance et al., 1999; Mansy et al., 1997, 1999; Mansy & Meilliez, 1993; Meilliez & Mansy, 1990). In France, the NPC coal basin extends across 85 km E–W from the Belgian border to the Artois region and 15 km N–S from the Brabant foreland to the frontal thrust zone. Toward the east, it extends in Belgium to the Hainaut and Namur basins (Figure 1). Its stratigraphy includes an Upper Mississippian - Middle Pennsylvanian (formerly Namurian-Westphalian, ca. 320–305 Ma) synorogenic sedimentary sequence (Figure 2). Fluvio-deltaic and paralic deposits consist of a succession of alternating layers of coal, sandstones and shales, having a total thickness

of up to 3.5 kilometers (Bouroz, 1969). In the south of the study area, the upper Carboniferous sequence and its underlying substratum form a large monocline dipping gently towards the south ($5\text{--}10^\circ$). It is largely underthrust below the Ardennes thrust wedge, which is generally referred to as the Ardennes Allochthonous Unit (Figure 3a). To the north, the Brabant Para-autochthonous Unit shows a clear localized flexure at the footwall of the frontal thrust zone, which allows the lower Paleozoic basement to be directly exhumed below the Cretaceous-Tertiary cover. This is the Orchies basement high located north of the NPC basin (Figure 1b). This feature has recorded the relative uplift of the Brabant foreland, that likely was coeval with the northward propagation of the thrust front (Minguely et al., 2008).

Some thrust sheets, characterized by particularly complex geometries and an overall overturned attitude of the sedimentary layers have often been observed between the Brabant Para-autochthonous Unit and the Ardennes Allochthonous Unit (Figure 3a) (Bouroz, 1969; Bouroz et al., 1961; Delmer, 1997, 2003; Lacquement et al., 1999, 2005; Mansy et al., 1997). The so-called “Overturned Thrust Sheets” are made of folded Silurian to upper Carboniferous sedimentary layers. These are frequently deformed by second-order, low-angle curved normal faults (Bouroz, 1950; Le Gall, 1994; Meilliez, 2019). The occurrence and kinematics of these faults have been observed in the coal mines (Bouroz, 1950). The OTS is a largely underconstrained body affected by a series of NNW-vergent thrust faults that hardly connect laterally. The extent of the thrust surface at the base of the OTS complex is defined here as the OTS basal thrust (OTSBT). In France, this OTS complex decreases or even vanishes west of Douai (Figure 1b).

To the south, the OTS and the Brabant Para-autochthonous Unit are overthrust by the Ardennes Allochthonous Unit along a major crustal-scale thrust fault (Figure 3a) that extends along more than 120 km to the south (Cazes et al., 1985; Mansy & Meilliez, 1993; Meilliez & Mansy, 1990; Raoult, 1986, 1988). This major thrust is named there the Allochton Main Basal Thrust (AMBT). Its shallow part is frequently referred to as the “Midi Fault” due to its recurrent position at the southern border of the coal basin (“Midi” meaning “South” in French, e.g., Meilliez, 2019). Unlike the OTS and Brabant units, the Ardennes Allochthonous Unit comprises a thick Lower Devonian sequence that was deposited in the distal rifted part of the southern Laurussian margin (Figure 2). In the Avesnois and Ardennes regions, this Lower Devonian to Dinantian sequence was intensely faulted and folded with an overall E-W to ENE-WSW strike (Khatir et al., 1988; Lacquement et al., 2005; Mansy & Lacquement, 2006; Mansy & Meilliez, 1993; Meilliez & Mansy, 1990; Moulouel, 2008). It is unconformably lying on a lower Paleozoic (Cambrian-Ordovician) slightly metamorphosed sedimentary basement that locally crops out along the frontal thrust zone. The basement crops out more substantially further south within the cores of several major thrust-related anticlinal highs such as the Rocroi, Serpont and Stavelot massifs (Figure 1b).

2.3. Current Views on the Kinematics of the Northern Variscan Front in Northern France

Restorations of geological sections and seismic profiles within the Northern Variscan thrust wedge have estimated an amount of shortening of at least 60–70 kilometers both in the Ardennes Massif (Le Gall, 1992) and at the French-Belgian border (Averbuch et al., 2018; Houchen, 1988; Lacquement, 2001; Lacquement et al., 1999; Mansy et al., 1999) (Figure 3b). A large part of the shortening is related to the major thrust zone at the base of the allochthonous unit (AMBT).

The kinematics of the AMBT has been recently documented from the interpretation and restoration of the M146 seismic profile in the Valenciennes region (Figure 3b) (Averbuch et al., 2018). The section restoration illustrates the control of the rift-related geometry of the Laurussian margin upon the Northern Variscan thrust wedge (Figure 1b and 3a). Particularly, the Devonian normal faults that formed during rifting of the Laurussian margin are likely to have localized deformation during the Variscan compression (Figure 3b) (Lacquement et al., 2005). The main border fault zone, which limits the Lower Devonian depositional area and forms a major vertical step-over in the margin geometry, is considered to have localized the main frontal ramp of the AMBT. The propagation of thrusting onto the AMBT would have induced the dissection of the crest of the related footwall block and formation of a footwall short-cut thereby inducing the transport of slices of basement and reduced Devonian-Carboniferous cover at the sole of the propagating thrust (i.e., the future OTS). The hangingwall unit (the future Ardennes Allochthonous Unit), detached on the thick basal Lower Devonian shales series, would have been displaced over the Brabant Para-autochthonous Unit forming a major thrust-related anticline, sequentially crosscut by out-of-sequence forelimb thrusts. This process

is considered to have induced the progressive shearing and overturn of the thrust-sheets involved in the initial forelimb of this major anticline. The last out-of-sequence thrust would correspond to the emergence of the AMBT along the “Midi fault zone.” This propagation of thrusting along the AMBT is shown by the thrust sequence 1, 2, 3 in the restored section (Figure 3b).

The geometry and kinematics of deformation within the Northern Variscan thrust front were strongly governed by the rheological contrasts within the Paleozoic sequence. The mechanical stratigraphy within the thrust wedge is illustrated in Figure 2. As defined by structural field studies in the Ardennes-Avesnois fold-and-thrust belt (e.g., Khatir et al., 1992; Lacquement, 2001; Lacquement et al., 2005; Moulouel, 2008), three major décollements are present (Figure 2). The basal one is the weak Lochkovian shales located at the base of the syn-rift sequence. The middle one is the weak Famennian shales, resting above the more resistant Frasnian limestone unit. The upper one is located at the transition between the Dinantian carbonates and the overlying Namurian shales at the base of the synorogenic sequence. Some second-order décollements have also been described adding locally some complexity to the primary structural fold-thrust pattern. These are located within (Figure 2): (a) the shaly intervals of the Lower Devonian silicoclastic sequence; (b) the Middle Devonian shales, alternating with limestones; and (c) the numerous layers of shales of the syn-orogenic Namurian-Westphalian coal-bearing succession. It is worth noting that décollements may also exist within the carbonate-dominated Dinantian, especially in the Viséan evaporitic intervals (e.g., Rouchy et al., 1986, 1987; De Putter, 1995) and in the lower part of the Tournaisian that includes shale formations, such as the homogeneous Pont d’Arcole Formation (e.g., Mortelmans and Bourguignon, 1954; Coen-Aubert et al., 1980; Poty et al., 2001; Hance and Poty, 2006).

3. Seismic and Well Data

During the 1960’s and the 1980’s, northern France was a target of significant onshore oil exploration by various oil and gas companies. These exploration surveys led to the acquisition of 189 seismic reflection profiles with a total length of 2,613 km. These data are essential to image the 3-D structure of the Northern Variscan Front buried under the Mesozoic-Cenozoic cover.

Our study is based on the reprocessing of 21 seismic reflection profiles acquired in the 1980’s of a total length of 532 km (Figure 4). These seismic profiles were selected based on their location, their orientation, the availability and the quality of the seismic data. The selected profiles cover an approximate surface of 5,130 km² (95 km long by 54 km wide). They extend over the southern allochthonous and northern para-autochthonous units of the Northern Variscan Front from the cities of Arras and Lens to the west to the Belgian border to the east. They intersect the study area with various orientations, and therefore provide the opportunity to crosscut the main regional structures and to image their lateral variations. Given the acquisition parameters used in these exploration surveys, mainly the frequency bandwidth of the seismic source and the recording length (up to 5 s), the estimated depth of investigation is around 7–8 km, with a vertical resolution of approximately 25–30 meters.

Seismic reprocessing of the selected lines used modern signal-processing algorithms in order to significantly improve the quality of the images obtained in the 1980’s. Efforts were focused on three key steps, repeated several times throughout the processing sequence: (a) computing primary and residual static corrections in order to remove the topographic and velocity effects of the superficial rock layer, strongly impacting the seismic signal; (b) detailed velocity analysis; and (c) various methods of organized and random noise attenuation. Pre-stack time migration enhanced the details of structural features and completed this reprocessing sequence before stacking the data.

In addition to the seismic data, three deep exploration wells have been selected and included into the database in order to provide geological information at depth along the seismic profiles. These are the Epinoy-1, Gouzeaucourt-101 and Jeumont-1 wells (Figure 4). They were selected based on their proximity to the seismic lines (less than 1 km), their depth, and the availability of well log data.

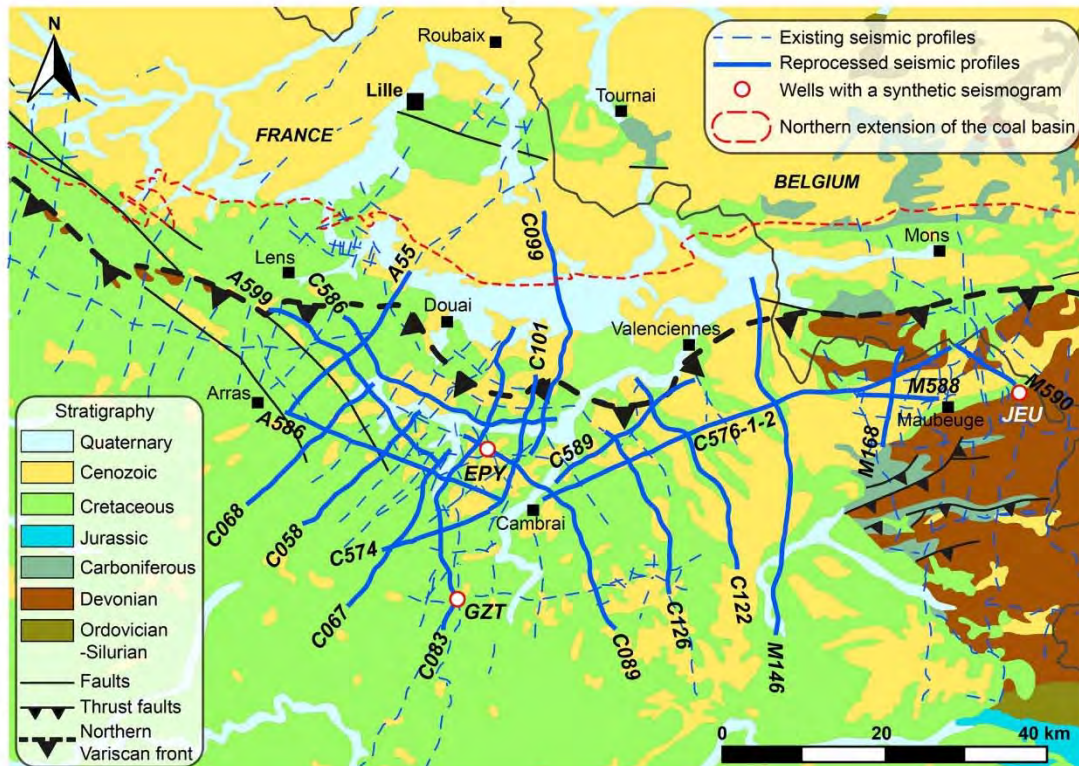


Figure 4. Simplified geological map of northern France extracted from the geological map of France (Chantraine et al., 2003) showing the location of reprocessed seismic profiles and available deep boreholes in the study area. The outline of the Northern Variscan Front corresponds to that defined before this study was conducted.

4. Seismic-Well Tie and Description of the Seismic Facies

Major stratigraphic and structural surfaces have been selected and interpreted to accurately decipher the structural framework of the thrust front. Thus, we preferentially picked the Top Paleozoic Unconformity (TPU), the AMBT, the tops of the Dinantian (T-Din), Famennian (T-Fam), Frasnian (T-Fra), Eifelian-Givetian (T-Giv) and, finally, the top of the lower Paleozoic basement (T-Sil) (Figure 5). The interpretation of the seismic data was carried out using the IHS Kingdom Software.

4.1. Seismic-Well Tie

The first step in this process was to calibrate and tie the targeted seismic markers to their corresponding geological surfaces. Two exploration wells were selected to produce synthetic seismograms: Epinoy-1 (EPY) and Jeumont-1 (JEU) (Figure 4). A synthetic seismogram is a theoretical seismic trace that models the changes in acoustic impedance in the different rock layers along a given borehole. It is generated by convolving the reflective coefficient, computed from sonic and density logs, with a seismic wavelet defining the amplitude variations of the synthetic seismogram and best representing the seismic signal.

The Epinoy and Jeumont boreholes are the only wells in the vicinity of the seismic lines that meet two important requirements: (a) the velocity data necessary for calculating a synthetic seismogram are available (sonic log, check-shots), and (b) the wells are deep enough to cross the targeted geological surfaces. Both wells drilled through the Mesozoic-Cenozoic cover, the Ardennes Allochthonous Unit and the OTS, but only the Jeumont borehole went through the entire underlying Para-autochthonous Unit and reached the

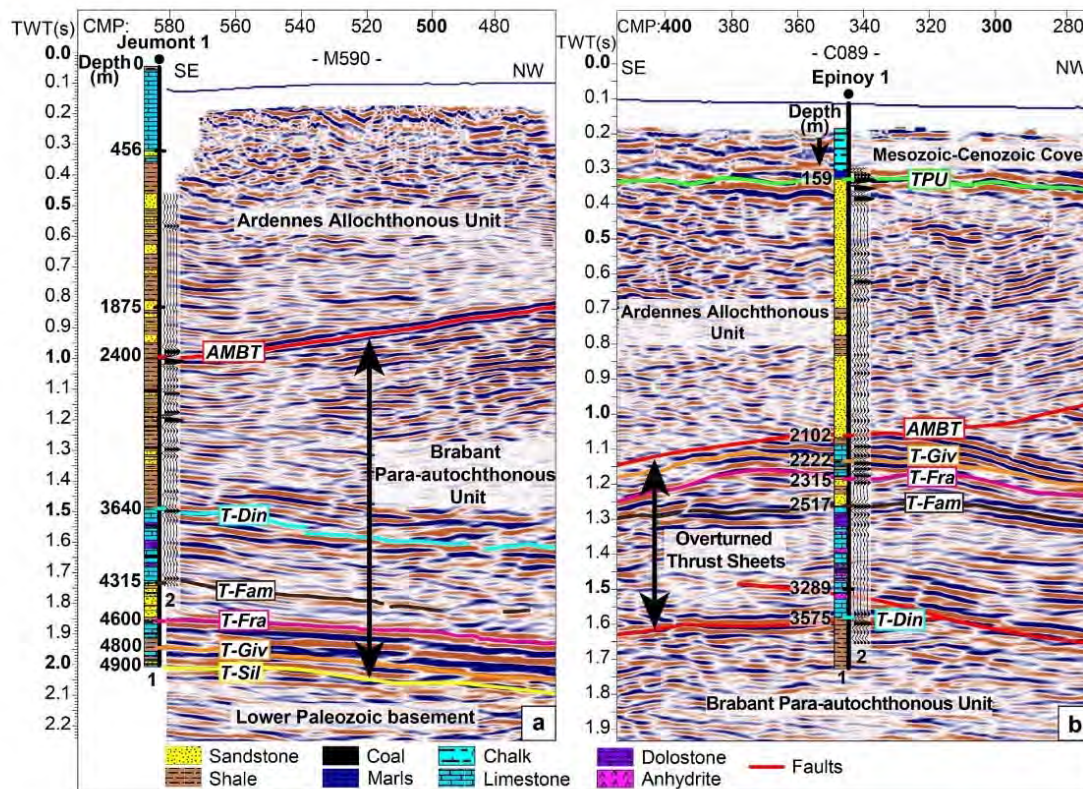
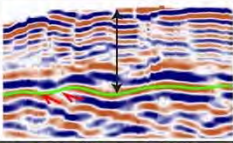
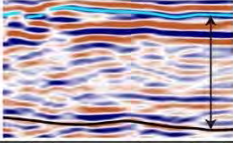
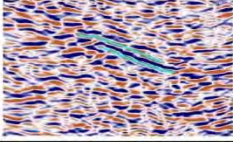
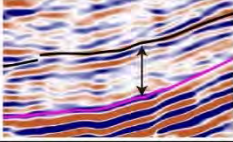
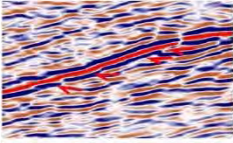
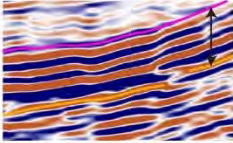
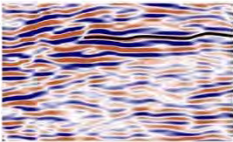
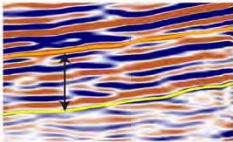
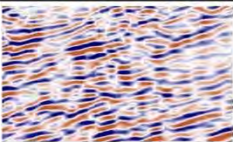
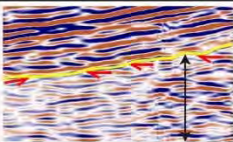


Figure 5. Seismic-well tie between (a) the Jeumont borehole and the M590 reprocessed seismic profile, and (b) the Epinoy borehole and the C089 reprocessed seismic profile. 1: Lithological log; 2: Synthetic seismogram. T-Din: Top Dinantian; T-Fam: Top Famennian; T-Fra: Top Frasnian; T-Giv: Top Givetian; T-Sil: Top Silurian; TPU: Top Paleozoic Unconformity.

Eifelian (Figure 5). Therefore, the Epinoy and Jeumont boreholes have been used as references to identify the seismic markers in the OTS and in the Para-autochthonous Unit.

Synthetic seismograms were generated following several steps: (a) quality control of the sonic log and removal of abnormal values; (b) integration of the velocity data (sonic log and check-shots); (c) generation of a time-depth chart that allowed us to convert the vertical scale of the well data from depth to time using integrated velocity data; (d) setting the density value to 1 g/cm^3 , as the density logs were not available; (e) computation of the acoustic impedance; (f) computation of the reflectivity coefficient; (g) generation of a seismic wavelet extracted from the seismic traces around the well and having a mean frequency of 35 Hz; (h) convolution of the reflectivity coefficient with a seismic wavelet. Once the synthetic seismograms were created for both wells, they were adjusted on the seismic profiles M590 (Jeumont) and C089 (Epinoy) so that they fit the seismic signal around the well, concluding the seismic-well tie process (Figure 5). The latter made it possible to calibrate and tie the geological surfaces of interest to the corresponding seismic markers, with the exception of the top of the Brabant basement that was never encountered in the boreholes.

Once the targeted horizons were identified near the Epinoy and Jeumont boreholes, they were correlated step by step from line to line by comparing the seismic facies and by checking the 3-D structural consistency. Structural surfaces, such as major thrust faults and normal faults were also interpreted and correlated from line to line. These faults usually appeared as discontinuities delimiting and truncating two sets of reflectors often having a different apparent dip. This sparse well data set could be seen as a source of interpretation uncertainties; this is however compensated by the lateral coherence of the seismic facies and structures throughout the study area, thereby helping the seismic interpretation process.

Geological level	Seismic facies	Reflection attributes	Geological level	Seismic facies	Reflection attributes
Mesozoic-Cenozoic cover		1) parallel to semiparallel 2) semicontinuous 3) variable amplitude 4) variable frequency	Dinantian		1) parallel to contorted 2) semicontinuous 3) low-medium amplitude, high amplitude at the top 4) variable frequency
Ardennes Allochthonous Unit		1) highly chaotic 2) discontinuous 3) mostly low to variable amplitude 4) variable frequency	Famennian		1) semiparallel 2) semicontinuous 3) low amplitude, medium amplitude at the top 4) high frequency
Allochthon Main Basal Thrust		1) parallel 2) continuous 3) high amplitude 4) high frequency	Frasnian		1) parallel 2) continuous 3) high amplitude 4) low-medium frequency
Overtuned Thrust Sheets		1) chaotic 2) discontinuous 3) variable amplitude 4) variable frequency	Middle Devonian		1) parallel to semiparallel 2) semicontinuous 3) high amplitude 4) low-medium frequency
Namurian-Westphalian coal basin		1) chaotic 2) discontinuous 3) low amplitude 4) medium to high frequency	Lower Paleozoic basement		1) chaotic 2) discontinuous 3) variable amplitude 4) variable frequency

Brabant Para-autochthonous Unit

Figure 6. Illustration and description of the characteristic seismic facies of the interpreted geological formations and units. Reflection attributes: a) configuration; b) continuity; c) amplitude; d) frequency. Giv. Limest.: Givetian limestones; T-Din: Top Dinantian; T-Fam: Top Famennian; T-Fra: Top Frasnian; T-Giv: Top Givetian; T-Sil: Top Silurian; TPU: Top Paleozoic Unconformity.

4.2. Seismic Facies

Seismic-well tie allowed to identify the targeted geological surfaces and to identify the overall seismic facies of the relevant geological units. They are described here and illustrated in Figure 6.

The Mesozoic-Cenozoic cover is represented by rather parallel to semiparallel reflectors, continuous, with high amplitude and low frequency in the lower part; in the upper part the reflectors are more or less continuous and display variable amplitude with high frequency (Figure 6). Due to the unconformable character of the Mesozoic-Cenozoic cover on the Paleozoic substratum, the Top Paleozoic Unconformity is usually identified by truncations below parallel, continuous and high amplitude reflectors (Figure 6).

The Ardennes Allochthonous Unit is located beneath the Mesozoic-Cenozoic sedimentary cover. It is characterized by an overall chaotic seismic sequence with discontinuous reflectors having variable amplitude and frequency (Figure 6). The intense deformation of the allochthonous series, which are affected by numerous faults and sometimes very steep or even vertical or overturned folds, generates strong dispersions of the seismic waves. This makes it difficult to obtain a good seismic imaging of this unit. However, some continuous, high-amplitude reflectors sporadically and locally appear on a few profiles (Figure 6). These have been interpreted as the Givetian limestones (Lacquement et al., 1999).

The AMBT, which is located at the base of the Allochthonous Unit, is usually clearly visible on the seismic profiles. It is represented by a series of few continuous and parallel reflectors of high amplitude and frequency, truncating locally reflectors at its footwall (the underlying OTS and Brabant Para-autochthonous Unit) (e.g., Raoult, 1986; Lacquement et al., 1999) (Figure 6).

Below the AMBT, the OTS are distinguished by rather chaotic facies associated with discontinuous reflectors of variable amplitude and frequency (Figure 6). The intense deformation of the OTS makes it difficult to image their internal geometry. However, continuous reflectors are visible in some areas (see Figure 5b). The OTS is not always easily visible on the profiles; its seismic facies vary laterally, depending on the impedance contrast between the footwall and hangingwall formations. In areas where there is a strong impedance contrast, for instance between Dinantian carbonates in the OTS and Namurian shales in the para-autochthonous unit, the OTS is represented by a series of parallel and rather continuous high amplitude reflectors. On the contrary, the weak impedance contrast created by the presence of Namurian deposits both in the hangingwall and footwall of the OTS results in a lower amplitude seismic facies of the OTS.

The Brabant Parautochthonous Unit is characterized by variable seismic facies: (a) the Namurian-Westphalian coal-bearing deposits are characterized by a chaotic seismic facies. The reflectors are discontinuous and usually have a low amplitude and a medium-to-high frequency (Figure 6). These chaotic facies can be related to the intense short-wavelength folding and faulting of the coal basin during the late Carboniferous, which is responsible for the strong dispersion of the seismic waves; (b) the underlying Dinantian carbonate platform is represented by a parallel to contorted facies, associated with semicontinuous reflectors of variable frequency and medium-to-low amplitude (Figure 6). In some areas, the Dinantian displays semi-transparent seismic facies associated with very low-amplitude reflections. At the top of the Dinantian, the reflectors are usually continuous and have a higher amplitude (Figure 6), illustrating a major impedance variation between the overlying Namurian coal-bearing deposits and the Viséan limestones; (c) Famennian sedimentary sequences, comprising mainly sandstones and shales, appear as semiparallel, semicontinuous, low-amplitude and high-frequency reflectors (Figure 6). The top of Famennian is usually visible on seismic lines because it appears as continuous medium-amplitude and high-frequency reflectors (Figure 6); (d) beneath the Famennian, the Frasnian limestones are marked by their stratified geometry associated with parallel, continuous, high-amplitude and low-frequency reflectors, easily visible on seismic data (e.g., Raoult, 1986; Lacquement et al., 1999) (Figure 6); (e) the underlying Eifelian-Givetian limestones have a similar seismic facies, although the reflectors are mostly semicontinuous (Figure 6).

At the base of the Brabant Para-autochthonous Unit, the Eifelian and Givetian limestones are unconformably lying above Silurian deposits of the lower Paleozoic basement. The latter is represented by a chaotic facies associated with discontinuous reflectors of variable amplitude and frequency (Figure 6). Poor imaging of the basement structure is due to the low penetration of seismic waves at such depths. The basement unconformity is poorly imaged on seismic lines. It can usually be identified as the limit between the chaotic facies of the basement and the semicontinuous high-amplitude reflectors of the Eifelian-Givetian limestones. Truncations of the basement reflectors below the Middle Devonian deposits are sometimes visible (Figure 6).

5. Seismic Interpretation

The interpretation of the seismic lines provides insights into the geometric and structural features of the Northern Variscan Front and its substratum. We were able to evidence the first-order geometry of major extensional and compressional structures and present it below. The description follows the structural model described above (cf., 2.2.), detailing the geometry of the Brabant Para-autochthonous Unit, the Overturned Thrust Sheet and the Ardennes Allochthonous Unit. In particular, we focus on lateral ramps within the thrust system.

5.1. Brabant Para-Autochthonous Unit

The relatively good quality of seismic data below the poorly imaged Ardennes Allochthonous Unit allows us to precisely interpret the deep structure of the buried Brabant Para-autochthonous Unit. In the following, we successively document the large underthrusting of the foreland basin below the AMBT, second order thrust faults, deep folding and then extensional structures in the Brabant Para-autochthonous Unit.

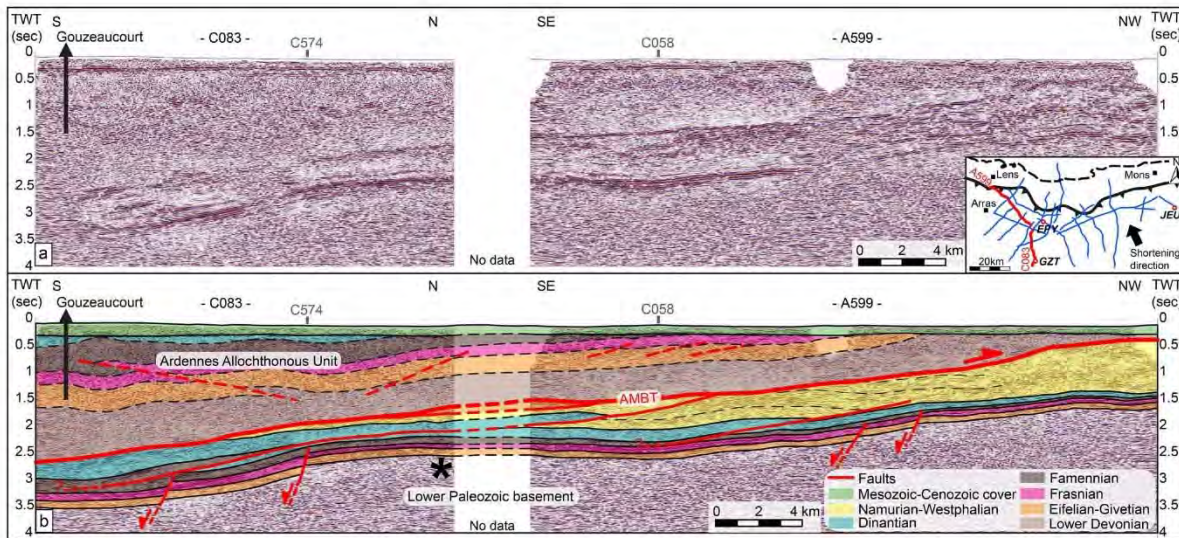


Figure 7. SE-NW composite seismic reflection profile with (a) reprocessed line and (b) geological interpretation. This profile is approximately parallel to the Variscan shortening direction (i.e., SE-NW). The dashed lines in the Namurian–Westphalian coal basin represent the overall geometry of the sedimentary layers. The asterisk marks the deep low-curvature folding of the Brabant Para-autochthonous Unit.

5.1.1. Extent of Foreland Basin Underthrusting

Seismic interpretation of profiles oriented parallel to the overall thrust transport direction (NNW-SSE) such as the A599–C083 composite seismic profile (Figure 7), highlights the large underthrusting of the Brabant Parautochthonous Unit below the Ardennes Allochthonous Unit. Identifying the cut-off line of the basal reflector of the Namurian–Westphalian foreland basin with the AMBT allowed us to quantify the relative minimum amount of underthrusting of the foreland basin beneath the allochthonous unit. It reveals that the sub-thrust foreland basin extends c. 20–25 km beyond the thrust front. More than half of the coal-basin region is therefore buried below the AMBT. This pattern observed on all seismic profiles in the study area (e.g., C122 profile in Figure 8) underlines highly localized displacement onto the AMBT and its subsidiary, the OTSBT.

5.1.2. Second-Order Variscan Thrust Faults

The interpretation of the C122 profile, trending parallel to the direction of the Variscan shortening, shows two major NW-verging thrust faults that deform the Brabant Para-autochthonous Unit below the AMBT (Figure 8). Truncations of the reflectors are clearly visible against the footwall of these faults. The upper thrust is truncated to the south by the AMBT and deforms the Namurian–Westphalian coal-bearing deposits. The lower thrust affects the coal basin, as well as the underlying Dinantian and Famennian platforms. Both thrusts show two flats and ramps. The geometry of the reflectors on the hangingwall of these faults indicates a major folding of the Brabant para-autochthonous sequence, especially in the coal basin. We interpreted those folds as fault-bend folds generated by the movement of the thrust sheets over the ramps (e.g., Suppe, 1983). Accordingly, these two thrusts formed along two of the main regional detachments: the upper one located at the limit between the Dinantian carbonates and the Namurian shales and sandstones and the lower one located within the Famennian shales, resting onto the Frasnian limestones (Figure 2). These compressional structures have been interpreted on numerous seismic profiles and are consistent in the entire study area.

The interpretation of the C058 profile (Figure 9), oriented almost perpendicularly to the regional thrust transport direction, provides another example of a deep thrust characterized by a detachment in the Famennian shales. This thrust has an apparent dip towards the SW and affects the Famennian to Namurian–Westphalian sequence.

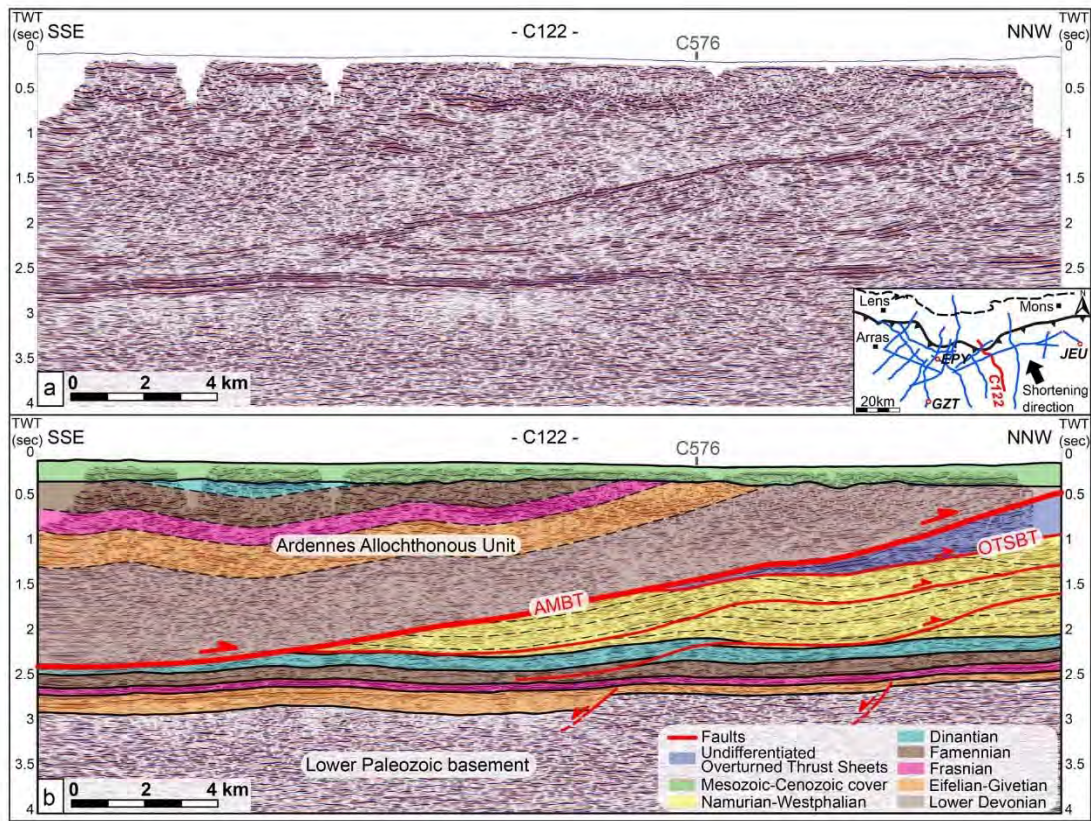


Figure 8. Seismic reflection profile C122 (in TWT) with (a) reprocessed line and (b) geological interpretation. This profile is almost parallel to the Variscan shortening direction (i.e., SE-NW). The dashed lines in the Namurian-Westphalian coal basin represent the overall geometry of the sedimentary layers. The dashed lines in the Ardennes Allochthonous Unit emphasize the simplified nature of the interpretation and the related uncertainties.

A similar geometry has also been observed on the C083 profile (Figure 10). A major thrust is visible on the entire profile and characterized by an apparent southward dip. It deforms the Famennian to Westphalian para-autochthonous sequence and is responsible for its northward displacement of at least 4 km. Truncations of the reflectors, both against the footwall and the hangingwall of this fault, allowed us to delineate its geometry made of one flat and two ramps. Deformation was rooted into the Famennian detachment at the southern end of the profile. The existence of a flat within the generally competent Dinantian carbonates is quite surprising, but its occurrence appeared reasonable in 3-D. The involved décollement in the Dinantian could correspond to the Visean evaporites or the shaly formations of the Tournaisian (e.g., Pont d'Arcole Formation) (Figure 2).

Thrust faults rooting within the Famennian shales and deforming the Famennian to upper Carboniferous series are visible on most seismic lines. Their generalized character along the Northern Variscan Front is particularly well illustrated on a WSW-ENE composite seismic profile (Figure 11) that crosses the entire study area. Since the composite profile is almost orthogonal with respect to the Variscan shortening direction (i.e., SE-NW), it is important to notice that structures are intersected at a high angle relative to the main plane of movement. Six of these highlighted thrusts have an apparent vergence towards the WSW and an apparent dip towards the ENE. The folded geometry of the reflectors in the hangingwall of some of these faults indicates the existence of thrust-related folds generated by movement of the thrust sheets over the ramps. A peculiar feature to note on this profile (Figure 11) is the existence of a thrust fault rooting down onto the Middle Devonian second-order décollement (Figure 2). It is also important to notice that this fault apparently nucleated against a Middle Devonian normal fault.

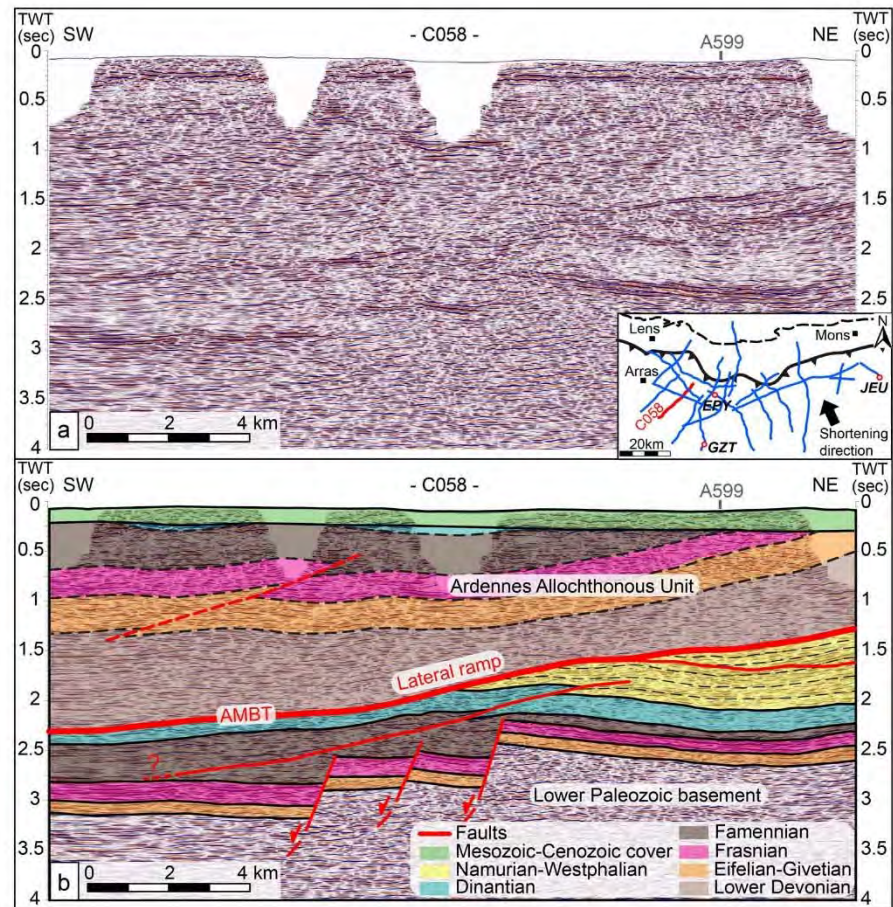


Figure 9. Seismic reflection profile C058 with (a) reprocessed line and (b) geological interpretation. This profile is highly oblique with respect to the direction of Variscan shortening (i.e., SE-NW). The dashed lines in the Namurian-Westphalian coal basin represent the overall geometry of the sedimentary layers. The dashed lines in the Ardennes Allochthonous Unit mark the simplified geometry of the interpretation and the related uncertainties.

5.1.3. Deep Folding of the Para-Autochthonous Unit

The interpretation of the C083 profile (Figure 10) illustrates the overall southward dip of the Brabant Para-autochthonous Unit, as well as some superimposed long-wavelength undulations of the basement and the overlying para-autochthonous series. A gentle antiform structure is observed west of Cambrai in the southern part of the profile (marked by an asterisk in Figure 10) at a depth over 2 s TWT. This long-wavelength, deep antiform affects the lower Paleozoic basement and the entire para-autochthonous sequence. Similar deep folding of the basement and the Brabant Para-autochthonous Unit has also been observed further west on the C058, C067 and C068 profiles. For instance, on the C058 profile (Figure 9), Devonian and Carboniferous layers at the footwall of the northernmost Devonian normal fault are dipping northward.

We do not view this peculiar geometry as a seismic artifact (pull-up effect) because there is no evidence of the presence of a high seismic velocity layer above the para-autochthonous unit. Seismic facies of the Ardennes Allochthonous Unit remain consistent across the profiles (Figure 10). Moreover, the AMBT does not seem to be affected by this uplift as it would be the case with a seismic pull up. Instead, we suggest that this basement dome corresponds to a deep anticline formed during the propagation of the Variscan thrust front. The lack of deformation of the AMBT, which truncates the folded para-autochthonous series

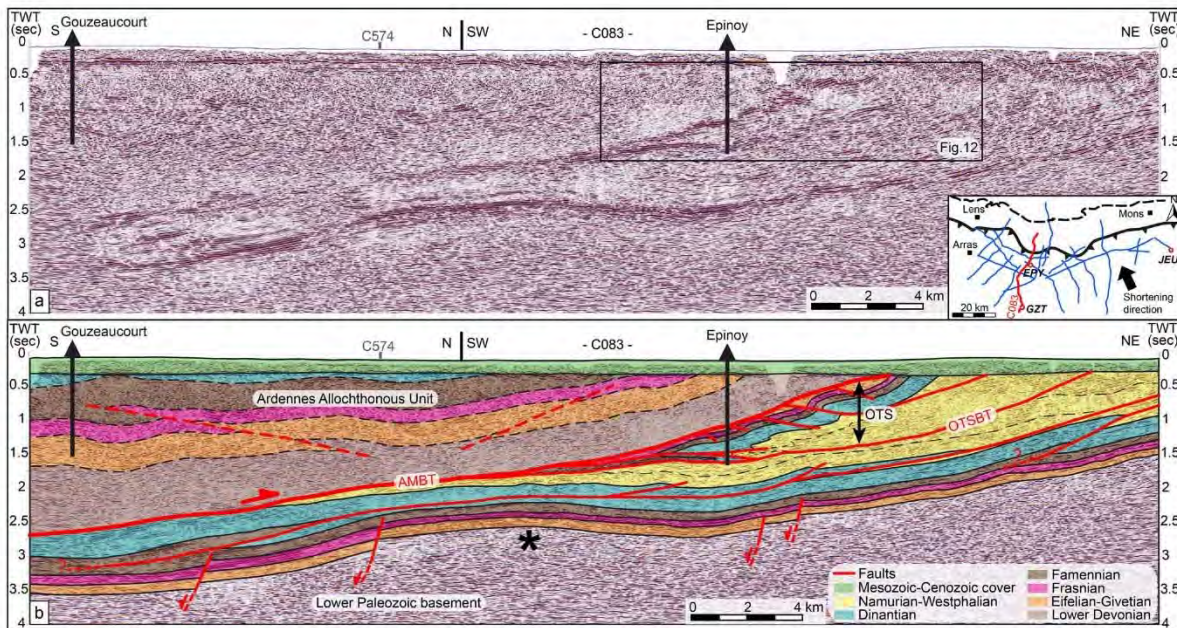


Figure 10. Seismic reflection profile C083 with (a) reprocessed line and (b) geological interpretation. This profile is mostly parallel to the Variscan shortening direction (i.e., SE-NW) in its southern part and highly oblique to the Variscan shortening direction in its northern part. The asterisk points out folding at depth of the Brabant para-autochthonous Unit. The black frame corresponds to an enlarged part of this profile focusing on the OTS internal structure, presented in Figure 12.

(Figure 10), suggests that the anticline formed before the terminal stage of the Variscan orogeny and the out-of-sequence dislocation of the frontal thrust zone in the Middle Pennsylvanian (i.e., late Westphalian).

5.1.4. Pre-Existing Extensional Structures

The clearly imaged deep reflectors below the AMBT provide useful insights on the prominent characteristics of the initial geometry of the Laurussian margin prior to its underthrusting. For example, this is illustrated by the C122 profile located south of Valenciennes (Figure 8). Analysis of the reflectors' continuity and the seismic facies variation shows two normal faults with an apparent southward dip. These faults affect the lower Paleozoic basement and offset the top of the basement. The southernmost normal fault is particularly well marked by the contrasting seismic facies of the Middle Devonian in its hangingwall (i.e., rather transparent facies) and footwall (i.e., higher amplitude reflectors). The Eifelian-Givetian deposits are thicker in the hangingwall of these faults, thus demonstrating the syn-sedimentary nature of these extensional structures (i.e., Middle Devonian in age). The continuity of the high amplitude reflectors of the Frasnian limestones above those faults suggests that deformation ended before the Late Devonian. Similar faults have been interpreted in the eastern part of the study area, especially on the M146 profile (Figure 3) (Lacquement et al., 1999).

Further west, south of Douai, our interpretation of the seismic lines C058 (Figure 9), C067, C068 and C083 (Figure 10) highlights a series of normal faults that have apparent dips towards the south or southwest. Large offsets of high-amplitude, usually continuous, reflectors of the Frasnian limestones are clearly visible on these profiles, especially the C058 one (Figure 9). The analysis of these offsets allowed to identify two to three major normal faults in the southern part of the profiles. These faults clearly deform the basement and the Middle Devonian sediments. Thickening of the Frasnian and mostly of the Famennian, is visible in their hangingwall, evidencing the apparent syn-sedimentary nature of these extensional structures (i.e., Late Devonian in age). Along the C058 (Figure 9) and C083 profiles (Figure 10), Devonian normal faults are particularly well imaged because the strike of the profiles (i.e., SW-NE) is orthogonal to the strike of the normal faults (i.e., NW-SE—see later in 6.3.).

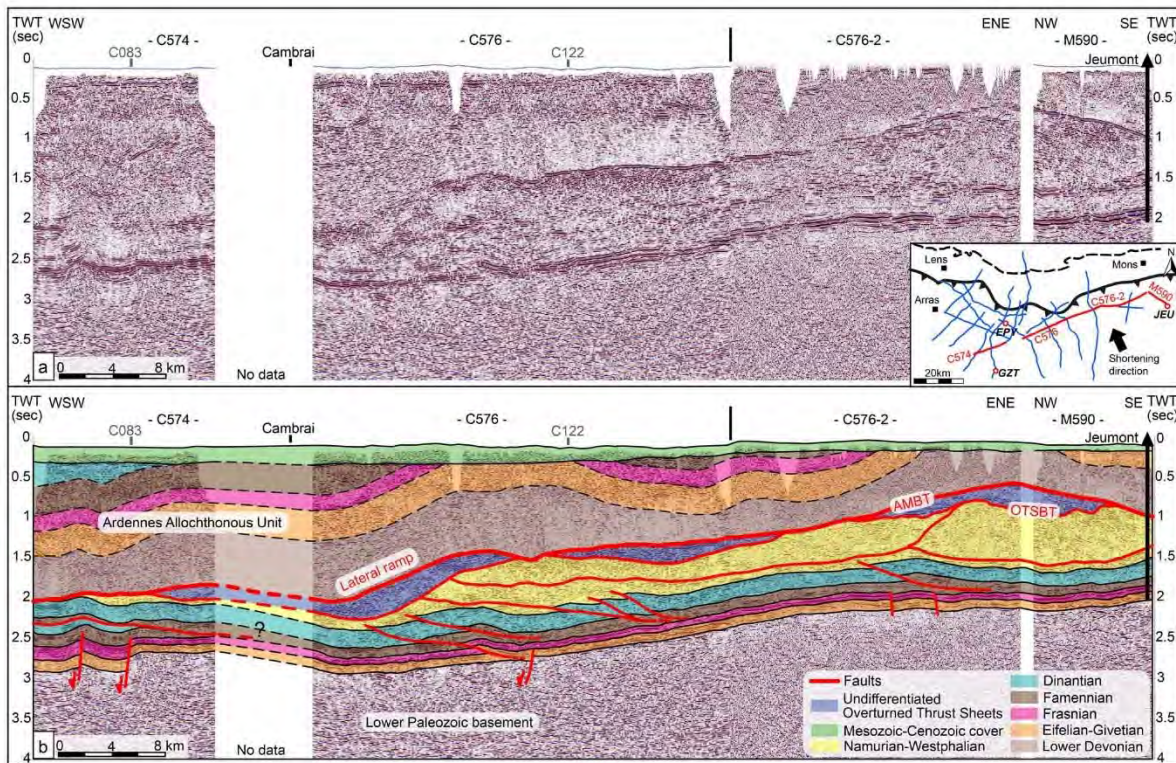


Figure 11. WSW-ENE composite seismic reflection profile with (a) reprocessed line and (b) geological interpretation. Note that the strike of this profile is orthogonal to the Variscan shortening direction (i.e., SE-NW), implying that structures are intersected very obliquely with respect to the direction of tectonic movement.

In summary, deep Devonian syn-sedimentary normal faults are visible on most of the interpreted profiles. These faults accommodated extension during the Mid-Late Devonian and represent first-order structures of the pre-orogenic Laurussian margin in its proximal part (Brabant border). These results suggest that extensional deformation persisted after the Early Devonian rifting phase associated with the opening of the Rheino-Hercynian Ocean and responsible for the first-order segmentation of the southern Laurussian margin. This post-rift extension, coeval with the overall thermal subsidence of the margin, may have had some impacts on its structure and the associated depocenters until the Famennian, at least in the most proximal part of the margin (the southern border of the Brabant massif). This result is in agreement with several studies carried out along the Northern Variscan Front (Ardennes, southern England) that evidenced some effects of extension on the sedimentation pattern up to the Middle and Late Devonian (e.g., Thorez & Dreesen, 1986; Pr at & Boulvain, 1988; Shail & Leveridge, 2009; Leveridge, 2011). Interestingly, an analysis of the faults' activity shows a diachronic pattern within the study area. Some faults were active during the Middle Devonian and others during the Late Devonian. The reason for such diachronism in northern France remains an open question. Similar diachronic segmentation of the Laurussian margin is also known in SW England where a progressive northward development of the Laurussian margin basins between the Emsian (Looe Basin) and the Famennian (Culm basin) has been highlighted (Leveridge, 2011; Shail & Leveridge, 2009).

Finally, comparison of the position of Devonian syn-sedimentary normal faults and Variscan thrust faults indicates that most ramps of the Variscan thrusts (both lateral and frontal) are located above Middle to Late Devonian syn-sedimentary normal faults. For instance, the ramps of both thrusts in the Para-autochthonous Unit on the C122 profile (Figure 8) are located above two Middle Devonian normal faults. Moreover, the lower detachment within the Famennian is located right above the southern normal fault. The same observation has been made on the C058 profile (Figure 9), where the lateral ramp of the AMBT and the

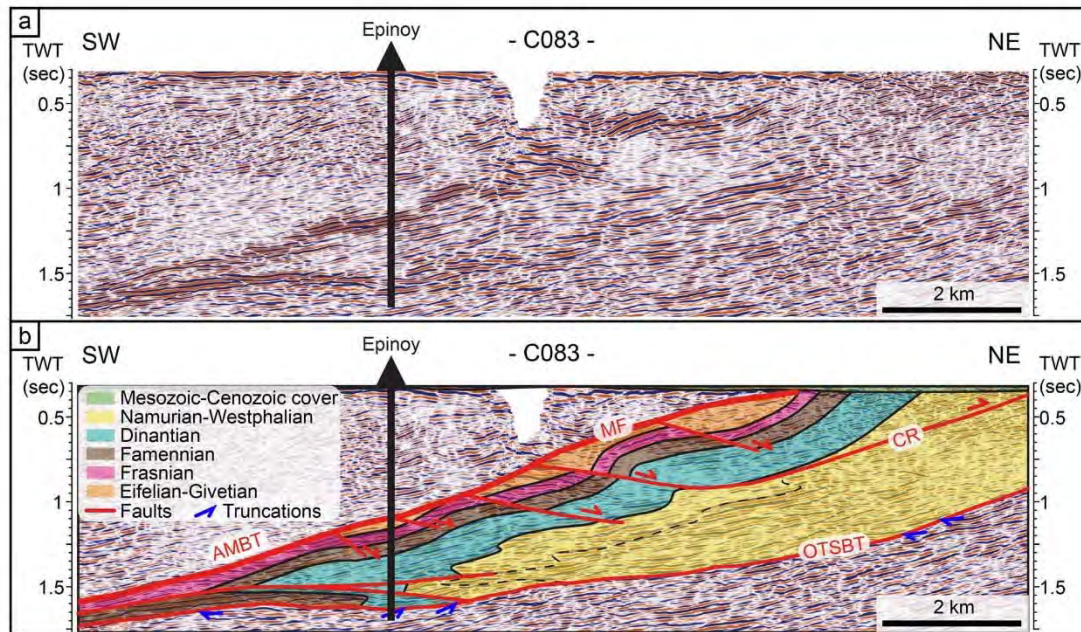


Figure 12. Details on the internal structure of the OTS on the seismic reflection profile C083; (a) reprocessed line and (b) geological interpretation. This part of the profile is oblique to the Variscan shortening direction (i.e., SE-NW). The structures are intersected obliquely with respect to the tectonic transport direction. Faults legend: CR: “Cran de Retour”; MF: “Midi Fault”.

ramp of the para-autochthonous thrust are located above a series of three Late Devonian syn-sedimentary normal faults. The same feature can be observed on the C083 profile (Figure 10) where both ramps of the major thrust fault in the Para-autochthonous Unit are located above Devonian normal faults.

5.2. Overturned Thrust Sheets

The OTS constitute one of the major and peculiar units of the Northern Variscan Front in the north of France. Owing to the seismic-well tie of the Epinoy borehole, we could link the overall and internal structure of the OTS between Douai and Cambrai cities (Figure 10 and 12). The OTS are bounded by two major thrusts characterized by high amplitude seismic facies. These are the out-of-sequence “Midi Fault” at the top, which corresponds to the shallower part of the AMBT, and the OTSBT that connects to the AMBT south of the profile.

The internal structure of the OTS (Figure 12) is interpreted on the basis of (a) the stratigraphic succession known from the Epinoy borehole, (b) the geometry of the reflectors, (c) the 3-D consistency with structures interpreted on all related seismic profiles, and (d) the consistency with the near surface structures in the coal basin area (Bouroz et al., 1963) (Figure 12). The interpretation of the C083 seismic line shows the overturned geometry of the Devonian-Carboniferous sequence that is deformed as a major recumbent syncline. It is worth mentioning that imaging of a recumbent fold in seismic data is limited, particularly in the hinge zone, where reflectors of both the upper and lower limbs intersect, creating mostly chaotic and discontinuous seismic patterns. Therefore, some uncertainties remain on the position of markers interpreted in the hinge zone of recumbent synclines, where interpretation choices have to be made to maintain a coherent geometry and kinematics.

The north-facing recumbent syncline is truncated to the south by the AMBT. It is characterized by a significant thickening of the sedimentary series across the hinge zone. This is especially the case for the Dinantian sequence observed in the Epinoy borehole whose thickness reaches at least a thousand meters. The overturned limb of the syncline is deformed by northward-dipping second-order low-angle curved normal faults

present in the coal basin (Bouroz, 1950; Le Gall, 1994; Meilliez, 2019). It is also truncated by a NE-verging thrust fault bounded to the south by the AMBT. This curved thrust has been identified as the “Cran de Retour” thrust (CR), described in the NPC coal basin literature (e.g., Bouroz et al., 1961; Becq-Giraudon, 1983).

5.3. Ardennes Allochthonous Unit

The Ardennes Allochthonous Unit is not well imaged on seismic data, mainly because of the combined effect of an overall lithological homogeneity of the sedimentary sequences (mostly alternating shales and sandstones) and intense internal deformation. Despite this, our interpretation is based on (a) the seismic-well tie of the Gouzeaucourt borehole (GZT) along with the C083 profile (Figure 10), (b) the interpretation of some sporadic and continuous high-amplitude reflectors that we assume to correspond to Givetian limestones (Lacquement et al., 1999; Raoult, 1986), (c) the geological sketch map of the Paleozoic substratum in northern France (C.F.P. et al., 1965; Figure 1b), (d) the 3-D coherence between profiles.

Our interpretations are greatly simplified compared with the present-day structure of the Allochthonous Unit, but they highlight locally some major Variscan folds and thrusts affecting the Lower Devonian to lower Carboniferous allochthonous sequence. For instance, a north-vergent thrust fault deforming the Lower to Upper Devonian layers has been interpreted on the C058 (Figure 9) and C083 (Figure 10) profiles. A back-thrust can also be seen on the C083 profile (Figure 10). It is characterized by a detachment in the Lower Devonian series (Figure 2) and it deforms the entire Devonian allochthonous sequence. Such back-thrusts in the Ardennes Allochthonous Unit have already been observed and described in the field in the Avesnois region (Moulouel, 2008).

5.4. Lateral Ramps in the Thrust System

In the area SE of Douai, near Cambrai, specific structural features along the AMBT are present and are illustrated on the composite WSW-ENE striking seismic line (Figure 11). In the eastern part of the C576 profile, the AMBT trace is mostly parallel to the surface and is only slightly tilted toward the south at a depth of approximately 1.2–1.5 s TWT. It then rapidly deepens westward at a depth of 2 s TWT. This phenomenon is associated with significant folding and thickening of the overlying Ardennes Allochthonous Unit. Considering that the orientation of this seismic profile is orthogonal to the direction of the Variscan shortening, we interpreted this change in geometry of the thrust fault as an evidence of a major lateral or oblique ramp in the western part of the profile. Lateral and oblique ramps are defined as thrust surfaces that are parallel or oblique to the direction of transport of the allochthonous thrust sheet (e.g., Butler, 1982; McClay, 1992). These have been observed and described in numerous fold-and-thrust belts, such as the Pyrenees (Averbuch et al., 1993; Frizon de Lamotte et al., 1995), Taiwan (Lacombe et al., 2003) or the Appalachians (Cook & Thomas, 2009).

The AMBT is characterized by a frontal ramp in the eastern part of the profile (south of Valenciennes). A similar example of a lateral or oblique ramp of the AMBT is visible to the west on the C058 profile that is oblique to the direction of Variscan shortening (Figure 9). Interestingly, on the C576 profile, the OTSBT has a similar lateral or oblique ramp geometry under the lateral ramp of the AMBT (Figure 11). This suggests that both thrusts may have been inherited from a similar 3-D geometry.

Finally, the underlying Para-autochthonous Unit shows a complex structure under those two superimposed lateral ramps (Figure 11). Indeed, the Middle-Upper Devonian and Carboniferous sequence is deformed by deep Variscan thrusts that have an apparent vergence towards the WSW and are associated with fault-related folds. These structures caused an overthickening of the Para-autochthonous Unit under the lateral ramps.

6. Structural Maps

Results of the seismic interpretation have been correlated and summarized on time structural maps (or isochron maps) for the key geological surfaces such as the AMBT, the OTSBT or the top of the Givetian sedimentary layer in the Brabant Para-autochthonous Unit. Structural surfaces were generated in two-way travel time (TWT time) using a minimum curvature algorithm, meaning that seismic data were interpolated

and extrapolated in 3-D based on the principle that two adjacent data points were assumed to lie along a circular arc. A medium smoothing was applied during the gridding process in order to improve the plotting quality of the isochrons while respecting the seismic data interpretation. A different grid cell size has been chosen to model the different structural horizons, depending on precision needed and structural complexity of the geological surface. For instance, we chose a 1500 × 1500 meters grid cell size to model the AMBT surface because this surface is quite homogeneous in 3-D. On contrary, we chose a 100 × 100 meters grid cell size to model the top Givetian horizon, which is much more deformed. It is important to mention a limitation associated with this modeling method. Indeed, since it is based on the interpolation of the seismic data interpretation, uncertainties increase in areas where seismic lines are located far from each other. Therefore, the results of gridding have to be considered with caution in areas with no closeby-located seismic data.

The structural maps obtained provide unprecedented regional images of the 3-D geometry of the Northern Variscan Front and the structure of the underthrust southern Laurussian margin in northern France. Furthermore, mapping of the cut-off lines of the base of the Namurian-Westphalian molasse (Figure 13a) and of the OTSBT (Figure 13b) allows to characterize the southern extent of the syn-orogenic deposits and the OTS complex below the Ardennes Allochthonous Unit. They also allow us to quantify the relative displacement on the AMBT and the related underthrusting of the Brabant Para-autochthonous Unit.

6.1. 3-D Geometry of the AMBT

The structural map of the AMBT between Arras and Maubeuge shows its general southward deepening (Figure 13a). It reaches time depths from 0.29 s TWT at the southern edge of the coal-bearing foreland basin down to 2.86 s TWT south of Cambrai (approximate depth range of 100–6.750 m, based on seismic-well ties). To the north, tight isochrons highlight a steeper dip of the AMBT near the surface, while spread isochrons to the south show a lower dip of the AMBT at depth. A comparison between map traces of the AMBT (black continuous line) and of the basal reflector of the Namurian-Westphalian sequence (dark pink dotted line) points out that the syn-orogenic deposits extend more than 20 km south of the frontal thrust zone below the Ardennes Allochthonous Unit. This configuration basically emphasizes a high degree of localization of displacement on the AMBT.

An important outcome is the lateral evolution of the strike of the AMBT from West (Arras) to East (Maubeuge) (Figure 13a). As mentioned above, the overall orientation of the Northern Variscan Front in northern France-southern Belgium changes laterally from WNW-ESE (N110–120°) in the Boulonnais and Artois regions, to ENE-WSW (N60–70°) in the Avesnois region and the Ardennes Massif. In our study area, these two major trends are visible at depth. South of Valenciennes and Lens, the AMBT trends N70–80° and is orthogonal to the Variscan shortening direction (i.e., SSE–NNW) (Figure 13a). This is consistent with the general strike of the Northern Variscan Front known in this area. Therefore, we consider the direction of Variscan shortening along the AMBT in these regions as frontal. However, south of Douai, the AMBT trends N130° and is almost parallel to the direction of Variscan shortening (Figure 13a). This major change in strike indicates the presence of a lateral thrust ramp relaying the two frontal thrust ramps to the south of Lens and Valenciennes. A second-order lateral ramp, striking N120°, is visible NE of Cambrai. An apparently oblique thrust ramp is also visible further east in the Maubeuge area, where the AMBT trends N110°. Unfortunately, seismic profiles are lacking in the southern part of this area, which would have allowed us to determine the actual trend of the basal thrust.

Another major outcome arising from the 3-D integration of the seismic data is the new map trace of the frontal thrust zone under the Mesozoic-Cenozoic cover between Douai and Valenciennes (Figure 13a). The latter does not represent the original geometry of the frontal thrust zone but its current state. Indeed, the frontal thrust zone continued further north during late Carboniferous times and was eroded afterward. The easily identifiable seismic facies of the AMBT allowed us to accurately interpret its northern extension on the seismic profiles A55, C083, C099, C101, C122, C586, and M146. East of the M146 profile and in the areas with no seismic data, the trace of the AMBT corresponds to the trace of the “Midi Fault” (Figure 1a). Some major changes have been made between Douai and Valenciennes, where seismic data are available. The interpretation of the eastern part of the C586 profile highlighted the presence of two distinct thrusts relaying at the base of the Ardennes Allochthonous Unit. The eastern thrust, trending N70° and characterized by a

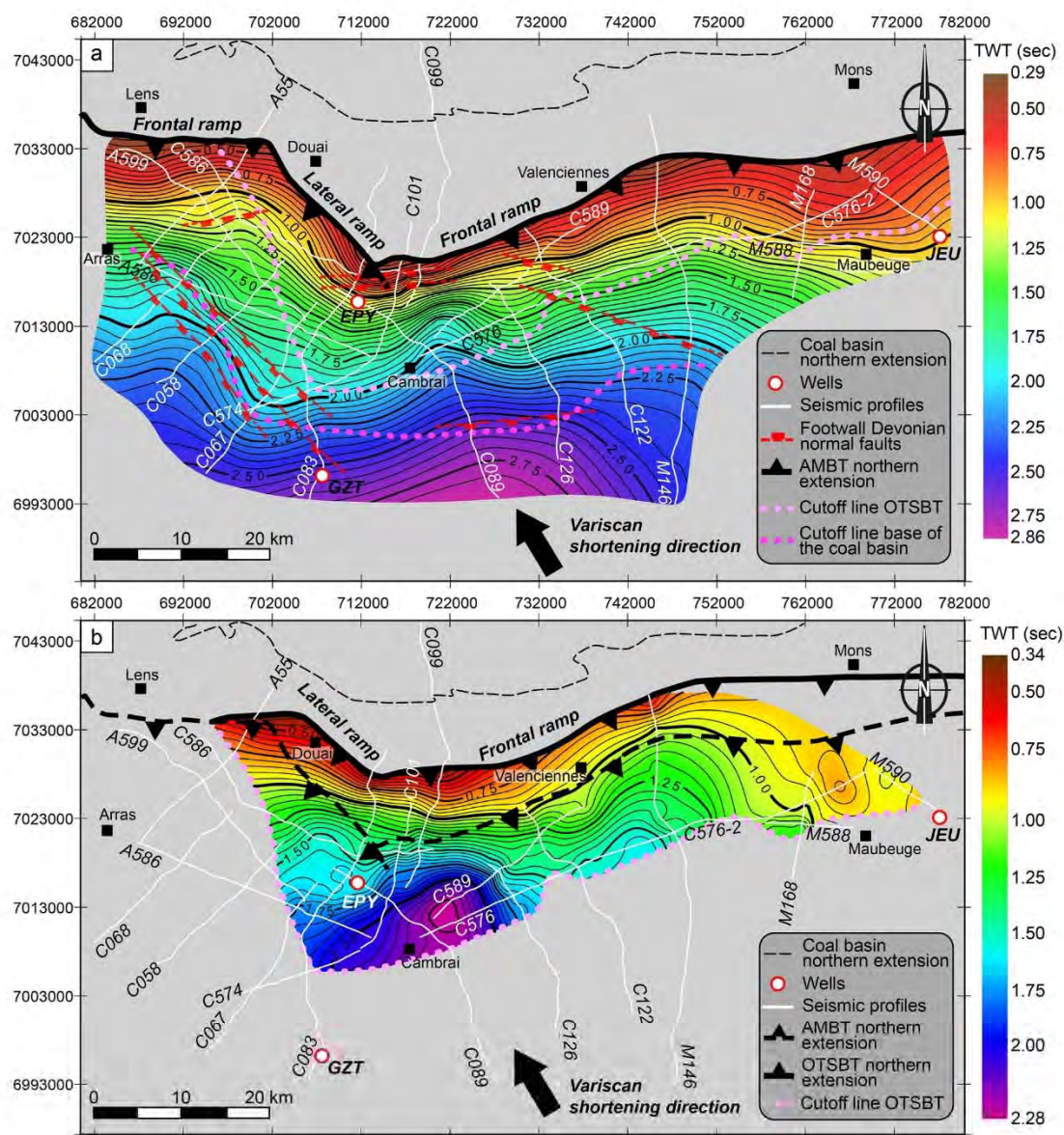


Figure 13. Isochron maps of (a) the Allochthon Main Basal Thrust (AMBT) (grid cell size of 1500×1500 meters) and (b) the Overturned Thrust Sheets Basal Thrust (OTSBT) (grid cell size of 500×500 meters), computed from seismic interpretation. Contour lines are every 0.05 s. The modeling was carried out using IHS Kingdom Software. Map coordinates are in French Lambert 93. A new outline of the AMBT truncated by the Mesozoic-Cenozoic cover is proposed, based on the results of the seismic interpretation.

frontal ramp geometry south of Valenciennes, is truncated to the west by a second thrust, trending $N130^\circ$ south of Douai (lateral ramp) and $N70-80^\circ$ south of Lens (frontal ramp) (Figure 13a). Therefore, this result indicates that the Northern Variscan Front appears to have a segmented geometry in northern France, rather than a continuous one (Figure 13a). The lateral ramp south of Douai relays two major frontal thrusts of a segmented Northern Variscan Front, trending generally WSW-ENE.

6.2. 3-D Geometry of the OTSBT

The structural map of the OTSBT indicates that this basal thrust deepens southward and reaches depths between 0.34 s TWT in the coal basin and 2.28 s TWT to the south (approximate depth range of 100–5,500 m, based on seismic-well ties), where it intersects the AMBT (Figure 13b). Its cut-off line is represented on the grids of both the AMBT (Figure 13a) and the OTSBT (Figure 13b). A striking feature on this map is the substantial southward extension of the OTS. Indeed, the OTSBT and consequently the OTS extend over 15–25 km between their northern limit in the coal basin and their cut-off line with the AMBT to the south.

Major strike variations are evidenced by the 3-D integration of seismic interpretation between Douai and Maubeuge cities, thus, illustrating the lateral evolution of the OTSBT geometry. To the east (area of Valenciennes), this thrust is orthogonal to the Variscan shortening direction (i.e., SSE–NNW) as it strikes approximately N70°. It follows therefore the overall structural trend of the Northern Variscan Front in the Avesnois region and the Ardennes Massif (i.e., WSW–ENE). The OTSBT strike changes progressively westward, from WSW–ENE to SE–NW (N110–130°) in the area of Douai. Accordingly, it highlights the transition from a frontal thrust ramp geometry near Valenciennes to an oblique and lateral thrust ramp geometry southeast of Douai. Local changes in strike are visible in a few areas. The transverse structure seems to be transferred east of Cambrai into a rather steep about N160 ramp as observed at the western end of the C576 profile (Figure 11). The related abrupt deepening delimits eastward a zone of maximum depth of the OTSBT, whereas it appears to be bounded by a N070 trending ramp along its northern border (close to the Epinoy borehole). Another lateral thrust ramp can be identified northwest of Maubeuge, where the OTSBT trends about N130°. However, seismic data crossing the thrust front at the eastern end of the study area are lacking and a precise description of the 3-D geometry in this area is not possible.

An interesting correlation appears when comparing the 3-D geometries of both the AMBT and the OTSBT. The lateral or oblique ramps of both thrusts are superimposed, as well as the frontal ramps. For instance, the second-order lateral ramp of the AMBT northeast of Cambrai, is superimposed to the lateral ramp of the OTSBT identified in this area (Figure 11). Likewise, the strike-deviation zone between Douai and Valenciennes coincides geographically with that of the AMBT, presented above (Figure 13a). This finding is important because it shows that both of these out-of-sequence thrusts were deformed along the same two main axes between Lens and the Belgian border. The first axis (N60–70°) is orthogonal to the Variscan shortening direction in the area of Valenciennes, whereas the second one (N110–130°) is parallel or oblique to the Variscan shortening direction in the areas of Douai, Maubeuge and northeast of Cambrai.

6.3. 3-D Geometry of the Southern Laurussian Margin

We computed a structural map of the top-Givetian limestone sequence at the base of the Brabant Para-autochthonous Unit (Figure 14). This map is the first 3-D image showing the structure of the underthrust, slightly deformed southern Laurussian margin in northern France. This map shows that the Givetian carbonates are present at a depth between 0.29 and 3.47 s TWT (approximate depth range of 50–8,500 m, based on seismic-well ties). They generally gently deepen southward in response to the thrust-loading flexural bending of the Brabant Parautochthonous Unit. To the north, in the coal basin area, the Middle Devonian carbonate sequence displays a steeper monoclinical geometry, as shown by the tightened and parallel isochrons. It strikes N120–130° in the area of Douai and N70° north of Valenciennes. South of the coal basin area, the southern Laurussian margin has a more irregular geometry as emphasized by the 3-D geometry of the top Givetian reflector. Between Maubeuge and Cambrai, it slowly deepens towards the south-west and is characterized by an alternation of quite flat levels with steeper-dipping levels, defining a staircase geometry striking around N130°. Between Lens and Cambrai, the southern Laurussian margin has an overall N50° orientation and deepens towards the south-east.

Seismic interpretation has shown that the Brabant Para-autochthonous Unit is deformed by major deep structures (both compressional and extensional) south of the coal basin area. Some of them have been correlated from line to line and are illustrated on the structural map of the Givetian top (Figure 14). Between Arras and Cambrai, the top-Givetian reflector is affected by a pair of anticline and syncline (orange folds axes) striking N120–130°. Those folds correspond to the deep anticline and associated syncline interpreted on the C083 seismic profile (Figure 10).

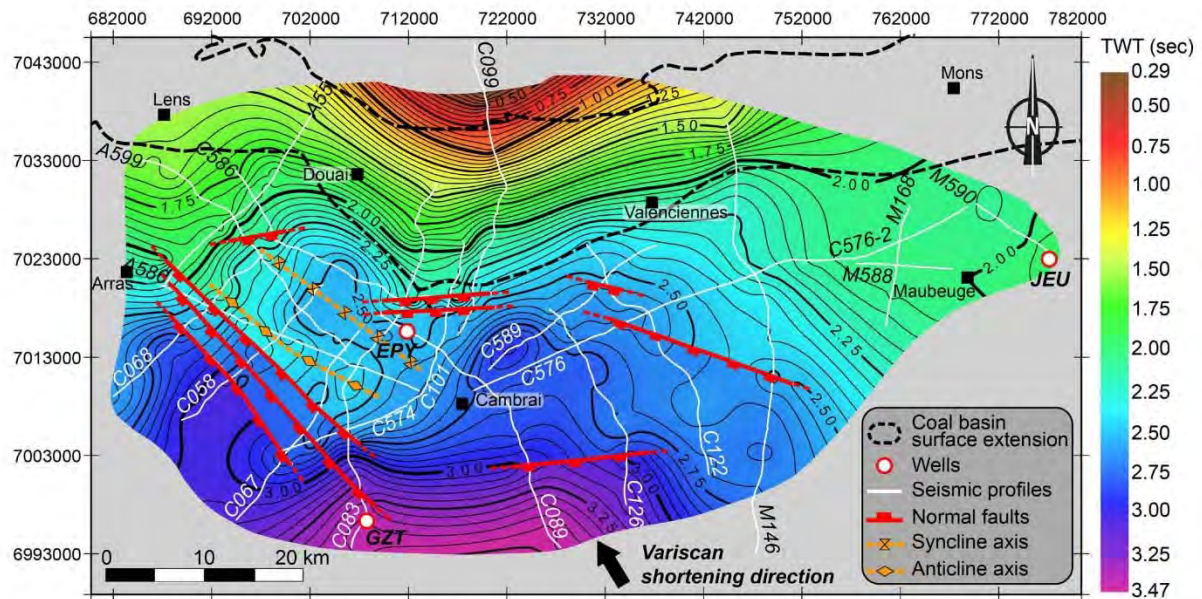


Figure 14. Isochron map of the top of the Givetian (grid cell size of 100×100 meters). This structural grid was modeled based on the seismic interpretation of the Givetian top. The modeling was carried out using IHS Kingdom Software. Equidistance is 0.05 s. Map coordinates are in French Lambert 93.

The syn-sedimentary normal faults inherited from the pre-orogenic Laurussian margin deformation have also been laterally correlated and illustrated on the structural map (Figure 14). In detail, three different sets of faults strikes can be distinguished from the east to west: a) $N120^\circ$ south of Valenciennes, b) $N130^\circ$ south of Douai-Lens and c) about $N70\text{--}80^\circ$ in the central region. Considering that the $N120^\circ$ and $N130^\circ$ striking sets cannot be regarded as significantly different fault systems, it can be inferred that the southern Laurussian margin was basically segmented by a system of normal faults striking $N70\text{--}80^\circ$ and $N120\text{--}130^\circ$. This finding is consistent with previous studies that suggest that the Laurussian margin in northern France-southern Belgium was segmented by a set of $N50\text{--}70^\circ$ and $N110\text{--}130^\circ$ trending normal faults during the syn-rift Devonian stage (e.g., Meilliez et al., 1991; Lacquement, 2001). These syn-sedimentary normal faults have significantly contributed to the southward deepening of the southern Laurussian margin and the associated thickening of the Devonian series. It is particularly visible southeast of Arras, where the $N130^\circ$ -trending normal faults are characterized by an important down-dip throw responsible for the substantial deepening of the Devonian layers towards the south-west and the associated thickening of the Upper Devonian sequence (Figure 9).

The superposition of Variscan structures and pre-existing Devonian normal faults is well illustrated in 3-D on the structural map of the AMBT (Figure 13a). Except for the region located south of Valenciennes, the geometry of the AMBT follows the strike of the Devonian normal faults in its footwall. Furthermore, comparison of the structural maps of the AMBT (Figure 13a) and OTSBT (Figure 13b) to the structural map of the Givetian top (Figure 14) reveals a spatial correlation between the geometry of the Variscan thrusts and the topography of the Devonian substratum in the footwall of these faults. Indeed, frontal thrust ramps of the AMBT (Figure 13a) and OTSBT (Figure 13b) developed where the rifted Laurussian margin was trending $N60\text{--}80^\circ$ and deepened southeastward, while the lateral and oblique thrust ramps developed, trending $N110\text{--}130^\circ$ and deepening southwestward. For instance, the $N130^\circ$ trend of the lateral ramp of the AMBT south of Douai matches the trend of the underlying Laurussian rifted margin. The strike-deviation zone between Douai and Valenciennes coincides with a major change in orientation of the underlying substratum. Northeast of Cambrai, the superimposed lateral ramps of the AMBT and OTSBT, both visible on the seismic data (Figure 11) and structural maps, developed above the edge of a topographic trough, trending SE-NW. Overall, the main Variscan thrusts seem to be molded on the topography of the Laurussian margin inherited from the Devonian Rheno-Hercynian extensional event.

7. Discussion

7.1. New Insights on the Geometry of the Northern Variscan Front in Northern France

Our seismic interpretation provides a new understanding of the 3-D geometry of the North Variscan Front in northern France, so far locally described from 2-D geological cross-sections. The along-strike lateral changes in the geometry of the thrust front and its controlling factors are discussed below.

7.1.1. Segmentation of the Thrust Front

Study of the 3-D geometry of the two main thrusts of the Northern Variscan Front (AMBT and OTSBT) demonstrates the existence of major lateral ramps south of Douai, relaying two frontal thrust segments: the first one located south of Valenciennes, and the second one south of Lens (Figure 13). This new finding corroborates several studies (Averbuch et al., 2002; Lacquement, 2001; Lacquement et al., 2005; Mansy & Meilliez, 1993; Meilliez, 1989; Raoult, 1986) that suggest that the zones of major change in strike observed along the Northern Variscan Front of NW Europe correspond to lateral or oblique thrust ramps relaying several major thrusts of a segmented front.

At a smaller scale, some previous studies focusing on a similar change in strike in the Meuse valley-Dinant recess (Ardennes Massif) (Lacquement et al., 2005; Szaniawski et al., 2003) have suggested that these lateral and oblique ramps, including the one located south of Douai, may have acted as transfer zones during the propagation of the thrust front in late Carboniferous times. They would have localized transpressional corridors that accommodated components of both right-lateral strike-slip deformation and oblique shortening. Such a process was evidenced by analog modeling experiments (e.g., Martinez et al., 2002; McClay et al., 2004) showing that convergence oblique with respect to the margin can lead to strain partitioning between margin-normal contraction and margin parallel strike-slip faulting. This could apply south of Douai where the Laurussian margin is parallel-to-oblique with respect to the direction of the Variscan shortening (Figure 14). The transverse shortening localized along the lateral ramps evidenced on the C576 seismic profile (Figure 11) is likely to reflect such transpressional deformation partitioned between different faults.

7.1.2. Structural Inheritance

Results of the seismic interpretation showed that Variscan thrust ramps localized above Devonian normal faults, therefore suggesting that these pre-existing extensional structures acted as areas of preferential nucleation of the subsequent contractional thrust ramps. We argue that such basement discontinuities focused contractional stress during the northward propagation of the thrust front in Late Mississippian-Middle Pennsylvanian and consequently had a buttressing effects that controlled the nucleation of subsequent thrust ramps. This phenomenon has been observed and described already in the 1980s (Butler, 1989; Gillcrist et al., 1987; Schedl & Wiltshcko, 1987; Wiltshcko & Eastman, 1983) in various fold-and-thrust belts, especially in the Appalachians (Konstantinovskaya et al., 2014; Thomas, 2001, 2007), in the Apennines (Butler et al., 2006; Scisciani, 2009; Tavarnelli, 1996, 1999), in the Jura Mountains (Malz et al., 2020; Ustaszewski & Schmid, 2006), in the Alps (Butler et al., 2006), in the Himalayas (Butler, 2020), and at the eastern end of the Variscan deformation front in Poland (Krzywiec et al., 2017; Kufraša et al., 2020), among others. The structure of the Northern Variscan Front in northern France provides a new example of the control exerted by inherited extensional basement structures on the deformation of a propagating thrust front.

At a regional scale, structural maps reveal that the 3-D geometry of the main Variscan thrusts (AMBT and OTSBT) (Figure 13) can be correlated to the topography of the underlying rifted structures of the Laurussian margin (Figure 14). Results show that the major lateral ramps of the AMBT and OTSBT south of Douai formed above the SW-deepening Laurussian margin segmented by N130° striking Devonian normal faults, parallel to the shortening direction. Various natural case studies (Amadori et al., 2019; Lacombe et al., 2003; Lacquement et al., 2005; Paulsen & Marshak, 1999; Ustaszewski & Schmid, 2006), and analog modeling experiments (e.g., Calassou et al., 1993) have emphasized the significant control exerted by inherited basement topography on the geometry and segmentation of thrust fronts along-strike, especially by localizing lateral or oblique ramps, salients and reentrants. Examples in the Jura Mountains (France) (Ustaszewski & Schmid, 2006), in the Sevier fold-thrust belt (Utah, USA) (Paulsen & Marshak, 1999) or in Taiwan (Lacombe et al., 2003) have shown that lateral or oblique thrust ramps of a propagating thrust front are likely to form above basement offsets (often fault-related) trending parallel or oblique with respect to the shortening

direction. By localizing both Variscan frontal and lateral ramps, the inherited structure of the southern Laurussian margin had a major impact on the 3-D geometry and along-strike segmentation of the Northern Variscan Front.

7.2. Synthesis of the Kinematic Evolution of the Northern Variscan Front in Northern France

Results of our seismic interpretation emphasize the main tectonic features of the Northern Variscan Front in northern France. We aim now at providing a regional scope to the structural and kinematic model of the thrust front previously described on the basis of local studies in the Valenciennes (M146 seismic profile, Figure 3) (Averbuch et al., 2018; Lacquement, 2001; Lacquement et al., 1999; Mansy et al., 1997) and Artois regions (Minguely et al., 2008) and attempt an unprecedented regional synthesis of the kinematic evolution of the Northern Variscan Front in northern France. It takes into account known elements from previous studies on the thrust front, as well as additional contributions from our study, in particular (a) the quantification of the regional underthrusting of the foreland basin, (b) the deep folding and thrusting of the Brabant Para-autochthonous Unit, and (c) the nucleation of thrusts above pre-existing basement faults. We present and detail a new conceptual tectonic model for the kinematic evolution of the thrust front showing the successive stages of deformation during the Late Mississippian-Middle Pennsylvanian (Figure 15). The evolution is divided into seven stages (from A to G), with A representing the early compressional stage of the Variscan foreland (Late Mississippian), and F the last compressional stage (Middle Pennsylvanian); stage G depicts the present-day situation. The specific tectonic features of the thrust front visible on this model are discussed below.

7.2.1. Localized Displacement of the Ardennes Allochthonous Unit Onto the AMBT

Our seismic interpretation has emphasized the high degree of localization of displacement onto the AMBT during the Variscan shortening stage. First-time regional quantification of the relative underthrusting of the foreland basin revealed the latter extends on average 20–25 km southward below the Ardennes Allochthonous Unit (Figure 13a). Based on the restoration of the M146 seismic section (Figure 3), and corroborated by the seismic profiles trending almost parallel the average transport direction presented above (Figures 7 and 8), a total displacement of at least 50 km can be estimated along the AMBT (stage F, Figure 15). However, these values are likely to be underestimated, considering that the thrust front extended further north in late Carboniferous times and was later eroded (stage G, Figure 15).

Similar examples of thrusts localizing important displacement exist in various fold-and-thrust belts. In the Southern Apennines (Italy), the Lagronegro allochthon accommodated more than 65 km of displacement (Butler, 2020; Butler et al., 2004), resulting in the large underthrusting of the Apulian foreland. In the Central Salt Range (Pakistan), the Salt Range Thrust localized about 25 km of displacement (Butler, 2020; Qayyum et al., 2015). Numerous studies based on analog modeling and studies of natural cases, argue that syn-kinematic sedimentation exerts a strong influence on the structural evolution of a thrust wedge (e.g., Storti & McClay, 1995; Barrier et al., 2002; Bonnet et al., 2008; Wu & McClay, 2011; Graveleau et al., 2012). Butler (2020) showed that if there is little or no sedimentation at the toe of an emergent thrust front, an individual emergent thrust having a low-angle dip can localize a large amount of slip and carry thrust allochthons, therefore creating a significant sub-thrust or underthrust foreland. If the sedimentation rate increases at the thrust front, the emergent thrust may steepen significantly therefore reducing its tendency to slip. Consequently, deformation may be transferred onto new additional structures in the thrusts hangingwall and footwall.

We, therefore hypothesize that surface processes may have had a significant influence on the geometry of the Northern Variscan Front in northern France. A low sedimentation rate at the toe of the propagating AMBT would provide a viable explanation for the high degree of localization of displacement on the AMBT (stages B and C, Figure 15). This would be consistent with the low-angle dip of the AMBT visible south of the frontal thrust zone (Figure 13a) and at the southern end of the seismic profiles. A later increase in sedimentation rate in the foreland basin may have had a significant influence on the steepening of the AMBT in the frontal thrust zone (Figure 13a), evolving from a footwall flat geometry with large displacement into a footwall ramp geometry with lower displacement (stages D, E, F, Figure 15).

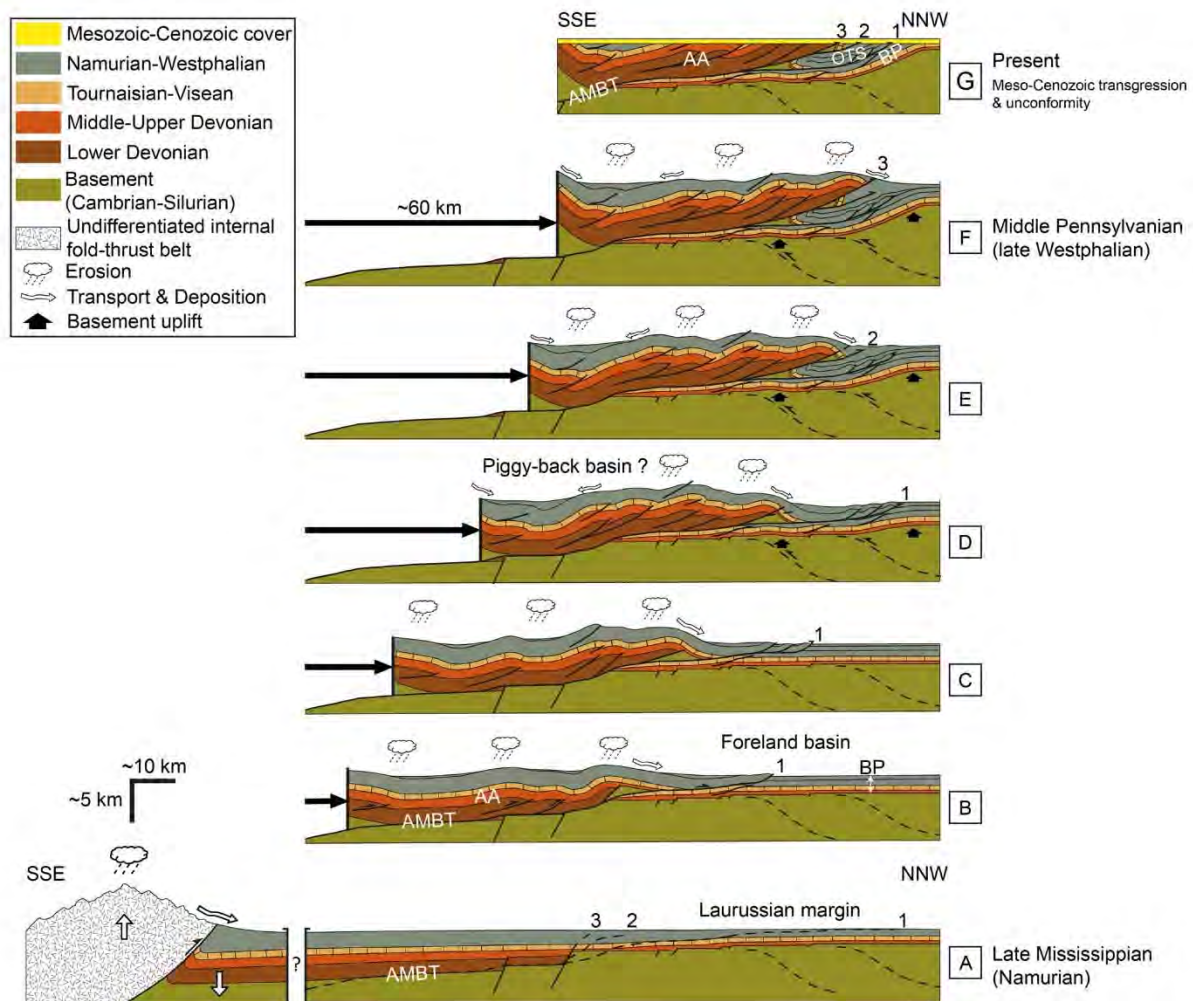


Figure 15. Conceptual kinematic model of the Northern Variscan Thrust Front in northern France (segment to the east of the Douai lateral ramp), integrating previous work (see Figure 3) and new insights from the present study. AA: Ardennes Allochthonous Unit, AMBT: Allochthon Main Basal Thrust, BP: Brabant Para-autochthonous Unit, OTS: Overturned Thrust Sheets. Numbers 1, 2 and 3 correspond to the order of activation of the different thrust faults, the OTS, the “Cran de Retour” thrust and the “Midi Fault,” illustrating the out-of-sequence deformation sequence of the Northern Variscan Front during late Westphalian times.

7.2.2. Out-Of-Sequence Dislocation of the Thrust Front

The detailed interpretation of the C083 profile (Figure 10 & 12) and the analysis of the structural map of the OTS (Figure 13b) demonstrated that the OTS have the overall geometry of a recumbent syncline north of Cambrai and are truncated by the AMBT at least 15 km south of the frontal thrust zone. The overturned limb of this recumbent syncline is likely to correspond to that of a major thrust-related anticline, whose progressive rotation and overturn was induced by the basal shear associated to the large displacement of the Allochthonous Unit on the AMBT (stages C, D, E, F, Figure 15). The existence of such an antiform was established in the “Condroz inlier” of the Belgian Ardennes, along the Meuse River Cross-section (Adams & Vandenberghe, 1999; Khatir et al., 1992; Le Gall, 1992; Raoult & Meilliez, 1987), where lower Paleozoic rocks are exposed. Within the OTS complex, internal strain is likely to have been accommodated by the formation of Riedel-type low-angle normal shear planes of minor scale, as observed in Figure 12 and in the coal-bearing molasse from the NPC basin (e.g., Bouroz, 1950; Le Gall, 1994; Meilliez, 2019). This kind of

structures represent relatively uncommon objects in mountain fronts and foreland basins but they were described in highly strained zones below forelimb thrusts in different foreland fold-thrust structures (i.e., the Jura, NE Pyrenees, Central Apennines) (Averbuch et al., 1992, 1995; Smeraglia et al., 2020). The particularly large horizontal simple-shear strain associated with the forward rotation of the forelimb of the thrust-related anticline developed above the frontal ramp of the AMBT is likely to account for the unusual mechanical conditions controlling the generation of such a low-angle normal fault (Frizon de Lamotte et al., 1995).

The anticline was sequentially cross-cut by out-of-sequence forelimb thrusts, identified in the region as the “Cran de Retour” thrust (2 in Figure 15) and the “Midi Fault” (3 in Figure 15), the latter being the last out-of-sequence thrust (stages D, E, F, Figure 15). Such an out-of-sequence dislocation of the frontal thrust zone can be explained in different ways. It may evidence an impossibility of the thrust front to propagate further north due to, for instance, an uplift of the Brabant Massif that acted as a buttress located in front of the propagating Variscan thrust wedge (Averbuch et al., 2004; Mansy et al., 1999). This mechanism is a feature predicted by analog modeling of basement asperity subduction (Dominguez et al., 2000; Lallemand et al., 1992). This could partly explain the observed re-entrant of the thrust front rearward of the deep Orchies anticline (Marshak, 2004). Such a mechanical locking is known in other natural cases as in the Central Sivas Basin (Turkey) where a topographic high, the crustal Kirshehir block, limited the propagation of the deformation front, resulting in a structural uplift of the fold-thrust belt through an antiformal stack (Legeay et al., 2020). Alternatively, the influence of large volume of syntectonic sedimentation in front of the active thrust front may have led to a backward sequence of thrusting and steepening of the thrust sheet (Barrier et al., 2002; Butler, 2020).

7.2.3. Variscan Reactivation of the Front of the Anglo-Brabant Deformation Belt

Seismic interpretations (C083 profile, Figure 10) and analysis of the structural map of the top-Givetian horizon (Figure 14) revealed the existence of a N120–130 trending deep anticline-syncline pair of folds within the Brabant Para-autochthonous Unit, west of Cambrai. Accounting for the close proximity of the Northern Variscan Front and the late Caledonian Anglo-Brabant deformation belt in the study area (Mansy et al., 1999; Pharaoh, 2018; Pharaoh et al., 1993; Van Grootel et al., 1997), we suggest that this deep anticline may have accommodated shortening associated with the Variscan reactivation of south-vergent thrusts of the Anglo-Brabant deformation front buried within the basement (stages D to F, Figure 15). This hypothesis is supported by the orientation of the WNW-ESE main structural trend of the Anglo-Brabant deformation belt (Mansy et al., 1999; Pharaoh, 2018; Pharaoh et al., 1993; Van Grootel et al., 1997). The pronounced flexure and monoclinical geometry of the Brabant Para-autochthonous Unit delimiting to the north the foreland basin (Figure 14), could possibly have the same origin (Figure 15).

The poor quality of the seismic data in the basement does not allow imaging the deep late Caledonian thrusts. Such structures have, however, been observed on seismic data further west in the Artois region (Minguely et al., 2008) (location in Figure 1a). In this area, north-verging Variscan thrusts and south-verging basement thrusts, interpreted as possible frontal thrusts of the Anglo-Brabant fold belt, form a peculiar frontal triangle zone that uplifted the foreland. Analog modeling experiments conducted for the Artois region (Minguely et al., 2008) and the northern Apennines (Toscani et al., 2014) investigated the mechanism of deformation of two interfering thrust fronts having opposite vergence. Results showed that the pre-existing thrusts (i.e., the late Caledonian thrusts) seems to be reactivated once the northern tip of the younger propagating thrust wedge (i.e., the Variscan thrust wedge) reached the pre-existing thrust front (i.e., the Anglo-Brabant thrust front). Analog modeling experiments (Minguely et al., 2008) argue that the reactivation of such deep inherited thrusts, forming part of a deep frontal triangle zone and resulting in the relative uplift of the Brabant foreland, would have exerted a major buttressing effect in front of the northward propagating Variscan thrust front. Such a process is likely to have enhanced both the localization of displacement on the single AMBT and the out-of-sequence dislocation of the hangingwall anticline developed previously at the tip of the propagating thrust front (stages D to F, Figure 15). Similar cases have been observed in emergent fold-and-thrust belts in the Alps (Ortner et al., 2015) or the Andes (Calderon et al., 2017). For example in the Alps (western Austria, southern Germany), the formation of a frontal triangle zone stopped the foreland propagation of the Alpine thrust front and initiated a break-back sequence of thrusting into the hinterland (Ortner et al., 2015).

8. Conclusions

Seismic profiles presented in this article show the 3-D structure and kinematics of the Northern Variscan Thrust Front in northern France. The frontal thrust zone (AMBT) is shown to localize the displacement of the Ardennes Allochthonous Unit over more than 50 km above the Laurussian margin referred here as the Brabant Para-autochthonous Unit. This large displacement induced underthrusting of the molassic foreland basin and its truncation by a major out-of-sequence thrust (the shallow part of the AMBT, frequently referred to as the Midi fault). An extensive complex of dominantly overturned thrust sheets (the OTS complex) at the sole of this thrust, is interpreted as the result of dissection of a previous major hangingwall anticline at the tip of the AMBT, its forelimb being successively cross-cut and overturned by basal shear along the footwall of the propagating out-of-sequence major thrust.

A major outcome of our 3-D approach is the characterization of a major NW-SE-trending lateral ramp, approximatively along a line Douai-Cambrai and that affects both the main frontal thrust (AMBT) and the OTSBT. This deep-seated ramp marks the western extent of the OTS complex. This is a major relay zone along the thrust front in between the eastern segment (trending ENE-WSW between Valenciennes and Douai), where the molassic foreland basin is largely underthrust (more than 20 km) below the Allochthonous Unit, and the western segment (trending WNW-ESE in the Boulonnais and Artois regions) where no underthrusting occurred. The way this transfer zone is accommodated in the foreland basin is poorly known and thus remains a major objective for future research.

Another key result is the 3-D characterization of the Brabant Para-autochthonous Unit. Along with the overlying Namurian-Westphalian synorogenic layers trapped in the Northern Variscan foredeep, these are deformed by a series of second-order north-verging thrust faults often associated with ramp-related folds developed at their hangingwall. The transition zones between (a) the Famennian shales and the underlying Frasnian limestones, and (b) the Namurian shales and the Dinantian carbonates form the main décollements within this unit.

We showed that at the base of the Brabant Para-autochthonous Unit, the Middle-Upper Devonian sequence has been deformed by syn-sedimentary normal faults. Those faults are responsible for the general thickening of the Devonian sequence towards the south or southwest. Their N060–080° and N110–130° trend corresponds precisely to the strike of the frontal and lateral ramps of the Variscan thrust wedge. Our seismic interpretations also confirm that numerous Variscan thrusts formed right above the Devonian syn-sedimentary normal faults. This observation is valid for both the frontal and lateral ramps and points out the impact of mechanical heterogeneities on the localization of later thrust ramps. Indeed, rift-related deformation in the southern Laurussian margin has exerted a major control on the dynamics of the thrust front by controlling the spacing between individual thrusts, the frictional conditions at the base of the thrust wedge and its along-strike segmentation.

Seismic interpretations revealed the presence of deep folds within the underthrust foreland affecting both the Para-autochthonous Unit and its lower Paleozoic substratum. We propose that their origin is associated with the activation of a deep-seated early Paleozoic backthrust in the basement. The pronounced flexure delimiting to the north the coal-bearing foreland basin and exhuming the lower Paleozoic basement could possibly have the same origin. Such deep foreland back-thrusts are likely to have exerted a major buttressing effect in front of the northward propagating Variscan thrust front, thereby possibly enhancing its out-of-sequence dislocation and the localization of slips along one single major thrust (i.e., the AMBT).

Finally, we propose a conceptual tectonic scenario that fits the main geometric and kinematic characteristics of the Variscan frontal thrust zone in northern France. Hopefully this scenario should benefit from further input of new field and subsurface data, and thus remains to be explored to better constrain the kinematic evolution of this ancient mountain front.

Data Availability Statement

According to French laws, the field seismic data are publically available at <http://www.minergies.fr/fr>. The reprocessed seismic data (SEG-Y) used in this paper belong to the BRGM, so they can be released only with a formal agreement with the BRGM.



Acknowledgments

This work is part of the Ph.D. thesis of Aurore Laurent, granted by the BRGM (French Geological Survey) and the Hauts-de-France region. It is based on the interpretation of 21 seismic lines reprocessed by the BRGM. The reprocessing of the seismic data was supported by the RGF program of the BRGM. Eight lines are presented in the paper, the others are not, but all of them have been used to produce the interpretations and maps presented here. This work benefited also from a financial support from the TelluS Program of the CNRS/INSU. IHS Markit is greatly acknowledged for the permission to use the Kingdom Suite software through an academic grant to the University of Lille. We also thank QGIS development team for providing the QGIS open-source software used during this study. The authors gratefully acknowledge the Editor L. Jolivet, the Associate Editor O. Lacombe and the reviewers P. Krzywiec, S. Mazur and an anonymous reviewer for their constructive comments that significantly improved the manuscript. We particularly thank B. Vendeville for his careful reading of this article and help in the improvement of the English style.

References

- Adams, R., & Vandenberghe, N. (1999). The Meuse section across the Condroz-Ardennes (Belgium) based on a predeformational sediment wedge. *Tectonophysics*, 309(1–4), 179–195. [https://doi.org/10.1016/S0040-1951\(99\)00138-9](https://doi.org/10.1016/S0040-1951(99)00138-9)
- Allen, P. A., Homewood, P., & Williams, G. D. (1986). Foreland Basins: An Introduction. In P. A. Allen, & P. Homewood (Eds.), *Foreland basins*. Special Publication of the International Association of Sedimentologists (Vol. 8, pp. 3–12). Blackwell Scientific Publications.
- Amadori, C., Toscani, G., Di Giulio, A., Maesano, F. E., D'Ambrogio, C., Ghielmi, M., & Fantoni, R. (2019). From cylindrical to non-cylindrical foreland basin: Pliocene–Pleistocene evolution of the Po Plain–Northern Adriatic basin (Italy). *Basin Research*, 31(5), 991–1015. <https://doi.org/10.1111/bre.12369>
- Averbuch, O., Frizon de Lamotte, D., & Kissel, C. (1992). Magnetic fabric as a structural indicator of the deformation path within a fold-thrust structure: A test case from the Corbières (NE Pyrenees, France). *Journal of Structural Geology*, 14(4), 461–474. [https://doi.org/10.1016/0191-8141\(92\)90106-7](https://doi.org/10.1016/0191-8141(92)90106-7)
- Averbuch, O., Frizon de Lamotte, D., & Kissel, C. (1993). Strain distribution above a lateral culmination: An analysis using microfaults and magnetic fabric measurements in the Corbières thrust belt (NE Pyrenees, France). *Annales Tectonicae*, 7(1), 3–21.
- Averbuch, O., Lacquement, F., Meilliez, F., Graveleau, F., Beccaletto, L., & Vendeville, B. (2018). *La chaîne varisque vue depuis son front nord: Dynamique du front de chaîne, sous-charriage crustal de la marge avalonienne et délamination associée de la lithosphère supra-subduction*. 26th Réunion des Sciences de la Terre, October 22, 2018.
- Averbuch, O., Lacquement, F., Szaniawski, R., Mansy, J. L., & Lewandowski, M. (2002). Segmentation of the Variscan thrust front (N France, S Belgium): Insights into the geometry of the Devonian Rheno-Hercynian Basin. *Aardkundige Mededelingen*, 12, 89–92.
- Averbuch, O., Mansy, J.-L., Lamarche, J., Lacquement, F., & Hlanot, F. (2004). Geometry and kinematics of the Boulonnais fold-and-thrust belt (N France): Implications for the dynamics of the Northern Variscan thrust front. *Geodinamica Acta*, 17(2), 163–178. <https://doi.org/10.3166/ga.17.163-178>
- Averbuch, O., Mattei, M., Kissel, C., Frizon de Lamotte, D., & Speranza, F. (1995). Cinématique des déformations au sein d'un système chevauchant aveugle; l'exemple de la Montagna dei Fiori (front des Apennins centraux, Italie). *Bulletin de la Société Géologique de France*, 166(5), 451–461. <https://doi.org/10.2113/gssgibull.166.5.451>
- Averbuch, O., & Piromallo, C. (2012). Is there a remnant Variscan subducted slab in the mantle beneath the Paris basin? Implications for the late Variscan lithospheric delamination process and the Paris basin formation. *Tectonophysics*, 558–559, 70–83. <https://doi.org/10.1016/j.tecto.2012.06.032>
- Ballèvre, M., Bosse, V., Ducassou, C., & Pitra, P. (2009). Palaeozoic history of the Armorican Massif: Models for the tectonic evolution of the suture zones. *Comptes Rendus Geoscience*, 341(2–3), 174–201. <https://doi.org/10.1016/j.crte.2008.11.009>
- Bally, A. W., Gordy, P. L., & Stewart, G. A. (1966). Structure, Seismic Data, and Orogenic Evolution of Southern Canadian Rocky Mountains. *Bulletin of Canadian Petroleum Geology*, 14(3), 337–381. <https://doi.org/10.35767/gscpgbull.14.3.337>
- Banks, C. J., & Warburton, J. (1986). "Passive-roof" duplex geometry in the frontal structures of the Kirthar and Sulaiman mountain belts, Pakistan. *Journal of Structural Geology*, 8(3–4), 229–237. [https://doi.org/10.1016/0191-8141\(86\)90045-3](https://doi.org/10.1016/0191-8141(86)90045-3)
- Barrier, L., Nalpas, T., Gapais, D., Proust, J. N., Casas, A., & Bourquin, S. (2002). Influence of syntectonic sedimentation on thrust geometry. Field examples from the Iberian Chain (Spain) and analogue modeling. *Sedimentary Geology*, 146(1–2), 91–104. [https://doi.org/10.1016/S0037-0738\(01\)00168-3](https://doi.org/10.1016/S0037-0738(01)00168-3)
- Becc-Giraudon, J.-F. (1983). *Synthèse structurale et paléogéographique du bassin houiller du Nord et du Pas-de-Calais*. Mémoire BRGM (No. 123). Editions du BRGM.
- Belanger, L., Delaby, S., Delcambre, B., Ghysel, P., Hiennebert, M., Laloux, M., et al. (2012). Redéfinition des unités structurales du front varisque utilisées dans le cadre de la nouvelle Carte géologique de Wallonie (Belgique). *Geologica Belgica*, 15(3), 169–175.
- Bonnet, C., Malavieille, J., & Mosar, J. (2008). Surface processes versus kinematics of thrust belts: Impact on rates of erosion, sedimentation, and exhumation – Insights from analogue models. *Bulletin de la Société Géologique de France*, 179(3), 297–314. <https://doi.org/10.2113/gssgibull.179.3.297>
- Bouroz, A. (1950). Sur quelques aspects du mécanisme de la déformation tectonique dans le bassin houiller du Nord de la France. *Annales de la Société Géologique du Nord*, 70, 2–55.
- Bouroz, A. (1969). Le Carbonifère du Nord de la France. *Annales de la Société Géologique du Nord*, 89(1), 47–65.
- Bouroz, A., Chalard, J., Dalinval, A., & Stiévenard, M. (1961). La structure du bassin houiller du Nord de la région de Douai à la frontière Belge. *Annales de la Société Géologique du Nord*, 81, 173–218.
- Bouroz, A., Stiévenard, M., Buisine, M., Chalard, J., Dalinval, A., Dollé, P., et al. (1963). *Houillères du Bassin du Nord et du Pas-de-Calais: Carte des zones stratigraphiques à la cote -300*. Institut Géographique National.
- Boyer, S. E., & Elliott, D. (1982). Thrust Systems. *AAPG Bulletin*, 66(9), 1196–1230. <https://doi.org/10.1306/03B5A77D-16D1-11D7-8645000102C1865D>
- Bultynck, P., Coen-Aubert, M., Dejonghe, L., Godefroid, J., Hance, L., Lacroix, D., et al. (1991). Les formations du Dévonien moyen de la Belgique. *Mémoires pour servir à l'Explication des Cartes Géologiques et Minières de la Belgique*, 30, 1–106.
- Burgess, P. M., & Gayer, R. A. (2000). Late Carboniferous tectonic subsidence in South Wales: Implications for Variscan basin evolution and tectonic history in SW Britain. *Journal of the Geological Society*, 157(1), 93–104. <https://doi.org/10.1144/jgs.157.1.93>
- Butler, R. W. H. (1982). The terminology of structures in thrust belts. *Journal of Structural Geology*, 4(3), 239–245. [https://doi.org/10.1016/0191-8141\(82\)90011-6](https://doi.org/10.1016/0191-8141(82)90011-6)
- Butler, R. W. H. (1987). Thrust sequences. *Journal of the Geological Society*, 144(4), 619–634. <https://doi.org/10.1144/gsjgs.144.4.619>
- Butler, R. W. H. (1989). The influence of pre-existing basin structure on thrust system evolution in the Western Alps. *Geological Society, London, Special Publications*, 44(1), 105–122. <https://doi.org/10.1144/GSL.SP.1989.044.01.07>
- Butler, R. W. H. (2020). Syn-kinematic sutura influence the structural evolution of emergent fold-thrust belts. *Geological Society, London, Special Publications*, 490(1), 57–78. <https://doi.org/10.1144/SP490-2019-14>
- Butler, R. W. H., Bond, C. E., Cooper, M. A., & Watkins, H. (2018). Interpreting structural geometry in fold-thrust belts: Why style matters. *Journal of Structural Geology*, 114, 251–273. <https://doi.org/10.1016/j.jsg.2018.06.019>
- Butler, R. W. H., Mazzoli, S., Corrado, S., Donatelli, M. D., Bucci, D. D., Gambini, R., et al. (2004). Applying Thick-skinned Tectonic Models to the Apennine Thrust Belt of Italy—Limitations and Implications. In K. R. McClay (Ed.), *Thrust tectonics and hydrocarbon systems* (Vol. 82, pp. 647–667). AAPG Memoir. <https://doi.org/10.1306/m82813c34>
- Butler, R. W. H., Tavarnelli, E., & Grasso, M. (2006). Structural inheritance in mountain belts: An Alpine–Apennine perspective. *Journal of Structural Geology*, 28(11), 1893–1908. <https://doi.org/10.1016/j.jsg.2006.09.006>

- Calassou, S., Larroque, C., & Malavieille, J. (1993). Transfer zones of deformation in thrust wedges: An experimental study. *Tectonophysics*, 221(3–4), 325–344. [https://doi.org/10.1016/0040-1951\(93\)90165-G](https://doi.org/10.1016/0040-1951(93)90165-G)
- Calderon, Y., Baby, P., Hurtado, C., & Brusset, S. (2017). Thrust tectonics in the Andean retro-foreland basin of northern Peru: Permian inheritances and petroleum implications. *Marine and Petroleum Geology*, 82, 238–250. <https://doi.org/10.1016/j.marpetgeo.2017.02.009>
- Cazes, M., Torrelles, G., Bois, C., Damotte, B., Galdeano, A., Hirn, A., et al. (1985). Structure de la croûte hercynienne du Nord de la France; premiers résultats du profil ECORS. *Bulletin de la Société Géologique de France*, 1(6), 925–941. <https://doi.org/10.2113/gssgibull.1.6.925>
- C.F.P.(M), COPESEI, R. A. P., & S. N. P. A. (1965). Contribution à la connaissance des bassins paléozoïques du Nord de la France. *Annales de la Société Géologique du Nord*, 85, 273–281.
- Chantraine, J., Autran, A., Caveller, C., Alabouvette, B., Barfèty, J.-C., Cecca, F., et al. (2003). *Carte géologique de la France à l'échelle du millionième, 6^e édition révisée*. BRGM.
- Chapple, W. M. (1978). Mechanics of thin-skinned fold-and-thrust belts. *GSA Bulletin*, 89(8), 1189–1198. [https://doi.org/10.1130/0016-7606\(1978\)89<1189:MOTFB>2.0.CO;2](https://doi.org/10.1130/0016-7606(1978)89<1189:MOTFB>2.0.CO;2)
- Cobert, C., Bacle, J.-M., Boulvais, P., Poujol, M., & Decrcé, S. (2018). Petrogenesis of the Mairupt microgranite: A witness of an Uppermost Silurian magmatism in the Rocroi Inlier, Ardennes Allochton. *Comptes Rendus Geoscience*, 350(3), 89–99. <https://doi.org/10.1016/j.crd.2017.12.001>
- Coen-Aubert, M., Groessens, E., & Legrand, R. (1980). Les formations paléozoïques des sondages de Tournai et de Leuzc. *Bulletin de la Société belge de Géologie*, 89(4), 241–275.
- Cook, B. S., & Thomas, W. A. (2009). Superposed lateral ramps in the Pell City thrust sheet, Appalachian thrust belt, Alabama. *Journal of Structural Geology*, 31(9), 941–949. <https://doi.org/10.1016/j.jsg.2009.06.001>
- Corfield, S. M., Gawthorpe, R. L., Gage, M., Fraser, A. J., & Besly, B. M. (1996). Inversion tectonics of the Variscan foreland of the British Isles. *Journal of the Geological Society*, 153(1), 17–32. <https://doi.org/10.1144/gsjgs.153.1.0017>
- Dahlen, F. A., Suppe, J., & Davis, D. (1984). Mechanics of fold-and-thrust belts and accretionary wedges: Cohesive Coulomb Theory. *Journal of Geophysical Research: Solid Earth*, 89(B12), 10087–10101. <https://doi.org/10.1029/JB089iB12p10087>
- Dahlstrom, C. D. A. (1969). Balanced cross sections. *Canadian Journal of Earth Sciences*, 6(4), 743–757. <https://doi.org/10.1139/e69-069>
- Davis, D., Suppe, J., & Dahlen, F. A. (1983). Mechanics of fold-and-thrust belts and accretionary wedges. *Journal of Geophysical Research: Solid Earth*, 88(B2), 1153–1172. <https://doi.org/10.1029/JB088iB02p01153>
- Debacker, T. N., Dewaele, S., Sintubin, M., Verniers, J., Muchez, P., & Boven, A. (2005). Timing and duration of the progressive deformation of the Brabant Massif, Belgium. *Geologica Belgica*, 8(4), 20–34.
- DeCelles, P. G., & Giles, K. A. (1996). Foreland basin systems. *Basin Research*, 8(2), 105–123. <https://doi.org/10.1046/j.1365-2117.1996.01491.x>
- Delmer, A. (1997). Structure tectonique du bassin houiller du Hainaut. *Annales de la Société Géologique du Nord*, 5(2), 7–15.
- Delmer, A. (2003). La structure tectonique transfrontalière entre les bassins houillers de Valenciennes (France) et du Hainaut belge. *Geologica Belgica*, 6(3–4), 171–180.
- Delmer, A., Dusaer, M., & Delcambre, B. (2001). Upper Carboniferous lithostratigraphic units (Belgium). *Geologica Belgica*, 4(1–2), 95–103. <https://doi.org/10.20341/gb.2014.045>
- Delmer, A., Leclercq, V., Marlière, R., & Robaszynski, F. (1982). La géothermie en Hainaut et le sondage de Ghlin (Mons - Belgique). *Annales de la Société Géologique du Nord*, 101, 189–206.
- De Putter, T. (1995). Etude sédimentologique de la Grande brèche viséenne ("V3a") du bassin de Namur-Dinant. *Mém. Expl. Cartes Géologiques et Minières de la Belgique*, 40, 1–272.
- Dominguez, S., Malavieille, J., & Lallemand, S. E. (2000). Deformation of accretionary wedges in response to seamount subduction: Insights from sandbox experiments. *Tectonics*, 19(1), 182–196. <https://doi.org/10.1029/1999TC900055>
- Farquharson, N., Schubert, A., & Steiner, U. (2016). Geothermal Energy in Munich (and Beyond) A Geothermal City Case Study. *GRC Transactions*, 40, 189–196.
- Fielitz, W., & Mansy, J.-L. (1999). Pre- and synorogenic burial metamorphism in the Ardennes and neighboring areas (Rhenohercynian zone, central European Variscides). *Tectonophysics*, 309(1–4), 227–256. [https://doi.org/10.1016/S0040-1951\(99\)00141-9](https://doi.org/10.1016/S0040-1951(99)00141-9)
- Fillon, C., Huisman, R. S., & van der Beek, P. (2013). Syntectonic sedimentation effects on the growth of fold-and-thrust belts. *Geology*, 41(1), 83–86. <https://doi.org/10.1130/G33531.1>
- Fitz-Diaz, E., Hudleston, P., & Tolson, G. (2011). Comparison of tectonic styles in the Mexican and Canadian Rocky Mountain Fold-Thrust Belt. *Geological Society, London, Special Publications*, 349(1), 149–167. <https://doi.org/10.1144/SP349.8>
- Ford, M. (2004). Depositional wedge tops: Interaction between low basal friction external orogenic wedges and flexural foreland basins. *Basin Research*, 16(3), 361–375. <https://doi.org/10.1111/j.1365-2117.2004.00236.x>
- Franke, W. (1992). Phanerozoic structures and events in Central Europe. In D. Blundell, R. Freeman, & S. Mueller (Eds.), *A continent revealed: The European geotraverse* (pp. 164–179). Cambridge University Press.
- Franke, W. (2000). The mid-European segment of the Variscides: Tectonostratigraphic units, terrane boundaries and plate tectonic evolution. *Geological Society, London, Special Publications*, 179(1), 35–61. <https://doi.org/10.1144/GSL.SP.2000.179.01.05>
- Franke, W. (2006). The Variscan orogen in Central Europe: Construction and collapse. *Geological Society, London, Memoirs*, 32(1), 333–343. <https://doi.org/10.1144/GSL.MEM.2006.032.01.20>
- Franke, W., Cocks, L. R. M., & Torvik, T. H. (2017). The Palaeozoic Variscan oceans revisited. *Gondwana Research*, 48, 257–284. <https://doi.org/10.1016/j.gr.2017.03.005>
- Franke, W., Dallmeyer, R. D., & Weber, K. (1995). Geodynamic Evolution. In R. D. Dallmeyer, W. Franke, & K. Weber (Eds.), *Pre-permian geology of central and eastern Europe* (pp. 579–593). Springer-Verlag. https://doi.org/10.1007/978-3-642-77518-5_57
- Frizon de Lamotte, D., Guezou, J.-C., & Averbuch, O. (1995). Distinguishing lateral folds in thrust-systems; examples from Corbières (SW France) and Betic Cordilleras (SE Spain). *Journal of Structural Geology*, 17(2), 233–244. [https://doi.org/10.1016/0191-8141\(94\)90035-w](https://doi.org/10.1016/0191-8141(94)90035-w)
- Gillerist, R., Coward, M., & Mugnier, J.-L. (1987). Structural inversion and its controls: Examples from the Alpine foreland and the French Alps. *Geodinamica Acta*, 1(1), 5–34. <https://doi.org/10.1080/09853111.1987.11105122>
- Golonka, J. (2002). Plate-Tectonic Maps of the Phanerozoic. *SEPM Special Publications*, 72, 21–75. <https://doi.org/10.2110/pcc.02.72.0021>
- Golonka, J. (2020). Late Devonian paleogeography in the framework of global plate tectonics. *Global and Planetary Change*, 186, 103129. <https://doi.org/10.1016/j.gloplacha.2020.103129>
- Golonka, J., & Gawęda, A. (2012). Plate Tectonic Evolution of the Southern Margin of Laurussia in the Paleozoic. In E. Sharkov (Ed.), *Tectonics-Recent advances* (pp. 261–282). InTech. <https://doi.org/10.5772/50009>
- Graveleau, F., Malavieille, J., & Dominguez, S. (2012). Experimental modeling of orogenic wedges: A review. *Tectonophysics*, 538–540, 1–66. <https://doi.org/10.1016/j.tecto.2012.01.027>

- Guillot, F., Averbuch, O., Dubois, M., Durand, C., Lanari, P., & Gauthier, A. (2020). Zircon age of vaugnerite intrusives from the Central and Southern Vosges crystalline massif (E France): Contribution to the geodynamics of the European Variscan belt. *BSGP - Parth Sciences Bulletin*, 191, 26. <https://doi.org/10.1051/bsgf/2020027>
- Gutscher, M.-A., Kukowski, N., Malavicille, J., & Lallemand, S. (1996). Cyclical behavior of thrust wedges: Insights from high basal friction sandbox experiments. *Geology*, 24(2), 135–138. [https://doi.org/10.1130/0091-7613\(1996\)024<0135:CBOTW>2.3.CO;2](https://doi.org/10.1130/0091-7613(1996)024<0135:CBOTW>2.3.CO;2)
- Hammerstein, J. A., Di Cuià, R., Cottam, M. A., Zamora, G., & Butler, R. W. H. (2020). *Fold and thrust belts: Structural Style, Evolution and Exploration*. Geological Society, London, Special Publications, 490(1). <https://doi.org/10.1144/SP490>
- Hance, L., Dejonghe, L., Ghysel, P., Laloux, M., & Mansy, J.-L. (1999). Influence of heterogeneous lithostructural layering on orogenic deformation in the Variscan Front Zone (eastern Belgium). *Tectonophysics*, 309(1–4), 161–177. [https://doi.org/10.1016/S0040-1951\(99\)00137-7](https://doi.org/10.1016/S0040-1951(99)00137-7)
- Hance, L., & Poty, E. (2006). Hastarian. *Geologica Belgica*, 9(1–2), 111–116.
- Houchen, M. A. (1988). *Structural modeling of the external Variscides of France and Belgium (Doctoral dissertation)*. National University of Ireland.
- Hughes, A. (2020). Mechanical controls on structural styles in shortening environments: A discrete-element modeling approach. *Geological Society, London, Special Publications*, 490(1), 33–55. <https://doi.org/10.1144/SP490-2019-114>
- Huigi, L., McClay, K. R., & Powell, D. (1992). Physical models of thrust wedges. In K. R. McClay (Ed.), *Thrust tectonics* (pp. 71–81). Springer. https://doi.org/10.1007/978-94-011-3066-0_6
- Jones, P. B. (1982). Oil and gas beneath east-dipping underthrust faults in the Alberta Foothills, Canada. *Geological Studies of the Cordilleran Thrust Belt*, 1, 61–74.
- Karner, G. D., & Watts, A. B. (1983). Gravity anomalies and flexure of the lithosphere at mountain ranges. *Journal of Geophysical Research: Solid Earth*, 88(B12), 10449–10477. <https://doi.org/10.1029/JB088B12p10449>
- Khatir, A., Mansy, J.-L., & Meilliez, F. (1988). Structures et déformation dans l'allochtone ardennaise en Avesnois (Nord). *Annales de la Société Géologique du Nord*, 108(2–3), 73–83.
- Khatir, A., Mansy, J.-L., & Meilliez, F. (1992). Structuration varisque en Ardenne occidentale: Une hiérarchie des niveaux de décollement. *Comptes rendus de l'Académie des sciences. Série 2. Mécanique, Physique, Chimie, Sciences de l'univers, Sciences de la Terre*, 314(4), 365–371.
- Kley, J., Monaldi, C. R., & Salfity, J. A. (1999). Along-strike segmentation of the Andean foreland: Causes and consequences. *Tectonophysics*, 301(1–2), 75–94. [https://doi.org/10.1016/S0040-1951\(98\)90223-2](https://doi.org/10.1016/S0040-1951(98)90223-2)
- Konstantinovskaya, E., & Malavicille, J. (2005). Accretionary orogens: Erosion and exhumation. *Geotectonics*, 39(1), 69–86.
- Konstantinovskaya, E., Malo, M., & Badina, F. (2014). Effects of irregular basement structure on the geometry and emplacement of frontal thrusts and duplexes in the Quebec Appalachians: Interpretations from well and seismic reflection data. *Tectonophysics*, 637, 268–288. <https://doi.org/10.1016/j.tecto.2014.10.012>
- Krzywiec, P., Mazur, S., Gagala, L., Kufraś, M., Lewandowski, M., Malinowski, M., & Buffenmyer, V. (2017). Late Carboniferous thin-skinned compressional deformation above the SW edge of the East European craton as revealed by seismic reflection and potential field data—Correlations with the Variscides and the Appalachians. In R. D. Law, J. R. Thigpen, A. J. Merschat, & H. H. Stowell (Eds.), *Linkages and Feedbacks in orogenic systems* (Vol. 213, pp. 20). Geological Society of America Memoir. [https://doi.org/10.1130/2017.1213\(14](https://doi.org/10.1130/2017.1213(14)
- Kufraś, M., Krzywiec, P., Gagala, L., Mazur, S., & Mikolajczak, M. (2020). Sequence of deformation at the front of an orogen: Lublin basin case study (Poland). *Journal of Structural Geology*, 141, 1–18. <https://doi.org/10.1016/j.jsg.2020.104211>
- Lacombe, O., Lavé, J., Roure, F. M., & Vergés, J. (2007). *Thrust belts and foreland basins - from fold kinematics to hydrocarbon systems*. Springer-Verlag. <https://doi.org/10.1007/978-3-540-69426-7>
- Lacombe, O., & Mouthereau, F. (2002). Basement-involved shortening and deep detachment tectonics in forelands of orogens: Insights from recent collision belts (Taiwan, Western Alps, Pyrenees). *Tectonics*, 21(4), 12–22. <https://doi.org/10.1029/2001TC901018>
- Lacombe, O., Mouthereau, F., Angelier, J., Chu, H.-T., & Lee, J.-C. (2003). Frontal belt curvature and oblique ramp development at an obliquely collided irregular margin: Geometry and kinematics of the NW Taiwan fold-thrust belt. *Tectonics*, 22(3), 1–16. <https://doi.org/10.1029/2002TC001436>
- Lacquement, F. (2001). *L'Ardenne Varisque. Déformation progressive d'un prisme sédimentaire pré-structuré, de l'affleurement au modèle de chaîne*. (Publication No. 29). Société Géologique du Nord.
- Lacquement, F., Averbuch, O., Mansy, J.-L., Szaniawski, R., & Lewandowski, M. (2005). Transpressional deformations at lateral boundaries of propagating thrust-sheets: The example of the Meuse Valley Recess within the Ardennes Variscan fold-and-thrust belt (N France–S Belgium). *Journal of Structural Geology*, 27(10), 1788–1802. <https://doi.org/10.1016/j.jsg.2005.05.017>
- Lacquement, F., Mansy, J.-L., Hanot, F., & Meilliez, F. (1999). Retraitement et interprétation d'un profil sismique pétrolier méridien au travers du Massif paléozoïque ardennais (Nord de la France). *Comptes Rendus de l'Académie des Sciences-Séries IIA: Earth and Planetary Science*, 329(7), 471–477. [https://doi.org/10.1016/S1251-8500\(00\)80020-8](https://doi.org/10.1016/S1251-8500(00)80020-8)
- Lallemand, S. E., Malavicille, J., & Calassou, S. (1992). Effects of oceanic ridge subduction on accretionary wedges: Experimental modeling and marine observations. *Tectonics*, 11(6), 1301–1313. <https://doi.org/10.1029/92TC00637>
- Le Gall, B. (1992). The deep structure of the Ardennes Variscan thrust belt from structural and ECORS seismic data. *Journal of Structural Geology*, 14(5), 531–546. [https://doi.org/10.1016/0191-8141\(92\)90155-P](https://doi.org/10.1016/0191-8141(92)90155-P)
- Le Gall, B. (1994). Deformation of the Nord-Pas-de-Calais Carboniferous Coalfield (France) in the Variscan Frontal Tectonic Pattern. In A. Mascle (Ed.), *Hydrocarbon and Petroleum geology of France*. Special Publication of the European Association of Petroleum Geoscientists (Vol. 4, pp. 379–398). Springer-Verlag. https://doi.org/10.1007/978-3-642-78849-9_27
- Legeay, E., Ringenbach, J.-C., Kergaravat, C., Pichat, A., Mohn, G., Vergés, J., et al. (2020). Structure and kinematics of the Central Sivas Basin (Turkey): Salt deposition and tectonics in an evolving fold-and-thrust belt. *Geological Society, London, Special Publications*, 490(1), 361–396. <https://doi.org/10.1144/SP490-2019-92>
- Legrand, R. (1968). Le Massif du Brabant. *Mémoires pour servir à l'Explication des Cartes Géologiques et Minières de la Belgique*, 9, 1–148.
- Leveridge, B. E. (2011). The Looe, South Devon and Tavy basins: The Devonian rifted passive margin successions. *Proceedings of the Geologists' Association*, 122(4), 616–717. <https://doi.org/10.1016/j.pgcga.2011.03.005>
- Licour, L. (2012). Relations entre la géologie profonde et le comportement hydrogéologique du réservoir géothermique du Hainaut (Belgique) - Caractérisation de l'aquifère dans la région de Saint-Ghislain (Doctoral dissertation). Mons, Belgium: Université de Mons.
- Malavicille, J. (2010). Impact of erosion, sedimentation, and structural heritage on the structure and kinematics of orogenic wedges: Analog models and case studies. *Geological Society of America Today*, 20(1), 4–10. <https://doi.org/10.1130/GSATG48A.1>
- Malz, A., Madritsch, H., Jordan, P., Meier, B., & Kley, J. (2020). Along-strike variations in thin-skinned thrusting style controlled by pre-existing basement structure in the easternmost Jura Mountains (Northern Switzerland). *Geological Society, London, Special Publications*, 490(1), 199–220. <https://doi.org/10.1144/SP490-2019-090>

- Mansy, J. L., Everaerts, M., & De Vos, W. (1999). Structural analysis of the adjacent Acadian and Variscan fold belts in Belgium and northern France from geophysical and geological evidence. *Tectonophysics*, 309(1–4), 99–116. [https://doi.org/10.1016/S0040-1951\(99\)00134-1](https://doi.org/10.1016/S0040-1951(99)00134-1)
- Mansy, J.-L., & Lacquement, F. (2006). Contexte géologique régional: L'Ardenne paléozoïque (Nord de la France et Sud de la Belgique). *Géologie de la France*, 1–2, 7–13.
- Mansy, J.-L., Lacquement, F., Meilliez, F., Hanot, F., & Everaerts, M. (1997). Interprétation d'un profil sismique pétrolier, sur le méridien de Valenciennes (Nord de la France). *Aardkundige Mededelingen*, 8, 127–129.
- Mansy, J.-L., Manby, G. M., Averbuch, O., Everaerts, M., Bergerat, F., Van Vliet-Lanoe, B., et al. (2003). Dynamics and inversion of the Mesozoic Basin of the Weald–Boulonnais area: Role of basement reactivation. *Tectonophysics*, 373(1–4), 161–179. [https://doi.org/10.1016/S0040-1951\(03\)00289-0](https://doi.org/10.1016/S0040-1951(03)00289-0)
- Mansy, J.-L., & Meilliez, F. (1993). Eléments d'analyse structurale à partir d'exemples pris en Ardenne-Avesnois. *Annales de la Société Géologique du Nord*, 2(2), 45–60.
- Marshak, S. (2004). Salients, Recesses, Arcs, Oroclines, and Syntaxes—A Review of Ideas Concerning the Formation of Map-view Curves in Fold-thrust Belts. In K. R. McClay (Ed.), *Thrust Tectonics and Hydrocarbon systems* (Vol. 82, pp. 131–156).
- Martínez, A., Malavieille, J., Lallemand, S., & Collot, J.-Y. (2002). Strain partitioning in an accretionary wedge, in oblique convergence: Analogue modeling. *Bulletin de la Société Géologique de France*, 173(1), 17–24. <https://doi.org/10.2113/173.1.17>
- Matte, P. (2001). The Variscan collage and orogeny (480–290 Ma) and the tectonic definition of the Armorica microplate: A review. *Terra Nova*, 13(2), 122–128. <https://doi.org/10.1046/j.1365-3121.2001.00327.x>
- Mazur, S., Aleksandrowski, P., Gagala, L., Krzywiec, P., Zaba, J., Gaidzik, K., & Sikora, R. (2020). Late Palaeozoic strike-slip tectonics versus oroclinal bending at the SW outskirts of Baltica: Case of the Variscan belt's eastern end in Poland. *International Journal of Earth Sciences*, 109(4), 1133–1160. <https://doi.org/10.1007/s00531-019-01814-7>
- McClay, K. R. (1992). Glossary of thrust tectonics terms. In K. R. McClay (Ed.), *Thrust tectonics* (pp. 419–433). Springer Science & Business Media.
- McClay, K. R. (2004). *Thrust Tectonics and Hydrocarbon Systems* (Vol. 82, pp. 667). AAPG Memoir. <https://doi.org/10.1306/M82813>
- McClay, K. R., Whitehouse, P. S., Dooley, T., & Richards, M. (2004). 3D evolution of fold and thrust belts formed by oblique convergence. *Marine and Petroleum Geology*, 21(7), 857–877. <https://doi.org/10.1016/j.marpetgeo.2004.03.009>
- Meilliez, F. (1989). Importance de l'événement calédonien dans l'allochtone ardennaise; essai sur une cinématique paléozoïque de l'Ardenne dans la chaîne Varisque (Doctoral dissertation). Le Mans, France: Université du Maine.
- Meilliez, F. (2019). La Faille du Midi, mythe et réalités. *Annales de la Société Géologique du Nord*, 26(2), 13–32.
- Meilliez, F., André, L., Blicke, A., Fieflitz, W., Goffette, O., Hance, L., et al. (1991). Ardenne-Brabant. *Sciences Géologiques. Bulletin*, 44(1–2), 3–29. <https://doi.org/10.3406/sgeol.1991.1864>
- Meilliez, F., & Mansy, J. L. (1990). Déformation pelliculaire différenciée dans une série lithologique hétérogène: le Dévono-Carbonifère de l'Ardenne. *Bulletin de la Société Géologique de France*, 6(1), 177–188. <https://doi.org/10.2113/gssgibull.VL1.177>
- Mingucly, B., Averbuch, O., Patin, M., Rolin, D., Hanot, F., & Bergerat, F. (2010). Inversion tectonics at the northern margin of the Paris basin (northern France): New evidence from seismic profiles and boreholes interpolation in the Artois area. *Bulletin de la Société Géologique de France*, 181(5), 429–442. <https://doi.org/10.2113/gssgibull.181.5.429>
- Mingucly, B., Folens, L., Averbuch, O., & Vendeville, B. C. (2008). Formation of deep-seated triangle zones by interaction between two orogenic thrust fronts having opposite vergence: Structural evidence from the Caledonian-Variscan system in Northern France and preliminary analogue modeling. *Bollettino Di Geofisica*, 49(2), 242–246.
- Moore, J. C. (1989). Tectonics and hydrogeology of accretionary prisms: Role of the décollement zone. *Journal of Structural Geology*, 11(1–2), 95–106. [https://doi.org/10.1016/0191-8141\(89\)90037-0](https://doi.org/10.1016/0191-8141(89)90037-0)
- Morley, C. K. (1986). A Classification of Thrust Fronts. *AAPG Bulletin*, 70(1), 12–25. <https://doi.org/10.1306/94885615-1704-11d7-864-5000102c1865d>
- Morley, C. K. (1988). Out-of-Sequence Thrusts. *Tectonics*, 7(3), 539–561. <https://doi.org/10.1029/TC007i003p00539>
- Mortelmans, G., & Bourguignon, P. (1954). *Partie I. La stratigraphie. Chapitre 61e Dinantien*. Annales de la Société géologique de Belgique, Special publications: Prodrome d'une description géologique de la Belgique, (pp. 217–321).
- Moulouel, H. (2008). Caractérisation cartographique d'une différenciation verticale et horizontale de la déformation: Application à la couverture sédimentaire de la plate-forme ardennaise. (Doctoral dissertation). Lille, France: Université des Sciences et Technologies de Lille.
- Needham, D. T., Matthews, S. J., & Butler, R. W. H. (2004). Oil and Gas in Compressional Belts. *Marine and Petroleum Geology*, 21(7), 783–964. <https://doi.org/10.1016/j.marpetgeo.2004.04.002>
- Nemcek, M., Schamel, S., & Gayer, R. (2005). *Thrustbelts: Structural architecture, thermal regimes and petroleum systems*. Cambridge University Press. <https://doi.org/10.1017/CBO9780511584244>
- Oncken, O., Plesch, A., Weber, J., Ricken, W., & Schrader, S. (2000). Passive margin detachment during arc-continent collision (Central European Variscides). *Geological Society, London, Special Publications*, 179(1), 199–216. <https://doi.org/10.1144/GSL.SP.2000.179.01.13>
- Oncken, O., von Winterfeld, C., & Dittmar, U. (1999). Accretion of a rifted passive margin: The Late Palaeozoic Rhenohercynian fold and thrust belt (Middle European Variscides). *Tectonics*, 18(1), 75–91. <https://doi.org/10.1029/98TC02763>
- Ortner, H., Aichholzer, S., Zerlauth, M., Pilsner, R., & Flügel, B. (2015). Geometry, amount, and sequence of thrusting in the Subalpine Molasse of western Austria and southern Germany, European Alps: Thrusting in the Alpine Foreland. *Tectonics*, 34(1), 1–30. <https://doi.org/10.1002/2014TC003550>
- Paulsen, T., & Marshak, S. (1999). Origin of the Uinta recess, Sevier fold–thrust belt, Utah: Influence of basin architecture on fold–thrust belt geometry. *Tectonophysics*, 312(2), 203–216. [https://doi.org/10.1016/S0040-1951\(99\)00182-1](https://doi.org/10.1016/S0040-1951(99)00182-1)
- Pharaoh, T. (2018). The Anglo-Brabant Massif: Persistent but enigmatic palaeo-relief at the heart of western Europe. *Proceedings of the Geologists' Association*, 129(3), 278–328. <https://doi.org/10.1016/j.pgeola.2018.02.009>
- Pharaoh, T. C., Molyneux, S. G., Merriman, R. J., Lee, M. K., & Vermiers, J. (1993). The Caledonides of the Anglo-Brabant Massif reviewed. *Geological Magazine*, 130(5), 561–562. <https://doi.org/10.1017/S0016756800020847>
- Plesch, A., & Oncken, O. (1999). Orogenic wedge growth during collision—constraints on mechanics of a fossil wedge from its kinematic record (Rhenohercynian FTB, Central Europe). *Tectonophysics*, 309(1–4), 117–139. [https://doi.org/10.1016/S0040-1951\(99\)00135-3](https://doi.org/10.1016/S0040-1951(99)00135-3)
- Poblet, J., & Lisle, R. J. (2011). Kinematic Evolution and Structural Styles of Fold-and-Thrust Belts. *Geological Society, London, Special Publications*, 349(1). <https://doi.org/10.1144/SP349.1>
- Poly, E., Hance, L., Lees, A., & Hennebert, M. (2001). Dinantian lithostratigraphic units (Belgium). *Geologica Belgica*, 4(1–2), 69–94. <https://doi.org/10.20341/gb.2014.044>

- Préat, A., & Boulvain, F. (1988). Excursion A-1. Middle and Upper Devonian carbonate platform evolution in Dinant and Namur basins (Belgium, France). In A. Herbosch (Ed.), *IAS 9th European regional meeting: Excursion guidebook leuven-Belgium* (p. 1–25). Belgium: Ministry of Economic Affairs, Belgian Geological Survey.
- Price, R. A. (1986). The southeastern Canadian Cordillera: Thrust faulting, tectonic wedging, and delamination of the lithosphere. *Journal of Structural Geology*, 8(3–4), 239–254. [https://doi.org/10.1016/0191-8141\(86\)90046-5](https://doi.org/10.1016/0191-8141(86)90046-5)
- Qayyum, M., Spratt, D. A., Dixon, J. M., & Lawrence, R. D. (2015). Displacement transfer from fault-bend to fault-propagation fold geometry: An example from the Himalayan thrust front. *Journal of Structural Geology*, 77, 260–276. <https://doi.org/10.1016/j.jsg.2014.10.010>
- Raoult, J.-F. (1986). Le front varisque du Nord de la France d'après les profils sismiques, la géologie de surface et les sondages. *Revue de Géologie Dynamique et de Géographie Physique*, 27(3–4), 247–268.
- Raoult, J.-F. (1988). Le front varisque du Nord de la France: Interprétation des principales coupes d'après les profils sismiques, la géologie de surface et les sondages. In M. Cazes, & G. Torrelles (Eds.), *Étude de la croûte terrestre par sismique profonde: Profil du Nord de la France* (pp. 171–196). Technip.
- Raoult, J.-F., & Meilliez, F. (1987). The variscan front and the midi fault between the channel and the meuse river. *Journal of Structural Geology*, 9(4), 473–479. [https://doi.org/10.1016/0191-8141\(87\)90122-2](https://doi.org/10.1016/0191-8141(87)90122-2)
- Ravaglia, A., Seno, S., Toscani, G., & Fantoni, R. (2006). Mesozoic extension controlling the Southern Alps thrust front geometry under the Po Plain, Italy: Insights from sandbox models. *Journal of Structural Geology*, 28(11), 2084–2096. <https://doi.org/10.1016/j.jsg.2006.07.011>
- Rouchy, J. M., Laumondais, A., & Groessens, E. (1987). The lower Carboniferous (Visean) evaporites in northern France and Belgium: Depositional, diagenetic and deformational guides to reconstruct a disrupted evaporitic basin. In T. M. Peryt (Ed.), *Evaporite basins* (Vol. 13, pp. 31–67). Springer-Verlag. <https://doi.org/10.1007/BFb0010099>
- Rouchy, J. M., Pierre, C., Groessens, E., Monty, C., Laumondais, A., & Moine, B. (1986). Les évaporites pré-permiennes du segment varisque franco-belge: Aspects paléogéographiques et structuraux. *Bulletin de la Société belge de Géologie*, 95(2–3), 139–149.
- Schedl, A., & Wiltshko, D. V. (1987). Possible effects of pre-existing basement topography on thrust fault ramping. *Journal of Structural Geology*, 9(8), 1029–1037. [https://doi.org/10.1016/0191-8141\(87\)90011-3](https://doi.org/10.1016/0191-8141(87)90011-3)
- Schulmann, K., Schaltegger, U., Jezek, J., Thompson, A. B., & Edel, J.-B. (2002). Rapid burial and exhumation during orogeny: Thickening and synconvergent exhumation of thermally weakened and thinned crust (Variscan orogen in Western Europe). *American Journal of Science*, 302(10), 856–879. <https://doi.org/10.2475/ajs.302.10.856>
- Scisciani, V. (2009). Styles of positive inversion tectonics in the Central Apennines and in the Adriatic foreland: Implications for the evolution of the Apennine chain (Italy). *Journal of Structural Geology*, 31(11), 1276–1294. <https://doi.org/10.1016/j.jsg.2009.02.004>
- Shail, R. K., & Leveridge, B. E. (2009). The Rhenohercynian passive margin of SW England: Development, inversion and extensional reactivation. *Comptes Rendus Geoscience*, 341(2–3), 140–155. <https://doi.org/10.1016/j.crte.2008.11.002>
- Sintubin, M., Debaecker, T. N., & Van Baelen, H. (2009). Early Palaeozoic orogenic events north of the Rhenic suture (Brabant, Ardennes): A review. *Comptes Rendus Geoscience*, 341(2), 156–173. <https://doi.org/10.1016/j.crte.2008.11.012>
- Smeraglia, L., Fabbri, O., Choulet, F., Buatier, M., Boulvais, P., Bernasconi, S. M., & Castorina, F. (2020). Synclonic fluid flow and deformation mechanisms within the frontal thrust of a foreland fold-and-thrust belt: Example from the Internal Jura, Eastern France. *Tectonophysics*, 778, 1–21. <https://doi.org/10.1016/j.tecto.2019.228178>
- Smit, J., van Wees, J.-D., & Cloetingh, S. (2018). Early Carboniferous extension in East Avalonia: 350 My record of lithospheric memory. *Marine and Petroleum Geology*, 92, 1010–1027. <https://doi.org/10.1016/j.marpetgeo.2018.01.004>
- Storti, F., & McClay, K. (1995). Influence of syntectonic sedimentation on thrust wedges in analogue models. *Geology*, 23(11), 999–1002. [https://doi.org/10.1130/0091-7613\(1995\)023<0999:iOSSOT>2.3.CO;2](https://doi.org/10.1130/0091-7613(1995)023<0999:iOSSOT>2.3.CO;2)
- Suppe, J. (1983). Geometry and kinematics of fault-bend folding. *American Journal of Science*, 283(7), 684–721. <https://doi.org/10.2475/ajs.283.7.684>
- Szaniawski, R., Lewandowski, M., Mansy, J.-L., Averbuch, O., & Jacques, F. (2003). Syn-folding remagnetization events in the French-Belgium Variscan thrust front as markers of the fold-and-thrust belt kinematics. *Bulletin de la Société Géologique de France*, 174(5), 511–523. <https://doi.org/10.2113/174.5.511>
- Tanner, D. C., Bense, F. A., & Ertl, G. (2011). Kinematic retro-modeling of a cross-section through a thrust-and-fold belt: The Western Irish Namurian Basin. *Geological Society, London, Special Publications*, 349(1), 61–76. <https://doi.org/10.1144/SP349.4>
- Tavernelli, E. (1996). The effects of preexisting normal faults on thrust ramp development: An example from the northern Apennines, Italy. *Geologische Rundschau*, 85, 363–371. <https://doi.org/10.1007/BF02422241>
- Tavernelli, E. (1999). Normal faults in thrust sheets: Pre-orogenic extension, post-orogenic extension, or both? *Journal of Structural Geology*, 21(8–9), 1011–1018. [https://doi.org/10.1016/S0191-8141\(99\)00034-6](https://doi.org/10.1016/S0191-8141(99)00034-6)
- Thomas, W. A. (2001). Mushwad: Ductile duplex in the Appalachian thrust belt in Alabama. *AAPG Bulletin*, 85(10), 1847–1869. <https://doi.org/10.1306/8626D08B-173B-11D7-8645000102C1865D>
- Thomas, W. A. (2007). Role of the Birmingham basement fault in thin-skinned thrusting of the Birmingham anticlinorium, Appalachian thrust belt in Alabama. *American Journal of Science*, 307(1), 46–62. <https://doi.org/10.2475/01.2007.03>
- Thorez, J., & Dreesen, R. (1986). A model of a regressive depositional system around the Old Red Continent as exemplified by a field trip in the Upper Famennian "Isammites du Condroz" in Belgium. *Annales de la Société Géologique de Belgique*, 109, 285–323.
- Toscani, G., Bonini, L., Ahmad, M. I., Di Bucci, D., Di Giulio, A., Seno, S., & Galuppo, C. (2014). Opposite verging chains sharing the same foreland: Kinematics and interactions through analogue models (Central Po Plain, Italy). *Tectonophysics*, 633, 268–282. <https://doi.org/10.1016/j.tecto.2014.07.019>
- Tozer, R. S. J., Butler, R. W. H., Chiappini, M., Corrado, S., Mazzoli, S., & Speranza, F. (2006). Testing thrust tectonic models at mountain fronts: Where has the displacement gone? *Journal of the Geological Society*, 163, 1–14. <https://doi.org/10.1144/0016-764904-140>
- Ustaszewski, K., & Schmid, S. M. (2006). Control of preexisting faults on geometry and kinematics in the northernmost part of the Jura fold-and-thrust belt. *Tectonics*, 25, 1–26. <https://doi.org/10.1029/2005TC001915>
- Van Grootel, C., Verniers, J., Geerckens, B., Laduron, D., Verhaeren, M., Hertogen, J., & De Vos, W. (1997). Timing of magmatism, foreland basin development, metamorphism and inversion in the Anglo-Brabant fold belt. *Geological Magazine*, 134(5), 607–616. <https://doi.org/10.1017/S0016756897007413>
- Van Hulten, F. F. N. (2012). Devonian-Carboniferous carbonate platform systems of the Netherlands. *Geologica Belgica*, 15(4), 284–296.
- Vann, I. R., Graham, R. H., & Hayward, A. B. (1986). The structure of mountain fronts. *Journal of Structural Geology*, 8(3–4), 215–227. [https://doi.org/10.1016/0191-8141\(86\)90044-1](https://doi.org/10.1016/0191-8141(86)90044-1)
- Verniers, J., Herbosch, A., Vanguestaine, M., Ceukens, E., Delcambre, B., Pingot, J.-L., et al. (2001). Cambrian-Ordovician-Silurian lithostratigraphic units (Belgium). *Geologica Belgica*, 4(1–2), 5–38.

- Von Hagke, C., & Malz, A. (2018). Triangle zones—Geometry, kinematics, mechanics, and the need for appreciation of uncertainties. *Earth-Science Reviews*, *177*, 24–42. <https://doi.org/10.1016/j.earscirev.2017.11.003>
- Wiltschko, D., & Fastman, D. (1983). Role of basement warps and faults in localizing thrust fault ramps. In R. D. Hatcher, Jr, H. Williams, & I. Zietz (Eds.), *Contributions to the Tectonics and Geophysics of Mountain Chains* (Vol. 158, pp. 177–190). GSA Memoirs. <https://doi.org/10.1130/mcm158-p177>
- Wu, J. E., & McClay, K. R. (2011). Two-dimensional Analog Modeling of Fold and Thrust Belts: Dynamic Interactions with Syncontractional Sedimentation and Erosion. In K. R. McClay, I. H. Shaw, & J. Suppe (Eds.), *Thrust Fault-Related Folding* (Vol. 94, pp. 301–333). AAPG Memoir.
- Ziegler, P. A. (1989). *Evolution of Laurussia: A study in late palaeozoic plate tectonics*. Kluwer Academic Publishers. <https://doi.org/10.1007/978-94-009-0469-9>
- Ziegler, P. A. (1990). *Geological atlas of western and central Europe*. Shell Internationale Petroleum Maatschappij B.V.
- Ziegler, P. A., Bertotti, G., & Cloetingh, S. (2002). Dynamic processes controlling foreland development - The role of mechanical (de)coupling of orogenic wedges and forelands. *Stephan Mueller Special Publication Series*, *1*, 17–56. <https://doi.org/10.5194/smeps-1-17-2002>

3.4.5. Modélisation 3D des réservoirs dinantiens - Publication 3

Laurent A., Beccaletto L., Averbuch O., Graveleau F., Lacquement F., Caritg S., Marc S. & Capar L. (2021) Modelling the 3D geometry of the Dinantian carbonate geothermal reservoir in northern France, *Z. Dt. Ges. Geowiss. (J. Appl. Reg. Geol.)*, 172 (3), 293-305. <https://doi.org/10.1127/zdgg/2021/0284>

Cette publication concrétise les travaux de thèse d'A.Laurent sur la modélisation en 3D de la géométrie du front nord varisque, en ciblant particulièrement les réservoirs carbonatés géothermiques dinantiens. Le modèle résultant, qui n'aurait pas vu le jour sans la démarche scientifique sous-jacente de compréhension tectonique du front nord varisque (publication 2), est largement scruté par les acteurs régionaux du monde de la géothermie, collectivités territoriales ou industriels. En complément de l'équipe d'encadrement Séverine Caritg-Monnot du BRGM a apporté son expertise de modélisatrice 3D.

Principaux résultats de la publication 3

- Présentation des données d'entrée au modèle 3D (e.g. interprétation converties en profondeur de 532 km de profils sismiques qui représentent l'ossature du modèle, 1128 forages), et de la méthodologie de modélisation 3D, spécifiquement adaptée à la structuration complexe du front nord-varisque.
- Le réservoir carbonaté dinantien présente régionalement une géométrie monoclinale due à la réponse flexurale de l'avant-pays varisque en conséquence de l'avancée des nappes de chevauchement. Il présente un pendage global vers le sud ou le sud-ouest sous le bassin houiller du Nord-Pas-de-Calais.
- Le réservoir a une superficie beaucoup plus grande qu'attendu sur l'ensemble du territoire, s'étendant sur une superficie d'environ 7675 km², jusqu'à au moins 30-40 km au sud du district houiller sous l'unité allochtone ardennaise. La limite méridionale de l'extension est définie par la surface de cut-off de la séquence dinantienne au niveau de certaines rampes frontales et latérales majeures de l'AMBT (Allochthonous Main Basal Thrust, nouvellement défini).
- Le réservoir dinantien est généralement situé à moins de 200 m de profondeur dans la métropole lilloise, mais il atteint 1000 à 3000 m de profondeur sous le district du bassin houiller et enfin une profondeur maximale d'environ 7000 m à l'extrémité sud de la zone d'étude.
- Le réservoir dinantien est déformé le long de deux directions principales orientées N70-80 et N110-130, selon la configuration initiale de la marge syn-rift laurussienne. Les événements de déformation postérieurs (i.e. l'extension fini carbonifère-permienne, ainsi que la phase d'inversion tertiaire liée aux raccourcissements far-field alpin-pyrénéen) n'ont produit que des structures localisées de second ordre (tels que les anticlinaux du Boulonnais-Artois et du Mélantais-Tournais).

Publication 3

Z. Dt. Ges. Geowiss. (J. Appl. Reg. Geol.), 172 (3), p. 293–305, 6 figs.

Published online September 2021

Article

Open Access



Modelling the 3D geometry of the Dinantian carbonate geothermal reservoir in northern France

Aurore Laurent¹, Laurent Beccaletto², Olivier Averbuch¹, Fabien Graveleau¹, Frédéric Lacquement², Séverine Caritg², Stéphane Marc² & Laure Capar^{2*}

Laurent, A., Beccaletto, L., Averbuch, O., Graveleau, F., Lacquement, F., Caritg, S., Marc, S. & Capar, L. (2021): Modelling the 3D geometry of the Dinantian carbonate geothermal reservoir in northern France. – Z. Dt. Ges. Geowiss., 172: 293–305, Stuttgart.

Abstract: The current research project aims at better characterising the 3D geometry of the main deep geothermal reservoir in northern France: the Dinantian karstic and brecciated limestones (lower Carboniferous, Mississippian). The detailed 3D geometry of this buried reservoir in the region has been investigated here through the integration of a large database including 1,128 boreholes and 532 km of reprocessed and interpreted seismic reflection profiles. This geological information was then interpolated in a 3D structural model using the GeoModeller software. Despite residual uncertainties related to the time-depth conversion procedure of the seismic data as well as the interpolation process, it provides an image of the 3D geometry of the Dinantian sequence at depth with an unprecedented resolution.

The 3D modelling indicates that the Dinantian reservoir is rather continuous and extends over an area of approximately 7,675 km² in northern France-southwestern Belgium. Interestingly, we document that the Dinantian reservoir extends at least 30 to 40 km south or southwest of the coal basin area as indicated by the geometry of its cut-off line with the major frontal and lateral ramps of the Allochthon Main Basal Thrust of the Northern Variscan Front. From the Lille metropolitan area, where the Dinantian is rather shallow (depth lower than 200 m), the Dinantian reservoir strongly deepens southward as it reaches 1,000–3,000 m depth beneath the coal basin district and a maximum depth of about 7,000 m at the southern end of the study area.

Keywords: 3D structural modelling, Dinantian geothermal reservoir, Northern Variscan thrust front

1. Introduction

Over the last few decades, growing societal awareness regarding the need to turn to renewable energies has led to the implementation of new energy policies. Following the Paris Agreements for climate change in 2015, governments are committed to massively invest into and develop renewable energies in the coming decades. Among this renewable energy package, geothermal energy is probably one of the less known, although it is locally of major importance. Numerous projects for the development of deep geothermal energy have thus been launched recently both at the European level, such as the Interreg North-West Europe DGE-ROLLOUT project, and at the regional scale, e.g. the Hauts-de-France region in northern France.

In the Hauts-de-France region (northern France), the populated Nord-Pas-de-Calais (NPC) coal basin district (1.5 million inhabitants), located above the fossil deformation front of the Variscan Orogen, constitutes an interesting target for the

development of low-temperature deep geothermal energy. Such orogenic fronts have long been favoured targets for the exploration and exploitation of hydrocarbons and coal. It was particularly the case of the NPC Molasse foreland basin explored and exploited for coal production during the 19th–20th centuries. More recently, however, they have raised major interest for deep geothermal applications. Indeed, in such geological setting, potential rock reservoirs can be buried at a few kilometres depth beneath the foreland basin, thereby creating favourable conditions for the generation of high-temperature waters. This is, for example, the case in Bavaria, Germany, near Munich, where high-temperature geothermal fluids (80–140 °C) are extracted beneath the Alpine molassic basin (Farquharson et al. 2016).

In late Carboniferous times, the development of the Variscan NPC Molasse foreland basin led to the burial of the pre-orogenic sequence up to few kilometres depth in northern France; the region-wide Dinantian (Lower Carboniferous) carbonate units are part of this buried pre-orogenic se-

*Addresses of the authors:

¹Univ. Lille, CNRS, Univ. Littoral Côte d'Opale, UMR 8187 – LOG – Laboratoire d'Océanologie et de Géosciences, F-59000 Lille, France (aurore.laurent@univ-lille.fr / olivier.averbuch@univ-lille.fr / fabien.graveleau@univ-lille.fr)

²BRGM, F-45060 Orléans, France (l.beccaletto@brgm.fr / f.lacquement@brgm.fr / s.caritg@brgm.fr / s.marc@brgm.fr / l.capar@brgm.fr)

© 2021 The authors

DOI: 10.1127/zdgg/2021/0284

E. Schweizerbartsche Verlagsbuchhandlung, Stuttgart, Germany, www.schweizerbart.de

quence. Due to their highly fractured and karstified character, they constitute the main target reservoir for the exploitation of deep geothermal energy in northern France. This reservoir is already exploited in Belgium in the Hainaut coal district area, that is the eastward prolongation of the NPC coal district area, where the water temperature in the three geothermal wells of Douvrain, Ghlin and Saint-Ghislain reaches 60–70 °C (e.g. Delmer 1982; Licour 2012). In northern France, the Dinantian reservoir has only been observed through boreholes and its geothermal potential is not well constrained. A few geothermal anomalies have been recorded in the NPC coal basin district at the source of Saint-Amand-les-Eaux (23 °C) and near Lens in the mining boreholes of Lens n°10 and Meurchin n°2 (40 °C at 240–335 metres depth; Becq-Giraudon 1983). During the 1980s, a geothermal exploration well was drilled at Condé-sur-l'Escaut, less than 20 kilometres from the Belgian productive geothermal wells, without finding any geothermal evidence. This highlighted the geographical variability of the geothermal potential in the region, most probably related to both the hydrodynamics within the Dinantian reservoir and the complex structure and fault network along the Northern Variscan Front.

In this general context, our study aims at defining the 3D geometry of the buried Dinantian carbonate reservoir in northern France. It is based on the 3D modelling of the structure of the Northern Variscan Front in northern France–southwestern Belgium, using the GeoModeller software. This 3D model integrates a large database, comprising 532 kilometres of reprocessed seismic reflection profiles, 1,128 boreholes as well as local structural data. A depth structural map of the top of the Dinantian reservoir in the study area has been generated as a result of the modelling process. This 3D modelling approach allows defining the extension and depth of the Dinantian carbonate reservoir with an unprecedented resolution and thereby represents the first step towards assessing the geothermal potential in the region.

2. Geological setting

2.1 The Dinantian carbonate sequence in northern France

In NW Europe, the Dinantian carbonate units (Lower–Middle Mississippian, 359–331 Ma) are known all around the lower Palaeozoic London-Brabant Massif. They extend from Ireland via England to the Netherlands and from northern France via Belgium to western Germany (Arndt 2021; Broothaers et al. 2021; Pharaoh et al. 2021; Pracht et al. 2021). In northern France, the Dinantian units and the entire Palaeozoic substratum are generally covered, unconformably, by a 100–200 metres thick Cretaceous-Tertiary sequence, deposited along the northern border of the Paris Basin (Fig. 1). The Dinantian sequence is thus mainly constrained through boreholes (see reference wells in Fig. 2a), and on a few outcrops localised in the Boulonnais (English

Channel borders) and Avesnois regions (western end of the Ardennes Massif) as well as in the Mons-Tournai area (southwestern Belgium) (Fig. 1).

In the NPC coal district area (northern France) and in the Hainaut region (southwestern Belgium), the known thickness of the complete Dinantian series varies between 600 m in the area of Jeumont (COPESEP 1965) and 2,600 m in the area of Saint-Ghislain (Groessens et al. 1982). The lower Dinantian or Tournaisian (Lower Mississippian, 359–347 Ma), is well documented in the boreholes Tournai, Vieux-Leuze (Coen-Aubert et al. 1980) and Saint-Ghislain (Groessens et al. 1982) (Fig. 2a). It consists of shales, calcareous shales with crinoidal beds and crinoidal limestones with argillaceous intervals and cherty layers (Poty et al. 2001; Hance 2006a) (Fig. 2c). At its base, the uppermost Devonian-lowermost Tournaisian is characterised by sandstones, dolomitic sandstones, shales, dolomitic limestones and sandy limestones. The upper Dinantian or Visean (Middle Mississippian, 347–331 Ma) consists mostly of bioclastic and crinoidal dolomites and limestones. It usually comprises thick intervals of brecciated limestones with stromatolitic levels (Groessens et al. 1982; Poty et al. 2001; Hance et al. 2006b; Fig. 2c). The extensive brecciated character of the Visean limestones is attributed to the polyphased, long-term dissolution of interstratified evaporite sequences during the successive events of burial of the Dinantian rocks (Rouchy et al. 1986, 1987; De Putter 1995; De Putter et al. 1994). Thick residual levels of anhydrite are locally preserved in the Visean series of the Epinoy and Saint-Ghislain boreholes (Delmer 1977; Rouchy et al. 1986, 1987; De Putter et al. 1991, 1994); where anhydritic levels are present, brecciated limestones are more scarce (Licour 2012). The heterogeneity and fractured character of the Visean brecciated limestone sequence together with its higher tendency for local karstification make this unit the main geothermal target in the N France-Hainaut area.

From a palaeogeographical point of view, the Dinantian series of northern France (Lille and NPC coal district area) and southwestern Belgium (Mons-Tournai area) were deposited in a marine shallow-water carbonate environment at the southern margin of the Laurussian continental block. Overall, it evolved from a south-facing ramp in the early Tournaisian to a rimmed shelf during the late Tournaisian-early Visean (Hance et al. 2001, 2006a; Poty et al. 2001). During the mid-late Visean, this carbonate sequence deposited on a broad shelf of regional extent. A polarity inversion occurred in the middle Visean (Livian): facies characteristics of a more restricted marine environment (e.g. anhydrite, stromatolitic facies) deposited to the south while open marine facies deposited to the north (Hance et al. 2001, 2006b; Poty et al. 2001). This change reflects the first effects of the northward propagating uplift associated to the tectonic inversion of the Laurussian margin and the subsequent development of the Variscan thrust front.

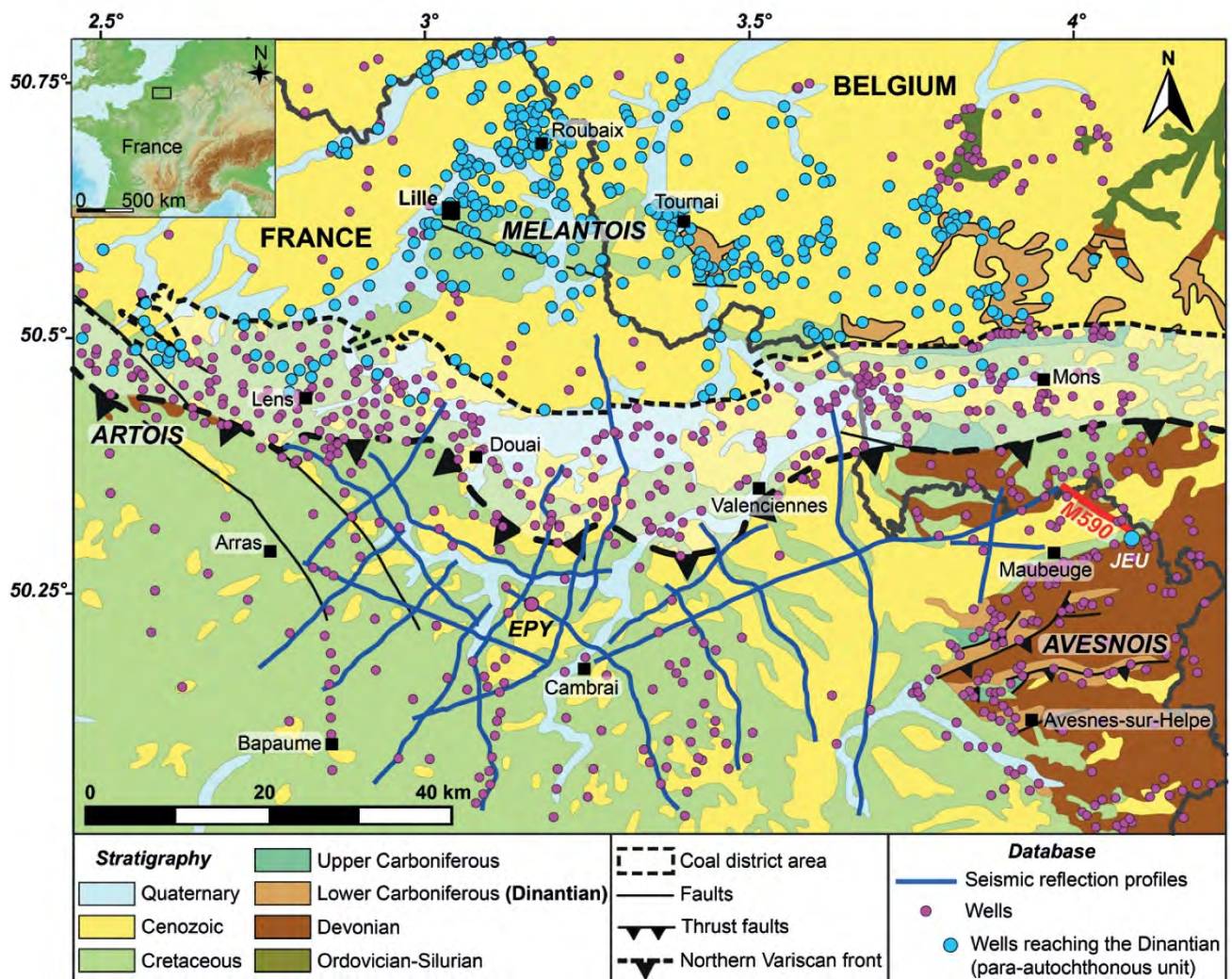


Fig. 1: Simplified geological map of the modelled area extracted from the geological map of France (Chantraine et al. 2003) reporting the location of the boreholes and seismic reflection profiles used to produce the 3D model. Dinantian outcrops in the Brabant Para-autochthonous Unit (Belgium) have been delimited by a thick black line. Borehole legend: EPY – Epinoy; JEU – Jeumont.

2.2 Structural framework

The Dinantian units developed as part of a large-scale post-rift transgressive carbonate platform onto the slowly subsiding southern Laurussian margin from the late Eifelian to the Viséan (Meilliez et al. 1991; Mansy et al. 1999). This large platform recorded the long-term thermal subsidence of the proximal southern margin of the Laurussian continent following a major rifting phase that took place from Early (Lochkovian) to Middle Devonian (Eifelian) (Meilliez et al. 1991; Franke 2000; Shail & Leveridge 2009). This rifting event triggered the opening of the Rheno-Hercynian Ocean in between the northern Laurussian margin and the southern Armorica-Saxo-Thuringia continental blocks. The syn-rift subsidence of the Laurussian margin was marked by normal faulting oriented along two main directions: i.e. N50-70° and N110-130° (Meilliez et al. 1991).

From Late Devonian times onward, tectonic kinematics changed and the subsequent N-S convergence between Avalonia and the Armorica-Gondwana accretion complex led to the progressive southward subduction and closure of the Rheno-Hercynian Ocean and to the collision of the surrounding margins during the middle Viséan (ca. 340 Ma; Cazes et al. 1985; Averbuch & Piromallo 2012; Franke et al. 2017). This Variscan collision stage, characterised by an overall NNW-SSE shortening, lasted about 35 Ma until the Middle Pennsylvanian (ca. 305 Ma) and led to the gradual tectonic inversion of the southern Laurussian margin (e.g. Oncken et al. 1999, 2000; Averbuch et al. 2004; Averbuch & Piromallo 2012). It resulted in the development of a north-vergent thrust system extending in northern France from the Channel borders (Boulonnais) to the Avesnois region (Maubeuge area in Fig. 2; Cazes et al. 1985; Raoult & Meilliez 1987; Averbuch et al. 2004).

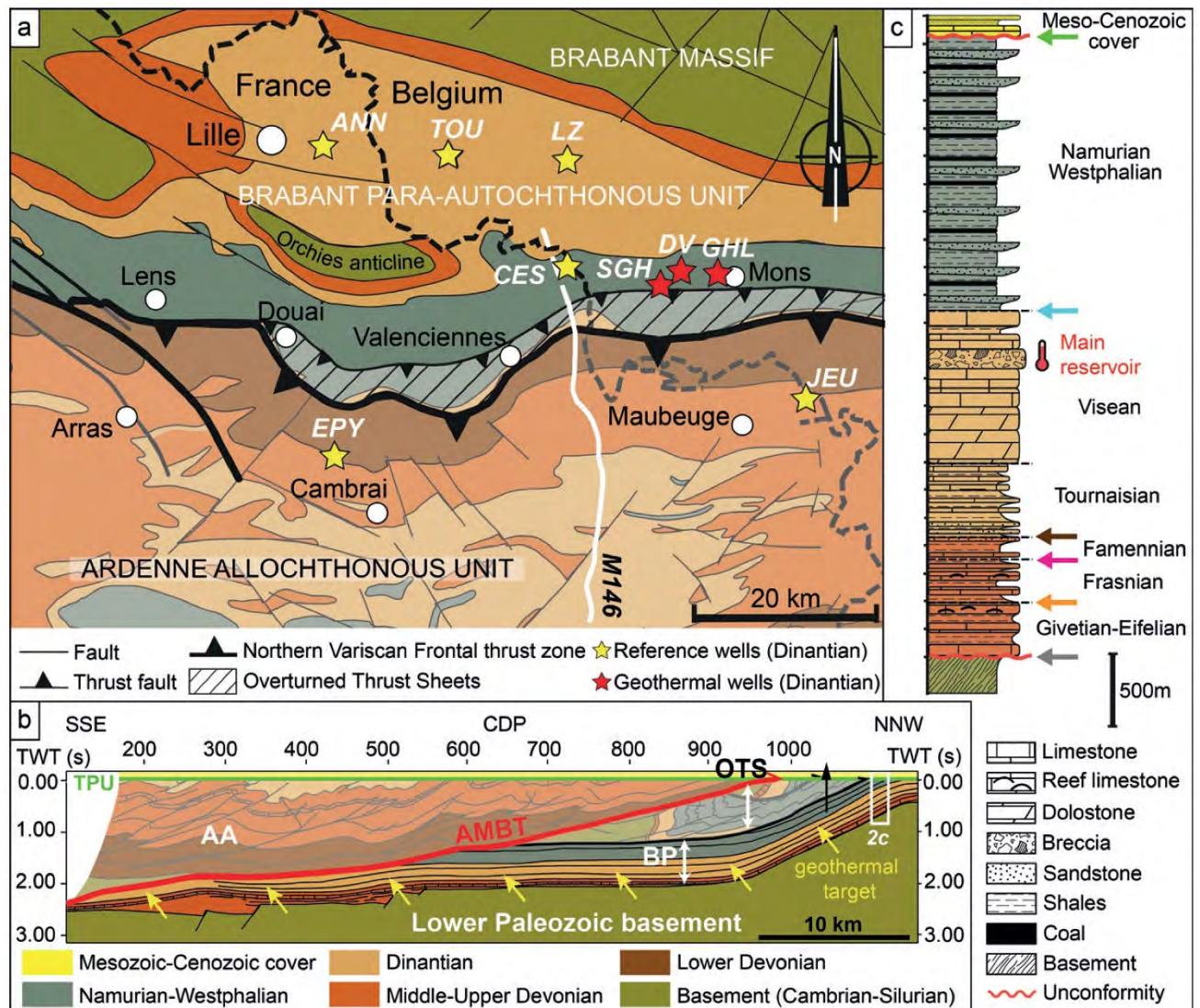


Fig. 2: (a) Structural map of the Variscan basement in the modelled area (modified from CFP et al. 1965 and Averbuch et al. 2004). Only the geological levels modelled in 3D are represented in full colours (i.e. Brabant Para-autochthonous Unit). The reference wells correspond to the deep boreholes used to define and describe the Dinantian in northern France-southwestern Belgium. Borehole legend: ANN – Annapes; CES – Condé-sur-l’Escaut; DV – Douvrain; EPY – Epinoy; GHL – Ghlin; JEU – Jeumont; LZ – Leuze; SGH – Saint-Ghislain; TOU – Tournai. (b) Interpretation of the M146 seismic profile (location in Fig. 2a), illustrating the structure of the Northern Variscan Front in the area of Valenciennes (modified from Lacquement et al. 1999 and Mansy & Lacquement 2006). AA – Ardennes Allochthonous Unit; AMBT – Allochthon Main Basal Thrust; BP – Brabant Para-autochthonous Unit; OTS – Overturned Thrust Sheets; TPU – Top Palaeozoic Unconformity. (c) Synthetic lithostratigraphic log of the Brabant Para-autochthonous Unit in northern France-southwestern Belgium. Indicated thicknesses have been defined based on the data of the reference boreholes in the region (Fig. 2a). The coloured arrows point at the geological surfaces interpreted in seismics (Fig. 3) and modelled in 3D. Main Dinantian geothermal reservoir is indicated.

The Dinantian carbonate units of northern France were primarily deformed during the Variscan orogenic cycle. Subsequent deformation events (i.e. the late Carboniferous-Permian and Late Jurassic-Early Cretaceous rifting episodes as well as the Tertiary inversion related to the far-field accommodation of the Alpine-Pyrenean shortening) produced only second-order structures, mostly localised along the Artois-

Boulonnais hills (western limit of the area under study) and the Mélançois dome (between Lille and Tournai) (e.g. Mansy et al. 2003; Minguely et al. 2010 and references herein). Beneath the Mesozoic-Cenozoic cover, the Dinantian series are incorporated within three major structural units involved in the northern Variscan thrust front (from north to south): the Brabant Para-autochthonous Unit, the Overturned Thrust

Sheets and the Ardennes Allochthonous Unit (Fig. 2a; Meilliez & Mansy 1990; Mansy et al. 1997, 1999; Lacquement et al. 1999).

The Brabant Para-autochthonous Unit corresponds to the slightly deformed part of the Laurussian continental margin. It is formed by the Middle Devonian to lower Carboniferous (late Eifelian–Visean) post-rift transgressive cover of the Brabant lower Palaeozoic basement and by the overlying synorogenic molasse (Fig. 2c), deposited along the Northern Variscan foredeep during the Late Mississippian–Middle Pennsylvanian (Namurian–Westphalian, 325–305 Ma; Fig. 2a). In northern France, this basin, known as the NPC coal basin, involves an up to 3.5 km thick molasse sequence made of an alternation of fluvio-deltaic and paralic deposits (Bouroz 1969; Becq-Giraudon 1983; Delmer et al. 2001). This structural unit displays an overall monoclinical geometry with a general gentle southward dip (5–10°; Fig. 2b) due to the flexural response of the foreland to thrust loading. North of the emergence of the frontal thrust zone, it displays however a major flexure allowing for the exhumation of the Palaeozoic substratum directly below the Mesozoic–Cenozoic cover (the Orchies anticline in Fig. 2a).

To the south, the Brabant Para-autochthonous Unit is overthrust by the Ardennes Allochthonous Unit along a major crustal-scale thrust zone (Figs. 2a, b; Raoult 1986; Meilliez & Mansy 1990; Mansy et al. 1997; Lacquement et al. 1999). The latter is referred to, in this paper, as the Allochthon Main Basal Thrust (AMBT). Its emerging part, which delimits the southern extension of the coal district area, is usually known as the Midi Fault (Meilliez 2019 and references herein). The Ardennes Allochthonous Unit is composed of a more complete and thicker Lower Devonian to Dinantian sequence than the Brabant Para-autochthonous Unit due to its more distal palaeogeographic position on the southern Laurussian margin. The allochthonous unit forms part of a typical fold-and-thrust belt with an overall E–W to ENE–WSW trend in the area under study (Khatir et al. 1988; Meilliez & Mansy 1990; Mansy & Meilliez 1993; Lacquement 2001; Moulouel 2008). In northern France, restoration of the margin geometry before compression suggests that the Ardennes Allochthonous Unit was displaced over at least 60–70 km northward along the main frontal thrust zone (Raoult & Meilliez 1987; Lacquement et al. 1999; Mansy et al. 1999; Laurent et al. 2021). This intense deformation is emphasised by the existence of thrust sheets characterised by a complex and overall overturned geometry between the Brabant Para-autochthonous Unit and the Ardennes Allochthonous Unit (Bouroz et al. 1961; Delmer 1997, 2003; Mansy et al. 1997; Lacquement et al. 1999; Fig. 2b). These so-called “Overturned Thrust Sheets” (OTS) consist of a folded Silurian to upper Carboniferous sequence affected by a series of second-order NNW-vergent forelimb thrusts (Bouroz 1950; Le Gall 1994; Meilliez 2019). This typical structural style is depicted in the N–S cross-section of Fig. 2b, based on the interpretation of the reference M146 seismic profile in the Valenciennes area (Mansy et al. 1997; Lacquement et al. 1999; Laurent et al. 2021).

3. Data and methodology

3.1 Selection of the seismic and well data

The 3D geometry of the Dinantian carbonate reservoir in the NPC coal district area and its southward extension below the Ardennes Allochthonous Unit has been investigated by modelling the 3D structure of the Northern Variscan Front in northern France and southwestern Belgium (Hainaut area). The study area extends over 125 km E–W, from the Hainaut coal basin district in the east to the Artois region in the west, and over 86 km N–S, from the northerly Roubaix–Tourcoing cities to the southern limit of the Nord-Pas-de-Calais region (Fig. 1). It represents a surface area of 10 750 km².

A large database including mainly seismic reflection and well data was compiled prior to the 3D modelling process. 21 seismic reflection profiles, acquired during the onshore oil exploration of the northern Paris Basin (France) in the 1980s, have been reprocessed by the BRGM–French Geological Survey (static corrections, velocity analysis, noise attenuation, pre-stack time migration) and interpreted within the scope of this study (Fig. 1). Given the acquisition parameters used in the surveys (recording length up to 5 seconds two-way-time), the estimated depth of investigation is around 7 to 8 km and the vertical resolution of seismic imaging is approximately 25–30 metres. Seismic lines represent a total length of 532 km and cover an area of approximately 5,130 km² over the allochthonous and para-autochthonous units (Fig. 1). The seismic profiles cross the region along various orientations allowing their interpretation to provide an updated image of the 3D structure of the Dinantian carbonate platform in the investigated area. The seismic interpretation was carried out using the IHS Kingdom Software. The targeted geological surfaces have been identified in seismics by calibrating and tying seismic and well data. Synthetic seismograms have been produced using the velocity data from the Epinoy and Jeumont boreholes (Fig. 1), which are the only wells of sufficient depth in the vicinity of the seismic lines to cross the targeted geological levels (see the example of the seismic-well tie between the Jeumont borehole and the M590 seismic profile in Fig. 3a). Several geological horizons and faults have been interpreted (Fig. 2c), with a special focus on the Dinantian carbonates and the regional structural pattern (see Laurent et al. 2021 for further details).

In addition to the seismic data, 1,128 boreholes reaching the Palaeozoic basement have been selected in northern France and southwestern Belgium and included in the database (Fig. 1). A methodical screening process limited to one borehole in a 500 m radius was applied in order to collect as much relevant well data as possible, while avoiding redundant and excessive information. Among the 1,128 selected boreholes, 389 reach the Dinantian in the Brabant Para-autochthonous Unit (Fig. 1). All but one (Jeumont) of these boreholes are located north of the Variscan front. South of the Variscan front, where the underthrust Dinantian units deepen below the thick Ardennes Allochthonous Unit, only the seismic data provides information at

depth, thus reflecting the complementarity of seismic and well data (Fig. 1).

Finally, our database was completed with structural data from the geological maps of France (1: 1,000,000; [Chantraine et al. 2003](#)) and Wallonia (Belgium) (1: 25,000, “Carte géologique de Wallonie”, Programme de révision de la Carte géologique de Wallonie), such as azimuth and dip values and stratigraphic contacts (see the Dinantian outcrops highlighted in Fig. 1). A digital elevation model (DEM) with a resolution of 25 metres (EU-DEM v1.1 from the Copernicus Land Monitoring Service), provided the required topographic information (Fig. 4).

3.2 Time-depth conversion of the seismic data

Seismic horizons interpreted in time (Fig. 3a) have been converted to depth before being integrated into the 3D model. To do so, several time-depth (TD) conversion methods have been tested: (1) time-depth conversion using the seismic stacking velocities, obtained from the reprocessing of the seismic profiles in time; (2) time-depth conversion based on the migration velocities used for the pre-stack depth migration (PSDM) of six seismic profiles, carried out as part of the

Interreg North-West Europe DGE-Rollout project; and (3) layer-cake time-depth conversion using interval velocities obtained from well data.

The accuracy of the different methods could only be checked and compared at the very few wells located in the vicinity of the seismic lines and deep enough to cross the geological surfaces of interest, particularly the Epinoy and Jeumont boreholes (Fig. 1). This relatively limited well control constitutes the main limitation of this procedure.

After comparing the results of all three methods, the layer-cake TD conversion was chosen to maintain 3D consistency between the profiles and the well data. This method is based on the principle that a constant velocity is attributed to each layer displaying similar velocity behaviour ([Marsden 1989](#)). The velocity behaviour is defined by lithologies and rock properties and the interval velocity of a given layer corresponds to the mean velocity within this layer:

$$V_{int} = \frac{Z_{base} - Z_{top}}{OWT_{base} - OWT_{top}} \quad \text{Eq. 1}$$

with OWT = one-way time, Z = depth.

We therefore considered every geological level of the stratigraphic pile of the model (see 3.1) as a distinct layer with a constant interval velocity in the entire study area (Fig.

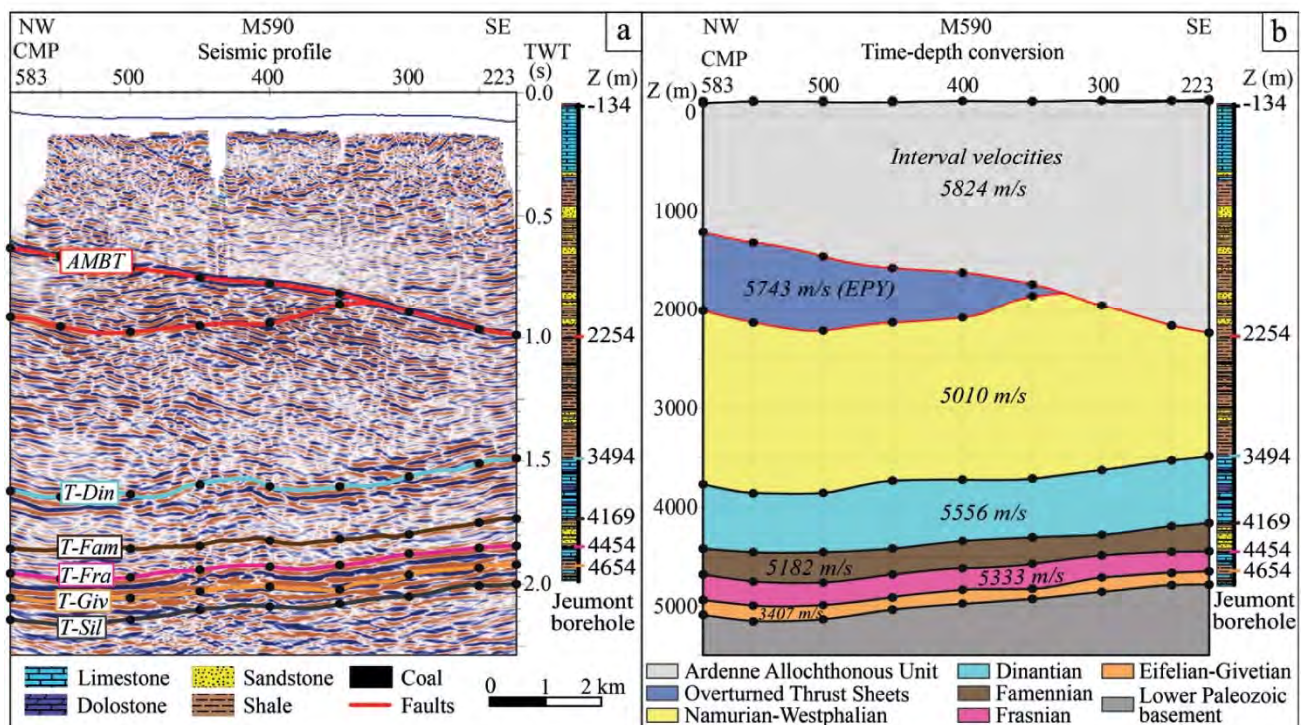


Fig. 3: (a) Geological interpretation of the M590 seismic reflection profile. The profile is highlighted in red in Fig. 1. The Jeumont borehole has been tied to the seismic line by generating a synthetic seismogram using well log data (Sonic log). The black dots show the time data points converted in depth using the interval velocities. AMBT – Allochthon Main Basal Thrust; T-Din – Top Dinantian; T-Fam – Top Famennian; T-Fra – Top Frasnian; T-Giv – Top Givetian; T-Sil – Top Silurian. (b) Time to depth conversion of the M590 seismic reflection profile using the interval velocities of the Jeumont borehole. Note that the interval velocity of the Overturned Thrust Sheets comes from the Epinoy borehole (EPY).

3b). The interval velocities in the Brabant Para-autochthonous Unit and in the Overturned Thrust Sheets have been computed from the data of the only two wells crossing these units, respectively the Jeumont and Epinoy boreholes (Fig. 1). The interval velocity in the Ardenne Allochthonous Unit corresponds to a mean value calculated from the data of both wells. Finally, to ensure a better geological consistency, a different interval velocity in the Mesozoic-Cenozoic cover has been computed for each line, using the data from nearby boreholes. The interpreted seismic horizons have then been converted to depth step by step from the shallowest (base of the Meso-Cenozoic cover) to the deepest one (top of the lower Palaeozoic basement), using a sampling rate of 50 CMP (common midpoint) (i.e. every 1,250 metres) along each seismic profile. Fig. 3b illustrates an example of TD conversion of the M590 profile, close to the Jeumont borehole.

Like any other TD conversion method, the layer-cake TD conversion has some limitation. First, because the interval velocities are computed based on the data of only two boreholes, the TD conversion of the seismic profiles does not take into account the potential lateral variations of lithologies and rock properties. Therefore, uncertainties increase as distance from the reference boreholes increases. However, considering the lithologies described in the boreholes, the facies variations are very likely not significant enough at the regional scale to have a major impact on the velocity behaviour of the different units.

3.3 3D modelling workflow

The 3D modelling of the Dinantian carbonate reservoir was carried out using the GeoModeller software developed by the French Geological Survey (BRGM) and Intrepid Geophysics Company (www.intrepid-geophysics.com). The modelling method used in this software, referred to as the “potential-field method” (Lajaunie et al. 1997), was specifically designed to compute the geological surfaces and volumes based on both stratigraphic contact points and orientation points (azimuth, dip and polarity values) from geophysical, structural and well data (Fig. 4). It uses a cokriging algorithm to interpolate a 3D potential-field scalar function describing the geology of the study area (Lajaunie et al. 1997; Chilès et al. 2004; Aug et al. 2005; McInerney et al. 2005; Calcagno et al. 2008; Maxelon et al. 2009).

A stratigraphic pile incorporating the main regional geological levels has been established in order to best define the 3D structure of the Northern Variscan Front. Each geological formation of the stratigraphic pile has been assigned to a rule, either “Erode” or “Onlap”, defining its relationship with older formations. The stratigraphic column includes from base to top: The lower Palaeozoic basement (onlap), the Middle Devonian (erode), the Frasnian (onlap), the Famennian (onlap), the Dinantian (onlap), the Namurian-Westphalian (onlap), the OTS (erode), the Ardenne Allochthonous Unit (erode) and the discordant Mesozoic-Cenozoic cover (erode) (see Figs. 2b, c). By defining the stratigraphic pile and the relationship

rules, the geological history of the study area is automatically taken into account during the modelling process, making it easy to try out different interpretations.

Once the stratigraphic pile of the model was created, the input database described above (3.1) was integrated to the GeoModeller Software (Fig. 4). The fault network and the fault interactions with the different series have been established using the specific features of the GeoModeller software. Stratigraphic horizons and faults were then modelled step by step so that they match structural, seismic and well data. In areas where the geometry of the modelled surfaces was geologically inconsistent, especially in areas with no or insufficient data, 3D construction points were added to the dataset on horizontal and vertical cross-sections. This ensured the 3D structural consistency of the model. At the end of the modelling process, depth structural maps have been extracted from the model using a grid cell size of 250 m (Fig. 4).

4. 3D geometry of the top of the Dinantian carbonate reservoir: results and discussion

The 3D geometry of the Dinantian carbonate reservoir in northern France-southwestern Belgium is presented in this paper through the detailed analysis of the 2D depth structural map of the top of the Dinantian limestones (Fig. 5). It is important to notice that the top of the Dinantian unit is of variable geological nature (domains [a], [b] and [c] in Fig. 5 inset) from south to north. The top Dinantian corresponds to the stratigraphic Dinantian-Namurian boundary in domain [b], it is a truncation limit southward in domain [a] and an erosive limit northward in domain [c]. To the south, the truncation limit corresponds to the tectonic contact between the Dinantian and the overthrusting Ardennes Allochthonous Unit, i.e. the AMBT. To the north, the top limit of the Dinantian series is eroded and truncated by the discordant Mesozoic-Cenozoic cover. Thereby, north of the truncation line (domain [c] in Fig. 5), the modelled geological surface represents the Dinantian-Cretaceous unconformity or Top Palaeozoic Unconformity (TPU).

In the study area, the Dinantian sequence extends over a surface area of approximately 7,675 km² (Fig. 5). Interestingly, it extends at least 30 to 40 kilometres south of the coal district area beneath the Ardenne Allochthonous Unit. Additionally, the Dinantian sequence is absent west of Arras, because it is truncated in the Artois region by the lateral ramp of the AMBT. The few tightened contour lines south of the cutoff line indicate a stronger dip of the truncated top of the Dinantian unit and therefore of the AMBT. These observations corroborate previous studies (Minguely 2007), showing that the main frontal thrust is steeper in the Artois region (20°) than in the NPC coal basin area (5–10°). To the north, beneath the unconformable Mesozoic-Cenozoic cover (area [c] in Fig. 5), the Dinantian extends beyond the Roubaix and Tournai cities and edges the Brabant Massif in Belgium.

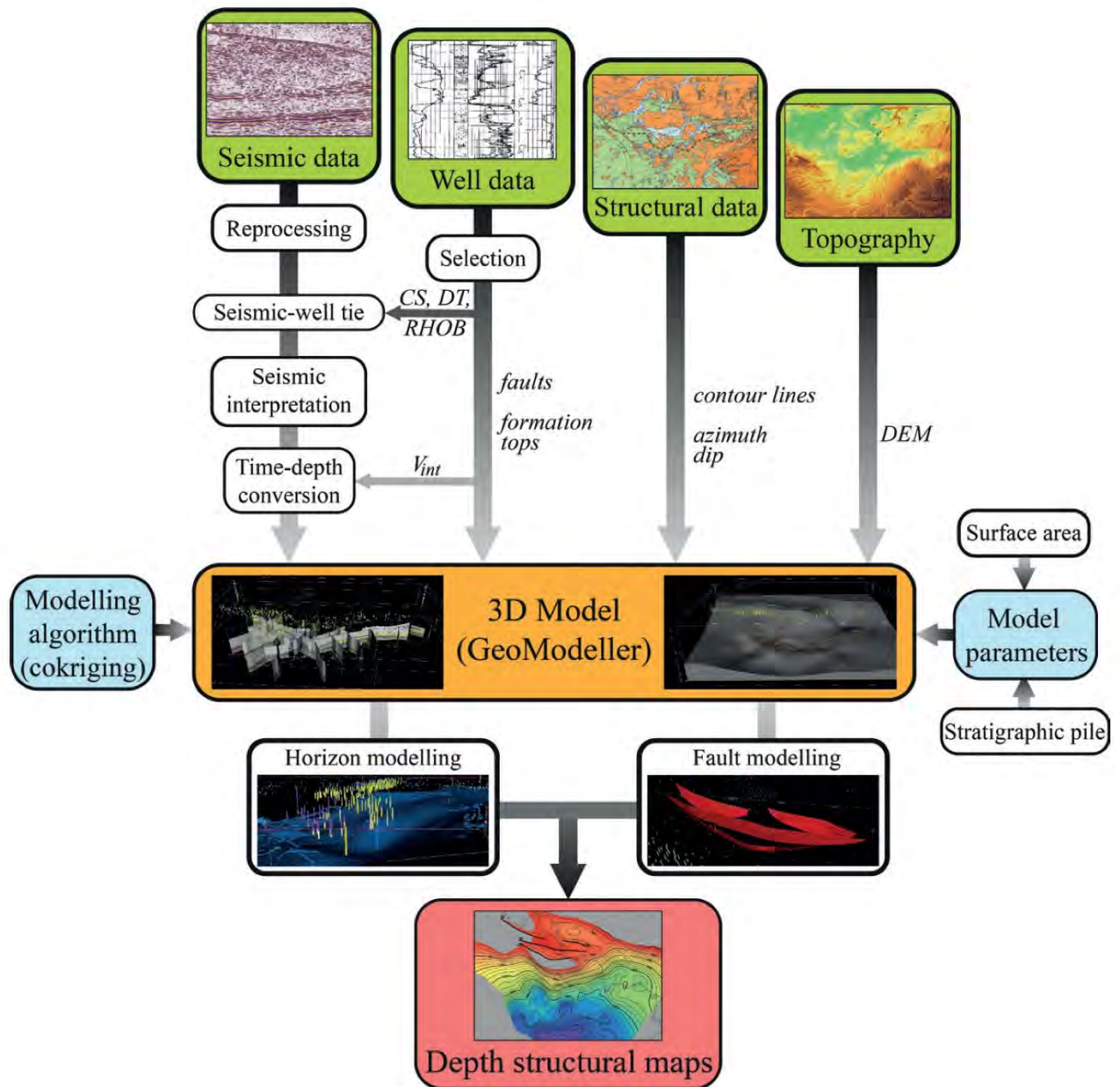


Fig. 4: Flow chart of the methodology implemented to model the 3D structure of the Dinantian reservoir. CS – checkshots; DEM – Digital Elevation Model; DT – sonic log; RHOB – density log; V_{int} – interval velocities.

Overall, the Dinantian series deepens southward. The modelled top-Dinantian surface has a maximum elevation of 122 metres in Belgium, northeast of Mons, and reaches a maximum depth of ~7,000 metres at the southern end of the study area. In the Lille-Tournai metropolitan area, where the Dinantian reservoir is exploited for its natural water resources, the structure of the Dinantian is well constrained by numerous wells (Fig. 5) and some localised outcrops (Tournai area, Belgium). Reservoir depth varies slightly and does not exceed 150 metres, which is related to the sub-tabular character of Dinantian layers (dips below 10°). Due to the shallow depth and slight dip variations, the modelled surface

appears flat in 3D at the regional scale (Fig. 6). In this area, the top of the Dinantian, as well as the entire Palaeozoic substratum and the Mesozoic-Cenozoic cover, forms a gentle dome (the Melantois-Tournais anticline) oriented along a $N100-110^\circ$ axis between Lille and Tournai (Fig. 5) (e.g. Hennebert & Doremus 1997a, b; Hennebert 1998). The Melantois-Tournais anticline is affected by two reverse faults of limited offset, oriented along a $N100-110^\circ$ direction: from north to south, the Gaurain-Ramecroix Fault (GRF) and the Haubourdin Fault (HF) (or Rumes Fault in Belgium). According to previous studies (e.g. Hennebert 1998; Minguely 2007), these faults initiated during a transtensive late Vari-

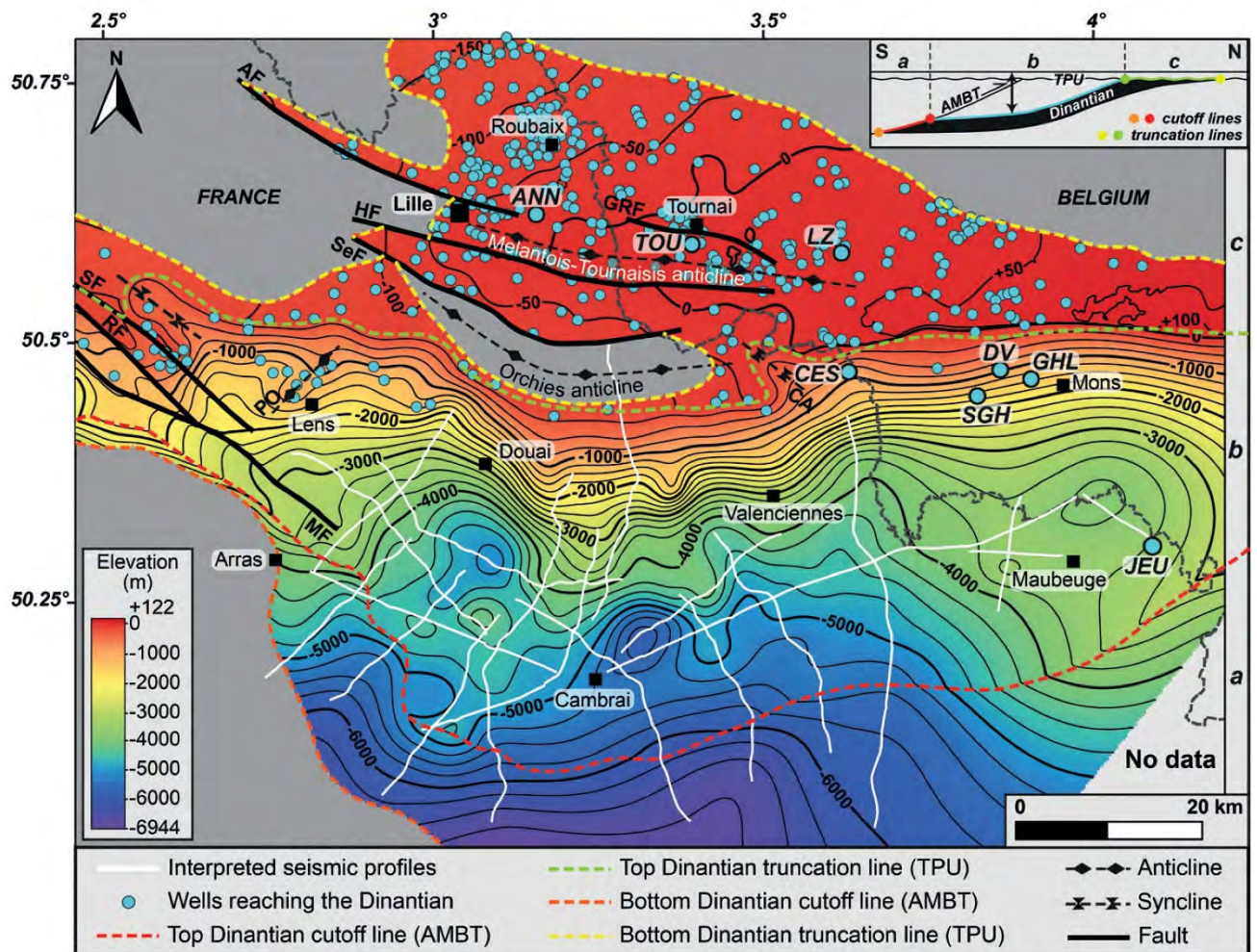


Fig. 5: Depth structural map of the top of the Dinantian, extracted from the 3D model. Grid cell size: 250 m. Faults and folds legend: AF – Armentieres Fault; CA – Chateau L’Abbaye syncline; GRF – Gaurain-Ramecroix Fault; HF – Haubourdin Fault; MF – Marqueffles Fault; PO – Poil d’Ours anticline; RF – Ruitz Fault; SF – Sains Fault; SeF – Seclin Fault. Borehole legend: same as Fig. 2a.

scan event and were reactivated as reverse faults during the Cenozoic as a result of the far-field accommodation of the Alpine-Pyrenean shortening. The general antiform would have developed as the result of this late shortening phase.

South of the Lille-Tournai metropolitan area, the monoclinical geometry of the Dinantian series rapidly deepens beneath the coal basin. According to our model, its depth ranges from 0 to approximately 3,000 metres between the northern and southern boundaries of the NPC coal district area. A major flexure is visible in the area of the NPC coal district, where the slope is steeper (10–30°) than in the rest of the region (5–10°), as shown by the tightened contour lines (Fig. 5). A slope break at the northern edge of the coal basin district is clearly apparent in 3D (top Dinantian truncation line in Fig. 6). Maximum dips ranging between 20 and 30° have been recorded near Douai and Valenciennes. This major flexure is associated to the exhumation of the Dinantian and Palaeozoic substratum directly below the Mesozoic-Cenozoic cover along the N90-120° striking Orchies anticline. This

anticline is bounded to the north by the north-dipping Seclin normal fault (SeF) having a similar orientation. It is suggested that this uplift of the Brabant foreland may have been caused by the Variscan reactivation as back-thrusts of deep south-vergent Caledonian thrusts in the basement (Minguely et al. 2008).

Localised folds are noticeable in some parts of the coal basin district, such as the Chateau L’Abbaye syncline (striking N120°) and the Poil d’Ours anticline (striking N50°) (Fig. 5). At the western end of the coal district area in the Artois region (west of Lens), the Dinantian carbonate reservoir is segmented by several steeply south-dipping faults striking N130°; from north to south: the Sains Fault (SF), the Ruitz Fault (RF) and the Marqueffles Fault (MF). Seismic studies in the Artois region (Minguely 2007; Minguely et al. 2010) suggested that these faults are rooting down onto Variscan thrusts at depth and that they were formed during the late Carboniferous-Permian extensional period by negative tectonic inversion of these Variscan thrusts. A second defor-

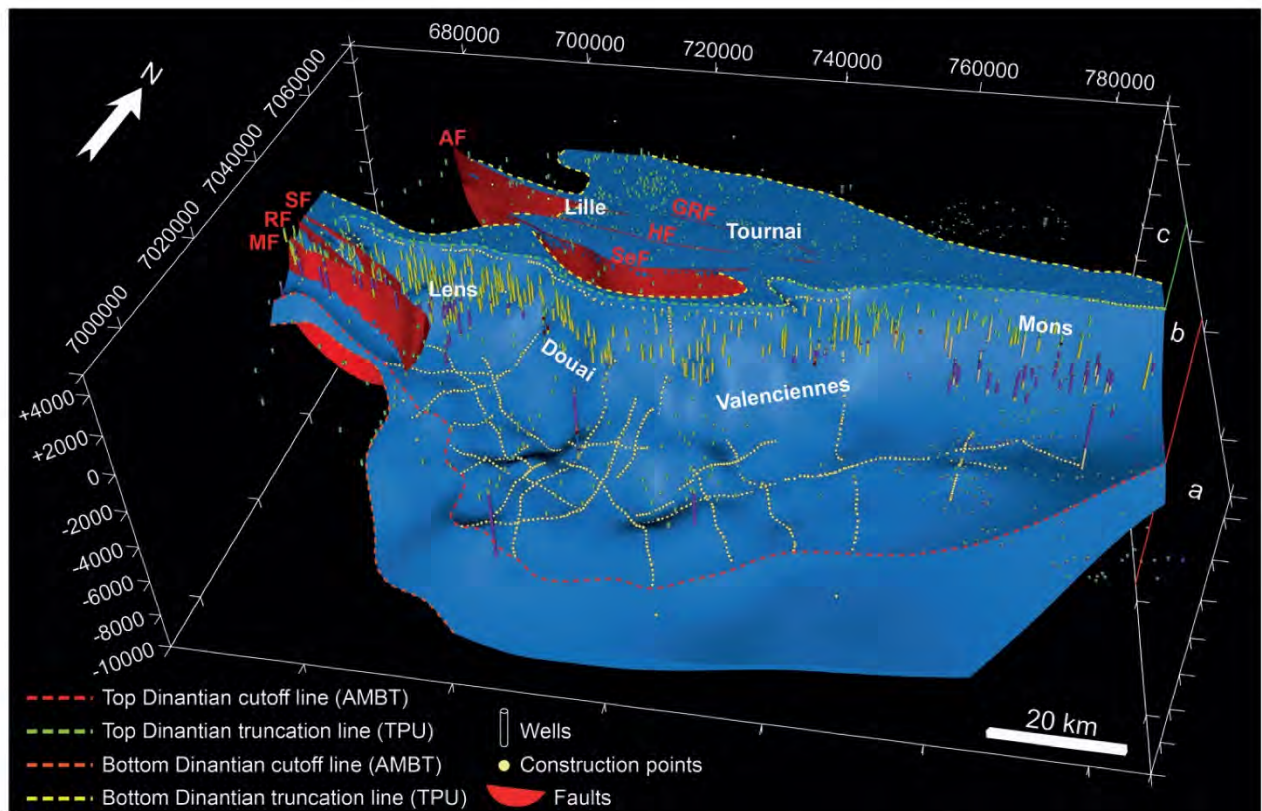


Fig. 6: 3D view of the top of the Dinantian modelled in the GeoModeller Software (grid cell size: 1,000 m, vertical exaggeration: x3). Coordinates are in French Lambert 93 and elevation values are in metres. Areas (a), (b) and (c) as well as the fault legend are defined in Fig. 5.

mation phase related to the far-field accommodation of the Alpine-Pyrenean shortening during the Tertiary would have resulted in the positive tectonic inversion of those faults as evidenced by the uplift of the Artois hills.

South of the coal district area, the Dinantian reservoir reaches depths approximately ranging from 3,000 to about 7,000 metres. The modelled geometry appears complex and irregular, especially in the Cambrai and Maubeuge areas. There, the interpretation of the deep seismic profiles revealed an intense deformation of the Dinantian series by deep Variscan thrusts. These thrusts would have a “décollement” level within the underlying Famennian shales and affected the entire para-autochthonous sequence (Laurent et al. 2021). At present-day, only the ramp-related fold structures at the hanging wall of those thrusts have been taken into account in our model, thus explaining the irregular geometry of the Dinantian series (the 3D modelling of the thrusts themselves and their implementation in the 3D model is still in progress).

Overall, in the study area, the top-Dinantian surface is structured along two main directions: N70-80° (e.g. the areas of Mons, Valenciennes, and Cambrai) and N110-130° (e.g. the area of Douai and SW of Maubeuge). Interestingly, our previous work based on the interpretation of the seismic data showed that the underlying southern Laurussian margin was

structured along the same structural axes in the study area (Laurent et al. 2021), which suggests that the Devonian syn-rift prestructuring of the southern Laurussian margin had a major influence on the 3D configuration of the Variscan thrusts and of the resulting flexural behaviour of the under-thrust foreland.

The 3D modelling of the base of the Dinantian reservoir shows a similar geometry and structural trends. Preliminary results suggest major thickness variations of the Dinantian reservoir in the study area. Their origin, whether sedimentary or tectonic, remains difficult to identify before the final completion of the 3D model, and are not discussed in the present paper.

Further improvements are needed to produce a final representation of the 3D geometry of the Dinantian reservoir in northern France. They will include the 3D modelling of (1) deep Variscan thrusts interpreted in seismics that are affecting the Dinantian reservoir south of the coal district area, and (2) second-order faults known in the Brabant foreland. Particular attention will be paid to the modelling of the internal structure of the coal basin, whose deformations directly affect the underlying para-autochthonous sequence, especially the Dinantian reservoir. Finally, an in-depth assessment of the uncertainties associated with the 3D modelling of the Dinantian reservoir will be carried out. A combined qualitative

and quantitative approach will help to evaluate the impact that each source of uncertainty can have on the output of the 3D modelling, whether they are associated to the borehole data (measured depth, trajectory, well logs, etc.), the seismic data (acquisition, reprocessing, resolution, horizons and faults picking, geological understanding, etc.), the time-depth conversion (velocity model, structural complexity, etc.) or the 3D modelling process itself (algorithm, resolution, data spatial distribution, geological understanding, etc.).

5. Conclusions

The 3D structural modelling of the Northern Variscan Front in northern France-southwestern Belgium, based on the integration and interpolation of data from 1,128 boreholes and 532 km of interpreted seismic reflection profiles, provides an unprecedented image of the 3D geometry of the buried Dinantian carbonate reservoir in the region. Our 3D approach highlights the main structural features of the reservoir at the regional scale and offers a first interpretation of its typical depth across the study area.

Overall, our results illustrate that the Dinantian carbonate reservoir has a general monoclinical geometry due to the flexural response of the Variscan foreland to thrust-loading. It displays an overall south- to southwestward dip underneath the NPC coal basin. We document the unprecedentedly appreciated subsurface presence of the reservoir across the territory as it extends over an area of approximately 7,675 km² and at least 30–40 km south of the coal district area, beneath the Ardenne Allochthonous Unit of the Northern Variscan Front. The southern limit of extension is defined by the cut-off surface of the Dinantian sequence at some major frontal and lateral ramps of the AMBT. The Dinantian reservoir is generally less than 200 m deep in the Lille metropolitan area but it reaches 1,000–3,000 m depth beneath the coal basin district and finally a maximum depth of approximately 7,000 m at the southern end of the study area. Our results document that the Dinantian reservoir is deformed along two main directions striking N70–80° and N110–130°. This structural pattern is the main result of Variscan thrusts moulded on the initial syn-rift configuration of the Laurussian margin. Subsequent deformation events (i.e. the late Carboniferous–Permian rifting as well as the Tertiary inversion phase related to the far-field accommodation of the Alpine-Pyrenean shortening) produced only localised second-order structures (i.e. Boulonnais-Artois and Melantois-Tournais anticlines).

The model still needs some improvements, for instance regarding the geometry of both the deep Variscan thrusts and the coal basin. Anyway, this 3D structural model provides an unprecedented representation of the regional 3D geometry of the Dinantian reservoir in northern France. Once completed, it may ultimately be used in hydrodynamic modelling studies and/or help to target specific areas of geothermal interest, prefiguring local investigations to determine the in-depth geothermal potential of the Dinantian reservoir.

6. Acknowledgements

This work is part of the PhD thesis of AL, granted by the BRGM (French Geological Survey) and the Hauts-de-France region. It also benefitted from a financial support from the TelluS Program of the CNRS/INSU. The reprocessing of the seismic profiles integrated in the database was supported by the RGF (Référentiel Géologique de la France) program of the BRGM. IHS Markit is greatly acknowledged for the permission to use the Kingdom Suite software through an academic grant to the University of Lille. The authors also thank the BRGM for providing the working licence of the GeoModeller software.

This study was also supported by the Interreg NWE Programme through the Roll-out of Deep Geothermal Energy in North-West Europe (DGE-ROLLOUT) Project (www.nweurope.eu/DGE-Rollout). The Interreg NWE Programme is part of the European Cohesion Policy and is financed by the European Regional Development Fund (ERDF).

The authors gratefully acknowledge the associate editor M. Arndt as well as the reviewers, E. Poty and an anonymous reviewer for their constructive comments on the preliminary version of this article.

7. References

- Arndt, M. (2021, this issue). 3D modelling of the Lower Carboniferous (Dinantian) as an indicator for the deep geothermal potential in North Rhine-Westphalia (NRW, Germany). [Journal of Applied and Regional Geology]. *Zeitschrift der Deutschen Gesellschaft für Geowissenschaften*, 172(3), 307–324. <https://doi.org/10.1127/zdgg/2021/0279>
- Aug, C., Chilès, J. P., Courrioux, G., & Lajaunie, C. (2005). 3D geological modelling and uncertainty: The potential-field method. In O. Leuangthong & C. V. Deutsch (Eds.), *Geostatistics Banff 2004* (pp. 145–154). Dordrecht: Springer. https://doi.org/10.1007/978-1-4020-3610-1_15
- Averbuch, O., & Piromallo, C. (2012). Is there a remnant Variscan subducted slab in the mantle beneath the Paris basin? Implications for the late Variscan lithospheric delamination process and the Paris basin formation. *Tectonophysics*, 558–559, 70–83. <https://doi.org/10.1016/j.tecto.2012.06.032>
- Averbuch, O., Mansy, J.-L., Lamarcheb, J., Lacquement, F., & Hannot, F. (2004). Geometry and kinematics of the Boulonnais fold-and-thrust belt (N France): Implications for the dynamics of the Northern Variscan thrust front. *Geodinamica Acta*, 17(2), 163–178. <https://doi.org/10.3166/ga.17.163-178>
- Becq-Giraudon, J.-F. (1983). Synthèse structurale et paléogéographique du bassin houiller du Nord et du Pas-de-Calais. *Mémoires du Bureau de Recherches Géologiques et Minières*, 123, 1–67.
- Bouroz, A. (1950). Sur quelques aspects du mécanisme de la déformation tectonique dans le bassin houiller du Nord de la France. *Annales de la Société Géologique du Nord*, 70(1), 2–55.
- Bouroz, A. (1969). Le Carbonifère du Nord de la France. *Annales de la Société Géologique du Nord*, 89(1), 47–65.
- Bouroz, A., Chalard, J., Dalinval, A., & Stiévenard, M. (1961). La structure du bassin houiller du Nord de la région de Douai à la frontière Belge. *Annales de la Société Géologique du Nord*, 81(1), 173–218.

- Broothaers, M., Lagrou, D., Laenen, B., Harcouët-Menou, V., & Vos, D. (2021, this issue). Deep geothermal energy in the Lower Carboniferous carbonates of the Campine Basin, northern Belgium: An overview from the 1950's to 2020. [Journal of Applied and Regional Geology]. *Zeitschrift der Deutschen Gesellschaft für Geowissenschaften*, 172(3), 211–225. <https://doi.org/10.1127/zdgg/2021/0285>
- Calcagno, P., Chilès, J. P., Courrioux, G., & Guillen, A. (2008). Geological modelling from field data and geological knowledge: Part I. Modelling method coupling 3D potential-field interpolation and geological rules. *Physics of the Earth and Planetary Interiors*, 171(1-4), 147–157. <https://doi.org/10.1016/j.pepi.2008.06.013>
- Cazes, M., Torreilles, G., Bois, C., Damotte, B., Galdeano, A., Hirn, A., ... Raoult, J.-F. (1985). Structure de la croute hercynienne du Nord de la France: Premiers résultats du profil ECORS. *Bulletin de la Société Géologique de France*, 1(6), 925–941. <https://doi.org/10.2113/gssgfbull.1.6.925>
- CFP – Compagnie Française de Pétrole, COPESEP – Compagnie des Pétroles du Sud-Est Parisien, RAP – Régie Autonome des Pétroles, & SNPA – Société Nationale des Pétroles d'Aquitaine. (1965). Contribution à la connaissance des bassins paléozoïques du Nord de la France. *Annales de la Société Géologique du Nord*, 85(1), 273–281.
- Chantraine, J., Autran, A., Cavelier, C., Alabouvette, B., Barfèty, J.-C., Cecca, F., ... Ternet, Y. (2003). *Carte géologique de la France à l'échelle du millionième*. Orléans: BRGM.
- Chilès, J. P., Aug, C., Guillen, A., & Lees, T. (2004). Modelling the geometry of geological units and its uncertainty in 3D from structural data: The potential-field method. In R. Dimitrakopoulos, & S. Ramazan (Eds.), *Orebody Modelling and Strategic Mine Planning* (pp. 313–320). Spectrum Series, 14. Carlton, Victoria: Australasian Institute of Mining and Metallurgy.
- Coen-Aubert, M., Groessens, E., & Legrand, R. (1980). Les formations paléozoïques des sondages de Tournai et de Leuze. *Bulletin de la Société Belge de Géologie*, 89(4), 241–275.
- COPESEP (1965). *Rapport de fin de sondage Jeumont-Marpent n°1 – "JEU. 1". N°14.3037* (23 pp.).
- Delmer, A. (1977). Le bassin du Hainaut et le sondage de St-Ghislain. *Geological Survey of Belgium. Professional Paper*, 6(143), 1–12.
- Delmer, A. (1982). Recherches géothermiques en Belgique. *Annales de la Société Géologique du Nord*, 102, 87–88.
- Delmer, A. (1997). Structure tectonique du bassin houiller du Hainaut. *Annales de la Société Géologique du Nord*, 5(2), 7–15.
- Delmer, A. (2003). La structure tectonique transfrontalière entre les bassins houillers de Valenciennes (France) et du Hainaut belge. *Geologica Belgica*, 6(3–4), 171–180.
- Delmer, A., Dusar, M., & Delcambre, B. (2001). Upper Carboniferous lithostratigraphic units (Belgium). *Geologica Belgica*, 4(1–2), 95–103.
- De Putter, T. (1995). Etude sédimentologique de la Grande brèche viséenne ("V3a") du bassin de Namur-Dinant. *Mémoires pour Servir à l'Explication des Cartes Géologiques et Minières de la Belgique*, 40, 1–272.
- De Putter, T., Groessens, E., & Herbosch, A. (1991). Le "V3a" anhydritique du sondage de Saint-Ghislain (150E387, Province du Hainaut, Belgique): Description macroscopique et structures sédimentaires. *Geological Survey of Belgium. Professional Paper*, 6(250), 1–22.
- De Putter, T., Rouchy, J.-M., Herbosch, A., Keppens, E., Pierre, C., & Groessens, E. (1994). Sedimentology and palaeo-environment of the Upper Viséan anhydrite of the Franco-Belgian Carboniferous basin (Saint-Ghislain borehole, southern Belgium). *Sedimentary Geology*, 90(1–2), 77–93. [https://doi.org/10.1016/0037-0738\(94\)90018-3](https://doi.org/10.1016/0037-0738(94)90018-3)
- Farquharson, N., Schubert, A., & Steiner, U. (2016). Geothermal energy in Munich (and beyond). A geothermal city case study. *Geothermal Resources Council. Transactions*, 40, 189–196.
- Franke, W. (2000). The mid-European segment of the Variscides: Tectonostratigraphic units, terrane boundaries and plate tectonic evolution. *Special Publication – Geological Society of London*, 179(1), 35–61. <https://doi.org/10.1144/GSL.SP2000.179.01.05>
- Franke, W., Cocks, L. R. M., & Torsvik, T. H. (2017). The Palaeozoic Variscan oceans revisited. *Gondwana Research*, 48, 257–284. <https://doi.org/10.1016/j.gr.2017.03.005>
- Groessens, E., Conil, R., & Hennebert, M. (1982). Le Dinantien du sondage de Saint-Ghislain. *Mémoires pour Servir à l'Explication des Cartes Géologiques et Minières de la Belgique*, 22, 1–137.
- Hance, L., Poty, E., & Devuyt, F.-X. (2001). Stratigraphie séquentielle du Dinantien type (Belgique) et corrélation avec le Nord de la France (Boulonnais, Avesnois). *Bulletin de la Société Géologique de France*, 172(4), 411–426. <https://doi.org/10.2113/172.4.411>
- Hance, L., Poty, E., & Devuyt, F.-X. (2006a). Tournaisien. In L. Dejonghe (Ed.), *Current status of chronostratigraphic units named from Belgium and adjacent areas*. *Geologica Belgica*, 9(1–2), 47–53.
- Hance, L., Poty, E., & Devuyt, F.-X. (2006b). Viséan. In L. Dejonghe (Ed.), *Current status of chronostratigraphic units named from Belgium and adjacent areas*. *Geologica Belgica*, 9(1–2), 55–62.
- Hennebert, M. (1998). L'anticlinal faillé du Mélantais-Tournaisien fait partie d'une "structure en fleur positive" tardi-varisque. *Annales de la Société Géologique du Nord*, 6(2), 65–78.
- Hennebert, M., & Doremus, P. (1997a). Antoing-Leuze. Carte géologique de Wallonie. Echelle 1/25.000. *Notice Explicative*, 37(7–8), 1–74.
- Hennebert, M., & Doremus, P. (1997b). Hertain-Tournai. Carte géologique de Wallonie. Echelle 1/25.000. *Notice Explicative*, 37(5–6), 1–66.
- Khatir, A., Mansy, J.-L., & Meilliez, F. (1988). Structures et déformation dans l'allochtone ardennais en Avesnois (Nord). *Annales de la Société Géologique du Nord*, 108(2–3), 73–83.
- Lacquement, F. (2001). L'Ardenne varisque. Déformation progressive d'un prisme sédimentaire pré-structuré; de l'affleurement au modèle de chaîne. *Société Géologique du Nord. Publication*, 29, 1–285.
- Lacquement, F., Mansy, J.-L., Hanot, F., & Meilliez, F. (1999). Retraitement et interprétation d'un profil sismique pétrolier méridien au travers du Massif paléozoïque ardennais (Nord de la France). *Comptes Rendus de l'Académie des Sciences Paris. Sciences de la Terre et des Planètes*, 329(7), 471–477.
- Lajaunie, C., Courrioux, G., & Manuel, L. (1997). Foliation fields and 3D cartography in geology: Principles of a method based on potential interpolation. *Mathematical Geology*, 29(4), 571–584. <https://doi.org/10.1007/BF02775087>
- Laurent, A., Averbuch, O., Beccaletto, L., Graveleau, F., Lacquement, F., Capar, L., ... Marc, S. (2021). 3-D structure of the Variscan Thrust Front in northern France: New insights from seismic reflection profiles. *Tectonics*, 40(7), e2020TC006642. <https://doi.org/10.1029/2020TC006642>
- Le Gall, B. (1994). Deformation of the Nord-Pas-de-Calais Carboniferous coalfield (France) in the Variscan frontal tectonic pattern. In A. Mascle (Ed.), *Hydrocarbon and petroleum geol-*

- ogy of France. *Special Publication of the European Association of Petroleum Geoscientists*, 4, 379–398.
- Licour, L. (2012). Relations entre la géologie profonde et le comportement hydrogéologique du réservoir géothermique du Hainaut (Belgique) – Caractérisation de l’aquifère dans la région de Saint-Ghislain. *Doctoral dissertation Université de Mons (Belgium)* (372 pp.).
- Mansy, J.-L., & Lacquement, F. (2006). Contexte géologique régional: L’Ardenne paléozoïque (Nord de la France et Sud de la Belgique). *Géologie de la France*, 1–2, 7–13.
- Mansy, J.-L., & Meilliez, F. (1993). Eléments d’analyse structurale à partir d’exemples pris en Ardenne-Avesnois. *Annales de la Société Géologique du Nord*, 2(2), 45–60.
- Mansy, J.-L., Lacquement, F., Meilliez, F., Hanot, F., & Everaerts, M. (1997). Interprétation d’un profil sismique pétrolier, sur le méridien de Valenciennes (Nord de la France). *Aardkundige Mededelingen*, 8, 127–129.
- Mansy, J.-L., Everaerts, M., & De Vos, W. (1999). Structural analysis of the adjacent Acadian and Variscan fold belts in Belgium and northern France from geophysical and geological evidence. *Tectonophysics*, 309(1–4), 99–116. [https://doi.org/10.1016/S0040-1951\(99\)00134-1](https://doi.org/10.1016/S0040-1951(99)00134-1)
- Mansy, J.-L., Manby, G. M., Averbuch, O., Everaerts, M., Bergerat, F., Van Vliet-Lanoe, B., . . . Vandycke, S. (2003). Dynamics and inversion of the Mesozoic basin of the Weald–Boulonnais area: Role of basement reactivation. *Tectonophysics*, 373(1–4), 161–179. [https://doi.org/10.1016/S0040-1951\(03\)00289-0](https://doi.org/10.1016/S0040-1951(03)00289-0)
- Marsden, D. (1989). Layer cake depth conversion, Part I. *The Leading Edge*, 8(1), 10–14. <https://doi.org/10.1190/1.1439561>
- Maxelon, M., Renard, P., Courrioux, G., Brändli, M., & Mancktelow, N. (2009). A workflow to facilitate three-dimensional geometrical modelling of complex poly-deformed geological units. *Computers & Geosciences*, 35(3), 644–658. <https://doi.org/10.1016/j.cageo.2008.06.005>
- McInerney, P., Guillen, A., Courrioux, G., Calcagno, P., & Lees, T. (2005). Building 3D geological models directly from the data? A new approach applied to Broken Hill, Australia. *Digital Mapping Techniques*, 2005, 119–130.
- Meilliez, F. (2019). La Faille du Midi, mythe et réalités. *Annales de la Société Géologique du Nord*, 26(2), 13–32.
- Meilliez, F., & Mansy, J.-L. (1990). Déformation pelliculaire différenciée dans une série lithologique hétérogène: Le Dévonien-Carbonifère de l’Ardenne. *Bulletin de la Société Géologique de France*, VI(1), 177–188. <https://doi.org/10.2113/gssgfbull.VI.1.177>
- Meilliez, F., André, L., Blicq, A., Fielitz, W., Goffette, O., Hance, L., . . . Verniers, J. (1991). Ardenne-Brabant. *Sciences Géologiques. Bulletin*, 44(1–2), 3–29. <https://doi.org/10.3406/sgeol.1991.1864>
- Minguely, B. (2007). Caractérisation géométrique 3-D de la couverture sédimentaire méso-cénozoïque et du substratum varisque dans le Nord de la France: Apports des données de sondages et des données géophysiques. *Doctoral dissertation Université de Lille* (231 pp.).
- Minguely, B., Folens, L., Averbuch, O., & Vendeville, B. C. (2008). Formation of deep-seated triangle zones by interaction between two orogenic thrust fronts having opposite vergence: Structural evidence from the Caledonian-Variscan system in Northern France and preliminary analogue modelling. *Bollettino di Geofisica Teorica ed Applicata*, 49(2), 242–246.
- Minguely, B., Averbuch, O., Patin, M., Rolin, D., Hanot, F., & Bergerat, F. (2010). Inversion tectonics at the northern margin of the Paris basin (northern France): New evidence from seismic profiles and boreholes interpolation in the Artois area. *Bulletin de la Société Géologique de France*, 181(5), 429–442. <https://doi.org/10.2113/gssgfbull.181.5.429>
- Moulouel, H. (2008). Caractérisation cartographique d’une différenciation verticale et horizontale de la déformation: Application à la couverture sédimentaire de la plate-forme ardennaise. *Doctoral dissertation Université de Lille* (205 pp.).
- Oncken, O., von Winterfeld, C., & Dittmar, U. (1999). Accretion of a rifted passive margin: The Late Paleozoic Rhenohercynian fold and thrust belt (Middle European Variscides). *Tectonics*, 18(1), 75–91. <https://doi.org/10.1029/98TC02763>
- Oncken, O., Plesch, A., Weber, J., Ricken, W., & Schrader, S. (2000). Passive margin detachment during arc-continent collision (Central European Variscides). *Special Publication – Geological Society of London*, 179(1), 199–216. <https://doi.org/10.1144/GSL.SP.2000.179.01.13>
- Pharaoh, T., Jones, D., Kearsey, T., Newell, A., Abesser, C., Randles, T., . . . Kendall, R. (2021, this issue). Early Carboniferous limestones of southern and central Britain: Characterisation and preliminary assessment of deep geothermal prospectivity. [Journal of Applied and Regional Geology]. *Zeitschrift der Deutschen Gesellschaft für Geowissenschaften*, 172(3), 227–249. <https://doi.org/10.1127/zdgg/2021/0282>
- Poty, E., Hance, L., Lees, A., & Hennebert, M. (2001). Dinantian lithostratigraphic units (Belgium). *Geologica Belgica*, 4(1–2), 69–94.
- Pracht, M., Rogers, R., & McConnell, B. J. (2021, this issue). Mississippian (Dinantian) of Ireland and its geothermal potential. [Journal of Applied and Regional Geology]. *Zeitschrift der Deutschen Gesellschaft für Geowissenschaften*, 172(3), 267–292. <https://doi.org/10.1127/zdgg/2021/0280>
- Raoult, J.-F. (1986). Le front varisque du Nord de la France d’après les profils sismiques, la géologie de surface et les sondages. *Revue de Géologie Dynamique et de Géographie Physique*, 27(3–4), 247–268.
- Raoult, J.-F., & Meilliez, F. (1987). The Variscan Front and the Midi Fault between the Channel and the Meuse river. *Journal of Structural Geology*, 9(4), 473–479. [https://doi.org/10.1016/0191-8141\(87\)90122-2](https://doi.org/10.1016/0191-8141(87)90122-2)
- Rouchy, J. M., Pierre, C., Groessens, E., Monty, C., Laumondais, A., & Moine, B. (1986). Les évaporites pré-permiennes du segment varisque franco-belge: Aspects paléogéographiques et structuraux. *Bulletin de la Société Belge de Géologie*, 95(2–3), 139–149.
- Rouchy, J. M., Laumondais, A., & Groessens, E. (1987). The Lower Carboniferous (Visean) evaporites in northern France and Belgium: Depositional, diagenetic and deformational guides to reconstruct a disrupted evaporitic basin. In T. M. Peryt (Ed.), *Evaporite basins. Lecture Notes in Earth Sciences*, 13(1), 31–67. <https://doi.org/10.1007/BFb0010099>
- Shail, R. K., & Leveridge, B. E. (2009). The Rhenohercynian passive margin of SW England: Development, inversion and extensional reactivation. *Comptes Rendus Geoscience*, 341(2–3), 140–155. <https://doi.org/10.1016/j.crte.2008.11.002>

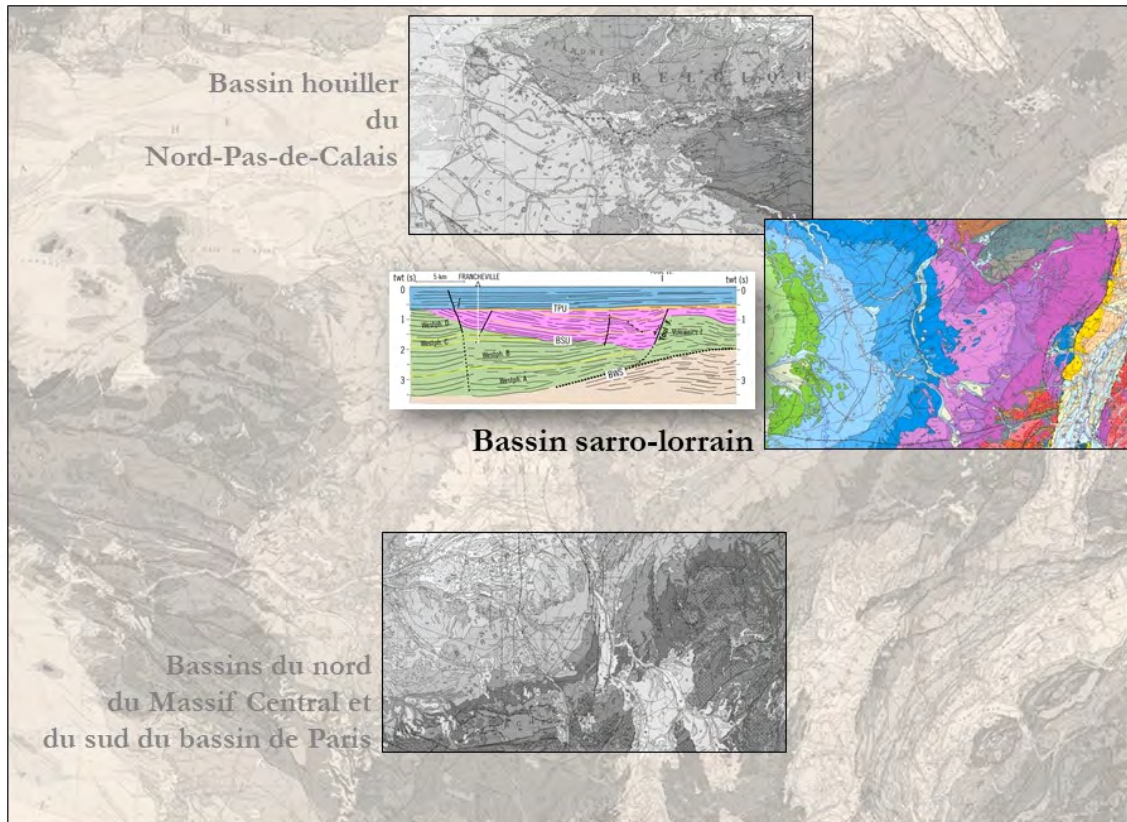
Manuscript received: 02.03.2021

Revisions required: 21.04.2021

Revised version received: 14.05.2021

Accepted for publication: 18.08.2021

3.5. Le bassin sarro-lorrain, transition syn- à -post-orogénique varisque



3.5.1. Cadre collaboratif

Les premières réflexions sur la compréhension tectonique du bassin sarro-lorrain et les incertitudes cinématiques et géodynamiques des modèles proposés dans la littérature ont été initiées par O. Averbuch (LOG, Université de Lille) au début des années 2010. Nous avons commencé à réfléchir ensemble à ces problématiques dans le cadre du projet INSU DELAM piloté par ce dernier et auquel je participais (DELAM pour Délamination lithosphérique tardi-orogénique : un modèle géodynamique intégrateur pour l'effondrement de la chaîne varisque et l'initiation du bassin de Paris ?). Je menais en parallèle des études pour l'ANDRA puis l'IRSN sur les séries carbonifères et permienes en Lorraine, études qui m'ont permis de me familiariser avec le contexte régional et les données sismiques industrielles disponibles. Il s'est très vite avéré que la réponse à nos interrogations se trouverait dans l'interprétation d'une sélection judicieusement choisie de ces profils recoupant le bassin.

Cette collaboration s'est élargie à R. Michels et A. Izart de GéoRessources Nancy - ouverts à des propositions tectoniques alternatives - et s'est concrétisée par le lancement du post-doc de R. Hemelsdaël cofinancé pour deux ans par le BRGM et le projet DeepSurf de Géoressources Nancy.

3.5.2. Problématiques appliquée et scientifique

Le sous-sol du bassin sarro-lorrain est actuellement convoité pour des usages qui peuvent être considérés comme complémentaires ou antagonistes. Historiquement les recherches ont ciblé le charbon, qui a été largement exploité jusqu'à la fin du 20^{ème} siècle dans les « Houillères de Lorraine » (voir la synthèse de Donsimoni, 1981). Les hydrocarbures ont à leur tour été recherchés dans les années 1980-90, donnant lieu à de multiples acquisitions sismiques, certains de ces profils ayant été retraités par le BRGM récemment. Le charbon et le pétrole sont passés de mode, mais le sous-sol lorrain n'en reste pas moins très sollicité. Sa partie occidentale est depuis les années 1990 le site du laboratoire souterrain de l'ANDRA pour le stockage des déchets radioactifs (projet Cigéo). Sa partie orientale est le siège de recherche menées par la Française de l'Energie pour l'exploitation future en subsurface de gaz de charbon (« Coal Bed Methane », projet ReGaLor FDE-Université Lorraine). Le bassin dans son ensemble est par ailleurs ciblé pour l'exploration de ressources géothermiques profondes (Barchi et al., 2008 et note interne BRGM) et le stockage de CO₂ en aquifères (Robelin, 2004 ; Fleury, 2022). Prendre des décisions sur l'utilisation du sous-sol lorrain nécessite donc (entre autre, mais à coup sûr) d'en avoir une meilleure connaissance géologique, en particulier (i) sur la géométrie des dépôts sédimentaires qui le constitue, (ii) la nature des failles contrôlant/recoupant ces derniers, (iii) l'organisation de l'ensemble en 3D, et (iv) une conception mise à jour des processus tectoniques sous-jacents, qui donnent une cohérence scientifique à l'ensemble. Le projet DeepSurf (Univ. Lorraine) cofinanceur du post de R. Hemelsdaël s'inscrit totalement dans cette démarche (« le projet IMPACT DEEPSURF est un projet de recherche qui s'intéresse aux échanges de chaleur et de matière entre les compartiments géologiques profonds, la zone critique et la surface, lors de leur utilisation pour la transition énergétique (i.e. stockages géologiques, exploitation de ressources fossiles à faible empreinte carbone, production de biomasse énergétique »).

En France, le bassin sédimentaire carbonifère-permien sarro-lorrain (prolongation orientale en subsurface du bassin affleurant de Saar-Nahe en Allemagne) se trouve sous les formations mésozoïques de l'est du bassin de Paris. Ce bassin pris dans sa globalité (bassin de Lorraine-Saar-Nahe) représente le plus grand bassin carbonifère-permien en Europe au cœur de l'orogène varisque (Schneider et Römer, 2010). Malgré de nombreuses investigations géologiques et géophysiques, son calendrier tectonique a toujours été débattu, et certaines incohérences subsistent entre ses parties orientales et occidentales pour ce qui concerne la cinématique des failles bordières principales (faille de Süd-Hunsrück, faille de Metz) et les différentes phases de déformation tectoniques rapportée au contexte géodynamique carbonifère varisque. L'interrogation principale demeure l'interprétation du remplissage sédimentaire Namuro-Westphalien puis Stéphano-Permien inférieur (séparés par une discordance régionale), le plus souvent considéré comme enregistrant une série syn-rift et donc un contexte extensif généralisé (Donsimoni, 1981 ; Henk, 1993; Oncken, 1998 ; Korsch & Schäfer, 1991, 1995; Schäfer, 2011; Becker et Schäfer, 2021). Mais alors comment s'enregistre dans le bassin la phase compressive varisque au Carbonifère supérieur ? Ce travail s'inscrit plus largement dans le champ d'étude des modalités du retour à l'équilibre d'une lithosphère orogénique sur-épaissie (« tectonic collapse » ; e.g. Dewey, 1988; Menard et Molnar, 1988; Malavielle et al, 1990; Burg et al, 1994) : il image en profondeur et démontre sur un exemple ancien le rôle décisif de la réactivation en extension de chevauchements majeurs préexistants

(inversion tectonique négative ; e.g. Smith et Bruhn, 1984; Williams et al, 1989; Mohapatra et Johnson, 1998; Minguely et al, 2010 ; Tari et al., 2023).

Les résultats de nos investigations sont rassemblés dans une publication soumise à *Tectonics*, en cours d'évaluation :

Hemelsdaël R., Averbuch O., **Beccaletto L.**, Izart, A. Marc S., Capar L., Michels R. (2023) A deformed wedge-top basin inverted during the collapse of the Variscan belt: the Permian-Carboniferous Lorraine Basin (NE France), soumise à *Tectonics*.

Cette publication concrétise les travaux de R. Hemelsdaël et de l'équipe d'encadrement sur la remise en question complète de l'évolution tectonique du bassin sarro-lorrain, que l'on considère maintenant comme enregistrant la transition syn- à post-orogénique varisque en position wedge-top du rétro-wedge saxothuringien. Le contexte géologique (en anglais, directement extrait de l'article), les données et les principaux résultats sont issus de cet article.

3.5.3. Contexte géologique du bassin de Lorraine-Saar-Nahe (BLSN)

The LSNB in the Variscan geodynamic context

Within the Variscan orogenic system, the LSNB (Lorraine-Saar-Nahe Basin) represents a major intramountain basin located just south of the mid-Carboniferous Rhenohercynian suture zone, i.e. the trace of the southward subducted Rhenohercynian oceanic slab and of the adjoining distal southern continental margin of Avalonia (SW part of Laurussia) below the Saxothuringian-Moldanubian units of the upper lithospheric plate (northern part of Gondwana) (e.g. Franke, 2000; Averbuch & Piromallo, 2012; Edel et al., 2013). This suture is characterized by the northward thrust units of the Northern Phyllite zone (SW Rhenish massif; Oncken, 1997; Franke & Dulce, 2017), a heterogeneous tectonic assemblage of rocks originating from the Lower Devonian-Early Carboniferous Rhenohercynian-Avalonian passive margin oceanic shelf succession (lower plate). These rocks were involved in the subduction zone but exhibit rather low peak-pressure conditions (i.e. only 6.5 kbar; Massonne, 1995) indicating a limited amount of burial within the subduction channel before their exhumation. The Northern Phyllite Zone locally outcrops at the northern border of the LSNB along the South-Hunsrück fault system (Figure 17; Anderle et al., 1995). To the north, the Hunsrück-Taunus massif forms the internal part of the Variscan Rhenohercynian zone, dominated by folded and thrust Early Devonian clastic shelf sediments, formerly deposited along the distal southern rifted margin of the Avalonian (Laurussia) continent (Oncken et al., 2000) [*NDLR: un équivalent latéral des séries de l'Allochtone ardennais vu précédemment, section 3.4*]. To the south-east, the LSNB lies upon the units of the Saxothuringian retro-wedge (i.e. the deformed upper-plate) and more specifically on its northern border referred to as the Mid-German Crystalline Rise (MGCR). The latter represents a main site for syn-orogenic magmatism and the resultant relief, a significant clastic source for the LSNB towards the NW. Southward subduction and closure of the Rhenohercynian ocean indeed resulted in the formation of a late Devonian–mid Carboniferous magmatic arc on the northern flank margin of the Armorican-Saxothuringian microplate (McCann, Skompski, et al., 2008). This magmatic arc formed a 75–100 km wide unit that can be traced along the strike of the suture zone over a distance of about 1000 km. Arc-related plutonism was particularly important in the mid-Carboniferous, but rocks also derived from Early Silurian-Early

Devonian magmatism, consistent with coeval opening of the Rhenohercynian ocean in a back-arc position (Averbuch & Piromallo, 2012; Zeh & Gerdes, 2010). The Vosges and Black Forest Massifs are the exposed remnants of the Mid-German Crystalline Rise (MGCR) south the Lorraine-Saar area (Stein, 2001).

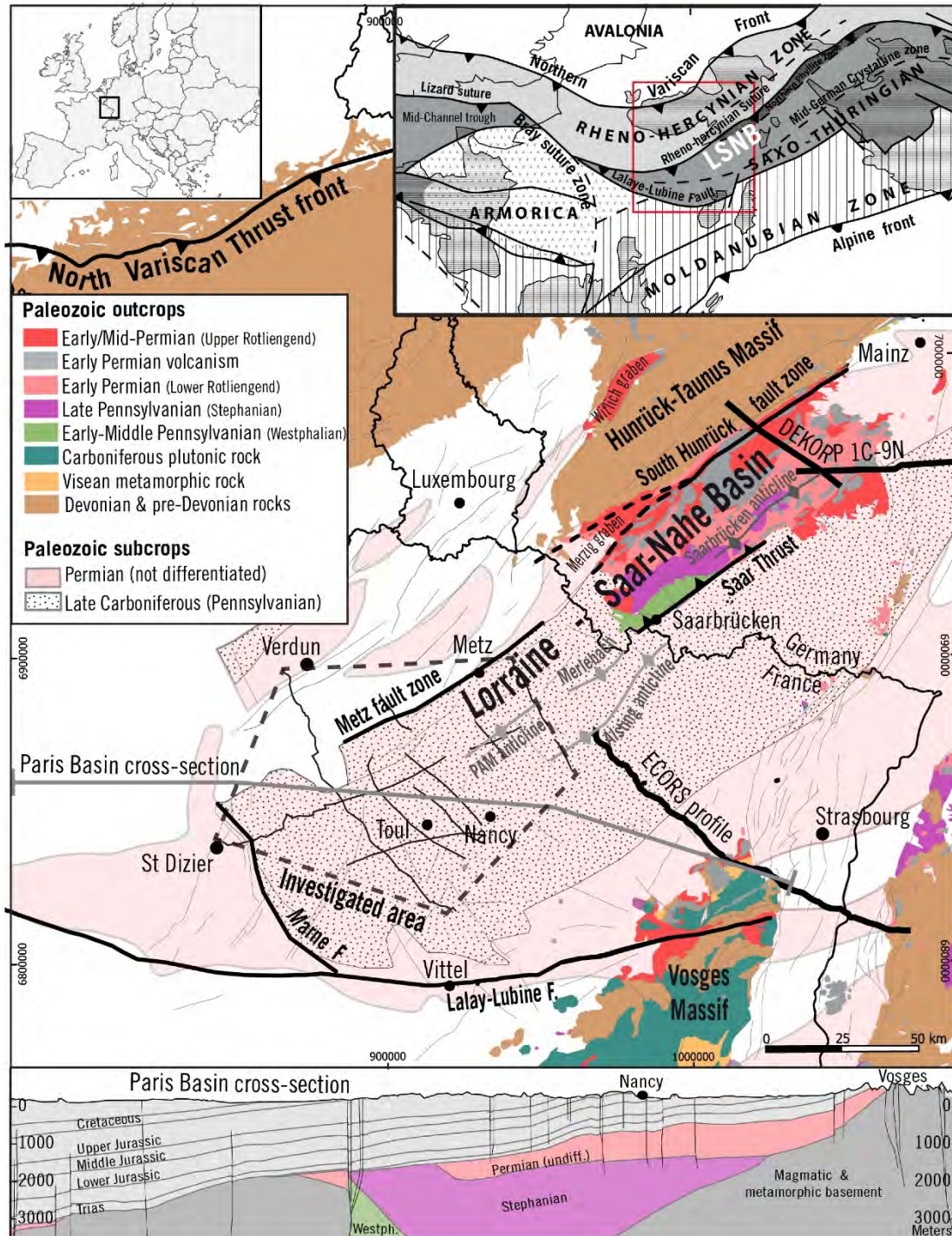


Figure 17 - Carte géologique de l'est de la France avec la couverture sédimentaire mésozoïque représentée en transparence. Les limites classiquement proposées pour les bassins carbonifères-permiens en subsurface sont également reportées (Delmas et al., 2002). Les transects correspondent aux profils sismiques ECORS et DEKORP ainsi qu'à la coupe du bassin de Paris représentée dessous. L'encart montre la localisation du bassin sarro-lorrain et de Saar-Nahe au sein des principaux domaines tectoniques varisques (**Hemelsdaël et al., 2022 soumis à Tectonics ; compilé à partir de Faure, 1995 ; Franke, 2014 ; Guillot et al., 2020 ; Schneider & Romer, 2010).

Stratigraphy of the LSNB

The LSNB is a limnic intramountain coal basin without any connection with the sea, and differs from paralic coal basins located in Northern France, Belgium and Germany deposited in the foredeep of the northern Variscan thrust front (Schneider et Römer, 2010; [NDLR: *par exemple le bassin Houiller du Nord-Pas-de-Calais, voir section 3.4*]). The stratigraphy of the LSNB is well documented in the Saar-1 borehole (Figure 18; Kelch & Reible, 1976), which traverses the most complete Permo-Carboniferous succession (i.e. about 4.7 km thick) down to the Middle Devonian. It is also well known from outcrops in the Saar-Nahe domain (Schäfer, 1989; Schäfer & Korsch, 1998; Becker & Schäfer, 2021). The Late Carboniferous stratigraphy is described here by using the Western European lithostratigraphic nomenclature and framework (Aretz et al., 2020; Lucas et al., 2022). The Westphalian unit is divided into different subunits A, B, C, D in France and Germany based on the identification of floral assemblages (Laveine, 1974). These substages correspond to the Langsettian, Duckmantian, Bolsovian and Asturian, respectively (Aretz et al., 2020). The limits of the Westphalian formations are however different in Lorraine and Saar-Nahe Basins, thus making difficult the regional stratigraphic correlation.

The initiation of the LSNB occurred in the latest Namurian-earliest Westphalian (Early Pennsylvanian) (both in France and Germany), with increased subsidence from Late Westphalian times onward (Korsch & Schäfer, 1995). The main sediment sources are located in the MGCR (as part of the uplifted Saxothüringian retro-wedge) to the South, and the Rhenohercynian range to the North (Anderle, 1987; Oncken, 1997). Major material input systems have been proposed, however, to change with time from N to S-SW, between Late Namurian-Westphalian and Stephanian-Early Permian times respectively (Schäfer, 2011).

In the Saar region, the rocks underlying the Carboniferous-Permian basin consist of a slightly deformed and metamorphosed Mid-Devonian to Visean marine sedimentary sequence interpreted to have been deposited in a forearc position during the ongoing southward subduction of the Rhenohercynian slab (Weber, 1995; von Seckendorff et al., 2004). The base of the basin is marked by a period of no deposition due to uplift and exhumation of the MGCR units (320-335 Ma cooling age after McCann, et al., 2008), associated to the Variscan collision stage by mid-Visean times, locally referred to as the classic Sudetian phase (Kneuper, 1976; Weber, 1995).

The late Carboniferous to Middle Permian sedimentary fill of the basin in the Saar-Nahe domain can be subdivided into four megasequences (Henk, 1993; Korsch & Schäfer, 1991): (i) an initial Uppermost Namurian-Westphalian (Lower-Middle Pennsylvanian) series, the controlling subsidence mechanism of which still remains unclear and thereby commonly ascribed to a “proto-rift” phase; (ii) a Stephanian (Upper Pennsylvanian) pre-volcanic syn-rift sequence; (iii) a subsequent Early Permian volcanic syn-rift sequence, (iv) a final late Early to Middle Permian post-rift sequence controlled by thermal subsidence (Stollhofen et al., 1999). This thick continental succession is disrupted by a large variety of igneous rocks (rhyolite, dacite) that were mainly emplaced over about 4 Myr from 296 to 293 Ma (i.e. Early Permian) (Königer et al., 2002; von Seckendorff et al., 2004). This volcanic event is assigned to the base of the ‘Upper Rotliegend’ sequence (Nahe Subgroup) and thereby would represent a late-rifting magmatic pulse marking the transition toward the post-rift thermal subsidence phase. The underlying ‘Lower Rotliegend’ (or Glan Subgroup) and Stephanian (Ottweiler Subgroup) non-volcanic syn-rift series are characterized

by localized horizons of ash layers that are likely to source from the Black Forest and Northern Vosges areas (some 100–150 km south of the LSNB) (Stollhofen et al., 1999). In the late stages of basin development, up to 3200 m of sediments were suggested to be eroded partly due to the Saalian compressional phase in the Saar region (Hertle & Littke, 2000). Izart et al (2016) estimated however a more limited amount of erosion in the Lorraine basin before deposition of the Triassic cover, i.e. about 1200 m.

In the Lorraine basin, the stratigraphic scheme (Figure 18) was originally defined for the purpose of mining excavation in the productive coal area at the French-German border, but also more westerly areas below the Mesozoic cover using deep boreholes such as the reference Gironville (5683 m) and Francheville (3859 m) boreholes. It consists of up to 6 km of preserved continental series deposited from Early Pennsylvanian to Permian; as in Saar, it contains abundant coal-bearing sediments, particularly in Westphalian successions.

The Westphalian succession (up to 3.5 km thick) is made of conglomerates, sandstones, claystones with abundant interbedded coal. Subdivision of the Westphalian succession (A-D) is based on paleobotanic markers and palynology (e.g. Laveine, 1974). The upper Westphalian succession (subunits C and D) is better known due to coal mining. Westphalian C and D (Bolsovian and Asturian) each consist of three to four fining-upward successions from braided river conglomerate and sandstone at the base, meandering fluvial sandstone and swamp deposits to lacustrine deposits at the top (Fleck et al., 2001; Izart et al., 2005).

The Stephanian unit mainly consists of grey sandstone and claystone with minor occurrence of coal beds. This unit is mainly known from its observation in Coumes and Francheville boreholes. As previously mentioned, the Westphalian and Stephanian strata are separated by an angular unconformity marking a sedimentary hiatus; the basin-wide deposition of the Holz conglomerates marks the resumption of sedimentation at the base of the Stephanian sequence (Weber, 1995). The stratigraphic gap at the base of the Stephanian unit (Cantabrian) corresponds to about 3 Ma between about 308.5 and 305.5 Ma (Schneider et al., 2020; Knight & Álvarez-Vázquez, 2021). Moreover, this Base Stephanian unconformity is interpreted as diachronous with the lower age varying from 307 to 306 in Saar and Lorraine region respectively (Burger et al., 1997).

The Permian red beds (mostly sandstones) are preserved with variable thickness (up to 1400 m), intercalated with volcanic rocks in some places. Rhyolites are found in the southern part of the basin (Chevraumont and Forcelles wells). Andesite and trachybasalt are found in the northern Lorraine Basin, east of the Metz Fault. Permian rocks are poorly dated in Lorraine and correlation with the Rotliegend Group in Germany is not clear. The («Upper Rotliegend» red beds likely correspond to the «Saxonian» levels in Lorraine (Guerrier and Pruvost, 1965). The «Lower Rotliegend» of Early Permian age is not defined in Lorraine.

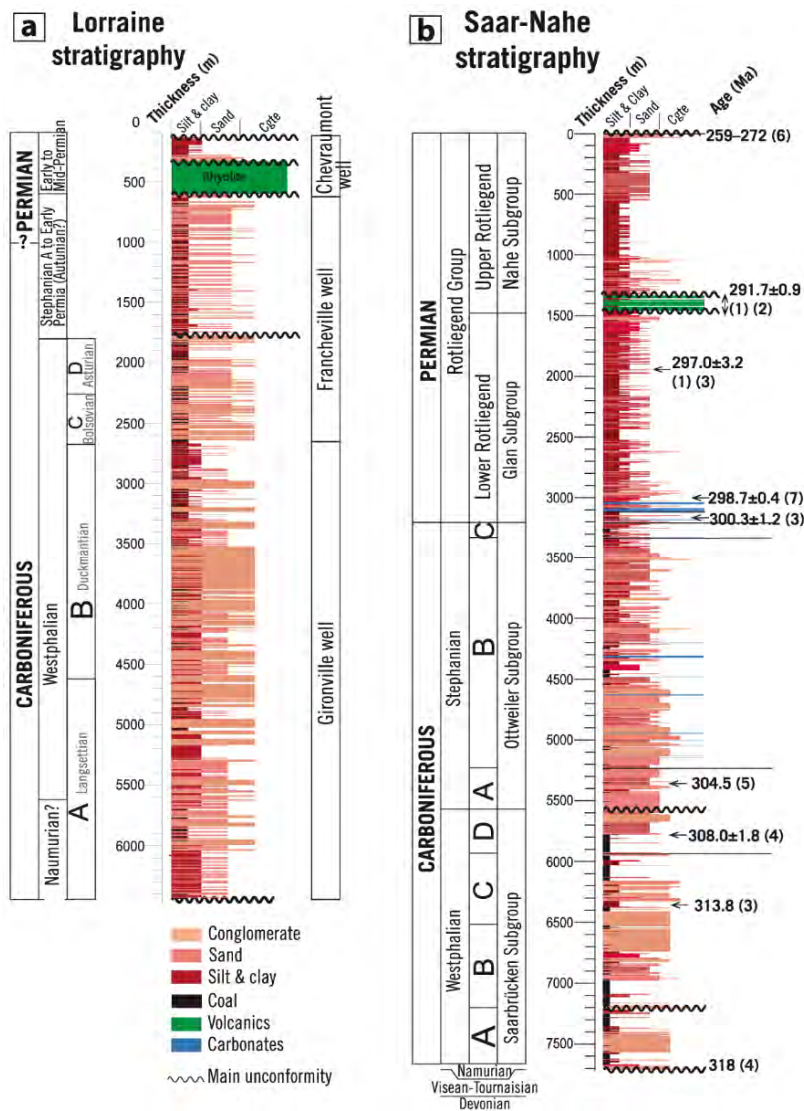


Figure 18 - Stratigraphie synthétique du Permo-Carbonifère du bassin Lorraine-Saar-Nahe (**Hemelsdaël et al., 2022 soumis à Tectonics).

3.5.4. Données sismiques et de forage, interprétation sismique

Comme dans l'étude du front nord-varisque, cette étude est basée sur le retraitement d'une sélection de 11 profils de sismique réflexion 2D acquis dans les années 1980 et représentant une longueur totale de 438 km (Figure 19). Ces profils sismiques orientés NNO-SSE et OSO-ENE se recoupent entre eux et recoupent les structures et dépoctrés principaux du Carbonifère supérieur au Permien.

En plus des données sismiques, 13 puits d'exploration sont intégrés au projet d'interprétation sismique pour fournir des informations géologiques en profondeur. Ils ont été sélectionnés en fonction de leur proximité avec les lignes sismiques (moins de trois km), de l'âge Paléozoïque des séries et de la disponibilité des données de lois de vitesse et de diaggraphie. Les forages sont principalement situés au sommet ou à proximité des cœurs des anticlinaux westphaliens.

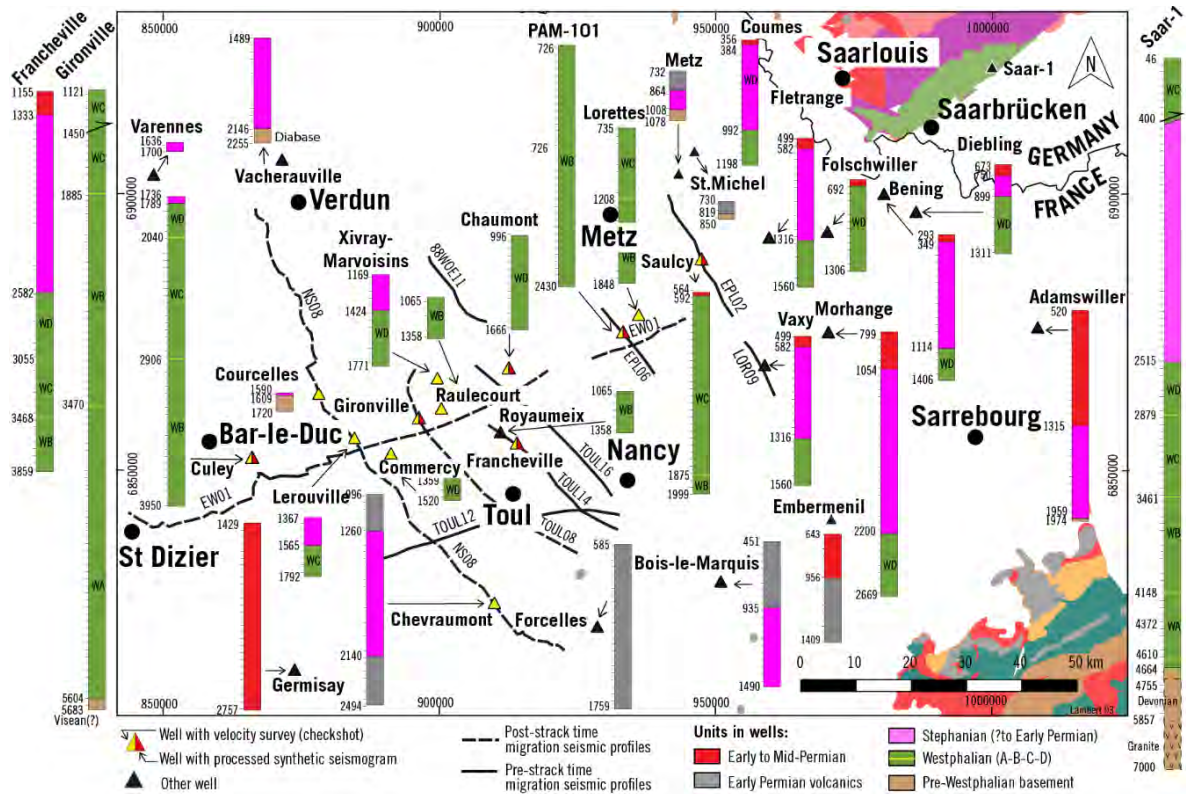


Figure 19 - Localisation des profils sismiques et des puits avec leur succession sédimentaire permo-carbonifères simplifiée (**Hemelsdaël et al., 2022 soumis à Tectonics).

Les profils sismiques imagent du bas en haut de la série (Figure 20) : (i) les séries syn-orogéniques plissées et basculées westphaliennes, au front de chevauchements à vergence nord ; (ii) le remplissage syn-rift (syn-extension post-orogénique) stéphanien-(permien inférieur ?) contrôlé par le jeu de failles normales se branchant sur les chevauchements, et reposant sur le Westphalien par l'intermédiaire d'une discordance angulaire majeure ; (iii) un remplissage post-rift peu épais permien inférieur ; et (iv) la base des séries mésozoïques, discordante sur tous les dépôts paléozoïques.

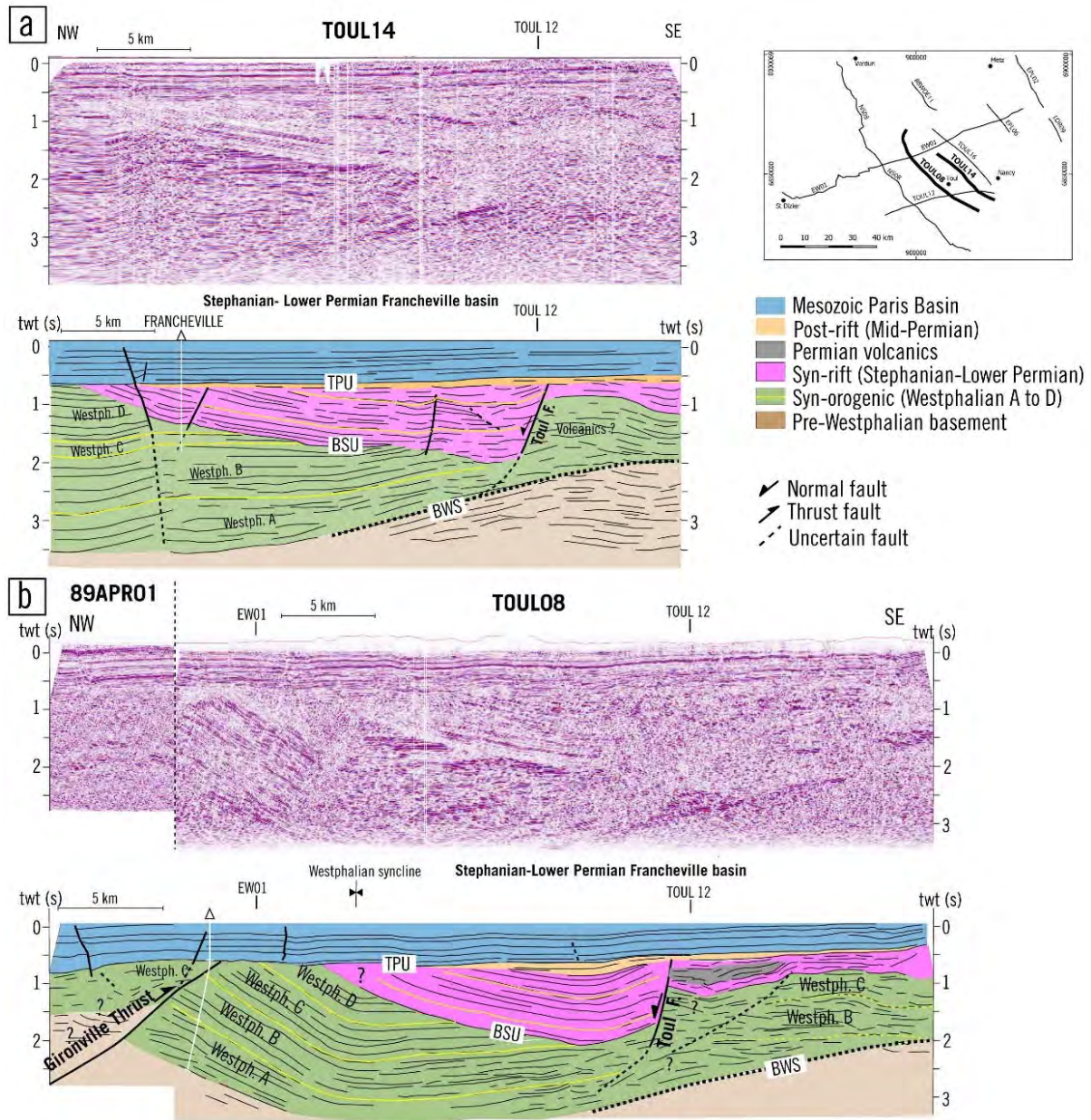


Figure 20 - Interprétation de deux profils transverses au bassin sarro-lorrain ; on note l'épaisseur maximale du dépocentre syn-rift au droit de la partie la plus érodée des séries westphaliennes plissées, témoignant d'un processus majeur d'inversion topographique et tectonique négative (**Hemelsdaël et al., 2022 soumis à Tectonics).

3.5.5. Principaux résultats

Les principaux résultats de nos travaux en Lorraine se résument comme suit :

- L'interprétation de 438 km de profils sismiques retraités dans le NE de la France fournit un nouveau cadre structural et une nouvelle évolution géodynamique du bassin de Lorraine-Saar-Nahe (BLSN). Ce dernier témoigne des processus géodynamiques à la transition entre les phases de collision et d'effondrement tectonique post-orogénique. Le BLSN, constitué de dépôts syn-orogéniques du Namurien supérieur-Westphalien, s'est formé au toit du rétro-prisme (« retro-wedge ») orogénique saxothuringien. Les chevauchements se sont propagés vers le SE pendant le Westphalien supérieur

(principalement le Westphalien D), comme le soulignent les structures de croissance dans les flancs inverses des plis.

- Après une brève période d'érosion des anticlinaux (plis sur rampe) qui se traduit par une importante discordance angulaire, la subsidence reprend à partir du Stéphanien jusqu'au Permien inférieur terminal. La subsidence est due à la reprise en extension (ou transtension) de la zone de suture (faille Süd-Hunsrück) et des chevauchements internes à vergence SE, traduisant une inversion tectonique négative majeure. Cette phase de rifting/extension est à l'origine de la géométrie générale en demi-graben du BLSN).
- Les lignes sismiques mettent en évidence le caractère segmenté du bassin, les dépôts syn-rifts étant localement décalés et contrôlés par des décrochements NNO-SSE (failles de transfert).
- La phase syn-rift tardive (Permien inférieur) se caractérise par des arrivées magmatiques le long des failles majeures. Cette activité magmatique est suivie par une réactivation locale des failles normales et des anciens chevauchements, déclenchant un uplift généralisée du bassin (compression saaliennne). Cette phase est moins marquée en Lorraine que dans le bassin de Saar-Nahe. La séquence post-rift (Rotliegend supérieur), contrôlée par une subsidence thermique régionale, se développe au-dessus de la surface d'érosion saaliennne. L'évolution cinématique du bassin sarro-lorrain est résumé sur la Figure 21.

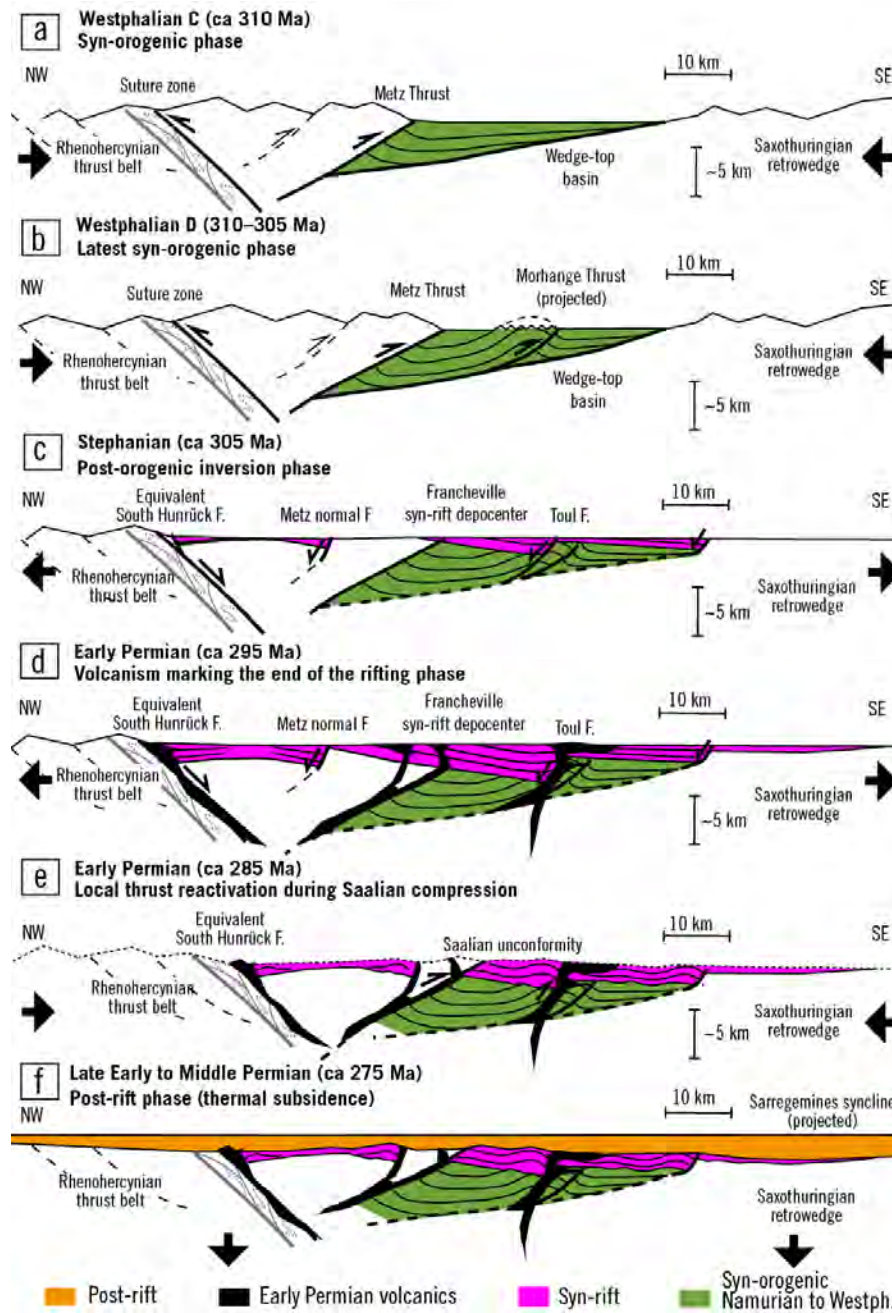


Figure 21 - Coupe schématique NW-SE illustrant le modèle d'évolution du bassin permo-carbonifère lorrain, subdivisé en 6 étapes: (a) développement d'un bassin syn-orogénique (ici au Westphalien C); (b) propagation de chevauchements à vergence SE et plissements associés pendant le Westphalien D; (c) inversion tectonique négative post-orogénique contrôlant le développement de dépocenters syn-rift (Stéphanien à Permien inférieur); (d) volcanisme syn-rift du Permien inférieur; (e) réactivation locale des chevauchements pendant la phase de compression saalienne; (f) subsidence thermique post-rift à la fin du Permien inférieur et au Permien moyen (**Hemelsdaël et al., 2022 soumis à Tectonics).

- La limite nord du bassin syn-orogénique est marquée par un rétro-chevauchement majeur à vergence SE (chevauchement de Metz). Cette zone de faille ne correspond pas à la prolongation directe de la faille Süd-Hunsrück, comme généralement proposé. L'équivalent de la faille Süd-Hunsrück, qui correspond à la zone de suture rhéno-hercynienne inversée pendant la phase post-orogénique, doit être recherché en Lorraine plus au nord (i.e. au nord du bassin stéphano-permien de Varennes-Vacherauville ; Figure 22).

- La distinction entre structures syn- et post-orogéniques dans le BLSN est un résultat majeur de notre étude. Cette dualité permet de proposer un scénario tectonique cohérent avec le contexte géodynamique varisque, en reliant le changement de régime tectonique et l'effondrement de la chaîne à des processus profonds (tel que l'élimination de la racine lithosphérique).

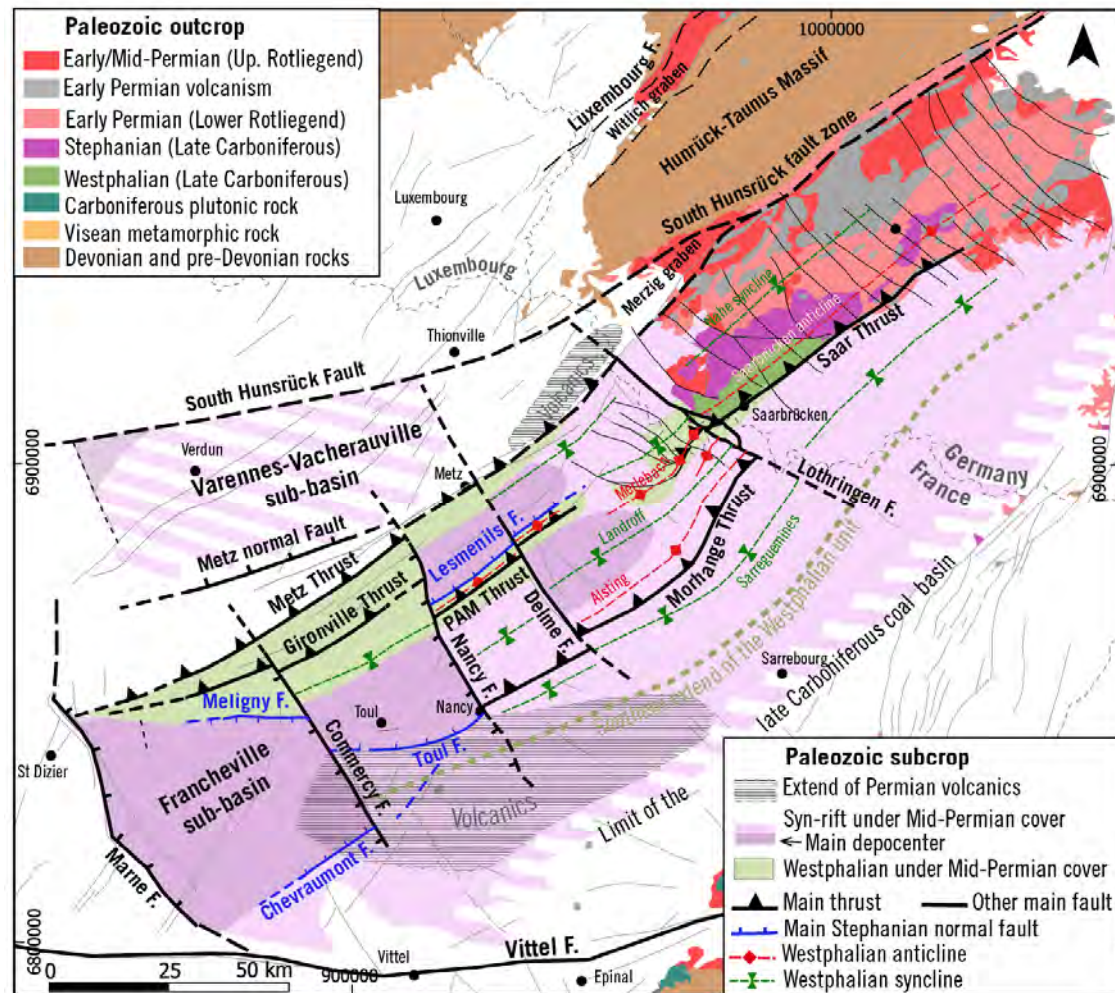
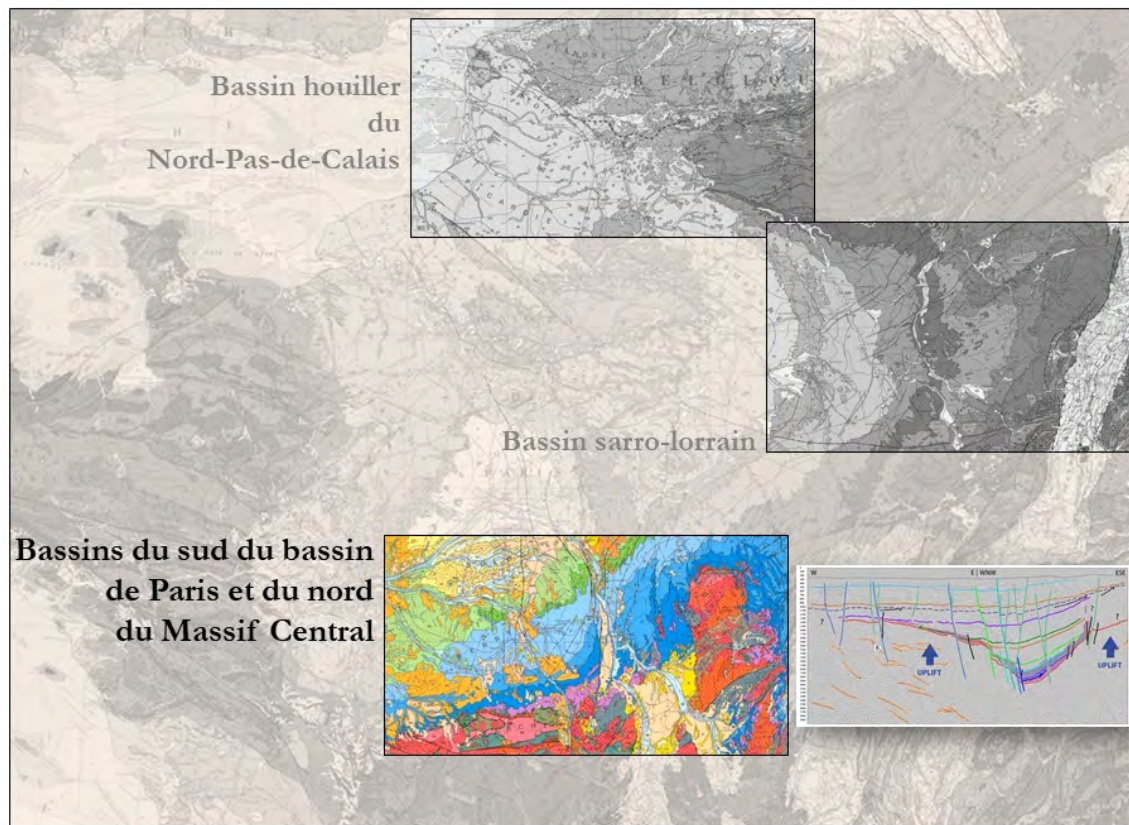


Figure 22 - Carte structurale révisée du bassin permio-carbonifère sarro-lorrain dans le prolongement du bassin Saar-Nabe (Allemagne), basée sur l'interprétation des profils sismiques (**Hemelsdaël et al., 2022 soumis à Tectonics).

3.6. Les bassins stéphano-permiens du sud du bassin de Paris et du nord du Massif Central, évolution structurale et paléo-environnements en contexte post-orogénique



3.6.1. Cadre collaboratif

Les bassins stéphano-permiens sous couverture méso-cénozoïque du sud du bassin de Paris resteront mon premier cas d'étude lorsque j'ai débuté en 2009 mes travaux sur les bassins carbonifères-permiens ; comme on le verra par la suite, le sujet n'est pas encore épuisé. Le BRGM venait de finaliser le levé aéromagnétique de la région Centre-Val-de-Loire, qui devait mettre à jour la connaissance sur le « socle » de la région. En complément, des retraitements sismiques ont été réalisés pour imaginer les bassins paléozoïques sus-jacents et la couverture sédimentaire méso-cénozoïque (*Beccaletto et al., 2015). Ce projet interne au BRGM est typique des études de synthèse que doit produire le Service Géologique National. Les investigations géophysiques sur le « socle » se sont traduites par le Master 2 de M. Bergé puis par la thèse de J. Baptiste, dont j'étais co-encadrant ; elles ont fait l'objet d'une publication (**Baptiste et al., 2016). Ma collaboration fructueuse avec S. Bourquin (Géosciences Rennes) a débuté par une mise à jour de la description sédimentologique et palynologique de la carotte du forage scientifique Couy-1 (M2 de J. Bureau, puis collaboration avec les collègues de l'Université de Vigo) ; une publication est sortie de ces travaux (*Juncal et al., 2018). Nous avons poursuivi notre collaboration avec l'idée de ré-investiguer à partir de données de carottes et sismiques les bassins d'Autun, de Lucenay-lès-Aix et d'Aumance, aboutissant au Master 2 de Ch. Hue, à la thèse de M. Mercuzot et au post-doc de C. Ducassou. La thèse de M. Mercuzot, soutenue en 2020, a bénéficié d'un cofinancement BRGM - région Bretagne,

et initié des collaborations avec les collègues de Biogéosciences de l'Université de Dijon (P ; Pellenard, E. Venin, Ch. Thomazo). Les résultats marquants de ces travaux sont présentés ci-après. En parallèle j'ai participé au montage du projet ICDP Deepdust de forages carottés dans le Permien aux USA et en Europe de l'ouest, piloté par L. Soreghan (Université Oklahoma, USA), et dont je suis le Co-PI responsable de la tâche forage dans le bassin de Paris ; ce projet au long cours sera développé le chapitre 5 « perspectives » ; je détaillerai aussi dans ce volet les collaborations naissantes sur les bassins permien avec 45-8 Energie (recherche d'hélium naturel dans le nivernais).

3.6.2. Problématiques appliquée et scientifique

Le contexte paléoclimatique autour de 300 Ma et les comparaisons avec l'actuel ont été notre premier point d'accroche, en mettant en exergue l'utilité de travailler sur des analogues anciens. Dans le cadre de la thèse de M. Mercuzot nous avons montré l'intérêt d'approfondir notre connaissance des interactions entre biosphère et géosphère depuis la fin du Carbonifère jusqu'au début du Trias - séquence/glaciation/réchauffement/aridification intense/récupération - en insistant sur l'analogie entre cette séquence et les changements climatiques actuels (Gastaldo et al., 1996). Notre objectif à terme est d'aboutir à des reconstitutions paléoclimatiques globales (volet modélisation climatiques du projet Deepdust). Quant aux problématiques touchant aux nouveaux usages du sous-sol, elles sont encore émergentes pour ce qui concerne les bassins stéphano-permiens du sud du bassin de Paris. Ces dernières années ont cependant vu pour la première fois les séries permien mentionnées comme cible potentielles pour la géothermie dans une réponse BRGM à un AAP de la région Centre Val-de-Loire. Le projet Deepdust comprend d'ailleurs un volet de caractérisation réservoir des séries gréseuses permien du bassin de Brécly dans la région de Bourges. Une autre piste prometteuse concerne la recherche d'hélium naturel, pour lequel les séries permien pourraient être un réservoir remarquable (voir section 5.1).

Il ne manque pas d'arguments pour reprendre les études sur les bassins stéphano-permiens dans le sud du bassin de Paris et le nord du Massif Central, les données étant là aussi anciennes (Marteau, 1983 ; Paquette, 1980 ; Donsimoni, 1990 ; Mathis et Brulhet, 1990). Beaucoup de questions scientifiques restent ouvertes, dont les plus prégnantes sont :

- Les relations entre le calendrier tectonique fini-varisque, la dynamique de rifting, et l'évolution des milieux de sédimentation. L'âge précis des bassins reste en effet largement méconnu (et leurs corrélations difficiles en raison de l'absence d'âges radiométriques fiables), tout comme leur mode d'ouverture (contrôle structural local vs subsidence régionale). Les milieux de dépôt doivent être réévalués (lac vs plaine d'inondation, Gilbert deltas vs réseaux fluviaux) et les sources rediscutées (part de la fraction volcanogène, source proche vs lointaine).
- Quels indices de changements paléoenvironnementaux et paléoclimatiques s'enregistrent dans les sédiments permo-carbonifères (indices et facteurs liés à la sédimentologie, la géochimie organique, la minéralogie des argiles, la cyclostratigraphie) ? Il s'agit de discuter des impacts de ces facteurs sur la sédimentation (en premier lieu le climat et ses variations à différentes échelles de temps), dont les interprétations restent largement contradictoires et doivent être confrontées au contexte tectonique: comment l'un et l'autre sont-ils enregistrés dans les sédiments ?

- Malgré le fait que de nombreuses inconnues existent, telles que l'altitude de ces bassins et leur taille initiale, est-ce possible de comparer/corréler les bassins entre eux ? Existe-t-il des connexions entre les différents bassins étudiés, ayant des implications paléogéographiques et paléoclimatiques de plus grande ampleur ?

Deux dépocentres stéphano-permiens (Contres-Brécy et Arpheuilles) étaient déjà identifiés sous la couverture méso-cénozoïque du bassin de Paris avant que je retravaille sur le secteur. Le nord du Massif Central est bordé quant à lui de trois bassins stéphano-permiens étudiés depuis bien plus longtemps (car exploités pour leur charbon) : les bassins de Decize-La Machine / Lucenay-lès-Aix, de l'Aumance, et d'Autun (Figure 23). Les résultats les plus significatifs sont énoncés par bassin après la présentation de leur contexte géologique.

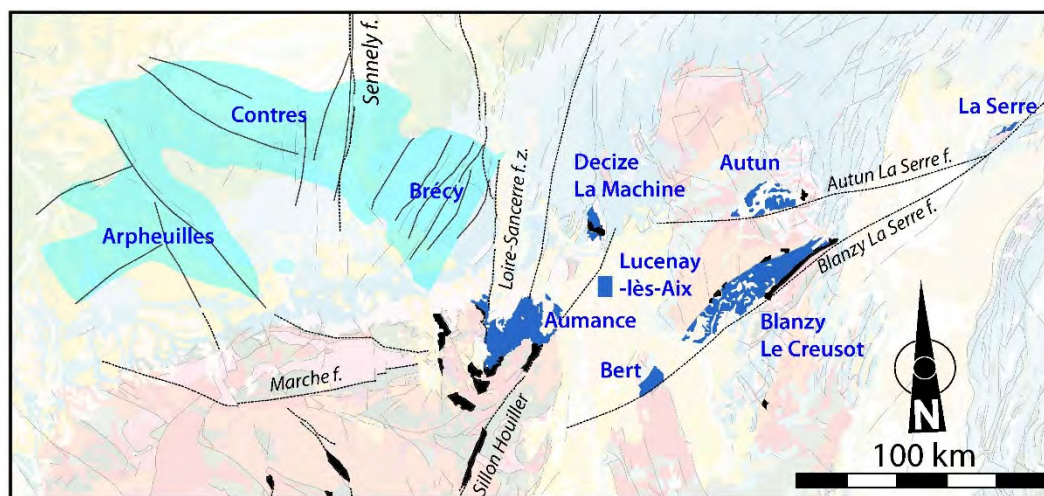


Figure 23 - Localisation des bassins stéphano-permiens du sud du bassin de Paris et du nord du Massif Central (en bleu foncé à l'affleurement, en bleu clair en subsurface).

3.6.3. Contexte géologique des bassins stéphano-permiens du sud du bassin de Paris et du nord du Massif Central

Les années 1980 ont vu la publication d'études spécifiques sur les bassins stéphano-permiens cachés sous la couverture sédimentaire mésozoïque du bassin de Paris (Donsimoni et al., 1980 ; Gréber, 1980; Lebreton, 1990), certaines d'entre elles sous l'angle de l'exploration-production d'hydrocarbures (Masclé, 1990; Perrodon et Zabek, 1991, Delmas et al., 2002). Ces auteurs s'accordaient sur la localisation approximative des bassins, et tous distinguaient le bassin de Contres-Brécy orienté ONO-ESE du bassin d'Arpheuilles d'extension plus réduite (Figure 23).

Les faciès sédimentaires de remplissage sont grossièrement décrits sur la base des rapports de forages pétroliers. Les faciès stéphaniens consistent principalement en une alternance de bancs conglomératiques et de charbon dans une matrice plus fine agilo-sableuse, similaires à ceux décrits dans les bassins affleurants alentours (voir ci-après), où ils sont attribués à des environnements alluviaux à palustres/lacustres. Ces faciès sont caractéristiques de l'initiation de ces bassins (Marteau, 1983; Courel et al., 1986; Vallé et al., 1988; Paquette et Feys, 1989). Les faciès autunien, saxonien et permien indifférencié sont assez similaires. Ils sont principalement constitués d'argile plus ou moins silto-sableuses, avec parfois de rares et fines passées de matériel sableux, carbonaté, conglomératique ou évaporitique; des passages de grès fin à grossier de plusieurs dizaines de mètres

d'épaisseur, avec des intercalations conglomératiques, sont aussi présentes. Là encore ces lithologies peuvent également être comparées à celles décrites dans les bassins environnants, où elles sont reliées à des environnements de type lacustre-playa à plaine d'inondation avec incursions fluviales (comblement du bassin, Paquette et Feys, 1989; Marteau, 1983; Gand, 2003; Roger et al., 2010). Aucun cadre structural n'était proposé pour expliquer le développement de ces séries finipaléozoïques sous couverture.

3.6.4. Evolution structurale et enregistrement sédimentaire des bassins stéphano-permiens du SO du bassin de Paris - Publication 4

Beccaletto L., Capar L., Serrano O., Marc S. (2015), Structural evolution and sedimentary record of the Stephano-Permian basins occurring beneath the Mesozoic sedimentary cover in the southwestern Paris basin (France), *Bull. Soc. géol. France*, t. 186, n°6, 429-450. <https://doi.org/10.2113/gssgfbull.186.6.429>

Ce travail est basé sur le retraitement et l'interprétation de 36 profils sismiques industriels acquis dans les années 1980 dans le SO du bassin de Paris et retraités par le BRGM (représentant une longueur de 1476 km). Ces dépocentres (bassins de Contres, Arpheuilles et Brécy) étaient déjà identifiés, mais de grandes incertitudes persistaient sur leur extension réelle et les épaisseurs des séries. De même aucune hypothèse n'avait été proposée concernant les modes de remplissage sédimentaires et leur histoire tectonique.

Principaux résultats issus de la publication 4

- Pour la première fois, (i) la géométrie interne et externe des trois bassins est décrite ; (ii) le cadre structural de chaque bassin est défini, et cinq directions structurales principales sont identifiées, correspondantes à des directions connues dans le substratum métamorphique et magmatique sous-jacent ; (iii) des cartes d'épaisseur en temps doubles et en profondeur ont été calculées pour les trois bassins ; (iv) les bassins s'ouvrent en deux temps, avec une phase initiale d'ouverture bien caractérisée (failles et éventails sédimentaires associés), suivie d'une phase d'uplift de bordure des bassins (subsidence différentielle) ; (v) cet uplift est estimé à environ 2000 m avant l'arrivée des premiers sédiments triasiques.
- L'évolution structurale des bassins stéphano-permiens se résume ainsi : (i) initiation de petits bassins plurikilométriques dans le bassin d'Arpheuilles contrôlés par des failles orientées NE-SO ; (ii) contrôle structural fort (failles normales avec jeu décrochant probable) à l'ouverture des bassins d'Arpheuilles, Contres et Brécy ; sédimentation de type conglomératique associée (avec passées de charbon) ; (iii) activité tectonique (décrochements dans le bassin d'Arpheuilles, uplift des bordures et subsidence différentielle dans les trois bassins) et remplissage sédimentaire associé à la suite de l'ouverture des bassins. Erosion régionale différentielle de toute la série stéphano-permienne avant le Trias. La plupart des failles ont ensuite été réactivées pendant le méso-cénozoïque.
- Les bassins de Contres, Arpheuilles et Brécy semblent comparables aux bassins connus à l'affleurement (même âges supposés et faciès sédimentaires similaires, cadre structural...), à la seule différence qu'ils sont bien plus étendus et épais, étant « fossilisés » depuis le Trias et n'ayant donc pas subi les phases de surrection/érosion postérieures.

Publication 4*Bull. Soc. géol. France*, 2015, t. 186, n° 6, pp. 429-450**Structural evolution and sedimentary record of the Stephano-Permian basins occurring beneath the Mesozoic sedimentary cover in the southwestern Paris basin (France)**LAURENT BECCALETTO¹, LAURE CAPAR¹, OLIVIER SERRANO¹ and STÉPHANE MARC¹*Key-words* – Paris basin, Stephano-Permian sedimentary basins, Seismic interpretation, Syn-tectonic sedimentation, Uplift, Erosion

Abstract. – Stephanian to Permian post-orogenic basins (SPB) outcrop in several limited locations in and around the present-day French Variscan basement. Little is known about their subsurface occurrences beneath the post-depositional sedimentary cover. Our work intends to decipher the structural evolution of the hidden SPB in the southwestern Paris basin, where only a few regional studies have aimed to determine their location beneath the Mesozoic sedimentary cover.

Our approach is based on the reprocessing and interpretation of 36 seismic lines (1480 km) acquired by the oil industry in the 1980s in the southwestern Paris basin. We first obtain a comprehensive view of the geometry of the SPB, based on (i) the interpretation of the base of the Stephano-Permian surface (lower limit) and the erosional base of the surface of the Triassic layers (upper limit) and (ii) the recognition of specific internal geometries and seismic facies. The interpreted faults are grouped into different categories according to their period of activity, with a focus on synsedimentary faults related to thickness variations of the Stephano-Permian deposits. We then propose a structural scheme containing faults that were active during the Stephano-Permian period, in relation to the late-Variscan structural pattern which has led to the recognition of five sets of faults: N140-trending faults associated with secondary N155- and N055-trending faults (Arpheuilles basin); N115-trending faults (Contres basin); N030-trending faults (Brécly basin); NS-trending faults (transition between the Contres and Brécly basins). Based on the seismic interpretation, thickness maps are calculated both in time and in meters, allowing a pseudo-3D view of the three identified SPB, with thicknesses up to 3000 m (Contres basin); these maps indicate that the preserved extents and thicknesses of the basins in the subsurface are systematically greater than those observed at outcrop.

Finally, we show that the SPB were filled during two different tectonic phases: (i) an initial period of opening of the Arpheuilles, Contres and Brécly basins, during which Stephanian conglomeratic/coal facies were deposited under a strong structural control (normal faulting with certainly a strike-slip component, wedge-shaped geometry of the sediments); (ii) a consecutive pre-Triassic tectonic activity (N155-trending strike-slip in the Arpheuilles basin, uplift of the margins of the three basins), at the origin of a significant part of the sedimentary filling of the basins; this vertical uplift may have reached 2000 m.

Evolution structurale et enregistrement sédimentaire des bassins stéphano-permiens présents sous la couverture mésozoïque du sud-ouest du bassin de Paris (France)

Mots-clés. – Bassin de Paris, Bassins sédimentaires stéphano-permiens, Interprétation sismique, Sédimentation syn-tectonique, Uplift, Erosion.

Résumé. – En France, les bassins sédimentaires post-orogéniques stéphano-permiens (SPB) affleurent localement à l'intérieur des grands domaines varisques. En revanche, il existe peu d'information sur leur présence en subsurface sous la couverture sédimentaire post-dépôt. Notre travail se propose de décrypter l'évolution structurale des bassins cachés dans le sud-ouest du bassin de Paris, où seulement quelques études se sont appliquées à préciser leur position sous la couverture sédimentaire mésozoïque.

Notre approche se base sur le retraitement et l'interprétation de 36 profils sismiques (1480 km) acquis en région Centre par l'industrie pétrolière dans les années 80. Nous présentons tout d'abord une vue détaillée de la géométrie des SPB, sur la base d'une compilation des données de forages, de l'interprétation sismique de la base du Stéphanien et de la base érosive du Trias (resp. limite inférieure et supérieure des bassins), de l'agencement des géométries internes et des faciès sismiques. Les failles interprétées ont été classées selon leur période d'activité, en mettant l'accent sur les failles syn-sédimentaires stéphano-permiennes. Ensuite, nous proposons un schéma structural des bassins stéphano-permiens en relation avec le contexte régional tardi-varisque; cinq ensembles de failles ont ainsi été identifiés: failles N140 associées à des failles N155, et failles N055 (bassin d'Arpheuilles); failles N115 (bassin de Contres); failles N030 (bassin de Brécly); failles N-S (dans la zone de transition entre les bassins de Contres et Brécly). Les interprétations sismiques permettent de calculer des cartes d'épaisseur en temps et en profondeur de ces bassins, ce qui permet d'obtenir une pseudo-vue 3D des trois SPB; les épaisseurs peuvent atteindre 3000 m (bassin de Contres). Ces cartes montrent que les bassins cachés sont systématiquement plus étendus et épais que les bassins affleurants.

¹ BRGM-French Geological Survey, Geology Division, 3 avenue Claude Guillemin, 45060 Orléans cedex 2, France, Email corresponding author: *l.beccaletto@brgm.fr*

Manuscript received on August 5, 2014 ; accepted on February 4, 2015.

Nous montrons enfin que les SPB se sont développés selon deux phases tectoniques distinctes: (i) une période initiale d'ouverture, reconnue dans les bassins d'Arpheuilles, de Contres et Brécy, pendant laquelle se sont déposés des faciès conglomératiques à intercalations de charbon (Stéphanien) sous contrôle structural marqué (failles à jeu normal avec certainement une composante décrochante, géométrie en éventail des dépôts sédimentaires); (ii) une activité tectonique pré-triasique marquée par une composante décrochante de direction N155 dans le bassin d'Arpheuilles, et par une surrection des bordures des trois bassins; cette surrection est à l'origine d'une partie significative du remplissage sédimentaire observé; le mouvement vertical a pu atteindre 2000 m.

INTRODUCTION

Late Carboniferous (Stephanian) to Permian basins (hereinafter referred to as Stephano-Permian basins, or SPB) outcrop in several limited locations in and around the present-day French Variscan basement, as shown for instance on the 1: 1,000,000 scale geological map of France [BRGM, 2003, fig. 1]. They are mostly considered as intramontane post-orogenic (Variscan) basins, developed in close relationships with crustal to lithospheric geological events [Echtler and Malavieille, 1990; Burg *et al.*, 1994; Praeg, 2004]. On the other hand, little is known about their subsurface occurrences beneath their post-depositional sedimentary covers. This is the case, for instance, in the Paris basin, where only a few regional studies attempted to locate them beneath the

Mesozoic sedimentary cover [e.g. Debeglia, 1980; Mascle, 1990; Delmas *et al.*, 2002]. There, the issues of their extension, thickness, sedimentary filling, internal geometry and structural control have hardly been addressed and therefore still remain open. Likewise, their preservation from the Mesozoic regional uplift phases and subsequent erosion of cover rocks opens a window on the post-Stephanian to pre-Triassic tectonic activity [Barbarand, 2003; Peyaud *et al.*, 2005; Barbarand *et al.*, 2013]. At the very end of the Variscan orogenic period, the SPB record the last sedimentation and erosion phases prior to the onset of the Mesozoic sedimentation, attesting the transition from the Palaeozoic Variscan cycle to the Mesozoic sedimentary cycle.

Our study addresses the poorly-known SPB located beneath the Mesozoic cover in the southwestern part of the

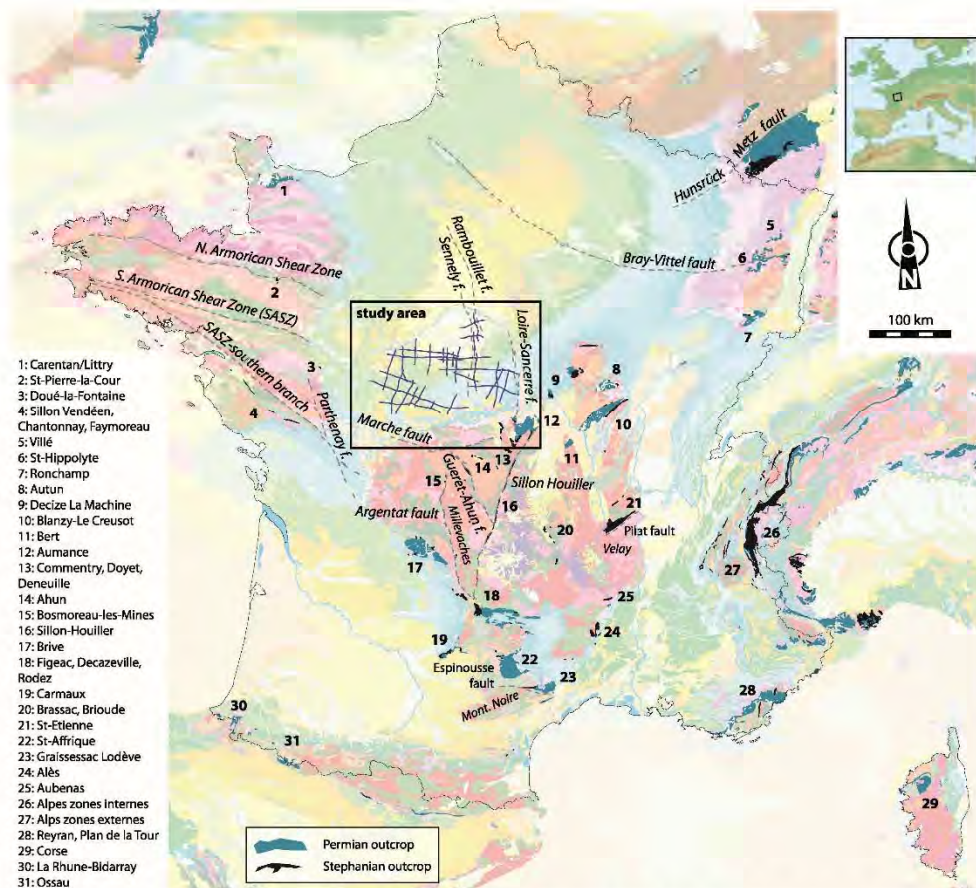


FIG. 1. – Location of the study area including the reprocessed/interpreted seismic lines (in blue). The map also shows the major Stephano-Permian basins outcropping in France [Vetter, 1986; Praeg, 2004], and the major late Variscan faults. The geological background is from the 1:1,000,000 geological map of France [BRGM, 2003]. Top-right inset: geographic position of the Paris basin in western Europe.

Paris basin (fig. 1). It is based on the interpretation of newly reprocessed seismic lines (about 1400 km in length) initially acquired by the oil industry in the 1980s. We firstly present an overview of the location of the SPB in the framework of the Variscan orogen, and focus on the occurrence of the SPB in France, both at outcrops and in the subsurface. The seismic and well data are then presented, before relying on the interpretation of the seismic lines to discuss some structural and general features of the SPB (fault nomenclature, structural pattern, basin thickness, and estimation of the pre-Triassic uplift). A simple geological scenario is proposed, from the initiation of the SPB in the late Carboniferous to the arrival of the first Triassic sediments. Our aim is to document and shed new light on these hidden geological objects, which display depositional and tectonic geometries that are inevitably lost in outcropping basins.

GEOLOGICAL BACKGROUND

The SPB in the framework of the Variscan orogen

Two main late orogenic extensional tectonic events have been identified in the Variscan belt of Western and Central Europe (fig. 2) [Faure and Becq-Giraudon, 1993; Burg *et al.*, 1994; Ziegler and Stampfli, 2001].

(1) A mid-Carboniferous (late Visean-mid Westphalian) tectonic event, mainly characterized by ductile shearing and rapid exhumation of deep crustal rocks, widespread derived crustal plutonism and volcanism, and local development of volcano-sedimentary basins [Faure *et al.*, 1990; Echtle and Chauvet, 1992; Rey *et al.*, 1991; Faure, 1995; Timmerman, 2004]. Based on numerous indicators of syn-metamorphic deformation and syn-tectonic plutons, the late Visean-mid Westphalian syn-orogenic extension was characterized in the French Massif Central and surroundings areas by a NW-SE maximum stretching direction [Faure, 1995].

(2) A late Carboniferous (Stephanian)-Early Permian tectonic event, which provides the space and time framework for our study. This period marks the final stage of the Variscan orogeny, with the collapse of the thickened and hot Variscan crust (post-orogenic collapse; Ménard and Molnar [1988], Malavieille [1993]). It was accompanied by the uplift of high-grade metamorphic domes and related faults and detachments, with the development of mainly half-graben or pull-apart types, multi-directional asymmetric intramontane coal basins [Van den Driessche and Brun, 1991; Malavieille, 1993; Costa and Rey, 1995]. The end of the Variscan orogeny was also accompanied in the internal zones and in the foreland by a widespread intrusive and extrusive magmatic activity [Doblas *et al.*, 1998; Timmerman, 2004]. This second phase of extension has generally been attributed to a "Basin and Range" style of post-orogenic evolution [Lorenz and Nicholls, 1976, 1984; Ménard and Molnar, 1988], although some authors contest this view on the basis of mechanical, geodynamic or surface process arguments [Ziegler, 1990; Ziegler and Stampfli, 2001; Malavieille, 2010].

SPB are therefore consistent with the extension and stretching of the Variscan crust at the end of the Variscan orogeny. However, many of these basins also contain indicators of one or more shortening phases and coeval sedimentation [Bonijoly and Castaing, 1983, 1986; Blès *et al.*, 1989; Ziegler, 1990; Genna and Debriette, 1994]. Preliminary explanations given for basins located in the French Massif Central argued in favor of a progressive rotation of the principal horizontal compressional stress axis from N-S to E-W [Bonijoly et Castaing, 1986; Gélard *et al.*, 1986; Blès *et al.*, 1989] in a regional wrench tectonic setting [Ziegler, 1990, 1992]. However, Faure and Becq-Giraudon [1993] and Faure [1995] proposed that all the structural features of the Massif Central basins (including the shortening ones) could be explained via a single extensional stress field characterized by a NE-SW maximum stretching direction. The extensional deformation propagated outwards with time, from the internal to the external zones of the orogen [Praeg, 2004].

Late orogenic SPB are widespread in present-day western Europe; they are known at outcrop in the internal and external zones of the orogen (e.g. around the French Massif Central, or the Sarre-Nahe basin) as well as in the northern foreland (e.g. Great Britain and North Sea-Poland basins) of the Variscan belt [see the synthesis of Praeg, 2004]. Their subsurface prolongation beneath the Mesozoic and Cenozoic sedimentary cover is mostly attested by well data and seismic scientific [Blundell, 1990; Bois *et al.*, 1991, 1994] or industrial surveys (oil and gas exploration-production). Indeed, apart from scientific research, SPB were extensively studied for their resources, such as oil, gas, coal, uranium or other ore deposits [Courel *et al.*, 1986; Mascle, 1990; Dill *et al.*, 1991; Delmas *et al.*, 2002; Bouchot *et al.*, 1997, 2005].

French SPB at outcrop and in the subsurface

French SPB at outcrop

Many SPB, ranging from less than one to several hundred square kilometers, are found in and around the present-day French Variscan basement, including the Alpine and Pyrenean

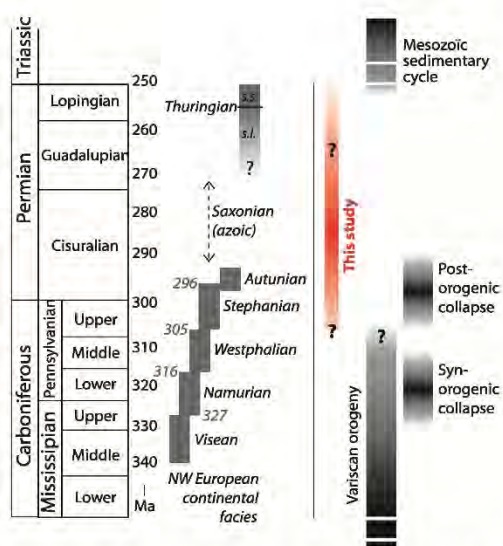


FIG. 2. – Location of the studied SPB at the transition between the Variscan Paleozoic cycle and the Mesozoic sedimentary cycle; ages and continental facies compiled from Menning *et al.* [1999], Cohen *et al.* [2013] and Durand [2014]. Refer to the text for a discussion on the age of the studied basins.

domains (fig. 1). They are closely related either to regional faults reactivated at the end of the Variscan orogeny (e.g. Sillon Houiller and Hunsrück-Metz fault [Vetter, 1971; Burg *et al.*, 1990; Korsch and Schäfer, 1995]) or to metamorphic domes and spatially-related faults or detachments (Velay, Millevache and Montagne Noire massifs [Malavieille *et al.*, 1990; Van den Driessche and Brun, 1992; Faure, 1995]).

South of the study area, the SPB of the Massif Central may be classified according to the direction of their border faults [Faure and Becq-Giraudon, 1993; Faure, 1995]. Pull-apart basins related to submeridian faults (Sillon Houiller and Argentat fault) are distinguished from half-graben basins related to NW-SE, E-W or NE-SW trending border faults. West of the study area in the Armorican domain, only rare small basins have been preserved along or near the northern and southern Armorican shear zones (fig. 1). The Permo-Carboniferous ages of the sedimentary deposits are usually based on biostratigraphic assemblages [BRGM, 1989]. Radiochronologic data controlling the formation of the SPB are scarce. The Stephanian Saint-Etienne basin developed along the Pilat detachment controlling the uplift of the Velay dome in Stephanian times (around 300 Ma, Ar-Ar ages from Costa [1991]; n°21 in fig. 1). More recently, Bruguier *et al.* [2003] dated fine-grained sediments of the Bosmoreau basin (n°15), showing that it was formed in close relationship with the Argentat fault according to two distinct sedimentary cycles (around 340 Ma and 296 Ma, K-Ar ages). In the South Armorican domain (Golfe du Morbihan), the extensional shear deformation – with no preserved basin – has been dated at *ca.* 300 Ma (Ar-Ar ages, Turrillot *et al.* [2011]).

The sedimentary filling of the French SBP indicates similar environments, despite local differences notably concerning their thickness or facies variations; the development of continental to deltaic-lacustrine-playa deposits several hundred meters thick is systematically controlled by the neighboring faults. Continental sediments are composed of alluvial fan conglomerates and fluvial sandstones, while lacustrine-playa to flood plain sediments consist of black to red shales, evaporites and minor sandstones and carbonates [BRGM, 1989 and references therein; Pochat and Van den Driessche, 2011]; bituminous shales and coal beds, which have been exploited in the past, are a common feature [Courel *et al.*, 1986].

Southeast of and closer to the study area, some isolated SPB outcrop over the deformed magmatic and metamorphic rocks of the French Massif Central (fig. 1). The closest basin is the Aumance basin (n° 12 in fig. 1), located 30 km southeast of the easterly seismic lines at the junction between the Loire-Sancerre and the Sillon Houiller fault zones [Bonnion *et al.*, 1983; Paquette and Feys, 1989]. The small Decize-La Machine horst (n° 9) outcrops northeast of the Aumance basin [Grangeon *et al.*, 1968], of which it could be the prolongation. Farther east, the Autun (n°8), Bert (n°11) and Blanzay-Le Creusot (n°10) basins are also present. These basins, which have been specifically studied in the 1980s (field and subsurface surveying), display a typical half-graben geometry, with a strong structural control during the continental and lacustrine to floodplain sedimentation; the main structural trends of the Autun and Blanzay-Le Creusot basins are respectively N080 and N060 [Paquette and Feys, 1989; Marteau, 1983; Feys and Gand,

1983; Vallé, 1986; Vallé *et al.*, 1988; Gand, 2003; Roger *et al.*, 2010].

French SPB in the subsurface – focus on the SW Paris basin

Subsurface investigations of the French pre-Mesozoic basement of the Paris, Aquitaine and South-East basins originated in the mid-20th century, following the development of geophysical methods together with the drilling of deep oil and gas wells with Palaeozoic and Mesozoic targets (for the Paris basin, see Goguel [1954] and Lienhardt [1961]). The first geological studies on the Paris basin were then published in the 1960s and 1970s [Sapin, 1967; Gérard, 1971; Héritier and Vuillemin, 1971; Weber, 1973], leading to several syntheses dealing with the location of the pre-Mesozoic units including the SPB [Autran *et al.*, 1980; Debeglia, 1980]. Similar syntheses were produced for the Aquitaine and southeastern basins [BRGM, 1974; Debrand-Passard *et al.*, 1984]. More recently, the acquisition and interpretation of gravimetric, aeromagnetic or seismic data gave birth to a new set of syntheses dedicated to the geodynamic and paleogeography of the western part of the Variscan belt [Matte and Hirn, 1988; Bois *et al.*, 1994; Edel, 2008].

From the 1980s on, specific studies on the SPB concealed beneath the Mesozoic sedimentary cover of the Paris basin have also been published [Donsimoni *et al.*, 1980; Greber, 1980; Lebreton, 1990], some of them from an exploration-production angle [Mascle, 1990; Perrodon and Zabek, 1990; Delmas *et al.*, 2002]. Figure 3 shows the locations of SPB in the SW Paris basin according to these studies. The authors agree about the rough location of the basins, and all distinguish the WNW-ESE elongated Contres-Brécly and the smaller Arpheuilles basins (nomenclature according to Delmas *et al.* [2002]). However, a rapid overview reveals many discrepancies between the different studies, for instance regarding the detailed location of the basins/depocenters, their outlines, and the possible subdivision of the Contres-Brécly basin. A striking feature of particular interest is the lack of structural information. Except for the Sennely and Loire-Sancerre faults, very few structural indications, with no reference to their source, is provided on the maps (similarly, ages and depositional environments are little discussed by the authors, probably due to the lack of related data). Only Lebreton [1990] indicated small fault segments related to the SPB, and initiated a discussion about their structural pattern from a partial seismic dataset. The seismic data provided in this paper bring new insights on these points.

Age and depositional environments of the pre-Mesozoic sedimentary deposits in the SW Paris basin

Trachy-andesites sampled at the bottom of the Stephano-Permian sediments of the Couy-1 well (fig. 4) yielded an Ar-Ar age of 301 Ma [Costa and Maluski, 1988]; this is the only absolute age from the studied series. Furthermore, the age determination of the sedimentary basins imaged on the seismic lines relies on the public drilling reports of ten oil exploration wells and one scientific well (Couy-1 from the GPF Project; fig. 4). Most of them were drilled in the 1960s except Bertray-1 and Couy-1, drilled in 1987. Four wells reach Stephanian facies, identified by plant debris and/or ostracods (Arpheuilles-1, Bertray-1, Ciran-1 and Brécly-1;

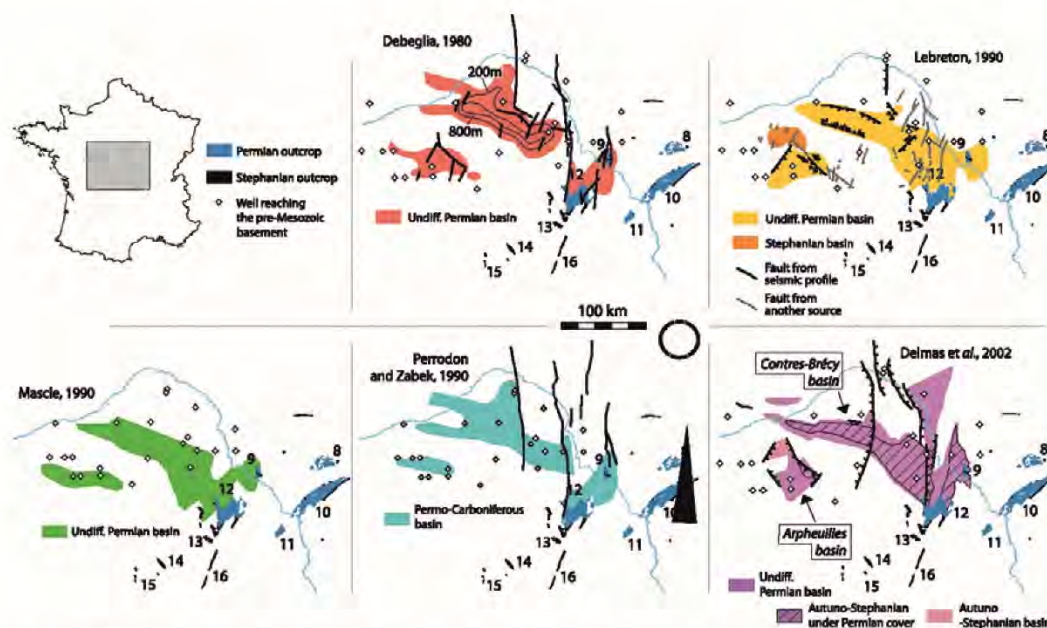


FIG. 3. – Location of the hidden Stephano-Permian basins in the southwestern Paris basin according to Debégliá [1980], Lebreton [1990], Mascle [1990], Perrodon and Zabeł [1990] and Delmas *et al.* [2002], with respect to the neighboring basins at outcrop. See figure 10 for a comparison with the present study.

fig. 4). Based on facies comparisons [Sapin, 1967; Chantraine *et al.*, 1992], two more wells are thought to reach Stephanian facies (Coyu-1 and Ligueil-1; fig. 4), one well contains Autunian facies (Arpheuilles-1; fig. 4), and four wells cut or reach Saxonian facies (Bossay/Claise-1b, St Georges/Moulon-1, Brécy-1 and Contres-1; fig. 4). In the absence of biostratigraphic argument, undifferentiated Permian or Permian-Triassic facies are considered within four wells (Bertray-1, Clion-1, Couy-1; Boussay-1; fig. 4).

The terms Stephanian, Autunian or Saxonian refer to facies and not ages [e.g. Broutin *et al.*, 1999; Menning *et al.*, 1999]. For instance, the boundary between the Stephanian and Autunian sediments is facies-dependent and diachronous [Broutin *et al.*, 1986; Menning *et al.*, 1999]. It is then problematic to propose a detailed age on the basis of these facies considerations [Durand, 2014]. Accordingly, the basins are considered to be Stephano-Permian in age (fig. 2), without further detail (consistent with the Couy-1 radiometric age). The traditional term Stephanian is intentionally retained, considering that it refers to a late Carboniferous age [Menning *et al.*, 1999] (fig. 2).

In the study area, the first Mesozoic sediments above the Paleozoic series are thought to be represented by Middle Triassic sediments with Buntsandstein facies of Anisian age [Bourquin *et al.*, 2002 and 2006].

The sedimentary facies of the SPB may be roughly described on the basis of the drilling reports. Stephanian facies mainly consist of alternating conglomeratic and coal beds in a finer shaly to sandy matrix. These lithologies are similar to those described in the surrounding outcropping basins, where they are attributed to alluvial fan to palustrine/lacustrine environments. These facies are a characteristic feature of the initiation of the SPB [Marteau, 1983; Courel *et al.*, 1986; Vallé *et al.*, 1988; Paquette and

Feys, 1989]. The Autunian, Saxonian and undifferentiated Permian facies are quiet similar. They mainly consist of clay/shale or silty to sandy clay/shale, with possible rare and thin beds composed of sandy, carbonated, conglomeratic or evaporitic material; occurrences of fine to coarse sandstone several tens of meters thick, with conglomeratic intercalations, could also occur. These lithologies may also be compared to those described in the surrounding basins, where they are related to lacustrine-playa to flood plain environments with fluvial incursions (filling up of the basin [Paquette and Feys, 1989; Marteau, 1983; Gand, 2003; Roger *et al.*, 2010]).

METHODOLOGY

Seismic data retrieval and processing

The study is based on the reprocessing of 36 seismic lines representing about 1476.5 km in length. The seismic raw data were historically recorded by the ESSOREP Company at the beginning of the 1980s (CHER and CLA surveys; for convenience sake CH and CL abbreviations are used in the figures for the line names, fig. 5). These old seismic data have been reprocessed using modern methods and algorithms, thereby significantly improving the quality of the resulting seismic section and leading to enhanced descriptions of the geological structures [Beccaletto *et al.*, 2011]. Twenty-five seismic lines were reprocessed using the standard Post-Stack Time Migration method, and 11 seismic lines were reprocessed using the Pre-Stack time migration (PSTM) method (fig. 5); the latter has the advantage of enhancing the details of the structural features. Particular attention has been paid to the static corrections in order to remove the topographic and velocity effects of the surficial rock layer along the seismic lines.

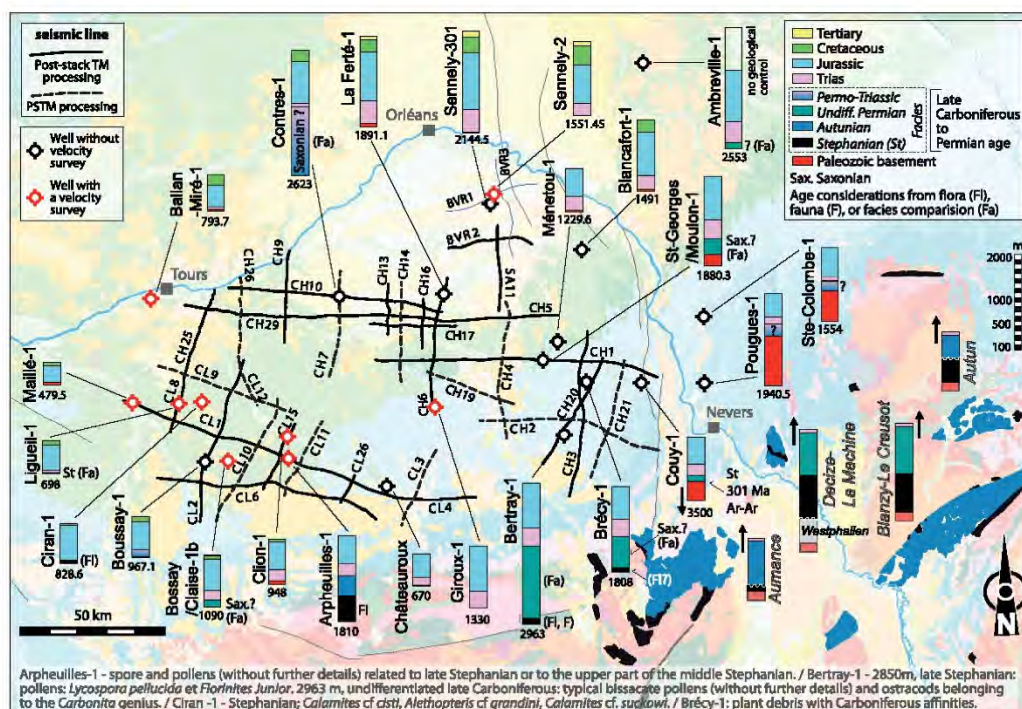


FIG. 4. – Location and designation of the reprocessed and interpreted seismic lines; location, name and schematic stratigraphic columns of the available wells; for outcropping basins: schematic stratigraphic column of the Aurance basin from Paquette and Feys [1989], of the Decize-La Machine horst from Roger *et al.* [2010] and Grangeon *et al.* [1968], of the Autun basin from Marteau and Feys [1989], of the Blanzy-Le Creusot basin from Gand [2003]. The geological background is from the 1:1,000,000 geological map of France [BRGM, 2003]. Biostratigraphic data from the oil company drilling reports.

The seismic images of the SPB are generally of good quality, with exceptions along some W-E-trending seismic lines in the northern area. Independently of the quality of the raw data, this may possibly be due to the similar orientation of the seismic lines and the main structural trends. Unsurprisingly, only the deepest zones below the Stephano-Permian basins are poorly imaged (the acquisition parameters were not tuned to image such deep places). When compared with the previously processed lines, the new ones display a better continuity and horizontal-vertical resolution of the seismic horizons or groups of horizons (especially the deep horizons above the base of the Stephano-Permian basins), and improved geometric characterization of faults and fault zones. This is particularly true for the PSTM-reprocessed lines.

Seismic data interpretation

The calibration and tie of the selected geological markers to the corresponding seismic horizons was achieved using well data, seismic facies and reflector geometries. The targeted surfaces were correlated from line to line and cross-correlated using the Seisvision software (© Landmark-Geographix). Twenty-two wells were used to calibrate and tie the geological markers to the corresponding seismic horizons and to compute the thickness maps; well data come from public drilling reports of exploration wells. Nine of them have velocity surveys, which are necessary to convert the well geological data from depth (in m) to time, and then

display the geological markers on the seismic lines (in ms two-way-time).

A synthetic seismogram has also been calculated for the Arpheuilles-1 well. Such a seismogram aims to model the acoustic response of the rock layers along a given well. It is generated by convolving the reflectivity derived from digitized acoustic and density logs with a specific wavelet. The result is therefore a seismic trace simulating the acoustic response of the well lithologies.

INTERPRETATION OF THE SEISMIC LINES

Targeted horizons and seismic facies

The base of the basins and the erosional base of the Triassic layers were targeted in order to obtain the SPB envelope. Figure 5 gives an overview of the various basins geometries based on the interpretations of a selection of seismic lines (note, for instance, their large thicknesses compared to the Mesozoic sedimentary cover).

The base of Stephano-Permian sedimentary fill corresponds to the top of the pre-Stephanian substratum. The latter is cut in fifteen wells, which show that it could be either sedimentary, metamorphic or plutonic (a weathered surface may occur as well). In most places the top of the pre-Stephanian substratum matches the top of the acoustic basement; however, some sets of reflectors, belonging to pre-Stephanian units, still appear locally below that horizon (fig. 5).

On many seismic lines, the bottom of the basins displays very typical low-frequency/high-amplitude, continuous to discontinuous reflectors (figs 6 and 7). The synthetic

seismogram of the Arpueilles-1 well indicates that these reflectors are correlated with Stephanian conglomeratic and coal beds (fig. 6). These seismic facies and related

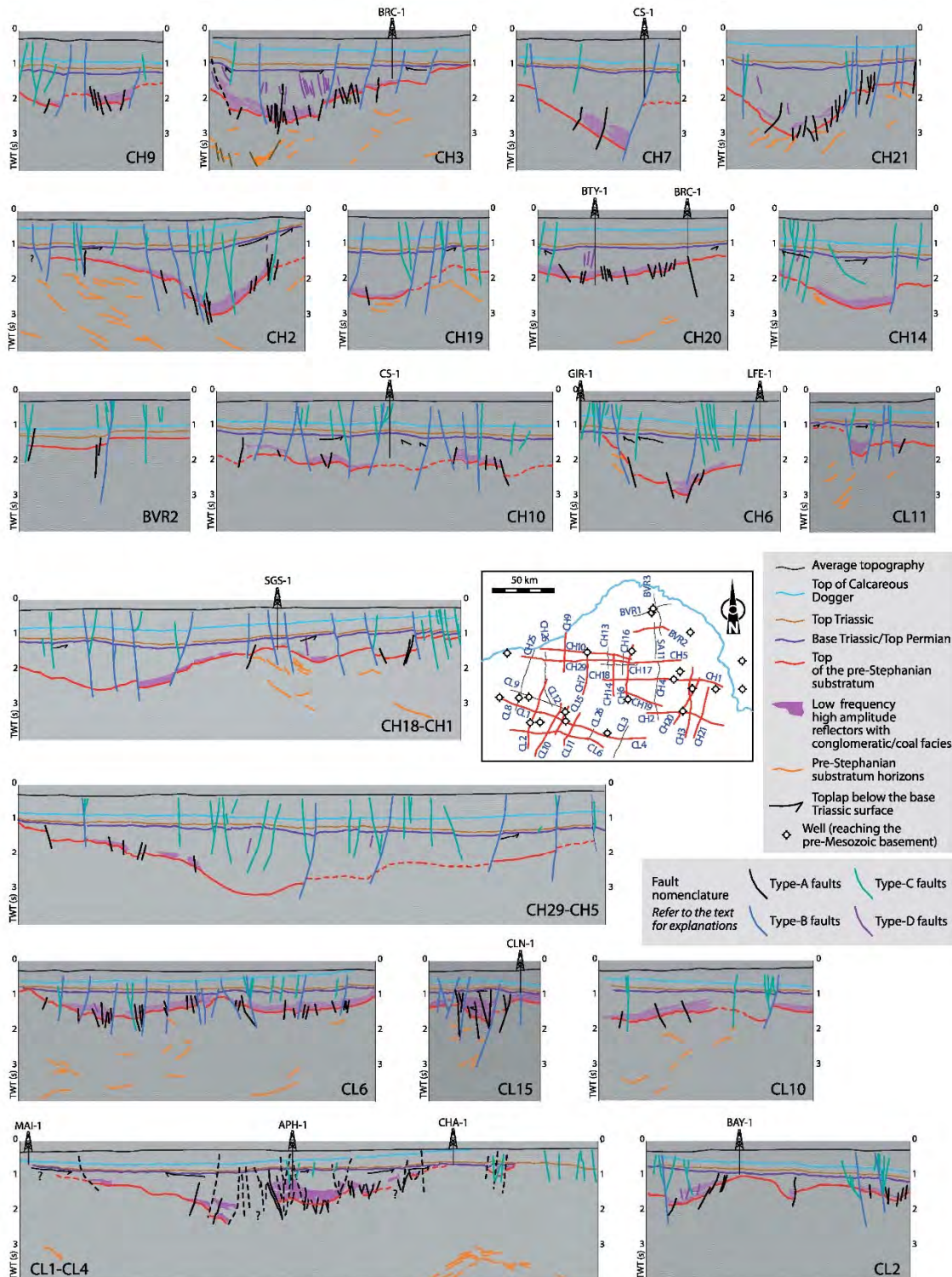


FIG. 5. – Interpretation of a selection of representative seismic lines (in red on the inset map), with the calibration wells. The fault nomenclature is explained in the text. For the N-S lines, the north is on the right; for the E-W lines, the west is on the left.

lithologies, lying at the bottom of the basins, are a characteristic feature of the initiation of the studied basins (see section “Structural evolution of the SBP”).

Seismic facies between the basal low-frequency/high-amplitude reflectors (when they occur) and the erosional base of the Triassic layers are usually stratified, roughly parallel, with continuous reflectors varying from low to high amplitudes and medium to high frequencies; chaotic or semi-transparent facies are also possible. This variety in seismic facies features – to be compared to the homogeneous basal facies described above – may be related to lithological variations. Characteristic geometries also locally

occur (onlaps, toplaps, progradation pattern...) recording particular sedimentation and structural processes (see section “Structural evolution of the SBP”).

The erosional base of the Triassic layers, which corresponds to the topmost preserved beds of the Stephano-Permian, is characterized by the development of toplap geometries of the Stephano-Permian reflectors below the Mesozoic sequence (figs 6 and 7). Although present throughout the whole studied area, these geometries are best seen in the southern part, where the low-frequency conglomeratic seismic facies are cut by the base Triassic sediments.

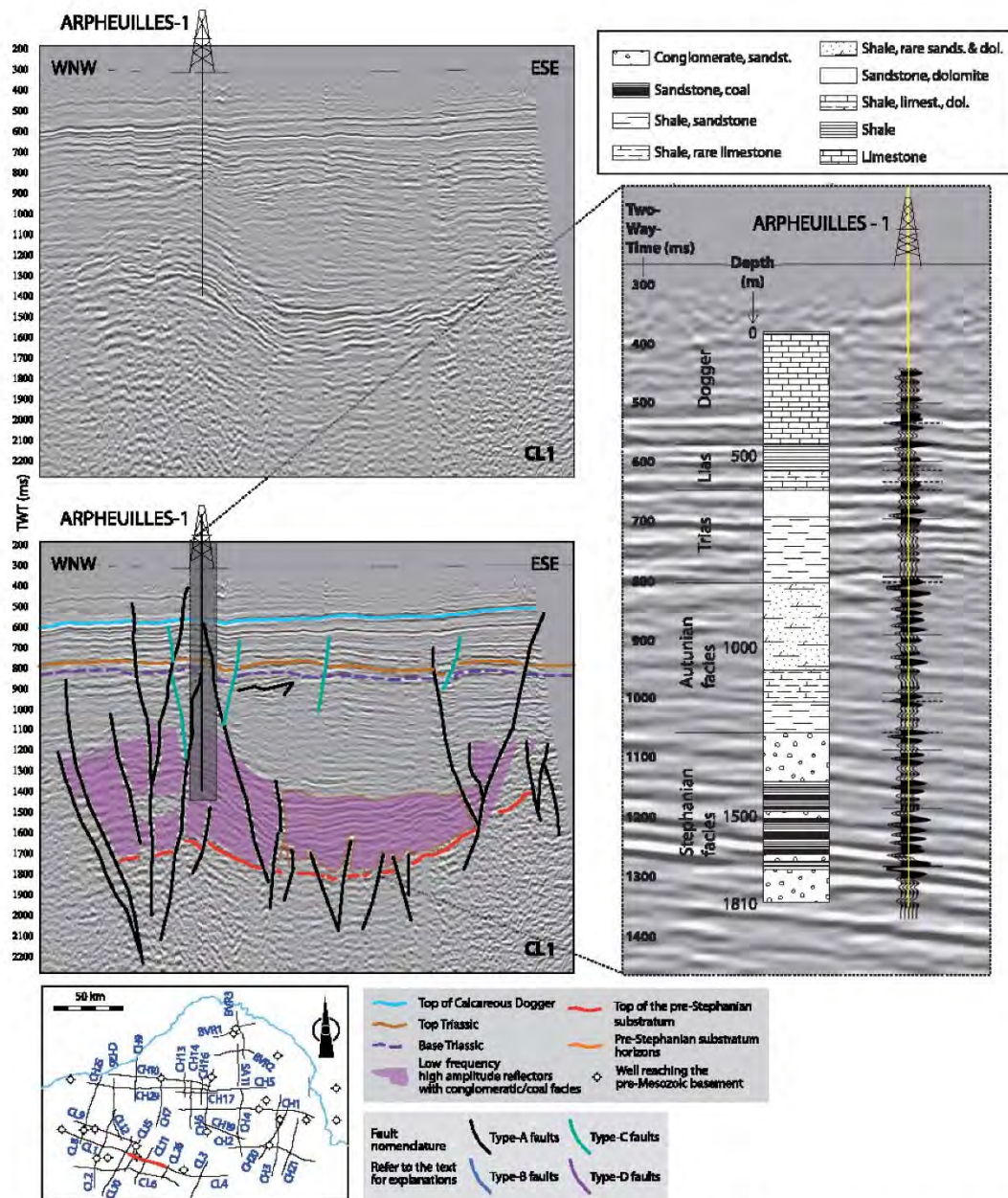


FIG. 6. – Seismic and geometric characteristics of the Stephano-Permian sedimentary filling, and geological meaning of the low-frequency/high-amplitude reflectors (correlation between the Arpheuilles-1 well and line CL1).

Finally, in order to image the Mesozoic sedimentary cover and provide a complete view of the sedimentary pile, the horizons corresponding to the top Triassic and the top calcareous Dogger have also been interpreted, and are displayed on the seismic lines (figs 5, 6, 7 and 11-16).

Fault nomenclature – Overprint of the Mesozoic tectonic activity

Faults are a striking feature of the seismic lines (fig. 5). An attractive way to use this information is to group them into different categories according to their activity period. Our classification is based on two simple criteria: (1) a given fault is said to be synsedimentary (i.e. it controlled the sedimentation), if a thickness variation of the sedimentary pile is spatially related to the fault; the occurrence of the low-frequency/high-amplitude conglomeratic/coal facies help to discriminate these faults; (2) a fault is said to be post-sedimentary if it cuts through the whole sedimentary pile. The

combined use of these two criteria led us to distinguish four types of individual faults (fig. 5; the various types of faults are identified on all the figures of the paper): (A) type-A faults cutting through the base of the Stephano-Permian sequence, and for the most part spatially related to thickness variations of the low-frequency/high-amplitude seismic reflectors (conglomeratic/coal lithology). This category also includes the faults cutting through the base of the Stephano-Permian unit with no indication of thickness variation (only a throw is observed); they do not cut the base Triassic layer; (B) type-B faults cutting through the base of the Stephano-Permian unit, and related to thickness variations of all the Stephano-Permian deposits, with a post Permian activity; (C) type-C more recent faults, with only a post-Permian (generally post-Triassic) activity and no evidence for Stephano-Permian activity; (D) type-D intra Stephano-Permian faults, sometimes cutting the base of the Triassic sediments; very rare faults with a pre-Stephanian activity have also been observed, only on the CH3 line.

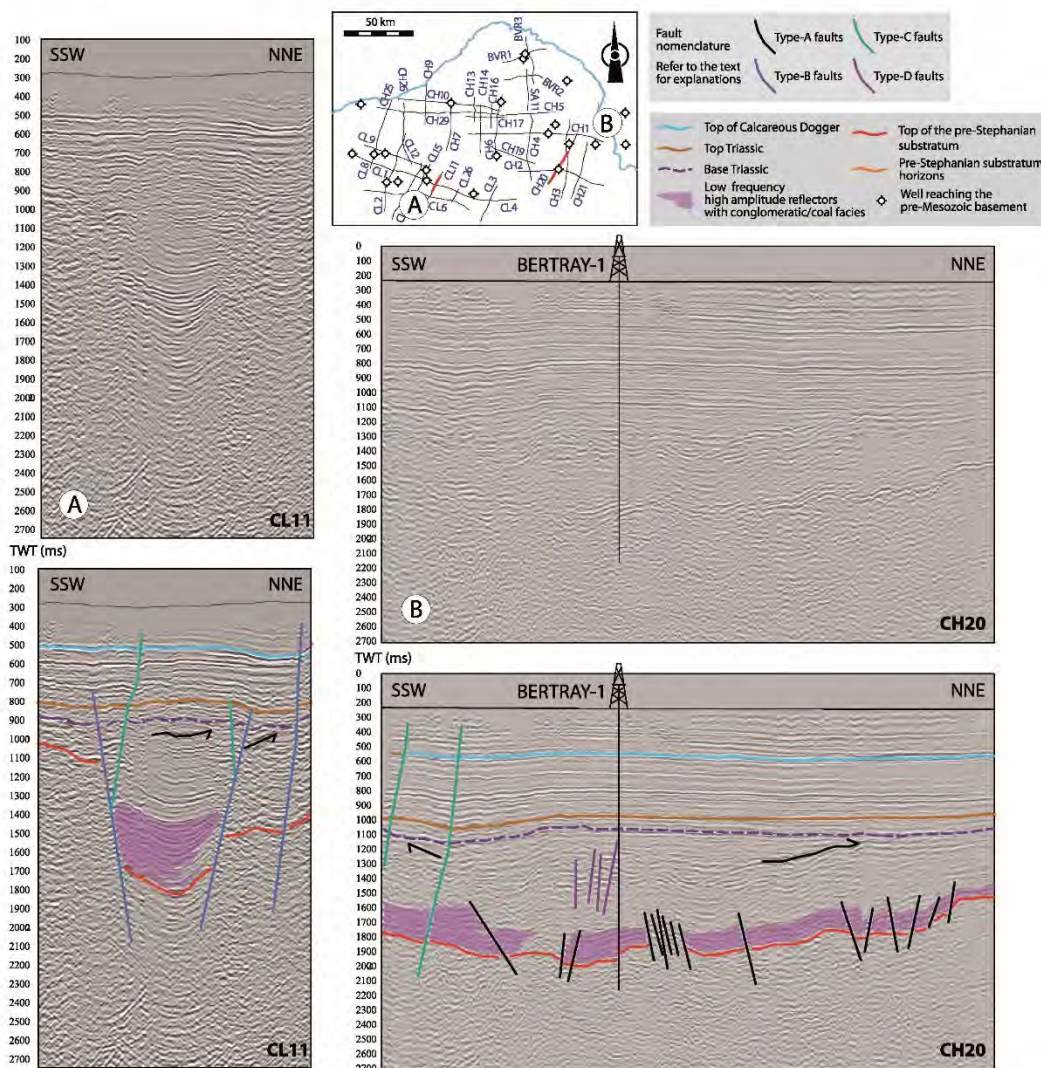


FIG. 7. – Seismic and geometric characteristics of the Stephano-Permian sedimentary filling; examples of lines CL11 (A) and CH20 (B).

on both sides, including the southern branch of the South Armorican dextral shear zone (SASZ-sb) [Rolin *et al.*, 2009]. They are also similar in direction to the Gueret-Ahun fault (GAF) in the Massif Central;

(2) N055-trending faults, visible in the southwestern portion of the study area. This fault direction does not correspond to any field-regional trend. They are cut by the N140-trending fault;

(3) N-S-trending faults, including the Sennely fault (SF) [Héritier and Villemain, 1971], visible in the northern part of the study area. This direction is parallel to the sinistral Loire-Sancerre fault zone (LSFZ);

(4) N115-trending faults, visible in the northwestern portion of the study area. This direction is similar to that of the dextral South and North Armorican shear zones (resp. SASZ and NASZ). These faults are cut by the N-S-trending faults;

(5) N030-trending faults, visible in the eastern portion of the study area. This direction is parallel to the northern trend of the sinistral Sillon Houiller fault zone (SH). Due to

a lack of data, their spatial relation with the neighboring fault sets (including the nearby N-S-trend) is unknown.

A relative chronology of the fault activity may be proposed from this structural scheme on the basis of cartographic intersection relationships between the various fault trends (fig. 9): the N055-trending faults were active first, prior to the N115 trending faults and N145/155-trending faults; the active fault set was subsequently the N-S-trending faults. As for the N030-trending ones, their exact place in the suggested chronology remains conjectural due to their isolated position.

No strike-slip component can be inferred from the seismic structural pattern alone, although some cartographic fault relationships may show possible regional Riedel geometries in a map view (N115 and N140/155 fault sets, fig. 9); this would be confirmed by their trend, which is similar to the strike-slip Armorican shear zones (SASZ and NASZ) and the Parthenay fault (PF). Similarly, a strike-slip component may be inferred for the N030-trending faults,

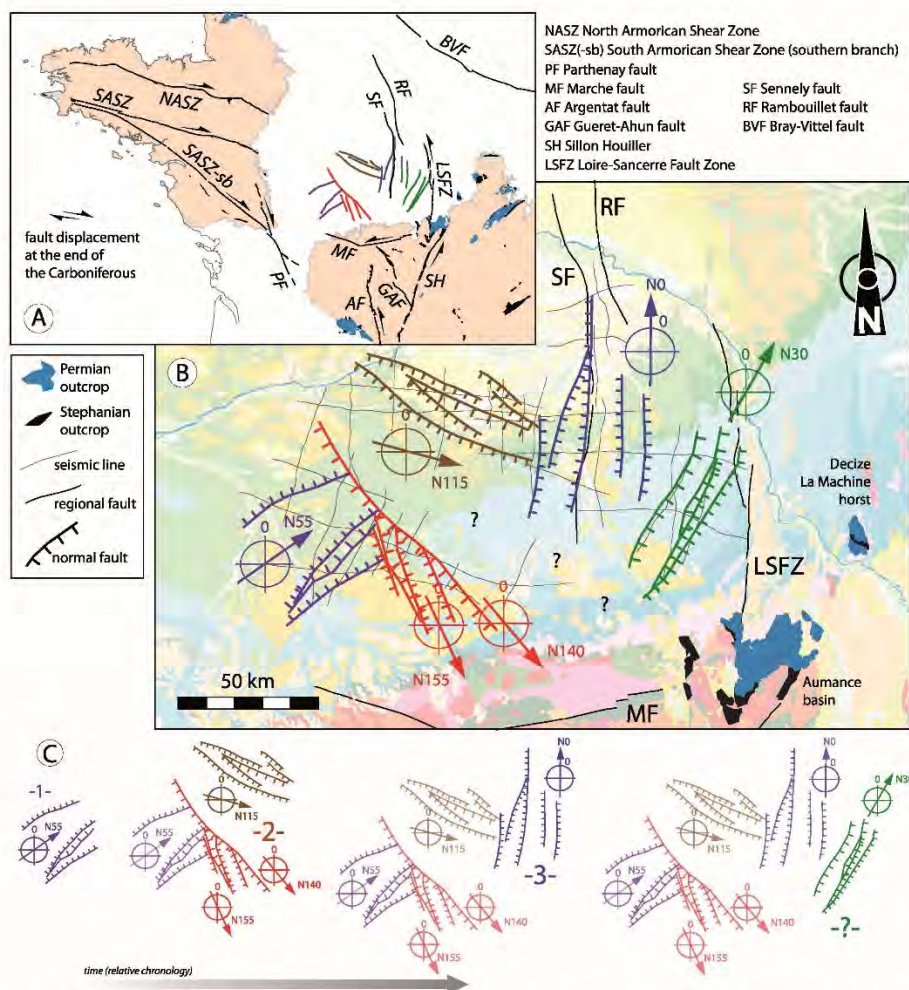


FIG. 9. – A: regional fault pattern at the end of the Carboniferous [Faure, 1995; Ballèvre *et al.*, 2009; Rollin *et al.*, 2009]. B: structural scheme with faults active during the Stephanian-Permian period. The colours correspond to the various fault strikes; a simplified version of the fault pattern is displayed in A. C: relative chronology of the faults activity. The geological background is from the 1:1,000,000 geological map of France [BRGM, 2003].

which have the same direction as the sinistral Sillon Houiller fault zone.

These fault directions, deduced from the interpretation of seismic lines, are generally compatible with anomalies and structural directions deduced from aeromagnetic and gravimetric data recently acquired and reprocessed in the

area (including the N055-trending faults; Martelet *et al.* [2013]). These aeromagnetic and gravimetric trends are thought to occur at deeper depths than the SPB story, suggesting a strong coupling between the structural style of the deeper basement and the late Carboniferous-Permian synsedimentary faults (structural inheritance).

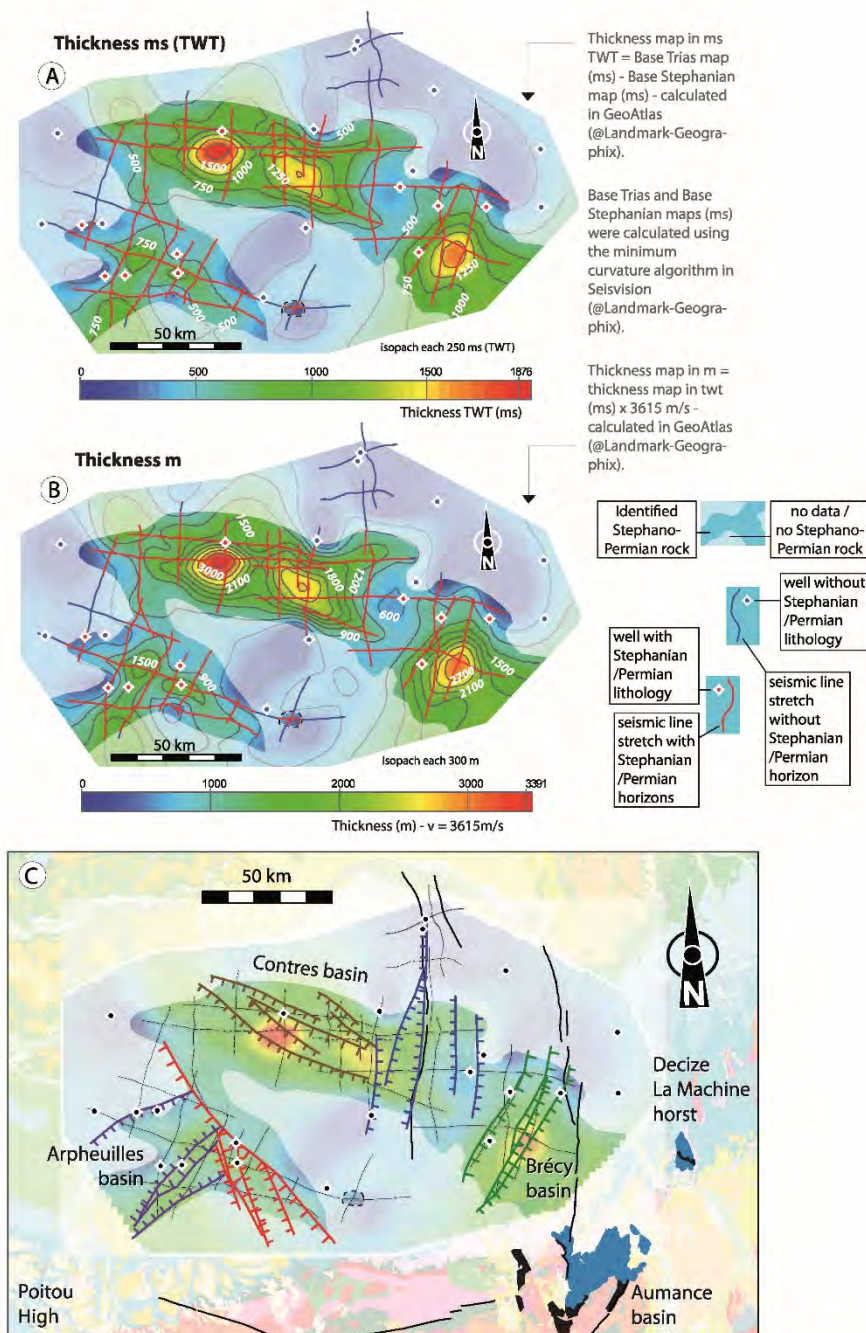


FIG. 10. – Thickness maps of the SBPs. A: thickness map in ms TWT (TWT: two-way-traveltime). B: thickness map in m. C: Synthesis map with the TWT-thicknesses (without the contour lines), the structural scheme and the location of the seismic lines; the Poitou high, the Aumance basin, the Decize-La Machine horst, and the wells reaching the pre-Mesozoic basement are indicated. The geological background is from the 1:1,000,000 geological map of France [BRGM, 2003]. Refer to figure 2 for a comparison with earlier studies.

Thickness maps – Location of the basins

Two simple thickness maps have been calculated for the whole Stephano-Permian sedimentary filling (fig. 10). (1) The thickness of the first map is in ms two-way-time (TWT) (fig. 10A); it has been calculated by subtracting the base Stephanian map from the base Trias map (these maps are calculated by interpolation of the corresponding seismic horizons and faults). The thickness map is based only on the seismic data (i.e. the outcrop geological contours have not been used as hanging points). Due to the interpolation processes, the map is hypothetical outside the zone where subsurface data are present. In order to obtain a more realistic map, a mask of the areas both without data and Stephano-Permian rocks has been drawn (fig. 10); by doing so, we get a map indicating the inferred location of the basins. (2) The second thickness map is in meters (fig. 10B). It has been calculated simply by multiplying the TWT-map by a constant velocity of 3615 m/s. This value corresponds to the mean velocity calculated from the velocity survey of the Arpheiltes-1 well (the only well cutting through both the Autunian sequence and reaching the Stephanian sediments); the same mask has been drawn. To help the discussion, a synthetic map including the TWT-thickness/location and geological maps, and also the faults active during the Stephanian-Permian period, has been added (fig. 10C).

Three main basins are clearly identified (to be compared to figure 3). (1) In the northern study area, the Contres basin has an elongated shape striking N115; it can be subdivided into two distinct depocenters, whose thickness may reach more than 3000 m for the westerly subbasin and 2500 for the easterly subbasin. (2) The Brécý basin has

an elongated shape striking N030 and may reach the thickness of 2700 m. (3) The Arpheiltes basin has a more complex array due to the interference between the N140/155 and N055 trending faults; thicknesses are smaller (maximum value around 1500 m).

As expected, the spatial distribution of the three basins fits with the trends of the related faults; however, the maps show that the Stephano-Permian sedimentary filling systematically extends beyond the areas where faults are present, suggesting that the sedimentation processes were also active later on independently of the normal fault activity.

The maximum preserved thicknesses of the basins in the subsurface are systematically greater than those observed at outcrop (Aumance, Decize La Machine, Autun and Blanzy Le Creusot, fig. 4). Similarly, the minimum extent of the subsurface basins is much larger than the neighboring basins at outcrop (fig. 10C). This might be explained by the preservation of the hidden basins from the Meso-Cenozoic regional uplift phases and subsequent erosion. This large volume of preserved sediments should therefore be taken into account in any work on the quantification of the erosion of the Variscan belt.

The three SPB appear to be connected by corridors with lower thickness values of Stephano-Permian deposits; in particular, the transitional zone between the Contres and Brécý basins extends through the N-S-trending fault area. The Brécý basin obviously opens southeastward to the Aumance and Decize La Machine outcrops. The calculated thicknesses suggest that the Contres basin may extend westward to northwestward (with the same strike as the St-Pierre-la-Cour basin, fig. 1). The Arpheiltes basin opens

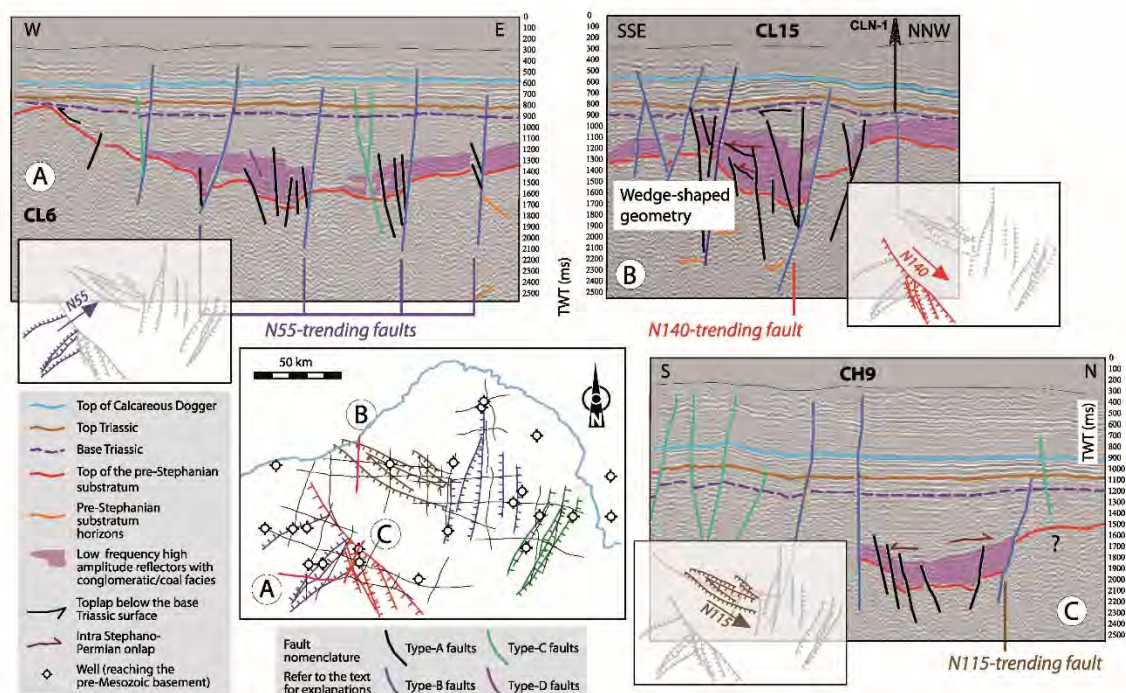


FIG. 11. – Opening of the SPB. A: small basins controlled by N055-trending faults. B: opening of the Arpheiltes basin along a N140-trending fault, with wedge-shaped geometry of the sediments. C: opening of the Contres basin along a N115-trending fault.

southwestwards towards the Poitou High but apparently stops before reaching it (no Stephanian or Permian outcrop is known there).

STRUCTURAL EVOLUTION OF THE SPB IN THE SW PARIS BASIN

The regional spatial and vertical distribution of the basins and related faults is now better understood; we rely on these results to propose a scenario for the structural evolution and sedimentary filling of the SPB based on selected interpreted seismic lines.

Opening of the SPB

Arpheuilles basin

The first indications of a tectonic subsidence and related sedimentation are found in the southwestern part of the study area. There, several very local basins, a few kilometers wide, developed along the N055-trending faults (fig. 11A). In addition to the latter faults, these local depocenters are controlled by smaller, generally antithetic

faults, which cut through the top of the pre-Stephanian substratum. The small basins are filled with coarse conglomeratic sediments, as illustrated by the occurrence of the low-frequency/high-amplitude reflectors with conglomeratic/coal facies. In the Arpheuilles area, the major subsidence phase is related to the normal activity of the N140/155-trending faults, which took over from the N055-trending faults. The syn-extensional tectonic activity results in the wedge-shaped geometry of the conglomeratic facies and related internal onlaps (fig. 11B, see also fig. 15). Additional antithetic or smaller faults, cutting through the top of the pre-Stephanian substratum, were also active.

Contres basin

The Contres basin displays nearly the same structural and sedimentary pattern as in the Arpheuilles basin. The opening of the basin is controlled by the activity of N115-trending normal faults with the deposition of the conglomeratic/coal facies (fig. 11C; see also lines CH6 and CH14 on fig. 5).

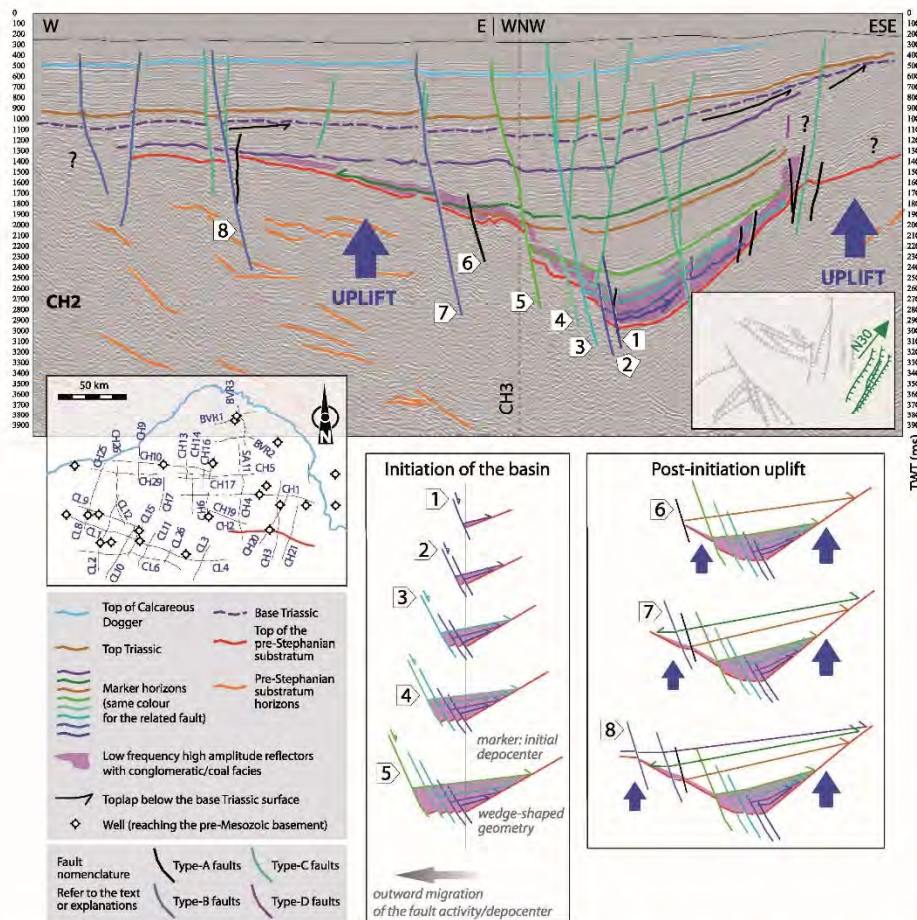


FIG. 12. – Opening of the Brécy basin controlled by N030-trending faults: interpreted seismic profile and diagrams explaining the initiation and post-initiation uplift of the basin (line CH2).

Brécý basin

The line CH2, which cuts the Brécý basin perpendicular to its longitudinal axis, offers the most spectacular image of a SPB (fig. 12; see also line CH3 in fig. 14). There, the opening is controlled by the westward migration of successive active N030-trending normal faults and their related depocenters, onlapping each other (faults 1 to 5 on fig. 12). The syn-tectonic filling consists of the conglomeratic/coal sediments as illustrated by the occurrence of the low frequency-high amplitude reflectors with conglomeratic/coal facies. Their wedge-shaped geometry, although disturbed by the post-opening tectonic activity, is still identifiable.

Post-opening pre-Triassic uplift recorded in the SPB

The interpreted seismic lines do not only allow the initiation of the three SPB and their related sedimentary filling to be observed. They also highlight a significant post-opening tectonic activity and sedimentation.

Contres basin

Seismic line CH6, perpendicular to the main axis of the Contres basin, displays the usual syn-opening conglomeratic seismic facies at the bottom of the Stephano-Permian sedimentary sequence (fig. 13). It also displays toplap geometries of the topmost reflectors below the base Triassic surface, together with a significant tilting and consecutive

truncation of the top of the pre-Stephanian substratum at the southern margin of the basin (fig. 13; see also line CH14 on fig. 5). These observations suggest that the southern margin of the basin was uplifted after the main opening phase, and prior to the deposition of the first Triassic sediments. Moreover, the angle between the toplap geometries of the topmost reflectors and the base Triassic surface decreases toward the top of the sedimentary succession (i.e. with time), indicating that the sedimentation was coeval with the progressive tilting (fig. 13).

Brécý basin

Seismic line CH3, parallel to the main axis of the basin, provides a convenient opportunity to decipher the post-opening tectonic activity coeval with Stephano-Permian sedimentation. In the same way as in the Contres basin, the northern and southern margins of the Brécý basin are uplifted before the arrival of the first Triassic sediments (fig. 14, see also line CH20 on fig. 5). Line CH3 has the advantage of affording a comprehensive view of the downstream sediment flux related to the uplift and consecutive erosion of the basin borders: the successive onlaps are well displayed, together with a pluri-kilometer scale, prograding sediment body, indicating a southward sediment supply. The uplift of the borders of the Brécý basin is also imaged on line CH2, perpendicular to line CH3 (fig. 12). There, the western and eastern borders of the basin are uplifted,

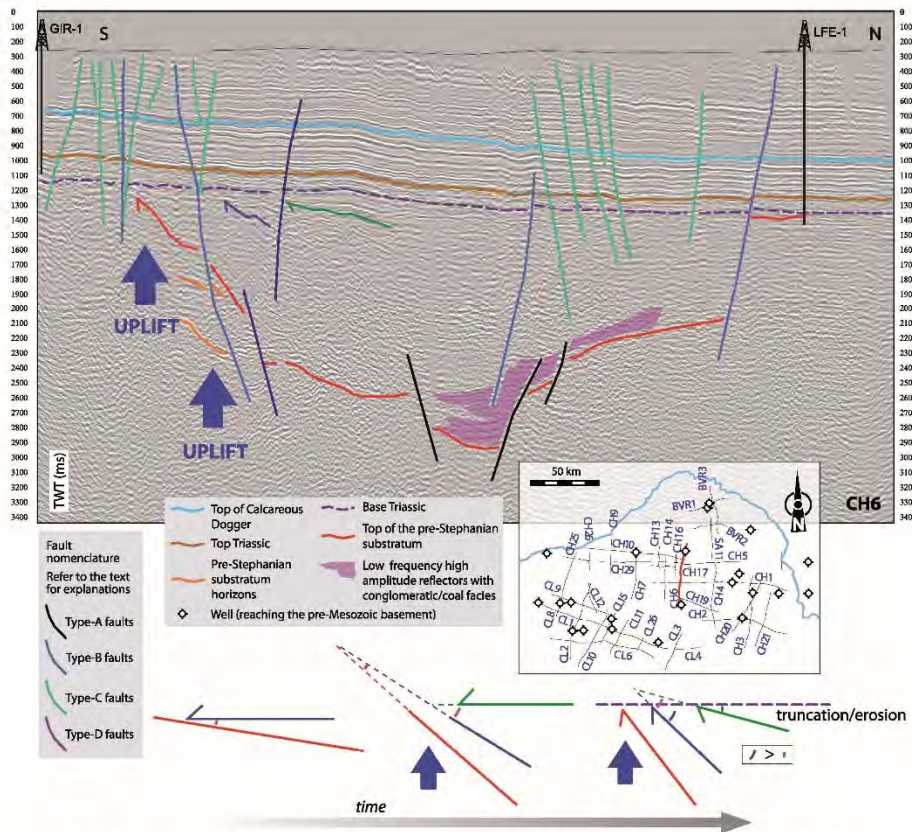


FIG. 13. – Uplift of the margins of the Contres basin: interpreted seismic profile and explanatory diagrams (line CH6).

resulting in the onlap of the resulting sediments. Faults number 6, 7, and 8 are coeval with the uplift of the borders, indicating that the widening basin was coeval with the uplift.

Arpheuilles basin

Seismic lines CL1 and CL4 illustrate a more complex structural situation compared to the examples taken from the Contres and Brécý basins (fig. 15). There, the syn-opening deposits (including the conglomeratic/coal facies with their wedge-shaped geometry and internal onlaps) are folded and uplifted. In detail, the antiformal geometry, visible around the Arpheuilles-1 well on seismic lines CL1 and CL6, is interpreted as the result of the transpressional strike-slip reactivation of N155-trending faults, leading to the development of a positive flower structure several kilometers wide. The uplift triggered the erosion of a significant part of the initial basin, of which an isolated indicator lies about 15 km away, east of the main depocenter; the truncations of the topmost reflectors below the base Triassic surface are still present (toplap geometries). A similar situation, although simpler, is observable on line CL6 (fig. 5). The available data do not allow the temporal relationships between the strike-slip deformation and the uplift to be deciphered.

These results call for several comments.

– The seismic lines do not only record the initial opening of the basins, represented by the conglomeratic/coal facies and wedge-shaped geometries. Indeed, two additional

tectonic phases, succeeding the initial extensional phase, are identified: (i) an uplift phase of the margins – and related sedimentary filling – of the Brécý, Contres and Arpheuilles basins; (ii) a strike-slip phase in the Arpheuilles area (but the temporal relationship with the uplift phase is not clear). The available well data are too sparse and imprecise to ascribe these deformation phases to a given age. However, they do occur after the deposition of the Stephanian conglomeratic seismic facies, and are sealed by the Triassic sediments.

– A direct implication of the above observations is that a significant part of the sedimentary filling of the basins occurs after the initial extensional phase, during the tectonic uplift event. Actually, this second phase contributes more than the first one to the total thickness of sediments (e.g. fig. 13 and 14). The available space is created by the uplift of the borders and the coeval subsidence of the on-going basin.

– The three SPB acquired their “basin shape” geometry (in cross-section) during the uplift phase, which was accompanied by the erosion of their uplifted borders. This final geometry was then sealed by the first Triassic sediments. A direct implication would be that the initial basin area (i.e. before the uplift) may have been larger than what is observed today.

– The uplift of the three basins seems to be partly accommodated by the activity of type-B faults (fig. 12, 13, 14 and 15). However, the observed throws along the fault planes are not great enough to explain the whole uplift,

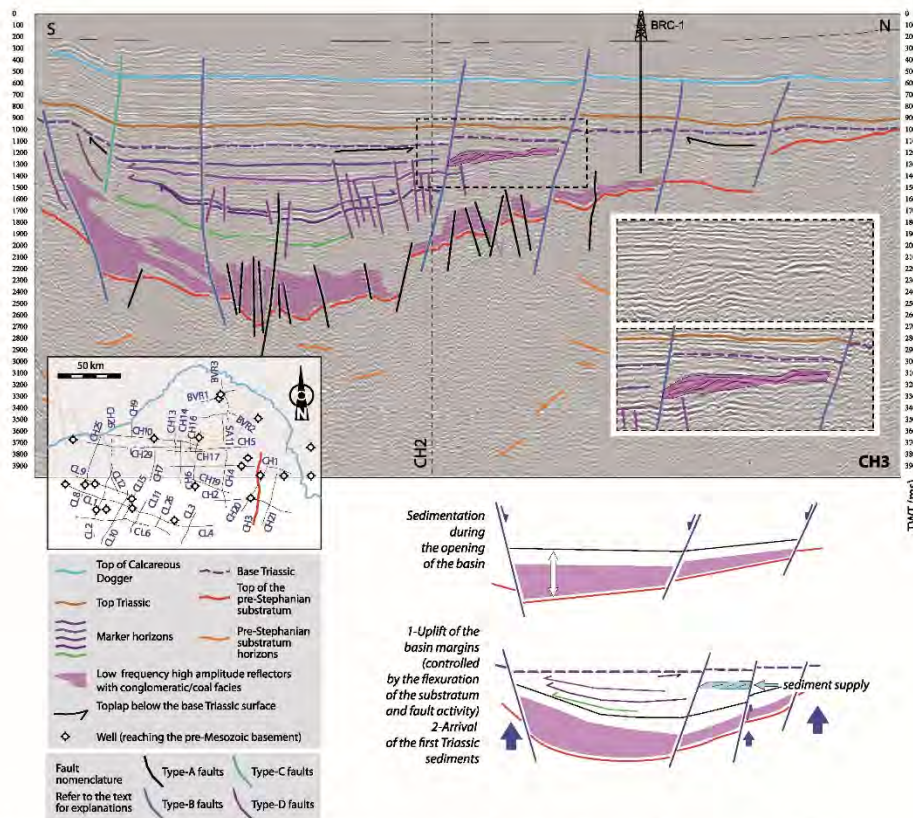


FIG. 14. – Uplift of the margins of the Brécý basin: interpreted seismic profile and explanatory diagrams (line CH3).

implying that the uplift was not only accommodated by such a localized mechanism. One hypothesis is that the uplift might also be accommodated in a more diffuse way by the flexure of the pre-Stephanian basement. The “basin shape” morphology itself – which result from the tilting of the basal surface of basins – supports this interpretation.

This pre-Triassic tectonic activity may be compared to what is recognized in the neighboring outcropping basins. An angular unconformity between Stephanian and Autunian deposits is observed in the Aumance and Autun basins [Bonnion *et al.*, 1983; Vetter, 1986; Paquette and Feys, 1989; Marteau, 1983; Marteau and Feys, 1989]. In the Aumance basin, the Stephanian beds are tilted at about 45° below the Autunian deposits. In the Autun basin, the Stephanian and Autunian facies are clearly unconformable and result from two different structural patterns [Marteau and Feys, 1989]. On the contrary, there is no unconformity

between the two facies in the Blanzy-Montceau-Le-Creusot basin and Decize-La Machine horst [Vallé, 1986; Vallé *et al.*, 1988; Gand, 2003; Feys and Gand, 1983; Courel *et al.*, 1986; Donsimoni, 1990]. However, Stephanian beds are folded and locally inverted in the Le Creusot sub-basin [Feys and Gand, 1983]. These data show that each basin has its own structural dynamics, possibly due to local lithological features or structural inheritance in the pre-Stephanian rocks. In all basins, the Triassic sediments unconformably overlie the Stephano-Permian beds. It is tempting to link these unconformities and deformations to the structural evolution observed in the Contres, Arpheilles and Brécý basins. However, points of comparison are scarce between subsurface and outcropping basins, and surrounding metamorphic and magmatic bodies, particularly regarding their timeframe, and further comparisons would be a matter of conjecture.

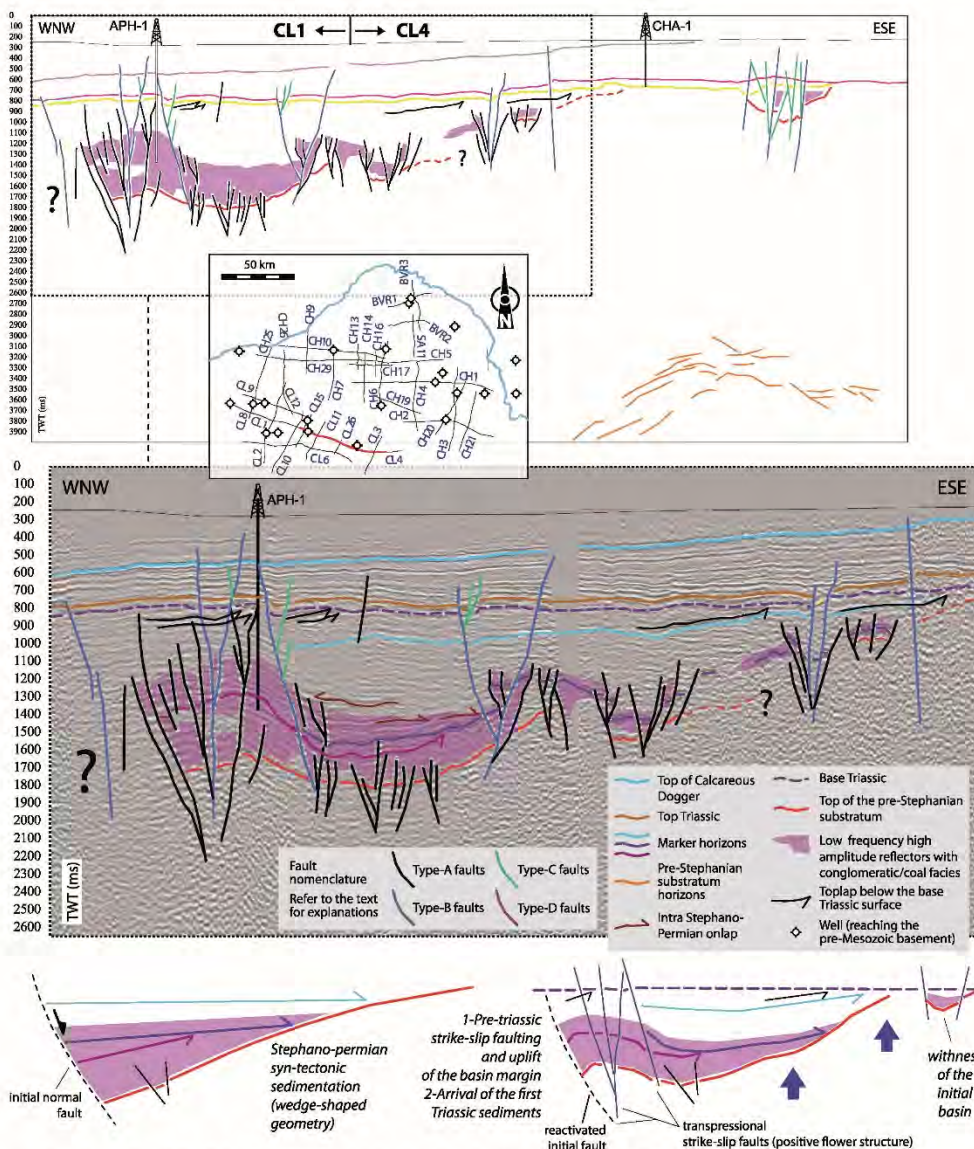


FIG. 15. – Opening, strike-slip and uplift of the margins of the Arpheilles basin: interpreted seismic profile and explanatory diagrams (lines CL1-CL4).

Vertical uplift versus preservation of the SPB in the SW Paris basin

The three basins record and preserve a phase of uplift of their future borders prior to the arrival of the first Triassic sediments (cf. the above section). Indeed, unlike the basins recognized in the field, the hidden SPB were preserved by their Mesozoic sedimentary cover from later Mesozoic-Cenozoic uplift and consecutive erosional processes [Guillocheau *et al.*, 2000; Barbarand *et al.*, 2013].

In addition to the local uplift observed for each basin, we also notice that, at the scale of the whole study area, the total thickness of the Stephanian-Permian sediments is lower on average in the southern part near the Variscan basement of the Massif Central than in the northern part (see Fig. 10). Two main explanations may come to mind: (1) either the SPB were thicker in the northern area than in the southern one prior to the (pre-?)Triassic erosion; the latter was then uniform at the regional scale and did not modify this original pattern; (2) or this regional thickness gradient is related to the occurrence of a late regional uplift and subsequent erosional phase, whatever the initial thickness of the basins (with the southern area uplifted as compared to the northern one). Unfortunately, we do not have convincing arguments allowing us to choose between these two possibilities. In the second hypothesis however, the late erosion of the SPB sediments might be seen as a possible source for the coarse clastic rocks of Early Triassic age, not

present in the study area but occurring farther east [Delmas *et al.*, 2002; Bourquin *et al.*, 2006].

Among the available seismic lines, lines CL6 and CL1-CL4 (Arpheuilles basin) are the most suitable ones to quantify in a simple way the final (total) amount of uplift, due to observation continuity, sufficient extension, and well-imaged uplift (fig. 16). The top of the pre-Stephanian substratum (= base of the Stephanian-Permian filling – conglomeratic/coal facies) is used as a reference marker. We assume that this surface was roughly horizontal at the beginning of the Stephanian-Permian filling over the considered distances. A simple difference between maximum and minimum depths (ms in TWT) reached by this marker yields a value corresponding to its finite vertical uplift. Using the only available velocity ($v=3615$ m/s), the vertical uplift is estimated along line CL6 at about 1300 m, and at about 2000 m along lines CL1-CL4. Unfortunately, there is no way to link this vertical motion to the amount of eroded sediments: no information is available on the lateral thickness variations of the syn-opening deposits prior to the uplift, which prevents us from having a reference thickness to make calculation.

Finally, an important implication of the above results is that they should now be considered when discussing the initiation of the subsidence of the Paris basin. Indeed, the initial thermal anomaly at the origin of the subsidence of the Paris basin is thought to be inherited from the late Carboniferous-Early Permian to post Variscan history [Prijac *et al.*, 2000]. Various mechanisms have been proposed to explain

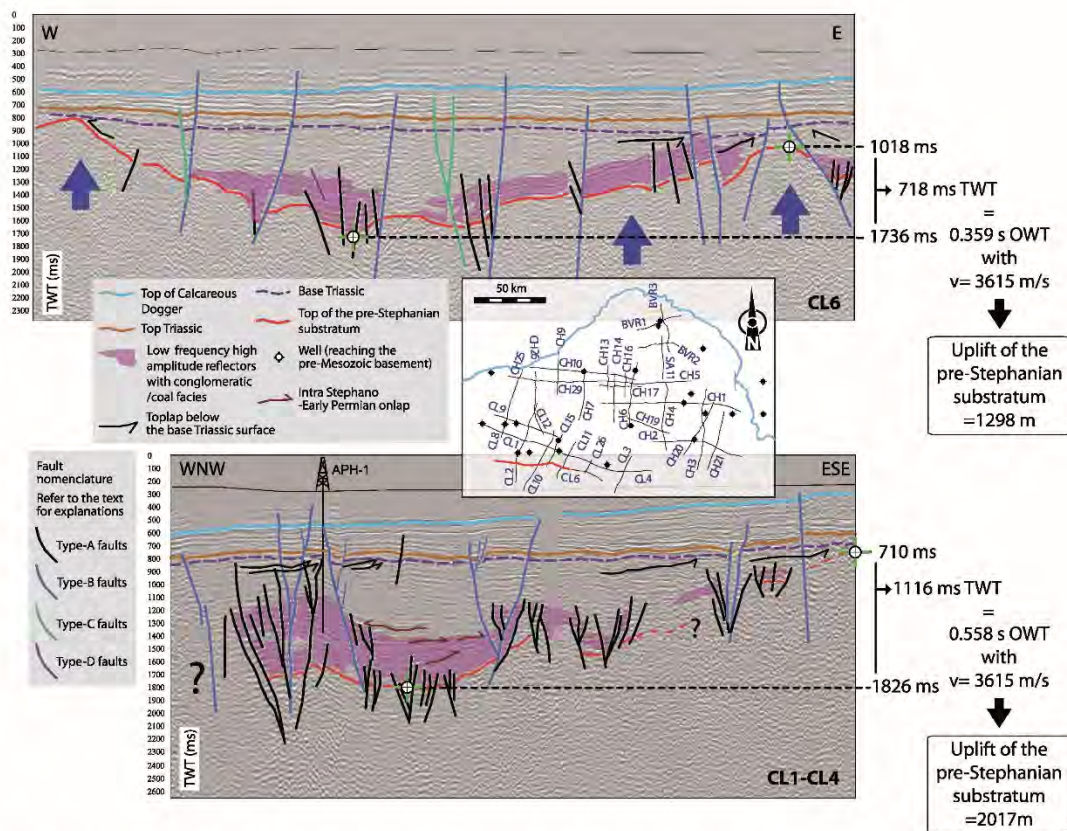


FIG. 16. – Quantification of the uplift of the pre-Stephanian substratum (Arpheuilles basin, line CL6).

this anomaly, such as the extensional post-orogenic Variscan collapse, the delamination of the mantle lithosphere below the Variscan belt, the detachment of the Variscan oceanic slab, or a combination thereof [Burg *et al.*, 1994; Le Solleuz *et al.*, 2004; Lorenz and Nicholls, 1984; Prijac *et al.*, 2000; Ziegler and Stampfli, 2001; Averbuch and Piromallo, 2012]. The pre-Triassic uplift phases, observed at the basin scale and possibly at the regional scale, should now be used as input data in the future post-Variscan to present subsidence scenarios, and confronted with the proposed mechanisms.

SUMMARY AND CONCLUSION

The reprocessing and interpretation of 1476.5 km of seismic lines acquired in the 1980s by the oil industry in the southwestern Paris basin has enabled us to considerably increase our knowledge concerning the Stephano-Permian basins hidden beneath the Meso-Cenozoic sedimentary cover basins (the Arpheuilles, Contres and Brécyc basins). Due to their preservation from further erosional processes, the SPB are larger and thicker than their equivalent at outcrop, giving an undistorted view of the geological reality at the very end of the Variscan orogeny.

For the first time, (1) a comprehensive view of the geometry of these basins has been obtained (well data compilation, interpretation of geological surfaces and internal geometries, specific facies); (2) five directional sets of faults active during the filling of the basins have been identified; (3) thickness maps both in time and in meters, allowing a pseudo-3D view of the three identified, have been calculated; (4) a two-phase formation of these basins (initial opening then uplift of the borders) and related sediment patterns (wedge-shaped geometry, then filling up of the basin), has been determined; and (5) the total vertical amount of vertical uplift prior to the arrival of the first Triassic sediments has also been estimated, with values up to 2000 m.

Taken altogether, previous observations and new results allow us to construct the following Stephano-Permian (pre-Triassic) structural history: (1) initiation of small basins in the Arpheuilles area, controlled by NE-SW faults;

these small basins and related faults are only known in the southwestern part of the study area; (2) strong structural control (normal faulting with certainly a strike-slip component) at the initiation of the Arpheuilles, Contres and Brécyc basins, and related syn-tectonic filling represented by the conglomeratic-coal facies; (3) tectonic activity (strike-slip in the Arpheuilles basin, uplift of the borders of the three basins) and related sedimentary filling after the initial extensional phase; possible later regional-scale erosion of the Permian and Stephanian beds prior to the deposition of the first Triassic sediments. Most of the faults were then re-activated during the Meso-Cenozoic period. This study also underlines the lack of available age data, which prevents us from going further in understanding the evolution of the basins and compare it with the outcropping basins.

The Contres, Arpheuilles and Brécyc basins are thus newly described SPB, comparable to those recognized in the field (similar ages and sedimentary facies, structural trends consistent with the regional ones...). However, due to their buried position, their study refines our understanding of their structural evolution and sedimentary record: previously unknown details are revealed, thereby greatly improving our understanding of the regional geological framework, together with our knowledge about this essential period. The resumption of studies on the outcropping basins will subsequently be a necessary step towards validating our findings.

Finally, this work sheds new light on these hidden geological basins and participates in renewing interest for the field and subsurface study of the French SPB. Indeed, these geological objects still have much to teach us about the transition from the Palaeozoic Variscan cycle to the Mesozoic sedimentary cycle – not to mention their industrial applications, which were the initial motivation for studying them.

Acknowledgments. – This work and publication were supported by the BRGM's Public Service division. We are greatly indebted to S. Bourquin and M. Faure for their constructive and thorough reviews, which noticeably improved the original manuscript. We also thank associate editor R. Augier for his positive comments. LB would like to express his thanks to BRGM and academic colleagues for sharing fruitful discussions; friendly thanks to E. Nitsch from the LGRB Freiburg. Seismic interpretation of the top Triassic and top Dogger were performed by F. Lenoir and M. Berger.

References

- AUTRAN A., DEBEGLIA N., DONSIMONTI M., FEYS R. & GREBER C. (1980). – Socle du bassin. In: MEGNIEN C., Ed., Synthèse géologique du bassin de Paris. Stratigraphie et paléogéographie. – *Mémoire BRGM*, **101**, 17-36.
- AVERBUCH O. & PIROMALLO C. (2012). – Is there a remnant Variscan subducted slab in the mantle beneath the Paris basin; implications for the late Variscan lithospheric delamination process and the Paris basin formation. – *Tectonophysics*, **558-559**, 70-83.
- BALLEVRE M., BOSSE V., DUCASSOU C. & PITRA P. (2009). – Palaeozoic history of the Armorican Massif; models for the tectonic evolution of the suture zones. – *Comptes Rendus Geoscience*, **341**, 174-201.
- BARBARAND J. (2003). – Apatite fission-track thermochronology in western Europe: search for weathered/eroded cover rocks on the Hercynian basement (method, results, limitations and perspectives). – *Géologie de la France*, **1**, 91-93.
- BARBARAND J., QUESNEL F. & PAGEL M. (2013). – Lower Paleogene denudation of Upper Cretaceous cover of the Morvan massif and southeastern Paris basin (France) revealed by AFT thermochronology and constrained by stratigraphy and paléosurfaces. – *Tectonophysics*, **608**, 1310-1327.
- BECCALETTO L., HANOT F., SERRANO O. & MARC S. (2011). – Overview of the subsurface structural pattern of the Paris basin (France). Insight from the reprocessing and interpretation of regional seismic lines. – *Marine and Petroleum Geology*, **28**, 861-879.

- BLES J.-L., BONIJOLY D., CASTAING C. & GROS Y. (1989). – Successive post-Variscan stress fields in the French Massif Central and its borders (western European plate); comparison with geodynamic data. – *Tectonophysics*, **169**, 79-111.
- BLUNDELL D.J. (1990). – Relationships between deep crustal structure and sedimentary basins around Britain. In: B. PINET & C. BOIS, Eds, The potential of deep seismic profiling for hydrocarbon exploration. – Technip, Paris, 317-333.
- BOIS C., GABRIEL O. & PINET B. (1991). – Les campagnes sismiques SWAT et WAM, leur réalisation et leur interprétation par une équipe du programme ECORS. – *Mémoires de la Société géologique de France*, **159**, 9-24.
- BOIS C., CAZES M., CHOUKROUNE P., GARIEL O., HIRN A., LE GALL B., LEFORT J.-P., MATTE P. & PINET B. (1994). – Seismic reflection images of the pre-Mesozoic crust in France and adjacent areas. In: J.D. KEEPPÉ, Ed., Pre-Mesozoic geology in France and related areas. – Springer-Verlag, Berlin, 3-48.
- BONIJOLY D. & CASTAING C. (1983). – Fracturation et genèse des bassins stéphanien du Massif central français en régime compressif. – *Annales Société Géologique du Nord*, **CIII**, 187-199.
- BONIJOLY D. & CASTAING C. (1986). – Ouverture et évolution structurale de quelques bassins houillers de directions orthogonales, dans le Massif central français. – *Annales Société Géologique du Nord*, **CVI**, 189-200.
- BONNION S., COUREL L., GELARD J.-P. & PAQUETTE Y. (1983). – L'organisation des dépôts de charbon et de stérile dans le bassin de l'Aumance (Allier) ; tectonique synsédimentaire et syndiagénétique. – *Mémoires Géologiques de l'Université de Dijon*, **8**, 87-97.
- BOUCHOT V., MILESI J.-P., LESCUYER J.-L. & LEDRU P. (1997). – Les minéralisations aurifères de la France dans leur cadre géologique autour de 300 Ma. – *Chronique de la Recherche Minière*, **528**, 13-62 (with map at 1/1,000,000).
- BOUCHOT V., LEDRU P., LEROUGE C., LESCUYER J.-L. & MILESI J.-P. (2005). – Late Variscan mineralizing systems related to orogenic processes: The French Massif Central. – *Ore Geology Reviews*, **27**, 169-197.
- BOURQUIN S., ROBIN C., GUILLOCHEAU F. & GAULIER J.-M. (2002). – Three dimensional accommodation analysis of the Keuper of the Paris basin: discrimination between tectonics, eustasy and sediment supply in the stratigraphic record. – *Marine and Petroleum Geology*, **19**, 469-498.
- BOURQUIN S., PERON S. & DURAND M. (2006). – Lower Triassic sequence stratigraphy of the western part of the Germanic basin (west of Black Forest): fluvial system evolution through time and space. – *Sedimentary Geology*, **186**, 187-211.
- BRGM, ELF, ESSO-REP, SNPA, Eds (1974). – Géologie du Bassin d'Aquitaine.
- BRGM (1989). – Synthèse géologique des bassins permien français. – *Mémoire BRGM*, **128**.
- BRGM (2003). – Carte géologique de la France au 1/1 000 000^{ème}, 6^{ème} édition révisée.
- BROUTIN J., DOUBINGER J., LANGIAUX J. & PRIMEY D. (1986). – Conséquences de la coexistence de flores à caractères stéphanien et autunien dans les bassins limniques d'Europe occidentale. – *Mémoires de la Société géologique de France, Nouvelle Série*, **149**, 15-25.
- BROUTIN J., CHATEAUNEUF J.-J., GALTIER J. & RONCHI A. (1999). – L'Autunien d'Autun reste-t-il une référence pour les dépôts continentaux du Permien inférieur d'Europe? Apport des données paléobotaniques. – *Géologie de la France*, **2**, 17-31.
- BRUGUIER O., BECQ-GIRAUDON J.-F., CLAUER N. & MALUSKI H. (2003). – From late Viséan to Stephanian; pinpointing a two-stage basinal evolution in the Variscan Belt; a case study from the Bosmoreau basin (French Massif Central) and its geodynamic implications. – *International of Earth Sciences*, **92**, 3, 338-347.
- BURG J.-P., BRUN J.-P. & VAN DEN DRIESSCHE J. (1990). – Le Sillon Houiller du Massif Central français; faille de transfert pendant l'aminissement crustal de la chaîne. – *Comptes Rendus de l'Académie des Sciences, Série 2, Mécanique, Physique, Chimie, Sciences de l'Univers, Sciences de La Terre*, **311**, 147-152.
- BURG J.-P., VAN DEN DRIESSCHE J. & BRUN J.-P. (1994). – Syn- to post-thickening extension in the Variscan belt of western Europe: modes and structural consequences. – *Géologie de la France*, **3**, 33-51.
- CHANTRAINE J., LORENZ C., MEGNIEN C., MILLON R. & LIENHARDT M.-J. (1992). – Forage scientifique de Sancerre-Couy (Cher): Synthèse d'études 1986-1992. – *Mémoire du Bureau de Recherches Géologiques et Minières, Géologie Profonde de la France*, **3**, 230 p.
- COHEN K.M., FINNEY S.C., GIBBARD P.L. & FAN J.-X. (2013; updated). – The ICS International Chronostratigraphic Chart. – *Episodes*, **36**, 199-204.
- COSTA S. (1991). – East-West diachronism of the collisional stage in the French Massif Central: implications for the European Variscan orogen. – *Geodinamica Acta*, **5**, 51-58.
- COSTA S. & MALUSKI H. (1988). – Datations par la méthode ³⁹Ar-⁴⁰Ar de matériel magmatique et métamorphique paléozoïque provenant du forage de Couy-Sancerre (Cher, France). Programme G.P.F. – *Compte Rendu Académie des Sciences*, Paris, **306**, II, 351-356
- COSTA S. & REY P. (1995). – Lower crustal rejuvenation and growth during post-thickening collapse: Insights from a crustal cross section through a Variscan metamorphic core complex. – *Geology*, **23**, 905-908.
- COUREL L., DONSIMONI M. & MERCIER D. (1986). – La place du charbon dans la dynamique des systèmes houillers intramontagneux. – *Mémoires de la Société géologique de France*, **149**, 37-50.
- DEBEGLIA N. (1980). – Carte du socle écorché anté-triasique. In: MEGNIEN C., Ed., Synthèse géologique du bassin de Paris. Atlas. – *Mémoire BRGM*, **102**.
- DEBRAND-PASSARD S., COURBOULEIX S. & LIENHARDT M.-J. (1984). – Synthèse géologique du Sud-Est de la France. – *Mémoire BRGM*, **125**, 615.
- DELMAS J., HOUEL P. & VIALLY R. (2002). – Paris Basin, Petroleum potential. – IFP regional report.
- DILL H., TESCHNER M. & WEHNER H. (1991). – Geochemistry and lithofacies of Permo-Carboniferous rocks from the southwestern edge of the Bohemian massif (Germany). A contribution to facies analysis of continental anoxic environments. – *International Journal of Coal Geology*, **18**, 251-291.
- DOBLAS M., OYARZUN R., LOPEZ-RUIZ J., CEBRIA J. M., YOUBI N., MAHECHA V., LAGO M., POCIVI A. & CABANIS B. (1998). – Permo-Carboniferous volcanism in Europe and northwest Africa: a superplume exhaust valve on the centre of Pangea? – *Journal of African Earth Sciences*, **26**, 1, 89-99.
- DONSIMONI M. (1990). – Le gisement de charbon de Lucenay-lès-Aix (Nièvre). – *Documents du BRGM*, **179**, 84 p.
- DONSIMONI M., FEYS R. & GREBER C. (1980). – Bassins carbonifères. In: Synthèse géologique du bassin de Paris, stratigraphie et paléogéographie. – *Mémoires BRGM*, **101**, 24-25.
- DURAND M. (2014). – Le bassin permien de Saint-Dié-Villé (Lorraine-Alsace) et sa couverture gréseuse triasique. – *Bulletin Information Géologie Bassin de Paris*, **51**, 3, 3-24.
- ECHTLER H.P. & CHAUVET A. (1992). – Carboniferous convergence and subsequent crustal extension in the southern Schwarzwald (SW Germany). – *Geodinamica Acta*, **5**, 37-49.
- ECHTLER H. & MALAVIEILLE J. (1990). – Extensional tectonics, basement uplift and Stephano-Permian collapse basin in a late Variscan metamorphic core complex (Montagne Noire, southern Massif Central). – *Tectonophysics*, **177**, 125-138.
- EDEL J.B. (2008). – Structure et nature du socle anté-permien du bassin de Paris d'après les données gravimétriques et magnétiques ; le problème de l'anomalie magnétique du bassin de Paris (AMBP). – *Géochronique*, **105**, 31-37.
- FAURE M. (1995). – Late orogenic Carboniferous extensions in the Variscan French Massif Central. – *Tectonics*, **14**, 132-153.
- FAURE M. & BECQ-GIRAUDON J.-F. (1993). – Sur la succession des épisodes extensifs au cours du désépaissement carbonifère du Massif central français. – *Compte Rendu Académie des Sciences*, Paris, **316**, 967-973.
- FAURE M., PROST A.E. & LASNE E. (1990). – Déformation ductile extensive d'âge namuro-westphalien dans le plateau d'Aigurande, Massif central français. Extensional ductile deformation of Namurian-Westphalian age in the Aigurande plateau, French Central Massif. – *Bulletin de la Société géologique de France*, **6**, 189-197.
- FEYS R. & GAND G. (1983). – Gisement houiller du Creusot ; une tectonique de serrage dans le sillon permo-houiller de Blanzay Creusot. – *Géologie de la France*, **1-2**, 97-122.

- GAND G. (2003). – Le bassin permien de Blanzay-Le Creusot et ses bordures carbonifères. – *Bulletin information des Géologues du bassin de Paris*, **40**, 3, 4-19.
- GELARD J.-P., CASTAING C., BONJOLY D. & GROLIER J. (1986). – Structure et dynamique de quelques houillers limniques du Massif central. – *Mémoires de la Société géologique de France, Nouvelle Série*, **149**, 57-72.
- GENNA A. & DEBRIETTE P.-J. (1994). – Structures en fleur dans le bassin houiller d'Ales ; implications structurales. – *Comptes Rendus de l'Académie des Sciences, Série II Sciences de la Terre et des Planètes*, **318**, 977-984.
- GERARD A. (1971). – Apports de la gravimétrie à la connaissance de la tectonique profonde du bassin de Paris. – *Bulletin du Bureau de Recherches Géologiques et Minières Section 1: Géologie de la France*, **2**, 75-87.
- GOGUEL J. (1954). – Levé gravimétrique détaillé du Bassin parisien. – *Bur. Recherches Géologiques Géophysiques et Minières*, **15**.
- GRANGEON M., FEYS R. & GREBER CH. (1968). – Géologie profonde de la région de Decize (Nièvre). – *Bulletin du BRGM*, **2**, 1, 1, 66 p.
- GREBER C. (1980). – Bassins permien. In: Synthèse géologique du bassin de Paris, stratigraphie et paléogéographie. – *Mémoires du BRGM*, **101**, 22-24.
- GUILLOCHEAU F., ROBIN C., ALLEMAND P., BOURQUIN S., BRAULT N., DROMART G., FRIEDENBERG R., GARCIA J., GAULIER J., GAUMET F., GROSDOY B., HANOT F., LE STRAT P., MÉTTRAUX M., NALPAS T., PRIJAC C., RIGOLLET C., SERRANO O. & GRANDJEAN G. (2000). – Meso-Cenozoic geodynamic evolution of the Paris Basin; 3D stratigraphic constraints. – *Geodynamica Acta*, **13**, 189-245.
- HÉRITIER F. & VILLEMEN J. (1971). – Mise en évidence de la tectonique profonde du bassin de Paris par l'exploration pétrolière. Evidence of deep tectonics in the Paris Basin from petroleum exploration. – *Bulletin du Bureau de Recherches Géologiques et Minières Section 1: Géologie de la France*, **2**, 11-30.
- KORSCH R. & SCHÄFER A. (1995). – The Permo-Carboniferous Saar-Nahe Basin, South-West Germany and Northeast France – Basin formation and deformation in a strike-slip regime. – *Geologische Rundschau*, **84**, 2, 293-318.
- LEBRETON M.-L. (1990). – Les bassins stéphano-permiens du sud du bassin de Paris: contrôle structural et sédimentologie. – Thèse de doctorat, Orsay, 155p.
- LENOIR F., GUILLOCHEAU F., ROBIN C., LASSEUR E., SERRANO O. & BECCALETTO L. (2014). – Seismic study of the Jurassic deformation and sedimentation of the southwestern Paris basin: a low subsiding domain transition to the Aquitaine basin. – *Bulletin de la Société géologique de France*, **185**, 3, 191-204.
- LE SOLLEUZ A., DOIN M.-P., ROBIN C. & GUILLOCHEAU F. (2004). – From a mountain belt collapse to a sedimentary basin development; 2-D thermal model based on inversion of stratigraphic data in the Paris basin. – *Tectonophysics*, **386**, 1-27.
- LIENHARDT M. (1961). – Etude stratigraphique, pétrographique et structurale du socle anté permien du bassin de Paris. – *Annales de la Société Géologique du Nord*, **81**, Part 3, 233-241.
- LORENZ V. & NICHOLLS I.A. (1976). – The Permo-Carboniferous basin and range province of Europe; an application of plate tectonics. – *NATO Advanced Study Institutes Series Series C: Mathematical and Physical Sciences*, **22**, 313-342.
- LORENZ V. & NICHOLLS I.A. (1984). – Plate and intraplate processes of Hercynian Europe during the late Paleozoic. – *Tectonophysics*, **107**, 25-56.
- MALAVIEILLE J. (1993). – Late orogenic extension in mountain belts; insights from the basin and range and the late Paleozoic Variscan belt. – *Tectonics*, **12**, 1115-1130.
- MALAVIEILLE J. (2010). – Impact of erosion, sedimentation, and structural heritage on the structure and kinematics of orogenic wedges: Analog models and case studies. – *GSA Today*, **20**, 1, 4-10.
- MALAVIEILLE J., GUIHOT P., COSTA S., LARDEAUX J.-M. & GARDIEN V. (1990). – Collapse of the thickened Variscan crust in the French Massif Central; Mont Pilat extensional shear zone and St. Etienne Late Carboniferous basin; Terranes in the Variscan belt of Europe and Circum-Atlantic Paleozoic orogens. – *Tectonophysics*, **177**, 139-149.
- MARTEAU P. (1983). – Le bassin permo-carbonifère d'Autun; Stratigraphie, sédimentologie et aspects structuraux. – *Documents B.R.G.M.*, **64**.
- MARTEAU P. & FEYS R. (1989). – Le bassin d'Autun. In: Synthèse géologique des bassins permien français. – *Mémoire du BRGM*, **128**, 65-71.
- MARTELET G., PERRIN J., TRUFFERT C. & DEPARIS J. (2013). – Fast mapping of magnetic basement depth, structure and nature using aeromagnetic and gravity data: combined methods and their application on the Paris basin. – *Geophysical prospecting*, **61**, 4, 857-873.
- MASCLE A. (1990). – Géologie pétrolière des bassins permien français ; Comparaison avec les bassins permien du Nord de l'Europe. Petroleum geology of French Permian basins; comparison with the Permian basins of northern Europe; Potential économique des bassins permien français. Economic potential of French Permian basins. – *Chronique de la Recherche Minière*, **499**, 69-86.
- MATTE P. & HIRN A. (1988). – Seismic signature and tectonic cross section of the Variscan crust in western France. – *Tectonics*, **7**, 141-155.
- MENARD G. & MOLNAR P. (1988). – Collapse of a Hercynian Tibetan plateau into a late Palaeozoic European basin and range province. – *Nature (London)*, **334**, 235-237.
- MENNING M., WEYER D., DROZDZEWSKI G., VAN AMEROM H.W.J. & WENDT I. (1999). – A Carboniferous time scale 2000; discussion and use of geological parameters as time indicators from Central and Western Europe. – *Geologisches Jahrbuch.Reihe A: Allgemeine Und Regionale Geologie BR Deutschland Und Nachbargebiete, Tektonik, Stratigraphie, Palaeontologie*, **156**, 3-44.
- PAQUETTE Y. & FEYS R. (1989). – Le bassin de Bourbon l'Archambault. In: Synthèse géologique des bassins permien français. – *Mémoires du BRGM*, **128**, 43-54.
- PERRODON A. & ZABEK J. (1990). – Paris basin; Interior cratonic basins. – *AAPG Memoir*, **51**, 633-679.
- PEYAUD J.-B., BARBARAND J., CARTER A. & PAGEL M. (2005). – Mid-Cretaceous uplift and erosion on the northern margin of the Ligurian Tethys deduced from thermal history reconstruction. – *International Journal of Earth Sciences*, **94**, 3, 462-474.
- PRAEG D. (2004). – Diachronous Variscan late-orogenic collapse as a response to multiple detachments; a view from the internides in France to the foreland in the Irish Sea. – *Geological Society Special Publications*, **223**, 89-138.
- POCHAT S. & VAN DEN DRIESSCHE J. (2011). – Filling sequence in Late Paleozoic continental basins: A chimera of climate change? A new light shed given by the Graissessac-Lodève basin (SE France). – *Palaeogeography, Palaeoclimatology, Palaeoecology*, **302**, 170-186.
- PRIJAC C., DOIN M.-P., GAULIER J.-M. & GUILLOCHEAU F. (2000). – Subsidence of the Paris basin and its bearing on the late Variscan lithosphere evolution; a comparison between plate and CHABLIS models. – *Tectonophysics*, **323**, 1-38.
- REY P., BURG J.-P. & CARON J.-M. (1991). – Tectonique extensive ductile et plutonisme viséo-namurien dans les Vosges. – *Comptes Rendus de l'Académie des Sciences, Série 2, Mécanique, Physique, Chimie, Sciences de l'Univers, Sciences de la Terre*, **312**, 1609-1616.
- ROGER J., GAUDRY F., MARTEAU P., QUESNEL F., CHEVREMENT P. & JAUFFRET D. (2010). – Notice explicative, Carte géol. France (1/50 000), feuille Decize (549). – Orléans, BRGM, 185 p.
- ROLIN P., MARQUER D., COLCHEN M., CARTANNAZ C., COCHERIE A., THIERY V., QUENARDEL J. & ROSSI P. (2009). – Famenco-Carboniferous (370-320 Ma) strike slip tectonics monitored by syn-kinematic plutons in the French Variscan belt (Massif Armoricain and French Massif Central). – *Bulletin de la Société géologique de France*, **180**, 231-246.
- SAPIN S. (1967). – Principaux résultats géologiques des travaux d'exploration réalisés par la Société Nationale des Pétroles d'Aquitaine dans le sud-ouest du bassin de Paris. – *Bulletin de la Société géologique de France*, **9**, 327-354.
- TIMMERMAN M.J. (2004). – Timing, geodynamic setting and character of Permo-Carboniferous magmatism in the foreland of the Variscan orogen, NW Europe. – *Geological Society Special Publications*, **223**, 41-74.
- TURRILLOT P., AUGIER R., MONIE P. & FAURE M. (2011). – Late orogenic exhumation of the Variscan high-grade units (South Armorican domain, western France), combined structural and ⁴⁰Ar/³⁹Ar constraints. – *Tectonics*, **30**, 5, TC5007.

- VALLE B. (1986). – Evolution structurale du fossé stephano-permien de Blanzky (Massif central, France) depuis la fin du Carbonifère ; implications tectoniques régionales. – *Comptes Rendus de l'Académie des Sciences, Série 2, Mécanique, Physique, Chimie, Sciences de l'Univers, Sciences de la Terre*, **302**, 593-598.
- VALLE B., COUREL L. & GELARD J.-P. (1988). – Les marqueurs de la tectonique synsédimentaire et syndiagénétique dans le bassin stéphanien à régime cisailant de Blanzky-Montceau (Massif central, France). – *Bulletin de la Société géologique de France*, **4**, 529-540.
- VAN DEN DRIESSCHE J. & BRUN J.-P. (1991). – Tectonic evolution of the Montagne Noire (French Massif Central): a model of extensional gneiss dome. – *Geodynamica Acta*, **5**, 85-92.
- VETTER P. (1971). – Le Carbonifère supérieur et le Permien du Massif central. Géologie, géomorphologie et structure profonde du Massif central français. – *Symp. J. Jung, Plein air service*, Cl-Fd, 169-213.
- VETTER P. (1986). – Les formations limniques du Carbonifère supérieur et de l'Autunien en France. – *Mémoires de la Société géologique de France*, **149**, 7-17.
- WEBER C. (1973). – Le socle antétriasique sous la partie sud du bassin de Paris d'après les données géophysiques. – *Bulletin du Bureau de Recherches Géologiques et Minières, Section 2: Géologie Appliquée, Chronique des Mines*, **3**, 219-292.
- ZIEGLER P.A. (1990). – Geological atlas of western and central Europe, 2nd edition. – Shell Internationale Petroleum Maatschappij B.V., The Hague, 239p, 56 enclosures.
- ZIEGLER P.A. (1992). – Plate tectonics, plate moving mechanisms and rifting. – *Tectonophysics*, **215**, 9-34.
- ZIEGLER P.A. & STAMPELLI G.M. (2001). – Late Palaeozoic-Early Mesozoic plate boundary reorganisation: collapse of the Variscan orogen and opening of Neotethys. – "Natura Bresciana" *Annuario Del Museo Di Scienze Naturali Di Brescia*, **25**, 17-34.

3.6.5. Le bassin de Decize-La Machine / Lucenay-lès-Aix

Contexte géologique

À l'ouest du Morvan, la série sédimentaire du horst de Decize-La Machine (Figure 23), d'une superficie d'environ 50 km², est composée de grès grossiers, de conglomérats polygéniques, de schistes à intercalations de grès et d'argilites noires (Roger et al., 2010) ; de rares passées carbonatées (microbialites) des veines de charbon et de rares tonsteins (i.e. cinérites) sont intercalés dans la série.

Le bassin a été exploité pour ses ressources en charbon et en pétrole, ce qui a conduit à mener des recherches dans ses environs pour localiser et caractériser des ressources additionnelles (réserves). Il s'avère que ce bassin s'étend en subsurface sous la couverture méso-cénozoïque au nord, jusqu'au horst de Saint-Saulge, et plus largement à l'est, à l'ouest et au sud (vers Lucenay-lès-Aix).

Le bassin de Lucenay-lès-Aix, située à environ 15 km au sud de Decize (Figure 23), a été le dernier à être exploré lors de l'inventaire national français des ressources en charbon mené par le BRGM de 1981 à 1986 (Donsimoni 1990, 2006). Cette campagne d'exploration a commencé par des études gravimétriques, avec une anomalie de Bouguer négative détectée dans la région de Lucenay-lès-Aix, montrant une accumulation de sédiments épais sur le socle varisque. Le bassin est défini comme un demi-graben bordé par une faille syn-sédimentaire orientée N-S contrôlant le dépo-centre principal vers l'est.

Géométrie et reconstitutions paléoenvironnementales du bassin de Decize-La Machine - Publication 5

Mercuzot M., Bourquin S., **Beccaletto L.**, Ducassou C., Rubi R., Pellenard P., (2021) Palaeoenvironmental reconstitutions at the Carboniferous Permian transition south of the Paris Basin, France: implications on the stratigraphic evolution and basin geometry, International Journal of Earth Sciences. <https://doi.org/10.1007/s00531-020-01940-7>

L'évolution spatio-temporelle des paléoenvironnements du secteur de Lucenay-lès-Aix au sud du bassin de Decize-La Machine est totalement réévaluée sur la base de douze forages diagraphiés. Parmi ces forages trois sont carottés permettant un calage faciès-électrofaciès fin essentiel aux corrélations. Les géométries d'ensemble sont calées par l'interprétation de profils sismique haute résolution acquis par le BRGM dans les années 1980 (comme les forages).

Principaux résultats issus de la publication 5

- Le secteur de Lucenay-lès-Aix montre des séries sédimentaires attribuées à des environnements de plaine alluviale, lacustres et deltaïques, sans preuve de d'environnements fluviaux.
- Les interprétations sismiques et les données de forages ont été importées dans un viewer 3D, afin de mieux contraindre les corrélations séquentielles. Sept cycles successifs progradant-rétrogradant sont identifiés et corrélés à l'échelle du bassin, traduits en termes de cartes paléogéographiques du secteur de Lucenay-lès-Aix à la limite Carbonifère-

Permien. Les dépôts, proximaux en base, sont de plus en plus lacustres vers le haut de de série.

- Il apparaît ainsi que (i) les environnements sont de plus en plus lacustres avec le temps (deltas progradants dans le bassin), les faciès les plus proximaux étant de plus en plus rares (cônes alluviaux et charbons) ; (ii) le bassin semble s'ouvrir vers l'est ; (iii) le secteur de Lucenay-lès-Aix est comparable en termes d'environnements de dépôts au bassin de l'Aumance situé quelques dizaines de kilomètres à l'ouest (systèmes lacustres à deltaïques riches en charbon).
- Les limites actuelles du bassin de Decize-La Machine sont érosives, suggérant que ce bassin était bien plus étendu qu'aujourd'hui, englobant celui de l'Aumance et peut-être même les bassins connus plus à l'est (Autun et Blanzay-Le Creusot). Si cela se confirmait, il faudrait totalement réévaluer les taille et l'épaisseur des bassins stéphano-permiens en France et sans doute proposer le même raisonnement pour les bassins similaires en Europe occidentale.

Publication 5

International Journal of Earth Sciences (2021) 110:9–33

<https://doi.org/10.1007/s00531-020-01940-7>

ORIGINAL PAPER



Palaeoenvironmental reconstitutions at the Carboniferous–Permian transition south of the Paris Basin, France: implications on the stratigraphic evolution and basin geometry

Mathilde Mercuzot¹ · Sylvie Bourquin¹ · Laurent Beccaletto² · Céline Ducassou¹ · Romain Rubi³ · Pierre Pellenard⁴

Received: 17 March 2020 / Accepted: 20 September 2020 / Published online: 13 October 2020

© Geologische Vereinigung e.V. (GV) 2020

Abstract

The late Carboniferous-to-Permian coal-bearing Decize-La Machine Basin, and more specifically the Lucenay-lès-Aix area, located south of the Paris Basin, has been investigated to reassess the palaeoenvironmental evolution and the basin architecture. The detailed sedimentological study has been carried out based on core data and digitised old mining data, i.e., seismic profiles and well-logs. An interpretation of well-logs without core data is proposed, based on a palaeoenvironmental interpretation from cores and their respective well-log data, and three depositional environments have been defined: an alluvial plain, an alluvial-fan, and deltaic and lacustrine environments. Correlations between wells have been performed using markers identified in seismic profiles, paired with sequence stratigraphic interpretations from well-log and core data. An evolution in seven major progradational–retrogradational stratigraphic cycles is proposed based on the evolution of the depositional environment observed at the basin scale, leading to a reconstruction of palaeogeographic maps at the Carboniferous–Permian transition. This new viewpoint shows that through time, the deposits, proximal at the base of the succession with coal preservation, become more lacustrine with the delta prograding into the basin. In consequence, the basin evolution shows a general retrogradational trend with increasing lacustrine deposits at the top of the succession eroded by the Permian–Triassic unconformity. Therefore, the current borders of the basin in the Lucenay-lès-Aix area are not representative of those at the time of the sedimentary filling, and thus, this area could be part of a larger one, perhaps encompassing all north-eastern French Massif Central late Carboniferous-to-Permian basins.

Keywords Carboniferous–Permian of Decize-la Machine Basin · Sedimentological analyses · Sequence stratigraphy · Depositional environment · Seismic and well-log data

Introduction

The Carboniferous-to-Permian transition is of great geological interest, because it records large internal and external geodynamic variations of the Earth. This period corresponds to the transition from the end of the Variscan orogen to the

breakup of Pangaea (Scotese and Langford 1995; Stampfli et al. 2013), and to the transition between the Late Palaeozoic Ice Age (LPIA) and the end-Permian-to-Triassic aridification (e.g., Bishop et al. 2010; Bourquin et al. 2011).

The Variscan orogen provides evidence for the collision between the southerly Gondwana and northerly Laurasia; the mountain belt was oriented E–W, and located in the Pangean equatorial-to-intertropical realm during the Carboniferous and Permian. In Europe, it results from the accretion of several microcontinents (e.g., Avalonia and Armorica) and intervening oceanic domains (Matte 1986; Franke et al. 2000; Lardeaux et al. 2001; Ballèvre et al. 2009; Martinez-Catalan et al. 2009), and is evidenced by high-pressure–low-temperature metamorphic rocks formed during subduction and nappe stacking (Paquette et al. 2017; Lotout et al. 2018). Because of the post-orogenic history footprints (collapse of the reliefs, late-orogenic extension,

Mathilde Mercuzot
mathilde.mercuzot@outlook.com

¹ Géosciences Rennes, UMR 6118, Univ Rennes, CNRS, 35000 Rennes, France

² BRGM, 45060 Orléans, France

³ Department of Physical Geography and Quaternary, University of Liège, Liège, Belgium

⁴ Biogéosciences UMR uB/CNRS 6282, Université Bourgogne Franche-Comté, 21000 Dijon, France

and late Alpine tectonics; Faure et al. 1995; Ballèvre et al. 2013), the geodynamic evolution of the Variscan belt is difficult to establish and is therefore not consensual (e.g., Ballèvre et al. 2014; Franke et al. 2017). The post-orogenic collapse of the thick and hot Variscan crust is reflected by high-grade metamorphic domes, detachments, and extensive faults reactivating ancient shear zones (Malavieille et al. 1990; Van Den Driessche and Brun 1992; Burg et al. 1994). Internal Pennsylvanian (i.e., late Carboniferous)-to-Permian European basins, considered as pull-apart or hemi-graben basins, developed in the late-orogenic extensional structural context (Ménard and Molnard 1988; Vallé et al. 1988; Van Den Driessche and Brun 1989, 1992; Burg et al. 1990; Malavieille et al. 1990; Faure and Becq-Giraudon 1993; Faure 1995; Becq-Giraudon et al. 1996; Genna et al. 1998; Choulet et al. 2012).

Paired with this tectonic context, these sedimentary basins could have also recorded the LPIA, marking the transition from a global icehouse to a greenhouse climate during the Permian. This climatic period corresponded to the latest wide-extent and long-lived glaciation on a vegetated Earth (Gastaldo et al. 1996; Michel et al. 2015). The specificity of this period is notably the lowest CO₂ and highest O₂ levels of the Phanerozoic (e.g., Berner 2006; Montanez et al. 2007, 2016), that lasted during dozens of millions of years, from the late Devonian to the Cisuralian–Guadalupian, i.e., early–middle Permian (Fielding et al. 2008). The LPIA witnessed long-lived but discrete ice sheets, diachronous at the scale of Gondwana, migrating eastward from the late Devonian to the early Permian (Isbell et al. 2003; Fielding et al. 2008; López-Gamundí and Buatois 2010; Montanez and Poulsen 2013), with an apex during the Pennsylvanian–Sakmarian.

The latest Variscan tectonic stages combined with the end of the LPIA and the transition to the greenhouse climate, from humid to arid conditions (Isbell et al. 2003; Roscher and Schneider 2006; Bourquin et al. 2011; Michel et al. 2015), are the prevalent driving factors controlling the sedimentary dynamic of Western European Carboniferous-to-Permian basins. This is the case for French intracontinental Carboniferous–Permian basins located south of the Variscan front, in the internal zones of the mountain belt, which result from late- to post-orogenic extensional processes (Malavieille et al. 1990; Costa and Rey 1995; Faure 1995; McCann et al. 2006), and record a period of destruction of the Variscan reliefs. Some of these sedimentary basins are located south of the Paris Basin, mainly known through subsurface and mining data, such as the Decize-La Machine Basin. For this basin, sediments partly crop out at the Decize-La Machine horst, but its western, eastern, and southern terminations are located under the Meso-Cenozoic sedimentary cover. The area of Lucenay-lès-Aix, located south of the Decize-La Machine horst (Fig. 1), has been

exploited since 1806. The latest investigations performed in the twentieth century and up to 1986 for the mining industry, aimed to characterise the coal resources in the subsurface. Old mining reports indicate a succession of fine and coarse-grained deposits attributed to lacustrine and fluvio-lacustrine sediments, in which coal seams are interbedded. The occurrence of altered volcanic ash layers (i.e., tonsteins) and microbial deposits have been documented and tentatively used to propose intrabasin correlations (Donsimoni 1990).

Here, we aim to reassess the sedimentary architecture and the palaeoenvironmental evolution in this area, based on updated data and methods. Stratigraphical and sedimentological re-evaluations are based on the investigation of three cored boreholes from the Lucenay area, well-logs, and seismic data acquired during the 1980s. The palaeoenvironmental evolution through time is assessed through facies and facies association determination using cores analysis and electrofacies characterisation on well-logs. Supported by seismic interpretation, stratigraphic correlations between the wells are performed in the Lucenay-lès-Aix area, highlighting the sedimentary architecture of the Decize-La Machine Basin. These results are then compared with data from adjacent areas, to document the basin geometry and environments throughout time and space and to better constrain the Carboniferous-to-Permian evolution of the internal zone of the Variscan orogen.

Geological setting

French late Carboniferous-to-Permian basins cropping out south of the Paris Basin

French Carboniferous-to-Permian basins are localised around the remnants of the Variscan belt, such as the Vosges, Alps, Pyrenees, Armorican Massif, and Massif Central (Fig. 1a), but are also known in the subsurface below the Aquitaine Basin and South-East Basin, and below the Meso-Cenozoic cover of the Paris Basin, to the south (Beccaletto et al. 2015) and to the north-east (Donsimoni 1981). In the north-eastern part of the Massif Central, several basins are exposed (the Aumance, Autun, Decize-La Machine, and Blanzay-Le Creusot basins, Fig. 1b) and, for some of them, may constitute the termination of the subsurface basins south of the Paris Basin (Beccaletto et al. 2015). Numerous lithological and palaeontological analyses were performed on these late Carboniferous-to-early Permian basins, which were investigated during the nineteenth and twentieth centuries for coal and oil mining. The sedimentary succession in these basins is attributed to the late Pennsylvanian–early Permian (i.e., upper Westphalian, Stephanian A, B, and C, Autunian and Saxonian regional sub-stages; Heckel and Clayton 2006; Menning et al. 2006; Schneider et al. 2020).

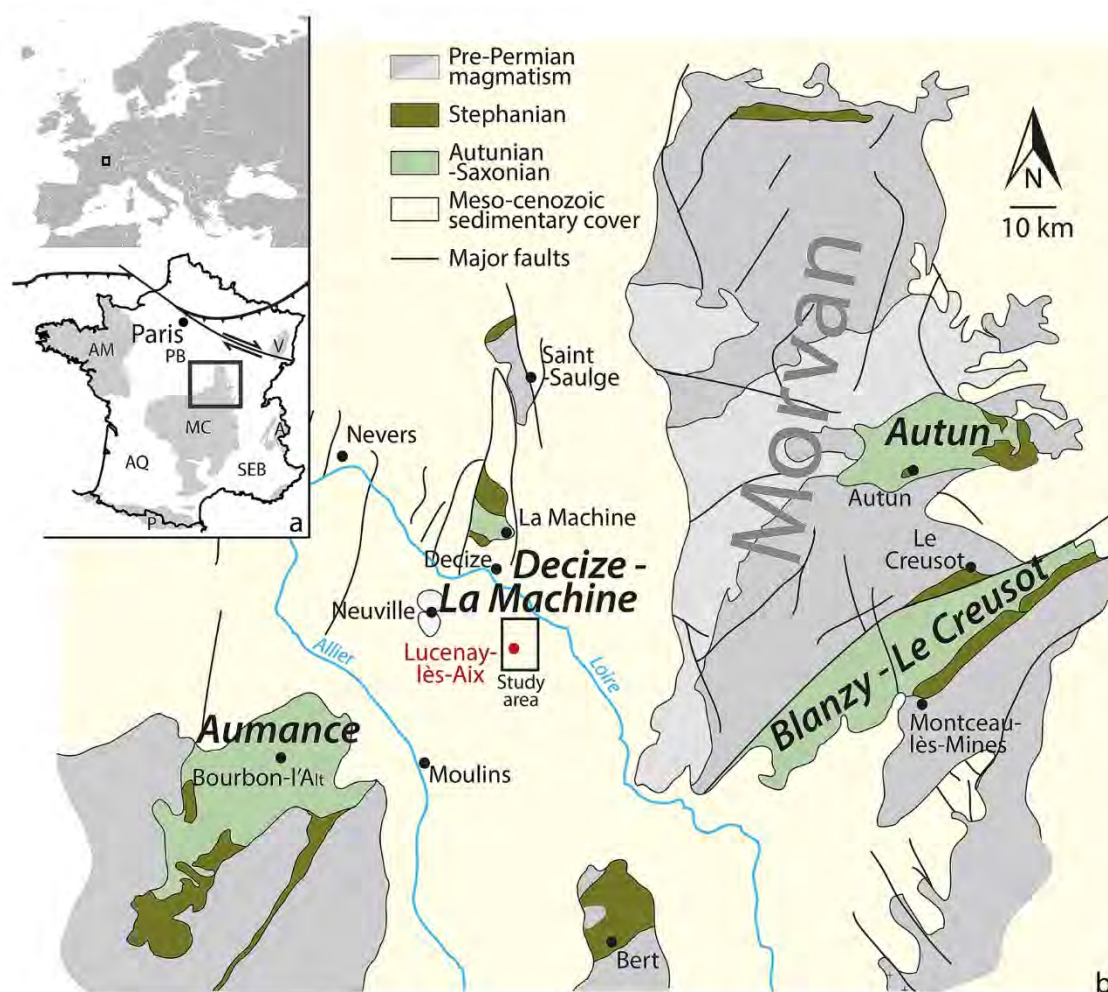


Fig. 1 Localisation of the late Carboniferous-to-Permian basins in the north-eastern Massif Central (modified from Elsass-Damon 1977). The Lucenay-lès-Aix area is located south of the outcropping Decize-

La Machine succession. *AM* Armorican Massif, *MC* Massif Central, *P* Pyrenees, *A* Alps, *V* Vosges, *AB* Aquitaine Basin, *SEB* South-East Basin, *PB* Paris Basin

The Westphalian and Stephanian are often attributed to the late Pennsylvanian, while the Autunian and Saxonian are considered to have a Permian affinity. However, it is difficult to correlate these stratigraphic units to the official marine stages, because their boundaries, defined using macroflora, palynomorphs, and fauna associations, are diachronous (Langiaux 1984; Broutin et al. 1986, 1990, 1999; Doubinger et al. 1979; Schneider et al. 2020). Thus, intra- and inter-basinal stratigraphic correlations based on available biostratigraphy should be cautiously considered due to large uncertainties, even when basins are separated by a short distance, due to depositional environment biases affecting macro- and microflora repartition. However, instantaneous aerial volcanic events are regularly recorded as thin tonstein deposits intercalated in the succession and could be used as correlation tools. In the French Autun and Lodève basins, such altered volcanic ash layers have been recently dated (Michel et al.

2015; Pellenard et al. 2017) by U–Pb on zircon using the chemical abrasion–isotope dilution–thermal ionisation mass spectrometry (CA–ID–TIMS) method. In the Lucenay-lès-Aix area, recent U–Pb ages using laser ablation–inductively coupled plasma–mass spectrometry (LA–ICP–MS) have been also performed by Ducassou et al. (2019), and correlations were then tentatively applied between these three basins. A late Gzhelian-to-early Asselian age could be attributed to the base of the Lucenay-lès-Aix succession (299 ± 2 Ma, Ducassou et al. 2019), which could therefore be correlated with the lower Autunian (Igornay Fm and Muse Fm) defined in the Autun Basin (299.9 ± 0.38 Ma to 298.05 ± 0.19 Ma; Pellenard et al. 2017), and either to a gap in the Lodève Basin (Michel et al. 2015) or to the Graissessac Fm (295.5 ± 5.1 ; Bruguier et al. 2003). The middle of the sedimentary succession from the Lucenay-lès-Aix area yielded a 295 ± 5 Ma age (Ducassou et al. 2019), and could be compared either with

the Tuilières-Loiras Fm and Viala Fm (293.94 ± 0.08 Ma to 290.96 ± 0.19 Ma using CA-ID-TIMS U–Pb dating by Michel et al. 2015) or to the Graissessac Fm (295.5 ± 5.1 ; using SIMS U–Pb dating by Bruguier et al. 2003).

The Decize-La Machine Basin

To the west of the Morvan Massif (Fig. 1), Palaeozoic units crop out near the localities of Saint-Saulges and Neuville (crystalline rocks), and near Decize and La Machine (sedimentary rocks), due to the activity of a post-Permian fault system. The sedimentary succession of the Decize–La Machine horst, covering an area of approximately 50 km^2 , is composed of coarse-grained sandstones, polygenic conglomerates, shales with sandstone intercalations, and black shale deposits, and shows evidence of microbial deposits and the occurrence of coal seams and tonstein layers. These sedimentary successions were exploited for coal and oil resources, leading to research being carried out in the surrounding areas to localise and characterise the amount of the potential resource. This basin extends in the subsurface under the Meso-Cenozoic cover (ca. 60–370 m in thickness) to the north, up to the Saint-Saulge horst, and more extensively to the east, west and south. However, the palaeogeographic boundaries of this basin at the time of sedimentation are not known, and it may have been connected with the Aumance Basin located to the west (Fig. 1b) (Grangeon et al. 1968; Châteauneuf and Farjanel 1989). The sedimentary succession is divided into the upper Westphalian, only found to the south-east, the Stephanian and the Autunian. However, these regional stages are biostratigraphically poorly documented in this area and may thus be only considered as lithostratigraphic units. The Stephanian and Autunian units are in stratigraphic continuity, but the Stephanian sedimentation area is more restricted compared to those of the Autunian which presents a larger extent. This indicates that the depocenters migrate and widen through time. The Triassic deposits unconformably overlie the Permian succession, following a huge erosional event. The cumulative thickness of the Palaeozoic sedimentary succession in this basin is thought to exceed 3000 m.

The Lucenay-lès-Aix area is located approximately 15 km south of Decize (Fig. 1), and is characterised by a relatively flat topography, with a mean altitude close to 220 m, peaking at 236 m. This sub-basin was the latest to be investigated in the Decize-La Machine Basin during the French national coal resource inventory from 1981 to 1986 (Donsimoni 1990, 2006). This exploration campaign began with gravimetric investigations, with a negative Bouguer anomaly detected in the Lucenay-lès-Aix area, showing a thick sedimentary accumulation over the crystalline basement (Donsimoni 1990, 2006). These investigations were completed with electric, seismic, and magnetotelluric surveys

based on rock resistivity, partially cored boreholes, and well-log data (Fig. 2a); 31 km of seismic lines were shot (Fig. 2a). The crystalline basement was not reached by the wells, but was estimated to be at a depth close to 1500 m (Donsimoni 1990). The eastern edge of the sub-basin was not investigated, but may be wider than the studied area. The sedimentary deposits were initially attributed to fluvial, palustrine, and lacustrine environments (Donsimoni 1990) but recently reattributed to deltaic and lacustrine deposits, from the LY-F core, by Ducassou et al. (2019) (Fig. 2a); the lithostratigraphy is defined by the productive La Machine and Lucenay formations, attributed to the Stephanian B and C, and separated by a discontinuity. In these two formations, a substantial amount of coal was evidenced at depths ranging between 200 and 600 m. Above, the more detrital “Grey Autunian” and “Red Permian” formations are assumed to be in stratigraphic continuity (Donsimoni 1990, 2006). The tectonic structure of the Lucenay-lès-Aix area was defined as a hemi-graben geometry, with a syn-sedimentary fault oriented ~N–S, governing the disposition with a thick sedimentary accumulation in the western part of the basin, and limited sedimentary inputs towards the east. The subsidence was thought to be heterogeneous with time throughout this area: high and fast subsidence favoured debris flow deposits, while more moderate and regular subsidence favoured palustrine-to-lacustrine deposits, including coal deposits (Donsimoni 1990).

Material and methods

Sedimentological descriptions (facies and electrofacies)

Among the 37 wells drilled during the exploration campaign of the Lucenay-lès-Aix area during the 1980s, only three cores are still available (property of the BRGM—French Geological Survey): the LY-F, LY-G, and LY-ZB wells (Fig. 2a). The LY-F core has already been investigated and dated by Ducassou et al. (2019) (Fig. 2b). The LY-F, LY-G, and LY-ZB cored boreholes were first described in this study in terms of lithology, sedimentary structure, grain composition and morphology, and colour (i.e., reflecting organic content and oxidation of the sediment). Each bed was then assigned to a sedimentary facies and to a depositional process (Tables 1 and 3). Finally, facies were associated to characterise the depositional environments along a depositional profile (facies associations, Table 2).

For the wells without core information, an electrofacies analysis from well-log data is necessary. Well-log data are used to calibrate electrofacies with sedimentary facies (e.g., Bourquin and Guillocheau 1996; Bourquin et al. 1998), but because only old well-log data are available in the

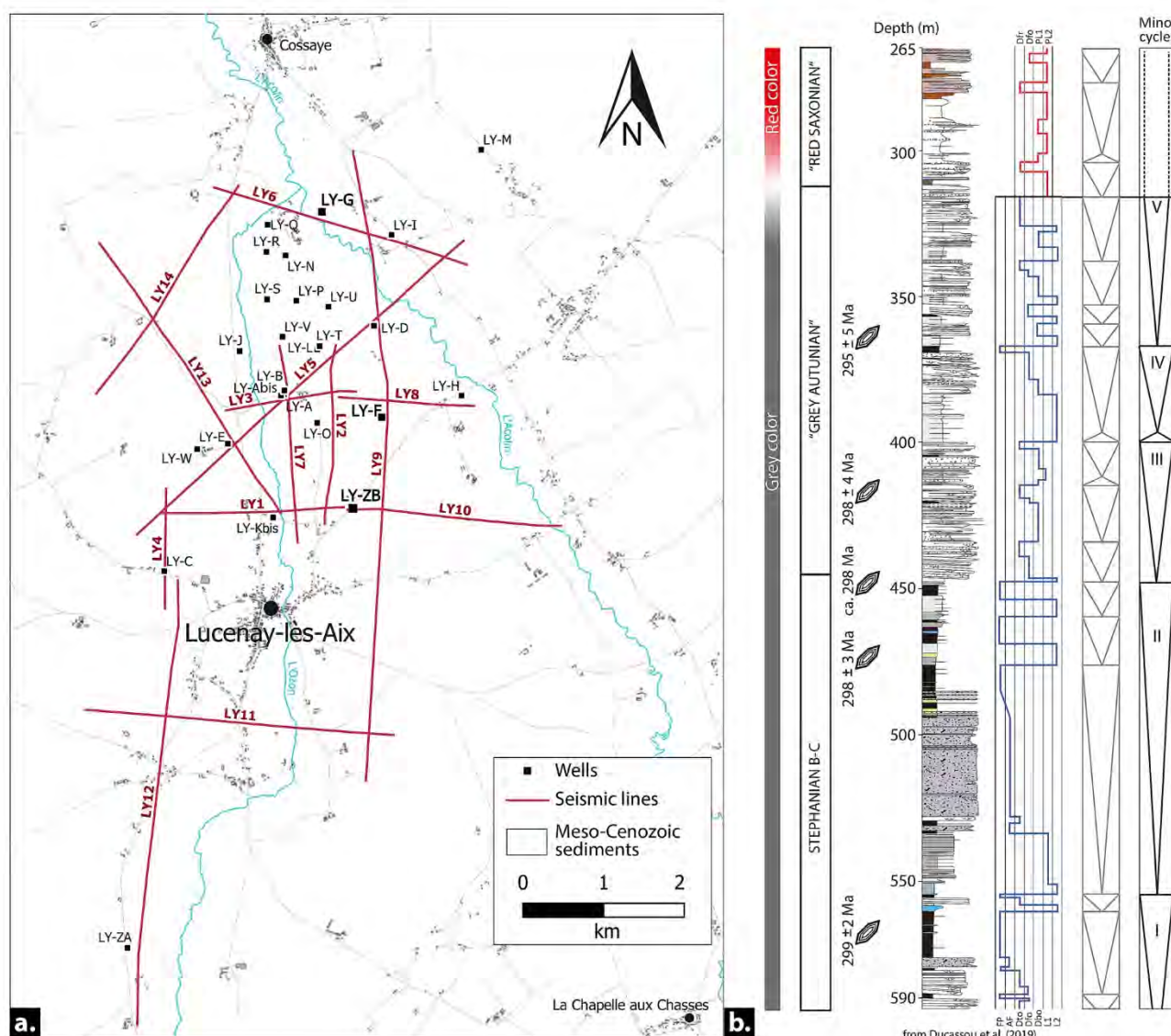


Fig. 2 **a** Map of the Lucenay-lès-Aix area, showing the location of the studied wells and the seismic lines. **b** Synthetic sedimentary column, depositional environments evolution, and stratigraphic cycles of

the LY-F core after Ducassou et al. (2019). *FP* floodplain, *AF* alluvial-fan delta, *Dfr* delta frontset, *Dfo* delta foreset, *Dbo* delta bottomset, *L* lake, *PL* playa lake

Lucenay-lès-Aix area, a precise facies/electrofacies characterisation is not possible. The depositional environments have been identified from the well-log data on the basis of (1) the former sedimentological descriptions of the cored boreholes of the Lucenay-lès-Aix area, performed during the 1980s, and (2) a comparison with the new descriptions of the LY-F, LY-G, and LY-ZB cored boreholes.

Sequence stratigraphy

Bathymetry curves were built based on the depositional environment evolution established for the three cored boreholes. Each stratigraphic surface was identified through

facies analysis, and used to propose a high-resolution sequence stratigraphy model, which depends, in continental environments, on the fluctuations of the stratigraphic base level (surface below which sediments accumulate and above which erosion takes place, i.e., accommodation combined with sediment supply; e.g., Bourquin et al. (2009) and references therein). In a general way, these base-level fluctuations are displayed as (1) periods of aggradation of the alluvial system (stratigraphic base-level rise, i.e., increasing accommodation space and/or decreasing sediment supply) and (2) periods of stacking of the fluvial system with erosion, by pass and/or palaeosol development (stratigraphic base-level fall, i.e., decreasing accommodation space and/

Table 1 Facies description and interpretation of the depositional processes of the different studied wells, based on facies descriptions of Ducassou et al. (2019)

Name	Lithology	Sedimentary structures	Depositional process interpretation
Fine-grained lithologies			
F (Table 3b,c)	Clay to silt Bed thickness: cm to dm	Massive Planar or inclined bed (iF, Table 3h)	Deposition from suspension or from low-density tail of turbidity current and settling of pelagic or hemipelagic particles; Te (settling of clays, Bouma 1962)
Ftc (Table 3a)	Heterolithic Clay to silt to very fine-grained sand, beds of fine to medium-grained sand exceptionally coarse-grained Sometimes: - Coal and plant fragments - Thin bed (cm) of carbonate - Bioturbation Bed thickness: cm to m	Thinly laminated in mm to cm beds, sandstone beds are either massive or contain planar lamination/current ripples or trough cross stratifications	Deposition from suspension alternating with tractive current, low-density turbidity current (Lowc 1982), or shear sorting of grains and floes Td (finely laminated Bouma 1962)
Sandstones and conglomerates			
SI (Table 3d,e)	Fine-to-medium-grained sand Well-sorted Bed thickness: cm to dm	Laminated (planar bedding) with sometimes symmetric ripples at top Normal grading Sometimes lenticular beds Erosive base	Tractive current, sometimes reworked by wave influences or Tb (laminated), Te (ripples) (Bouma 1962)
GSm (Table 3j)	Poorly sorted, disorganized, ungraded conglomerates Mostly clast-supported Poorly sorted matrix composed of almost all finer size sand fractions Bed thickness: dm to several m Same facies as GSm	Massive bed Erosive base which can display a cm-thick basal unit with inverse grading	Massive freezing, cohesive debris flow deposits or high-density turbidity current (Lowc 1982; Davies and Walker 1974; Walker 1975; Postma 1984, 1990; Postma and Cartigny 2014)
IGSm (Table 3h)	Same facies as GSm	Inclined sedimentary bed from 15 to 25°	Debris flow on foreset (Davies and Walker 1974; Walker 1975; Postma 1990; Postma and Cartigny 2014)
GSi (Table 3f,g)	Well sorted and clast-supported conglomerates, gravels to pebbles and medium- to coarse-grained sandstones Bed thickness: dm	Horizontal bedding, erosive base. Individual beds are well sorted	Laminar supercritical flows, traction carpet driven by streamflow (Postma 1990). Alternating periods of erosion and deposition (Cartigny et al. 2014; Postma et al. 2014; Rubi et al. 2018)
GSt (Table 3i)	Well-sorted conglomerates to medium-grained sandstones Bed thickness: dm to m	Trough cross stratification Erosive base	Tractive current and 3D megaripple migration (Miall 1978; Davies and Walker 1974; Walker 1975)
IGSt	Same lithology as the GSt facies Bed thickness: dm to m	Cyclic steps Inclined beds from 15° to 25° Erosive base	Hydraulic jump (Cartigny et al. 2014; Postma et al. 2014) on the lee side (Breda et al. 2007; Clarke et al. 2012; Dietrich et al. 2016; Clarke 2016; Rubi et al. 2018)
GSmm (Table 3k)	Very poorly sorted, disorganized, ungraded matrix-supported conglomerates Clast sizes ranging from gravel to boulder Matrix composed of silt to coarse-grained sand Bed thickness: dm to m	Massive beds Erosive base which can display a cm-thick basal unit with inverse grading	Hyperconcentrated debris flow (Walker 1975; Postma 1990; Mulder and Alexander 2001)—aerial or aquatic non-cohesive debris flow/masse freezing (Walker 1975; Lowc 1982; Postma 1990; Miall 1996)

Table 1 (continued)

Name	Lithology	Sedimentary structures	Depositional process interpretation
GSFd (Table 3l,m)	Heterolithic Consolidated sediments of various lithologies, from conglomerates to silts Bed thickness: dm to m	Chaotic deposits of folded and brecciated blocks Deformed beds	Slump and slides
Other facies			
C (Table 3n, p)	Coal with plant fragments and mm to cm beds of fine to medium-grained sand Bed thickness: dm to m	Massive or thinly laminated	Coal deposits alternating with overbank
T/Tr (Table 3o, p)	White to ochre clay sometimes with coal chips Bed thickness: cm to m	Massive (T) or thinly laminated with trough cross stratifications, planar bedding and plants fragments (Tr)	Tonsteins: altered volcanic ashes (T), (Bohor and Triplehorn 1993) sometimes reworked by tractive current (Tr)
Cs (Table 3q)	Massive carbonates Bed thickness: dm to m	Undulatory bedding	Microbial deposits

Table 2 Facies associations and their attribution to depositional environments based on facies associations determined by Ducassou et al. (2019)

Code	Facies association	Depositional environment
AP	C, Fm, Flc, T, Tr, thin layers of SI	Swamp deposits within a floodplain/coastal plain
AF	GSmm, Fm, Flc, C, T Rare GSFd	Alluvial fan within a swamp or lake (Blair and McPherson 1994; Miall 1996)
Dlo	GSm, GSu, GSI, SI, Fm, Flc, C, T Rare GSmm, GSFd	Topset of delta deposits with coal preservation (Postma 1990; Dietrich et al. 2016; Bhattacharya 2010)
Dfo	IGSm, IGSt, Fm, Flc, Rare GSmm, GSFd, C	Foreset and hydraulic jump of delta deposits (Postma and Roep 1985; Dietrich et al. 2016; Rubi et al. 2018)
Dbo	GSFd, GSm, GSI, GSmm, SI, Fm, Flc Rare C	Bottom set of delta deposits (Postma and Roep 1985; Rubi et al. 2018)
L1	Fm, Flc, thin layers of sandstones (SI, GSI, GSm), GSFd	Lake environment with sediment supply deposited laterally to the delta deposits
L2	Fm, Flc, Cs, C, GSFd, rare SI	Lake environment with a weak sediment supply and soft-sediment deformations, or more rarely with microbial deposits (carbonates)

Table 3 Illustrations of the main facies described in Table 1 and in the text

See Table 1 for the facies code

or increasing sediment supply). In consequence, two stratigraphic surfaces can be recognised: (1) the maximum flooding surfaces (MFS) that end the stratigraphic base-level rise, i.e., end of the retrogradational trend, which represents an extensive lacustrine sedimentation or alluvial plain deposits in humid depositional environments, and (2) the end of the stratigraphic base-level fall, i.e., end of the progradational trends, that could be defined as a maximum regressive surface (MRS) in lake environments.

Stratigraphic cycles are defined from depositional environments based on facies and electrofacies analysis. In sequence stratigraphy, these cycles can be either autocyclic, resulting from internal processes, or allocyclic, resulting from local or global external factors (climate and tectonics). Although stratigraphic cycles are identified on all the available cored boreholes and on well-log data, correlations between one well and another are not possible due to the lack of reference timelines (absence of biostratigraphic data and radiometric dating); only the LY-F well is currently dated with 5 LA-ICP-MS U–Pb ages obtained from zircons and apatites collected in tonstein deposits (Ducassou et al. 2019). Additionally, the cycle definition is more precise for the wells for which core data are available. Consequently, we used a seismic analysis to constrain stratigraphic surfaces and large-scale correlations between wells.

Well-logs and seismic data

In a first step, the 14 seismic lines acquired in the 1980s and originally in paper format were digitised in seg-y format (i.e., dedicated to seismic softwares). Well-logs are available for 28 wells in the Lucenay-lès-Aix area (including the LY-F, LY-G, and LY-ZB wells), each one with at least two and sometimes three parameters recorded: gamma-ray (GR, total natural radioactivity), neutron (N), and gamma-gamma (GG, density), each of them measured in counts per second. In a second step, the three wells with core data were relocated on the nearest seismic lines (LY-6, LY-9, and LY-10; Fig. 2) (1) to propose correlations for the geological markers at the different scales (i.e., seismic, well-logs, and facies association), and (2) to reveal the large-scale geometry and evolution of the depositional environment through time and space, between the defined timelines. In a third step, the seismic profiles were integrated into a 3D GeoModeller software (Skua-GoCad software, Paradigm) for 3D visualisation and interpretation. Each profile was interpreted individually through seismic line-drawing to underlain sedimentary and structural architectures. The main seismic reflectors, discontinuities, and faults were drawn on the seismic profiles. The wells with their respective well-logs were entered in the project after a depth-to-time conversion using the mean

velocity law based on five well data (LY-B, LY-C, LY-D, LY-E, and LY-ZA).

Results

Sedimentological descriptions and depositional environments

Detailed sedimentary logs were drawn for the LY-G and LY-ZB cored boreholes to complete the previous descriptions of the LY-F core provided by Ducassou et al. (2019). The LY-G and LY-ZB cores display similar facies to the LY-F core (i.e., Ducassou et al. 2019); the facies of Ducassou et al. (2019) have been refined and regrouped into 13 facies (Table 1): eight conglomerate and sandstone facies, two fine-grained facies, and three additional facies (coal, volcanic ashes and carbonates), each of them deposited through specific processes. The facies are illustrated on Table 3. The depositional palaeoenvironments were determined through seven facies associations (Table 2). The detailed logs were then summed up into synthetic logs (Fig. 3) to propose a vertical evolution of the sedimentary environments along a depositional profile.

Facies associations and depositional environments

When the cores are mostly composed of coal deposits (C facies, Table 3n, p), with interbedded tonstein layers (T, Tr, Table 3o, p) within fine facies (Fm, Flc, Table 3a, b, c) and few sandstones (SI, Table 3d, e), sedimentation occurs in a swamp environment in a humid restricted alluvial plain (CP facies association). The second facies association comprises the GSmm facies in metric to plurimetric beds, interpreted as mass-freezing, cohesive debris flow deposits, reworking volcanic gravels to pebbles, intercalated with some coal levels. This facies is often associated with swamp deposits (F, Flc, C, T, Table 3a, b, c, n, p), which indicates that it developed in a proximal environment, probably near the interface between air and water, and suggesting a volcanoclastic alluvial-fan delta environment (AF facies association). The environment is attributed to a delta topset (Dto association) when the dominant facies are dominated by tractive processes, marked by horizontal beds of conglomerates and sandstones (upper plan beds, trough cross stratifications, current ripples; GSI, GSt, SI, Table 3d, e, f, i), sometimes stacked together, with some Soft-Sedimentary Deformation (SSD) occurrences (e.g., slumps, shearing, load casts, ball and pillows; GSFd facies, Table 3l, m), and with some debris flow deposits (GSm, GSmm, Table 3j, k), plant remains, and coal intercalations (Flc, C, Table 3a, n, p). The fourth facies association (Dfo) is composed of inclined beds of sandstones to conglomerates (IGSm, IGSt, Table 3h) alternating with

inclined beds of fine-grained facies (Flc, Table 3a), marking settling periods, and with few coal levels (C, Table 3n, p). The inclined beds, gravity processes, and slump occurrences (GSFd, Table 3l, m) are attributed to deltaic foresets. The fifth facies association corresponds to the bottomset environment (Dbo), characterised by conglomerates and sandstones corresponding to gravity deposits (GSm, GSmm facies, Table 3j, k) or tractive currents (SI, GSI, Table 3d, e, f, g), and by fine-grained facies (Flc facies, Table 3a), sometimes affected by some SSDs (GFd facies, Table 3l, m). The two last facies associations record lacustrine conditions; one of them is composed of fine-grained lithologies (Flc, F, Table 3a) interbedded with some sandstone facies attributed to turbidity flow (SI, GSm, GSI, Table 3d, e, f, g, j) with few SSDs (GSFd, Table 3l, m), marking periods of detrital input into a lake environment (facies association L1). The second one (facies association L2) shows only a weak detrital supply (SI facies reworked by wave influence and few GSFd, Table 3l, m) and is characterised by the same fine facies as the L1 facies association. Some occurrences of microbial deposits (Cs facies, Table 3q) have been observed in this L2 environment when the water column is low. With all these facies associations, the evolution of depositional environments for each cored borehole can thus be proposed (Fig. 3).

Well-log facies characterisation and depositional environment

Four depositional environments have been identified from the well-log data (Fig. 4): lake, delta, volcanoclastic alluvial-fan, and alluvial plain.

The coal deposits usually display a low GR and N, and a high GG. Sometimes, GR is high when either coal contains uranium or is mixed with clays. This electrofacies association corresponds to the CP facies association (Table 2).

The lake environment is characterised by a fluctuating but mainly high GR, a low N, and a low-to-high GG, depending on the clay content or uranium adsorbed on organic matter. This electrofacies association corresponds to L1 and L2 sedimentary facies associations (Table 2).

The alluvial-fan delta deposits display a moderate but constant GR and N, and a low GG. This electrofacies association corresponds to the AF sedimentary facies association (Table 2).

Finally, the deltaic environments are characterised by a fluctuating GR, depending on the clay levels, and by fluctuating, but generally very high N and low GG. This electrofacies association corresponds to the sedimentary facies associations Dto, Dfo, and Dbo (Table 2) without distinction between the proximal or distal depositional environment. To dissociate the topset, foreset, and bottomset, it is necessary to pair the well-logs with the mining report descriptions to find indications on the sedimentary features observed when

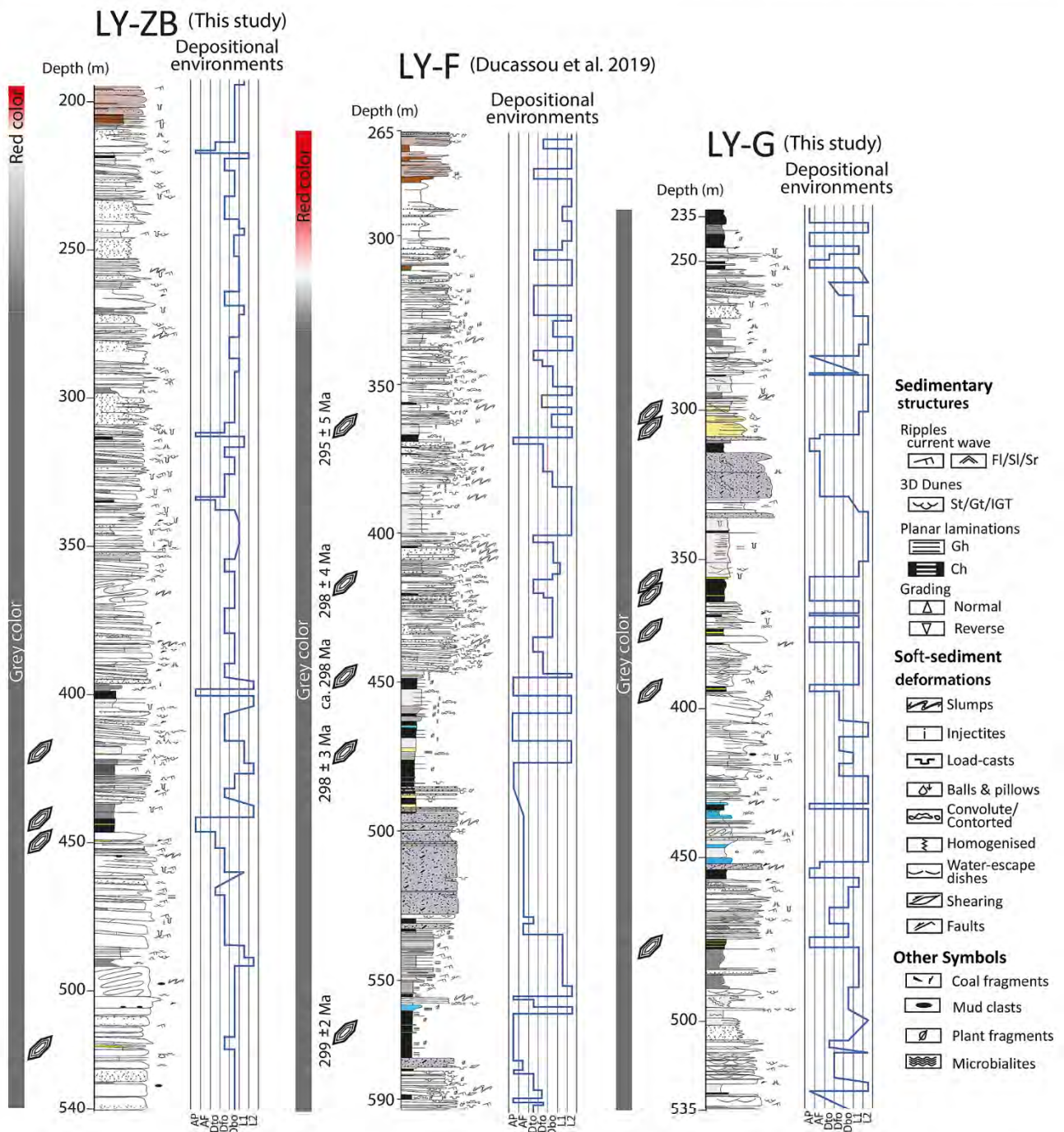


Fig. 3 Sedimentary logs of the LY-ZB (this study), LY-F (modified from Ducassou et al. 2019), and LY-G (this study) wells, with their respective depositional environment evolution. The log caption is available in Ducassou et al. (2019)

the cores were still available (e.g., stratifications, slump and slide occurrences, alternating coarse and fine granulometry, and dip of the deposits). The LY-I well is shown as an example (Fig. 5) to illustrate the sedimentary facies associations inferred from the electrofacies. For this example, we

distinguished three deltaic poles (proximal, medium, and distal delta, Fig. 5), based on both the well-logs and the descriptions from the mining reports, that correspond to the topset, foreset, and bottomset, respectively.

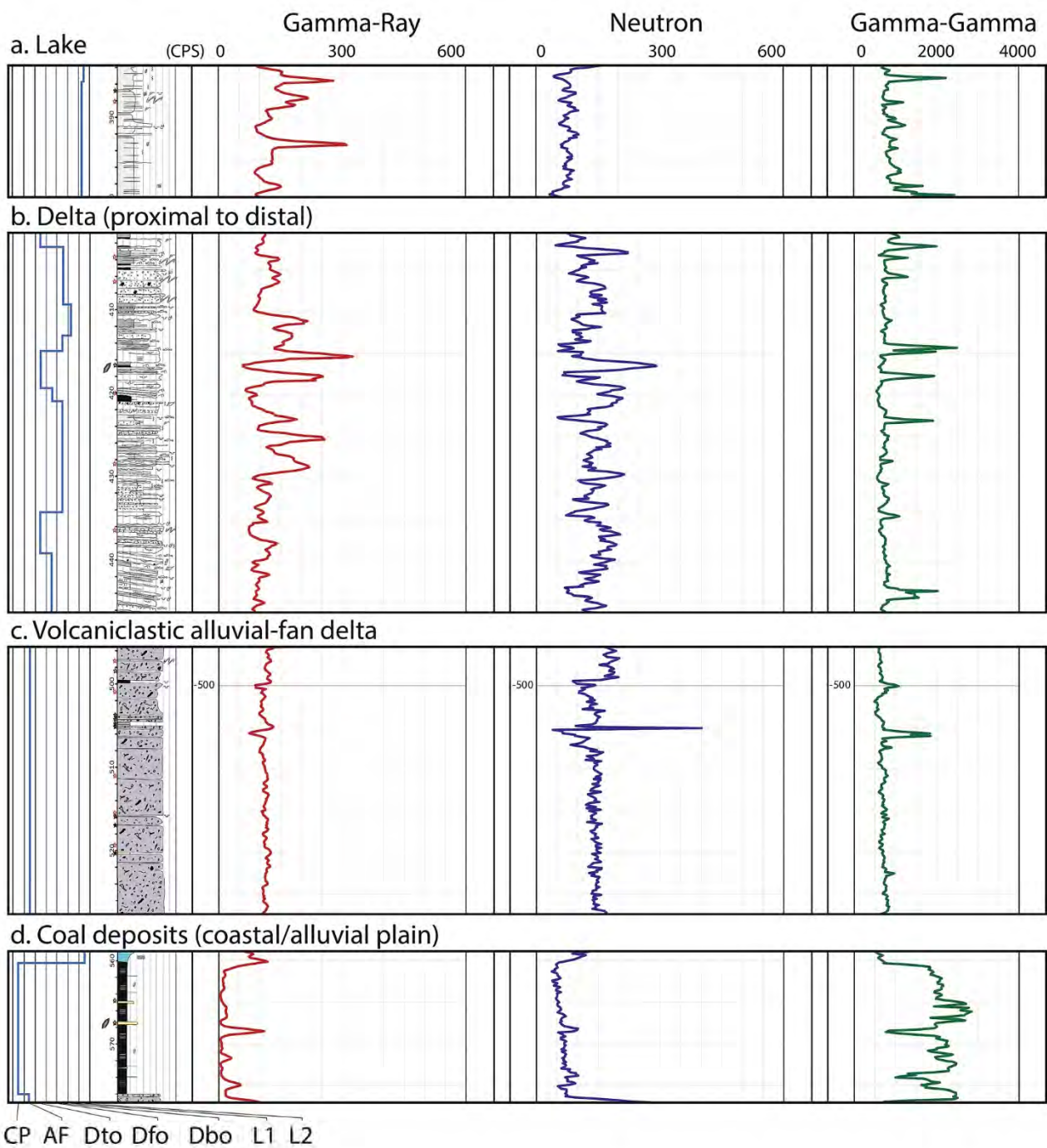


Fig. 4 Electrofacies and sedimentary facies correspondence for the alluvial plain, the volcaniclastic alluvial-fan delta, the delta and the lake environments. The sedimentary profile is from the LY-F well (Ducassou et al. 2019)

Sequence stratigraphy on cores and well-log and seismic correlations

Core, well-log, and seismic interpretations

The basin geometry and large-scale architectures are best imaged along five seismic profiles: one oriented north–south

(LY9, Fig. 6b), three oriented approximately west–east (LY6, LY8, and LY10, Fig. 6c), and one oriented SW-NE (LY5, Fig. 6c). The west–east basin architecture can be seen in Fig. 6c, displaying the four approximately west–east seismic lines (with north to south LY6, LY5, LY8, and LY10). The main seven seismic reflectors, identified on at least two seismic lines, are highlighted with specific colours.

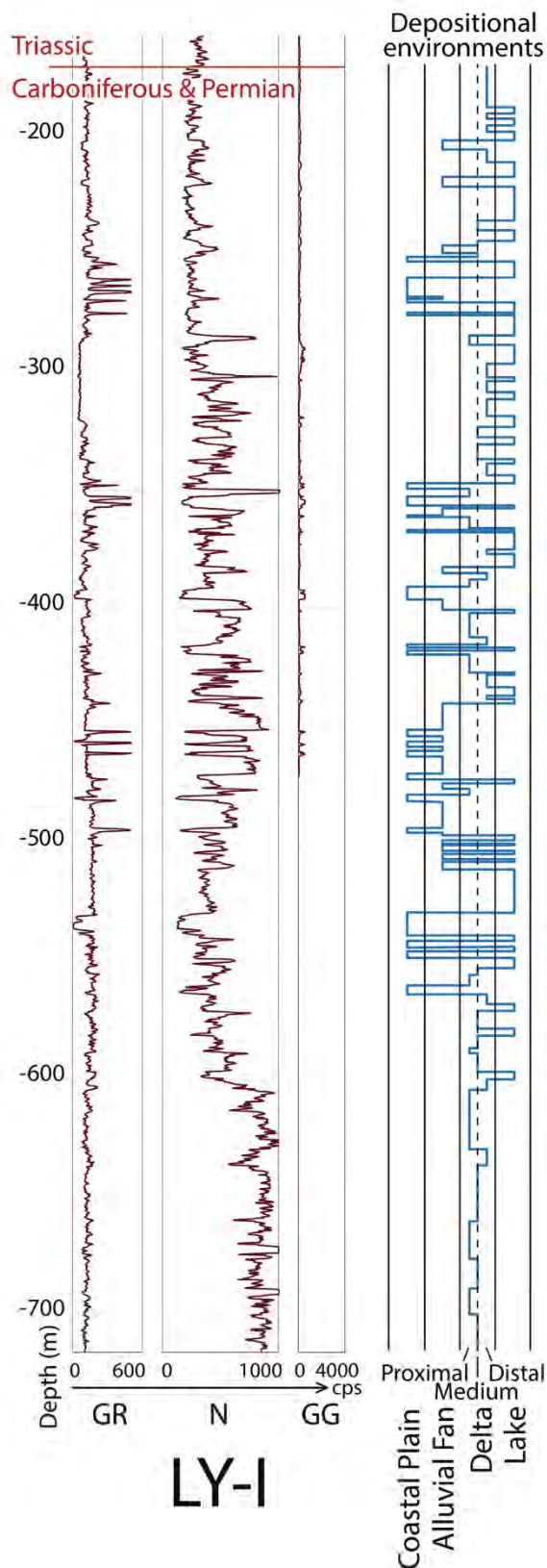


Fig. 5 Calibration of the depositional environments of the LY-I well based on well-log analyses

Seismic reflectors which can be seen on only one seismic line were drawn in black. The major unconformity between the Carboniferous and Permian deposits and the overlying the Meso-Cenozoic sedimentary cover is well-defined by toplap geometries below the unconformity, and is underlined in red in Fig. 6. The seismic interpretations reveal a synclinal morphology induced by a post-depositional tectonic deformation of the sediments as represented on profile LY10 (Fig. 6c), yet the boundaries of the basin are not visible on the seismic profiles.

Therefore, we used the seismic profiles to track some time-markers between the wells. Because of the poor quality of the seismic profiles, it is difficult to associate seismic facies and sedimentary facies. However, the seismic profiles show some continuous markers (particularly above the blue marker, Fig. 6b, c). Given the resolution of the seismic data, these main markers are recognised only in the central and eastern part of the Lucenay-lès-Aix area; the following discussion will therefore focus only on wells from this location. The seismic data interpretations show, from the base to the top of the Carboniferous–Permian deposits, seven main markers. Each marker was reported on the well-logs, displayed directly in the GeoModeller software, of the LY-ZB, LY-F, LY-D, LY-I, and LY-G wells (Fig. 7) and of the LY-D, LY-U, LY-T, and LY-L wells (Fig. 8). Units between these markers were named units A to H from the base to the top. As represented on the seismic profiles, these units are nearly isopach, except for unit C in the LY-ZB and LY-F wells (Fig. 6b), indicating an onlap geometry, and between the orange and the blue markers (unit B, Figs. 6b, c and 7). In a last stage, the evolution of depositional environments is obtained by combining well-log and core data for each unit identified through the seismic profiles (Fig. 9).

Correlations of wells and 3D depositional environment evolution

In unit A (below the orange marker), mostly proximal facies are observed. The alluvial-fan delta is dominant, and is alternating with some coal deposits and some lake facies in the LY-F well (Fig. 9), but also on the LY-L, LY-T, and LY-U well-logs (Fig. 8). To the contrary, the LY-D well shows more distal facies, with mostly deltaic sequences and few coal deposits (Figs. 7 and 8).

In unit B (Figs. 7, 8, and 9), the deltaic environment dominates the succession of the LY-F, LY-G, LY-I, and LY-ZB wells, and is alternating with few lacustrine facies. In the northern part of the area (LY-U, LY-T, LY-L, Figs. 6 and 8), some coal deposits indicate a more proximal environment. This trend towards a more proximal pole is confirmed in unit C (in the LY-F and LY-ZB wells) which displays only deltaic and lacustrine deposits. Units B and C are not isopach, but show a compensated geometry that may be explained

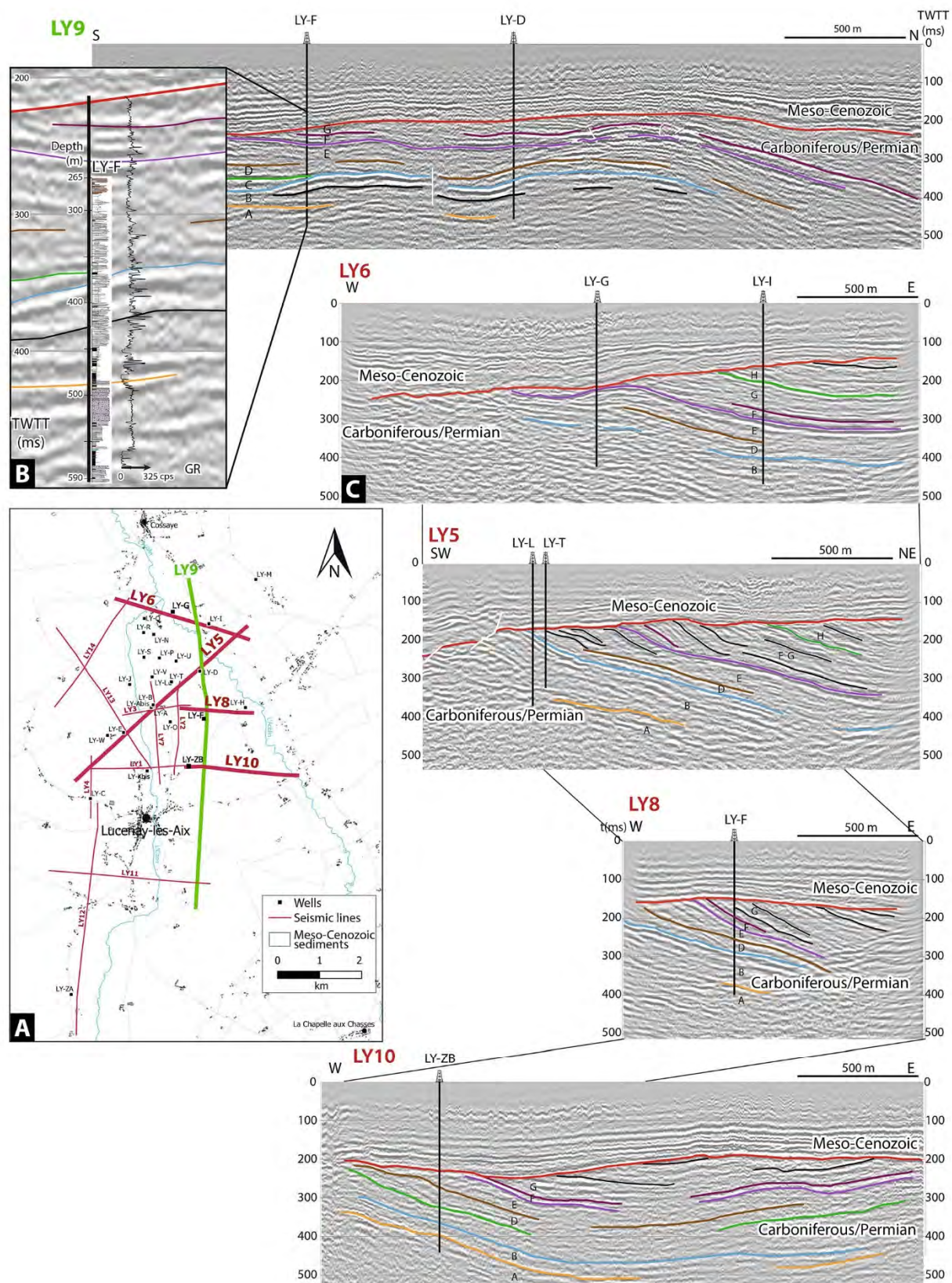


Fig. 6 A. Localisation of the seismic profiles and wells in the Lucenay-lès-Aix area. B. Calibration of the LY-F well-log along the LY-9 seismic profile. C. Interpretation of the seismic profiles LY-6, LY-5, LY-8, and LY-10

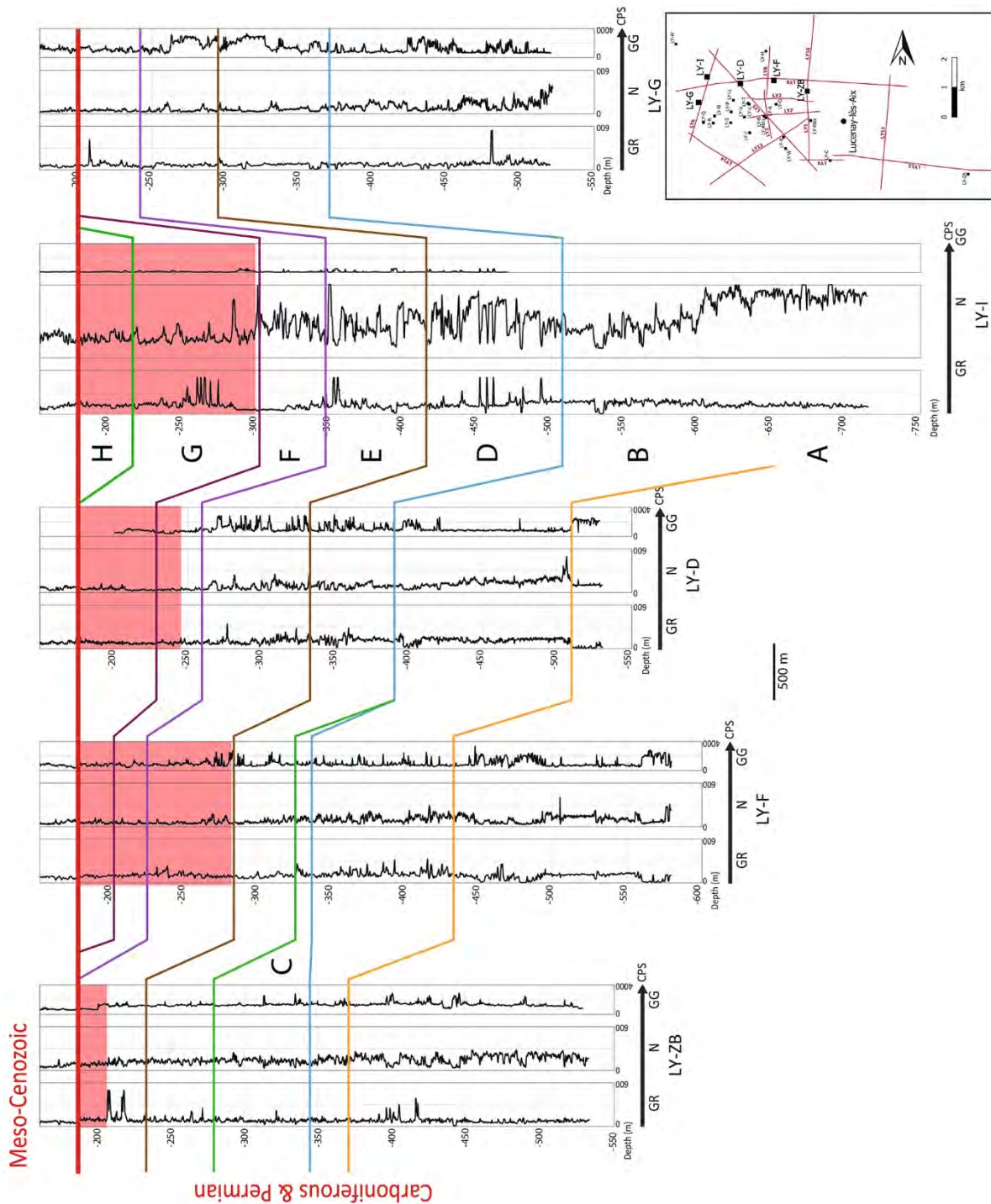


Fig. 7 Correlations based on seismic markers of the LY-ZB, LY-F, LY-D, LY-I, and LY-G wells. When observed, the “Red Permian” is represented in red at the top of the wells

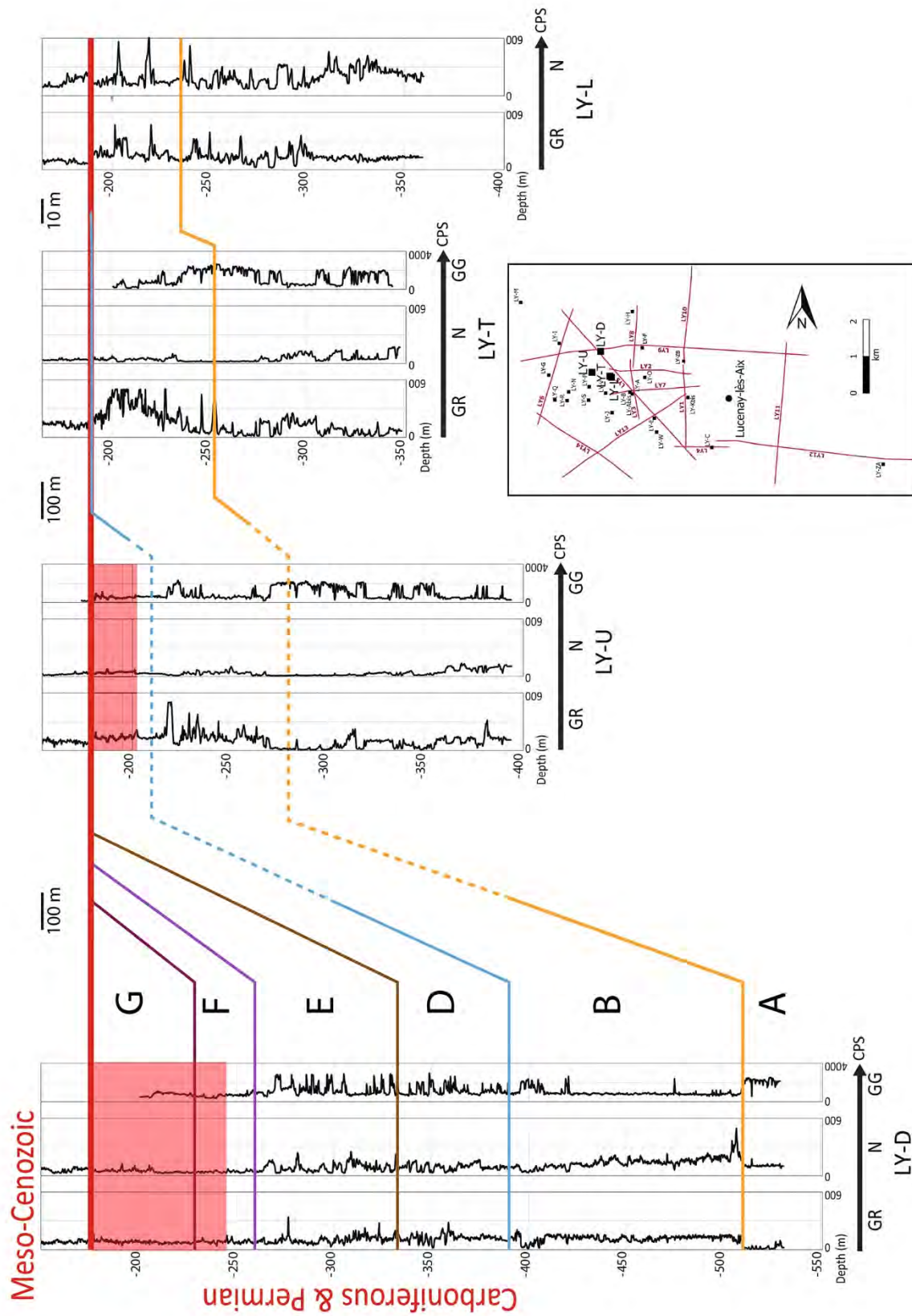


Fig. 8 Correlations between the LY-D, LY-U, LY-T, and LY-L wells based on the seismic markers. When observed, the "Red Permian" is represented in red at the top of the wells

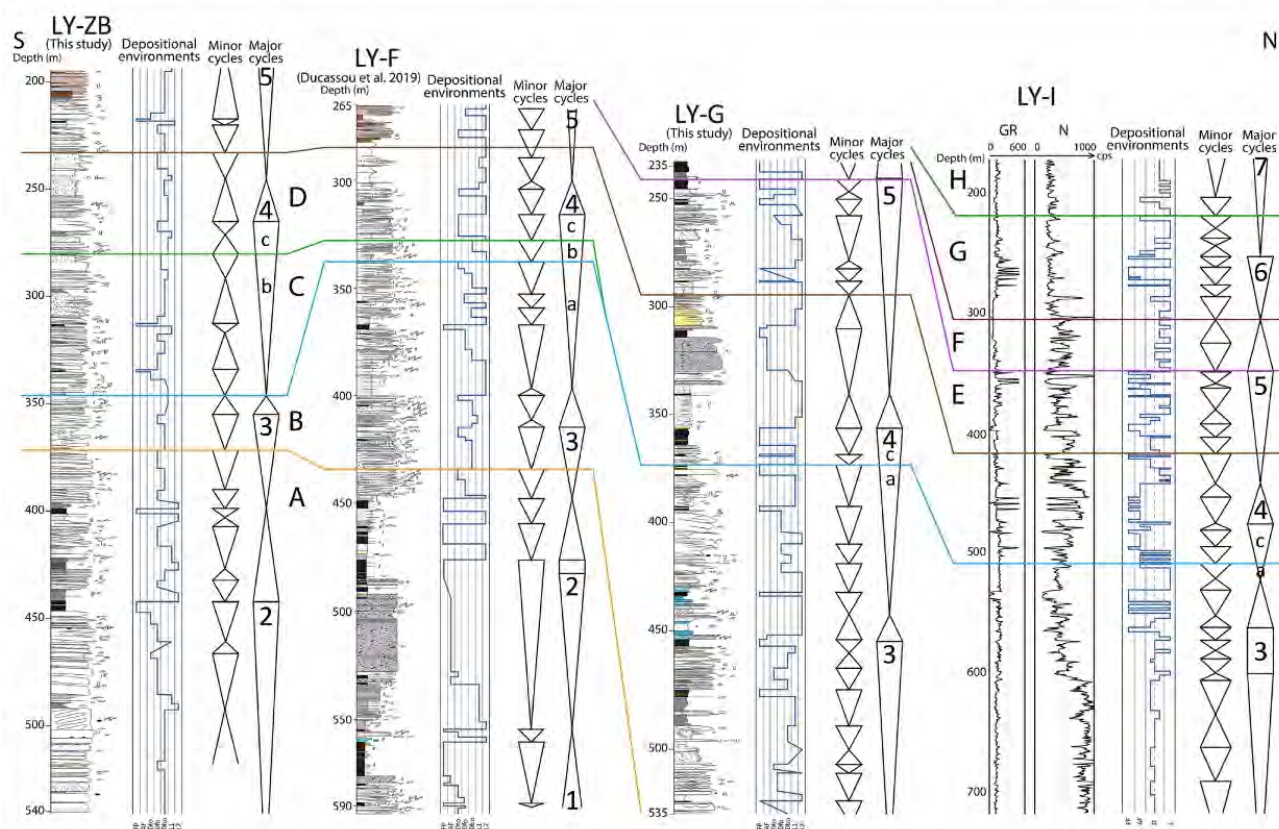


Fig. 9 Correlations between the LY-ZB, LY-F, LY-G, and LY-I wells based on seismic interpretations and stratigraphic cycles

by the deltaic progradations. Westward (LY-P, LY-R, and LY-N wells, Fig. 6a), the wells are far from the seismic profiles, and the location of the seismic markers on the well-logs is therefore uncertain. However, the 3D visualisation shows that these successions belong to units A and/or B (i.e., located below the blue marker) and are dominated by alluvial plain and alluvial-fan facies. This assumption is supported by the electrofacies analysis, as the LY-E and LY-J well-logs display similar facies to the LY-F well. This is confirmed by the correlations with the LY-F well and by the well-logs of the LY-E and LY-J wells which show the same facies. In unit D (Figs. 7, 8, and 9), proximal facies are developed to the north of the area (LY-D, LY-G, LY-I, and LY-U wells) and are alternating with lacustrine levels, whereas to the south, lacustrine conditions dominate and are interbedded with few deltaic facies (LY-F and LY-ZB). In unit E (Figs. 7, 8, and 9), the lake and the delta facies are more developed to the east (LY-D, LY-F, LY-I, and LY-ZB wells), whereas to the west (LY-U well), lake deposits alternate with coal. The F and G units, only observed in the LY-D, LY-F, and LY-I wells (Figs. 7 and 9), consist of lacustrine environments northward, and mixed lacustrine to deltaic environments southward. Finally, in unit H (LY-I well, Figs. 7 and 9), the deltaic facies dominate. The major

unconformity at the top of the succession, like in most of the Carboniferous–Permian basins in Europe (e.g., Bourquin et al. 2006, 2011; Durand 2006), is well observed and a large part of the sediments have been eroded mainly in the western part of the Lucenay-lès-Aix area (Figs. 6c and 8). This depositional environment evolution observed at the basin scale from stratigraphic markers defined by seismic profiles (units A–H) is compared with minor stratigraphic cycles observed from core and well-log data. Thus, an evolution in seven major progradational–retrogradational stratigraphic cycles is illustrated in the LY-ZB, LY-F, LY-G, and LY-I wells (Fig. 9).

Sequence stratigraphy and basin evolution

Figure 10 illustrates the depositional environment evolution in time and space, from three wells from west to east (LY-U to LY-F) and from south to north (LY-F to LY-I). The first sequence stratigraphy cycle, denoted 1 (Fig. 10, LY-U and LY-F wells), is incomplete and only constituted by a retrogradational trend from a proximal environment (alluvial plain and alluvial-fan delta) to a lake environment. In the second cycle, located below the orange marker (denoted 2 on Figs. 9 and 10) and observed in the LY-U, LY-ZB, and

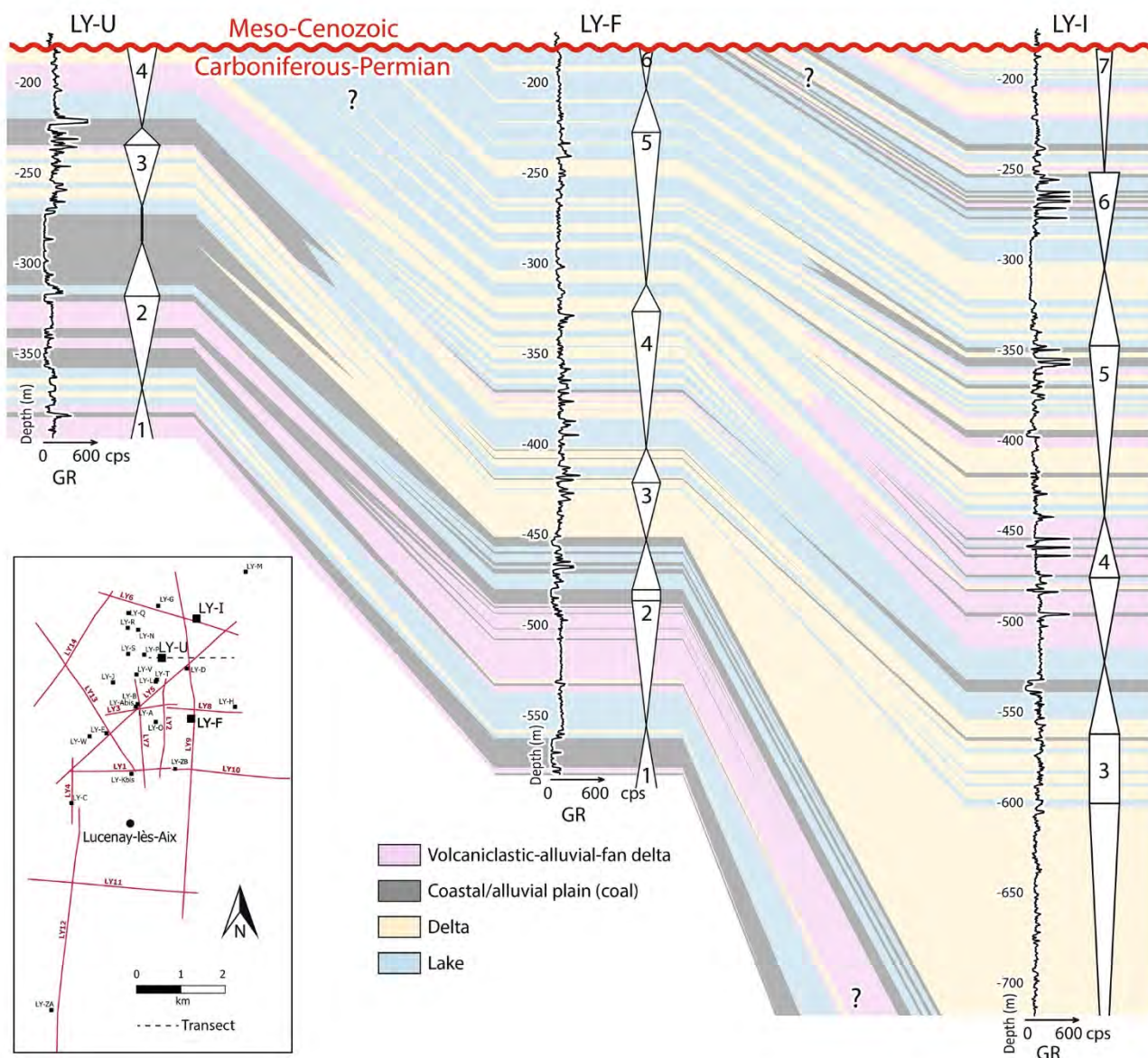


Fig. 10 Correlations between the LY-U, LY-F and LY-I wells, showing the depositional environment variations in space and time

LY-F wells, the progradational trend is more developed than the retrogradational one. This cycle is expressed through different facies with (1) alluvial-fan deposits alternating with a few coal levels in the LY-U well, (2) mostly alluvial-fan deposits in the LY-F well, and (3) mostly bottomset deposits displaying deltaic progradations in the LY-ZB well. The retrogradational trend is characterised by a greater preservation of the coal deposits in the LY-U well, occurrence of coal levels and deltaic deposits in LY-ZB well, and of lake deposits interbedded with coal in the LY-F well. Indeed, a base-level rise is necessary to preserve these coal deposits. The maximum flooding surface is characterised by the occurrence of lake deposits. In the LY-N, LY-P, LY-R, and LY-T wells (located westward, Fig. 6a), this second cycle displays

some coal levels alternating with alluvial-fan deposits. The third cycle, denoted 3, is recognised in five wells: LY-U, LY-F, LY-I, LY-ZB, and LY-G. The well-developed progradational trend is mostly represented by deltaic deposits, up to a more or less-developed coal level. The retrogradational trend is marked by thick lacustrine accumulations (up to a well-developed lacustrine level in the LY-ZB, LY-F, LY-G, and LY-I wells), and by the preservation of coal in this base-level-rise context mainly in the northern part (LY-U, LY-I). This third sequence should also be present in the short LY-N, LY-P, and LY-R wells, as it is recognised in the LY-U well located close by, but due to the lack of seismic profiles in this area, this cannot be confirmed. The fourth cycle, denoted 4 (Figs. 9 and 10), shows a well-developed progradational

trend from lake to delta or alluvial plain environments in the LY-ZB, LY-F, LY-G, and LY-I wells, and the occurrence of alluvial-fan deposits in the northern area, i.e., LY-U and LY-I wells. This progradational trend can be divided into three parts (4a, 4b, and 4c, Fig. 9), separated by the blue and green seismic markers. These three parts are well preserved in the LY-F well, with the 4a part located in unit B, the 4b part in unit C, and the 4c part in unit D. In the LY-ZB well, as unit B is tightened compared to the LY-F well, the lower part of the progradational trend (4a; Fig. 9) is absent, stacked with the top of cycle 3, while the 4b part is well developed. This geometry could reflect a compensated architecture of delta deposits (Figs. 6, 8, 9 and 10), with the presence of two and half minor cycles preserved in the LY-ZB well, compared to only one half in the LY-F well (Fig. 9). Similarly, part 4a is well developed in the LY-F and LY-G wells, and part 4b is missing in the LY-G and LY-I wells, due to the stacking of the blue and green markers (Fig. 9). Because of the Permian–Mesozoic unconformity, the retrogradational trend of the fourth cycle and the following cycles (denoted 5–7, Fig. 10) are not present in the LY-U well, nor in the short wells from the same area (i.e., LY-N, LY-P, LY-R, and LY-T wells, Figs. 6, 7 and 8). The retrogradational trend of cycle 4 is short in each well, representing only one minor cycle (on core and well-log data), with a termination in a lake environment (Fig. 9). The fifth cycle is characterised by a large progradational trend as shown in the LY-G and LY-I wells, up to the top of the E unit (Fig. 9). Toward the north, this trend is materialised by lake, delta and alluvial plain (coal) deposits, whereas in the LY-F and LY-ZB wells, to the south, the facies are more distal, mostly with lacustrine or bottomset deposits. The retrogradational trend is displayed only in the LY-I and LY-F wells (Figs. 9 and 10), whereas the deltaic deposits observed in the LY-I well are replaced by lacustrine deposits in the LY-F well (Figs. 9 and 10). The maximum flooding surface between cycles 5 and 6 is located at the top of the F unit (Figs. 9 and 10). The progradational trend of the sixth cycle is observed in the northern part (i.e., LY-I well), whereas more south, i.e., in the LY-F well, this trend is topped by the Permian–Triassic unconformity (Fig. 10). Finally, the seventh cycle (units G and H) is only represented in the LY-I well, showing the progradation of the deltaic deposits. Despite the fact that the LY-M well is far away from the seismic profiles and thus cannot be correlated with the other wells (Fig. 6a), it presents distal facies (i.e., deltaic and lacustrine, without coal occurrence), indicating that proximal deposits are not extending toward the east.

To sum up, because of the tectonic structure of the basin, units E, F, G, and H are not present in the wells located in the western part of the studied area (Fig. 6b). The seven stratigraphic cycles show a general retrogradational trend with increasing lacustrine deposits in sequences 1–6, with well-extended lacustrine deposits between the MFS of

sequences 5 and 6, suggesting an extended lake at the top of the succession (Fig. 10). The correlations of seismic and well data therefore suggest that the synclinal morphology observed from the seismic lines is a post-depositional structure and that the present-day boundaries of the basin are not representative of the boundaries at the time of the sedimentary filling.

Discussion

Refining the depositional environments of the Decize-La Machine basin

Three type of depositional environments were previously described in the first studies of the Decize-La Machine basin: palustrine, fluvial, and lacustrine (Donsimoni 1990). Our study shows that these depositional environments need to be reassessed in the light of the new sedimentological descriptions and available methods. As stated in Ducassou et al. (2019), the facies and facies association descriptions have shown that the sediments were mainly deposited in an aquatic environment with deltaic influences. Only the coal-bearing sequences and alluvial-fan deposits reflect a subaerial environment. The main argument in favour of subaquatic deposits is the presence of large-scale turbidite deposits and soft sedimentary deformations in the sandy to conglomerate facies, such as slumps, convolutes, injectites, and load features, characteristic of sediments deposited under a certain water column. Indeed, such deformations result either of a high sediment supply or from gravitational instabilities along a slope, as envisaged in delta foresets (e.g., Pisarska-Jamroz and Weckwerth 2013). These kinds of depositional environments were already mentioned for the Aumance Basin, located westward to the Decize-La Machine Basin, where deltaic progradations are shown, with distributaries coming from the west and south-east (Mathis and Brulhet 1990).

Within this sedimentary context, sequence stratigraphy correlations from only well-log and core data are tricky to realise in both continental successions and post-depositional deformed basins. Moreover, in a deltaic palaeoenvironmental context with progradation of deltaic systems, the minor cycles (auto or allocyclic, Fig. 7) are not stacked vertically but laterally (e.g., recent deltaic system of Corinth, Rohais et al. 2007; Rubi et al. 2018). In consequence, a combined analysis including subsurface data (core and well-logs) and seismic profiles is required to perform basin-scale sequence stratigraphy correlations. The major cycles defined in previous work (Ducassou et al. 2019) only reflect the 1D evolution without integrating the entire basin evolution. In the present study, the stratigraphic cycles initially defined by Ducassou et al. (2019) for the LY-F well (Fig. 2b) have

therefore been reassessed considering both the available well-log at the top of the well (in the part without core data) and the pattern of progradational–retrogradational trends obtained from the facies analysis of the other cored wells (Fig. 10). In the Lucenay area, most of the minor sequences observed are not complete, and display only progradational trends, and only a minority of sequences show both a progradational and a retrogradational trend (Fig. 9). This study highlights the progradational feature of deltaic systems in the Lucenay-lès-Aix area, with delta compensation beneath the green marker (Fig. 9).

Figure 11 shows palaeogeographic maps displaying the depositional environment evolution through time, between the defined timeline seismic markers which can be correlated at the scale of the studied area. These palaeogeographic maps were built by selecting the most representative environments in each unit. The alluvial-fan delta deposits are either under the lake water (when the GSmm facies presents some slump and slide and injectite occurrences, Fig. 11a, c), or above the lake level, in the alluvial plain, where it is associated with the coal deposits (Fig. 11b). This palaeogeographic evolution shows that the depositional environments are more and more dominated by the lake and the delta through time. The direction of progradation of the deltaic systems is poorly known, but the facies distribution seems to indicate a sediment supply coming from the southwest (Fig. 11a–e) and from the north (Fig. 11c–e), whereas the alluvial-fan delta would come from the north-west (Fig. 11a–c). Moreover, Ducassou et al. (2019) suggested that there is one main episode of volcanoclastic alluvial-fan deposits; our study, through the correlations between wells based on seismic data, shows that there are rather two episodes (Figs. 9 and 10, cycles 1–2 and cycle 4), although it is uncertain if they can be directly attributed to several contemporaneous volcanic events or be linked to previous volcanic material reworking (e.g., Ducassou et al. 2019 for discussion). From the ages obtained for the LY-F well (Figs. 2b and 11, Ducassou et al. 2019), we consider that the succession of the Lucenay-lès-Aix area between cycles 1 and 4 correspond to the boundary between the Carboniferous and Permian, with a late Gzhelian-to-early Asselian age, and could therefore be correlated with the lower Autunian (Igornay Fm or Muse Fm) defined in the Autun Basin (299.9 ± 0.38 Ma to 298.05 ± 0.19 Ma; Pellenard et al. 2017).

In some basins of Western Europe, the terms Grey and Red Permian are used as stratigraphic units to date the sedimentary succession, as it is the case for the Decize-La Machine Basin (Donsimoni 1990). This nomenclature implies that the boundary between the grey and red deposits is synchronous at the scale of the basin and constitutes a limit between two distinct depositional environments: one dominated by a reduced grey facies and the other allowing the deposition and preservation of more oxidised red

facies (e.g., Ducassou et al. 2019, LY-F well). The use of the difference in colour as a timeline should be possible only if, by definition, the change from the grey to red colour is synchronous within and between all the relevant basins. However, by working on several wells in the Lucenay-lès-Aix area (Figs. 7, 8 and 9), it is clear that the boundary between the grey and red facies cannot be correlated between the wells using the sequence stratigraphy proposed and is therefore diachronous. This highlights that (1) the previously described Grey and Red Autunian units are not representative of a real stratigraphic unit that can be applied to continental successions, and (2) the red colour is most probably the effect of differential diagenesis. In the study of Ducassou et al. (2019), the change from grey to red colour was attributed to a change in the depositional environment, from a lacustrine to a playa-lake environment (Fig. 2). By refining the facies description, and integrating this study at the basin scale, we actually do not observe any drastic change in the depositional environments (Fig. 10). The red deposits present similar facies to the grey deposits, aside the colour, and are therefore attributed to lacustrine to deltaic deposits, later affected by diagenesis. Thus, the depositional profile of the LY-F core was modified from Ducassou et al. (2019) in Fig. 7, and the depositional profile of the red part of the LY-ZB core was drawn accordingly. Moreover, it has been shown in Germany that the grey (coal) and red deposits (“wet red beds”) were deposited synchronously, for example between the Thuringian Forest and Saale basins, demonstrating that the red Permian is not necessary younger than the grey Permian (Schneider and Scholze 2018).

The Decize-La Machine Basin: part of a larger Carboniferous–Permian basin?

The Lucenay-lès-Aix area is described as a hemi-graben basin bounded by a major syn-sedimentary fault, oriented ~N–S and located to the west of the basin, which controls, with another minor syn-sedimentary fault at the centre of the area, the type and thickness of the sedimentation (e.g., phytogenic sedimentation, Donsimoni 1990). However, by interpreting the seismic profiles, no fault has been evidenced, except one on the LY-11 profile, oriented ~N–S, but affecting both the Carboniferous–Permian succession and the Meso-Cenozoic ones, and therefore considered as a post-depositional fault. Our new correlations indicate that the apparent difference in the thickness of the coal deposits observed between the eastern and western part of the area is in reality only due to the post-sedimentation deformation affecting the succession: the well-developed coal deposits preserved in the western part of the Lucenay-lès-Aix area are in fact correlated with the base of the succession of the eastern part (i.e., unit A, Figs. 6 and 10), which were not systematically cored (e.g., LY-I well, Fig. 10).

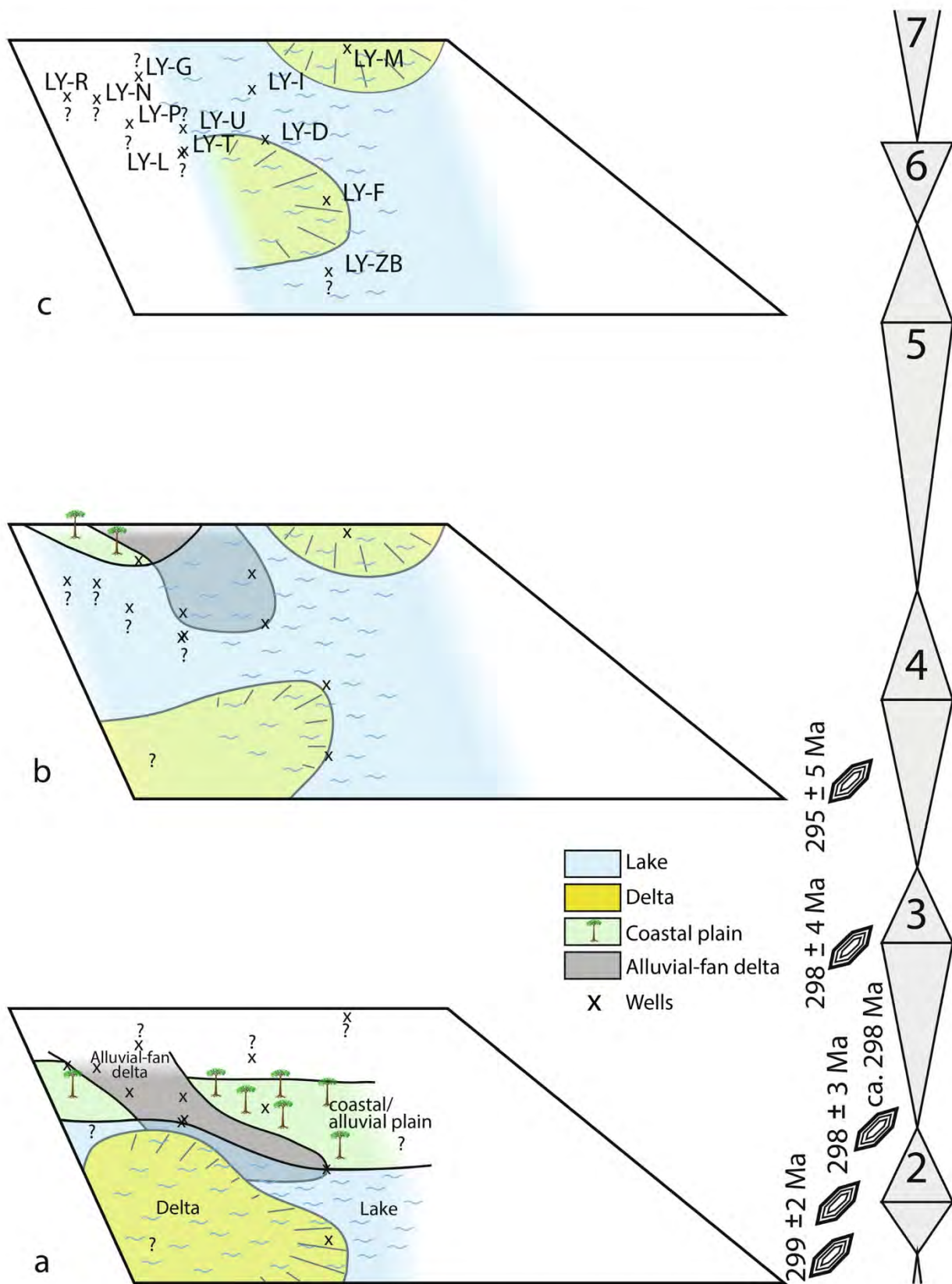


Fig. 11 Palaeogeographic maps showing the depositional environment evolution through time at the scale of the basin

Based on these new data, the initially inferred hemi-graben structure is not demonstrated. The structuration of the basin (i.e., synclinal morphology, Fig. 6) is given by a post-depositional deformation that took place either during Permian (post-lower Permian, e.g. Saalian or Altmark phases, Glennie et al. 2003), or after the Permian but before the Triassic (Bourquin et al. 2011). South of the Paris Basin, close to our study area, large-sized Carboniferous–Permian basins (Contres, Brécy, and Arpheuilles basins) have also been detected under the Meso-Cenozoic sedimentary cover since the 1980s (Debégliá 1980; Lebreton 1990; Mascle 1990; Perrodon and Zábek 1990; Delmas et al. 2002), and were recently re-evaluated through seismic data interpretations (Beccaletto et al. 2015); the latter demonstrate that these subsurface basins experienced several deformation events both during and after their sedimentation. For instance, this is the case for the Brécy Basin, where the edges were uplifted during Permian (Beccaletto et al. 2015), giving the basin a synclinal morphology and triggering the subsequent erosion of the edges, followed by the deposition of the Triassic succession.

Beccaletto et al. (2015) also show that the Aumance Basin (located 30 km to the west of our study area) could be an outcropping termination of these large subsurface basins. Given the very close proximity between the Decize-La Machine Basin and the Aumance Basin, it is highly possible that the Decize-La Machine Basin was also formed in the continuation of these large basins. Besides the location of the Lucenay-lès-Aix area south to the outcropping Decize-La Machine Basin, some other deep cored wells have indicated that the Carboniferous and Permian deposits also extend north, west and east to the Decize-La Machine area. Moreover, seismic data for the Lucenay-lès-Aix area (this study) do not show the boundaries of the basin (such as a major fault between the magmatic basement and the sedimentary succession, or an onlap over the basement), except perhaps in the eastern part of the area, as suggested by the synclinal morphology observed on the LY-10 profile (Fig. 6). Finally, the study of the depositional environments has highlighted that the more proximal deposits are located in the western part of the area (CP and AF), and that the lacustrine and deltaic deposits are mostly in the eastern part, indicating that the basin opens towards the east (Fig. 11). For instance, the LY-M well, located in the easternmost part of the study area, does not display any coal deposits.

If the connection with the Aumance Basin to the west is probable, it would be interesting to look for a possible connection with another Carboniferous-to-Permian basin toward the east, such as the Autun and Blanzay-Le Creusot basins

located, respectively, only 60 km and 40 km east of the study area (Fig. 12), and displaying distal lacustrine facies (black shales). If the connection between several sub-basins or the existence of one large basin south of the Paris Basin during the Carboniferous and Permian time is proven, this would have significant geodynamic implications, in terms of tectonics (amount of eroded rocks), and perhaps climate (atmospheric CO₂ storage in organic matter).

Conclusion

The Decize-La Machine Basin, particularly the Lucenay-lès-Aix area, displays sedimentary successions attributed to alluvial plain, lacustrine and deltaic environments without evidence of fluvial environments. This basin was structured after the sedimentation, as shown by its W–E synclinal morphology. This structuration, and the fact that continental deposits display a strong lateral variability in terms of facies, means that direct correlations cannot be made between the available wells based only on the facies descriptions. Thus, a multidisciplinary approach has been used in this study to make intrabasinal correlations: the well-log data from 12 wells were paired with three detailed sedimentary logs and facies descriptions to determine the palaeoenvironmental evolution through time and space, and to define a reliable sequence stratigraphical scheme across the Lucenay-lès-Aix area. By visualising the data on a 3D seismic viewer (i.e., seismic profile and well-log data), some major markers (considered as timelines) have been reported on the logs and well-logs to make correlations, confirmed by the use of sequence stratigraphy. These results show that (1) the Lucenay-lès-Aix area is comparable to the Aumance Basin, with coal deposits and development of delta into a lacustrine system, (2) the environments become more lacustrine through time, with the disappearance of the more proximal facies (coal and alluvial-fan delta deposits), and (3) the basin seems to open towards the east. Finally, the current boundaries of the Decize-La Machine Basin are only erosive, suggesting that this basin could be part of a larger one, encompassing the Aumance basin and perhaps even the more eastern Autun and Blanzay-Le Creusot basins. Occurrences of such wide basins would lead us to greatly re-evaluate the size and thickness of Carboniferous–Permian basins and related sedimentation in France and Western Europe. A next step would be to deconvolute the sedimentary record, to distinguish the role of tectonic and climatic controlling parameters—i.e., to discuss the respective impact of erosional processes at the end of the Variscan orogeny and in the end-Palaeozoic climate dynamic.

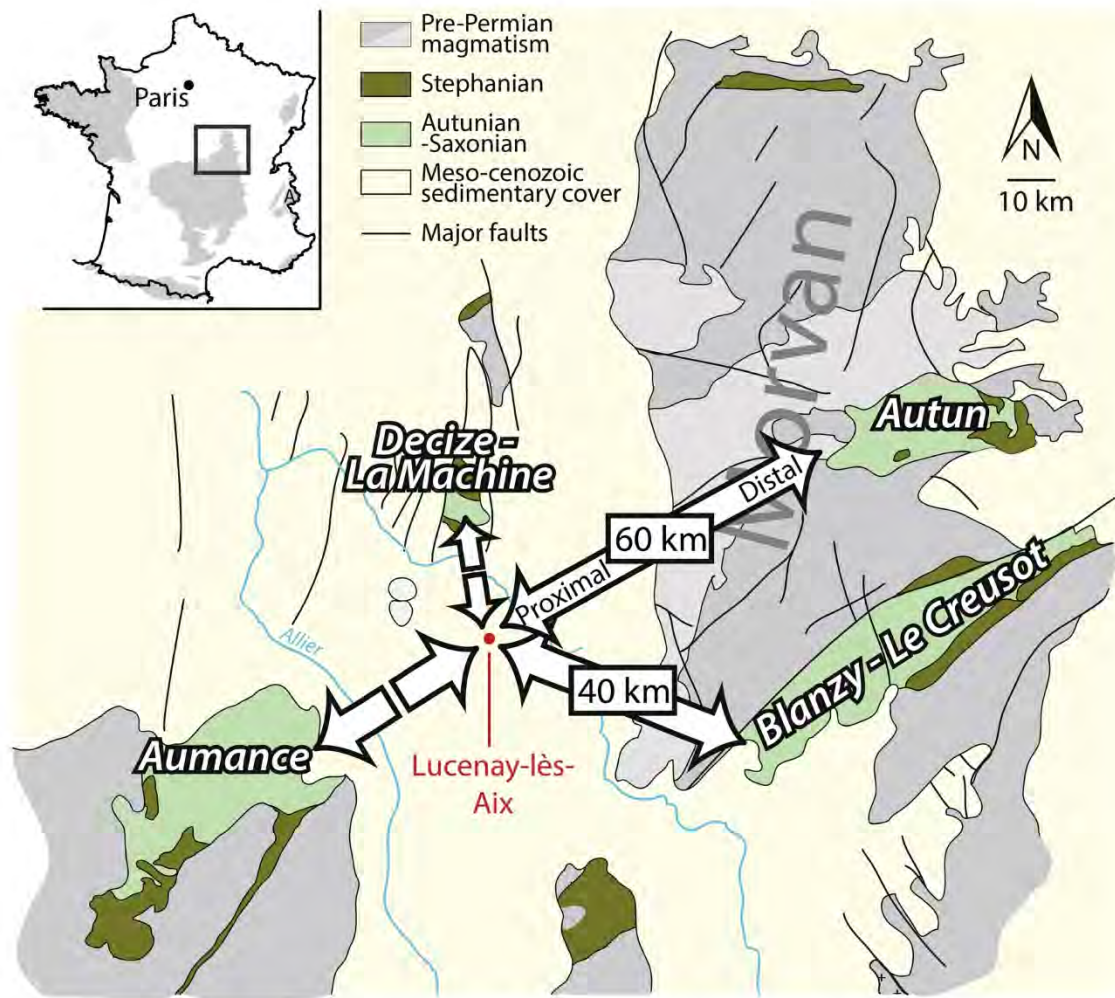


Fig. 12 Geographic map showing the proximity between the Decize-La Machine, Aumance, Autun, and Blanzay-Le Creusot basins. The distances between the Decize-la Machine Basin and the Autun and Blanzay-Le Creusot basins are indicated

Acknowledgements We are grateful to the French geological survey (BRGM) and the Bretagne region (France) for financial support (Mathilde Mercuzot's PhD). This work was also supported by the TelluS Program of CNRS/INSU. The authors also thank Christian Le Carlier de Veslud for assistance for the GoCad GeoModeller software, Sara Mullin for the English proofreading, and Thomas Voigt and Frank Scholze for their detailed comments, which have greatly improved the manuscript.

References

- Ballèvre M, Bosse V, Ducassou C, Pitra P (2009) Palaeozoic history of the Armorican Massif: models for the tectonic evolution of the suture zones. *C R Géosci* 341:174–201
- Ballèvre M, Catalán JRM, López-Carmona A, Pitra P, Abati J, Fernández RD, Ducassou C et al (2014) Correlation of the nappe stack in the Ibero-Armorican arc across the Bay of Biscay: a joint French-Spanish project. *Geol Soc Lond Spec Publ* 405:77–113
- Balleve M, Bosse V, Dabard MP, Ducassou C, Fourcade S, Paquette JL, Peucat JJ, Pitra P (2013) Histoire géologique du Massif armoricain: actualité de la recherche. *Bulletin de la Société Géologique et Minéralogique de la Bretagne, Société géologique et minéralogique de Bretagne* 10:5–96
- Beccaletto L, Capar L, Serrano O, Marc S (2015) Structural evolution and sedimentary record of the Stephano-Permian basins occurring beneath the Mesozoic sedimentary cover in the southwestern Paris basin (France). *Bulletin de la Société Géologique de France* 186:429–450
- Becq-Giraudon JF, Montenat C, Van Den Driessche J (1996) Hercynian high-altitude phenomena in the French Massif Central: tectonic implications. *Palaeogeogr Palaeoclimatol Palaeoecol* 122:227–241
- Berner RA (2006) Geological nitrogen cycle and atmospheric N₂ over Phanerozoic time. *Geology* 34:413–415
- Bhattacharya JP (2010) Delta. In: James NP, Dalrymple RW (eds) *Facies models 4*. Geological Association of Canada, St. John's, pp 233–264
- Bishop JW, Montañez IP, Osleger DA (2010) Dynamic Carboniferous climate change, Arrow Canyon, Nevada. *Geosphere* 6:1–34
- Blair TC, McPherson JG (1994) Alluvial fans and their natural distinction from rivers based on morphology, hydraulic processes,

- sedimentary processes, and facies assemblages. *J Sediment Res* 64:450–489
- Bohor BF, Triplehorn DM (1993) Tonsteins: altered volcanic ash layers in coal-bearing sequences, special paper, 285th edn. Geological Society of America, Washington
- Bouma AH (1962) Sedimentology of some flysch deposits. A graphic approach to facies interpretation. Elsevier Publishing Company, Amsterdam
- Bourquin S, Guillocheau F (1996) Keuper stratigraphic cycles in the Paris Basin and comparison with cycles in other Peritethyan basins (German Basin and Bresse-Jura Basin). *Sediment Geol* 105:159–182
- Bourquin S, Rigollet C, Bourges P (1998) High-resolution sequence stratigraphy of an alluvial fan–delta environment: stratigraphic and geodynamic implications—an example from the Keuper Chaunoy Sandstones, Paris Basin. *Sediment Geol* 121:207–237
- Bourquin S, Peron S, Durand M (2006) Lower Triassic sequence stratigraphy of the western part of the Germanic Basin (west of Black Forest): fluvial system evolution through time and space. *Sediment Geol* 186:187–211
- Bourquin S, Guillocheau F, Péron S (2009) Braided rivers within an arid alluvial plain (example from the Lower Triassic, western German Basin): recognition criteria and expression of stratigraphic cycles. *Sedimentology* 56:2235–2264
- Bourquin S, Bercovici A, López-Gómez J, Diez JB, Broutin J, Ronchi A et al (2011) The Permian–Triassic transition and the onset of Mesozoic sedimentation at the northwestern peri-Tethyan domain scale: palaeogeographic maps and geodynamic implications. *Palaeogeogr Palaeoclimatol Palaeoecol* 299:265–280
- Breda A, Mellere D, Massari F (2007) Facies and processes in a Gilbert-delta-filled incised valley (Pliocene of Ventimiglia, NW Italy). *Sediment Geol* 200:31–55
- Broutin J, Doubinger J, Langiaux J, Primey D (1986) Conséquences de la coexistence de flores à caractères stéphaniens et autuniens dans les bassins limniques d'Europe occidentale. *Mémoires de la Société géologique de France* 149:15–25
- Broutin J, Doubinger J, Farjanel G, Freyret P, Kerp H (1990) Le renouvellement des flores au passage Carbonifère Permien: approches stratigraphique, biologique, sédimentologique. *Comptes rendus de l'Académie des sciences. Série 2. Mécanique, Physique, Chimie, Sciences de l'univers, Sciences de la Terre* 311:1563–1569
- Broutin J, Châteauneuf JJ, Galtier J, Ronchi A (1999) L'Autunien d'Autun reste-t-il une référence pour les dépôts continentaux du Permien inférieur d'Europe? Apport des données paléobotaniques. *Géologie de la France* 2:17–31
- Bruquier O, Becq-Giraudon JF, Champenois M, Deloule E, Ludden J, Mangin D (2003) Application of in situ zircon geochronology and accessory phase chemistry to constraining basin development during post-collisional extension: a case study from the French Massif Central. *Chem Geol* 201:319–336
- Burg JP, Brun JP, Van Den Driessche J (1990) Le sillon houiller du Massif Central français: faille de transfert pendant l'amincissement crustal de la chaîne. *Comptes rendus de l'Académie des sciences. Série 2 Mécanique, Physique, Chimie, Sciences de l'univers, Sciences de la Terre* 311:147–152
- Burg JP, Van den Driessche J, Brun JP (1994) Syn- to post-thickening extension in the Variscan Belt of Western Europe: modes and structural consequences. *Géologie de la France* 3:33–51
- Cartigny MJ, Ventra D, Postma G, van Den Berg JH (2014) Morphodynamics and sedimentary structures of bedforms under supercritical-flow conditions: new insights from flume experiments. *Sedimentology* 61:712–748
- Catalán JRM, Aller J, Alonso JL, Bastida F (2009) The Iberian Variscan orogen. Spanish geological frameworks and geosites: an approach to Spanish geological heritage of international relevance. *IGME, Madrid*, pp 13–27
- Châteauneuf JJ, Farjanel G (1989) Synthèse géologique des bassins permien français. Éditions du BRGM, Paris
- Choulet F, Faure M, Fabbri O, Monié P (2012) Relationships between magmatism and extension along the Autun–La Serre fault system in the Variscan Belt of the eastern French Massif Central. *Int J Earth Sci* 101:393–413
- Clarke JEH (2016) First wide-angle view of channelized turbidity currents links migrating cyclic steps to flow characteristics. *Nat Commun* 7:1–13
- Clarke JH, Brucker S, Muggah J, Hamilton T, Cartwright D, Church I, Kuus P (2012) Temporal progression and spatial extent of mass wasting events on the Squamish prodelta slope. *Landslides and engineered slopes: protecting society through improved understanding*. Taylor and Francis Group, London, pp 1091–1096
- Costa S, Rey P (1995) Lower crustal rejuvenation and growth during post-thickening collapse: insights from a crustal cross section through a Variscan metamorphic core complex. *Geology* 23:905–908
- Davies IC, Walker RG (1974) Transport and deposition of resedimented conglomerates; the Cap Enrage Formation, Cambro-Ordovician, Gaspé, Quebec. *J Sediment Res* 44:1200–1216
- Debeglia N, Debrand-Passard S (1980) Principaux accidents tectoniques issus des corrélations entre les données de géophysique et les données de terrain (au sens large), dans le Sud-Ouest du bassin de Paris. *Bulletin de la Société géologique de France* 7:639–646
- Delmas J, Houel P, Vially R (2002) Paris basin, petroleum potential. IFP, Mumbai
- Dietrich P, Ghienne JF, Normandeau A, Lajeunesse P (2016) Upslope-migrating bedforms in a proglacial sandur delta: cyclic steps from river-derived underflows? *J Sediment Res* 86:112–122
- Donsimoni M (1981) Synthèse géologique du bassin houiller lorrain. *Mémoires du B.R.G.M., Paris*, p 117
- Donsimoni M (1990) Le gisement de charbon de Lucenay-lès-Aix (Nièvre). *Documents du BRGM* 179:84
- Donsimoni M (2006) Le gisement de charbon de Lucenay-lès-Aix (Nièvre). In: *Etat des connaissances acquises par le B.R.G.M. entre 1981 et 1986—Rapport final—Projet n°PDI06CDG54 (No. BRGM/RC-54694-FR)*. Rapports du B.R.G.M. Orléans.
- Doubinger J, Elsass P (1979) Le bassin Permo-Carbonifère d'Autun. Nouvelles données stratigraphiques et palynologiques. *Bulletin Trimestriel de la Société d'Histoire Naturelle et des Amis du Muséum d'Autun* 91:9–25
- Ducassou C, Mercuzot M, Bourquin S, Rossignol C, Pellenard P, Beccaletto L et al (2019) Sedimentology and U–Pb dating of Carboniferous to Permian continental series of the northern Massif Central (France): Local palaeogeographic evolution and larger scale correlations. *Palaeogeogr Palaeoclimatol Palaeoecol* 533:109228
- Durand M (2006) The problem of the transition from the Permian to the Triassic Series in southeastern France: comparison with other Peritethyan regions. *Geol Soc Lond Spec Publ* 265:281–296
- Elsass-Damon FE (1977) Les « schistes bitumineux » du bassin d'Autun: pétrographie, minéralogie, cristallographie, pyrolyse. *Dissertation, Université de Bourgogne*
- Faure M (1995) Late orogenic carboniferous extensions in the Variscan French Massif Central. *Tectonics* 14:132–153
- Faure M, Becq-Giraudon JF (1993) Sur la succession des épisodes extensifs au cours du désépaississement carbonifère du Massif Central français. *Comptes rendus de l'Académie des sciences. Série 2 Mécanique Physique Chimie Sciences de l'univers Sciences de la Terre* 316:967–973
- Fielding CR, Frank TD, Isbell JL (2008) The late Palaeozoic ice age—a review of current understanding and synthesis of global climate patterns. *Resolving the late Palaeozoic ice age in time and space*, vol 441. Geological Society of America, Washington, pp 343–354

- Frank W, Haak V, Oncken O, Tanner D (2000) Orogenic processes: quantification and modelling in the Variscan belt. *Geol Soc Lond Spec Publ* 179:1–3
- Franke W, Cocks LRM, Torsvik TH (2017) The Palaeozoic Variscan oceans revisited. *Gondwana Res* 48:257–284
- Gastaldo RA, DiMichele WA, Pfefferkorn HW (1996) Out of the ice-house into the greenhouse: a late Paleozoic analogue for modern global vegetational change. *Gsa Today* 6:2–7
- Genna A, Roig JY, Debrieite PJ, Bouchot V (1998) Le bassin houiller d'Argentan (Massif Central français), conséquence topographique d'un plissement de son substratum varisque. *Comptes Rendus de l'Académie des Sciences Series IIA Earth Planet Sci* 327:279–284
- Glennie KW, Higham J, Stemmerik L (2003) The Permian of the Northern North Sea. *Millennium Atlas: petroleum geology of the Central and Northern North Sea*. Geological Society of London, London, pp 91–103
- Grangeon M, Feys R, Greber CH, Raymond AL (1968) Géologie profonde de la région de Decize (Nièvre). *Essai de synthèse d'après les sondages profonds*. *Bull Bur Rech Géol Min* 4:43–108
- Heckel PH, Clayton G (2006) The Carboniferous System. Use of the new official names for the subsystems, series, and stages. *Geologica Acta* 4:403–407
- Isbell JL, Miller MF, Wolfe KL, Lenaker PA (2003) Timing of late Paleozoic glaciation in Gondwana: was glaciation responsible for the development of northern hemisphere cyclothems? *Spec Pap Geol Soc Am* 370:5–24
- Langiaux J (1984) Flores et faunes des formations supérieures du Stéphanien de Blanzy-Montceau (Massif Central français): stratigraphie et paléooécologie. *Rev La Physiophile Soc Et Sci Nat H ist Montceau* 100:1–270
- Lardeaux JM, Ledru P, Daniel I, Duchene S (2001) The Variscan French Massif Central—a new addition to the ultra-high pressure metamorphic 'club': exhumation processes and geodynamic consequences. *Tectonophysics* 332:143–167
- Lebreton ML (1990) Les bassins stephano-permiens du sud du bassin de paris: controle structural et sedimentologique. *Dissertation, University of Paris 11*
- López-Gamundí OR, Buatois LA (eds) (2010) Late Paleozoic glacial events and postglacial transgressions in Gondwana. *Geological Society of America, Washington*, p 468
- Lotout C, Pitra P, Poujol M, Anczkiewicz R, Van Den Driessche J (2018) Timing and duration of Variscan high-pressure metamorphism in the French Massif Central: a multimethod geochronological study from the Najac Massif. *Lithos* 308:381–394
- Lowe DR (1982) Sediment gravity flows; II, depositional models with special reference to the deposits of high-density turbidity currents. *J Sediment Res* 52:279–297
- Malavieille J, Guihot P, Costa S, Lardeaux JM, Gardien V (1990) Collapse of the thickened Variscan crust in the French Massif Central: Mont Pilat extensional shear zone and St. Etienne Late Carboniferous basin *Tectonophysics* 177:139–149
- Mascle A (1990) Géologie pétrolière des bassins permien français. Comparaison avec les bassins permien du Nord de l'Europe. *Chronique de la recherche minière* 499:69–86
- Mathis V, Brulhet J (1990) Les gisements uranifères du bassin permien de Bourbon-l'Archambault (nord du Massif Central français). *Chronique de la recherche minière* 499:19–30
- Matte P (1986) La chaîne varisque parmi les chaînes paléozoïques péri atlantiques, modèle d'évolution et position des grands blocs continentaux au Permo-Carbonifère. *Bulletin de la Société géologique de France* 2:9–24
- McCann T, Pascal C, Timmerman MJ, Krzywiec P, López-Gómez J, Wetzel L et al (2006) Post-Variscan (end Carboniferous-Early Permian) basin evolution in western and central Europe. *Geol Soc Lond Memoirs* 32:355–388
- Ménard G, Molnar P (1988) Collapse of a Hercynian Tibetan plateau into a late Palaeozoic European Basin and Range province. *Nature* 334:235–237
- Menning M, Alekseev AS, Chuvashov BI, Davydov VI, Devuyt FX, Forke HC et al (2006) Global time scale and regional stratigraphic reference scales of central and west Europe, east Europe, Tethys, south China, and North America as used in the Devonian–Carboniferous–Permian Correlation Chart 2003 (DCP 2003). *Palaeogeogr Palaeoclimatol Palaeoecol* 240:318–372
- Miall AD (1978) Tectonic setting and syndepositional deformation of molasse and other nonmarine-paralic sedimentary basins. *Can J Earth Sci* 15:1613–1632
- Miall AD (1996) The geology of fluvial deposits. *Sedimentary facies, basin analysis, and petroleum geology*. Springer, Berlin
- Michel LA, Tabor NJ, Montañez IP, Schmitz MD, Davydov VI (2015) Chronostratigraphy and palaeoclimatology of the Lodève Basin, France: evidence for a pan-tropical aridification event across the Carboniferous–Permian boundary. *Palaeogeogr Palaeoclimatol Palaeoecol* 430:118–131
- Montañez IP, Poulsen CJ (2013) The Late Paleozoic ice age: an evolving paradigm. *Annu Rev Earth Planet Sci* 41:629–656
- Montañez IP, Tabor NJ, Niemeier D, DiMichele WA, Frank TD, Fielding CR et al (2007) CO₂-forced climate and vegetation instability during Late Paleozoic deglaciation. *Science* 315:87–91
- Montañez IP, McElwain JC, Poulsen CJ, White JD, DiMichele WA, Wilson JP et al (2016) Climate, pCO₂ and terrestrial carbon cycle linkages during late Palaeozoic glacial–interglacial cycles. *Nat Geosci* 9:824–828
- Mulder T, Alexander J (2001) The physical character of subaqueous sedimentary density flows and their deposits. *Sedimentology* 48:269–299
- Paquette JL, Ballèvre M, Peucat JJ, Cornen G (2017) From opening to subduction of an oceanic domain constrained by LA-ICP-MS U–Pb zircon dating (Variscan belt, Southern Armorican Massif, France). *Lithos* 294:418–437
- Pellenard P, Gand G, Schmitz M, Galtier J, Broutin J, Stéyer JS (2017) High-precision U–Pb zircon ages for explosive volcanism calibrating the NW European continental Autunian stratotype. *Gondwana Res* 51:118–136
- Perrodon A, Zabek J (1990) Paris basin. Interior cratonic basins. *AAPG Memoir* 51:633–679
- Pisarska-Jamroz M, Weckwerth P (2013) Soft-sediment deformation structures in a Pleistocene glaciolacustrine delta and their implications for the recognition of subenvironments in delta deposits. *Sedimentology* 60:637–665
- Postma G (1984) Mass-flow conglomerates in a submarine canyon: Abrijoa fan-delta, Pliocene, southeast Spain. *Sedimentol Gravels Conglom Memoir* 10:237–256
- Postma G (1990) An analysis of the variation in delta architecture. *Terra Nova* 2:124–130
- Postma G, Cartigny MJ (2014) Supercritical and subcritical turbidity currents and their deposits—a synthesis. *Geology* 42:987–990
- Postma G, Roep TB (1985) Resedimented conglomerates in the bottomsets of Gilbert-type gravel deltas. *J Sediment Res* 55:874–885
- Postma G, Kleverlaan K, Cartigny MJ (2014) Recognition of cyclic steps in sandy and gravelly turbidite sequences, and consequences for the Bouma facies model. *Sedimentology* 61:2268–2290
- Rohais S, Eschard R, Ford M, Guillocheau F, Moretti I (2007) Stratigraphic architecture of the Plio-Pleistocene infill of the Corinth Rift: implications for its structural evolution. *Tectonophysics* 440:5–28
- Roscher M, Schneider JW (2006) Permo-Carboniferous climate: early Pennsylvanian to Late Permian climate development of central Europe in a regional and global context. *Geol Soc Lond Spec Publ* 265:95–136

- Rubi R, Rohais S, Bourquin S, Moretti I, Desaubliaux G (2018) Processes and typology in Gilbert-type delta bottomset deposits based on outcrop examples in the Corinth Rift. *Mar Pet Geol* 92:193–212
- Schneider JW, Scholze F (2018) Late Pennsylvanian–Early Triassic conchostracan biostratigraphy: a preliminary approach. *Geol Soc Lond Spec Publ* 450:365–386
- Schneider JW, Lucas SG, Scholze F, Voigt S, Marchetti L, Klein H, Opluštil S, Werneburg R, Golubev VK, Barrick JE, Nemyrovska T, Ronchi A, Day MO, Silantiev VV, Rößler R, Saber H, Linneemann U, Zharinova V, Shen S (2020) Late Palaeozoic–early Mesozoic continental biostratigraphy—links to the Standard Global Chronostratigraphic Scale. *Palaeoworld* 29:186–238
- Scotese CR, Langford RP (1995) Pangea and the palaeogeography of the Permian. *The Permian of Northern Pangea*. Springer, Berlin, pp 3–19
- Stampfli GM, Hochard C, Vérard C, Wilhem C (2013) The formation of Pangea. *Tectonophysics* 593:1–19
- Vallé B, Courel L, Gelard JP (1988) Les marqueurs de la tectonique synsédimentaire et syndiagénétique dans le bassin stéphanien à régime cisailant de Blanzay-Montceau (Massif Central, France). *Bulletin de la Société géologique de France* 4:529–540
- Van Den Driessche J, Brun JP (1989) Un modèle cinématique de l’extension paléozoïque supérieur dans le Sud du Massif Central. *Comptes rendus de l’Académie des sciences. Série 2. Mécanique, Physique, Chimie, Sciences de l’univers, Sciences de la Terre* 309:1607–1613
- Van Den Driessche J, Brun J (1992) Structure and evolution of late Variscan extensional gneiss dome (Montagne Noire, southern Massif Central, France). *Geodin Acta* 5:85–99
- Walker RG (1975) Generalized facies models for resedimented conglomerates of turbidite association. *Geol Soc Am Bull* 86:737–748

3.6.6. Le bassin d'Autun

Contexte géologique

Le bassin d'Autun, situé au sud du Morvan, couvre une superficie d'environ 250 km² (Figure 23). Il repose en discordance sur un substratum magmatique/métamorphique et sédimentaire du Dévonien au Carbonifère (Carrat, 1969). Il consiste en une série sédimentaire d'environ 1200 m d'épaisseur, composée d'une alternance de lithologies très largement silicoclastiques à grains moyens/grossiers et de lithologies à grains fins, ces dernières comprenant des séquences houillères et de schistes bitumineux (i.e. black-shales ; Marteau, 1983 ; Garel et al., 2017). Le calage temporel des dépôts a récemment été précisé sur la base d'âges U-Pb CA-ID-TIMS sur tonsteins (cinérites) interstratifiés dans la série (depuis la fin du Ghzélien (Carbonifère terminal) au début de l'Assélien (Permien basal ; Pellenard et al. 2017)).

Le bassin est décrit comme un demi-graben (Marteau 1983; BRGM, 1989), dont la subsidence au stéphano-permien est supposée contrôlée (au moins partiellement) par une faille normale possiblement identifiée sur sa bordure méridionale (faille d'Autun ; Marteau, 1983; Choulet et al. 2012). Historiquement le bassin d'Autun a été largement étudié pour son contenu paléontologique (flore et faune) et ses ressources minérales (charbon, pétrole, schistes bitumineux et uranium ; Pruvost, 1942 ; Elsass-Damon, 1977, Marteau, 1983). Les investigations sédimentologiques et reconstitutions paléoenvironnementales les plus récentes avaient été principalement réalisées par Marteau (1983), qui a attribué les sédiments laminés à grain fin et les schistes bitumineux à des environnements palustres/lacustres, tandis que les sédiments plus grossiers (incluant les grès et les conglomérats à mégarides 3D), ont été interprétés comme typiques de systèmes fluviaux.

Le bassin d'Autun : faciès, stratigraphie séquentielle et paléoenvironnements - Publication 6

Mercuzot M., Bourquin S., Pellenard P., Beccaletto L., Schnyder J., Baudin F., Ducassou C. ; Garel S., Gand G. (2022) Reconsidering Carboniferous–Permian continental paleoenvironments in eastern equatorial Pangea: facies and sequence stratigraphy investigations in the Autun Basin (France), International Journal of Earth Sciences, 111, 1663-1696. <https://doi.org/10.1007/s00531-022-02200-6>

Ce travail est basé sur des descriptions sédimentologiques de quatre forages carottés traduites en terme de stratigraphie séquentielle, complétée par une étude terrain de quelques affleurements clés. Il a permis de complètement réévaluer les paléoenvironnements de dépôts du bassin d'Autun.

Principaux résultats issus de la publication 6

- La base du remplissage sédimentaire du bassin d'Autun, précédemment attribué à des environnements strictement fluviaux alternant avec des milieux et palustres-lacustres, correspond plutôt à une alternance de dépôts deltaïques progradant dans un environnement lacustre (sans préservation de dépôts fluviaux). Elle apporte donc la preuve qu'à la fin du Carbonifère et au début du Permien (~ 299 Ma), le bassin d'Autun a été soumis à des épisodes de variation d'accommodation, soit en réponse au climat, soit en réponse à des variations de subsidence, dont les rôles respectifs restent à déterminer.

- Pendant les périodes de haut niveau lacustre (i.e. accommodation importante), la préservation des sédiments riches en matière organique a été favorisée par le développement de conditions dysoxiques/anoxiques, également atteintes pendant les épisodes de bas niveau du lac lorsque les environnements de dépôt étaient protégés des apports détritiques. Ces conditions, quand elles sont associées à une faible turbidité de l'eau, ont également permis de développer la photosynthèse microbienne se traduisant par la minéralisation des tapis microbiens (microbialites). En outre, la présence d'arbres en position de vie et de paléosols indique que certaines parties du bassin étaient occasionnellement émergées, notamment à proximité de la limite entre le Gzhélien-Assélien.
- La présence de dépôts lacustres profonds en bordure actuelle du bassin d'Autun, ainsi que l'absence de transition latérale entre le système deltaïque-lacustre et les zones en érosion en amont, indiquent que ces limites ne sont qu'érosives et ne correspondent donc pas aux limites initiales du bassin au moment de son remplissage sédimentaire. Ceci suggère que les bassins carbonifères-permiens du nord-est du Massif Central étaient plus larges que les aires de sédimentation préservées aujourd'hui, et qu'ils ont pu être connectés pour former un bassin plus étendu, comme le confirment également les données sismiques et la paléobiogéographie (*Beccaletto et al., 2015 ; Fisher et al., 2013).
- Plus généralement, ce travail met en évidence une possible sous-estimation de l'étendue et de l'épaisseur des systèmes sédimentaires dans l'est de la Pangée équatoriale à la fin du Carbonifère et au début du Permien. Ces régions constituaient probablement un puits de CO₂ atmosphérique grâce au stockage du carbone organique dans les sédiments, jouant un rôle déterminant dans les variations climatiques connues à cette époque.

Publication 6

International Journal of Earth Sciences
<https://doi.org/10.1007/s00531-022-02200-6>

ORIGINAL PAPER



Reconsidering Carboniferous–Permian continental paleoenvironments in eastern equatorial Pangea: facies and sequence stratigraphy investigations in the Autun Basin (France)

Mathilde Mercuzot^{1,2} · Sylvie Bourquin¹ · Pierre Pellenard² · Laurent Beccaletto³ · Johann Schnyder⁴ · François Baudin⁴ · Céline Ducassou¹ · Sylvain Garel^{5,6} · Georges Gand²

Received: 27 August 2021 / Accepted: 25 April 2022
 © Geologische Vereinigung e.V. (GV) 2022

Abstract

The late Carboniferous–early Permian represents a key period in the Phanerozoic history, given the major global geodynamic and climate modifications. The aim of this work is to better understand the context and characteristics of the sedimentation recorded in the continental environments of eastern equatorial Pangea at this time, through the example of the Autun Basin (northeastern Massif Central, France). The Autun Basin contains the historical stratotype of the Autunian continental stage, and its stratigraphy was recently improved by accurate numerical ages. This basin formed in an extensional tectonic context during the latest stages of the Variscan orogeny, and it is essential to study its paleoenvironmental evolution to provide new insights into the sedimentary evolution of contemporaneous surrounding basins. Using field and subsurface data, we propose a refined sedimentological model for the Autun Basin, relying on updated facies interpretations, organic matter content fluctuations, and sequence stratigraphy concepts and correlations. The continental environments of the lower sedimentary succession of the Autun Basin, previously considered to be fluvial and lacustrine, are herein re-interpreted as mainly lacustrine, comprising fine-grained organic matter-rich deposits, and supplied by coarser-grained deltaic siliciclastic sediments, without preservation of strict fluvial sedimentation. The determination of the sequence stratigraphy cycles, strengthened by the quantification of the organic matter content, and reflected by the temporal succession of progradational and retrogradational trends, is used to determine new correlations between several sections, as well as to reconstruct the paleoenvironment evolution at the Carboniferous–Permian transition. This study provides evidence that the sedimentation area of the Autun Basin at the time of its filling was much larger than the preserved basin area, and suggests connections with contemporaneous neighboring French basins, pointing to a large sedimentary system in the northeastern Massif Central area rather than narrow and isolated basins.

Keywords Gzhelian · Asselian · Continental delta environments · Late-Variscan basin · Paleoenvironment · Paleogeography

✉ Mathilde Mercuzot
mathilde.mercuzot@outlook.com

¹ Univ Rennes, CNRS, Géosciences Rennes - UMR 6118, 35000 Rennes, France

² Biogéosciences UMR uB/CNRS 6282, Université Bourgogne Franche-Comté, 21000 Dijon, France

³ BRGM, 45060 Orléans, France

⁴ Institut des Sciences de la Terre de Paris (ISTeP), UMR 7193 CNRS, Sorbonne Université, 75005 Paris, France

⁵ Energy and Geoscience Institute, The University of Utah, Salt Lake City, UT 84108, USA

⁶ CVA Engineering, 6 Avenue Eiffel, 78420 Carrières-sur-Seine, France

Introduction

The late Carboniferous–early Permian (CP) is a key period in the Phanerozoic history, due to large-scale geodynamic modifications, including the latest Variscan orogeny stages and the onset of the breakup of Pangea (e.g., Ménard and Molnar 1988; Stampfli and Kozur 2006), as well as a major climate upheaval marked by the acme of the Late Paleozoic Ice Age (LPIA), constituting a turning point in the climate modes of the Paleozoic (e.g., Gastaldo et al. 1996; Montañez et al. 2007). Given the presence of large tropical rainforests (Cleal and Thomas 2005) and the tremendous rates of organic carbon burial in sediments at that time (i.e., coal and black-shale deposits), intertropical areas constituted a major

Published online: 28 May 2022

Springer

atmospheric CO₂ sink. It is, therefore, of utmost importance to explore paleointertropical basins, because their sensitivity to climate forcings has been underestimated in paleoclimate scenarios (e.g., Soreghan et al. 2020). At that time, intertropical latitudes are mainly considered as a mountainous region submitted to tropical weathering (e.g., Godd ris et al. 2017), and therefore mainly in erosion; active sedimentation areas are not fully considered in either the terrestrial paleogeography reconstructions or in the climate modeling. Continental sediments accumulated during the CP period are preserved in Western and Central Europe, in basins developed in an extensional tectonic setting, linked with the syn- to late-orogenic Variscan stages (e.g., Faure et al. 2009; Kroner and Romer 2013). In France, these sedimentary successions are considered as having been deposited in a multitude of small unconnected basins (e.g., Schneider and Scholze 2018), such as those found in the northeastern part of the Massif Central (Aumance, Decize–La Machine, Blanzay–Le Creusot and Autun basins, Fig. 1), presenting roughly similar sedimentary patterns and hosting detrital sediments mostly derived from the erosion of the Variscan mountain belt (Vall  et al. 1988; Van den Driessche and Brun 1989; Burg et al. 1990; Malavieille et al. 1990; Faure and Becq-Giraudon 1993; Brun and van den Driessche 1994; Faure 1995; Becq-Giraudon et al. 1996; Genna et al. 1998).

Among these basins, the Autun Basin, containing the historical regional stratotype of the Autunian continental stage (Mayer-Eymar 1881; Gaudry 1883; Bergeron 1889; Munier-Chalmas and de Lapparent 1893), was mostly studied for its carbonaceous resources and outstanding paleontological record (e.g., Gaudry 1883; Sauvage 1890; Renault 1896; Landriot 1936; Doubinger 1970; Bouroz and Doubinger 1975; Elsass-Damon 1977; Gand et al. 2011, 2012, 2014). This basin was recently dated using the U–Pb method on interbedded volcanic layers, allowing to precisely assign the Gzhelian and Asselian stages to the regional stratigraphy (Pellenard et al. 2017) and thereby enabling additional correlations with other Carboniferous–Permian basins and global events. However, few detailed sedimentological studies have been carried out since the seminal work of Marteau (1983), all arguing in favor of fluvial, palustrine and lacustrine depositional environments. More recent studies of neighboring CP basins, using modern concepts and analytical tools, including integrative sedimentological studies and sequence stratigraphy principles, along with well-log and seismic data as well as geochemical proxies, suggest that the depositional setting and environmental model of the northeastern Massif Central CP basins, including the Autun Basin, should be reconsidered (Aumance Basin, Mathis and Brulhet 1990; Decize–La Machine and Autun basins, Mercuzot et al. 2021a, b).

In a wider view, these northeastern Massif Central basins are in a key position between the Central European Permian

Basin and the southern (e.g., Lod ve, Saint-Affrique, Rodez, Brive or Pyrenean/South Alpine) basins. Therefore, reevaluated data from the Autun Basin would help to (i) accurately characterize the sedimentary dynamics and the nature of the sediments preserved in this equatorial continental system (i.e., through paleoenvironment reconstructions), (ii) specify the size of the initial sedimentation areas, allowing to thereafter integrate paleoenvironments into paleogeography reconstructions, something which has so far been challenging (e.g., Glennie et al. 2003; Roscher and Schneider 2006; Schneider and Scholze 2018), and lastly (iii) improve our knowledge on the dynamics of equatorial terrestrial systems during the CP period.

Therefore, we propose herein to re-evaluate the depositional model of the Autun Basin, based on modern sedimentological concepts including both facies and sequence stratigraphy analyses, performed on core and outcrop sections. Last, we aim to explain the variability of the lithological succession in terms of the paleoenvironmental evolution through time and space and to provide new constraints on the extent of the sedimentation areas during the CP period in the northeastern French Massif Central.

Geological setting of the Autun Basin

The CP Autun Basin is located in Burgundy (France), south of the Morvan Massif, in the northeastern part of the Massif Central (Fig. 1). It covers an area extending over ~250 km² and overlies a Devonian to Carboniferous magmatic/metamorphic and sedimentary substratum (Carrat 1969). It displays a sedimentary succession that is approximately 1.2 km thick, composed of alternating medium-to-coarse and fine-grained lithologies; the latter includes coal-bearing sequences and black-shale deposits, i.e., oil-shale beds (OSBs) (Marteau 1983). The depositional time frame has recently been constrained to a time period ranging from the late Gzhelian (latest Carboniferous) to the early Asselian (earliest Permian, Pellenard et al. 2017; Fig. 1c), using high-resolution chemical abrasion–isotope dilution–thermal ionization mass spectrometry (CA–ID–TIMS) U–Pb ages from interbedded tonsteins, i.e., distal volcanic ash-fall layers deposited in continental environments, and altered in clay minerals, dominated by kaolinite (Spears 2012). The structure of the basin was described as a half-graben, later deformed due to an episode of tectonic flexure (e.g., Delafond 1889; Feys and Greber 1972; Marteau 1983; Ch teau-neuf and Farjanel 1989). Along the straight-lined southern margin, it is inferred that a brittle normal fault, named the Autun fault, partly controlled the CP subsidence of the basin (Marteau 1983; Choulet et al. 2012); today, it separates the sedimentary succession of the Autun Basin from a southerly Carboniferous (Westphalian) granitic pluton

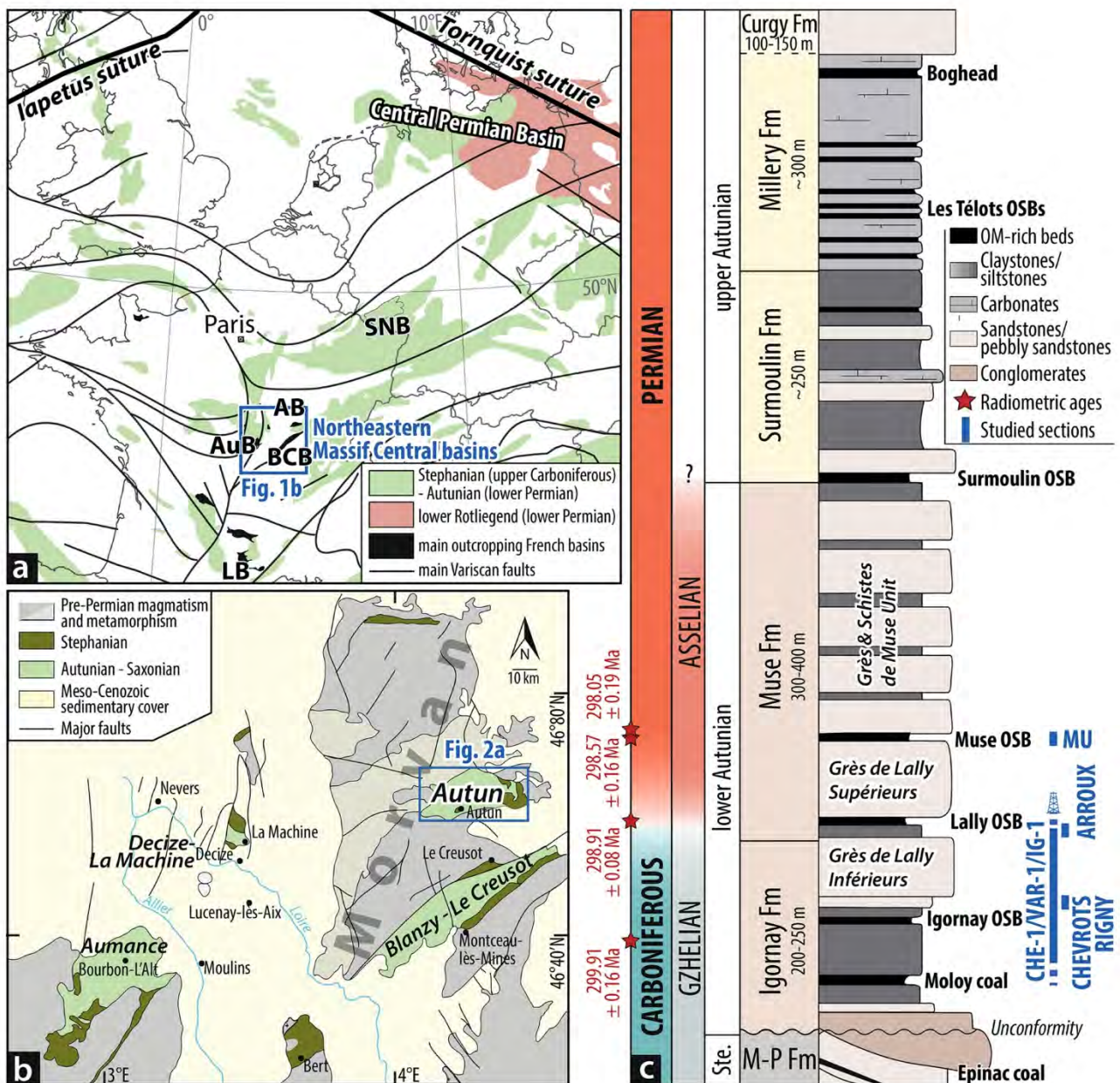


Fig. 1 **a** Map of Western Europe showing the main Variscan tectonic structures and the surface and subsurface Permian basins (modified from Beccaletto et al. 2015 and Schneider and Scholze 2018). **b** Geological map of the northeastern Massif Central, France, with the location of the late Carboniferous to early Permian basins. Modified from Elsass-Damon 1977. **c** Synthetic sedimentary succession and stratigraphy of the Autun Basin including the radiometric ages reported by Pellencard et al. (2017), the lithostratigraphic divisions (formations and units), the major oil-shale beds, and the studied sections. SNB Saar-Nahe Basin, AB Autun Basin, BCB Blanzay–Le Creusot Basin, AuB Aumance Basin, LB Lodève Basin, Ste. Stephanian, OSB oil-shale bed, OM organic matter, M-P Fm Mont-Pelé formation

raphy of the Autun Basin including the radiometric ages reported by Pellencard et al. (2017), the lithostratigraphic divisions (formations and units), the major oil-shale beds, and the studied sections. SNB Saar-Nahe Basin, AB Autun Basin, BCB Blanzay–Le Creusot Basin, AuB Aumance Basin, LB Lodève Basin, Ste. Stephanian, OSB oil-shale bed, OM organic matter, M-P Fm Mont-Pelé formation

(Mesvres Granite, Fig. 2a). Along the northern basin's margin, Permian deposits unconformably overlie the Viséan Lucenay-Lévêque Massif. To the east, the contact between the magmatic basement and the Paleozoic sedimentary units is partly covered by the Mesozoic series, and to the west, the basin is limited by the Saint-Honoré-les-Bains Massif (Marteau 1983, Fig. 2a).

The sedimentary succession of the Autun Basin (Fig. 1c) encompasses two continental regional stages, the Stephanian and the Autunian, originally defined by their floristic content, and separated by an unconformity (e.g., Roche 1881; see Gand et al. 2017 for details). The Stephanian is represented by the Épinac Formation (Fm), including coal beds and OSBs, and is topped by the Mont-Pelé

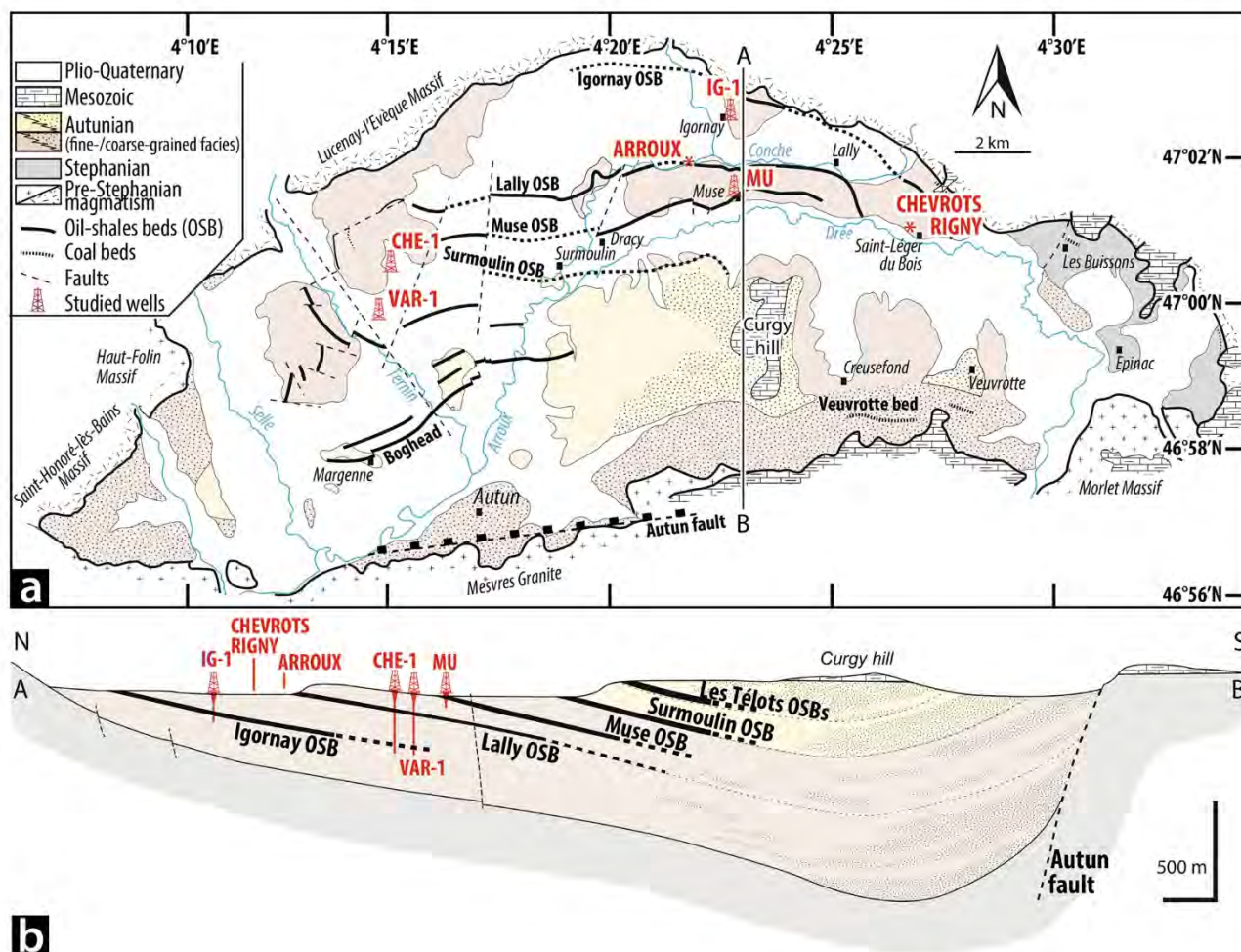


Fig. 2 **a** Geological map of the Autun Basin including the lithostratigraphic divisions (same Fm colors as in Fig. 1c) and the studied subsurface and outcrop sections. Modified from Gand et al. (2007). **b** Cross-section of the Autun Basin displaying the lithostratigraphic

divisions and the studied wells and sections. The VAR-1, CHE-1, Rigny and Chevrots sections are projected given their approximate position in the stratigraphy. IG-1 Igornay well, CHE-1 Chevrey well, VAR-1 Varolles well, MU Muse well and section

Fm, immediately below the base of the Autunian series (Fig. 1c). The sedimentation area of the Stephanian Épinac Fm is restricted to the Épinac area, in the eastern part of the Autun Basin (Fig. 2a), whereas the Autunian deposits are preserved towards the center and the western part of the basin, where they directly lie on the magmatic substratum (Fig. 2). This Autunian succession is subdivided into the lower and upper Autunian, the latter being only preserved in the center of the basin (Pruvost 1942; Marteau 1983; Gand et al. 2017). The lithostratigraphic units were first described by Delafond (1889), followed by Pruvost (1942) and Marteau (1983), who distinguished five units that are equivalent to the present-day formations: (i) the Igornay Fm (200–250 m thick, lower Autunian), composed of claystones and siltstones with organic matter (OM)-rich beds, i.e., the Moloy coal and the Igornay OSB, and topped by the sandy *Grès de Lally Inférieurs* Unit

(Fig. 1c), (ii) the Muse Fm (300–400 m thick, lower Autunian), subdivided into the sandy *Grès de Lally Supérieurs* Unit, with the Lally OSB at its base and the Muse OSB at its top, and the *Grès et Schistes de Muse* Unit (Fig. 1c), (iii) the Surmoulin Fm (~250 m thick, upper Autunian), mainly fine-grained, with the Surmoulin OSB at the base and some dolomitic levels (Fig. 1c), (iv) the Millery Fm (~300 m thick, upper Autunian), composed of claystones with carbonate beds, some OM-rich deposits including the Les Télots OSBs and the pure algal-coal Boghead bed, as well as analcimolite beds in the upper part of the formation (Fig. 1c), and (v) the Curgy Fm (~100–150 m thick, uppermost Autunian), mainly composed of sandstones (Fig. 1c). The thickness of the upper Autunian is roughly estimated, as it is based only on descriptions of previous boreholes obtained from mining exploration, given that outcrops are very sparse and incomplete.

In Curgy Hill, in the center of the basin (Fig. 2), some Mesozoic sedimentary successions are preserved (Triassic and Lower Jurassic), lying above the CP succession (Courel 1970). Due to an erosional event between the Permian and Triassic (Bourquin et al. 2011), it is likely that upper Permian sediments were deposited in the Autun Basin but are no longer preserved.

The Autun Basin has been extensively investigated for its paleontological content (flora and fauna) and its mineral resources (coal, oil and uranium) since the eighteenth century, as described by Pruvost (1942), Elsass-Damon (1977) and Marteau (1983). More recently, studies on OM have attempted to characterize the current alteration of fossil-bearing shales (Odin et al. 2015a, b), as well as to describe the types of OM found in the sediments, their variations in the stratigraphy, particularly in the main OM-rich levels of the basin, as well as the dynamics of the carbon and nitrogen cycles (Garel et al. 2017; Mercuzot et al. 2021b).

Sedimentologically based paleoenvironmental reconstructions in the Autun Basin have mostly been carried out by Marteau (1983), who attributed the fine-grained laminated sediments and OSBs to palustrine/lacustrine environments based on “varve” features (i.e., seasonal alternations of dark- and light-colored laminae), whereas the medium-to-coarse-grained sediments, including sandstones and conglomerates with trough cross-stratifications have been interpreted as strict fluvial systems.

Material and methods

Core and field sections of the Autun Basin

Four unoriented cores drilled in the Autun Basin have been studied: the Chevrey (CHE-1), Varolles (VAR-1), Igornay (IG-1) and Muse (MU) cores (Fig. 2). The IG-1 core, drilled in 1965 by the Génie Rural (French rural engineering) in the village of Igornay (47°2'37.67"N, 4°22'48.70"E; 200 m thick), encompasses a large part of the Igornay Fm, from the Igornay OSB to the *Grès de Lally Inférieurs* Unit (Fig. 1c). The CHE-1 core (47°0'13.17"N, 4°16'11.01"E; 366 m thick) and the VAR-1 core (47°0'0.31"N, 4°16'5.34"E; 266 m thick), located approximately 10 km from the IG-1 well, were drilled in 1982 by the French Geological Survey (BRGM), with the original goal being to cross over the whole lower Autunian succession. The MU core (47°1'36.85"N, 4°22'54.56"E, 8 m thick) was drilled in the village of Muse to complete the observations on the historical Muse outcrop which has been excavated since 2010 for paleontological studies (Gand et al. 2011, 2014, 2015). It encompasses the uppermost part of the *Grès de Lally Supérieurs* Unit at the base of the well, and the totality of the Muse OSB.

Lastly, to complete the analysis of the core data, outcrops of the *Grès de Lally Inférieurs* Unit (Figs. 1c, 2) have been studied at the former Les Chevrots (47°1'15.81"N, 4°26'25.81"E; 8 m thick) and Rigny quarries (47°1'14.35"N, 4°26'4.06"E; 15 m thick), and at the Arroux viaduct section (47°1'57.36"N, 4°21'52.86"E; 6 m thick). The Rigny and Chevrots sections have been previously studied by Marteau (1983), who assigned their medium-to-coarse-grained clastic sediments to a fluvial environment, either meandering or braided, as trough cross-stratifications are found together with beveled sedimentary geometries.

Facies analysis to reconstruct the evolution of the depositional environments

All of the studied sections (i.e., cores and outcrops) belong to the first half of the lower Autunian sedimentary succession (Igornay and Muse fms, Figs. 1c, 2), and have been described according to their granulometry and sedimentary features, at a scale of 1:50 for the MU, IG-1 and CHE-1 cores, and 1:100 for the VAR-1 core.

Each determined sedimentary facies corresponds to a depositional process; the facies are grouped into facies associations, and are then ascribed to depositional environments, i.e., along the succession from a landward to a basinward position (Table 2).

All of the facies codes (Table 1) are largely based on the classifications provided by Miall (1978) and Postma (1990), established for fluvial and delta deposits, respectively. As some facies present in the Autun Basin were not described by these authors (because they are related to other depositional processes), these classifications have therefore been extended in this work, as already done in the works of Ducassou et al. (2019) and Mercuzot et al. (2021a) in the neighboring Decize–La Machine CP Basin.

The granulometry is divided into three grain sizes: fine-grained facies with clays (<4 µm, i.e., claystones) and silts (<63 µm, i.e., siltstones), medium-grained facies with sands (fine sand <0.25 mm < medium sand <0.5 mm < coarse sand <2 mm, i.e., sandstones), and coarse-grained facies, with gravels and some pebbles (<2 cm and >2 cm, respectively, i.e., conglomerates). The grain size is indicated by a capital letter (F for fine-grained facies, S for sands, G for conglomerates; and two capital letters are used for heterolithic facies), preceded by an I when the sets are inclined, and followed by lowercase letters indicating the main sedimentary features or deformations (m for massive, mm for matrix supported, l for horizontal to sub-horizontal laminations, r for current ripples, w for wave ripples, t for trough cross-stratifications, mud for mudclasts, clast for clasts of various nature, i for injectites, and d for deformed structures). T and C represent the tonstein and carbonate levels, respectively.

Table 1 Description of facies observed in the studied sections with their lithologies, sedimentary features and depositional processes

Name	Lithology and Sedimentary structures	Occasional features	Depositional process	Deformations
<i>Fine to medium-grained facies</i>				
F (Figs. 3a, 5b, 6a, d, e, f)	Organic-rich claystones and siltstones to very fine-grained sandstones, massive, sometimes bioturbated or finely laminated (Fig. 6e)	Red laminae (siderite, Fig. 6c), coprolites (Fig. 6f), fish scales, macrophytes fragments, coal fragments, siderite nodules, pyrite, phosphate and dolomitic nodules	Deposition of low-density tails of turbidity currents (Tc, Bouma 1962) or settling of fine-grained particles	Load, micro-slumps (cm-thick beds), fractures, normal and listric faults, convolutes, micro-injectites
F/Sm (Fig. 5b)	Finely-laminated or massive claystones to siltstones, black to gray with thin massive fine-grained sandstone levels	Siderite laminae, coprolites, fish scales, bioturbations siderite nodules, numerous mm-large phyto-clasts in the sandy levels, mudclasts, contacts sometimes gradational	Deposition of low-density tails of turbidity currents and settling of pelagic or hemipelagic particles (Tc, Bouma 1962) alternating with traction carpets/high-density turbidity current (Lowe 1982)	Injectites, convolutes, load, micro-slumps, convolutes, normal faults
F/Sr (Fig. 6b, c)	Black/gray/red finely laminated claystones to siltstones and sandy levels with 2D current ripples (Fig. 6b). Containing numerous mm-large phytoclasts (Fig. 6b)	3D current ripples	Turbidity currents with Tc (ripples) and Td (laminations) Bouma divisions (Bouma 1962)	Load (flames, undulations, ball-and-pillows), micro-slumps, injectites, convolutes, listric, normal and reverse faults
Sm/F (Fig. 5b) – ISm/F	Massive sandstones alternating with massive or laminated fine-grained lithologies (Sm/F), sometimes inclined (ISm/F)	Normal grading, when very fine-grained, the sand can be laminated, mm-large phytoclasts, mudclasts, siderite laminae	High density turbidity currents or grainflows (Mulder and Alexander 2001), sometimes in active foresets (cf. ISm, Ducassou et al. 2019), alternating with settling of particles	Load, faults, boudinage, micro-injectites, convolutes
Su/F	dam to m sandy beds with trough cross-stratifications or planar bedding alternating with fine-grained beds	Siderite laminae in siltstones, mud-clasts, mm-large phytoclasts and coal fragments, aligned gravels	3D megaripple migration (Miall 1996; Davis and Walker 1974; Walker 1975) followed by settling of particles	Load
SF	Lenses of sandstones (50%) alternating with gray siltstones (50%). Both can be either massive or with horizontal laminations, or discrete current ripples. Contacts often gradational	mm-large phytoclasts, bioturbations, nodules, mudclasts or white clasts, rare cm gravel levels	Hyperconcentrated debris flow (Walker 1975; Postma 1990; Mulder and Alexander 2001)/Non-cohesive debris flow (Walker 1975; Lowe 1982; Postma 1990; Miall 1996)	Load, convolutes, normal faults
Fclast	Black siltstones with mm-size white clasts floating or aligned	Coprolites, beefs	Deposition of low-density tails of turbidity currents and settling of pelagic or hemipelagic particles (Tc, Bouma 1962)	Micro-slumps, injectites, load (ball-and-pillows), rare normal faults
<i>Medium to coarse-grained facies</i>				
Sw (Fig. 3d)	Dm thick fine to medium-grained sandstone beds, displaying symmetric ripples at their top (wave-length ~ 5 cm)	–	Oscillatory current influence (waves)	–

Table 1 (continued)

Name	Lithology and Sedimentary structures	Occasional features	Depositional process	Deformations
GSm (Figs. 3a, b, 4b, 5b, 6a) – IGSm (Figs. 4a, c, 5a)	Massive pebbles or sandstones without sedimentary features, sometimes inclined (IGSm). Erosive contact at the base	Matrix or floating pebbles, normal or inverse grading, rare cm fine-grained levels between the beds	Cohesive grain/debris flow deposits (sometimes on active foresets) or high-density turbidity current (Lowe 1982; Davis and Walker 1974; Walker 1975; Postma 1990) or back-set deposits (Breda et al. 2007)	Load, micro-slumps
GSI (Figs. 3b, 4b, 5a) – IGSI (Figs. 4a, c, 5a)	Planar-bedded sandstones or grain-supported conglomerates, sometimes inclined (IGSI). Erosive contact at the base	Mudclasts, mm-large phytoclasts or coal fragments, current ripples	Laminar supercritical flows, traction carpet driven by streamflow (Postma 1990). Alternating periods of erosion and deposition (Cartigny et al. 2014; Postma et al. 2014; Rubi et al. 2018), sometimes in active foresets	Load
GSt (Figs. 3a, b, 4c)	Sandstones to gravelly conglomerates with trough cross-stratifications	Mudclasts, gravel alignments, mm-large phytoclasts, rare bioturbations, pyrite	3D megaripple migration (Miall 1996; Davis and Walker 1974; Walker 1975) or hydraulic jump (active bottomsets, Breda et al. 2007; Clarke et al. 2012; Cartigny et al. 2014; Postma et al. 2014; Dietrich et al. 2016; Clarke 2016)	Micro-injectites, normal faults, micro-slumps
GSB (Fig. 5c)	cm to m beds of normal-graded gravels to fine sandstones, up to siltstones and claystones. Erosive and massive at the base, then laminated and ending with current ripples. Containing numerous mm-large phytoclasts	Mudclasts at the top, siderite nodules, coal fragments	Hyperconcentrated turbidity flow (Ta, Tb and Tc Bouma sequence, Bouma 1962), sometimes settling of fine-grained particles (low-density tail of turbidity current, Te)	Normal faults, load (flames, ball-and-pillows), micro-injectites, injectites, convolutes, micro-slumps
GSmm/F (Fig. 4c) – IGSmm/F	cm to dm beds of massive medium to coarse sandstones to gravels, poorly sorted in gray to black fine-grained matrix, with gradational, flat or erosive base. Floating or aligned white clasts in the black matrix. Sometimes separated by dm levels of fine-grained material	Normal grading, coal fragments, pebbles, mudclasts, mm-large phytoclasts	Hyperconcentrated debris flow (Walker 1975; Postma 1990; Mulder and Alexander 2001)/Non-cohesive debris flow (Walker 1975; Lowe 1982; Postma 1990; Miall 1996), sometimes in active foresets (Ducasseu et al. 2019)	Deformations/homogenization, micro-slumps, micro-injectites, load, boudinage, normal faults, fractures, rare injectites
Smud (Fig. 5b, d)	Well-sorted massive sandstones containing cm to dm mudclasts and rip-up clasts with sometimes gray-to black matrix and white gravels	Coal fragments, siderite clasts and nodules, mudclasts, mm-large phytoclasts,	Non-cohesive debris flow (Walker 1975; Lowe 1982; Postma 1990; Miall 1996)	Injectites, micro-injectites, load (flames), micro-slumps, convolutes
<i>Deformed facies</i> SFI	Massive-sand injection, 3D networks in fine-grained facies	Sills or dykes	Hydrofracturing and injection, clay leaching	Injectites

Table 1 (continued)

Name	Lithology and Sedimentary structures	Occasional features	Depositional process	Deformations
GSPd	Deformed heterolithic facies, with a loss of information on the primary facies	Coarse-grained facies dominate (sand to pebbles)	Slump and slide	Slumps, load
<i>Other facies</i>				
T	Gray to ochre clay or fine-grained sandstones, massive or thinly laminated	–	Tonsteins: altered volcanic ashes in continental environment	Load
Cs	Massive or laminated carbonates	Bird's eyes, pyrite, nodules. Sometimes encrusting remains of trunks (Fig. 3c)	Microbialites or MSS—organomineralization (Dupraz et al. 2009)	Undulations, fractures, faults
Ca	Dolomitic nodules or horizons	Pyrite, carbonate veins, rare clasts and nodules	Diagenetic carbonate precipitation	Fractures, faults

Organic matter characterization

Claystone and siltstone samples from the IG-1 core (215 samples), CHE-1 core (331 samples) and MU core (36 samples) were analyzed using the Rock–Eval thermal analysis method described by Behar et al. (2001) at the IStEP laboratory (Sorbonne Université, Paris). Several measurements were obtained from the successive pyrolysis and oxidation of ~60 mg of powder. Only the total organic carbon (TOC, expressed in wt.%), calculated as the sum of the pyrolyzed and residual organic carbon, is presented here, with an estimated uncertainty of ± 0.05 wt.%.

Sequence stratigraphy

High-resolution sequence stratigraphy principles have been applied to the studied sedimentary succession of the Autun Basin, based on the observed stacking pattern of the smallest stratigraphic units, i.e., parasequences or genetic units (e.g., Cross 1988; Van Wagoner et al. 1988; Mitchum and Van Wagoner 1991; Cross et al. 1993). In continental sedimentary successions, genetic units are defined using a high-resolution reconstruction of the depositional environment evolution, i.e., by determining the position of the deposits along a landward–basinward transect. Therefore, it allows to identify larger-scale progradational–retrogradational cycles (i.e., stratigraphic cycles). These cycles are separated by the maximum regressive surface (MRS, lowest lake level, at the end of the progradational trend), and topped by the maximum flooding surfaces (MFS, highest lake level, at the end of the retrogradational trend, Wheeler 1964; Cross et al. 1993). Stratigraphic cycles depend on variations of the accommodation space 'A' combined with changes in sediment supply 'S', both of which are driven by climate (i.e., precipitation vs. evaporation rates, driving lake expansion/contraction phases) and deformation (tectonic processes, subsidence of the basin, e.g., Cross 1988; Jervey 1988; Galloway 1989; Galloway and Williams 1991; Mutto and Steel 2002; Péron et al. 2005; Bourquin et al. 2009); the trend is retrogradational when $A/S > 1$ and progradational when $A/S < 1$.

In a mixed alluvial and lacustrine depositional environment, MFSs can reliably be used to recognize, delineate, and correlate genetic sequences (e.g., Bourquin et al. 1998), and the quantification of the OM content makes it easier to identify them. Sedimentary OM content (i.e., OM preservation, reflected by the TOC values), depending on OM production minus OM degradation, versus OM dilution (Bohacs 1990; Bohacs et al. 2000), is at its maximum in the most profundal lacustrine deposits (corresponding to MFSs) where the sedimentation rates are low, and where the sediments and the base of the water column remain dysoxic or anoxic, preventing the remineralization of OM. On the contrary,

MRSs are defined where the most landward environments are observed, most of the time associated with low OM content due to effective oxidation.

Re-evaluation of the paleoenvironments

Determination of the depositional environments from facies associations

The sedimentary description of both the field sections and the cored wells of the Autun Basin has highlighted a total of 19 facies, detailed in Table 1 and pictured in

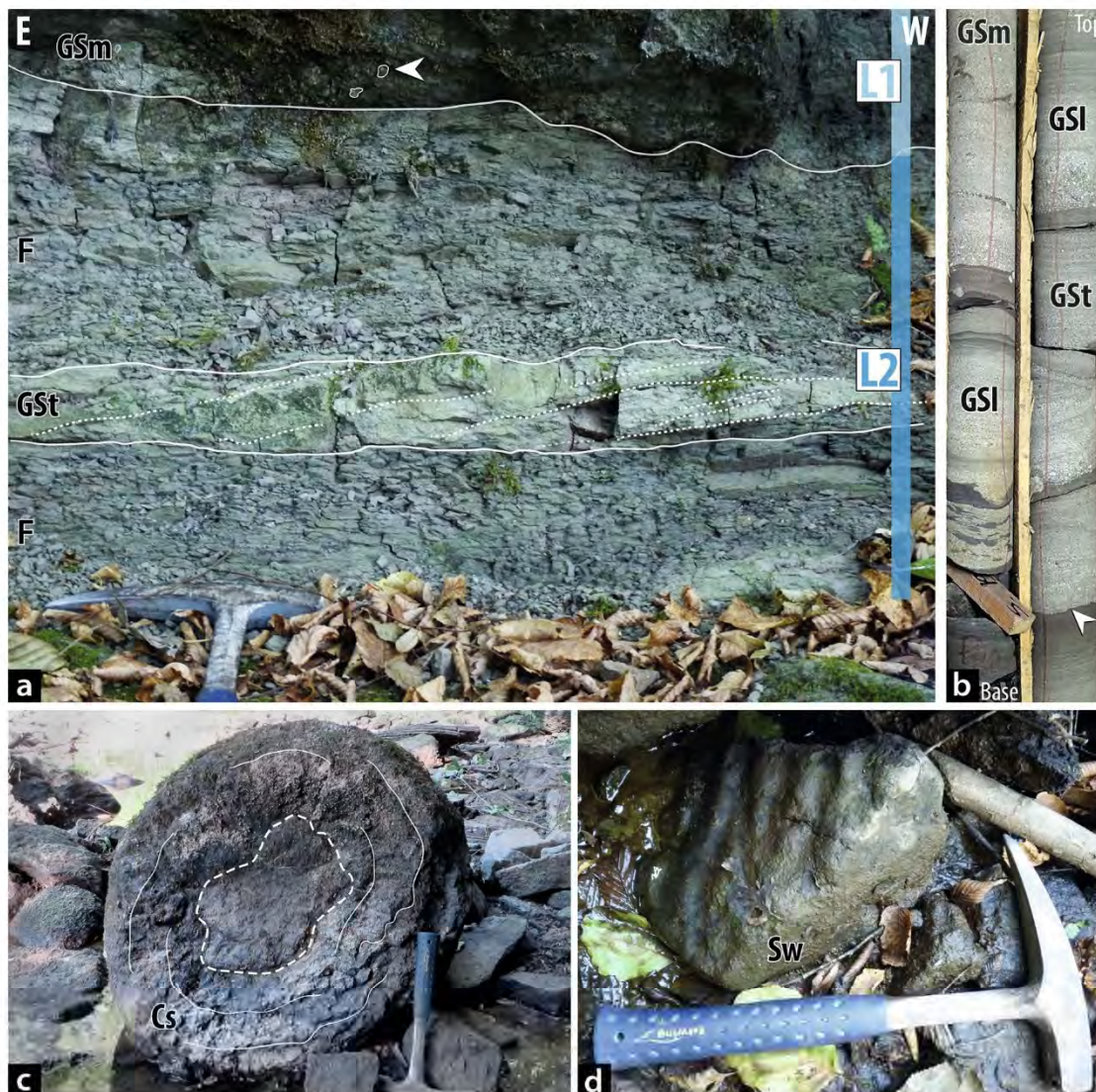
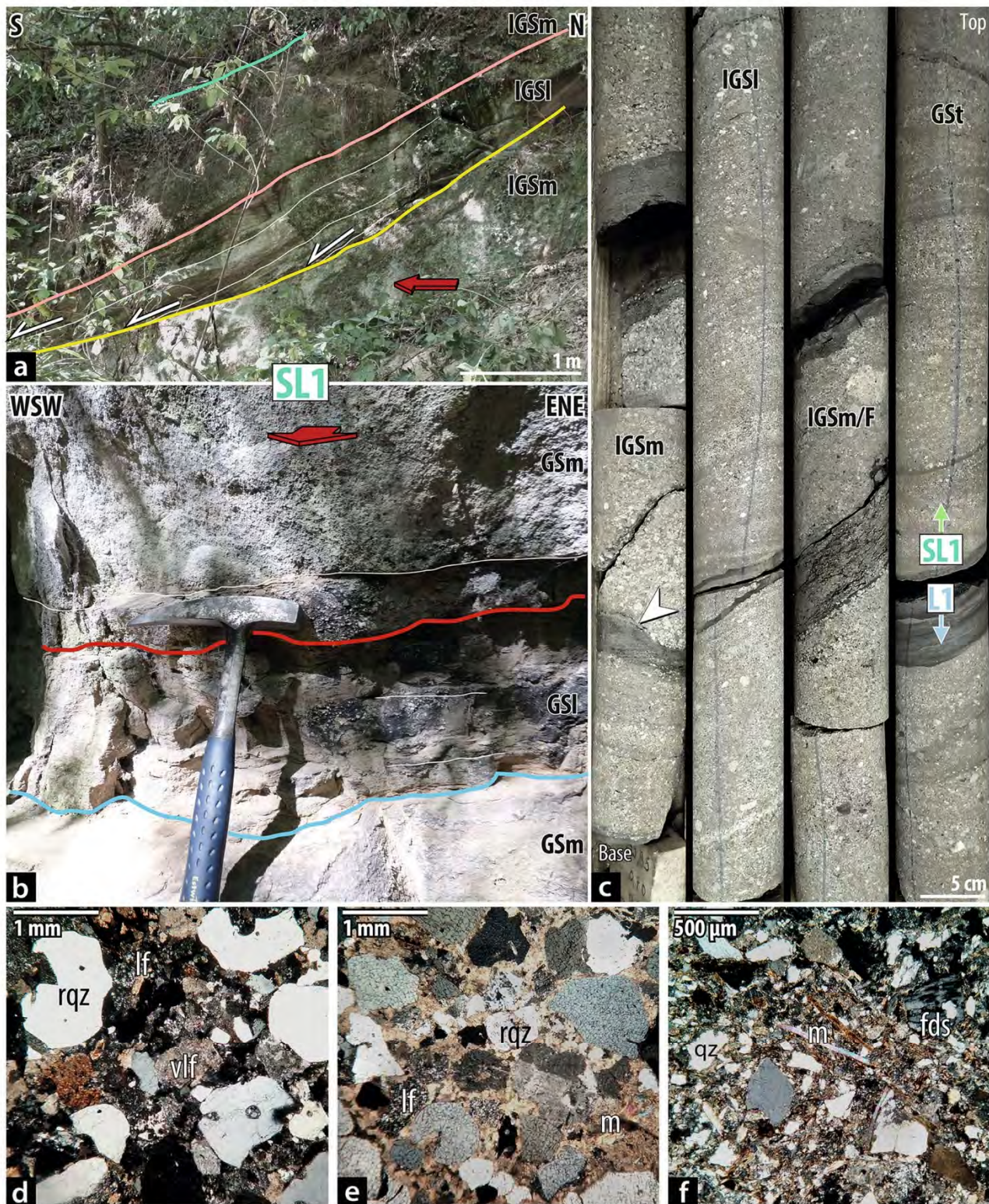


Fig. 3 Illustration of the facies associations corresponding to the littoral lake environments (L1 and L2 facies associations; see Table 1 for the facies codes). **a** Outcrop of the Arroux section displaying fine-grained facies (F facies, low sedimentary fluxes) alternating with medium-to-coarse-grained facies, massive or with trough cross-stratifications (GSm and GST facies, high sedimentary fluxes), and attributed to the succession of shallow and protected lake and deltaic topset deposits, in a littoral lake environment. The white arrow indicates centimetric gravels. **b** Interval from the CHE-1 core (located

at ~186 m, Fig. 13) displaying sandy facies, massive (GSm), laminated (GSI) with fining-upward trends and erosional bases (white arrow) and with trough cross-stratifications (GST), representing deltaic topset deposits in a littoral lake environment (L1 facies association, Fig. 13). **c** Transversal section of microbial carbonates (Cs facies) encrusting a trunk (dashed line-tilted) near the Arroux section. **d** Reworked fragment of a sandstone bed with wave ripples (Sw facies, found at the base of the cliff of the Arroux section, Fig. 10)



Figs. 3, 4, 5 and 6, ranging from fine-grained to coarse-grained facies, either homolithic or heterolithic, with a mean grain size of ~2–5 mm, and a maximum grain size

of ~5 cm (rare levels). The observation of thin sections, taken from facies composed of fine sands to gravels, has provided evidence for a wide diversity in detrital grains,

Fig. 4 Illustration of the SL1 facies association (sublittoral lake environment, deltaic foresets; see Table 1 for the facies codes). **a** Chevrons section (cf. map location in Fig. 2b and location on the outcrop in Fig. 8): zoom on inclined facies, massive (IGSm) and laminated (IGSl), the latter presenting downlap geometries (white arrows). The current direction is indicated by the red arrow. **b** Photograph of a similar interval, taken perpendicularly to the current (red arrow; cf. location on the outcrop in Fig. 8). **c** Illustration of inclined homolitic and heterolithic facies of the CHE-1 core (located at ~194 m, Fig. 13) attributed to the SL1 environment, and topped with the GSt facies (trough cross-stratifications) characterizing the L1 facies association, i.e., littoral lake environment with deltaic topsets. The white arrow highlights an erosional surface. **d, e, f** Thin sections illustrating various facies of the IG-1 core, showing immature sandstones (i.e., litharenites) with subangular to angular grains of quartz, feldspars and lithic fragments. **d** Poorly sorted GSl facies presenting small lithic fragments (lf), sometimes of volcanic origin (vlf, altered rhyolites), and large rhyolitic quartz grains (rqz) displaying typical corrosion gullies. **e** GSmm facies presenting a better sorting, containing lithic fragments, rhyolitic quartz grains and some micas (muscovite, m). **f** Thin section of a fine-sand levels from the heterolithic Sm/F facies, with a poorly sorting, angular grains, including detrital quartz (qz), feldspars (fds) and muscovite (m)

dominated by rhyolitic quartz, feldspars and lithic fragments (Fig. 4c, d, e). The grains are subangular to angular, therefore indicating immature material, moderate transport, and a sediment source that is likely quite close to the sedimentation area.

The facies are grouped into facies associations, used to interpret depositional environments (Table 2). The facies associations are named according to the lacustrine classification of Bohacs et al. (2000) that defines depositional environments based on the bathymetry of the deposits, depending on the subdivisions established for lacustrine water column, i.e., epilimnion (superficial waters), thermocline (physical–chemical transition zone) and hypolimnion (bottom waters). Thus, this classification depends on the position of the deposits along a landward-to-basinward (i.e., proximal–distal) transect: the littoral lake (L) environment encompasses facies deposited at epilimnion-interval bathymetries, the sublittoral lake (SL) environment encompasses facies deposited at thermocline-interval bathymetries, and the profundal lake (P) environment includes facies deposited at hypolimnion-interval bathymetries. These positions were then subdivided by considering the sediment supply variations and the main depositional processes in each of them (Table 2), with a total of seven facies associations; these subdivisions are represented in the theoretical depositional model presented in Fig. 7. The facies associations are described below, followed by the sedimentary descriptions of the field sections, where the facies, facies associations and their relationships (sedimentary architectures) are displayed; then, the facies associations in cored wells, and the related environmental evolution, are presented.

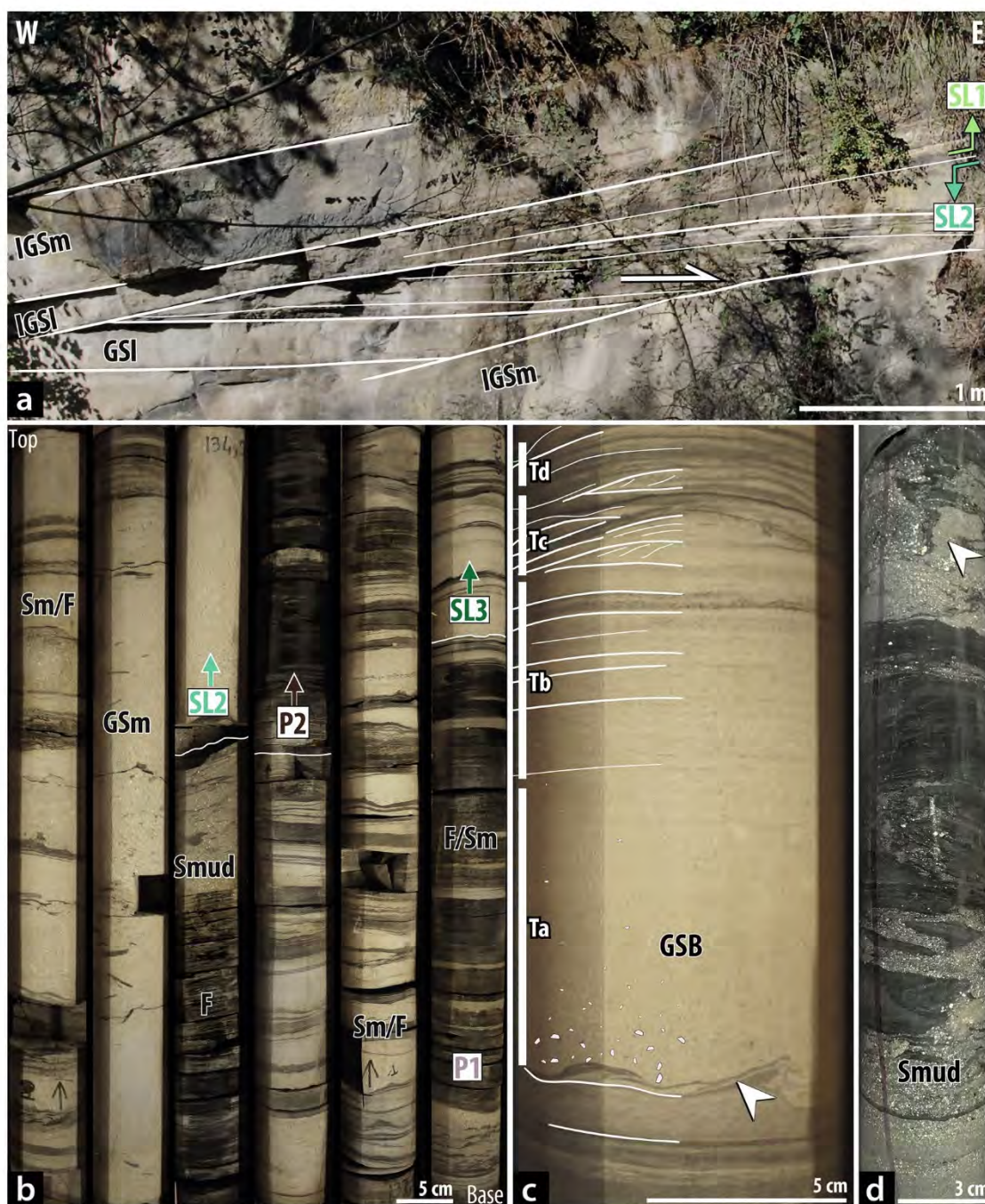
Facies association L1

The L1 facies association, illustrated in Fig. 3, is dominated by medium-to-coarse-grained facies (i.e., coarse sands to pebbles), organized in beds that are one to several meters thick, either planar-laminated (GSl facies, Table 1, Fig. 3b), with trough cross-stratifications (GSt facies, Table 1, Figs. 3b), or massive (GSmm facies, Table 1, Figs. 3a, b). Given this range of granulometries, the planar bedding indicates high-energy tractive currents, and the trough cross-stratifications are interpreted as 3D megaripple migration. However, less common heterolithic facies, such as the SF facies (silt to coarse-sand m-thick levels, often lenticular and without marked contacts, Table 1), the St/F facies (medium-to-coarse-sand dm-thick levels with trough cross-stratifications, alternating with clayey to silty material, Table 1), and the GSmm/F facies (dm-thick coarse sands to gravels in a fine-grained matrix, alternating with fine-grained levels, Table 1), indicate more contrasted periods in terms of sediment fluxes, with calmer episodes allowing for the settling of the finest-grained particles. However, homolitic claystone and siltstone beds (F facies, Table 1) are scarce and relatively thin (dm-thick levels). Bioturbations can be found at the top of some GSt-facies beds, indicating that this was a favorable environment for subaquatic life, and oxygenated waters, at least up to the water/sediment interface.

This facies association, showing high-energy current features, together with the dominant medium-to-coarse granulometries, and the frequent erosional surfaces, reflects high detrital inputs into the basin. A fluvial environment could be considered here, but the total absence of emersion evidence or pedogenic features (i.e., root traces, pedogenic nodules, slickensides, etc.) instead suggests a strictly subaquatic, yet shallow environment, i.e., a littoral lake environment (Fig. 7) with characteristics of deltaic topset deposits (e.g., Nemeč 1990; Postma 1990; Bhattacharya 2006; Rohais et al. 2008; Table 2).

Facies association L2

The L2 facies association, represented in Fig. 3, is predominantly composed of fine-to-medium-grained facies, as well as carbonate deposits. The claystone to siltstone facies (F facies, several meters thick, Fig. 3a) are mostly massive, sometimes laminated, with an OM content up to 21 wt.%. These facies are associated with carbonate levels, either massive, likely diagenetic (cm-thick, Ca facies, Table 1), or they display very fine irregular laminae, sometimes encrusting remains of trunks, and are attributed to a microbial activity (Cs facies, dm-thick, Table 1, Fig. 3c). Some dm- to m-thick levels present a coarser-grained lithology (fine to medium sand, rarely coarse), displaying wave-ripples (Sw facies, Fig. 3d), or forming lenticular bodies included in a



silty material (SF facies), reflecting periods of sedimentary inputs, although very low. Only rare cm- to dm-thick sandy beds, showing planar or trough cross-stratifications, indicate periods of deposition under a tractive current influence (GSI and GSt facies, fine to medium sand, Fig. 3a).

According to Burne and Moore (1987), Visscher et al. (1998) and Dupraz et al. (2009), microbial carbonate deposits are organomineralized structures formed by the association of benthic micro-organisms, some of which use photosynthetic metabolisms in most reported cases. Therefore,

their presence implies a low water column (euphotic zone) with reduced sediment supply (no turbidity), allowing for chemical or biologically induced carbonate precipitation when the concentration in carbonate and calcium ions is sufficient. Some carbonate microbial deposits have already been described in French CP basins, and assigned to shallow aquatic environments, either marginal lacustrine or fluvial, based on sedimentological evidence (features reflecting shallow environments, like mudcracks or root marks, oncoids or oolites) and biological evidence (photosynthetic

Fig. 5 Illustration of the facies associations (SL1–SL3 environments, see Table 1 for the facies codes) corresponding to the sublittoral lake environments (prodelta). **a** Rigny section (see map location in Fig. 2b and location on the outcrop in Fig. 9): zoom on an alternation of inclined facies attributed to deltaic foresets (SL1 facies association) with sandy prodelta deposits (SL2 facies association), characterized by the horizontal GSI facies overlapping the IGSm facies of the deltaic foreset. **b** Interval from the IG-1 core (located at ~135 m, Fig. 12) displaying facies from the profundal lake environment (P1 facies association) at the base, followed by the sublittoral prodelta SL3 facies association, and by profundal lake deposits (P2 facies association, dominated by organic-rich claystones) and prodelta deposits (SL2 facies association) towards the top. The SL3 prodelta deposits (Sm/F) are broadly finer-grained than the SL2 prodelta deposits, with a higher proportion of fine-grained granulometries; in the prodelta SL2 facies association, the sandy beds (Sm/F and GSm facies) are thicker. **c** Zoom on a sandy to clayey turbiditic level of the IG-1 core, displaying four terms of the Bouma sequence, i.e., Ta (massive and fining-upward sand), Tb (medium to fine sand, high-energy planar laminae), Tc (ripple bedding) and Td (low-energy planar laminae composed of clay to silt material). The white arrow shows the erosive surface at the base as well as fluid escape features. **d** Photograph of the Smud facies of the CHE-1 core, attributed to debris flow deposits in rather profundal environments (sublittoral lake SL3, or sometimes profundal lake P1 environments). Pluricentimetric rip-up clasts of various facies and mudclasts are contained in a coarse-sand matrix, sometimes very dark. Fluid escape (white arrow) or injectite features are often observed

metabolisms, e.g., Frey et al. 1992, 1999, 2000; Gand et al. 1993; Stapf and Gand 1994).

The above-mentioned facies dominated by very low-energy deposits, in association with the microbial deposits, are, thus, attributed to a quiet littoral lake environment (Table 2), i.e., a shallow lake where the detrital sediment fluxes are minimal, either because of limited erosion in the watershed, or because they are located laterally from the main distributaries (Fig. 7). Some OM-rich levels preserved in the Autun Basin have already been attributed to such a shallow lake environment by Garel et al. (2017).

Facies association SL1

The SL1 facies association, displayed in Fig. 4, is mainly composed of inclined facies, presenting a large range of granulometries, from claystones to pebbly conglomerates. The medium-to-coarse-grained facies are dominant, in dm- to m-thick beds with erosive bases, either homolithic massive (IGSm facies, Table 1, Figs. 4a, c, 5a) or laminated (IGSI facies, Table 1, Figs. 4a, c, 5a), or heterolithic (IGSm/F facies, Table 1, Fig. 4c), sometimes matrix-supported (IGSmm/F facies, Table 1). These heterolithic facies are dominated by sandstones and conglomerates, organized in m-thick beds, and are topped by cm to dm-thick fine-grained beds (claystones to siltstones). Some fining-upward sandstone levels, sometimes beginning with gravels, followed by planar-lamination and ripple intervals, are interpreted as hyperconcentrated turbidite deposits, displaying

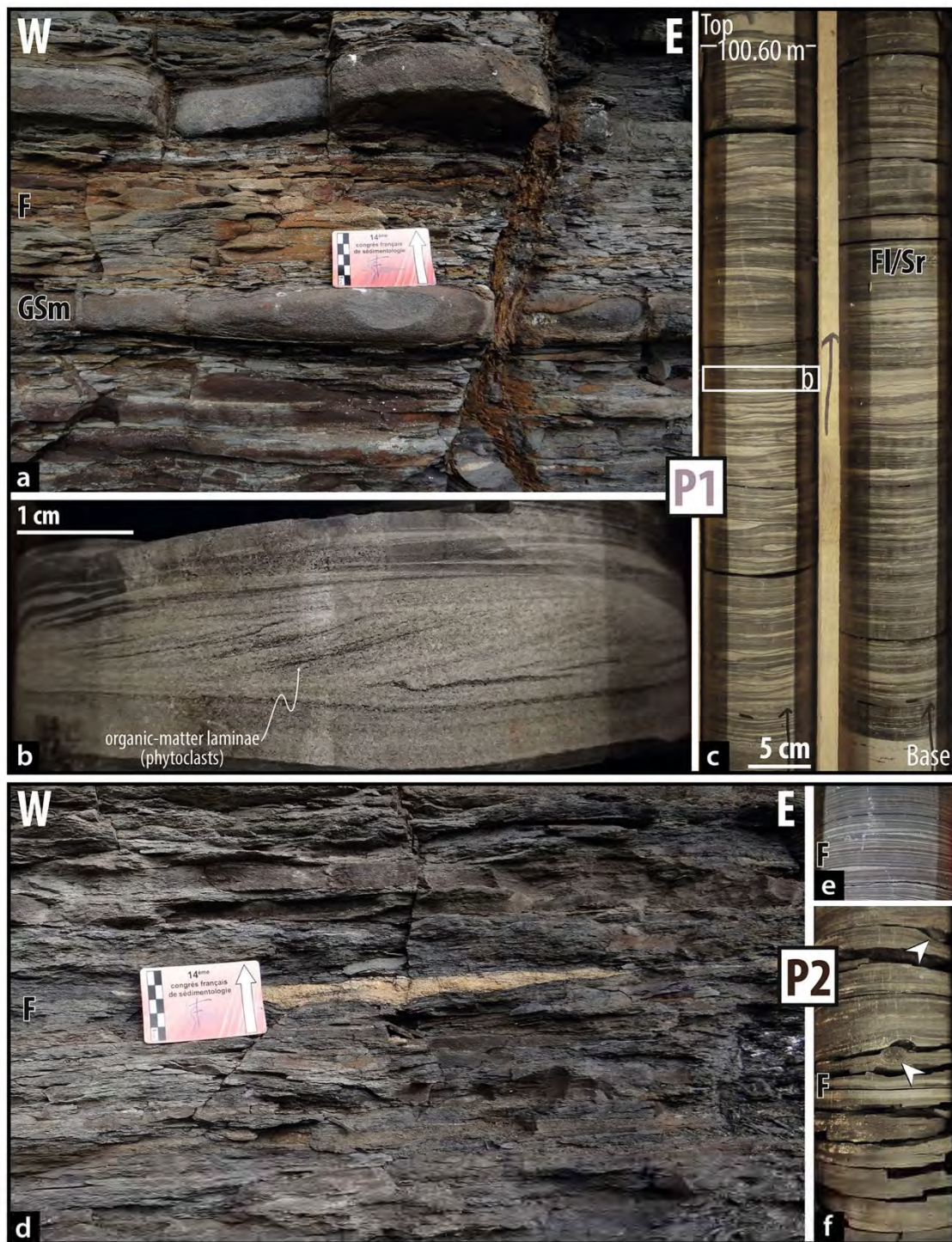
parts of the Bouma sequence (GSB facies, with the Ta, Tb and Tc Bouma divisions, respectively, Bouma 1962, Table 1). Some matrix-supported coarse-grained lithologies, interbedded with fine-grained levels, are interpreted as debris flow deposits, alternating with calmer periods of settling of clays or silts (GSmm/F facies).

The inclination of the dominant facies of the SL1 facies association is attributed to a sedimentary dip rather than a tectonic tilting, given their association with numerous gravity-flow deposits, the absence of faults (either syn-sedimentary or post-depositional), and their observation at both the large (i.e., outcrops) and small scale (i.e., cores). The sedimentary dip, together with the dominant facies reflecting high sedimentary fluxes alternating with phases of settling of fine-grained particles, and with the turbidite and the debris flow deposits, likely indicate deltaic foresets (e.g., Lowe 1982; Postma 1984; Colella et al. 1987; Kostaschuk and McCann 1989; Nemeč 1990; Massari 1996; Breda et al. 2007; Rubi et al. 2018) that are prograding into a sublittoral lake environment (Table 2).

Facies association SL2

The dominant facies of the SL2 facies association, represented in Fig. 5, are sandy to gravelly, dominated by dm- to m-thick massive beds, with erosive or planar basal contacts (GSm facies, Fig. 5b), attributed either to cohesive debris flows or to high-density turbidite deposits. Numerous dm- to m-thick beds, with erosive bases and showing a vertical organization with fining-upward trends from gravels to coarse sands, planar bedding, current ripples and settling of fine-grained particle intervals are also displayed, attributed to the GSB facies, with the divisions of the Bouma sequence (Ta to Te, Bouma 1962, Fig. 5c). This facies indicates hyperconcentrated to low-density turbidity currents, here interpreted as relatively proximal along a landward–basinward transect, given their significant thickness and the medium-to-coarse-grained Ta division. Deformed beds measuring several meters thick, mixing fine-to-coarse-grained material and frequently showing folding structures (GSF_d facies, Table 1), are interpreted as slump and slide deposits. Some sandstone to conglomerate beds, displaying planar laminations (GSI facies, Fig. 5a, mostly dm-thick), or trough cross-stratifications (GSt facies, mostly m-thick), are included in this SL2 facies association, reflecting high-energy tractive currents. Other scarcer facies are also included, consisting in heterolithic alternations of medium-to-coarse-grained lithologies, sometimes matrix-supported, with fine-grained lithologies, reflected by the GSm_m/F, Sm/F (Fig. 5b), F/Sm and FS facies (Table 1). Some periods of settling of fine-grained particles are also displayed, reflected by the F facies.

The GSt facies, associated with slumps, thick coarse-grained turbidites and heterolithic facies, is interpreted



as hydraulic jump deposits formed at a slope break (e.g., Simons and Richardson 1963; Middleton 1965; Breda et al. 2007). It reflects a delta toset geometry, i.e., the tangential transition from the deltaic foreset to the bottomset in a sublittoral lake environment, and/or gravelly bottomsets (i.e., Postma and Roep 1985; Rohais et al. 2008; Gobo et al. 2014; Rubi et al. 2018), therefore indicating prodelta deposits, i.e.,

the transition between the inclined foresets and the strict lacustrine environment.

Facies association SL3

This facies association, illustrated in Fig. 5b, presents similarities with the facies association SL2, with numerous

◀**Fig. 6** Illustration of deposits corresponding to the profundal lake environments (P1 and P2 facies associations, see Table 1 for the facies codes). **a** Photograph of a small section located in the Saint-Léger-du-Bois village, ~800 m from the Chevrots and Rigny sections (Fig. 2a) displaying the Igornay oil-shale beds, that are also reached by the IG-1 well (Fig. 12). Fine-grained OM-rich deposits (F facies) alternate with coarser-grained levels (GSm facies), indicating a profundal lake environment, yet including clastic sediment supply events (P1 facies association). **b** Current ripples in fine sandstone from the Fl/Sr facies (zoom of Fig. 6c), reworking millimetric phytoclasts (black laminae). **c** Heterolithic fine-grained facies Fl/Sr from the IG-1 core (~100 m), showing alternation of organic matter-rich clayey deposits and thin fine-grained sandy turbidites attributed to the profundal lake environment (P1 facies association). **d** Fine-grained facies, laminated and OM-rich (F facies), with minor sedimentary fluxes represented as centimetric fine-sand lenses, attributed to the most distal lacustrine environment (P2 facies association, Saint-Léger-du-Bois outcrop). **e, f** Examples of the F facies in the IG-1 core. **e** F facies with colored millimetric laminae (clays, silts and very fine sand, located at 179.50 m, Fig. 12). **f** OM-rich F facies with very thin black laminations in the IG-1 core (located at 182.50 m, Fig. 12). The white arrows indicate phosphate-fish coprolites

turbidite deposits reflected by the GSm and GSB facies (Fig. 5c), and tractive current influence reflected by the planar-laminated GSl facies. The main differences are: (i) the sandy-to-gravelly beds are thinner and scarcer on average (mostly dm-thick), in favor of more heterolithic facies, displaying thicker levels of fine-grained lithology, such as GSm/F, Sm/F (Fig. 5b), F/Sm and FS facies, (ii) the basal granulometry of the coarser turbiditic levels (i.e., GSm, GSB) does not exceed the medium to coarse sands, and (iii) the Fl/Sr facies (Table 1), absent in the SL2 facies association, likely reflects alternations between periods of moderate tractive current (i.e., current ripple intervals) and of settling of fine-grained particles. Some relatively scarce dm- to m-thick levels of matrix-supported conglomerates, constituted by large mudclasts (cm- to dm-sized) floating in a fine- to medium-sand gray-to-black matrix (Smud facies, Table 1, Fig. 5d), are interpreted as distal debris flows given that the eroded material partly comes from the fine-grained facies.

Accordingly, the SL3 facies association is characterized by more distal turbidite deposits than the SL2 facies association, that alternate with more significant calm periods of settling of fine-grained particles. Therefore, this facies association indicates fine-grained prodelta deposits (e.g., Gilbert 1885; Postma and Roep 1985; Rubi et al. 2018), still in a sublittoral lake environment (Table 2, Fig. 7), but more distal than the SL2 facies association.

Facies association P1

Facies association P1, detailed in Fig. 6, comprises both homolithic and heterolithic fine-grained facies. The homolithic F facies (Fig. 6a) dominates in intervals spanning several meters and is either massive or finely laminated (i.e.,

alternation of millimeter-thick clays, silts and siderite laminae); the latter is interpreted as varve deposits by Marteau (1983), yet without clear evidence of a seasonal control. It often contains fish fossils or remains (scales and coprolites), and sometimes presents OM enrichments. It alternates with the heterolithic F/Sm facies (cm-thick massive sandy levels interbedded in massive claystones to siltstones, Fig. 5b), and the laminated Fl/Sr facies (Fig. 6c), where the sandy levels contain current ripple marks (Figs. 6b, c). Tonstein levels (T facies) are frequently found embedded in the fine-grained beds. Some dm-thick medium-to-coarse-grained beds with erosive bases, either massive (facies GSm, Fig. 6a) or with large mudclasts (facies Smud), are intercalated in the fine-grained facies, and are interpreted as debris flows or grain flows; some dm-thick levels of GSB facies, mostly fine to medium grained are also found and are interpreted as distal turbidites (Bouma sequence). Sometimes, some interbedded massive cm- to dm-thick sandy levels in fine-grained intervals (claystones–siltstones) show injection patterns (SFi facies, Table 1), due to differential compaction, given the contrasted lithologies.

This facies association, dominated by fine-grained sediments deposited in a calm environment, yet presenting some gravity flow deposits (i.e., distal turbidites, debris flows and grain flows), is attributed to a profundal lake environment, with low sediment fluxes (Table 2, Fig. 7).

Facies associations P2 and P2a

Facies association P2, represented in Fig. 6, presents strong similarities with facies association P1. The fine-grained facies dominate, but the homolithic facies (F facies, Figs. 5d, 6d, e, f) are more present than the heterolithic facies. They are sometimes finely laminated (Fig. 6e), may contain scarce thin sandy lenses (Fig. 6d), and are very rich in fish remains (e.g., scales, coprolites, Fig. 6f), even containing selachian coprolites (freshwater sharks, already found in Western European CP basins such as the Aumance, Blanzay–Le Creusot, Autun, or Saar-Nahe basins, Fischer et al. 2013; Schneider and Zajic 1994; Schneider et al. 2000; Luccisano et al. 2021). The heterolithic facies are constituted by massive claystones to siltstones alternating with fine-to-medium-grained sandstones, always massive (i.e., F/Sm facies), never showing current features, but sometimes showing bioturbations (Table 1). The coarsest levels are only represented by (i) the mm- to cm-thick sandy levels of the F/Sm facies, the cm-thick fine-to-medium-grained sandy beds attributed to grain flows (GSm facies) or to distal turbidites when showing Bouma sequence divisions (GSB facies), (ii) the rare m-thick dark siltstone beds, containing some mm-sized floating grains and interpreted as low-density tails of turbidity currents (Fclast facies, Te division of the Bouma sequence; Bouma 1962), and (iii) the rare dm-thick debris flows (Smud

Table 2 Facies associations observed in the studied sections, corresponding to depositional environments

Name	Facies association (sort by frequency: prevalent , common, rare)	Depositional environment
L1	GSI, GSt, GSm, SF, Sl/F, GSmm/F, F	Deltaic topsets in a littoral lake environment with maximal sediment fluxes
L2	F, Ca, Cs, SF, Sw, GSI, GSt	Shallow protected littoral lake, sometimes dysoxic/anoxic with microbial deposits, protected from major sediment fluxes
SL1	IGSm, IGSI, ISm/F, IGSm/F, GSB, GSmm/F	Deltaic foresets in a sublittoral lake environment
SL2	GSm, GSB, GSFd, GSI, GSt, GSmm/F, Sm/F, F/Sm, SF, F	Prodelta deposits in a sublittoral lake environment, sometimes differentiated into deltaic toesets or gravelly bottomsets (i.e., proximal bottomset deposits), showing proximal turbidites and grain flows
SL3	GSm, GSB, GSI, GSmm/F, Sm/F, F/Sm, Smud, Fl/Sr, SF	Fine-grained prodelta deposits in a sublittoral lake environment, showing distal turbidites and grain flows (i.e., distal bottomset deposits)
P1	F, F/Sm, Fl/Sr, Smud, T, GSm, GSB, SFi	Profundal lake environment with low sediment fluxes (turbidites, debris flows)
P2 – P2a	F, F/Sm, T, GSm, GSB, Fclast, Smud	Profundal lake environment (i.e., P2) sometimes dysoxic or anoxic (i.e., P2a), with minimal sediment fluxes

For the facies descriptions, see Table 1

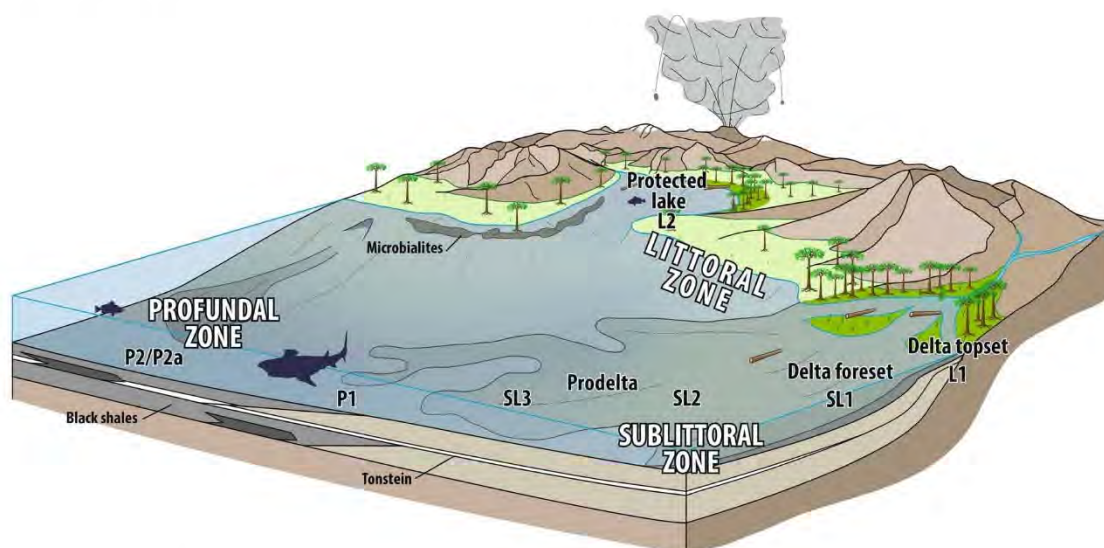


Fig. 7 Conceptual model of the Autun Basin showing the depositional environments determined from the subsurface and outcrop data. This model does not represent a snapshot of the basin but rather

a combination of all the depositional environments found through time. See Table 2 for the facies association codes

facies), thus indicating minimal sediment fluxes. This interpretation is also supported by the highest OM enrichment in the F facies with TOC values up to 21.5 wt.%, reflecting periods of dysoxic to anoxic bottom waters and sediments under a sustained water-column stratification (chemocline/thermocline). Like for the P1 facies association (profundal lake environment with low sediment fluxes), tonstein layers (T facies) are observed since these low hydrodynamic environments are prone to fine-grained material preservation.

Therefore, this facies association is attributed to a profundal lake environment in its most distal part, with minimal sediment supply preventing the homogenization of the

water column and favoring OM preservation when dysoxic to anoxic conditions are reached (P2a facies association, Table 2, Fig. 7), as evidenced by Mercuzot et al. (2021b).

Architectures and depositional environment evolution based on field sections

The Chevrots section

This outcrop section (Fig. 8), located above an OM-rich level attributed to the Igornay OSB, based on mining work and cartography (Fig. 2), represents the base of the *Grès*

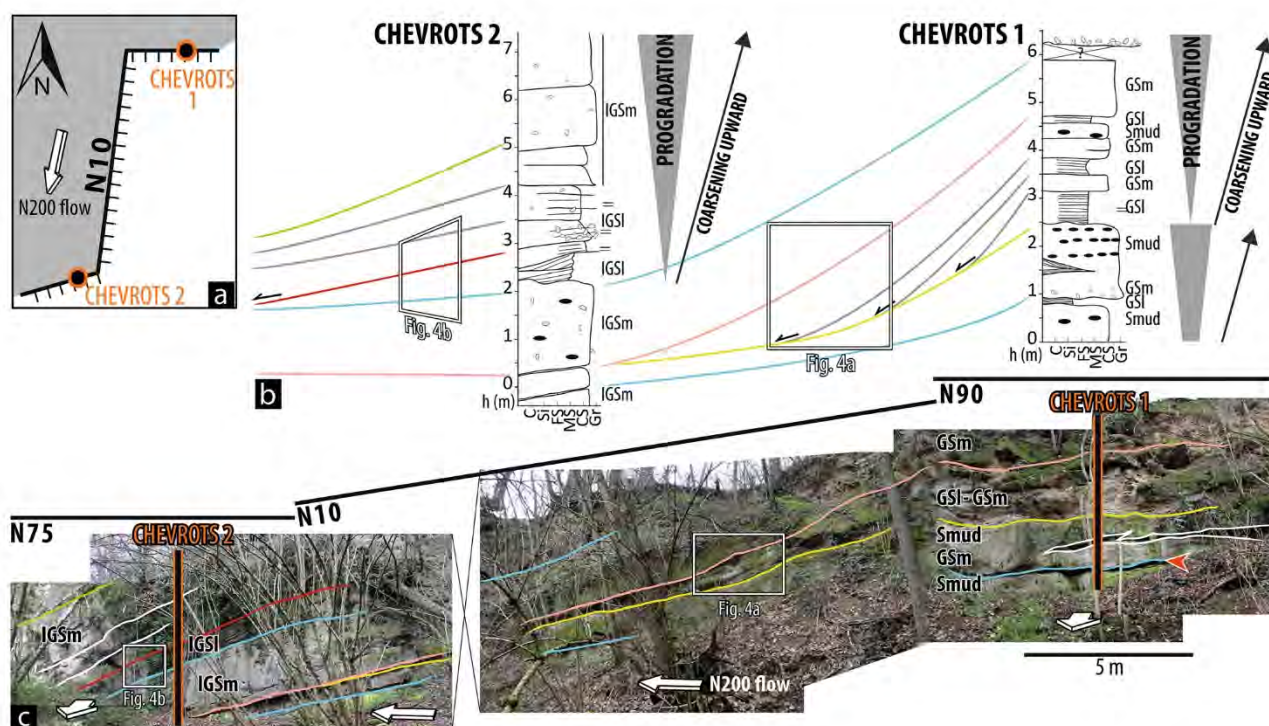


Fig. 8 Les Chevrots section (see Figs. 1c and 2 for the position in the stratigraphy and location on a map, and Table 1 for the facies codes). **a** Top view of the Chevrot quarry showing the orientations of the available outcrops and two sections used for detailed logs. **b** Sedimentary logs of the E–W sections, correlated together (see Fig. 10 for the log caption; the colors of the sedimentary geometries are the same as those used in Fig. 8c). **c** claystone, *Si* siltstone, *Fs* fine sand,

Ms medium sand, *Cs* coarse sand, *Gr* gravel. The sedimentary features display coarsening-upward beds and the sedimentary architecture displays downlap and progradational structures. **c** E–W, ENE–WSW and E–W views of the outcrop (from the left to the right), showing the deltaic geometries. The ENE–WSW view is approximately parallel to the flow. The red arrow on the right E–W section indicates the N200-oriented flute cast

de Lally Inférieurs Unit (Fig. 1c), and displays a 3D view with two E–W-oriented sections (Chevrots 1 and Chevrots 2; Fig. 8) and one WSW–ENE-oriented section. In the Chevrots 1 E–W section (Fig. 8), lenticular sandstone bodies are observed, with massive coarse-grained sands to gravels at the base (GSm facies) and with mudclasts highlighting horizontal bedding at the top (Smud facies, Fig. 8), alternating with planar laminated fine-grained lithologies (fine to medium sand, GSI facies, high-energy planar bedding). The top of the medium-to-coarse-grained levels is undulated to irregular (Fig. 8), indicating either an erosional event, the eroded material being deposited basinward, or a stasis in the sedimentation before the deposition of fine-grained lithologies filling the depressions. The coarse-grained layers also display thickening-upward and coarsening-upward sequences. The WSW–ENE section shows downlap structures, with inclined laminated and massive facies (IGSI, IGSm facies, Fig. 8), and an evolution from fine-grained to coarse-grained lithologies is observed from the base to the top of the outcrop (Fig. 8). On the Chevrots 2 E–W section (Fig. 8), the beds become coarser towards the top, and the thickening-upward pattern of the strata reflects a

progradational architecture. Altogether, the sedimentary features observed in the Chevrots section indicate a progradation of the sandstone bodies towards the WSW (almost parallel to the WSW–ENE section), also supported by a N200-oriented flute cast observed at the base of a coarse-grained bed in the Chevrots 1 section (Fig. 8c), rather than lateral accretion processes in a fluvial channel, as previously interpreted by Marteau (1983).

Although it is not possible to accurately restore the original sedimentary dip of these strata due to the subsequent moderate tectonic activity affecting the basin (i.e., post-early Permian faulting and tilting), all of the sedimentological characteristics observed on this outcrop indicate deltaic foreset deposits that can be attributed to a sublittoral lake SL1 environment (Table 2).

The Rigny section

The Rigny section is located 450 m away from the Chevrots section and is representative of the same stratigraphic interval. This former quarry is suitable to observe the layer relationships and geometries, but cannot be used to provide

a precise description of the facies as it is difficult to access the outcrop (height, vegetal cover). Although detailed sedimentary logs are not available, the strata displayed on the Rigny outcrop undoubtedly show a general coarsening-upward trend, from fine-grained sandstones at the base of the outcrop, to conglomerates at the top. The strata are thickening-upward and their general thickening towards the west, together with the inclined geometries, indicate progradational features (Fig. 9). Three major architectural characteristics are also observed: (i) onlap structures at the base of the prograding sets, interpreted as backset deposits, formed under a turbulent flow (hydraulic jump) in the deltaic toeset (i.e., sublittoral lake SL2 environment, displayed on Fig. 5a), (ii) inclined strata towards the west, and (iii) an erosional surface filled by sandy material, attributed to a chute-fill structure eroding the underlying set. The two latter geometries indicate prograding deltaic sets, i.e., deltaic foreset deposits in the sublittoral lake SL1 environment, with

a roughly WSW/SW flow direction, given that the outcrop is almost parallel to the prograding sets. Towards the top of the outcrop, the dip of the stratification is lower and the lithologies are dominated by conglomerates, likely massive with erosive bases. This interval can be attributed to deltaic topset deposits in a littoral lake L1 environment (Fig. 9).

The Arroux section (ARR)

The base of the Arroux section (Fig. 10) is characterized by a massive m-thick coarse-sand level (GSm facies) containing trunk casts filled by sand and encrusted by microbial carbonate deposits (Cs facies, Figs. 3c, 10). Then, erosive sandy beds, fine- to medium-grained, homolithic with planar laminations (GSI facies) or heterolithic (Sm/F facies), alternate with fine-grained facies (F facies, siltstones dominant) containing plant fragments. At the top of the section, another sandy level (very coarse sand, GSm facies) was

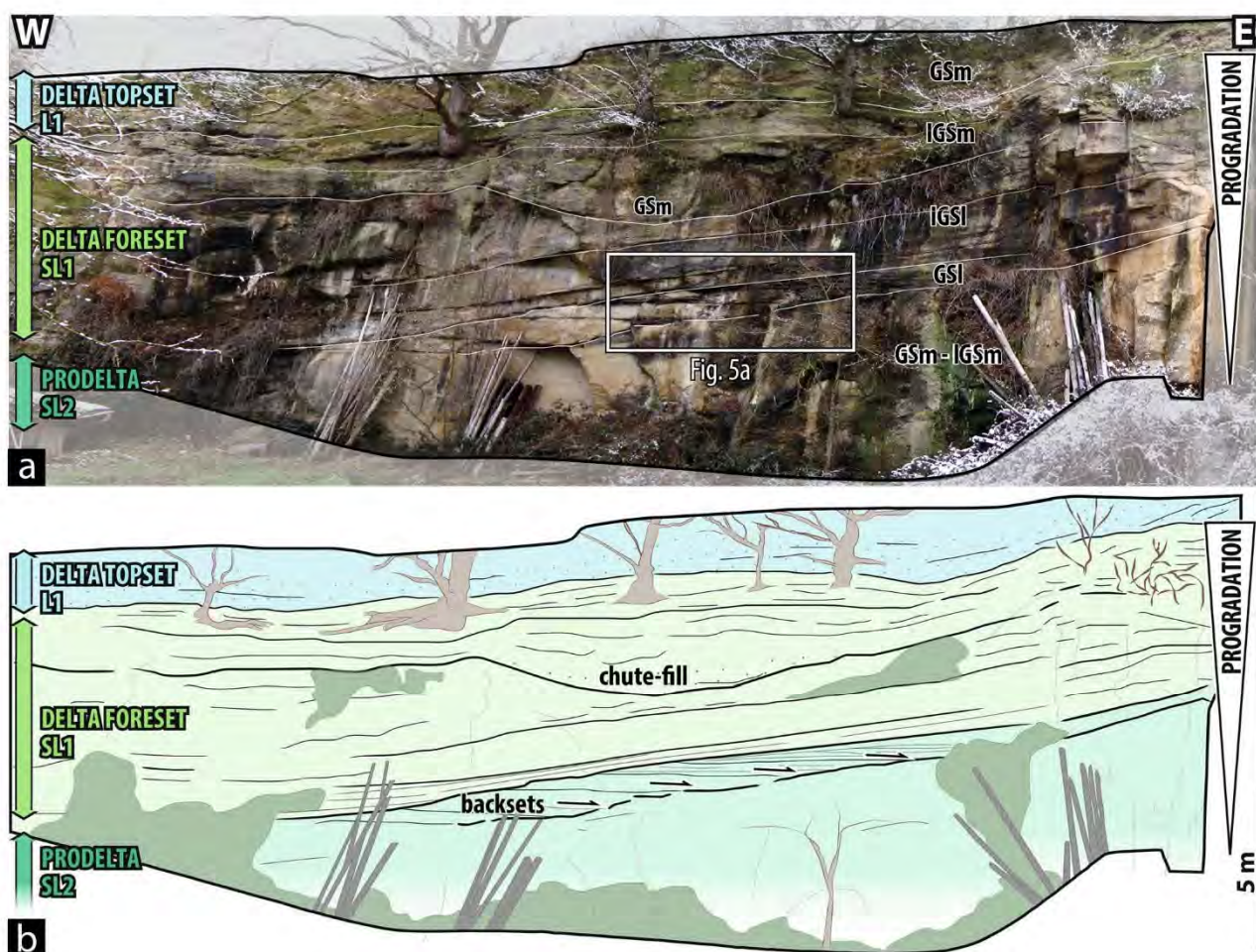


Fig. 9 a Photograph of the Rigny section (see Figs. 1c and 2 for the position in the stratigraphy and location on a map, and Table 1 for the facies codes), oriented W–E. b Interpretation of the photograph high-

lighting deltaic architectures, notably with chute-fill and backset features, reflecting foreset and prodelta (toeset/bottomset) environments, respectively, and overlain by a conglomeratic topset

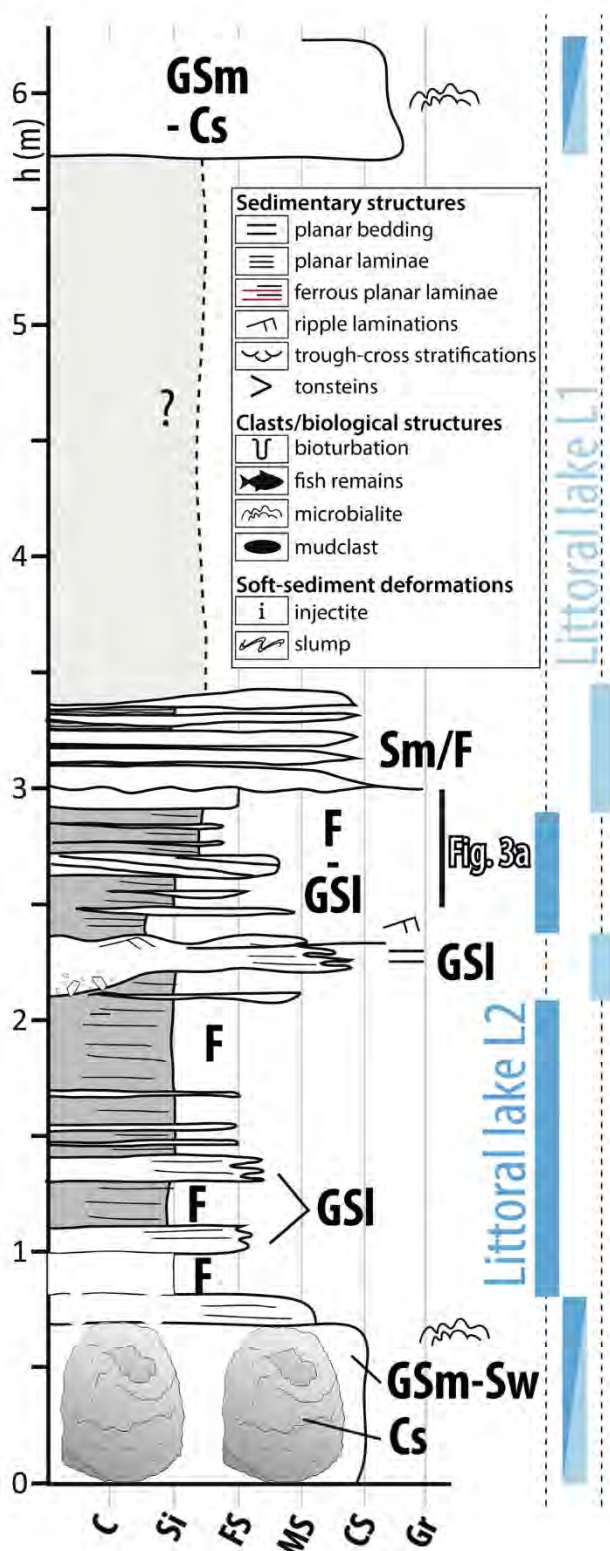


Fig. 10 Sedimentary log of the Arroux section (see Figs. 1c and 2 for the position in the stratigraphy and location on a map, and Table 1 for the facies codes) showing the evolution of the depositional environments

found, associated with microbial deposits. Considered all together, the trunks preserved in living position, the wave ripples (Fig. 3d) in the sandy facies, and the associated microbial deposits indicate a marginal lake environment. Therefore, this facies succession corresponds to an alternation between a littoral lake environment, when sediment fluxes are minimal (fine-grained lithologies, protected lake environment L2), and a littoral lake L1, during periods of higher sediments fluxes (high-energy sandy facies).

The Muse section and well (MU)

The Muse section is only composed of the Muse OSB, whereas the MU well encompasses the Muse OSB and the uppermost part of the *Grès de Lally Supérieurs* Unit (Fig. 1b). The core displays 3D megaripple structures (GSt facies, Table 1) at its base, indicating a littoral lake L1 environment (deltaic topsets, Fig. 11). Then, medium-to-coarse-grained planar laminated facies (GSI facies), rich in floating higher plant debris, indicate a sublittoral SL2/SL3 environment, and are followed by a littoral lake L2 environment, marked by massive fine-grained lithologies (i.e., claystones to very fine-grained sandstones), also rich in plant fragments. At the top of the core, the black shales (facies F) indicate a deeper lacustrine environment (P2) with a sustained water-column stratification, allowing for dysoxic/anoxic conditions at the base of the water column and in the sediments, as shown by the high TOC content (up to 28 wt.%). The coarse-grained lithologies in the MU well are oxidized, probably due to recent weathering as material from this core is close to the surface.

Evolution of the depositional environments inferred from subsurface data

The Igornay core (IG-1)

The IG-1 core (Fig. 12) presents an overall trend from dominantly fine-grained to coarse-grained facies. The association of fine-grained facies, either homolithic, sometimes OM-rich, or heterolithic, with scarce medium-to-coarse-grained lithologies reflecting turbidites or debris flows, indicates intervals of profundal lake environments that are more or less distal (P2–P1 environments, Table 2) depending on the frequency, thickness and granulometry of the coarsest-grained levels. When displaying dysoxia to anoxia features (laminated OM-rich facies), the facies association is instead representative of the P2a environment (Table 2), as was the case at the base of the core and between 155 and 148 m (i.e., Igornay OSB, Figs. 1b, 12).

These profundal-lake facies associations are often interbedded with intervals of coarser-grained facies, occurring in dm-thick to several meters thick beds from sandstones to

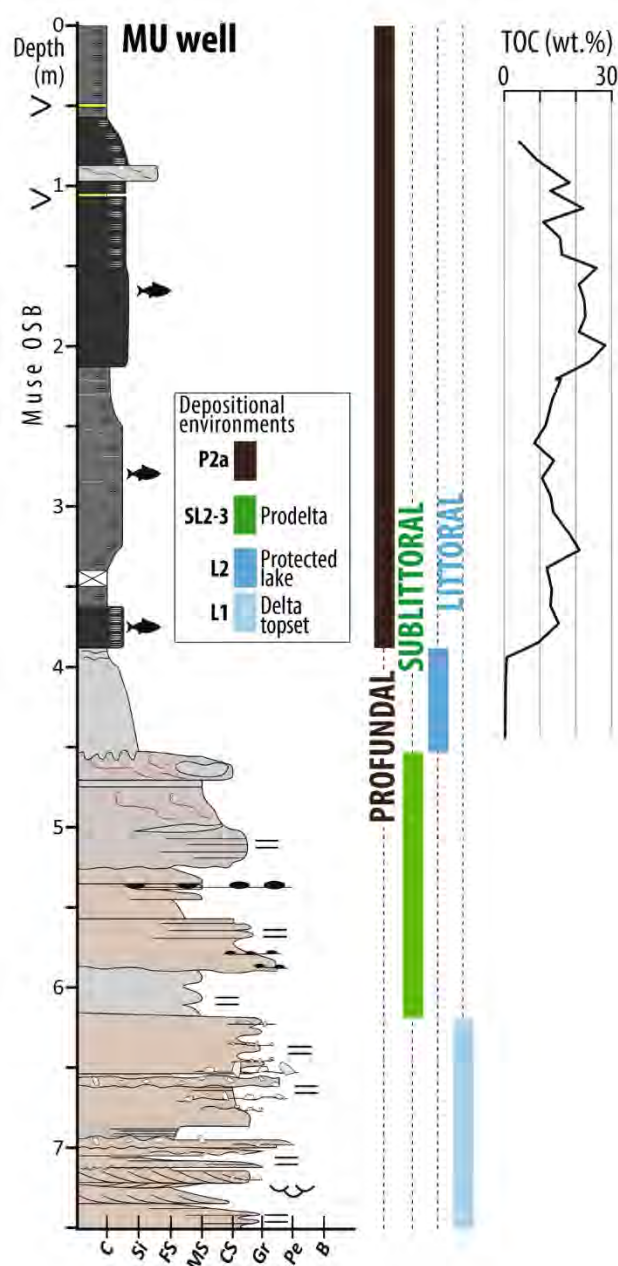


Fig. 11 Sedimentary log of the MU core (see Figs. 1c and 2 for the position in the stratigraphy and location on the map, Fig. 10 for the log caption, and Table 2 for the facies association codes) showing the evolution of the depositional environments. The TOC content has been measured for the Muse OSB only. *TOC* total organic carbon

conglomerates, either thickening-upward (i.e., at the expense of the finest-grained facies) as shown at the base of the core, or thinning-upward above the Igornay OSB (Fig. 12). These intervals are composed of massive facies, sometimes matrix-supported or containing large mudclasts (i.e., debris flows), or displaying Bouma sequence divisions reflecting turbidite deposits, both of them indicating a sublittoral lake

environment with significant or moderate sediment fluxes, reflecting prodelta deposits (SL2 and SL3 environments, respectively, Table 2). Some energetic medium-grained facies, with planar bedding and trough cross-stratifications, mark substantial flows and are interpreted as deposited in gravelly bottomsets or through hydraulic jumps occurring in deltaic toesets, respectively (SL2 environment, prodelta, Table 2).

The coarsest lithologies of the IG-1 core (medium-to-coarse-grained facies) are located in the upper third of the core (Fig. 12). Some intervals display inclined facies with current features alternating with thin beds of finer-grained facies deposited during periods of fine-grained particle settling, as well as thickening-upward sequences and interbedded slump levels, thus indicating deltaic foreset progradations in a sublittoral lake environment (SL1, Table 2). Other intervals present planar-bedded facies or trough cross-stratifications, indicating maximal sediment fluxes and 3D megaripple migration and, therefore, an even shallower environment, i.e., a sublittoral lake environment displaying deltaic topsets (L1 environment, Table 2). However, these facies are alternating with periods of very low-energy and sediment fluxes reflected by fine-grained levels, often OM-rich, sometimes bioturbated or containing some microbial carbonate deposits, marking a protected littoral lake environment (L2).

The Chevrey core (CHE-1)

The lower half of the CHE-1 core displays an alternation between the fine-grained homolithic facies, containing some whitish tonstein levels and heterolithic facies (Fig. 13). Some dm-thick coarser-grained facies, reflecting distal turbidites or debris flows, are also displayed. The dominant fine-grained facies mostly indicate profundal lake P1 (when some detrital fluxes are deciphered by cm- to dm-thick turbidite levels) and P2 environments, and sometimes P2a environments when dysoxic/anoxic conditions are reached (i.e., OM-rich deposits at ~330 m, Fig. 13, Table 2). Several periods of slightly enhanced sediment fluxes (dm-thick sandstone beds with current features, alternating with fine-grained lithologies, on 1–2 m thick intervals) indicate prodelta deposits in sublittoral lake SL2 and SL3 environments (Table 2). Embedded in this interval of dominantly profundal and sublittoral lake environment deposits, a ~30 m thick interval of mostly sandy to conglomeratic facies is found around 200 m, sometimes displaying trough cross-stratifications indicating 3D megaripple migrations in a littoral lake L1 environment (major sediment supply in deltaic topsets), or sometimes with inclined facies, indicating a sublittoral lake SL1 environment (active deltaic foresets, Table 2).

The upper half part of the core begins with a ~25 m thick OM-rich interval composed of fine-grained facies attributed to the Lally OSB (Fig. 13), indicating a profundal lake P2a.

Above, another alternation between deposits from profundal (fine-grained facies, from claystones to fine-grained sandstones) and sublittoral environments (frequent turbidites and grain flows, SL2 and SL3 prodelta deposits) is observed. However, the sandy to conglomeratic facies representing prodelta deposits are dominant over the fine-grained facies, with a thickening-upward trend. Two ~8 m thick intervals, dominated by coarse-grained facies with planar stratifications indicating high-energy currents, and reflecting deltaic topsets in a littoral lake L1 environment, are observed in this upper half part of the core.

The Varolles core (VAR-1)

The depositional environment evolution in the VAR-1 core is displayed in Fig. 14. This core is dominated by an alternation between intervals of fine-grained facies, dominant at the base of the core, and intervals of medium-to-coarse-grained facies which, conversely, become dominant towards the top of the core.

The fine-grained facies are mostly characterized by laminated claystones to siltstones, sometimes finely laminated and OM-rich, reflecting a low-energy environment, assigned to a P2 profundal lake when the sediment fluxes are minimal (cm-thick fine to medium sandy levels), or to a P1 profundal lake environment when they are slightly more substantial, reflected by distal turbidites (heterolithic fine-grained facies, sometimes with Tb, Tc or Te divisions of the Bouma sequence) and scarce grain flows or debris flows. Close to the top of the core, a ~20 m thick interval composed of very fine-grained laminated black facies is displayed, with numerous fish remains, and is attributed to a dysoxic/anoxic profundal lake environment P2a, representing the Lally OSB according to Marteau (1983).

The second end-member, in terms of the facies association, is composed by ~5 m thick sets, either (i) dominated by fine-to-medium-grained heterolithic facies or homolithic facies, mainly massive or with planar bedding, and attributed to grain flows or turbidites deposited in a prodelta, in the sublittoral lake environment (SL2/SL3 facies associations), or (iii) showing inclined medium-to-coarse-grained facies (grain flows and debris flows), sometimes deformed (i.e., slumps), reflecting deltaic foresets (sublittoral lake SL1 environment, Table 2), which have a much higher representation in the VAR-1 core compared to the IG-1 and CHE-1 cores.

Scarce plurimetric intervals displaying medium-to-coarse-grained facies, with high-energy planar bedding or trough cross-stratifications, are attributed to deltaic topsets (littoral lake L1 environment), and narrow intervals of fine-grained facies (claystones to siltstones), either finely laminated or massive, sometimes showing horizontal and vertical burrows, likely indicate a shallow low-energy environment,

i.e., a protected littoral lake (L2 environment; Fig. 14, Table 2). These most landward facies associations are only found in the lower third of the core.

Basin-scale sequence stratigraphy correlations

Stratigraphic cycles based on the evolution of the depositional environments and organic matter accumulation rates

The Igornay well (IG-1)

In the IG-1 well, the TOC content values vary between 0.12 and 20.36 wt.% (Fig. 12), and the highest values can be used to determine the location of the MFSs in the sequence stratigraphy analysis. This core displays five intervals with very high TOC values: (i) at the base of the core (TOC ~15–17 wt.%), (ii) around 150 m, where the highest values are found (TOC up to 20 wt.%), (iii) around 85 m (TOC up to 12 wt.%); between 35 and 40 m (TOC up to 16 wt.%) and around 22 m (TOC up to 13 wt.%). All of these intervals are associated with black fine-grained lithologies, mostly deposited in a profundal lake environment (P2 facies association, Fig. 12), or in a protected littoral lake environment (L2 facies association, Fig. 12).

Based on the depositional environment evolution described above and on these OM-content variations, four stratigraphic cycles have been identified in the IG-1 core (Fig. 12). The first one, from 200 to 152 m, encompasses a large progradational trend from a profundal dysoxic/anoxic lacustrine environment (P2a facies association) to a sublittoral lake environment (SL2 facies association, gravelly bottomsets in a prodelta), up to the MRS located at 162 m. This trend is then reversed, with a retrogradational trend ending by a MFS at 152 m, within an anoxic/dysoxic profundal lake P2a environment, corresponding to the Igornay OSB (Marteau 1983). The second cycle, from 152 to 87 m, is progradational up to 128 m, from the previous profundal dysoxic/anoxic lake P2a environment, to the sublittoral lake SL2 environment constituting the MRS. The retrogradational trend, up to 87 m, bounded by a MFS in a 1 m thick interval of profundal lake P2a deposits, is gradual and displays several occurrences of sublittoral lake SL3 deposits (i.e., fine-grained prodelta deposits), between the profundal lake P1 and the sublittoral lake SL2 (toesets/gravelly bottomsets in a prodelta) endmembers. The third cycle, from 87 to 40 m, is progradational up to the MRS located at 53 m, corresponding to a littoral lake L1 environment (deltaic topset deposits), and then retrogradational, up to a dysoxic/anoxic protected littoral lake L2 environment. The fourth cycle,

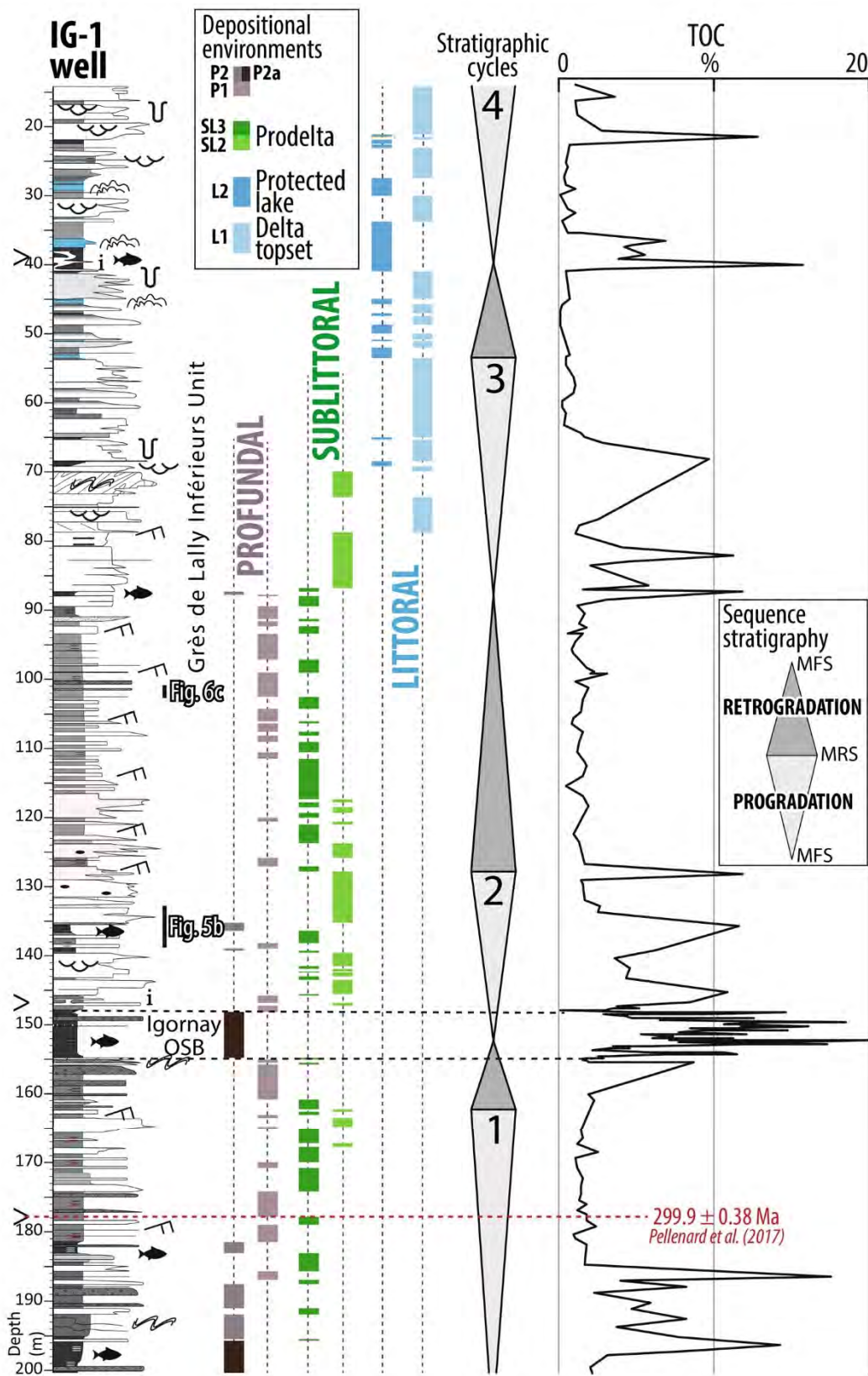


Fig. 12 Sedimentary log of the IG-1 well (see Figs. 1c and 2 for the position in the stratigraphy and location on a map, Fig. 10 for the log caption, and Table 2 for the facies association codes), evolution of the depositional environment, stratigraphic cycles and OM content (total organic carbon TOC) variation through time. OSB oil-shale bed, a anoxia

from 40 m to the top of the core, is only progradational, with increasing occurrences of coarse-grained littoral lake L1 deposits (deltaic topsets). Cycles 2–4 correspond to the *Grès de Lally Inférieurs* Unit (Fig. 12).

The Chevrey well (CHE-1)

The TOC values in the CHE-1 well range between 0.18 and 20.98 wt.% (Fig. 13). Intervals with significant TOC values are displayed around 325 m (TOC up to 10 wt.%) and between 130 and 155 m (TOC up to 21 wt.%), in the same dark and fine-grained facies as in the IG-1 core, and occasionally in very thin intervals interbedded in coarser lithologies (Fig. 13).

For the CHE-1 core, seven stratigraphic cycles have been identified (Fig. 13). The first one, from the base of the core to 324 m, shows a retrogradational trend, with the transition from a sublittoral lake environment (SL2 and SL3, prodelta deposits) to a profundal dysoxic/anoxic lake P2a environment comprising the MFS. The second cycle, from 324 to 228 m, displays high-frequency transitions between the profundal P1 and P2 and sublittoral SL3 lake environments, with a MRS characterized by a 2 m thick interval of sublittoral lake SL2 deposits, located at 245 m, and a MFS in OM-rich deposits (TOC of ~6 wt.%). The third cycle, from 228 to 176 m, is progradational up to a littoral lake L1 environment (deltaic topsets), with a MRS at 190 m, and retrogradational up to a profundal lake P2 environment (TOC values of 7 wt.%). The fourth cycle, from 176 to 140 m, is progradational up to a sublittoral lake SL2 environment at 162 m, constituting the MRS, and then retrogradational to a dysoxic/anoxic profundal lake P2a environment constituting a ~20 m thick interval with the highest OM content of the core (TOC up to 21 wt.%). The fifth cycle, from 140 to 96 m, is progradational up to 103 m, up to a littoral lake L1 environment (deltaic topsets), and retrogradational up to another interval of dysoxic/anoxic profundal lake P2a environment (TOC values up to 5 wt.%). The sixth cycle, from 96 to 31 m, is only progradational, up to a littoral lake L1 environment, and is followed by the seventh cycle, also beginning by profundal lake P2 deposits, and progradational up to 21 m, followed by a retrogradational trend up to a profundal lake P1 environment at ~15 m.

The Varolles well (VAR-1)

In the VAR-1 core, no TOC values have been measured, making it impossible to precisely place the MFSs within the more distal deposit intervals at the end of the retrogradational trends. Five stratigraphic cycles have been identified based on sedimentological data (Fig. 14). The first one is progradational from the base of the core to 230 m with a transition from a profundal lake P2 environment to a sublittoral lake SL1 environment (deltaic foresets) constituting the MRS at 237 m, and then retrogradational up to a profundal lake P2 environment. The second cycle is from 230 to 149 m, with a progradational trend up to the littoral environments (L1, deltaic topsets, and L2, protected lake) and a retrogradational trend up to the profundal lake, probably dysoxic to anoxic given the very fine-grained black facies (P2a environment). The third cycle is from 149 to 102 m, with a progradational trend up to a sublittoral lake SL1 environment (deltaic foresets) at 130 m, and a retrogradational trend up to the profundal lake environment, again likely dysoxic/anoxic. The fourth cycle spans from 102 to 44 m, and displays the same depositional environments along its progradational/retrogradational trends than the previous cycle, with a MRS placed at 62 m, and a MFS in the middle of the 20 m thick interval, likely enriched in OM (very dark finely laminated claystones comprising lot of fish remains, as observed in the IG-1 and CHE-1 OM-rich deposits). The fifth cycle, from 44 m to the top of the core, only displays a progradational trend, possibly incomplete, from the profundal lake P2a environment to the sublittoral SL2 environment (gravelly bottomsets in a prodelta).

Correlations between deep-cored wells

Together with the present sequence stratigraphy analysis and some previous interpretations of Marteau (1983), it is possible to reliably make correlations between the three deep wells presented in Fig. 15. The IG-1 core encompasses the Igornay OSB (from ~155 to 145 m, Fig. 12), with overlying deposits corresponding to the *Grès de Lally Inférieurs* Unit (Marteau 1983, Fig. 1c). No other significant OM-rich deposits are identified up to the top of the core, which means that the Lally OSB, located at the top of the *Grès de Lally Inférieurs* Unit, was not drilled. The CHE-1 core displays the *Grès de Lally Supérieurs* Unit at its top (Figs. 1c, 12), and the OM-rich interval between 130 and 155 m is attributed to the Lally OSB (Marteau 1983), thus indicating that the underlying deposits belong to the *Grès de Lally Inférieurs* Unit. Given the thickness between the Lally OSB and the OM-rich interval between 334 and 320 m (i.e., representing 165 m), these OM-rich deposits likely correspond to the Igornay OSB, since the maximum thickness of the *Grès de Lally Inférieurs* Unit

Fig. 13 Sedimentary log of the CHE-1 well (see Figs. 1c and 2 for the position in the stratigraphy and location on the map, Fig. 10 for the log caption, and Table 2 for the facies association codes), evolution of the depositional environments, stratigraphic cycles and evolution of the TOC content. *TOC* total organic carbon

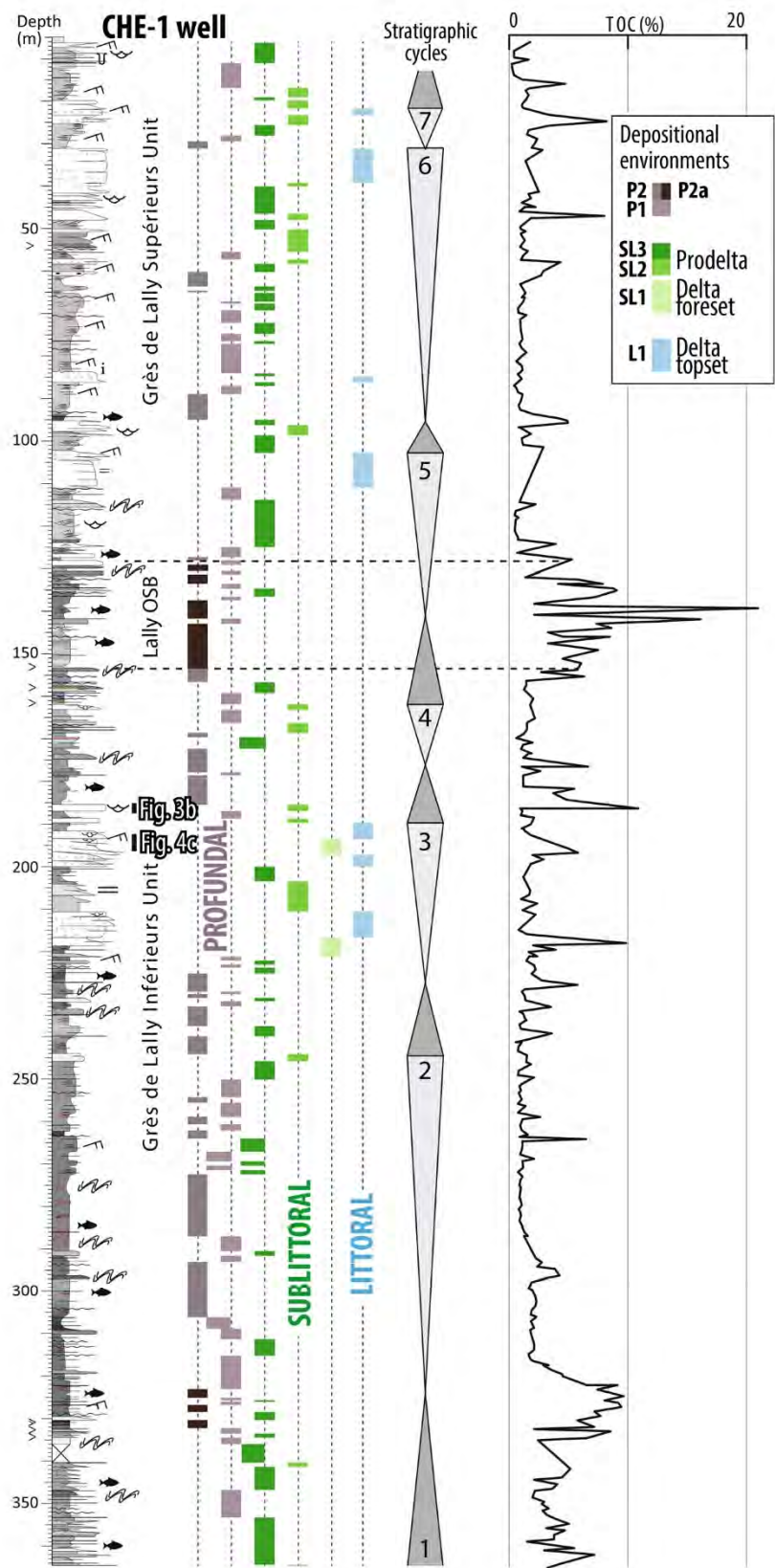
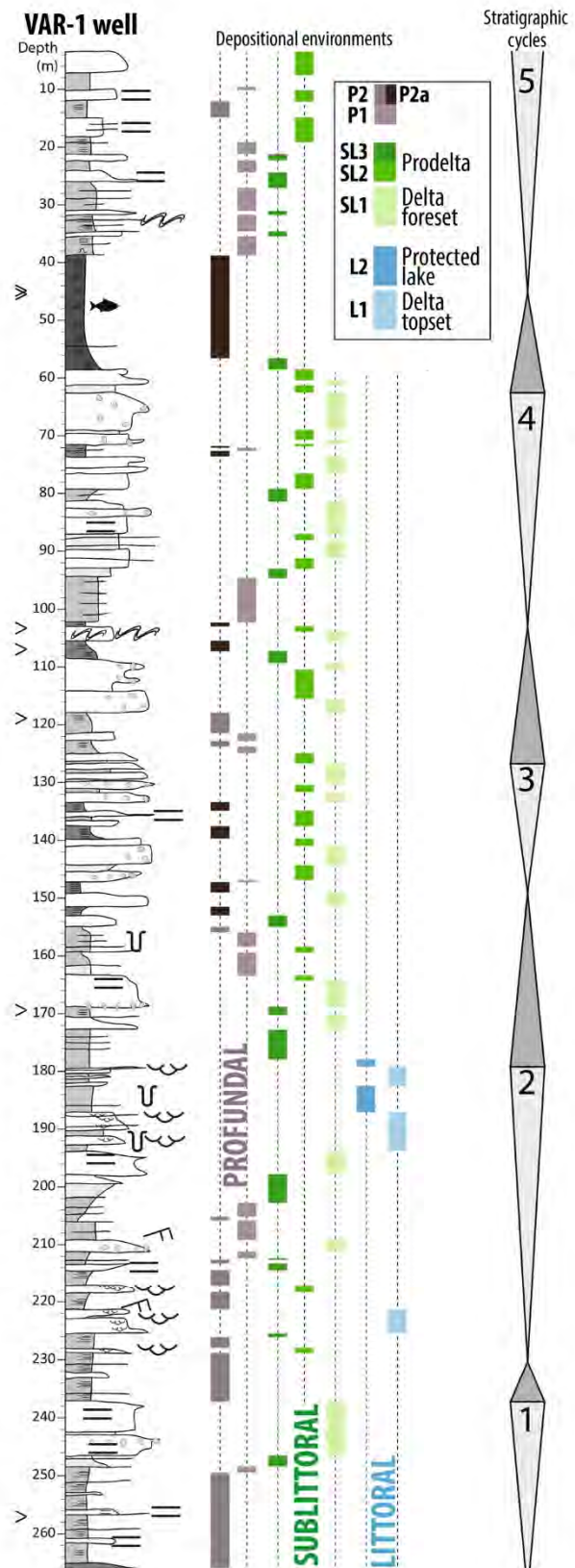


Fig. 14 Sedimentary log of the VAR-1 well (see Figs. 1c and 2 for the position in the stratigraphy and location on the map, Fig. 10 for the log caption, and Table 2 for the facies association codes), depositional environment evolution and stratigraphic cycles

throughout the Autun Basin is estimated to be ~ 150 m (Fig. 1c). Thus, it seems likely that the OM-rich intervals containing the MFSs, combined with the previously determined stratigraphic cycles, can be reliably used to provide accurate correlations between the IG-1 and CHE-1 wells, as represented in Fig. 15. The Igornay OSB comprises the MFS separating cycles 1 and 2 in these two wells, allowing to correlate the subsequent cycles as follows: the second major flooding located at 85 m in the IG-1 core corresponds to the flooding observed at 228 m in the CHE-1 core (top of cycle 2, Figs. 12, 13, 15), and the MFS located at 40 m in the IG-1 core corresponds to the MFS at 176 m in the CHE-1 core (top of cycle 3, Figs. 12, 13, 15). In these two wells, profundal and sublittoral lake environments dominate at the base of the Igornay Fm, i.e., from the base to 80 m in the IG-1 core, and to 220 m in the CHE-1 core. The medium-to-coarse-grained lithologies between 40 and 90 m in the IG-1 core, attributed to sublittoral SL2 to littoral lake L1 environments and assigned to the *Grès de Lally Inférieurs* Unit, can be correlated with the medium-to-coarse-grained facies of the CHE-1 core between ~ 190 and 220 m.

The CHE-1 and VAR-1 wells are located 850 m from each other (Fig. 2), at a similar altitude (310 m and 315 m, respectively) and, according to Marteau (1983), the local dip of the series is 2.5° to the north, likely due to a local tectonic tilting, whereas the main regional dip is towards the south (Fig. 2b). The Lally OSB is well identified in these two wells in the work of Marteau (1983), thus constituting an accurate correlating level (i.e., the MFS between cycles 4 and 5 in the two wells, Figs. 13, 14 and 15). However, considering the short distance between the two wells and the slight local dip, the substantial depth of the Lally OSB in the CHE-1 core (i.e., 130 m, Figs. 13, 15) compared to the one in the VAR-1 core (i.e., 40 m, Figs. 14, 15), likely reflects a fault between the two wells. Despite the proximity of these two boreholes, the sedimentological descriptions also show that the VAR-1 facies are broadly coarser than the CHE-1 facies, possibly due to a higher sediment supply in the VAR-1 core location, and therefore indicating more proximal environments, with respect to the sediment sources. However, based on the recognition of the progradational-retrogradational cycles, it is possible to make correlations between these two wells (Fig. 15). Based on these new correlations, it is likely that the Igornay OSB has also been reached by the VAR-1 well, considering the dark laminated fine-grained facies deposited in a profundal lake P2 environment between 226 and 236 m; this hypothesis could be strengthened by additional TOC content analyses. Lastly,



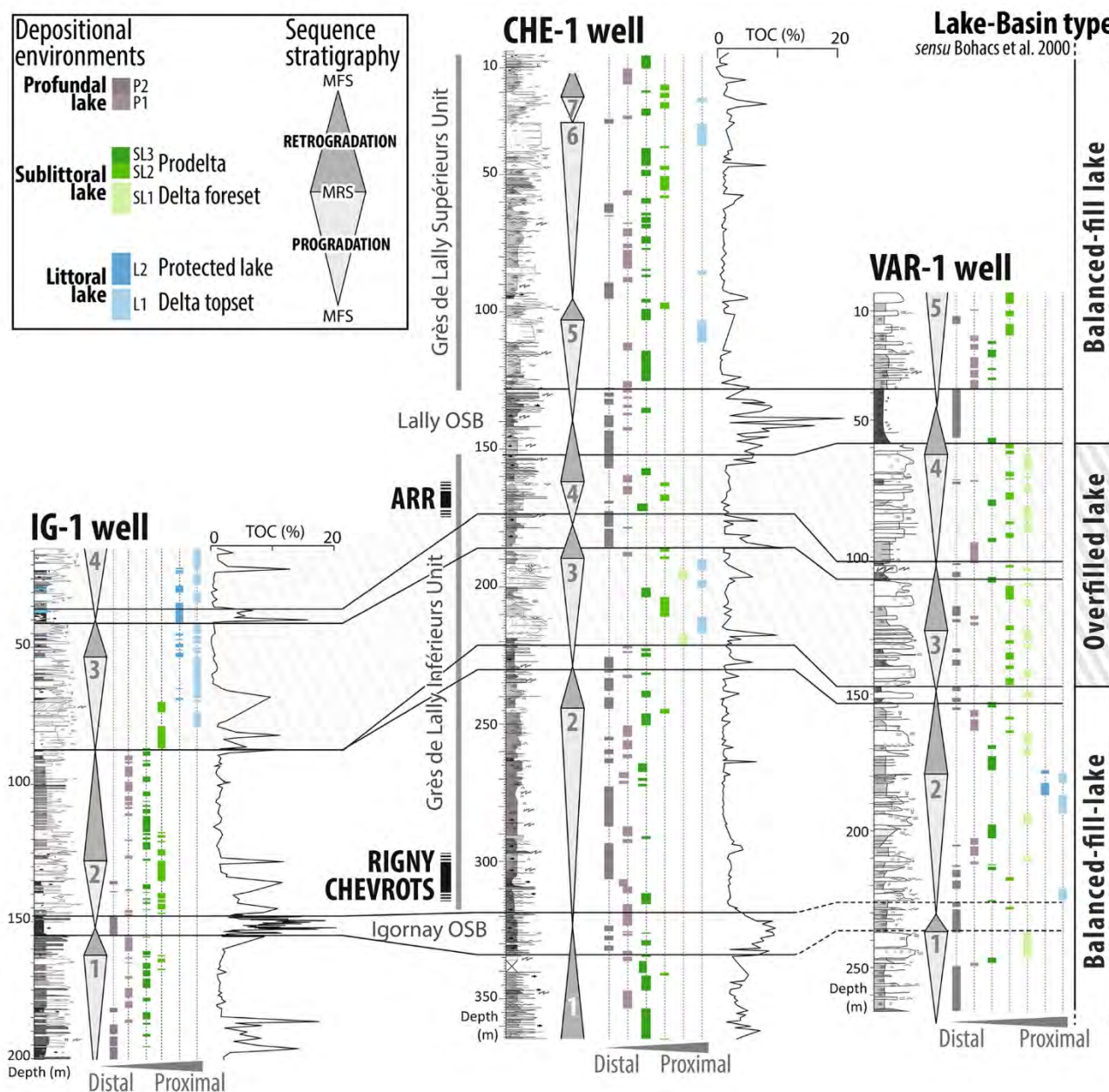


Fig. 15 Correlations between the IG-1, CHE-1 and VAR-1 wells. The Arroux, Chevrots and Rigny sections have been replaced at the base and top of the Grès de Lally Inférieurs Unit, respectively. The MU core is not figured as this section is stratigraphically above the Grès

de Lally Inférieurs Unit (i.e., Muse OSB, not reached by the three wells). See Fig. 2 for the location of the wells and sections on a map, and Fig. 10 for the log caption. OSB oil-shale bed; MFS maximum flooding surface; MRS maximum regressive surface

correlations between VAR-1 and CHE-1 are in agreement with some previous observations of Marteau (1983).

Correlations between subsurface data and field sections

Outcrop sections can be correlated to the three deep cores IG-1, CHE-1 and VAR-1, since the Chevrots and Rigny

sections are stratigraphically located between the Igornay and Lally OSBs (i.e., in the Grès de Lally Inférieurs Unit), based on cartographic positions (Fig. 2). Moreover, based on field data, they are located only several meters above the Igornay OSB, indicating that the deltaic facies associations from topsets (L1 environment) to gravelly bottomsets (SL2 environment, prodelta) of these outcropping sections correspond to the prodelta SL2 to SL3 facies associations

displayed in the IG-1 core. Based on the correlation between the cored wells, it also suggests that the Chevrots and Rigny sedimentary successions correspond to the profundal lake P1 and P2 facies associations in the CHE-1 core, and to either the marginal-lake (littoral lake L1) or distal (profundal lake) facies associations in the VAR-1 core, when considering a roughly constant thickness of the Igornay Fm throughout the basin (200–250 m, Fig. 1c).

The Arroux section, containing some alternations of medium-to-coarse and fine-grained lithologies, as well as microbial deposits, can be correlated with the interval showing microbial deposits in the IG-1 core (~37–28 m, i.e., the base of the progradational trend of cycle 4, Fig. 12). The MU core, encompassing the Muse OSB, is located higher up in the stratigraphic column (Muse Fm, Fig. 1c) and, therefore, cannot be correlated with any of the cores or outcrops.

Discussion

Refining the paleoenvironments of the Autun Basin

Sedimentological facies analyses suggest that the sediments of the Autun Basin were deposited in three positions along a landward–basinward transect, namely the littoral, sublittoral and profundal lakes (as defined by Bohacs et al. 2000). These positions are divided into seven depositional environments, depending on the sedimentary flux intensity, highlighting (i) periods dominated by high sediment supply in the basin, indicated by deltaic topset, foreset and prodelta deposits (topsets/bottomsets), and (ii) periods of low sediment supply, i.e., reflected by fine-grained laminated sediments attributed either to profundal or shallow-protected littoral lacustrine deposits, depending on their association with low-water column sedimentary features (e.g., microbial deposits, trunks, wave ripples).

The two first stratigraphic cycles in the three deep-cored wells (Figs. 12, 13, 14 and 15) present an evolution from a dominantly profundal lake to sublittoral lake environments (i.e., prodelta deposits), yet with some scarce sublittoral to littoral lake deposits in the VAR-1 core. In the lower part of the cores, the profundal lacustrine conditions are determined through the presence of OSBs (i.e., Igornay OSB) interbedded with turbidites, and the laminated fine-grained deposits containing alternations of dark, light and sometimes red laminae, possibly linked with seasonal physical and chemical modifications in the water column. The OSBs either indicate a decreased sediment supply in the basin, and/or a deepening of the lake, marked by a chemical or thermal stratification of the water column, leading to dysoxia/anoxia in the bottom waters.

The sedimentary architectures observed in the *Grès de Lally Inférieurs* Unit in the deep cores (IG-1, CHE-1 and

VAR-1 wells), and on the Chevrots and Rigny outcrops, together with the numerous rapid transitions between profundal lacustrine deposits (i.e., fine-grained lithologies and OSBs) and more proximal deposits with respect to the sediment source areas (i.e., coarse-grained sandstones to conglomerates), without pronounced unconformities, do not support transitions from a lacustrine to a strict fluvial environment, as suggested by several previous studies of the Autun Basin (e.g., Marteau 1983; Delfour et al. 1991, 1995), but also in the Decize–La Machine Basin (Donsimoni 1990, 2006). Instead, the refined sedimentological data, with the coarsest-grained facies displaying deltaic features (e.g., inclined foresets, toeset and bottomsets deposits), paired with the use of sequence stratigraphy concepts, indicate deltaic progradations into a lacustrine environment, i.e., sedimentary succession dominated by subaquatic or lacustrine-marginal environments exclusively, rather than strictly fluvial vs. lacustrine environments. The fluvial or alluvial system feeding this delta-lake system is therefore not preserved in the parts of the basin or the sedimentary intervals studied here. These interpretations are also in line with the deltaic environments described in the recent studies of the neighboring Decize–La Machine Basin performed by Ducassou et al. (2019) and Mercuzot et al. (2021a), based on the core descriptions and seismic profiles, as well as in the study carried out by Mathis and Brulhet (1990) in the sedimentary succession of the Aumance Basin (location in Fig. 1b).

The Arroux section (ARR), close to the top of the *Grès de Lally Inférieurs* Unit (i.e., progradational trend of the cycle 4, Fig. 15), contains the most proximal facies observed in the studied lower Autunian, as indicated by the wave ripples and the trunks preserved in living position (Figs. 3c, d), reflecting periods of contraction of the lake and the lowest lake level of the studied interval.

At the top of the IG-1 core (i.e., retrogradational trend of the third cycle and the whole fourth cycle, Fig. 15), thin OSBs are associated with some microbial deposits (Fig. 12), thus indicating a shallow water column in a littoral lake L2 environment protected from major sediment inputs. They are, therefore, different from the Igornay OSB, which is interpreted as profundal lake deposits. Two conditions are necessary to preserve such black shales in a shallow marginal part of the lake: (1) protection from sediment supply either due to the formation of a topographic or phytogenic barrier, or a quiet sedimentation taking place laterally from the main deltaic system (Fig. 7); and (2) stagnant water preventing the oxidation and remineralization of the OM.

Above the *Grès de Lally Supérieurs* Unit (i.e., the fifth, sixth and seventh stratigraphic cycles from the CHE-1 and VAR-1 cores; Fig. 15), up to the MU core deposits, the sedimentary succession, still belonging to the *Grès de Lally Supérieurs* Unit, is no longer available through surface or subsurface data. However, some silicified trunks and roots

(e.g., *Stigmaria flexuosa* and *Dadoxylon*) have been found in living position, indicating the presence of paleosols (Renault 1888; Marguerier and Pacaud 1980), and therefore other periods of low lake level in the Autun Basin, with the possibility of fluvial deposit preservation. In the uppermost sediments observed in the stratigraphy (i.e., the Muse section and MU core), the very high OM content found in the Muse OSB suggests a return to more distal environments, with profundal lacustrine facies deposited under dysoxic to anoxic conditions. The overlaying series are poorly known because of the lack of outcrops or core data (several tens of meters to hundreds of meters are possibly missing).

Lastly, when comparing the three deep cores (IG-1, CHE-1 and VAR-1 wells), the environments are generally more proximal in the IG-1 and VAR-1 cores than in the CHE-1 core, with respect to the sediment source areas. The more distal conditions recorded in the CHE-1 core may have prevented erosional events, resulting in a better preservation of the OM-rich fine-grained sediments of the Igornay OSB. This also indicates that the IG-1 core is located in a more proximal area of the basin than the CHE-1 core, and partly explains the absence of microbial deposits in the CHE-1 core.

To sum up, in the Autun Basin, the most profundal lacustrine environments are dominant in the late Gzhelian (cf. Fig. 1c), with identification of developed intervals of very finely and regularly laminated levels as well as OSBs, corresponding to periods of dysoxia/anoxia of the bottom waters and in the sediment. Then, these profundal lacustrine conditions evolve towards more proximal environments along a landward-to-basinward transect during the early Asselian, where deltaic systems are displayed, whereas the OM can still be preserved if the depositional environment is protected from the sediment supply. Lastly, the most proximal environments recorded in the studied sections, i.e., the closest to the sediment source areas, marked by carbonate-mineralized microbial deposits and trees, are described close to the Gzhelian/Asselian boundary (CP boundary, Fig. 1c).

Basin-fill evolution

A lake basin-type classification has been established by Bohacs et al. (2000) that distinguishes underfilled, balanced-fill and overfilled lake-basins, depending on the variations of the sediment supply and of the available accommodation space. Considering the characteristics listed above, three main intervals are displayed along the lower Autunian succession of the Autun Basin, and can be distinguished as per this classification (Fig. 15): (i) the two first stratigraphic cycles, dominated by sublittoral to profundal environments, thus displaying very low to moderate sediment fluxes, can be attributed to a balanced-fill lake-basin type, i.e., where the accommodation space exceeds the sediment supply,

either induced by a climatically driven high lake level or by high subsidence rates; (ii) the third and fourth stratigraphic cycles, representing the most landward environments of the studied succession, with the highest sediment fluxes, are attributed to an overfilled lake-basin type, i.e., high sediment supply exceeding the accommodation rates; and (iii) the fifth to seventh stratigraphic cycles, displaying depositional environments comparable to the first two cycles, are also considered as periods of balanced-fill lake-basin type, either because of a decrease in the sediment fluxes and/or an increase in the subsidence.

This basin-fill evolution, therefore, reflects variations in the relative lake level over time, triggered either by climate or tectonic variations. Further work is required to determine the respective control of these two factors, notably through precise correlations with adjacent basins, which is only possible through the acquisition of precise radiometric ages.

An isolated or connected lake system?

The Autun Basin is one of the four CP basins cropping out in the northeastern Massif Central, together with the Blanzay–Le Creusot, Aumance, and Decize–La Machine basins (Fig. 1b), formed and filled in a similar geodynamic setting. The tectono-sedimentary history of the Autun Basin is reconstructed in Fig. 16. At the beginning of the basin filling, the deposition of CP sediments was driven by the Autun fault, and the distal facies extended further north (Fig. 16a). The subsequent tilting of the basin and the uplift of its borders then prevented the deposition of the post-early Permian and basal Triassic sediments (Fig. 16b). The currently preserved sediments are known from the Middle Triassic onwards—belonging to the Meso-Cenozoic cover of the Paris Basin—and are no longer controlled by any fault (i.e., regional subsidence, Fig. 16c). They were then partly eroded during the Late Cretaceous to Tertiary uplift phases (Fig. 16d). In the present day, erosion is still occurring, resulting in a Meso-Cenozoic succession that is almost totally eroded in the Autun Basin area (Fig. 16e). Thus, the present-day borders of the basin are erosive, and the observed deposits are partially preserved from the post-lower Permian uplifts and subsequent erosions because they were protected by the overlaying Mesozoic sediments. This difference in position between the present-day northern border of the preserved sedimentary area and the initial border of the basin shows that the initial sedimentary area was much broader.

This is also observed in the Decize–La Machine Basin (Mercuzot et al. 2021a), where the most distal facies (i.e., profundal lacustrine facies) crop out near the present-day borders of the basin (Figs. 2, 16e), indicating that the shoreline of the lake at the time of sedimentation is not preserved. Furthermore, recent studies of this basin (Ducassou et al.

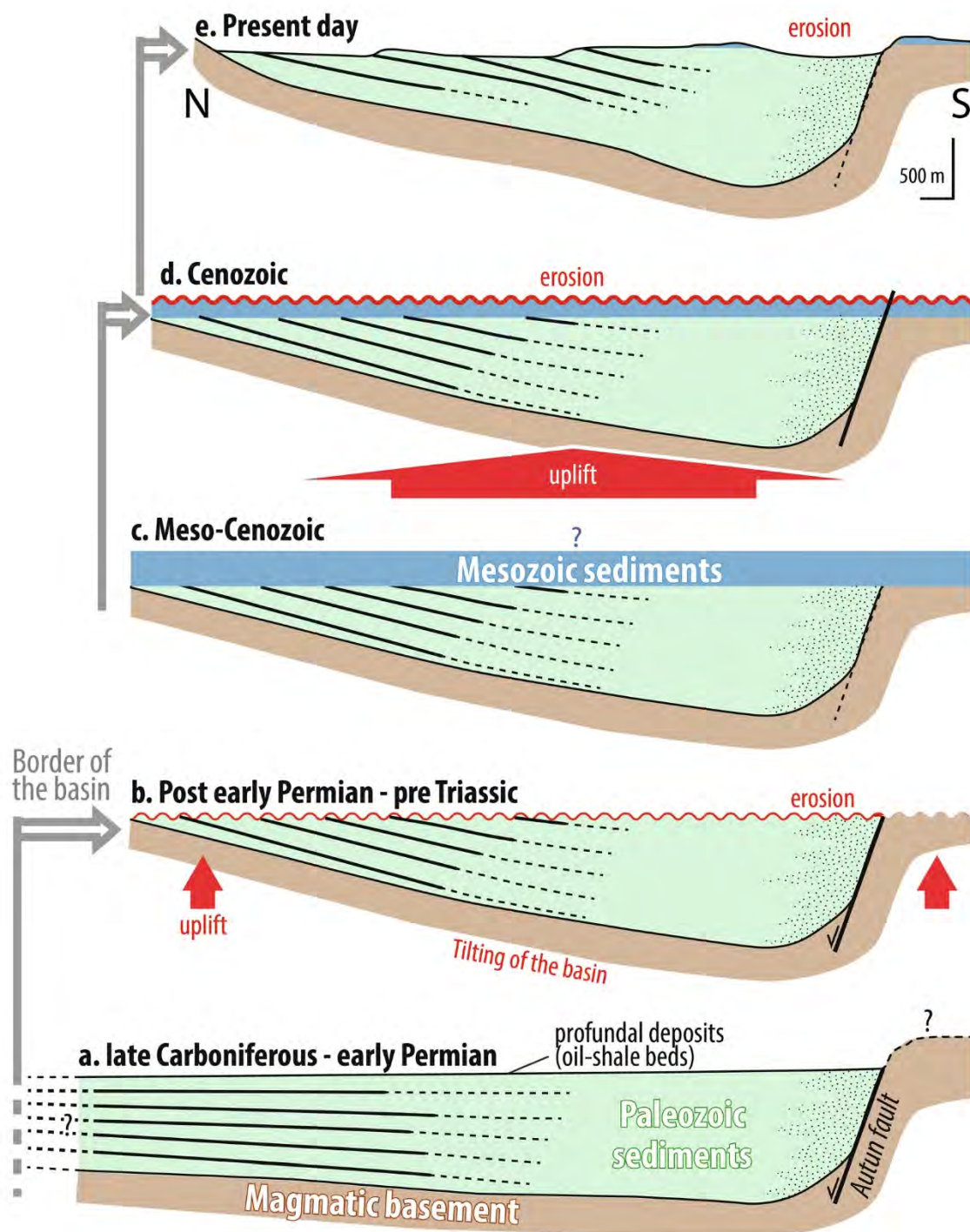


Fig. 16 Simplified tectono-sedimentary history of the Autun Basin through time. **a** Filling of the basin during the late Carboniferous and the early Permian, driven by the Autun fault activity. **b** Tilting of the basin, uplift of its borders, erosion. **c** Meso-Cenozoic sedimentation,

no longer controlled by the Autun fault. **d** Tertiary regional uplift and erosion, with a probable reactivation of the Autun fault. **e** Present-day configuration, with erosion

2019; Mercuzot et al. 2021a), also evidenced large deltaic systems prograding into a lacustrine environment, but highlighted more proximal depositional environments with

respect to the sediment source areas than in the Autun Basin, i.e., floodplain with coal deposits, coarse-grained alluvial fan or Gilbert-type deltaic lithologies, and an absence of

varves and black-shale deposits. On a landward-to-basinward depositional profile, these features indicate that the Decize–La Machine Basin is overall more proximal than the Autun Basin, and that its active sedimentation area was deepening towards the east, i.e., in the direction of the Autun Basin (cf. Figure 1b), thus suggesting a possible connection between these two basins. This hypothesis is strengthened by the new age models of the Decize–La Machine and Autun basins, provided by Ducassou et al. (2019) and Pellenard et al. (2017), respectively, showing that the sedimentary successions of these two basins are contemporaneous (i.e., centered around the CP boundary).

As suggested by Mercuzot et al. (2021a), the Decize–La Machine and Aumance basins could be part of a much larger basin, through connections with the subsurface Brécy, Contres and Arpheuilles basins, evidenced in the southern Paris Basin through seismic data by Beccaletto et al. (2015), and the Autun Basin would, therefore, be part of this larger system. This suggests a Permian basin spanning several hundreds of kilometers in length, with a roughly west–east extension, partly hidden beneath the Meso-Cenozoic sedimentary cover of the Paris Basin. This is also in agreement with paleobiogeography data, as highlighted by the studies performed by Schneider and Zajic (1994) and Schneider et al. (2000). During the uppermost Carboniferous (i.e., Gzhelian), some sharks, the fossils of which (e.g., teeth, coprolites) are found in the Autun and Aumance basins amongst others, had a uniform species association within the European basins (e.g., Puertollano Basin, Saar-Nahe Basin, Saale Basin and Central Bohemian Basin), implying connections between them.

It is, therefore, highly probable that the French CP basins of the northeastern Massif Central were connected at some point during their filling, likely with a shared drainage system with fluvial connections, rather than connections with the marine realm, as the paleoecology of the fossil sharks, investigated by Fischer et al. (2013) indicates a freshwater living environment for these species. This calls into question the use of the term “basin”, which would be not relevant anymore when mentioning French CP sedimentary successions or, more broadly, European CP successions, as each present-day individual basin could actually represent several distinct depocenters of larger former basins.

Conclusion

Based on sedimentological descriptions paired with sequence stratigraphy concepts, this study reveals that the lower Autun Basin sedimentary successions, previously ascribed to environments alternating between strictly fluvial and palustrine–lacustrine, correspond instead to an

alternation of deltaic deposits prograding into a lacustrine environment, without evidence of strict fluvial deposit preservation. It therefore provides evidence that during the late Carboniferous and the earliest Permian (~299 Ma), the Autun Basin was subjected to episodes of fluctuating accommodation space, either in response to climate or to subsidence variations, the respective roles of which still need to be determined.

During periods of high lake level (i.e., high accommodation space), the preservation of OM-rich sediments was favored by the development of dysoxic/anoxic conditions, also reached during episodes of low lake levels, when the depositional environment was protected from detrital supply. These conditions, when coupled with low water turbidity, also made efficient microbial photosynthesis possible, and thus the mineralization of microbial mats. Moreover, the presence of trees in living position and evidence of paleosols indicate that parts of the basin were occasionally emerged, notably close to the Gzhelian/Asselian boundary.

Lastly, the presence of profundal lacustrine deposits cropping out along the present-day borders of the Autun Basin, together with the missing lateral transition between the delta-lake system and the areas in erosion, indicate that these borders are only erosive, and thus do not correspond to the initial limits of the basin at the time of its infill. This implies that the Carboniferous–Permian basins of the northeastern Massif Central were broader than the present-day preserved sedimentary areas, and that they might have been connected to form a larger basin, as also supported by seismic data and paleobiogeography. It highlights a potential underestimation of the extent and thickness of sedimentary systems in eastern equatorial Pangea during the late Carboniferous and the early Permian. As these areas likely constituted a considerable atmospheric CO₂ sink through the storage of organic carbon in sediments, they would have constituted a major driving factor on the climate, especially at that time (e.g., Montañez et al. 2016; Richey et al. 2020). Given the sensitivity of the equatorial continental areas to climate forcing (e.g., Soreghan et al. 2020), these results and their implications should help constrain future paleoclimate reconstructions.

Acknowledgements This work is part of the PhD thesis of Dr. M. Mercuzot and was funded by the BRGM and the Région Bretagne. The authors thank C. Hue, M. Buisson, T. Boucher, M. Boussaid and A. Saloume for participating in the core logging and Rock-Eval analyses, D. Chabard (director of the Natural History Museum of Autun) for access to the cores, Prof. E. Vennin for providing field section photographs, and Dr. S. Mullin for proofreading the English content. The authors also thank the two reviewers (Dr. T. Voigt and Prof. J. Schneider) who provided constructive comments, greatly improving the manuscript.

References

- Bhattacharya JP (2006) Deltas. In: Posamentier HW, Walker RG (eds) Facies models revisited. SEPM (Society for Sedimentary Geology) Special Publication 84, Tulsa, pp 237–292
- Beccaletto L, Capar L, Serrano O, Marc S (2015) Structural evolution and sedimentary record of the Stephano-Permian basins occurring beneath the Mesozoic sedimentary cover in the southwestern Paris basin (France). *Bulletin De La Société Géologique De France* 186:429–450. <https://doi.org/10.2113/gssgfbull.186.6.429>
- Becq-Giraudon JF, Montenat C, Van Den Driessche J (1996) Hercynian high-altitude phenomena in the French Massif Central: tectonic implications. *Paleogeogr Paleoclimatol Paleocool* 122:227–241. [https://doi.org/10.1016/0031-0182\(95\)00081-X](https://doi.org/10.1016/0031-0182(95)00081-X)
- Behar F, Beaumont V, Pentecado HDB (2001) Rock-Eval 6 technology: performances and developments. *Oil Gas Sci Technol* 56:111–134. <https://doi.org/10.2516/ogst.2001013>
- Bergeron G (1889) Etude géologique du Massif ancien situé au sud du Plateau Central. Dissertation, Paris
- Bohacs KM (1990) Sequence stratigraphy of the Monterey Formation, Santa Barbara County: integration of physical, chemical, and biofacies data from outcrop and subsurface. SEPM Core Workshop 14, San Francisco, California, pp 139–201
- Bohacs KM, Carroll AR, Neal JE, Mankiewicz PJ (2000) Lake-basin type, source potential, and hydrocarbon character: an integrated sequence-stratigraphic-geochemical framework. *Lake Basins Space Time* 46:3–34
- Bouma AH (1962) Sedimentology of some flysch deposits. A graphic approach to facies interpretation. *Dev Sedimentol* 3:247–256. [https://doi.org/10.1016/S0070-4571\(08\)70967-1](https://doi.org/10.1016/S0070-4571(08)70967-1)
- Bouroz A, Doubinger J (1975) Les relations entre le Stéphanien et l'Autunien d'après le contenu de leur stratotype. *Comptes Rendus De L'Académie Des Sciences De Paris* 279:1745–1748
- Bourquin S, Rigollet C, Bourges P (1998) High-resolution sequence stratigraphy of an alluvial fan—fan delta environment: stratigraphic and geodynamic implications—example of the Chauvoy Sandstones, Keuper of the Paris Basin. *Sed Geol* 121:207–237. [https://doi.org/10.1016/S0037-0738\(98\)00081-5](https://doi.org/10.1016/S0037-0738(98)00081-5)
- Bourquin S, Guillocheau F, Péron S (2009) Braided river within an arid alluvial plain (example from the early Triassic, western German Basin): criteria of recognition and expression of stratigraphic cycles. *Sedimentology* 56:2235–2264. <https://doi.org/10.1111/j.1365-3091.2009.01078.x>
- Bourquin S, Bercovici A, López-Gómez J, Diez JB, Broutin J, Ronchi A, Durand M, Arché A, Linol B, Amour F (2011) The Permian-Triassic transition and the onset of Mesozoic sedimentation at the northwestern peri-Tethyan domain scale: paleogeographic maps and geodynamic implications. *Paleogeogr Paleoclimatol Paleocool* 299:265–280. <https://doi.org/10.1016/j.paleo.2010.11.007>
- Breda A, Mellere D, Massari F (2007) Facies and processes in a Gilbert-delta-filled incised valley (Pliocene of Ventimiglia, NW Italy). *Sed Geol* 200:31–55. <https://doi.org/10.1016/j.sedgeo.2007.02.008>
- Brun JP, Van Den Driessche J (1994) Extensional gneiss domes and detachment fault systems; structure and kinematics. *Bulletin De La Société Géologique De France* 165:519–530
- Burg JP, Brun JP, Van Den Driessche J (1990) Le sillon houiller du Massif Central français : faille de transfert pendant l'amincissement crustal de la chaîne. *Comptes rendus de l'Académie des sciences. Série 2. Mécanique, Physique, Chimie, Sciences De L'univers, Sciences De La Terre* 311:147–152
- Burne RV, Moore LS (1987) Microbialites; organosedimentary deposits of benthic microbial communities. *Palaio* 2:241–254
- Carrat HG (1969) Le Morvan cristallin. Etude pétrographique, géochimique et structurale. Position de l'uranium. Dissertation, Faculté des Sciences de l'Université de Nancy
- Cartigny MJ, Ventra D, Postma G, Van Den Berg JH (2014) Morphodynamics and sedimentary structures of bedforms under supercritical-flow conditions: new insights from flume experiments. *Sedimentology* 61:712–748. <https://doi.org/10.1111/sed.12076>
- Châteauneuf JJ, Farjanel G (1989) Synthèse Géologique des Bassins Permians Français. Éditions du BRGM, Orléans
- Choulet F, Faure M, Fabbri O, Monié P (2012) Relationships between magmatism and extension along the Autun–La Serre fault system in the Variscan Belt of the eastern French Massif Central. *Int J Earth Sci* 101:393–413. <https://doi.org/10.1007/s00531-011-0673-z>
- Clarke JEH (2016) First wide-angle view of channelized turbidity currents links migrating cyclic steps to flow characteristics. *Nat Commun* 7:1–13. <https://doi.org/10.1038/ncomms11896>
- Clarke JH, Brucker S, Muggah J, Hamilton T, Cartwright D, Church I, Kuus P (2012) Temporal progression and spatial extent of mass wasting events on the Squamish prodelta slope. Landslides and engineered slopes: protecting society through improved understanding. Taylor and Francis Group, London, pp 1091–1096
- Cleal CJ, Thomas BA (2005) Palaeozoic tropical rainforests and their effect on global climates: is the past the key to the present? *Geobiology* 3:13–31. <https://doi.org/10.1111/j.1472-4669.2005.00043.x>
- Colella A, De Boer PL, Nio SD (1987) Sedimentology of a marine intermontane Pleistocene Gilbert-type fan-delta complex in the Crati Basin, Calabria, southern Italy. *Sedimentology* 34:721–736. <https://doi.org/10.1111/j.1365-3091.1987.tb00798.x>
- Courel L (1970) Trias et rhétien de la bordure nord et est du Massif Central français: modalités de la transgression mésozoïque. Dissertation, Université de Bourgogne
- Cross TA (1988) Controls on coal distribution in transgressive-regressive cycles, Upper Cretaceous, Western Interior, USA. In: Wilgus CK, Hastings BS, Kendall CGStC, Posamentier HW, Ross CA, Van Wagoner JC (eds) Sea-level changes: an integrated approach. SEPM Spec Publ 42, pp 371–380
- Cross TA, Baker MR, Chapin MA, Clark MS, Gardner MS, Hanson MA, Lessenger LD, Little LD, Mc Donough KJ, Sonnenfeld MD, Valesk MR, Williams MR, Witter DN (1993) Applications of high-resolution sequence stratigraphy to reservoir analysis. In: Eschard R, Doligez B (Eds) Subsurface Reservoir Characterization from Outcrop Observations, Paris, pp 11–33
- Davies IC, Walker RG (1974) Transport and deposition of reworked conglomerates; the cap enrage formation, Cambro-Ordovician, Gaspé, Quebec. *J Sediment Res* 44:1200–1216. <https://doi.org/10.1306/212F6C76-2B24-11D7-8648000102C1865D>
- Delafond F (1889) Bassin houiller et permien d'Autun et d'Épinac : stratigraphie. In: Etude des Gîtes Minéraux de la France, Bassin Houiller et Permien d'Autun et Epinac. Quantin
- Delfour J, Arène J, Clozier L, Carroue JP, Cornet J, Delance JH, Feys R, Lemièrre B (1991) Notice explicative de la carte géologique d'Autun au 1:50000. Bureau de recherches géologiques et minières, Orléans
- Delfour J, Clozier L, Cornet J, Lablanche G, Feys R (1995) Notice explicative de la carte géologique de Lucenay-L'Évêque au 1:50000. Bureau de recherches géologiques et minières, Orléans
- Dietrich P, Ghienne JF, Normandeau A, Lajeunesse P (2016) Upslope-migrating bedforms in a proglacial sandur delta: cyclic steps from river-derived underflows? *J Sediment Res* 86:112–122. <https://doi.org/10.2110/jsr.2016.4>
- Donsimoni M (1990) Le gisement de charbon de Lucenay-lès-Aix (Nièvre). Documents du BRGM 179, 84 pp.

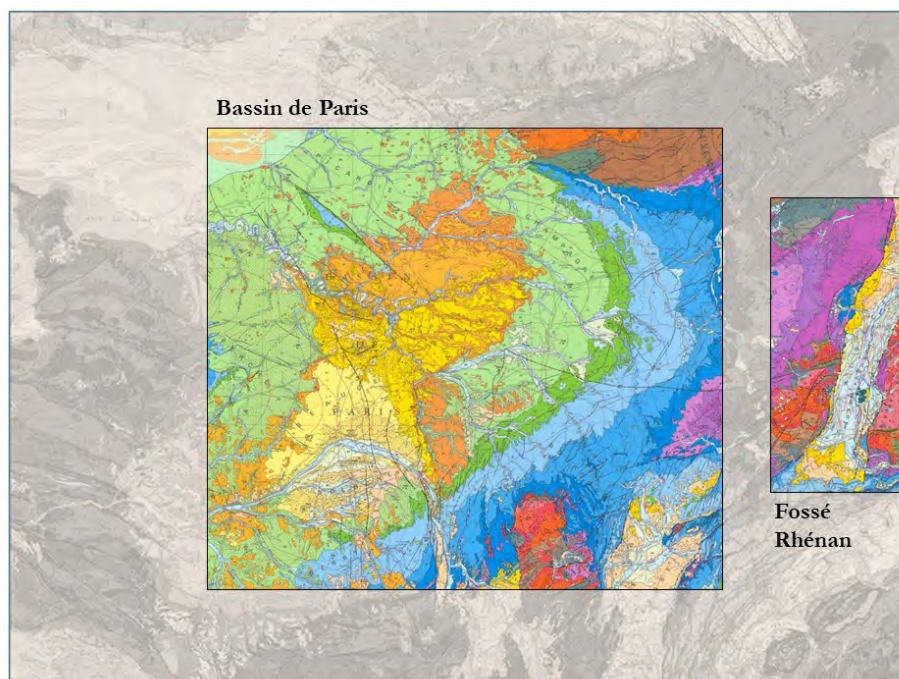
- Donsimoni M (2006) Le gisement de charbon de Lucenay-lès-Aix (Nièvre). Etat des connaissances acquises par le B.R.G.M. entre 1981 et 1986. Rapports du B.R.G.M., Orléans
- Doubinger J (1970) Réflexions sur la flore du Mont-Pelé (Bassin d'Autun). Colloque sur la Stratigraphie du Carbonifère. Les Congrès Et Colloques De L'université De Liège 55:275–284
- Ducassou C, Mercuzot M, Bourquin S, Rossignol C, Pellenard P, Beccaletto L, Pujol M, Hallot E, Pierson-Wickmann AC, Hue C, Ravier E (2019) Sedimentology and U-Pb dating of Carboniferous to Permian continental series of the northern Massif Central (France): local paleogeographic evolution and larger scale correlations. *Paleogeogr Paleoclimatol Paleocool* 533:109228. <https://doi.org/10.1016/j.paleo.2019.06.001>
- Dupraz C, Reid RP, Braissant O, Decho AW, Norman RS, Visscher PT (2009) Processes of carbonate precipitation in modern microbial mats. *Earth Sci Rev* 96:141–162. <https://doi.org/10.1016/j.earscirev.2008.10.005>
- Elsass-Damon FE (1977) Les « schistes bitumineux » du bassin d'Autun : pétrographique, minéralogie, cristallogénie, pyrolyse. Dissertation, Université de Paris VI
- Faure M (1995) Late orogenic carboniferous extensions in the Variscan French Massif Central. *Tectonics* 14:132–153. <https://doi.org/10.1029/94TC02021>
- Faure M, Becq-Giraudon JF (1993) Sur la succession des épisodes extensifs au cours du désépaissement carbonifère du Massif central français. Comptes rendus de l'Académie des sciences. Série 2. Mécanique, Physique, Chimie, Sciences De L'univers, Sciences De La Terre 316:967–973
- Faure M, Lardeaux JM, Ledru P (2009) A review of the pre-Permian geology of the Variscan French Massif Central. *Comptes Rendus Géosciences* 341:202–213. <https://doi.org/10.1016/j.crte.2008.12.001>
- Feyls R, Greber C (1972) L'Autunien et le Saxonien en France. In: Falke H (Eds) *Rotliegend. Essays on European Lower Permian*. Brill EJ Publisher, Leiden, pp 114–136
- Fischer J, Schneider JW, Voigt S, Joachimski MM, Tichomirowa M, Tütken T, Götze J, Berner U (2013) Oxygen and strontium isotopes from fossil shark teeth: environmental and ecological implications for Late Paleozoic European basins. *Chem Geol* 342:44–62. <https://doi.org/10.1016/j.chemgeo.2013.01.022>
- Freytet P, Lebreton ML, Paquette Y (1992) The carbonates of the Permian Lakes of North Massif Central, France. *Carbonates Evap* 7:122–131
- Freytet P, Toutin-Morin N, Broutin J, Debriette P, Durand M, El Wartiti M, Gand G, Kerp H, Orszag F, Paquette Y, Ronchi A, Sarfati J (1999) Palaeoecology of non marine algae and stromatolites: Permian of France and adjacent countries. *Annales De Paléontologie* 85:99–153. [https://doi.org/10.1016/S0753-3969\(99\)80010-X](https://doi.org/10.1016/S0753-3969(99)80010-X)
- Freytet P, Broutin J, Durand M (2000) Distribution and palaeoecology of freshwater algae and stromatolites: III, some new forms from the Carboniferous, Permian and Triassic of France and Spain. *Annales De Paléontologie* 86:195–241. [https://doi.org/10.1016/S0753-3969\(01\)80001-X](https://doi.org/10.1016/S0753-3969(01)80001-X)
- Galloway WE (1989) Genetic stratigraphic sequences in basin analysis I: architecture and genesis of flooding-surface bounded depositional units. *AAPG Bull* 73:125–142. <https://doi.org/10.1306/703C9AF5-1707-11D7-8645000102C1865D>
- Galloway WE, Williams TA (1991) Sediment accumulation rates in time and space: Paleogene genetic stratigraphic sequences of the northwestern Gulf of Mexico basin. *Geology* 19:986–989. [https://doi.org/10.1130/0091-7613\(1991\)019%3c0986:SAR-ITA%3e2.3.CO;2](https://doi.org/10.1130/0091-7613(1991)019%3c0986:SAR-ITA%3e2.3.CO;2)
- Gand G, Stapf KR, Broutin J, Debriette P (1993) The importance of silicified wood, stromatolites, and conifers for the paleoecology and the stratigraphy in the Lower Permian of the northeastern Blanzay-Lc Creusot Basin (Massif Central, France). *Newsl Stratigr* 28:1–32. <https://doi.org/10.1127/nos/28/1993/1>
- Gand G, Châteauneuf JJ, Durand M, Chabard D, Passaqui JP (2007) Early Permian Continental environments in the Autun basin. In: Gand G, Châteauneuf JJ, Durand M, Chabard D, Passaqui JP (eds) *Pre-symposium fieldtrip guide: Autun*. Publ ASF 56, Paris, pp 35
- Gand G, Steyer S, Chabard D (2011) Reprise des fouilles paléontologiques dans un gîte bourguignon célèbre : les « schistes bitumineux » de l'Autunien de Muse (bassin d'Autun). Bilan 2010 et perspective. *Revue Scientifique Bourgogne-Nature* 12:11–29
- Gand G, Steyer JS, Chabard D (2012) Les fouilles paléontologiques de Muse: bilan 2011, projets 2012. *Bulletin De La Société D'histoire Naturelle Et Des Amis Du Muséum D'autun* 202:33–43
- Gand G, Steyer S, Chabard D, Pellenard P, Glé L, Van Waveren I (2014) Études géologiques 2013 et projets 2014 sur l'Autunien du bassin d'Autun. *Bulletin De La Société D'histoire Naturelle D'autun* 206:7–20
- Gand G, Steyer S, Pellenard P, Bethoux O, Odin G, Rouchon V, Van Waveren I, Plogde G, Chabard D (2015) Le stratotype Autunien (Permien) du bassin d'Autun : résultats préliminaires des travaux réalisés en 2014 sur les niveaux de la couche de Muse (Saône-et-Loire). *Bulletin De La Société D'histoire Naturelle D'autun* 207:12–31
- Gand G, Pellenard P, Galtier J, Broutin J, Steyer JS (2017) Le stratotype Autunien du bassin d'Autun (Bourgogne-France): évolution de la stratigraphie et des âges. *Bulletin De La Société D'histoire Naturelle D'autun* 211:19–36
- Garel S, Behar F, Schnyder J, Baudin F (2017) Palaeoenvironmental control on primary fluids characteristics of lacustrine source rocks in the Autun Permian Basin (France). *Bulletin De La Société Géologique De France* 188:1–29. <https://doi.org/10.1051/bsgf/2017187>
- Gastaldo RA, DiMichele WA, Pfefferkorn H (1996) Out of the icehouse into the greenhouse: a late Paleozoic analog for modern global vegetational change. *GSA Today* 6:1–7
- Gaudry A (1883) *Les Enchaînements du Monde Animal dans les Temps Géologiques*. Masson, Paris. <https://doi.org/10.5962/bhl.title.61801>
- Genna A, Roig JY, Debriette PJ, Bouchot V (1998) Le bassin houiller d'Argentat (Massif Central français), conséquence topographique d'un plissement de son substratum varisque. *Comptes Rendus De L'académie Des Sciences - Series IIA-Earth and Planetary Science* 327:279–284. [https://doi.org/10.1016/S1251-8050\(98\)80086-4](https://doi.org/10.1016/S1251-8050(98)80086-4)
- Gilbert GK (1885) *The topographic features of lake shores*. US Government Printing Office
- Glennic KW, Higham J, Stemmerik L (2003) The Permian of the Northern North Sea. In: Evans D, Graham C, Armour A, Bathurst P (eds) *The Millennium Atlas: petroleum geology of the Central and Northern North Sea*. Geological Society London, pp 91–103
- Gobo K, Ghinassi M, Nemeč W (2014) Reciprocal changes in foreset to bottomset facies in a gilbert-type delta: response to short-term changes in base level. *J Sediment Res* 84:1079–1095. <https://doi.org/10.2110/jsr.2014.83>
- Goddéris Y, Donnadieu Y, Carretier S, Aretz M, Dera G, Macouin M, Regard V (2017) Onset and ending of the late Paleozoic ice age triggered by tectonically paced rock weathering. *Nat Geosci* 10:382–386. <https://doi.org/10.1038/ngeo2931>
- Jervey MT (1988) Quantitative geological modelling of siliciclastic rock sequences and their seismic. In: Wilgus CK, Hastings BS, Kendall CGStG, Posamentier HW, Ross CA, Van Wagoner JC (eds) *Sea-level Changes: an integrated approach*. SEPM Spec. Publ. 42, pp 47–70

- Kostaschuk RA, McCann SB (1989) Submarine slope stability of a fjord delta; Bella Coola, British Columbia. *Géogr Phys Quaternaire* 43:87–95. <https://doi.org/10.7202/032756ar>
- Kroner U, Romer RL (2013) Two plates—many subduction zones: the Variscan orogeny reconsidered. *Gondwana Res* 24:298–329. <https://doi.org/10.1016/j.jr.2013.03.001>
- Landriot JB (1936) Notice géologique sur la Formation des Schistes de Muse. In: *Compte-Rendus des travaux de la Société Edienne, des Lettres, Sciences et Arts*. Autun, pp 117–138
- Lowe DR (1982) Sediment gravity flows; II, depositional models with special reference to the deposits of high-density turbidity currents. *J Sediment Res* 52:279–297. <https://doi.org/10.1306/212F7F31-2B24-11D7-8648000102C1865D>
- Luccisano V, Pradel A, Amiot R, Gand G, Steyer J-S, Cuny G (2021) A new Triodus shark species (Xenacanthidae, Xenacanthiformes) from the lowermost Permian of France and its paleobiogeographic implications. *J Vertebr Paleontol* 41:e1926470. <https://doi.org/10.1080/02724634.2021.1926470>
- Malavieille J, Guihot P, Costa S, Lardeaux JM, Gardien V (1990) Collapse of the thickened Variscan crust in the French Massif Central: Mont Pilat extensional shear zone and St. Etienne Late Carboniferous Basin Tectonophysics 177:139–149. [https://doi.org/10.1016/0040-1951\(90\)90278-G](https://doi.org/10.1016/0040-1951(90)90278-G)
- Marguerier J, Pacaud G (1980) La 3e zone de bois silicifiés de L'Autunien du bassin d'Autun (France): nouvelles données sur un gisement de bois silicifiés, Caractères paléobotaniques. *Bulletin De La Société D'histoire Naturelle D'autun* 95:1–54
- Marteau P (1983) Le bassin permio-carbonifère d'Autun: stratigraphie, sédimentologie et aspects structuraux. Dissertation, Université de Bourgogne
- Massari F (1996) Upper-flow-regime stratification types on steep-face, coarse-grained, Gilbert-type progradational wedges (Pleistocene, Southern Italy). *SEPM J Sediment Res* 66:364–375. <https://doi.org/10.1306/D426834C-2B26-11D7-8648000102C1865D>
- Mathis V, Brulhet J (1990) Les gisements uranifères du bassin permien de Bourbon-l'Archambault (nord du Massif central français). *Chronique De La Recherche Minière* 499:19–30
- Mayer-Eymar C. (1881) Classification internationale des terrains sédimentaires, S.L., Arch. Soc. Géol. Fr. 1–15
- Ménard G, Molnar P (1988) Collapse of a Hercynian Tibetan plateau into a late Paleozoic European Basin and Range province. *Nature* 334:235–237. <https://doi.org/10.1038/334235a0>
- Mercuzot M, Bourquin S, Beccaletto L, Ducassou C, Rubi R, Pellenard P (2021a) Paleoenvironmental reconstitutions at the Carboniferous-Permian transition south of the Paris Basin, France: implications on the stratigraphic evolution and basin geometry. *Int J Earth Sci* 110:9–33
- Mercuzot M, Thomazo C, Schnyder J, Pellenard P, Baudin F, Pierson-Wickmann AC, Sans-Jofre P, Bourquin S, Beccaletto L, Santoni AL, Gand G, Buisson M, Glé L, Munier T, Saloume A, Boussaid M, Boucher T (2021b) Carbon and nitrogen cycle dynamic in continental late-Carboniferous to early Permian basins of eastern Pangea (northeastern Massif Central, France). *Front Earth Sci*. <https://doi.org/10.3389/feart.2021.705351>
- Miall AD (1978) Tectonic setting and syndepositional deformation of molasse and other nonmarine-paralic sedimentary basins. *Can J Earth Sci* 15:1613–1632
- Miall AD (1996) The geology of fluvial deposits. Sedimentary facies, basin analysis, and petroleum geology. Springer, Berlin
- Middleton GV (1965) Antidune cross-bedding in a large flume. *J Sediment Res* 35:922–927. <https://doi.org/10.1306/74D713AC-2B21-11D7-8648000102C1865D>
- Mitchum RM, Van Wagoner JC (1991) High-frequency sequences and their stacking patterns: sequence-stratigraphic evidence of high-frequency eustatic cycles. *Sed Geol* 70:131–160. [https://doi.org/10.1016/0037-0738\(91\)90139-5](https://doi.org/10.1016/0037-0738(91)90139-5)
- Montañez IP, Tabor NJ, Niemeier D, DiMichele WA, Frank TD, Fielding CR, Isbell JL, Birgenheier LP, Rygel MC (2007) CO₂-forced climate instability and linkages to tropical vegetation during late Paleozoic deglaciation. *Science* 315:87–91. <https://doi.org/10.1126/science.1134207>
- Montañez IP, McElwain JC, Poulsen CJ, White JD, DiMichele WA, Wilson JP, Griggs G, Hren MT (2016) Climate, pCO₂ and terrestrial carbon cycle linkages during late Palaeozoic glacial-interglacial cycles. *Nat Geosci* 9:824–828. <https://doi.org/10.1038/ngco2822>
- Mulder T, Alexander J (2001) The physical character of subaqueous sedimentary density flows and their deposits. *Sedimentology* 48:269–299. <https://doi.org/10.1046/j.1365-3091.2001.00360.x>
- Munier-Chalmas E, de Lapparent A (1893) Note sur la nomenclature des terrains sédimentaires. *Bull Soc Géol Fr* 3:454
- Muto T, Steel RJ (2002) Role of autoretreat and A/S changes in the understanding of deltaic shoreline trajectory: a semi-quantitative approach. *Basin Res* 14:303–318. <https://doi.org/10.1046/j.1365-2117.2002.00179.x>
- Nemec W (1990) Aspects of sediment movement on steep delta slopes. In: Colella A, Prior D (eds) *Coarse-grained Deltas*. Blackwell Publishing Ltd, Oxford, pp 29–73. <https://doi.org/10.1002/978144303858.ch3>
- Odin GP, Cabaret T, Mertz JD, Menendez B, Etienne L, Wattiaux A, Rouchon V (2015a) Alteration of fossil-bearing shale (Autun Basin, France; Permian), part I: characterizing iron speciation and its vulnerability to weathering by combined use of Mössbauer spectroscopy, X-ray diffraction, porosimetry and permeability measurements. *Annales De Paléontologie* 101:75–85. <https://doi.org/10.1016/j.annpal.2015.01.002>
- Odin GP, Vanmeert F, Farges F, Gand G, Janssens K, Romero-Sarmiento MF, Steyer JS, Vantelon D, Rouchon V (2015b) Alteration of fossil-bearing shale (Autun, France; Permian), part II: Monitoring artificial and natural ageing by combined use of S and Ca K-edge XANES analysis, Rock-Eval pyrolysis and FTIR analysis. *Annales De Paléontologie* 101:225–239. <https://doi.org/10.1016/j.annpal.2015.03.001>
- Pellenard P, Gand G, Schmitz M, Galtier J, Broutin J, Stéyer JS (2017) High-precision U-Pb zircon ages for explosive volcanism calibrating the NW European continental Autunian stratotype. *Gondwana Res* 51:118–136. <https://doi.org/10.1016/j.gr.2017.07.014>
- Péron S, Bourquin S, Fluteau F, Guillocheau F (2005) Paleoenvironment reconstructions and climate simulations of the Early Triassic: impact of the water and sediment supply on the preservation of fluvial system. *Geodin Acta* 18:431–446. <https://doi.org/10.3166/ga.18.431-446>
- Postma G (1984) Mass-flow conglomerates in a submarine canyon: Abrijoja fan-delta, Pliocene, Southeast Spain. *Sedimentol Gravels Conglomerates Memoir* 10:237–256
- Postma G (1990) Depositional architecture and facies of river and fan deltas: a synthesis. In: Colella A (ed) *Coarse-grained Deltas*. Blackwell, Oxford, pp 13–27
- Postma G, Roep TB (1985) Resedimented conglomerates in the bottomsets of Gilbert-type gravel deltas. *J Sediment Res* 55:874–885
- Pruvost P (1942) Etude Géologique du Bassin Permo-Carbonifère d'Autun. Rapport du Bureau de recherches géologiques et minières, Orléans
- Renault B (1888) Notice sur les Sigillaires. *Bulletin de la Société d'Histoire Naturelle d'Autun* 1:121–199
- Renault B (1896) Bassin houiller et permien d'Autun et d'Epinaç. In: *Etudes des gîtes minéraux de la France*, Paris
- Richey JD, Montañez IP, Goddérès Y, Looy CV, Griffiths NP, DiMichele WA (2020) Influence of temporally varying weatherability on CO₂-climate coupling and ecosystem change in the late Paleozoic. *Clim Past* 16:1759–1775. <https://doi.org/10.5194/cp-16-1759-2020>

- Roche E (1881) Sur les fossiles du terrain permien d'Autun (Saône-et-Loire). *Bulletin De La Société Géologique De France* 9:7–83
- Rohais S, Eschard R, Guillocheau F (2008) Depositional model and stratigraphic architecture of rift climax Gilbert-type fan deltas (Gulf of Corinth, Greece). *Sediment Geol* 210:132–145. <https://doi.org/10.1016/j.sedgeo.2008.08.001>
- Roscher M, Schneider JW (2006) Permo-Carboniferous climate: Early Pennsylvanian to late Permian climate development of central Europe in a regional and global context. In: Lucas SG, Cassinis G, Schneider JW (eds) Non-marine Permian biostratigraphy and biochronology. Geological Society London Special Publications, London, pp 95–136
- Rubi R, Rohais S, Bourquin S, Moretti I, Desaubliaux G (2018) Processes and typology in Gilbert-type delta bottomset deposits based on outcrop examples in the Corinth Rift. *Mar Pet Geol* 92:193–212. <https://doi.org/10.1016/j.marpetgeo.2018.02.014>
- Sauvage HE (1890) Recherches sur les poissons du terrain Permien d'Autun; bassin houiller et permien d'Autun et d'Épinac. *Études des gîtes minéraux de la France* 3.
- Schneider JT, Zajić J (1994) Xenacanthiden (Pisces, Chondrichthyes) des mitteleuropäischen Oberkarbon und Perm-Revision der Originale zu Goldfuss 1847, Beyrich 1848, Kner 1867 und Fritsch 1879–1890. *Freib Forsch* 452:101–151
- Schneider JW, Scholze F (2018) Late Pennsylvanian–Early Triassic conchostracan biostratigraphy: a preliminary approach? *Geol Soc Lond* 450:365–386 (**Spec. Publ**)
- Schneider JW, Hampe O, Soler-Gijón R (2000) The Late Carboniferous and Permian: aquatic vertebrate zonation in southern Spain and German basins. *Courier-Forschungsinstitut Senckenberg* 543–562.
- Simons DB, Richardson EV (1963) A study of variables affecting flow characteristics and sediment transport in alluvial channels. In: Miss J (eds) Proceedings, Federal Interagency Sedimentation Conference, US Department of Agriculture, Washington, D.C., pp. 193–206.
- Soreghan GS, Beccaletto L, Benison KC, Bourquin S, Hamamura N, Hamilton M, Heavens NG, Hinnov L, Huttenlocker A, Looy C, Pfeifer LS, Pochat S, Sardar Abadi M, Zambito J (2020) Report on ICDP deep dust workshops: probing continental climate of the Late Paleozoic Icehouse-greenhouse transition and beyond. *Sci Drill* 28:93–112. <https://doi.org/10.5194/sd-28-93-2020>
- Spears DA (2012) The origin of tonsteins, an overview, and links with seatearths, fireclays and fragmental clay rocks. *Int J Coal Geol* 94:22–31. <https://doi.org/10.1016/j.coal.2011.09.008>
- Stampfli GM, Kozur HW (2006) Europe from the Variscan to the Alpine cycles. In: Gec DG, Stephenson RA (eds) European lithosphere dynamics. *Memoir of the Geological Society, London*, pp 57–82
- Stapf K, Gand G (1994) The stromatolites from the Lower Permian of Montceau-les-Mines (Massif Central-France). In: Poplin C, Heyler D (eds) Quand le Massif Central était sous l'Équateur. Un écosystème carbonifère à Montceau-les-Mines. Comité des travaux historiques et scientifiques, Paris, pp. 87–92
- Vallé B, Courel L, Gelard JP (1988) Les marqueurs de la tectonique synsédimentaire et syndiagénétique dans le bassin stéphanien à régime cisailant de Blanzay-Montceau (Massif central, France). *Bulletin De La Société Géologique De France* 4:529–540. <https://doi.org/10.2113/gssgfbull.IV.4.529>
- Van Den Driessche J, Brun JP (1989) Un modèle cinématique de l'extension paléozoïque supérieur dans le Sud du Massif Central. *Comptes rendus de l'Académie des sciences. Série 2. Mécanique, Physique, Chimie, Sciences De L'univers, Sciences De La Terre* 309:1607–1613
- Van Wagoner JC, Posamentier HW, Mitchum RMJ, Vail PR, Sarg JF, Loutit TS, Hardenbol J (1988) An overview of the fundamentals of sequence stratigraphy and key definitions. In: Wilgus CK et al. (eds) Sea-level Changes: an Integrated Approach. *Soc. Econ. Paleontol. Mineral. Spec. Publ.* 42:39–46
- Visscher PT, Reid RP, Bebout BM, Hocft SE, Macintyre IG, Thompson JA (1998) Formation of lithified micritic laminae in modern marine stromatolites (Bahamas); the role of sulfur cycling. *Am Miner* 83:1482–1493. <https://doi.org/10.2138/am-1998-1109>
- Walker RG (1975) Generalized facies models for resedimented conglomerates of turbidite association. *Geol Soc Am Bull* 86:737–748. [https://doi.org/10.1130/0016-7606\(1975\)86%3c737:GFM-FRC%3e2.0.CO;2](https://doi.org/10.1130/0016-7606(1975)86%3c737:GFM-FRC%3e2.0.CO;2)
- Wheeler HE (1964) Base level, lithosphere surface, and time stratigraphy. *Geol Soc Am Bull* 75:599–610. [https://doi.org/10.1130/0016-7606\(1964\)75\(599:BLSAT\)2.0.CO;2](https://doi.org/10.1130/0016-7606(1964)75(599:BLSAT)2.0.CO;2)

4. Volet 3 - La couverture sédimentaire méso- cénozoïque : interprétation sismique et nouveaux usages du sous-sol

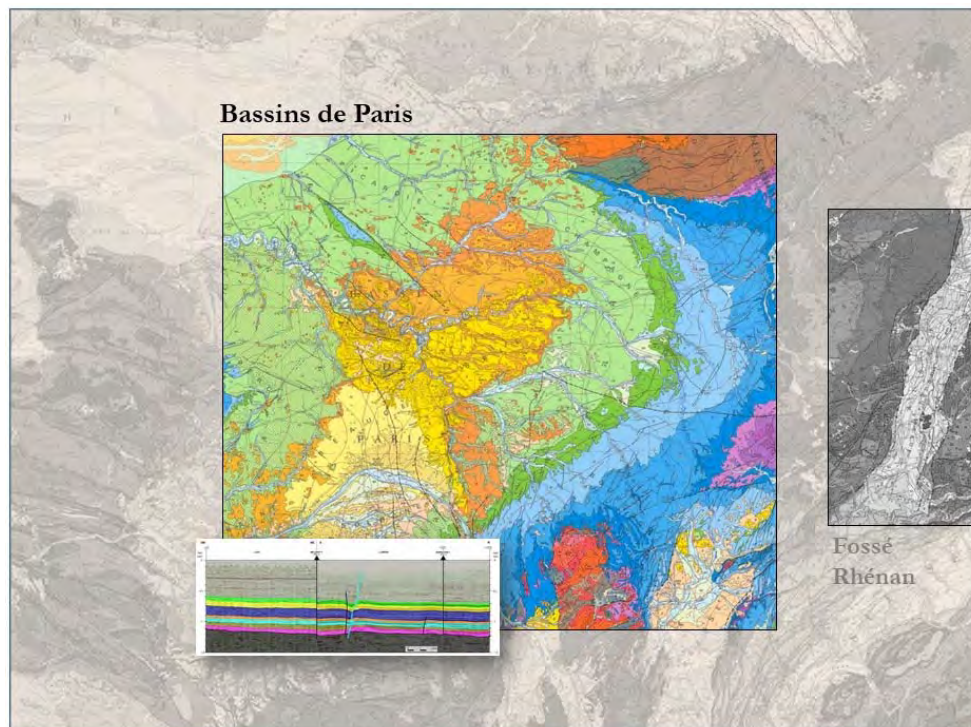
Exemple du bassin de Paris et du fossé Rhénan



Les profils sismiques sur lesquels je travaille imagent souvent les séries paléozoïques et méso-cénozoïques. Ce volet thématique bénéficie par conséquent directement de mes travaux sur les bassins carbonifères-permiens. Ces derniers représentent le substratum sur lequel se développent pour partie les séries sédimentaires méso-cénozoïques, impliquant des relations génétiques entre les deux phases de remplissages et leurs contrôles structuraux (notion d'héritage structural).

Ce volet regroupe quelques cas d'études dans le bassin de Paris et le fossé Rhénan où l'interprétation de profils sismiques retraités apporte une plus-value décisive pour la résolution de problèmes scientifiques (structuration, cinématique) en relation avec leurs ressources (géométrie des réservoirs).

4.1. Le Mésozoïque du bassin de Paris



4.1.1. Cadre collaboratif

J'ai commencé à travailler sur la structuration du bassin de Paris dès mon arrivée au BRGM dans le cadre d'un projet interne de retraitement et interprétation de transects sismiques régionaux dans le bassin de Paris, et de projets avec l'ANDRA (catalogue des failles principales dans le bassin). La publication 1 sur le bassin de Paris en début de manuscrit est la traduction scientifique de ces projets. J'ai travaillé au BRGM pendant de nombreuses années dans le cadre d'un projet interne sur tout ce qui touche à l'interprétation sismique dans le bassin de Paris (appui retraitement sismique, mise à jour de la base de données de forages profonds (horizons géologiques, lois de vitesses, déviations...), projets d'interprétations locales...). L'ensemble des connaissances acquises a déclenché plusieurs collaborations sous la forme d'appui expertise à des étudiants en thèse ou Master 2 dont les sujets étaient orientés vers les usages du sous-sol, et dont le point commun était le besoin de connaissance structurale en subsurface dans le bassin ; toutes mes interventions se sont soldées par des publications dont je suis co-auteur : (i) thèse de F. Lenoir (encadrement Géosciences Rennes/BRGM ; **Lenoir et al., 2014); (ii) thèse J. Dentzer (encadrement Mines Paris Tech/BRGM/ENS Paris, **Dentzer et al., 2018) ; (iii) thèse de P.-A. Reninger (encadrement BRGM/ISTOrléans ; **Reninger et al., 2014) ; (iv) Master 2 de P. Mas (encadrement BRGM, **Mas et al., 2022). Les collaborations sur la structuration du bassin de Paris se poursuivent actuellement avec la thèse de S. Brown (structuration tertiaire, collab. Université Cergy-Pontoise et Paris-Saclay).

4.1.2. Problématiques appliquée et scientifique

L'entité géologique « bassin de Paris » s'étend de la Normandie à la Lorraine et du Centre-Val-de-Loire aux Hauts-de-France. Cette vaste étendue regroupe la plus grande densité de population en France (Ile-de-France et métropoles régionales comme Orléans, Lille, Reims, Nancy...) et nombres d'industries. Il n'est donc pas étonnant que le développement de la géothermie ait débuté dans cette région dès le début des années 1970, en réaction au premier choc pétrolier. Après une période creuse, l'activité a repris à la fin des années 1990 à la suite de l'accord de Kyoto et du "Programme de relance de la géothermie en Ile-de-France" à la fin des années 2000 (Lopez et al., 2010). Cette région comprend actuellement 50 installations géothermiques profondes (doublets) dédiées au chauffage urbain (sur plus de 70 en France), dont la plupart ciblent l'aquifère du Dogger (Jurassique moyen ; Figure 24). L'avenir de cette filière passe entre autres par (i) la recherche de nouveaux aquifères (e.g. Trias, Lusitanien, Albien) là où celui du Dogger est saturé (problème de bulle froide depuis le puits d'injection), et (ii) l'implantation de nouvelles installations dans les secteurs sous-dotés (Hamm et al., 2021). En parallèle, depuis le début des années 2000, certains aquifères sont ciblés pour développer le stockage du CO₂ (Dogger carbonaté et Trias silicoclastique ; Fabriol et al., 2008). Sans compter les problématiques d'approvisionnement en eau, le sous-sol du bassin étant le siège de nombreux aquifères depuis le Trias jusqu'à la craie, sans compter les multiples aquifères tertiaires (e.g. Goncalves et al. 2004 ; Salquèbre et al., 2009).

Le développement de tels projets d'exploitation des aquifères (énergie géothermique, stockage de CO₂, hydrogéologie...), parfois géographiquement proches, nécessite donc de disposer d'informations géologiques en subsurface fiables (géométrie, fracturation...) et multi-échelles (bassin vs réservoir).

L'apport de l'interprétation sismique est incontestable pour aborder ce type de problématique, que ce soit à une échelle régionale (tout le bassin), ou plus locale (une métropole). Cette approche grande maille manquait dans le bassin de Paris, les études structurales étant anciennes et lacunaires en raison d'un manque de données adéquates (e.g. BRGM, 1980). Mon apport a ainsi généralement consisté à déterminer la continuité latérale (ou non) des aquifères principaux et à caractériser leur déformation cassante ou flexurale (*Beccaletto et al., 2011, publication 1). En particulier la mise à jour du schéma structural du bassin de Paris permet de mieux comprendre l'influence de la fracturation à grande échelle sur la localisation des réservoirs géothermiques profonds. Ces failles représentent des drains potentiels et il est essentiel d'avoir une idée précise de leur localisation, et des séries sédimentaires affectées (**Dentzer et al., 2018). Ce raisonnement vaut aussi à plus petite échelle, que ce soit pour des problématiques géothermiques (**Mas et al., 2022) ou hydrogéologiques (**Reninger et al., 2014). Ces études sont présentées ci-après, une fois le contexte géologique posé. Ces travaux s'inscrivent plus largement dans le champ d'étude de la déformation et l'enregistrement sédimentaire du bassin de Paris comme témoin passif des déformations lointaines (« far-field » ; Lacombe et Mouthereau, 1999 ; Guillocheau et al., 2000 ; Robin et al., 2000 ; Briaux et al., 2016).

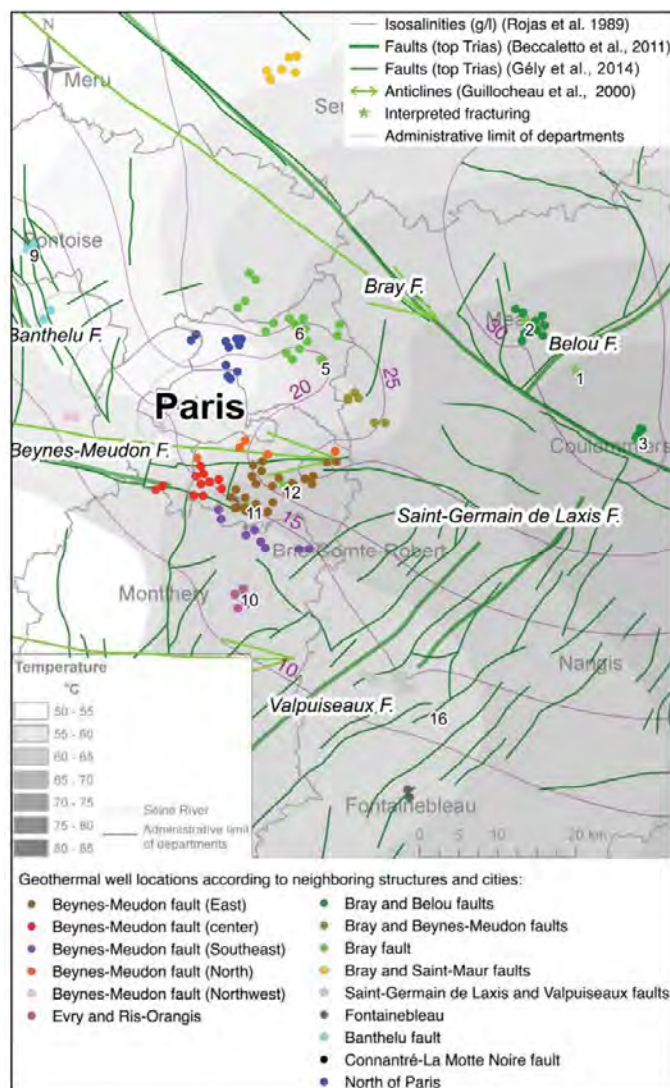


Figure 24 - Regroupement des doublets géothermiques au Bathonien suivant leur distribution spatiale et la présence de structures tectoniques (**Dentzer et al., 2018).

4.1.3. Contexte géologique du bassin de Paris

Héritage varisque et subsidence mésozoïque

La structure profonde du bassin de Paris, héritée des orogènes varisque et cadomienne, a été récemment étudiée par J. Baptiste, dont j'ai co-encadré la thèse (**Baptiste et al., 2016 ; Figure 25). Du nord vers le sud, le remplissage post-varisque repose sur les quatre ensembles paléogéographiques suivants : la zone rhéno-hercynienne, la zone saxothuringienne, le domaine armoricain et la marge nord-Gondwaniennne. Les témoins de ces grands ensembles se retrouvent à l'affleurement sur les bordures du bassin (à l'ouest, le massif Armoricain, au sud le Massif Central, à l'est les Vosges et au nord-ouest, le massif des Ardennes). Les bassins carbonifères-permiens discutés en détail dans le volet 2, qu'ils soient syn- et/ou post-varisques, se trouvent à l'interface entre ce qu'on appelait autrefois le « socle déformé » et le remplissage méso-cénozoïque (Figure 14).

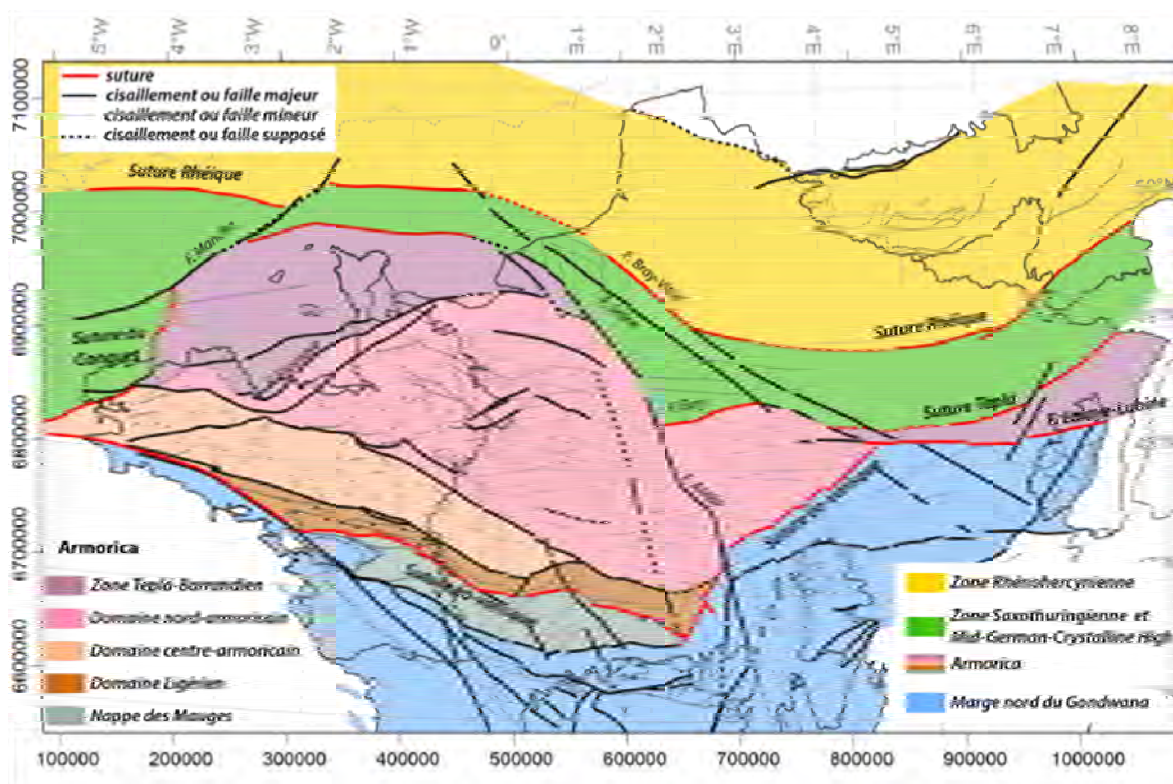


Figure 25 - Schéma structural de la zonation de la chaîne varisque sous le bassin de Paris méso-cénozoïque et ses bordures varisques et cadomiennes (Baptiste, 2016).

Le bassin de Paris est considéré comme un exemple type d'un bassin intracratonique (Pomerol, 1978; Brunet et Le Pichon, 1982; Perrodon et Zabeck, 1991), caractérisé par un régime de subsidence thermique initié après l'effondrement de la chaîne varisque se prolongeant durant le Mésozoïque (Brunet et Le Pichon, 1982, Perrodon et Zabek, 1991, Loup et Wildi, 1994 ; Prijac et al. 2000). Plusieurs phases tectoniques de courte durée, liées à la déformation de la partie occidentale de la plaque eurasiennne se superposent à cette subsidence long-terme (Loup et Wildi, 1994, Robin et al., 2000). Cette double évolution (subsidence à long terme vs à court terme) contrôle le développement de la plupart des bassins intracratoniques ouest-européens (Loup et Wildi, 1994 ; Ziegler et Dèzes, 2007). Ce régime mixte de subsidence s'est traduit dans le bassin de Paris par le dépôt de plus de 3000 mètres de sédiments continentaux et marins. Ce remplissage est initié au Permien et s'achève au Miocène, période au cours de laquelle le bassin est affecté par un flambage lithosphérique lié à la compression alpine (Guillocheau et al., 2000 et Bourgeois et al., 2007, Briaies et al., 2016).

Remplissage sédimentaire et déformations

Le remplissage sédimentaire du bassin de Paris est brièvement décrit en terme de lithostratigraphie et d'aquifères, et les grandes phases tectoniques sont mentionnées (Figure 26 et Figure 27).

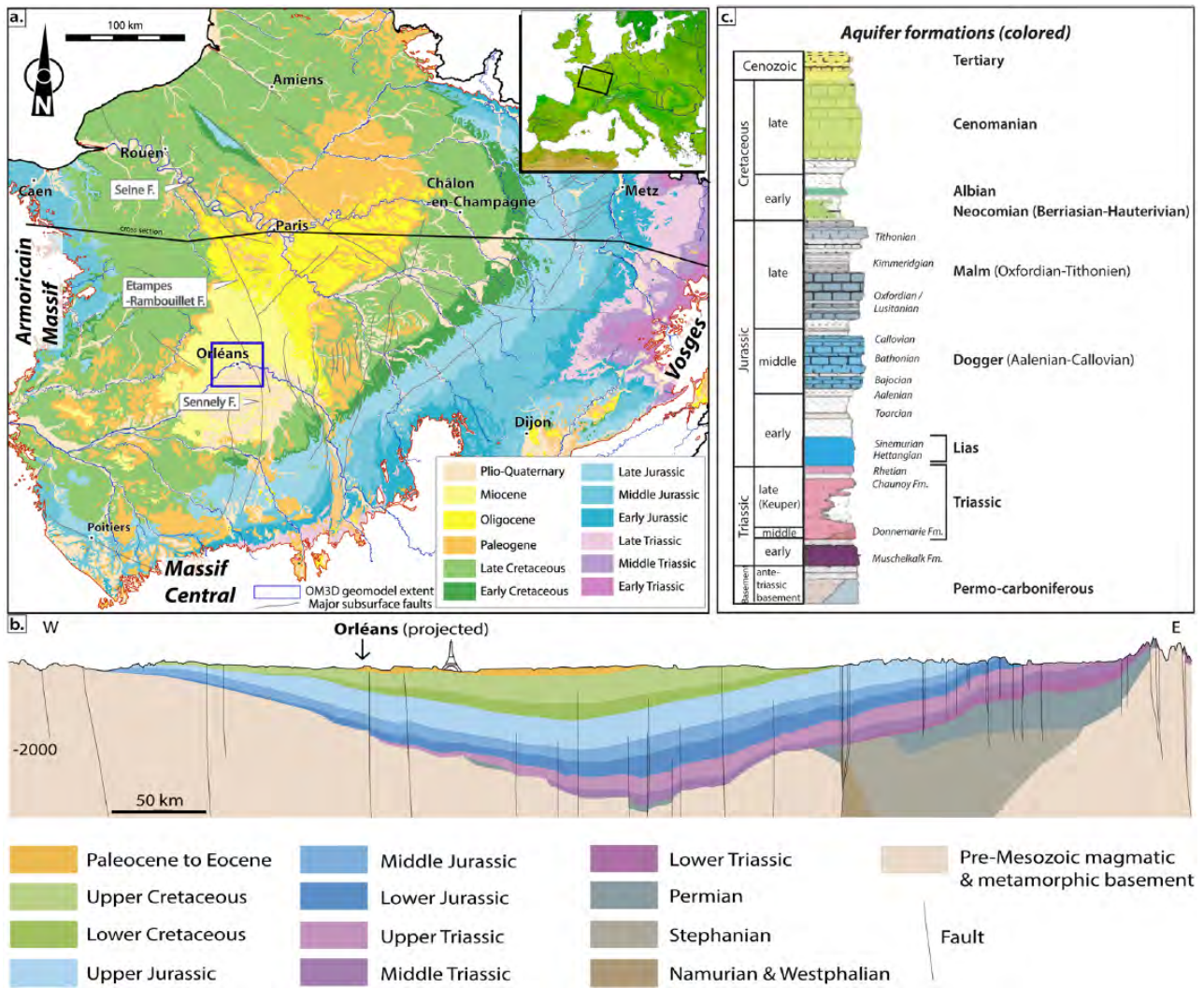


Figure 26 - Le bassin de Paris (**Mas et al., 2022). Carte géologique localisant les failles principales (*Beccaletto et al., 2011). Coupe ouest-modifiée de AGBP (2014). Log lithostratigraphique avec les principaux aquifères (modifié de Delmas et al., 2002).

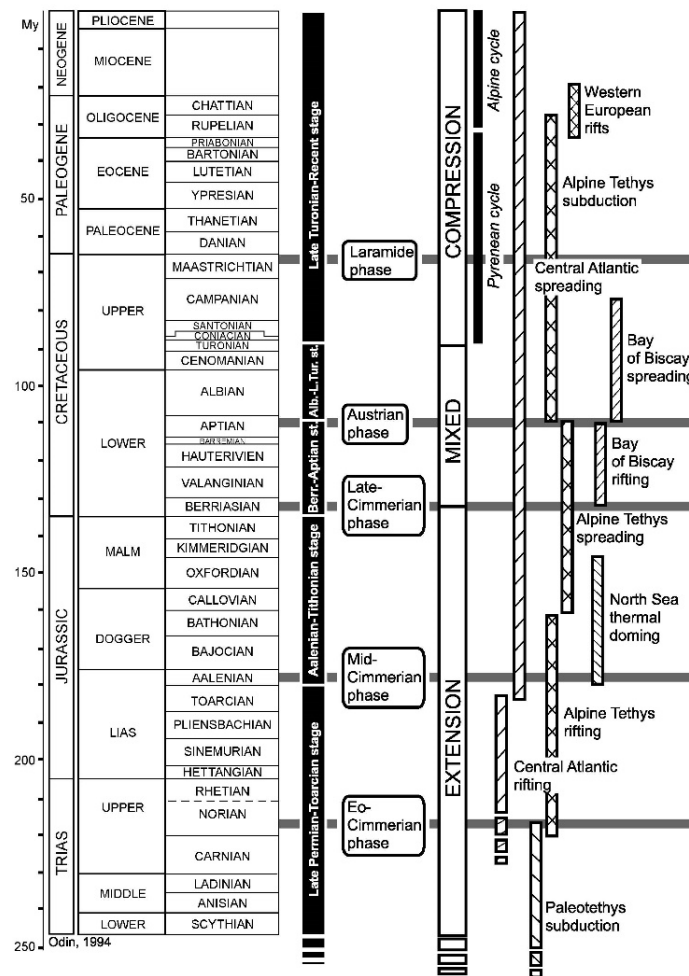


Figure 27 - Evolution géodynamique du bassin de Paris (*Beccaletto et al., 2011).

Du Trias au Crétacé inférieur, le bassin de Paris reste généralement en régime tectonique extensif (subsidence ponctuée de mouvements verticaux). Les dépôts triasiques sont constitués à la base de faciès de cônes alluviaux, passant aux faciès du Muschelkalk (inondation ladinienne) puis aux grès du Keuper (Trias moyen à supérieur). Ces derniers sont composés de deux ensembles fluviatiles séparées par un intervalle argileux (Bourquin et al., 1998): les grès de Donnemarie à la base et les grès de Chaunoy au sommet. Les grès du Keuper constituent la principale formation aquifère du Trias (Bugarel et al., 2019). Le Keuper voit se mettre en place d'épais dépôts salifères sous contrôle tectonique (Guillocheau et al., 2000; Bourquin et al., 2009). Les derniers dépôts triasiques consistent en des marnes et dolomies, passant à des alternances de marnes, argiles et dolomies au début de Lias (Guillocheau et al., 2000).

A partir du Trias supérieur/Lias, une seconde inondation atteint le Bassin de Paris et le Toarcien correspond à l'inondation maximale (« maximum flooding »), avec des dépôts marins ouverts (marnes, argilites à débris de crinoïdes ou gastéropodes). Ces « schistes carton » correspondent à un niveau aquitard bien identifié régionalement. Le Lias correspond à une période d'extension (E-O à NO-SE) en réponse à la phase de rifting de la Téthys Alpine (Stampfli et Hochard, 2009).

La limite Lias/Dogger marque la mise en place des premières plates-formes carbonatées (Guillocheau et al., 2000; Robin et al., 2000). Les axes de subsidence sont orientés NNE-SSO. La discontinuité Mid-Cimmérienne (Ziegler, 1990) à la limite Toarcien-Aalénien (Robin, 1997) est contemporaine de l'accrétion océanique de la Téthys Alpine (Stampfli et Kozur, 2006) et du bombement thermique de la mer du Nord.

Le Dogger est divisé en trois unités: (i) l'Aalénien, représenté par des marnes grises contenant des éléments bioclastiques et localement des alternances de calcaires argileux. La proportion est inversée dans le Bajocien inférieur; (ii) le Bajocien supérieur et le Bathonien, qui représentent les principaux niveaux aquifères du Dogger et principalement constitués de calcaires oolithiques et bioclastiques (« oolithe blanche »); (3) les dépôts calloviens sus-jacents, constitués de calcaires oolithiques plus fins ou de marnes à fragments bioclastiques (Perrodon et Zabeck, 1990).

Les deux principales formations aquifères du Jurassique supérieur sont: (i) l'Oxfordien moyen et tardif (Lusitanien), composé d'une plate-forme carbonatée micritique progradante (**Lenoir et al., 2014), limitée à son sommet par les marnes de l'Oxfordien inférieur et le Kimméridgien ; (ii) les calcaires du Tithonien témoignent d'une plate-forme carbonatée aggradante se terminant par des évaporites de plaine côtière (Guillocheau et al., 2000; **Lenoir et al., 2014).

La discontinuité fini-Cimmérienne à la limite Jurassique-Crétacé (Ziegler, 1990), décrite sur l'ensemble de la plaque ouest-européenne, est contemporaine de l'ouverture de l'océan Atlantique et du rifting en mer du Nord. Le Crétacé inférieur marque le passage à des systèmes terrigènes (environnements deltaïques et de plaine côtière ; Mégnien et Mégnien, 1980; Guillocheau et al., 2000). Les axes de subsidence sont orientés NO-SE.

Le Crétacé supérieur est caractérisé par une réorganisation majeure de la paléogéographie du bassin de Paris (ouverture du Golfe de Gascogne, et dans un contexte plus large ouverture de l'Atlantique sud ; Guillocheau et al., 2000 ; phase autrichienne de Ziegler, 1990). A l'Albien, les systèmes de type silicoclastiques dominés par des dépôts deltaïques passent à des faciès marins ouverts à l'Albien moyen/supérieur (aquifère albien). Au Cénomaniens, les dépôts sont principalement dominés par des plates-formes carbonatées crayeuses, elles aussi aquifères (transgression cénomaniens ; Lasseur, 2007).

L'apparition de grandes flexures au cours du Crétacé supérieur sont rapportées au mouvement de l'Ibérie et au début de l'orogène pyrénéen (Lasseur, 2007). La limite Crétacé-Tertiaire est marquée par une phase d'émersion-érosion généralisée (Pomerol, 1989), associée à l'orogène pyrénéen (Guillocheau et al., 2000 ; phase Laramide de Ziegler, 1990).

Le Tertiaire est la période correspondant à la « fermeture » du bassin. Les faciès marins du Lutétien (Gély et Lorenz ; 1991, Briais, 2015) passent à des faciès lacustres à l'Oligocène puis à des faluns (Miocène inférieur) correspondant aux derniers dépôts marins. Des systèmes alluviaux se mettent en place au cours du Miocène (Mégnien et Mégnien, 1980) uniquement dans la partie SO du bassin. Le Miocène correspond à la fin de la sédimentation du bassin de Paris (Briais, 2015). Ces dépôts tertiaires typiques d'une faible subsidence caractérisent des aquifères peu épais, déconnectés et peu profonds.

4.1.4. Résultats

Schéma structural du bassin de Paris

Je complète ici les résultats des travaux menés sur la structuration du bassin de Paris, déjà abordés dans la publication 1, qui aurait eu toute sa place dans ce volet (e.g. rôle prépondérant des failles tardi-varisques polyphasées, failles monophasées typiques de l'activité tectonique tertiaire, déformations dans le bassin mises en regard de l'évolution géodynamique ; *Beccaletto et al., 2011). Il s'agit d'un schéma structural consolidé issu de mes premiers projets d'interprétation sismique au BRGM et d'une compilation de nombreuses données connexes (Beccaletto et al., 2008). Les failles recoupant les toits du Trias, du Dogger et du Kimméridgien sont identifiées à l'échelle du bassin (Figure 28). Leur tracé est vérifié (indice de confiance) et les rejets en mètres sont estimés le long de leur tracé. Pour chaque faille, les coordonnées et cotes des intersections entre les failles et les toits des trois surfaces géologiques sont disponibles; ce qui signifie qu'il est possible d'utiliser directement ces failles en données d'entrée pour des modélisations géologiques 3D. Ce schéma structural est utilisé dans de nombreux projet de recherche académique (Master et thèses, e.g. ANR UPGEO en cours) ou appliquée (modélisations à visées réservoir, e.g. Bader et al., 2014 pour le stockage du CO₂).

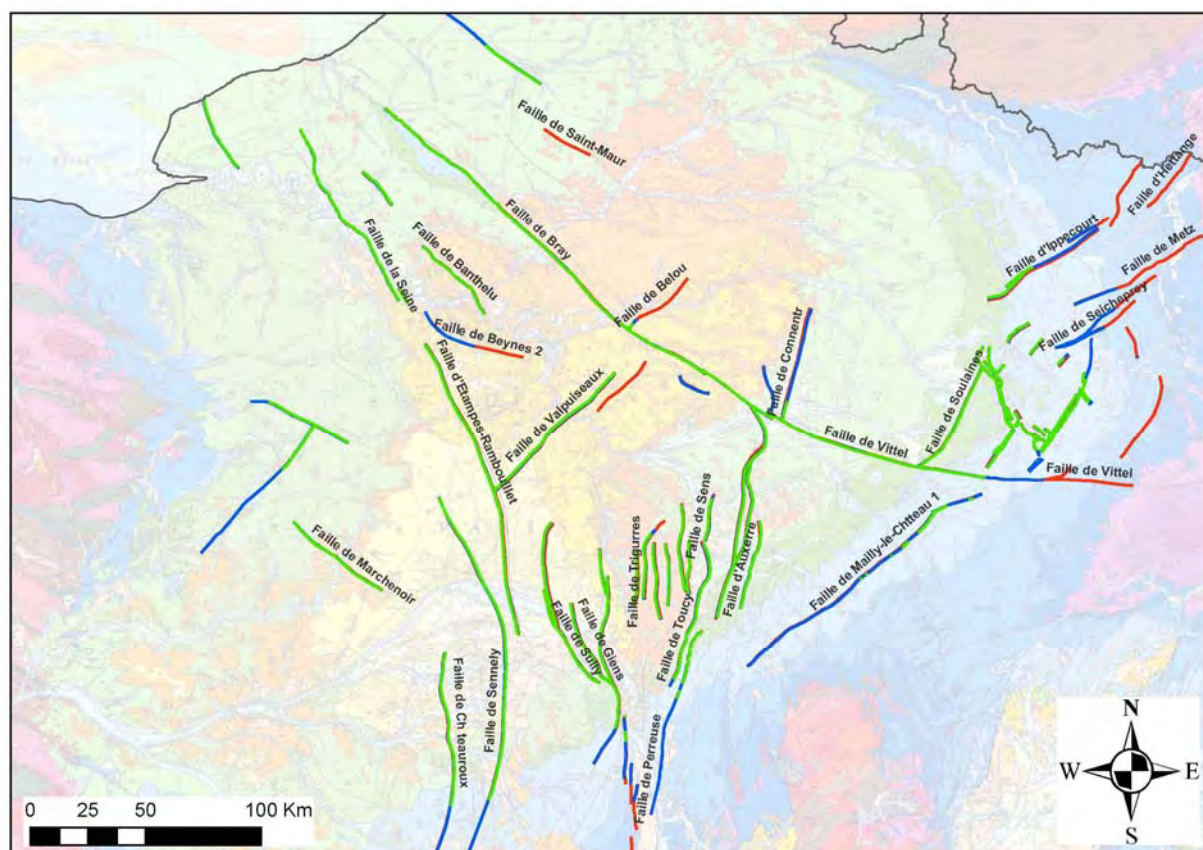


Figure 28 - Schéma structural consolidé du bassin de Paris ; en rouge, failles au toit du Trias ; en bleu failles au toit du Dogger Calcaire, en vert failles au toit du Kimméridgien ; en fond carte géologique de la France au 1/1000000^{ème} (BRGM, 2003).

Impact des structures géologiques sur les anomalies thermiques du bassin de Paris

Je présente ici les résultats originaux tirés de la publication suivante (thèse de J. Dentzer):

Dentzer J., Bruel D., Delescluse M., Chamot-Rooke N., **Beccaletto L.**, Lopez S., Courrioux G., Violette S. (2018) Thermal and seismic hints for chimney type cross-stratal fluid flow in onshore basins, Nature Scientific Reports. <http://dx.doi.org/10.1038/s41598-018-33581-x>

On observe au sein du bassin de Paris une différence de température de l'ordre de 20°C à quelques kilomètres de distance entre le sud et le nord de Paris, et ce dans la même formation aquifère du Bathonien à même profondeur. L'idée initiale était de rechercher le rôle de failles et des zones fracturées dans la distribution spatiale de cette hétérogénéité de température. Je suis intervenu pour travailler les profils sismiques retraités à l'occasion de cette thèse (Figure 29). J'ai mis l'accent sur l'interprétation de certains horizons mésozoïques caractéristiques (base et toit Trias, base et toit Dogger Calcaire, limite Berriasien inférieur/supérieur, et toit de l'Albien), sur les structures géologiques observables (plis et failles), leur résolution verticale et leur extension latérale.

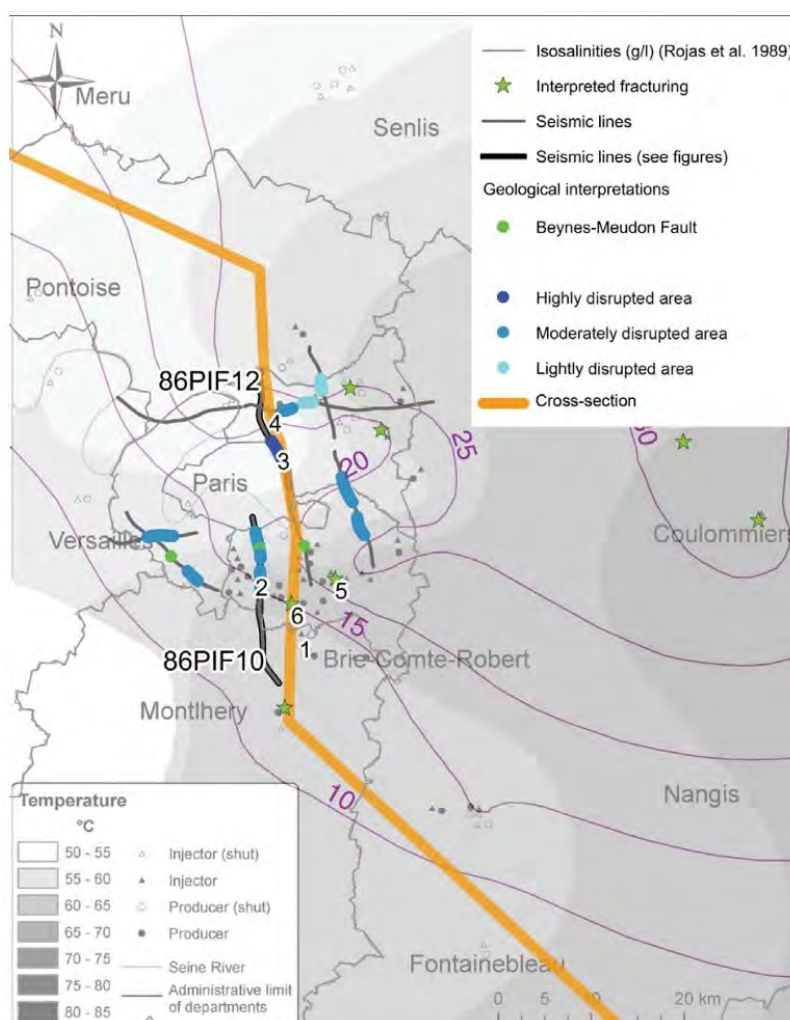


Figure 29 - Structuration et anomalies thermiques dans le bassin de Paris ; (i) des isothermes ; (ii) des isosalinités au Bathonien ; (iii) des propositions d'interprétations géologiques (en vert et bleu) à partir des lignes sismiques ; (iv) de la coupe de référence 2D en orange (Dentzer, 2016).

Cela s'est traduit par (i) une définition accrue de la structure plissée de l'anticlinal de Beynes-Meudon et la faille associées (plis sur faille) ; (ii) la mise en évidence le long des profils sismiques de zones de plus faible amplitude et à faciès sismiques transparents ; ces structures larges d'un à deux kilomètres n'avaient jamais été décrites auparavant (Figure 30). Elles sont interprétées en terme de conduits verticaux fracturés à une échelle infra-sismique (« chimneys »), à l'image de conduits similaires connus en domaines offshore (e.g. Karsten et al., 2015).

Les horizons et structures interprétées ont ensuite été convertis en profondeur et intégrés dans le Geomodeller[®] du BRGM pour construire un modèle 3D de la région considéré (\approx l'Ile-de-France). Une coupe géologique orientée NS et donc perpendiculaire aux structures géologiques a été extraite de ce modèle géométrique. Cette coupe de référence a servi de support pour des modélisations thermiques pour tester le rôle des failles et conduits fracturés sur les distributions de température. Les différents scénarios de modélisation de failles et zones de fractures montrent clairement leur contribution à l'hétérogénéité de température observée dans le bassin (les fluides chauds circulent préférentiellement via ces conduits). En plus de ce résultat singulier, cette étude constitue la première quantification de l'impact thermique des écoulements au sein de failles et zones fracturées dans le bassin de Paris. L'idée à terme est de rechercher davantage ces conduits, mieux comprendre leur origine et évaluer leur impact sur les écoulements, le transport de la chaleur et des éléments en solution.

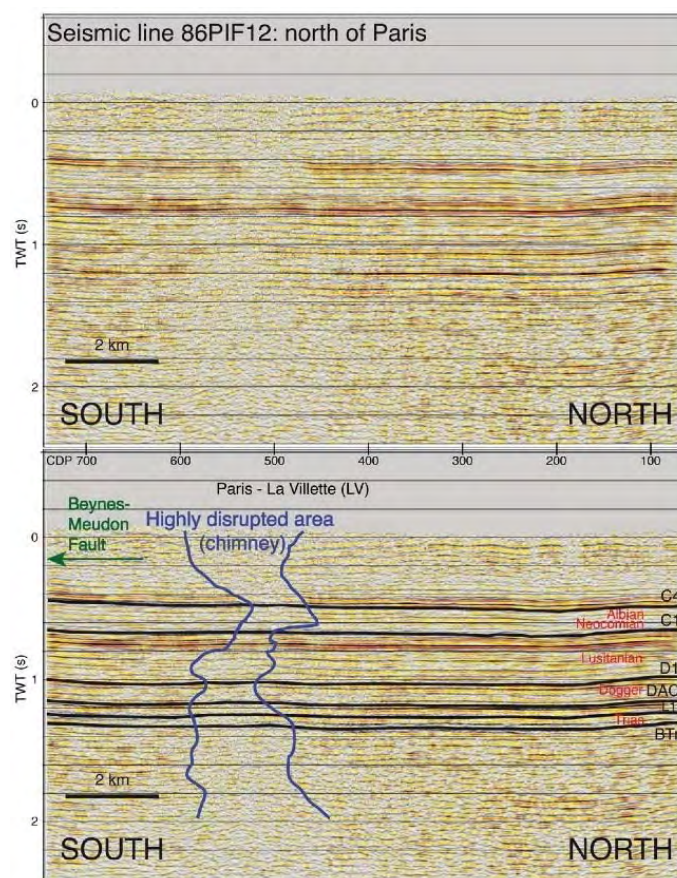


Figure 30 - Ligne sismique interprétée au nord de Paris montrant en bleu un conduit subvertical caractérisé par un faciès sismique transparent ; horizons interprétés en noir ; BTr base Trias, L1 toit Trias, Dac toit des Marnes à Ostrea Acuminata, D1 toit du Dogger calcaire « Dalle nacrée », C1 limite Bérriasien inférieur/supérieur, C4 toit de l'Albien (**Dentzler et al., 2018).

Modélisation 3D à visée géothermique des aquifères en région Centre-Val-de-Loire - Publication 7

Mas P., Calcagno P., Caritg-Monnot S., **Beccaletto L.**, Capar L. & Hamm V. (2022) A 3D geomodel of the deep aquifers in the Orléans area of the southern Paris Basin (France), Scientific Data, <https://doi.org/10.1038/s41597-022-01876-4>

Un nombre croissant de villes s'intéresse à la géothermie profonde afin d'augmenter la part des énergies renouvelables dans leurs réseaux de chauffage urbain. Pour réduire les risques liés à l'exploitation de la géothermie profonde (« de-risking »), des modèles numériques fiables sont nécessaires. Ils permettent de prédire la profondeur des aquifères loin des forages existants, ainsi que leur évolution thermique et hydrologique en simulant des flux d'eau et de chaleur.

Contrairement aux habituelles publications en Géosciences, Scientific Data se propose de publier et mettre à disposition de ses lecteurs toutes sortes de modèles, géologiques ou autres (médecine, biologie...). Le but de cet article, issu du stage 3A de P. Mas (ENSEGID), est donc de fournir à la communauté un modèle géologique 3D étayé du sous-sol de la région orléanaise, et non pas de discuter, par exemple, de son évolution géologique. L'idée sous-jacente est de montrer comment construire un modèle géologique qui sera utile pour l'exploration géothermique.

Ce modèle 3D est très largement basé sur l'interprétation de profils sismiques retraités dans le cadre d'un projet interne au BRGM sur la géothermie en région Centre-Val-de-Loire. Je suis venu en appui de P. Mas pour interpréter ces profils, affiner le schéma structural et valider la conversion en profondeur de l'ensemble.

Résumé de la publication 7

- Après avoir posé brièvement le cadre géologique, les données d'entrées au modèle sont présentées dans un souci d'exhaustivité et de reproductibilité : données sismiques, cartes géologiques, MNT, données de forages, modèle 3D grande maille préexistant.
- La méthodologie employée est détaillée : setup du modèle dans le Geomodeller® du BRGM, interprétation sismique, préparation des données et import dans le Geomodeller®, processus de modélisation 3D, export des surfaces modélisées (important pour que le modèle puisse être réutilisé). L'étape d'interprétation sismique est particulièrement détaillée : déstockage et retraitement des profils, import des profils et forages dans le logiciel Gverse GeoGraphix®, identification des horizons et des failles, modèle de vitesse et conversion temps-profondeur des horizons interprétés.
- Une validation technique du modèle est proposée afin de démontrer sa fiabilité (qualité des données, expertise géologique, avantages du Geomodeller®, cohérence avec d'autres données géophysiques...).

scientific data



OPEN

DATA DESCRIPTOR

A 3D geomodel of the deep aquifers in the Orléans area of the southern Paris Basin (France)

Perrine Mas^{1,2}✉, Philippe Calcagno¹, Séverine Carity-Monnot¹, Laurent Beccaletto¹, Laure Capar¹ & Virginie Hamm¹

An increasing number of cities are interested in deep geothermal energy in order to increase the share of renewable energies in their district heating networks. To reduce the risks related to deep geothermal energy operations, reliable digital models are needed: they make it possible to predict the depth of aquifers away from borehole locations, and their thermal and hydrological evolution by supporting detailed water and heat flow simulations. This paper presents a 3D geomodel developed for this purpose in the southern Paris Basin of France in the Orléans area. The 3D geomodel integrates various data such as reprocessed and interpreted seismic lines, well data, and a pre-existing larger-scale and lower-resolution 3D geological model. The resulting 3D geomodel gives a new and reliable representation of the main aquifers underlying the study area. Within the framework of the project, hydrological and thermal simulations were then performed based on this 3D geomodel. Other environmental investigations (e.g. CO₂ storage) and teaching/communication activities could also benefit from the dataset.

Background & Summary

Three-dimensional geological and reservoir models have become a very common tool in many applications in earth sciences over recent decades^{1,2}. They are used to better understand the geology of an area by constructing a coherent interpretation of the structures and by merging 2D data in a 3D space. In the underground exploration, engineering or management industries, geological models are the basis for calculations, such as predictive fluid flow simulations and resource evaluations^{1,3–5}. Therefore, geological models are currently commonly used in, among other domains: applications related to geotechnics⁶, hydrogeology^{7,8}, seismic hazard assessments⁹, energy resources^{10,11} (e.g. geothermal energy and hydrocarbons), and underground storage¹² (e.g. heat, gas, CO₂, and waste). In addition, geological models are also really useful for communication and educational purposes by visualizing 3D subsurface information^{3,13}.

Geothermal development in the Paris Basin started in the early-1970s in reaction to the first oil crisis¹⁴. After a period of withdrawal, there was a boost of activity at the end of the 1990s following the Kyoto Agreement, and the “Geothermal Energy in Ile-de-France Revival Program” in the late 2000s^{14,15}. This region presently includes 50 out of the more than 70 deep geothermal energy installations dedicated to urban heating in France, most of which target the Dogger (middle Jurassic) aquifer. The installations are mostly “doublets” which comprise a production and an injection well, forming an open loop system¹⁵. One of the major issues in geothermal energy in the Paris Basin is the “thermal breakthrough”, which is the arrival of the low temperature front from the injector well¹⁵. South-east of the Paris Basin, the doublet installations are located quite close to one another, increasing the risk of thermal breakthrough induced by another operation. In some areas of the Paris Basin (e.g. south-east of Paris) targeting the Dogger aquifers leads its exploitation to saturation at these places: another installation cannot be implanted without being affected by a thermal breakthrough caused by another doublet. Therefore, the prospection of other underlying or overlying aquifers has begun to further develop geothermal energy in these areas. On an other hand, since the beginning of the 2000s a secondary interest for the aquifers targeted by geothermal energy has appeared to develop CO₂ storage: studies targeting the carbonate Dogger formation and the saline aquifers in Triassic silico-clastic formations have been conducted with a view to eventually create a “geological carbon sink”^{16,17}. The development of such aquifer exploitation projects (geothermal energy, CO₂

¹Bureau de Recherches Géologiques et Minières (BRGM), Orléans, France. ²Géosciences Paris-Saclay, Université Paris-Saclay, CNRS, Orsay, France. ✉e-mail: perrine.mas@universite-paris-saclay.fr

storage...), sometimes geographically close, reinforces the need to have the most reliable geological models possible.

In response to this challenge, a 3D geomodel was built using the BRGM's GeoModeller software (see the "Code Availability" section) and as part of a collaboration between two interdisciplinary projects. It was called the Orléans Métropole geomodel (thereafter "OM3D geomodel") and is located in the southern Paris basin of France in the Orléans area.

The aim of the first project (called "Orléans Métropole") was to study and assess the deep geothermal potential of the subsurface beneath the metropolis of Orléans in the Centre-Val de Loire French administrative region. The goal of the second project (called "GEOCO2"¹⁸) was to assess the feasibility of an innovative method of dissolved CO₂ storage in aquifers¹⁶ in the same region. The OM3D geomodel was part of the exploratory phase for both projects. Using well and seismic data, it aimed to better characterise the reservoirs and to reduce economic risk of the operations. Its purpose was then to obtain a local-scale, updated and reliable 3D geomodel of the vicinity of Orléans, representing a step forward compared to a pre-existing larger-scale lower-resolution 3D geological model (the SIGES model, see Table 1) covering the entire Centre-Val de Loire region¹⁹.

The target aquifers for the "Orléans Métropole" and "GEOCO2" projects are the Triassic Sandstones and Dogger (Bajocian-Bathonian) Limestones²⁰, and the overlying Tithonian and Lusitanian (Oxfordian) Limestones²¹, respectively. The OM3D geomodel was specifically built to provide the best possible representation of the geometry of these deep aquifers. The aim of this paper is to share the OM3D geomodel so that it can be reused, refined, or modified irrespective of the application domain. Within the "Orléans Métropole" project, the OM3D geomodel was used as a basis for hydrothermal simulations and ultimately for the assessment of the geothermal potential^{22,23}. Within the "GEOCO2" project it was used to study the feasibility of CO₂ storage²¹. However, it could also be used for future applications, e.g. it could be a tool for groundwater management, or energy resources and waste storage for the Orléans metropolis, or as a communication and teaching tool for local representatives and geosciences students. In addition to sharing the geomodel, another objective of this paper is also to provide a methodology that can be applied to other case studies where similar types of data are available^{24,25}.

The workflow followed to create the OM3D geomodel is shown in Fig. 1. The core steps are: (1) model setup, (2) seismic interpretation, (3) data preparation and import for geomodelling, (4) 3D geomodel processing, including the iterative process of quality control and adjustments which mostly involved comparing the OM3D geomodel to the pre-existing larger-scale lower-resolution 3D geological model, and (5) OM3D geomodel export. These core steps are developed in the "Methods" section.

Geological and Hydrogeological Contexts

The Meso-Cenozoic Paris Basin is an intracratonic sedimentary basin lying unconformably over a Paleozoic Variscan basement^{26,27}. Both the sedimentary (from open marine to fluvial-continental environments through evaporitic systems, with subsequent major erosional unconformities) and structural (fault activity, long- to short- wavelength folding) patterns successively record the Mesozoic opening of the Alpine Tethys, Atlantic Ocean and Bay of Biscay, and Late Cretaceous-Cenozoic Pyrenean and Alpine orogenies^{28–32}. This long-term geological evolution results in the occurrence of major aquifers (Fig. 2) and faults (Fig. 3) in the southwestern part of the Paris Basin and Orléans area.

Stratigraphy and major aquifers in the orléans area. From the Triassic to the Early Cretaceous, the Paris Basin underwent an overall extensional tectonic regime. Triassic deposits are made of alluvial fan sediments at their base, gradually changing to the Keuper Sandstones (Middle to Late Triassic). The latter are composed of two fluvial bodies separated by a clayey interval³³: the Donnemarie Sandstones lower body, and the Chaunoy Sandstones upper one. The former is made of proximal to median alluvial fan-type coarse sandstones and conglomerate deposits, whereas the latter is composed of finer sandstones, characteristic of alluvial fans to braided channel systems³⁴. The Keuper Sandstones are the major aquifer formation within the Triassic²⁰ (Fig. 2). The uppermost Triassic consists of marls and dolomites, which continue to the Lias (Early Jurassic), where an alternation of clays or marls with clayey and often dolomitic limestones are found²⁹.

The Toarcian recorded the maximal flooding period, made of open marine deposits such as marls or shales with shell debris, crinoids, or gastropods. This aquitard level corresponds to the "Schistes Carton" also found further to the east of the basin²⁹.

The Dogger is divided into three units (Fig. 2): (1) The Aalenian, represented by grey marl containing bioclastic elements and possibly alternating shaly limestone. The proportion is inverted in the lower-Bajocian, formed by shaly limestones with shaly interbeds; (2) The upper Bajocian and the Bathonian, composing the main water-productive levels and mostly consisting of oolitic, gravelly and bioclastic limestones; their light color gave them the name of "Oolithe Blanche"; (3) The overlying Callovian deposits, made of thinner oolitic limestones or marls with bioclastic fragments, and containing a stratigraphic reference level of ferruginous oolites found everywhere in the Paris Basin³³.

The two main aquifer formations of the Late Jurassic (Malm) are as follows (Fig. 2): (1) the middle and late Oxfordian (Lusitanian), which is composed of a muddy progradational carbonate platform³⁵ bounded by the impermeable marls of the early Oxfordian at the base, and the Kimmeridgian at the top³⁶, and (2) the Tithonian limestones recording an aggradational muddy carbonate platform ending with coastal plain evaporites^{29,35}.

The Lower Cretaceous marks the end of the extensive phase of the basin. The uplift of the basin gave birth to the sandy sediments of the Neocomian and Albian aquifers, deposited over the tilted and truncated Jurassic deposits^{26,35} (Fig. 2). The sea level then rose drastically to cover the whole basin again (global Cenomanian transgression), essentially characterized by chalky aquifer deposits^{29,37}. Lastly, the Cenozoic records very low subsidence rates leading to thin and laterally varying sedimentary deposits, forming numerous small-scale shallow aquifers.

Type	Name	Original Operator/Institute	Acquisition/Issue date	Notes
Seismic lines	Chartres	Petroleum Exploration Company (CEP)	acquisition: 1963 reprocessing: 2008	Selected lines: CH09, CH11, CH12 and CH13
	Loury-Villeny	EURAFREP	acquisition: 1964 reprocessing: 2020	Selected lines: LV03, LV09 and LV14
	Loiret 1982/Loiret 1983	Esso	acquisition: 1982–1984 reprocessing: 2020	Selected lines: LOIR1, LOIR8, LOIR9, LOIR10, LOIR15, LOIR16, LOIR17, LOIR18, LOIR19, LOIR22
Geological maps	BD Charm-50 [®]	BRGM (French Geological Survey)	2005	1/50 000 geological map of the Loire department and (for identification of the formation contours)
	BD Million-Géol [®]		2006	1/1 000 000 geological of the French metropolitan territory (for the fault traces) The geological maps were harmonized, simplified and the Sennely fault trace was modified after Beccaletto <i>et al.</i> , 2008.
Digital Terrain Model (DTM)	BD ALTI [®]	National Institute of Geographic and Forest Information (IGN)	2018	Spatial resolution 25 m
Well data	Marilly-en-Vilette 1	FROPEX	1959	Petroleum exploration well Reaches the Portlandian (TVD = 585 m) no velocity survey
	Saint-Sigismond 1	SAFREP	1963	Petroleum exploration well Reaches the Basement (TVD = 1299 m) velocity survey recorded
	Rebréchien 1	Petroleum Exploration Company (CEP)	1964	Petroleum exploration well Reaches the Basement (TVD = 1518 m) velocity survey recorded
	Melleray 1	BRGM (French Geological Survey)	1979	Geothermal well Reaches the Basement (TVD = 1668 m) no velocity survey
	Melleray 2	BRGM (French Geological Survey)	1980	Geothermal well (deviated from 890 m) Reaches the Basement (TVD = 1161 m) no velocity survey
	Pre-existing larger-scale lower-resolution 3D geological model	SIGES Centre Val-de-Loire 3D geological model	BRGM (French Geological Survey)	2019

Table 1. Datasets used as input during the development of the OM3D gemodel. TVD = True Vertical Depth (of the Bottom Hole)

For this study, a stratigraphic division was employed to better distinguish the main aquifers from their overlying aquitards (Fig. 2). Each major aquifer formation was then treated individually, whereas the aquitard formations were grouped together. It should be noted that this study focused mainly on the deep aquifers that may present an interest for geothermal energy or storage, and therefore the upper Cretaceous and overlying Cenozoic deposits were not modelled.

Tectonic setting in the orléans area. The Mesozoic deposits of the southwestern part of the Paris Basin are affected by reactivated Variscan faults, separating the center of the basin to the east from the Variscan Armorican massif to the west^{27,38,39} (Fig. 2). These faults belong to the Seine-Etampes-Rambouillet-Sennely fault system, oriented along a N-S axis in the studied area, turning to a NNW trend in its northern section. They were initiated as strike-slip faults at the end of the Variscan orogeny in Carboniferous times, then reactivated as normal faults during the Permian at the time of the collapse of the Hercynian chain³⁹. During the Meso-Cenozoic, these faults mostly act as normal faults with local minor compressional features⁴⁰.

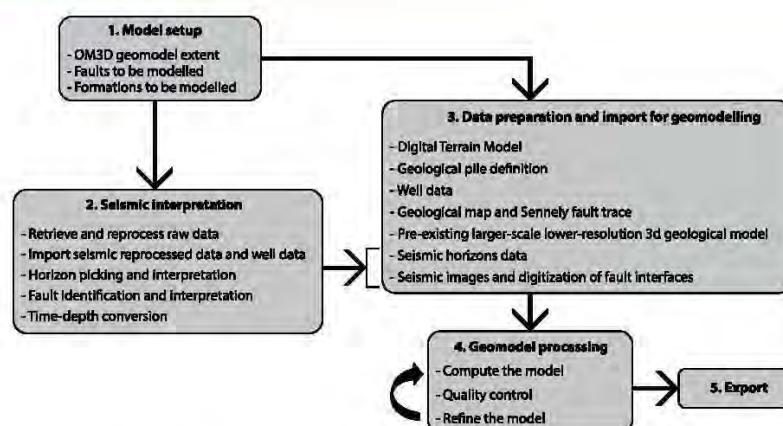


Fig. 1 Workflow followed to develop the OM3D geomodel.

The Seine, Rambouillet and Etampes faults are arranged in a relay zone, and they form a Y-shape with the Sennely fault to which they connect to the south-east of Orléans (Fig. 2). The Sennely fault is important for the realization of the OM3D geomodel because it crosses through the metropolis' territory. According to Héritier and Villemain³⁸, it is unlikely to be a continuous fault, but rather a network of relayed segmented faults, along a meridian direction, with a slight trend towards the north-west north of Rambouillet. The dip generally strongly inclined towards the north-west; the offsets are smaller in the northern part of the fault occurrence, whereas they can reach 500 m in the southern part^{38,40}.

Input Data

The Paris Basin is among the most extensively studied sedimentary basins in the world²⁹. Between the 1950s and 1980s, a large amount of subsurface data was acquired during petroleum exploration, leading to better knowledge of the basin's geology³². Numerous hydrocarbon exploration wells were drilled, and seismic acquisition campaigns were conducted. From the 1970s onwards, tens of geothermal doublets were also drilled.

The input data for the OM3D geomodel are: (1) 17 seismic lines, (2) a geological map with the digitized Sennely fault trace, (3) a Digital Terrain Model (DTM), (4) data from five wells (survey reports with geological logs) and (5) a pre-existing 3D larger-scale and lower-resolution 3D geological model which covers a much wider area than the metropolis' territory (Fig. 3). These data sources are presented in Table 1.

Seismic data. As mentioned above, many oil companies carried out seismic acquisition campaigns in the Paris Basin during the 1950–1960s and 1980s. For our study, seismic lines acquired around Orléans were retrieved from the oil companies that carried out the campaigns⁴¹. These seismic data originate from three different acquisition campaigns: (1) Loiret 1982 and Loiret 1983, (2) Loury-Villeny, and (3) Chartres (Fig. 3). Within these raw data sets, only the closest lines to the Orléans metropolis, and those located near the Sennely fault, were selected for interpretation to reduce processing costs. These lines were reprocessed and reinterpreted using up-to-date techniques to give better results than the original processing carried out decades ago. These reprocessed data are the seismic data that were interpreted (for the deposits's geometry as well as the structural elements) and used for the geomodelling.

Only the datasets from the Chartres and Loury-Villeny campaigns were reprocessed during the projects because the Loiret 1982/Loiret 1983 datasets were already reprocessed in 2008. Some of the lines are outside of the OM3D geomodel domain (Fig. 3), but they were used to better constrain the Sennely fault (especially its northern part) that crosses all of them.

Geological map. The geological map displayed in Fig. 3 comes from the harmonization of two BRGM (French Geological Survey) geological map datasets: the BD Charm-50⁴² (1/50 000 vectorized geological map of the Loiret department) and the BD Million-Géol⁴³ (1/1 000 000 geological map of the entire French metropolitan territory). The Sennely fault was improved and modified after Beccaletto *et al.*⁴⁰ to provide a more reliable fault interpretation. This new fault line was used in the construction of the geomodel to complement the seismic data where no lines were available.

It can be noted that no aquifer formation outcrops in this area, the groundwater recharge coming from the outcropping aquifer formations in the south-west of the Paris Basin. The consequence is also that the geological map cannot be used to constrain the geometry of the modelled formations at the surface, contrary to the modelled faults: the Sennely fault traced on the geological map is very useful to constrain the fault on the topographic section.

Digital terrain model (DTM). The BD ALTI[®] digital terrain model (DTM), provided by the French National Institute of Geographic and Forest Information⁴⁴ (IGN), is a raster dataset with a horizontal cell resolution of 25 m. A higher resolution was not necessary since the altitude variation of the study area is low (the

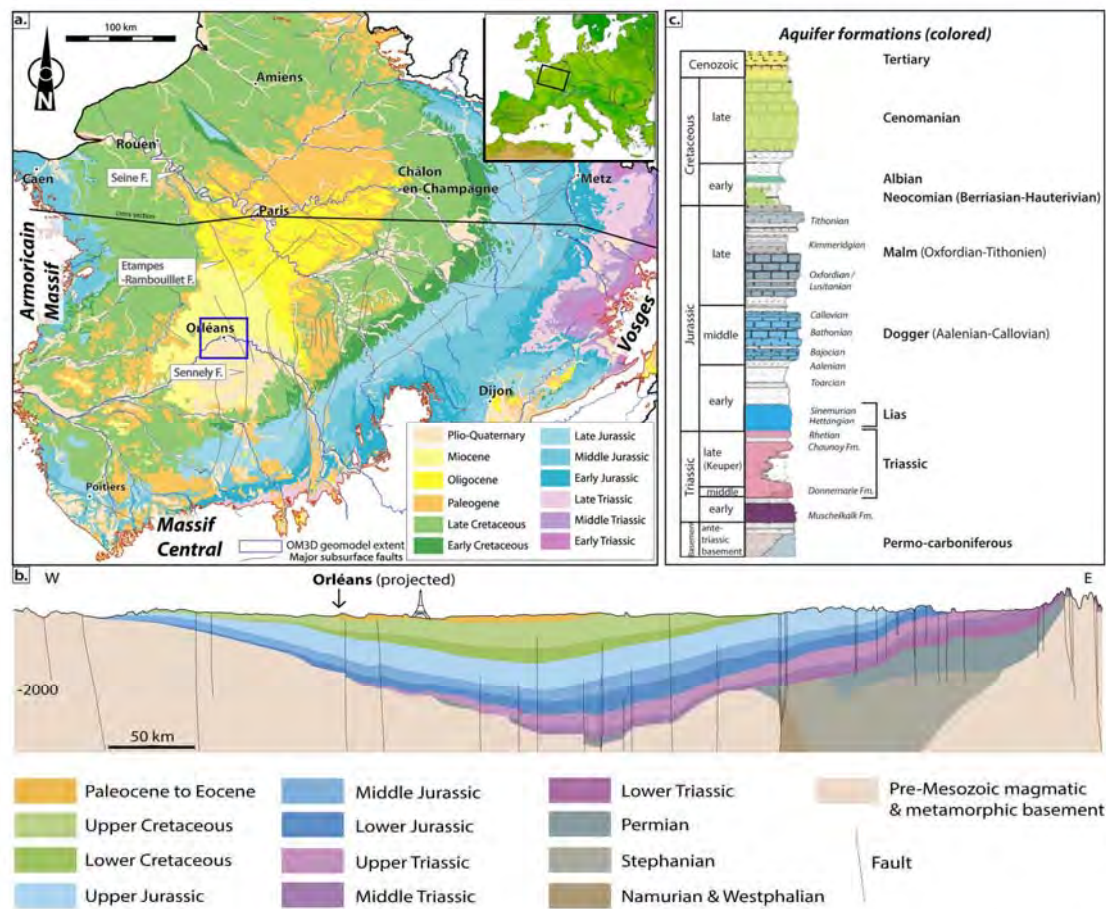


Fig. 2 (a) Geological overview of the Paris Basin featuring the major subsurface faults. The faults are compiled from Héritier and Villemin³⁸, Mégnien and Mégnien²⁶, Perrodon and Zabeck³³ and Delmas *et al.*³², redrawn and modified by Beccaletto *et al.*⁴⁰. The geological background is from the 1:1 000 000 geological map of France (Chantraine *et al.*). Top-right inset: the Paris Basin in Western Europe. (b) Cross section modified after Gély *et al.* (c) The stratigraphic log of the Paris Basin with the major aquifer (colored) and aquitard (uncolored) formations is modified after Delmas *et al.*³².

altitudes range between 80 and 150 m above the sea). It represents the ground surface elevation without vegetation or buildings.

Well data. Geological information beneath the Orléans area is also constrained by well log information⁴⁵. Five wells, including three petroleum ones and one geothermal doublet, are located relatively close to the metropolis and their survey reports contain lithological logs (Fig. 3). They provide information on the sedimentary formation properties based on both logging and testing, as well as on the depth of the tops of the geological formations. The latter are used to tie seismic data to wells, convert the seismic horizons to depth and they were also directly integrated in the 3D geomodel (Table 2 and Fig. 6).

Pre-existing larger-scale and lower-resolution 3D geological model. A pre-existing larger-scale and lower-resolution 3D geological model exists at the scale of the Centre-Val de Loire region (approximately 40,000 km²), also covering the area of Orléans; its cell resolution of 500 m is not accurate enough for a deep geothermal application at the scale of a metropolis. This 3D geological model (SIGES) was initiated in 2012 and modified and completed in 2019, using the GDM-Multilayer BRGM software¹⁹. It is composed of surfaces representing the tops of the main aquifers (down to the basement) in the Centre-Val de Loire region and was created by interpolating data from 12,941 wells throughout the entire region, but with only five deep wells covering the study area (and no seismic data). This model was mainly used for adjusting the Sennely fault geometry in the south-east of the OM3D geomodel (and the formations top near the boundaries of the model).

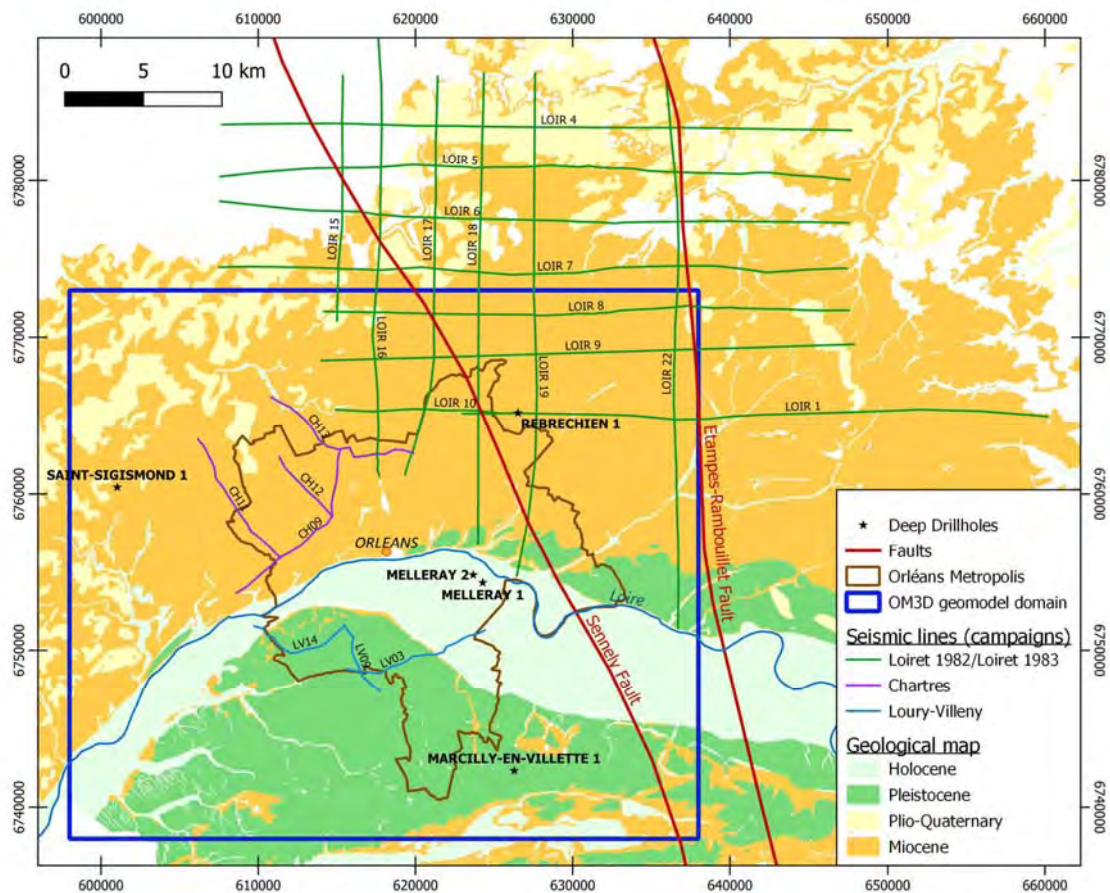


Fig. 3 Location of the different input datasets for the development of the OM3D geomodel. The geological background is modified from the 1:50 000 geological map of the Loiret campaign (BD CHARM-50¹², BRGM). The RGF93/Lambert-93 coordinate system is used.

Methods

Model setup. The OM3D geomodel domain, i.e. the 3D bounding box, was chosen based on literature data^{10,42,43} to meet two imperatives: (1) the OM3D geomodel's extent must cover the metropolis' territory, and (2) the OM3D geomodel domain must contain as much input data as possible. The area is a rectangle spanning 40 km by 35 km centered on the metropolis (Fig. 3, blue box). Its coordinates are given in Table 3. The Rambouillet-Etampes fault was not included, as it is far enough from the metropolis and lies on the eastern limit of the OM3D geomodel extent.

The choice of the formations to be identified on the seismic lines and to be modelled was made based on the main aquifer and aquitard formations of the Paris Basin identified in the well reports (see the "Geological and Hydrogeological Contexts" section). Some of the connected aquifer or aquitard formations need to be grouped together to simplify the stratigraphy and due to seismic vertical resolution issues. Some formations, although identified in the wells (Table 2), are not thick enough to be visible on seismic (vertical resolution of approximately 20 m, see the "Horizon picking and interpretation" part of the "Methods" section below) nor to be considered as reservoir or aquitard formations (see the "Geological pile definition" part of the "Methods" section below). From bottom to top, the aquifer (A) and aquitard (a) formations are: the Basement (a), Triassic Sandstones (A), Liassic and Triassic Marls (a), Liassic Limestones (A), Toarcian Shale (a), Dogger Limestones (A), Callovo-Oxfordian Shale (a), Lusitanian Limestones (A), Kimmeridgian Marls (a) and the Tithonian Limestones (A) and the sandy lower Cretaceous (A). With regards to the faults, only the newly interpreted Sennely fault was modelled, because it is the only one that falls within the model extent.

Seismic interpretation. Seismic reflection is a geophysical method for obtaining 2D images of the subsurface geological structures. There is contrast in rock properties between the different geological units where the acoustic waves bounce off, hence generating reflection. These surfaces are called "reflectors" and are represented by "reflections" on the seismic image. They are recorded in Two-Way-travel-Time (TWT), usually s or ms, which refers to the travel time that takes the acoustic waves from the source to reflect on the interface and be received at the surface receiver.

www.nature.com/scientificdata/

WELL	X_L93	Y_L93	Wellhead Elevation (m above sea level)	Total Depth (m)	Top Depth (m)	Floor Depth (m)	AQUIFERS/AQUITARDS
RBHI	626516	6765181	133.5	1518	0	624.5	Undifferentiated Cover
RBHI	626516	6765181	133.5	1518	624.5	725	Tithonian Limestones
RBHI	626516	6765181	133.5	1518	725	832	Kimmeridgian Marls
RBHI	626516	6765181	133.5	1518	832	1124	Lusitanian Limestones
RBHI	626516	6765181	133.5	1518	1124	1166	Callovo-Oxfordian Shale
RBHI	626516	6765181	133.5	1518	1166	1311.5	Dogger Limestones
RBHI	626516	6765181	133.5	1518	1311.5	1352	Toarcian Shale
RBHI	626516	6765181	133.5	1518	1352	1385.8	Liassic Limestones
RBHI	626516	6765181	133.5	1518	1385.8	1392.5	Triassic-Liassic Marls
RBHI	626516	6765181	133.5	1518	1392.5	1494	Triassic Sandstones
RBHI	626516	6765181	133.5	1518	1494	1518	Basement
SG1	601036	6760435	113.8	1299.5	0	450	Undifferentiated Cover
SG1	601036	6760435	113.8	1299.5	450	535	Tithonian Limestones
SG1	601036	6760435	113.8	1299.5	535	631.5	Kimmeridgian Marls
SG1	601036	6760435	113.8	1299.5	631.5	907	Lusitanian Limestones
SG1	601036	6760435	113.8	1299.5	907	971	Callovo-Oxfordian Shale
SG1	601036	6760435	113.8	1299.5	971	1125.5	Dogger Limestones
SG1	601036	6760435	113.8	1299.5	1125.5	1212	Toarcian Shale
SG1	601036	6760435	113.8	1299.5	1212	1221	Liassic Limestones
SG1	601036	6760435	113.8	1299.5	1221	1238.5	Triassic-Liassic Marls
SG1	601036	6760435	113.8	1299.5	1238.5	1285	Triassic Sandstones
SG1	601036	6760435	113.8	1299.5	1285	1299.5	Basement
GMY1	624281	6754320	96	1668.75	0	512	Undifferentiated Cover
GMY1	624281	6754320	96	1668.75	512	612	Tithonian Limestones
GMY1	624281	6754320	96	1668.75	612	730	Kimmeridgian Marls
GMY1	624281	6754320	96	1668.75	730	1027	Lusitanian Limestones
GMY1	624281	6754320	96	1668.75	1027	1063	Callovo-Oxfordian Shale
GMY1	624281	6754320	96	1668.75	1063	1237	Dogger Limestones
GMY1	624281	6754320	96	1668.75	1237	1336	Toarcian Shale
GMY1	624281	6754320	96	1668.75	1336	1410	Liassic Limestones
GMY1	624281	6754320	96	1668.75	1410	1436	Triassic-Liassic Marls
GMY1	624281	6754320	96	1668.75	1436	1618	Triassic Sandstones
GMY1	624281	6754320	96	1668.75	1618	1668.8	Basement
GMY2D	623676	6754815	96	1661	0	512	Undifferentiated Cover
GMY2D	623676	6754815	96	1661	512	608	Tithonian Limestones
GMY2D	623676	6754815	96	1661	608	725	Kimmeridgian Marls
GMY2D	623676	6754815	96	1661	725	1021	Lusitanian Limestones
GMY2D	623676	6754815	96	1661	1021	1061	Callovo-Oxfordian Shale
GMY2D	623676	6754815	96	1661	1061	1226	Dogger Limestones
GMY2D	623676	6754815	96	1661	1226	1326	Toarcian Shale
GMY2D	623676	6754815	96	1661	1326	1391	Liassic Limestones
GMY2D	623676	6754815	96	1661	1391	1418	Triassic-Liassic Marls
GMY2D	623676	6754815	96	1661	1418	1582	Triassic Sandstones
GMY2D	623676	6754815	96	1661	1582	1661	Basement
MV1	626284	6742320	129	585	0	537	Undifferentiated Cover
MV1	626284	6742320	129	585	537	585	Tithonian Limestones

Table 2. Aquifers/aquitards formation tops and floors depths for each well. The RGF93/Lambert-93 coordinate system is used.

Retrieve and reprocess raw data. Once retrieved, the seismic data was prepared to a numerical format to be reprocessed. The Loury-Villeny and Chartres seismic campaigns were acquired in the 1960s and therefore their raw data (recorded during the seismic acquisition) were recorded on analogic tapes. It was first necessary to transcribe them into a numeric format. The quality and consistency of the raw data was checked to ensure that the digitized seismic signal, the recording report and the source and receiver coordinates were consistent and to avoid an inadequate reprocessing and subsequent seismic imaging. Once checked, the seismic lines from the Loury-Villeny and Chartres datasets were reprocessed to convert the raw seismic data into a seismic image suitable for geological interpretation. The main objective is to obtain the best image of the sub-surface, given the

	Northing (m)	Easting (m)	Elevation (m above sea level)
Minimum	6 738 000	598 000	-2000
Maximum	6 773 000	638 000	500

Table 3. OM3D geomodel domain extent. The RGF93/Lambert-93 coordinate system is used.

vintage data available. Seismic reprocessing used modern signal-processing algorithms to significantly improve the quality of the images obtained in the 1960's (see examples in the Paris Basin in Beccaletto *et al.*^{39,46} and Laurent *et al.*⁴⁷). Several steps were necessary to obtain a satisfactory seismic image of the sub-surface. The first involved updating the acquisition geometry. It geographically positions the sources, receivers and seismic traces. A processing sequence is then applied that is comprised of spherical divergence compensation, velocity picking, noise attenuation, surface consistent deconvolution, surface consistent amplitude compensation, refraction and residual statics, stack and migration^{48,49}.

Efforts were focused on three key steps that were repeated several times throughout the processing sequence: (a) the calculation of primary and residual static corrections in order to remove the topographic and velocity effects of the superficial rock layer, which strongly impact the seismic signal; (b) a detailed velocity analysis (migration); and (c) various methods of organized and random noise attenuation.

As a last step, the resulting reprocessed seismic lines were then exported in SEG-Y format - SEG-Y as this is the standard format for storing and using seismic data, read by all seismic processing and interpretation software⁵⁰.

Import seismic reprocessed data and well data. The reprocessed seismic data were imported into the seismic interpretation module Geophysics in the GVERSE software⁵¹. The seismic lines from the Chartres and Loury-Villeny campaigns were merged with the Loiret 1982/Loiret 1983 lines by modifying their datum elevation. The vertical resolution of the reprocessed seismic lines is around 20 m.

The five wells were also integrated into the project in GVERSE's Wellbase module to be used as a reference for the accurate depths and stratigraphy. Information from their survey report about their coordinates, head elevation, total well depth, formation top depths, deviation surveys and velocity surveys were entered. Since the seismic lines were in two-way travel time, it was necessary to convert the formation top depths to time. When a velocity survey was available (Table 1), it was also imported to convert the well to two-way travel time and thus, allow the seismic to well tie. Otherwise, the velocity survey of the nearest well was used.

Horizon picking and interpretation. Seismic interpretation consists of recognizing seismic reflectors. The presence of nearby wells, converted in two-way travel time, (e.g. Rebréchien) makes it possible to match a formation top to a reflection, checking for consistency with the amplitude of the seismic signal, which provides information on the rock properties contrast. The reflection can then be tracked laterally and all the points of a picked reflection form a "seismic horizon" (Fig. 4). Reflections were associated with the formation tops selected for geomodelling (see the "Model setup" part of the "Methods" section above) (Fig. 4), from the base to the top: top Basement, top Triassic, top Lias (i.e. top Bathonian (i.e. Top Dogger Limestones), top Callovo-Oxfordian Marls, top Lusitanian Limestones (Oxfordian), top Kimmeridgian Marls, and top Tithonian Limestones.

Regarding the seismic to well tie and resolution issues, the geophysical properties of the rocks in the main aquifers and aquitards (and thus their reflections) are significant enough to discriminate them on the seismic lines despite their relatively low thickness. The seismic horizons are therefore clearly identified on the seismic lines with continuous and well-defined seismic facies.

The high density and regular spacing of the seismic lines in the western part of the model area, together with the relatively simple geological context (few faults, horizontal layers, well-defined geological formation, strong impedances contrasts), minimize the errors during the interpretation process.

The horizons thus created provide information on the "depth" of the formation tops between wells in two-way travel time (TWT), which are used for the OM3D geomodel development once converted into depths.

Fault identification and interpretation. The seismic interpretation has been used to define the geometry of the Sennely fault, which crosses the study area; it was identified on the seismic lines of the Loiret 1982/Loiret 1983 campaigns.

Since the Sennely fault is a relay fault³⁸, some characteristics were studied on the seismic lines to identify the different segments: (1) the vertical extent, (2) the maximal apparent vertical offset, and (3) the approximate dip of the fault (not a real dip as the lines are in TWT). With regards to the two former characteristics, the deformation field of a fault is an ellipsoid, the offset and the vertical extent are smaller at the extremities than in the middle of the fault segment. The apparent dip is assumed to be constant for a given segment.

It can be noticed that there are flexures near the fault between two seismic lines where the fractured rocks thickness and offsets are the lowest. These flexures are located on either one side of the fault or the other depending on the line. One hypothesis is that these flexures could be the ends of fault segments that appear respectively on the other line, forming a relay. The flexures are more developed at depth, meaning that the ends of the fault are anchored deeper.

This case can be observed between lines LOIR7 and LOIR16 as well as between lines LOIR17 and LOIR10 (Fig. 5). Consequently, the fault was divided into three individual segments for the OM3D geomodel. The three

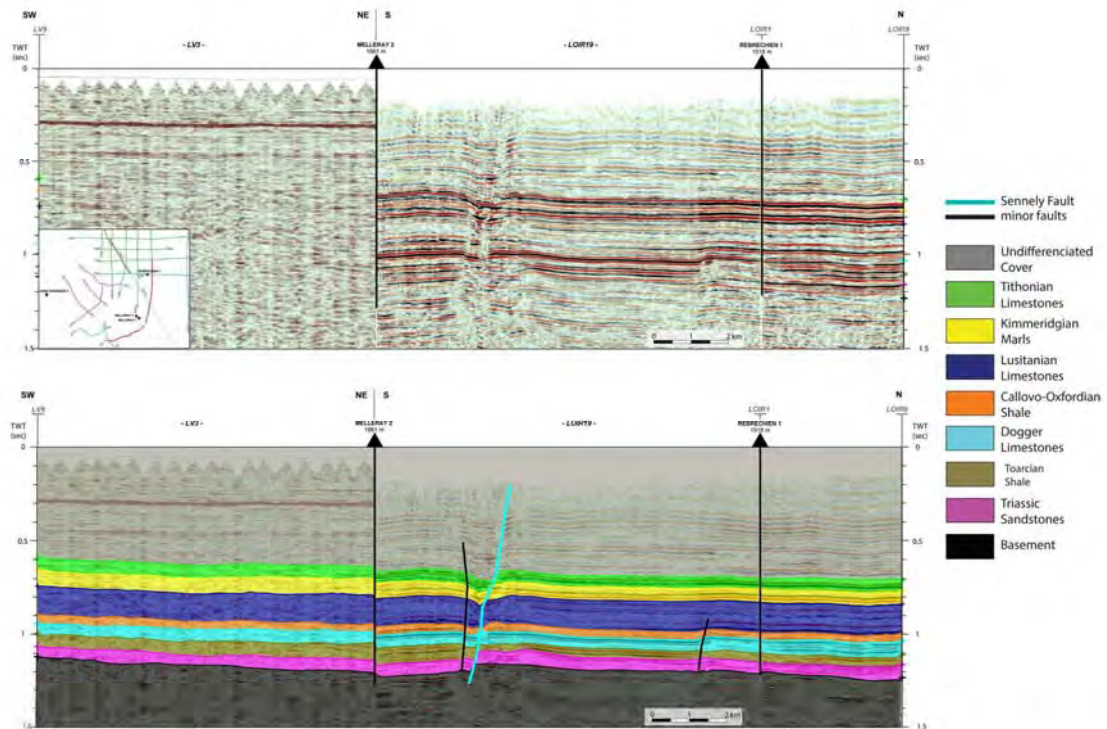


Fig. 4 Snapshot of the composite seismic line LV03-LOIR19 showing the Sennely fault (blue), conjugate faults (black) and the projection of the Melleray 2 well on the composite line.

segments of the fault have the same direction of 150° SE. Figure 5 also shows that the fault dip increases towards the south-east, which is consistent with the regional structural context.

Lastly, it can be noticed that the Sennely fault is not noticeable on all lines, meaning the offset is below seismic resolution of these lines. This is consistent with the aforementioned observations and the description of the relayed fault network provided by Héritier and Villemin³⁸.

Velocity model and time-depth conversion. Seismic lines contain information in two-way travel time (TWT) and the seismic horizons interpreted in time have therefore been converted to depth using a velocity model before being integrated into the 3D model. This is a key step, and it is directly dependent on the seismic velocities in the underground.

Since there was no velocity survey for each well, the velocity model was established by first combining the depth of the formation tops in the wells and the horizon picking in two-way travel time in order to obtain a velocity value per formation at the well location. These local velocity values were then interpolated throughout the whole area (minimum curvature algorithm, cells spanning 250 m²), resulting in a velocity model with varying velocities for a given geological interval.

We used interval velocities rather than average velocities, as is usually done in the Paris Basin when depth-converted seismic horizons are the input data for 3D modelling (its advantage is that it avoids the converted horizons from crossing each other^{52,53}).

Generally speaking, the interval velocity of a given formation corresponds to the mean velocity within this formation:

$$V_{int} = \frac{Z_{base} - Z_{top}}{OWT_{base} - OWT_{top}}$$

where OWT = one-way time, Z = depth.

As a result, we considered every geological formation of the stratigraphic pile of the model as a distinct layer with a varying interval velocity in the entire study area. This calculation was performed in the GVERSE Geophysics software. Velocities mostly range from approximately 2000 m/s to approximately 4000 m/s for all of the formations, which are typical values in this area of the Paris Basin³⁵. For each formation, the thickness values for the interval between the current and previous horizon were calculated using the velocity values associated with that interval. The final depths were calculated by successively adding the thicknesses of the formation calculated in this way. The interpreted seismic horizons have then been converted to depth step by step from the shallowest (Top Tithonian) to the deepest one (Top Basement).

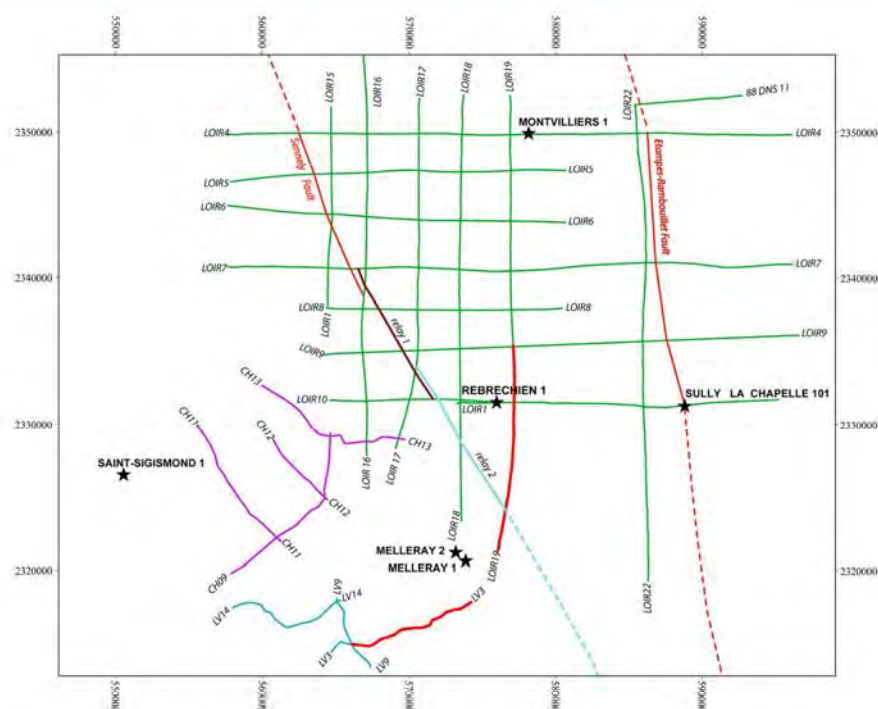


Fig. 5 Map featuring the geometry of the Sennely fault following the interpretation in the relay fault. Note that the map is not centered around the OM3D geomodel domain (represented in blue). The RGF93/Lambert-93 coordinate system is used.

Like any other TD conversion method, this interval velocity conversion method has some limitations. Because the interval velocities are first calculated based on data from five boreholes (before being interpolated at the scale of the 3D model), the TD conversion of the seismic horizons does not consider the potential lateral variations of lithologies and rock properties. Therefore, the uncertainties increase as the distance from the reference boreholes increases. However, given the similar lithologies for each layer (as described in the boreholes and from regional geology, e.g. Guillocheau *et al.*²⁰, Lenoir *et al.*²³), the facies variations are very likely not significant enough at the regional scale to have a major impact on the velocity behavior of the different units.

At the end of the process, a selection of data points (X, Y, Z in meters) along the seismic lines of all the depth converted horizons were exported from GVERSE Geophysics in a table format, ready to use in GeoModeller. On average, the spacing of the points in X, Y is 800 m.

Data preparation and import for geomodelling. *Digital terrain model.* Once the domain was defined, the BD ALTI® digital terrain model (IGN) was imported into GeoModeller to constrain and form the topographic surface of the OM3D geomodel.

Geological pile definition. The “geological pile” refers to the sequence of lithological formations and allows an automatic management of the relationships between the geological bodies during the geomodelling process (see the “Code Availability” section). Several individual formations can be grouped together, forming a “series”²⁴. The geological pile and series were composed for a hydrogeological purpose (see the “Model setup” part of the “Methods” section above). Consequently, the formations were grouped together according to the main aquifers and aquitards. Formations at the top were grouped to form the “Undifferentiated Cover”, because they cover the aquitard lying over the upper targeted reservoir and do not need to be differentiated. The final geological pile is shown in Fig. 6.

Well data. Well data were imported in GeoModeller from the spreadsheet containing information about their coordinates, formation names, and depths of the formation tops. These pieces of information were recovered from the borehole survey reports.

Geological map and sennely fault trace. The georeferenced geological map with the Sennely fault trace (Fig. 3) was imported into GeoModeller and wedged in the topographic section.

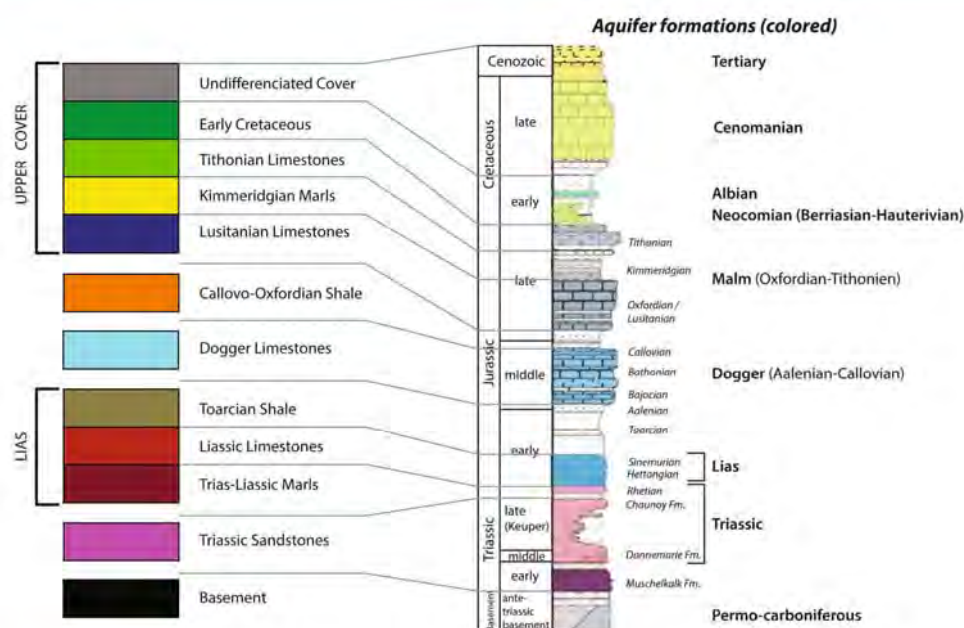


Fig. 6 Geological pile defined for the OM3D geomodel development and the corresponding levels on the stratigraphical log of the Paris Basin with the major aquifer (colored) and aquitard (uncolored) formations (modified after Delmas *et al.*³²). Some formations were grouped together to form “series” to identify aquifers and aquitards.

Pre-existing larger-scale lower-resolution 3D geological model. The surfaces of the pre-existing larger-scale lower-resolution 3D geological model corresponding to the formation tops to be modelled were integrated in the GeoModeller project.

Seismic horizons data. In GeoModeller, the seismic data import involves two steps: the broken-line cross-sections corresponding to the seismic lines were first created using their coordinates, and the picking points of the time-depth converted horizons were then integrated into the 3D software (Fig. 7).

During import, each horizon was associated with the corresponding formation of the previously created geological pile to constrain the interpolation of the formation’s geometry.

Seismic images and digitalization of fault interfaces. Aside from the tops of the formations, the Sennely fault is the second type of geological object to be modelled. The GVERSE Geophysics software does not enable the fault points to be exported because the time-depth conversion cannot be applied to this type of geological features. It was therefore necessary to adopt another approach to integrate these data into the GeoModeller in two steps: (1) georeferencing and vertical stretching of the seismic image: each seismic line including a trace of the Sennely fault was entered as a screen shot in the seismic interpretation software and then georeferenced. The key problem was to match the images of the seismic lines shot in two-way time within the OM3D geomodel cross-sections in real depth. This was accomplished using the previously integrated horizon points: interpreted seismic line images were vertically adjusted to match the horizon points projected in the cross-sections. (2) digitizing the subsurface fault interfaces: once the seismic line images were fitted to the horizons, the fault lines were digitized (Fig. 8) and the orientation data were placed according to the fault trace on the image to better constrain the fault geometry. However, the image adjustment does not allow for a perfect match of every horizon in a given cross-section. To ensure optimal stretching, a seismic line image was fitted horizon by horizon, involving several calibrations per line.

To the south-west of the OM3D geomodel, where there is no seismic data, contact points and orientation data were given by the Sennely fault digitized following Beccaletto *et al.*⁴⁰. These data points were added to the topographic section.

3D geomodel processing. The potential field method implemented in GeoModeller was used to interpolate the OM3D geomodel. This method allows to infer the geological formation for any 3D points (x,y,z), and produces a continuous geomodel (see Calcagno *et al.*³⁴ and the “Code Availability” section).

The sedimentary filling of the area to the south-west of the Paris Basin is relatively continuous, and the geological data of the Orléans region did not reveal any major discontinuity. Consequently, the ‘Onlap’ relationship was assigned to every series in the geological pile, meaning that a given series simply ‘onlaps onto’ the older ones (see the “Usage Notes” section). Likewise, the links between the Sennely fault and geological series were defined

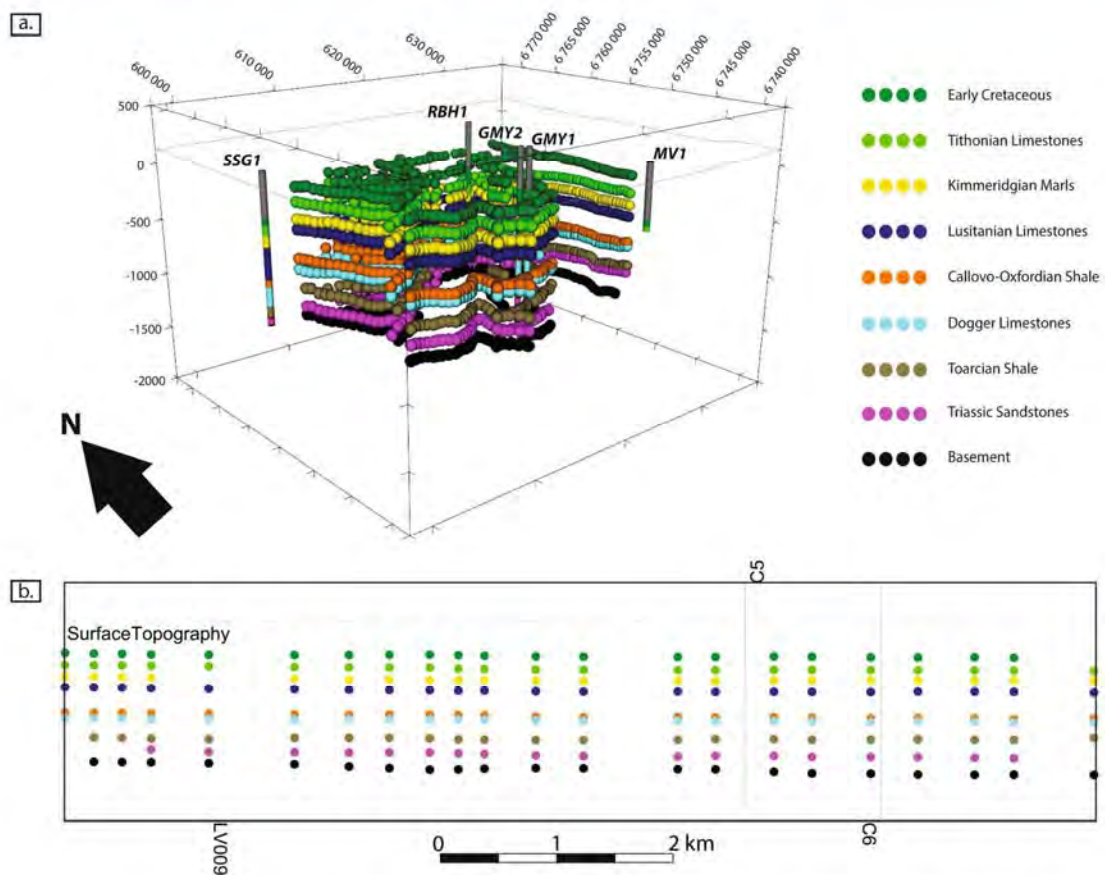


Fig. 7 (a) 3D view of the horizon picking points integrated in GeoModeller (note that the formations of the undifferentiated cover are not shown), (b) 2D view of the horizon picking points projected in the LV03 cross-section (Fig. 3; note that the formations of the undifferentiated cover series are shown). The RGF93/Lambert-93 coordinate system is used.

to state that the fault affects the whole series, as observed on the seismic lines. Moreover, the two segments of the Sennely fault included in the OM3D geomodel's domain were modelled by two finite faults to obtain a reliable representation of the relay: finite fault boundaries are modelled as elliptic surfaces, since the displacement decreases towards its limits (see Calcagno *et al.*⁵⁴ for more information). The radius of the ellipsoids was defined to match the seismic interpretation (see Fig. 5 and the "Fault identification and interpretation" part of the "Methods" section above), i.e. the extent was adjusted so that each fault segment crosses only the seismic lines where it has been observed. The parameters used in GeoModeller to constrain the finite faults are given in the Table 4.

The seismic and wells data used for the construction of the OM3D geomodel are mostly located in the north-east and in the center of the study area. Elsewhere, the formations architecture and fault geometry were constrained by the pre-existing larger-scale and lower-resolution 3D geological model: eight additional cross-sections were constructed for this purpose and additional control points were added to them. In the south-east of the OM3D geomodel, it was completed by the revised cartographic data for the delineation of the Sennely fault (see the "Geological map" part of the "Input Data" section above).

Export. Once it was determined that the OM3D geomodel is an acceptable representation of reality (see the "Technical Validation" section), it was saved in its native format and can thus be opened, visualized, or modified directly in this software (Figs. 9,10). Since GeoModeller also has geophysical and geothermal modules, further modelling processes can be performed in the software.

In addition, the OM3D geomodel was exported in several formats (see the "Usage Notes" section) with a grid cell resolution of $100\text{ m} \times 100\text{ m} \times 10\text{ m}$. These export formats can be used as base models for further modelling or simulations. A 3D PDF was produced. This format is very practical because it can be opened and accessed from most PDF reader softwares. The geomodel can be manipulated, and the geological volumes and interfaces can be shown or hidden. Therefore, this format is useful for communication purposes.

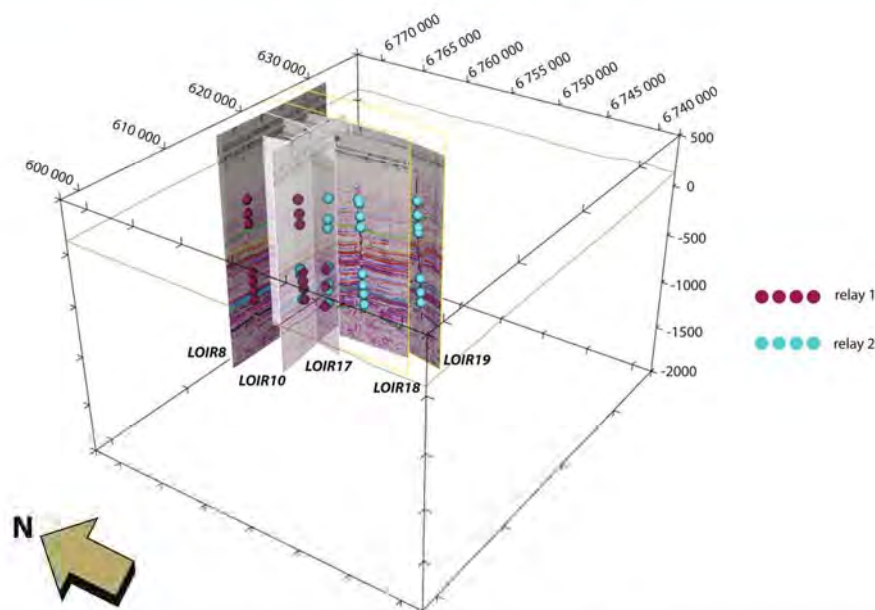


Fig. 8 3D view showing the projected seismic lines in the cross-sections and the digitized points associated with the Sennely fault. The blue and red dots show the location of the two segments of the fault. The RGF93/Lambert-93 coordinate system is used.

	Relay 1	Relay 2
Horizontal Radius (m)	7500	26000
Vertical Radius (m)	1500	2500
Influence Radius (m)	1500	5000
Center	Mean Center	User specified (x=632133.5; Y=6749049.102; Z=-1700)

Table 4. Parameters used to model the two finite faults representing the Sennely fault relay located in the OM3D geomodel extent.

3D shapes were also exported in two format types: the first one is the TSurf format that can be imported in many modeling or simulation softwares, and the second one is the ParaView VTK (i.e. Visualization ToolKit) Poly Data format that can be visualized in the open-source 3D visualization software ParaView. The formation interface surfaces can be loaded as polygonal meshes and processed by the ParaView tools.

Data Records

The OM3D geomodel⁵⁵ is recorded in the Zenodo repository under the Creative Commons Attribution 4.0 International (CC BY 4.0) license. The geomodel comes with a metadata sheet in pdf format which summarizes the technical parameters related to the model such as location, description, and contact.

The OM3D geomodel is made of 11 formations in total, grouped in six series overlapping on top of each other. Two finite faults represent the two segments of the Sennely fault crossing the study area and forming a relay (Fig. 10).

The OM3D geomodel should be considered as a “data augmentation exercise” as proposed by Thornton *et al.*²⁴. It shows how a multi-disciplinary integration allows for the knowledge of the subsurface to be refined. This work delivers a geomodel that is particularly suitable at the scale of the metropolis that can be used as a base for various future calculations, such as hydrothermal simulations. It would enable the metropolis to have a representation of its subsurface that can be updated when new data are acquired.

Technical Validation

Several considerations were taken into account during the seismic interpretation and the modelling steps to ensure the reliability of the OM3D geomodel: the quality of the input data, the methodology used for the modelling and the continuous checking of the geological plausibility of the results.

First, most of the input data, seismic lines, and boreholes, were acquired by petroleum companies between the 1960s and the 1980s. These data are particularly suitable for the identification and modelling of the main aquifers of the Orléans metropolis’ area as these companies were targeting mostly the same reservoirs. Moreover, the reprocessing techniques used for this study have improved the quality of the resulting seismic

www.nature.com/scientificdata/

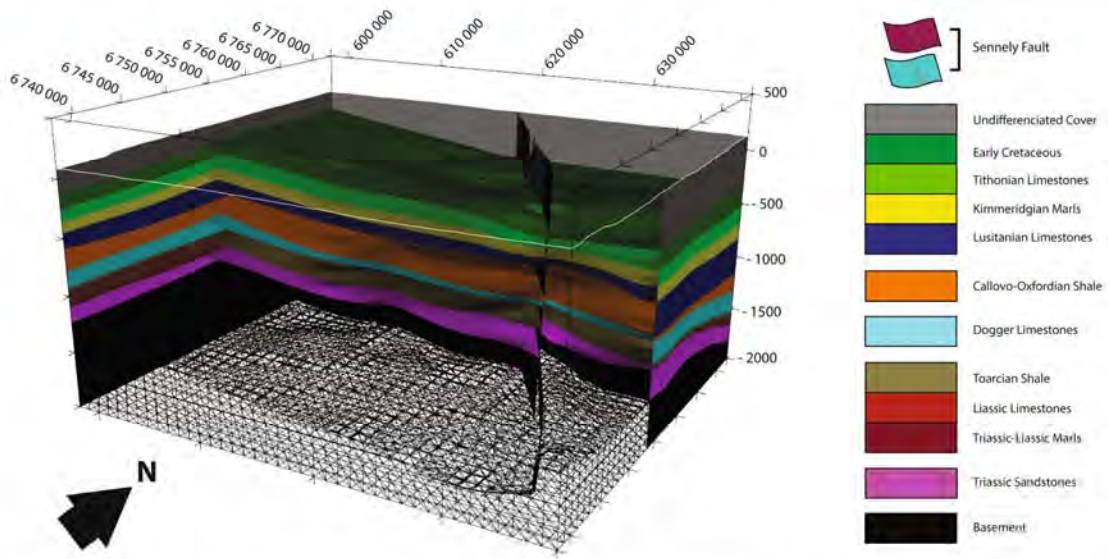


Fig. 9 View from the southwest of the OM3D geomodel in the 3D Window of GeoModeller. The RGF93/Lambert-93 coordinate system is used.

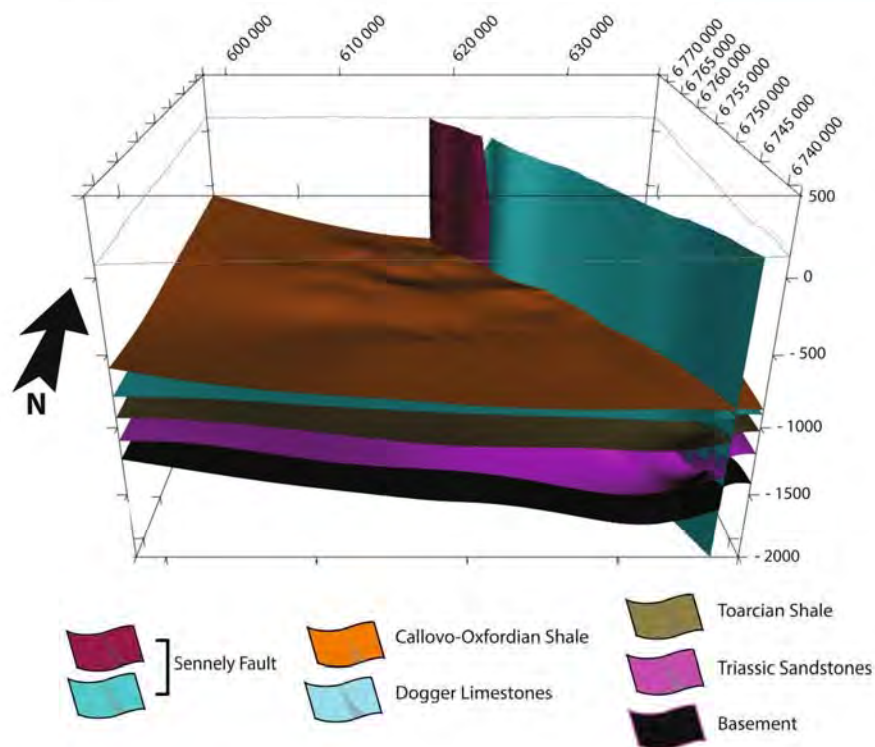


Fig. 10 View from the south of the OM3D geomodel in the 3D Window of GeoModeller showing the main aquifer formation tops; note the relay geometry of the subvertical Sennely fault. The top right inset is the topographic section of the geomodel displaying the geological map and the modelled Sennely fault on the surface. The RGF93/Lambert-93 coordinate system is used.

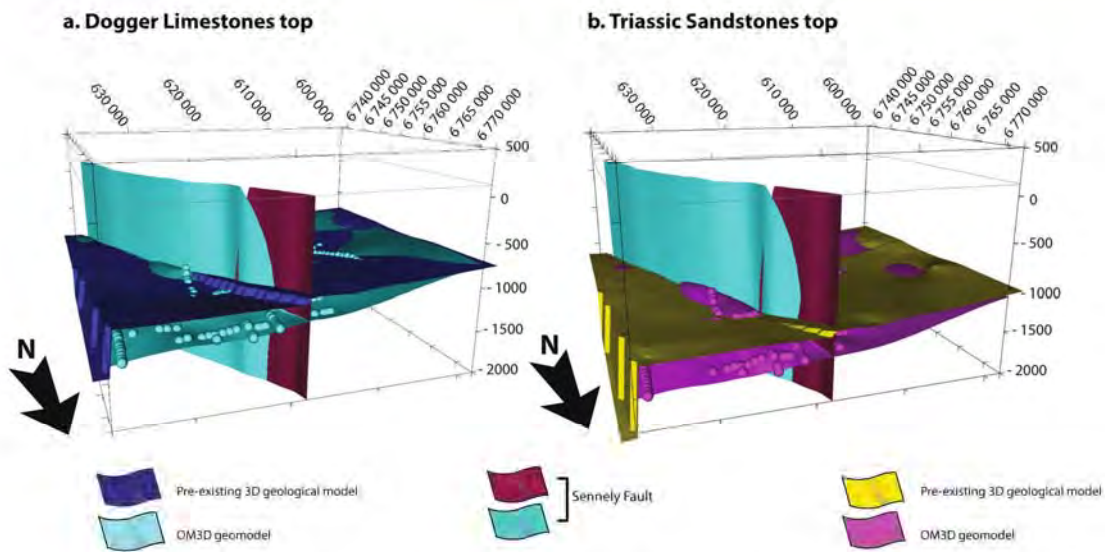


Fig. 11 Comparison between the surfaces of the Dogger Limestones (left) and the Triassic Sandstones (right) extracted from the OM3D geomodel and the pre-existing larger-scale lower-resolution 3D geological model. The dots represent the horizon picking points of the formation tops. The RGF93/Lambert-93 coordinate system is used.

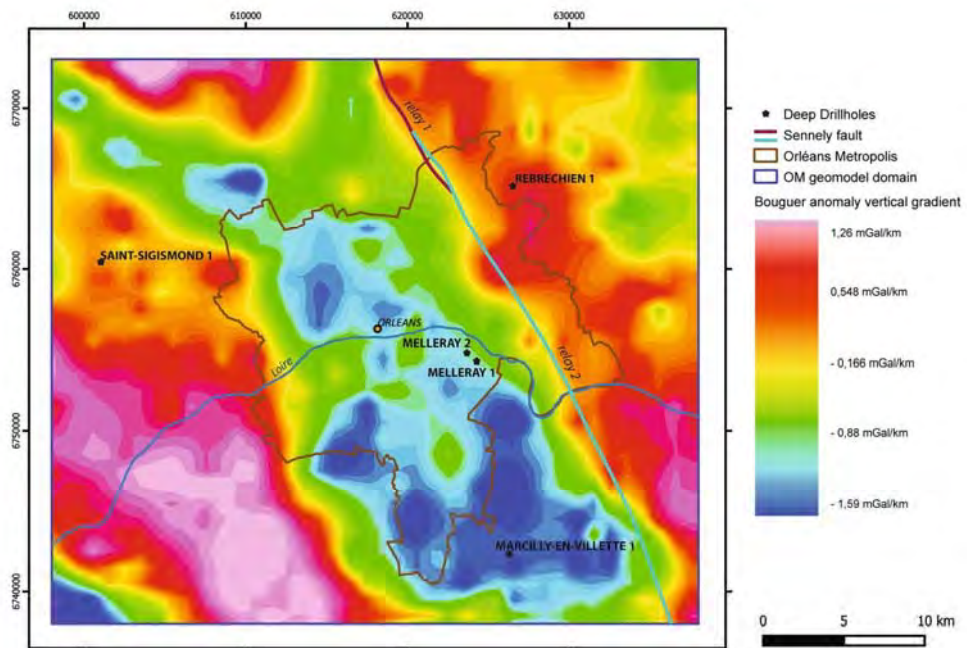


Fig. 12 The gravimetric map shows a graben structure to the south-west of the modelled area, in accordance with the structure in the OM3D geomodel. Modified after Martelet *et al.*⁵⁹. The Sennely fault trace displayed on the map originates from a section of the OM3D geomodel at a depth of 1000 m.

images, making the identification of the geological interfaces easier and more accurate compared to the original processing.

The wells are located on (or very close to) the seismic lines, and some of them have velocity surveys. This is very important (1) to display the wells in depth on the seismic lines in TWTT, and (2) to ensure the accuracy of the horizon's location in real depth for the time to depth conversion. Moreover, the geological context is

File format	Software
GeoModeller	GeoModeller, https://www.geomodeller.com
PDF 3D	Standard Adobe pdf reader, https://get.adobe.com/fr/reader/
TSurf	GocadTSurfaceReader, https://www.opengeosys.org/docs/tools/fileio/gocadtsurfacereader/
VTK	Paraview, https://www.paraview.org/download/

Table 5. OM3D geomodel file formats available on the Zenodo repository and software to read them.

very appropriate for the depth-conversion process: the layers are quite tabular and horizontal, and the structural aspect is relatively simple. Those conditions improve the reliability of the time to depth conversion⁵⁶. The interval velocity method has also been chosen as the most robust one to ensure the reliability of the horizons converted to depth. A quality control has been performed when importing the well and seismic data in the OM3D geomodel to compare the depths of the formation tops in the wells with the resulting horizons converted in depth.

Furthermore, the approach and methodology used to create the OM3D geomodel helped improve its reliability: many independent data types and datasets were integrated such as well data, seismic data, a Digital Terrain Model (DTM) and a pre-existing larger-scale and lower-resolution 3D geological model. The crossing of these data improves the consistency and reliability of the OM3D geomodel.

Regarding the validity and accuracy of the OM3D geomodel calculation by the GeoModeller software, it has been demonstrated that its algorithm correctly takes the input data into account^{24,57,58}. Consequently, the objects modelled using this methodology give a realistic description of the geology, in accordance with the input data and without creating uncertainties.

This is also ensured by the geological expertise of the operators during the modelling process, who can validate or not the results and the geomodel plausibility based on their knowledge of the geological features represented. As a consequence, the modelling of the Sennely fault is in accordance with the state of knowledge on its geometry^{38,40}.

As a result of this interdisciplinary methodology, the OM3D geomodel highlights the added value of the use of seismic data. The surfaces of the Dogger and the Triassic tops of the OM3D geomodel are better constrained thanks to the seismic data which improve the location of these geological interfaces. They appear deeper than those of the pre-existing larger-scale and lower-resolution 3D geological model in the north-east corner which is, as a reminder, the only one covering this study area and with a larger scale. This difference can reach 500 m in depth but is very local (Fig. 11). Another improvement of the OM3D geomodel concerns the northern part of the Sennely fault. From a structural point of view, the OM3D geomodel gives a more detailed representation of the Sennely fault with a better-defined geometry which is also consistent with the geological reality of late Variscan faults (Fig. 11).

In another validation phase, the OM3D geomodel was compared with a gravimetric survey. Gravimetry is a geophysical method for detecting variations in gravity, which can be related to variations in the density of deposits. Negative gravimetric anomalies represent density deficits, corresponding to cavities or lighter geological formations. Positive gravimetric anomalies represent excesses of density, corresponding to the presence of minerals, faults or massive terrain rising close to the surface.

A vertical gradient of the vertical anomaly map from Martelet *et al.*⁵⁹ (Fig. 12) shows negative anomalies to the south-east of the modelled area which could be explained by both the deepening of the basement and the over-thickness of the overlying sedimentary series in relation to the westward downthrow of the Sennely normal fault offset²⁷. From a structural point of view, this can be interpreted as a regional horst and graben structure: the NW-SE axis horst is delimited between the Sennely and Etampes-Rambouillet faults and a semi-graben is located to the west of the Sennely fault.

A sedimentary thickening is present in the south-west of the OM3D geomodel, in accordance with the gravimetric map (Figs. 9,10). Even if the gravimetric map and the OM3D geomodel give a representation of two different objects (the basement for the former and the sedimentary cover for the latter), they show similar trends and features, validating the accuracy of the OM3D geomodel at a large scale.

Some challenges were encountered during the development of the OM3D geomodel. Its limitations are mainly based on the distribution and density of the primary data: there are fewer seismic or borehole data in the north-west, south-west and south-east corners of the OM3D geomodel and within the metropole; as a consequence, a pre-existing larger-scale lower-resolution 3D geological model, which is a result of a prior interpretation work, was used to constrain the OM3D geomodel. Lastly, the ideal technical validation would be new drilling operations to check and assess the reliability and specify the OM3D geomodel since no data have been withheld, as discussed in Thornton *et al.*²⁴.

Usage Notes

Formats. The geomodel available in the Zenodo repository is in the original GeoModeller format, PDF 3D, TSurf, and VTK. The file formats can be read using the tools listed in Table 5.

Code availability

GeoModeller. GeoModeller is a proprietary software developed by the French Geological Survey (BRGM) in collaboration with Intrepid Geophysics. It has been designed for three-dimensional interpretation and modelling based on the integration of various types of data, such as field observations and geophysical measurements. The calculation of the model is based on geological rules. These rules are defined in a geological pile that manages the

relationships between the geological formations to be modelled⁵⁴. Data are associated with formations and faults to constrain their geometry. The modelling of these geological objects relies on the interpolation of the input data. GeoModeller's interpolation method produces a scalar field where iso-values represent the geological interfaces. The scalar field is interpolated by co-kriging two types of data: (1) 3D points that are the location of observed or interpreted geological interfaces and faults, and (2) orientation data that are 3D vectors representing the dip of geological formations. These two types of data are respectively associated with the iso-values and the gradients of the scalar field to be interpolated^{54,60}. GeoModeller also enables direct and inverse geophysical calculations to improve and refine the geomodels⁶¹.

For further information, see: <https://www.geomodeller.com>

The GeoModeller version used for this study is the following:

GeoModeller Version: 4.0.7

Build Date: May 22, 2019

Build Number: 27eee3dc31ba

The default parameters of GeoModeller were used for the interpolation of the geomodel presented in this paper.

Received: 15 November 2021; Accepted: 30 November 2022;

Published online: 24 December 2022

References

- Houlding, S. *3D geoscience modeling: computer techniques for geological characterization*. (Springer-Verlag, 1994).
- Jones, R. *et al.* Integration of regional to outcrop digital data: 3D visualisation of multi-scale geological models. *Comput. Geosci.* **35**, (2009).
- Pan, D., Xu, Z., Lu, X., Zhou, L. & Li, H. 3D scene and geological modeling using integrated multi-source spatial data: Methodology, challenges, and suggestions. *Tunn. Undergr. Space Technol.* **100**, (2020).
- Sala, P., Frehner, M., Tisato, N. & Pfiffner, O. A. Building a three-dimensional near-surface geologic and petrophysical model based on borehole data: A case study from Chémery, Paris Basin, France. *AAPG Bull.* **97**, 1303–1324 (2013).
- Keith Turner, A., Kessler, H. & van der Meulen, M. *Applied Multidimensional Geological Modeling: Informing sustainable human interactions with the shallow subsurface.*, <https://doi.org/10.1002/9781119163091> (Wiley, 2021).
- Dong, M., Neukum, C., Hu, H. & Azzam, R. Real 3D geotechnical modeling in engineering geology: a case study from the inner city of Aachen, Germany. *Bull. Eng. Geol. Environ.* **74**, 281–300 (2015).
- Lelliott, M. R., Bridge, D. M. C., Kessler, H., Price, S. J. & Seymour, K. J. The application of 3D geological modelling to aquifer recharge assessments in an urban environment. *Q. J. Eng. Geol. Hydrogeol.* **39**, 293–302 (2006).
- Robins, N. S., Davies, J. & Dumbleton, S. Groundwater flow in the South Wales coalfield: historical data informing 3D modelling. *Q. J. Eng. Geol. Hydrogeol.* **41**, 477–486 (2008).
- Boon, D., Dellow, G., Van Dissan, R., Perrin, N. & Rattenbury, M. Advancement of 3D modeling methodologies for seismic hazard assessment: a study of potential site effects in the Lower Hutt Basin, New Zealand. *Geophys. Res. Abstr.* **15**, (2013).
- Sbrana, A., Fulignati, P., Marianelli, P. & Ciani, V. Mt. Amiata hydrothermal system (Italy): 3D geological and geothermal modeling. *Ital. J. Geosci.* **134**, 291–303 (2015).
- Lipparini, L., Trippetta, F., Ruggieri, R., Brandano, M. & Romi, A. Oil distribution in outcropping carbonate-ramp reservoirs (Maiella Mountain, Central Italy): Three-dimensional models constrained by dense historical well data and laboratory measurements. *AAPG Bull.* **102**, 1273–1298 (2018).
- Klapperer, S., Moeck, I. & Norden, B. Regional 3D geological modeling and stress field analysis at the CO₂ storage site of Ketzin, Germany. *Trans. Geotherm. Resour. Coun.* **35**, 419–423 (2011).
- Branscombe, P. & MacCormack, K. Delivering to the client; communication and delivery for successful application of 3D models. *Workshop extended abstracts: Illinois State Geological Survey*, 24–27, 2142/101426 (2018).
- Laplaige, P. *et al.* Geothermal resources in France. Current situation and prospects. in *Proceedings world geothermal congress 24–29* (2005).
- Lopez, S. *et al.* 40 years of Dogger aquifer management in Ile-de-France, Paris Basin, France. *Geothermics* **39**, 339–356 (2010).
- Fabriol, H. *et al.* *Géocarbonate Monitoring. Rapport Final*. Report No. BRGM/RP-56640-FR (Bureau de Recherches Géologiques et Minières, 2008).
- Fabriol, H. *et al.* Results of investigations to design a monitoring program for a CO₂ storage project in the Paris Basin (France). *Energy Procedia* **1**, 2285–2291 (2009).
- Kervevan, C. GEOCO₂. <https://co2-dissolved.brgm.fr/page/geoco2> (2019).
- Salquière, D., Husson, F., Jozja, N., Klinka, T. & Tourlière, B. *Système d'Information pour la Gestion des Eaux Souterraines (SIGES) en région Centre-Val de Loire - Bilan de la phase 3 (2017–2019)*. Report No. BRGM/RP- 69591-FR (Bureau de Recherches Géologiques et Minières, 2019).
- Bugarel, E., Salquière, D. & Hamm, V. *Etude du potentiel de la géothermie profonde sur le territoire d'Orléans Métropole - Volet 1: conditions d'accès à la ressource (modèle du Dogger en région Ile-de-France) et retours d'expérience sur les opérations au Trias*. Report No. BRGM/RP-69450-FR (Bureau de Recherches Géologiques et Minières, 2019).
- Caritg, S. *et al.* *Rapport de synthèse: calculs de pré-dimensionnement d'une installation CO₂-DISSOLVED sur le site Orvaède (Saran, France). Rapport final (Confidentiel)*. Report No. BRGM/RP-71518-FR (Bureau de Recherches Géologiques et Minières, 2022).
- Hamm, V., Capar, L., Mas, P., Calcagno, P. & Caritg-Monnot, S. Characterisation of the Dogger and Trias deep resources in Orleans Metropolis, Centre-Val de Loire region, France: 3D geomodel and first geothermal potential assessment. in EGU General Assembly 2021, <https://doi.org/10.5194/egusphere-egu21-14465> (2021).
- Capar, L., Hamm, V., Mas, P., Calcagno, P. & Caritg-Monnot, S. *Etude du potentiel de la géothermie profonde sur le territoire d'Orléans Métropole - Volet 2: réalisation d'un modèle géologique 3D du Dogger et Trias et évaluation du potentiel géothermique - Rapport final - BRGM/RP-70363-FR*. Report No. BRGM/RP-70363-FR (Bureau de Recherches Géologiques et Minières, 2020).
- Thornton, J. M., Mariethoz, G. & Brunner, P. A 3D geological model of a structurally complex Alpine region as a basis for interdisciplinary research. *Sci. Data* **5**, 180238 (2018).
- Calcagno, P., Trumpy, E., Gutiérrez-Negrín, L. C. & Liotta, D. A collection of 3D geomodels of the Los Humeros and Acoculco geothermal systems (Mexico). *Sci. Data* **9**, 280 (2022).
- Megnien, C. & Megnien, E. *Synthèse Géologique du Bassin de Paris. Volume I. Stratigraphie et paléogéographie*. (Bureau de Recherches Géologiques et Minières, 1980).
- Baptiste, J. *et al.* Mapping of a buried basement combining aeromagnetic, gravity and petrophysical data: The substratum of southwest Paris Basin, France. *Tectonophysics* **683**, 333–348 (2016).
- Stampfli, G. & Marchant, R. Geodynamic evolution of the Tethyan margins of the Western Alps. in (1997).
- Guillocheau, E. *et al.* Meso-Cenozoic geodynamic evolution of the Paris Basin: 3D stratigraphic constraints. *Geodin. Acta* **13**, 189–245 (2000).

30. Briais, J. Le Cénozoïque du bassin de Paris: un enregistrement sédimentaire haute résolution des déformations lithosphériques en régime de faible subsidence. (Université Rennes 1, 2015).
31. Robin, C. Stratigraphic measurement of deformation; application to Jurassic evolution of the Paris Basin. *Mém. Géosciences Rennes* (1997).
32. Delmas, J., Houel, P. & Vially, R. *Paris Basin, Petroleum potential* (IFP regional report, 2002).
33. Perrodon, A. & Zabeck, J. Paris Basin: Chapter 32: Part II. Selected Analog Interior Cratonic Basins: Analog Basins. *AAPG Spec. Vol.* **134**, 633–679 (1990).
34. Bouchot, V., Badet, A.-G., Bialkowski, A. & Bonté, D. *CLASTIQ-2: programme de recherche sur les ressources géothermales des réservoirs clastiques en France (Bassin de Paris et Fossé Rhénan) - Rapport final*. Report No. BRGM/RP-61472-FR (Bureau de Recherches Géologiques et Minières, 2012).
35. Lenoir, F. *et al.* Seismic study of the Jurassic deformation and sedimentation of the southwestern Paris basin: a low subsiding domain transition to the Aquitaine basin. *Bull. Société Géologique Fr.* **185**, 191–204 (2014).
36. Carity-Monnot, S., Bourguin, B., Foissard, D. & Lopez, S. *Evaluation du potentiel géothermique du Lusitanien du bassin de Paris pour la production de chaleur: mise en adéquation entre ressource et besoins*. Report No. BRGM/RP-63244-FR (Bureau de Recherches Géologiques et Minières, 2014).
37. Lasseur, E. La Craie du Bassin de Paris (Cénomaniens-Campanien, Crétacé supérieur). Sédimentologie de faciès, stratigraphie séquentielle et géométrie 3D. (Université Rennes 1, 2007).
38. Héritier, F. & Villemin, J. Evidence of deep tectonics in the Paris Basin from petroleum exploration. *Bull. Bur. Rech. Geol. Min. Sect. 1 Geol. Fr.* **2**, 11–30 (1971).
39. Beccaletto, L., Capar, L., Serrano, O. & Marc, S. Structural evolution and sedimentary record of the Stephano-Permian basins occurring beneath the Mesozoic sedimentary cover in the southwestern Paris basin (France). *Bull. Société Géologique Fr.* **186**, 429–450 (2015).
40. Beccaletto, L., Hanot, F. & Robelin, C. *Cartographie structurale et caractérisation des failles majeures dans le Bassin de Paris (Confidentiel)*. Report No. BRGM/RP-56305-FR (Bureau de Recherches Géologiques et Minières, 2008).
41. BRGM Bureau de Recherches Géologiques et Minières. Banque du sous-sol (BSS). <http://infoterre.brgm.fr/page/banque-sol-bss>.
42. BRGM Bureau de Recherches Géologiques et Minières. BD Charm-50 | InfoTerre. <http://infoterre.brgm.fr/formulaire/telechargement-cartes-geologiques-departementales-150-000-bd-charm-50>.
43. BRGM Bureau de Recherches Géologiques et Minières. Bd Million-Géol | InfoTerre. <http://infoterre.brgm.fr/formulaire/telechargement-carte-geologique-metropolitaine-11-000-000>.
44. IGN Institut National Géographique. BD ALTI® Digital Terrain Model. <https://geoservices.ign.fr/documentation/diffusion/telechargement-donnees-libres.html#les-modeles-num%C3%A9riques-3d>.
45. BRGM Bureau de Recherches Géologiques et Minières. Minergies. <http://www.minergies.fr/fr>.
46. Beccaletto, L., Hanot, F., Serrano, O. & Marc, S. Overview of the subsurface structural pattern of the Paris Basin (France): Insights from the reprocessing and interpretation of regional seismic lines. *Mar. Pet. Geol.* **28**, 861–879 (2011).
47. Laurent, A. *et al.* 3-D Structure of the Variscan Thrust Front in Northern France: New Insights From Seismic Reflection Profiles. *Tectonics* **40**, (2021).
48. Yilmaz, Ö. & Doherty, S. M. *Seismic data processing*. (Society of Exploration Geophysicists, 1987).
49. Yilmaz, Ö., Doherty, S. M. & Yilmaz, Ö. *Seismic data analysis: processing, inversion, and interpretation of seismic data*. (Society of Exploration Geophysicists, 2001).
50. Barry, K. M., Cavers, D. A. & Kneale, C. W. Recommended standards for digital tape formats. *Geophysics* **40**, 344–352 (1975).
51. LMK Resources Inc. GVERSE Geophysics. <https://www.gverse.com/ProductPackages/geophysics>.
52. Thion, I. *Projet Picoref - Interprétation sismique - Rapport intermédiaire*. Report No. BRGM/RP-55632-FR (Bureau de Recherches Géologiques et Minières, 2007).
53. Dentzer, J. *et al.* Thermal and seismic hints for chimney type cross-stratal fluid flow in onshore basins. *Sci. Rep.* **8**, 15330 (2018).
54. Calcagno, P., Chilès, J. P., Courrioux, G. & Guillen, A. Geological modelling from field data and geological knowledge: Part I. Modelling method coupling 3D potential-field interpolation and geological rules. *Phys. Earth Planet. Inter.* **171**, 147–157 (2008).
55. Mas, P. *et al.* A 3D geomodel of the deep aquifers in the Orléans area of the southern Paris Basin (France). *Zenodo* <https://doi.org/10.5281/zenodo.5643266> (2022).
56. Jardin, A., Rakotoarisoa, H., Broto, K. & Thibaut, M. Pitfalls in Seismic Time to Depth Conversion for Geological Modelling. in *cp-22-00020*, <https://doi.org/10.3997/2214-4609.201403036> (European Association of Geoscientists & Engineers, 2006).
57. Meixner, A. J., Lane, R., Czarnota, K. & Cassidy, K. Constructing geologically-constrained 3D models using 3D Geomodeler: An example from the Paterson Orogen. Report No. 2006/20 (Geoscience Australia, (2006).
58. Olaniran, O., Smith, R. S. & Lafrance, B. Regional 3D geophysical investigation of the Sudbury Structure. *Interpretation* **3**, SL63–SL81 (2015).
59. Martelet, G., Pajot, G. & Debeglia, N. *Nouvelle carte gravimétrique de la France; RCGF09 - Réseau et Carte Gravimétrique de la France, 2009*. Report No. BRGM/RP-57908-FR (Bureau de Recherches Géologiques et Minières, 2009).
60. Lajaunie, C., Courrioux, G. & Manuel, L. Foliation fields and 3D cartography in geology: Principles of a method based on potential interpolation. *Math. Geol.* **29**, 571–584 (1997).
61. Guillen, A., Calcagno, P., Courrioux, G., Joly, A. & Ledru, P. Geological modelling from field data and geological knowledge. *Phys. Earth Planet. Inter.* **171**, 158–169 (2008).

Acknowledgements

The work was conducted as part of the “Contribution du BRGM au développement de la géothermie sur le Territoire d’Orléans Métropole” project led by Alain Saada and co-funded by Orléans Métropole and the BRGM (French Geological Survey), contract n M18348G. Seismic line reprocessing was enabled through collaboration with the GEOCO2 project led by Christophe Kervevan, conducted by the BRGM and co-funded by the Centre-Val de Loire (CVL) Region. The field seismic data used in the paper are publicly available at <http://www.minergies.fr/fr>. The authors gratefully acknowledge Stéphane Marc for his valuable work regarding the retrieving of the seismic data and the reviewers for their careful reading and constructive comments that significantly improved the manuscript and the English style.

Author contributions

Perrine Mas: seismic interpretation, 3D modelling work, writing – original draft. Philippe Calcagno: supervision, advice on data processing and geomodelling, writing – original draft, supervision. Séverine Carity-Monnot: realization and evaluation of the 3D geomodel, writing – review and editing. Laurent Beccaletto: advice on seismic lines interpretation, writing – Outline of the geology of the Paris Basin and Tectonic Setting in the Orléans area, time-depth conversion methodology. Laure Capar: reprocessing of the seismic lines, advice on the seismic interpretation, writing – review and editing. Virginie Hamm: supervision, evaluation of the 3D geomodel, its preparation for hydrothermal simulations, writing – review and editing.

www.nature.com/scientificdata/

Competing interests

The authors declare no competing interests.

Additional information

Correspondence and requests for materials should be addressed to P.M.

Reprints and permissions information is available at www.nature.com/reprints.

Publisher's note Springer Nature remains neutral with regard to jurisdictional claims in published maps and institutional affiliations.



Open Access This article is licensed under a Creative Commons Attribution 4.0 International License, which permits use, sharing, adaptation, distribution and reproduction in any medium or format, as long as you give appropriate credit to the original author(s) and the source, provide a link to the Creative Commons license, and indicate if changes were made. The images or other third party material in this article are included in the article's Creative Commons license, unless indicated otherwise in a credit line to the material. If material is not included in the article's Creative Commons license and your intended use is not permitted by statutory regulation or exceeds the permitted use, you will need to obtain permission directly from the copyright holder. To view a copy of this license, visit <http://creativecommons.org/licenses/by/4.0/>.

© The Author(s) 2022

Ressource en eau - Caractérisation d'un système karstique dans la craie du sud du bassin de Paris

Je présente ici les résultats tirés de la publication suivante (thèse de P.-A. Reninger):

Reninger P-A., Martelet G., Lasseur E., **Beccaletto L.**, Deparis J., Perrin J., Chen Y. (2014) Geological environment of karst within chalk using airborne time domain electromagnetic data cross-interpreted with boreholes, Journal of Applied Geophysics. <https://doi.org/10.1016/j.jappgeo.2014.04.020>

Cette étude montre l'intérêt de croiser des informations géologiques de surface (cartes géologiques) et de subsurface (forages et profils sismiques) avec les données issues d'un levé hélicoptéré électromagnétique (TDEM, Time Domain Electro Magnetic) pour imager des hétérogénéités plurikilométriques de l'aquifère de la craie dans le sud du bassin de Paris (Courtenay ; Figure 31). Cela permet ensuite de discuter de leurs implications pour le développement du système karstique local et son comportement hydrogéologique ; en effet ce dernier dépend des propriétés pétrophysiques de la craie qui est localement fortement altérée et karstifiée.

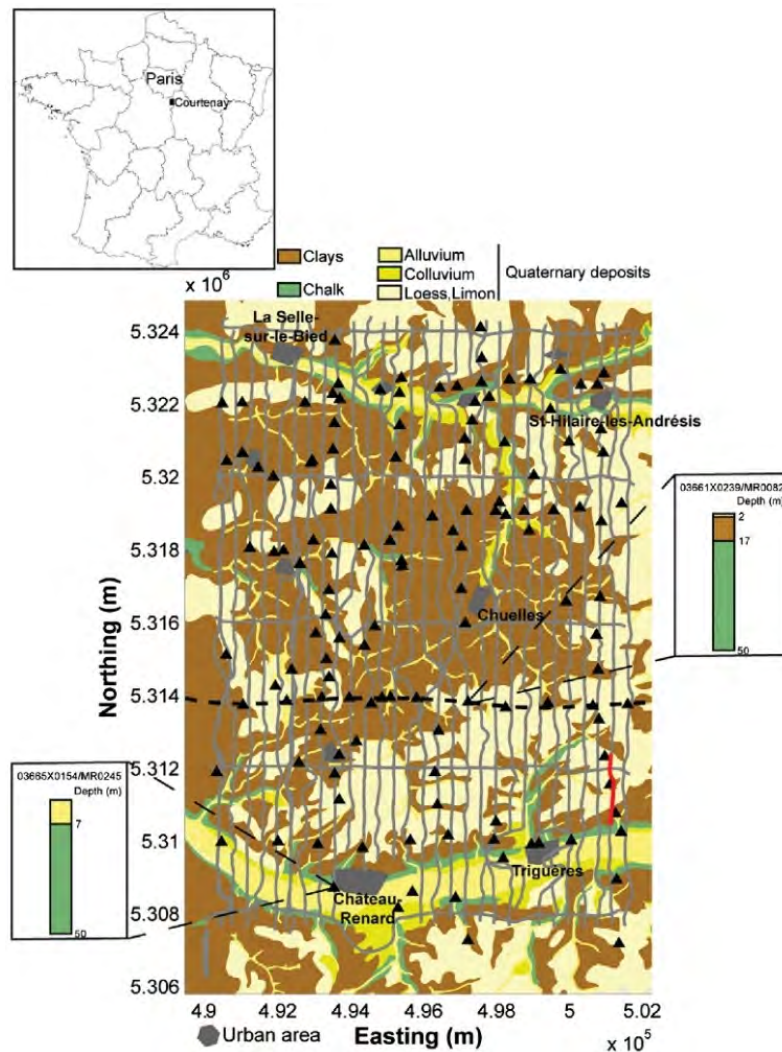


Figure 31 - Carte géologique simplifiée de la zone d'étude ; les lignes de vol de l'acquisition TDEM sont représentées en gris ; triangles noirs : forages ; ligne noire en pointillés : une des lignes sismiques interprétées (** Reninger et al., 2014).

De nombreux forages et plusieurs profils sismiques ont été utilisés pour contraindre les interprétations TDEM, qui donnent quant à elles des informations sur les variations de résistivité dans le sous-sol. Je suis intervenu pour interpréter ces profils en ciblant divers horizons géologiques et les nombreuses failles présentes dans le secteur (Figure 32), et en tirer un schéma structural local. Les failles sont orientées NS et leur prolongation vers la surface est corrélée avec les variations topographiques du secteur (à noter qu'aucune faille n'est connue en surface sur la carte géologique au 1 :50000^{ème}). Ces failles sont aussi et surtout corrélées avec des zones dans la craie de résistivité intermédiaire (traitement et de l'interprétation des données TDEM).

Ces zones de résistivité intermédiaire sont interprétées en terme d'altération de la craie due à l'activité des failles (couloirs d'érosion), ce qui permet par ailleurs d'affiner le réseau de failles dans les 150 premiers mètres (i.e. la profondeur d'investigation de l'EM, complémentaire de celle de la sismique industrielle, qui est plus profonde).

Il a ensuite été possible d'imager des géométries en ondulation à grande échelle dans la craie orientées SO-NE, direction cohérente dans tout le bassin de Paris (e.g. Quine et Bosence, 1991). Il apparaît que ces géométries ont révélé dans la région de Courtenay deux dépôts crayeux distincts C1 et C2 en terme de résistivité, C1 est plus résistant que C2.

Enfin, le modèle de résistivité a été comparé aux mesures piézométriques acquises dans le cadre d'études hydrologiques antérieures sur le secteur de Courtenay, ce qui permet de proposer un cadre géologique pour le développement de son système karstique: en effet le drainage karstique semble se développer dans le dépôt de craie C1 et la plupart des dômes piézométriques semblent être associés à des zones de résistivité intermédiaire dans C1, interprétées comme altérées.

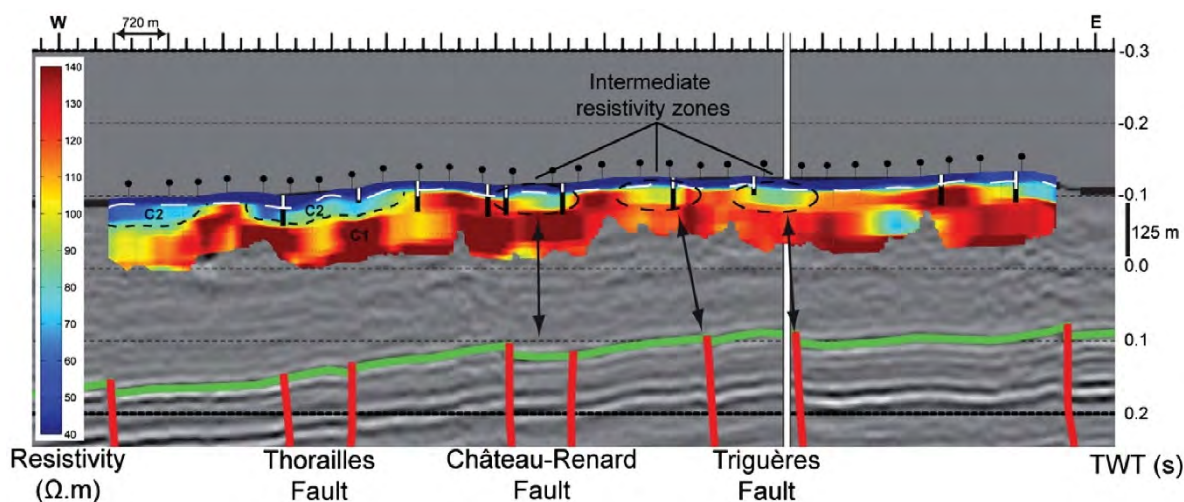
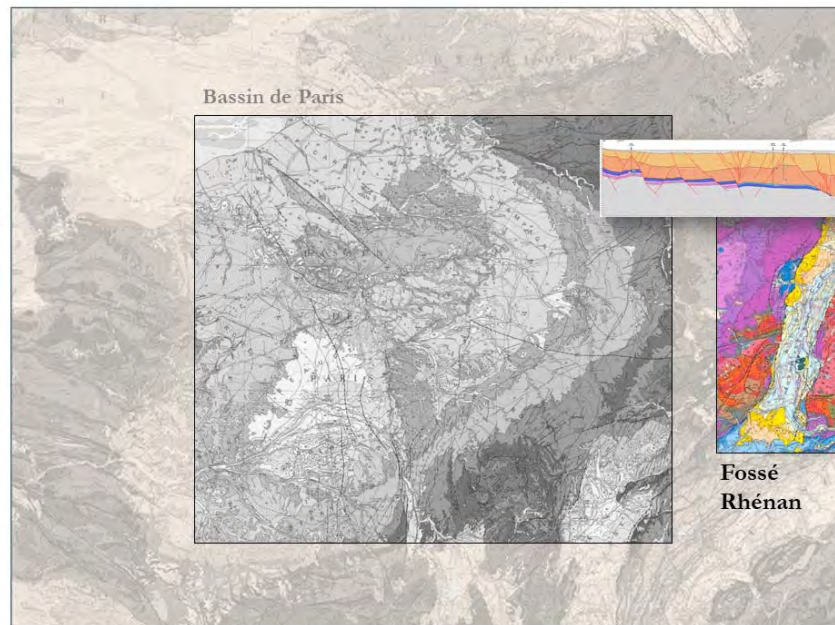


Figure 32 - Comparaison entre un profil de résistivité et la ligne sismique E-O (localisation sur la Figure 31). Les forages situés à une distance de 50 m du profil sont également représentés. Les argiles sont représentées en blanc dans les forages et la craie en noir. Les lignes pointillées blanches et noires représentent le sommet interprété de la craie et l'interface entre C1 et C2 respectivement. Les contours noirs en pointillés et les flèches noires mettent en évidence les zones de résistivité intermédiaire et leur lien suggéré avec les failles interprétées en sismique (** Reninger et al., 2014).

4.2. Le fossé Rhénan



4.2.1. Cadre collaboratif

J'ai inauguré mes travaux sur le fossé Rhénan en participant de 2009 à 2013 au projet européen GeORG (programme Interreg IV). Ce projet transfrontalier sur le potentiel géologique profond du fossé Rhénan (géothermie, stockage du CO₂) a impliqué une trentaine de collègues français, allemands et suisses représentant nombres de disciplines des Géosciences. Le livrable principal était un mapserver public (<https://maps.geopotenziale.eu>) basé sur un modèle géologique 3D, lui-même s'appuyant sur l'interprétation de plus de 5000 km de profils sismiques, tâche pour laquelle j'étais responsable (supervision de 7 géologues), en complément de ma responsabilité de géologue référent pour la France. La fin du projet GeORG en 2013 a correspondu avec le lancement du programme Référentiel Géologique de la France (RGF) du BRGM, et de son démonstrateur Vosges-fossé Rhénan. Nous avons alors travaillé au sein de mon unité Géologie des Bassins Sédimentaires sur la géométrie et le contrôle structural des dépôts syn-rifts du fossé (2013-2014). Je suis actuellement impliqué dans l'encadrement de la thèse de L. Tchang-Tchong qui travaille sur la modélisation thermique des séries pré- syn- et post-rifts du fossé à partir de la géochimie de la matière organique (collab. Géoresources Nancy).

4.2.2. Problématique scientifique et appliquée

La région de Pechelbronn située dans le nord du fossé Rhénan entre Haguenau et Wissembourg résume à elle seule les enjeux industriels et scientifiques qui le caractérisent. C'est tout d'abord, historiquement, une terre d'exploration-production d'hydrocarbures (e.g. le champ de Pechelbronn ; Schwarz, 2021). C'est aussi un champ géothermal étudié depuis la fin du 19^{ème} siècle, siège aujourd'hui de l'usine géothermique de Soultz-Sous-Forêts qui produit de l'électricité à partir de forages atteignant un granite varisque à plus de 5000 m de profondeur (Gérard et Kappelmeyer, 1987). Plus récemment, toujours dans le même secteur, des recherches sont activement menées

pour extraire du lithium des saumures géothermales (Fries et al., 2022). Sans compter l'intérêt croissant des industriels du fossé Rhénan pour le stockage de CO₂ en aquifères profonds. L'exploration puis l'exploitation du sous-sol profond pour produire de l'électricité peut aussi se traduire par des risques importants de sismicité induite (e.g. le site Fonroche de Vendenheim). Le rappel de ces quelques faits montre à quel point la mise à jour de la connaissance géologique du sous-sol profond du fossé Rhénan est un sujet d'actualité.

De nombreux travaux ont été menés sur le remplissage et la dynamique sédimentaire du fossé (e.g. Blanc-Valleron, 1991 ; Düringer, 1988 ; Roussé, 2006). Plus récemment les études ont ciblé les relations substratum granitique - couverture sédimentaire (Vidal, 2017 ; Aicholzer, 2019). La fracturation a la plupart du temps été étudiée à l'échelle du secteur de Soultz-Sous-Forêts (Valley, 2007; Dylkowski, 1985). De rares études basées sur l'interprétation de profils sismiques industriels ont caractérisé la structuration syn- ou post-rift (Rotstein et Schaming, 2008, 2011), mais le schéma structural du fossé n'avait pas été mis à jour depuis la années 1970-80 (Illies et Grener, 1979 ; Villemin, 1986). Par ailleurs, les anomalies thermiques du fossé ont aussi été largement investiguées en raison de leur importance pour l'exploration géothermique, mais plutôt en termes de processus et de compréhension des circulations actuelles des fluides chauds (e.g. Bailleux et al., 2013 ; Guillou-Frottier et al., 2013 ; Armandine-Les-Landes et al., 2019 ; Freymark et al., 2019).

Mon activité de recherche sur le fossé Rhénan a par conséquent consisté (i) à redéfinir son schéma structural d'ensemble à partir de l'interprétation de profils sismiques et en tirer des enseignements remettant en cause son cadre tectonique général, et (ii) comprendre son évolution thermique régionale avant et pendant le rifting, c'est-à-dire sur le temps long.

4.2.3. Contexte géologique du fossé Rhénan

Le fossé Rhénan (ou « Upper Rhine Graben », URG) appartient au système de rifts cénozoïques européens (« European Cenozoic Rift System », ECRIS ; Figure 33), long de 1100 km et initié à l'Éocène, et s'étendant de la mer du Nord à la Méditerranée occidentale (Dèzes et al., 2004). Le fossé Rhénan, d'orientation NNE-SSO, s'étend sur 300 km du Massif Rhénan au nord jusqu'au Jura au sud. Sa géométrie actuelle correspond à un ensemble de demi-grabens asymétriques et antithétiques, reliés par des zones de transfert héritées des structures paléozoïques varisques (Schumacher, 2002; Derer et al., 2003; Roussé, 2006; Hinsken et al., 2007; Grimmer et al., 2017). Son développement a été contrôlé par les dynamiques orogéniques pyrénéennes et alpines (Schumacher, 2002; Dèzes et al., 2004), se traduisant par une évolution tectonique polyphasée associée à une phase de sédimentation syn-rift passant à un remplissage post-rift (Laubscher, 1987; Sissingh, 1998, 2006; Schumacher, 2002).

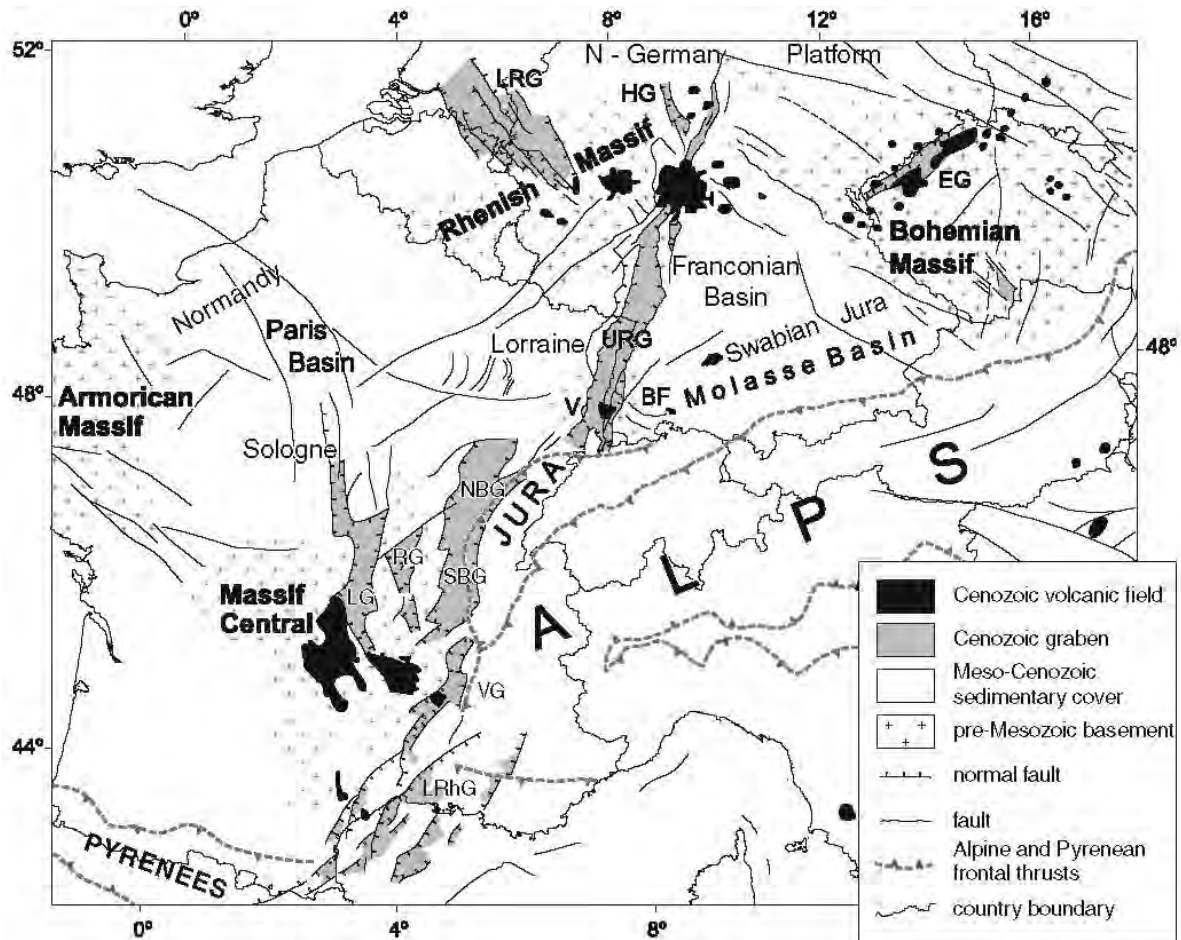


Figure 33 - Schéma structural de l'ECRIS (Modifié de Dèzes et al. (2004) dans Bourgeois et al., 2007) ; BF Black Forest, EG Eger Graben, FP Franconian Platform, HG Hessian grabens, LG Limagne Graben, LRG Lower Rhine (Roer Valley) Graben, LRhG Lower Rhône; Grabens, NBG Northern Bresse Graben, RG Roanne Graben, SBG ; Southern Bresse Graben, URG Upper Rhine Graben, V Vosges, VG ; Valence Graben.

Evolution pré-rift du fossé Rhénan

Le substratum paléozoïque du fossé Rhénan est issu de l'orogène Varisque (Edel et Fluck, 1989; Lardeaux et al., 2014). Au cours du Carbonifère terminal et du Permien inférieur, la région a subi l'effondrement de l'orogène varisque (Schumacher, 2002; Ziegler et Dèzes, 2005), accompagnée du dépôt de sédiments clastiques continentaux dans des bassins extensifs (bassins du Kraichgau ; Boigk et Schöneich, 1970; voir le volet 2). L'héritage varisque sur la structuration tertiaire du fossé Rhénan est bien documenté (Edel et al., 2007, Schumacher, 2002). Depuis la fin du Permien jusqu'au Jurassique moyen au moins, cette région a subi ensuite une subsidence thermique post-orogénique, à l'égal du bassin de Paris et de la plate-forme franconienne (section 4.1.3 ; Cloethingh et Ziegler, 2007).

Les premiers dépôts mésozoïques sont principalement représentés par les grès fluviaux discordants du Buntsandstein (Bourquin et Guillocheau, 1996), évoluant vers les faciès argileux, calcaires et dolomitiques du Trias moyen (faciès Muschelkalk; Ménillet et al., 2015). Au Trias supérieur, la sédimentation évolue vers des dépôts évaporitiques (faciès Keuper) lié à la régression marine du bassin germanique (Bourquin et Guillocheau, 1996; Bourquin et al., 2002). La

transgression téthysienne au Jurassique inférieur entraîne le dépôt de carbonates et d'argilites pendant l'Hettangien-Sinemurien, suivi de séries argileuses épaisses du Pliensbachien à l'Aalénien (Schnaebele, 1948; Megnien, 1980). Ces formations ont été suivies par les carbonates du Dogger jusqu'à la transgression du Callovien-Oxfordien, marquée par des dépôts marneux (Wetzel et al., 2003; Blaise et al., 2011; Landrein et al., 2013). Le fossé Rhéna (et l'est du bassin de Paris) ne montre pas de dépôts crétacés (Sittler, 1985). Toute la région (y compris en Allemagne) est soulevée (Schumacher, 2002), avant d'être affectée par une phase compressive à la limite Crétacé/Paléocène (phase Laramide connue aussi dans le bassin de Paris ; Ziegler, 1990). Elle se traduit par des plis de grande longueur d'onde et un basculement vers le sud de la série mésozoïque, déclenchant leur érosion et leur karstification avant le début de la sédimentation syn-rift (Sittler, 1967; Ziegler, 1990; Lutz et Cleintuar, 1999; Bourgeois et al., 2007; Grimmer et al., 2017). Contrairement à ce qui est connu dans le centre et l'ouest du bassin de Paris, la majeure partie du Malm et la totalité des dépôts crétacés ne se retrouvent pas sous les dépôts syn-rift de l'URG (les sédiments pré-rift les plus jeunes sont d'âge Oxfordien-Kimmeridgien; Wannesson, 1998).

Evolution syn- et post-rift du fossé Rhéna

La phase syn-rift initiale (« early-rift ») commence à l'Eocène moyen (Lutétien; Schumacher, 2002; Lutz et al., 2013; Figure 34). Des argiles résiduelles et des dépôts sidérolithiques issus de l'altération des carbonates mésozoïques forment les premiers sédiments (Sittler, 1965; Düringer, 1988; Schumacher, 2002; Düringer et al., 2019). Ces produits d'érosion sont souvent associés à des sédiments lacustres riches en lignite (Fm. de Bouxwiller; Sittler, 1965; Ménillet et al., 2015). Cette reprise de la subsidence se poursuit au Bartonien avec le dépôt de formations marneuses et calcaires dans deux bassins de type pull-apart orientés ENE (Schumacher, 2002 ; Châteauneuf and Ménillet, 2014; Düringer et al., 2019).

La phase syn-rift s.s. début à l'Oligocène inférieur avec la mise en place d'un régime de subsidence mixte thermique et tectonique dans un contexte extensif ONO/ESE (Schumacher 2002). Le Groupe de Pechelbronn (nord du fossé) et les formations salifères successives (sud du fossé), d'âge Priabonien-Rupélien, représentent les dépôts syn-rifts. La transition avec la phase post-rift est marquée par la Fm. des Marnes à Foraminifères en base de la Série Grise ; elle est reconnue sur l'ensemble du fossé et témoigne d'une inondation marine généralisée intra-rupélienne en provenance de la Mer du Nord. A la fin de l'Oligocène (Chattien), la connexion marine est rompue et se met en place temporairement un régime décrochant dextre (Schumacher, 2002; Sissingh, 2006). Une réorientation majeure des contraintes au début du Miocène se traduit ensuite par un régime décrochant sénestre à l'origine d'une structuration importante du fossé, proche de celle connue actuellement (Schumacher 2002; *Beccaletto et al. 2013; *Team GeORG 2013). La propagation du bulge alpin au Miocène moyen se traduit par un soulèvement du sud du fossé alors soumis à l'érosion, tandis que le nord est toujours en subsidence (remplissage sédimentaire aquitain-burdigalien ; Dèzes et al. 2004; Berger et al. 2005; Bourgeois et al. 2007). La période du Pliocène supérieur à l'actuel se caractérise par des dépôts fluviaux et lœssiques (Ménillet 2015; Düringer et al. 2019), toujours sous l'influence de la tectonique alpine.

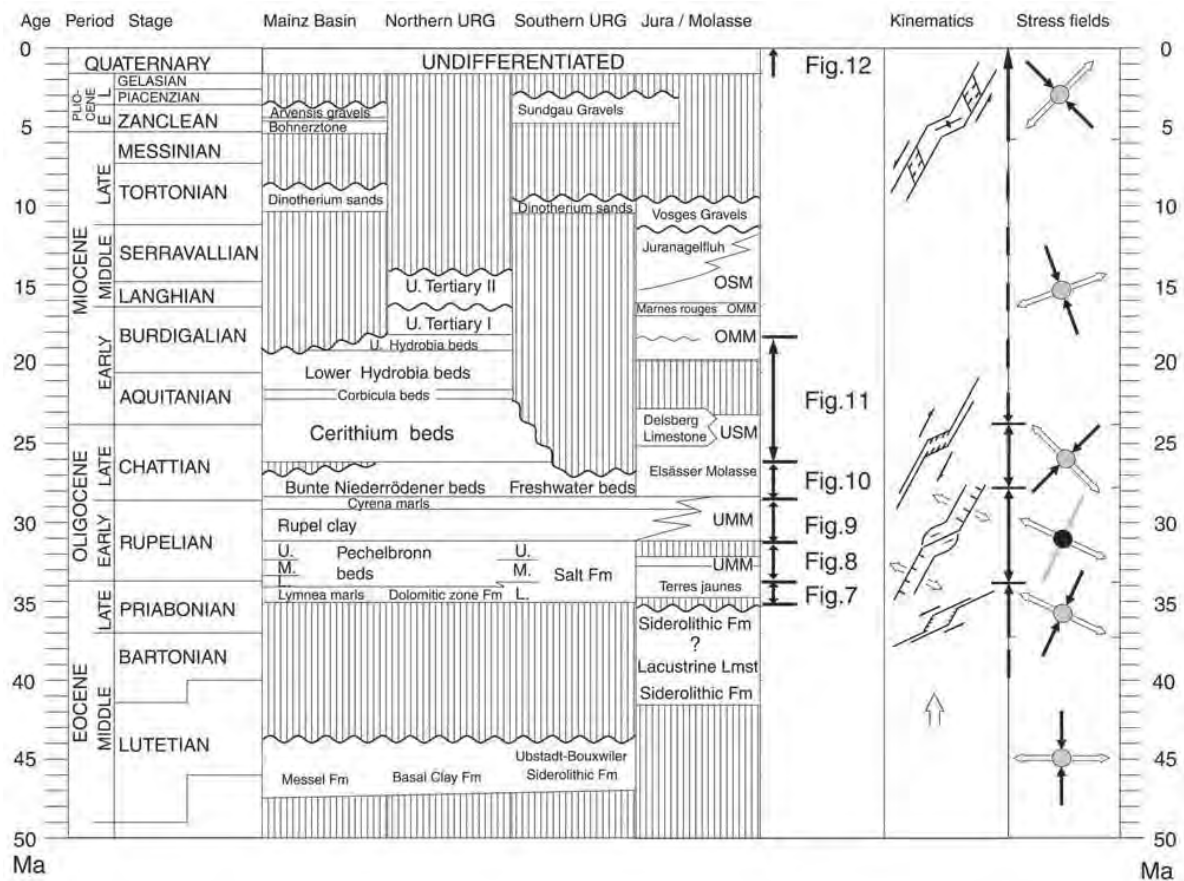


Figure 34 - Remplissage sédimentaire cénozoïque du fossé Rhénan, cinématique et champ de contraintes régionaux (σ_1 en noir, σ_2 en gris, σ_3 en blanc) (Schumacher, 2002).

4.2.4. Résultats

Schéma structural, héritage structural, failles bordières et calendrier des déformations

La construction du modèle géologique du fossé Rhénan en 3D dans le cadre du projet GeORG a nécessité la construction d'un nouveau schéma structural, véritable ossature du modèle. Sa construction en 3D (dans SKUA-GOCAD[®]) s'est appuyée sur toutes les informations de surface et de subsurface disponibles dans la région, aussi bien du côté français que du côté allemand et suisse, en particulier sur le retraitement et l'interprétation de plus de 5000 km de profils sismiques (kilométrage total pour les trois partenaires allemand, suisse et français), dont plus de 1700 km du côté français. Quinze cartes structurales correspondant à quinze surfaces géologiques repères ont été produites (cf. Figure 35 pour le schéma structural à la base du Tertiaire). Ce schéma transfrontalier détaillé est depuis largement utilisé par les collègues en interne au BRGM (e.g. Armandine-Les-Landes et al., 2019) ou en externe (e.g. Böcker et al., 2017 ; Aicholzer, 2019 ; Bossenec et al., 2021).

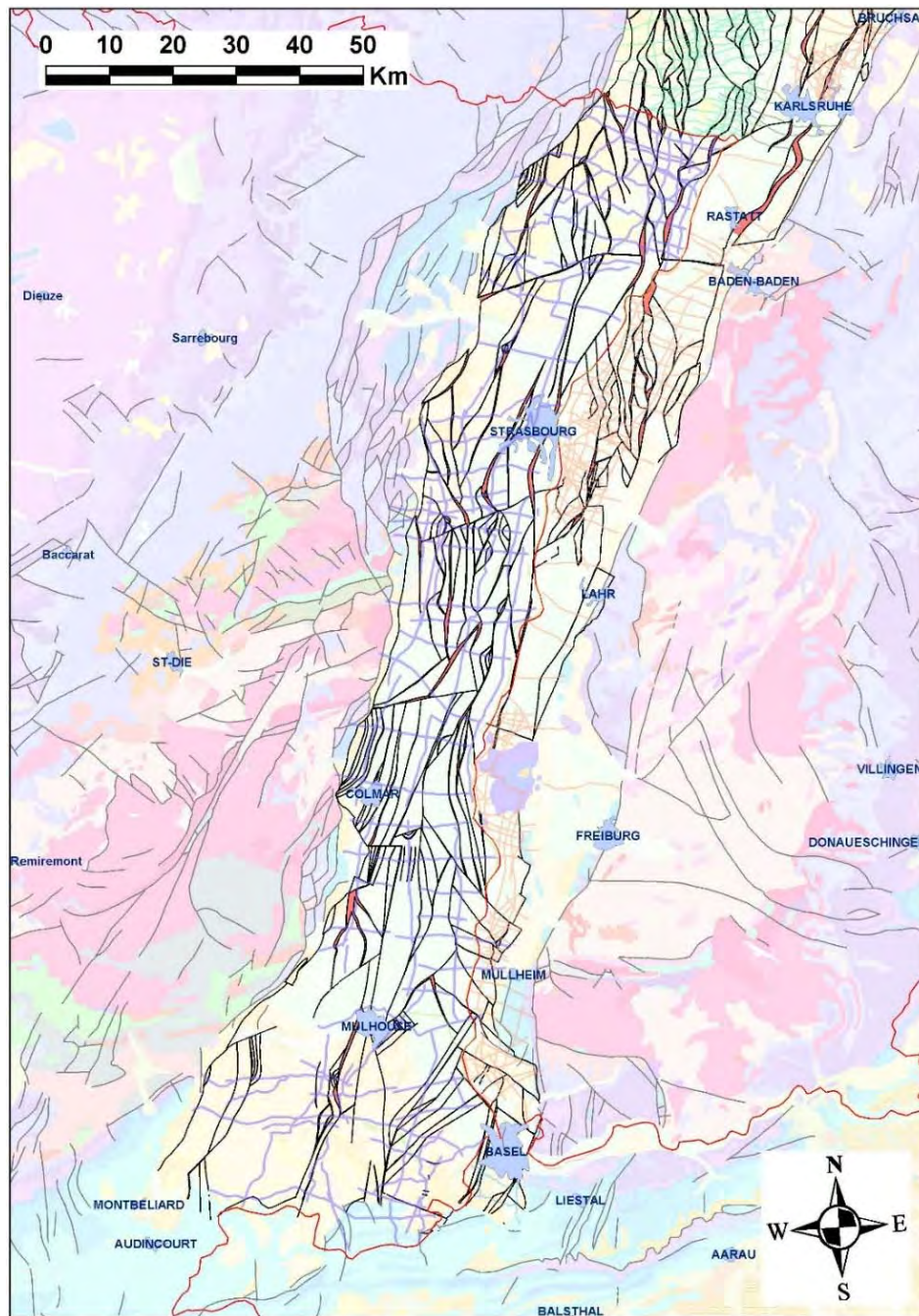


Figure 35 - Schéma structural du fossé Rhénan pour la base du Tertiaire (projet GeORG); en arrière-plan, profils sismiques interprétés en mauve, orange et vert ; en fond, carte géologique au 1/1000000^{ème} de l'Allemagne (BGR, 1993).

Voici les principaux résultats issus de l'interprétation des profils sismiques (Beccaletto et al., 2012).

- La grande majorité des failles vues sur les profils sismiques recoupe la pile sédimentaire dans son ensemble (séries pré- syn- et post-rifts ; Figure 36). Cette observation fondamentale signifie que la plupart des failles du « rift rhénan » sont post-rift.
- Les failles, donc post-rifts pour la plupart, s'organisent souvent en structures tectoniques transtensives (de type structure en fleur négatives, Figure 36 et Figure 37).

- Les épaisseurs des séries syn-rifts varient peu le long des profils sismiques transverses au fossé ; les variations d'épaisseur significatives des dépôts syn-rifts sont seulement visibles à proximité de quelques failles (Figure 36 et Figure 37).

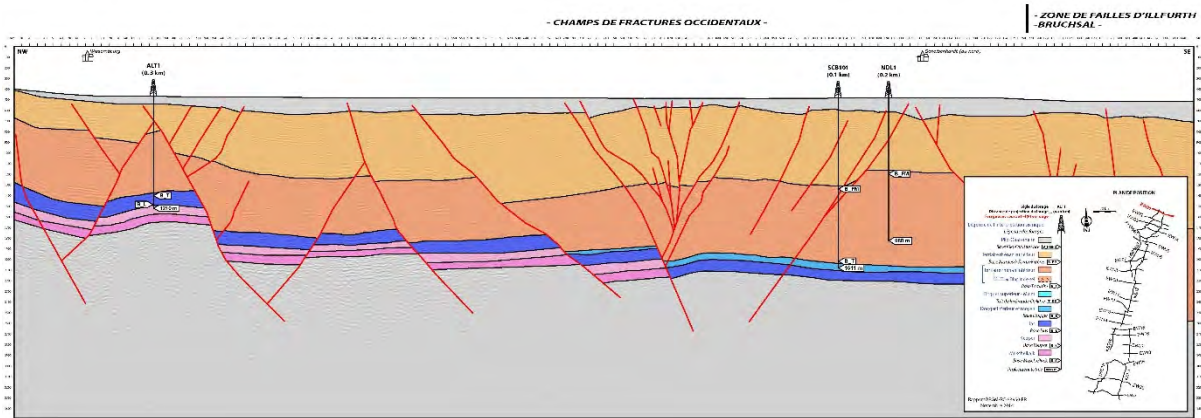


Figure 36 - Profil sismique interprété dans le nord du Fossé rhénan ; séries syn-rift en orange foncé (Beccaletto et al., 2014, confidentiel).

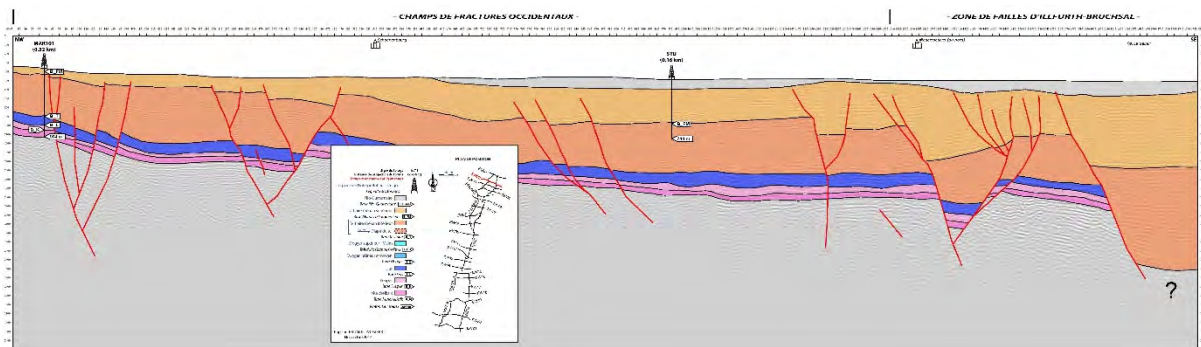


Figure 37 - Profil sismique interprété dans le nord du Fossé rhénan ; séries syn-rift en orange foncé (Beccaletto et al., 2014, confidentiel).

- La faille varisque de Lalaye-Lubine-Baden-Baden (e.g. Wickert et Eisbacher, 1988) est décrite dans le fossé Rhénan ; des segments de cette faille recoupent les séries post-rifts selon un jeu décrochant sénestre (Figure 38). D'autres failles post-rifts de même orientation (N60) ont été reconnues plus au nord et au sud, témoignant d'un héritage structural varisque fort sur la dynamique tectonique post-rift.

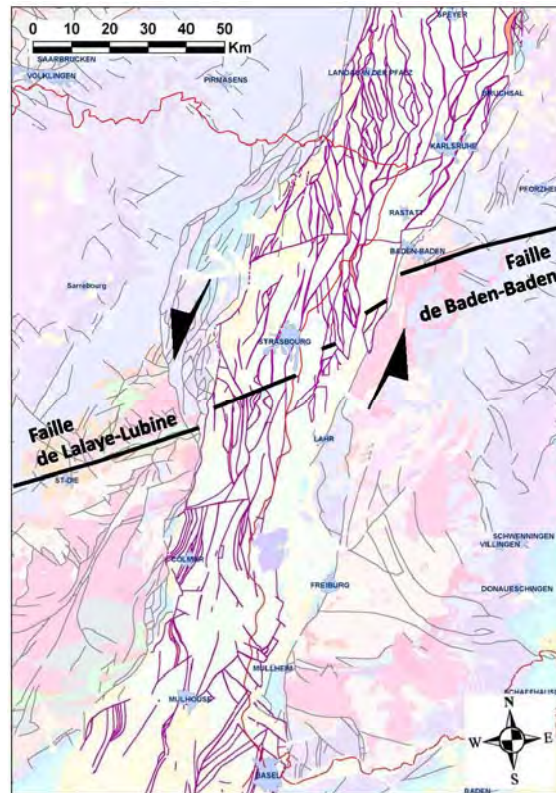


Figure 38 - Schéma structural du fossé Rhénan pour la base de la série post-rift (projet GeORG); en noir tracé de la faille de Lalaye-Lubine-Baden-Baden ; en fond carte géologique au 1/1000000^{ème} de l'Allemagne (BGR, 1993).

- La faille bordière actuelle est segmentée et n'est pas systématiquement liée à des corps conglomératiques syn-rifts (Düringer, 1988), et encore moins à des éventails sédimentaires syn-rifts (Figure 39). Ceci suggère qu'elle n'est pas la faille bordière syn-rift tout le long de son tracé et qu'une grande partie de son activité est postérieure au rifting.

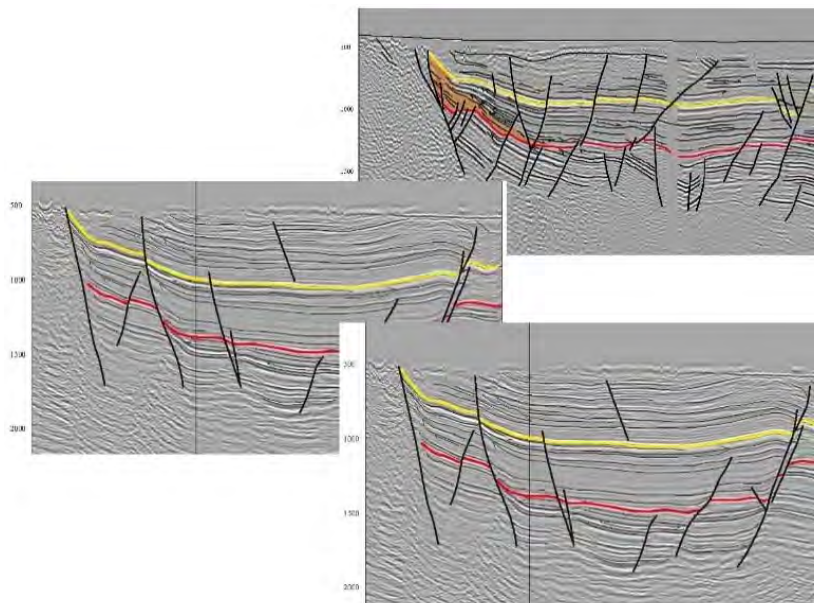


Figure 39 - Différentes géométries de la faille bordière occidentale du fossé Rhénan (à gauche sur les profils) ; série syn-rift entre les horizons rouges et jaunes (Beccaletto et al., 2013).

Les observations précédentes, réalisées de part et d'autre du Rhin, nous ont permis de proposer une hiérarchisation simplifiée des failles dans le fossé Rhénan en regard du contexte géodynamique ouest-européen, en distinguant (Figure 40):

- Les failles mésozoïques scellées par la discordance en base des premiers dépôts tertiaires, développées principalement en relation avec la phase de rifting liasique (Stampfli & Hochard, 2009).
- Les failles bordières originelles contrôlant les premiers dépocentres, préservées aujourd'hui en bordure du fossé (e.g. champ de fractures de Saverne), en relation avec l'orogénèse pyrénéenne (Sissingh, 2006 ; Bourgeois et al., 2007).
- Les failles héritées tardi-varisques, réactivées pendant les phases syn- et post-rift (Grimmer et al., 2017).
- Le méga-réseau décrochant sénestre (transtensif) orienté N20 d'Illfurth-Bruchsal, suivi sur plus de 200 km de long et 30 km de large le long des profils sismiques. Actif à partir de 15-18 Ma et réactivé jusqu'au Plio-Pléistocène, il recoupe l'ensemble des structures préexistantes et donne au fossé sa géométrie actuelle. Il se caractérise structuralement par des relais de structures en fleurs négatives et l'initiation des mouvements halocinétiques dans le sud du fossé (diapirs et murs des évaporites syn-rifts), développés en relation avec la collision alpine (Schumacher, 2002).



Figure 40 - Schéma structural hiérarchisé du fossé Rhénan (Team GeORG, 2013).

Conditions thermiques pré-rift du fossé Rhénan - Publication 8

Tchang-Tchong L., Michels R., Beccaletto L., Bossennec C., Lorgeoux C., Faure P. (2023) Pre- to early-rift thermal conditions of the Upper Rhine Graben using geological and organic geochemical controls, Marine & Petroleum Geology, 151. <https://doi.org/10.1016/j.marpetgeo.2023.106202>

Cette publication concrétise les travaux de thèse de L. Tchang-Tchong sur l'évolution thermique pré-rift du fossé Rhénan à partir de modélisations géochimiques de la matière organique. L'enfouissement et l'histoire thermique du fossé sont approchés via l'étude des roches mères liasiques, sources principale du pétrole dans la région. La maturité de ces roches dépend de trois inconnues : (i) le hiatus de sédimentation de plus de 120 Ma du Jurassique supérieur au Paléocène; (ii) les enfouissement syn- et post-rift; et (iii) les forts gradients géothermiques actuels et les cellules convectives hydrothermales associées. Ainsi, pour reconstruire l'histoire thermique et d'enfouissement du bassin, la part liée au hiatus du Jurassique supérieur/Paléocène doit d'abord être résolue (inconnue (i)). Les échantillons analysés proviennent du champ de fracture de Saverne, considéré comme témoins de la phase pré à early-rift du fossé Rhénan (Ménillet et al., 1979, 2015; Genre, 1981). Cette étude, combinant l'enfouissement du bassin et la modélisation thermique 1D sur la base de la géochimie des biomarqueurs du champ de fractures de Saverne, améliore la connaissance de l'histoire thermique du fossé Rhénan avant et au début du rift. Je suis intervenu tout au long du processus de modélisation pour contrôler les paramètres géologiques de premier ordre des modèles. Les travaux se poursuivent par la modélisation thermique 2D de la période syn- à post-rift par le biais de coupes géologiques de référence issus des interprétations sismiques.

Principaux résultats issus de la publication 8

- Les roches mères liasiques du champ de fractures de Saverne sont immatures. Les valeurs d'équilibre du rapport homohopane $22S/(22S+22R)$ C_{31} indiquent que le début de la fenêtre à huile est atteint dans le Trias.
- Les mesures de maturité thermique calculées à partir des rapports $22S/(22S+22R)$ C_{31} homohopane et $20S/(20S+20R)$ C_{29} $\alpha\alpha\alpha$ stéranes ont été intégrées dans le logiciel PetroMod[®] comme valeurs d'étalonnage. Sur la base (i) d'une colonne lithostratigraphique synthétique de référence pour le champ de fractures de Saverne, et (ii) le test de plusieurs scénarios d'enfouissement et de modélisation thermique à l'aide du logiciel PetroMod[®], il apparaît que l'épaisseur cumulée de sédiments érodés au-dessus de la série du Dogger est de 300 m au maximum. Il n'est pas possible de démontrer si cette valeur est attribuée aux seuls dépôts du Malm, ou au Malm plus le Crétacé. Les modélisations montrent que l'épaisseur maximale cumulée du Crétacé devait être faible (≤ 100 m).
- Ces conclusions peuvent être transposées à l'est du bassin de Paris, qui a enregistré la même histoire thermique que le pré-rift du fossé Rhénan du Permien au Crétacé/Paléocène.
- La mesure de la maturité thermique des lignites de Bouxwiller (Lutétien) combinée à la modélisation thermique indique que, lors des premiers stades du rifting (early-rift), les

sédiments mésozoïques ont pu à nouveau être enfouis sous 250 m de sédiments cénozoïques, avec une influence négligeable sur leur signature thermique.

- Par conséquent, la maturité thermique des roches mères liasiques du fossé Rhénan n'a jamais été suffisante pour atteindre la fenêtre à huile pendant la phase pré-rift. Leur maturation dans les parties plus profondes du fossé pour atteindre les fenêtres à huile et à gaz ne serait que la conséquence de leur enfouissement syn-rift à post-rift, avec la possible influence d'anomalies géothermiques locales.

Publication 8

Marine and Petroleum Geology 151 (2023) 106202



Contents lists available at ScienceDirect

Marine and Petroleum Geology

journal homepage: www.elsevier.com/locate/marpetgeo

Pre- to early-rift thermal conditions of the Upper Rhine Graben using geological and organic geochemical controls

Laurie Tchang-Tchong^{a,b,*}, Raymond Michels^a, Laurent Beccaletto^c, Claire Bossennec^d, Catherine Lorgeoux^a, Pierre Faure^b^a Université de Lorraine, CNRS, GeoRessources, UMR 7359, Nancy, France^b Université de Lorraine, CNRS, LIEC, UMR 7360, Nancy, France^c BRGM, F 45060, Orléans, France^d Institute of Applied Geosciences, Geothermal Science and Technology, Technische Universität Darmstadt, Schnittspahnstraße 9, 64287, Darmstadt, Germany

ARTICLE INFO

Keywords:

Upper Rhine Graben
 Basin thermal modelling
 Paleoburial
 Pre-rift
 Cretaceous hiatus
 Toarcian Posidonia Shale
 Homohopanes
 Steranes

ABSTRACT

The Toarcian Posidonia Shale and Hettangian/Sinemurian Formation are the two main Mesozoic source rocks of the Upper Rhine Graben (URG). Their thermal maturities are measured and used to reconstruct the thermal history of the URG. However, the thermal maturity of these source rocks was impacted by: 1) the pre-rift burial history which includes a 120 My hiatus from Upper Jurassic to the Paleocene; 2) the syn- and post-rift burial histories; and 3) the current high geothermal gradients and associated hydrothermal convective cells. In this study, the Saverne Fracture Field is considered the pre-rift analogue of the URG and therefore bears witness to the pre-rift thermal history. It was isolated from the graben upon its opening, i.e. in the Priabonian, and contains the same Mesozoic rocks, which, in contrast to the URG, are currently outcropping. As the source rocks in the Saverne Fracture Field were not buried as in the URG, their thermal maturities should be a consequence of the Upper Jurassic/Cretaceous burial only. Organic geochemistry results indicate that they are of pre-oil window thermal maturity. Calibration of the Saverne Fracture Field thermal model for the pre-rift period of the URG allows us to estimate that during the Upper Jurassic/Cretaceous hiatus additional burial did not exceed about 300 m. The additional sediments cannot be attributed specifically to the Upper Jurassic or Cretaceous. However, simulation results indicate that if Cretaceous sediments were deposited, they had to be preserved until the Paleocene, and their maximum cumulative thickness must have been at most 100 m. In addition, thermal modelling indicates that during the very first onset of the URG, Mesozoic sediments could have been buried again by about 250 m of Cenozoic sediments, with negligible effect of the pre-rift thermal signature. These geochemical and geological constraints are key input for further URG thermal modelling. Indeed, such constraints on the pre-rift thermal history should allow future assessment of the syn-rift burial and recent hydrothermal convective cells impact on the Mesozoic source rocks maturity.

1. Introduction

The Upper Rhine Graben (URG) is a Cenozoic intracontinental rift with significant local thermal anomalies. Historically, it was the focus for research on hydrocarbon resources and more recently on deep geothermal energy (e.g., Frey et al., 2022a, 2022b). This is precisely the case for the Pechelbronn sub-basin, located in the western central part of the URG, which was mentioned as early as the end of the 15th century for its hydrocarbon resources (Schwarz, 2021) and hosts a geothermal field studied since the end of the 19th century (Gérard and Kappelmeyer,

1987). Deep geothermal energy is a key renewable energy (e.g., Frey et al., 2022a) that raises other strategic challenges, such as the extraction of lithium from geothermal brines (e.g., Fries et al., 2022; Sanjuan et al., 2022). As a result, understanding and evaluating the diagenesis, porosity and permeability properties of geothermal reservoirs is of major importance. The evolution of these properties is controlled by burial and the thermal history of the basin (Schmoker and Gautier, 1988; Schmoker and Hester, 1989; Kuzec et al., 1997). In addition, the same control factors are involved in evaluating petroleum systems, which depend on burial, time and temperature (e.g., Philippi, 1965; Welte, 1966; Bajor

* Corresponding author. Université de Lorraine, CNRS, GeoRessources, UMR, 7359, France.
 E-mail address: laurie.tchang-tchong@univ-lorraine.fr (L. Tchang-Tchong).

<https://doi.org/10.1016/j.marpetgeo.2023.106202>

Received 22 November 2022; Received in revised form 9 February 2023; Accepted 25 February 2023

Available online 28 February 2023

0264-8172/© 2023 Elsevier Ltd. All rights reserved.

et al., 1969). Consequently, because the URG is one of the main targets of geothermal projects in Central Europe (Frey et al., 2022a), it is essential to reconstruct the evolution of its burial and thermal history. Generally, thermal maturity assessment of organic matter allows calibration of the burial and thermal reconstructions. As the primary source rocks of the URG are of Liassic age (Böcker and Litke, 2016, and references therein), they experienced the burial history of the eastern Paris Basin prior to that of the URG (i.e., prior to the Priabonian). Their maturities can be at least attributed to three superimposed unknowns of burial and thermal conditions: 1) the sedimentation hiatus of more than 120 My from the Upper Jurassic to the Paleocene (Schnaebele, 1948; Ziegler, 1990; Ménéillet et al., 2015); 2) the syn- and post-rift burial histories (Schumacher, 2002; Buchmann and Connolly, 2007; and the references therein); and 3) the current high geothermal gradients and associated hydrothermal convective cells (e.g., Kohl et al., 2000; Baillicieux et al., 2013). Thus, to reconstruct the full burial and thermal history of the basin, the part related to the Upper Jurassic/Paleocene hiatus must be resolved first.

The Saverne Fracture Field is adjacent to the Pechelbronn sub-basin and is part of the current western margin of the URG (Fig. 1; Genre, 1981; Sissingh, 2006). The Saverne Fracture Field has been isolated

from the URG since its opening (Ménéillet et al., 1979, 2015; Genre, 1981) and Liassic source rocks are preserved as outcrops today (Chantraine et al., 1996). Their thermal maturities acquired during the Upper Jurassic to Paleocene (represented today by a stratigraphic hiatus) have not been affected by the syn- and post-rift burial histories and the current high geothermal gradients and associated hydrothermal convective cells. The Saverne Fracture Field thus provides the opportunity to evaluate the maximum burial depth reached by the Mesozoic pre-rift sediments during Upper Jurassic/Cretaceous times, prior to the onset of the URG rifting.

In this study, the thermal maturity data measured on outcropping Mesozoic rock samples from the Saverne Fracture Field are used to calibrate thermal basin models to estimate the maximum burial depth reached before the development of the URG *sensu stricto*, i.e. before the Priabonian. By analogy, this provides geological and geochemical conditions of the URG pre-rift thermal history. The work proposes burial models based on: 1) a bibliographical synthesis of the tectono-sedimentary history of the URG, in particular its pre-rift period; 2) the characterization and assessment of the thermal maturity of the organic matter contained in Mesozoic rocks; and 3) the integration of the results into the PetroMod® Software to calibrate the URG pre-rift thermal

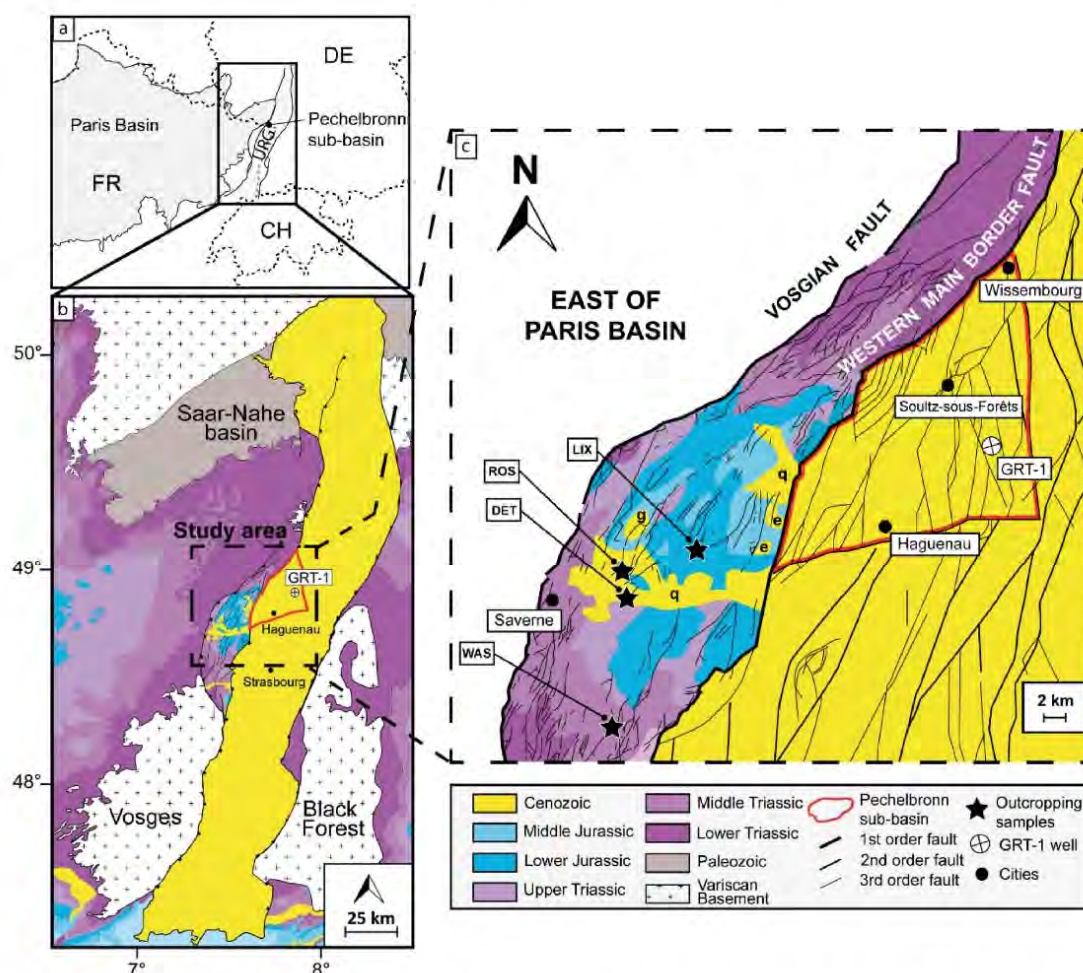


Fig. 1. Location of studied area. a. Simplified map of the borders between France, Germany, Switzerland with east Paris Basin, the URG and location of the Pechelbronn sub-basin. b. Simplified geological map of the URG surroundings with limits of the study area and Pechelbronn sub-basin. Location of the geothermal GRT-1 well (crossed circle). c. Zoom on the study area represented by a schematic structural map with the outcropping formations of the Saverne Fracture Field. Black stars: sampling locations. q: Plio-Quaternary; g: Oligocene; e: Eocene; LIX: Lixhausen quarry; ROS: Rosenwiller; DET: Dettwiller; WAS: Wasselonne quarry. Based on Équipe du projet GeORG (2013) and the geological map of France 1/1 000 000, BRGM (Chantraine et al., 1996).

history, by adjusting the paleoburial.

2. Geological background of the URG

2.1. General geological features of the URG

The URG belongs to the European Cenozoic Rift System (ECRS), a 1100 km long rift system initiated in the Eocene and extending from the North Sea to the Western Mediterranean (Dèzes et al., 2004). The NNE/SSW trending URG extends over 300 km from the Rhenish Massif to the north to the Jura Mountains and its current geometry corresponds to a set of asymmetrical and antithetical half-grabens, connected by transfer zones inherited from Paleozoic basement structures (Schumacher, 2002; Derer, 2003; Roussé, 2006; Hinsken et al., 2007; Grimmer et al., 2017). It is limited to the west by the Vosges Mountains, the eastern Paris Basin and the Saverne Fracture Field, and to the east by the corresponding units of the Black Forest, Odenwald and Franconian Platform. The present-day URG is limited by the Western and Eastern Main Border Faults. Its opening and development were controlled by the Pyrenean and Alpine orogen dynamics (Schumacher, 2002; Dèzes et al., 2004), resulting in a polyphase tectonic rift evolution and related syn-to post-rift sedimentation (Laubscher, 1987; Sissingh, 1998, 2006; Schumacher, 2002).

2.2. The Saverne Fracture Field

This study focuses on the western central part of the URG, corresponding to the Saverne Fracture Field and the easterly adjacent Pechelbronn sub-basin within the Haguenau block as defined by the GeORG project (Fig. 1c; *Équipe du projet GeORG*, 2013). The Saverne Fracture Field is a crescent-shaped 90 km long and up to 20 km wide highly-faulted structure located between the URG and the eastern Paris Basin (Fig. 1b and c). The Paris Basin and the Franconian Platform are intracratonic basin systems, where up to 2–3 km of sediments accumulated during Triassic and Jurassic (Ziegler and Dèzes, 2005, and references therein). The sedimentary deposits in these basins were eroded to the Lower Triassic (Buntsandstein), while preserved in the Saverne Fracture Field which contains both pre-rift sediments from Lower Triassic to Bajocian formations and Middle Eocene early-rift sediments (Fig. 1b and c; Ménillet et al., 1979, 2015; Chantraine et al., 1996).

2.3. Pre-rift and early-rift tectono-sedimentary history of the URG and the surrounding areas

The oldest rocks in the area are known in the Vosges, the Black Forest and Odenwald massifs and are related to the pre- and syn-Variscan orogeny (Edel and Fluck, 1989; Lardeaux et al., 2014). During the latest Carboniferous-early Permian, the area of the future URG, the Saverne Fracture Field, the eastern Paris Basin and the Franconian Platform experienced disruption and collapse of the Variscan orogen (Schumacher, 2002; Ziegler and Dèzes, 2005). Uppermost Carboniferous to Lower Permian continental clastics were deposited in vast fault-controlled basins, such as the Lorraine-Saar-Nahe and the Kraichgau basins, known either at outcrops or identified beneath the Mesozoic cover of the Paris and Germanic basins (Boigk and Schöneich, 1970; Donsimoni, 1981; Scheck-Wenderoth et al., 2008).

From the Late Permian until at least the mid-Jurassic, this area underwent post-orogenic thermal subsidence (Clothingh and Ziegler, 2007). This tectonic regime led to the formation of the Paris Basin and Franconian Platform, both belonging to the same epicontinental paleogeographic domain, namely the southern part of the Central Europe Basin System located north of the passive northern margin of the Alpine Tethys (Ziegler, 1990; Geyer et al., 1991; Bourquin et al., 2006; Scheck-Wenderoth et al., 2008). The area experienced a limited geological evolution, only determined by eustatic sea-level changes, low-grade regional subsidence and diffuse crustal stretching (Ziegler

and Dèzes, 2005; Scheck-Wenderoth et al., 2008).

The first Mesozoic deposits are represented mainly by the fluvial Buntsandstein sandstones (Bourquin and Guillocheau, 1996; Bourquin et al., 2006, 2009), grading into Middle Triassic claystones, limestones and dolostones (Muschelkalk facies) (Fig. 2; Ziegler, 1990; Ménillet et al., 2015). In the Late Triassic, the sedimentation evolved to evaporitic deposits (Keuper facies) due to marine regression from the Germanic Basin (Bourquin and Guillocheau, 1996; Bourquin et al., 2002). The Tethysian transgression at the Early Jurassic led to the deposition of carbonates and shales during Hettangian-Sinemurian, followed by thick shales from Pliensbachian to Aalenian (Fig. 2; Schnaebeler, 1948; Schirardin, 1960; Megnien, 1980). These Liassic deposits contain the main source rocks of the URG, also extending over the entire Central Europe Basin System (Littke et al., 2008). These formations were followed by Dogger carbonates until the Callovian-Oxfordian transgression, which was marked by marl deposits (Wetzel et al., 2003; Blaise et al., 2011; Landrein et al., 2013). The end of Jurassic is characterized by carbonate platform deposits of Upper Oxfordian, Kimmeridgian and Tithonian (Curnelle and Dubois, 1986; Landrein et al., 2013).

The eastern Paris Basin, the Saverne Fracture Field, the URG and the Franconian Platform do not show evidence of Cretaceous sedimentation (Fig. 1). The absence of Cretaceous deposits may result from a combination of a low eustatic sea level during the Early Cretaceous (Scheck-Wenderoth et al., 2008) and the uplift of the “Rhenish Shield” (Cloos, 1939; Illies, 1975; Düringer, 1988; Geyer et al., 1991; Ziegler, 1994; Walter, 1995; Schumacher, 2002; Le Roux and Harmand, 2003; Timar-Geng et al., 2006; Bourgeois et al., 2007; Scheck-Wenderoth et al., 2008). The large uplifted domain involves notably the future URG (Schumacher, 2002) and the Saverne Fracture Field areas, which were then affected by the intraplate so-called “Laramide” compression during the late Cretaceous/Paleocene (Ziegler, 1987). This slight compressional phase led to moderate folding and southward tilting of the Mesozoic series in the whole area, triggering their erosion before syn-rift sedimentation (Sittler, 1967; Ziegler, 1990; Lutz and Cleintuar, 1999; Bourgeois et al., 2007; Grimmer et al., 2017). Indeed, in contrast to the central and western Paris Basin, most of the Malm and all of the Cretaceous deposits are not found in the URG beneath the syn-rift deposits (the youngest pre-rift sediments are Oxfordian-Kimmeridgian) (Wannesson, 1998).

The early-rift phase started in Middle Eocene (Lutetian) and is evidenced by volcanic activity (Schumacher, 2002; Lutz et al., 2013), e.g. the Basalte de Gundershoffen Formation in the study area (Ménillet et al., 2015; and references therein). The first Cenozoic sediments correspond to siderolitic formations and residual clays resulting from weathering of the Mesozoic carbonates (Sittler, 1965; Düringer, 1988; Schumacher, 2002; Düringer et al., 2019). These weathering products are locally associated with lignite-rich Lutetian lacustrine sediments, e.g. the Bouxwiller Formation in the Saverne Fracture Field and the URG (Figs. 1 and 2; Sittler, 1965; Ménillet et al., 2015; and references therein). This slight resumption of subsidence marks the early rifting phase and is characterized by the deposition of marly clays and calcareous formations of Bartonian age (Châteauneuf and Ménillet, 2014; Düringer et al., 2019). These sediments are sparsely recorded in the Saverne Fracture Field (Châteauneuf and Ménillet, 2014) and certainly correspond to the last sediments deposited before its isolation from the URG (Ménillet et al., 1979, 2015; Genre, 1981). The onset of the rifting was initiated following this period, probably at Priabonian (Düringer, 1988; Berger et al., 2005; Derer et al., 2005; Ménillet et al., 2015). During the early Oligocene, the URG was episodically flooded by marine incursions, as reflected by the deposition of fossil-rich marine marls, referred as the Middle Pechelbronn layers in its central part (Martini and Reichenbacher, 2007). The Pechelbronn Gp. of Rupelian age (Early Oligocene) is made of siliciclastic and evaporitic rocks representing the syn-rift stage. The transition to the post-rift stage is then marked by the deposition of the Marnes à Foraminifères Formation at the base of the Série Grise (Fig. 2), whose uniform facies and thickness throughout the

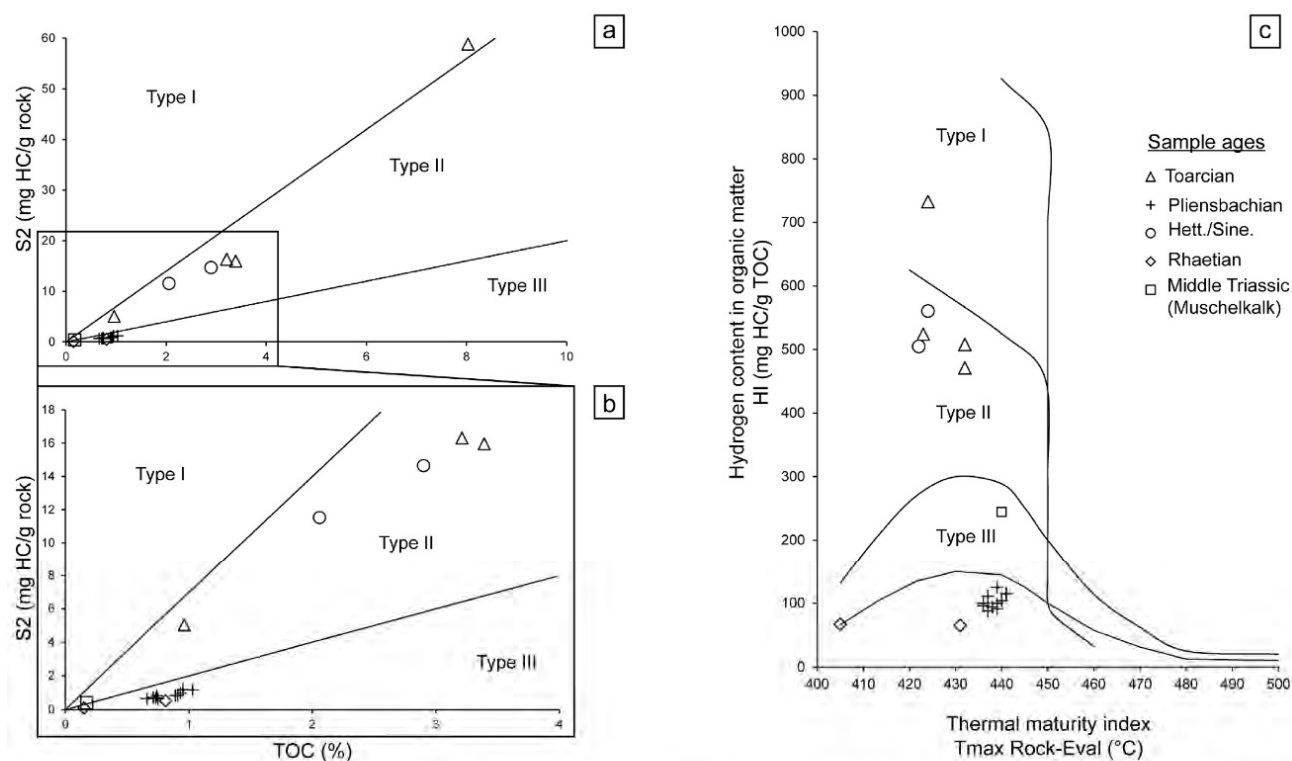


Fig. 3. Rock-Eval data of outcrop samples collected in the Saverne Fracture Field. a. Plot of S2 Rock-Eval (mg HC/g rock) versus TOC (%) indicating kerogen types (Late Triassic sample not indicated). b. Zoom of plot 3a for TOC < 4%. c. Plot of Hydrogen Index (mg HC/g TOC) versus T_{max} Rock-Eval ($^{\circ}$ C) indicating kerogen types and thermal maturity. Same legend for all illustrations.

URG testify to a general flooding from middle to late Rupelian (Oligocene) (Schumacher, 2002).

3. Sampling and analytical procedures

Nineteen fresh outcrop rock samples collected along the Paris-Strasbourg high-speed train worksites (Toarcian, Pliensbachian, Hettangian/Sinemurian, Late and Middle Triassic – respectively Keuper and Muschelkalk facies - ages) and two quarries (Pliensbachian, Hettangian/Sinemurian and Middle Triassic - Muschelkalk facies - ages) in the Saverne Fracture Field (Fig. 1c) were selected. The facies and stratigraphic level of the samples are presented in Table 1.

The rock samples were crushed, sieved (<180 μ m mesh) and analyzed by Rock-Eval pyrolysis at the Institut des Sciences de la Terre d'Orléans (ISTO) laboratory (France) (Table 1; analytical procedure described in Le Meur et al., 2021). Powered rock samples (20–30 g) were also extracted with dichloromethane (DCM) using an Accelerated Solvent Extractor (ASE 350, Dionex) at 100 bar and 130 $^{\circ}$ C (Li et al., 2002; Hautevelle et al., 2006; Biache et al., 2015). The organic extracts were dried, weighed and taken up in hexane for the SARA fractionation method (analytical procedure described in Abuhelou et al., 2017). Using the automated ASPEC GX-274 (Gilson), fractionation was carried out using Strata CN cartridges (500 mg, 3 mL, Phenomenex) to which 1 g of activated silica was added. The aliphatic fractions were analyzed for biomarkers using an Agilent Technologies 8890 GC equipped with a silica DB5-MS column (60 m \times 0.25 mm id \times 0.25 μ m film thickness) coupled to an Agilent Technologies Triple Quadrupole 7000/7010 MS operating in alternated full scan/single-ion monitoring (SIM) mode. The oven temperature was programmed as follows: 70 $^{\circ}$ C (held 2 min) to 130 $^{\circ}$ C at 15 $^{\circ}$ C/min, then 130–315 $^{\circ}$ C at 4 $^{\circ}$ C/min, and then 325 $^{\circ}$ C (held 25 min). The carrier gas was helium at 1.4 mL/min constant flow. The injection was set in splitless mode at 300 $^{\circ}$ C. Biomarkers were

identified using GC-MS/MS and according to the literature.

4. Modelling procedures

4.1. Synthetic lithostratigraphy column based on the GRT-1 geothermal well

The 1D thermal modelling was performed using the PetroMod[®] software, version 2022.1. Numerical and maturity modelling concepts were previously published by Waples et al. (1992b, 1992a), Yakin et al. (1997), and Poelchau et al. (1997). The primary inputs are listed in Table 2 and Table 3. The stratigraphic formations were based on the description of the geothermal well GRT-1 from (Fig. 2; Düringer et al., 2019). Stratigraphic ages were derived from the same publication and based on the international chrono-stratigraphic chart revised in 2019 (Cohen et al., 2013). The lithological mixes were derived from the explanatory note of the Haguenau geological map (Ménillet et al., 2015). The stratigraphic formations thicknesses are based on the measured depth (Düringer et al., 2019) as corrected for the slight well deviation (Baujard et al., 2017), providing the true vertical depth (Genter, personal communication). As visible in the GRT-1 well, the Bajocian was partially eroded to approximately 30 m of preserved rock. As deduced from Landrein et al. (2013), the thickness eroded was evaluated to 50 m and added into the burial model (bringing the total initial thickness to 80 m). Moreover, as the Bathonian and the Callovian units were deposited across the whole Jurassic carbonate platform, these formations were added to the synthetic stratigraphic column (Table 2), i.e. 50 m and 60 m, respectively (Böcker, 2015).

For all model strategies, organic thermal maturity markers were used to calibrate the thermal history (Burrus, 1986; Makhous and Galushkin, 2004; Hantschel and Kauerauf, 2009), considering fixed time-temperature couples. This assumption was made possible as time is

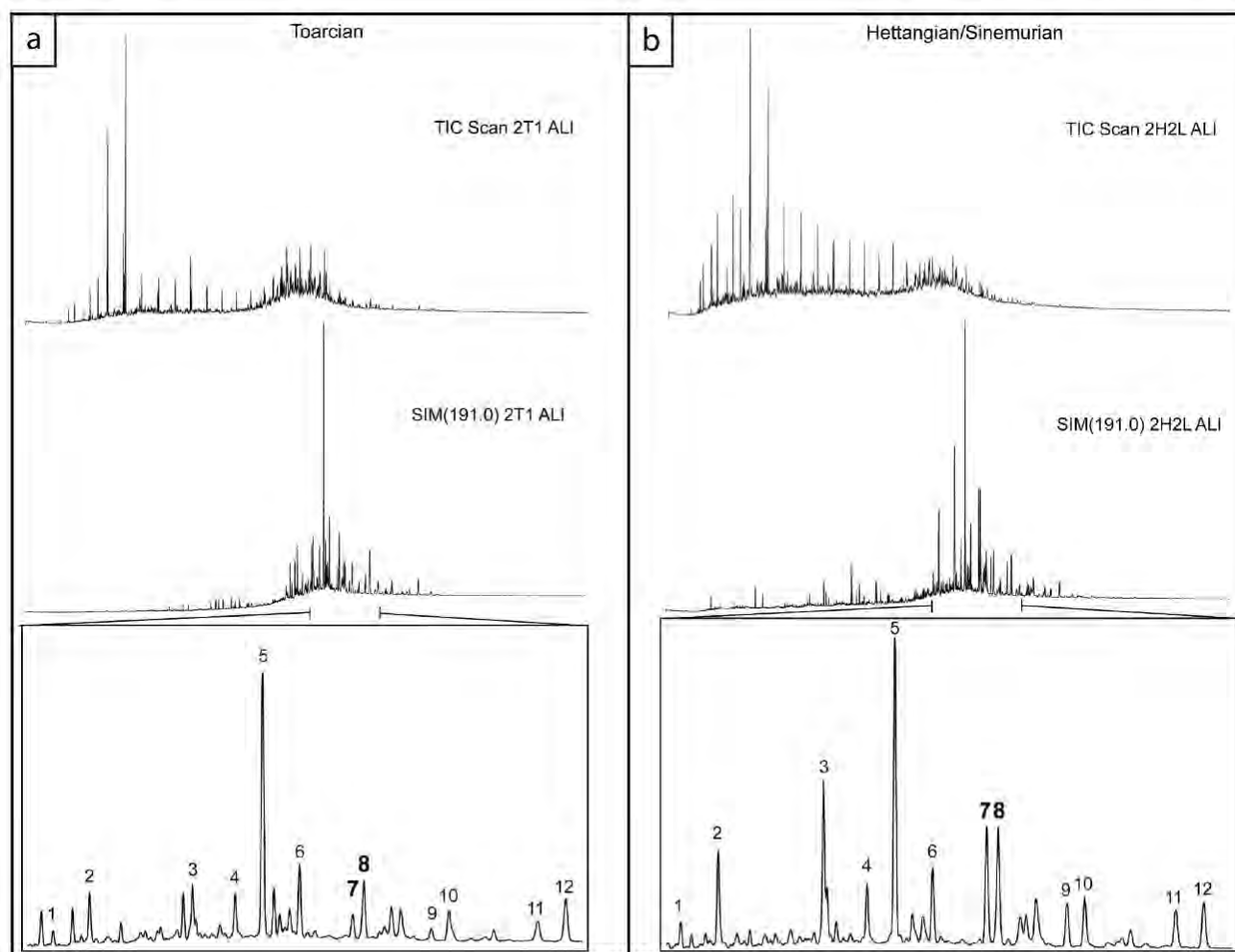


Fig. 4. Saturated fractions gas chromatograms (TIC: Fullscan Total Ion chromatogram; SIM m/z 191: Selected ion chromatogram, and partial m/z 191 showing the distributions of hopanes of selected outcrop samples.

a. Toarcian sample 2T1; b. Hettangian/Sinemurian sample 2H2L; Peak assignments: 1: $18\alpha(\text{H}), 22,29,30$ -Trisnorneohopane (Ts); 2: $17\alpha(\text{H}), 22,29,30$ -Trisnorhopane (Tm); 3: $17\alpha(\text{H}), 21\beta(\text{H})$ -30-Norhopane ($\text{C}_{29} \alpha\beta$); 4: $17\beta(\text{H}), 21\alpha(\text{H})$ -30-Norhopane ($\text{C}_{29} \beta\alpha$); 5: $17\alpha(\text{H}), 21\beta(\text{H})$ -Hopane ($\text{C}_{30} \alpha\beta$); 6: $17\beta(\text{H}), 21\alpha(\text{H})$ -Hopane ($\text{C}_{30} \beta\alpha$); 7: $17\alpha(\text{H}), 21\beta(\text{H})$ -22S homohopane ($\text{C}_{31} \alpha\beta \text{ S}$); 8: $17\alpha(\text{H}), 21\beta(\text{H})$ -22R homohopane ($\text{C}_{31} \alpha\beta \text{ R}$); 9: $17\alpha(\text{H}), 21\beta(\text{H})$ -22S bis-homohopane ($\text{C}_{32} \alpha\beta \text{ S}$); 10: $17\alpha(\text{H}), 21\beta(\text{H})$ -22R bis-homohopane ($\text{C}_{32} \alpha\beta \text{ R}$); 11: $17\alpha(\text{H}), 21\beta(\text{H})$ -22S tris-homohopane ($\text{C}_{33} \alpha\beta \text{ S}$); 12: $17\alpha(\text{H}), 21\beta(\text{H})$ -22R tris-homohopane ($\text{C}_{33} \alpha\beta \text{ R}$).

determined from the lithostratigraphic description (Cohen et al., 2013; Düringer et al., 2019) and temperature from the boundary conditions (see subsection 4.2). Input data were adjusted to fit the simulated and measured maturity markers values by adding or removing sediment thickness of Upper Jurassic and presumed Cretaceous age. After estimating the maximum thickness of sediments, modelling was conducted considering the onset of the URG at the late Eocene. Lutetian and Bartonian layers were added to the model after consideration of the associated Eocene thermal peak (Table 3).

4.2. Boundary conditions

To calculate the temperature gradient and resulting paleo-heat flow within a basin, model boundary conditions (heat convection, heat conduction and radiogenic heat production) have to be defined (Brunns et al., 2016). The software systematically calculated the radiogenic heat production in the sedimentary column according to the lithological mix. The sediment-water interface temperature (SWIT, in $^{\circ}\text{C}$) and the paleo-water depth (PWD, in m) were used to estimate the temperature at

the top of the sedimentary column through time. Finally, the evolution of the basal heat flow over time is based on Bossennec et al. (2021; see below).

In this study, the PWD data from the Permian to the Upper Jurassic (145 Ma) were derived from Blaise (2012). Its evolution varies between 0 m and 100 m accordingly to paleo-environments, e.g., 100 m corresponding to the Liassic clay-rich facies. PWD values were considered as 0 m, from the end of the Jurassic to the Paleocene, followed by the deposition of exclusively continental paleo-environments during Middle Eocene (Ménillet et al., 2015; Düringer et al., 2019). The SWIT was determined according to Bruss (2000), who compiled temperature data based on palynological and palynofacies studies of the URG from Stahmer (1980), Schuler (1990) and Sittler and Ollivier-Pierre (1994). Finally heat flow from Bossennec et al. (2021) were used. These authors estimated its value by calibrating the temperature derived from $\delta^{18}\text{O}$ measured in quartz overgrowths of URG Buntsandstein samples with burial temperature profiles modelled under OpenFlow $^{\circ}$ and based on Böcker (2015). For the pre-rift period, the following scenario was used: Heat flow of 65 mW/m^2 at the beginning of the Permian, progressively

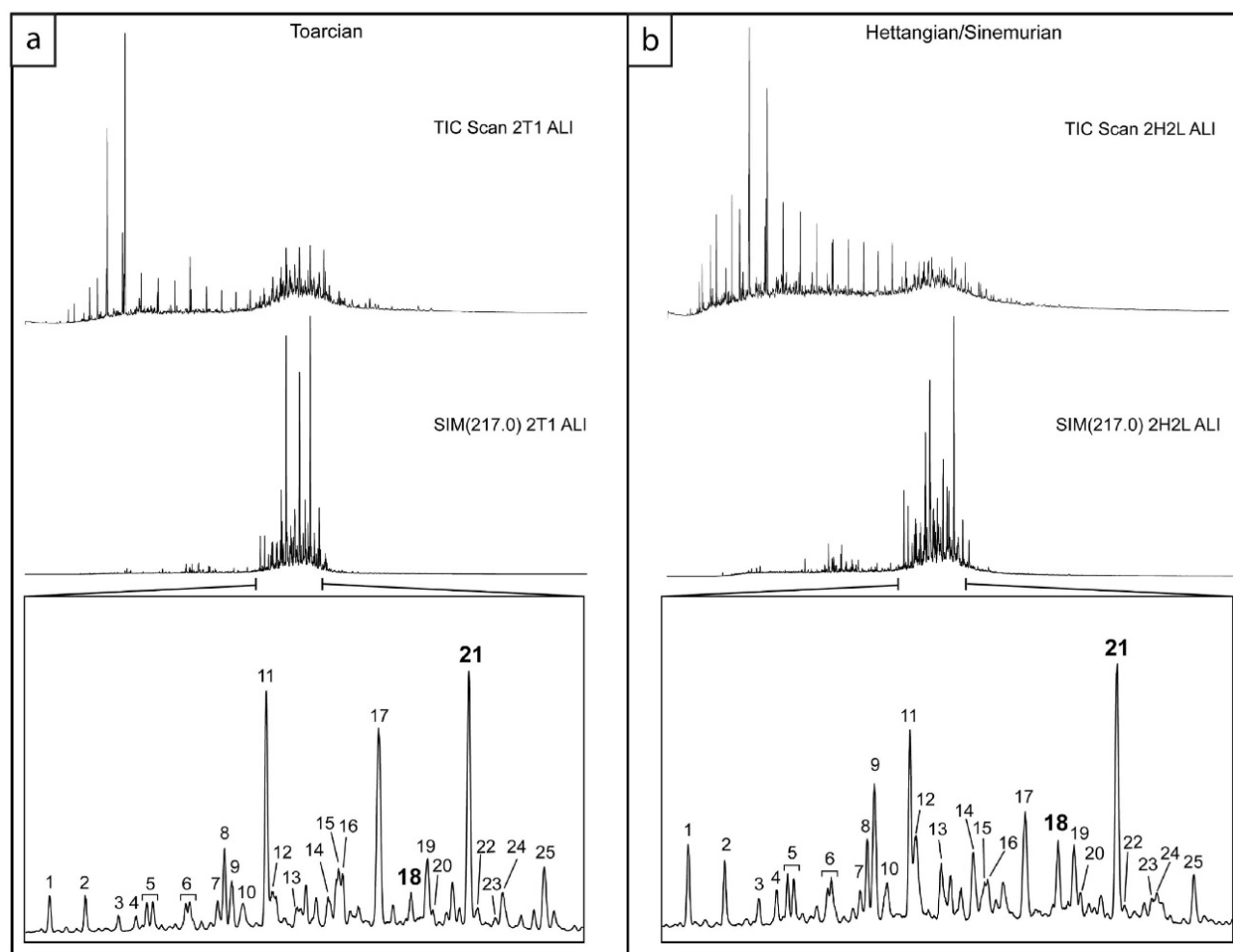


Fig. 5. Saturated fractions gas chromatograms (TIC: Fullscan Total Ion chromatogram; SIM m/z 217: Selected ion chromatogram, and partial m/z 217 showing the distributions of steranes of selected outcrop samples.

5a: Toarcian sample 2T1; 5b: Hettangian/Sinemurian sample 2H2L. Peak assignments: 1: C_{27} $\beta\alpha$ 20S; 2: C_{27} $\beta\alpha$ 20R; 3: C_{27} $\alpha\beta$ 20S; 4: C_{27} $\alpha\beta$ 20R; 5: C_{28} $\beta\alpha$ 20S*; 6: C_{28} $\beta\alpha$ 20R*; 7: C_{28} $\alpha\beta$ 20S; 8: C_{27} $\alpha\alpha$ 20S; 9: C_{27} $\alpha\beta\beta$ 20R– C_{29} $\beta\alpha$ 20S; 10: C_{27} $\alpha\beta\beta$ 20S– C_{28} $\alpha\beta$ 20R*; 11: C_{27} $\alpha\alpha\alpha$ 20R; 12: C_{29} $\beta\alpha$ 20R; 13: C_{29} $\alpha\beta$ 20S; 14: C_{28} $\alpha\alpha\alpha$ 20S*; 15: C_{28} $\alpha\beta\beta$ 20R; 16: C_{28} $\alpha\beta\beta$ 20S; 17: C_{28} $\alpha\alpha\alpha$ 20R; 18: C_{29} $\alpha\alpha\alpha$ 20S; 19: C_{29} $\alpha\beta\beta$ 20R; 20: C_{29} $\alpha\beta\beta$ 20S; 21: C_{29} $\alpha\alpha\alpha$ 20R; 22: C_{30} $\alpha\alpha\alpha$ 20S; 23: C_{30} $\alpha\beta\beta$ 20R; 24: C_{30} $\alpha\beta\beta$ 20S; 25: C_{30} $\alpha\alpha\alpha$ 20R; $\beta\alpha$, $\alpha\beta$, $\alpha\alpha\alpha$ and $\alpha\beta\beta$ denote 13 β (H),17 α (H)-diasteranes, 13 α (H),17 β (H)-diasteranes, 5 α (H),14 α (H),17 α (H)-steranes and 5 α (H),14 β (H),17 β (H)-steranes, respectively. *isomeric peaks (24S and 24R).

increasing to 80 mW/m^2 at 180 Ma, decreasing to 73–72 mW/m^2 at the end of the Jurassic, and an almost constant value (≈ 70 mW/m^2) until 90 Ma. With the URG opening, the heat flow increased to 100 mW/m^2 during the Paleocene from 60 to 50 Ma, and remained constant until the Priabonian.

4.3. Biomarker kinetic parameters

Organic matter (OM) deposited in sedimentary basins is transformed during geological history in response to burial, temperature and time (Philippi, 1965; Welte, 1966; Bajor et al., 1969). Constituents of the transformed OM, e.g. the biomarkers, record information about the thermal history of sedimentary basins. Biomarker reactions depend on time and temperature and are therefore characterized by their kinetic parameters (Seifert and Moldowan, 1980; Mackenzie and McKenzie, 1983; Gallagher and Evans, 1991; Marzi, 1992; Landais and Elie, 1999).

In this study, the kinetic parameters for the isomerization of hopanes at C_{22} (activation energy: 0.016 s^{-1} ; pre-exponential factor: 91 $kJ\ mol^{-1}$) and steranes at C_{20} (activation energy: $6 \cdot 10^{-3}$ s^{-1} ; pre-

exponential factor: 91 $kJ\ mol^{-1}$) from Mackenzie and McKenzie (1983) were used for calibration. Modelling was performed using the C_{31} -homohopanes and C_{29} -steranes S/(S + R) isomerization ratios.

4.4. Thermal simulations strategies

As conducted using PetroMod© software, burial and thermal modelling consisted of comparing the evolution of the C_{31} -homohopanes and C_{29} -steranes S/(S + R) isomerization ratios determined on the sample set (Fig. 6) with simulated values as a function of depth. For the basin modelling of pre-rift and early-rift periods, a synthetic reference stratigraphic column was constructed (Table 2) between the top of the basement at 259.8 Ma to the Marnes et Calcaires d'Ettendorf Formation at 170 Ma (layer 47 Bajocian, in Table 2). A short Induan age hiatus follows the Permian deposits, then from the Grès Vosgien Gp. (250 Ma) to the Toarcian, the domain was gradually buried by thermal subsidence. After the Cimmerian tectonic phase (Toarcian-Aalenian limit) (Robin, 1995; Guillocheau et al., 2000), the Marnes et Calcaires d'Ettendorf Formation was deposited, indicating the development of

Table 1

Rock-Eval pyrolysis and molecular geochemistry results measured on outcrop samples from the Saverne Fracture Field. Locality abbreviations: ROS: Rosenwiller; LIX: Lixhausen quarry; DET: Dettwiller; WAS: Wasselonne quarry. Rock-Eval pyrolysis parameters and biomarkers ratios abbreviations: HI: Hydrogen Index; OI: Oxygen Index; Biomarkers maturity parameters : RC₃₀ (%): $\beta\alpha/(\beta\alpha + \alpha\beta)$ C₃₀ hopane; RC₃₁ (%): 22S/(22S + 22R) C₃₁ homohopane; RC₃₂ (%): 22S/(22S + 22R) C₃₂ homohopane; RC₂₉ (%): 20S/(20S + 20R) C₂₉ 5 α (H),14 α (H),17 α (H) steranes; R²C₂₉ (%): $\beta\beta/(\beta\beta + \alpha\alpha)$ C₂₉ steranes.

Sample	Locality	Stratigraphic formation	Facies	Stage/Age	Rock-Eval pyrolysis data						Biomarkers ratios				
					TOC (%)	Tmax (°C)	S1 (mg HC/g rock)	S2 (mg HC/g rock)	HI (mg HC/g TOC)	OI (mg HC/g TOC)	RC ₃₀ (%)	RC ₃₁ (%)	RC ₃₂ (%)	RC ₂₉ (%)	R ² C ₂₉ (%)
2T4	ROS.	Couches à <i>Dactyloceras</i>	Laminated marl, clay-rich facies	Toarcian	3.39	432	0.02	15.96	471	13	31	22	18	14	29
2T3	id.	Schistes carton	id.	id.	3.21	432	0.02	16.31	508	15	30	22	17	8	24
2T2	id.	id.	Laminated marl, carbonate facies	id.	0.96	423	0.02	5.03	524	43	20	29	25	15	26
2T1	id.	id.	Laminated marl, organic-rich facies	id.	8.03	424	0.19	58.85	733	15	22	27	26	10	23
2P7	id.	Calcaire de Kirrwiller	Marls	Pliensbachian	0.66	439	0.01	0.66	100	11	46	24	14	14	27
2P5	id.	Marnes à <i>Septaria</i>	id.	id.	0.75	437	0.01	0.66	88	15	45	25	15	16	24
2P4	id.	id.	id.	id.	0.89	438	0.01	0.84	94	28	46	25	15	17	24
2P3	id.	id.	id.	id.	0.95	439	0.06	1.19	125	8	43	28	18	18	19
2P2	id.	id.	id.	id.	1.03	441	0.01	1.18	115	10	45	25	15	14	23
2P1	id.	id.	id.	id.	0.93	440	0.01	0.97	104	11	44	26	16	12	20
2P18	LIX.	Marnes à Ovoïdes	id.	id.	0.71	436	0.01	0.71	100	14	41	37	21	24	21
2P13	id.	id.	id.	id.	0.73	436	0.01	0.7	96	5	41	37	22	21	20
2P8	id.	id.	id.	id.	0.74	437	0.02	0.82	111	14	40	36	22	20	22
2H	DET.	Calcaires et marnes à Gryphées	id.	Hett./Sine.	2.9	422	0.21	14.65	505	22	23	44	35	22	28
2H21.	LIX.	id.	id.	Hett./Sine.	2.06	424	0.05	11.54	561	51	20	48	46	24	26
2R1	DET.	Argiles de Levallois	Oxidized siltstone	Rhetian	0.15	405	0.02	0.1	67	127	40	57	49	26	17
2R2	id.	Grès Rhétiens	Clayey siltstone	id.	0.81	431	0.01	0.53	65	4	41	59	56	28	31
2K	id.	Marnes irisées Supérieures	Marls	Late Triassic	–	–	–	–	–	–	14	57	61	24	45
2M	WAS.	Couches à Cératites	Limestone	Middle Triassic	0.17	440	0.01	0.42	245	116	20	60	58	45	43

carbonate platforms.

The first strategy (strategy No.1, Table 4) aimed to evaluate the maximum thickness of sediment deposited during the hiatus. Böcker (2015) speculated 400 m of Malm in his thermal model. Based on the literal interpretation of the literature, five simulations considered the deposition of 0 m, 100 m, 200 m, 300 m or 400 m of Malm followed by a hiatus period from 140 to 70 Ma. The simulation ended with the partial erosion of Bajocian and the complete erosion of Bathonian, Callovian and Malm during the Paleocene (from 60 to 50 Ma) (Fig. 6a and b).

The second strategy (strategy No.2, Table 4) aimed to assign the estimated sediment thickness to a stratigraphic age, i.e. to the Jurassic or Cretaceous. In this perspective, a first simulation considered gradual sediment deposition from 160 to 70 Ma with 200 m of Malm and 100 m of continental to coastal facies sediments of Cretaceous age, followed by the partial erosion of Bajocian and the complete erosion (from 60 to 50 Ma) of Cretaceous, Malm, Callovian and Bathonian (red curve on Fig. 6c and d). The second simulation considered the deposition of 300 m of Malm (from 160 to 145 Ma) followed by a hiatus period from 140 to 70 Ma, which ended with the partial erosion of Bajocian and the complete erosion of Malm, Callovian and Bathonian from 60 to 50 Ma (black curve on Fig. 6c and d). The third simulation considered the deposition of 200 m of Malm followed by alternations of deposition and erosion episodes during Cretaceous. Maximum cumulative thickness considered was 100 m (as to have an expected impact on biomarkers thermal maturity)

before start of erosion at 60 Ma (green curve on Fig. 6c and d).

The third strategy (strategy No.3, Table 4) considered the early-rift period (Table 3) as a sensitivity test on the simplest simulated pre-rift model (black curve on Fig. 6c and d). This strategy considered the presence of Eocene deposits in the Saverne Fracture Field (Fig. 1c) and its isolation from the URG at the beginning of Priabonian (Fig. 7). This was tested with regard to the thickness of 253 m of Lutetian and Bartonian deposits from the GRT-1 well (Fig. 2; Düringer et al., 2019).

5. Results

5.1. Geochemical characteristics of source rock samples

The characteristics of the source rocks in this sample set can be summarized as follows: the Hettangian/Sinemurian Formation (Calcaire et marnes à Gryphées - Lias α ; TOC range 2.06–2.9%; HI range 505–561 mgHCs/gTOC) and the Toarcian Posidonia Shale (Schistes carton - Lias ϵ ; TOC range 0.96–8.03%; HI range 471–733 mgHCs/gTOC) (Fig. 3; Ronov, 1958; Tissot et al., 1974; Katz, 1995). Organic matter in these samples is well-preserved type II (marine) kerogen. For the other samples of Jurassic and Triassic ages, the TOC values are <1% with HI values that do not exceed 125 mgHCs/gTOC. An exception is the Muschelkalk limestone for which the HI = 245 mgHCs/gTOC.

Organic matter preservation was also examined using the molecular

Table 2

Input data for the pre-rift burial model of the URG. Stratigraphic formations and thicknesses from [Dürringer et al. \(2019\)](#); Ages in Ma based on the international chrono-stratigraphic chart ([Cohen et al., 2013, 2019](#) revised); Lithological mixes based on the explanatory note of the Haguenau geological map ([Ménillet et al., 2015](#)). Abbreviations: E: Erosion; H: Hiatus; D: Deposition; C: Conglomerate; Ss: Sandstone; shSs: Shaly sandstone; doSs: Dolomitic sandstone; Si: Silstone; Sh: Shale; bSh: Black shale; ssSh: Sandy shale; siSh: Silty shale; Li: Limestone; siLi: Silty limestone; shLi: Shaly limestone; Ml: Marls; Do: Dolomite; Ml: Mica; PY: Pyrite; GY: Gypsum; KAO: Kaolinite; Il: Illite; Cl: Chlorite; AP: Apatite; KE: Kerogen; GL: Glauconite; CA: Calcite; Ch: Chert; DO: dolomite; AN: Anhydrite.

PRE-RIFT MODEL							
Stratigraphic formation	Modelled layer name	Age (Ma)	Thickness (m)	Eroded thickness (m)	Event (type)	Lithological Mix (%)	
-	63 Selandian	60	0	-(?) m	E	-	
-	62 Maastrichtian	to 70	0	(?)	H	-	
-	55 Berriasian	from 140					
-	54 Tithonian	145.1	0	(?)	D		
-	53 Tithonian	150	0	(?)	D	-	
-	52 Kimmeridgian	155	0	(?)	D	-	
-	51 Oxfordian	160	0	(?)	D	(?)	
Not differentiated	50 Callovian	165	0	60	D	Ml(50),Sh(20),Si(10),Sh(10),Ss(10)	
Not differentiated	49 Bathonian	167	0	50	D	Ml(35),Sh(25),Si(15),Li(10),Ss(10),Sh(5)	
Grande Oolithe	48 Bajocian	169	0	50	D	shLi(72),Sh(26),PY(2)	
SYNTHETIC REFERENCE STRATIGRAPHIC COLUMN							
Marnes et Calcaires d'Ettendorf	47 Bajocian	170	32	-	D	Li(90),Ml(10)	
Argiles Sableuses	46 Aalenian	171	4	-	D	Sh(85),Ss(15)	
Formation de Schalkendorf	45 Aalenian	172	39	-	D	Si(50),Ss(22),Sh(8),Li(8),Ml(8),PY(6)	
Formation de Gundershoffen	44 Aalenian	174	39	-	D	Sh(45),Si(15),Li(15),Ss(12),PY(5),GY,KAO,IL&CH(3 ea.)	
Formation de Printzheim	43 Aalenian	175	32	-	D	Ml(60),Si(25),bSh(10),PY(3),GY(2)	
Marnes de Schillersdorf	42 Toarcian	177.5	6	-	D	Ml(70),Li(15),AP(15)	
Couches à <i>Dactyloceras</i> c.	41 Toarcian	180	3	-	D	bSh(75),Li(25)	
Schistes carton	40 Toarcian	182	9	-	D	bSh(80),Ml(10),Li(10)	
Calcaire de Kirrwiller	39 Pliensbachian	183.5	1	-	D	Li(85),Ml(15)	
Marnes à <i>Septaria</i>	38 Pliensbachian	184.5	7	-	D	Ml(90),Li(35),PY(5)	
Marnes à Ovoïdes	37 Pliensbachian	185.5	52	-	D	id.	
Marnes feuilletées	36 Pliensbachian	186.5	5	-	D	id.	
Calcaire de Zinswiller	35 Pliensbachian	188.5	5	-	D	siLi(80),Ml(20)	
Formation de Bossendorf	34 Pliensbachian	189.5	4	-	D	Ml(100)	
Calcaire de Gundershoffen	33 Sinemurian	191.5	1	-	D	Li(88),Ml(12)	
Formation d'Obermodern	32 Sinemurian	195.5	29	-	D	siLi(80),Ss(5),Si(5),IL(4),PY&MI(3 ea.)	
Calcaires et Marnes à Gryphées	31 Hettangian	199.5	21	-	D	Ml(40),Li(28),Sh(15),Si(15),KE(2)	
Argiles de Levallois	30 Rhaetian	202	9	-	D	Sh(72),Li(18),Si(5),IL&KAO(2.50 ea.)	
Grès Rhétiens	29 Rhaetian	205	9	-	D	Ss(40),Si(40),Sh(14),Co(5),PY(1)	
Argiles Bariolées dolomitiques	28 Norian	209	27	-	D	siLi(50),Ml(35),Do(15)	
Argiles de Chanville	27 Carnian	227.3	16	-	D	Sh(68),AN(20),Ss(10),Li(2)	
Dolomie de Beaumont	26 Carnian	229	5	-	D	Do(100)	
Argiles Bariolées Intermédiaires	25 Carnian	232	5	-	D	Ml(60),Li(15),Ss(9),Do(5),GY(3)	
Grès à Roseaux	24 Carnian	235	7	-	D	id.	
Marnes Irisées inférieures	23 Carnian	237	97	-	D	Id.	
Dolomie Limite	22 Ladinian	242	1	-	D	Do(100)	
Argiles de la Lettenkohle	21 Anisian	242.5	21	-	D	Sh(35),Si(25),Ss(20),Do(15),doSs(5)	
Dolomie inférieure	20 Anisian	243	11	-	D	Do(50),Sh(25),Si(15),DO(8),GL(2)	
Calcaire à Térébratules	19 Anisian	243.5	2	-	D	Li(80),shLi(20)	
Couches à Cératites	18 Anisian	244	38	-	D	shLi(60),Sh(20),Ml(20)	
Calcaire à Entroques	17 Anisian	244.5	9	-	D	Li(92),Ml(8)	
Dolomie à Lingules	16 Anisian	245	10	-	D	Do(45),Ml(25),Ch(20),CA&CHE(5 ea.)	
Marnes Bariolées	15 Anisian	245.5	37	-	D	AN(50),Ml(30),Do(20)	
Orb.-Schaumkalk-Wellenkalk	14 Anisian	246	14	-	D	shLi(32),Do(23),Sh(22.5),siSh(22.5)	
Wellenmergel-C. Térébratules	13 Anisian	246.5	16	-	D	Ss(26),Do(26),Si(26),DO(7),CA(5)	

(continued on next page)

Table 2 (continued)

PRE-RIFT MODEL							
Couches à <i>Myacites</i>	12 Anisian	247	11			D	Si(45),siSh(35),doSs(15),MI(5)
Grès Coquillier	11 Olenekian	247.3	8	–		D	doSs(75),Si(15),siSh(10)
Grès à <i>Voltzia</i> (G. argileux)	10 Olenekian	247.4	9			D	Ss(35),shSs(35),Sh(30)
Grès à <i>Voltzia</i> (G. à Meules)	9 Olenekian	247.5	9	–		D	id.
Couches Intermédiaires	8 Olenekian	248	41	–		D	doSs(55),siSh(30),Si(10),Do(5)
Poudingue de Sainte-Odile	7 Olenekian	248.5	20	–		D	Co(100)
Couches de Karlstal	6 Olenekian	249	100			D	Ss(80),Co(20)
Couches de Rehberg	5 Olenekian	249.5	79	–		D	Ss(60),Co(40)
Couches de Trifels	4 Olenekian	250	91	–		D	Ss(50),Co(50)
Gap of Induan	3 Induan	252	–	–		H	–
Grès d'Annweiler	2 Changhsingian	253	41	–		D	shSs(80),ssSh(20)
Grès Anté-Annweiler	1 Changhsingian	254	10	–		D	Ss(60),Co(30),Sh(10)
Top basement	0 Wuchiapingian	259.8					

Table 3

Input data for the early-rift burial model of the URG. Stratigraphic formations and thicknesses after [Duminger et al. \(2019\)](#); Ages in Ma are based on the international chrono-stratigraphic chart ([Cohen et al., 2013](#), 2019 revised); Lithological mixes based on the explanatory note of the Haguenau geological map ([Meruliet et al., 2015](#)). Abbreviations: E: Erosion; H: Hiatus; D: Deposition; Co: Conglomerate; Ss: Sandstone; Si: Silstone; Sh: Shale; Li: Limestone; shLi: Shaly limestone; MI: Marls; Do: Dolomite; PY: Pyrite; AN: Anhydrite.

EARLY-RIFT MODEL							
Stratigraphic formation	Modelled layer name	Age (Ma)	Thickness (m)	Eroded thickness (m)	Event type	Lithological Mix (%)	
Marnes Vertes à Limnées	66 Bartonian	39	92	0	D	MI(70),Ss(12),Co(8),Do(8),AN(2)	
Marnes Calcaires Grises à Anhydrite	65 Bartonian	40	159	0	D	MI(75),AN(25)	
Zone de transition	64 Lutetian	45	2	0	D	MI(40),Sh(40),Li(15),PY(5)	
–	63 Selandian	60	–	–160	E	–	
DISCUSSED STRATIGRAPHIC CONTRIBUTION	–	62	70	–	0	H	
–	Maastrichtian	–	–	–	–	–	
–	61 Campanian	80	–	0	II	–	
–	60 Turonian	90	–	0	H	–	
–	59 Cenomanian	100	–	0	H	–	
–	58 Albian	110	–	0	H	–	
–	57 Aptian	120	–	0	H	–	
–	56 Hauterivian	130	–	0	H	–	
–	55 Berriasian	140	–	0	H	–	
–	54 Tithonian	145.1	0	75	D	Li(50),MI(30),Sh(10),Si(10)	
–	53 Tithonian	150	0	75	D	Li(50),MI(30),Sh(10),Si(10)	
–	52	155	0	75	D	Li(50),MI(30),Sh(10),Si(10)	
–	Kimmeridgian	–	–	–	–	–	
–	51 Oxfordian	160	0	75	D	Li(50),MI(30),Sh(10),Si(10)	
Not differentiated	50 Callovian	165	0	60	D	MI(50),Sh(20),Si(10),Sh(10),Ss(10)	
Not differentiated	49 Bathonian	167	0	50	D	MI(35),Sh(25),Si(15),Li(10),Ss(10),Sh(5)	
Grande Oolithe	48 Bajocian	169	0	50	D	shLi(72),Sh(26),PY(2)	
INTEGRATION OF THE SYNTHETIC REFERENCE STRATIGRAPHIC COLUMN							

geochemistry of aliphatic and aromatic fractions determined by GC-MS, especially regarding rocks with low TOC contents. All samples showed well-preserved hydrocarbon distributions (Figs. 4 and 5; data not shown except for Toarcian and Hettangian/Sinemurian samples).

5.2. Thermal maturity of rock samples

Hydrogen Index values as a function of T_{max} (°C) are shown in Fig. 3c. Most samples have T_{max} values below 435 °C and are immature (Peters, 1986). For the Pliensbachian samples, the values cluster around 440 °C and TOC values are lower than <1%.

Biomarker maturity ratios using hopanes (Fig. 4 and Table 1) and steranes (Fig. 5 and Table 1) were calculated on m/z 191 and m/z 217 chromatograms. Specific ratios included: $\beta\alpha/(\alpha\beta + \beta\alpha)$ C_{30} hopanes ratio

(C_{21} isomerization); $S/(S + R)$ ratios for C_{31} and C_{32} homohopanes (C_{22} isomerization); $\beta\beta/(\beta\beta + \alpha\alpha)$ C_{29} steranes ratio; and $S/(S + R)$ C_{29} 5α (H), 14α (H), 17α (H) steranes ratio (C_{20} isomerization).

The $\beta\alpha/(\alpha\beta + \beta\alpha)$ C_{30} hopanes ratios for these samples are distributed over a wide range within the same formation (Table 1). These results and those from the $\beta\beta/(\beta\beta + \alpha\alpha)$ C_{29} steranes ratio do not show any correlation with depth. In contrast, $22S/(22S + 22R)$ C_{31} and C_{32} homohopane ratios (Table 1) increase respectively from 22 to 60% and 18–61% following the stratigraphic age of the deposits (and hence paleo-depth) from Liassic to Muschelkalk (Table 1; Fig. 6). However, the C_{32} homohopane ratio results display a discrepancy between Argiles de Levallois Formation (Rhaetian) and Muschelkalk. The $20S/(20S + 20R)$ C_{29} $\alpha\alpha\alpha$ steranes ratio increases from 14 to 45%, from Liassic to Muschelkalk (Table 1; Fig. 6), following the stratigraphic age of the

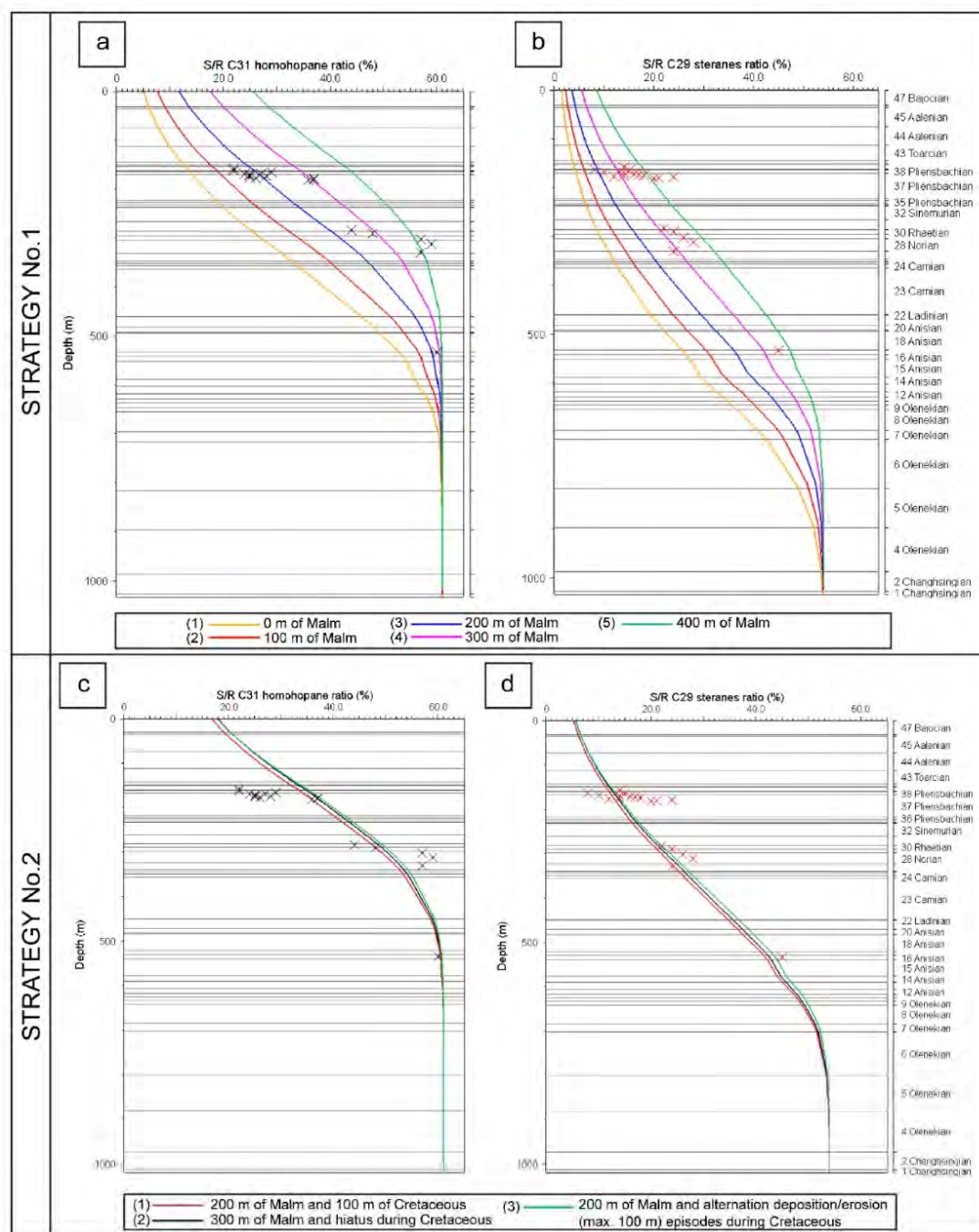


Fig. 6. Thermal maturity calibration using modelled (curves) vs. measured (crosses) S/(S + R) ratios (%) versus depth (m) for the strategies No.1 and No.2 using PetroMod© software. Isomerization kinetic parameters are from Mackenzie and McKenzie (1983). Lithostratigraphic column as in Table 2 a. S/(S + R) C₃₁ homohopane ratio (%) evolutions testing 0, 100, 200, 300 and 400 m of Malm (see Table 4). b. S/(S + R) C₂₉ steranes ratio (%) versus depth (m) evolutions testing various thicknesses of Malm (same as for 6a; Table 4). c. S/(S + R) C₃₁ homohopane ratio (%) versus depth (m) evolutions testing (1) (in red) a gradually deposition from 160 to 70 Ma of 200 m of Malm and 100 m of Cretaceous and subsequent partial erosion of Bajocian and the full erosion of Bathonian, Callovian, Malm and Cretaceous from 60 to 50 Ma; (2) (in black) the deposition of 300 m of Malm followed by a hiatus period from 140 Ma to 70 Ma and subsequent partial erosion of Bajocian and full erosion of the Bathonian, Callovian and Malm from 60 to 50 Ma; (3) (in green) deposition of 200 m of Malm followed by an alternation of deposition/erosion episodes of Cretaceous (paleoburial max. of 100 m) followed by erosion to Bajocian (60-50 Ma). d. S/(S + R) C₂₉ steranes ratio (%) versus depth (m) evolutions testing same simulations as in Fig. 6c.

Table 4
 Synthesis of the simulations tested on PetroMod® software and refers to the figures where the associated results are represented. S/(S + R) C₃₁ H referred to the 22S/(22S + 22R) C₃₁ homohopane ratio (%) and S/(S + R) $\alpha\alpha\alpha$ C₂₉ S to the 20S/(20S + 20R) $\alpha\alpha\alpha$ C₂₉ steranes ratio (%), both simulated using Mackenzie and McKenzie (1983) kinetic parameters.

PRE-RIFT MODEL				EARLY-RIFT MODEL			
Strategy No.1: Estimation of the maximum depth of paleoburial by adding eroded sediment thicknesses				Strategy No.2: Assignment of the estimated maximum cumulative thickness to the Upper Jurassic and/or Cretaceous			
Simulation Results	Simulated curves		Synthesis of simulation tests	Simulation Results	Simulated curves		Synthesis of simulation tests
	Run nb.	Color			Run nb.	Color	
Fig. 6a, using S/(S+R) C ₃₁ H	1	Orange	Adding 0 m of Malm (160–145.1 Ma) followed by a hiatus period (140–70 Ma), ended by the partial erosion of Bajocian (50 m) and complete erosion of Bathonian, Callovian and Malm in the Paleocene (60–50 Ma)	Fig. 6c, using S/(S+R) C ₃₁ H	1	Red	Adding a gradual deposition of 200 m of Malm (160–145.1) and 100 m of Cretaceous (140–70 Ma), followed by the partial erosion of Bajocian (50 m) and complete erosion of Bathonian, Callovian, Malm and Cretaceous (60–50 Ma)
	2	Red			2	Black	
	3	Blue			3	Green	
	4	Purple			3	Green	
	5	Green			3	Green	
Fig. 6b, using S/(S+R) $\alpha\alpha\alpha$ C ₂₉ S	1	Orange	Same as in Fig. 6a	Fig. 6d, using S/(S+R) $\alpha\alpha\alpha$ C ₂₉ S	1	Red	Same as in Fig. 6c
	2	Red			2	Black	
	3	Blue			3	Green	
	4	Purple			3	Green	
	5	Green			3	Green	

deposits.

Thermal maturity of the Lutetian sediments in the Saverne Fracture Field (for which no outcrops are currently available) could be estimated from Arpino (1973). The m/z 191 chromatogram of lignite from the Complexe Inférieur argileux de Bouxwiller Formation when compared with the Messel shale (e.g., Kimble et al., 1974; Sugden and Abbott, 2002; Adam and Schaeffer, personal communication) has a very low abundance of the C₃₁ homohopane S-configuration compared to the R-configuration. The estimated 22S/(22S + 22R) C₃₁ homohopane ratio (based on Arpino (1973); Adam and Schaeffer, personal communication) is equal to 1.2%.

5.3. Pre-rift modelling: results of the strategies No.1 and No.2

The first step of the study considered only the pre-rift period to evaluate the maximum burial depth reached during the Upper Jurassic and the Cretaceous (Tables 2 and 4). Since the Malm in the study area was deposited and then eroded, an estimate of its initial thickness is

required. Strategy No.1 is represented by the graphs in Fig. 6a and b. Fig. 6a compares measured to modelled values of C₃₁ homohopane isomerization ratio (expressed as %) as a function of depth by considering (1) 0 m, (2) 100 m, (3) 200 m, (4) 300 m and (5) 400 m thickness of Malm (Table 4). Fig. 6b compares measured to modelled values of C₂₉ $\alpha\alpha\alpha$ 20S/(20S + 20R) sterane isomerization ratios (expressed as %) as a function of depth by considering the same Malm thicknesses as previously, i.e., (1) 0 m, (2) 100 m, (3) 200 m, (4) 300 m and (5) 400 m (Table 4). The best fit between simulated and measured 22S/(22S + 22R) C₃₁ homohopane and 20S/(20S + 20R) C₂₉ $\alpha\alpha\alpha$ steranes ratios versus depth is obtained for a Malm thickness ranging from 200 to 300 m and from 300 to 400 m, respectively. Thus, a value of 300 m of Malm was chosen for further modelling (Fig. 6c and d; Fig. 7).

Fig. 6c and d show the three simulated curves of strategy No.2 (Table 4). The gradual deposition of sediments during the Malm and Cretaceous is represented by the curve in red; the exclusive deposition of Malm followed by a Cretaceous hiatus period is represented by the second curve in black; and the deposition of Malm followed by an

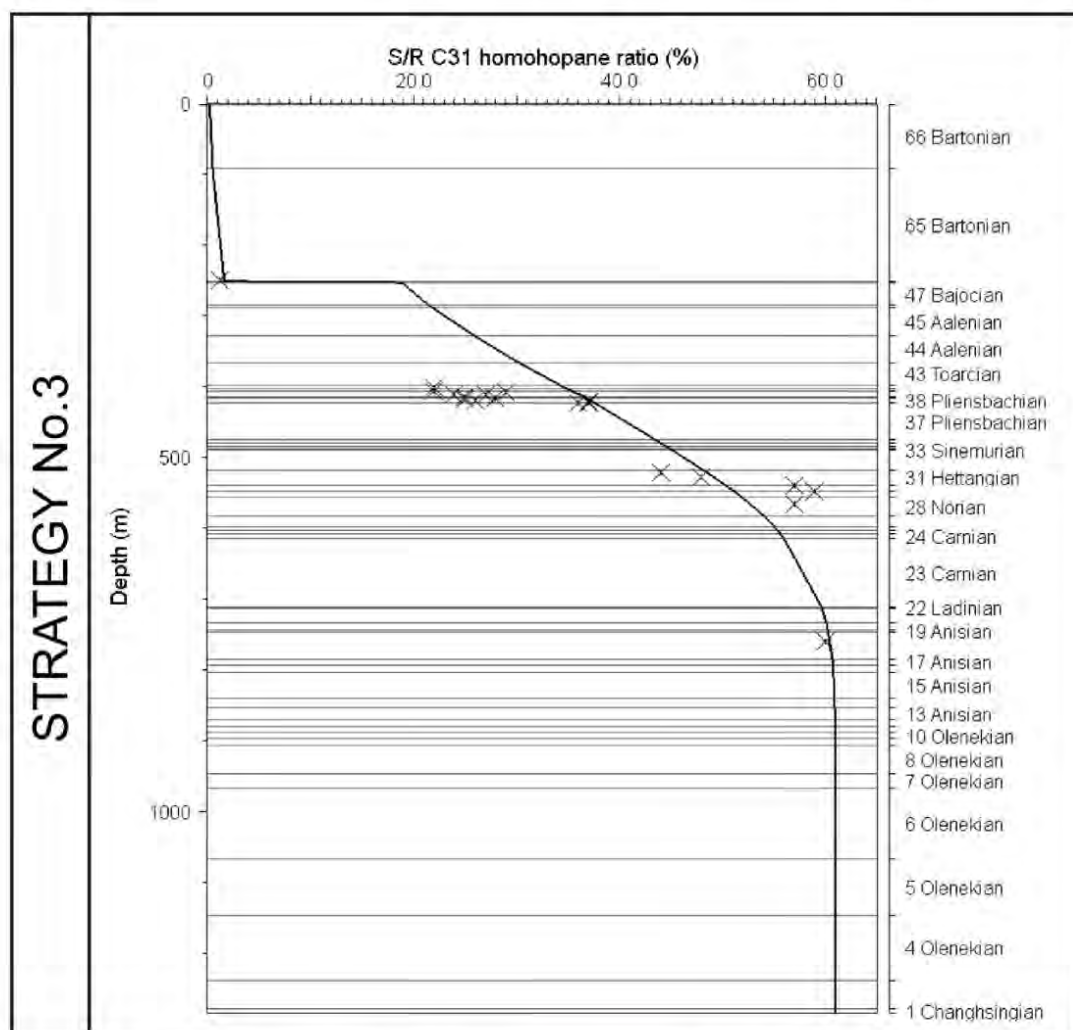


Fig. 7. Thermal maturity calibration using modelled (curve) vs. measured (crosses) S/(S+R) C₃₁ homohopane ratio (%) versus depth (m) for the strategy No.3 using PetroMod® software. Isomerization kinetic parameters are from Mackenzie and McKenzie (1983). Lithostratigraphic column as in Table 3. S/(S + R) C₃₁ homohopane ratio (%) versus depth (m) evolution based on the simulation represented by the black curve on Fig. 6c and d, including deposition of 253 m of Middle Eocene.

alternating deposition/erosion of Cretaceous by the curve in green (Fig. 6c and d), according to the simulation strategies described in subsection 4.4 and summarized in Table 4. It appears that the three curves are almost indistinguishable.

5.4. Early-rift modelling: results of the strategy No.3

The modelling results corresponding to the early-rift period are represented by Figs. 7 and 8. 253 m of Middle Eocene were added to the pre-rift burial model (black curve in Fig. 6c and d) which considered 300 m of Malm followed by a hiatus period from 140 to 70 Ma, ended by the complete erosion of Malm, Callovian, Bathonian and the partial erosion of Bajocian (60–50 Ma) (Table 4). Fig. 7 presents the values of C₃₁ homohopane isomerization ratio (expressed as %) as a function of depth, measured on the Mesozoic formations and estimated for the Bouxwiller lignite (see subsection 5.2).

6. Discussion

6.1. The Saverne Fracture Field source rocks

Rock-Eval pyrolysis results of the Saverne Fracture Field outcrop samples indicate that only the Hettangian/Sinemurian Formation and the Toarcian Posidonia Shale have source rock characteristics (Table 1; see subsection 5.1). This conclusion for the Saverne Fracture Field source rocks is similar to Röhl et al. (2001), Frimmel (2003), and Böcker and Littke (2016), who studied source rock properties in the URG. For samples with TOC below 1% (especially the Pliensbachian samples), matrix effects are expected during Rock-Eval pyrolysis and can lead to unreliable T_{max} values (Peters, 1986; Blaise et al., 2011). In addition, variations in the type of OM and its preservation affect T_{max} (Böcker and Littke, 2016), especially for pre-oil window maturity levels (Peters, 1986; di-Giovanni et al., 1998). Yang and Horsfield (2020) list the numerous factors that can influence maturity evaluation using T_{max}. For these reasons, the thermal models were not calibrated using T_{max}.

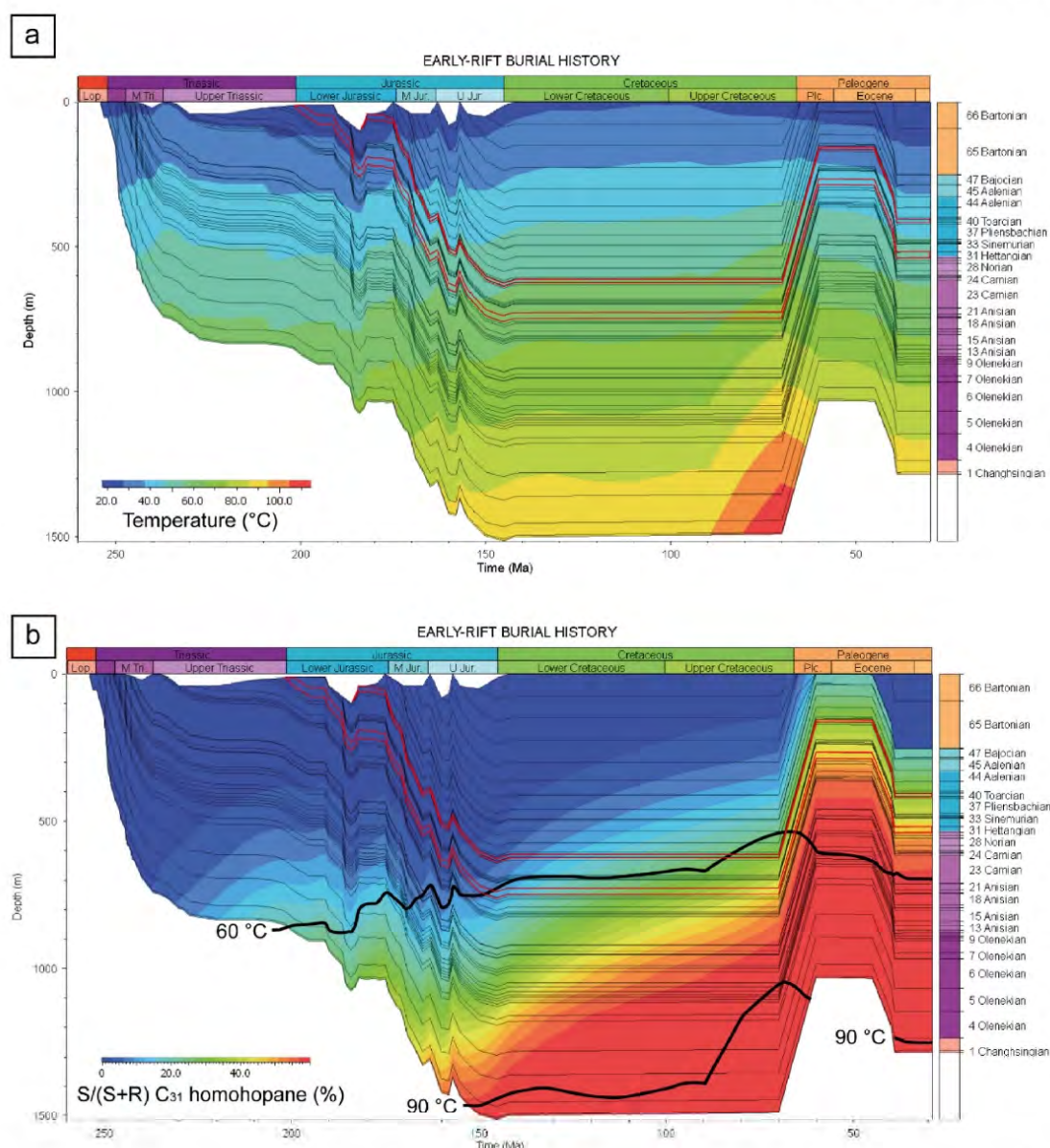


Fig. 8. 1D basin burial history of the early-rift stage considering the pre-rift model represented by the black curve in Fig. 6a and d, followed by the deposition of 253 m of Lutetian and Bartonian according to Düringer et al. (2019) (PetroMod® software). a. The two main source rocks are outlined in red and the colored overlay applied correspond to the temperature from 20 to 110 °C. b. The two main source rocks are outlined in red, the isotherms 60 °C and 90 °C are represented by black curves and the colored overlay applied correspond to the simulated thermal maturity of S/(S + R) C₃₁ homohopane ratio (%) using Mackenzie and McKenzie (1983) kinetic parameters.

6.2. Thermal maturity recorded for the Saverne Fracture Field rock samples

No clear correlation was found between maturity and depth concerning $\beta\beta/(\beta\beta + \alpha\alpha)$ C₂₉ steranes and $\beta\alpha/(\alpha\beta + \beta\alpha)$ C₃₀ hopane ratios (Table 1). The $\beta\alpha/(\alpha\beta + \beta\alpha)$ C₃₀ hopane ratio may be significantly influenced by depositional environment and organic matter input (Moldovan et al., 1986; Rullkötter and Marzi, 1988). The $\beta\beta/(\beta\beta + \alpha\alpha)$ C₂₉ steranes ratio is described in the literature as rather independent of organic matter source (Seifert and Moldovan, 1986). Yet, its evolution as a function of thermal maturation is most effective within oil window. Conversely, a good correlation was found between maturity and depth using the 20S/(20S + 20R) C₂₉ $\alpha\alpha\alpha$ steranes ratio.

At lower maturity levels, homohopanes isomerization occurs earlier than for many other biomarker maturity parameters. The 22S/(22S + 22R) homohopanes ratio increases from 0 to an equilibrium value of 55–62% at onset of oil window (Seifert and Moldovan, 1980; Zumberge, 1987; Marzi, 1992). This ratio when measured on the sample set increases from 22 to 60%, following the stratigraphic age of the deposits (Table 1). Same ranges of thermal maturity values were measured in the corresponding stratigraphic formations of the eastern Paris Basin (Blaise et al., 2011). The variable data for the Triassic clay and sandstone samples are a consequence of a low signal-to-noise ratio related to low biomarker content which led to the overestimation of maturity. In any case, isomerization ratio equilibrium values increase with stratigraphic depth up to 60% for Triassic which has therefore reached the onset of oil

window (Fig. 6; Seifert and Moldovan, 1980; Zumberge, 1987; Marzi, 1992). The same conclusion is obtained for the $20S/(20S + 20R)$ C_{29} $\alpha\alpha\alpha$ sterane ratios, which increases from 14 to 45% (Table 1). This means that the Liassic petroleum source rocks did not generate oil before the opening of the URG. Their immaturity level is, therefore, a significant constraint to the determination by modelling of the maximum burial depth (reached during the Jurassic/Cretaceous hiatus; Fig. 8).

6.3. Estimation of the maximum cumulative thickness of Jurassic/Cretaceous eroded sediments

The best fit between measured and modelled data using C_{31} $22S/(22S + 22R)$ homohopane ratio (%) is obtained for a sediment thickness ranging from 200 to 300 m. Meanwhile, the best fit between measured and modelled data using C_{29} $20S/(20S + 20R)$ sterane ratio (%) is obtained for a sediment thickness ranging from 300 to 400 m. This leads to a mean estimated value of 300 m thickness of Malm (Fig. 6a and b). This thickness is relatively low compared to the approximately 700 m of Malm in the central Paris Basin (Guillocheau et al., 2000) or approximately 500–550 m in the Southwest German Basin (Thomas and Schulz, 2007). Mazurek et al. (2006) proposed that in the Swiss Molasse Basin, 600–700 m of late Jurassic and Cretaceous sediments were deposited.

In his model (1D thermal model of Mingolsheim 1986 Well, URG), Böcker (2015) speculated a deposit of 400 m of Malm and 200 m of Cretaceous sediments, presumably corresponding to the total cumulative thickness of sediments deposited during the sedimentary hiatus. Thermal modelling allows the estimation of the maximum depth of paleoburial by adding thickness of sediments that thermally impacted the underlying layers, i.e. the maximum cumulative thickness.

If the Cretaceous was deposited, it happened with alternating depositional and erosional periods, as discussed in Böcker (2015) and references therein (e.g., Meyer, 1976; Haq, 2014). In addition, during this period, the study area was uplifted (Cloos, 1939; Illies, 1975) and elevated above the depositional level (Scheck-Wenderoth et al., 2008; Ménillet et al., 2015). Since the “depositional duration” variable strongly impacts the source rock maturation, the total cumulative thickness of Cretaceous sediments is not representative of the maximum cumulative thickness. In addition, as the Upper Jurassic-Early Cretaceous correspond to a Europe-wide sea-level fall, the marine regression resulted in the isolation of depositional basins (Ruffell, 1991), which prevents the straightforward comparison of the Saverne Fracture Field (the future URG area) with the surrounding basins. However, whether the maximum cumulative thickness of about 300 m (Fig. 6a and b) can be attributed to Malm sediments only or to Malm and Cretaceous needs to be tested.

6.4. Assignment of the estimated maximum cumulative thickness to the Upper Jurassic and/or Cretaceous

Table 4 summarizes simulations testing the hypothesis of Cretaceous deposition: (1) the first simulated curve (red curve in Fig. 6c and d) corresponds to a gradual deposition of 200 m of Malm and 100 m of Cretaceous (from 160 to 70 Ma), followed by the partial erosion of Bajocian and the complete erosion of Bathonian, Callovian and Malm (from 60 to 50 Ma); (2) the second curve (black curve on Fig. 6c and d) corresponds to a deposition of 300 m of Malm followed by a hiatus period (from 140 to 70 Ma), and then by the partial erosion of Bajocian and complete erosion of Bathonian, Callovian and Malm (from 60 to 50 Ma); and (3) the third curve (green curve on Fig. 6c and d) corresponds to a deposition of 200 m of Malm followed by an alternation of deposition/erosion episodes of Cretaceous (maximum cumulative thickness of 100 m), followed by the partial erosion of Bajocian and the complete erosion of Bathonian, Callovian and Malm (from 60 to 50 Ma).

The models based on strategy No.2 testing the hypothesis of Cretaceous deposition show that all the tested burial conditions are consistent with the measured data (Fig. 6c and d). However, if the Cretaceous

deposited, it must not have accumulated significant thicknesses (maximum cumulative thickness ≤ 100 m; simulation results not shown). Indeed, although the Cretaceous exists in the Paris Basin, it is absent in the southwestern part of Germany (Geyer et al., 1991; LGRB, 1998; Lahner and Toloczky, 2004). Blaise et al. (2011, 2014) estimated its thickness to decrease eastward within Paris Basin. In this sense, it appears that the paleo-shoreline was very likely at the eastern end of the Paris Basin (Ziegler, 1990), at the border of the future URG area in progressive uplift (Cloos, 1939). Given the geodynamics of the Upper Jurassic/Cretaceous period (e.g., Ziegler, 1987; Hibsich et al., 1995), the multiplication of tectonic events and the strong structural inheritance of the study area (Schumacher, 2002; Sissingh, 2006; Edel et al., 2007), the sediments were likely not deposited continuously (as considered for the red curve in Fig. 6c and d). As mentioned above, for some authors if the Cretaceous was deposited, it happened with alternating depositional and erosional periods. It turns out that the simulation of alternating deposition/erosion of Cretaceous sediments might be accredited regarding the simulation results (green curve on Fig. 6c and d), although there is no evidence of Cretaceous deposition and subsequent erosion. For this reason, the estimation of alternating deposited and eroded sediments during Cretaceous is questionable. Because the simulation results are the same, it seems more relevant from a modelling perspective to use the simplest simulation represented by the black curve, i.e., the exclusive deposition of Malm followed by a Cretaceous hiatus period before erosion (black curve in Fig. 6c). For all simulations, maximum temperatures of the Posidonia Shale and the Hettangian/Sinemurian Formation reached before the onset of the URG are about 65 °C and 72 °C, respectively. These values were reached during Late Cretaceous (70 Ma) (Fig. 8a).

6.5. Consideration of the burial and thermal histories of the early-rift period

To consider an influence of the very first stages precursor to the URG main onset, the modelling represented in Figs. 7 and 8 is based on a simulation adding 253 m of early-rift sediments (deduced from the GRT-1 well and in agreement with the presence of sparse Eocene deposits in the Saverne Fracture Field) to the burial history represented by the black curve of Fig. 6c and d (see Table 4). This modelling corresponds to a sensitivity test of the simplest pre-rift model (black curve on Fig. 6c and d). Its burial history and the associated evolution of the $22S/(22S + 22R)$ C_{31} homohopane over time is represented in Fig. 8b. The evolution of this ratio according to depth reveals a shift in the simulated trend between the pre-rift and the early-rift series (Fig. 7). This is a consequence of the Upper Jurassic/Cretaceous erosion and the transition from pre-rift geothermal history to rift initiation. Such shift is also observed in thermal maturity measurements within wells of the Pechelbronn sub-basin (Robert, 1985; Böcker, 2015; and references therein). For Mesozoic sediments, the considered scenario induces a slight shift towards the higher conversion of $22S/(22S + 22R)$ C_{31} homohopane ratio in response to additional burial and heating during the early-rift, within acceptable range of measured data. The Bouxwiller lignite estimated $S/(S + R)$ C_{31} homohopane value of 1.2% is in complete agreement with the early-rift sediment thickness of the well GRT-1 (Pechelbronn sub-basin). Note that the approximately 250 m thickness can be attributed actually to Eocene deposits alone or to Eocene deposits plus additional Oligocene alluvial fans, in response to the later activity of the faults (Ménillet et al., 1979; Genre, 1981).

7. Conclusion

This study combining basin burial and thermal modelling, as well as biomarker geochemistry from the Saverne Fracture Field, improves the knowledge of the URG pre-rift and early-rift thermal history. First, the results show that the Liassic source rocks of the Saverne Fracture Field are immature. The $22S/(22S + 22R)$ C_{31} homohopane ratio equilibrium

values indicate that the onset of the oil window is reached in the Triassic stratigraphic levels. The thermal maturity measurements calculated from the $22S/(22S + 22R)$ C_{31} homohopane and $20S/(20S + 20R)$ C_{29} $\alpha\alpha\alpha$ steranes ratios were integrated into PetroMod© software as calibration values. The reconstruction of a synthetic reference stratigraphic column for the Saverne Fracture Field and the testing of several burial scenarios and thermal modelling using PetroMod© software proposes a maximum cumulative thickness of 300 m of eroded sediments above the Dogger series. In contrast, it could not be demonstrated whether this value should be attributed to Malm deposits solely or to Malm and Cretaceous. However, in regards to literature and burial sensitivity tests, the maximum cumulative thickness of Cretaceous must have been low (≤ 100 m). These conclusions can be transposed to the eastern Paris Basin, which recorded the same thermal history from the Permian to the Cretaceous/Paleocene. In addition, the thermal maturity measurement of the Bouxwiller Lutetian lignites combined with thermal modelling indicates that, during the very first onset of the URG, the Mesozoic sediments could have been buried again by about 250 m of Cenozoic sediments, with negligible influence on the pre-rift thermal signature. As a consequence, the thermal maturity of the Liassic source rocks within the URG was never sufficient to reach the oil window during the pre-rift stage. Their maturation in the deeper parts of the URG to reach the oil-to-gas windows would then only be the consequence of syn-rift to post-rift burial, with the potential (local) additional influence of geothermal anomalies. Thanks to this study, the determination of their respective contribution to the overall thermal effect on the URG source rocks can now be further investigated.

Declaration of competing interest

The authors declare that they have no known competing financial interests or personal relationships that could have appeared to influence the work reported in this paper.

Data availability

Data will be made available on request.

Acknowledgements

The authors would like to thank ÉS-Geothermie and especially A. Genter for sharing their data on well GRT-1 and scientific discussions, as well as P. Adam and P. Schaeffer (University of Strasbourg) for sharing GC-MS data on the aliphatic fraction of the Messel shale. We also thank Schlumberger for providing the PetroMod© academic license. Dr. B. Katz and T. Blaise are thanked for their thorough and detailed review as well as Prof. P. Philp for English spelling and clarity advisory. Their respective contributions greatly improved our manuscript. The Université de Lorraine is acknowledged for funding this research through the "Lorraine Université d'Excellence" initiative (DEEPSURF project), reference ANR-15-IDEX-04-LUE.

References

Abuhelou, F., Mansuy-Huault, L., Lorgeoux, C., Catteloin, D., Collin, V., Bauer, A., Kanbar, H.J., Gley, R., Manceau, L., Thomas, F., 2017. Suspended particulate matter collection methods influence the quantification of polycyclic aromatic compounds in the river system. *Environ. Sci. Pollut. Control Ser.* 24 (28), 22717–22729.

Arpino, P., 1973. Les lipides de sédiments lacustres éocènes. Doctoral Dissertation, Université de Strasbourg, p. 107.

Baillieux, P., Schill, F., Edel, J.-B., Mauri, G., 2013. Localization of temperature anomalies in the Upper Rhine Graben: insights from geophysics and neotectonic activity. *Int. Geol. Rev.* 55 (14), 1744–1762.

Bajor, M., Roquebert, M., Van der Weide, B., 1969. Transformation de la matière organique sédimentaire sous l'influence de la température. *Bull. Centre Recherches Pau-SNPA* 3 (1), 113–124.

Baujard, C., Genter, A., Dalmais, E., Maurer, V., Hehn, R., Rosillette, R., Vidal, J., Schmittbuhl, J., 2017. Hydrothermal characterization of wells GRT-1 and GRT-2 in

Rittershoffen, France: implications on the understanding of natural flow systems in the Rhine Graben. *Geothermics* 65, 255–268.

Berger, J.-P., Reichenbacher, B., Becker, D., Grimm, M., Grimm, K., Picot, L., Storni, A., Pirkenseer, C., Derer, C., Schaefer, A., 2005. Paleogeography of the upper rhine graben (URG) and the Swiss Molasse Basin (SMB) from Eocene to Pliocene. *Int. J. Earth Sci.* 94 (4), 697–710.

Blache, C., Lorgeoux, C., Andriatsihoarana, S., Colombano, S., Faure, P., 2015. Effect of pre-heating on the chemical oxidation efficiency: implications for the PAH availability measurement in contaminated soils. *J. Hazard Mater.* 286, 55–63.

Blaise, T., 2012. Histoire thermique et interactions fluides-roches dans l'Est du Bassin de Paris. Doctoral Dissertation, Université de Lorraine, p. 348.

Blaise, T., Izart, A., Michels, R., Suarez-Ruiz, I., Cathelineau, M., Landrein, P., 2011. Vertical and lateral changes in organic matter from the Mesozoic, eastern Paris Basin (France): variability of sources and burial history. *Int. J. Coal Geol.* 88 (2–3), 163–178.

Blaise, T., Barbarand, J., Kars, M., Ploquin, F., Aubourg, C., Brigaud, B., Cathelineau, M., El Albani, A., Gautheron, C., Izart, A., Janots, D., Michels, R., Pagel, M., Pozzi, J.-P., Boiron, M.-C., Landrein, P., 2014. Reconstruction of low temperature (< 100 °C) burial in sedimentary basins: a comparison of geothermometer in the intracontinental Paris Basin. *Mar. Petrol. Geol.* 53, 71–87.

Böcker, J., 2015. Petroleum System and Thermal History of the Upper Rhine Graben: Implications from Organic Geochemical Analyses, Oil-Source Rock Correlations and Numerical Modelling. Doctoral Dissertation, Fakultät für Georesourcen und Materialtechnik der Rheinisch-Westfälischen Technischen Hochschule Aachen, p. 104.

Böcker, J., Littke, R., 2016. Thermal maturity and petroleum kitchen areas of liassic black shales (lower jurassic) in the central upper rhine graben, Germany. *Int. J. Earth Sci.* 105 (2), 611–636.

Böcker, J., Littke, R., Forster, A., 2016. An overview on source rocks and the petroleum system of the central Upper Rhine Graben. *Int. J. Earth Sci.* 106 (2), 707–742.

Boigk, H., Schöneich, H., 1970. Die Tiefenlage der Permbasis im nördlichen Teil des Oberrheingrabens. *Graben Probl.* 27, 48–55.

Bossenne, C., 2019. Évolution des propriétés de transfert des grès par diagenèse et déformation: application aux formations du Buntsandstein Gp., Graben du Rhin. Doctoral Dissertation, Université de Lorraine, p. 580.

Bossenne, C., Géraud, Y., Böcker, J., Klug, B., Mattioni, L., Sizun, J.-P., Sudo, M., Moretti, I., 2021. Evolution of diagenetic conditions and burial history in Buntsandstein Gp. fractured sandstones (Upper Rhine Graben) from in-situ $\delta^{18}O$ of quartz and $40Ar/39Ar$ geochronology of K-feldspar overgrowths. *Int. J. Earth Sci.* 110 (8), 2779–2802.

Bourgeois, O., Ford, M., Diraison, M., Veslud, C., Gerbault, M., Pik, R., Ruby, N., Bonnet, S., 2007. Separation of rifting and lithospheric folding signatures in the NW-Alpine foreland. *Int. J. Earth Sci.* 96 (6), 1003–1031.

Bourquin, S., Guillocheau, F., 1996. Keuper stratigraphic cycles in the Paris Basin and comparison with cycles in other peritethyan basins (German Basin and bresse-jura basin). *Sediment. Geol.* 105 (3–4), 159–182.

Bourquin, S., Robin, C., Guillocheau, F., Gaulier, J.-M., 2002. Three-dimensional accommodation analysis of the Keuper of the Paris Basin: discrimination between tectonics, eustasy and sediment supply in the stratigraphic record. *Mar. Petrol. Geol.* 19 (4), 469–498.

Bourquin, S., Peron, S., Durand, M., 2006. Lower Triassic sequence stratigraphy of the western part of the Germanic Basin (west of Black Forest): fluvial system evolution through time and space. *Sediment. Geol.* 186 (3–4), 187–211.

Bourquin, S., Guillocheau, F., Péron, S., 2009. Braided rivers within an arid alluvial plain (example from the Lower Triassic, western German Basin): recognition criteria and expression of stratigraphic cycles. *Sedimentology* 56 (7), 2235–2264.

Bruns, B., Littke, R., Gasparik, M., van Wees, J., Nelkamp, S., 2016. Thermal evolution and shale gas potential estimation of the Wealden and Posidonia Shale in NW-Germany and The Netherlands: a 3D basin modelling study. *Basin Res.* 28 (1), 2–33.

Bruss, D., 2000. Zur Herkunft der Erdöle im mittleren Oberrheingraben und ihre Bedeutung fuer die Rekonstruktion der Migrationsgeschichte und der Speichergesteinsdiagenese. Doctoral Dissertation, Universität Erlangen-Nürnberg, Forschungszentrum Jülich. Ber. Des. Forschungszentrums Jülich 3831, 222.

Buchmann, T.J., Connolly, P.T., 2007. Contemporary kinematics of the Upper Rhine Graben: a 3D finite element approach. *Global Planet. Change* 58 (1–4), 287–309.

Burrus, J., 1986. Thermal Modeling in Sedimentary Basins: 1st IHP Exploration Research Conference, Carcans, France. Editions Technip. June 3-7, 1985.

Chantraine, J., Autran, A., Cavellier, C., Alabouvette, B., Barféty, J., Cecca, F., Clozier, L., Debrand-Passard, S., Dubreuilh, J., Feybesse, J., 1996. Carte géologique de la France à 1/1 000 000. BRGM Orléans.

Châteauneuf, J.-J., Ménillet, F., 2014. Découverte d'une microflore bartonienne dans le Fossé rhénan supérieur: la formation de Mictesheim (Bas-Rhin, Alsace, France). *Géologie de la France* 1, 3–20.

Cloethingh, S., Ziegler, P.A., 2007. Tectonic models for the evolution of sedimentary basins, in crust and lithosphere dynamics. In: Watts, A.B. (Ed.), *Treatise on Geophysics*, pp. 486–611.

Cloos, H., 1939. Hebung-Spaltung-Vulkanismus, Elemente einer geometrisch in Analyse irdischer Crossformen. *Geol. Rundsch.* 30, 406–527.

Cohen, K.M., Finney, S.C., Gibbard, P.L., Fan, J.-X., 2013. The ICS international chronostratigraphic chart. *Episodes* 36, 199–204 (updated).

Cumelle, R., Dubois, P., 1986. Évolution mésozoïque des grands bassins sédimentaires Français: bassins de Paris, d'Aquitaine et du Sud-Est. *Bull. Soc. Geol. Fr.* 2 (4), 529–546.

Derer, C.E., 2003. Tectono-sedimentary Evolution of the Northern Upper Rhine Graben (Germany), with Special Regard to the Early Syn-Rift Stage. Doctoral Dissertation, Rheinischen Friedrich-Wilhelms-Universität Bonn, p. 103.

- Derer, C.E., Schumacher, M.E., Schäfer, A., 2005. The northern Upper Rhine Graben: basin geometry and early syn-rift tectono-sedimentary evolution. *Int. J. Earth Sci.* 94 (4), 640–656.
- Dèzes, P., Schmid, S.M., Ziegler, P.A., 2004. Evolution of the European Cenozoic Rift System: interaction of the alpine and pyrenean orogens with their foreland lithosphere. *Tectonophysics* 389 (1–2), 1–33.
- di-Giovanni, C., Disnar, J.R., Bichet, V., Campy, M., Guillet, B., 1998. Geochemical characterization of soil organic matter and variability of a postglacial detrital organic supply (Chailloux Lake, France). *Earth Surf. Process. Landforms: J. British Geomorphol. Group* 23 (12), 1057–1069.
- Donsimoni, M., 1981. Le bassin houiller lorrain: synthèse géologique. *Mém. BRGM, Orléans* 117, 102.
- Équipe du projet GeORG, 2013. Potentiel géologique profond du Fossé rhénan supérieur. Rapport scientifique et technique du projet Interreg GeORG. Part 1-4; Internet (PDF-document): <http://www.geopotenziale.eu>.
- Düringer, P., 1988. Les conglomérats des bordures du rift Cénozoïque Rhénan. Dynamique sédimentaire et contrôle climatique. Doctoral Dissertation, Université de Strasbourg, p. 328.
- Düringer, P., Aichholzer, C., Orciani, S., Genter, A., 2019. The complete lithostratigraphic section of the geothermal wells in Rittershoffen (Upper Rhine Graben, eastern France): a key for future geothermal wells. *BSGF-Earth Sci. Bulletin* 190 (1), 13.
- Edel, J., Fluck, P., 1989. The upper Rhenish Shield basement (Vosges, Upper Rhinegraben and Schwarzwald): main structural features deduced from magnetic, gravimetric and geological data. *Tectonophysics* 169 (4), 303–316.
- Edel, J.-B., Schulmann, K., Rotstein, Y., 2007. The variscan tectonic inheritance of the upper rhine graben: evidence of reactivations in the Lias, late eocene–oligocene up to the recent. *Int. J. Earth Sci.* 96 (2), 305–325.
- Frey, M., Bär, K., Stober, J., Reinecker, J., van der Vaart, J., Sass, I., 2022a. Assessment of deep geothermal research and development in the Upper Rhine Graben. *Geoth. Energy* 10, 1–67.
- Frey, M., van der Vaart, J., Bär, K., Bossennc, C., Calcagno, P., Dezayes, C., Sass, I., 2022b. Techno-economic assessment of geothermal resources in the variscan basement of the northern upper rhine graben. *Nat. Resour. Res.* 1–22.
- Fries, D., Lebouil, S., Maurer, V., Martin, C., Baujard, C., Ravier, G., Boguais, R., Amari, S., 2022. Lithium Extraction through Pilot Scale Tests under Real Geothermal Conditions of the Upper Rhine Graben. Presented at the Proceedings European Geothermal Congress, p. 7.
- Frimmel, A., 2003. Hochauflösende Untersuchungen von Biomarkern an epikontinentalen Schwarzschiefern des Unteren Toarciums (Posidonienschiefer, Lias ε [Lias-epsilon]) von SW-Deutschland. Doctoral dissertation. Eberhard-Karls-Universität Tübingen, p. 109.
- Gallagher, K., Evans, E., 1991. Estimating kinetic parameters for organic reactions from geological data: an example from the Gippsland Basin, Australia. *Appl. Geochem.* 6 (6), 653–664.
- Genre, C., 1981. BRGM Carte géologique de la France au 1: 50 000 Feuille Saverne. *Norois* 110 (1), 237–238.
- Gérard, A., Kappelmeyer, O., 1987. The Soutz-sous-Forêts project. *Geothermics* 16 (4), 393–399.
- Geyer, O.F., Gwinner, M.P., Geyer, M., Nitsch, E., Simon, T., 1991. Geologie von baden-württemberg. Schweizerbart, Stuttgart, Germany, p. 472.
- Grimmer, J., Ritter, J., Eisbacher, G., Fielitz, W., 2017. The late Variscan control on the location and asymmetry of the Upper Rhine Graben. *Int. J. Earth Sci.* 106 (3), 827–853.
- Guillocheau, F., Robin, C., Allemand, P., Bourquin, S., Brault, N., Dromart, G., Friedenberg, R., Garcia, J.-P., Gauthier, J.-M., Gaumet, F., 2000. Meso-Cenozoic geodynamic evolution of the Paris Basin: 3D stratigraphic constraints. *Geodin. Acta* 13 (4), 189–245.
- Hantschel, T., Kauerauf, A.I., 2009. Fundamentals of Basin and Petroleum Systems Modeling. Springer Science & Business Media, p. 476.
- Haq, B.U., 2014. Cretaceous eustasy revisited. *Global Planet. Change* 113, 44–58.
- Hauteville, Y., Michels, R., Malartre, F., Trouillier, A., 2006. Vascular plant biomarkers as proxies for palaeoflora and palaeoclimatic changes at the Dogger/Malm transition of the Paris Basin (France). *Org. Geochem.* 37 (5), 610–625.
- Hibsch, C., Jarrige, J.-J., Cushing, F.M., Mercier, J., 1995. Palaeostress analysis, a contribution to the understanding of basin tectonics and geodynamic evolution. Example of the Permian/Cenozoic tectonics of Great Britain and geodynamic implications in western Europe. *Tectonophysics* 252 (1–4), 103–136.
- Hinsken, S., Ustaszewski, K., Wetzal, A., 2007. Graben width controlling syn-rift sedimentation: the Palaeogene southern Upper Rhine Graben as an example. *Int. J. Earth Sci.* 96 (6), 979–1002.
- Illies, J., 1975. Recent and paleo-intraplate tectonics in stable Europe and the Rhinegraben rift system. In: *Developments in Geotectonics*, vol. 9. Elsevier, pp. 251–264.
- Katz, B.J., 1995. Petroleum source rocks—an introductory overview. In: Katz, B.J. (Ed.), *Petroleum Source Rocks*. Casebooks in Earth Sciences. Springer, Berlin, Heidelberg, pp. 1–8.
- Kimble, B., Maxwell, J., Philp, R., Fglinton, G., Albrecht, P., Ensminger, A., Arpino, P., Ourisson, G., 1974. Tri- and tetraterpenoid hydrocarbons in the Messel oil shale. *Geochem. Cosmochim. Acta* 38 (7), 1165–1181.
- Kohl, T., Bächler, D., Rybach, L., 2000. Steps towards a Comprehensive Thermo-Hydraulic Analysis of the HDR Test Site Soutz-Sous-Forêts. Presented at the Proceedings World Geothermal Congress. Kyushu-Tohoku Japan, pp. 2671–2676.
- Kupecz, J.A., Gluyas, J., Bloch, S., 1997. Reservoir Quality Prediction in Sandstones and Carbonates: an Overview, vol. 69. AAPG Memoir, pp. VII–XXIV.
- Lahner, L., Toloczyki, M., 2004. Geowissenschaftliche Karte der Bundesrepublik Deutschland 1: 2.000. 000. Geologie, Bundesanstalt für Geowissenschaften und Rohstoffe, Hannover.
- Landais, P., Elie, M., 1999. Utilisation de la géochimie organique pour la détermination du paléoenvironnement et de la paléothermicité dans le Callovo-Oxfordien du site de l'Est de la France. *FDP Sci.* 1999, 35–58.
- Landrein, P., Vigneron, G., Delay, J., Lebon, P., Pagel, M., 2013. Lithologie, hydrodynamisme et thermicité dans le système sédimentaire multicouche recoupé par les forages Andra de Montiers-sur-Saulx (Meuse). *Bull. Soc. Geol. Fr.* 184 (6), 519–543.
- Lardeaux, J., Schulmann, K., Faure, M., Janoušek, V., Lexa, O., Skrzypek, E., Edel, J., Štípská, P., 2014. The moldanubian zone in the French Massif Central, Vosges/Schwarzwald and Bohemian Massif revisited: differences and similarities. *Geol. Society, London, Spec. Publ.* 405 (1), 7–44.
- Laubscher, H., 1987. Die tektonische entwicklung der Nordschweiz. *Eclogae Geol. Helv.* 80 (2), 287–303.
- Le Meur, M., Boussafir, M., Le Milbeau, C., Debure, M., Claret, F., Robinet, J.-C., Lerouge, C., 2021. Organic matter oxidation of the légulines clay formation, (Paris Basin, France): spatial heterogeneities. *Appl. Geochem.* 134, 105093.
- Le Roux, J., Harmand, D., 2003. Origin of the hydrographic network in the eastern Paris Basin and its border massifs. *Géologie de la France* 1, 105–110.
- LGRB, 1998. Geologische Übersichtskarte von Baden-Württemberg 1:300,000 (GÜ 300) [Geological map of the state of Baden-Württemberg 1:300,000. Landesamt für Geologie, Rohstoffe und Bergbau Baden-Württemberg (LGRB)].
- Li, Y., Michels, R., Mansuy, L., Fleck, S., Faure, P., 2002. Comparison of pressurized liquid extraction with classical solvent extraction and microwave-assisted extraction-application to the investigation of the artificial maturation of Mahakam coal. *Fuel* 81 (6), 747–755.
- Litke, R., Bayer, U., Gajewski, D., Nelskamp, S. (Eds.), 2008. Dynamics of Complex Intracontinental Basins: the Central European Basin System. Springer, pp. 227–290.
- Lutz, M., Cleintuar, M., 1999. Geological results of a hydrocarbon exploration campaign in the southern upper rhine graben (alsace centrale, France). *Bull. Angew. Geol. Bull. Appl. Geol.* 4, 3–80.
- Lutz, H., Lorenz, V., Engel, T., Häfner, F., Haneke, J., 2013. Paleogene phreatomagmatic volcanism on the western main fault of the northern upper rhine graben (kisselwörth diatreme and nierstein-aßtheim volcanic system, Germany). *Bull. Volcanol.* 75 (7), 1–11.
- MacKenzie, A., McKenzie, D., 1983. Isomerization and aromatization of hydrocarbons in sedimentary basins formed by extension. *Geol. Mag.* 120 (5), 417–470.
- Makhov, M., Galushkin, Y., 2004. Basin Analysis and Modeling of the Burial, Thermal and Maturation Histories in Sedimentary Basins. Editions OPHRYS, p. 360.
- Martini, E., Reichenbacher, B., 2007. Nannoplankton und fisch-otolithen in den Mittleren Pechelbronn-Schichten (Unter-Oligozän, Oberrheingraben/Mainzer Becken). *Geol. Abh. Hess.* 116, 235–273.
- Marzi, R., 1992. Qualitative und quantitative evolution and kinetics of biological marker transformations-laboratory experiments and application to the Michigan Basin. In: Moldowan, J.M., Albrecht, P., Philp, R.P. (Eds.), *Biological Markers in Sediments and Petroleum*. Prentice-Hall, Englewood Cliffs, NJ, pp. 18–41.
- Mazurek, M., Hurford, A.J., Leu, W., 2006. Unravelling the multi-stage burial history of the Swiss Molasse Basin: integration of apatite fission track, vitrinite reflectance and biomarker isomerisation analysis. *Basin Res.* 18 (1), 27–50.
- Megnien, C., 1980. Tectogenese du Bassin de Paris; etapes de l'évolution du bassin. *Bull. Soc. Geol. Fr.* 7 (4), 669–680.
- Ménillet, F., Vogt, H., Reichelt, R., Schumacher, E., Van Werveke, L., Haug, E., Bucking, H., Gross, J., Schirardin, J., Thévenin, A., 1979. Carte Géologique France (1/50 000), Feuille Bouxwiller (197) Orléans, vol. 59. BRGM.
- Ménillet, F., Durand, M., Genter, A., Party, J., 2015. Notice explicative de la carte géologique de France (1/50 000), Feuille Haguenau (198, 2e éd. BRGM, Orléans.
- Meyer, R., 1976. Continental sedimentation, soil genesis and marine transgression in the basal beds of the Cretaceous in the east of the Paris Basin. *Sedimentology* 23 (2), 235–253.
- Moldowan, J.M., Sundararaman, P., Schoell, M., 1986. Sensitivity of biomarker properties to depositional environment and/or source input in the Lower Toarcian of SW-Germany. *Org. Geochem.* 10 (4–6), 915–926.
- Peters, K.E., 1986. Guidelines for evaluating petroleum source rock using programmed pyrolysis. *AAPG Bull.* 70 (3), 318–329.
- Philippi, G., 1965. On the depth, time and mechanism of petroleum generation. *Geochem. Cosmochim. Acta* 29 (9), 1021–1049.
- Poelchau, H., Baker, D., Hantschel, T., Horsfield, B., Wygrala, B., 1997. Basin simulation and the design of the conceptual basin model. In: *Petroleum and Basin Evolution*. Springer, pp. 3–70.
- Robert, P., 1985. Histoire géothermique et diagenèse organique. Bulletin des Centres de Recherches Exploration-Production ELF-Aquitaine, Pau, Mém. 8, 345.
- Robin, C., 1995. Mesure stratigraphique de la déformation: application à l'évolution Jurassique du Bassin de Paris: Application à l'évolution jurassique du Bassin de Paris. Doctoral Dissertation, Université de Rennes 1, vol. 77. Mém. Géosciences-Rennes, p. 293.
- Röhl, H.-J., Schmid-Röhl, A., Oschmann, W., Frimmel, A., Schwark, L., 2001. The Posidonia Shale (Lower Toarcian) of SW-Germany: an oxygen-depleted ecosystem controlled by sea level and palaeoclimate. *Palaeogeogr. Palaeoclimatol. Palaeoecol.* 165 (1–2), 27–52.
- Ronov, A., 1958. Organic carbon in sedimentary rocks (in relation to the presence of petroleum). *Geochemistry* 5, 497–509.
- Roussé, S., 2006. Architecture et dynamique des séries marines et continentales de l'oligocène moyen et supérieur du sud du fossé rhénan: Evolution des milieux de

- dépôt en contexte de rift en marge de l'avant-pays alpin. Doctoral Dissertation, Université de Strasbourg, p. 474.
- Ruffell, A., 1991. sea-level events during the early cretaceous in western Europe. *Cretac. Res.* 12 (5), 527–551.
- Rullkötter, J., Marzi, R., 1988. Natural and artificial maturation of biological markers in a Toarcian shale from northern Germany. *Org. Geochem.* 13 (4–6), 639–645.
- Sanjuan, B., Gourcerol, B., Millot, R., Rettenmaier, D., Jeandel, E., Rombaut, A., 2022. Lithium-rich geothermal brines in Europe: an up-date about geochemical characteristics and implications for potential Li resources. *Geothermics* 101, 102385.
- Scheck-Wenderoth, M., Krzywiec, P., Zühlke, R., Maystrenko, Y., Froitzheim, N., 2008. Permian to cretaceous tectonics. In: *The Geology of Central Europe, umc 2*. The Geological Society Publishing House, London, pp. 999–1030. Mesozoic and Cenozoic.
- Schirardin, J., 1960. Sur la limite du Toarcien et de l'Aalénien en Alsace. *Sciences Géologiques, bulletins et mémoires* 13 (3), 95–126.
- Schmoker, J.W., Gautier, D.L., 1988. Sandstone porosity as a function of thermal maturity. *Geology* 16 (11), 1007–1010.
- Schmoker, J.W., Hester, T.C., 1989. Regional Trends of Sandstone Porosity versus Vitrinite Reflectance—A Preliminary Framework. In: Presented at the AAPG Rocky Mountain Section Meeting, vol. 73. AAPG Bulletin, Albuquerque, NM (USA. CONF-8910195-).
- Schnaebelé, R., 1948. Monographie géologique du champ pétrolier de Pechelbronn. *Mém. Serv. Carte géol. Als. Lorr.* 7, 254.
- Schuler, M., 1990. Environnements et paléoclimats paléogènes. Palynologie et biostratigraphie de l'Eocène et de l'Oligocène inférieur dans les fossés rhénan, rhodanien et de Hesse, vol. 190. Documents B.R.G.M., p. 503
- Schumacher, M.F., 2002. Upper Rhine Graben: role of preexisting structures during rift evolution. *Tectonics* 21 (1), 6–1.
- Schwarz, F., 2021. Le pays de Pechelbronn. Un territoire façonné par l'industrie pétrolière. *Rev. Alsace* (147), 239–268.
- Seifert, W.K., Moldovan, J.M., 1980. The effect of thermal stress on source-rock quality as measured by hopane stereochemistry. *Phys. Chem. Earth* 12, 229–237.
- Seifert, W., Moldovan, J., 1986. Use of biological markers in petroleum exploration. *Methods Geochem. Geophys.* 24, 261–290.
- Sissingh, W., 1998. Comparative tertiary stratigraphy of the rhine graben, bresse graben and Molasse Basin: correlation of alpine foreland events. *Tectonophysics* 300 (1–4), 249–284.
- Sissingh, W., 2006. Syn-kinematic palaeogeographic evolution of the West European Platform: correlation with Alpine plate collision and foreland deformation. *Neth. J. Geosci.* 85 (2), 131–180.
- Sittler, C., 1965. Le Paléogène des fossés rhénan et rhodanien. *Etudes sédimentologiques et paléoclimatiques, Mém. Serv. Carte Géol. Alsace Lorraine* (24), 329.
- Sittler, C., 1967. Le soubassement et le remplissage sédimentaire du Fossé Rhénan au niveau du Bassin de Pechelbronn et du Seuil d'Erstein. In: *Coupes géologiques à travers le fossé rhénan. Abh. Geol. Landesamt Baden-Württemberg*, 6, Freiburg et Publ. Serv. Carte géol. Als. Lorr., vol. 1967. The Rhinegraben Progress Report, Strasbourg, pp. 69–80.
- Sittler, C., Ollivier-Pierre, M.-F., 1994. Palynology and palynofacies analyses: some essential clues to assess and identify West-European Tertiary depositional environments in terms of relative high or lowstands. Application to the case of three Eocene and Oligocene sections in France. *Bull. Cent. Rech. Explor.-Prod. Elf-Aquitaine* 18 (2), 475–488.
- Stahmer, G., 1980. Stratigraphie des Oberrheingraben-Tertiärs und seiner nördlichen Fortsetzungen. (Interne Bericht). Wintershall AG, Kassel.
- Sugden, M.A., Abbott, G.D., 2002. The stereochemistry of bound and extractable pentacyclic triterpenoids during closed system pyrolysis. *Org. Geochem.* 33 (12), 1515–1521.
- Thomas, R., Schulz, R., 2007. Facies differentiation of the Malm by interpretation of reflection seismic profiles and a moving source VSP experiment. Presented at the Proceedings European Geothermal Congress 2007 (Unterhaching, Germany).
- Timar-Geng, Z., Fügenschuh, B., Wetzel, A., Dresmann, H., 2006. Low-temperature thermochronology of the flanks of the southern upper rhine graben. *Int. J. Earth Sci.* 95 (4), 685–702.
- Tissot, B., Durand, B., Espitalié, J., Combaz, A., 1974. Influence of nature and diagenesis of organic matter in formation of petroleum. *AAPG (Am. Assoc. Pet. Geol.) Bull.* 58 (3), 499–506.
- Walter, R., 1995. *Geologie von mitteleuropa*. Schweizerbart, Stuttgart, Germany, p. 566.
- Wannesson, J., 1998. *Alsace-Rapport Régional D'évaluation Pétrolière*, vol. 96. Institut Français du pétrole, Technical report, p. 62.
- Waples, D.W., Kamata, I., Suizu, M., 1992a. The art of maturity modeling, part 1: finding a satisfactory geologic model. *AAPG Bull.* 76 (1), 31–46.
- Waples, D.W., Suizu, M., Kamata, I., 1992b. The art of maturity modeling. Part 2: alternative models and sensitivity analysis. *AAPG Bull.* 76 (1), 47–66.
- Welte, D.H., 1966. Kohlenwasserstoffgenese in Sedimentgesteinen: untersuchungen über den thermischen Abbau von Kerogen unter besonderer Berücksichtigung der n-Paraffinbildung. *Geol. Rundsch.* 55 (1), 131–144.
- Wetzel, A., Allenbach, R., Allia, V., 2003. Reactivated basement structures affecting the sedimentary facies in a tectonically "quiescent" epicontinental basin: an example from NW Switzerland. *Sediment. Geol.* 157 (1–2), 153–172.
- Yalcin, M., Lütke, R., Sachsenhofer, R., 1997. Thermal history of sedimentary basins. In: *Petroleum and Basin Evolution*. Springer, pp. 71–167.
- Yang, S., Horsfield, B., 2020. Critical review of the uncertainty of Tmax in revealing the thermal maturity of organic matter in sedimentary rocks. *Int. J. Coal Geol.* 225, 103500.
- Ziegler, P.A., 1987. Late Cretaceous and Cenozoic intra-plate compressional deformations in the Alpine foreland—a geodynamic model. *Tectonophysics* 137 (1–4), 389–420.
- Ziegler, P.A., 1990. Geological Atlas of Western and Central Europe. *Shell Int. Pet. Maatschappij. Geol. Soc. Publ. House, Bath, UK*, p. 239.
- Ziegler, P.A., 1994. Cenozoic rift system of Western and Central-Europe: an overview. *Geol. Mijnbouw* 73 (2–4), 99–127.
- Ziegler, P.A., Dèzes, P., 2005. Evolution of the lithosphere in the area of the rhine Rift System. *Int. J. Earth Sci.* 94 (4), 594–614.
- Zumberge, J.E., 1987. Terpenoid biomarker distributions in low maturity crude oils. *Org. Geochem.* 11 (6), 479–496.

5. Perspectives de recherche

Mes perspectives de recherche pour les années à venir (court-moyen terme) s'inscrivent dans la continuité des trois volets qui constituent le corps de mon manuscrit ; elles s'articulent autour de trois axes principaux:

(i) Mes travaux ont montré l'importance de retraiter et interpréter les profils sismiques industriels pour comprendre la formation des bassins carbonifères-permiens et de leur couverture méso-cénozoïque. L'objectif est donc de poursuivre le travail initié de mise à jour de la connaissance, chère au BRGM, en recherchant les modalités structurales de mise en place de ces objets.

(ii) La réévaluation des environnements de dépôts et de l'extension/épaisseur des bassins stéphano-permiens permet de discuter des conditions paléoenvironnementales locales et régionales prévalant à la limite Carbonifère-Permien ; le projet ICDP Deepdust formalise ces réflexions en élargissant le champ de recherche à la Pangée équatoriale.

(iii) Dans un optique ressources et usages du sous-sol, il est nécessaire d'appréhender les géométries des corps sédimentaires et approcher leur paramètres « réservoir ». Je souhaite en particulier appliquer aux bassins carbonifères-permiens de nouvelles approches (Interprétation Quantitative), issues du monde de l'Exploration-Production des hydrocarbures.

Afin de respecter le plan du manuscrit je présenterai tout d'abord mes perspectives de recherche sur les bassins carbonifères-permiens (les plus nombreuses), puis celles concernant leur couverture méso-cénozoïque. Les collaborations potentielles sont mentionnées, ainsi que les possibles sujets de thèse associés. Je laisserai volontairement de côté les réflexions en cours au BRGM sur des sujets de recherche appliquée dans lesquels je vais être amené à apporter mon expertise scientifique « bassins profonds » dans les années qui viennent (PEPR Sous-sol, synthèse géothermique des bassins métropolitains, stockage du CO₂...).

Je profite de ce chapitre pour ajouter quelques lignes sur mon approche et les enjeux de la direction des jeunes chercheurs (étudiants en thèse, post-doctorants). L'important est leur avenir et il en va bien sûr de notre responsabilité de les préparer au monde de la recherche, mais aussi de les aider à anticiper les autres possibilités qui s'offrent à eux (c'est dire importance d'inscrire la thèse dans une trajectoire professionnelle).

Ma conviction est qu'encadrer, c'est en premier lieu enseigner et donner au jeune chercheur les clés pour obtenir son diplôme de doctorat ; par exemple la thèse est un apprentissage complexe de compétences techniques et scientifiques, de façons de se comporter et d'appréhender le milieu scientifique et plus largement professionnel. Le jeune chercheur a tout intérêt à développer son autonomie (pour produire des idées scientifiques et des connaissances nouvelles, pour organiser son travail...). Il faut qu'il considère sa thèse ou son post-doc comme un véritable projet

opérationnel dont il est le chef de projet (je parle ici sans doute sous l'influence de mon expérience au BRGM). L'implication de l'encadrant consiste alors à le guider et non pas diriger, avec autant d'exigence envers soi-même qu'envers le jeune chercheur. Je considère par ailleurs que l'attention et l'empathie auront toujours la primeur sur de quelconques nécessités de pressions.

L'objectif est donc de donner au jeune chercheur les outils pour poursuivre sa carrière dans le monde de la recherche s'il le souhaite, mais pas seulement. Lors de mes discussions avec les doctorants j'insiste souvent sur le fait qu'en plus de devenir spécialistes d'un domaine scientifique, ils acquièrent de nombreuses compétences transverses. Ces qualités de synthèse, de capacité rédactionnelle, d'expression orale, pour n'en citer que quelques-unes, seront tout à fait utiles dans n'importe quel autre domaine que celui qu'ils ont côtoyé pendant leur projet de recherche. C'est important qu'ils en prennent pleinement conscience, ce qui n'est pas toujours le cas. Car ces jeunes chercheurs ont toute leur place à prendre dans la révolution énergétique en route, à l'Université ou ailleurs.

5.1. Perspectives de recherche sur les bassins sédimentaires carbonifères-permiens

5.1.1. Mise à jour de la connaissance et modalités de mise en place des bassins stéphano-permiens sur le pourtour du Massif Central

Les bassins en bordure occidentale du Massif Central

Il n'existe pas à ma connaissance d'étude récente publiée sur le mode de remplissage et le cadre structural des bassins stéphano-permiens de Brive, Figeac-Decazeville-Rodez et Quercy-Albigeois-La Grésigne, les derniers travaux étant publiés dans la synthèse du BRGM de 1989. Une mission de reconnaissance du BRGM dans le bassin de Brive a montré l'intérêt de reprendre les descriptions sédimentologiques et rediscuter le découpage lithostratigraphique en vigueur (Feys, 1989). Nous disposons par ailleurs d'un jeu de profils sismiques déjà retraités qui imagent les bassins permien sous-couverture méso-cénozoïques du bassin d'Aquitaine (Figure 41) ; ces données pourraient être complétées par le retraitement de profils supplémentaires afin de mieux imaginer les bassins sous couverture. Ces bassins pourraient alors servir de cas d'étude à un ambitieux programme de recherche, à l'image de celui en cours dans le sud du bassin de Paris et le nord du Massif Central. Une thèse pourrait être lancée pour défricher le secteur, visiter les affleurements et interpréter les profils sismiques ; chaque méthode d'observation apportant son lot d'information (pour faire simple les faciès sédimentaire et environnements de dépôts à partir des affleurements, géométrie et structuration des bassins à partir de la sismique). Il sera intéressant de vérifier si ces bassins sont plutôt similaires (en terme d'environnements de dépôts, de contrôle structural et de contexte géodynamique) aux bassins géographiquement proches (Saint-Affrique, Lodève) ou aux bassins plus lointains du nord du Massif Central.

Les bassins en bordure orientale du Massif Central et la phase saaliennne

Il est reconnu depuis longtemps que certains bassins stéphano-permiens enregistrent une (ou plusieurs) phase(s) compressive(s) (Bonijoly et Castaing, 1983, 1986; Blès et al., 1989; Ziegler, 1990; Genna et Debriette, 1994), à l'image du bassin d'Alès (Figure 41), malgré de nombreuses remises en questions (e.g. Delenin et al., 1988 ; Djarar et al., 1996). Plus au nord le bassin de St-Etienne (Figure 41) montre lui aussi des structures plissées de son remplissage stéphanien, diversement interprétées (Mattaier et Matte, 1998). Au nord du bassin de St-Etienne, le bassin de Blanzay-Le Creusot (Figure 41) - qui préserve à la différence des deux précédents une épaisse série sédimentaire permienne - montre lui aussi des indices de plissement sur ses bordures (Feys et Gand, 1983). Ces structures existent bel et bien mais ne sont pas connus pour les autres bassins situés plus à l'ouest (i.e. ceux discutés dans le volet 2). Il sera fondamental pour la compréhension de la dynamique tardi-varisque d'en comprendre leur origine ; soit « locale » en raison par exemple de jeux décrochants compressifs d'échelle réduite, soit régionale en relation avec la phase compressive saaliennne (Permien inférieur), observée en Lorraine et encore plus exprimée dans les bassins carbonifères-permiens en Allemagne (Gebhardt et al., 1991 ; Schneider et Romer, 2010). Ce projet de réévaluation des bassins stéphano-permiens à structures compressive pourrait lui aussi prendre

la forme d'une thèse de géologie structurale ; j'ai déjà évoqué cette possibilité avec les collègues structuralistes du BRGM (F. Lacquement, S. Caritg-Monnot, C. Allanic) travaillant depuis longtemps dans le bassin d'Alès en compagnie de P. H. Leloup (ENS Lyon, qui connaît le bassin d'Alès mais aussi celui de St-Etienne). Le recherche de cinérites (connues dans ces bassins, e.g. Gardien et al., 2022) pour dater les séries sera aussi un objectif important pour corréliser les dépôts et déformations.

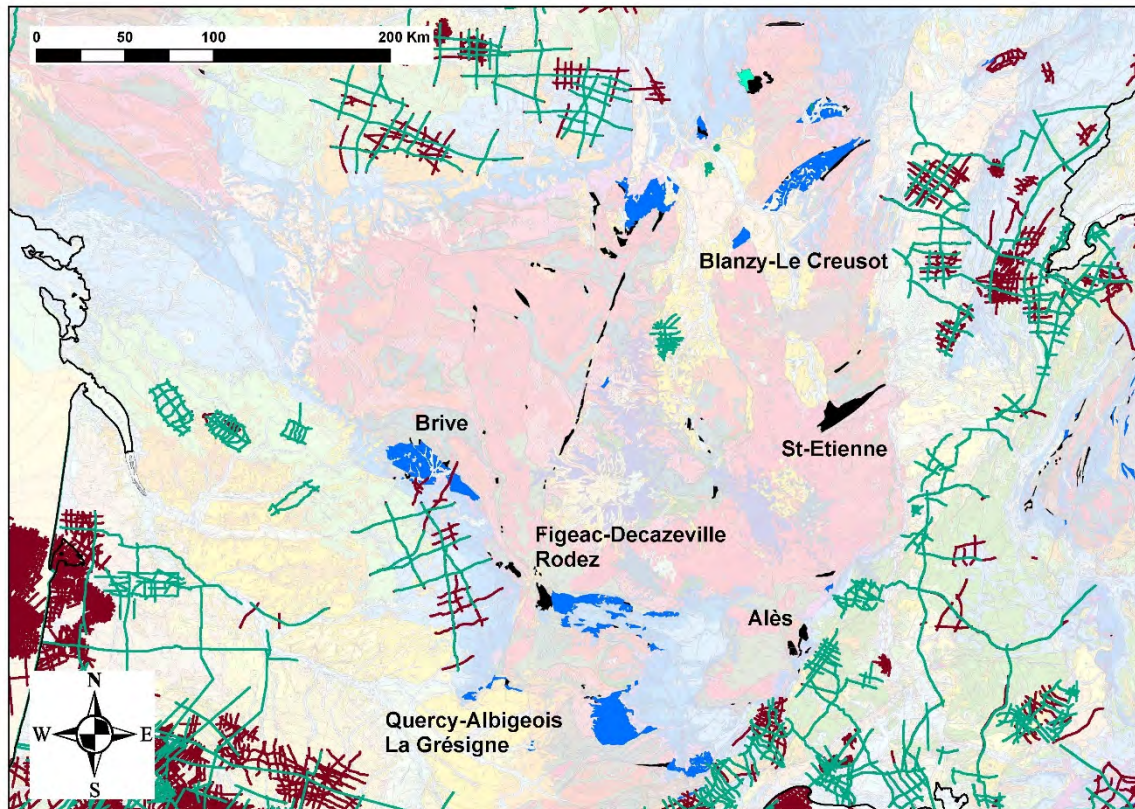


Figure 41 - Localisation des bassins permien (en bleu) et stéphaniens (en noir) de Brive, Blanzzy-Le Creusot, St-Étienne et Alès. Plan de position des profils sismiques retraités au BRGM en vert, disponibles pour retraitement en marron. En fond carte géologique de la France au 1:1000000^{ème} (BRGM, 2003).

Les bassins du sud du Massif Central, connexions Lodève-Alès

La bordure sud/sud-est du Massif Central est affectée par des déformations tertiaires bien exprimées, ce qui est moins le cas sur ses autres bordures. En résumé, la phase pyrénéenne (Crétacé terminal, Eocène moyen ; e.g. Arthaud et Laurent, 1995) se traduit par des chevauchements orientés OE à vergence nord, repris pour parti en extension à l'Oligocène avec le développement de failles normales orientés NO-SE (e.g. Séranne et al., 1995 ; Séranne et al., 2021 ; Hemelsdaël et al., 2021). Ces déformations d'abord reconnus en domaine onshore sont aussi identifiées en offshore (e.g. Lacombe et Jolivet, 2005). Elles dominent le style structural de la région et oblitèrent le signal tectonique et sédimentaire anté-pyrénéen.

Des observations préliminaires sur des profils retraités ces dernières années par le BRGM permettent cependant d'observer localement sous la couverture méso-cénozoïque déformée des réflecteurs attribuables au Carbonifère-Permien. L'idée est ici de passer en revue tous les profils

sismiques et les données de forage disponibles (hydrocarbures et BSS) pour rechercher ces bassins afin d'estimer leur extension initiale et les replacer paléogéographiquement (restauration) en les raccordant aux bassins affleurants (Lodève, Alès). Il s'agira aussi de discuter les connections entre ces deux bassins en terme d'âge et de déformation (extension sous le Causses du Larzac, rôle de la faille des Cévennes dans les déformations compressives post-stéphanienne à Alès...). Enfin il sera intéressant de discuter de la déformation de ces bassins sous-couverture lors des phases tectoniques tertiaires (enracinement des structures, transport passif lors de la tectonique chevauchante ; voir Espurt et al. (2019) pour une discussion similaire en Provence).

Ces réflexions préliminaires devront être poursuivie avec les collègues de Géosciences Montpellier de l'équipe Géologie des Réservoirs et Ressources qui maîtrisent le cadre tectonique régional (e.g. M. Séranne).

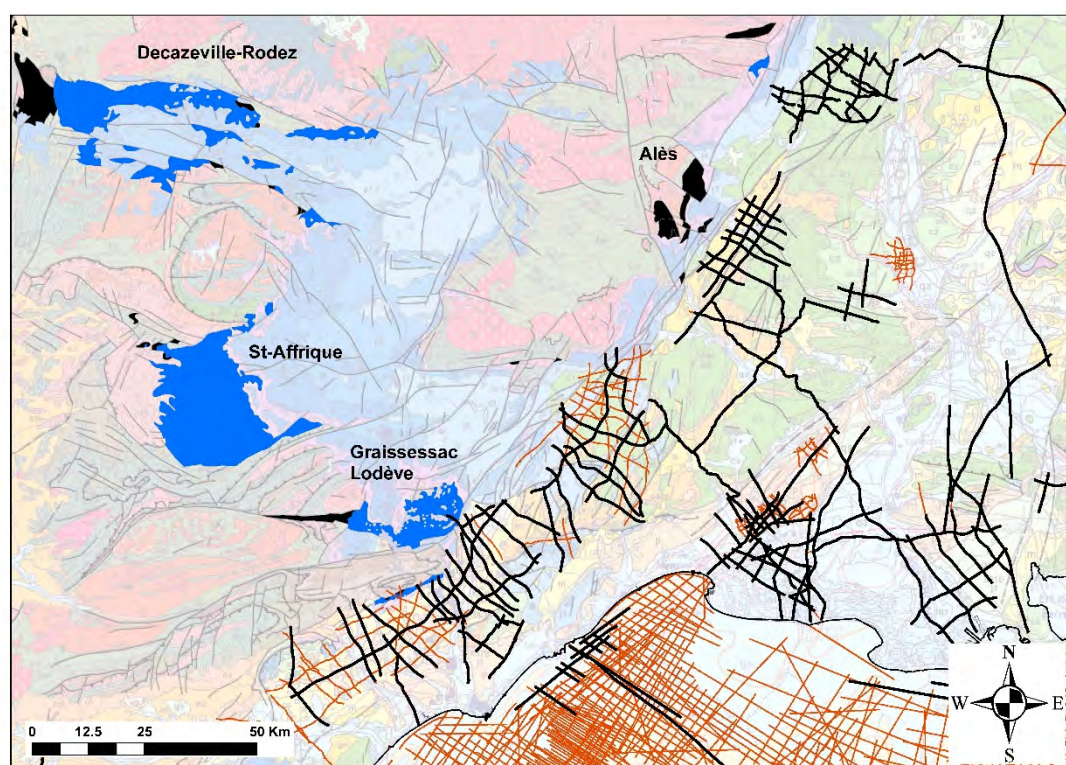


Figure 42 - Localisation des bassins permien (en bleu) et stéphanien (en noir) de Decazeville-Rodez, St-Affrique, Graissessac-Lodève et Alès. Plan de position des profils sismiques retraités au BRGM en noir, disponibles pour retraitement en marron. En fond carte géologique de la France au 1:1000000^{ème} (BRGM, 2003).

Datations absolues et corrélations inter-bassins

Nous avons vu dans le volet 2 que la transition Carbonifère-Permien se caractérise par des changements géodynamiques internes et externes majeurs (fin du cycle varisque, Late Paleozoic Ice Age). La mise en place des bassins syn- à post-orogéniques s'est accompagnée d'un volcanisme explosif qui s'est enregistré dans les bassins sous la forme de cinérites interstratifiées dans les séries silicoclastiques ; elles sont aujourd'hui complètement altérées lors de processus diagénetiques en argiles riches en kaolinite appelées tonsteins (Spears, 2012). Ces tonsteins sont connus depuis longtemps et ont servi de guide pour tenter de corréliser entre eux les différents bassins carbonifères-permiens (Bouroz, 1967, 1968), mais sans être datés, ce qui limitait les extrapolations. Les

nombreuses corrélations existantes entre ces bassins reposent plutôt sur l'utilisation d'étages continentaux. Cependant, elles sont largement controversées car leur définition est principalement basée sur des biozonations floristiques et faunistiques souvent peu précises ; en effet les évolutions de la macroflore, des spores et pollen, et des insectes dépendent très largement de leur environnement, ce qui introduit une faible résolution temporelle et un diachronisme potentiel des biozonations (e.g. Broutin et al., 1999).

L'effort récent de la communauté française pour donner des âges absolus aux cinérites des bassins carbonifères-permiens français - auquel je participe - commence à porter ses fruits (datations U/Pb des zircons en LA-ICP-MS : *Ducassou et al. (2019), *Poujol et al. (2023), ou CA-ID-TIMS : Pellenard et al. (1997) ; Figure 43). Ces premiers résultats montrent des dépôts sédimentaires pendant des intervalles plus courts qu'escomptés et donc des taux de sédimentation élevés. Il s'agit maintenant de multiplier les études pour réaliser de véritables corrélations temporelles inter-bassins pour caler les séries aux événements globaux.

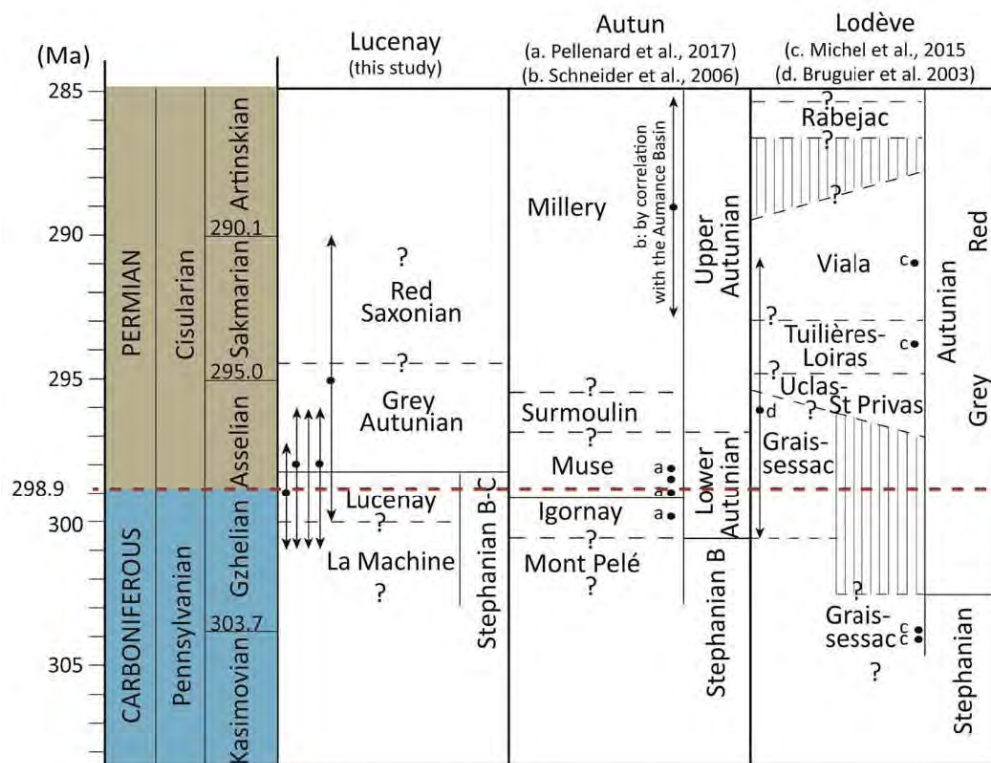


Figure 43 - Exemple de corrélations inter-bassins entre les bassins de Lucenay-lès-Aix, d'Autun et de Lodève (**Ducassou et al., 2019).

A très court terme, il est prévu une publication sur la datation absolue en CA-ID-TIMS des séries fini-paléozoïques des bassins de l'Aumance et de Decize-la-Machine (collab. avec les collègues de Géoscience Rennes, Biogéosciences Dijon, Department of Earth Atmospheric and Planetary Sciences du MIT, du Dipartimento di Scienze Chimiche e Geologiche de l'Università de Cagliari).

Je participe aussi à des investigations en cours et à venir sur les tonsteins du bassin sarro-lorrain, échantillonnés dans le cadre du post-doc de R. Hemelsdaël (cf. section 3.5). Le bassin étant sous couverture méso-cénozoïque du côté français, les accès aux données sont plus difficiles et il

manque cruellement de datations absolues comparé au côté allemand (e.g. Königer et al., 2002; Königer & Lorenz, 2002 ; Voigt et al., 2022). Cependant le contexte favorable de la reprise des investigations de subsurface dans ce bassin a permis d'échantillonner pour la première fois des tonsteins de carottes traversant les séries westphaliennes, stéphaniennes et permienes en Lorraine (collab. avec les collègues de Géoressources Nancy et IStEParis).

A plus long terme, je souhaite initier la datation absolue du bassin houiller du Nord-Pas de Calais et des séries permienes des Vosges. En effet j'ai retrouvé récemment des échantillons de cinérites du bassin houiller du Nord-Pas-de-Calais dans la lithothèque du BRGM; après inventaire et tests méthodologiques, la datation de ces cinérites apporterait pour la première fois un cadre temporel absolu au remplissage de ce bassin et donc à la dynamique du front de chaîne varisque dans le nord de la France.

Dans le même ordre d'idée, le BRGM stocke dans sa Géothèque trois carottes de forages recoupant les séries permienes du bassin de Villé dans les Vosges (Figure 44). Je souhaite (i) réévaluer les faciès sédimentaires et environnements de dépôts, à l'image des travaux menés dans les bassins du nord du Massif Central, et (ii) dater les cinérites interstratifiées dans les sédiments et identifiées sur les logs simplifiés disponibles. Ces données seront alors comparées aux résultats attendus en Lorraine et à ceux connus en Allemagne, et permettront de se caler temporellement dans les séries post-rifts identifiées dans la région.

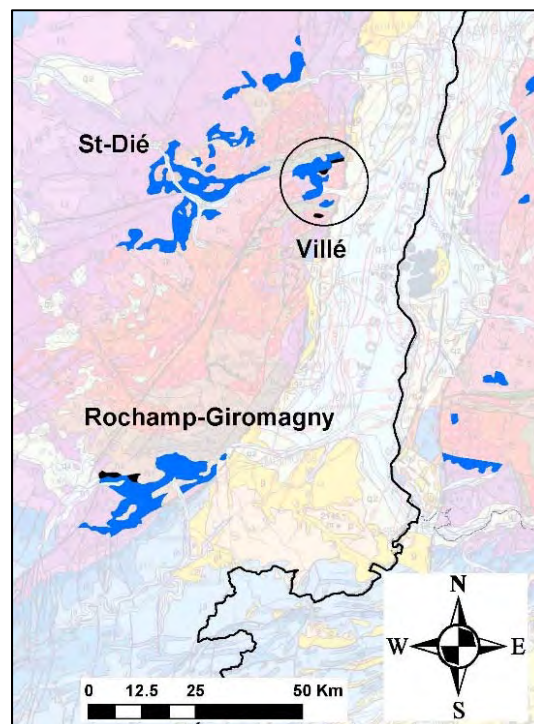


Figure 44 - Localisation des bassins permienes (en bleu) et stéphaniens (en noir) des Vosges. En fond carte géologique de la France au 1 :1000000^{ème} (BRGM, 2003).

5.1.2. Le projet Deepdust - Explorer le climat continental à la transition icehouse-greenhouse de la fin du Paléozoïque

L'ICDP (International Continental Scientific Drilling Program) est un programme de recherche international qui sponsorise et finance en partie des forages carottés en domaine continental pour répondre à des questions scientifiques fondamentales (e.g. processus géodynamiques) ou appliquées (e.g. risques naturels, géoressources). C'est le pendant onshore du programme IODP (Integrated Ocean Drilling Program).

Deepdust est un projet ICDP initié en 2017 par L. Soreghan (Oklahoma University, USA) dont les objectifs ciblent les paléoclimats et paléoenvironnements permien et les conditions propices à la vie microbienne permienne et actuelle. L'originalité de ce projet d'ampleur est de forer une section permienne la plus complète possible en deux localités éloignées appartenant à la Pangée équatoriale (Figure 45) : une aux USA en Oklahoma (dans un premier temps), l'autre en Europe occidentale, dans le bassin de Paris (dans un second temps).

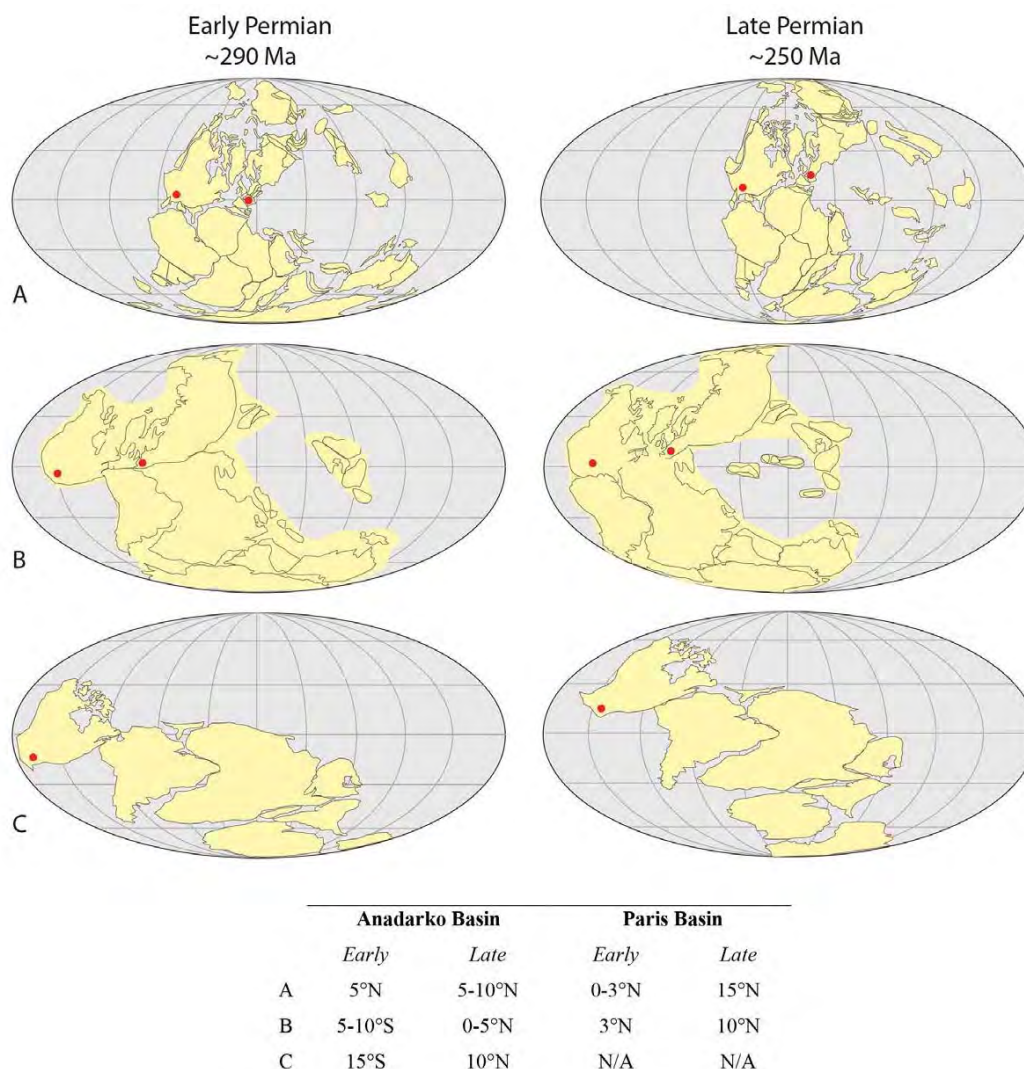


Figure 45 - Paléogéographie au Permien inférieur et supérieur, d'après les reconstructions de (A) Domeier et Torsvik (2014), (B) Muttoni et Kent (2019), et (C) Tomaszoli et al. (2018). Les points rouges indiquent les 2 cibles de forages en Pangée équatoriale (USA et Europe occidentale), dans *Soreghan et al., 2020).

Les thèmes scientifiques que nous aborderons sont:

- Le paléoclimat depuis la fin du Carbonifère et pendant le Permien, son évolution depuis le pic icehouse jusqu'aux conditions greenhouse au Permien terminal.
- L'influence des poussières atmosphériques (« dust ») sur les variabilités climatiques.
- La nature de la biosphère microbienne actuelle et passée.
- La sédimentologie et ses relations à la tectonique, qui m'intéressent plus particulièrement.
- La recherche de sections de références paléomagnétiques et magnétostratigraphiques.
- Des objectifs appliqués qui concernent plusieurs équipes du BRGM: sismicité induite, géothermie, hydrogéologie.

L'équipe de projet Deepdust est constituée de quatre PI et dix Co-PIs représentant sept nationalités, et je suis le Co-Pi responsable de la cible française dans le SO du bassin de Paris (bassin de Brécy, Figure 46). J'ai donc coordonné la préparation du dossier de forage depuis la reconnaissance en subsurface (retraitement et interprétation sismique, profondeur et épaisseur de la cible) jusqu'au programme technique de forage (design de puit, réalisé par CFG, filiale du BRGM). Une publication sur les avancées scientifiques à l'issue de ces travaux sur le bassin de Brécy est en cours de préparation (Beccaletto et Bourquin, in prép.).

Les projets ICDP s'inscrivent dans la durée (une dizaine d'années) et Deepdust n'échappe pas à la règle. A ce jour nous avons obtenu la labellisation officielle de notre projet par l'ICDP ainsi qu'une participation financière importante pour lancer le premier forage, à charge à l'équipe projet de trouver les financements complémentaires. A suivre...

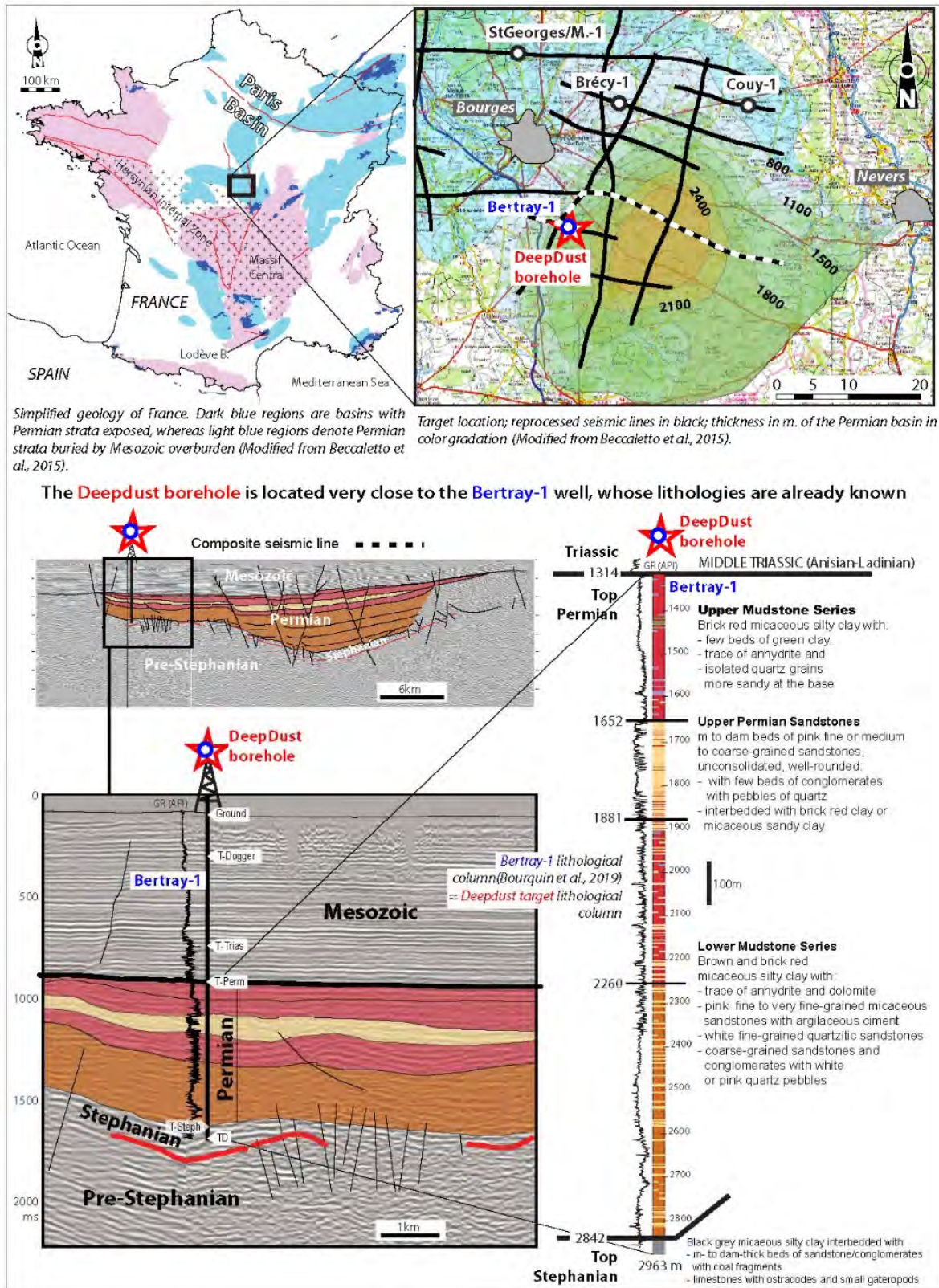


Figure 46 - Fiche synthétique pour la cible Deepdust en France (Source : full proposal ICDP, 2021).

5.1.3. Bassins carbonifères-permiens et ressources

L'Interprétation Quantitative appliquée aux bassins carbonifères-permiens

L'approche régionale sur la base de profils sismique a montré tout sa pertinence pour caractériser géométriquement les bassins carbonifères-permiens et proposer un cadre structural et cinématique pour leur évolution. L'idée est maintenant d'aller plus loin dans le détail du remplissage sédimentaire, d'approcher les géométries internes aux bassins, les variations latérales de faciès le long des profils sismiques et in fine les propriétés réservoirs des grandes unités sédimentaires.

Définition

L'interprétation quantitative des données de sismique réflexion consiste à utiliser l'information contenue dans l'amplitude du signal sismique (après retraitement) pour dériver des informations sur les caractéristiques du milieu traversé par ces ondes. Elle se donne pour objectif d'évaluer des propriétés pétrophysiques des roches dans le sous-sol (e.g. porosité, perméabilité, volume d'argile). L'avantage est le changement d'échelle dans l'information obtenue, en raison de sa couverture spatiale, l'interprétation quantitative des données de sismique réflexion vient en complément de l'analyse ponctuelle des diagraphies. Cette méthode est largement utilisée dans le milieu pétrolier pour identifier les réservoirs et leurs contenus, et l'idée est de l'appliquer à la géothermie (Capar et al., 2021). En effet connaître la variabilité latérale de propriétés comme la porosité ou la perméabilité est un facteur de succès important de l'exploration géothermique.

Principe

Lors de la propagation des ondes sismiques dans le sous-sol, une multitude d'effets modifie leurs amplitudes et leurs phases. Un de ces effets est la séparation de l'énergie de l'onde sismique, lorsque celle-ci rencontre des couches géologiques aux propriétés élastiques différentes (e.g. la densité, la vitesse des ondes sismiques), entre la partie réfléchiée du signal vers la surface et la partie transmise qui continue à se propager en profondeur (Figure 47). La séparation de l'énergie dépend des propriétés élastiques du sous-sol elles-mêmes dépendantes des propriétés pétrophysiques du réservoir. L'amplitude du signal enregistrée en surface contient donc des informations sur le milieu traversé et surtout sur les couches sur lesquelles il se réfléchit.

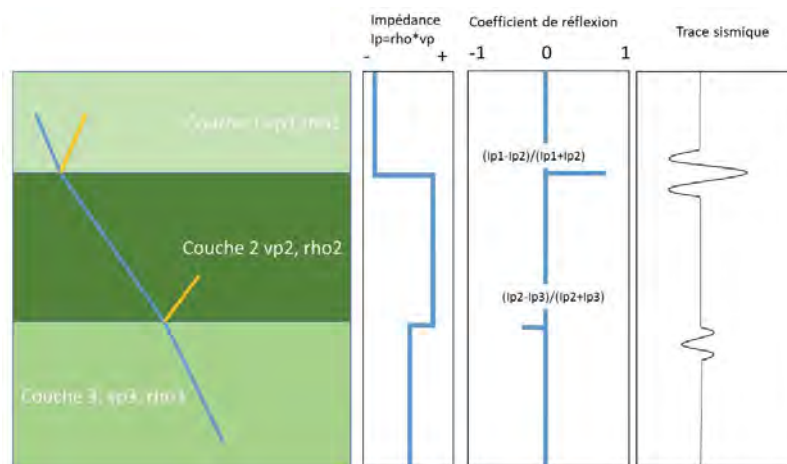


Figure 47 - Illustration simplifiée de la réflexion et de la transmission d'une onde sismique dans le sous-sol. L'interprétation quantitative consiste à retrouver les propriétés du sous-sol à partir de la trace sismique (Capar et al., 2021).

En mettant en relation les propriétés élastiques du milieu à ses propriétés pétrophysiques, issues notamment des diagraphies enregistrées dans les puits, il est donc possible d'utiliser la sismique pour obtenir des propriétés caractéristiques du réservoir comme la lithologie (Figure 48) ou la porosité. Les données sismiques doivent être préparées de telle sorte à ce que les variations d'amplitude liées à la propagation dans le sous-sol soient préservées, et que toutes autres variations, liées à l'acquisition, par exemple, soient atténuées, voir éliminées.

Les diagraphies (Gamma Ray, V_p et V_s , Densité, Neutron) jouent un rôle crucial dans l'interprétation quantitative, car elles permettent de remonter directement à l'information pétrophysique au droit du forage, avant de l'étendre le long d'un profil sismique.

Il existe deux types d'approche permettant de passer de la sismique aux propriétés réservoirs : une méthode d'inversion sismique acoustique classique et une méthode plus exploratoire, basée sur l'entraînement de réseaux de neurones (Capar et al., 2021).

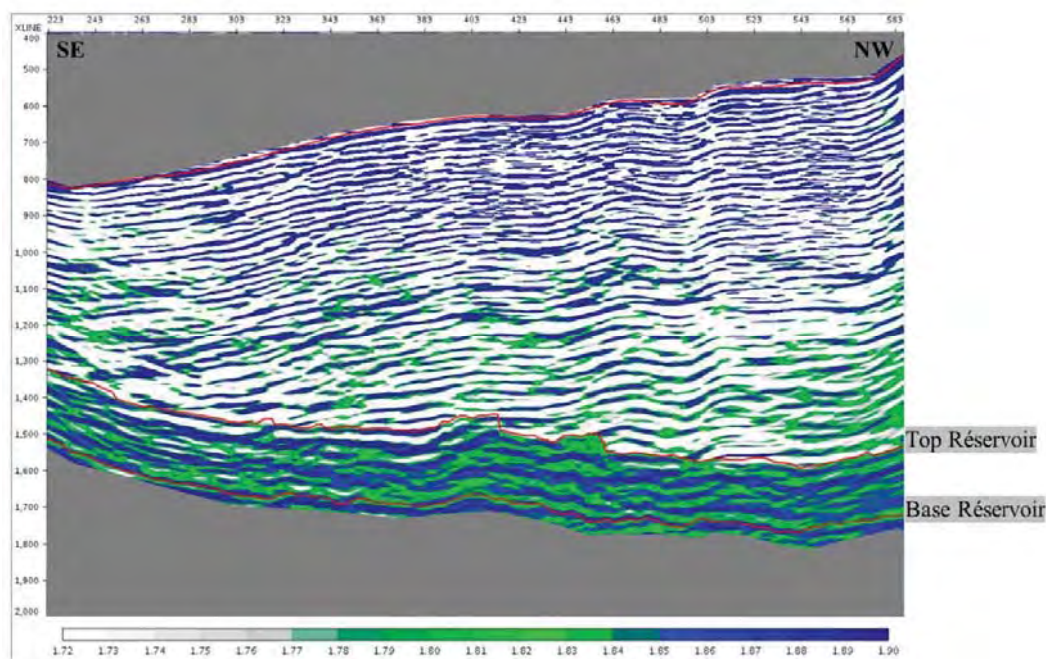


Figure 48 - Exemple d'Interprétation Quantitative sur une zone test dans le bassin houiller du Nord-Pas-de-Calais ; les couleurs bleu vert blanc correspondent à trois lithologies (Toussaint, 2020).

Le bassin sarro-lorrain se prêterait parfaitement à cette approche géophysique ; outre les données sismiques disponibles, il possède en effet un nombre de forages suffisants avec les diagraphies adéquates. Cette méthode prometteuse doit encore être testée et calibrée aux données anciennes et incomplètes dont on dispose en général pour ce type de bassins. Cependant il est certain qu'elle apportera des informations encore inaccessibles, que ce soit en terme de lithologies et de propriétés réservoir grande maille.

La structuration du bassin houiller du Nord-Pas-de-Calais, entre géothermie profonde et hydrogéologie

La thèse d'A. Laurent a raffiné la géométrie du front nord-varisque et proposé pour la première fois un modèle d'évolution cinématique intégrant données de surface et de subsurface (section 3.4). C'est un point de départ déterminant pour avancer plus finement dans la connaissance, en particulier des séries houillère s.s., non étudiés en détail au cours de cette thèse.

J'ai initié avec les collègues du LOG de Lille et du BRGM des réflexions qui ont abouti à un projet intégré abordant la thématique hydrogéologie en complément de l'approche géothermique. En effet l'aquifère de la craie, reposant en discordance sur les séries houillères carbonifères, est affectée par des failles souvent très mal connues héritées des séries sous-jacentes. Une partie de ces failles peut avoir perturbé la sédimentation des formations tertiaires et quaternaires sus-jacentes qui représentent les terrains affleurants (Minguely, 2007).

Ce projet prendrait la forme d'une thèse qui envisagerait le bassin houiller comme un objet géologique essentiel pour la compréhension des enjeux scientifiques (structuration nord varisque) et territoriaux (géothermie et hydrogéologie) dans les Hauts-de-France (Figure 49). Tout d'abord en mettant à jour les connaissances sur ce bassin d'avant-pays varisque (en particulier le schéma structural), ce qui apportera à coup sûr des éléments nouveaux sur la dynamique syn-orogénique. En effet de nombreuses données (e.g. plan de mines) restent encore à dépouiller et interpréter en terme de concepts tectoniques modernes des fronts de chaîne (**Laurent et al. 2021, et référence incluses). Ensuite en construisant un modèle géologique 3D du bassin houiller qui intégrera ces nouvelles données au cadre structural issus de la thèse d'A. Laurent. Ce nouveau modèle 3D devra mieux définir le substratum du bassin houiller (i.e. les réservoirs géothermiques dinantiens) et sa couverture (aquifère de la craie), et les relations entre eux (prolongations de failles vers le bas ou le haut ?).

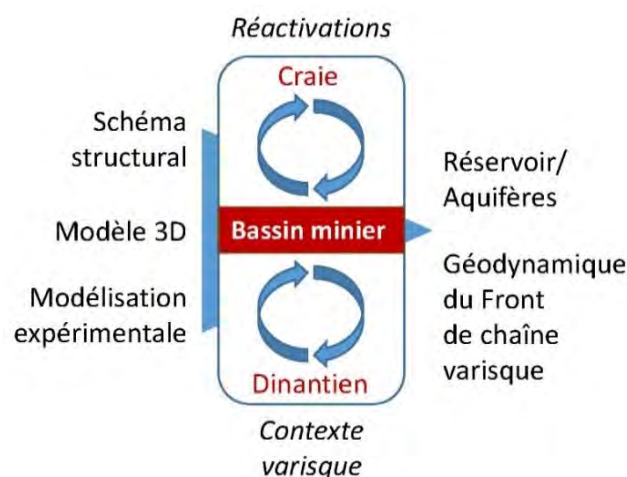


Figure 49 - Géothermie et hydrogéologie dans le bassin houiller du Nord-Pas-de-Calais, une démarche intégrée.

Ces réflexions déjà bien avancées seront nourries par des travaux qui viennent de débuter sur l'interprétation transfrontalière du bassin houiller, de son substratum réservoir géothermique dinantien et de sa couverture aquifère crétacée. Ce projet, impliquant les collègues lillois, du BRGM et de l'Université de Mons en Belgique (O. Kaufman), se propose d'avoir une vision encore plus

complète du front nord varisque en l'étudiant pour la première fois de manière continue à travers la frontière franco-belge sur la base de l'interprétation de profils sismiques (nouvellement retraités et/ou acquis).

Le bassin sarro-lorrain comme cible géothermique ?

Nous avons vu que les épaisseurs cumulées de la série silicoclastique carbonifère et permienne du bassin sarro-lorrain sont de l'ordre de plusieurs milliers de mètres, en particulier les séries westphaliennes (4509 m dans le forage de Gironville-1). En conséquence, pour un gradient thermique normal (35°C/km) typique du bassin de Paris s.s. sus-jacent (Bonté et al., 2010), on estime qu'une température de 150°C, favorable à la production d'électricité, serait atteinte dans les formations sédimentaires carbonifères vers 4000 m de profondeur.

Le post-doc de R. Hemelsdaël a permis de complètement réévaluer le contexte cinématique et géodynamique du bassin sarro-lorrain (Hemelsdaël et al., soumis à *Tectonics*), dévoilant la complexité structurale du secteur. Cette histoire tectonique polyphasée et la géométrie des dépôts résultants est certainement favorable au développement d'une intense fracturation multi-échelle, notamment à proximité des failles transverses réactivées pendant l'orogénèse alpine (Henk, 1993). Quant aux questionnements sur les lithologies réservoirs et les perméabilités matricielles attendues, elles pourraient être abordés via l'Interprétation Quantitative du signal sismique (voir la section dédiée).

J'ai participé récemment au montage d'un projet de recherche BRGM qui pourrait faire l'objet d'une thèse dans les années à venir (collab. Géoressources Nancy et géothermiciens du BRGM), dont les grandes étapes se résument ainsi:

- Construire un modèle géologique 3D du bassin sarro-lorrain sur la base des résultats du post-doc (interprétations sismiques converties en profondeur, lithostratigraphie des forages mise à jour... ; Figure 50).
- Estimer les propriétés réservoirs des formations permo-carbonifères - porosité, perméabilité, salinité -, à partir de l'interprétation des données de forages pétroliers existants (description lithologique, échantillonnage sur carottes, diagraphie) et de l'Interprétation Quantitative.
- Estimer et modéliser les températures le long de coupes géologiques issues du modèle 3D (voire en 3D) en identifiant la présence de possibles convections, compte tenu de l'intense fracturation caractérisant le bassin (e.g. le long des failles transverses).

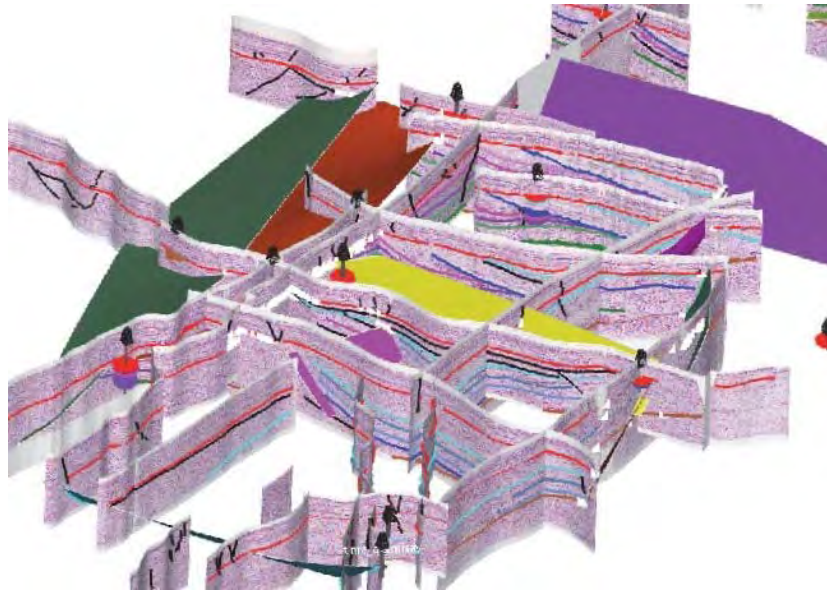


Figure 50 - Profils sismiques interprétés dans le bassin sarro-lorrain vus en 3D (source Post-doc R. Hemelsdaël).

Les bassins carbonifères-permiens comme réservoir d'hélium naturel

Je contribue activement à la définition d'un programme de recherche et d'exploration d'hélium mené conjointement par le BRGM et 45-8 Energie, une entreprise pionnière dans ce domaine.

Les premières investigations au nord du Massif Central (PER Fonts-Bouillants dans la Nièvre) ont montré que les bassins stéphano-permiens sont des cibles potentielles pour ce gaz, tout comme certains faciès sédimentaires mésozoïques sus-jacents (Hauville et al., 2021 ; Jacob et al., 2021 ; Figure 51).

Les questions posées sont celles déjà exposées dans le volet 2, dans une optique d'exploration: quelles sont leur épaisseur, jusqu'à quel point sont-ils en continuité latérale, quels types de sédiments les remplissent ? Un autre challenge, auquel je viens en appui en tant géologue expert de ces bassins, est de choisir les meilleures méthodes d'investigation géophysique pour détecter ces bassins sous couverture (gravimétrie, électromagnétisme, tomographie de résistivité électrique, sismique HR...).

Il est aussi prévu à court terme que j'intervienne dans une thèse CIFRE en cours (financements 45-8 Energie - Géorressources Nancy) qui cherche à caractériser (i) le bassin permien nouvellement identifié dans la Nièvre, et (ii) les systèmes géologiques de l'hélium naturel à plus grande échelle et l'évaluation de son potentiel exploratoire.

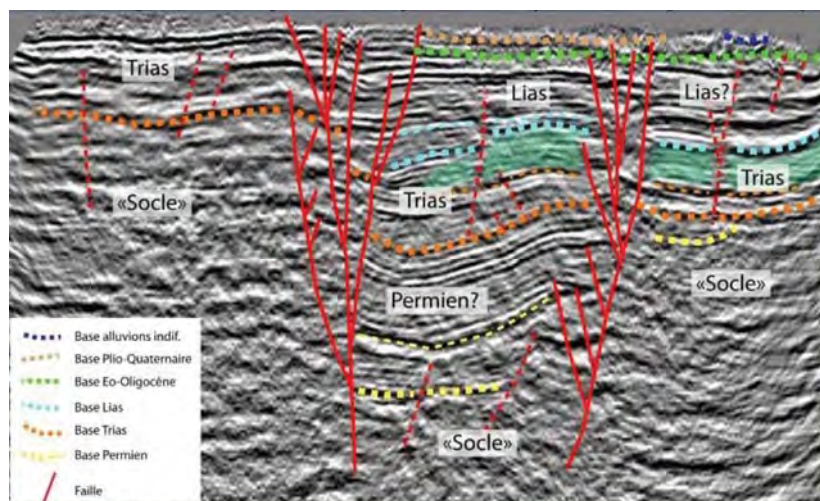


Figure 51 - Dépocentre permien identifié sous couverture méso-cénozoïque ; le profil sismique correspond à une longueur de quelques kilomètres (Jacob et al., 2021).

5.1.4. Pour aller plus loin

L'objectif à long terme, au-delà d'établir des corrélations précises entre les bassins carbonifères-permiens, est de poursuivre les efforts pour comprendre les interconnexions entre :

- Les résultats issus des projets précédents à l'échelle métropolitaine et ouest-européenne (contexte structural, modalités des remplissages sédimentaires, géométries et faciès, datations absolues).

Et

- Les évènements géodynamiques internes et externe d'échelle globale prévalant à cette époque :
 - Les changements notables de la paléogéographie en relation avec la géodynamique globale (fin du cycle varisque, fermeture de la Paléotéthys), induisant des modifications majeures de la circulation océanique et atmosphériques (Blakey, 2003; Tabor & Montañez 2002).
 - L'altitude de la chaîne Varisque (et par extension du système Varisque-Mauritanides-Ouachita-Appalaches), son effondrement et son érosion en contexte post-orogénique (Rowley et al., 1985; Tabor & Montañez, 2004; Dusséault et al., 2021).
 - Les cycles de glaciations-déglaciations à la transition permo-carbonifère (Poulsen et al., 2007; Isbell et al., 2008), et l'augmentation des températures et de l'aridité au cours du Permien inférieur traduisant le passage graduel d'un climat icehouse à greenhouse (Tabor & Montañez, 2004).
 - L'influence du volcanisme généralisé sur les remplissages sédimentaires et les paramètres paléoclimatiques (Timmermann, 2004, Soreghan et al., 2019).

Peut-être alors pourrions-nous apporter de nouvelles réponses à la question des modalités de fonctionnement et d'enregistrement sédimentaire de ces bassins, et discuter sur des bases solides la part de la tectonique vs celle du climat (cf. Michel et al., 2015 ; Pochat & Van Den Driessche, 2016) ? Nous pourrions aussi tenter de quantifier des volumes de sédiments déposés et remonter aux volumes de roches érodées et altérées (rôle du climat, approche Source-to-Sink) lors des processus syn- et post-orogéniques.

5.2. Perspectives de recherche sur la couverture sédimentaire méso-cénozoïque

5.2.1. Les déformations multi-échelles cénozoïques du bassin de Paris

Ce travail déjà en cours est une collaboration BRGM-GE Cergy-GEOParis-Saclay, qui prend la forme d'une thèse RGF Chantier bassin de Paris (thèse de S. Brown).

L'objectif de la thèse est d'établir un corpus régional des déformations cénozoïques du bassin de Paris (répartition spatiale, géométries, densités, âges et liens avec les architectures de dépôts sédimentaires) et d'intégrer ce modèle dans un contexte géodynamique plus large, intégrant les systèmes alpins, pyrénéens, et les rifts ouest européens (déformation « far-field »; Lacombe et Mouthereau, 1999 ; Guillocheau et al., 2000 ; Robin et al., 2000 ; Briais et al., 2016). La réalisation de cette étude repose sur :

- L'acquisition de données structurales à toutes les échelles, depuis l'échelle régionale (plis et failles) jusqu'à la micro-échelle (micro-fracturation, anisotropies magnétique et acoustique et macles de la calcite), en passant par les observations et mesures de terrain (Figure 52).
- La datation absolue des structures tectoniques (U/Pb sur calcites syn-cinématiques).

L'équipe s'est d'abord concentrée sur les lithologies du Tertiaire les plus susceptibles d'enregistrer la déformation: calcaires daniens, lutétiens, bartoniens et priaboniens, grès rupéliens et calcaires aquitaniens. Les formations mésozoïques, qui ont elles aussi enregistré cette déformation, sont également investiguées, notamment les séries crétacées (craie) et jurassiques.

La caractérisation de la déformation repose sur une approche multi-échelles et donc nécessairement multi-techniques: géophysique (interprétation des lignes sismiques retraitées précédemment par le BRGM, tâche qui me concerne plus directement), géologie structurale (acquisition de données sur le terrain), pétrophysique (caractérisation des microdéformations) et géochimique (datation U-Pb des calcites syn-cinématiques). Ces quatre approches complémentaires permettront d'effectuer le saut d'échelle entre l'échelle régionale et l'échelle microscopique.

Les premiers résultats concernant les âges de calcites syn-cinématiques sont en cours de publication à Terra Nova. A la suite de la thèse le travail se poursuivra au moins interne au BRGM jusqu'en 2027, dernière année du chantier RGF-Bassin de Paris.

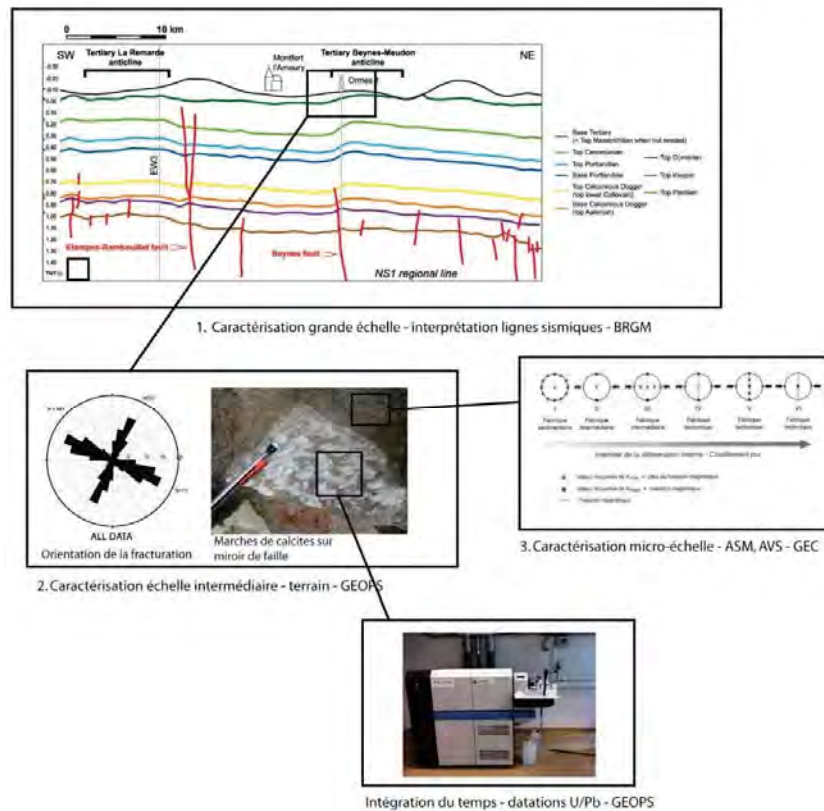


Figure 52 - Approche multi-échelles et multi-techniques pour établir le corpus structural du bassin de Paris pour le Tertiaire.

5.2.2. Tectonique du Trias évaporitique et carbonaté du Haut-Var - Implications en terme d'aléa gravitaire (effondrement-dissolution)

La Provence présente une géologie très complexe avec une succession d'épisodes tectoniques, thermiques, de phases d'érosion/d'aplanissement généralisé, et d'enfouissement depuis la fin du Paléozoïque: (Delfaud et al., 1989; Hippolyte et al., 1993; Laurent et al., 2000; Champion et al., 2000; Besson, 2005; Balansa et al., 2022), le tout entremêlé avec une tectonique salifère en relation avec les évaporites-carbonates triasiques déformées de manière totalement dysharmonique (Mennessier et al., 1969, 1975; Angelier et Aubouin, 1976; de Graciansky et Lemoine, 1988; Espurt et al., 2019; Wicker et Ford, 2021).

Dans la région Provence-Alpes-Côte d'Azur et plus particulièrement dans le nord du département du Var (Haut-Var), le Trias supérieur, principalement évaporitique (gypse et sels du Keuper) est concerné par des phénomènes de dissolution de gypse continue pouvant engendrer la création de vides souterrains à l'origine de désordres fréquents en surface (effondrements, affaissements). De même, le Trias moyen calcaire sous-jacent (Muschelkalk) pourrait être associé à des phénomènes de fracturation et de karstification générant des effondrements. La stratégie régionale Provence-Alpes-Côte d'Azur des risques naturels hydrauliques et miniers 2022-2024 prévoit l'accompagnement des collectivités pour gérer ce risque. En effet, les événements récents et désordres associés (le Luc-en-Provence en 2014, Clapiers en 2016) ou plus anciens mais marquants (le Peyruis à Bargemon en 1992) font peser un poids économique de plus en plus important sur les communes, les habitants et les assurances.

Je suis impliqué depuis plusieurs années dans un projet de recherche et d'appui aux politiques publiques piloté par le BRGM sur l'aléa dissolution de gypse dans une commune du Var (Marçot et al., 2022). Les résultats montrent le rôle central de l'information géologique pour l'établissement de cartes de sensibilité au risque (e.g. alignement N110 des fontis au cœur de l'axe anticlinal principal ; Figure 53), en complément des approches hydrogéologiques et géophysiques. Ils nous confortent dans la nécessité d'aller plus loin dans la compréhension des mécanismes notamment géologiques et structuraux de mise en place de ces formations. En particulier, il est important de lever les verrous scientifiques liés à la profondeur et la géométrie des horizons géologiques à risque (gypse et calcaire), c'est-à-dire au seuil de profondeur à partir duquel les phénomènes de dissolution peuvent avoir un impact en surface et générer in fine des désordres).

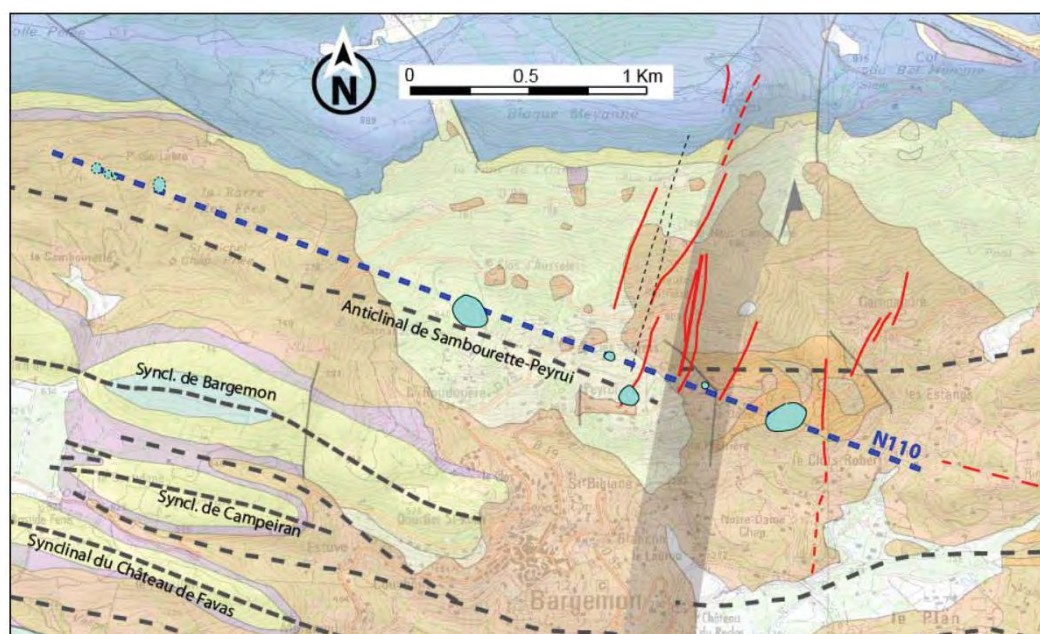


Figure 53 - Alignement selon une direction N110 des fontis sur la commune de Bargemon (Marçot et al., 2022) ; en fond carte géologique harmonisée au 1/50000^{ème} (source BRGM).

Je participe ainsi au montage d'un projet de recherche impliquant des géophysiciens et ingénieurs « risque naturels » du BRGM et des collègues universitaires (e.g. N. Espurt de GEOAZUR Université de Nice). Ce projet pluriannuel s'appuiera en partie sur une thèse dont les grandes lignes sont résumées ici :

- Cartographie, construction et équilibrage de coupes ciblées autour des zones identifiées comme étant à risque.
- Datation U-Pb des calcites de faille et cinématique de déformation, afin de déchiffrer l'histoire cinématique complexe de la déformation du Muschelkalk carbonaté (plissement vs. fracturation).
- Thermicité Raman (RSCM) des séries évaporitiques-carbonatées du Trias, afin d'avoir des réponses sur la température maximale associée aux déformations du Muschelkalk.
- Discussion et implications en termes d'aléa effondrement ; les trois volets ci-dessus apporteront les éléments scientifiques indispensables pour affiner (i) la cartographie géologique détaillée sur les secteurs ciblés, (ii) la description/compréhension de la déformation du Muschelkalk peu travaillé jusqu'à présent, (iii) le rôle des fluides, en y ajoutant une troisième dimension verticale le long des coupes géologiques.

Plus largement, nous sommes convaincus que toute amélioration de la connaissance du Trias évaporitique/carbonaté se traduira par une meilleure compréhension de l'aléa effondrement-dissolution dans la région.

5.2.3. Pour aller plus loin

L'objectif à long terme est de continuer à confronter :

- La structuration de la couverture méso-cénozoïque (en lien avec l'héritage varisque) et les remplissages sédimentaires associés.

Avec

- La variabilité du contexte géodynamique pendant cette période (e.g. Ziegler, 1990 ; Stampfli et Hochard, 2009).

Autrement dit, préciser comment ces bassins enregistrent le passage d'un système plutôt extensif (ouverture de l'Atlantique Central, de la Téthys Alpine, du Golfe de Gascogne) à un système plutôt compressif (phases orogéniques pyrénéennes et alpines).

A ce titre le Tertiaire m'intéresse particulièrement : quelles sont les relations génétiques entre les phases de déformations orogéniques ou extensives en limite de plaques (« far-field ») et les enregistrements tectoniques et sédimentaires dans le bassin de Paris et le fossé Rhénan, et plus largement le système de rift ouest-européen (e.g. comment ce dernier influence la propagation des contraintes alpines vers le bassin de Paris et au-delà) ?

Références bibliographiques

- AGBP.** 2014. Le Bassin parisien, un nouveau regard sur la géologie, Bull. Inf. Géol. Bass. Paris, mémoire hors-série n°9, 228 p
- Aichholzer, C.,** 2019. Le log complet de la stratigraphie de la zone rhénane ainsi que les modalités stratigraphiques, sédimentaires et structurales de la transition « socle-couverture ». Application à la géothermie profonde. Thèse Université de Strasbourg
- Anderle, H.J.,** 1987. The evolution of the South Hunsrück and Taunus Borderzone. *Tectonophysics* 137, 101–114. [https://doi.org/10.1016/0040-1951\(87\)90317-9](https://doi.org/10.1016/0040-1951(87)90317-9)
- Anderle, H.-J., Franke, W., Schwab, M.,** 1995. Stratigraphy, in: Dallmeyer, R.D., Franke, W., Weber, K. (Eds.), *Pre-Permian Geology of Central and Eastern Europe*. Springer Berlin Heidelberg, Berlin, Heidelberg, pp. 99–107. https://doi.org/10.1007/978-3-642-77518-5_9
- Angelier, J., Aubouin, J.,** 1976. Contribution à l'étude géologique des bandes triasiques provençales: de Barjols (Var) au bas Verdon. *Bulletin du BRGM*, (2), I, n° 3, 187–217
- Armandine Les Landes, A., Guillon, T., Peter-Borie, M., Blaisonneau, A., Rachez, X., Gentier, S.,** 2019. Locating Geothermal Resources: Insights from 3D Stress and Flow Models at the Upper Rhine Graben Scale. *Geofluids* 2019, 1–24. <https://doi.org/10.1155/2019/8494539>
- Arnold, J., Jacoby, W.R., Schmeling, H., Schott, B.,** 2001. Continental collision and the dynamic and thermal evolution of the Variscan orogenic crustal root: 3D numerical models. *Journal of Geodynamics*.
- Arthaud, F., Laurent, P.,** 1995. Contraintes, déformation et déplacement dans l'avant-pays Nord-pyrénéen du Languedoc méditerranéen. *Geodynamica Acta* 8: 142–157
- Arthaud, F., Matte, Ph.,** 1975. Les décrochements tardi-hercyniens du sud-ouest de l'Europe. Géométrie et essai de reconstitution des conditions de la déformation. *Tectonophysics* 25, 139–171. [https://doi.org/10.1016/0040-1951\(75\)90014-1](https://doi.org/10.1016/0040-1951(75)90014-1)
- Averbuch, O., Mansy, J.-L., & Lamarche, J.,** 2001. Déformations tardi-paléozoïques au front septentrional de la chaîne varisque : l'exemple des massifs paléozoïques du Boulonnais (N France). *Annales de la Société Géologique du Nord*, Tome 9 (2ème série), 13–24
- Arthaud, F., & Matte, P.,** 1977. Late Paleozoic strike-slip faulting in southern Europe and northern Africa: Result of a right-lateral shear zone between the Appalachians and the Urals. *Geological Society of America Bulletin*, 88, 1305–1320
- Averbuch, O., Piromallo, C.,** 2012. Is there a remnant Variscan subducted slab in the mantle beneath the Paris basin? Implications for the late Variscan lithospheric delamination process and the Paris basin formation. *Tectonophysics* 558–559, 70–83. <https://doi.org/10.1016/j.tecto.2012.06.032>
- Bader, A.G., Thiébeau, S., Vincké, O., Delprat Jannaud, F., Saysset, S., Joffre, G.H., Giger, F.M., David, M., Gimenez, M., Dieulin, A., Copin, D.,** 2014. CO2 Storage Capacity Evaluation in Deep Saline Aquifers for an Industrial Pilot Selection. Methodology and Results of the France Nord Project. *Energy Procedia* 63, 2779–2788. <https://doi.org/10.1016/j.egypro.2014.11.300>
- Balansa, J., Espurt, N., Hippolyte, J.-C., Philip, J., Caritg, S.,** 2022. Structural evolution of the superimposed Provençal and Subalpine fold-thrust belts (SE France). *Earth-Science Reviews* 227, 103972. <https://doi.org/10.1016/j.earscirev.2022.103972>
- Ballèvre, M., Bosse, V., Ducassou, C., & Pitra, P.,** 2009. Palaeozoic history of the Armorican Massif: Models for the tectonic evolution of the suture zones. *Comptes Rendus Géoscience*, 341(2–3), 174–201. <https://doi.org/10.1016/j.crte.2008.11.009>
- Ballèvre, M., Manzotti, P., Dal Piaz, G.V.,** 2018. Pre-Alpine (Variscan) Inheritance: A Key for the Location of the Future Valaisan Basin (Western Alps). *Tectonics* 37, 786–817. <https://doi.org/10.1002/2017TC004633>
- Ballèvre, M., Martínez Catalán, J.R., López-Carmona, A., Pitra, P., Abati, J., Fernández, R.D., Ducassou, C., Arenas, R., Bosse, V., Castiñeiras, P., Fernández-Suárez, J., Gómez Barreiro, J., Paquette, J.-L., Peucat, J.-J., Poujol, M., Ruffet, G., Sánchez Martínez, S.,** 2014. Correlation of the nappe stack in the Ibero-Armorican arc across the Bay of Biscay: a joint French–Spanish project. *SP 405*, 77–113. <https://doi.org/10.1144/SP405.13>
- Baptiste, J.,** 2016. Cartographie structurale et lithologique du substratum du Bassin parisien et sa place dans la chaîne varisque de l'Europe de l'Ouest - Approches combinées : géophysiques, pétrophysiques, géochronologiques et modélisations 2D, Thèse de doctorat, Université d'Orléans, 296 p.
- Baptiste, J., Martelet, G., Faure, M., Beccaletto, L., Reninger, P.-A., Perrin, J., Chen, Y.,** 2016. Mapping of a buried basement combining aeromagnetic, gravity and petrophysical data:

- The substratum of southwest Paris Basin, France. *Tectonophysics* 683, 333–348. <https://doi.org/10.1016/j.tecto.2016.05.049>
- Barchi, P., Cartannaz, C., Fourniguet, G.**, 2008. PROJET MINEWATER Géologie du bassin houiller lorrain et potentialité géothermique BRGM/RP-56096-FR, 53 p
- Beccaletto, L., Capar L., Badinier G., Marc S.**, 2014. Étude sismique Non-Exclusive du Fossé rhénan français, BRGM/RC-63950-FR, 147p. (Confidentiel)
- Beccaletto, L., Capar, L., Serrano, O., Marc, S.**, 2015. Structural evolution and sedimentary record of the Stephano-Permian basins occurring beneath the Mesozoic sedimentary cover in the southwestern Paris basin (France). *Bulletin de la Société Géologique de France* 186, 429–450. <https://doi.org/10.2113/gssgfbull.186.6.429>
- Beccaletto, L., Hanot, F., Serrano, O., Marc, S.**, 2011. Overview of the subsurface structural pattern of the Paris Basin (France): Insights from the reprocessing and interpretation of regional seismic lines. *Marine and Petroleum Geology, Thematic Set on the Implications of basin dynamics on petroleum systems* 28, 861–879. <https://doi.org/10.1016/j.marpetgeo.2010.11.006>
- Beccaletto, L., Lasseur, E., Paquet, F., Capar, L.**, 2013. Géométrie et contrôle structural des dépôts syn-rifts du Fossé rhénan: Démonstrateur RGF Vosges/Fossé rhénan. Rapport final BRGM/RP-62896-FR
- Beccaletto, L., Nitsch, E., Anders, B., Dresmann, H., Rupf, I., Tesch, J., Zumsprekel, H., Capar, L. & The Georg Project Team**, 2012. 3D structural modelling of a wrench rift basin: the Upper Rhine Graben of NW Europe as a case study - Contribution of the EU GeORG project. 34IGC, Brisbane, Australia
- Beccaletto, L., Robelin, C., Hanot, F.**, 2008. Cartographie structurale de surfaces géologiques de référence, caractérisation des failles majeures, Rapport BRGM/RP56355-FR, 379 p. (Confidentiel)
- Beccaletto, L., Steiner, C.**, 2005. Evidence of two-stage extensional tectonics from the northern edge of the Edremit Graben, NW Turkey. *Geodinamica Acta* 18, 283–297. <https://doi.org/10.3166/ga.18.283-297>
- Becker, A., Schäfer, A.**, 2021. Evolution of the Saar-Nahe Basin in the late Palaeozoic. *jber_oberrh* 103, 211–233. <https://doi.org/10.1127/jmogv/103/0006>
- Becq-Giraudon, J.-F.**, 1983. Synthèse géologique du bassin Houiller Nord-Pas-de-Calais, Mémoire BRGM 123
- Belanger, I., Delaby, S., Delcambre, B., Ghysel, P., Hennebert, M., Laloux, M., et al.**, 2012. Redéfinition des unités structurales du front varisque utilisées dans le cadre de la nouvelle Carte géologique de Wallonie (Belgique). *Geologica Belgica*, 15(3), 169–175
- Berger, J.-P., Reichenbacher, B., Becker, D., Grimm, M., Grimm, K., Picot, L., Storni, A., Pirkenseer, C., Derer, C., Schaefer, A.**, 2005. Paleogeography of the Upper Rhine Graben (URG) and the Swiss Molasse Basin (SMB) from Eocene to Pliocene. *Int J Earth Sci (Geol Rundsch)* 94, 697–710. <https://doi.org/10.1007/s00531-005-0475-2>
- Besson, D.**, 2005. Architecture du bassin rhodano-provençal miocène (Alpes, SE France), Relations entre déformation, physiographie et sédimentation dans un bassin molassique d'avant-pays, PhD thesis, 438 pp., Ecole des Mines de Paris
- BGR**, 1993. Geologische Karte der Bundesrepublik Deutschland, 1:1000000
- Blaise, T., Izart, A., Michels, R., Suarez-Ruiz, I., Cathelineau, M., Landrein, P.**, 2011. Vertical and lateral changes in organic matter from the Mesozoic, eastern Paris Basin (France): variability of sources and burial history. *Int. J. Coal Geol.* 88 (2–3), 163–178. Blaise, T., Barbarand
- Blakey, R. C., Wong, T. E.**, 2003. Carboniferous–Permian paleogeography of the assembly of Pangaea. In *Proceedings of the XVth International Congress on Carboniferous and Permian Stratigraphy*, Utrecht, Vol. 10, p. 16
- Blanc-Valleron, M. M.**, 1990. Les formations paléogènes évaporitiques du bassin potassique de Mulhouse et des bassins plus septentrionaux d'Alsace (Doctoral dissertation, Strasbourg 1)
- Blès, J.-L., Bonijoly, D., Castaing, C. & Gros, Y.**, 1989. Successive post-Variscan stress fields in the French Massif Central and its borders (western European plate); comparison with geodynamic data. *Tectonophysics*, 169, 79–111
- Böcker, J., Littke, R., Forster, A.**, 2017. An overview on source rocks and the petroleum system of the central Upper Rhine Graben. *Int J Earth Sci (Geol Rundsch)* 106, 707–742. <https://doi.org/10.1007/s00531-016-1330-3>
- Boigk, H., Schöneich, H.**, 1970. Die Tiefenlage der Permian im nördlichen Teil des Oberrheingrabens. *Graben Probl.* 27, 48–55
- Bonijoly, D., Castaing, C.**, 1983. Fracturation et genèse des bassins stéphaniens du Massif central français en régime compressif. - *Annales Société Géologique du Nord*, CIII, 187–199

- Bonijoly, D. & Castaing, C.**, 1986. Ouverture et évolution structurale de quelques bassins houillers de directions orthogonales, dans le Massif central français. - *Annales Société Géologique du Nord*, CVI, 189-200
- Bonté, D., Guillou-Frottier, L., Garibaldi, C., Bourguine, B., Lopez, S., Bouchot, V., & Lucazeau, F.**, 2010. Subsurface temperature maps in French sedimentary basins: new data compilation and interpolation. *Bulletin de la Société géologique de France*, 181(4), 377-390.
- Bossennec, C., Géraud, Y., Böcker, J., Klug, B., Mattioni, L., Sizun, J.-P., Sudo, M., Moretti, I.**, 2021. Evolution of diagenetic conditions and burial history in Buntsandstein Gp. fractured sandstones (Upper Rhine Graben) from in-situ $\delta^{18}\text{O}$ of quartz and $40\text{Ar}/39\text{Ar}$ geochronology of K-feldspar overgrowths. *Int J Earth Sci (Geol Rundsch)* 110, 2779–2802. <https://doi.org/10.1007/s00531-021-02080-2>
- Bourgeois, O., Ford, M., Diraison, M., Veslud, C.L.C. de, Gerbault, M., Pik, R., Ruby, N., Bonnet, S.**, 2007. Separation of rifting and lithospheric folding signatures in the NW-Alpine foreland. *Int J Earth Sci (Geol Rundsch)* 96, 1003–1031. <https://doi.org/10.1007/s00531-007-0202-2>
- Bouroz, A.**, 1967. Corrélations des tonsteins d'origine volcanique entre les bassins houillers de Sarre-Lorraine et du Nord - Pas-de-Calais. *Comptes Rendus de l'Académie des Sciences* 264, série D
- Bouroz, A.**, 1968. Corrélations entre quelques bassins stéphaniens du Massif Central par le moyen des niveaux cinéritiques. *Comptes Rendus de l'Académie des Sciences* 266, série D
- Bouroz, A.**, 1969. Le Carbonifère du Nord de la France. *Annales de la Société Géologique du Nord*, 89(1), 47–65
- Bouroz, A., Chalard, J., Dalinval, A., Stiévenard, M.**, 1961. La structure du bassin houiller du Nord de la région de Douai à la frontière Belge. *Annales de la Société Géologique du Nord*, 81, 173–218
- Bourquin, S., Guillocheau, F.**, 1996. Keuper stratigraphic cycles in the Paris basin and comparison with cycles in other peritethyan basins (German basin and Bresse-Jura basin). *Sedimentary Geology* 105, 159–182. [https://doi.org/10.1016/0037-0738\(95\)00153-0](https://doi.org/10.1016/0037-0738(95)00153-0)
- Bourquin, S., Guillocheau, F., Pâron, S.**, 2009. Braided rivers within an arid alluvial plain (example from the Lower Triassic, western German Basin): recognition criteria and expression of stratigraphic cycles. *Sedimentology* 56, 2235–2264. <https://doi.org/10.1111/j.1365-3091.2009.01078.x>
- Bourquin, S., Rigollet, C., Bourges, P.**, 1998. High-resolution sequence stratigraphy of an alluvial fan–fan delta environment: stratigraphic and geodynamic implications – An example from the Keuper Chaunoy Sandstones, Paris Basin. *Sedimentary Geology* 121, 207–237. [https://doi.org/10.1016/S0037-0738\(98\)00081-5](https://doi.org/10.1016/S0037-0738(98)00081-5)
- Bourquin, S., Robin, C., Guillocheau, F., Gaulier, J.-M.**, 2002. Three-dimensional accommodation analysis of the Keuper of the Paris Basin: discrimination between tectonics, eustasy and sediment supply in the stratigraphic record. *Marine and Petroleum Geology* 19, 469–498. [https://doi.org/10.1016/S0264-8172\(02\)00008-9](https://doi.org/10.1016/S0264-8172(02)00008-9)
- BRGM**, 1980. Synthèse géologique du Bassin de Paris, II, Atlas. In: Mémoires du BRGM n° 102
- BRGM**, 1984. Synthèse géologique du Sud-Est de la France. Mémoire BRGM n°126
- BRGM**, 1989. Synthèse géologique des bassins permien français. - Mémoire BRGM n°128
- BRGM**, 2003. Carte géologique de la France au 1/1000000^{ème}, 6^{ème} édition révisée
- Briais, J.**, 2015. Le Cénozoïque du bassin de Paris : un enregistrement sédimentaire haute résolution des déformations lithosphériques en régime de faible subsidence. Thèse Université Rennes 1
- Briais, J., Guillocheau, F., Lasseur, E., Robin, C., Châteauneuf, J.J., Serrano, O.**, 2016. Response of a low-subsiding intracratonic basin to long wavelength deformations: the Palaeocene–early Eocene period in the Paris Basin. *Solid Earth* 7, 205–228. <https://doi.org/10.5194/se-7-205-2016>
- Broutin, J., Châteauneuf, J.-J., Galt, J., Ronchi, A.**, 1999. L'Autunien d'Autun reste-t-il une référence pour les dépôts continentaux du Permien inférieur d'Europe? 16.
- Brunet, M.-F., Le Pichon, X.**, 1982. Subsidence of the Paris Basin. *J. Geophys. Res.* 87, 8547. <https://doi.org/10.1029/JB087iB10p08547>
- Bugarel, F., Salquière, D. & Hamm, V.**, 2019. Etude du potentiel de la géothermie profonde sur le territoire d'Orléans Métropole - Volet 1 : conditions d'accès à la ressource (modèle du Dogger en région Ile-de-France) et retours d'expérience sur les opérations au Trias. Report No. BRGM/RP-69450-FR
- Burg, J.P., Van Den Driessche, J., Brun, J.P.**, 1994. Syn- to post-thickening extension: mode and consequences. *Comptes Rendus de l'Académie des Sciences - Series IIA - Earth and Planetary Science* 319 (2), 1019–1032

- Burger, K., Hess, J. C., & Lippolt, H. J.**, 1997. *Tephrochronologie mit Kaolin-Koblensteinen: Mittel zur Korrelation paraisischer und limnischer Ablagerungen des Oberkarbons*. Schweizerbart
- Butler, R.W.H.**, 1989. The influence of pre-existing basin structure on thrust system evolution in the Western Alps. SP 44, 105–122. <https://doi.org/10.1144/GSL.SP.1989.044.01.07>
- Butler, R.W.H., Tavarnelli, E., Grasso, M.**, 2006. Structural inheritance in mountain belts: An Alpine–Apennine perspective. *Journal of Structural Geology* 28, 1893–1908. <https://doi.org/10.1016/j.jsg.2006.09.006>
- Capar L., Darnet M., Issautier B., Marc S. et Stopin A.**, 2021. Valorisation des données de sismique réflexion et de puits, des années 80, pour de l'interprétation quantitative, sur le réservoir géothermique du Dogger dans le Bassin parisien. Rapport final. BRGM/RP-70726-FR, 69 p
- Carrat, H.**, 1969. Le Morvan cristallin : étude pétrographique, géochimique et structurale : position de l'uranium. Ph.D. thesis. Université de Nancy-Faculté des sciences
- Cazes, M., Torreilles, G., Bois, C., Damotte, B., Galdeano, A., Hirn, A., Mascle, A., Matte, P., Van Ngoc, P., Raoult, J.F.**, 1985. Structure de la croûte hercynienne du Nord de la France; premiers résultats du profil ECORS. *Bulletin de la Société Géologique de France I*, 925–941. <https://doi.org/10.2113/gssgfbull.I.6.925>
- Champion, C., Choukroune, P., Clauzon, G.**, 2000. La déformation post-Miocène en Provence occidentale. *Geodin. Acta*, 13, 67–85
- Choulet, F., Faure, M., Fabbri, O., Monié, P.**, 2012. Relationships between magmatism and extension along the Autun–La Serre fault system in the Variscan Belt of the eastern French Massif Central. *Int J Earth Sci (Geol Rundsch)* 101, 393–413. <https://doi.org/10.1007/s00531-011-0673-z>
- Cleal, C.J., Thomas, B.A.**, 2005. Palaeozoic tropical rainforests and their effect on global climates : is the past the key to the present ? *Geobiology* 3, 13_31
- Cloethingh, S., Ziegler, P.A.**, 2007. Tectonic models for the evolution of sedimentary basins, in crust and lithosphere dynamics. In: Watts, A.B. (Ed.), *Treatise on Geophysics*, pp. 486–611
- Cohen, K.M., Finney, S.C., Gibbard, P.L. & Fan, J.-X.**, 2013; updated. The ICS International Chronostratigraphic Chart. *Episodes* 36: 199-204
- Costa, S., Rey, P.**, 1995. Lower crustal rejuvenation and growth during post-thickening collapse: Insights from a crustal cross section through a Variscan metamorphic core complex. *Geol* 23, 905. [https://doi.org/10.1130/0091-7613\(1995\)023<0905:LCRAGD>2.3.CO;2](https://doi.org/10.1130/0091-7613(1995)023<0905:LCRAGD>2.3.CO;2)
- Courel, L., Valle, B., Branchet, M.**, 1986. Le bassin houiller de Blanzay-Montceau ; cadre géologique et structural ; succession et dynamique des paléoenvironnements. *Bulletin trimestriel de la Société d'histoire naturelle et des amis du Muséum d'Autun*, 7-26
- de Graciansky, P. C., Lemoine M.**, 1988. Early Cretaceous tectonics in the southwestern French Alps: A consequence of North Atlantic rifting during Tethyan spreading, *Bull. Soc. Geol. Fr.*, 5, 733–737
- Delenin, P., Clermonté, J., Courel, L., Dumain, M., Laversanne J.**, 1988. Remise en cause des charriages dans le bassin houiller des Cévennes (Gard, France), *C. R. Acad. Sci. Paris*, t. 307, Série II, p. 1237-1243
- Delfaud, J., Toutin-Morin, N., Morin, R.**, 1989. Un cône alluvial en bordure d'un bassin intramontagneux: La formation permienne du Rocher de Roquebrune (Bassin du Bas- Argens, Provence orientale). *C. R. Acad. Sci., Ser. II: Mec., Phys., Chim., Sci. Terre Univers* 309, 1811–1817
- Delmer, A.**, 1997. Structure tectonique du bassin houiller du Hainaut. *Annales de la Société Géologique du Nord*, 5(2), 7–15.
- Delmer, A.**, 2003. La structure tectonique transfrontalière entre les bassins houillers de Valenciennes (France) et du Hainaut belge. *Geologica Belgica*, 6(3–4), 171–180
- Delmer, A.**, 2004. Tectonique du front varisque en Hainaut et dans le Namurois. *Memoirs of the Geological Survey of Belgium*, 50, 1–62
- Delmer, A., Duser, M., & Delcambre, B.**, 2001. Upper Carboniferous lithostratigraphic units (Belgium). *Geologica Belgica*, 4(1–2), 95–103. <https://doi.org/10.20341/gb.2014.045>
- Delmas, J., Houël, P., Vially, R.**, 2002. Paris Basin, Petroleum potential. - IFP regional report
- Dentzer, J.**, 2016. Forçages environnementaux et contrôles structuraux sur le régime thermique actuel du bassin de Paris - Enjeux pour la compréhension du potentiel géothermique en Île-de-France, Thèse de doctorat, Université Pierre et Marie Curie, 144 p.
- Dentzer, J., Bruel, D., Delescluse, M., Chamot-Rooke, N., Beccaletto, L., Lopez, S., Courrioux, G., Violette, S.**, 2018. Thermal and seismic hints for chimney type cross-stratal fluid flow in onshore basins. *Sci Rep* 8, 15330. <https://doi.org/10.1038/s41598-018-33581-x>
- Derer, C., Kosinowski, M., Luterbacher, H.P., Schäfer, A., Süß, M.P.**, 2003. Sedimentary response to tectonics in extensional basins: the Pechelbronn Beds (Late Eocene to early

- Oligocene) in the northern Upper Rhine Graben, Germany. SP 208, 55–69. <https://doi.org/10.1144/GSL.SP.2003.208.01.03>
- Dewey, J.F., Holdsworth, R.E., Strachan, R.A.**, 1998. Transpression and transtension zones. SP 135, 1–14. <https://doi.org/10.1144/GSL.SP.1998.135.01.01>
- Dèzes, P., Schmid, S.M., Ziegler, P.A.**, 2004. Evolution of the European Cenozoic Rift System: interaction of the Alpine and Pyrenean orogens with their foreland lithosphere. *Tectonophysics* 389, 1–33. <https://doi.org/10.1016/j.tecto.2004.06.011>
- Domeier, M., Torsvik, T.H.**, 2014. Plate tectonics in the late Paleozoic. *Geoscience Frontiers* 5, 303–350. <https://doi.org/10.1016/j.gsf.2014.01.002>
- Donsimoni, M.**, 1981. Le bassin houiller Lorrain, synthèse géologique, Mémoire BRGM 117
- Donsimoni, M.**, 1990. Le gisement de charbon de Lucenay-lès-Aix (Nièvre). Documents du BRGM 179
- Donsimoni, M.**, 2006. Le gisement de charbon de Lucenay-lès-Aix (Nièvre). Etat des connaissances acquises par le B.R.G.M. entre 1981 et 1986 (confidentiel)
- Donsimoni, M., Feys, R., Greber, C.**, 1980. Bassins carbonifères. *In: Synthèse géologique du bassin de Paris, stratigraphie et paléogéographie. – Mémoires BRGM*, **101**, 24-25
- Doornenbal, J.C., Stevenson, A.G.**, (editors), 2010. Petroleum Geological Atlas of the Southern Permian Basin Area. EAGE Publications b.v. (Houten)
- Ducassou, C., Mercuzot, M., Bourquin, S., Rossignol, C., Pellenard, P., Beccaletto, L., Poujol, M., Hallot, E., Pierson-Wickmann, A.C., Hue, C., Ravier, E.**, 2019. Sedimentology and U-Pb dating of Carboniferous to Permian continental series of the northern Massif Central (France): Local palaeogeographic evolution and larger scale correlations. *Palaeogeography, Palaeoclimatology, Palaeoecology* 533, 109228. <https://doi.org/10.1016/j.palaeo.2019.06.001>
- Düringer, P.**, 1988. Les conglomérats des bordures du rift Cénozoïque Rhénan. Dynamique sédimentaire et contrôle climatique. Doctoral Dissertation, Université de Strasbourg, p. 328
- Dusséaux, C., Gébelin, A., Ruffet, G., Mulch, A.**, 2021. Late Carboniferous paleoelevation of the Variscan Belt of Western Europe. *Earth and Planetary Science Letters* 569, 117064. <https://doi.org/10.1016/j.epsl.2021.117064>
- Dylikowski, J.**, 1985. Etude en stratigraphie sismique de remplissage tertiaire de la région de Pechelbronn (Fossé Rhénan) - Application au développement pétrolier en domaine de fossé d'effondrement. Thèse Université Paris-Sud Centre Orsay
- Echtler, H., Malavieille, J.**, 1990. Extensional tectonics, basement uplift and Stephano-Permian collapse basin in a late Variscan metamorphic core complex (Montagne Noire, Southern Massif Central). *Tectonophysics* 177, 125–138. [https://doi.org/10.1016/0040-1951\(90\)90277-F](https://doi.org/10.1016/0040-1951(90)90277-F)
- Edel, J., Fluck, P.**, 1989. The upper Rhenish Shield basement (Vosges, Upper Rhinegraben and Schwarzwald): main structural features deduced from magnetic, gravimetric and geological data. *Tectonophysics* 169 (4), 303–316
- Edel, J.B., Schulmann, K., Skrzypek, E., Cocherie, A.**, 2013. Tectonic evolution of the European Variscan belt constrained by palaeomagnetic, structural and anisotropy of magnetic susceptibility data from the Northern Vosges magmatic arc (eastern France). *JGS* 170, 785–804. <https://doi.org/10.1144/jgs2011-138>
- Elsass Damon, F.**, 1977. Les schistes bitumineux du bassin d'Autun : pétrographie, minéralogie, cristallographie, pyrolyse, thèse docteur Ingénieur, Université Paris VI
- Espurt, N., Wattellier, F., Philip, J., Hippolyte, J.-C., Bellier, O., Bestani, L.**, 2019. Mesozoic halokinesis and basement inheritance in the eastern Provence fold-thrust belt, SE France. *Tectonophysics* 766, 60–80. <https://doi.org/10.1016/j.tecto.2019.04.027>
- Fabriol H., Becquey M., Charmoille A., Deflandre J.P., Gal F., Huguet F., Le Pierres K., Lescanne, Pajot G., M., Pironon J., Pokryszka Z., Tocqué E. et Vu Hoang, D. et l'équipe projet**, 2008. Géocarbonate Monitoring Rapport final. BRGM/RP-56640-FR
- Faure, M.**, 1995. Late orogenic carboniferous extensions in the Variscan French Massif Central. *Tectonics* 14, 132–153. <https://doi.org/10.1029/94TC02021>
- Feys, R.**, 1989. Le bassin de Brive, dans Synthèse géologique des bassins permien français, Mémoire BRGM, 128
- Feys, R., Gand, G.**, 1983. Gisement houiller du Creusot ; une tectonique de serrage dans le sillon permo-houiller de Blanzay Creusot. – *Géologie de la France*, **1-2**, 97-122
- Fielding, C.R., Frank, T.D., Isbell, J.L.**, 2008. The late Paleozoic ice age—A review of current understanding and synthesis of global climate patterns, in: Fielding, C.R., Frank, T.D., Isbell, J.L. (Eds.), *Resolving the Late Paleozoic Ice Age in Time and Space*. Geological Society of America, p. 0. [https://doi.org/10.1130/2008.2441\(24\)](https://doi.org/10.1130/2008.2441(24))
- Fielitz, W., Mansy, J.-L.**, 1999. Pre- and synorogenic burial metamorphism in the Ardenne and neighbouring areas (Rhenohercynian zone, central European Variscides). *Tectonophysics* 309, 227–256. [https://doi.org/10.1016/S0040-1951\(99\)00141-9](https://doi.org/10.1016/S0040-1951(99)00141-9)

- Finger, F., Gerdes, A., René, M., Riegler, G., 2009.** The Saxo-Danubian Granite Belt: magmatic response to post-collisional delamination of mantle lithosphere below the southwestern sector of the Bohemian Massif (Variscan orogen). *Geologica Carpathica* 60, 205–212. <https://doi.org/10.2478/v10096-009-0014-3>
- Fischer, J., Schneider, J.W., Voigt, S., Joachimski, M.M., Tichomirowa, M., Tütken, T., Götze, J., Berner, U., 2013.** Oxygen and strontium isotopes from fossil shark teeth: Environmental and ecological implications for Late Palaeozoic European basins. *Chemical Geology* 342, 44–62. <https://doi.org/10.1016/j.chemgeo.2013.01.022>
- Fleck, S., Michels, R., Izart, A., Elie, M., Landais, P., 2001.** Palaeoenvironmental assessment of Westphalian fluvio-lacustrine deposits of Lorraine (France) using a combination of organic geochemistry and sedimentology. *International Journal of Coal Geology* 48, 65–88. [https://doi.org/10.1016/S0166-5162\(01\)00048-9](https://doi.org/10.1016/S0166-5162(01)00048-9)
- Fleury, T., 2022.** Atteindre la neutralité carbone en 2050 : quelles opportunités pour le stockage souterrain de CO₂ en France ? Rapport stage Université de Lorraine, Club CO₂, CNRS. 43 p
- Fries, D., Lebouil, S., Maurer, V., Martin, C., Baujard, C., Ravier, G., Boguais, R., Amari, S., 2022.** Lithium Extraction through Pilot Scale Tests under Real Geothermal Conditions of the Upper Rhine Graben. Presented at the Proceedings European Geothermal Congress, p. 7
- Franke, W., 2000.** The mid-European segment of the Variscides: tectonostratigraphic units, terrane boundaries and plate tectonic evolution. *SP* 179, 35–61. <https://doi.org/10.1144/GSL.SP.2000.179.01.05>
- Franke, W., Cocks, L.R.M., Torsvik, T.H., 2017a.** The Palaeozoic Variscan oceans revisited. *Gondwana Research* 48, 257–284. <https://doi.org/10.1016/j.gr.2017.03.005>
- Franke, W., Dulce, J.-C., 2017b.** Back to sender: tectonic accretion and recycling of Baltica-derived Devonian clastic sediments in the Rheno-Hercynian Variscides. *Int J Earth Sci (Geol Rundsch)* 106, 377–386. <https://doi.org/10.1007/s00531-016-1408-y>
- Freyermark, J., Bott, J., Cacace, M., Ziegler, M., Scheck-Wenderoth, M., 2019.** Influence of the Main Border Faults on the 3D Hydraulic Field of the Central Upper Rhine Graben. *Geofluids* 2019, 1–21. <https://doi.org/10.1155/2019/7520714>
- Gand, G., 2003.** Le bassin permien de Blanzay-Le Creusot et ses bordures carbonifères. - *Bulletin information des Géologues du bassin de Paris*, 40, 3, 4-19
- Gapais, D., Brun, J.-P., Gumiaux, C., Cagnard, F., Ruffet, G., Le Carlier De Veslud, C., 2015.** Extensional tectonics in the Hercynian Armorican belt (France). An overview. *Bulletin de la Société Géologique de France* 186, 117–129. <https://doi.org/10.2113/gssgfbull.186.2-3.117>
- Gardien, V., Martelat, J.-E., Leloup, P.-H., Mahéo, G., Bevilard, B., Allemand, P., Monié, P., Paquette, J.-L., Grosjean, A.-S., Faure, M., Chelle-Michou, C., Fellah, C., 2022.** Fast exhumation rate during late orogenic extension: The new timing of the Pilat detachment fault (French Massif Central, Variscan belt). *Gondwana Research* 103, 260–275. <https://doi.org/10.1016/j.gr.2021.10.007>
- Gastaldo, R.A., 1996.** Out of the Icehouse into the Greenhouse: A Late Paleozoic Analog for Modern Global Vegetational Change. *GSA TODAY*.
- Gebhardt U., Schneider J., Hoffmann N., 1991.** Modelle zur Stratigraphie und Beckenwicklung im Rotliegend der Norddeutschen Senke, *Geol. Jb.* A127, 405-427
- Gély, J. and Lorenz, C., 1991.** Analyse séquentielle de l'Eocène et de l'Oligocène du Bassin de Paris (France), *Oil and Gas Science and Technology-Rev. IVP.*, 46, 713-747.
- Genna, A., Debriette, P. J., 1994.** Structures en fleur dans le bassin houiller d'Alès. Implications structurales. *Comptes Rendus de l'Académie Des Sciences. Série 2. Sciences de La Terre et Des Planètes*, 318(7), 977–984
- Genre, C., 1981.** BRGM Carte géologique de la France au 1: 50 000 Feuille Saverne. *Norv. 110(1)*, 237-238
- Gérard, A., Kappelmeyer, O., 1987.** The Soultz-sous-Forêts project. *Geothermics* 16 (4), 393–399
- Glennie, K., Higham, J., Stemmerik, L., 2003.** Permian, in *The Millennium atlas: Petroleum geology of the Central and Northern North Sea*, Evans D., Graham C., Armour A. and Bathurst P. (éds), The geological Society of London
- Golonka, J., 2002.** Plate-Tectonic Maps of the Phanerozoic. *SEPM Special Publications*, 72, 21–75s
- Golonka, J., Gaweda, A., 2012.** Plate Tectonic Evolution of the Southern Margin of Laurussia in the Paleozoic, in: Sharkov, E. (Ed.), *Tectonics - Recent Advances*. InTech. <https://doi.org/10.5772/50009>
- Gonçalvès, J., Violette, S., Guillocheau, F., Robin, C., Pagel, M., Bruel, D., de Marsily, G., Ledoux, E., 2004.** Contribution of a three-dimensional regional scale basin model to the study of the past fluid flow evolution and the present hydrology of the Paris basin, France. *Basin Research* 16, 569–586. <https://doi.org/10.1111/j.1365-2117.2004.00243.x>

- Greber C.**, 1980. Bassins permien. - In: Synthèse géologique du bassin de Paris, Stratigraphie et Paléogéographie. - Mémoires du BRGM, 101, 22-24
- Grimmer, J.C., Ritter, J.R.R., Eisbacher, G.H., Fielitz, W.**, 2017. The Late Variscan control on the location and asymmetry of the Upper Rhine Graben. *Int J Earth Sci (Geol Rundsch)* 106, 827–853. <https://doi.org/10.1007/s00531-016-1336-x>
- Guerrier, R., Pruvost, P.**, 1965. La limite septentrionale du bassin houiller de la Lorraine. *Comptes Rendu de Académie des Sciences de Paris*, 261, 5349-5553
- Guillocheau, F., Robin, C., Allemand, P., Bourquin, S., Brault, N., Dromart, G., Friedenber, R., Garcia, J.-P., Gaulier, J.-M., Gaumet, F., Grosdoy, B., Hanot, F., Le Strat, P., Mettraux, M., Nalpas, T., Prijac, C., Rigoltet, C., Serrano, O., Grandjean, G.**, 2000. Meso-Cenozoic geodynamic evolution of the Paris Basin: 3D stratigraphic constraints. *Geodinamica Acta* 13, 189–245. <https://doi.org/10.1080/09853111.2000.11105372>
- Guillot, F., Averbuch, O., Dubois, M., Durand, C., Lanari, P., Gauthier, A.**, 2020. Zircon age of vaugnerite intrusives from the Central and Southern Vosges crystalline massif (E France): contribution to the geodynamics of the European Variscan belt. *BSGF - Earth Sci. Bull.* 191, 26. <https://doi.org/10.1051/bsgf/2020027>
- Guillou-Frottier, L., Carré, C., Bourguine, B., Bouchot, V., Genter, A.**, 2013. Structure of hydrothermal convection in the Upper Rhine Graben as inferred from corrected temperature data and basin-scale numerical models. *Journal of Volcanology and Geothermal Research* 256, 29–49. <https://doi.org/10.1016/j.jvolgeores.2013.02.008>
- Gutscher, M.-A., Kukowski, N., Malavieille, J., Lallemand, S.**, 1996. Cyclical behavior of thrust wedges: Insights from high basal friction sandbox experiments. *Geol* 24, 135. [https://doi.org/10.1130/0091-7613\(1996\)024<0135:CBOTWI>2.3.CO;2](https://doi.org/10.1130/0091-7613(1996)024<0135:CBOTWI>2.3.CO;2)
- Hamm, V., Capar, L., Mas, P., Calcagno, P., Caritg-Monnot, S.**, 2021. Characterisation of the Dogger and Trias deep resources in Orleans Metropolis, Centre-Val de Loire region, France: 3D geomodel and first geothermal potential assessment. in *EGU General Assembly 2021*, <https://doi.org/10.5194/egusphere-egu21-14465>
- Handy, M.R., Franz, L., Heller, F., Janott, B., Zurbriggen, R.**, 1999. Multistage accretion and exhumation of the continental crust (Ivrea crustal section, Italy and Switzerland). *Tectonics* 18, 1154–1177. <https://doi.org/10.1029/1999TC900034>
- Hauville, B., Laine, C., Pélissier, N., Boka Mene, M., Jacob, T., Coppo, N.**, 2021. Exploration d'hélium en France : avancées du projet Fonts-Bouillants dans la Nièvre et résultats apportés par de multiples acquisitions géophysiques et géochimiques, 27^{ème} RST Lyon
- Hemelsdaël, R., Séranne, M., Husson, E., Ballas, G.**, 2021. Structural style of the Languedoc Pyrenean thrust belt in relation with the inherited Mesozoic structures and with the rifting of the Gulf of Lion margin, southern France. *BSGF - Earth Sci. Bull.* 192, 46. <https://doi.org/10.1051/bsgf/2021037>
- Henk, A.**, 1999. Did the Variscides collapse or were they torn apart?: A quantitative evaluation of the driving forces for postconvergent extension in central Europe. *Tectonics* 18, 774–792. <https://doi.org/10.1029/1999TC900014>
- Henk, A.**, 1993. Late orogenic Basin evolution in the Variscan internides: the Saar-Nahe Basin, southwest Germany. *Tectonophysics* 223, 273–290. [https://doi.org/10.1016/0040-1951\(93\)90141-6](https://doi.org/10.1016/0040-1951(93)90141-6)
- Henk, A., von Blanckenburg, F., Finger, F., Schaltegger, U., Zulauf, G.**, 2000. Syn-convergent high-temperature metamorphism and magmatism in the Variscides: a discussion of potential heat sources. *SP* 179, 387–399. <https://doi.org/10.1144/GSL.SP.2000.179.01.23>
- Hermann, J.**, 1997. The Braccia gabbro (Malenco, Alps): Permian intrusion at the crust to mantle interface and Jurassic exhumation during rifting (PhD Thesis). ETH Zurich
- Hertle, M., Littke, R.**, 2000. Coalification pattern and thermal modelling of the Permo-Carboniferous Saar Basin ŹSW-Germany/.
- Hibsch, C., Cushing, E. M., Cabrera, J., Mercier, J., Prasil, P., & Jarrige, J. J.**, 1993. Evolution des paléo-contraintes en Grande-Bretagne du Permien au Cénozoïque : approche géodynamique de l'évolution des bassins méridionaux du Royaume-Uni. *Bulletin Des Centres de Recherches Exploration - Production Elf-Aquitaine*, 17(2), 303–330
- Hinsken, S., Ustaszewski, K., Wetzel, A.**, 2007. Graben width controlling syn-rift sedimentation: the Palaeogene southern Upper Rhine Graben as an example. *Int J Earth Sci (Geol Rundsch)* 96, 979–1002. <https://doi.org/10.1007/s00531-006-0162-y>
- Hippolyte, J.-C., Angelier, J., Nury, D., Bergerat, F., Guieu, G.**, 1993. Tectonic-stratigraphic record of paleostress time changes in the Oligocene basins of the Provence, southern France. *Tectonophysics* 226, 15–35
- Illies, J. H., Greiner, G.**, 1979. Holocene movements and state of stress in the Rhinegraben rift system *Tectonophysics*, 52 (1979) 349-359

- Isbell, J. L., Cole, D. I., Catuneanu, O.**, 2008. Carboniferous-Permian glaciation in the main Karoo Basin, South Africa: Stratigraphy, depositional controls, and glacial dynamics. In *Resolving the Late Paleozoic ice age in time and space* (Vol. 441, pp. 71-82). *Geol. Soc. Am. Special Paper*
- Izart, A., Barbarand, J., Michels, R., Privalov, V.A.**, 2016. Modelling of the thermal history of the Carboniferous Lorraine Coal Basin: Consequences for coal bed methane. *International Journal of Coal Geology* 168, 253–274. <https://doi.org/10.1016/j.coal.2016.11.008>
- Jacob, T., Portal, A., Gal, F., Beccaletto, L., Bitri, A., Gaudot, I.**, 2021. Acquisitions géophysiques et Radon le long d'un linéaire au sein du PÉR « Fonts-Bouillants » - Phase II (Saint-Parize-le-Châtel, 58). Rapport final. BRGM/RC-70801-FR (confidentiel)
- Juncal, M.A., Bourquin, S., Beccaletto, L., Diez, J.B.**, 2018. New sedimentological and palynological data from the Permian and Triassic series of the Sancerre-Couy core, Paris Basin, France. *Geobios* 51, 517–535. <https://doi.org/10.1016/j.geobios.2018.06.007>
- Karstens, J., Berndt, C.**, 2015. Seismic chimneys in the Southern Viking Graben – Implications for palaeo fluid migration and overpressure evolution. *Earth Planet. Sci. Lett.* **412**, 88–100
- Kelch, H.-J., & Reible, P.**, 1976. Beschreibung der Spülproben and Kerne der Bohrung Saar 1. *Geol. Jb.*, **A27**, 29-89
- Khatir, A., Mansy, J.-L., Meilliez, F.**, 1988. Structures et déformation dans l'allochtone ardennais en Avesnois (Nord). *meille Annales de la Société Géologique du Nord*, **108**(2–3), 73–83
- Kneuper, G.**, 1976. Regional Geologische Folgerungen aus der Bohrung Saar-1, 27, 417-428
- Knight, J.A., Alvarez-Vázquez, C.**, 2021. A summary of upper Pennsylvanian regional substages defined in NW Spain – the chronostratigraphic legacy of Robert H. Wagner. nos 54, 275–300. <https://doi.org/10.1127/nos/2021/0616>
- Königer, S., Lorenz, V.**, 2002a. Geochemistry, tectonomagmatic origin and chemical correlation of altered Carboniferous–Permian fallout ash tuffs in southwestern Germany. *Geol. Mag.* **139**. <https://doi.org/10.1017/S0016756802006775>
- Königer, S., Lorenz, V., Stollhofen, H., Armstrong, R.**, 2002b. Origin, age and stratigraphic significance of distal fallout ash tuffs from the Carboniferous-Permian continental Saar-Nahe Basin (SW Germany). *International Journal of Earth Sciences* **91**, 341–356. <https://doi.org/10.1007/s005310100221>
- Korsch, R.J., Schäfer, A.**, 1991. Geological interpretation of DEKORP deep seismic reflection profiles 1C and 9N across the variscan Saar-Nahe Basin southwest Germany. *Tectonophysics* **191**, 127–146. [https://doi.org/10.1016/0040-1951\(91\)90236-L](https://doi.org/10.1016/0040-1951(91)90236-L)
- Korsch, R.J., Schäfer, A.**, 1995. The Permo-Carboniferous Saar-Nahe Basin, south-west Germany and north-east France: basin formation and deformation in a strike-slip regime. *Geol Rundsch* **84**. <https://doi.org/10.1007/BF00260442>
- Lacombe, O., Jolivet, L.**, 2005. Structural and kinematic relationships between Corsica and the Pyrenees-Provence domain at the time of the Pyrenean orogeny. *Tectonics* **24**: TC1003
- Lacquement, F., Mansy, J.-L., Hanot, F., Meilliez, F.**, 1999. Retraitement et interprétation d'un profil sismique pétrolier méridien au travers du Massif paléozoïque ardennais (Nord de la France). *Comptes Rendus de l'Académie des Sciences - Series IIA - Earth and Planetary Science* **329**, 471–477. [https://doi.org/10.1016/S1251-8050\(00\)80020-8](https://doi.org/10.1016/S1251-8050(00)80020-8)
- Landrein, P., Vigneron, G., Delay, J., Lebon, P., Pagel, M.**, 2013. Lithologie, hydrodynamisme et thermicité dans le système sédimentaire multicouche recoupé par les forages Andra de Montiers-sur-Saulx (Meuse). *Bull. Soc. Geol. Fr.* **184** (6), 519–543
- Lasseur, E.**, 2007. La Craie du Bassin de Paris (Cénomaniens-Campanien, Crétacé supérieur). *Sédimentologie de faciès, stratigraphie séquentielle et géométrie 3D*, Université Rennes 1
- Laubscher, H.**, 1987. Die tektonische entwicklung der Nordschweiz. *Eclogae Geol. Helv.* **80** (2), 287–303
- Laurent, A., Averbuch, O., Beccaletto, L., Graveleau, F., Lacquement, F., Capar, L., Marc, S.**, 2021. 3-D Structure of the Variscan Thrust Front in Northern France: New Insights From Seismic Reflection Profiles. *Tectonics* **40**. <https://doi.org/10.1029/2020TC006642>
- Laurent, O., Couzinié, S., Zeh, A., Vanderhaeghe, O., Moyen, J.-F., Villaros, A., Gardien, V., Chelle-Michou, C.**, 2017. Protracted, coeval crust and mantle melting during Variscan late-orogenic evolution: U–Pb dating in the eastern French Massif Central. *Int J Earth Sci (Geol Rundsch)* **106**, 421–451. <https://doi.org/10.1007/s00531-016-1434-9>
- Laurent, O., Stéphan, J.-F., Popoff, M.**, 2000. Modalités de la structuration miocène de la branche sud de l'arc de Castellane (chaîne subalpines méridionales), *Géologie de la France*, **3**, 33-65
- Lebreton M.-L.**, 1990. Les bassins stéphano-permiens du sud du bassin de Paris: contrôle structural et sédimentologie. - Thèse de doctorat, Orsay, 155p
- Legrand, R.**, 1968. Le Massif du Brabant. Mémoires pour servir à l'Explication des Cartes Géologiques et Minières de la Belgique, **9**, 1–148

- Lenoir, F., Guillocheau, F., Robin, C., Lasseur, E., Serrano, O., Beccaletto, L.**, 2014. Seismic study of the Jurassic deformation and sedimentation of the southwestern Paris basin: a low subsiding domain transition to the Aquitaine basin. *Bulletin de la Société Géologique de France* 185, 191–204. <https://doi.org/10.2113/gssgfbull.185.3.191>
- Lopez, S., Hamm, V., Le Brun, M., Schaper, L., Boissier, F., Cotiche, C., Giuglaris, E.**, 2010. 40 years of Dogger aquifer management in Ile-de-France, Paris Basin, France, *Geothermics* 39, 339–356
- Lorenz, V., Nicholls, I.A.**, 1984. Plate and intraplate processes of Hercynian Europe during the late paleozoic. *Tectonophysics* 107, 25–56. [https://doi.org/10.1016/0040-1951\(84\)90027-1](https://doi.org/10.1016/0040-1951(84)90027-1)
- Loup, B., Wildi, W.**, 1994. Subsidence analysis in the Paris Basin: a key to Northwest European intracontinental basins? *Basin Research* 6, 159–177.
- Lucas, S. G., Schneider, J. W., Nikolaeva, S., Wang, X.**, 2022. The Carboniferous chronostratigraphic scale: history, status and prospectus. *Geological Society, London, Special Publications*, 512(1), 19-48. <https://doi.org/10.1144/SP512-2020-210>
- Lutz, M., Cleintuar, M.**, 1999. Geological results of a hydrocarbon exploration campaign in the southern upper rhine graben (alsace centrale, France). *Bull. Angew Geol. Bull. Appl. Geol.* 4, 3–80
- Lutz, H., Lorenz, V., Engel, T., Häfner, F., Haneke, J.**, 2013. Paleogene phreatomagmatic volcanism on the western main fault of the northern upper rhine graben (kisselwörth diatreme and nierstein–astheim volcanic system, Germany). *Bull. Volcanol.* 75 (7), 1–11
- Malavieille, J.**, 1993. Late Orogenic extension in mountain belts: Insights from the basin and range and the Late Paleozoic Variscan Belt. *Tectonics* 12, 1115–1130. <https://doi.org/10.1029/93TC01129>
- Malavieille, J., Guihot, P., Costa, S., Lardeaux, J.M., Gardien, V.**, 1990. Collapse of the thickened Variscan crust in the French Massif Central: Mont Pilat extensional shear zone and St. Etienne Late Carboniferous basin. *Tectonophysics* 177, 139–149. [https://doi.org/10.1016/0040-1951\(90\)90278-G](https://doi.org/10.1016/0040-1951(90)90278-G)
- Mansy, J.-L., Lacquement, F.**, 2006. Contexte géologique régional : l'Ardenne paléozoïque (Nord de la France et Sud de la Belgique). *Géologie de la France*, 1–2, 7–13
- Mansy, J.-L., Lacquement, F., Meilliez, F., Hanot, F., Everaerts, M.**, 1997. Interprétation d'un profil sismique pétrolier, sur le méridien de Valenciennes (Nord de la France). *Aardkundige Mededelingen*, 8, 127–129.
- Mansy, J.-L., Meilliez, F.**, 1993. Eléments d'analyse structurale à partir d'exemples pris en Ardenne-Avesnois. *Annales de la Société Géologique du Nord*, 2(2), 45–60
- Marçot, N., Genevier, M., Abad, J., Aslan, G., Beccaletto, L., Bitri, A., Coueffe, R., De Michele, M., Equilbey, E., Gaudot, I., Portal, A., Lombard, M., Ibba, M., Ladouche, B., Maurice B., Wright, R.**, 2022. Gestion du risque affaissement-effondrement lié à la dissolution de gypse - Commune de Bargemon (Var). Rapport final BRGM/RP-71427-FR
- Marteau, P.**, 1983. Le bassin permo-carbonifère d'Autun; Stratigraphie, sédimentologie et aspects structuraux. - Documents s- B.R.G.M., 64
- Martínez Catalán, J.R., Collett, S., Schulmann, K., Aleksandrowski, P., Mazur, S.**, 2020. Correlation of allochthonous terranes and major tectonostratigraphic domains between NW Iberia and the Bohemian Massif, European Variscan belt. *Int J Earth Sci (Geol Rundsch)* 109, 1105–1131. <https://doi.org/10.1007/s00531-019-01800-z>
- Mas, P., Calcagno, P., Caritg-Monnot, S., Beccaletto, L., Capar, L., Hamm, V.**, 2022. A 3D geomodel of the deep aquifers in the Orléans area of the southern Paris Basin (France). *Sci Data* 9, 781. <https://doi.org/10.1038/s41597-022-01876-4>
- Masclé, A.**, 1990. Géologie pétrolière des bassins permien français; Comparaison avec les bassins permien du Nord de l'Europe; Potentiel économique des bassins permien français. *Chronique de la Recherche Minière*, 499, 69-86
- Massonne, H.-J.**, 1995. Metamorphic Evolution, in: Dallmeyer, R.D., Franke, W., Weber, K. (Eds.), *Pre-Permian Geology of Central and Eastern Europe*. Springer Berlin Heidelberg, Berlin, Heidelberg, pp. 132–137. https://doi.org/10.1007/978-3-642-77518-5_12
- Mathis, V., Brulhet, J.**, 1990. Les gisements uranifères du bassin permien de Bourbon-l'Archambault (nord du Massif central français).
- Mattauer, M., Matte, P.**, 1998. Le bassin Stéphaniens de St-Etienne ne résulte pas d'une extension tardi-hercynienne généralisée: c'est un bassin pull-apart en relation avec un décrochement dextre. *Geodinamica Acta* 11, 23–31. <https://doi.org/10.1080/09853111.1998.11105309>
- Matte, P.**, 2001. The Variscan collage and orogeny (480-290 Ma) and the tectonic definition of the Armorica microplate: a review. *Terra Nova* 13, 122–128. <https://doi.org/10.1046/j.1365-3121.2001.00327.x>
- Matte, P.**, 1986. Tectonics and plate tectonics model for the Variscan belt of Europe. *Tectonophysics* 126, 329–374. [https://doi.org/10.1016/0040-1951\(86\)90237-4](https://doi.org/10.1016/0040-1951(86)90237-4)

- McCann, T., Skompski, S., Poty, E., Duser, M., Vozarova, A., Schneider, J., Wetzel, A., Krainer, K., Kornpohl, K., Schafer, A., Krings, M., Oplustil, S., Tait, J., 2008. Carboniferous, in: McCann, T. (Ed.), *The Geology of Central Europe Volume 1: Precambrian and Palaeozoic*. The Geological Society of London, pp. 411–529. <https://doi.org/10.1144/CEV1P.9>
- Mégnien, C., 1980. Tectogenese du Bassin de Paris; etapes de l'évolution du bassin. *Bull. Soc. Geol. Fr.* 7 (4), 669–680
- Mégnien, C., Mégnien, F., 1980. Synthèse géologique du Bassin de Paris. In: *Geological synthesis of the Paris Basin; Volume I, Stratigraphy and paleogeography*, Bureau de Recherches Géologiques et Minières, (BRGM): Paris, France
- Meilliez, F., 2019. La Faille du Midi, mythe et réalités. *Annales de la Société Géologique du Nord*, 26(2), 13–32.
- Meilliez, F., Mansy, J.L., 1990. Deformation pelliculaire différenciée dans une série lithologique hétérogène; le Dévonien-Carbonifère de l'Ardenne. *Bulletin de la Société Géologique de France* VI, 177–188. <https://doi.org/10.2113/gssgfbull.VI.1.177>
- Ménard, G., Molnar, P., 1988. Collapse of a Hercynian Tibetan plateau into a late Palaeozoic European Basin and Range province. *Nature*, 334(6179), 235–237
- Menessier, G., de Lapparent, A.-F., Bordet, P., 1969. Carte géologique détaillée de la France à 1/50 000: Draguignan, 2^{ème} édition. BRGM, Orléans (1023, carte et notice explicative)
- Ménillet F., Durand M., Genter A., Party J., 2015. Notice explicative de la carte géologique de France (1/50 000). Feuille Haguenau (198) (2^{ème} éd.), BRGM, Orléans
- Ménillet F., Vogt H., Reichelt R., Schumacher E., Van Werweke L., Haug E., Bucking H., Gross J., Schirardin J., Thévenin A., 1979. Carte géologique France (1/50 000), feuille Bouxwiller (197) Orléans: BRGM
- Mercuzot, M., Bourquin, S., Beccaletto, L., Ducassou, C., Rubi, R., Pellenard, P., 2021. Palaeoenvironmental reconstitutions at the Carboniferous–Permian transition south of the Paris Basin, France: implications on the stratigraphic evolution and basin geometry. *Int J Earth Sci (Geol Rundsch)* 110, 9–33. <https://doi.org/10.1007/s00531-020-01940-7>
- Minguely, B., 2007. Caractérisation géométrique 3-D de la couverture sédimentaire Méso-Cénozoïque et du substratum varisque dans le Nord de la France, thèse USTLille
- Minguely, B., Averbuch, O., Patin, M., Rolin, D., Hanot, F., Bergerat, F., 2010. Inversion tectoniques at the northern margin of the Paris basin (northern France): new evidence from seismic profiles and boreholes interpolation in the Artois area. *Bulletin de la Société Géologique de France* 181, 429–442. <https://doi.org/10.2113/gssgfbull.181.5.429>
- Moix, P., Beccaletto, L., Kozur, H.W., Hochard, C., Rosselet, F., Stampfli, G.M., 2008. A new classification of the Turkish terranes and sutures and its implication for the paleotectonic history of the region. *Tectonophysics* 451, 7–39. <https://doi.org/10.1016/j.tecto.2007.11.044>
- Monjoie, P., Bussy, F., Schaltegger, U., Mulch, A., Lapierre, H., Pfeifer, H.-R., 2007. Contrasting magma types and timing of intrusion in the Permian layered mafic complex of Mont Collon (Western Alps, Valais, Switzerland): evidence from U/Pb zircon and ⁴⁰Ar/³⁹Ar amphibole dating. *Swiss j geosci* 100, 125–135. <https://doi.org/10.1007/s00015-007-1210-8>
- Montañez, I.P., Poulsen, C.J., 2013. The Late Paleozoic Ice Age: An Evolving Paradigm. *Annual Review of Earth and Planetary Sciences* 41, 629–656. <https://doi.org/10.1146/annurev.earth.031208.100118>
- Montañez, I. P., Tabor, N. J., Niemeier, D., DiMichele, W. A., Frank, T. D., Fielding, C. R., Isbell, J.L., Birgenheier, L. P., Rygel, M. C., 2007. CO₂-forced climate and vegetation instability during Late Paleozoic deglaciation. *Science* 315(5808), 87–91.
- Muttoni, G., Kent, D., 2019. Adria as promontory of Africa and its conceptual role in the Tethys twist and Pangea B to Pangea A transformation in the Permian, *Rivista Italiana di Paleontologia e Stratigrafia* vol. 125(1): 249–269
- Neumann, E.-R., Wilson, M., Heeremans, M., Spencer, E.A., Obst, K., Timmerman, M.J., Kirstein, L., 2004. Carboniferous–Permian rifting and magmatism in southern Scandinavia, the North Sea and northern Germany: a review. *SP* 223, 11–40. <https://doi.org/10.1144/GSL.SP.2004.223.01.02>
- Oncken, O., 1998. Orogenic mass transfer and reflection seismic patterns — evidence from DEKORP sections across the European Variscides (central Germany). *Tectonophysics* 286, 47–61. [https://doi.org/10.1016/S0040-1951\(97\)00254-0](https://doi.org/10.1016/S0040-1951(97)00254-0)
- Oncken, O., 1997. Transformation of a magmatic arc and an orogenic root during oblique collision and its consequences for the evolution of the European Variscides (Mid-German Crystalline Rise). *Geologische Rundschau* 86, 2–20. <https://doi.org/10.1007/s005310050118>
- Oncken, O., Plesch, A., Weber, J., Ricken, W., Schrader, S., 2000. Passive margin detachment during arc-continent collision (Central European Variscides). *SP* 179, 199–216. <https://doi.org/10.1144/GSL.SP.2000.179.01.13>

- Paquette, Y.**, 1980. Le Bassin autunien de l'Aumance (Allier) : sédimentologie (charbon, cinérites...), tectonique syndiagénétique. Ph.D. thesis
- Paquette, Y., Feys, R.**, 1989. Le bassin de Bourbon l'Archambault. - In: Synthèse géologique des bassins permien français. - Mémoires du BRGM, 128, 43-54
- Pellenard, P., Gand, G., Schmitz, M., Galtier, J., Broutin, J., Stéyer, J.-S.**, 2017. High-precision U-Pb zircon ages for explosive volcanism calibrating the NW European continental Autunian stratotype. *Gondwana Research* 51, 118–136. <https://doi.org/10.1016/j.gr.2017.07.014>
- Perrodon, A., Zabek, J.**, 1991. Paris basin; Interior cratonic basins. - *AAPG Memoir*, 51, 633-679
- Pharaoh, T.**, 2018. The Anglo-Brabant Massif: Persistent but enigmatic palaeo-relief at the heart of western Europe. *Proceedings of the Geologists' Association* 129, 278–328. <https://doi.org/10.1016/j.pgeola.2018.02.009>
- Plesch, A., Oncken, O.**, 1999. Orogenic wedge growth during collision — constraints on mechanics of a fossil wedge from its kinematic record (Renohercynian FTB, Central Europe). *Tectonophysics* 309, 117–139. [https://doi.org/10.1016/S0040-1951\(99\)00135-3](https://doi.org/10.1016/S0040-1951(99)00135-3)
- Pochat, S., Van Den Driessche, J.**, 2011. Filling sequence in Late Paleozoic continental basins: A chimera of climate change? A new light shed given by the Graissessac–Lodève basin (SE France). *Palaeogeography, Palaeoclimatology, Palaeoecology* 302, 170–186. <https://doi.org/10.1016/j.palaeo.2011.01.006>
- Pomerol, C.**, 1978. Evolution paléogéographique et structurale du Bassin de Paris, du Précambrien à l'Actuel, en relation avec les régions avoisinantes, *Geol. Mijnbouw*, 57 (4), 533-543.
- Pomerol, C.**, 1989. Stratigraphy of the Palaeogene; hiatuses and transitions, *Proceedings of the Geologists' Association*, 100, 313-324
- Poujol, M., Mercuzot, M., Lopez, M., Bourquin, S., Bruguier, O., Hallot, E., Beccaletto, L.**, 2023. Insights on the Permian tuff beds from the Saint-Affrique Basin (Massif Central, France): an integrated geochemical and geochronological study. *Comptes Rendus. Géoscience* 355, 1–25. <https://doi.org/10.5802/crgeos.184>
- Poulsen, C. J., Pollard, D., Montañez, I. P., Rowley, D.**, 2007. Late Paleozoic tropical climate response to Gondwanan deglaciation. *Geology* 35(9), 771-774.
- Prijac, C., Doin, M.P., Gaulier, J.M., Guillocheau, F.**, 2000. Subsidence of the Paris Basin and its bearing on the late Variscan lithosphere evolution: a comparison between Plate and Chablis models. *Tectonophysics* 323, 1–38. [https://doi.org/10.1016/S0040-1951\(00\)00100-1](https://doi.org/10.1016/S0040-1951(00)00100-1)
- Pruvost, P.**, 1942. Etude géologique du bassin permo-carbonifère d'Autun. Rapport inédit - Archives BRGM.
- Quine, M., Bosence, D.**, 1991. Stratal geometries, facies and sea-floor erosion in Upper Cretaceous Chalk, Normandy, France. *Sedimentology* 38, 1113–1152
- Raoult, J.-F.**, 1986. Le front varisque du Nord de la France d'après les profils sismiques, la géologie de surface et les sondages. *Revue de Géologie Dynamique et de Géographie Physique*, 27(3–4), 247–268
- Raoult, J.-F.**, 1988. Le front varisque du Nord de la France : interprétation des principales coupes d'après les profils sismiques, la géologie de surface et les sondages. In M. Cazes & G. Torrelles (Eds.), *Etude de la croûte terrestre par sismique profonde : profil du Nord de la France*. (pp. 171–196). Paris, France: Technip
- Ravaglia, A., Seno, S., Toscani, G., Fantoni, R.**, 2006. Mesozoic extension controlling the Southern Alps thrust front geometry under the Po Plain, Italy: Insights from sandbox models. *Journal of Structural Geology* 28, 2084–2096. <https://doi.org/10.1016/j.jsg.2006.07.011>
- Reninger, P.-A., Martelet, G., Lasseur, E., Beccaletto, L., Deparis, J., Perrin, J., Chen, Y.**, 2014. Geological environment of karst within chalk using airborne time domain electromagnetic data cross-interpreted with boreholes. *Journal of Applied Geophysics* 106, 173–186. <https://doi.org/10.1016/j.jappgeo.2014.04.020>
- Robelin, C.**, 2004. Filière du charbon propre en France - Etude de Faisabilité d'un pilote de séquestration du CO2 pour les centrales thermiques au charbon - Bassin Houiller de Lorraine, Rapport BRGM/RP53943-FR
- Robin, C.**: Mesure stratigraphique de la déformation: Application à l'évolution jurassique du Bassin de Paris, Thèse de doctorat, 1997.
- Robin, C., Guillocheau, F., Allemand, P., Bourquin, S., Dromart, G., Gaulier, J.-M., Prijac, C.**, 2000. Echelles de temps et d'espace du contrôle tectonique d'un bassin flexural intracratonique; le bassin de Paris. *Bulletin de la Société Géologique de France* 171, 181–196. <https://doi.org/10.2113/171.2.181>
- Roger, J., Gaudry, F., Marteau, P., Quesnel, F., Chevremont, P., Jauffret, D.**, 2010. Notice explicative, Carte géol. France (1/50 000), feuille Decize (549). Orléans : BRGM, 185 p. Carte géologique par Gaudry F., Roger J., Marteau P., Quesnel F., Chevremont P., 2010

- Rotstein, Y., Schaming, M.**, 2011. The Upper Rhine Graben (URG) revisited: Miocene transtension and transpression account for the observed first-order structures: TRANSPRESSION IN THE UPPER RHINE GRABEN. *Tectonics* 30, n/a-n/a. <https://doi.org/10.1029/2010TC002767>
- Roussé, S.**, 2006. Architecture et dynamique des séries marines et continentales de l'oligocène moyen et supérieur du sud du fossé rhénan : Evolution des milieux de dépôt en contexte de rift en marge de l'avant-pays alpin. Doctoral Dissertation, Université de Strasbourg, p. 474
- Rowley, D. B., Raymond, A., Parrish, J. T., Lottes, A. L., Scotese, C. R., Ziegler, A. M.**, 1985. Carboniferous paleogeographic, phytogeographic, and paleoclimatic reconstructions. *Int. J. Coal Geol.*, 5(1-2), 7-42
- Salquèbre, D., Husson, F., Jozja, N., Klinka, T. & Tourlière, B.**, 2009. Système d'Information pour la Gestion des Eaux Souterraines (SIGES) en région Centre-Val de Loire - Bilan de la phase 3 (2017–2019). Report No. BRGM/RP- 69591-FR
- Saspiturry, N., Cochelin, B., Razin, P., Leleu, S., Lemirre, B., Bouscary, C., Issautier, B., Serrano, O., Lasseur, E., Baudin, T., Allanic, C.**, 2019. Tectono-sedimentary evolution of a rift system controlled by Permian post-orogenic extension and metamorphic core complex formation (Bidarray Basin and Ursuya dome, Western Pyrenees). *Tectonophysics* 768, 228180. <https://doi.org/10.1016/j.tecto.2019.228180>
- Schäfer, A.**, 2011. Tectonics and sedimentation in the continental strike-slip Saar-Nahe Basin (Carboniferous-Permian, West Germany). *zdgg* 162, 127–155. <https://doi.org/10.1127/1860-1804/2011/0162-0127>
- Schäfer, A.**, 1989. Variscan molasse in the Saar-Nahe Basin (W-Germany), Upper Carboniferous and Lower Permian. *Geol Rundsch* 78, 499–524. <https://doi.org/10.1007/BF01776188>
- Schäfer, A., Korsch, R.J.**, 1998. Formation and sediment fill of the Saar-Nahe Basin (Permo-Carboniferous, Germany). *zdgg_alt* 149, 233–269. <https://doi.org/10.1127/1860-1804/1998/149/233>
- Schnaebelen, R.**, 1948. Monographie géologique du champ pétrolifère de Pechelbronn. *Mém. Serv. Carte géol. Als. Lorr.* 7, 254
- Schneider, J.W., Lucas, S.G., Scholze, F., Voigt, S., Marchetti, L., Klein, H., Opluštil, S., Werneburg, R., Golubev, V.K., Barrick, J.E., Nemyrovska, T., Ronchi, A., Day, M.O., Silantiev, V.V., Rößler, R., Saber, H., Linnemann, U., Zharinova, V., Shen, S.-Z.**, 2020. Late Paleozoic–early Mesozoic continental biostratigraphy - Links to the Standard Global Chronostratigraphic Scale. *Palaeoworld* 29, 186–238. <https://doi.org/10.1016/j.palwor.2019.09.001>
- Schneider, J., Romer, R.L.**, 2010. The Late Variscan Molasses (Late Carboniferous to Late Permian) of the Saxo-Thuringian Zone. In Linnemann, U. & Romer, R.L. (eds.) *Pre-Mesozoic Geology of Saxo-Thuringia - From the Cadomian Active Margin to the Variscan Orogen*. Schweizerbart, Stuttgart, pp. 323-346
- Schneider, J.W., Scholze, F.**, 2018. Late Pennsylvanian–Early Triassic conchostracan biostratigraphy: a preliminary approach. *SP 450*, 365–386. <https://doi.org/10.1144/SP450.6>
- Schott, B., Schmeling, H.**, 1998. Delamination and detachment of a lithospheric root. *Tectonophysics* 296, 225–247. [https://doi.org/10.1016/S0040-1951\(98\)00154-1](https://doi.org/10.1016/S0040-1951(98)00154-1)
- Schulmann, K.**, 2002. Rapid burial and exhumation during orogeny: Thickening and synconvergent exhumation of thermally weakened and thinned crust (Variscan orogen in Western Europe). *American Journal of Science* 302, 856–879. <https://doi.org/10.2475/ajs.302.10.856>
- Schumacher, M.E.**, 2002. Upper Rhine Graben: Role of preexisting structures during rift evolution: UPPER RHINE GRABEN EVOLUTION. *Tectonics* 21, 6-16–17. <https://doi.org/10.1029/2001TC900022>
- Schwarz, F.**, 2021. Le pays de Pechelbronn. Un territoire façonné par l'industrie pétrolière. *Rev. Alsace* (147), 239–268
- Scotese, C.**, 2002. Paleomap. Updated at <http://www.scotese.com>
- Séranne, M., Benedicto, A., Truffert, C., Pascal, G., Labaume, P.**, 1995. Structural style and evolution of the Gulf of Lion Oligo-Miocene rifting: Role of the Pyrenean orogeny. *Marine and Petroleum Geology* 12: 809–820
- Séranne, M., Couëffé, R., Husson, E., Baral, C., Villard, J.**, 2021. The transition from Pyrenean shortening to Gulf of Lion rifting in Languedoc (South France) – A tectonic-sedimentation analysis. *BSGF - Earth Sci. Bull.* 192, 27. <https://doi.org/10.1051/bsgf/2021017>
- Shail, R.K., Alexander, A.C.**, 1997. Late Carboniferous to Triassic reactivation of Variscan basement in the western English Channel: evidence from onshore exposures in south Cornwall. *Journal of the Geological Society* 154, 163–168. <https://doi.org/10.1144/gsjgs.154.1.0163>

- Sissingh, W.**, 2006. Syn-kinematic palaeogeographic evolution of the West European Platform: correlation with Alpine plate collision and foreland deformation. *Neth. J. Geosci.* 85 (2), 131–180
- Sittler, C.**, 1967. Le soubassement et le remplissage sédimentaire du Fossé Rhénan au niveau du Bassin de Pechelbronn et du Seuil d'Erstein. In: Coupes géologiques à travers le fossé rhénan. Abh. Geol. Landesamt Baden-Württemberg, 6, Freiburg et Publ. Serv. Carte géol. Als. Lorr., vol. 1967. The Rhinegraben Progress Report, Strasbourg, pp. 69
- Sittler C.**, 1985. Les hydrocarbures d'alsace dans le contexte historique et géodynamique du fossé rhénan. *Bull. Centres Rech. Explor. Prod. Elf-Aquitaine* 9
- Smith, R.B., Bruhn, R.L.**, 1984. Intraplate extensional tectonics of the Eastern basin-Range: Inferences on structural style from seismic reflection data, regional tectonics, and thermal-mechanical models of brittle-ductile deformation. *J. Geophys. Res.* 89, 5733–5762. <https://doi.org/10.1029/JB089iB07p05733>
- Soreghan, G.S., Beccaletto, L., Benison, K.C., Bourquin, S., Feulner, G., Hamamura, N., Hamilton, M., Heavens, N.G., Hinnov, L., Huttenlocker, A., Looy, C., Pfeifer, L.S., Pochat, S., Sardar Abadi, M., Zambito, J., the Deep Dust workshop participants**, 2020. Report on ICDP Deep Dust workshops: probing continental climate of the late Paleozoic icehouse–greenhouse transition and beyond. *Sci. Dril.* 28, 93–112. <https://doi.org/10.5194/sd-28-93-2020>
- Soula, J.-C.**, 1984. Genèse de bassins sédimentaires en régime de cisaillement transcurrent : modèles expérimentaux et exemples géologiques. *Bulletin de La Société Belge de Géologie*, 93(1–2), 83–104
- Spears, D.A.**, 2012. The origin of tonsteins, an overview, and links with seatearths, fireclays and fragmental clay rocks. *International Journal of Coal Geology, Minerals and Trace Elements in Coal* 94, 22–31. <https://doi.org/10.1016/j.coal.2011.09.008>
- Spillmann, P., Büchi, H.J.**, 1993. The Pre-Alpine Basement of the Lower Austro-Alpine Nappes in the Bernina Massif (Grisons, Switzerland; Valtellina, Italy), in: von Raumer, J.F., Neubauer, F. (Eds.), *Pre-Mesozoic Geology in the Alps*. Springer Berlin Heidelberg, Berlin, Heidelberg, pp. 457–467. https://doi.org/10.1007/978-3-642-84640-3_27
- Stampfli, G.M., Hochard, C.**, 2009. Plate tectonics of the Alpine realm. *SP 327*, 89–111. <https://doi.org/10.1144/SP327.6>
- Stein, E.**, 2001. The geology of the Odenwald Crystalline Complex. *Mineralogy and Petrology* 72, 7–28. <https://doi.org/10.1007/s007100170024>
- Stollhofen, H.**, 1998. Facies architecture variations and seismogenic structures in the Carboniferous–Permian Saar–Nahe Basin (SW Germany): evidence for extension-related transfer fault activity. *Sedimentary Geology* 119, 47–83. [https://doi.org/10.1016/S0037-0738\(98\)00040-2](https://doi.org/10.1016/S0037-0738(98)00040-2)
- Tabor, N. J., Montañez, I. P.**, 2002. Shifts in late Paleozoic atmospheric circulation over western equatorial Pangea: Insights from pedogenic mineral $\delta^{18}\text{O}$ compositions. *Geology*, 30(12), 1127–1130
- Tabor, N. J., Montañez, I. P.**, 2004. Permo-Pennsylvanian alluvial paleosols (north-central Texas): High-resolution proxy records of the evolution of early Pangean paleoclimate. *Sedimentology*, 51, 851–884
- Tari, G., Connors, C., Flinch, J., Granath, J., Pace, P., Sobornov, K., Soto, J.I.**, 2023. Negative structural inversion: an overview. *Marine and Petroleum Geology* 152, 106223. <https://doi.org/10.1016/j.marpetgeo.2023.106223>
- Tchang-Tchong, L., Michels, R., Beccaletto, L., Bossennec, C., Lorgeoux, C., Faure, P.**, 2023. Pre- to early-rift thermal conditions of the Upper Rhine Graben using geological and organic geochemical controls. *Marine and Petroleum Geology* 151, 106202. <https://doi.org/10.1016/j.marpetgeo.2023.106202>
- Team GeORG**, 2013. Potentiel géologique profond du Fossé rhénan supérieur. Rapport scientifique et technique du projet Interreg GeORG. Part 1-4; Internet (PDF-document: <http://www.geopotenziale.eu>)
- Timmerman, M.J.**, 2004. Timing, geodynamic setting and character of Permo-Carboniferous magmatism in the foreland of the Variscan Orogen, NW Europe. *SP 223*, 41–74. <https://doi.org/10.1144/GSL.SP.2004.223.01.03>
- Toussaint, E.**, 2021. Caractérisation du réservoir géothermique carbonaté du Dinantien dans les hauts-de-France, Rapport stage 3A ENSG-BRGM.
- Tribuzio, R., Renna, M.R., Braga, R., Dallai, L.**, 2009. Petrogenesis of Early Permian olivine-bearing cumulates and associated basalt dykes from Bocca di Tenda (Northern Corsica): Implications for post-collisional Variscan evolution. *Chemical Geology* 259, 190–203. <https://doi.org/10.1016/j.chemgeo.2008.10.045>

- Tribuzio, R., Thirlwall, M.F., Messiga, B.**, 1999. Petrology, mineral and isotope geochemistry of the Sondalo gabbroic complex (Central Alps, Northern Italy): implications for the origin of post-Variscan magmatism. *Contributions to Mineralogy and Petrology* 136, 48–62. <https://doi.org/10.1007/s004100050523>
- Valle, B., Courel, L., Gelard, J.P.**, 1988. Les Marqueurs de la tectonique synsedimentaire et syndiagenetique dans le bassin stephanien a regime cisailant de Blanzky-Montceau (Massif Central, France). *Bulletin de la Société Géologique de France* IV, 529–540. <https://doi.org/10.2113/gssgfbull.IV.4.529>
- Valley B.**, 2007. The relation between natural fracturing and stress heterogeneities in deep-seated crystalline rocks at Soultz-sous-Forêts (France), Published thesis: Université ETH-Zürich, Switzerland. p. 260
- Vanderhaeghe, O., Laurent, O., Gardien, V., Moyen, J.-F., Gébelin, A., Chelle-Michou, C., Couzinié, S., Villaros, A., Bellanger, M.**, 2020. Flow of partially molten crust controlling construction, growth and collapse of the Variscan orogenic belt: the geologic record of the French Massif Central. *BSGF - Earth Sci. Bull.* 191, 25. <https://doi.org/10.1051/bsgf/2020013>
- Verniers, J., Herbosch, A., Vanguetaine, M., Geukens, F., Delcambre, B., Pingot, J.-L., et al.**, 2001. Cambrian-Ordovician-Silurian lithostratigraphic units (Belgium). *Geologica Belgica*, 4(1–2), 5–38.
- Vidal I.** 2017. Altérations hydrothermales associées aux zones de fractures à l'interface de la couverture sédimentaire et du socle cristallin dans le fossé rhénan supérieur. Thèse Université de Strasbourg
- Vielzeuf, D., Pin, C.**, 1989. Geodynamic implications of granulitic rocks in the Hercynian belt. *SP* 43, 343–348. <https://doi.org/10.1144/GSL.SP.1989.043.01.29>
- Villemin, T.**, 1986. Tectonique en extension, fracturation et subsidence: Le Fossé Rhénan et le bassin Sarro-Lorrain, Thèse de Doctorat, 270 pp., Univ. Pierre et Marie Curie, Paris
- Voigt, S., Schindler, T., Tichomirowa, M., Käßner, A., Schneider, J.W., Linnemann, U.**, 2022. First high-precision U–Pb age from the Pennsylvanian-Permian of the continental Saar–Nahe Basin, SW Germany. *Int J Earth Sci (Geol Rundsch)* 111, 2129–2147. <https://doi.org/10.1007/s00531-022-02222-0>
- von Raumer, J.F., Finger, F., Veselá, P., Stampfli, G.M.**, 2014. Durbachites-Vaugnerites - a geodynamic marker in the central European Variscan orogen. *Terra Nova* 26, 85–95. <https://doi.org/10.1111/ter.12071>
- von Raumer, J.F., Stampfli, G.M., Bussy, F.**, 2003. Gondwana-derived microcontinents — the constituents of the Variscan and Alpine collisional orogens. *Tectonophysics* 365, 7–22. [https://doi.org/10.1016/S0040-1951\(03\)00015-5](https://doi.org/10.1016/S0040-1951(03)00015-5)
- von Seckendorff, V., Arz, C., Lorenz, V.**, 2004. Magmatism of the late Variscan intermontane Saar-Nahe Basin (Germany): a review. *SP* 223, 361–391. <https://doi.org/10.1144/GSL.SP.2004.223.01.16>
- Wannesson, J.**, 1998. *Alsace-Rapport Régional D'évaluation Pétrolière*, vol. 96. Institut Français du Pétrole, Technical report, p. 62.
- Weber, K.**, 1995. The Saar-Nahe Basin, in: Dallmeyer, R.D., Franke, W., Weber, K. (Eds.), *Pre-Permian Geology of Central and Eastern Europe*. Springer Berlin Heidelberg, Berlin, Heidelberg, pp. 182–185. https://doi.org/10.1007/978-3-642-77518-5_18
- Wetzel, A., Allenbach, R., Allia, V.**, 2003. Reactivated basement structures affecting the sedimentary facies in a tectonically “quiescent” epicontinental basin: an example from NW Switzerland. *Sedimentary Geology* 157, 153–172. [https://doi.org/10.1016/S0037-0738\(02\)00230-0](https://doi.org/10.1016/S0037-0738(02)00230-0)
- Wicker, V., Ford, M.**, 2021. Assessment of the tectonic role of the Triassic evaporites in the north Toulon fold-thrust belt. *BSGF-Earth Sci. Bull.* 192, 51
- Williams, G.D., Powell, C.M., Cooper, M.A.**, 1989. Geometry and kinematics of inversion tectonics. *SP* 44, 3–15. <https://doi.org/10.1144/GSL.SP.1989.044.01.02>
- Zeh, A., Gerdes, A.**, 2010. Baltica- and Gondwana-derived sediments in the Mid-German Crystalline Rise (Central Europe): Implications for the closure of the Rheic ocean. *Gondwana Research* 17, 254–263. <https://doi.org/10.1016/j.gr.2009.08.004>
- Ziegler, P. A.**, 1990. *Geological Atlas of Western and Central Europe*. The Hague, Netherlands: Shell Internationale Petroleum Maatschappij B.V
- Ziegler, P.A., Bertotti, G., Cloetingh, S.**, 2002. Dynamic processes controlling foreland development – the role of mechanical (de)coupling of orogenic wedges and forelands. *Stephan Mueller Spec. Publ. Ser.* 1, 17–56. <https://doi.org/10.5194/smsps-1-17-2002>
- Ziegler, P.A., Dèzes, P.**, 2007. Cenozoic uplift of Variscan Massifs in the Alpine foreland: Timing and controlling mechanisms. *Global and Planetary Change* 58, 237–269. <https://doi.org/10.1016/j.gloplacha.2006.12.004>

Annexes

Annexe 1

Publication 9

Moix P., **Beccaletto L.**, Kozur H.W., Hochard C., Rosselet F., Stampfli G.M. (2008) A New Classification of the Turkish Terranes and Sutures and its Implication for the Paleotectonic History of the Region, *Tectonophysics* 451, 7–39. <https://doi.org/10.1016/j.tecto.2007.11.044>

Available online at www.sciencedirect.com

Tectonophysics 451 (2008) 7–39

TECTONOPHYSICS

www.elsevier.com/locate/tecto

A new classification of the Turkish terranes and sutures and its implication for the paleotectonic history of the region

Patrice Moix^{a,*}, Laurent Beccaletto^b, Heinz W. Kozur^c, Cyril Hochard^a,
François Rosselet^d, Gérard M. Stampfli^a

^a Institut de Géologie et de Paléontologie, Université de Lausanne, CH-1015 Lausanne, Switzerland

^b BRGM, Service GÉologie / Géologie des Bassins Sédimentaires, 3 Av. Cl. Guillemin - BP 36009, FR-45060 Orléans Cedex 2, France

^c Rézsü u. 83, H-1029 Budapest, Hungary

^d IHS Energy, 24, chemin de la Mairie, CH-1258 Perly, Switzerland

Received 15 October 2007; accepted 6 November 2007

Available online 14 December 2007

Abstract

The Turkish part of the Tethyan realm is represented by a series of terranes juxtaposed through Alpine convergent movements and separated by complex suture zones. Different terranes can be defined and characterized by their dominant geological background. The Pontides domain represents a segment of the former active margin of Eurasia, where back-arc basins opened in the Triassic and separated the Sakarya terrane from neighbouring regions. Sakarya was re-accreted to Laurasia through the Balkanic mid-Cretaceous orogenic event that also affected the Rhodope and Strandja zones. The whole region from the Balkans to the Caucasus was then affected by a reversal of subduction and creation of a Late Cretaceous arc before collision with the Anatolian domain in the Eocene. If the Anatolian terrane underwent an evolution similar to Sakarya during the Late Paleozoic and Early Triassic times, both terranes had a diverging history during and after the Eo-Cimmerian collision. North of Sakarya, the Küre back-arc was closed during the Jurassic, whereas north of the Anatolian domain, the back-arc type oceans did not close before the Late Cretaceous. During the Cretaceous, both domains were affected by ophiolite obduction, but in very different ways: north directed diachronous Middle to Late Cretaceous mélange obduction on the Jurassic Sakarya passive margin; Senonian synchronous southward obduction on the Triassic passive margin of Anatolia. From this, it appears that the Izmir-Ankara suture, currently separating both terranes, is composite, and that the passive margin of Sakarya is not the conjugate margin of Anatolia. To the south, the Cimmerian Taurus domain together with the Beydağları domain (part of the larger Greater Apulian terrane), were detached from north Gondwana in the Permian during the opening of the Neotethys (East-Mediterranean basin). The drifting Cimmerian blocks entered into a soft collision with the Anatolian and related terranes in the Eo-Cimmerian orogenic phase (Late Triassic), thus suturing the Paleotethys. At that time, the Taurus plate developed foreland-type basins, filled with flysch-molasse deposits that locally overstepped the lower plate Taurus terrane and were deposited in the opening Neotethys to the south. These olistostromal deposits are characterized by pelagic Carboniferous and Permian material from the Paleotethys suture zone found in the Mersin mélange. The latter, as well as the Antalya and Mamonia domains are represented by a series of exotic units now found south of the main Taurus range. Part of the Mersin exotic material was clearly derived from the former north Anatolian passive margin (Huğlu-type series) and re-displaced during the Paleogene. This led us to propose a plate tectonic model where the Anatolian ophiolitic front is linked up with the Samail/Baçr-Bassit obduction front found along the Arabian margin. The obduction front was indented by the Anatolian promontory whose eastern end was partially subducted. Continued slab roll-back of the Neotethys allowed Anatolian exotics to continue their course southwestward until their emplacement along the Taurus southern margin (Mersin) and up to the Beydağları promontory (Antaya-Mamonia) in the latest Cretaceous–Paleocene. The supra-subduction ocean opening at the back of the obduction front (Troodos-type Ocean) was finally closed by Eocene north–south shortening between Africa and Eurasia. This brought close to each other Cretaceous ophiolites derived from the north of Anatolia and those obducted on the Arabian promontory. The latter were sealed by a Maastrichtian platform, and locally never affected by Alpine tectonism, whereas those located on the eastern Anatolian plate are strongly deformed and metamorphosed, and affected by Eocene arc magmatism. These observations help to reconstruct the larger frame of the central Tethyan realm geodynamic evolution.

© 2007 Elsevier B.V. All rights reserved.

Keywords: Asia; Turkey; Tethys; Mesozoic; Terranes; Sutures; Ophiolites

* Corresponding author. Tel.: +41 21 692 43 58; fax: +41 21692 43 05.
E-mail address: Patrice.Moix@unil.ch (P. Moix).

1. Introduction

This paper proposes a new terrane subdivision of the Turkish Tethyan domain and its implications for the geological evolution of that region. This new scheme is based on recent field investigations carried out by a team of geologists from our university over the past 10 years. The new subdivision also incorporates previous concepts published in French language during the 1970–80's as PhD theses mainly done under the direction of Prof. Brunn by teams of scientists from Paris-Orsay. More recent input from Turkish geologists offers a series of well-constrained data on the ophiolites, with precise and modern dating of the magmatic and metamorphic events. Each structural/paleogeographic domain is described in order to precise their main geological characteristics. Unpublished new data related to the Mersin mélanges characterize the new South-Taurides exotic domain. The latter, integrated in a larger tectonic framework can explain synthetically the origin of the Turkish nappes, reconciling ideas on a northern versus southern origin of the nappes.

2. Terranes, sutures and paleo-oceanic domains of Turkey and adjacent areas

Ophiolitic bodies are widespread in Turkey. The eastern Mediterranean region as a whole exhibits a fascinating diversity of ophiolites and related oceanic magmatic units of mainly Triassic, Jurassic and Cretaceous ages (Fig. 1). Turkey is also made of several continental and oceanic fragments assembled during the Late Cretaceous–Early Tertiary period in consequence of the closure of different Tethyan oceanic basins. The first assembly of terranes was realized during the Variscan orogeny with an amalgamation of Gondwana and Laurasia-derived elements. In Late Triassic times, this was repeated during the Eo-Cimmerian orogenic event with the final closure of the Paleotethys Ocean. This paper is mainly centered on younger amalgamation events. For the Paleozoic dynamics and origin of the Turkish terranes, the reader is referred to recent publications on the Variscan (e.g. Stampfli and Borel, 2002) and Paleotethys sutures in the Tethyan realm (e.g. Stampfli et al., 2003; Stampfli and Kozur, 2006).

One of the outstanding challenges for the interpretation of the western Tethyan realm is to solve the problem of the origin of the Anatolian-Tauric nappes. Some authors assumed that the nappes (including the ophiolitic series) were derived from the closure of a single major ocean located to the north of the Tauric carbonate platform during the Late Cretaceous. Analogies of facies on both flanks of the Bolkar Mountains (i.e. “Taurus limestone axis”), and similarities between the para-autochthonous sequences in the Taurides and the Arabian platform were the starting point of the nappe/window interpretation of Ricou et al. (1974, 1975) and Brunn et al. (1976). Other authors assumed that several oceanic basins were separated by microcontinents (Robertson and Woodcock, 1981; Şengör and Yılmaz, 1981; Stampfli et al., 1991). Northerly units were derived from a northern oceanic basin, i.e. the Inner Taurides Ocean (Dilek et al., 1999; Özer et al., 2004) or northern branch

of Neotethys (Robertson and Woodcock, 1981; Şengör and Yılmaz, 1981). Southerly units came from a southern oceanic basin, i.e. the southern branch of the Neotethys (Robertson and Woodcock, 1981; Şengör and Yılmaz, 1981; Dilek et al., 1999). More recently, some authors supported both a northern and a southern origin for these ophiolitic nappes (Göncüoğlu et al., 1997; Robertson, 1998, 2000; Stampfli et al., 2001). Considering several oceanic basins, the Lycian Nappes, the Beyşehir-Hoyran Nappes, the Hadım Nappes, the Pınarbaşı and Munzur domains are typical northerly-derived units. On the other hand, southerly-derived units are represented by the Antalya Nappes, the Baër-Bassit ophiolite (Syria), the Mamonia Complex (Cyprus) and the Mersin ophiolite and its related mélanges.

In our new plate tectonic approach of this problem, and with the exception of the peri-Arabian ophiolites, all Turkish ophiolites south of the Izmir-Ankara suture are regarded as originating from the north. At some stage, they formed a unified obduction front with the peri-Arabian ophiolites, the latter progressively indented by the Anatolian-Tauric promontory.

2.1. Previous subdivision

Anatolia (Turkey) was previously subdivided into four major orogenic belts, namely the Pontides (Laurasian realm), the Anatolides, the Taurides and the Border folds (Gondwana realm) (Ketin, 1966). Three distinct ophiolitic belts were recognized some three decades ago (Gansser, 1974; Brinkmann, 1976; Juteau, 1980): from north to south, there are (1) the North Anatolian or northern ophiolitic belt associated with HP-LT sediments (Okay et al., 1998; Önen, 2003), (2) the Tauric ophiolitic belt, divided into four sub-parallel zones along the orogenic belt (Dilek et al., 1999) and (3) the peri-Arabian or southern ophiolitic belt, outlining the border with the Arabian plate and continuing eastward through the Zagros Range in Iran (Kermanshah and Neyriz ophiolites) and the Samail Nappes in Oman.

2.2. New subdivision

Recent geologic subdivisions of Turkey based on paleogeography and plate tectonics were made by Okay and Tüysüz (1999) and Bozkurt and Mittwede (2001). Based on proper terranes definitions and geologic descriptions of the main sutures, microcontinental blocks, and oceanic domains, we develop this concept further. Presently, the Izmir-Ankara-Erzincan suture divides Turkey into two main tectonic units, the Pontides and the Anatolides-Taurides platform (Şengör and Yılmaz, 1981; Okay et al., 1996) (Fig. 1). In the north, the Pontides comprise the Sakarya, Istanbul, Zonguldak and Rhodope-Strandja zones. All of them belonged to Laurasia and, except the Zonguldak zone, were affected by the Variscan metamorphic–plutonic events. South of the suture, the Anatolides-Taurides platform belonged for its southern part (Taurus terrane) to Gondwana, at least until the Permian, whereas the Anatolian terrane has Eurasian affinities. To the southeast, the Tertiary SE Turkish suture (Robertson et al., 2006) separates the Taurides-Anatolides domain from the

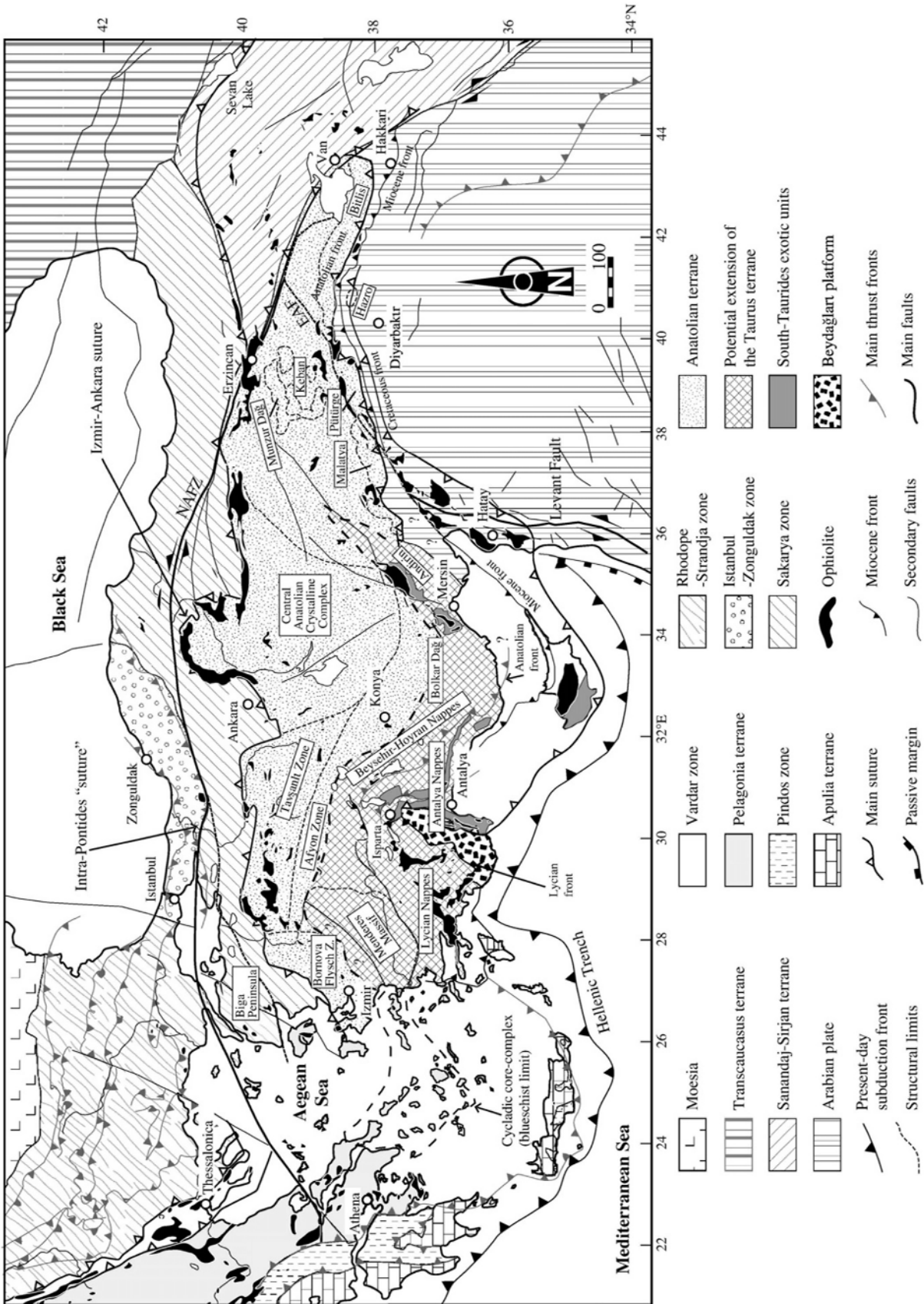


Fig. 1. Tectonic map of Turkey and surrounding regions. See the explanations in the text. NAFZ: North Anatolian Fault zone. EAF: East Anatolian Fault.

Arabian platform. Therefore, five main domains with contrasting geodynamic evolutions are differentiated: from north to south, there are (1) the Pontides domains, including the intra-Pontides and Izmir-Ankara-Erzincan sutures; (2) the Anatolian terrane and related ophiolitic nappes; (3) the Taurus Cimmerian terrane; (4) the South-Taurides exotic units and (5) the peri-Arabian domain. The composite Taurides-Anatolides domain is here subdivided into the Anatolian and Taurus terranes (Stampfli, 2000; Stampfli and Borel, 2002). These two terranes were not sealed by a common platform before the Late Triassic. Before that, the two blocks show a drastically different evolution and origin. All major domains are now reviewed in some detail (see Sections 3–7), presenting a summary of published and newly acquired field data.

3. The Pontides domain

The composite Pontides domain was affected by numerous terranes amalgamations from the Variscan times until the Cretaceous–Paleocene opening of the Black Sea basins. Generally speaking, this domain was often located within a context of an active margin with widespread arc-related volcanic activity. This resulted in the formation and superposition of metamorphic–plutonic complexes. This zone is also linked on both ends with similar areas, such the Balkanic orogenic complex in the west and the Caucasus orogenic system eastward.

3.1. The Rhodope-Strandja zone (Fig. 2)

The Strandja zone of Turkey represents the eastern continuation of the Rhodope Massif of northeastern Greece and southeastern Bulgaria (Fig. 1). Stratigraphically, it consists of a Variscan (Eurasian) basement of highly deformed metamorphosed rocks in the amphibolite facies, intruded by Late Variscan extensional Permian granitoids (Okay et al., 2001) (Fig. 2). This basement is unconformably overlain by a Triassic transgressive sequence comprising continental to shallow marine metasediments, extending up to the Middle Jurassic in its Bulgarian part (Chatalov, 1988). The Late Jurassic–Early Cretaceous interval corresponds to an important deformational regime involving all the previous units (Austrian phase or Balkanic orogeny (Georgiev et al., 2001)). This deformation is characterized by northward thrusting and is sealed by Cenomanian conglomerates and shallow marine limestones, followed by Senonian arc-related magmatic rocks. The magmatic arc is related to the Late Cretaceous final closure and northward subduction of the Jurassic Vardar Ocean beneath the Rhodope margin. The related Vardar suture, located in Greece, separates the Rhodope and circum-Rhodope zones from the Pelagonian terrane.

The Rhodope area is also characterized by the occurrence of *mélange*-like units in the allochthonous nappes of northern Greece and eastern Bulgaria (e.g. Boyanov and Russeva, 1989; Bonev and Stampfli, 2003). These oceanic remnants are correlated with similar units found in the Biga peninsula of northwest Turkey, e.g. the Çetmi *mélange* of Albian age (Beccaletto et al., 2005). Before the Cenomanian, both were

obducted northward onto the Rhodope margin during the Balkanic orogeny (Beccaletto, 2004). At a regional scale, this event may be related to a similar northward obduction process known in eastern Turkey and in the Caucasus (Sevan). There, accretionary complexes were obducted northward onto the Sakarya margin during the Cenomanian–Turonian interval (see Section 3.4). Finally, this implies a general northward obduction onto the Eurasian Rhodope-Sakarya margin, starting from the Albian in the west to the Turonian–Campanian in the east.

3.2. The Istanbul and Zonguldak zones (Fig. 3)

The Istanbul and Zonguldak zones are small continental fragments located southwest of the Black Sea. These zones are bounded to the east by the West Crimean Fault, and to the west by the West Black Sea Fault (Okay, 1989). They are separated from the southerly Sakarya zone by the Intra-Pontides “suture”/North Anatolian Fault system (Fig. 1). The Istanbul and Zonguldak zones were generally regarded as a single unit. However, as shown by Demirtaşlı (1989), Göncüoğlu and Kozur (1998) and Kozur and Göncüoğlu (1999), both terranes have a very different Paleozoic and Mesozoic development.

In the Zonguldak zone (Çamdağ, Zonguldak, Amasra and Safranbolu regions), a low-grade metamorphic Cadomian basement is present (Ustaömer and Robertson, 1997; Ustaömer et al., 2005) (Fig. 3A). One characteristic of the Zonguldak zone is the absence of Variscan overprint. The oldest rocks above the Cadomian basement are siliciclastic rocks of Tremadoc age (Dean et al., 2000). In the basal Arenig, a rapid deepening occurred and the Arenig to Ashgill consist of graptolite-bearing mudstones and siltstones with few limestones. The Baltic-type conodonts show a strong thermal alteration (CAI=5–6). The Silurian consists of graptolite-bearing shales and mudstones, with few limestones in the upper part. The youngest Silurian rocks occur below an angular disconformity and belong to the Pridoli. The Pridoli and Ludlow rocks are often removed below this angular disconformity. Up to the uppermost Silurian, the conodonts show a strong thermal alteration (CAI=5). In the Çamdağ Unit, the Ordovician consists of siliciclastic sediments and the Silurian is probably absent. Above the angular disconformity, the Devonian sequence begins with Pragian to Lower Emsian siliciclastic rocks, overlain by shallow water limestones and dolomites without Variscan alteration (CAI=2). Shallow water limestones and dolomites continue throughout the Mississippian (until Namurian A). Conodonts show the absence of Variscan metamorphism (CAI=1). Namurian B, C and Westphalian sequences consist of continental beds with coals and Euramerican flora. Continental beds without coals continued until the Stephanian. The Paleozoic development in the Zonguldak zone is similar to the Malopolski terrane in southeast Poland. The Triassic of the Zonguldak zone is continental (Görür et al., 1997). After a long gap, the Oxfordian transgression brought shallow marine sandstones and limestones. In the Cretaceous, shales, siltstones, and limestones prevail and Upper Cretaceous volcanics are present. In the Upper Maastrichtian, an unconformity is also present.

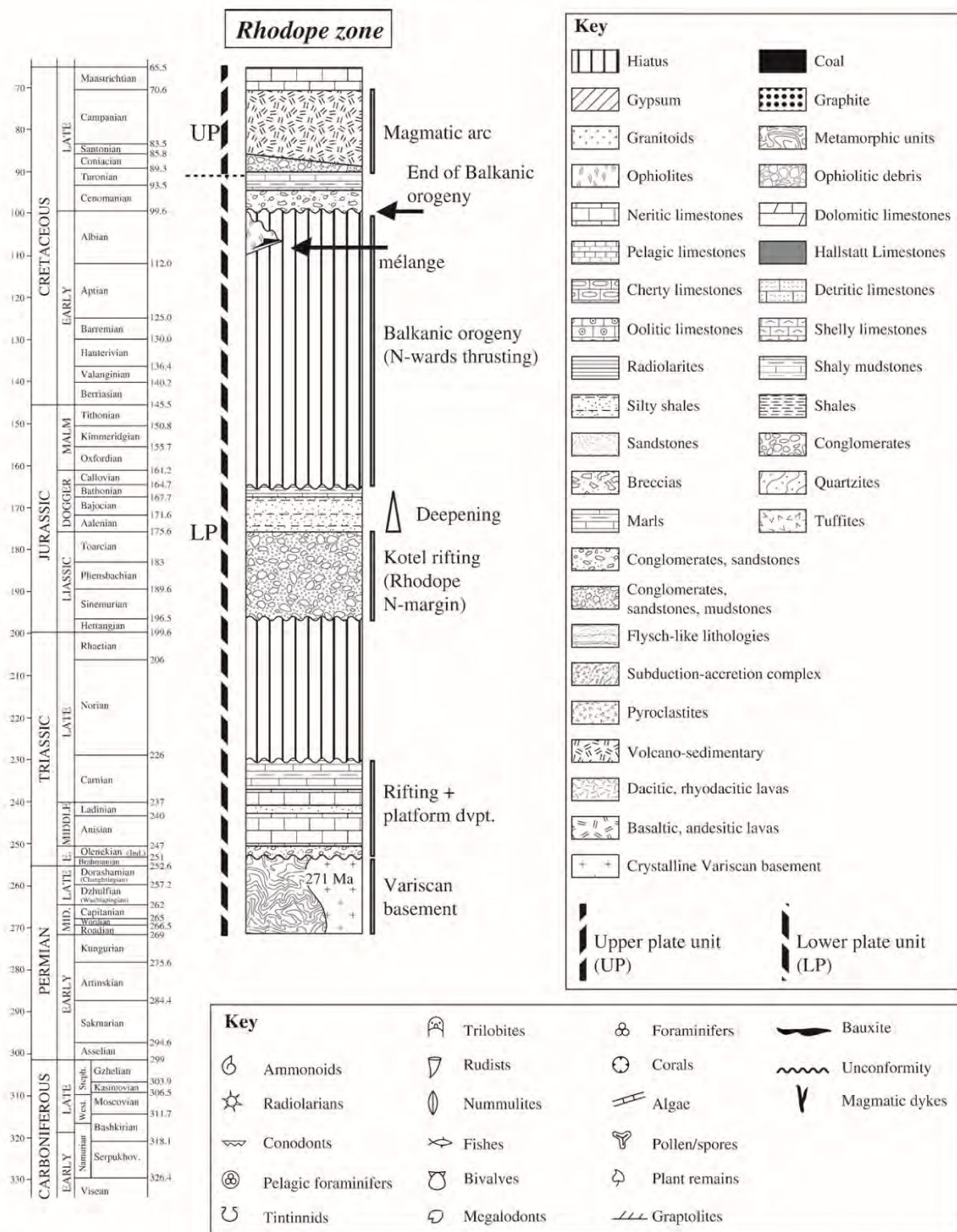


Fig. 2. Rhodope-Strandja zone: synthetic lithostratigraphic section and main geodynamic events. Section compiled from Georgiev et al. (2001) and Okay et al. (2001). The key refers to Figs. 2, 3, 4, 6, 7, 8, 9, 10, 11 and 12. For the Carboniferous, Lower Permian, Jurassic and Cretaceous, the geologic time scale is after Gradstein et al. (2004); for the Middle and Late Permian, and the Triassic, the geologic time scale is after Kozur (2003a,b). The same geological time scale is used on Figs. 4, 6, 7, 11 and 12.

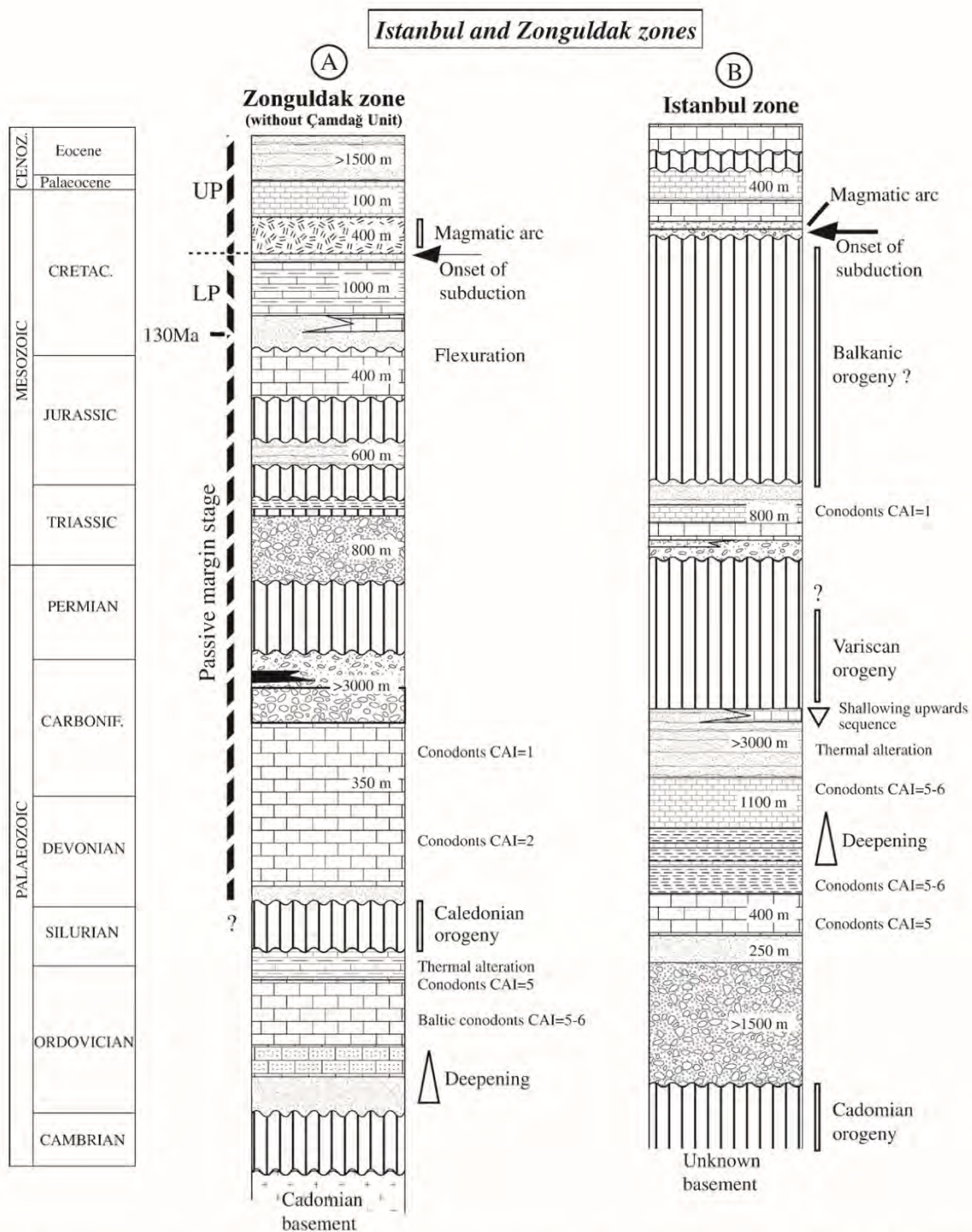


Fig. 3. Istanbul and Zonguldak zones: synthetic lithostratigraphic sections and main geodynamic events. Sections compiled from Okay and Tüysüz (1999) and Kozur (1999b). Key on Fig. 2.

The series in the Istanbul zone are different (Fig. 3B). The sedimentation began during the Arenig and the Ordovician and Llandovery rocks consist of shallow water clastics. The rocks ranging from the Wenlock to the Pridoli are represented by shallow water limestones. The thermal alteration of the conodonts

(CAI=5) in the Devonian was caused by Variscan metamorphism. Lochkovian to Lower Emsian rocks are represented by shallow water limestones, shales, greywackes and sandstones. A rapid deepening occurred within the Emsian. Pelagic nodular limestones and shales with paleopsychrosphaeric deep water

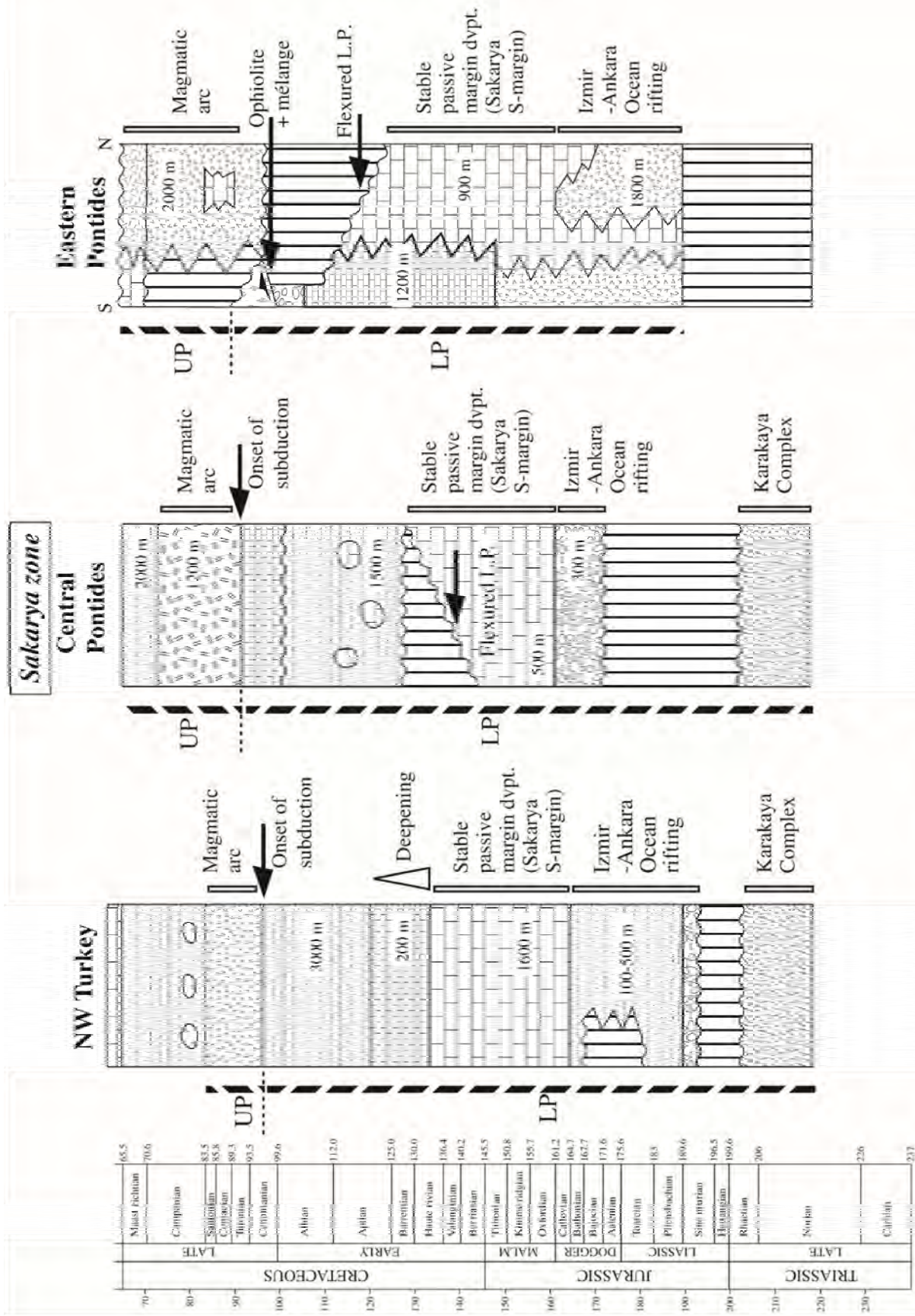


Fig. 4. Sakarya zone: synthetic lithostratigraphic sections and main geodynamical events. Sections modified from Okay and Tüysüz (1999). K₀₁ on Fig. 2.

ostracods and conodonts (CAI=4–5) were deposited up to the top of the Devonian. The Tournaisian is characterized by radiolarites and shales followed by the Hercynian flysch (greywackes and shales), which age ranges up to the Namurian A. A rapid shallowing in the Namurian B and C results in the deposition of the Cebeciköy Limestones, followed by the Hercynian unconformity. Following a Lower Triassic transgression, shallow water conglomerates, sandstones, limestones, and marls were deposited. A strong deepening occurred in the Spathian. From this time to the end of the Middle Triassic, pelagic, partly nodular limestones, Ammonitico Rosso, and some shallow water carbonates were deposited. The conodonts are unaltered (CAI=1). Carnian rocks are made of siliciclastic turbidites, which end in a shallowing upward sequence with Norian reefal limestones and sandstones. After a long gap, conglomerates, marls and rudist-bearing limestones mark the Campanian transgression. The absence of Jurassic and Lower Cretaceous rocks may be related to the influence of the Balkanic orogeny. Upper Cretaceous volcanics are also not present.

Both faunistic and paleomagnetic data demonstrate a Laurasian affinity for the Istanbul and Zonguldak zones during the Paleozoic (Görür et al., 1997) and the Early Triassic (Kerey et al., 1986; Saribudak et al., 1989). Senonian arc-related rocks, widespread in the northern part of the Zonguldak zone, are related to the closure of a southerly oceanic domain (Phrygian Ocean, see below), subducting northward beneath the Sakarya and Istanbul zones. This subduction also triggered the Late Cretaceous back-arc opening of the West Black Sea oceanic basin, leading to the southward translation of the Istanbul continental fragment away from the Odessa Shelf (Okay et al., 1994).

3.3. The Intra-Pontides “suture”

The Intra-Pontides “suture” (Şengör et al., 1980) separates the Istanbul and Zonguldak zones in the north from the Sakarya zone in the south (Fig. 1). The “suture” is a tectonic mixture of several units coming both from the Istanbul, Zonguldak and Sakarya zones, plus various metamorphic rocks and dismembered metaophiolitic bodies. However, the “suture” directly coincides with the major post-Miocene strike-slip North Anatolian Fault zone (Barka, 1992; Armijo et al., 1999). All the pre-Miocene structural relations between the Istanbul/Zonguldak and the Sakarya zones are thus disrupted. Besides this neotectonic problem, the lack of reliable field data (ages of metamorphic and ophiolitic rocks) prevents a clear understanding of the “suture” zone. For instance, there is still a debate on the age of the Almacık metaophiolite, considered either as Paleozoic (Abdüsselamoğlu, 1959; Gözübol, 1980; Yiğitbaş et al., 1999) or Late Cretaceous (Yılmaz et al., 1982, 1995; Robertson and Ustaömer, 2004).

As field evidences for an Intra-Pontides “suture” are scarce, the evolution of the corresponding Intra-Pontides Ocean remains highly speculative and controversial (Robertson and Ustaömer, 2004; Elmas and Yiğitbaş, 2005; Ustaömer and Robertson, 2005). For instance, there are no data for the age of its opening, nor any recognized passive margin sequences. The

age of its closure, generally based on the first transgressive sediments, is either placed in the Late Cretaceous (Yılmaz et al., 1995; Robertson and Ustaömer, 2004), the Paleocene–Eocene (Şengör and Yılmaz, 1981), the Early Eocene (Okay et al., 1994; Wong et al., 1995), or Early Eocene to Oligocene (Görür and Okay, 1996). Finally, data from Tüysüz (1999) favour a juxtaposition of the Istanbul and Sakarya zones during the Cenomanian, much earlier than previously suggested. Because of these discrepancies, and following the view of Elmas and Yiğitbaş (2001), we ignore the existence of a Mesozoic or Tertiary Intra-Pontides Ocean in the paleogeographic reconstructions.

3.4. The Sakarya zone (Fig. 4)

The Sakarya zone represents an east–west trending continental fragment. It is bordered to the northwest by the Rhodope–Strandja, Istanbul, and Zonguldak zones along the Intra-Pontides “suture”/North Anatolian Fault system and to the northeast by the Black Sea. To the south, the Sakarya zone is bounded by the composite Anatolian–Tauric block along the mélanges and ophiolites of the Izmir–Ankara–Erzincan zone (Fig. 1). The basement of the Sakarya zone (Okay et al., 1996) consists of a widespread Triassic subduction–accretion series, called the Karakaya Complex in its western part (Bingöl et al., 1975; Tekeli, 1981; Okay et al., 1991; Okay and Göncüoğlu, 2004). The Karakaya Complex may be seen as a fore-arc/foreland basin related to the northward subduction of the Paleotethys along the southern margin of Eurasia (Stampfli and Kozur, 2006). The various units of the Karakaya Complex are unconformably overlain by Liassic terrigenous to shallow marine clastic sedimentary rocks (Altner et al., 1991) (Fig. 4). These clastics are unconformably overlain by Middle–Upper Jurassic platform-type neritic limestones and Lower Cretaceous pelagic limestones. The whole series is interpreted as a syn- to post-rift sequence, related to the opening of the Izmir–Ankara Ocean along the southern margin of the Sakarya microcontinent (Görür et al., 1983). This ocean extended eastward to the Sevan south Caspian oceanic domain (Stampfli and Borel, 2002, 2004). It is regarded as a marginal ocean of the Neotethys, opening through the subduction of the latter since the latest Triassic.

During the Middle Cretaceous, this Jurassic–Cretaceous passive margin took all the characteristics of a flexural margin. Regional landward erosion and karstification, seaward deepening and local occurrence of accretion-related mélanges and ophiolites at the top of them are outstanding features (Altner et al., 1991; Koçyiğit et al., 1991; Okay and Şahintürk, 1997; Rojay and Altner, 1998; Okay and Tüysüz, 1999) (Fig. 4). In the Central Pontides, the flexuration is pre-Aptian. In the eastern Pontides, it is pre-Albian and even younger (Cenomanian) in the Sevan region (Bergougnan, 1987). In the eastern Pontides, an accretionary complex was emplaced at the top of the flexured margin during the Cenomanian–Turonian interval (Bergougnan, 1975; Okay and Şahintürk, 1997). As pointed out by Okay and Tüysüz (1999), this Middle Cretaceous northward obduction of accretionary complexes is a characteristic feature

of the Sakarya zone, and therefore must be integrated in any geodynamic scenario. Following this event, the Sakarya continental fragment and the Istanbul/Zonguldak zones flipped from a lower plate to an upper plate position. The development of a widespread Senonian volcanic arc indicates that the southerly ocean responsible for the former ophiolite obduction started to subduct northward sometime after the obduction. Moreover, the Triassic sequences in Crimea are similar to those found in the basement of the Sakarya zone, thus indicating that the latter was appended to Laurasia during the Jurassic and Cretaceous periods (Okay et al., 1996). Paleomagnetic data also indicate that the Sakarya zone was close to the Laurasian margin, at least during Liassic and Late Cretaceous times (Channell et al., 1996).

Another important feature of the Sakarya zone is the Küre Unit located close to the boundary with the Zonguldak zone. This unit comprises thrust-imbriated siliciclastic sediments interleaved with tectonic slices of a dismembered ophiolite (Ustaömer and Robertson, 1994, 1997). It is interpreted as a remnant of a back-arc basin (Küre) opened in the Early Triassic in response to the northward subduction of the Paleotethys (Kozur et al., 2000; Stampfli, 2000; Stampfli and Kozur, 2006). The Küre Ocean was closed in the Late Jurassic (Ustaömer and Robertson, 1997) after its southward subduction beneath the Sakarya zone (Kozur et al., 2000). Its northward roll-back in the Jurassic is the triggering mechanism for the opening of the Izmir-Ankara Ocean.

3.5. The Izmir-Ankara-Erzincan suture (Fig. 5)

The 2000 km long east–west trending Izmir-Ankara-Erzincan suture separates the Sakarya zone in the north from the Anatolian-Tauric block in the south (Fig. 1). The suture zone is made of ophiolitic rocks associated with accretionary mélangé units. The ophiolites occur mainly as peridotite massifs, lacking a complete ophiolitic sequence. Radiochronologic data from the sub-ophiolitic amphibolitic soles are rare and suggest Albian-Cenomanian ages for the intra-oceanic subduction (Önen and Hall, 1993; Harris et al., 1994) (Fig. 5). Striking similarities in the age of the metamorphic sole, at least for the ophiolites of southern Turkey, Cyprus, and Syria should be also noted.

The mélangés, (the Ankara mélangé of Bailey and McCallien (1950)), show dissimilar ages, origin, facies and size, generally with strong tectonic imbrications. The age of the blocks ranges from Carboniferous to Eocene (Çapan and Buket, 1975; Norman, 1993; Tüysüz et al., 1995). As pointed out by Okay and Tüysüz (1999), some ophiolites and accretionary complexes were obducted directly onto the flexural Sakarya margin along north verging thrust contacts (Bergougnan, 1975; Okay and Şahintürk, 1997). Two complexes should therefore be distinguished: one marking the northward obduction and the other related to the northward subduction and closure of the obducted ocean (Phrygian Ocean) after a flip of subduction polarity. This closure juxtaposed the Anatolian ophiolitic root zone to the Sakarya block and its mélangé (Karakaya and

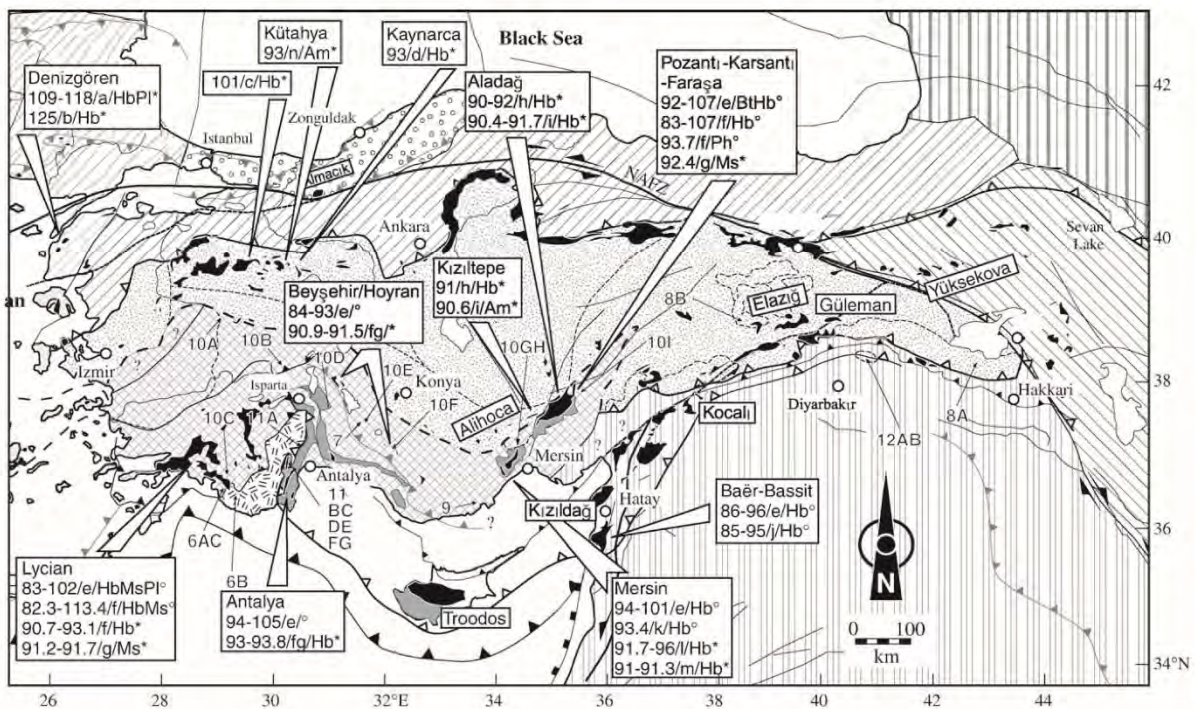
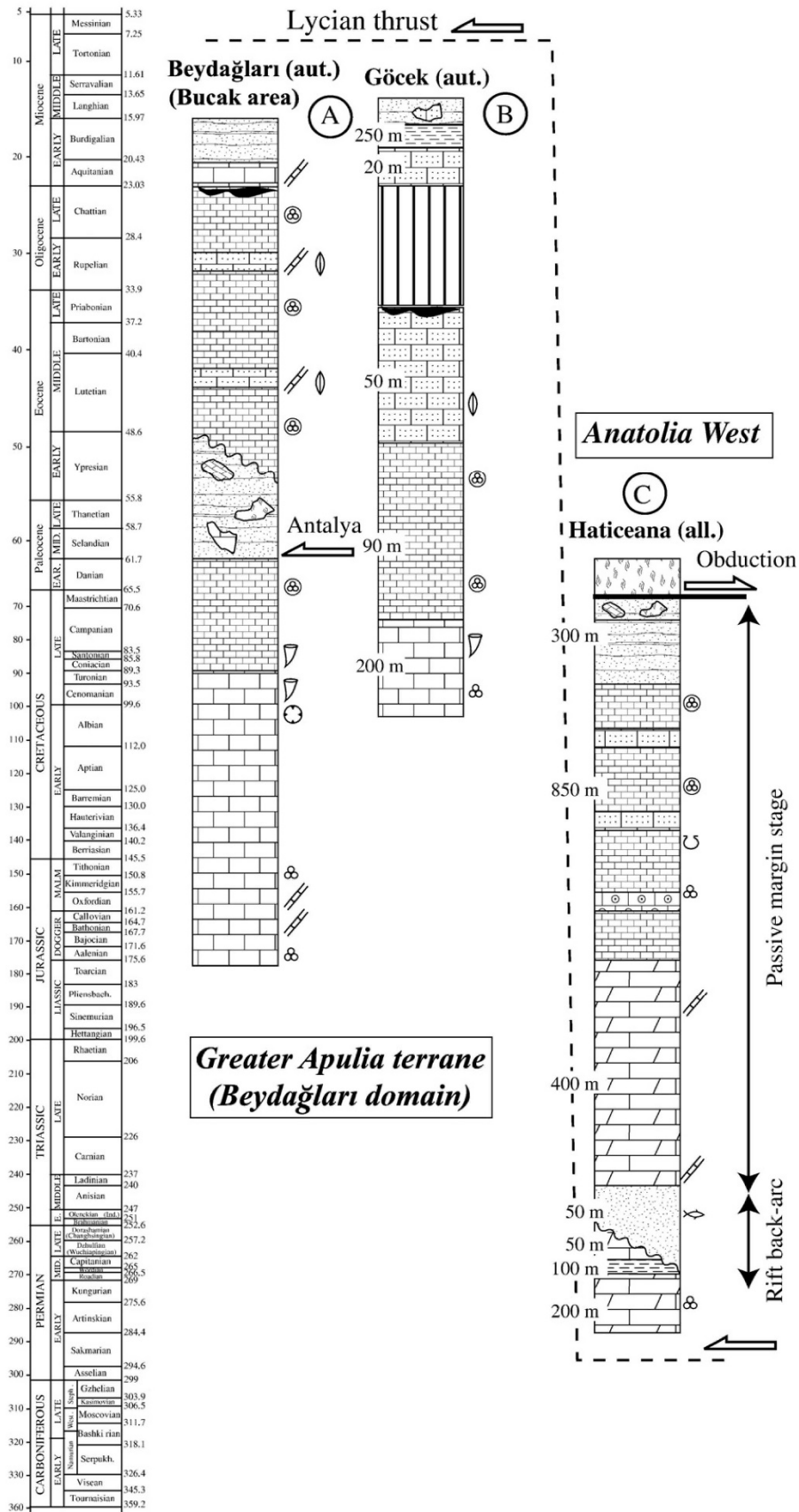


Fig. 5. Main ophiolitic massifs of Turkey, with the ages of their metamorphic soles, when published and location of the sections of Figs. 6, 7, 8, 9, 10, 11 and 12. Hb: hornblende; Bt: biotite; Pl: plagioclase; Ms: muscovite; Ph: phengite; Am: amphibole; *K–Ar method; *Ar–Ar method; (a) Okay et al. (1996); (b) Beccaletto and Jenny, 2004; (c) Önen and Hall, 2000; (d) Harris et al. (1994); (e) Thuizat et al. (1981); (f) Çelik, 2002; (g) Çelik et al. (2006); (h) Dilek and Whitney, 1997; (i) Dilek et al. (1999); (j) Delaloye and Wagner, 1984; (k) Parlak et al. (1995); (l) Parlak and Delaloye (1996); (m) Parlak and Delaloye (1999); (n) Öncü, 2003. Same key as Fig. 1.



Cretaceous ophiolitic mélangé of Norman (1993)), both areas being imbricated until the Eocene.

The oceanic domain related to the Izmir-Ankara-Erzincan suture is generally known as the Izmir-Ankara Ocean. The latter opened in the Liassic as shown by the syn-rift sequences observed in the Sakarya zone (Şengör and Yılmaz, 1981; Görür et al., 1983). Upper Triassic radiolarian cherts locally associated with pillow-lavas are common in the Izmir-Ankara mélanges and were considered as an evidence for a Late Carnian opening of this ocean (Tekin et al., 2002; Göncüoğlu et al., 2003). In view of the merging of the two mélanges found on the Sakarya basement (Triassic Karakaya Complex and Upper Cretaceous ophiolitic mélangé), lithologies older than Jurassic are likely derived from the Karakaya Complex (Norman, 1993). Therefore, the Anatolian block northern margin (characterized by Late Triassic volcanics) was not the southern conjugate margin of the Izmir-Ankara Ocean, both areas being juxtaposed only during the Late Cretaceous (Stampfli and Borel, 2004).

4. The Anatolian terrane (Figs. 6, 7, and 8)

The Tavşanlı and Afyon zones of Okay (1984, 1986) correspond to the Anatolides of Ketin (1966) which include also the Menderes Massif (Fig. 1). The Tavşanlı zone is characterized by a Late Cretaceous blueschist metamorphism (Okay et al., 1998; Sherlock et al., 1999). It represents the northward subducted continental margin of the Anatolian platform. It is thrust over the Afyon zone, composed of Devonian to Paleocene metamorphosed sedimentary rocks in the greenschist facies (Okay, 1986; Okay et al., 1996). Eastward, the Central Anatolian Crystalline Complex (Niğde, Akdağ and Kirşehir massifs) may be seen pro parte as a core complex within the Anatolian zone (Whitney and Dilck, 1997, 1998, 2000). The CACC was formerly covered by ophiolitic nappes found in most areas of the Anatolian terrane. In that regard, the “Inner Taurides suture” does not exist, these ophiolites now surrounding the CACC being formerly located on top of it before the unroofing processes.

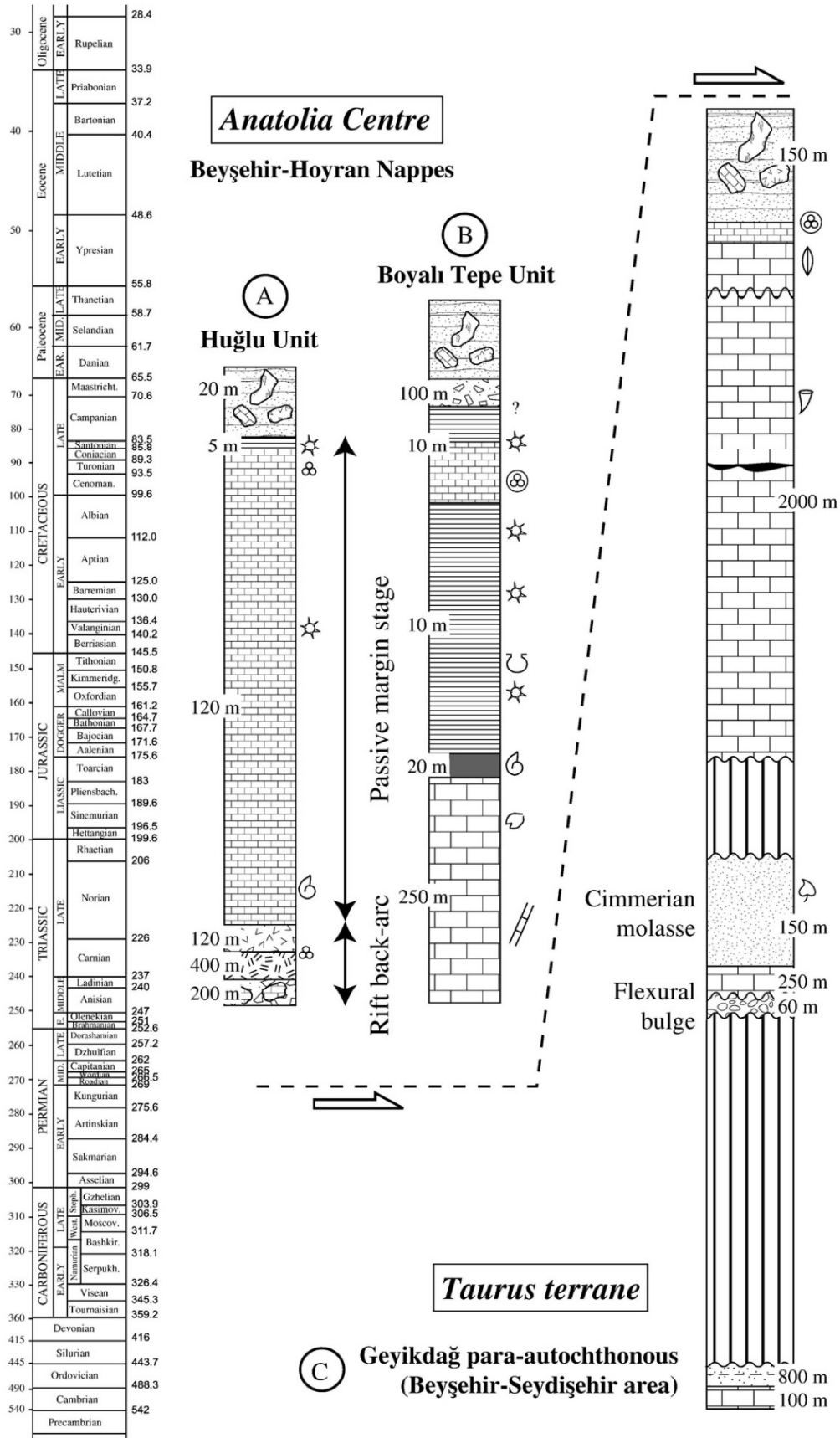
The Anatolian terrane is of Eurasian origin and joined the Taurus terrane during the Carnian–Early Norian closing of the Paleotethys (Stampfli et al., 2003). Before that, the slab roll-back of the Paleotethys detached the Anatolian terrane from Eurasia through the opening of a series of back-arc basins within the Eurasian active margin. The rapid collapse of the Variscan cordillera started in most places during the Permian. Active rifting leading to sea-floor spreading in the back-arc basins can be placed in Early to Middle Triassic times. This led to the formation of the northern Anatolian passive margin whose remnants are found as dismembered tectonic units (nappes) resting on the Taurus terrane. Characteristic deposits are open marine syn-rift sediments associated with widespread

volcanic activity (Huğlu-type series). These events can be correlated with the Pietra Verde event of the Hellenides, Dinarides, and northern Italy (e.g. Ziegler and Stampfli, 2001).

The substratum of the Anatolian passive margin is observed only in very few places: the Karaburun area in western Turkey (e.g. Kozur, 1995a, 1998a,b, 1999a,b, 2000b; Stampfli et al., 2003), thrust sheets at the base of the Lycian Nappes (Kozur et al., 1998; Kozur and Şenel, 1999), the Konya region (Göncüoğlu et al., 2000; Eren et al., 2004), and the Bitlis Massif (Bergougnan, 1987). In these areas, the substratum of the Anatolian terrane is made of a series of pelagic, clastic, and volcanic rocks ranging from Silurian to Carboniferous. In the Lycian Nappes, we recently confirmed the presence of a Carnian wildflysch including Upper Carboniferous seamounds and a Lower Carboniferous mélangé including MORBs, pelagic limestones, and radiolarites. Most of these sequences can be replaced in a context of a Carboniferous fore-arc basin evolving toward a Late Permian to Triassic arc. The Triassic arc is a characteristic feature of the sequences belonging to the Anatolian terrane and is totally absent from the Taurus terrane. The Anatolian terrane can be correlated westward to the Sitia-Arna terrane of the external Hellenides, representing the southern passive margin of the Triassic back-arc Pindos Ocean (Champod et al., 2003; Stampfli et al., 2003). Hence, the ocean bordering the northerly Anatolian-Sitia terrane will be referred to here as the Huğlu-Pindos Ocean. Eastward, in its former pre-Triassic position (Stampfli and Borel, 2004), the Anatolian terrane continued into the Sakarya terrane. The latter is also located to the south of another Triassic back-arc basin, the Küre Ocean, which opened in the region of the present Black Sea (Kozur et al., 2000).

Some of the nappe systems defined by Brunn et al. (1971) in southern Turkey represent allochthonous parts of the Anatolian terrane. These are the Lycian Nappes (Fig. 6A–C) lying on the Beydağları/Menderes autochthonous in the west (de Graciansky, 1972; Bernoulli et al., 1974; Poisson, 1977; Gutnic et al., 1979; Ricou et al., 1979); the Beyşehir-Hoyran Nappes (Fig. 7A–C) lying on the Geyikdağ autochthonous in the central part (Özgül, 1976, 1997; Monod, 1977; Gutnic et al., 1979; Andrew and Robertson, 2002; Andrew, 2003) and the Bitlis domain (Fig. 8A–B) in the east (Özgül, 1976; Özgül and Turşucu, 1984; Pampal and Kurtman, 1984; Perinçek and Kozlu, 1984; Yazgan, 1984; Bergougnan, 1987; Özer et al., 2004). There, the ophiolites and related imbricate structures are clearly sealed by Maastrichtian shallow water limestones. The underlying para-autochthonous (e.g. Beydağları, Geyikdağ) of all these nappes belongs generally to the Taurus terrane flexured in the Eocene. A flysch development preceded the emplacement of the Anatolian Nappes with their ophiolites, the latter corresponding to a synchronous Late Cretaceous obduction event generally sealed by a Maastrichtian carbonate platform (Fig. 5).

Fig. 6. Anatolia West: synthetic lithostratigraphic sections of the autochthonous (aut.) and one allochthonous (all.) series. (A) is compiled from Gutnic et al. (1979); (B) is modified from de Graciansky (1972); (C) is compiled from de Graciansky (1972) and Monod and Akay (1984). Key on Fig. 2 and location of the sections on Fig. 5.



5. The Taurus terrane (Figs. 9 and 10)

This terrane is a typical Cimmerian block (Şengör, 1979) recording the rifting/opening of the Paleotethys north of it in the Devonian and of the Neotethys south of it in the Permian (Fig. 1). Both periods correspond to locally large stratigraphic gaps and unconformities, but without major deformation or metamorphism. It shows an evolution similar to the Cimmerian–Iranian blocks located east of it. West of it, it corresponds to the most external part of the Hellenides. It comprises the Beydağları domain of southwest Turkey, forming altogether the Cimmerian Greater Apulian terrane (Stampfli et al., 1991, 2003) (Fig. 1). The Taurus terrane consists of a pre-Cambrian basement and a Paleozoic–Mesozoic cover mainly represented by carbonate platform-type sediments (Fig. 9). Together with the Pan-African Menderes Massif which is part of it (Şengör, 1984; Hetzel and Reischmann, 1996; Dannat and Reischmann, 1998, 1999), the Taurus terrane presents no Variscan deformations. On the contrary, it records the opening of the Neotethys south of it during its separation from the Gondwana in Permian times (Stampfli, 2000; Stampfli et al., 2001). This event and its related rift shoulder uplift created locally large-scale unconformities between the Permo-Triassic and older Paleozoic series. This is often regarded as “Variscan” unconformities, but no flysch, metamorphism or folding is observed.

The major event characterizing the Tauric sequence is the Eo-Cimmerian tectonic event (Fig. 10A–I) and associated sediments and deformation (Carbonian–Early Norian closing of the Paleotethys). This Eo-Cimmerian phase of deformation is mainly recorded in the Taurus terrane (Monod and Akay, 1984), with major clastic input, unconformities, and flysch-like deposits (Gutnic et al., 1979). It is sealed by a Late Triassic widespread molassic sequence, and followed by the development of Upper Triassic–Liassic carbonate platforms, found both on the Taurus and Anatolian terranes. A similar evolution is also found in the adjacent Cimmerian domains of Greece and Iran (Krahl et al., 1983; Baud and Stampfli, 1989; Bagheri et al., 2003; Stampfli et al., 2003). In these two regions, the subduction of the Paleotethys was toward the north, the Eurasian margin being the active one and the Cimmerian margin being passive. The carbonate platform sealing this orogenic event usually started in the Late Triassic or locally not before the Middle Jurassic. In most places, the Tauric series would proceed with little interruption up to the Middle Eocene flysch deposits (Monod, 1977). At that time, it was overthrust by the Anatolian Nappes. In the Late Miocene, most of the Tauric sedimentary cover was detached from its basement and displaced to its present position. This was made following a subduction progradation into the East-Mediterranean realm and the Middle Miocene closure of the space between the Taurus–Menderes and the Beydağları domains (Gutnic et al., 1979). Before that, the southern border of the Taurus terrane was the site of emplacement of ophiolitic mélanges, from the latest

Cretaceous through the Paleocene. These sequences define a South-Taurides exotic domain (see below), in which mélanges were juxtaposed to the Taurus or Greater Apulian terranes (i.e. Beydağları), as found in the Antalya Nappes.

The Taurus terrane presents several contrasting sequences. This is due to the Eo-Cimmerian deformation events which can be followed throughout the Taurus (Fig. 10A–I). The terrane being in lower plate position during its collision with the Anatolian terrane, it developed a flexural basin that was locally inverted in the Late Triassic. During the Late Cretaceous obduction of the ophiolites onto the Anatolian domain, the obducted nappes locally reached the Taurus terrane, and even went over it in its eastern segment. The ophiolites were then caught up in a westward slab retreat of the East-Mediterranean Ocean and redistributed along the southern margin of the Taurus domain mainly during the Paleocene. Typical Tauric sedimentary sequences are represented by the Geyikdağ Unit (Özgül, 1976) (Fig. 7C). The Tauric sedimentary sequences start usually in the Cambrian/Ordovician and end in the Late Cretaceous or later, depending on the proximity of the Anatolian ophiolitic front. The Taurus sequences closest to the Anatolian obduction front are found near Pınarbaşı (Altıner, 1981). There, the para-autochthonous sequence mainly presents a Devonian to Late Cretaceous neritic sedimentation. The sequence is interrupted during the Upper Triassic by the Eo-Cimmerian event accompanied by clastic input. This sequence is overthrust by allochthonous ophiolitic and sedimentary sequences. The neo-autochthonous cover is characterized by three successive sequences: the first one is composed of Upper Maastrichtian–Paleocene conglomerates derived from the allochthonous series; the second one is mainly made of Lutetian limestones and lays unconformably over the conglomerates; the third one is characterized by Upper Miocene conglomerates (Altıner, 1981).

On a more external position (between Silifke and Anamur), the autochthonous sequences of the Taurus terrane present a sedimentation ranging from the Cambrian to the Late Cretaceous/Paleocene (Demirtaşlı, 1984a,b), or even from the infra-Cambrian to the Middle Miocene (Koç et al., 1997). The Pınarbaşı sequence (Fig. 9) described by Demirtaşlı (1984a,b) can be closely compared with the Alborz series in northern Iran, recording the opening of both Paleo- and Neotethys. The Late Ordovician pebbly sandstone formation mark the Hirnantian glacial event (Monod et al., 2003). We associate it with the onset of the Paleotethys rifting, the rift shoulders being elevated and covered by temporary ice-sheets. A Lower Silurian black shale episode follows the glacial event and suggests a deposition in a restricted basin within the rift zone. This detrititic event can be related to the erosion of the Paleotethys rift shoulder, following thermal expansion uplift related to the onset of oceanic spreading. Subsequent thermal subsidence allowed the unconformable deposition of the Middle to Late Devonian series. This sequence marks the passive margin stage that lasted up to the Early Permian, when thermal uplift related to the opening of the

Fig. 7. Anatolia Centre: synthetic lithostratigraphic sections of a para-autochthonous and some allochthonous series. (A) compiled from Gökdeniz (1981), Monod (1977) and Özgül (1984); (B) modified from Monod (1977); (C) compiled from Özgül (1976, 1984). Key on Fig. 2 and location of the sections on Fig. 5.

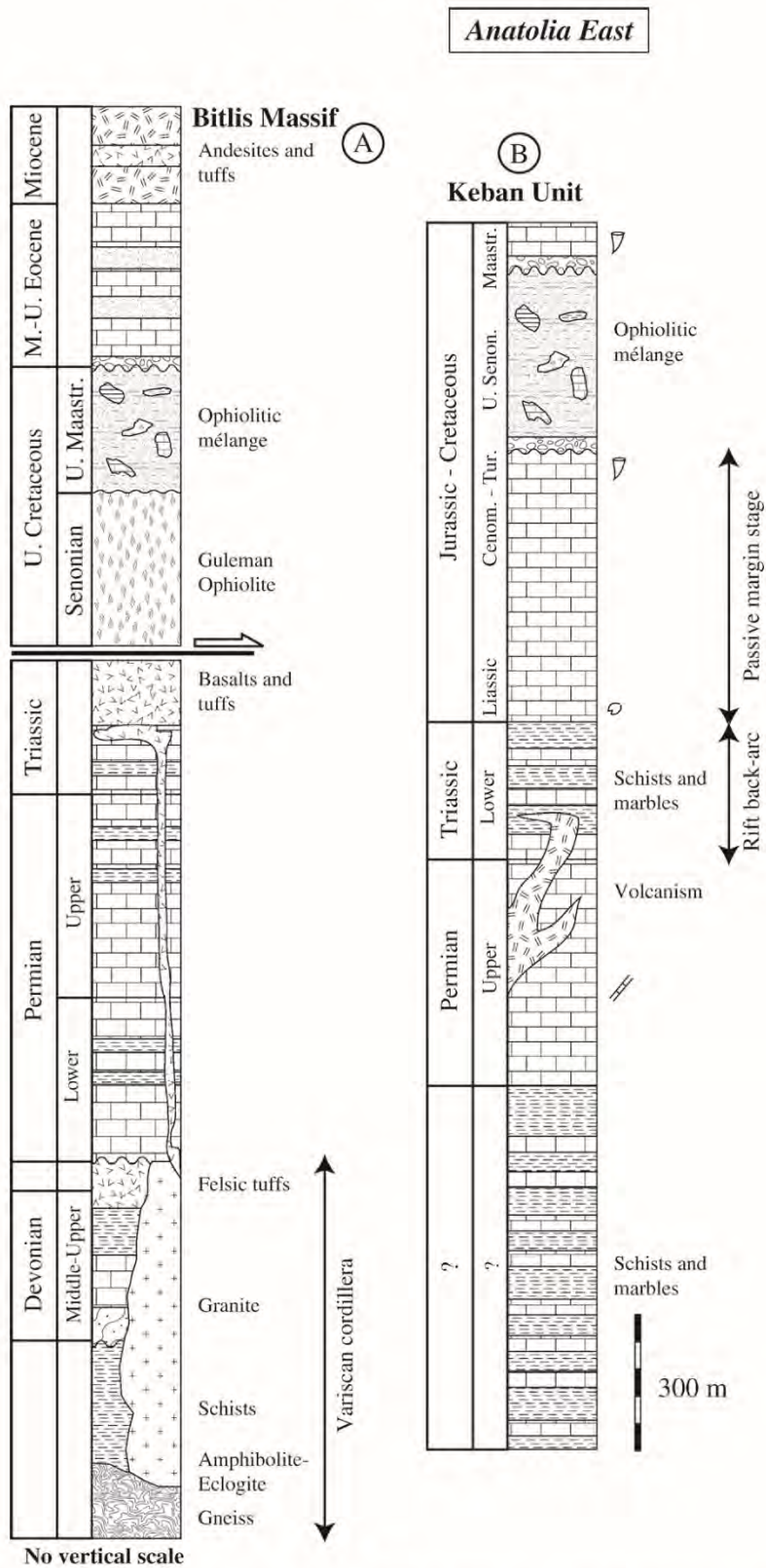


Fig. 8. Anatolia East: synthetic lithostratigraphic sections of the Bitlis Massif and the Keban Unit. (A) compiled from Bergougnan (1987) and Göncüoğlu and Turhan (1984); (B) compiled from Bergougnan (1987) and Özgül and Turşucu (1984). Key on Fig. 2 and location of the sections on Fig. 5.

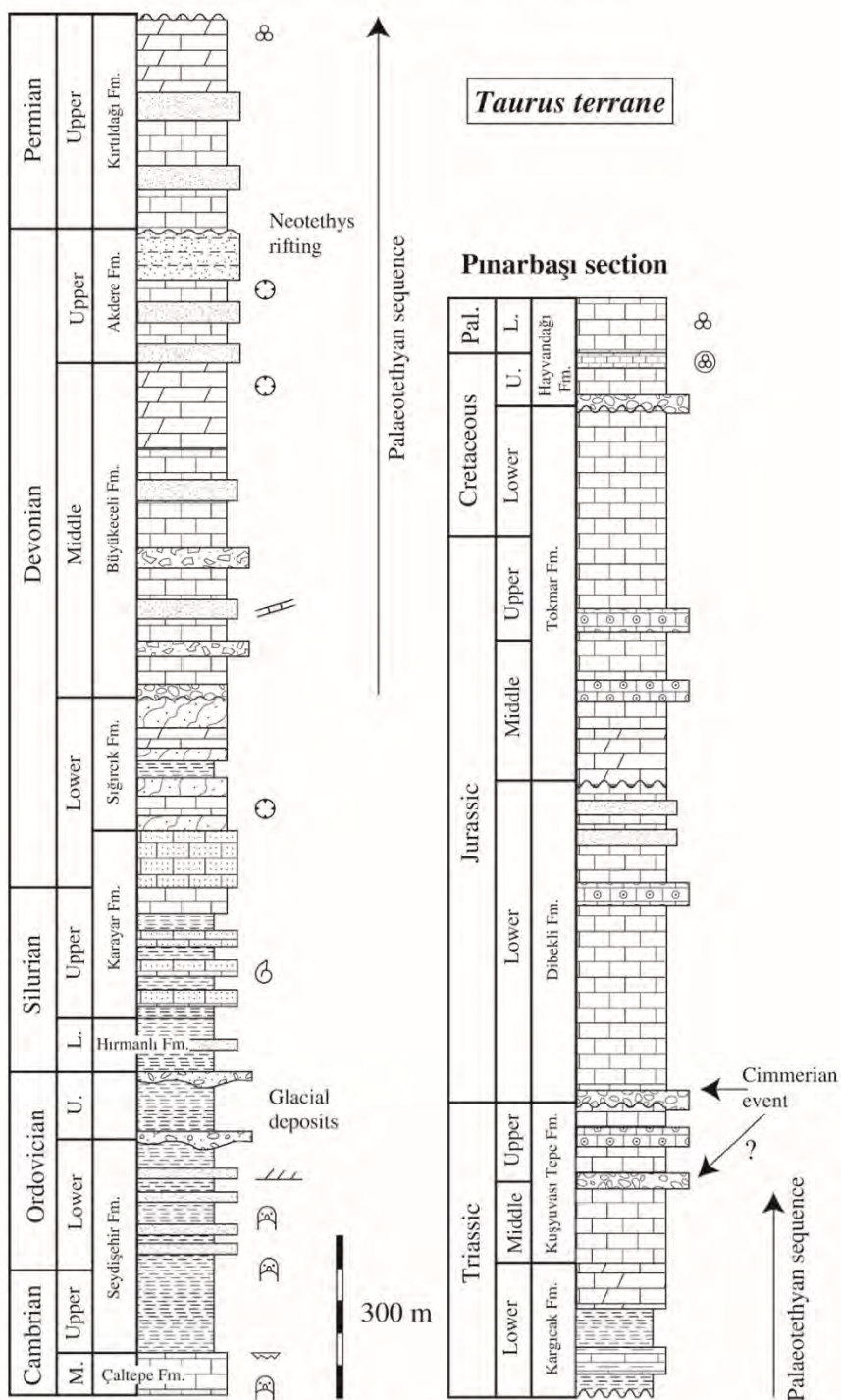


Fig. 9. Taurus terrane: synthetic lithostratigraphic section of a typical Tauric series between Silifke and Anamur (Pınarbaşı section). Compiled from Demirtaşlı (1984a,b). Key on Fig. 2 and location of the section on Fig. 5.

Neotethys created again major erosion and unconformities. The Carboniferous sequence is therefore often lacking. Locally, the Upper Permian made of limestones and quartzitic sandstones, overlies unconformably the Devonian. It corresponds to the

flooding of the Neotethyan rift shoulder and to the onset of a new (Neotethyan) passive margin sequence. The subsequent Eo-Cimmerian event (Fig. 10A–I) is characterized by large-scale unconformities, flysch/molasse deposits during the Late

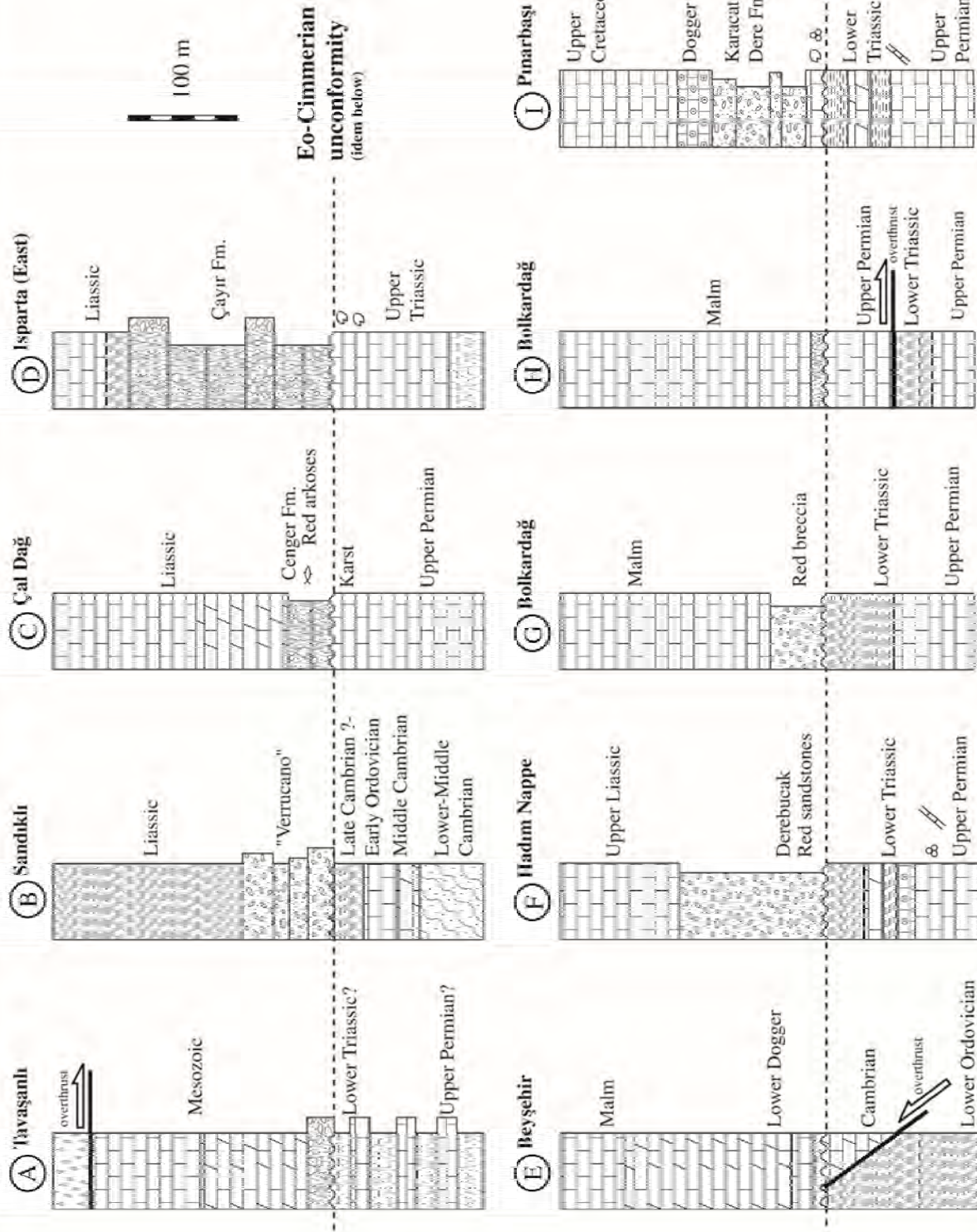


Fig. 10. The Eo-Cimmerian unconformities in the Taurus terrane. All sections are modified from Monvil and Akay (1984), except (B) compiled also from Dean and Özgül (1994) and Erdoğan et al. (2004) and except (E) compiled also from Akay (1981). Key on Fig. 2 and location of the sections on Fig. 5.

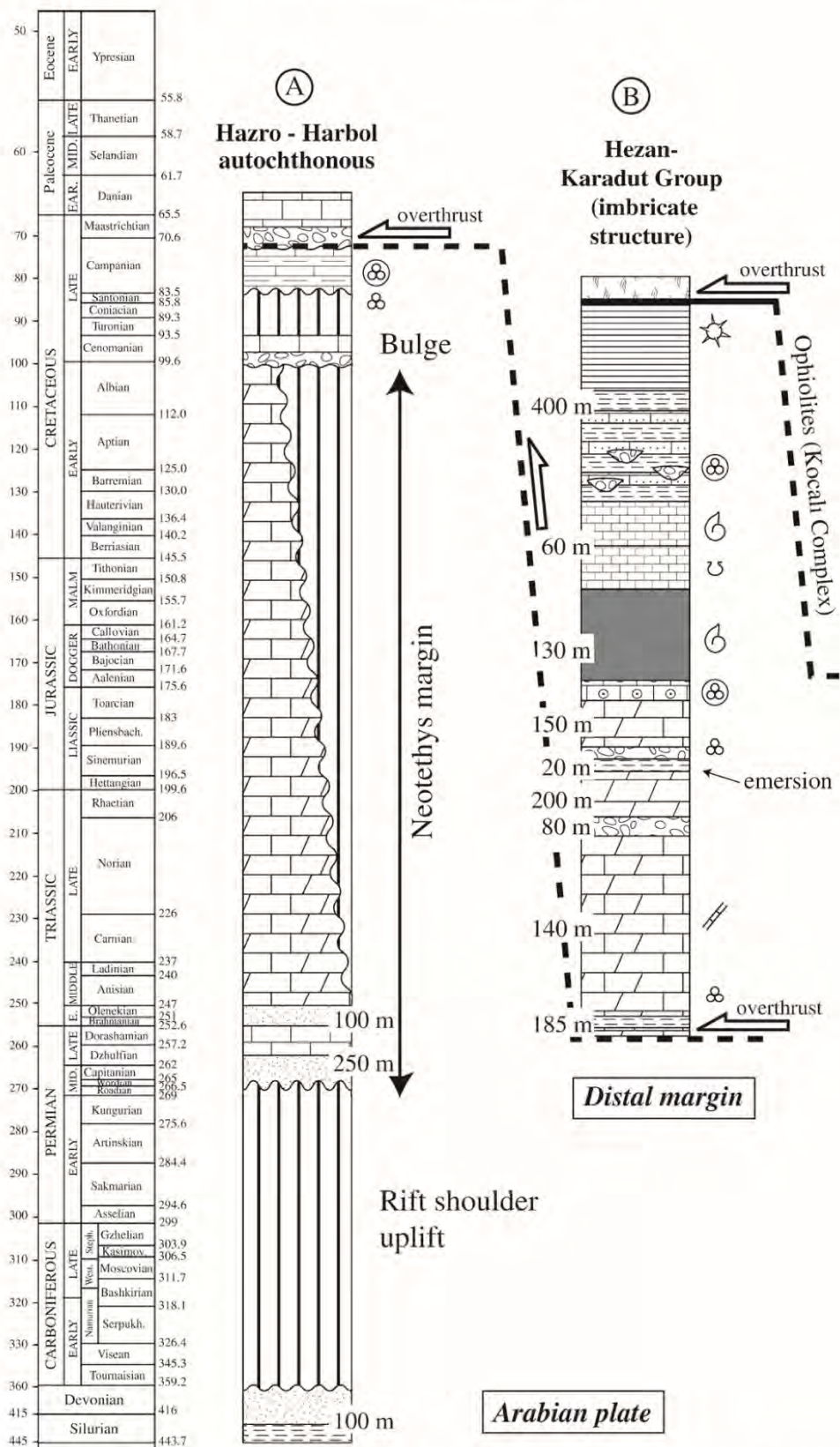


Fig. 12. Arabian plate: synthetic lithostratigraphic sections of the Hazro-Harbol autochthonous (A) and the Hezan-Karadut Group (B). Both sections modified from Fontaine (1981). Key on Fig. 2 and location of the sections on Fig. 5.

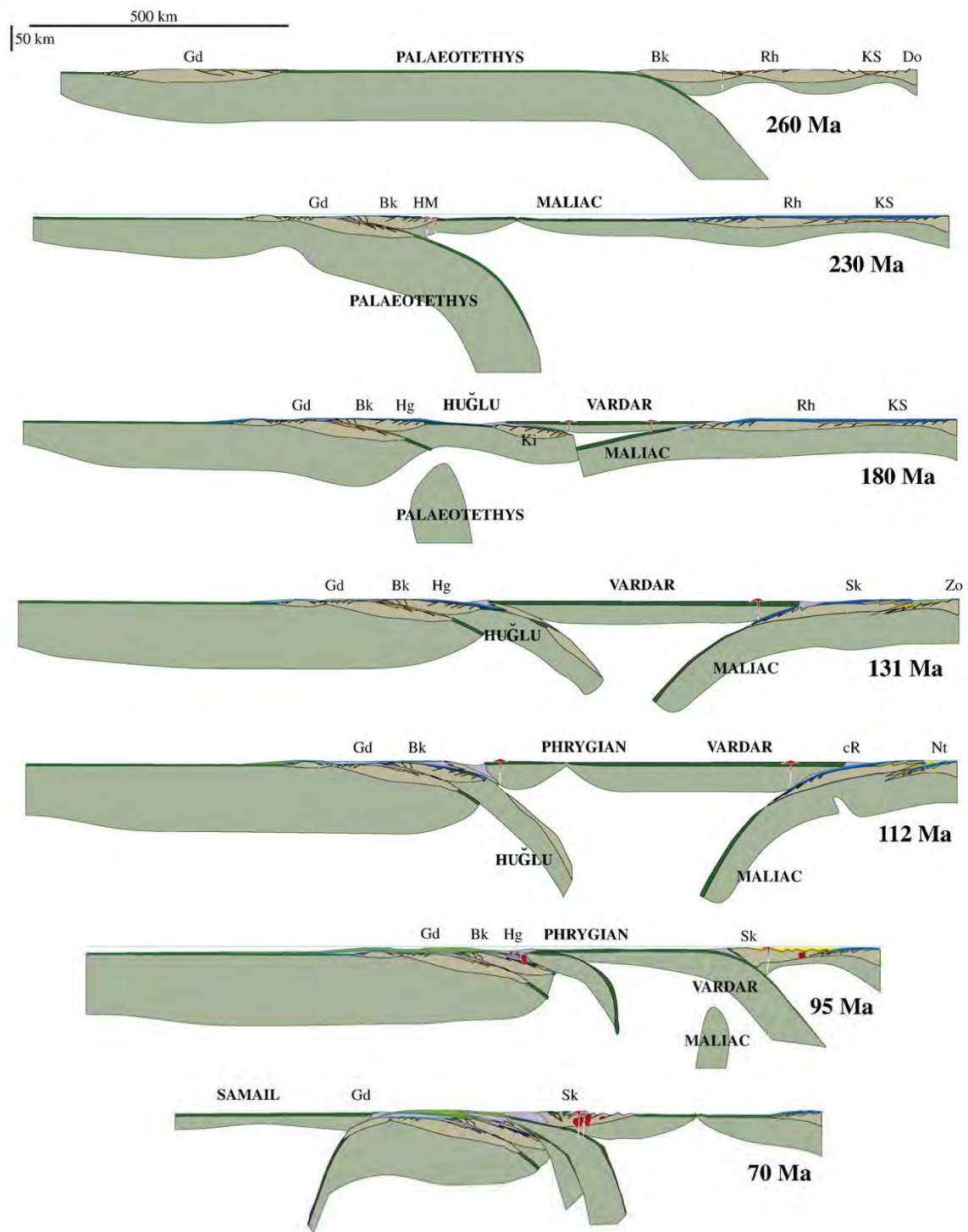


Fig. 13. Late Permian to Eocene palinspastic cross-sections through the East-Mediterranean realm. Traces of the palinspastic sections are on Figs. 14, 15, 16 and 17. Key on Fig. 14.

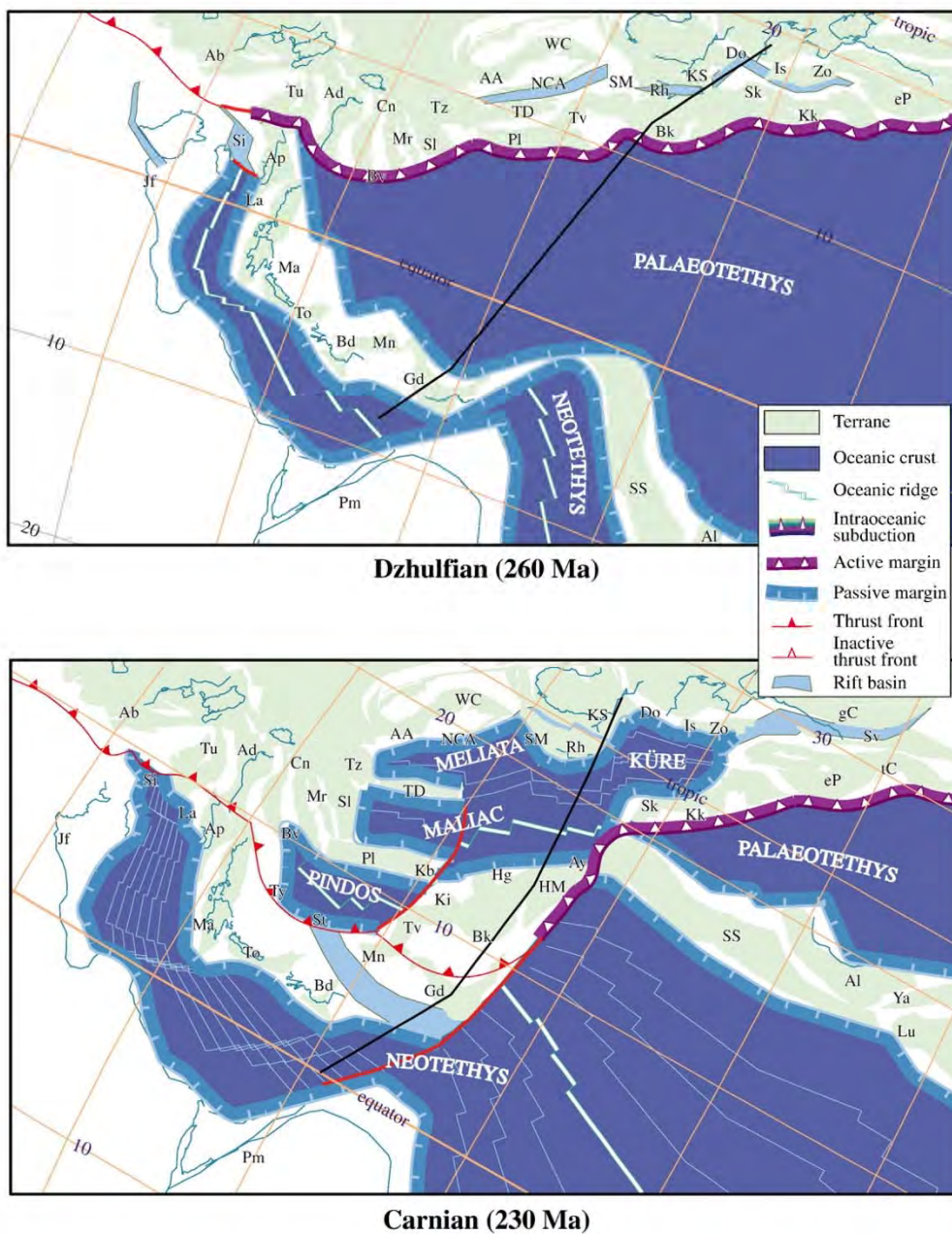
Triassic/Early Jurassic times, and pre-Jurassic thrusting (Gutnic et al., 1979; Akay, 1981; Monod and Akay, 1984). The Cimmerian molasse is mainly characterized by sandstones,

locally associated with plant remains, and conglomerates with rhyolites, lydites, crystalline limestones, quartzites, schists, and quartz as main elements. Possible origins of the pebbles might be

either one of the Paleozoic formations situated between Isparta and Seydişehir within the Taurus domain, their Pan-African basement, or the Anatolian domain, rich in lydites and volcanic formations. Some pelagic limestone and chert pebbles were recently dated and gave Paleozoic/Mesozoic ages, most likely derived from the Paleotethys oceanic series (Moix et al., 2007a).

In the sequence described by Demirtaşlı (1984a,b) (Fig. 9), the Eo-Cimmerian event is followed by the deposition of Lower Jurassic conglomerates and limestones. Locally, the Middle Jurassic seals major thrust faults. The Middle Jurassic to Upper Cretaceous sedimentation is characterized by the development of

thick platform-type deposits in a stable environment. Finally, the Upper Cretaceous–Paleocene rests unconformably over the underlying sequences. It usually starts with a basal conglomerate with blocks ranging in age from the Cretaceous to the Lower Paleozoic. It is followed by shallow water limestones during the Upper Cretaceous passing upward to pelagic limestones during the uppermost Cretaceous. This erosion/deepening event is related to the flexure of the margin. The sedimentation became again neritic (benthic foraminifera) during the Paleocene. Thus, and despite its flexure, this continuous Cretaceous–Paleocene sequence precludes the passage of the ophiolitic nappes over that



part of the Tauric autochthon. A similar conclusion was drawn in the central Tauric series by Baudin et al. (1994).

5.1. The Pan-African Menderes metamorphic Massif

The Menderes Massif is a core complex exhumed in the Late Tertiary (e.g. Bozkurt and Oberhänsli, 2001; Gessner et al., 2001; Işık et al., 2004). The Izmir-Ankara-Erzincan suture bounds it to the north (including the Bornova flysch zone), the Lycian Nappes to the south, and the Afyon zone to the east (Fig. 1). In its southern region, the stratigraphy of the Menderes Massif was subdivided into two tectono-stratigraphic units: the core and the cover units (Şengör, 1984), which are themselves subdivided in more detail (Özgül, 1976; Dora et al., 2001; Özer et al., 2001; Rimmelé et al., 2003). The core series comprise Precambrian to Cambrian gneisses, schists, metagranites, migmatites and metagabbros belonging to the Pan-African basement, plus eclogite and granulite relics (Hetzl and Reischmann, 1996). The cover series comprise schists attributed to the Ordovician to Devonian period, with channels filled by metaconglomerates consisting mainly of quartzite and granite pebbles. They also comprise Permo-Carboniferous metaquartzites with metacarbonates alternation including graphite veins. The latter are followed by Upper Triassic metaconglomerates with quartzite pebbles and quartzite/schist intercalations. The cover series continues with Jurassic to Cretaceous platform-type marbles, including bauxite pockets around the Jurassic–Cretaceous boundary and rudists at the top. The Campanian/Maastrichtian interval is then represented by thin-bedded red pelagic marbles. An ophiolitic metaolistostrome and flysch, containing serpentinites, metagabbros, eclogites, and varied marble blocks embedded in a chlorite/albite schist matrix, was deposited during the Late Maastrichtian/Early Paleocene. Paleocene and Ypresian sediments including Nummulites (Gutnic et al., 1979) were found below the ophiolitic olistostrome (Boray et al., 1973). Both the core and the cover units are tectonically overlain by the Lycian Nappes and the stratigraphic sequence is cut by

Early Triassic leucocratic metagranites and Miocene granitoid stocks (Dora et al., 2001).

In the Sandıklı-Afyon region, the Pan-African basement (Gutnic et al., 1979; Dean and Özgül, 1994; Gürsu and Göncüoğlu, 2001; Gürsu et al., 2004) of probable Menderes affinity yielded ages of 543 ± 7 Ma (Kröner and Şengör, 1990) and 541.3 ± 10.9 Ma (M. Satır in Gürsu and Göncüoğlu, 2006) and is overlain by Cambro-Ordovician series. These series are unconformably covered by Liassic clastics grading to a Middle Jurassic carbonate platform. We interpret this contact as a typical Eo-Cimmerian unconformity, thus confirming the Tauric affinity of the Menderes Massif and suggesting that large areas of the massif may have been totally eroded during the Triassic period. Some “cover series” of the Menderes Massif (e.g. Çarık göl and Tekkeçal Tepe sections of Sarp, 1976) are quite different and are characterized by the Late Cretaceous ophiolite obduction. Other units also include Triassic magmatic events (Dora et al., 2001). Therefore, we do not regard these “cover series” as Menderes-Tauric “sedimentary cover” of the Pan-African basement, but as slivers of metamorphic Anatolian Nappes at the base of the Lycian Nappes.

6. The South-Taurides exotic units (Fig. 11)

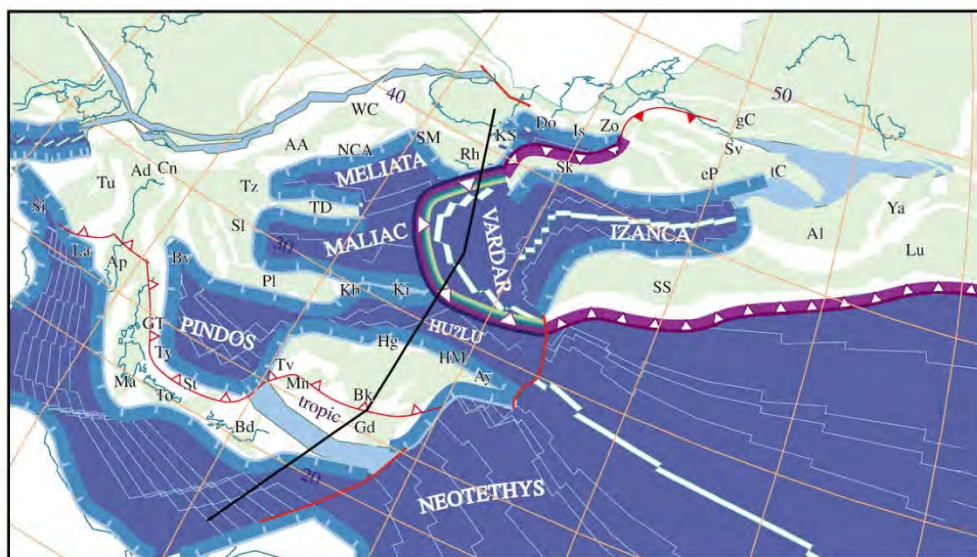
The Mersin Ophiolitic Complex (Demirtaşlı et al., 1984; Pampal, 1987; Parlak, 1996; Masset and Moix, 2004; Özer et al., 2004; Parlak and Robertson, 2004; Moix et al., 2007a,b) is a key point in the development of the new South-Taurides exotic units (Fig. 1). Other key units are found in the Pozantı–Karsantı–Faraşa Massif (Demirtaşlı et al., 1984; Tekeli et al., 1984; Dilek and Whitney, 1997; Dilek et al., 1999), the Antalya Nappes (Lefèvre, 1967; Gutnic et al., 1979; Marcoux, 1987a,b) (Fig. 11/A–G) and the Troodos-Mamonia Complex in Cyprus (Lapierre, 1975; Robertson, 1977; Robertson and Woodcock, 1979; Swarbrick and Robertson, 1980; Malpas et al., 1993; Riquhart and Banner, 1994). This new domain is made of exotic elements of the Anatolian terrane now found south of the Taurus terrane. They are

Fig. 14. Dzhulfian (260 Ma) and Carnian (230 Ma) paleotectonic reconstructions. As the Paleotethys subduction came to a final stage, slab roll-back along its northern margin accelerated and was marked by the opening of oceanic back-arc basins. There was still enough space available to open successive back-arc basins south of Meliata, the Maliac, then Pindos basin, before the final closure of Paleotethys in Carnian or Early Norian times. A detailed account of these opening is given in Stampfli and Kozur (2006). To the east, back-arc rifting was very active also in the Caucasus (Svanetia) and north Iran (Agh-Darband). The Nilüfer seamount was colliding with the Karakaya fore-arc basin, and both soon collided with the Cimmerian terranes. This induced soon after the closing of the Küre back-arc along a south-directed subduction. The East-Mediterranean part of the Neotethys was still spreading. A position around 10°N of the Taurus and Anatolian terranes is in agreement with Théveniaut et al. (1993) for the Bakırlı section. The Greater Apulia-Taurus Cimmerian block is being separated from the Beydağları. In the Late Triassic the Paleotethys was completely closed from Greece to the Himalayas. In Iran, this closing generated the development of a large molassic basin (Shemshak) followed by subduction progradation to the northern side of Neotethys, and the onset of subduction-related volcanism in the Sanandaj-Sirjan and Lut blocks, already in the Late Triassic. On an Anatolian-Tauric transect, there was no subduction progradation and the spreading in the Pindos back-arc stopped; the Eo-Cimmerian orogenic zone was rapidly eroded and covered by large carbonate platforms. Key areas: AA, Austro-Alpine; Ab, Alboran; Ad, Adria s. str.; Al, Alborz; Ap, Apulia s. str.; Ay, Antalya; Bd, Beydağları; Bc, Betic; Bf, Baft ophiolite; BH, Baçr-Bassit-Hatay ophiolites; Bk, Bozdağ-Konya fore-arc; Br, Briançonnais; Bu, Bucovinian; Bv, Budva; Ca, Calabria; cB, central Bosnia; Cn, Carnic; Da, Dacides; Db, Dent-Blanche; Do, Dobrogea; EBS, Eastern Black Sea; El, Elazığ-Guleman ophiolites and arc; eP, east Pontides; Er, Eratosthen; gC, great Caucasus; Gd, Geyikdağ-Anamas-Akseki; GT, Gavrovo-Tripolitza; Hg, Huğlu-Boyalı Tepe; hK, high Karst; HM, Huğlu-Mersin; Is, Istanbul; Jf, Jeffara rift; Kb, Karaburun; Ki, Kırşehir; Kk, Karakaya fore-arc; Ko, Korab; Kr, Kermanshah ophiolite; KS, Kotel-Strandja rift; Ky, Kabylies; La, Lagonegro; Li, Ligurian; Lu, Lut; Ma, Mani; Mk, Mangyshlak rift; Mm, Mamonia accretionary Complex; Mn, Menderes; MP, Mersin-Pozantı ophiolites; Mr, Mrzlevodice fore-arc; NC, North Caspian; NCA, North Calcareous Alps; Nn, Nain ophiolite; Ny, Neyriz ophiolite; Oz, Öztal-Silvretta; Pa, Panormides; Pi, Piemontais; Pl, Pelagonian; Pm, Palmyra rift; Pn, Pienniny rift; Rh, Rhodope; Ri, Rif internal; sB, sub-Betic rim basin; sC, Scythian platform; SC, South Caspian; Si, Sicilian; Sl, Slavonian; Sk, Sakarya; SM, Serbo-Macedonian; SS, Sanandaj-Sirjan; St, Sitia E-Crete; Sv, Svanetia rift; Sz, Sabzevar ophiolite; tC, trans-Caucasus; TD, Transdanubian; Tk, Tuarkyr; To, Talea Ori; Tp, Troodos ophiolite; Tu, Tuscan; Tv, Tavas Nappe; Ty, Tyros fore-arc; Tz, Tizia; UM, Umbria-Marches; Va, Valais trough; WBS, Western Black Sea; WC, West Carpathian; Ya, Yazd; Zo, Zonguldak.

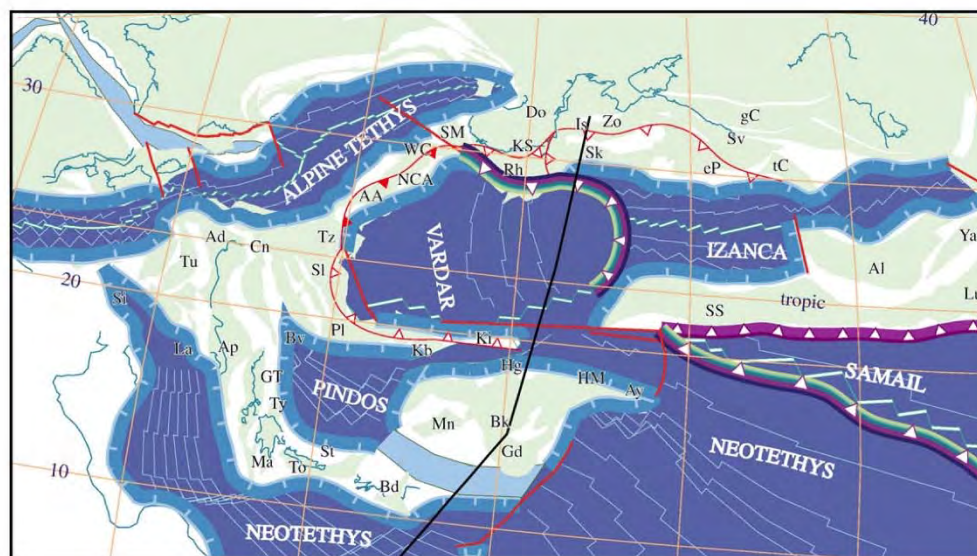
juxtaposed to elements derived from the Neotethys/Taurus terrane, and emplaced onto the Taurus southern margin (Mersin) or Beydağları domain (Antalya) in the Paleocene (Fig. 1). The main Anatolian elements are represented by sequences belonging to the northern margin of the Anatolian terrane, i.e. the Triassic syn-rift volcanic event (Huğlu-type series) and the Late Cretaceous obducted ophiolitic sequences (Fig. 5). Tauric elements are represented by Eo-Cimmerian flysch-like sequences including Paleotethyan material (Moix et al., 2007a) intercalated in Neotethyan series. This mixture of Anatolian and Tauric elements, emplaced onto more external platforms, is locally sealed by

nummulitic limestones like in the Egridir region (Gutnic et al., 1979).

Similar mélanges are found in Cyprus (Mamonia Complex) and Syria (Baër-Basit). Therefore, an arc-like accretionary front joined at some time the southern Taurus domain to the Arabian promontory, cutting across the Neotethyan East-Mediterranean Basin (see discussion below). As in the Anatolian domain, the peri-Arabian ophiolitic obduction is sealed by a Maastrichtian platform, whereas the Mersin-Antalya-Cyprus accretionary domain continued its westward migration at least until the Paleocene. Closing of the accretionary orocline on itself took



Toarcian (180 Ma)



Hauterivian (131 Ma)

place during the Eocene–Miocene interval, generating arc magmatism to the north (e.g. Maden Complex) (Aktaş and Robertson, 1984; Perinçek and Kozlu, 1984; Yazgan, 1984; Bergougnan, 1987; Robertson et al., 2006) and finally juxtaposing peri-Arabian elements to Anatolian elements around the Arabian promontory. As a consequence, the Tauric and South-Taurides elements have been nearly totally subducted or tectonically eroded during the collision processes in that region. The suture zone between these two domains is also found in Cyprus between the Kyrenia Range (Taurus terrane) and the Troodos-Mamonia Complex (Baroz, 1976, 1980; Robertson and Woodcock, 1986).

7. The peri-Arabian domain (Fig. 12)

In eastern Turkey, the peri-Arabian domain (Fig. 1) is represented by the Hazro-Harbol autochthonous overthrust by the Hezan-Karadut imbricate structures (Fontaine, 1981; Bergougnan, 1987; Fontaine et al., 1989) (Fig. 12A–B) and by the Kızıldağ ophiolite in Hatay (Ricou, 1971; Pişkin et al., 1986; Robertson, 1986; Dilek and Delaloye, 1992; Dilek et al., 1999). Elsewhere, it is also represented by the Baçr-Basit ophiolitic massif in Syria (Lapierre and Parrot, 1972; Delaune-Mayère et al., 1977; Parrot, 1980; Delaune-Mayère, 1984; Pişkin et al., 1986; Al-Riyami and Robertson, 2002; Al-Riyami et al., 2002) and the Samail ophiolite in Oman (Glennie et al., 1974; Béhenneç, 1988; Béhenneç et al., 1990; Le Métour et al., 1995; Pilleveit et al., 1997; Stampfli et al., 2001; Stampfli and Borel, 2002). Since the Permian, the peri-Arabian domain represents the northern Gondwana passive margin after the drifting of the Cimmerian blocks and concomitant opening of Neotethys (Al-Belushi et al., 1996; Angiolini et al., 2003a,b). This segment of the southern Neotethys Ocean passive margin is characterized by Lower Permian syn-rift sequences and volcanics. These series are found in Sicily, Greece, Iran, Oman, the Tethys Himalaya, and north of Australia (Catalano et al., 1991, 1992; Stampfli et al., 2001; Langhi and Borel, 2005; Kock et al., 2007), witnessing a simultaneous opening of the Neotethys all along the Gondwana border. A large rift shoulder

uplift (up to 2 km of erosion) was followed by a Middle to Late Permian transgression onto Pan-African Paleozoic or even Neoproterozoic sequences (Gass et al., 1990; Béhenneç et al., 1993). In Hazro-Harbol (Fig. 12A), the Middle Permian is transgressive onto the Early Carboniferous. Thereafter, a passive margin sequence, dominated by carbonates, lasted until the Late Cretaceous obduction of the Samail-type ophiolitic nappes, found in Oman, Iran, Iraq, Syria and Turkey (Fig. 5). These were sealed by a short lived Maastrichtian platform. In Oman, part of Turkey and Syria the nappes were never re-displaced during the Alpine collisional events. On the contrary, in the Iranian and Iraqian Zagros and southeast Turkey, the Cretaceous ophiolites and parts of their Gondwanan basement are included in the Tertiary Alpine Nappes.

8. Discussion

The Turkish segment of the Tethysides is subdivided into several terranes, separated by complex suture zones of different ages. Before the mainly north–south displacements marking the Late Cretaceous and Cenozoic period, the different terranes of Turkey underwent large lateral displacements in a roughly east–west direction since the Triassic. This resulted in the duplication of major suture zones (Stampfli and Borel, 2004). Major strike–slip movements during the Variscan orogenic cycle created the first juxtaposition of terranes. These were subsequently dispersed during the collapse of the Variscan cordillera and opening of Triassic back-arc basins (e.g. Küre back-arc in Stampfli and Kozur, 2006). In Late Triassic times, the southernmost Eurasia-derived block (Anatolian terrane) was assembled by the Cimmerian collage with Gondwana-derived terranes (Cimmerian terranes: Greater Apulia, Taurus terranes). Some terranes were finally emplaced only during the Late Cretaceous–Early Tertiary, such as the Antalya-Cyprus exotic domain derived from the Lycian-Anatolian-Samail obduction front, and the Apulia-derived Beydağları domain. The last juxtaposition was realized during the Alpine north–south shortening. The east–west shortening (2000 km) in the Tethyan region is in direct relation to the opening of the Central Atlantic Ocean. This can be measured

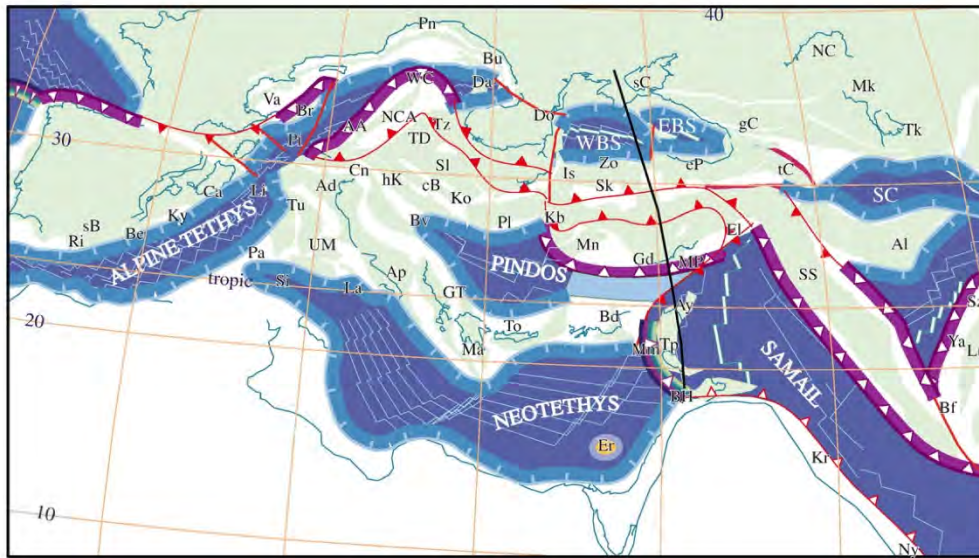
Fig. 15. Toarcian (180 Ma) and Hauterivian (131 Ma) palaeotectonic reconstructions. Diverging slab roll-back, both in Küre and in the Neotethys, induced the opening of the Izmir-Ankara Ocean. This opening prograded eastward up to the south Caspian region in Middle Jurassic times. The Central Atlantic rift widened and spreading started in the Toarcian (Steiner et al., 1998), the Alpine Tethys rift started to spread in Bajocian times, finally breaking the Pangea super-continent. The opening of the Vardar corresponds to the subduction progradation from the Küre domain toward the Maliac domain. The roll-back of the Maliac sea-floor generated westward spreading of the Vardar Basin in a scenario of intra-oceanic subduction, the Vardar progressively replacing in situ the Maliac-Meliata Ocean. The closure of the Küre Ocean induced a collision in the Black Sea domain and around the Rhodope promontory. During the Oxfordian, spreading in the Alpine Tethys Ocean reached the Carpathian domain. In the process, Moesia was detached from Europe by only a few hundred kilometers. The Küre Ocean was closed and the collision of its arc–trench system with the Rhodope was causing the first phases of the Balkanic orogeny accompanied by inversion of former rift zones. The Vardar arc–trench system was soon to collide with the Pelagonian–Dinaric landmass. This east–west shortening in the Maliac–Vardar domain was due also to the anti-clockwise rotation of Gondwana with respect to Europe, inducing the inception of an intra-oceanic subduction zone in the Vardar. Differential movement between Africa and India reactivated a Neotethys former N–S transform, separating the future Indian plate from Africa. Along this feature, intra-oceanic subduction took place and was at the origin of the Samail Ocean. In the Valanginian–Hauterivian, accelerating anti-clockwise rotation of Gondwana was responsible for the obduction of part of the Vardar mid-ocean ridge system onto the Pelagonian, Dinaric and Tizia blocks. Simultaneously, the Vardar arc–trench system collided with the northern margin of Meliata, detaching the future North Calcareous Alps domain from its basement (internal Austroalpine). Collision of the Vardar arc–trench system continued also in the Balkans, where parts of the Rhodope cover and basement were transported northward and thrust onto the Nish-Troyan trough (Boney and Stampfli, 2003, 2008). The major changes affecting the Neotethyan domain brought to an end the opening of the Izmir-Ankara Ocean (south Caspian) back-arc basin system. Then, the Izmir-Ankara slab started retreating eastward inducing the opening of a new supra-subduction spreading centre north of the Anatolian plate (Phrygian Ocean). This system was linked eastward with the opening supra-subduction Samail Ocean. Key on Fig. 14.

precisely through the magnetic anomalies of the Atlantic, and it is a key factor for any plate tectonic reconstruction of that area (e.g. Dewey et al., 1989).

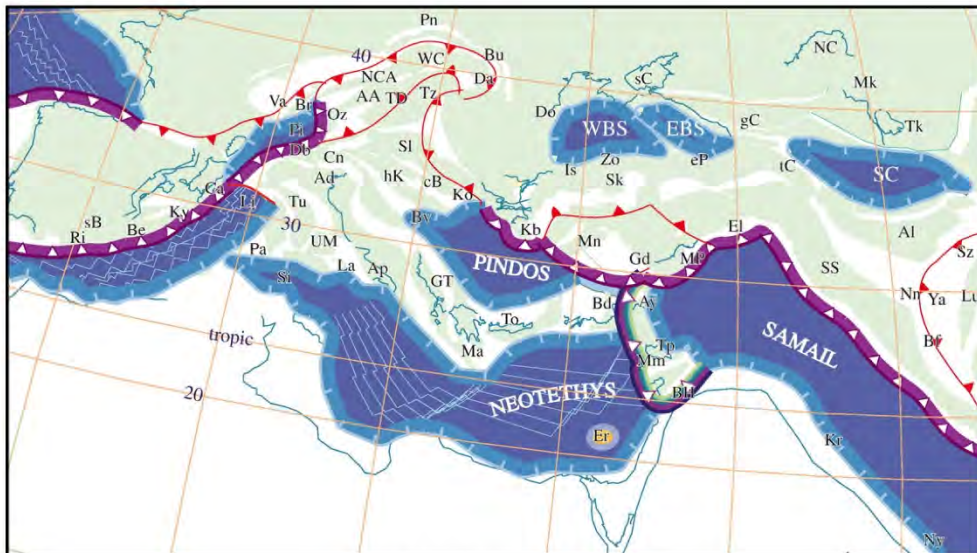
The following are some of the main points regarding the plate tectonic evolution of the region:

- (1) The Taurus terrane was detached from Gondwana together with other Cimmerian blocks in Permian times during the opening of the Neotethys and the East-Mediterranean oceans. Permian pelagic material found in Sicily (Kozur, 1990, 1991, 1995b; Catalano et al., 1991, 1992) were also found as exotic blocks at the base of the Mersin mélanges. Other important geological and geophysical arguments for this Permian opening of the Neotethys/East-Mediterranean Basin have been recently published (Stampfli et al., 2001; Finetti, 2005; Kock et al., 2007);
- (2) The Tauric block collided during the Middle Triassic with the Anatolian terrane, thus, sea-floor spreading in the East-Mediterranean Basin ended in the Middle Triassic or in the Carnian. From the Late Triassic onward, the Taurus domain and the Anatolian terrane were again part of the African plate. It is only since the Eocene–Miocene that these terranes were progressively detached, through subduction, from the African plate and accreted to Laurasia. It means that the wander path of the Tauric-Anatolian plate from the Triassic to the Miocene was the same as Africa;
- (3) In the north, the Pontides domain was detached from Eurasia in latest Early Triassic through the opening of the Küre Ocean, the closure of which took place in Late Triassic–Middle Jurassic times (Stampfli and Kozur, 2006). From that time until the Late Cretaceous, the Pontides were part of Eurasia. During the Cenomanian, they were detached again from Laurasia through the opening of the Black Sea basins. This opening was short lived, and from the Paleocene onward, the Pontides wander path is similar to that of Eurasia;
- (4) The southern margin of the Izmir-Ankara Ocean is not known in Turkey and is regarded as an element that may have left this region. The Anatolides northern margin is usually regarded as such, but, it was not due south of the Pontides when the Izmir-Ankara Ocean opened in the Liassic, the separation between the two domains being on the order of 2000 km in an east–west direction (Stampfli and Borel, 2002). Thus, the northern margin of Anatolia is not the conjugate margin of the southern Pontides margin. On the contrary, the Anatolian northern margin is a clear Triassic margin, not Jurassic, from which many segments are known in the Anatolian Nappes. Therefore, the southern margin of the Izmir-Ankara Ocean must have been either totally subducted or displaced laterally. We regard the Sanandaj-Sirjan domain of Iran and eastern Turkey as representing part of that margin, displaced eastward during the closing of the Izmir-Ankara Ocean and the opening of the peri-central Iranian microplate ocean in the Cretaceous;
- (5) The Cyprus-Baër-Bassit domain and their ophiolites were mainly derived from an intra-oceanic subduction zone inside the large Neotethys Ocean, their supra-subduction geochemical character being quite clear (Pearce et al., 1984). This domain extends eastward to the peri-Arabian ophiolites up to Oman. Guyots of Triassic age are found at their sole in exotic mélanges, together with Permian to Cretaceous pelagic sequences derived from the Neotethys sea-floor (e.g. Pilleveit et al., 1997). These ophiolites were first obducted onto the Arabian plate, at that time quite far from the Tauric-Anatolian domain. Then, during the Late Tertiary, the Arabian promontory was brought in contact with this domain. This was done during the closing of a remnant Samail Ocean, inducing the development of a Cenozoic arc along its northern margin, found from Turkey (e.g. Maden-type sequence) to Iran, and creating the Zagros orogen;
- (6) In the Eocene, the Tauric-Anatolian plate became a free moving plate, whereas the Greater Apulian domain (e.g. external zones of the Hellenides) was still moving with Africa. The last remnant of that, i.e. the Puglia-Adria part of Apulia in Italy, is still attached to Africa. An east to west diachronous transformation of the East-Mediterranean northern margin from passive to active is therefore demonstrated. The easternmost promontory of Greater Apulia is represented by the Beydağları domain of southwest Turkey. A collision of the Beydağları promontory with the Taurus domain was accompanied by a flysch basin found along the northern side of the Beydağları (Gutnic et al., 1979). This indicates a clear re-displacement of the ophiolitic Lycian Nappes onto the Beydağları platform in Miocene times. The presence of a migrating flexural bulge and development of a foreland basin show that the Tauric-Anatolian domain and Beydağları-Apulian domain were separated at least by a few hundred kilometers. We put this separation in the Middle Carnian (Kozur, 2000a);
- (7) The Late Cretaceous partial closure of the remnant eastern Huğlu-Pindos Ocean is witnessed by the first Pindos flysch (Neumann and Zacher, 1996; Wagreich, 1996), in which chrome-spinels have been found (Faupl et al., 2006). The Pindos Basin in the Cretaceous was bordered by major carbonate platforms to the south (Ionian-Mani), to the west (Karst-Budva), and to the north (Pelagonia-Parnassos). Therefore, flysch deposits can only come from the east (Anatolian-Tauric domain), from an orogenic domain related to the emplacement of the Lycian ophiolites (Bemoulli et al., 1974). The Pindos s. str. basin was finally closed only in the Oligocene (Richter et al., 1993; Degnan and Robertson, 1998).

Elements being subducted in space and time along the Eurasian margin are of continental or oceanic types. In the Cenozoic, oceanic domains such as the Pindos basin or the remnant Samail Ocean and continental elements such as the Beydağları or Arabian promontories were subducted simultaneously. Oceanic elements accompanied by slab roll-back induced major extensional events and formation of core



Maastrichtian (70 Ma)



Lutetian (48 Ma)

Fig. 17. Maastrichtian (70 Ma) and Lutetian (48 Ma) paleotectonic reconstructions. In the Maastrichtian, continued counterclockwise rotation of Africa was responsible for the obduction of the Samail Ocean onto Arabia (from Oman to Syria), and of the Phrygian Ocean onto the Anatolian block. A Maastrichtian platform seals the obduction in both areas; however, some ophiolitic massifs were re-displaced during the Paleocene and finally emplaced along the south-Tauric margin up to the eastern Beydağları. This resulted in the mixing of Neotethyan, Tauric and Anatolian elements as exotic material (e.g. Antalya, Mersin and Mamonia) at the base of the advancing Cyprus arc. In the eastern Taurus Mountains, the obduction passed over the Anatolian-Tauric plate before to reach the Neotethys. East-west shortening was still very active in the Alpine and Vardar domains. The latter is now totally closed, whereas roll-back of the remnant Phrygian slab allows the opening of the East Black Sea back-arc basin. By Eocene times, the Anatolian-Tauric plate was becoming a free moving entity, pulled westward by roll-back in the Pindos Ocean. Then most Turkish crustal elements were detached from their lithospheric root to form an orogenic complex. The Antalya (Pamphylian) suture zone is going to be the result of the closing of the Cyprus back-arc domain. This resulted in the juxtaposing of peri-Arabian ophiolites to Anatolian derived ophiolites in eastern Turkey. Key on Fig. 14.

centered on the Turkish area. For a larger picture, the reader is referred to the above-cited publications. These models differ from models that have been proposed so far, which are essentially continental drift models. These are constructed on

the basis of field observations and compiled literature about the whole Tethyan realm and are inserted into plate tectonics frameworks in which plate movements are constrained in space and time at a global scale.

9. Conclusions

The detailed study of exotic material found associated to the Mersin ophiolite (Masset and Moix, 2004; Moix et al., 2007b) led to the discovery of mixed origins for this material. Some blocks or series are clearly part of a passive margin formerly located north of the Anatolian domain and whose remnants are also found in other places such as the Huğlu series in the Beyşehir-Hoyran Nappes. This margin is interpreted as emerging from the collapse of the former Variscan cordillera and opening of major back-arc type basins along the northern active margin of the Paleotethys during the Triassic and can be correlated with similar events in Greece and in Iran. Other types of exotic material clearly do not belong to this passive margin sequence, such as pelagic Carboniferous and Permian sediments, but to sequences related to the Paleotethys suture zone, and reworked as major olistostromes in the Neotethys basin during the Eo-Cimmerian orogenic event. From these observations, it became necessary to develop a coherent model of terrane definition and dispersion for the Turkish and surrounding areas between the Late Paleozoic and the Tertiary. Thus, we have re-defined several terranes/domains whose geological history is clearly different through space and time; they consist of: (1) the Pontides domain; (2) the Anatolian terrane; (3) the Taurus terrane; (4) the south Taurides exotic units and (5) the peri-Arabian domain. These terranes, characterized by contrasting stratigraphy and geodynamic evolution, can be easily replaced in the larger paleotectonic frame of the western Tethyan realm. The main point we tried to convey is that the present juxtaposition of these terranes is far from their original places. This is due to major east–west translation and shortening of the Tethyan space in the Mesozoic, where the Beydağları, Taurus and Arabian domains moved with Gondwana/Africa, whereas the wander path of the Pontides is similar to Eurasia. In between, the Anatolian terrane was detached from Eurasia to be accreted to the Taurus Cimmerian domain in the Late Triassic and then moved with Gondwana. The detailed studies of the passive/active margins of these terranes in space and time is the key element of this new geodynamic scheme, as well as a plate tectonic reconstruction model, departing from the continental drift models used so far.

Detailed field studies carried out since the 1960's are at the base of these new proposals. Although modern analytical techniques and mainly absolute dating methods play an important role in the deciphering of a complicated geological puzzle that Turkey and surrounding areas represent. Only further classical field studies will help ameliorate the proposed models. Vast areas in eastern Turkey, Iraq, and western Iran are still under-explored, and a better investigation of these regions is necessary to go further in the understanding of the central Tethyan realm.

Acknowledgements

P.M. would like to express his thanks to J. Marcoux and L. Krystyn for the shared information and stimulating discussions, especially during field work carried out in the Taurides. The authors are very obliged to the Institute of Geology and Paleontology, Lausanne University, Switzerland for making available laboratory facilities. P.M. is also very grateful to Shell International

Exploration and Production for the financial support. We also want to express here our recognition for the excellent pioneering work done by a generation of mainly French geologists who deciphered the geology of Turkey in 1960 s–80's, and extend this to the new generation of excellent Turkish geologists who carry out systematic field work in an on-going effort to better understand the geology of this fascinating part of the Tethyan realm. The manuscript has benefited greatly from thorough reviews by A.I. Okay and an anonymous reviewer. E. Heydari and R. Sorkhabi (guest editors) are gratefully acknowledged for their stimulating reviews and comments.

References

- Abdüsselamoğlu, M.S., 1959. Geology of the Almacıkdağı and the region between Mudurnu and Göynük. *Istanbul Üniversitesi Fen Fakültesi Monografileri* 14, 1–94.
- Akay, E., 1981. Beyşehir yöresinde (Orta Toroslar) olası Alt Kimmeriyen dağoluşumu izleri. *Türkiye Jeoloji Kurumu Bülteni* 24, 25–29 (in Turkish, with English abstract).
- Aktaş, G., Robertson, A.H.F., 1984. The Maden Complex, SE Turkey: evolution of a Neotethyan active margin. In: Dixon, J.E., Robertson, A.H.F. (Eds.), *The geological evolution of the eastern Mediterranean*. Geological Society of London Special Publication, vol. 17, pp. 375–402.
- Al-Belushi, J., Glennie, K.W., Williams, B.P.J., 1996. Permo-Carboniferous glaciogenic Al Khlata Formation, Oman: a new hypothesis for origin of its glaciation. *GeoArabia* 1, 389–403.
- Al-Riyami, K., Robertson, A.H.F., 2002. Mesozoic sedimentary and magmatic evolution of the Arabian continental margin, northern Syria: evidence from the Baër-Bassit Mélange. *Geological Magazine* 139 (4), 395–420.
- Al-Riyami, K., Robertson, A.H.F., Dixon, J., Xenophontos, C., 2002. Origin and emplacement of the Late Cretaceous Baër-Bassit ophiolite and its metamorphic sole in NW Syria. *Lithos* 65 (1–2), 225–260.
- Altner, D., 1981. Recherches stratigraphiques et micropaléontologiques dans le Taurus Oriental au NW de Pınarbaşı (Turquie). PhD Thesis, Université de Genève, 450 pp.
- Altner, D., Koçyiğit, A., Farinacci, A., Nicosia, U., Conti, M.A., 1991. Jurassic, Lower Cretaceous stratigraphy and paleogeographic evolution of the southern part of northwestern Anatolia. *Geologica Romana* 18, 13–80.
- Andrew, T., 2003. Mesozoic to Early Tertiary tectonic-sedimentary evolution of the Northern Neotethys Ocean: evidence from the Beyşehir-Hoyran-Hadım Nappes, S.W. Turkey. PhD Thesis, University of Edinburgh. College of Science and Engineering. School of GeoSciences, Edinburgh, 217 pp.
- Andrew, T., Robertson, A.H.F., 2002. The Beyşehir-Hoyran-Hadım Nappes: genesis and emplacement of Mesozoic marginal and oceanic units of the northern Neotethys in southern Turkey. *Journal of the Geological Society of London* 159, 529–543.
- Angiolini, L., Balini, M., Garzanti, E., Nicora, A., Tintori, A., 2003a. Gondwanan deglaciation and opening of Neotethys: the Al Khlata and Saiwan Formations of Interior Oman. *Palaeogeography, Palaeoclimatology, Palaeoecology* 196 (1–2), 99–123.
- Angiolini, L., Balini, M., Garzanti, E., Nicora, A., Tintori, A., Crasquin-Soleau, S., Muttoni, G., 2003b. Permian climatic and paleogeographic changes in Northern Gondwana: the Khuff Formation of Interior Oman. *Palaeogeography, Palaeoclimatology, Palaeoecology* 191 (3–4), 269–300.
- Armijo, R., Meycr, B., Hubert, A., Barka, A., 1999. Westward propagation of the North Anatolian fault into the northern Aegean: Timing and kinematics. *Geology* 27 (3), 267–270.
- Bagheri, S., Kozur, H.W., Stampfli, G.M., 2003. The Paleotethys suture in NE Iran and its displaced continuation in Central Iran (Anarak-Nakhlak area). 22nd IAS Meeting, International Association of Sedimentology. Zbornik radova proceedings, Opatija, Croatia. pp. 9.
- Bailey, E.B., McCallien, W.J., 1950. The Ankara Mélange and the Anatolian Thrust. *Nature* 166, 938–940.

- Barka, A.A., 1992. The North Anatolian fault zone. *Annales Tectonicae* VI, 164–195 (Special Issue).
- Baroz, F., 1976. Caracteres petrographiques et geochemiques des deux series volcaniques potassiques du Pentadaktylos (Chypre). *Sciences de la Terre, Nancy* 20 (3), 295–332.
- Baroz, F., 1980. Volcanism and continent–island arc collision in the Pentadaktylos Range, Cyprus. In: Panayiotou, A. (Ed.), *Ophiolites; Proceedings, International ophiolite symposium. Republic of Cyprus, Ministry of Agriculture and Natural Resources, Geological Survey Department, Nicosia, Cyprus*, pp. 73–85.
- Baud, A., Stampfli, G.M., 1989. Tectonogenesis and evolution of a segment of the Cimmerides: the volcano-sedimentary Triassic of Aghdarban (Kopet-Dagh, North-East Iran). In: Şengör, A.M.C. (Ed.), *Tectonic evolution of the Tethyan region. Kluwer Academic Publishers, Amsterdam*, pp. 265–275.
- Baudin, F., Monod, O., Bégouën, V., Laggoun-Defarge, F., Person, A., 1994. Caractérisation et diagenèse de la matière organique du Jurassique supérieur du Taurus occidental (Turquie méridionale). Reconstitution paléoenvironnementale et conséquences tectoniques. *Bulletin de la Société Géologique de France* 165 (2), 134–145.
- Beccaletto, L., 2004. Geology, correlations, and geodynamic evolution of the Biga peninsula (NW Turkey). *Mémoires de Géologie (Lausanne)* 43, 145 pp.
- Beccaletto, L., Jenny, C., 2004. Geology and correlation of the Ezine zone: a Rhodope fragment in NW Turkey? *Turkish Journal of Earth Sciences* 13 (2), 145–176.
- Beccaletto, L., Bartolini, A.C., Martini, R., Hochuli, P.A., Kozur, H.W., 2005. Biostratigraphic data from the Çetmi Melange, northwest Turkey: palaeogeographic and tectonic implications. *Palaeogeography, Palaeoclimatology, Palaeoecology* 221, 215–244.
- Béchehennec, F., 1988. Géologie des nappes Hawasina dans les parties orientale et centrale des montagnes d'Oman. *Mémoires du Bureau de Recherches Géologiques et Minières Orléans* 127, 474 pp.
- Béchehennec, F., Le Métour, J., Platel, J.P., Roger, J., 1993. Geological map of the Sultanate of Oman. Explanatory notes. Ministry of Petroleum and Minerals, Directorate General of Minerals, Sultanate of Oman, Muscat, 93 pp.
- Béchehennec, F., Le Métour, J., Rabu, D., Bourdillon-de-Grissac, C., de Wever, P., Beurrier, M., Villey, M., 1990. The Hawasina Nappes: stratigraphy, palaeogeography and structural evolution of a fragment of the south-Tethyan passive continental margin. In: Robertson, A.H.F., Searle, M.P., Ries, A.C. (Eds.), *The Geology and Tectonics of the Oman Mountains. Geological Society of London Special Publication*, vol. 49, pp. 213–224.
- Bergougnan, H., 1975. Dispositif des ophiolites nord-est anatoliennes, origine des nappes ophiolitiques et sud-pontiques, jeu de la faille nord-anatolienne. *Comptes Rendus de l'Académie des Sciences de Paris, Série II* 281, 107–110.
- Bergougnan, H., 1987. Etudes géologiques dans l'Est-Anatolien. PhD Thesis, Université Pierre et Marie Curie, Paris VI, 606 pp.
- Bernoulli, D., de Graciansky, P.-C., Monod, O., 1974. The extension of the Lycian Nappes (SW Turkey) into the southeastern Aegean Islands. *Eclogae Geologicae Helveticae* 67 (1), 39–90.
- Bingöl, E., Akyürek, B., Korkmaz, B., 1975. Geology of the Biga Peninsula and some characteristics of the Karakaya blocky series. In: Doyuran, S. (Ed.), *Papers of congress of Earth Sciences on the occasion of the 50th anniversary of the Turkish Republic. Maden Tetkik ve Arama Enstitüsü, Ankara*, pp. 71–77.
- Bonev, N., Stampfli, G.M., 2003. New structural and petrological data on Mesozoic schists in the Rhodope (Bulgaria): geodynamic implications. *Comptes Rendus Geosciences* 335, 691–699.
- Bonev, N. and Stampfli, G.M., 2008. Petrology, geochemistry and geodynamic implications of Jurassic island arc magmatism as revealed by mafic volcanic rocks in the Mesozoic low-grade sequence, eastern Rhodope, Bulgaria. *Lithos* 100 (1–4), 210–233.
- Boray, A., Akat, U., Akdeniz, N., Akçoren, Z.Ç., Çağlayan, A., Guncy, E., Korkmaz, B., Öztürk, E.M., Sav, H., 1973. Some geological problems and their possible solutions along the southern border of the Menderes Massif. In: Doyuran, S. (Ed.), *Papers of congress of Earth Sciences on the occasion of the 50th anniversary of the Turkish Republic. Maden Tetkik ve Arama Enstitüsü, Ankara, Turkey*, pp. 11–20.
- Boyantov, I., Russeva, M., 1989. Lithostratigraphy and tectonic position of the Mesozoic rocks in the East Rhodopes. *Geologica Rhodopica* 1, 22–34.
- Bozkurt, E., Oberhänsli, R., 2001. Menderes Massif (Western Turkey): structural, metamorphic and magmatic evolution — a synthesis. *International Journal of Earth Sciences* 89, 679–708.
- Bozkurt, E., Mittweide, S.K., 2001. Introduction of the geology of Turkey — a synthesis. *International Geology Review* 43 (7), 578–594.
- Brinkmann, R., 1976. *Geology of Turkey*. Elsevier scientific publishing company, Amsterdam. Oxford–New York 158 pp.
- Brunn, J.H., Dumont, J.-F., de Graciansky, P.-C., Gutnic, M., Juteau, T., Marcoux, J., Monod, O., Poisson, A., 1971. Outline of the geology of the Western Taurides. In: Campbell, A.S. (Ed.), *Geology and History of Turkey. Petroleum Exploration Society of Lybia, Tripoli, Lybia*, pp. 225–255.
- Brunn, J.H., Argyriadis, I., Ricou, L.-E., Poisson, A., Marcoux, J., de Graciansky, P.-C., 1976. Eléments majeurs de liaison entre Taurides et Hellénides. *Bulletin de la Société Géologique de France* 18 (2), 481–497.
- Çapan, U., Buket, E., 1975. Aktepe-Gökdere bölgesinin jeolojisi ve ofiyolitli melanj. *Türkiye Jeoloji Bülteni* 18 (1–2), 11–16 (in Turkish, with English abstract).
- Catalano, R., di Stefano, P., Kozur, H.W., 1991. Permian circumcaspian deep-water faunas from the western Tethys (Sicily, Italy) — new evidence for the position of the Permian Tethys. *Palaeogeography, Palaeoclimatology, Palaeoecology* 87 (1–4), 75–108.
- Catalano, R., di Stefano, P., Kozur, H.W., 1992. New data on Permian and Triassic stratigraphy of western Sicily. *Neues Jahrbuch für Geologie und Paläontologie, Abhandlungen* 184 (1), 25–61.
- Çelik, Ö.F., 2002. Geochemical, petrological and geochronological observations on the metamorphic rocks of the Tauride Belt Ophiolites (S. Turkey). PhD Thesis, Université de Genève, 257 pp.
- Çelik, Ö.F., Delaloye, M., Féraud, G., 2006. Precise ⁴⁰Ar–³⁹Ar ages from the metamorphic sole rocks of the Tauride Belt Ophiolites, southern Turkey: implications for the rapid cooling history. *Geological Magazine* 143, 213–227.
- Champod, E., Kock, S., Colliard, B., Stampfli, G.M., 2003. The Permian–Triassic evolution of the Tethyan margins in the external Hellenides. 6th Alpshop workshop. *Annales Universitatis Scientiarum Budapestinensis, Sopron*, pp. 145–146.
- Channell, J.E.T., Tüysüz, O., Bektaş, O., Şengör, A.M.C., 1996. Jurassic–Cretaceous paleomagnetism and paleogeography of the Pontides (Turkey). *Tectonics* 15 (1), 201–212.
- Chatalov, G.A., 1988. Recent development in the geology of the Strandzha Zone in Bulgaria. *Bulletin of the Technical University of Istanbul* 41, 433–465.
- Dannat, C., Reischmann, T., 1998. Geochronological, geochemical and isotopic data on granitic gneisses from the Menderes Massif, SW Turkey. 3rd International Turkish Geology Symposium. Middle East Technical University, Ankara, Turkey, p. 282.
- Dannat, C., Reischmann, T., 1999. Single zircon ages of migmatites from the Menderes Massif, SW Turkey, EUG 10. European Union of Geosciences. Cambridge Publications, Strasbourg, p. 805.
- de Graciansky, P.-C., 1972. Recherches géologiques dans le Taurus Lycien. PhD Thesis, Paris Sud–Centre d'Orsay, Paris, 571 pp.
- Dean, W.T., Özgül, N., 1994. Cambrian rocks and faunas, Hüdaı area, Taurus Mountains, southwestern Turkey. *Bulletin de l'Institut Royal des Sciences Naturelles de Belgique* 64, 5–20.
- Dean, W.T., Monod, O., Rickards, R.B., Demir, O., Bultynck, P., 2000. Lower Palaeozoic stratigraphy and palaeontology, Karadere-Zirze area, Pontu Mountains, northern Turkey. *Geological Magazine* 137, 555–582.
- Degnan, P.J., Robertson, A.H.F., 1998. Mesozoic–Early Tertiary passive margin evolution of the Pindos Ocean (NW Peloponnese, Greece). *Sedimentary Geology* 117, 33–70.
- Delaloye, M., Wagner, J.-J., 1984. Ophiolites and volcanic activity near the Arabian plate edge. In: Dixon, J.E., Robertson, A.H.F. (Eds.), *The Geological Evolution of the Eastern Mediterranean. Geological Society of London Special Publication*, vol. 17, pp. 225–234.
- Delaune-Mayère, M., 1984. Evolution of a Mesozoic passive continental margin: Baër-Bassit (NW Syria). In: Dixon, J.E., Robertson, A.H.F. (Eds.), *The geological evolution of the Eastern Mediterranean. Geological Society of London Special Publication*, vol. 17, pp. 151–159.
- Delaune-Mayère, M., Marcoux, J., Parrot, J.-F., Poisson, A., 1977. Modèle d'évolution mésozoïque de la paléo-marge tethysienne au niveau des nappes radiolaritiques et ophiolitiques du Taurus Lycien d'Antalya et du Baër-Bassit. In: Biju-Duval, B., Montadert, L. (Eds.), *Structural history of the Mediterranean basins. Editions Technip, Paris*, pp. 79–94.

- Demirtaşlı, E., 1984a. Stratigraphic evidence of Variscan and early Alpine tectonics in southern Turkey. In: Dixon, J.E., Robertson, A.H.F. (Eds.), *The Geological Evolution of the Eastern Mediterranean*. Geological Society of London Special Publication, vol. 17, pp. 129–146.
- Demirtaşlı, E., 1984b. Stratigraphy and tectonics of the area between Silifke and Anamur, central Taurus Mountains. In: Tekeli, O., Göncüoğlu, C.M. (Eds.), *Geology of the Taurus Belt. Maden Tetkik ve Arama Enstitüsü, Ankara, Turkey*, pp. 101–118.
- Demirtaşlı, E., 1989. Stratigraphic correlation forms of Turkey. In: Sassi, F.P., Zanferrari, A. (Eds.), *Pre-Variscan and Variscan events in the Alpine-Mediterranean belts, Stratigraphic correlation forms*. Rendiconti della Società geologica Italiana, vol. 12–2. Società Geologica Italiana, Roma, pp. 183–211.
- Demirtaşlı, E., Turhan, N., Bilgin, A.Z., Selim, M., 1984. Geology of the Bolkar mountains. In: Tekeli, O., Göncüoğlu, M.C. (Eds.), *Geology of the Taurus belt. Maden Tetkik ve Arama Enstitüsü, Ankara, Turkey*, pp. 125–141.
- Dewey, J.F., Helman, M.L., Turco, E., Hutton, D.H.W., Knott, S.D., 1989. Kinematics of the western Mediterranean. In: Coward, M.P., Dietrich, D., Park, R.G. (Eds.), *Alpine tectonics*. Geological Society of London Special Publication, vol. 45, pp. 265–284.
- Dilek, Y., Delaloye, M., 1992. Structure of the Kızıldağ ophiolite, a slow-spread Cretaceous ridge segment north of the Arabian promontory. *Geology* 20, 19–22.
- Dilek, Y., Whitney, D.L., 1997. Counterclockwise P – T – t trajectory from the metamorphic sole of a Neo-Tethyan ophiolite (Turkey). *Tectonophysics* 280 (3–4), 295–310.
- Dilek, Y., Thy, P., Hacker, B., Grundvig, S., 1999. Structure and petrology of Tauride ophiolites and mafic intrusions (Turkey): implications for the Neotethyan Ocean. *Geological Society of America Bulletin* 111 (8), 1192–1216.
- Dora, O.Ö., Candan, O., Kaya, O., Koray, E., Dürr, S., 2001. Revision of “Leptite-gneisses” in the Menderes Massif: a suprastructural metasedimentary origin. *International Journal of Earth Sciences* 89 (4), 836–851.
- Elmas, A., Yiğitbaş, E., 2001. Ophiolite emplacement by strike-slip tectonics between the Pontides Zone and the Sakarya Zone in northwestern Anatolia, Turkey. *International Journal of Earth Sciences* 90, 257–269.
- Elmas, A., Yiğitbaş, E., 2005. Comment on “Tectonic evolution of the Intra-Pontide suture zone in the Armutlu Peninsula, NW Turkey” by Robertson and Ustaömer. *Tectonophysics* 405 (1–4), 213–221.
- Erdoğan, B., Uchman, A., Güngör, T., Özgül, N., 2004. Lithostratigraphy of the Lower Cambrian metaclastics and their age based on trace fossils in the Sandıklı region, southwestern Turkey. *Geobios* 37 (3), 346–360.
- Eren, Y., Kurt, H., Rosset, F., Stampfli, G.M., 2004. Palaeozoic deformation and magmatism in the northern area of the Anatolide block (Konya), witness of the Palaeozoic active margin. *Eclogae Geologicae Helveticae* 97 (2), 293–306.
- Faupl, P., Pavlopoulos, A., Klötzli, U., Petrakakis, K., 2006. On the provenance of mid-Cretaceous turbidites of the Pindos zone (Greece): implications from heavy mineral distribution, detrital zircon ages and chrome spinel chemistry. *Geological Magazine* 143 (3), 329–342.
- Finetti, I.R., 2005. *Crop-crustal Seismic Exploration of the Central Mediterranean and Italy*. Atlases in Geoscience 1. Elsevier Science Publishers, 500 pp.
- Fontaine, J.-M., 1981. *La plate-forme arabe et sa marge passive au Mésozoïque: l'exemple d'Hazro (SE Turquie)*. PhD Thesis, Paris Sud-Centre d'Orsay, 270 pp.
- Fontaine, J.-M., Monod, O., Braud, J., Perinçek, D., 1989. The Hezan units: a fragment of the South Neo-Tethyan passive continental margin in SE Turkey. *Journal of Petroleum Geology* 12 (1), 29–50.
- Gansser, A., 1974. The ophiolitic mélange, a world-wide problem on Tethyan examples. *Eclogae Geologicae Helveticae* 67 (3), 479–507.
- Gass, I.G., Ries, A.C., Shackleton, R.M., Smewing, J.D., 1990. Tectonics, geochronology and geochemistry of the Precambrian rocks of Oman. In: Robertson, A.H.F., Searle, M.P., Ries, A.C. (Eds.), *The geology and tectonics of the Oman region*. Geological Society of London Special Publication, vol. 49, pp. 585–599.
- Georgiev, G., Dabovski, C., Stanisheva-Vassileva, G., 2001. East Srednogie-Balkan rift Zone. In: Ziegler, P.A., Cavazza, W., Robertson, A.H.F., Crasquin-Soleau, S. (Eds.), *Peri-Tethys Memoir 6: Peri-Tethyan Rift/Wrench Basins and Passive Margins*. Mémoires du Muséum d'Histoire Naturelle de Paris, Paris, pp. 259–293.
- Gessner, K., Piazzolo, S., Güngör, T., Ring, U., Kröner, A., Passchier, C.W., 2001. Tectonic significance of deformation patterns in granitoid rocks of the Menderes nappes, Anatolide belt, southwest Turkey. *International Journal of Earth Sciences* 89, 766–780.
- Glennie, K.W., Boeuf, M.G.A., Hughes Clarke, M.W., Moody-Stuart, M., Pilaart, W.F.H., Reinhart, B.M., 1974. *Geology of the Oman mountains. part one: text*. Verhandelingen van het Koninklijk Nederlandsgeologisch Mijnbouwkundig Genootschap, p. 423 pp.
- Gökdeniz, S., 1981. *Recherches géologiques dans les Taurides occidentales entre Karaman et Ermenek, Turquie. Les séries à “tuffites vertes” triasiques*. PhD Thesis, Université de Paris Sud, centre d'Orsay, Paris, 202 pp.
- Göncüoğlu, C.M., Turhan, N., 1984. *Geology of the Bitlis metamorphic belt*. In: Tekeli, O., Göncüoğlu, C.M. (Eds.), *Geology of the Taurus Belt. Maden Tetkik ve Arama Enstitüsü, Ankara, Turkey*, pp. 237–244.
- Göncüoğlu, C.M., Kozur, H.W., 1998. Remarks to the pre-Variscan development in Turkey. In: Linnemann, U., Huc, T., Fatka, O., Kraft, P., Brocke, R., Erdtmann, B.-D. (Eds.), *Pre-Variscan terrane analysis of “Gondwanan Europe”*. Schriften des Staatlichen Museums für Mineralogie und Geologie, Dresden, pp. 137–138.
- Göncüoğlu, C.M., Dirik, K., Kozlu, H., 1997. Pre-Alpine and Alpine terranes in Turkey: explanatory notes to the terrane map of Turkey. In: Papanikolaou, D., Sassi, F.P. (Eds.), *IGCP Project n°276: Paleozoic domains and their alpidic evolution in the Tethys*. Annales Géologiques des Pays Helléniques, pp. 515–536.
- Göncüoğlu, C.M., Turhan, N., Tekin, U.K., 2003. Evidence for the Triassic rifting and opening of the Neotethyan Izmir-Ankara Ocean and discussion on the presence of Cimmerian events at the northern edge of the Tauride-Anatolide Platform, Turkey. In: Decandia, F.A., Cassinis, G., Spina, A. (Eds.), *Late Palaeozoic to early Mesozoic events of Mediterranean Europe, and additional regional reports; proceedings*. Società Geologica Italiana, Rome, Italy.
- Göncüoğlu, C.M., Kozur, H.W., Turhan, N., Göncüoğlu, Y., 2000. Stratigraphy of the Silurian–Lower Carboniferous rock units in Konya area (Kütahya-bolkardağ Belt, Central Turkey). VIII International Meeting of IGCP 421 in 1st Congresso Iberico de Paleontologia, Evora, Portugal, pp. 227–228.
- Görür, N., Okay, A.I., 1996. A fore-arc origin for the Thrace Basin, NW Turkey. *Geologische Rundschau* 85 (4), 662–668.
- Görür, N., Şengör, A.M.C., Akkok, R., Yılmaz, Y., 1983. Sedimentological data regarding the opening of the northern branch of Neotethys in the Pontides. *Türkiye Jeoloji Kurumu Bülteni* 26 (11–20).
- Görür, N., Monod, O., Okay, A.I., Şengör, A.M.C., Tüysüz, O., Yiğitbaş, E., Sakinc, M., Akkok, R., 1997. Paleogeographic and tectonic position of the Carboniferous rocks of the western Pontides (Turkey) in the frame of the Variscan belt. *Bulletin de la Société géologique de France* 168 (2), 197–205.
- Gözübol, A.M., 1980. *Geological investigation of the Mudurnu-Dokurcun-Abant area (Bolu Province) and the structural behaviour of the North Anatolian Transform Fault*. Istanbul Üniversitesi Fen Fakültesi Mecmuası 45 (B), 9–34.
- Gradstein, F.M., Ogg, J.G., Smith, A.G., Agterberg, F.P., Bleeker, W., Cooper, R.A., Davydov, V., Gibbard, P., Hinno, L., House, M.R., Lourens, L., Luterbacher, H.P., McArthur, J., Melchior, M.J., Robb, L.J., Shergold, J., Villeneuve, M., Wardlaw, B.R., Ali, J., Brinkhuis, H., Hilgen, F.J., Hooker, J., Howarth, R.J., Knoll, A.H., Laskar, J., Monechi, S., Plumb, K.A., Powell, J., Raffi, I., Roehl, U., Sanfilippo, A., Schmitz, B., Shackleton, N.J., Shields, G.A., Strauss, H., van Dam, J., van Kolfshoten, T., Veizer, J., Wilson, D., 2004. *A geological time scale 2004*. Miscellaneous Report — Geological Survey of Canada. Geological Survey of Canada, Ottawa, ON, Canada. 1 pp.
- Gürsu, S., Göncüoğlu, M.C., 2001. Characteristic features of the Late Precambrian felsic magmatism in Western Anatolia: implications for the Pan-African evolution in NW Perigondwana. *Gondwana Research* 4 (2), 169–170.
- Gürsu, S., Göncüoğlu, C.M., 2006. Petrogenesis and tectonic setting of Cadomian felsic igneous rocks, Sandıklı area of the western Taurides, Turkey. *International Journal of Earth Sciences* 95, 741–757.
- Gürsu, S., Göncüoğlu, C.M., Bayhan, H., 2004. Geology and geochemistry of the pre-Early Cambrian rocks in the Sandıklı area: implications for the Pan-African evolution of NW Gondwanaland. *Gondwana Research* 7 (4), 923–935.
- Gutnic, M., Monod, O., Poisson, A., Dumont, J.-F., 1979. *Géologie des Taurides occidentales (Turquie)*. Mémoire de la Société Géologique de France, vol. 137. Société Géologique de France, Paris. 109 pp.

- Harris, N.B., Kelley, S., Okay, A.I., 1994. Post-collision magmatism and tectonics in northwest Anatolia. *Contribution to Mineralogy and Petrology* 117 (3), 241–252.
- Hetzl, R., Reischmann, T., 1996. Intrusion age of Pan-African augengneisses in the southern Menderes massif and age of cooling after Alpine ductile extensional deformation. *Geological Magazine* 133, 565–572.
- İşik, V., Tekeli, O., Seyitoğlu, G., 2004. The 40Ar–39Ar age of extensional ductile deformation and granitoid intrusion in the northern Menderes core complex: implications for the initiation of extensional tectonics in western Turkey. *Journal of Asian Earth Sciences* 23 (4), 555–566.
- Juteau, T., 1980. Ophiolites of Turkey. *Ophioliti* 2, 199–238.
- Kerey, I.E., Kelling, G., Wagner, R.H., 1986. An outline stratigraphy and palaeobotanical records from the Middle Carboniferous rocks of north-west Turkey. *Annales de la Société Géologique du Nord* 55, 203–216.
- Ketin, I., 1966. Tectonic units of Anatolia (Asia Minor). *Bulletin of the Mineral Research and Exploration Institute of Turkey* 66, 23–34.
- Koç, H., Özer, E., Özsayar, T., 1997. Aydınçık (İçel) yöresinin jeolojisi. *Geosound* 30, 417–427 (in Turkish, with English abstract).
- Kock, S., Martini, R., Reischmann, T., Stampfli, G.M., 2007. Detrital zircon and micropalaeontological ages as new constraints for the lowermost tectonic unit (Talea Ori unit) of Crete, Greece. *Palaeogeography, Palaeoclimatology, Palaeoecology* 243 (3–4), 307–321.
- Koçyiğit, A., Altınır, D., Farinacci, A., Nicosia, U., Conti, M.A., 1991. Late Triassic–Aptian evolution of the Sakarya divergent margin: implications for the opening history of the northern Neotethys, in Northwestern Anatolia. *Geologica Romana* 27, 81–99.
- Kozur, H.W., 1990. Deep-Water Permian in Sicily and its possible connection with the Himalaya–Tibet region. 5th Himalaya–Tibet–Karakorum workshop. Dipartimento di Scienze della Terra, Università di Milano, Milano, Italy.
- Kozur, H.W., 1991. Permian deep-water ostracods from Sicily (Italy). Part I: Taxonomy. *Geologisch Paläontologische Mitteilungen Innsbruck. Sonderband*, vol. 3, pp. 1–24.
- Kozur, H.W., 1995a. New stratigraphic results on the Paleozoic of the western parts of the Karaburun peninsula, western Turkey. In: Pişkin, O., Ergün, M., Savaşcin, M.Y., Tarcan, G. (Eds.), *Proceedings of International Earth Sciences Colloquium on the Aegean region*, Izmir, pp. 289–308.
- Kozur, H.W., 1995b. First evidence of Middle Permian Ammonitico Rosso and further new stratigraphic results in the Permian and Triassic of the Sosio Valley area, Western Sicily. 1st Croatian Geological congress. *Zbornik radova proceedings, Opatija*, pp. 307–310.
- Kozur, H.W., 1998a. The age of the siliciclastic series (“Karareis formation”) of the western Karaburun peninsula, western Turkey. In: Szaniawski, H. (Ed.), *Proceedings of the 6th European Conodont Symposium*. *Paleontologia Polonica*, pp. 172–187.
- Kozur, H.W., 1998b. Opening and closing times of Paleozoic and early Mesozoic deep water basins in Turkey. 3rd International Turkish Geology Symposium, Ankara, p. 105.
- Kozur, H.W., 1999a. A review of the systematic position and stratigraphic value of Muçlerisphaerida. In: Tongiorgi, M., Playford, G. (Eds.), *Studies in Palaeozoic palynology*. *Bollettino della Società di Paleontologia Italiana*, pp. 197–206.
- Kozur, H.W., 1999b. The Variscan Carboniferous of Turkey, XIV ICCP. International Congress on the Carboniferous–Permian, Calgary, Alberta, Canada, p. 78.
- Kozur, H.W., 2000a. Northern origin of the Antalya and Alanya Nappes (Western Taurus, Turkey) and causes for the end of the tethyan faunal provincialism during the middle Carnian. In: Vlahović, I., Biondić, R. (Eds.), 2nd Croatian Geological Congress. *Zbornik radova, Zagreb*, pp. 275–282.
- Kozur, H.W., 2000b. Carboniferous and Permian of Turkey. *Schriften des Staatlichen Museums der Mineralogie und Geologie, Dresden*, p. 81.
- Kozur, H.W., 2003a. Integrated Permian ammonoid, conodont, fusulinid, marine ostracod and radiolarian biostratigraphy. *Permophiles* 42, 24–33.
- Kozur, H.W., 2003b. Integrated Permian ammonoid, conodont and radiolarian zonation of the Triassic. *Halleches Jahrbuch für Geowissenschaften*, B 25, 49–79.
- Kozur, H.W., Şenel, M., 1999. Carboniferous oceanic sequences in the Lycian nappes of southern Turkey. XIV ICCP, International Congress on the Carboniferous–Permian, Calgary, Alberta, Canada, 79.
- Kozur, H.W., Göncüoğlu, M.C., 1999. Differences in the geological evolution of the Istanbul and Zonguldak terranes, northern Turkey. In: Talent, J., Khan, F., Mawson, R. (Eds.), *IGCP 421: Mid-Palaeozoic bioevent/biogeography patterns in relation to crustal dynamics*. North Ryde (Macquarie University Printery), Peshawar, Pakistan, pp. 16–18.
- Kozur, H.W., Şenel, M., Tekin, K., 1998. First evidence of Hercynian Lower Carboniferous deep-water sediments in the Lycian Nappes, SW Turkey. *Geologica Croatica* 51 (1), 15–22.
- Kozur, H.W., Aydın, M., Demir, O., Yakar, H., Göncüoğlu, M.C., Kuru, F., 2000. New stratigraphic and paleogeographic results from the Paleozoic and Early Mesozoic of the Middle Pontides (Northern Turkey) in the Azdavay, Devrekani, Küre and Inebolu areas: implications for the Carboniferous–Early Cretaceous geodynamic evolution and some related remarks to the Karakaya oceanic rift basin. *Geologica Croatica* 53 (2), 209–268.
- Krahl, J., Kauffmann, G., Kozur, H.W., Richter, D., Förster, O., Heinritzi, F., 1983. Neue Daten zur biostratigraphie und zur tektonischen Lagerung der Phyllit-Gruppe und der Trypali-Gruppe auf der Insel Kreta (Griechenland). *Geologische Rundschau* 72 (3), 1147–1166.
- Kröner, A., Şengör, A.M.C., 1990. Archean and Proterozoic ancestry in late Precambrian to early Palaeozoic crustal elements of southern Turkey as revealed by single-zircon dating. *Geology* 18, 1186–1190.
- Langhi, L., Borel, G.D., 2005. Influence of the Neotethys rifting on the development of the Dampier Sub-basin (North West Shelf of Australia), highlighted by subsidence modelling. In: Marotta Anna, M., Bayer, U. (Eds.), *Integration of geophysical and geological data and numerical models in basins*. Elsevier, Amsterdam, Netherlands, pp. 93–111. 2005.
- Lapierre, H., 1975. Les formations sédimentaires et éruptives des Nappes de Mamonia et leurs relations avec le massif du Troodos. *Mémoires de la Société Géologique de France* 123, 1–132.
- Lapierre, H., Parrot, J.-F., 1972. Identité géologique des régions de Paphos (Chypre) et du Baër-Bassit (Syrie). *Comptes Rendus de l’Académie des Sciences de Paris* 268, 1999–2002.
- Le Métour, J., Michel, J.C., Béchenec, F., Platel, J.-P., Roger, J., 1995. Geology and mineral wealth of the Sultanate of Oman. Ministry of Petroleum and Minerals, Directorate General of Minerals, Oman. 285 pp.
- Lefèvre, R., 1967. Un nouvel élément de la géologie du Taurus lycien: les Nappes d’Antalya. *Comptes Rendus de l’Académie des Sciences de Paris* 265, 1365–1368.
- Malpas, J., Calon, T., Squires, G., 1993. The development of a late Cretaceous microplate suture zone in SW Cyprus. In: Prichard, H.M., Alabaster, T., Harris, N.B.W., Neary, C.R. (Eds.), *Magmatic Processes and Plate Tectonics*. Geological Society of London Special Publication, vol. 76, pp. 177–195.
- Marcoux, J., 1987a. Histoire et topologie de la Neo-Tethys - Tome 2 (sélection de publications 1970–1987). PhD Thesis, Université Pierre et Marie Curie — Paris 6, Paris, 569 pp.
- Marcoux, J., 1987b. Histoire et topologie de la Neo-Tethys — Tome 1 (introduction générale). PhD Thesis, Université Pierre et Marie Curie — Paris VI, Paris, 73 pp.
- Masset, O. and Moix, P., 2004. Les mélanges de l’ophiolite de Mersin (Turquie du Sud). unpublished MSc. Thesis, Lausanne, 143 pp.
- Moix, P., Kozur, H.W., Stampfli, G.M., 2007a. Evidence for Palaeotethyan origin of a part of the Mersin Mélange (southern Turkey) EGU2007 Geophysical Research Abstracts 9 08739 Vienna.
- Moix, P., Kozur, H.W., Stampfli, G.M., Mostler, H., 2007b. New palaeontological, biostratigraphical and palaeogeographical results from the Triassic of the Mersin mélange, SE Turkey. In: Lucas, S.G., Spielmann, J.A. (Eds.), *The Global Triassic*. New Mexico Museum of Natural History and Science Bulletin, vol. 41, pp. 282–311.
- Monod, O., 1977. Recherches géologiques dans le Taurus occidental au Sud de Beyşehir (Turquie). PhD Thesis, Université de Paris-Sud, Orsay.
- Monod, O., Akay, E., 1984. Evidence for a Late Triassic–Early Jurassic orogenic event in the Taurides. In: Dixon, J.E., Robertson, A.H.F. (Eds.), *The geological evolution of the Eastern Mediterranean*. Geological Society of London Special Publication, vol. 17, pp. 113–122.
- Monod, O., Kozlu, H., Ghienne, J.-F., Dean, W.T., Günay, Y., Le Hérisse, A., Paris, F., Robardet, M., 2003. Late Ordovician glaciation in southern Turkey. *Terra Nova* 15, 249–257.
- Neumann, P., Zacher, W., 1996. Multistratigraphic investigations and sedimentary cycles in the Upper Cretaceous of the Olanos-Pindos

- Zone (Greece): palaeogeography, facies and basin development. In: Reitner, J., Neuweiler, F., Gunkel, F. (Eds.), *Global and regional controls on biogenic sedimentation. Cretaceous sedimentation research reports. Göttinger Arbeiten zur Geologie und Paläontologie*, Göttingen, pp. 123–126.
- Norman, T.N., 1993. Remobilization of two mélanges in Central Anatolia. *Geological Journal* 28, 267–275.
- Okay, A.I., 1984. Distribution and characteristics of the northwest Turkish blueschists. In: Dixon, J.E., Roberston, A.H.F. (Eds.), *The geological evolution of the Eastern Mediterranean*. Geological Society of London Special Publication, vol. 17, pp. 455–466.
- Okay, A.I., 1986. High-pressure/low temperature metamorphic rocks of Turkey. In: Evans, B.W., Brown, E.H. (Eds.), *Blueschists and eclogites*. American Association of Petroleum Geologists Memoir, pp. 333–347.
- Okay, A.I., 1989. Tectonic units and sutures in the Pontides, northern Turkey. In: Şengör, A.M.C. (Ed.), *Tectonic evolution of Tethyan region*. Kluwer Academic Publications, Dordrecht, pp. 109–115.
- Okay, A.I., Şahintürk, Ö., 1997. Geology of the eastern Pontides. In: Robinson, A.G. (Ed.), *Regional and petroleum geology of the Black Sea and surrounding region*. American Association of Petroleum Geologists Memoir, vol. 68, pp. 291–311.
- Okay, A.I., Tüysüz, O., 1999. Tethyan sutures of northern Turkey. In: Durand, B., Jolivet, L., Horvath, F., Seranne, M. (Eds.), *Mediterranean Basins: Tertiary extension within the Alpine Orogen*. Geological Society of London Special Publication, vol. 156, pp. 475–515.
- Okay, A.I., Göncüoğlu, C.M., 2004. The Karakaya Complex; a review of data and concepts. *Turkish Journal of Earth Sciences* 13 (2), 77–95.
- Okay, A.I., Siyako, M., Bürkan, K.A., 1991. Geology and tectonic evolution of the Biga Peninsula, northwest Turkey. *Bulletin Technique de l'Université d'Istanbul* 44, 191–255.
- Okay, A.I., Şengör, A.M.C., Görür, N., 1994. Kinematic history of the opening of the Black Sea and its effect on the surrounding regions. *Geology* 22, 267–270.
- Okay, A.I., Satir, M., Maluski, H., Siyako, M., Monié, P., Metzger, R., Akyüz, S., 1996. Palaeo- and Neo-Tethyan events in northwestern Turkey: geologic and geochronologic constraints. In: Yin, A., Harrison, T.M. (Eds.), *The Tectonic Evolution of Asia*. Cambridge University Press, pp. 420–441.
- Okay, A.I., Harris, N.B.W., Kelley, S.P., 1998. Exhumation of blueschists along a Tethyan suture in northwest Turkey. *Tectonophysics* 285 (3–4), 275–299.
- Okay, A.I., Satir, M., Tüysüz, O., Akyüz, S., Chen, F., 2001. The tectonics of the Strandja Massif; late Variscan and mid-Mesozoic deformation and metamorphism in the northern Aegean. *International Journal of Earth Sciences* 90 (2), 217–233.
- Önen, A.P., 2003. Neotethyan ophiolitic rocks of the Anatolides of NW Turkey and comparison with Tauride ophiolites. *Journal of the Geological Society of London* 160 (6), 947–962.
- Önen, A.P., Hall, R., 1993. Ophiolites and related metamorphic rocks from the Kütahta region, north-west Turkey. *Geological Journal* 28, 399–412.
- Önen, A.P., Hall, R., 2000. Sub-ophiolite metamorphic rocks from NW Anatolia, Turkey. *Journal of Metamorphic Geology* 18, 483–495.
- Özer, S., Sözbilir, H., Özkaz, I., Toker, V., Sarı, B., 2001. Stratigraphy of Upper Cretaceous–Palaeogene sequences in the southern and eastern Menderes Massif (Western Turkey). *International Journal of Earth Sciences* 89 (4), 852–866.
- Özer, E., Koç, H., Özsayar, T.Y., 2004. Stratigraphical evidence for the depression of the northern margin of the Menderes-Tauride Block (Turkey) during the Late Cretaceous. *Journal of Asian Earth Sciences* 22 (5), 401–412.
- Özgül, N., 1976. Torosların bazı temel jeoloji özellikleri. *Türkiye Jeoloji Kurumu Bülteni* 19, 65–78 (in Turkish, with English abstract).
- Özgül, N., 1984. Stratigraphy and tectonic evolution of the central Taurides. In: Tekeli, O., Göncüoğlu, M.C. (Eds.), *Geology of the Taurus belt*. Maden Tetkik ve Arama Enstitüsü, Ankara, Turkey, pp. 77–90.
- Özgül, N., 1997. Bozkır-Hadım-Taşkent (orta toroslar'ın kuzey kesimi) dolayında yer alan tektono-stratigrafik birliklerin stratigrafisi. *Maden Tetkik ve Arama Dergisi* 119, 113–174 (in Turkish).
- Özgül, N., Turşucu, A., 1984. Stratigraphy of the Mesozoic carbonate sequence of the Munzur Mountains (Eastern Turkey). In: Tekeli, O., Göncüoğlu, C.M. (Eds.), *Geology of the Taurus Belt*. Maden Tetkik ve Arama Enstitüsü, Ankara, Turkey, pp. 173–180.
- Pampal, S., 1987. Güzeloluk-Sorgun (Mersin) yöresinin jeolojisi. *Gazi Üniversitesi-Mühendislik mimarlık fakültesi dergisi* 1 (2), 143–174 (in Turkish, with English abstract).
- Pampal, S., Kurtman, F., 1984. New data on the Neo-tethys rifting in the Eastern Taurus region. In: Tekeli, O., Göncüoğlu, C.M. (Eds.), *Geology of the Taurus Belt*. Maden Tetkik ve Arama Enstitüsü, Ankara, Turkey, pp. 217–222.
- Parlak, O., 1996. Geochemistry and geochronology of the Mersin ophiolite within the eastern Mediterranean tectonic frame (southern Turkey). PhD Thesis, Université de Genève, Genève, 242 pp.
- Parlak, O., Delaloye, M., 1996. Geochemistry and timing of postmetamorphic dike emplacement in the Mersin ophiolite (southern Turkey): new age constraints from ⁴⁰Ar–³⁹Ar geochronology. *Terra Nova* 8, 585–592.
- Parlak, O., Delaloye, M., 1999. Precise ⁴⁰Ar–³⁹Ar ages from the metamorphic sole of the Mersin ophiolite (southern Turkey). *Tectonophysics* 301 (1–2), 145–158.
- Parlak, O., Robertson, A.H.F., 2004. The ophiolite-related Mersin Mélange, southern Turkey; its role in the tectonic-sedimentary setting of Tethys in the Eastern Mediterranean region. *Geological Magazine* 141 (3), 257–286.
- Parlak, O., Delaloye, M., Bingöl, E., 1995. Origin of sub-ophiolitic metamorphic rocks beneath the Mersin ophiolite, Southern Turkey. *Ofioliti* 20 (2), 97–110.
- Parrot, J.-F., 1980. The Baër-Bassit (Northwestern Syria) ophiolitic area. In: Rocci, G. (Ed.), *Tethyan ophiolites*. *Ofioliti*, Special Issue, pp. 279–295.
- Pearce, J.A., Lippard, S.J., Roberts, S., 1984. Characteristics and tectonic significance of supra-subduction zone ophiolites. In: Kokelaar, B.P., Howels, M.F. (Eds.), *Marginal basin geology*. Geological Society of London Special Publication, vol. 16, pp. 77–94.
- Perinçek, D., Kozlu, H., 1984. Stratigraphy and structural relations of the units in the Afşin-Elbistan-Doğanshehir region (Eastern Taurus). In: Tekeli, O., Göncüoğlu, M.C. (Eds.), *Geology of the Taurus Belt*. Maden Tetkik ve Arama Enstitüsü, Ankara, Turkey, pp. 181–198.
- Pillecuit, A., Marcoux, J., Stampfli, G.M., Baud, A., 1997. The Oman exotics; a key to the understanding of the Neotethyan geodynamic evolution. *Geodinamica Acta* 10 (5), 209–238.
- Pişkin, O., Delaloye, M., Selçuk, H., Wagner, J.-J., 1986. Guide to Hatay geology (SE Turkey). *Ofioliti* 11, 87–104.
- Poisson, A., 1977. *Recherches géologiques dans les Taurides occidentales (Turquie)*. PhD Thesis, Paris-Sud (centre d'Orsay), Paris, 795 pp.
- Richter, D., Müller, C., Mihm, A., 1993. Die Flysch-Zonen Griechenlands; V. Zur Stratigraphie des Flysches der Pindos-Zone im nördlichen Pindos-Gebirge zwischen der albanischen Grenze und der Querzone von Kastaniotikos (Griechenland). *Neues Jahrbuch für Geologie und Paläontologie, Monatshefte* 5, 257–291.
- Ricou, L.-E., 1971. Le croissant ophiolitique péri-arabe: une ceinture de nappes mises en place au Crétacé supérieur. *Revue de Géographie Physique et de Géologie Dynamique* 13–4, 327–349.
- Ricou, L.-E., Argyriadis, I., Lefèvre, R., 1974. Proposition d'une origine interne pour les nappes d'Antalya et le massif d'Alanya (Taurides occidentales, Turquie). *Bulletin de la Société Géologique de France* 16 (2), 107–111.
- Ricou, L.-E., Argyriadis, I., Marcoux, J., 1975. L'axe calcaire du Taurus, un alignement de fenêtres arabo-africaines sous des nappes radiolaritiques, ophiolitiques et métamorphiques. *Bulletin de la Société Géologique de France* 17 (6), 1024–1044.
- Ricou, L.-E., Marcoux, J., Poisson, A., 1979. L'allochtone des Bey Dağları orientaux. Reconstruction paléogéographique des Taurides occidentales. *Bulletin de la Société Géologique de France* 11 (2), 125–133.
- Rimmelé, G., Oberhänsli, R., Goffé, B., Jolivet, L., Candan, O., Cetinkaplan, M., 2003. First evidence of high-pressure metamorphism in the "Cover Series" of the southern Menderes Massif. Tectonic and metamorphic implications for the evolution of SW Turkey. *Lithos* 71 (1), 19–46.
- Robertson, A.H.F., 1977. Tertiary uplift history of the Troodos massif, Cyprus. *Geological Society of America Bulletin* 88, 1763–1772.
- Robertson, A.H.F., 1986. The Hatay ophiolite (Southern Turkey) in its Eastern Mediterranean tectonic context: a report on some aspects of the field excursion. *Ofioliti* 11, 105–119.
- Robertson, A.H.F., 1998. Mesozoic–Tertiary tectonic evolution of the eastern-most Mediterranean area: integration of marine and land evidence. In:

- Robertson, A.H.F., Emeis, K.-C., Richter, C., Camerlenghi, A. (Eds.), Proceedings of the Ocean Drilling Program, Scientific Results.
- Robertson, A.H.F., 2000. Mesozoic–Tertiary tectonic-sedimentary evolution of a South Tethyan oceanic basin and its margins in Southern Turkey. In: Bozkurt, E., Winchester, J.A., Piper, J.D.A. (Eds.), *Tectonics and Magmatism in Turkey and the Surrounding Area*. Geological Society of London Special Publication, vol. 173, pp. 97–138.
- Robertson, A.H.F., Woodcock, N.H., 1979. Mamonía Complex, southwest Cyprus: evolution and emplacement of a Mesozoic continental margin. *Geological Society of America Bulletin* 90 (1), 651–665.
- Robertson, A.H.F., Woodcock, N.H., 1981. Gödene Zone, Antalya Complex, SW Turkey: volcanism and sedimentation on Mesozoic marginal ocean crust. *Geologische Rundschau* 70, 1177–1214.
- Robertson, A.H.F., Woodcock, N.H., 1986. The role of the Kyrenia Range Lineament, Cyprus, in the geological evolution of the eastern Mediterranean area. *Philosophical Transactions of the Royal Society of London, Series A: Mathematical and Physical Sciences* A317 (1539), 141–177.
- Robertson, A.H.F., Ustaömer, T., 2004. Tectonic evolution of the Intra-Pontide suture zone in the Armutlu Peninsula, NW Turkey. *Tectonophysics* 381, 175–209.
- Robertson, A.H.F., Ustaömer, T., Parlak, O., Unlugenc, U.C., Taşlı, K., Inan, N., 2006. The Berit transect of the Tauride thrust belt, S Turkey: Late Cretaceous–Early Cenozoic accretionary/collisional processes related to closure of the Southern Neotethys. *Journal of Asian Earth Sciences* 27 (1), 108–145.
- Rojay, F.B., Altner, D., 1998. Middle Jurassic–Lower Cretaceous biostratigraphy in the Central Pontides (Turkey): remarks on paleogeography and tectonic evolution. *Rivista Italiana di Paleontologia e Stratigrafia* 104, 167–180.
- Saribudak, M., Sanver, M., Ponat, E., 1989. Location of the western Pontides, NW Turkey, during Triassic time: preliminary palaeomagnetic results. *Geophysical Journal International* 96 (1), 43–50.
- Sarp, H., 1976. Etude géologique et minéralogique du cortège ophiolitique de la région située au NW de Yeşilova (Burdur, Turkey). PhD Thesis, Université de Genève, Genève.
- Şengör, A.M.C., 1979. Mid-Mesozoic closure of Permo-Triassic Tethys and its implications. *Nature* 279, 590–593.
- Şengör, A.M.C., 1984. Timing of tectonic events in the Menderes massif, Western Turkey: implications for tectonic evolution and evidence for Pan-African basement in Turkey. *Tectonics* 3 (7), 693–707.
- Şengör, A.M.C., Yılmaz, Y., 1981. Tethyan evolution of Turkey: a plate tectonic approach. *Tectonophysics* 75, 181–241.
- Şengör, A.M.C., Yılmaz, Y., Ketin, I., 1980. Remnants of a pre-Late Jurassic ocean in the northern Turkey: fragments of Permian–Triassic Paleo-Tethys? *Geological Society of America Bulletin* 91 (1), 599–609.
- Sherlock, S., Kelley, S.P., Inger, S., Harris, N., Okay, A.I., 1999. 40Ar–39Ar and Rb–Sr geochronology of high-pressure metamorphism and exhumation history of the Tavşanlı Zone, NW Turkey. *Contribution to Mineralogy and Petrology* 137, 46–58.
- Stampfli, G.M., 2000. Tethyan oceans. In: Bozkurt, E., Winchester, J.A., Piper, J.D.A. (Eds.), *Tectonics and magmatism in Turkey and surrounding area*. Geological Society of London Special Publication, vol. 173, pp. 1–23.
- Stampfli, G.M., Borel, G.D., 2002. A plate tectonic model for the Paleozoic and Mesozoic constrained by dynamic plate boundaries and restored synthetic oceanic isochrons. *Earth and Planetary Science Letters* 196, 17–33.
- Stampfli, G.M., Borel, G.D., 2004. The TRANSMED transects in space and time: constraints on the paleotectonic evolution of the Mediterranean domain. In: Cavazza, W., Roubé, F., Spakman, W., Stampfli, G.M., Ziegler, P. (Eds.), *The TRANSMED Atlas: the Mediterranean Region from Crust to Mantle*. Springer Verlag, pp. 53–80.
- Stampfli, G.M., Kozur, H.W., 2006. Europe from the Variscan to the Alpine cycles. In: Gee, D.G., Stephenson, R.A. (Eds.), *European lithosphere dynamics*. Memoir of the Geological Society, London, pp. 57–82.
- Stampfli, G.M., Marcoux, J., Baud, A., 1991. Tethyan margins in space and time. In: Channell, J.E.T., Winterer, E.L., Jansa, L.F. (Eds.), *Palaeogeography and paleoceanography of Tethys*. Palaeogeography, Palaeoclimatology, Palaeoecology. Elsevier, Amsterdam, pp. 373–409. Netherlands.
- Stampfli, G.M., Mosar, J., Favre, P., Pilleveit, A., Vannay, J.-C., 2001. Permo-Mesozoic evolution of the western Tethyan realm: the Neotethys/East-Mediterranean connection. In: Ziegler, P.A., Cavazza, W., Robertson, A.H.F., Crasquin-Soleau, S. (Eds.), *Peri-Tethys memoir 6: Peritethyan rift/wrench basins and passive margins*. IGCP 369 Mémoires du Muséum National d'Histoire Naturelle, Paris, pp. 51–108.
- Stampfli, G.M., Vavassis, I., De Bono, A., Rossetti, F., Matti, B., Bellini, M., 2003. Remnants of the Palaeotethys oceanic suture-zone in the western Tethyan area. In: Cassinis, G., Decandia, F.A. (Eds.), *Stratigraphic and structural evolution on the Late Carboniferous to Triassic continental and marine successions in Tuscany (Italy): regional reports and general correlation*. Bollettino della Società Geologica Italiana, Volume speciale, pp. 1–24.
- Steiner, C.W., Hobson, A., Favre, P., Stampfli, G.M., Hernandez, J., 1998. The Mesozoic sequence of Fuerteventura (Canary islands): witness of an Early to Middle Jurassic sea-floor spreading in the Central Atlantic. *Geological Society of America Bulletin* 110 (10), 1304–1317.
- Swarbrick, R.E., Robertson, A.H.F., 1980. Revised stratigraphy of the Mesozoic rocks of southern Cyprus. *Geological Magazine* 117 (6), 547–563.
- Tekeli, O., 1981. Subduction complex of pre-Jurassic age, northern Anatolia, Turkey. *Geology* 9, 68–72.
- Tekeli, O., Aksay, A., Ürgün, B.M., Işık, A., 1984. Geology of the Aladağ mountains. In: Tekeli, O., Göncüoğlu, M.C. (Eds.), *Geology of the Taurus belt*. Maden Tetkik ve Arama Enstitüsü, Ankara, Turkey, pp. 143–158.
- Tekin, U.K., Göncüoğlu, M.C., Turhan, N., 2002. First evidence of Late Carnian radiolarians from the Izmir-Ankara suture complex, central Sakarya, Turkey: implications for the opening age of the Izmir-Ankara branch of Neo-Tethys. *Geobios* 35, 127–135.
- Théveniaut, H., Gallet, Y., Besse, J., Krystyn, L., Marcoux, J., 1993. Origin and Evolution of Turkish blocks during the Late Triassic from magnetostratigraphic data. *Exploration Geophysics* 24, 295–300.
- Thuizat, R., Whitechurch, H., Montigny, R., Juteau, T., 1981. K–Ar dating of some infra-ophiolitic metamorphic soles from the Eastern Mediterranean: new evidence for oceanic thrustings before obduction. *Earth and Planetary Science Letters* 52, 302–310.
- Tüysüz, O., 1999. Geology of the Cretaceous sedimentary basins of the Western Pontides. *Geological Journal* 34, 75–93.
- Tüysüz, O., Dellaloğlu, A.A., Terzioğlu, N., 1995. A magmatic belt within the Neo-Tethyan suture zone and its role in the tectonic evolution of northern Turkey. *Tectonophysics* 243, 173–191.
- Urquhart, E., Banner, F.T., 1994. Biostratigraphy of the supra-ophiolite sediments of the Troodos Massif, Cyprus: the Cretaceous Perapedhi Kannaviou, Moni and Kathikas formations. *Geological Magazine* 131 (4), 499–518.
- Ustaömer, P.A., Mundil, R., Renne, P.R., 2005. U/Pb and Pb/Pb zircon ages for arc-related intrusions of the Bolu Massif (W Pontides, NW Turkey): evidence for late Precambrian (Cadomian) age. *Terra Nova* 17 (3), 215–223.
- Ustaömer, T., Robertson, A.H.F., 1994. Late Palaeozoic marginal basin and subduction-accretion: the Palaeotethyan Küre complex, Central Pontides, northern Turkey. *Journal of the Geological Society of London* 151, 291–305.
- Ustaömer, T., Robertson, A.H.F., 1997. Tectonic-sedimentary evolution of the North Tethyan margin in the Central Pontides of Northern Turkey. In: Robinson, A.G. (Ed.), *Regional and petroleum geology of the Black sea and surrounding region*. American Association of Petroleum Geologists Memoir, vol. 68, pp. 255–290.
- Ustaömer, T., Robertson, A.H.F., 2005. Tectonic evolution of the Intra-Pontides suture zone in the Armutlu Peninsula, NW Turkey; reply. *Tectonophysics* 405 (1–4), 223–231.
- Wagreich, M., 1996. Age and significance of Upper Cretaceous siliciclastic turbidites in the central Pindos Mountains, Greece. *Geological Magazine* 133 (3), 325–331.
- Whitechurch, H., 1993. Les ophiolites tethysiennes de la chaîne du Taurus (Turquie): de l'accrétion océanique à l'obduction. PhD Thesis, Université Louis Pasteur, Strasbourg, 366 pp.
- Whitney, D.L., Dilek, Y., 1997. Core complex development in Central Anatolia, Turkey. *Geology* 25 (11), 1023–1026.
- Whitney, D.L., Dilek, Y., 1998. Metamorphism during Alpine crustal thickening and extension in central Anatolia, Turkey: the Niğde metamorphic core complex. *Journal of Petrology* 39 (7), 1385–1403.
- Whitney, D.L., Dilek, Y., 2000. Andalusite–sillimanite–quartz veins as indicators of low-pressure–high-temperature deformation during late-stage

- unroofing of a metamorphic core complex, Turkey. *Journal of Metamorphic Geology* 18 (1), 59–66.
- Wong, H.K., Lüdmann, T., Ulug, A., Görür, N., 1995. The Sea of Marmara: a plate boundary sea in an escape tectonic regime. *Tectonophysics* 244, 231–250.
- Yazgan, E., 1984. Geodynamic evolution of the Eastern Taurus region. In: Tekeli, O., Göncüoğlu, M.C. (Eds.), *Geology of the Taurus Belt*. Maden Tetkik ve Arama Enstitüsü, Ankara, Turkey, pp. 199–208.
- Yiğitbaş, E., Elmas, A., Yılmaz, Y., 1999. Pre-Cenozoic tectono-stratigraphic components of the Western Pontides and their geological evolution. *Geological Journal* 34, 55–74.
- Yılmaz, Y., Gözübol, A.M., Tüysüz, O., 1982. Geology of an area in and around the northern Anatolian Transform Fault Zone between Bolu and Akyazı. In: Işıkara, A., Vogel, A. (Eds.), *Multidisciplinary approach to earthquake prediction*. Vieweg & Sohn, Braunschweig, pp. 45–65.
- Yılmaz, Y., Genç, S.C., Yiğitbaş, E., Bozcu, M., Yılmaz, K., 1995. Geological evolution of the Late Mesozoic continental margin of northwestern Anatolia. *Tectonophysics* 243, 155–171.
- Ziegler, P.A., Stampfli, G.M., 2001. Late Palaeozoic–Early Mesozoic plate boundary reorganisation: collapse of the Variscan orogen and opening of Neotethys. In: Cassinis, R. (Ed.), *The continental Permian of the southern Alps and Sardinia (Italy): regional reports and general correlations*. Annali Museo Civico Science Naturali, Brescia, pp. 17–34.

Annexe 2

Publication 10

Beccaletto L. and Steiner C. (2005) Evidences of Two-stage Extensional Tectonics from the Northern Edge of the Edremit Graben (NW Turkey). *Geodinamica Acta* 18/3-4, 283-297. <https://doi.org/10.3166/ga.18.283-297>

Evidence of two-stage extensional tectonics from the northern edge of the Edremit Graben, NW Turkey

Laurent Beccaletto *, Christian Steiner

Institute of Geology and Paleontology, BFSH-2 Geosciences and Environment Faculty, Lausanne University, CH-1015 Lausanne, Switzerland

Abstract

Western Turkey is a place of active continental extension, characterized by the occurrence of several WNW-ESE-trending major grabens. The central part of the northern edge of the Edremit Graben is delineated by various geological units, namely the metamorphic Kazdağ Massif, the Mid-Cretaceous Çetmi mélange, the sedimentary Küçükkuş formation, and loose Plio-Quaternary deposits. Detailed structural and sedimentological study suggests a two-stage extensional evolution of the area, separated by a short break in the tectonic regime. The first stage, possibly related to back-arc extension and/or orogenic collapse, is marked by the activity of a newly described low-angle detachment fault, the Şelale detachment fault, from the latest Oligocene onward. The fault plane, separating the mylonitized rocks of the Kazdağ Massif in the footwall from the unmetamorphosed Çetmi mélange and Küçükkuş formation in the hanging wall, must have played a significant role in the initial exhumation processes of the Kazdağ Massif at that time. The Lower Miocene syntectonic Küçükkuş formation has recorded the initiation and filling up of a small basin, which has developed in a typical supra-detachment basin, above the detachment fault. After a short phase of possible compression and erosion, the second stage—which marks the onset of neotectonic activity—is marked by the development of Plio-Quaternary step-like normal faults, which cut through all the previous units. Coarse, loose sediments were deposited following the fault activity. These local results are extrapolated to apply to the entire Edremit Graben. In that case, its evolution is seen as the succession of two extensional stages, characterized by distinct structural and sedimentological patterns, and possibly separated by a short compressional phase.

© 2005 Lavoisier SAS. All rights reserved.

Keywords: Northwestern Anatolia; Kazdağ Massif; Edremit Graben; extensional tectonics; detachment fault; two-stage extension

1. Introduction

The Aegean domain (Fig. 1), and specially western Turkey, displays one of the most active extensional tectonic regimes of the world, as shown by seismic and geodetic data [1-5]. This Late Tertiary regime has endured enough to develop typical extensional structures, such as core complexes, grabens, and their associated sedimentary basins (e.g., [6-14]). The most striking feature is the occurrence in western Turkey of about ten WNW-ESE-trending Neogene grabens, whose timing and origin of formation are the subjects of a long-lived debate (e.g., [15-27]).

The origins of crustal extension in the Aegean are set forth in four different models: (i) the “orogenic collapse” model, characterized by the spreading and thinning of an overthickened crust during the latest Oligocene-Early Miocene (e.g., [28-30]); (ii) the “back-arc spreading” or “slab-roll back” model, related to the southward rollback of the Mediterranean slab and consecutive southward migration of the Hellenic trench (e.g., [1, 31, 32]). These two models are related to late- or post-orogenic extension processes [33, 34]; (iii) the “tectonic escape” model, where the extension results from the westward extrusion of Anatolia since the late Serravalian, following the collision between

* Corresponding author.

E-mail address: laurent.beccaletto@igp.unil.ch (L. Beccaletto)

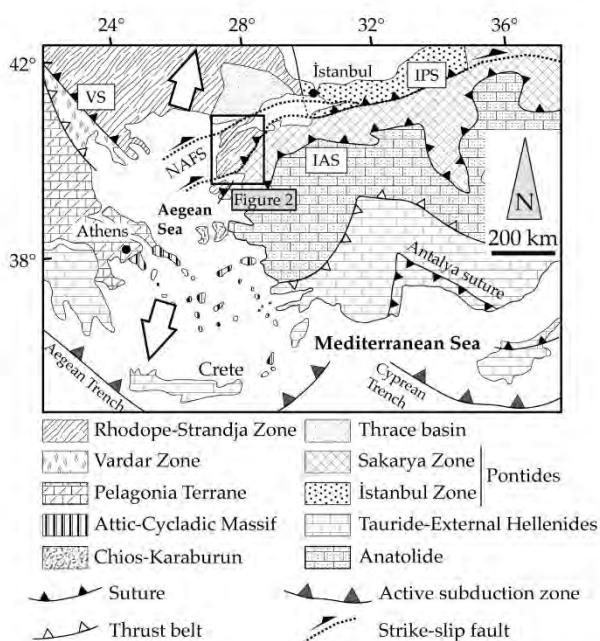


Fig. 1 Structural map of the Aegean domain, with the main sutures and neotectonic features; white arrows show the present-day extensional regime. NAFS- North Anatolian Fault System; VS- Vardar suture; IPS- Intra-Pontide suture; IAS- İzmir-Ankara Suture; modified from Bozkurt and Mittwede [80] and Okay *et al.* [82].

Arabia and the Taurides [35, 36]; (iv) the “episodic, two-stage graben” model, which combines two or more of the above mechanisms; in this model, the last phase of Plio-Quaternary extension followed an earlier phase due to orogenic collapse during the latest Oligocene-Middle Miocene times [17]; the two phases of extension are thought to be separated by a short interval, characterized by a N-S compressional event (e.g., [17, 23, 27]).

Therefore, to gain a better comprehension of the Late Tertiary extensional tectonic regime in western Turkey, one must answer the two central questions about (1) its continuous or discontinuous nature, and (2) the driving mechanism at its origin. The field recognition and the timing of the extensional structures in western Turkey, as well as their structural relationships, are of major interest to answer these questions. The present paper focuses on the central part of the northern edge of the Edremit Gulf, northwestern Turkey (Fig. 2). We first give a description of the three main geological units: the metamorphic Kazdağ Massif, which represents a core-complex of Late Oligocene-Early Miocene age [9, 37], the Tethyan accretion-related Çetmi mélangé, and the Küçükkuşu sedimentary basin (Küçükkuşu formation). We then describe for the first time a large-scale detachment fault, the Şelale detachment fault, which separates the high-grade metamorphic rocks of the Kazdağ Massif in the footwall, from the unmetamorphosed rocks of the Çetmi mélangé associated with the overlying

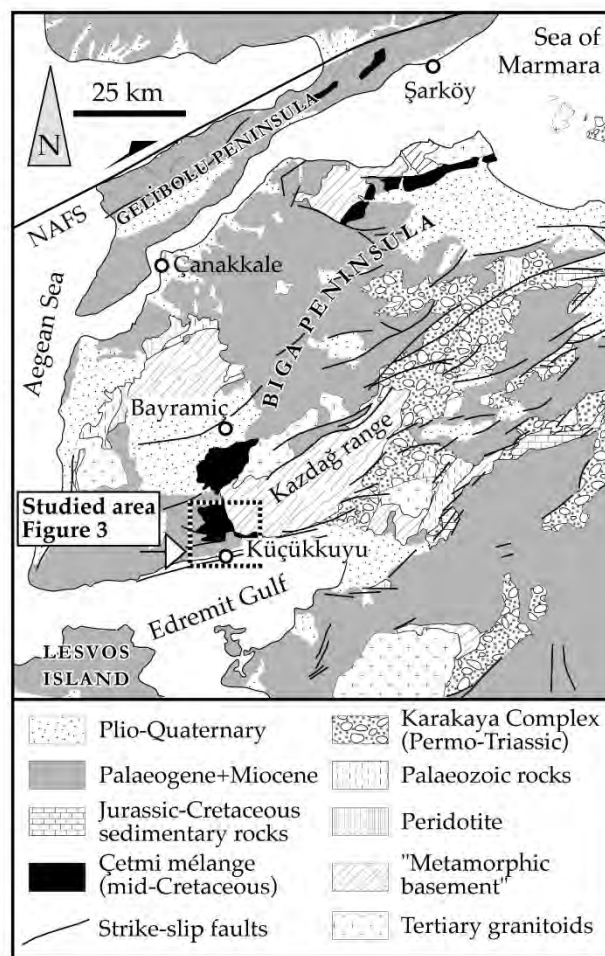


Fig. 2 Geological map of the Biga Peninsula, with the location of the studied area. NAFS- North Anatolian Fault System; modified from Siyako *et al.* [42].

Küçükkuşu basin in the hanging wall. The role of the latter is reassessed as a syntectonic sedimentary basin (supradetachment basin). A special focus is made on the structural relationships between the Şelale detachment fault and later high-angle normal faults, which leads us to suggest an episodic two-stage extensional process at the initiation of the formation of the Edremit Graben. The last part discusses the possible driving mechanism at the onset of Late Tertiary-Quaternary crustal extension in western Turkey and, by extrapolation, in the whole Aegean domain.

2. Geological Units

The three main geological units of this study, the Kazdağ Massif, the Çetmi mélangé, and the Küçükkuşu formation, are separately described below. The description is based on detailed field mapping of the area at the 1/15000 scale (Fig. 3; [38]).

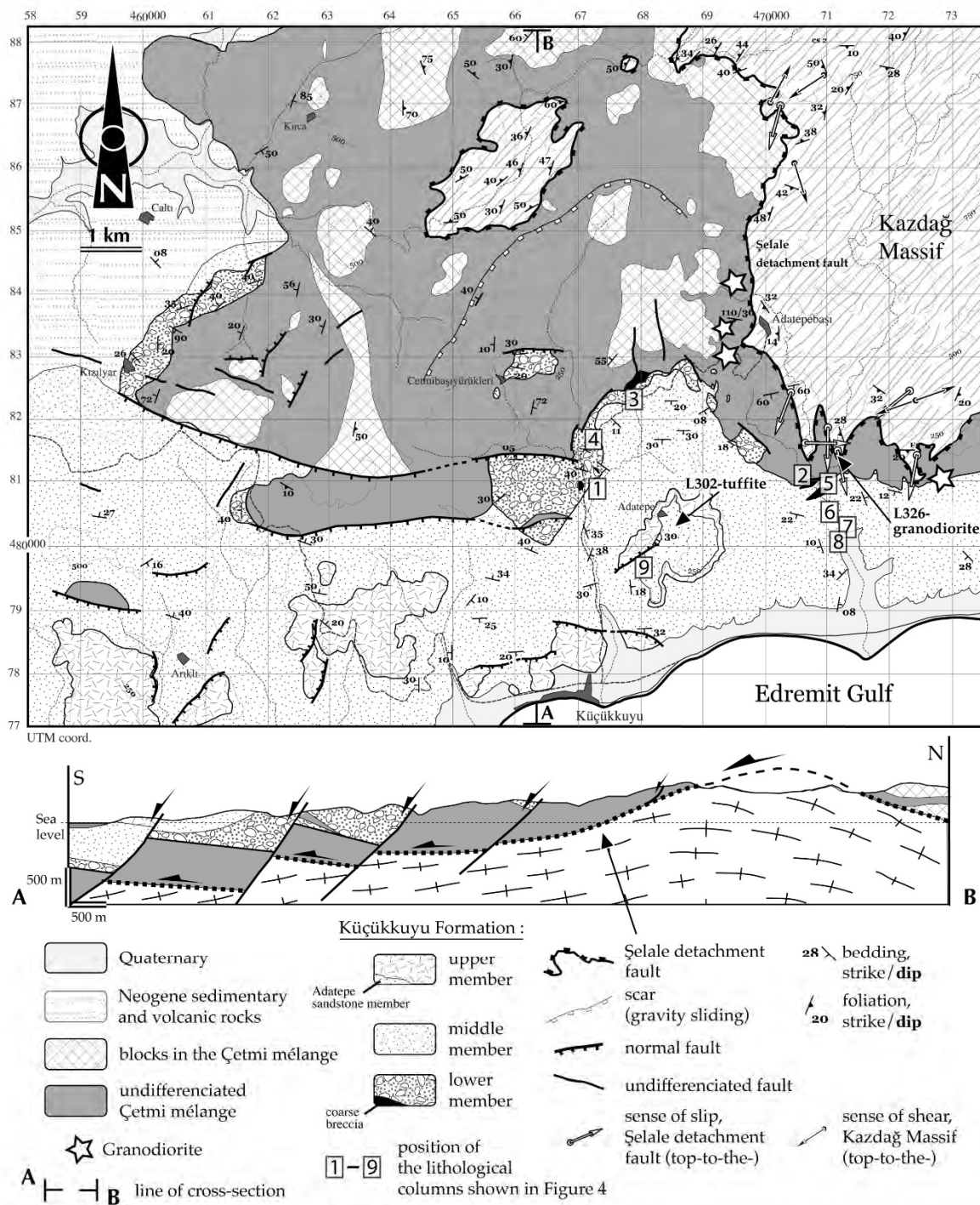


Fig. 3 Geological map and cross section of the studied area, showing the structural relationships between the Kazdağ Massif, the Çetmi mélangé, and the Küçükkuuyu formation.

2.1. The Kazdağ Massif

The Kazdağ Massif, bordering the northern side of the Edremit Gulf, is an NE-trending structural dome approximately 50-km long and 20-km wide. Metamorphosed ultramafic rocks and metagabbro occur in the core of the

dome, and are enveloped by a marble-rich sequence, which passes upward into felsic gneisses with marble and amphibolite intercalations. In its western part, the Kazdağ Massif consists of an intercalation of felsic gneiss, calc-silicate gneiss, amphibolite, marble and minor migmatite [37, 39]. The metamorphic assemblage, typical of the amphibolite

facies, is thought to be of latest Oligocene age, contemporaneous with core-complex formation (24 Ma, Rb/Sr method on micas, [9]), with Carboniferous inherited zircon ages (308 ± 16 Ma, Pb evaporation method, [40]).

The present study is limited to the southwestern end of the Kazdağ Massif, where the massif is in tectonic contact with the overlying unmetamorphosed Çetmi mélangé along a low-angle detachment fault (Fig. 3); the mélangé is then overlain by the sedimentary rocks of the Küçükkuş formation. In the north of the study area, the mélangé tectonically overlies the Kazdağ Massif along an intervening mylonitic zone [37]; the age of the mylonites (at least locally) is Late Palaeocene–Early Eocene (55.05 ± 6.2 Ma, Ar/Ar method on micas, [41]); thus, they may predate the deformations discussed here [38]. East of the study area, the southern side of the Kazdağ Massif is in tectonic contact with Plio-Quaternary deposits along a large fault scarp (section 3.3).

2.2. The Çetmi Mélangé

The Çetmi mélangé is an unmetamorphosed Tethyan accretion-related tectonic mélangé [38]; the mélangé also crops out in the northern Biga Peninsula north of the city of Biga. In order of decreasing abundance, it is made of slices/blocks of altered basic and pyroclastic rocks, blocks of upper Triassic limestones, and some various lithologies such as eclogite, serpentinite and listwaenite, Triassic pelagic limestone and radiolarite; the matrix consists of an alternation of greywacke and shale. The geodynamic evolution of the mélangé ended in the mid-Cretaceous with its emplacement on the Rhodope margin, so that it has passively suffered the Tertiary deformations [38]. The Çetmi mélangé is overlain along a tectonic contact by the sedimentary rocks of the Küçükkuş formation.

2.3. The Küçükkuş formation

The Küçükkuş formation [42] comprises the filling of a small sedimentary basin (c. 20-km long and 5-km wide), closely surrounding the Çetmi mélangé north of the town of Küçükkuş. The stratigraphy of the basin is shown through nine detailed lithological columns established from key areas (Figs 4, 5).

2.3.1. Stratigraphy of the Küçükkuş formation

The Küçükkuş formation is divided into three different members, based on facies associations and similarities.

The *lower member* crops out in a narrow zone (less than 1-km wide) directly above the Çetmi mélangé; its thickness is estimated to be a maximum of 150 m. Small syn-sedimentary normal faults with metre-scale throw affect this sequence. The *lower member* consists of a volcano-detrital sequence, with coarse reddish to greyish sandstone and conglomerate (Fig. 6a), alternating with tuff, tuffite and acidic lava flow, also red-pink in colour (Fig. 4, column 1). Towards the top, near the transition with the *intermediate member*, the sequence becomes carbonate-rich (marl and

limestone alternation, carbonaceous cement in microconglomerate, column 2). Columns 5 and 6 show a lateral equivalent, comprising green to red marls, alternating with grey-greenish limestone with charophytes and ostracods, interpreted as local lacustrine sediments. The whole member is characteristic of continental fluvial depositional environment (braided-river type) with alluvial-fan affinities, possibly grading laterally and towards the top into a proximal lake environment.

A striking feature of the lower member is the occurrence of breccias at its top, marking locally the transition to the *intermediate member* (columns 2, 3 and 4). Columns 7 and 8 show a progressive transition from the lacustrine deposits to carbonated sandy layers, and then to the *intermediate member*. Indeed, it is not clear from field relationships whether the breccias overlie the lacustrine deposits, or whether they are lateral equivalents. In the latter case, a 2-3-metre-thick conglomeratic episode may be a good lateral equivalent (column 7). The breccias are overwhelmingly monogenic, with cm to multi-dm angular blocks, without any organization (chaotic aspect). The fabric is block-supported, and matrix, where present, consists of the sandy fraction of the same material as the blocks. They are interpreted as subaerial foot-scarp deposits, following local fault activity.

The *lower member* is similar in facies and occurrence to the Kızılyar formation, described farther west near the Kızılyar village ([42], and Fig. 3). The presence of fan deposits, volcanic and tectonic activity, fault breccias, as well as the narrowness of the member, all suggest that a strong extensional tectonic activity controlled the sedimentation of the *lower member*. A similar active tectonic setting has been proposed for the Kızılyar formation [43]; because of their same lithology, depositional environment, structural position and spatial proximity, the Kızılyar formation is treated as an equivalent of our *lower member* and is incorporated into it.

The *intermediate member* of the Küçükkuş formation, c. 400 m in thickness, is made of rhythmic alternations of yellowish oxidized silty shale and siltstone-sandstone turbidites (column 9, and Fig. 6b). The contact with the lower member is conformable for the most part.

The proportion of fine-grained material is more important than the sandy material (in a ratio higher than 3 to 1). The layers are generally thin (less than 10 cm), with rare thicker beds (up to 3 m). They generally have carbonate cements. Erosional sole casts are scarce, whereas load casts occur more abundant. The sandstone layers show typical A, B and C Bouma sequences, and the flow structures all indicate a southward direction of transport. Near the base of the sequence, sandstone beds rework cm to dm fibrous wood fragments. Some slump structures and syn-sedimentary normal faulting have been observed. In the western part of the area, the base of the sequence comprises yellowish dolomitic silty laminated limestones, alternating with locally bituminous shales.

Towards the top of the sequence, there is renewed input of volcanogenic components (ash, feldspar) in the sediment; as a result, the rocks become more tuffitic, locally with a

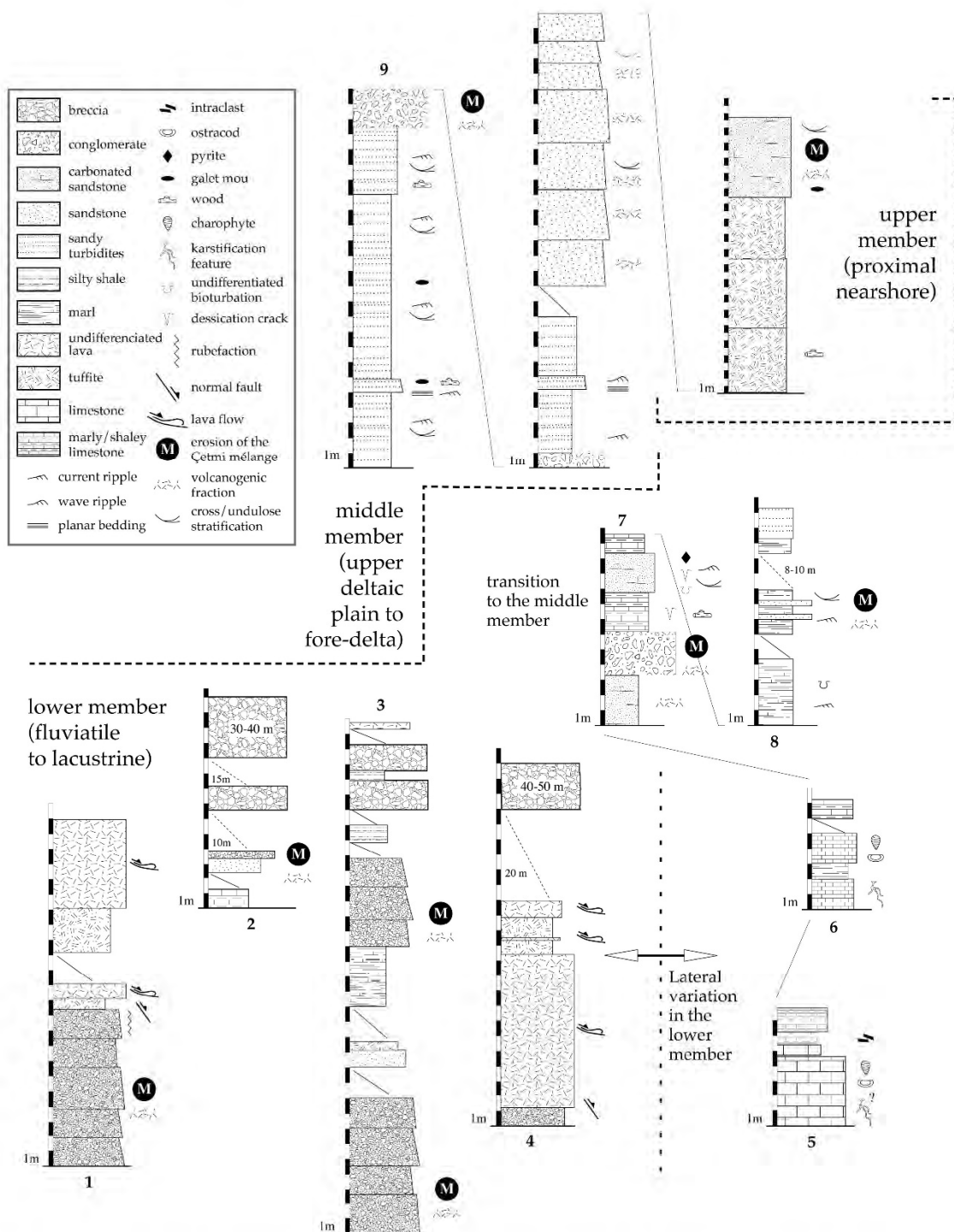


Fig. 4 Detailed lithological columns of the Küçükuyu formation and their vertical distribution (location of the columns on Figure 3).

greenish colour. Near Adatepe village, the transition to the *upper member* is made through a 20-m-thick succession of massive coarse sandstone/microconglomerate beds, with a clear tuffitic component (column 9).

Palynomorph assemblages from the base of the *intermediate member* (det. Prof. P. Hochuli, ETH Zürich), found in

the more dolomitic sequence, suggests a fresh-brackish water environment indicating a lacustrine environment (characteristic dinoflagellate, confirming the results of İnci [44]). The *intermediate member* is therefore interpreted as a turbiditic, progressive filling of a lake basin, with increasing volcanic activity towards the top of the sequence.

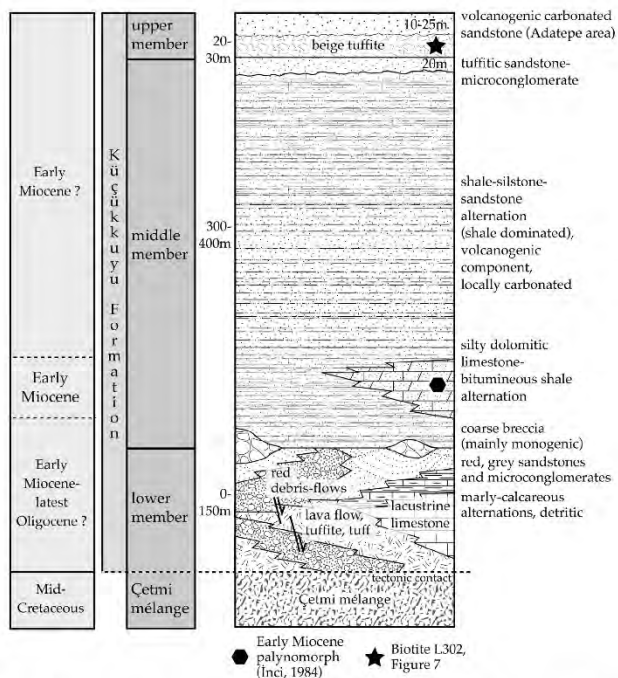


Fig. 5 Synthetic lithostratigraphic column of the Küçükkuyu formation.

The *upper member* comprises 20-30 m of beige-yellowish amalgamated tuffite deposits (Fig. 6c). At the base, abundant oxidized wood fragments, green mud balls and detrital feldspar, suggest moderately high-energy hydrodynamic features. This thick tuffitic bed is a discontinuous marker bed, invariably found at the top of the Küçükkuyu formation. Near Adatepe village, the tuffites progressively grade into coarse carbonate-rich sandstones, with a strong volcanicogenic component. All these features are characteristic of a detrital shallow-water environment, deposited in a more proximal setting than the *intermediate member*.

We therefore interpret the whole Küçükkuyu formation as follows: the *lower member* records strong volcanic and extensional tectonic activity, that were concomitant with the development of a small basin. The latter was progressively filled by shale-dominated lake turbidites (*intermediate member*). Such a rhythmic infill, together with slump and normal fault structures, suggests continuing tectonic control on sedimentation. The end of the filling and the starvation of the lake are marked by the *upper member*, which also confirms the re-initiation of volcanic activity in proximity to the basin.

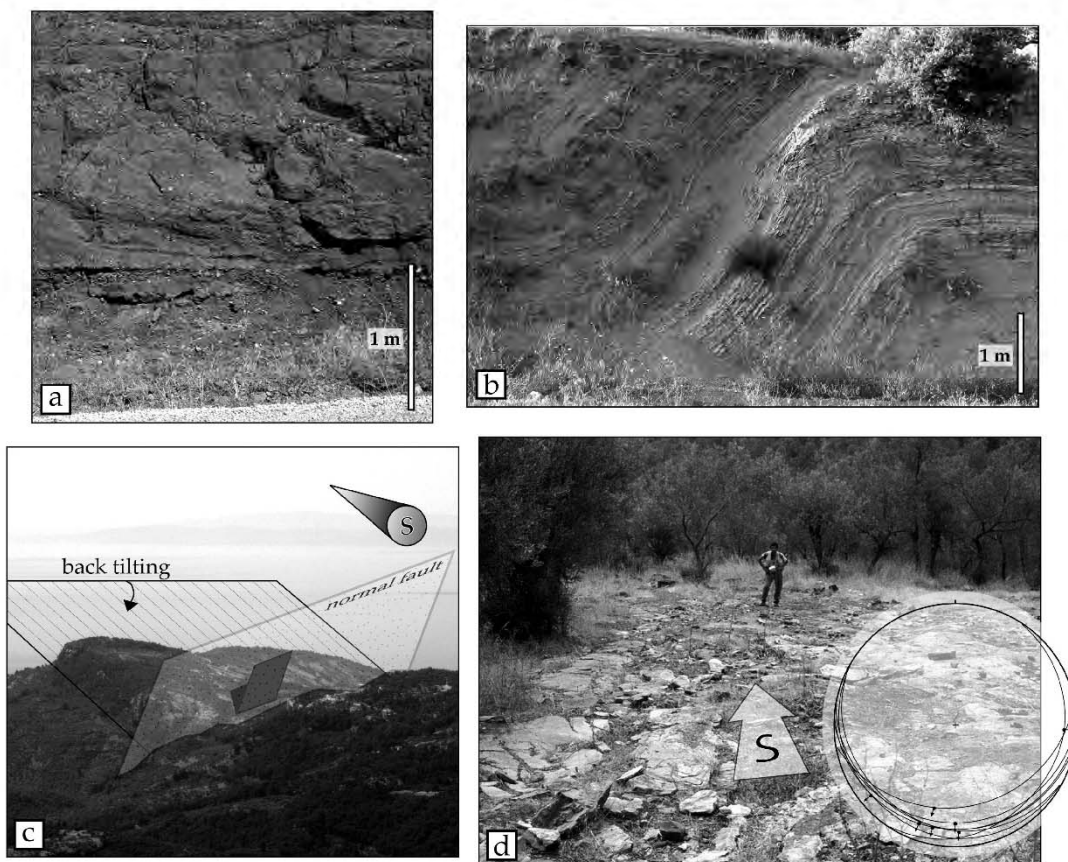


Fig. 6 Pictures of typical outcrops, Küçükkuyu area. (a) Red coarse fluvial conglomerate of the *lower member* of the Küçükkuyu formation; note the cross stratification and the white spots corresponding to centimetric quartz pebbles; (b) folding in the turbidites of the *middle member* of the Küçükkuyu formation; (c) back-tilted thick tuffite layers of the *upper member* of the Küçükkuyu formation; (d) detail of one of the major fault planes of the Şelale detachment fault. Insert: slip planes and senses of displacement of the upper plate (equal area lower hemisphere projection); man is 1.75 meter high.

The lithologies from the underlying Çetmi mélangé are systematically reworked in the *lower*, *middle*, and *upper members* of the Küçükuyu formation (see Fig. 4). Because of their resistant nature, the red radiolarite clasts are good markers of the continuous upstream presence of the Çetmi mélangé during basin evolution. Another source of the detritus was volcanic rocks, deposited close to the basin. A crucial point is that no lithologies from the Kazdağ Massif have been found in the Küçükuyu formation. Moreover, the occurrence of erosional products derived from the Çetmi mélangé in the Early Miocene implies that the latter was cropping out over a much larger area than today. As for younger Miocene rocks, they are absent in the study area, and are scattered in the neighbourhood without any direct geographic link to the Küçükuyu formation; they consist of calc-alkaline intermediate lava and pyroclastic rocks of Early-Middle Miocene age, with scarce carbonated and detrital intercalated sequences (Ayvacık and Balabanlı volcanics, [43, 45, 46] and references therein).

2.3.2. Age of the Küçükuyu formation

The age of the Küçükuyu formation is Early Miocene [44], based on a palynomorph association from bituminous shales that alternate with the dolomitic silty limestones in the western part of the *intermediate member* (equivalent to the Nüsrathı formation of İnci [44]).

We dated a biotite grain sampled from a detritic tuffite of the *upper member* of the Küçükuyu formation using the $^{40}\text{Ar}/^{39}\text{Ar}$ method (performed in Montpellier University by

P. Monié); the result shows a confident age of 34.4 ± 1.2 Ma (Fig. 7 and Table 1). This latest Eocene age (Priabonian) does not fit with the age of the fauna of the *intermediate member*, and is thus not interpreted as the age of the deposit, but as the age of the source of the detrital material for the *upper member*. Similar ages have been found in autochthonous acidic volcanic rocks in the Biga Peninsula (Eocene Balıklıçesme volcanics and Upper Eocene-Oligocene Çan volcanics; [46]). The source was probably the andesitic to rhyolitic rocks of the Çan volcanics, in so far as they are much closer to the present Küçükuyu basin.

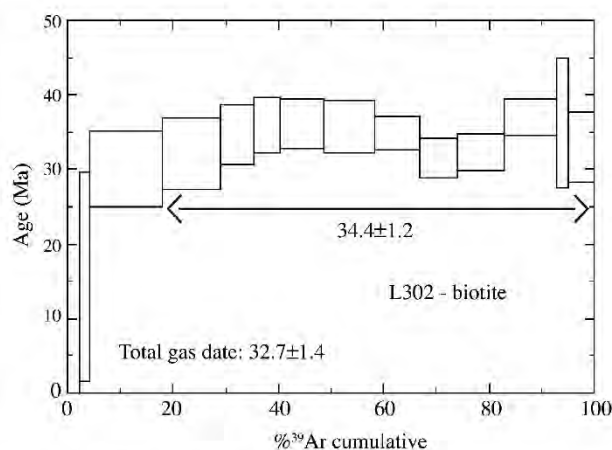


Fig. 7 $^{39}\text{Ar}/^{40}\text{Ar}$ age spectra for sample L302 from the tuffitic upper member of the Küçükuyu formation (sample's location on Figure 3).

Table 1

$^{39}\text{Ar}/^{40}\text{Ar}$ analytical data for *in situ* laser ablation analyses from the tuffite sample (L302) belonging to the upper member of the Küçükuyu formation.

L302	$^{40}\text{Ar}/^{39}\text{Ar}$	$^{36}\text{Ar}/^{40}\text{Ar}$ x 1000 J = 0.014283	$^{39}\text{Ar}/^{40}\text{Ar}$	$^{37}\text{Ar}/^{39}\text{Ar}$	% ^{39}Ar	% Atm.	Age (Ma)	error
1	0.612	3.163	0.1063	0.291	4.1	93.4	15.7	14.1
2	1.177	2.731	0.1639	0.044	18.1	80.7	30.1	5.0
3	1.256	2.255	0.2655	0.015	29.0	66.6	32.1	4.8
4	1.362	2.015	0.2967	0.000	35.4	59.5	34.8	4.0
5	1.406	1.752	0.3428	0.000	40.4	51.7	35.9	3.7
6	1.418	1.735	0.3436	0.139	48.8	51.3	36.2	3.3
7	1.400	1.797	0.3349	0.139	58.3	53.1	35.7	3.5
8	1.367	1.925	0.3154	0.069	67.0	56.9	34.9	2.2
9	1.232	1.842	0.3696	0.155	73.9	54.4	31.5	2.6
10	1.268	1.710	0.3901	0.134	83.0	50.5	32.4	2.4
11	1.451	1.084	0.4683	0.163	92.7	32.1	37.0	2.4
12	1.419	1.599	0.3717	0.041	95.1	47.2	36.2	8.7
13	1.295	0.293	0.7056	0.051	100.0	8.6	33.1	4.7
Total age =							32.7 ± 1.4	

3. Structural Pattern

We describe now the major tectonic features of the area, which include (i) the Şelale detachment fault, between the Kazdağ Massif on one side and the Çetmi mélangé and Küçükkuyu formation on the other side; (ii) folds in the Küçükkuyu formation; and (iii) numerous steeply dipping normal faults cutting through all the previous units.

3.1. The Şelale detachment fault

A major south-dipping low-angle (15–20°)—and presently inactive—detachment fault, the Şelale detachment fault, occurs between the Kazdağ Massif (footwall or lower plate) and the Çetmi mélangé/Küçükkuyu formation (hanging wall or upper plate).

This structure displays well-developed fault planes, with SSW-trending slip lineations, indicating southward to southwestward sense of movement (scarps and striations, Fig. 6d). The fault planes generally show brecciation of the marbles or gneisses of the Kazdağ Massif. In map view, the Şelale detachment fault displays typical corrugations, a characteristic feature of many detachment faults. The present-day topography of the southern flank of the Kazdağ Massif in the area is still controlled by the low-angle geometry of the Şelale detachment fault, as the general topography of the hills gently slopes seaward at an angle of about 10°, parallel to the detachment plane.

The rocks of the lower plate are the metamorphic rocks of the Kazdağ Massif; they have generally developed a mylonitic fabric, with their foliation running roughly parallel to the Şelale detachment fault, and dipping towards it. Five oriented samples from gneisses, amphibolite and metasediment have been collected; two have a broad top-to-the southwest shear sense, one top-to-the northeast, one has two opposite shear senses, and one is inconclusive (Fig. 3). These preliminary results, plus field observations, point toward a general top-to-the-south sense of shear in the mylonites. The bulk of the shear deformation took place in the greenschist facies, suggesting a retrograde metamorphism from the amphibolite to the greenschist facies towards the detachment; evidence for this is the systematic crystallization of chlorite in the shear bands, chloritization of biotite, and pre-deformation garnet partially replaced by chlorite and calcite in the deformation zone.

The upper-plate rocks, relative to the Şelale detachment fault, are made by the various lithologies of the Çetmi mélangé. In the vicinity of the detachment, the lithologies consist mainly of spilite and minor marble. Above the fault plane, at a thickness of several tens of metres or more, the spilites (and other lithologies where present) are systematically brecciated, with strong siliceous alteration, and more sporadically, carbonatization. In this area, the mélangé appears to be totally disorganized, and to have lost its already complex primary features. Some secondary south-dipping low-angle faults occur in the mélangé, highlighting

strong rheological contrast between lithologies; they are interpreted as smaller-scale detachment faults, co-genetic with the main Şelale detachment fault. The mélangé is then overlain along tectonic contacts by the Küçükkuyu formation of Early Miocene age.

3.1.1. Age of the Şelale detachment activity

Several small elliptical granitoid bodies (150 m maximum length for the longitudinal axis) crop out very near the detachment fault in the mélangé. These bodies are internally undeformed but show evidence of strong mineral alteration. They are interpreted as pre-dating the detachment activity, because: (i) one of these intrusions (granodiorite, sample L326, Fig. 3) is clearly cut by the Şelale detachment fault, and (ii) they are not randomly distributed but occur only in the upper plate near the detachment plane (for instance, they do not intrude the Kazdağ Massif). Selected zircons from the granodiorite that is cut by the Şelale detachment fault have been dated using the U-Th-Pb *in situ* ion-microprobe method (performed at the CRPG Nancy, by D. Bosch, Montpellier University). Because of the expected young age of the granodiorite (i.e., Tertiary), there was some doubt as to the amount of radiogenic Pb, and hence concerning the feasibility of the dating method. However, an extremely accurate U-Pb concordia age of 29.94 ± 0.37 Ma has been obtained from 18 spots on 16 grains (Fig. 8 and Table 2). This latest Early Oligocene age (late Rupelian) is considered as a lower limit for the activity of the Şelale detachment fault.

Moreover, a latest Oligocene age from a mylonitic marble of the Kazdağ Massif, taken west of Adatepebaşı village, has been reported by Lips (26.7 ± 2.8 Ma, Ar-Ar method on white mica, [41]); this age is in agreement with the post-Rupelian age of activity on the Şelale detachment fault.

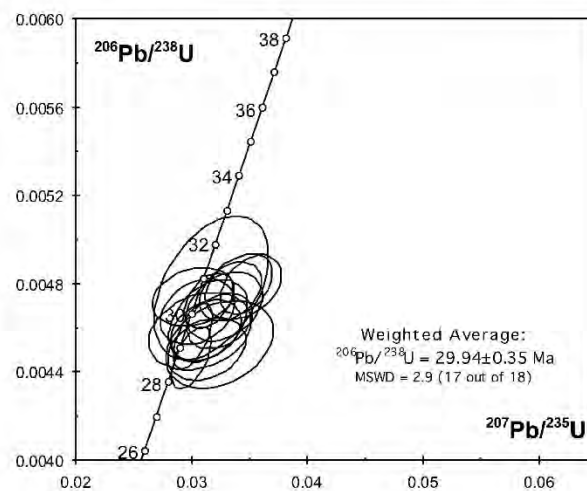


Fig. 8 Concordia diagram for zircons from the granodiorite cut by the Şelale detachment fault (sample L326, location on Figure 3).

Table 2
U–Th–Pb microprobe analytical data from the granodiorite (sample L326) cut by the Şelale detachment fault.

Grain	U	Pb*	Th	Th/	²⁰⁶ Pb/	²⁰⁸ Pb/		²⁰⁶ Pb/	±	²⁰⁷ Pb/	±	²⁰⁷ Pb/	±	²³⁸ U/	±	²³⁵ U/	±
area	ppm	ppm	ppm	U	²⁰⁴ Pb	²⁰⁶ Pb	±	²³⁸ U	(1s)	²³⁵ U	(1s)	²⁰⁶ Pb	(1s)	²⁰⁶ Pb	(1s)	²⁰⁷ Pb	(1s)
#1-1	425	1.9	494	1.16	334	0.271	0.063	0.00522	0.00021	0.0411	0.0074	0.0570	0.0100	33.59	1.34	40.85	7.19
#2-1	510	2.0	557	1.09	1,623	0.264	0.018	0.00459	0.00006	0.0312	0.0012	0.0493	0.0019	29.52	0.36	31.22	1.22
#2-2	834	3.4	1,363	1.63	1,513	0.390	0.014	0.00467	0.00006	0.0305	0.0013	0.0474	0.0020	30.05	0.39	30.52	1.30
#3-1	444	1.8	484	1.09	1,317	0.260	0.023	0.00474	0.00005	0.0302	0.0014	0.0461	0.0021	30.48	0.35	30.16	1.42
#4-1	633	2.5	928	1.47	1,993	0.348	0.014	0.00463	0.00005	0.0324	0.0012	0.0508	0.0017	29.78	0.33	32.42	1.13
#5-1	795	3.5	572	0.72	49	0.180	0.411	0.00509	0.00072	0.0211	0.0221	0.0301	0.0312	32.73	4.61	21.20	21.73
#6-1	458	1.9	527	1.15	1,574	0.272	0.017	0.00476	0.00005	0.0334	0.0011	0.0508	0.0015	30.64	0.35	33.33	1.06
#7-1	511	2.1	574	1.12	2,071	0.270	0.019	0.00479	0.00006	0.0345	0.0013	0.0522	0.0019	30.79	0.39	34.40	1.31
#8-1	718	2.9	1,008	1.40	2,532	0.337	0.009	0.00472	0.00005	0.0315	0.0008	0.0484	0.0012	30.38	0.33	31.48	0.83
#8-2	477	2.0	501	1.05	3,269	0.254	0.011	0.00479	0.00005	0.0347	0.0009	0.0526	0.0012	30.83	0.35	34.68	0.89
#9-1	612	2.5	858	1.40	2,079	0.335	0.014	0.00470	0.00006	0.0328	0.0014	0.0507	0.0020	30.20	0.41	32.79	1.33
#10-1	563	2.2	847	1.50	1,607	0.355	0.015	0.00463	0.00008	0.0314	0.0014	0.0492	0.0020	29.79	0.49	31.42	1.35
#11-1	403	1.6	434	1.08	1,276	0.238	0.023	0.00458	0.00007	0.0307	0.0018	0.0486	0.0028	29.49	0.46	30.73	1.78
#12-1	422	1.6	441	1.04	1,391	0.257	0.026	0.00452	0.00008	0.0324	0.0019	0.0520	0.0029	29.10	0.52	32.40	1.85
#13-1	1202	4.6	2,143	1.78	5,049	0.418	0.013	0.00446	0.00006	0.0300	0.0007	0.0487	0.0009	28.71	0.37	30.00	0.69
#14-1	753	3.0	1,230	1.63	2,763	0.386	0.009	0.00456	0.00006	0.0301	0.0007	0.0479	0.0009	29.34	0.39	30.13	0.68
#15-1	577	2.2	809	1.40	1,442	0.332	0.012	0.00450	0.00006	0.0313	0.0014	0.0504	0.0021	28.97	0.37	31.30	1.35
#16-1	539	2.2	633	1.17	1,578	0.238	0.041	0.00478	0.00013	0.0317	0.0020	0.0481	0.0027	30.75	0.85	31.68	1.98

Both data suggest that the Şelale detachment fault was active at least in the latest Oligocene, but without any direct constraint on the end of its activity. It appears then that the Şelale detachment fault must have played an important role in the first exhumation processes of the western end of the Kazdağ Massif in latest Oligocene time.

3.2. Folds

In addition to the syn-sedimentary faulting mentioned in section 2.3, the sediments of the Küçükuyu formation show evidence of folding. The dip and directional data from the bedding of the lithologies of the narrow *lower member* suggest large open folding. Moreover, well-developed fold structures occur in the *intermediate member*, where turbidites show many open to gentle small-scale folds (Fig. 6b). These features can be observed along the various roads and tracks crossing the field area. Although they have not been mapped in detail, preliminary observations indicate no preferential orientations for the fold axes. On the other hand, the massive tuffitic beds of the *upper member* of the Küçükuyu formation show no folding, possibly because of its discontinuous nature and its more competent lithology, compared to the underlying turbidites.

3.3. Step-like normal faults

The Şelale detachment fault, the Küçükuyu formation and the Çetmi mélange are cut by numerous roughly east–west-trending, south-dipping high-angle normal faults (Fig. 3). A striking piece of evidence for this is the southward back-tilting of the discontinuous massive tuffitic beds of the *upper member* of the Küçükuyu formation (Fig. 6c), and the juxtaposition of these tuffitic beds with the lithologies of the Çetmi mélange.

The normal faults, parallel to the Edremit Graben, have also been described in the Kazdağ Massif north and west of the Şelale detachment fault [47], and farther west and east of the field area, where they are related to the Late Pliocene–Quaternary opening of the Edremit Graben [24, 43]. All of these steeply dipping normal faults, bordering the northern side of the Gulf of Edremit, are grouped together under the generic name Edremit fault zone. The Plio–Quaternary graben infill, whose deposition was controlled by activity of the Edremit fault zone, consists of loose coarse clastics, characteristic of fan and alluvial deposits. These lithologies are observed at the surface only east of the study area, toward the end of Edremit Gulf, and also for several hundred metres in an exploration well drilled in the eastern part of the

gulf [42, 43]. However, over a small part of the field area east of Küçükuyu, similar red coarse clastics with reworked Kazdağ pebbles have been found, overlying turbidites of the Küçükuyu formation along a north-tilted low-angle unconformity (c. 10°). The Plio-Quaternary Edremit Graben is co-genetic with the E–W-trending Bayramiç Graben, located north of the Kazdağ Massif and Çetmi mélange [43]; its Plio-Quaternary infill is also made up of coarse red conglomerates that have reworked the metamorphic lithologies of the Kazdağ Massif, as well as Upper Miocene-Lower Pliocene limestones.

4. Discussion and conclusions

The southwestern part of the Kazdağ Massif (footwall) is tectonically overlain by the unmetamorphosed Çetmi mélange and Küçükuyu formation (hanging wall) along the Şelale detachment fault. The Küçükuyu formation is a syn-tectonic sedimentary basin of Early Miocene age, which developed simultaneously with the detachment activity. Tectonic control of the sedimentary processes, recorded in the rapid deepening and consecutive infilling of the Küçükuyu basin, is a strong argument for interpreting the Küçükuyu formation as a typical supra-detachment basin developed above the low-dipping detachment plane [48]. Note that the presently low dip angle of the detachment plane may have been different at the time of deformation; for instance, this angle may have been modified by the later activity of the steep normal faults. However, if the hypothesis of the Küçükuyu formation as a supra-detachment basin is accepted, then the dip of the Şelale detachment fault must not have been much higher than it is today. The sedimentation was synchronous with ongoing deformation in the footwall (mylonitization of the Kazdağ Massif), along the southward dipping Şelale detachment fault, but also in the Çetmi mélange; unlike many areas, the overlying sedimentary basin is not in direct contact with the detachment fault, but with an intermediate unit (the Çetmi mélange), which accommodated part of the extension. This particular feature may be related to the weak rheological competence of the already disrupted Çetmi mélange at the time of deformation.

As noted in the introduction, a key question with regard to regional tectonics is the continuous or episodic aspect of the extensional process in western Turkey. We provide here structural, stratigraphic and metamorphic arguments supporting a two-stage evolutionary model [20, 21, 23, 25, 27], before discussing the driving mechanism for this tectonic activity.

(i) The step-like normal faults clearly cut and displace the Şelale detachment fault, the Kazdağ Massif, the Çetmi mélange, and the Küçükuyu formation; hence, they cannot be genetically related to the detachment in so far as they postdate its activity (Fig. 9).

(ii) The erosional products found in the Lower Miocene Küçükuyu formation and the Pliocene-Quaternary infill of the Edremit Graben are different; the former is recycled pebbles from the Çetmi mélange, without any pebbles from the Kazdağ Massif. On the contrary, the first metamorphic pebbles from the Kazdağ Massif are encountered in the fluvial conglomerates of the Edremit and Bayramiç basins, whose deposition is linked to the activity of the step-like normal faults. This observation implies that the Kazdağ Massif only reached the surface from Plio-Quaternary times onward, under the control of the brittle activity of the normal faults.

(iii) The brittle-ductile deformation along and on either side of the Şelale detachment fault occurred in the greenschist facies (retrogression of the amphibolite facies), whereas the brittle normal faults were active (and remain active) near or at the surface; this implies that the detachment was active at a deeper structural level than the step-like normal faults, and must have been brought passively to the surface by their activity.

(iv) The recognition of a break in the extensional regime would be a strong argument for the two-stage model. Two signs of such a break may be found in and around the study area; the first is the presence of remnants of a flat-top plateau at the top of the Kazdağ mountains, representing a flat-lying erosional surface [43]. This surface, developed above the Upper Miocene-Lower Pliocene units, is proof of tectonic stability and (brief) cessation of the extensional regime. The other sign of a break in the extensional regime is the occurrence of a possible phase of compression in the region, characterized by the folding observed in the Küçükuyu formation.

(v) From the point of view of the updoming of the Kazdağ Massif, a continuous exhumation from the latest Oligocene to the Present would be quite slow. A depth of c. 14 km for the amphibolite-facies metamorphism, as proposed by Okay and Satır [9], would imply an exhumation rate of 0.56 mm per year, much less than generally expected in core-complex exhumation processes (several mm per year, e.g., [49]). The concentration of the extension in two shorter phases of exhumation (latest Oligocene-Early Miocene and Plio-Quaternary) would increase the exhumation rate.

All of these arguments strongly suggest that the extensional processes in the study area follow a two-stage model, regardless of what happened in the intervening period. We discuss now the possible driving mechanisms at the beginning of this tectonic evolution.

In latest Oligocene-Early Miocene, the Şelale detachment fault was controlling at least a part of the exhumation of the western Kazdağ Massif, with a top-to-the south to southwest sense of shear. The Çetmi mélange, which occurs as an intermediate unit in the hanging wall, was simultaneously accommodating a part of the shear deformation. The *lower member* of the Küçükuyu formation was recording the onset of the tectonic activity, whereas the *middle* and *upper members* were recording the filling of the newly created basin. It

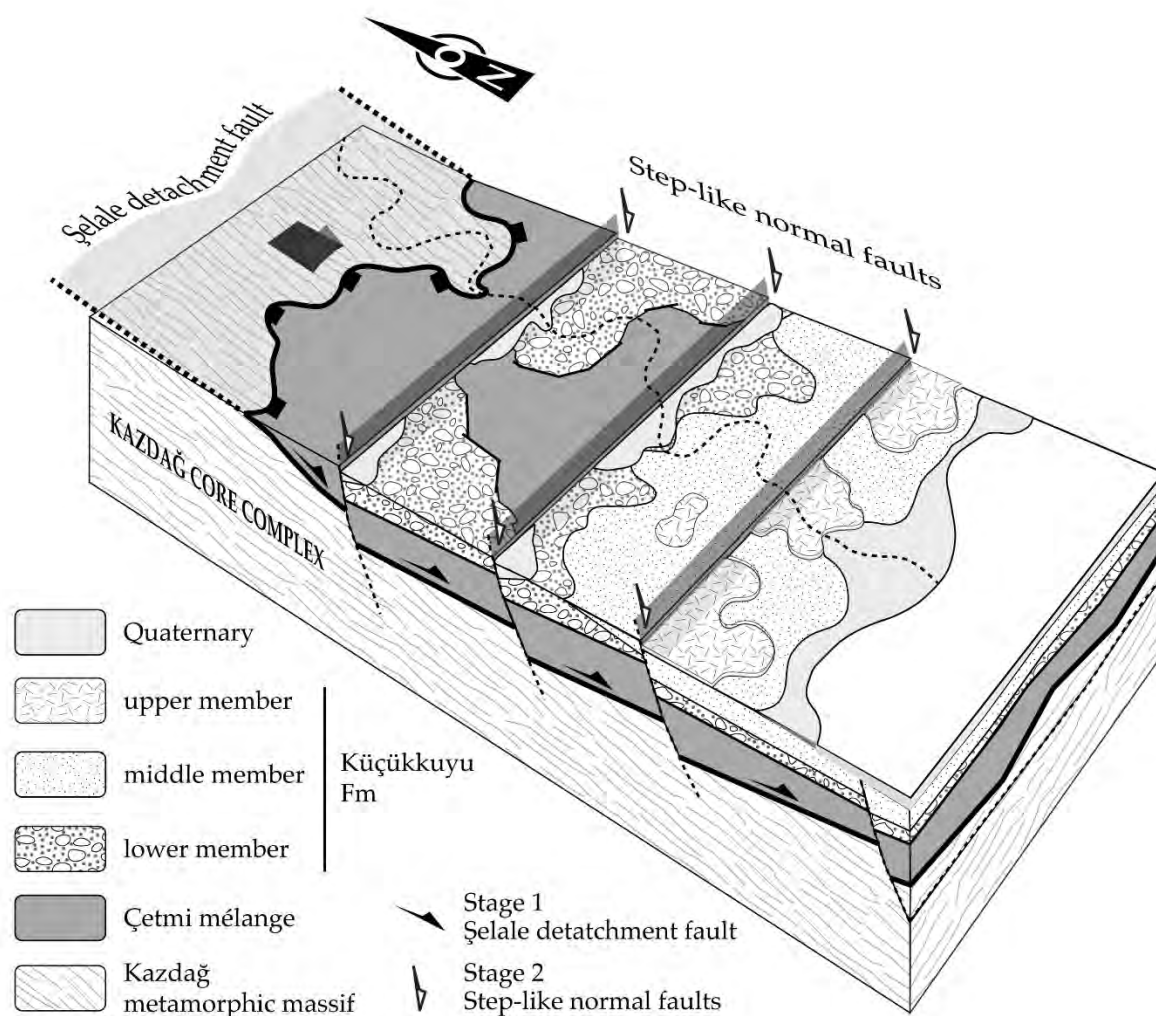


Fig. 9 3D synthetic diagram of the studied area, showing (1) the structural relationships between the Şelale detachment fault and the step-like normal faults, and (2) the distribution of the sedimentation according to the structural frame.

is quite difficult from these local data to resolve the question of the driving mechanisms of the extensional regime in western Turkey in the Late Oligocene–Early Miocene times (see the introduction for the various proposed models). Moreover, the discussion concerns more the timing of the various mechanisms than the mechanisms themselves ([23, 30] and references therein). The “tectonic escape” model fails because extension in western Turkey began prior to the Middle Miocene, and generally the two preferred mechanisms are orogenic collapse versus the back-arc extension of the upper plate due to roll-back of the Mediterranean slab.

We would like first to make two comments: (i) the “orogenic collapse” model requires, in order to be efficient, a free edge along one of the borders of the orogenic area, like a retreating subduction zone, in order to control the extensional processes [28]. In the case of the Aegean domain, a good candidate for the free edge would be the subduction of the Mediterranean slab and its consecutive roll-back; (ii) the

“orogenic collapse” model does not imply very high altitudes, as a consequence of an important overthickened continental crust, as in the Tibet area; a thick continental crust, with moderate altitudes, would also try to reach its equilibrium by spreading and thinning, if boundary forces permit [28]. It means, therefore, that the two mechanisms are not exclusive (or that both are compatible). However, whereas the orogenic collapse is more efficient if accompanied by a roll-back process, the latter can occur regardless of the initial thickness of the crust.

Several indisputable arguments point towards a roll-back of the Mediterranean subducting slab starting in Late Oligocene time, such as the arc signature of the calc-alkaline magmatism in NW Turkey [45, 50, 51], the length of the subducting Mediterranean slab [31, 52], and/or the southward migration of extension-related magmatism and metamorphism in the Aegean (for a detailed discussion, see [9]).

On the other hand, the continental nature of the sedimentation (alluvial fans, rivers and lakes, possibly interconnected) during Early-Middle Miocene time throughout western Turkey, with no marine incursion, suggests intramontane palaeomorphology (this work; [29, 53, 54], possibly related to the presence of relatively high topography. Moreover, another interpretation of the widespread magmatism, mentioned above, claims that it is characterized by a high amount of crustal component, possibly related to an over-thickened crust [55–58]. Lastly, from a geodynamic point of view, the whole Aegean domain was characterized in Palaeocene-Oligocene times by the closure of the Pindos oceanic domain (Palaeocene to Oligocene flysch, Richter and Müller [59, 60]), accompanying the diachronous collision of the Greater Apulia terrane (Apulia, External Hellenides and Bey Dağları, [61]) with the Pelagonian-Tauride Platform [62]. This collision may have initiated thickening of the continental crust in the region, such that consecutive Late Oligocene subduction and roll-back of the Mediterranean slab may have affected a thicker-than-normal crust. These three arguments possibly suggest that north-western Turkey was characterized by a relatively thick crust prior to the inception of extension.

Therefore, all of the previous arguments put together indicate that back-arc spreading, as a consequence to roll-back of the Mediterranean slab, may have affected a (moderately) thick upper plate, leading to its orogenic collapse. Therefore, we propose a combination of the “orogenic collapse” and “back-arc spreading” models to explain the initiation of extension in western Turkey in Late Oligocene-Early Miocene times.

It is difficult to give a regional significance to the folds occurring in the study area, as they are not time-constrained. However, they could be related to compressional structures, found about ten kilometres west of the study area, where Lower-Middle Miocene successions were deformed under a N-S shortening phase at the end of the Middle Miocene [43]. At a smaller scale, both episodes may then be related to the compressional phase observed in the northern Menderes Massif and neighbouring areas, considered to be late Middle Miocene-Early Pliocene in age ([20, 63] and references therein; [64–66]). As for the erosional surface, it appears to be a region-wide time marker, as it is also found farther south in the Menderes Massif, and even farther south yet [24]. Therefore, cessation of the extensional regime may be seen as a regional feature [67] that affected the whole of western Turkey. This event could be related to a late Alpine compressional pulse due to Middle-Late Miocene oceanic suturing between the Tauride block and the Arabian plate [68, 69]. Therefore, the first extensional stage possibly ended with a phase of compression preceding a phase of erosion [20, 23, 67, 70].

The extensional tectonic activity resumed at the end of the Early Pliocene [20, 67]; it is characterized in the study area by the activity of normal faults (belonging to the Edremit fault zone) cutting through all the previous units; it is also

marked by the coeval deposition of coarse sediments with the first pebbles from the Kazdağ Massif, which reached the surface at that time. The Edremit fault zone is located at a crossroad between two major tectonic regimes; first, it marks the western end of the dextral southern branch of the North Anatolian Fault System, whose activity in the region was contemporaneous with the opening of the Plio-Quaternary Edremit Graben [71–73]. Moreover, as seen before, it underwent the influence of a roughly north/south extensional regime in Plio-Quaternary times. The cause of the extensional regime can directly be found in the roll-back of the Mediterranean oceanic lithosphere in the Aegean region, which was active at that time [32, 74]; and minimum age known from the literature, 5 Ma, [75]). The Edremit fault zone had, therefore, a transtensional composite regime, and may be seen as a transfer zone between the strike-slip regime of the North Anatolian Fault System and the extensional regime of the Aegean region. This tectonic pattern is still active today, as seen from GPS and seismicity measurements [76–78]. At a smaller scale, the Plio-Quaternary tectonic regime falls into the complex geodynamic pattern of the eastern Mediterranean domain, which combined the effects of the northward motion of Arabia, the westward lateral escape of Anatolia, and the southward roll-back of the Mediterranean slab.

The structural relationships between the Şelale detachment fault and the late, steeply dipping normal faults clearly underlines the episodic aspect of the extensional tectonics at the onset of basin filling southwest of the Kazdağ Massif (Küçükkuyu formation and Plio-Quaternary infill). Moreover, the two-stage model agrees with the general idea of a two-phase exhumation process for the Kazdağ Massif [9], even if the mechanisms are different for the first stage. An important implication of this work is related to the newly described Şelale detachment fault, and by extension to the formation of the Edremit Graben. We have seen that the Plio-Quaternary deposits crop out only east of the study area, south of the top of the Kazdağ mountains, where the Edremit fault zone is marked inland by a big and steep cliff. In the same way, the older Çetmi mélange and Küçükkuyu formation only crop out at the southwestern end of the Kazdağ Massif and are absent eastward. These characteristics may be due to a differential uplift of the Kazdağ Massif (more important in the east), which produced a differential erosion of the overlying lithologies. A direct consequence is that the Çetmi mélange, the Küçükkuyu formation and Şelale detachment fault were certainly cropping out more extensively than today. This implies that the Şelale detachment fault, because of its inferred geographic extension, would have played a more significant role than expected in the first exhumation phase of the Kazdağ Massif. In that case, and if we apply the same reasoning to the whole southwestern flank of the Kazdağ Massif as for the study area, the evolution of the Edremit Graben appears to have been episodic, with two distinct stages (core-complex mode, then rift mode). Following this hypothesis, the graben was filled by

two successive and distinct sedimentary sequences, under the close control of two separate tectonic phases, whose underlying process was the roll-back of the Mediterranean slab. These general features have already been described farther south in western Turkey, for the Gediz and Büyük Menderes grabens, whose structural evolution follows the “episodic, two-stage graben” model [20–23, 27, 79].

In conclusion, this new work emphasizes (i) the importance of the field recognition of structural and deformational features in the study of extensional basins, as well as (ii) the distinction between sedimentation associated with detachment faults and that related to younger normal fault. Finally, only the combination of structural and stratigraphic data provides a powerful tool for unravelling the evolution of extensional basins.

Acknowledgements

The authors would like to thank G.M. Stampfli for fruitful discussions and original comments. The authors are indebted to E. Bozkurt for his constructive scientific and editorial comments, and express their sincere thanks to A. Okay and A. Koçyiğit for their helpful reviews, which greatly improved the original manuscript. This work was supported by the Swiss National Science Foundation, grant n° 20-53646.98.

References

- [1] X. Le Pichon, J. Angelier, The Hellenic arc and trench system: a key to the neotectonic evolution of the eastern Mediterranean area, *Tectonophysics* 60 (1979) 1–42.
- [2] A. Zanchi, J. Angelier, Seismotectonics of western Anatolia: regional stress from geophysical and geological data, *Tectonophysics* 222 (1993) 259–274.
- [3] H.G. Kahle, C. Straub, R. Reilinger, S. McClusky, R. King, K. Hurst, G. Veis, K. Kastens, P. Cross, The strain rate field in the eastern Mediterranean region, estimated by repeated GPS measurements, *Tectonophysics* 294 (1998) 237–252.
- [4] P. England, The alignment of Earthquake T-axes with the principal axes of geodetic strain in the Aegean region, *Turkish J. Earth Sci.* 12 (2003) 47–54.
- [5] O. Lenk, A. Türkezer, S. Ergintav, A.İ. Kurt, A. Belgen, Monitoring the kinematics of Anatolia using permanent GPS network stations, *Turkish J. Earth Sci.* 12 (2003) 55–66.
- [6] E. Bozkurt, R.G. Park, Southern Menderes Massif: an incipient metamorphic core complex in western Anatolia, Turkey, *J. Geo. Soc., London* 151 (1994) 213–216.
- [7] E. Bozkurt, R.G. Park, Evolution of a mid-Tertiary extensional shear zone in the southern Menderes Massif, Western Turkey, *Soc. Géol. France Bull.* 168 (1997) 3–14.
- [8] E. Bozkurt, M. Satir, New Rb–Sr geochronology from the southern Menderes Massif (southwestern Turkey) and its tectonic significance, *Geo. Jour.* 35 (2000) 285–296.
- [9] A.İ. Okay, M. Satir, Coeval plutonism and metamorphism in a latest Oligocene metamorphic core complex in northwest Turkey, *Geo. Mag.* 137 (2000) 495–516.
- [10] E. Bozkurt, Neotectonics of Turkey – a synthesis, *Geodinam. Acta* 14 (2001) 3–30.
- [11] E. Bozkurt, R. Oberhänsli, Menderes Massif (western Turkey): structural, metamorphic and magmatic evolution – a synthesis, *Inter. J. Earth Sci.* 89 (2001) 679–708.
- [12] A.L.W. Lips, D. Cassard, H. Sözbilir, H. Yılmaz, J.R. Wijbrans, Multistage exhumation of the Menderes Massif, western Anatolia (Turkey), *Inter. J. Earth Sci.* 89 (2001) 781–792.
- [13] H. Sözbilir, Extensional tectonics and the geometry of related macroscopic structures: Field evidence from the Gediz detachment, western Turkey, *Turkish J. Earth Sci.* 10 (2001) 51–67.
- [14] Ö.F. Güreş, Y. Yılmaz, Geology of the Ören and surrounding regions, SW Turkey, *Turkish J. Earth Sci.* 11 (2002) 2–18.
- [15] E. Arpat, E. Bingöl, The rift system of the western Turkey; thoughts on its development, *MTA Bull.* 73 (1969) 1–9.
- [16] G. Seyitoğlu, B.C. Scott, C.C. Rundle, Timing of Cenozoic extensional tectonics in west Turkey, *J. Geo. Soc., London* 149 (1992) 533–538.
- [17] G. Seyitoğlu, A. Koçyiğit, H. Yusufoglu, E. Bozkurt, Evidence from the Gediz graben for episodic two-stage extension in western Turkey; discussion and reply, *J. Geo. Soc., London* 156 (1999) 1240–1242.
- [18] G. Seyitoğlu, İ. Çemen, O. Tekeli, Extensional folding in the Alaşehir (Gediz) Graben, western Turkey, *J. Geo. Soc., London* 157 (2000) 1097–1100.
- [19] G. Seyitoğlu, O. Tekeli, İ. Çemen, Ş. Şen, V. Işık, The role of the flexural rotation/rolling hinge model in the tectonic evolution of the Alaşehir Graben, western Turkey, *Geo. Mag.* 139 (2002) 15–26.
- [20] A. Koçyiğit, H. Yusufoglu, E. Bozkurt, Evidence from the Gediz graben for episodic two stage extension in western Turkey, *J. Geo. Soc., London* 156 (1999) 605–616.
- [21] E. Bozkurt, Timing of Extension on the Büyük Menderes Graben, Western Turkey and its tectonic implications, in: E. Bozkurt, J.A. Winchester, J.D.A. Piper, (Eds), *Tectonics and Magmatism in Turkey and the Surrounding Area*. Geo. Soc. London, Spec. Publ. 173, 2000, pp. 385–403.
- [22] E. Bozkurt, Late Alpine evolution of the central Menderes Massif, western Anatolia, Turkey, *Inter. J. Earth Sci.* 89 (2001) 728–744.
- [23] E. Bozkurt, Origin of NE-trending basins in western Turkey, *Geodinam. Acta* 16 (2003) 61–81.
- [24] Y. Yılmaz, Ş.C. Genç, O.F. Güreş, M. Bozcu, K. Yılmaz, Z. Karacık, Ş. Altunkaynak, A. Elmas, When did the western Anatolian grabens begin to develop? in: E. Bozkurt, J.A. Winchester, J.D.A. Piper, (Eds), *Tectonics and Magmatism in Turkey and the Surrounding Area*. Geo. Soc. London, Spec. Publ. 173, 2000, pp. 353–384.
- [25] E. Bozkurt, G. Seyitoğlu, İ. Çemen, O. Tekeli, Extensional folding in the Alaşehir (Gediz) Graben, western Turkey; discussion and reply, *J. Geo. Soc. London* 159 (2002) 105–109.
- [26] H. Sözbilir, Geometry and origin of folding in the Neogene sediments of the Gediz Graben, western Anatolia, Turkey, *Geodinam. Acta* 15 (2002) 277–288.
- [27] E. Bozkurt, H. Sözbilir, Tectonic evolution of the Gediz Graben: field evidence for an episodic, two-stage extension in western Turkey, *Geol. Mag.* 141 (2004) 63–79.
- [28] J.F. Dewey, Extensional collapse of orogens, *Tectonics* 7 (1988) 1123–1139.
- [29] G. Seyitoğlu, B.C. Scott, Late Cenozoic crustal extension and basin formation in west Turkey, *Geo. Mag.* 128 (1991) 155–166.
- [30] G. Seyitoğlu, B.C. Scott, The cause of N–S extensional tectonics in western Turkey: Tectonic escape vs back-arc spreading vs orogenic collapse, *J. Geodynam.* 22 (1996) 145–153.
- [31] J.E. Meulenkeamp, W.J.R. Wortel, W.A. van Wamel, W. Spakman, E. Hoogerduyn Strating, On the Hellenic subduction zone and geodynamic evolution of Crete in the late middle Miocene, *Tectonophysics* 146 (1988) 203–215.
- [32] L. Jolivet, M. Patriat, Ductile extension and the formation of the Aegean Sea, in: B. Durand, L. Jolivet, F. Horvath, M. Seranne (Eds), *Mediterranean Basins: Tertiary Extension within the Alpine Orogen*. Geo. Soc. London, Spec. Publ. 156, 1999, pp. 427–456.

- [33] J. Malavielle Normal faulting and exhumation of metamorphic rocks in mountain belts, in: S. Sengupta (ed), *Evolution of Geological Structures in Micro- to Macro-scales*. Chapman & Hall, London, 1997, pp. 47-57.
- [34] L. Jolivet, B. Goffé, Les dômes métamorphiques extensifs dans les chaînes de montagne; extension syn-orogénique et post-orogénique. *Comptes R. l'Académ. Sci. Paris* 330 (2000) 739-751.
- [35] A.M.C. Şengör, The North Anatolian Transform Fault: its age, offset and tectonic significance. *J. Geo. Soc. London* 13 (1979) 268-282.
- [36] A.M.C. Şengör, Cross-faults and differential stretching of hanging-walls in regions of low-angle normal faulting: examples from western Turkey, in: M.P. Coward, J.F. Dewey, P.L. Hancock (Eds), *Continental Extensional Tectonics*, vol. 28, Geo. Soc. London, Spec. Publ., 1987, pp. 575-589.
- [37] A.İ. Okay, M. Siyako, K.A. Bürkan, Geology and tectonic evolution of the Biga Peninsula, northwest Turkey. *Bull. Technique de l'Université d'Istanbul* 44 (1991) 191-255.
- [38] L. Beccaletto, Geology, Correlations, and Geodynamic Evolution of the Biga Peninsula (NW Turkey). *Mémoires de Géologie* 43, 2004, Lausanne, Switzerland.
- [39] M. Duru, Ş. Pehlivan, Y. Şentürk, F. Yavaş, H. Kar, Lithostratigraphy of the Kazdağ Massif in Northwest Turkey. *Turkish J. Earth Sci.* 13 (2004) 177-186.
- [40] A.İ. Okay, M. Satır, M. Siyako, P. Monie, R. Metzger, S. Akyüz, Paleo- and Neo-Tethyan events in northwestern Turkey: Geologic and geochronologic constraints. In: A. Yin, T.M. Harrison (Eds), *The Tectonic Evolution of Asia* Cambridge University Press, 1996, pp. 420-441.
- [41] A.L.W. Lips, Temporal Constraints on the Kinematics of the Destabilization of an Orogen – Syn- to Post-Orogenic Extensional Collapse of the Northern Aegean Region, PhD thesis, 1998, Vrije University, Netherlands, Amsterdam.
- [42] M. Siyako, K.A. Bürkan, A.İ. Okay, Tertiary geology and hydrocarbon potential of the Biga and Gelibolu Peninsula, *Turkish Assoc. Petrol. Geol. Bull.* 1 (1989) 183-199.
- [43] Y. Yılmaz, Z. Karacık, Geology of the northern side of the Gulf of Edremit and its tectonic significance for the development of the Aegean grabens, *Geodinam. Acta* 14 (2001) 31-43.
- [44] U. İnci, The stratigraphy and organic properties of Demirci and Burhaniye bituminous shales, *Geol. Congress Turkey Proceedings* 5 (1984) 27-40 [in Turkish with English abstract].
- [45] S. Borsi, G. Ferrari, F. Innocenti, R. Mazzuoli, Geochronology and petrology of recent volcanics in the eastern Aegean Sea west Anatolia and Lesbos Island, *Bull. Volcan.* 36 (1972) 473-496.
- [46] T. Ercan, M. Satır, G. Steinitz, A. Dora, E. Sarıfakoğlu, C. Adis, H.-J. Walter, T. Yıldırım, Biga yarımadası ile Gökçeada, Bozcaada ve Tavşan adalarındaki (KB Anadolu) Tersiyer volkanizmasının özellikleri. *MTA Bull.* 117 (1995) 55-86 [in Turkish with English abstract].
- [47] M.Z. Gözler, Geologic and petrographic investigation of Mihli dere valley (Kazdağ, northwestern Turkey), *Bull. Geo. Soc. Turkey* 29 (1986) 133-142 [in Turkish with English abstract].
- [48] S.J. Friedmann, D.W. Burbank, Rift basins and supradetachment basins: intracontinental extensional end members, *Basin Res.* 7 (1995) 109-127.
- [49] R. Caby, D. Hammor, C. Delor, Metamorphic evolution, partial melting and Miocene exhumation of lower crust in the Edough metamorphic core complex, West Mediterranean orogen, eastern Algeria, in: O. Vanderhaeghe (Ed), *Partial Melting of Crust and Flow of Orogens*. Elsevier, Amsterdam, 2001 pp. 239-273.
- [50] M. Fytikas, O. Giuliani, F. Innocenti, G. Maarinelli, R. Mazzuoli, Geochronological data on Recent magmatism of the Aegean Sea, *Tectonophysics* 31 (1976) 29-34.
- [51] G. Pe-Piper, D.J.W. Piper, Spatial and temporal variation in late Cenozoic back-arc volcanic rocks, Aegean Sea region, *Tectonophysics* 169 (1989) 113-34.
- [52] W. Spakman, M.J.R. Wortel, N.J. Vlaar, The Hellenic subduction zone: a tomographic image and its geodynamic implications, *Phys. Earth Planet. Int.* 79 (1988) 3-74.
- [53] L. Benda, Principles of the subdivision of the Turkish Neogene, *Newslet. Stratig.* 1 (1971) 23-26.
- [54] U. İnci, Depositional evolution of Miocene coal successions in the Soma coalfield, western Turkey, *Inter. J. Coal Geol.* 51 (2002) 1-29.
- [55] A.M.C. Şengör, W.S.F. Kidd, Post-collisional tectonics of Turkish-Iranian plateau and a comparison with Tibet, *Tectonophysics* 55 (1979) 361-376.
- [56] Y. Yılmaz, An approach to the origin of young volcanic rocks of western Turkey, in: A.M.C. Şengör (Ed), *Tectonic Evolution of the Tethyan Region*. Kluwer Academic Publisher 259, 1989, pp. 159-190.
- [57] Y. Yılmaz, Comparison of young volcanic associations of western and eastern Anatolia under compressional regime; a review, *J. Volcan. Geoth. Res.* 44 (1990) 69-87.
- [58] Y. Yılmaz, Ş.C. Genç, Z. Karacık, S. Altunkaynak, Two contrasting magmatic association of NW Anatolia and their tectonic significance, *J. Geodynam.* 31 (2001) 243-271.
- [59] D. Richter, C. Müller, Der "Erste Flysch" in der Pindos-Zone (Griechenland), *Neues Jahr. Geol. Paläont., Monatshefte* 4 (1993) 209-226.
- [60] D. Richter, C. Müller, Die Flysch-Zonen Griechenlands VI. Zur Stratigraphie des Flysches der Pindos-Zone zwischen der Querzone von Kastaniotikos und dem Südpeloponnes (Griechenland), *Neues Jahr. Geol. Paläont., Monatshefte* 8 (1993) 449-476.
- [61] G.M. Stampfli, Tethyan oceans, in: E. Bozkurt, J.A. Winchester, J.D.A. Piper (Eds), *Tectonics and Magmatism in Turkey and the Surrounding Area*, Geo. Soc. London, Spec. Publ. 173, 2000, 1-23.
- [62] G.M. Stampfli, G. Borel, The TRANSMED transects in space and time: constraints on the paleotectonic evolution of the Mediterranean domain, in: W. Cavazza, F. Roure, W. Spakman, G.M. Stampfli, P. Ziegler (Eds), *The TRANSMED Atlas: the Mediterranean Region from Crust to Mantle*. Springer Verlag, 2004, pp.
- [63] M. Gutnic, O. Monod, A. Poisson, J.-F. Dumont, *Géologie des Taurides occidentales (Turquie)*. Mémoires de la Société Géologique de France 137 (1979).
- [64] S.C. Genç, Ş. Altunkaynak, Z. Karacık, M. Yazman, Y. Yılmaz, The Çubukdağ graben, south of Izmir: its tectonic significance in the Neogene geological evolution of western Anatolia, *Geodinam. Acta* 14 (2001) 45-56.
- [65] F.Ö. Gürer, M. Bozcu, K. Yılmaz, Y. Yılmaz, Neogene basin development around Söke-Kuşadası (western Anatolia) and its bearing on tectonic development of the Aegean region, *Geodinam. Acta* 14 (2001) 57-70.
- [66] O. Kaya, E. Ünay, G. Saraç, S. Eichhorn, S. Hassenrück, A. Knappe, A. Pekdeğer, S. Mayda, Halitpaşa transpressive zone: implications for an Early Pliocene compressional phase in central western Anatolia, Turkey, *Turkish J. Earth Sci.* 13 (2004) 1-13.
- [67] A. Koçyiğit, E. Ünay, G. Saraç, Episodic graben formation and extensional neotectonic regime in west central Anatolia and the Isparta Angle; a case study in the Akşehir-Afyon Graben, Turkey, in: E. Bozkurt, J.A. Winchester, J.D.A. Piper, (Eds), *Tectonics and Magmatism in Turkey and the Surrounding Area*. Geo. Soc. London, Spec. Publ. 173, 2000, pp. 405-421.
- [68] A.M.C. Şengör, Y. Yılmaz, Tethyan evolution of Turkey: a plate tectonic approach, *Tectonophysics* 75 (1981) 181-241.
- [69] J.F. Dewey, M.R. Hempton, W.S. Kidd, F. Şaroğlu, A.M.C. Şengör, Shortening of continental lithosphere: the neotectonics of eastern Anatolia – a young collision zone, in: A.C. Reis (Ed), *Collisional Tectonics*. Geo. Soc. London, Spec. Publ. 19, 1986, pp. 2-36.
- [70] A. Koçyiğit, A. Özacar, Extensional neotectonic regime through the NE edge of outer Isparta Angle, SW Turkey: new field and seismic data, *Turkish J. Earth Sci.* 12 (2003) 67-90.
- [71] A.A. Barka, The North Anatolian fault zone, *Annales Tectonicae* VI (1992) 164-195.

- [72] R. Armijo, B. Meyer, A. Hubert, Westward propagation of the North Anatolian fault into the northern Aegean: Timing and kinematics, *Geology* 27 (1999) 267-270.
- [73] R. Westaway, Kinematics of the Middle East and Eastern Mediterranean updated, *Turkish J. Earth Sci.* 12 (2003) 5-46.
- [74] L. Jolivet, C. Faccena, Mediterranean extension and the Africa-Eurasia collision, *Tectonics* 19 (2000) 1095-1106.
- [75] C. Kissel, C. Laj, The Tertiary geodynamical evolution of the Aegean arc: a paleomagnetic reconstruction, *Tectonophysics* 146 (1988) 183-201.
- [76] M. Pfister, W. Balderer, E. Greber, H.G. Kahle, D. Mayer-Rossa, S. Mueller, L. Rybach, C. Schindler, S. Sellami, C. Straub, Synthesis of the Marmara Poly-Project, in: M. Pfister (ed), *Active Tectonics of Northwestern Anatolia – The Marmara Poly-Project. A Multidisciplinary Approach by Space-Geodesy, Geology, Hydrogeology, Geothermics and Seismology.* vdf Hochschulverlag AG an der ETHZ, Zürich, 1997, pp. 539-565.
- [77] C. Straub, H.G. Kahle, Recent crustal deformation and strain accumulation in the Marmara Sea region, NW Anatolia, inferred from repeated GPS measurements, in: M. Pfister (Ed), *Active Tectonics of Northwestern Anatolia – The Marmara Poly-Project. A Multidisciplinary Approach by Space-Geodesy, Geology, Hydrogeology, Geothermics and Seismology.* vdf Hochschulverlag AG an der ETHZ, Zürich, 1997, pp. 418-447.
- [78] B. Üçer, H. Eyidoğan, C. Gürbüz, A.A. Barka, Ş. Barış, Seismic investigations in the Marmara region. in: M. Pfister (Ed), *Active Tectonics of Northwestern Anatolia – The Marmara Poly-Project. A Multidisciplinary Approach by Space-Geodesy, Geology, Hydrogeology, Geothermics and Seismology.* vdf Hochschulverlag AG an der ETHZ, Zürich, 1997, pp. 90-99.
- [79] E. Bozkurt, Granitoid rocks of the southern Menderes Massif (southwestern Turkey): field evidence for Tertiary magmatism in an extensional shear zone, *Inter. J. Earth Sci.* 93 (2004) 52-71.
- [80] E. Bozkurt, S.K. Mittweide, Introduction to the geology of Turkey – a synthesis, *Inter. Geol. Rev.* 43 (2001) 578-594.
- [81] A.İ. Okay, İ. Tansel, O. Tüysüz, Obduction, subduction and collision as reflected in Upper Cretaceous-Lower Eocene sedimentary record of western Turkey, *Geo. Mag.* 138 (2001) 117-142.

Les bassins carbonifères-permiens et leur couverture méso-cénozoïque - Mise à jour des connaissances, applications et perspectives

Résumé - Ce mémoire d'HDR met en lumière mes travaux de recherche au cours des 15 dernières années sur les bassins sédimentaires carbonifères-permiens et leur couverture méso-cénozoïque sur le territoire métropolitain. (i) Un premier volet méthodologique présente le retraitement et l'interprétation de profils sismiques réflexions industriels. Véritable matière de mon travail, ces profils couplés aux données de forages adéquates sont cruciaux pour imager et comprendre le mode de formation et l'évolution de ces bassins et de leur couverture au cours des temps géologiques. (ii) Un second volet expose mes travaux sur les bassins carbonifères-permiens, au cœur de mon manuscrit. Il s'agit en premier lieu de préciser leurs caractéristiques tectoniques et sédimentaires (localisation sous couverture, profondeur, épaisseur, calage temporel, style structural, mode de remplissage). Je montre ensuite, sur la base de scénarios cinématiques, comment ils enregistrent la transition syn- à post-orogénique varisque (syn-orogénique : bassin houiller des Hauts-de-France ; transition syn à post-orogénique : bassin houiller lorrain ; post-orogénique : bassins du nord du Massif Central et du SO du bassin de Paris). (iii) En utilisant les mêmes données de subsurface (profils sismiques et forages, cf. volet 1), le troisième volet présente mes recherches sur leur couverture sédimentaire méso-cénozoïque, à l'exemple de mes travaux dans le bassin de Paris et le fossé Rhéan. Sur la base de schémas structuraux mis à jour, je précise l'impact grande maille des structures sur les réservoirs/aquifères, et leur déformation en réponses aux événements géodynamiques subis par la plaque ouest-européenne. (iv) Je présente dans une dernière partie mes perspectives de recherches, en insistant sur la nécessité de continuer de mettre à jour la connaissance sur les bassins sédimentaires carbonifères-permiens et leur couverture, à travers de nouveaux cas d'études ou des nouvelles approches méthodologiques. En effet, la transition énergétique en cours nous impose de mieux connaître notre sous-sol, afin de définir et répondre à ses nouveaux usages (géothermie, hydrogéologie, hélium naturel, stockage profond...).

Carboniferous-Permian basins and their Meso-Cenozoic cover - scientific update, applications, and prospects

Abstract - This HDR thesis highlights my research work over the last 15 years on Carboniferous-Permian sedimentary basins and their Meso-Cenozoic cover in France. (i) A first methodological section presents the reprocessing and interpretation of industrial seismic reflection profiles. These profiles, coupled with appropriate borehole data, are crucial for imaging and understanding the mode of formation and evolution of these basins and their cover over geological time. (ii) A second section describes my work on the Carboniferous-Permian basins, at the heart of my manuscript. Firstly, I describe their tectonic and sedimentary characteristics (location under cover, depth, thickness, temporal setting, structural style, mode of filling). I then show, based on kinematic scenarios, how they record the syn- to post-orogenic Variscan transition (syn-orogenic: Hauts-de-France coal basin; syn- to post-orogenic transition: Lorraine coal basin; post-orogenic: basins of the northern Massif Central and SW Paris Basin). (iii) Using the same subsurface data (seismic profiles and boreholes, see section 1), the third section presents my research on their Meso-Cenozoic sedimentary cover, based on my work in the Paris Basin and Rhine Graben. Using updated structural schemes, I describe the large-scale impact of structures on reservoirs/aquifers, and their deformation in response to geodynamic events of the West European plate. (iv) In the final section, I present my research prospects, emphasizing the need to continue updating our knowledge of Carboniferous-Permian sedimentary basins and their cover, through new case studies or new methodological approaches. Indeed, the current energy transition requires us to understand our subsurface better, in order to define and respond to its new uses (geothermal energy, hydrogeology, natural helium, deep storage, etc.).